

METATÉRIOS PALEÓGENOS E NEÓGENOS DA AMAZÔNIA OCIDENTAL : SISTEMÁTICA E HISTÓRIA EVOLUTIVA

Narla Shannay Stutz

▶ **To cite this version:**

Narla Shannay Stutz. METATÉRIOS PALEÓGENOS E NEÓGENOS DA AMAZÔNIA OCIDENTAL : SISTEMÁTICA E HISTÓRIA EVOLUTIVA. Systematics, Phylogenetics and taxonomy. Université de Montpellier; Universidade do Rio Grande do Sul – Porto Alegre (Brésil), 2023. Portuguese. ⟨NNT : 2023UMONG108⟩. ⟨tel-05092416⟩

HAL Id: tel-05092416

https://theses.hal.science/tel-05092416v1

Submitted on 2 Jun 2025

HAL is a multi-disciplinary open access archive for the deposit and dissemination of scientific research documents, whether they are published or not. The documents may come from teaching and research institutions in France or abroad, or from public or private research centers.

L'archive ouverte pluridisciplinaire **HAL**, est destinée au dépôt et à la diffusion de documents scientifiques de niveau recherche, publiés ou non, émanant des établissements d'enseignement et de recherche français ou étrangers, des laboratoires publics ou privés.



HAL Authorization

THÈSE POUR OBTENIR LE GRADE DE DOCTEUR DE L'UNIVERSITÉ DE MONTPELLIER

En Paléobiologie

École doctorale GAIA

Unité de recherche UMR 5554 - ISEM - Institut des Sciences de l'Evolution - Montpellier

En partenariat international avec le Programa de Pós-Graduação em Geociências, Universidade Federal do Rio Grande do Sul. Brésil

Métathériens paléogènes et néogènes d'Amazonie occidentale : systématique et histoire évolutive

Présentée par Narla Shannay Stutz

Le 08 mai 2023

Sous la direction de Pierre-Olivier ANTOINE et d'Ana Maria RIBEIRO

Devant le jury composé de

Analia M. FORASIEPI, Directrice de Recherche, Instituto Argentino de Nivología, Glaciología y Ciencias Ambientales, Centro de Investigaciones Científicas y Técnicas (CCT CONICET Mendoza)	Rapporteur
Darin CROFT, Professeur, Case Western Reserve University School of Medicine	Rapporteur
Silane A. F. da SILVA-CAMINHA, Professeur, Universidade Federal de Mato Grosso	Examinateur
Marie-Pierre LEDRU, Directrice de Recherche, Institut de Recherche pour le Développement	Examinateur
César L. SCHULTZ, Professeur, Universidade Federal do Rio Grande do Sul	Examinateur
Pierre-Olivier ANTOINE, Professeur, Université de Montpellier	Directeur de thèse
Ana Maria RIBEIRO, Directrice de Recherche, Museu de Ciências Naturais, Secretaria do Meio Ambiente e Infraestrutura RS	Co-Directeur de thèse

UNIVERSITÉ DE MONTPELLIER

UNIVERSIDADE FEDERAL DO RIO GRANDE DO SUL
INSTITUTO DE GEOCIÊNCIAS
PROGRAMA DE PÓS-GRADUAÇÃO EM GEOCIÊNCIAS

METATÉRIOS PALEÓGENOS E NEÓGENOS DA AMAZÔNIA OCIDENTAL: SISTEMÁTICA E HISTÓRIA EVOLUTIVA

NARLA SHANNAY STUTZ

ORIENTADORA – Profª. Drª. Ana Maria Ribeiro

ORIENTADOR – Prof. Dr. Pierre-Olivier Antoine

Volume 1

Porto Alegre, 2023

UNIVERSIDADE FEDERAL DO RIO GRANDE DO SUL
INSTITUTO DE GEOCIÊNCIAS
PROGRAMA DE PÓS-GRADUAÇÃO EM GEOCIÊNCIAS

METATÉRIOS PALEÓGENOS E NEÓGENOS DA AMAZÔNIA OCIDENTAL (PERU E BRASIL): SISTEMÁTICA E HISTÓRIA EVOLUTIVA

NARLA SHANNAY STUTZ

ORIENTADORA – Profª. Drª. Ana Maria Ribeiro
ORIENTADOR – Prof. Dr. Pierre-Olivier Antoine
BANCA EXAMINADORA
Dra. Analia M. Forasiepi – Instituto Argentino de Nivología, Glaciología y Ciencias Ambientales, Centro de Investigaciones Científicas y Técnicas (CCT CONICET Mendoza), Mendoza, Argentina - *revisora*
Prof. Dr. César L. Schultz – Departamento de Paleontologia e Estratigrafia, Instituto de Geociências, Universidade Federal do Rio Grande do Sul, Porto Alegre, Brasil - *examinador*
Prof. Dr. Darin Croft – Department of Anatomy, Case Western Reserve University School of Medicine, Cleveland, OH, Estados Unidos - *revisor*
Profa. Dra. Silane A. F. da Silva-Caminha – Faculdade de Geociências, Universidade Federal de Mato Grosso, Cuiabá, Mato Grosso, Brasil – *examinadora*
Dra. Marie-Pierre Ledru – Institut de Recherche pour le Développement, Montpellier, França - *examinadora*

Volume 1

Tese de Doutorado apresentada como requisito parcial para a obtenção do Título de Doutora em Ciências.

Porto Alegre, 2023

CIP - Catalogação na Publicação

Stutz, Narla Shannay
METATÉRIOS PALEÓGENOS E NEÓGENOS DA AMAZÔNIA OCIDENTAL: SISTEMÁTICA E HISTÓRIA EVOLUTIVA / Narla Shannay Stutz. -- 2023.
756 f.
Orientadora: Ana Maria Ribeiro.

Coorientador: Pierre-Olivier Antoine.

Tese (Doutorado) -- Universidade Federal do Rio Grande do Sul, Instituto de Geociências, Programa de Pós-Graduação em Geociências, Porto Alegre, BR-RS, 2023.

1. Marsupial. 2. Eoceno. 3. Oligoceno. 4. Mioceno. 5. Polydolopimorphia. I. Ribeiro, Ana Maria, orient. II. Antoine, Pierre-Olivier, coorient. III. Título.

Elaborada pelo Sistema de Geração Automática de Ficha Catalográfica da UFRGS com os dados fornecidos pelo(a) autor(a).

A minha tia Manoca, por todo o amor que pudemos partilhar antes da tua partida.

Como um rio

Ser capaz, como um rio
que leva sozinho
a canoa que se cansa,
de servir de caminho
para a esperança.
E de lavar do límpido
a mágoa da mancha,
como o rio que leva,
e lava.

Crescer para entregar
na distância calada
um poder de canção,
como o rio decifra
o segredo do chão.

Se tempo é de descer,
reter o dom da força
sem deixar de seguir.
E até mesmo sumir
para, subterrâneo,
aprender a voltar
e cumprir, no seu curso,
o ofício de amar.

Como um rio, aceitar
essas súbitas ondas
feitas de água impuras
que afloram a escondida
verdade nas funduras.

Como um rio, que nasce
de outros, saber seguir
junto com outros sendo
e noutros se prolongando
e construir o encontro
com as águas grandes
do oceano sem fim.

Mudar em movimento,
mas sem deixar de ser
o mesmo ser que muda.
Como um rio.

Thiago de Mello, no livro "Mormaço na floresta". Civilização Brasileira, 1981.

AGRADECIMENTOS

Gostaria de agradecer primeiramente à oportunidade de, durante a graduação e pós-graduação, ter cursado um ensino superior gratuito e de qualidade no Brasil, e a todos os professores, servidores técnico-administrativos e terceirizados que possibilitaram que minha jornada acadêmica culminasse nesta tese de doutorado. Também gostaria de agradecer aos órgãos de fomento, Conselho Nacional de Desenvolvimento Científico e Tecnológico (CNPq), Coordenação de Aperfeiçoamento de Pessoal de Nível Superior (CAPES) e o programa CAPES-COFECUB Te 924/18/ 88881.143095/2017–01 “Paléo-Amazone: evolution Néogène de l’Amazonie Brésilienne/O PALEO AMAZONAS: evolução neogênica da Amazônia Brasileira” pelas bolsas que recebi e que possibilitaram o desenvolvimento dos meus trabalhos científicos e subsistência.

Gostaria de agradecer sobretudo aos meus orientadores de tese: Profa. Dra. Ana Maria Ribeiro, obrigada por me acompanhar em minha trajetória desde o mestrado, aceitar e incentivar meus projetos e pelos ensinamentos; Prof. Dr. Pierre-Olivier Antoine, obrigada por ter aceitado orientar uma pessoa desconhecida, por ter oferecido seu grande conhecimento e amizade nesta jornada, mesmo nos momentos difíceis. Um agradecimento especial também a meu orientador não-oficial Dr. Laurent Marivaux, sem quem certamente o doutorado não teria se desenrolado tão fruitiva e amigavelmente. Também agradeço a minha primeira orientadora, Profa. Dra. Patrícia Hadler (UFSC), por ter me abertos as portas e me ensinado os caminhos da ciência.

Agradeço igualmente aos colegas de campo, Michele, Martin, Aldo, Walter, Julia, Ricardo, Roberto, André, Tiago, Emmanuelle e, em especial François Pujos, além dos que auxiliaram na logística, por terem tornado o trabalho árduo uma vivência

de aprendizados e companheirismo. Também gostaria de agradecer aos coautores das minhas publicações, em especial Myriam Boivin, por suas contribuições e convites, pelos aprendizados e enriquecimento científico.

Agradeço imensamente aos meus amigos Mariana Gomes, Jaqueline, Júlia, Gabriel, Maiara, Carol, Mariana Bessel, Daniel, Renato, Cleiton, Dudu, Pâmela, Lívia, Kellen, Sabrina, Andrey, Pedro e Rafa, além de meus amigos no momento um tanto distantes, Leïla, Elena, Laly, Atacan, Léa, Marina, Lila, Amanda, Rémy, Diego, Sebástian, por serem sempre minha base e refúgio. Agradeço também a todos meus colegas de laboratório, PPGGEO e UFRGS, Ângela, Brodsky, Thaís, Ana Rita, Fernanda, Tiago, Mariana, Simone, Maiara, Thamiris, Camila, Morgan, Paulo, Marcel, Adriana, Catherine, Bruno e Vladmir, pelos momentos de companheirismo e amizade, tanto na tristeza quanto na alegria.

E por fim, agradeço imensamente a minha família, em especial meus pais, Odesio e Marcia, por todo o amor, incentivo e carinho que sempre compartilhamos.

REMERCIEMENTS

Je voudrais remercier les deux universités impliquées dans cette thèse, Université de Montpellier et Universidade Federal do Rio Grande do Sul, pour l'accès et l'infrastructure fournies pour la réalisation de ce projet, en spécial à l'Institut des Sciences de l'Évolution de Montpellier, je n'aurais pas pu imaginer un meilleur cadre pour développer ma thèse en France. Je remercie également les agences de financement, Conselho Nacional de Desenvolvimento Científico e Tecnológico (CNPq), Coordenação de Aperfeiçoamento de Pessoal de Nível Superior (CAPES) et le programme CAPES-COFECUB Te 924/18/ 88881.143095/2017–01 "Paléo-Amazone: evolution Néogène de l'Amazonie Brésilienne/O PALEO AMAZONAS: evolução neogênica da Amazônia Brasileira", ainsi que les autres impliquées dans les projets menés par mes collègues, d'avoir fourni les moyens pour ma subsistance et pour la réalisation de la recherche.

Je remercie aussi mes deux directeurs de thèse : Prof. Dr. Ana Maria Ribeiro, merci de m'avoir accompagné pendant cette longue trajectoire depuis le master et d'avoir soutenu mes projets ; Prof. Dr. Pierre-Olivier Antoine, merci beaucoup d'avoir accepté d'encadrer une inconnue, d'avoir été plus qu'un encadrant, mais aussi un ami, que ce soit pendant les moments joyeux ou les plus durs. Et un grand merci à mon directeur de thèse non-officiel Dr. Laurent Marivaux, meilleur collègue de bureau, avec qui j'ai tant appris et sans qui je n'aurai pas développé ce projet entourée de tant d'amitié et bienveillance.

Je remercie également mes collègues de terrain, Michele, Martin, Aldo, Walter, Julia, Ricardo, Roberto, André, Tiago, Emmanuelle et, spécialement François Pujos, d'avoir transformé ces durs périples en des moments joyeux et enrichissants. Je voudrais aussi remercier les coauteurs de mes papiers, en spécial Myriam Boivin, pour

leurs contributions et invitations, qui m'ont tant appris et enrichi mes connaissances scientifiques. Je voudrais remercier aussi les Profs. Drs. Brigitte Meyer-Berthaud et Robin Beck, ainsi que les membres de la direction de l'ISEM, de m'avoir accompagné pendant les comités de suivi de thèse et d'aider à améliorer mon projet.

Un grand merci aussi à tous les permanents de l'ISEM, en spécial à ceux de l'équipe Palénto, ainsi que Frédéric, Fabien, Julien-Claude, Camille, Marie-ka et Christelle, de m'avoir aussi bien accueillie au laboratoire et fait de mon séjour une expérience dont je garderai des très bons souvenirs. En spécial, je remercie à Catherine Girard, pour l'amitié et bienveillance.

Un grand merci à mes collègues non-permanents de l'ISEM, en spécial Alex, Amira, Félix, Léa, Alice, Louise, Manon, Nicolas, Selim, Céline, Nathan, Quentin, Sophie, Mehdi, Laura, Katerine et Daniely, de m'avoir accueillie et partagé tant de bons moments avec moi. Je remercie aussi mes amis en France et en Europe, Leïla, Elena, Atacan, Léa, Marina, Laly, Diego, Rémy, Amanda, Sebástian, Érika, Tomas, Murielle, Mathilde, Lila, Fanny, Cristina, ainsi qu'à ma famille d'accueil, de m'avoir toujours bien reçue et me faire sentir chez moi en Europe, de m'avoir soutenue et accompagné pendant la joie et la tristesse.

Et, finalement, je remercie ma famille, spécialement mes parents, Odesio et Marcia, pour tout l'amour, support et tendresse.

RESUMO

Metatheria, grupo-irmão dos placentários dentre os mamíferos, provavelmente se originou no Jurássico no que seria hoje a Ásia–América do Norte. Posteriormente, o grupo de difundiu por todo o Hemisfério Norte, sendo registrados na América do Norte, Europa e Ásia até o Mioceno e no Eoceno e Oligoceno da África. No Neocretáceo, um ou mais clados de metatérios dispersaram-se da América do Norte para a América do Sul, tendo seu registro mais antigo neste continente no início do Paleoceno da Argentina. Em seguida, provavelmente no Paleoceno, uma ou mais linhagens de metatérios americanos migrou em direção à Austrália, passando pela Antártica. As relações filogenéticas de Metatheria permanecem objeto de pesquisas e debates, principalmente a composição e afinidades de seus maiores subclados. O grupo-coroa, Marsupialia, que compreende todos os metatérios viventes, é dividido em: Australidelphia, com as ordens atuais (Dasyuromorphia, Peramelemorphia, Diprotodontia e Notoryctemorphia) e uma ordem fóssil (Yalkaparidontia) de distribuição na Australásia, além da ordem sul-americana Microbiotheria e possivelmente Polydolopimorphia (atualmente extintos); e “Ameridelphia”, táxon polifilético contendo as ordens Didelphimorphia e Paucituberculata, de ocorrência sobretudo na América do Sul. Ademais, a América do Sul contou com notável diversidade pretérita de metatérios, com táxons basais considerados “Ameridelphia” *incertae sedis*, incluindo a ordem Sparassodonta, atualmente extintos. A história evolutiva dos metatérios na América do Sul no Cenozoico é marcada por distintas fases, com períodos de diversificação e extinções, registradas em alguns sítios excepcionais, em especial na porção sul do continente. Contudo, observam-se grandes lacunas no registro fóssil de Metatheria na América do Sul, principalmente para a porção norte do continente, Região Amazônica, onde são reportados para alguns depósitos do Eoceno–Mioceno do Peru, Brasil, Venezuela e Colômbia. Neste sentido, a presente tese objetivou a identificação de restos fósseis de metatérios provenientes de localidades brasileiras (Estado do Acre, Alto Rio Juruá e Rio Envira, Formação Solimões, Bacia do Acre) e peruanas (regiões de Contamana, Bacia do Huallaga e Atalaya) da Região Amazônica, abrangendo o intervalo Eoceno–Mioceno, com o objetivo de contribuir para o conhecimento da sistemática e história evolutiva de Metatheria. Na localidade TAR-31, Departamento de San Martín, Peru, final do Mesomioceno (Laventense, ~13 Ma), três táxons de metatérios foram identificados: o didelfídeo (ordem Didelphimorphia) '*Thylamys*' cf. '*T.*' *colombianus*, e os membros da ordem Paucituberculata aff. *Palaeothentes* e *Pitheculites ipururensis* sp. nov. Nas

localidades investigadas no Acre foram encontrados quatro táxons de didelfídeos na localidade PRE 06, Rio Envira: Marmosini cf. *Marmosa*, *Didelphis* cf. *D*. *solimoensis*, '*Thylamys*' *colombianus*, além de didelfídeos não identificados, o que amplia significativamente a diversidade conhecida desta família no Mioceno do Acre. Nas localidades do Alto Rio Juruá, foram identificados dois táxons de Paucituberculata: Palaeothentidae Palaeothentinae indet. (PRJ 25 e PRJ 33', ambos fora de contexto estratigráfico) e Abderiditae *Abderites* sp. (PRJ 33, *in situ*). De acordo com as faunas de mamíferos associados, os didelfídeos de PRE 06 indicam uma idade início do Neomioceno para este afloramento. Já *Abderites* sp. sugere uma idade mais antiga para PRJ 33, Mesomioceno. Trata-se dos primeiros registros de Paucituberculata para o Mioceno da Amazônia brasileira. Comparações destas associações de metatérios com faunas temporalmente correlatas da Região Amazônica indicam grande similaridade entre TAR-31 e o Acre, assim como com La Venta, confirmando que a Amazônia Ocidental era uma região biogeográfica única e consistente para os mamíferos terrestres durante o Mesomioceno, na margem ocidental do Sistema Pebas. Com relação às localidades paleógenas estudadas, foram estudados apenas os membros da ordem Polydolopimorphia, com a identificação de 11 táxons representando unicamente a subordem Bonapartheriiformes, tanto com Bonapartherioidea Prepidolopidae, quanto com Argyrolagoidea Argyrolagidae. Ademais, também se registra o gênero *Wamradolops* e um novo gênero e espécie de relações filogenéticas incertas dentro de Polydolopimorphia, além de polidolopimórfios não identificados. Observou-se que as assembleias de Polydolopimorphia nas distintas regiões estudadas no Peru se assemelham em termos de composição taxonômica quando temporalmente correlatas, além de se assemelharem a fauna local de Santa Rosa (Eooligoceno, Peru) e às assembleias do Eo- e Mesoeoceno do noroeste Argentino. Através dos resultados obtidos na presente tese, em comparação com a literatura, grandes mudanças (*turnovers*) na composição das comunidades de metatérios da Região Amazônica ocorrem ao longo do intervalo Eoceno–Mioceno. Nota-se que as associações de metatérios no Mesoeoceno eram predominantemente compostas por membros da ordem Polydolopimorphia, com grande diversidade e abundância. Um primeiro *turnover* ocorre em torno da transição Eoceno–Oligoceno, caracterizado pela diminuição da abundância e diversidade de polidolopimorfios nas assembleias, com praticamente o desaparecimento dos Prepidolopidae e presença de Argyrolagidae, assim como o aumento da quantidade de restos e de táxons de Paucituberculata. Estes eram representados unicamente pela superfamília

Palaeothentoidea e apresentavam grande diversidade e abundância durante o Oligoceno. No Eomioceno aparecem os primeiros registros de membros provadamente da ordem Didelphimorphia e no Neomioceno ocorre o segundo *turnover*. As comunidades de metatérios passam a ser então constituídas praticamente unicamente por didelfídeos, os quais são representados por táxons já derivados e bastante semelhantes aos grupos atuais. Registra-se apenas um Argyrolagidae no final do Neomioceno, único e último representante da grande diversidade de Polydolopimorphia que existiu anteriormente na Região Amazônica. Estes resultados salientam o papel da Região Amazônica no que diz respeito à história evolutiva e paleobiogeografia dos metatérios durante o final do Paleógeno e início do Neógeno.

Palavras-chave: Marsupial, Didelphimorphia, Paucituberculata, Polydolopimorphia, Eoceno, Oligoceno, Mioceno.

RÉSUMÉ

Les Metatheria, le groupe frère des placentaires au sein des mammifères, sont probablement apparus au Jurassique dans l'actuelle Asie–Amérique du Nord. Par la suite, le groupe s'est répandu dans tout l'hémisphère nord, et a été enregistré en Amérique du Nord, en Europe et en Asie jusqu'au Miocène, ainsi qu'à l'Éocène et à l'Oligocène en Afrique. Au Crétacé Supérieur, un ou plusieurs clades de métathériens se sont dispersés de l'Amérique du Nord vers l'Amérique du Sud, leur premier registre sur ce continent remontant au début du Paléocène en Argentine. Ensuite, probablement au Paléocène, un ou plusieurs groupes de métathériens américains ont gagné l'Australie, en passant par l'Antarctique. Les relations phylogénétiques des Metatheria restent un sujet de recherche et de débat, en particulier la composition et les affinités de ses principaux sous-clades. Le groupe couronne, Marsupialia, qui comprend tous les métathériens vivants, est divisé en : Australidelphia, avec les ordres existants (Dasyuromorphia, Peramelemorphia, Diprotodontia et Notoryctemorphia) et un ordre fossile (Yalkaparidontia) de l'Australasie, plus l'ordre sud-américain Microbiotheria et peut-être les Polydolopimorphia (actuellement éteint) ; et "Ameridelphia", un taxon polyphylétique contenant les ordres Didelphimorphia et Paucituberculata, principalement documentés en Amérique du Sud. En outre, l'Amérique du Sud a connu dans le passé une remarquable diversité de métathériens, avec des taxons basaux "Ameridelphia" *incertae sedis*, dont l'ordre Sparassodonta, actuellement éteints. L'histoire évolutive des métathériens au Cénozoïque en Amérique du Sud est marquée par des phases distinctes, avec des périodes de diversification et d'extinction, enregistrées dans quelques sites exceptionnels, en particulier dans la partie méridionale du continent. Cependant, le registre fossile des Metatheria en Amérique du Sud présente de grandes lacunes, principalement dans le nord du continent, la région amazonienne, où ils sont signalés dans quelques gisements de l'Éocène–Miocène des Pérou, Brésil, Venezuela et Colombie. Dans cette perspective, la présente thèse avait pour but identifier les restes fossiles de Metatheria provenant de localités brésiliennes (État d'Acre, rivières Juruá et Envira, Formation Solimões, Bassin de l'Acre) et péruviennes (Contamana, Bassin de Huallaga et Atalaya) de la région amazonienne, couvrant l'intervalle Éocène–Miocène, afin de contribuer à la connaissance de la systématique et de l'histoire évolutive des Metatheria. Dans la localité TAR-31, Département de San Martin, Pérou, fin du Miocène moyen (Laventien, ~13 Ma), trois taxons de Metatheria ont été identifiés : le didelphidé (ordre Didelphimorphia) "*Thylamys*" cf. "*T.*" *colombianus*, et des membres

de l'ordre Paucituberculata aff. *Palaeothentes* et *Pitheculites ipururensis* sp. nov. Dans les localités de l'Acre étudiées, quatre taxons de didelphidés ont été trouvés dans la localité PRE 06, rivière Envira : Marmosini cf. *Marmosa*, *Didelphis* cf. *D. solimoensis*, '*Thylamys*' *colombianus*, en plus de didelphidés non identifiés, ce qui augmente considérablement la diversité connue de cette famille dans le Miocène de l'Acre. Dans les localités de la rivière Juruá, deux taxons de Paucituberculata ont été identifiés : Palaeothentidae Palaeothentinae indet. (PRJ 25 et PRJ 33', tous deux hors contexte stratigraphique) et l'abdéritidé *Abderites* sp. (PRJ 33, *in situ*). D'après les faunes de mammifères associées, les didelphidés de PRE 06 indiquent un âge Miocène supérieur basal pour cet affleurement. *Abderites* sp. suggère un âge plus ancien, Miocène moyen, pour PRJ 33. Il s'agit des premiers registres de Paucituberculata pour le Miocène de l'Amazonie brésilienne. La comparaison de ces associations de métathériens avec des faunes temporellement corrélées de la région amazonienne indique une grande similitude entre TAR-31 et l'Acre, ainsi qu'avec La Venta, confirmant que l'Amazonie occidentale était une région biogéographique unique et cohérente pour les mammifères terrestres au cours du Miocène moyen, sur la marge occidentale du Système Pebas. En ce qui concerne les localités paléogènes étudiées, seuls les membres des Polydolopimorphia ont été étudiés, avec l'identification de 11 taxons représentant uniquement le sous-ordre Bonapartheriiformes, avec des Bonapartherioidea Prepidolopidae et des Argyrolagoidea Argyrolagidae. De plus, le genre *Wamradolops* et un autre nouveau genre et nouvelle espèce, d'affinités phylogénétiques incertaines, ainsi que des polidolopimorphes non-identifiés ont été registrés. Les assemblages de Polydolopimorphia dans les différentes localités étudiées au Pérou se ressemblent en termes de composition taxonomique lorsqu'ils sont temporellement corrélés. Ils ressemblent également à la faune locale de Santa Rosa (Oligocène inférieur, Pérou) et aux assemblages de l'Éocène inférieur et moyen du nord-ouest de l'Argentine. Les résultats obtenus dans la présente thèse, en comparaison avec la littérature, montrent que des changements majeurs se sont produits dans la composition des communautés de métathériens de la région amazonienne au cours de l'intervalle Éocène–Miocène. Les assemblages de métathériens de l'Éocène moyen sont principalement composés de polydolopimorphes, avec de grandes diversité et abondance. Un premier changement se produit autour de la transition Éocène–Oligocène, caractérisé par une diminution de l'abondance et de la diversité des polydolopimorphes, avec la presque disparition des Prepidolopidae et le maintien des Argyrolagidae, contrebalancés par

l’augmentation du nombre de restes et de taxons de paucituberculés. Ces derniers ne sont représentés que par les Palaeothentoidea et présentent des diversité et abondance significatives pendant l'Oligocène. Au Miocène inférieur, les premiers membres non-ambigus des Didelphimorphia sont identifiés, et au Miocène supérieur, le deuxième changement a lieu. Les communautés de métathériens sont alors presque entièrement composées de didelphidés, représentés par des taxons dérivés très similaires aux groupes actuels. Un seul taxon d’argyrolagidé est enregistré au Miocène supérieur basal, le seul et dernier représentant de la grande diversité de Polydolopimorphia qui existait auparavant dans la région amazonienne. Tous ces résultats soulignent le rôle important de la région amazonienne dans l'histoire évolutive et la paléobiogéographie des métathériens au cours de la fin du Paléogène et du début du Néogène.

Mots-clés: Marsupial, Didelphimorphia, Paucituberculata, Polydolopimorphia, Eocène, Oligocène, Miocène.

ABSTRACT

Metatheria, the sister-group of the placentals among the mammals, was probably originated in the Jurassic in today's Asia–North America. Later, the group spread throughout the Northern Hemisphere, being recorded in North America, Europe and Asia until the Miocene and in the Eocene and Oligocene of Africa. In the Late Cretaceous, one or more clades of metatherians dispersed from North America to South America, being recorded for the first time in the early Paleocene of Argentina. Then, probably in the Paleocene, one or more lineages of American metatherians migrated toward Australia, passing through Antarctica. The phylogenetic relationships of Metatheria remain a subject of research and debate, especially the composition and affinities of its major subclades. The crown-group, Marsupialia, which includes all living metatherians, is divided into: Australidelphia, with the extant orders (Dasyuromorphia, Peramelemorphia, Diprotodontia and Notoryctemorphia) and a fossil order (Yalkaparidontia) distributed in Australasia, plus the South American order Microbiotheria and possibly the Polydolopimorphia (currently extinct); and "Ameridelphia," a polyphyletic taxon containing the orders Didelphimorphia and Paucituberculata, mainly inhabiting South America. Furthermore, South America had a remarkable past diversity of metatherians, with basal taxa "Ameridelphia" *incertae sedis*, including the order Sparassodonta, currently extinct. The Cenozoic evolutionary history of metatherians in South America is marked by distinct phases, with periods of diversification and extinctions, recorded in some exceptional sites, especially in the southern portion of the continent. However, there are large gaps in the fossil record of Metatheria in South America, mainly for the northern portion of the continent, the Amazon Region, where they are reported for some Eocene–Miocene deposits from Peru, Brazil, Venezuela and Colombia. In this sense, the present thesis aimed to identify fossil remains of Metatheria from Brazilian (Acre State, Upper Juruá and Envira Rivers, Solimões Formation, Acre Basin) and Peruvian (Contamana, Huallaga and Atalaya regions) localities of the Amazon region, covering the Eocene–Miocene interval, in order to contribute to the knowledge of Metatheria systematics and evolutionary history. At the locality TAR-31, San Martín Department, Peru, late Middle Miocene (Laventan, ~13 Ma), three Metatheria taxa were identified: the didelphid (order Didelphimorphia) '*Thylamys*' cf. '*T*.' *colombianus*, and members of the order Paucituberculata aff. *Palaeothentes* and *Pitheculites ipururensis* sp. nov. In the investigated localities in Acre, four taxa of didelphids were found at the locality PRE 06, Envira River: Marmosini cf. *Marmosa*, *Didelphis* cf. *D*. *solimoensis*, '*Thylamys*'

colombianus, besides unidentified didelphids, which considerably increase the known diversity of this family in the Miocene of Acre. In the localities of the Upper Juruá River, two taxa of the order Paucituberculata were identified: Palaeothentidae Palaeothentinae indet. (PRJ 25 and PRJ 33', both out of stratigraphic context) and the Abderiditae *Abderites* sp. (PRJ 33, *in situ*). According to the associated mammal faunas, the didelphids from PRE 06 indicate an early Late Miocene for this outcrop. *Abderites* sp. suggests an older age for PRJ 33, Middle Miocene. These are the first records of Paucituberculata for the Miocene of the Brazilian Amazon. Comparisons of these metatherian associations with temporally correlated faunas from the Amazon Region indicate great similarity between TAR-31 and Acre, as well as with La Venta, confirming that Western Amazonia was a unique and consistent biogeographic region for terrestrial mammals during the Middle Miocene, on the western margin of the Pebas Mega-Wetland System. Concerning the Paleogene localities studied, only members of the order Polydolopimorphia were studied, with the identification of 11 taxa representing the suborder Bonapartheriiformes, with both Bonapartherioidea Prepidolopidae and Argyrolagoidea Argyrolagidae. In addition, the genus *Wamradolops* and another new genus and new species of uncertain phylogenetic affinities, as well as unidentified polydolopimorphians were recorded. We observed that the Polydolopimorphia assemblages in the different localities studied in Peru resemble each other in terms of taxonomic composition when temporally correlated. They also resemble the Santa Rosa local fauna (early Oligocene, Peru) and the early and middle Eocene assemblages of Northwestern Argentina. Through the results obtained in the present thesis, in comparison with the literature, major turnovers occurred during the Eocene–Miocene interval in the composition of the metatherian communities from the Amazon Region. The metatherian associations in the middle Eocene were predominantly composed by members of polydolopimorphians, with high diversity and abundance. A first turnover occurred around the Eocene–Oligocene transition, characterized by a decrease in the abundance and diversity of polydolopimorphians, with practically the disappearance of the Prepidolopidae, the Argyrolagidae remaining, offset by an increase in the amount of specimens and taxa of paucituberculatans. These were solely represented by the superfamily Palaeothentoidea and had great diversity and abundance during the Oligocene. In the early Miocene, the first unambiguously members of the order Didelphimorphia are recorded, and in the Late Miocene the second turnover occurs. The metatherian communities are then almost entirely composed of didelphids, which are represented

by derived taxa very similar to the current groups. Only one Argyrolagidae is recorded in the early Late Miocene, the only and last representative of the great diversity of Polydolopimorphia that existed previously in the Amazon region. These results highlight the significant role of the Amazon region regarding the evolutionary history and paleobiogeography of metatherians during the late Paleogene and early Neogene.

Keywords: Marsupial, Didelphimorphia, Paucituberculata, Polydolopimorphia, Eocene, Oligocene, Miocene.

LISTA DE FIGURAS

Figura 1. Filogenia molecular calibrada de 5.911 espécies de mamíferos viventes e distribuídas ao redor do globo..... 5
Figura 2. Árvore filogenética consenso simplificada de Theria e linhagens fósseis de mamíferos basais..... 6
Figura 3. Árvore filogenética das ordens viventes de marsupiais (em vermelho) baseada em dados de *retrotransposons*..... 9
Figura 4. A, fêmea adulta de *Monodelphis domestica*; **B**, fêmea com ninhada de 10 filhotes aproximadamente 36 horas após seu nascimento (esta espécie não possui marsúpio); **C**, filhotes de B em detalhe; **D**, neonato, menos de 10 horas após o nascimento..... 14
Figura 5. Comparação entre os membros inferiores direitos de três metatérios (*Metachirus*, *Phalanger* e *Hypsiprymnodon*) e um eutério (*Tupaia*) demonstrando as diferenças na articulação do tornozelo entre Metatheria e Eutheria..... 15
Figura 6. Homologias entre dentes pós-caninos de mamíferos: Theria basal, metatério e eutério basal..... 16
Figura 7. Diversidade de espécies de metatérios (roxo) e eutérios (laranja) na Ásia e América do Norte, durante o Cretáceo..... 18
Figura 8. Distribuição dos Metatheria no Cenozoico da África e Eurásia. Peradectidae: **1**, Chambi, Tunísia; **2**, Fayum, Egito; **3**, Taqah, Omã; **4**, Bacia de Li, Tailândia; **5**, Sonlinzhuang, China. Herpetotheriidae: **6**, Bacia de Zaissan, Cazaquistão; **7**, Mina de lignite Vastan, Índia; **8**, Bugti Hills, Paquistão; **9**, B, Shanghuang e C, Jiangsu, China. Metatérios de afinidades incertas: **7**, Mina de lignite Vastan, Índia; **10**, Formação Kartal, Turquia..... 21
Figura 9. Molares superiores (esquerdos) e inferiores (a, e, direitos; c, d, f, h, i, esquerdos) de marsupiais: **a**, marsupial primitivo; **b**, Didelphimorphia (*Monodelphis*); **c**, Paucituberculata (*Caenolestes*); **d**, Dasyuromorphia (*Sminthopsis*); **e**, Microbiotheria (*Dromiciops*); **f**, Peramelemorphia (*Perameles*); **g**, Notoryctemorphia (*Notoryctes*); **h**, Diprotodontia (*Phascolarctos*); **i**, Diprotodontia (*Simosthenurus*)..... 22
Figura 10. Árvore filogenética dos táxons de Metatheria do Cretáceo e Paleógeno..... 25
Figura 11. Árvore filogenética de Metatheria obtida por Chornogubsky & Goin (2015).....26
Figura 12. Relações filogenéticas de Metatheria segundo Beck (2017)..... 27

Figura 13. Diagrama representando cladograma mais parcimonioso de Metatheria obtido através de dados morfológicos por Horovitz *et al*. (2009)..... 28
Figura 14. Árvore filogenética gerada com 50% de consenso através de análises Bayesianas datadas realizadas por Beck *et al*. (2022)..... 31-32
Figura 15. *Cocatherium lefipanum* (Metatheria, Polydolopimorphia), Formação Lefipán, Paleoceno, Argentina, molar inferior em vista **A**, labial; **B**, lingual; **C**, oclusal; **D**, anterior oclusal; **E**, posterior oclusal..... 34
Figura 16. "Ameridelphia" *incertae sedis*: molares inferiores, **A**, *Guggenheimia crocheti* (esquerdos); molares superiores, **B**, *Protodidelphis vanzolinii* (direitos), **C** e **D**, *Carolocoutoia ferigoloi* (esquerdos)..... 36
Figura 17. A, Vista lateral do crânio e dentário de *Thylacosmilus atrox* (Thylacosmilidae), de comprimento total 210 mm; **B**, Vista ventral do crânio de *Artodictis sinclari* (Borhyaenidae)..... 39
Figura 18. Representantes de Didelphimorphia, de cima para baixo, fora de escala, *Caluromys derbianus*, *Monodelphis brevicaudata*, *Marmosa robinsoni*, *Chironectes minimus*, *Metachirus nudicaudatus*..... 43
Figura 19. Representantes da ordem Paucituberculata, família Abderitidae: **A–P***, Pitheculites minimus*; **Q**, *P*. *rothi*; **R**, *P*. *chenche*..... 48
Figura 20. *Dromiciops gliroides*, *D. bozinovici* e *D. mondaca*..... 51
Figura 21. Pré-molares superiores e M1 de: **a**, *Epidolops ameghinoi*; **b**, *Bonapartherium hinakusijum*; **c**, *Gashternia carioca*; **d**, *Polydolops thomasi*; **e**, *Anargyrolagus primus*..... 55
Figura 22. Molares superiores e inferiores de Polydolopidae da Antártica: **a–d**, *Antarctodolops dailyi*; **e-f**, *A*. *mesetaense*; **g**, *Antarctodolops* sp..... 60
Figura 23. Representantes das famílias de Dasyuromorphia: Dasyuridae **A**, *Planigale subtilíssima*; **B**, *Dasyurus maculatus*; **C**, Thylacinidae, *Thylacinus cynocephalus*†; **D**, Myrmecobiidae, *Myrmecobius fasciatus*..... 61
Figura 24. Representantes das famílias da ordem Peramelemorphia: **A**, Thylacomyidae, *Macrotis lagotis*; **B**, Peramelidae, *Perameles gunni*; **C**, Peroryctidae, *Microperoryctes longicaudata*..... 62
Figura 25. Representantes das famílias da ordem Diprotodontia: **A**, Phascolarctidae, *Phascolarctos cinereus*; **B**, Vombatidae, *Vombatus ursinus*; **C**, Pseudocheiridae, *Pseudocheirus archeri*; **D**, Macropodidae, *Macropus parryi*; **E**, Phalangeridae, *Spilocuscus maculatus*; **F**, Acrobatidae, *Acrobates pygmaeus*; **G**, Burramyidae, *Cercartetus nanus*..... 63

Figura 26. Representante da ordem Notoryctemorphia, família Notoryctidae, *Notoryctes typhlops*..... 64
Figura 27. Holótipo de *Didelphis solimoensis*, em vista: **A**, labial; **B**, oclusal; **C**, lingual..... 74
Figura 28. *Chulpasia mattaueri*, holótipo, M1 ou M2 esquerdo, par estéreo..... 77
Figura 29. Metatérios fósseis da Formação Guabirotuba, Bacia de Curitiba: *Nemolestes* sp., dentário esquerdo, **a**, vista lateral, **b**, vista oclusal; Paleothentoidea gen. et sp. indet., p3 e m1, **c**, vista oclusal; Argyrolagoidea gen. et sp. indet., dentário esquerdo, **d**, vista lateral; **e**, vista oclusal..... 79
Figura 30. Nomenclatura das estruturas dentárias dos molares de metatérios de acordo com Goin *et al*. (2016): **A**, molar superior esquerdo; **B**, molar inferior esquerdo..... 85
Figura 31. Representação dos padrões dos molares de Argyrolagoidea e a respectiva nomenclatura das estruturas dentárias: **A**, vista oclusal de m2s esquerdos, da esquerda para direita: *Praedens aberrans*, *Klohnia major*, *Proargyrolagus bolivianus* e *Anargyrolagus primus*; **B**, vista oclusal de M2s esquerdos, a esquerda *Klohnia major* e a direita *Proargyrolagus bolivianus*..... 86
Figura 32. Desenhos esquemáticos da morfologia oclusal e nomenclatura das estruturas dos molares superiores e inferiores de Palaeothentidae e Abderitidae. **A**, *Palaeothentes primus,* M1 esquerdo; **B–C**, *Pitheculithes minimus*, **B**, M2 esquerdo, **C**, m2 direito; **D**, *Palaeothentes minutus*, m1–2 direitos..... 87
Figura 33. Parte do norte da América do Sul, com as principais bacias sedimentares brasileiras assinaladas, dentre elas a Bacia do Acre..... 90
Figura 34. Carta estratigráfica da Bacia do Acre..... 92
Figura 35. Mapa com a localização dos afloramentos onde foram encontrados os espécimes fósseis de metatérios na Formação Solimões, Estado do Acre, Brasil. Alto Rio Juruá: **A**, PRJ 25; **B**, PRJ 33. Rio Envira: **C**, PRE 06..... 95
Figura 36. Mapa dos das localidades visitadas e amostradas nas expedições de campo no Alto Rio Juruá, Acre, Brasil..... 96
Figura 37. A, Seção estratigráfica sintética e **B–C** fotografias da localidade PRJ 25, com a Formação Solimões como substrato, localizada na margem esquerda do Rio Juruá, Estado do Acre, Brasil..... 98
Figura 38. A, Seção estratigráfica sintética e **B**, fotografia da localidade PRJ 33, Mioceno, Formação Solimões, localizada na margem esquerda do Rio Juruá, Estado do Acre, Brasil..... 100

Figura 39. A, Fotografia e **B–C**, seções estratigráficas sintéticas da localidade PRE 06, Neomioceno, Formação Solimões, localizada na margem direita do Rio Envira, Estado do Acre, Brasil…… 102
Figura 40. A, Mapa da América do Sul apontando a localização de Contamana, Peru. **B**, Localização dos perfis cenozoicos na região de Contamana..... 104
Figura 41. Mapa geológico da região de Contamana, Peru..... 105
Figura 42. Seção estratigráfica sintética dos depósitos cenozoicos na região de Contamana, Peru..... 106
Figura 43. Afloramentos do Membro Inferior da Formação Pozo, final do Mesoeoceno, na região de Contamana, Peru. **A**, CTA-27 e **B**, CTA-47…….. 109
Figura 44. Afloramentos do Membro Inferior da Formação Pozo, final do Mesoeoceno, na região de Contamana, Peru. **A**, CTA-29 e **B**, CTA-51……..… 109
Figura 45. Afloramento CTA-66, Formação Pozo, final do Mesoeoceno, região de Contamana, Peru..... 110
Figura 46. Afloramento CTA-43, Formação Pebas, final do Neomioceno, região de Contamana, Peru…… 111
Figura 47. A, Mapa mostrando a localização das seções estratigráficas paleógenas de Juanjui e Balsayacu, próximas às cidades de Juanjui e Balsayacu, respectivamente. **B–C**, mapas aproximados com a localização dos afloramentos das seções estratigráficas de Juanjui e Balsayacu, Bacia do Huallaga, Peru..... 113
Figura 48. Localidades **A**, TAR-44 e **B**, TAR-45, da seção paleógena de Juanjui, Bacia do Huallaga, Peru…… 115
Figura 49. A, Mapa com a localização das cidades prospectadas na região da Bacia do Huallaga, Peru, com destaque para Balsayacu; **B**, mapa da região da seçãoc paleógena de Balsayacu, indicando a localização dos afloramentos; **C**, seção estratigráfica sintética dos afloramentos da seção de Balsayacu, com a indicação dos níveis fossilíferos onde foram encontrados restos de roedores caviomorfos..... 115
Figura 50. Localidades **A**, TAR-55 e **B**, TAR-56, da seção paleógena de Balsayacu, Bacia do Huallaga…… 116
Figura 51. Mapa com a localização das cidades de Tarapoto e Shapaja, Bacia do Huallaga, Peru……. 117
Figura 52. Mapa das localidades da seção paleógena de Shapaja, Bacia do Huallaga, Peru..... 118
Figura 53. Localidades **A**, TAR-01 e **B**, TAR-21, círculo amarelo e TAR-72, círculo azul, seção paleógena de Shapaja, Bacia do Huallaga, Peru……..……..…….. 118

Figura 54. Diagrama crono e bioestratigráfico sintético das assembleias fossilíferas da Seção de Shapaja, Neoeoceno–Eooligoceno, Departamento de San Martín, Peru, representando os dados paleontológicos e de análises de quimioestratigrafia apresentados em Antoine *et al*. (2021), com curva de paleotemperaturas adaptadas de Westerhold *et al*. (2020) e de nível do mar adaptadas de Miller *et al*. (2020).... 119
Figura 55. Hipótese de atribuição temporal das seções de Shapaja, Balsayacu e Juanjui em relação às principais faunas já descritas para o Eoceno e Oligoceno da Amazônia peruana..... 120
Figura 56. Localidade TAR-14, afloramento da Formação Chambira, Bacia do Huallaga, Peru……..……. 121
Figure 57. A, Mapa da localização da localidade TAR-31, Formação Ipururo, próximo a cidade de Tarapoto, distrito de Juan Guerra, Departamento de San Martín, Peru. **B**, Fotografia do afloramento, situado na margem esquerda do Rio Mayo, indicando a posição do nível fossilífero……..…….. 122
Figura 58. Localidades **A**, TMB-01, afloramento da Formação Pozo, e **B**, URU-210, afloramento da Formação Chambira, Atalaya, Peru..... 123
Figura 59. Gráficos representando a quantidade relativa de metatérios, por ordem, presentes nos afloramentos estudados do Mesoeoceno ao Neomioceno das regiões de Contamana, Bacia do Huallaga e Atalaya, Peru, e Acre, Brasil..... 133

LISTA DE QUADROS

Quadro 1. Lista de táxons de “Ameridelphia” *incertae sedis*, de acordo com Goin *et al*. (2016), de ocorrência na América do Sul..... 37
Quadro 2. Lista de táxons de Sparassodonta, segundo Goin *et al*. (2016), de ocorrência na América do Sul..... 40
Quadro 3. Lista de táxons de Didelphimorphia, de acordo com Gardner (2007), Forasiepi *et al*. (2009), Voss & Jansa (2009) e Goin *et al*. (2016), de ocorrência na América do Sul..... 45-46
Quadro 4. Lista de táxons de Paucituberculata, de acordo com Abello (2007), Rincón *et al*. (2015), Goin *et al*. (2016) e Stutz *et al*. (2022), de ocorrência na América do Sul..... 49
Quadro 5. Lista de táxons de Microbiotheria, de acordo com Goin *et al*. (2016) e D’Elía *et al*. (2016), de ocorrência na América do Sul e Antártica..... 52
Quadro 6. Lista de táxons de Polydolopimorphia, de acordo com Goin & Candela (2004) e Goin *et al*. (2016), de ocorrência no Hemisfério Sul..... 56–58
Quadro 7. Metatérios fósseis da fauna de Santa Rosa, Peru, segundo Goin & Candela (2004)..... 72
Quadro 8. Metatérios fósseis da fauna de La Venta, Colômbia, segundo Goin (1997) e Suárez Gómez (2019)..... 75
Quadro 9. Metatérios fósseis das formações Tremembé (Bacia de Taubaté) e Guabirotuba (Bacia de Curitiba), segundo Couto-Ribeiro (2010) e Sedor *et al*. (2017)..... 78
Quadro 10. Registros de Didelphimorphia, família Didelphidae, para o Quaternário do Brasil..... 80-81
Quadro 11. Quantidade de restos fósseis de metatérios por afloramento da região de Contamana, Peru, com as respectivas idades sugeridas dos afloramentos..... 83
Quadro 12. Quantidade de restos fósseis de metatérios por afloramento da Bacia do Huallaga, Peru e as respectivas idades dos afloramentos..... 83
Quadro 13. Afloramentos da região de Contamana, Peru contendo fósseis de metatérios da ordem Polydolopimorphia..... 108
Quadro 14. Localidades da Bacia do Huallaga, Peru, contendo fósseis de metatérios..... 114

LISTA DE SIGLAS E ABREVIATURAS

AC: Estado do Acre

AP: antes do presente

C: canino

DP5: 5º pré-molar superior decíduo

dp5: 5º pré-molar inferior decíduo

FABI: Primeiro Intercâmbio Biótico das Américas

GIBA: Grande Intercâmbio Biótico das Américas

I: incisivo

I1; I2; I3; I4; I5: 1º; 2º; 3º; 4º; 5º incisivos superiores

i1; i2; i3; i4: 1º; 2º; 3º; 4º incisivos inferiores

K–Pg: limite Cretáceo–Paleógeno

LACM: *Natural History Museum of Los Angeles County*

M: molar

M1; M2; M3; M4: 1º; 2º; 3º; 4º molares superiores

m1; m2; m3; m4: 1º; 2º; 3º; 4º molares inferiores

Ma: milhões de anos

MLP: *Museo de La Plata*

MUSM: *Museo de Historia Natural, Universidad Nacional Mayor de San Marcos*

NALMA: Idades de Mamíferos Terrestres Norte-Americanos

P: pré-molar

p1; p2; p3: 1º; 2º; 3º pré-molares inferiores

PR: Paraná

PRJ: Ponto Rio Juruá

PRE: Ponto Rio Envira

RCSB: Rift Continental do Sudeste do Brasil

RJ: Rio de Janeiro

SALMA: Idades de Mamíferos Terrestres Sul-Americanos

SP: São Paulo

UFAC: Universidade Federal do Acre

UFAC-CS: Universidade Federal do Acre, campus Floresta, Cruzeiro do Sul.

UFSC: Universidade Federal de Santa Catarina, Florianópolis.

SUMÁRIO

ESTRUTURA DA TESE.....3
PARTE I – TEXTO INTEGRADOR.....4
1 INTRODUÇÃO.....4
2 OBJETIVOS.....12
2.1 OBJETIVO GERAL.....12
2.2 OBJETIVOS ESPECÍFICOS.....12
3 ESTADO DA ARTE.....13
3.1 METATHERIA HUXLEY, 1880.....13
3.1.1 Metatheria no Cretáceo.....17
3.1.2 Metatheria do Cenozoico do Hemisfério Norte.....19
3.2 MARSUPIALIA ILLIGER, 1811..... 21
3.3 PANORAMA FILOGENÉTICO DE METATHERIA..... 23
3.4 METATHERIA NA AMÉRICA DO SUL..... 33
3.4.1 "Ameridelphia" *incertae sedis*..... 35
3.4.1.1 Ordem Sparassodonta..... 38
3.4.2 Ordem Didelphimorphia..... 41
3.4.3 Ordem Paucituberculata..... 47
3.4.4 Ordem Microbiotheria..... 50
3.4.5 Ordem Polydolopimorpha..... 52
3.5 METATHERIA NA ANTÁRTICA E AUSTRALÁSIA..... 59
3.6 REGISTRO FÓSSIL DE METATHERIA NA AMÉRICA DO SUL..... 64
3.6.1 História evolutiva dos Metatheria na América do Sul..... 64
3.6.2 O registro fóssil de Metatheria na Região Amazônica.... 68
3.6.3 O registro fóssil de Metatheria no Brasil e Peru..... 76
4 MATERIAL E MÉTODOS..... 82
4.1 MATERIAL..... 82
4.2 COLETA..... 84
4.3 ANÁLISE..... 84
4.4 IMAGEAMENTO..... 88

5 CONTEXTO GEOLÓGICO DA ÁREA DE ESTUDO.....89
5.1 BRASIL.....90
5.1.1 Alto Rio Juruá.....96
5.1.2 Rio Envira.....100
5.2 PERU.....102
5.2.1 Contamana.....103
5.2.2 Bacia do Huallaga.....111
5.2.3 Atalaya.....122
6 DISCUSSÃO INTEGRADORA E CONCLUSÕES.....124
6.1 SÍNTESE DOS ARTIGOS.....124
6.2 EVOLUÇÃO E COMPARAÇÃO DA PALEODIVERSIDADE DE METATÉRIOS.....126
6.3 CONCLUSÕES E PERSPECTIVAS.....130
7 REFERÊNCIAS BIBLIOGRÁFICAS.....135
PARTE II – ARTIGOS.....157
1 ARTIGO 1 – LATE MIDDLE MIOCENE METATHERIA (MAMMALIA: DELPHIMORPHIA AND PAUCITUBERCULATA) FROM JUAN GUERRA, SAN MARTÍN DEPARTMENT, PERUVIAN AMAZONIA.....157
2 ARTIGO 2 – NEW RECORDS OF MARSUPIALS FROM THE MIOCENE OF WESTERN AMAZONIA, ACRE, BRAZIL.....207
3 ARTIGO 3 – NEW RECORDS OF POLYDOLOPIMORPHIAN METATHERIA FROM THE PALEOGENE OF PERUVIAN AMAZONIA.....253

ESTRUTURA DA TESE

Esta tese de doutorado está estruturada em dois volumes. No Volume 1, estão presentes: i) texto introdutório; ii) um artigo publicado no *Journal of South American Earth Sciences* e iii) um artigo submetido (pendendo as correções enviadas pelos revisores) na *Acta Palaeontologica Polonica*, periódicos classificados nos estratos Qualis-CAPES A3 e A2, respectivamente. Ademais, um artigo adicional, o qual será aprimorado e valorizado em forma de publicação(ões) após a defesa, é apresentado. No Volume 2 encontram-se os complementos. Assim, a organização da tese de doutorado compreende as seguintes partes principais:

Volume 1

i) PARTE I – TEXTO INTEGRADOR:

Texto Integrador composto pelos seguintes capítulos: a) introdução com a formulação do problema de investigação e a hipótese; b) objetivos da pesquisa; c) o estado da arte do tema da pesquisa; d) os materiais e métodos utilizados; e) o contexto geológico da área; f) resumo dos principais resultados obtidos, interpretações desenvolvidas nos artigos e discussão integradora dos resultados; g) conclusões; h) referências bibliográficas.

ii) PARTE II – ARTIGOS:

Corpo Principal da Tese, constituído do(s) artigo(s) conforme os itens 1.1; 1.2 e/ou 1.3 da norma 118 do Programa de Pós-Graduação em Geociências da Universidade Federal do Rio Grande do Sul.

Volume 2

iii) PARTE III – COMPLEMENTOS:

Anexos, compreendendo: histórico escolar, certificados, resumos publicados em eventos e outros artigos em que a doutoranda é primeira autora ou coautora, produzidos durante o Curso de Doutorado.

PARTE I – TEXTO INTEGRADOR

1 INTRODUÇÃO

Os mamíferos, classe Mammalia *sensu* Rowe (1988), compõem um clado compreendendo o ancestral comum mais recente dos monotremados, marsupiais e placentários viventes e todos os seus descendentes (Figura 1). Trata-se de um táxon constituído de diversas linhagens extintas, além de três táxons viventes: os Australosphenida (i.e., monotremados); Metatheria (representados atualmente pelos marsupiais); e Eutheria (i.e., mamíferos placentários) (Upham *et al*., 2019). A origem de Mammalia segue sendo motivo de debates, assim como a das diversas linhagens que a compõe. Segundo análises moleculares, utilizando ou não calibração com dados fósseis, as estimativas do aparecimento dos mamíferos (não incluindo os mamaliaformes basais – *stem mammaliaforms*) variam entre o Mesotriássico e Mesojurássico, muito provavelmente Eojurássico (Upham *et al*., 2019). Em suas primeiras fases de diversificação, as linhagens fundamentais de Mammalia já se separaram, com, por exemplo, Australosphenida divergindo de Theriimorpha, além de diversas outras linhagens hoje extintas situadas filogeneticamente entre estes dois grupos, sendo que muito desta diversificação inicial ocorreu no que hoje é a Ásia. O clado Theriimorpha é constituído de diversos clados extintos, além de Trechnotheria, o qual compreende os Boreosphenida, grupo no qual se desenvolveu o molar tribosfênico (padrão básico dos molares dos mamíferos térios atuais, com molares inferiores com trigônido e talônido em forma de bacia). Dentro de Boreosphenida situa-se o clado Theria, constituído pelo ancestral comum mais recente dos marsupiais e placentários viventes e todos os seus descendentes (Metatheria e Eutheria) (Williamson *et al*., 2014; Brusatte & Luo, 2016).

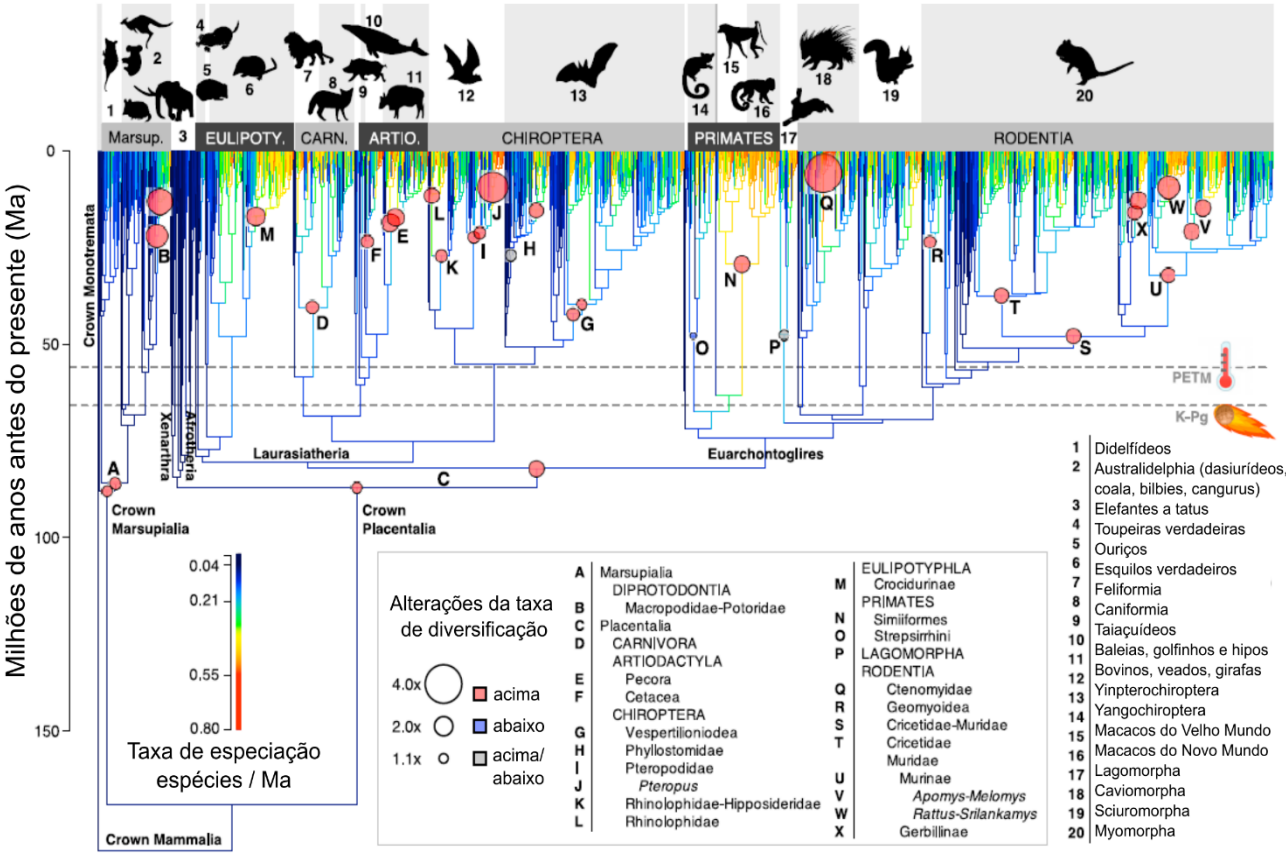


Figura 1. Filogenia molecular calibrada de 5.911 espécies de mamíferos viventes e distribuídas ao redor do globo. A confiabilidade dos clados é indicada pela coloração dos ramos, de acordo com as taxas de especiação (taxas de especiação *tip-level – tip DR metric*), e marcados com as taxas de diversificação brutas específicas dos ramos através dos círculos (método BAMM). Abreviações: **Artio**., Artiodactyla; **Carn**., Carnivora; **Eulipoty**., Eulipotyphla; **K-Pg**, limite Cretáceo-Paleógeno 66 Ma; **Ma**, milhões de anos antes do presente; **Marsup**., Marsupialia; **PETM**, máximo térmico do Paleoceno-Eoceno 56 Ma. Modificado de Upham *et al*. (2021).

A divergência das duas linhagens de mamíferos térios, Metatheria e Eutheria, também permanece não bem definida, com estimativas derivadas de análises moleculares sugerindo uma ampla gama temporal, entre o final do Triássico e o início do Cretáceo, mais provavelmente no Jurássico (Bi *et al*., 2018). No entanto, poucas evidências fósseis foram até hoje encontradas quanto aos primeiros representantes destes clados. No caso, três táxons considerados eutérios foram descritos para este intervalo de tempo da divergência dos térios (*Jurumaia*, 160 Ma, nordeste da China; *Durlstotherium* e *Durlstodon*, 145 Ma sul da Inglaterra). *Sinodelphys*, um táxon também do nordeste da China, porém mais recente que *Jurumaia* (*Sinodelphys* de 125 Ma), foi considerado como sendo o primeiro metatério quando de sua descoberta,

suportando uma origem asiática do grupo. No entanto, análises filogenéticas mais recentes demonstraram que, em realidade, *Sinodelphys* seria um eutério. Assim, se considera que os primeiros metatérios seriam pertencentes aos sub-clados Deltatheroidea e Marsupialiformes, provenientes do Aptiano-Albiano da América do Norte, os quais são conhecidos por restos fragmentários de dentes e mandíbulas (Figura 2) (Bi *et al*., 2018; Beck *et al*., 2022).

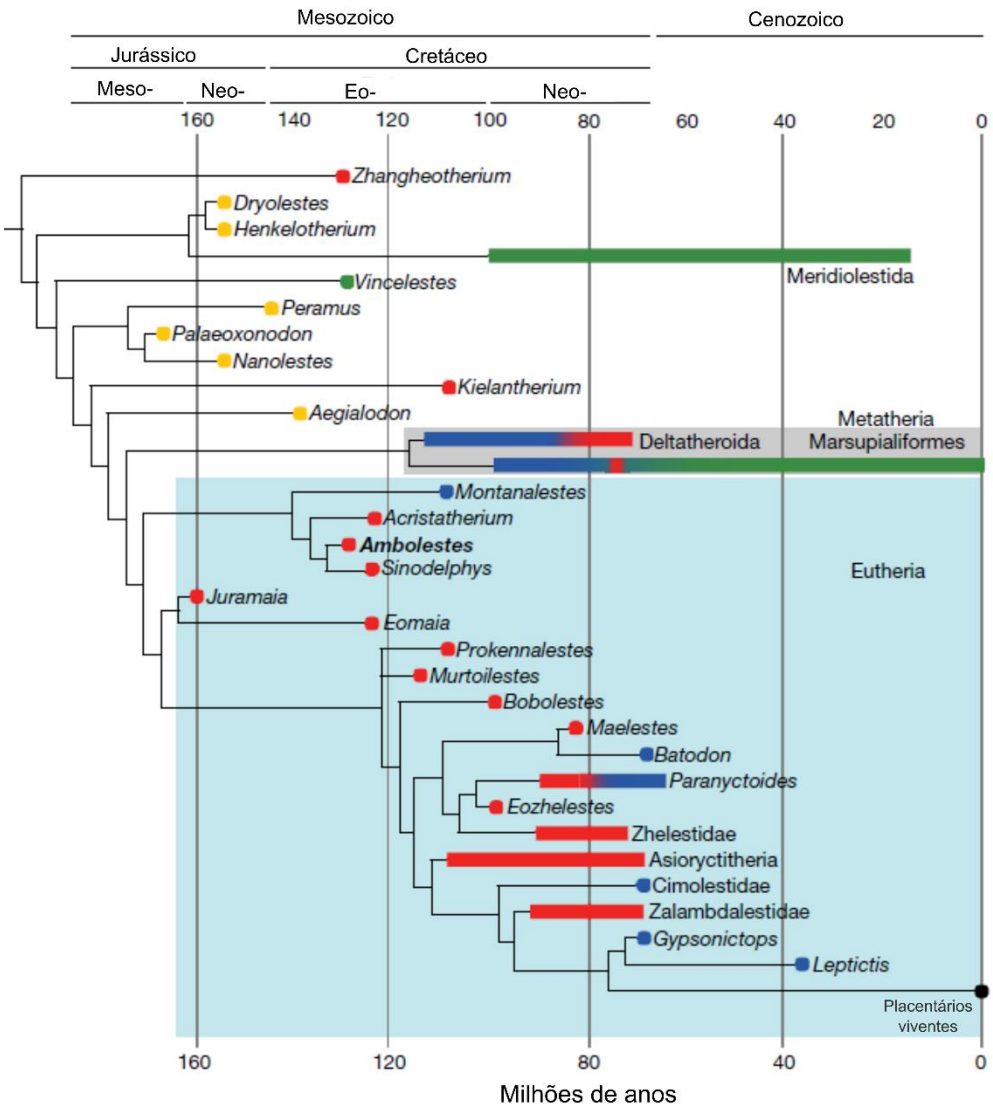


Figura 2. Árvore filogenética consenso simplificada de Theria e linhagens fósseis de mamíferos basais. As cores indicam o continente atual onde se encontraram os espécimes estudados, com exceção de Placentalia, sendo: Ásia, vermelho; Europa, amarelo; América do Sul, verde; América do Norte, azul. Já Deltatheroidea, Marsupialiformes e *Paranyctoides* provêm de distintos continentes. Modificado de Bi *et al*. (2018).

O clado Metatheria constitui uma infraclasse de Mammalia, abrangendo os mamíferos térios mais próximos dos marsupiais viventes do que de Eutheria (mamíferos placentários), incluindo táxons basais (*stem* metatérios), os Deltatheroidea e Marsupialiformes. Marsupialiformes, por sua vez, contém os Marsupialia (*crown group*, grupo-coroa, que inclui os marsupiais viventes) e metatérios basais mais próximos de Marsupialia do que de Deltatheroidea. Todos estes metatérios não-marsupiais mencionados encontram-se atualmente extintos (Kemp, 2005; Williamson *et al*., 2014).

As características utilizadas para a distinção entre Metatheria e Eutheria são, em grande parte, baseadas em caracteres observados em táxons viventes e seus tecidos moles, dificultando sua aplicação em fósseis. Destacam-se as notáveis diferenças no modo reprodutivo, visto que em Metatheria, na gestação, fêmeas possuem placenta vitelínica e o período intrauterino do embrião é mais curto. Em diversos grupos de marsupiais uma bolsa de tecido (marsúpio) está presente na barriga das fêmeas, protegendo os filhotes durante o período de lactação. O tamanho relativamente pequeno do cérebro e a estrutura do trato urogenital (útero e vagina pareados), também são considerados características diagnósticas dos marsupiais (Kemp, 2005; Williamson *et al*., 2014). Ademais, caracteres cranianos, pós-cranianos e de dentição, estes últimos mais facilmente aplicados aos fósseis, também podem ser utilizados para distinção de metatérios e eutérios (vide Seção 3 Estado da Arte; Luo *et al*., 2003; Williamson *et al*., 2014).

Após o surgimento de Metatheria, tal como mencionado acima, com os Deltatheroidea e Marsupialiformes, estes grupos passaram por eventos significativos de diversificação na Ásia e América do Norte, durante o Cretáceo (Goin *et al*., 2016). No Neocretáceo, os metatérios constituíam um grupo diverso, com formas basais e derivadas, morfologicamente diversificado e amplamente distribuído pelos continentes boreais da Laurásia, sendo até mesmo mais abundantes e taxonomicamente diversos que os eutérios na América do Norte (Williamson *et al*., 2014). A grande crise do limite Cretáceo–Paleógeno (K–Pg) atingiu severamente a radiação de metatérios norte-americanos, causando extinções significativas (Williamson *et al*., 2014). No Paleoceno, os únicos sobreviventes neste continente são *Peradectes* e algumas formas relacionadas. Estes metatérios persistiram na América do Norte até

possivelmente o Mioceno, tendo igualmente migrado para a Europa (registrados do Eoceno ao Mioceno), África (Eoceno e Oligoceno) e Ásia (Eoceno ao Mioceno), porém nunca atingindo grande diversidade taxonômica nestes continentes (Kemp, 2005; Cáceres, 2012).

Considera-se que uma ou mais linhagens de metatérios da América do Norte migraram em direção à América do Sul muito provavelmente no Neocretáceo. Em seguida, durante o Paleógeno, ocorre no continente uma grande diversificação de Metatheria, a qual é considerada um importante momento de sua história evolutiva, com a origem dos ancestrais mais próximos do grupo-coroa Marsupialia. Em seguida, supõe-se que a dispersão dos metatérios até a Austrália tenha sido completada antes do Eoceno (Goin *et al*., 2016). Posteriormente, com o Grande Intercâmbio Biótico das Américas (GIBA), no Pleistoceno, didelfídeos migraram da América do Sul para a América Central e América do Norte (Goin *et al*., 2016).

Atualmente, os marsupiais viventes são todos pertencentes ao grupo-coroa Marsupialia e são classificados em sete ordens e aproximadamente 91 gêneros e 385 espécies, distribuídos pela América do Norte, América Central, América do Sul e Australásia (Mammal Diversity Database, 2022). Na América do Sul, os marsupiais representam aproximadamente 10% da fauna de mamíferos terrestres (Goin *et al*., 2016), sendo, em conjunto com morcegos e roedores, os principais componentes das comunidades de pequenos mamíferos (Fonseca *et al*., 2003), contando com aproximadamente 22 gêneros e 134 espécies, pertencentes a três ordens: i) Paucituberculata, representada atualmente somente pela família Caenolestidae (três gêneros e sete espécies); ii) Microbiotheria, com uma família, Microbiotheriidae (um gênero e duas espécies); e iii) Didelphimorphia, hoje constituída exclusivamente pela família Didelphidae (18 gêneros e 125 espécies), a qual compreende a maior parte dos marsupiais viventes da América do Sul. Na Australásia se concentra o restante da diversidade de marsupiais viventes, com quatro ordens, sendo elas: i) Notoryctemorphia (um gênero e duas espécies); ii) Peramelemorphia (oito gêneros e 22 espécies); iii) Dasyuromorphia (19 gêneros e 77 espécies); e iv) Diprotodontia, ordem com maior diversidade e abundância (41 gêneros e 150 espécies) (Mammal Diversity Database, 2022). As relações filogenéticas entre as distintas ordens de marsupiais viventes e os agrupamentos internos de cada uma permanecem objeto de

intensos debates e estudos (May-Collado *et al*., 2015), contudo é de grande consenso que a ordem sul-americana Microbiotheria forma, juntamente com as ordens da Australásia, o clado Australidelphia (Figura 3) (vide Seção 3 Estado da Arte; Nilsson *et al*., 2010).

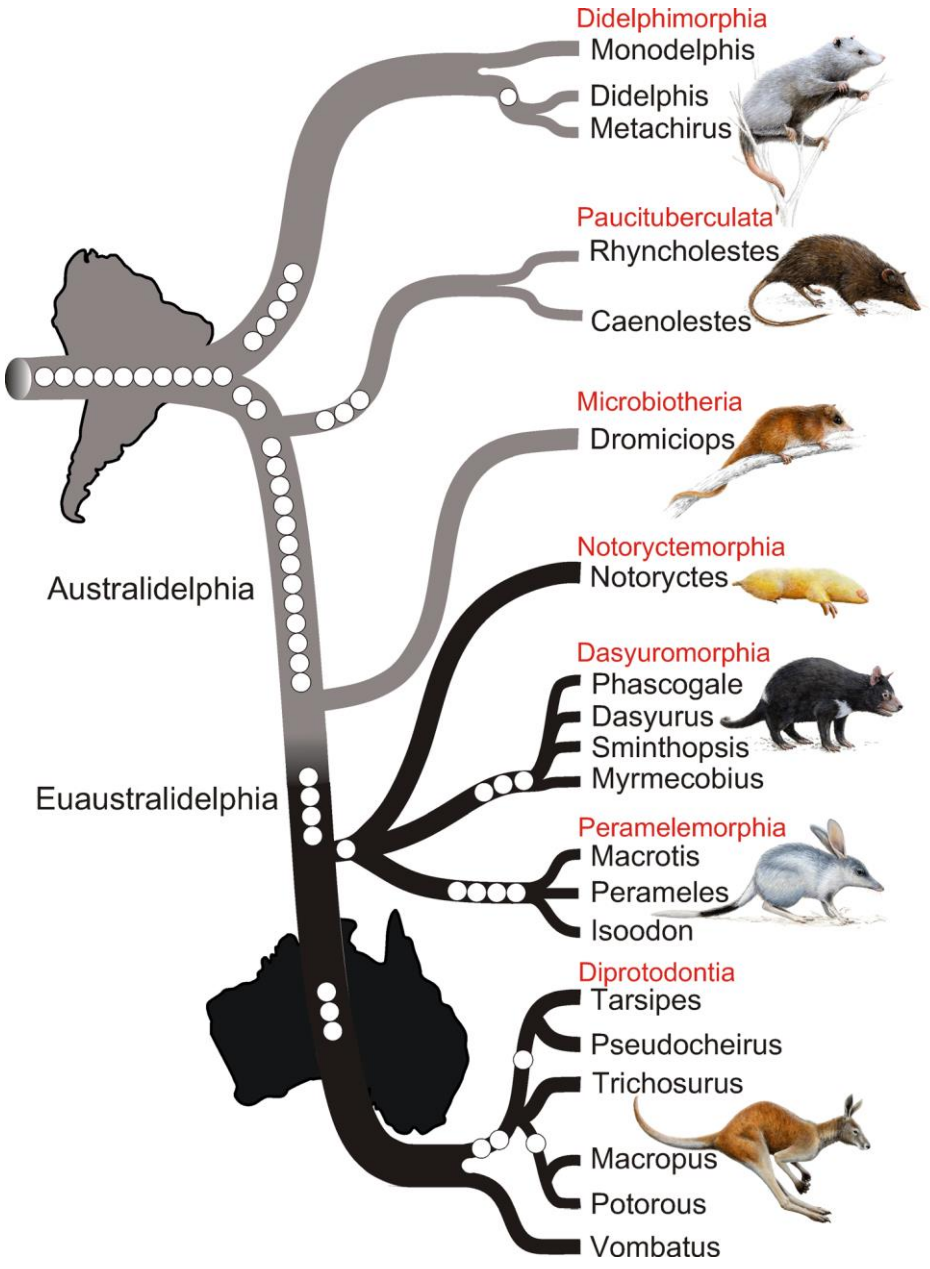


Figura 3. Árvore filogenética das ordens viventes de marsupiais (em vermelho) baseada em dados de *retrotransposons*. Linhas em cinza designam espécies com distribuição na América do Sul e linhas pretas indicam marsupiais da Australásia. Fonte: Nilsson *et al*. (2010).

Com relação ao registro fóssil de Metatheria no continente sul-americano, destacam-se sítios fossilíferos excepcionais na Patagônia argentina (e.g., Tejedor *et al*., 2009; Goin *et al*., 2010), na Bolívia (e.g., Goin *et al*., 2007a; Rincón *et al*., 2015; Muizon & Ladevèze, 2020), no Chile (Flynn *et al*., 2003) e no Brasil (Oliveira & Goin, 2011), os quais demonstraram a diversidade pretérita significativa dos metatérios na América do Sul. *Cocatherium lefipanum*, do início do Paleoceno do oeste da Patagônia, é o mais antigo metatério conhecido até o presente na América do Sul (Goin *et al*., 2016). Já com relação aos restos fósseis mais antigos de Metatheria na Austrália, estes datam do início do Eoceno (possivelmente final do Paleoceno), mas são escassos até o final do Oligoceno, quando o registro se torna mais diverso e abundante (Kemp, 2005).

Apesar da existência de localidades fossilíferas com grande diversidade e abundância de metatérios, além de espécimes excepcionalmente preservados, o registro fossilífero de Metatheria é considerado extremamente incompleto, tanto espacial quando temporalmente (Bennet *et al*., 2018). No caso da América do Sul, em especial, apesar de ter desempenhado um papel significativo na história filogenética, evolutiva e biogeográfica de Metatheria, o registro fóssil do grupo no continente é repleto de lacunas, tanto temporais quanto geográficas, em especial ao longo do Eoceno e Oligoceno da porção norte da América do Sul, sobretudo na região ocupada hoje pela Floresta Amazônica (Goin *et al*., 2016). Mais especificamente, o estudo de Goin & Candela (2004) sobre os depósitos de Santa Rosa, Peru, Eooligoceno, revelaram grande diversidade e abundância de metatérios. Contudo, trata-se do único estudo aprofundado realizado até o presente sobre os metatérios da proto-Amazônia no Paleógeno médio, sugerindo que diversidade deste clado possa estar subestimada e ainda desconhecida nesta região. No decorrer da última década, diversos trabalhos de campo revelaram faunas inéditas paleógenas e neógenas na Região Amazônica do Peru, nas regiões de Contamana, Bacia do Huallaga e Atalaya. Tais faunas se destacam por sua notável abundância de restos e diversidade taxonômica, tanto do ponto de vista de espécie quanto na escala de ordens e famílias (Antoine *et al*., 2016, 2017, 2021). Em especial, restos abundantes de Metatheria foram encontrados nos afloramentos peruanos, os quais foram, até o presente, apenas preliminarmente estudados. Ademais, em escavações realizadas no Alto Rio Juruá e Rio Envira,

Estado do Acre, Brasil, em afloramentos neógenos da Formação Solimões, também foram encontrados fragmentos fósseis de metatérios, os quais permanecem não descritos (Ribeiro *et al*., 2013).

Por conseguinte, a continuidade dos estudos e pesquisas sobre metatérios fósseis é de grande significatividade, especialmente para os períodos e regiões onde há extrema carência dos mesmos. Neste contexto, esta tese objetiva a identificação dos restos fósseis de metatérios mencionados acima, provenientes de afloramentos do Paleógeno e Neógeno da Amazônia Ocidental, no Brasil e Peru, buscando dar a conhecer novos registros de táxons já conhecidos na literatura, além da descrição de novos táxons, visando: i) contribuir para o conhecimento da riqueza e diversidade pretéritas de metatérios da América do Sul, em especial na porção norte do continente; ii) contribuir para a compreensão do registro fóssil de Metatheria em intervalos de tempo ainda demasiado desconhecidos, particularmente para o norte da América do Sul; iii) contribuir para o entendimento das relações destes metatérios fósseis amazônicos com táxons de faunas correlatas de outras partes do continente. Desse modo, espera-se que os dados levantados acerca destes novos registros de metatérios para o Paleógeno e Neógeno da Região Amazônica possam auxiliar a elucidar aspectos da sistemática, paleobiogeografia e história evolutiva de Metatheria como um todo.

2 OBJETIVOS

2.1 OBJETIVO GERAL

Avaliar e dar a conhecer a diversidade taxonômica dos Metatheria do Paleógeno e Neógeno da Amazônia Ocidental (Peru e Brasil), contribuindo para o entendimento da história evolutiva e paleobiogeográfica do grupo na América do Sul.

2.2 OBJETIVOS ESPECÍFICOS

i) Descrever e identificar taxonomicamente os fragmentos de Metatheria (ordens Didelphimorphia e Paucituberculata) provenientes da Formação Solimões, Bacia do Acre, regiões do Alto Rio Juruá e Rio Envira, Estado do Acre, Brasil;

ii) Descrever e identificar taxonomicamente os fragmentos de Metatheria (ordens Didelphimorphia e Paucituberculata) encontrados na localidade TAR-31, Formação Ipururo, Bacia do Huallaga, distrito de Juan Guerra, Departamento de San Martín, Peru;

iii) Descrever e identificar taxonomicamente os restos fósseis, constituídos essencialmente por dentes, de Metatheria da ordem Polydolopimorphia oriundos da região de Contamana, Departamento de Loreto, Peru;

iv) Descrever e identificar taxonomicamente os restos fósseis, em sua maioria dentes isolados, de Polydolopimorphia da Bacia do Huallaga, Departamento de San Martín, Peru;

v) Descrever e identificar taxonomicamente os restos fósseis (dentes isolados) de Polydolopimorphia de Atalaya, Departamento de Ucayali, Peru;

vi) Correlacionar, sistematicamente e/ou temporalmente, se possível, as faunas de metatérios da Amazônia Ocidental (Brasil e Peru).

3 ESTADO DA ARTE

3.1 METATHERIA HUXLEY, 1880

O clado Metatheria compreende o ancestral comum de todos os marsupiais viventes, assim como todos os táxons de mamíferos extintos mais próximos dos atuais marsupiais do que dos placentários viventes. Assim, inclui: táxons basais de metatérios, os Deltatheroida e os Marsupialiformes. Marsupialiformes, por sua vez, compreende Marsupialia, grupo-coroa (*crown group*) dos metatérios, além dos táxons basais de metatérios mais próximos de Marsupialia do que de Deltatheroida (Williamson *et al*., 2014).

Como mencionado acima, as diferenças mais contundentes observadas entre metatérios e eutérios atuais estão relacionadas ao modo reprodutivo de cada grupo. Em Metatheria, as fêmeas possuem um curto período de gestação e dão à luz a filhotes em estágio prematuro de desenvolvimento, os quais completam seu desenvolvimento agarrados à mãe por um longo tempo, muitas vezes dentro uma bolsa de pele (marsúpio, presente em diversos táxons; Figura 4). Este desenvolvimento intrauterino mais curto está relacionado a diferenças nos tecidos maternos e do feto em desenvolvimento. Nos metatérios nota-se a ausência de trofoblasto, presença de corpo lúteo de vida curta e, na maioria das espécies, placenta vitelínica (corioalantoide apenas em alguns casos, mas sem as vilosidades típicas dos eutérios). Tais características levam ao reconhecimento imunológico e rejeição dos filhotes pelo corpo da mãe, com o parto ocorrendo prematuramente quando comparado ao dos eutérios. Ademais, fêmeas possuem vagina e útero duplos e machos saco escrotal anterior ao pênis (exceto em Notoryctidae), além de abertura urogenital comum (Kielan-Jaworoska *et al*., 2004; Cáceres & Cherem, 2012). Tal estratégia de reprodução foi por muito tempo considerada menos derivada comparada a dos mamíferos placentários. No entanto, tal visão vem sendo contestada, sugerindo-se mais recentemente que estratégias do tipo dos placentários, com intenso contato entre mãe e feto, seriam na realidade a condição ancestral dos térios, já encontradas em grupos basais (*stem* Theria), como os Multituberculata (Weaver *et al*., 2022).



Figura 4. A, fêmea adulta de *Monodelphis domestica*; **B**, fêmea com ninhada de 10 filhotes aproximadamente 36 horas após seu nascimento (esta espécie não possui marsúpio); **C**, filhotes de B em detalhe; **D**, neonato, menos de 10 horas após o nascimento. Fonte: OpossumBase.

No que se refere ao esqueleto, este é bastante similar entre eutérios e metatérios. Nota-se nestes últimos a presença de ossos epipúbicos associados à cintura pélvica, ausentes em Eutheria, mas que seriam uma condição primitiva, visto que também são encontrados nos primeiros eutérios (Kielan-Jaworoska *et al*., 2004). A estrutura do tornozelo dos metatérios é característica e seria bastante semelhante à do ancestral comum dos térios. Nela se observa, na articulação do tornozelo superior, um menisco proeminente contendo ossificações (lúnulas) entre as facetas articulares astrágalo-fibulares da fíbula e do astrágalo (Szalay, 1994) (Figura 5).

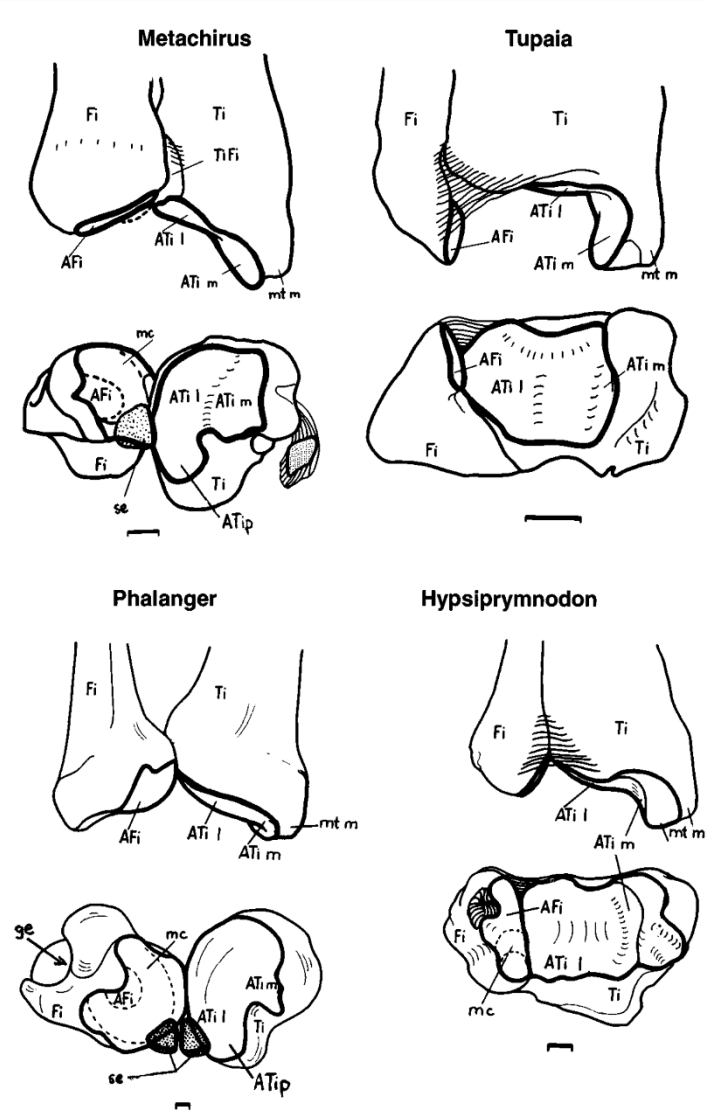


Figura 5. Comparação entre os membros inferiores direitos de três metatérios (*Metachirus*, *Phalanger* e *Hypsiprymnodon*) e um eutério (*Tupaia*) demonstrando as diferenças na articulação do tornozelo entre Metatheria e Eutheria. Escalas = 1 mm. Abreviaturas: **AFi**, articulação astrágalo-fibular; **ATil**, articulação astrágalo-tibial lateral; **ATim**, articulação astrágalo-tibial medial; **ATip**, articulação astrágalo-tibial posterior; **Fi**, fíbula; **ge**, sulco para extensores; **me**, menisco; **mtm**, maléolo tibial medial; **se**, sesamoide; **Ti**, tíbia; **TiFi**, articulação tíbio-fibular distal. Fonte: Szalay (1994).

O crânio dos metatérios possui algumas características diagnósticas, tais como: bula auditiva formada em parte pelo osso esfenoide, ausência de sulco para a artéria estapediana no promontório (Kielan-Jaworoska *et al*., 2004), presença de plataforma massetérica posterior no dentário, exposição ventral do pré-esfenoide e processo angular do dentário atingindo metade do comprimento total do ramo do dentário,

porém menor que este (Williamson *et al*., 2014). Comumente, também se nota que o crânio dos metatérios, à diferença de grande parte dos eutérios, possui grande área facial e pequena caixa craniana, palato fenestrado e processo angular do dentário voltado medialmente. A dentição dos Metatheria é representada pela fórmula dentária ancestral I5/4: C1/1: P3/3: M4/4 e os molares possuem o padrão tribosfênico básico, também observado em eutérios, com um grande contraste morfológico entre pré-molares e molares. Os metatérios apresentam também redução da difiodontia, na qual a substituição dentária pós-natal é limitada ao terceiro pré-molar. Neste sistema, o último pré-molar decíduo é retido e possui uma morfologia molariforme, o que, associado à sua posição, faz com que este dente seja tradicionalmente referido como sendo o M1/m1 (Figura 6). Tal padrão de substituição dentária é considerado uma modificação da condição ancestral presente entre os mamíferos térios cretácicos, tendo sido observado em diversos metatérios deste período e, portanto, inferido como o padrão compartilhado por todos os Metatheria. Ademais, grande parte dos marsupiais viventes e fósseis possuem túbulos em sua microestrutura dentária, o que não é encontrado em placentários (Kielan-Jaworoska *et al*., 2004; Cáceres & Cherem, 2012; Williamson *et al*., 2014).

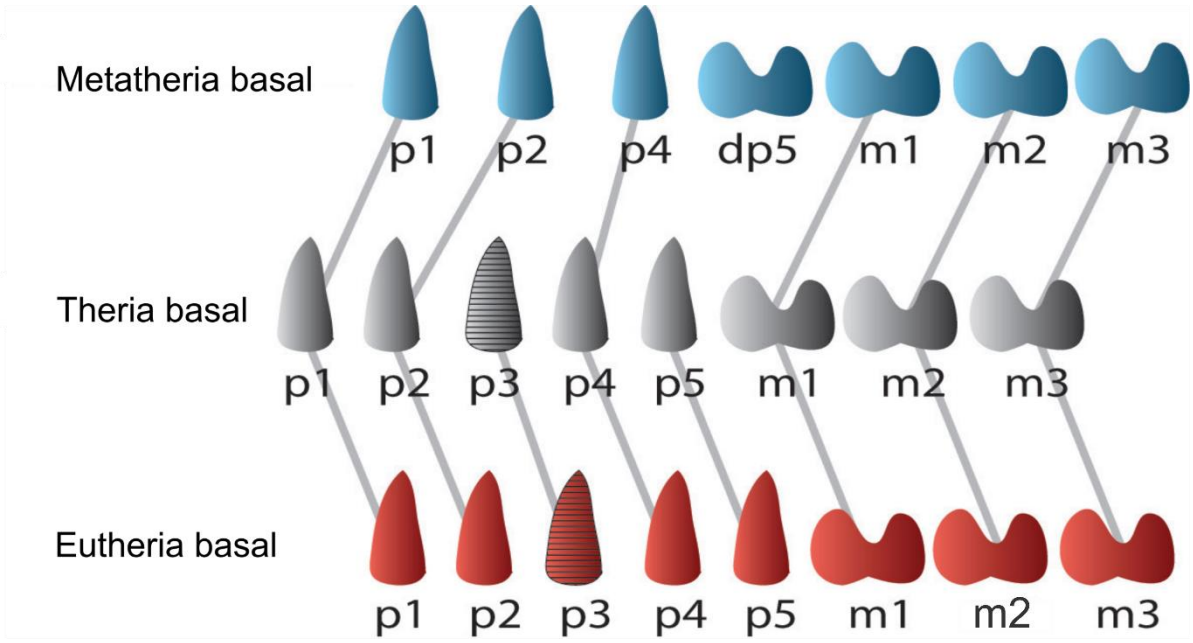


Figura 6. Homologias entre dentes pós-caninos de mamíferos: Theria basal, metatério e eutério basal. Modificado de Williamson *et al*. (2014).

3.1.1 Metatheria no Cretáceo

Como mencionado anteriormente, supõe-se que o clado Metatheria se originou no que seria hoje a América do Norte ou Ásia, muito provavelmente durante o Jurássico. No entanto, seus primeiros registros fósseis datam do Eocretáceo. Estes registros indicam que os primeiros metatérios eram pequenos animais compondo ecossistemas diversos, os quais também incluíam dinossauros, anfíbios, répteis e outros mamíferos (Williamson *et al*., 2014).

Até o final do Cretáceo, os metatérios distribuíam-se exclusivamente pela Laurásia. Nesta, os padrões de diversificação iniciais de Eutheria e Metatheria têm se revelado diferentes entre a América do Norte e a Eurásia. Na Eurásia, Eutheria foi o táxon predominante durante grande parte do Cretáceo. Contudo, não estavam presentes na América do Norte durante este período, só atingindo diversidade considerável no território norte-americano nos últimos 10 Ma do Neocretáceo (Cifelli & Davis, 2003). Já os metatérios foram pouco diversos no Cretáceo da Eurásia e notavelmente mais diversos na América do Norte, possuindo, neste continente, maior riqueza e abundância quando comparados aos eutérios (Figura 7). Na América do Norte, inclusive se observa, ao longo do Cretáceo, a diversificação de numerosas linhagens de Metatheria, com aumento da massa corporal média destes organismos no Neocretáceo, compreendendo táxons com tamanho de pequenos esquilos até outros com tamanho aproximado de gatos. Os metatérios norte-americanos igualmente possuíam, já por volta do Neocretáceo, dietas e hábitos locomotores variados (Williamson *et al*., 2014).

São reconhecidas atualmente 67 espécies válidas de metatérios para o Cretáceo, seis Deltatheroida e 61 espécies basais de Marsupialiformes, do Barremiano ao Maastrichtiano da Europa, Ásia e América do Norte. Os Deltatheroida são um grupo controverso, que somente recentemente foi reconhecido como parte de Metatheria. São registrados principalmente no Cretáceo da Ásia, com alguns registros na América do Norte. Já seu grupo irmão, Marsupialiformes, compreende grande parte da diversidade de metatérios, incluindo o grupo-coroa Marsupialia. Tanto Deltatheroida quanto Marsupialiformes possuem seus primeiros registros fósseis no Eocretáceo (Williamson *et al*., 2014; Bi *et al*., 2018).

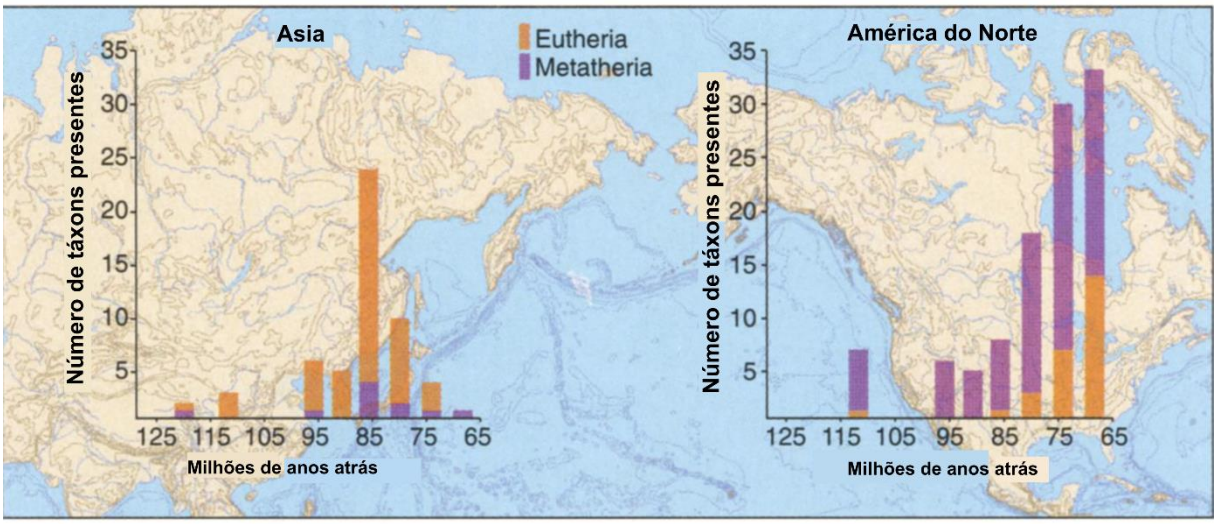


Figura 7. Diversidade de espécies de metatérios (roxo) e eutérios (laranja) na Ásia e América do Norte, durante o Cretáceo. Modificado de Cifelli & Davis (2003).

Dentro de Marsupialiformes, se reconhece os seguintes clados para o Cretáceo: i) Stagodontidae, pequeno clado de grandes metatérios com distribuição na América do Norte; ii) Pediomyidae, clado com forte suporte filogenético, de diversidade taxonômica e morfológica considerável, distribuído na América do Norte; iii) Glasbiidae (*sensu* Williamson *et al*., 2014), restrito ao gênero *Glasbius* da América do Norte; iv) "Alphadontidae", clado que tradicionalmente contém táxons relacionados a *Alphadon marshi*, considerado atualmente para ou polifilético; e v) Asiatheriidae, clado de distribuição na Ásia com caracteres primitivos. Somam-se a estes diversos táxons não compreendidos nestes clados, como, por exemplo, *Adelodelphys*, *Sinbadelphys*, *Kokopellia*, *Arcantiodelphys*, *Anchistodelphys*, *Aenigmadelphys*, *Eoalphadon*, *Apistodon*, *Iugomortiferum* e *Bistius*. Ademais, a origem de outros dois clados de Marsupialiformes, os quais teriam atravessado o limite K–Pg e perdurado durante o Paleógeno, ocorreu supostamente no Cretáceo, sendo eles: i) Herpetotheriidae, clado com alguns representantes basais no Cretáceo e que em seguida se tornou um dos mais especiosos do Paleógeno da América do Norte; e ii) "Peradectidae", clado muito abrangente e com pouco suporte filogenético, compreendendo principalmente táxons pós-cretácicos (Kielan-Jaworoska *et al*., 2004; Williamson *et al*., 2014).

3.1.2 Metatheria do Cenozoico do Hemisfério Norte

A grande extinção que marca o limite K–Pg foi bastante impactante sobre os táxons de metatérios norte-americanos, causando um grande declínio e extinção de numerosas linhagens cretácicas. Subsequentemente, os metatérios foram rapidamente suplantados por mamíferos placentários e não recobraram seus níveis de diversidade na América do Norte. Dentre as linhagens cretácicas mencionadas acima, encontram-se presentes no Paleógeno da América do Norte os “Peradectidae” (*Peradectes minor*, *Peradectes coproxeches*, *Peradectes elegans* e *Peradectes chesteri* no Paleoceno; *Peradectes gulottai*, *Peradectes protinnominatus*, *Mimoperadectes labrus*, *Mimoperadectes houdei*, *Armintodelphys dawsoni* e *Armintodelphys blacki* no Eoceno; e *Peradectes californicus* no Oligoceno) e os Herpetotheriidae (*Golerdelphys stock* no Paleoceno; *Copedelphys innominata*, *Herpetotherium comstocki*, *Herpetotherium edwardi*, *Herpetotherium marsupium* e *Herpetotherium knighti* no Eoceno; e *Herpetotherium fugax* no Oligoceno). Além destes, também estavam presentes na América do Norte os marsupialiformes *Thylacodon montanensis*, *Thylacodon pusillus*, *Swaindelphys encinensis* e *Swaindelphys johansoni*, todos do Paleoceno (Williamson *et al*., 2014). Os Metatheria persistiram na América do Norte até, possivelmente, o Mioceno, quando desapareceram totalmente deste continente. Em seguida, no Plioceno/Pleistoceno, quando do Grande Intercâmbio Biótico das Américas (GIBA), marsupiais da ordem Didelphimorphia, família Didelphidae, provindos da América do Sul, voltam a ocupar a América Central e do Norte, com, por exemplo, a espécie *Didelphis virginiana*, maior espécie de didelfídeo atual, a qual ocorre do Canadá a Costa Rica (Jones *et al*., 2003; Williamson *et al*., 2012).

Na Europa, por sua vez, após o Cretáceo, encontram-se formas de metatérios possivelmente descendentes de ancestrais provenientes da América do Norte. Os metatérios permaneceram como componentes modestos da fauna europeia, não atingindo grandes níveis de diversidade. Os Peradectinae (*sensu* Szalay, 1994) são registrados do Eoceno ao Mioceno na Europa (França, Bélgica, Alemanha), com táxons com morfologia dentária muito próxima àquela das formas que teriam vindo da América do Norte (Szalay, 1994). Outro clado registrado na Europa é

Herpetotheriidae, que atingiu sua maior diversidade neste continente no início do Eoceno e desapareceu no Mioceno médio, sendo registrado na França, Alemanha, Suíça, Áustria, República Tcheca e Espanha (Furió *et al*., 2012).

Já na Ásia, os táxons de metatérios do Cretáceo não são encontrados nas faunas paleógenas e o registro fóssil do grupo no Cenozoico é mal documentado. Supõe-se que um estoque de metatérios europeus teria migrado para a Ásia e África no Paleógeno, levando a uma exígua multiplicação de linhagens, sem grande diversificação (Szalay, 1994). O soerguimento dos Himalaias, o qual teria constituído uma importante barreira física, pode ter influenciado a história evolutiva e paleobiogeográfica dos metatérios na Ásia, visto que os registros dos Herpetotheriidae se encontram ao norte do complexo himalaio, enquanto que os Peradectidae se distribuem ao sul. Reportam-se esparsos restos de Metatheria para o Eoceno da China, Índia, Cazaquistão, Paquistão (Herpetotheriidae) e Turquia (*Anatoliadelphys*, Marsupialiformes não-Marsupialia + possivelmente Herpetotheriidae, afinidades incertas), Oligoceno Inferior de Omã (Peradectidae) e registros para o Mioceno da Tailândia e China (ambos Peradectidae). Na África, os metatérios somente são registrados no Cenozoico no norte do continente, especificamente no Eoeoceno da Tunísia e Eooligoceno do Egito (Peradectidae) (Figura 8) (Crochet *et al*., 2007; Murat Maga & Beck, 2017).

É importante ressaltar que todos estes táxons de metatérios do Cretáceo e início do Cenozoico não são ainda bem compreendidos com relação ao seu posicionamento filogenético, sendo considerados ou táxons basais (*stem*) do grupo-coroa Marsupialia, ou membros questionáveis do mesmo (Beck *et al*., 2022).

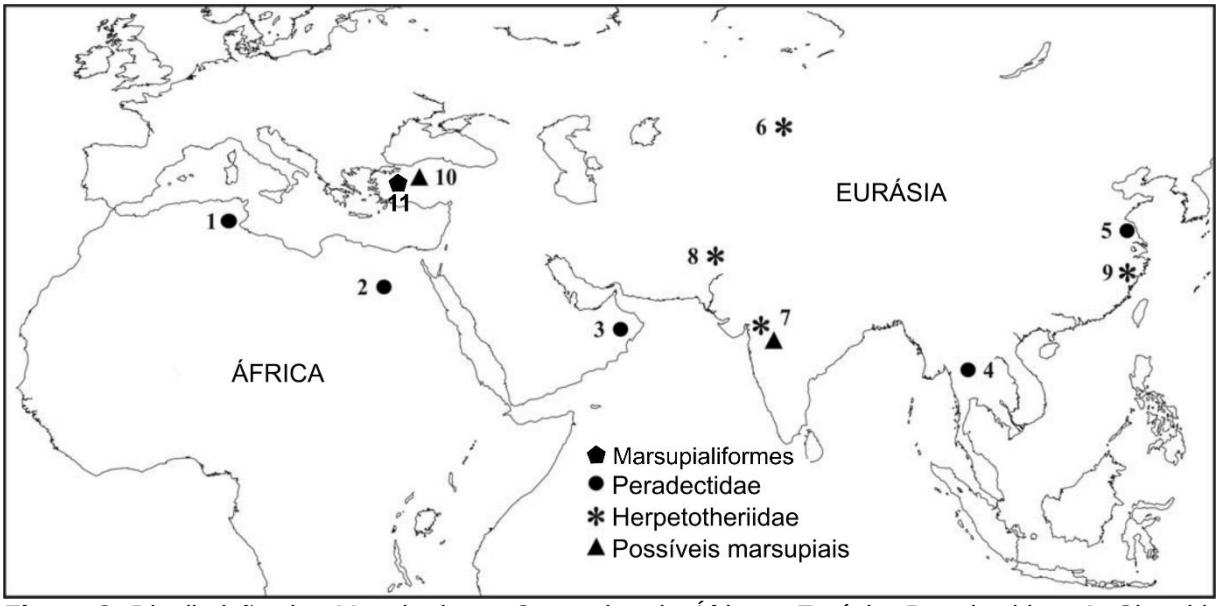


Figura 8. Distribuição dos Metatheria no Cenozoico da África e Eurásia. Peradectidae: **1**, Chambi, Tunísia; **2**, Fayum, Egito; **3**, Taqah, Omã; **4**, Bacia de Li, Tailândia; **5**, Sonlinzhuang, China. Herpetotheriidae: **6**, Bacia de Zaissan, Cazaquistão; **7**, Mina de lignite Vastan, Índia; **8**, Bugti Hills, Paquistão; **9**, Shanghuang e Jiangsu, China. Marsupialiformes: **11**, Uzunçarşidere Formation, Turquia. Marsupiais de afinidades incertas: **7**, Mina de lignite Vastan, Índia; **10**, Formação Kartal, Turquia. Modificado de Crochet *et al*. (2007) e Murat Maga & Beck (2017).

3.2 MARSUPIALIA ILLIGER, 1811

No que se refere ao grupo-coroa de Metatheria, Marsupialia, estima-se através de relógios moleculares que este teria se originado no Neocretáceo (Upham *et al*., 2019), ou mais recentemente entre o final do Paleoceno-início do Eoceno (Beck *et al*., 2022). Táxons indiscutivelmente considerados como pertencentes a Marsupialia são conhecidos apenas para o Cenozoico e com distribuição exclusiva no Gondwana, com exceção dos didelfídeos, que posteriormente migraram da América do Sul para a América do Norte durante o GIBA. O único carácter craniodental considerado como sinapomorfia do grupo seria a ausência de cingulídeo posterior nos molares inferiores. No entanto, um cingulídeo posterior já foi reportado para molares inferiores de alguns táxons de marsupiais, inclusive de didelfídeos (Beck *et al*., 2022).

Os membros da supercoorte Marsupialia, comumente denominados marsupiais, são tradicionalmente divididos em duas grandes coortes “Ameridelphia” e Australidelphia. Dentro de “Ameridelphia” estariam duas ordens com representantes atuais na América do Sul, Didelphimorphia e Paucituberculata. Já Australidelphia

compreende quatro ordens com distribuição atual na Australásia (Dasyuromorphia, Peramelemorphia, Notoryctemorphia e Diprotodontia) e uma ordem fóssil do Mioceno da Austrália, Yalkaparidontia. Ademais, também se inclui em Australidelphia a ordem sul-americana Miocrobiotheria (com representantes atuais e fósseis) e possivelmente a ordem fóssil Polydolopimorphia, que conta com registros na América do Sul e Antártica (exemplos de morfologias dentárias de representantes da maioria destas ordens na Figura 9). Praticamente todos os táxons conhecidos de Marsupialia até o presente podem ser classificados em uma destas sete ordens. Não obstante, é importante ressaltar que estudos recentes apontam o clado “Ameridelphia” como não monofilético (Voss & Jansa, 2009; Black *et al*., 2012; May-Collado *et al*., 2015; Goin *et al*., 2016).

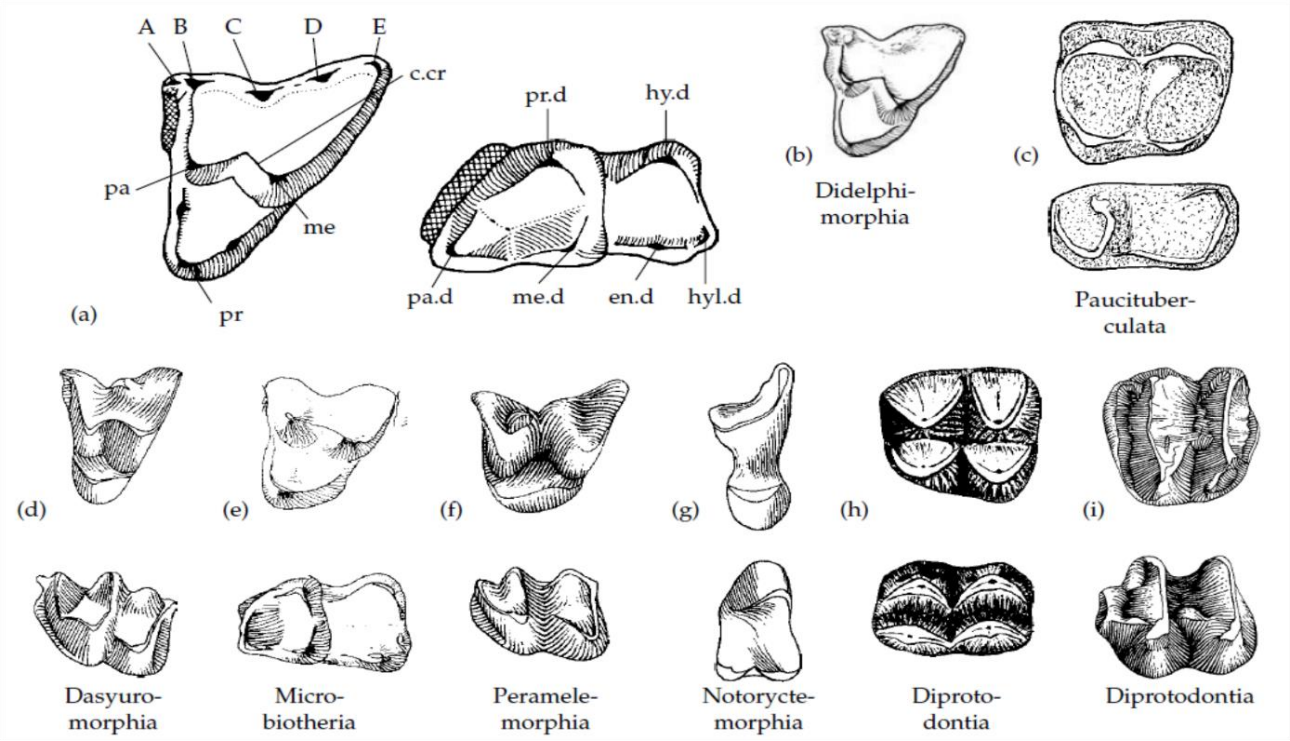


Figura 9. Molares superiores (esquerdos) e inferiores (a, e, direitos; c, d, f, h, i, esquerdos) de marsupiais: **a**, marsupial primitivo; **b**, Didelphimorphia (*Monodelphis*); **c**, Paucituberculata (*Caenolestes*); **d**, Dasyuromorphia (*Sminthopsis*); **e**, Microbiotheria (*Dromiciops*); **f**, Peramelemorphia (*Perameles*); **g**, Notoryctemorphia (*Notoryctes*); **h**, Diprotodontia (*Phascolarctos*); **i**, Diprotodontia (*Simosthenurus*). Abreviaturas: c.cr, centrocrista; en.d, entocônido; hy.d, hipocônido; hyl.d, hipoconúlido; m, metacone; me.d, metacônido; pa, paracone; pa.d, paracônido; pr, protocone; pr.d, protocônido. Modificado de Kemp (2005).

Sugere-se que o clado Marsupialia evoluiu na América do Sul e em seguida teriam se dispersado pela Antártica, Austrália e Nova Guiné (Voss & Jansa, 2009). Os mais antigos restos fósseis considerados como de fato pertencentes a Marsupialia permanecem motivo de debate. Sugere-se que †*Djarthia* e um calcâneo isolado, com morfologia intermediária entre a de um "Ameridelphia" e um Australidelphia, ambos provenientes da fauna local de Tingamarra, na Austrália, datada em ~54 Ma, seriam os mais antigos Marsupialia conhecidos até o presente (Beck *et al*., 2022). Já os restos indubitavelmente de Marsupialia da América do Sul são de Laguna Fría e La Barda, 47–49 Ma AP, Argentina, com *Bardalestes* (Paucituberculata), microbiotérios e tarsos de Australidelphia. De acordo com Muizon & Ladevèze (2020), táxons de Sparassodonta e outros "Ameridelphia" *incertae sedis* basais, assim como das ordens Polydolopimorphia e Microbiotheria já são encontrados na fauna de Tiupampa, Eopaleoceno da Bolívia. Segundo Beck (2017), na fauna de Itaboraí (Eoeoceno, Brasil) não são encontrados táxons seguramente Marsupialia, enquanto que na fauna de Santa Rosa (Eooligoceno, Peru) estão presentes restos de Paucituberculata e Microbiotheria. Contudo, segundo Oliveira & Goin (2011), a fauna de Itaboraí já incluiria sim diversos representantes de Marsupialia, com as ordens Didelphimorphia, Paucituberculata, Microbiotheria e Polydolopimorphia. Nota-se assim que, devido às divergentes concepções relacionadas a quais grupos pertencem ou não à Marsupialia, os primeiros registros deste clado permanecem incertos.

3.3 PANORAMA FILOGENÉTICO DE METATHERIA

Os metatérios são menos numerosos em termo de espécies quando comparados aos eutérios. Não obstante, sua longa e complexa história evolutiva, a qual compreende importantes períodos de isolamento (comumente na América do Sul e Australásia no início do Cenozoico), resultou em diversidade morfológica e ecológica bastante comparável àquela observada em eutérios. A história evolutiva de Metatheria é de fato marcada por episódios de radiação adaptativa em diferentes níveis taxonômicos, ocupação progressiva de zonas adaptativas, além de evolução convergente entre diferentes táxons de metatérios e entre metatérios e eutérios (Springer *et al*., 1997).

Segundo Goin *et al*. (2016), as radiações no seio de Metatheria foram desencadeadas por fases de aquecimento global (ótimos climáticos) não somente no Cenozoico, como também no Cretáceo. As relações filogenéticas de Metatheria têm sido objeto de intensa pesquisa, as quais utilizam as mais variadas metodologias (Goin *et al*., 2016). Na análise de Cardillo *et al*. (2004), por exemplo, foram encontradas 154 árvores filogenéticas, incluindo todas ou algumas linhagens de Metatheria, publicadas em 107 artigos de 1980 a 2004. No entanto, as relações entre grande parte dos maiores subclados de Metatheria permanecem a ser esclarecidas (Williamson *et al*., 2014). Ademais, poucos estudos incluem táxons fósseis em suas análises, e, quando incluem, estes são em pequena quantidade, dificultando a compreensão das relações filogenéticas a maiores níveis taxonômicos, a análise da evolução de caracteres e aspectos paleobiogeográficos (Beck *et al*., 2022). De acordo com Beck *et al*. (2022), como mencionado acima, todas estas formas de metatérios do Mesozoico como †*Asiatherium*, Deltatheroidea, “Alphadontidae”, ”Pediomyidae,” Stagodontidae, †Herpetotheriidae e †Peradectidae, assim como táxons basais da América do Sul como Pucadelphyidae, Protodidelphidae, Caroloameghinidae, Derorhynchidae, Sparassodonta e Polydolopimorphia não podem ser seguramente considerados como pertencentes ao grupo-coroa Marsupialia.

Com relação aos metatérios basais não-Marsupialia, Williamson *et al*. (2012, 2014) proveram importantes análises filogenéticas, baseadas em caracteres dentários, utilizando grande parte dos táxons do Cretáceo e início do Paleógeno, sobretudo da América do Norte (Figura 10). Apenas três táxons sul-americanos estão presentes nas análises destes autores: *Roberthoffstetteria nationalgeographica*, *Szalinia gracilis* e *Pucadelphys andinus*, todos do Eopaleoceno de Tiupampa, Bolívia. Os táxons de metatérios cretácicos e do início do Paleógeno são conhecidos principalmente através de restos dentários, o quê, apesar de permitir sua identificação e o reconhecimento de certas características paleobiológicas, dificulta os estudos de taxonomia e filogenia em nível superior ao de gênero. Assim, suas relações são pouco resolvidas e há pouco suporte filogenético para a maioria dos clados cretácicos. Segundo Williamson *et al*. (2012), os Pediomyidae, Peradectidae e Herpetotheriidae, também suspostamente presentes na América do Sul, seriam parte de um clado derivado de Metatheria, comparado aos “Alphadontidae”, e nele estariam inclusos os

táxons *Szalinia* e *Pucadelphys*, os quais são considerados “Ameridelphia” *incertae sedis*, e *Roberthoffstetteria*, um Polydolopimorphia. Ademais, segundo os mesmos autores, *Roberthoffstetteria* seria filogeneticamente próximo do gênero norte-americano *Glasbius* (família Glasbiidae).

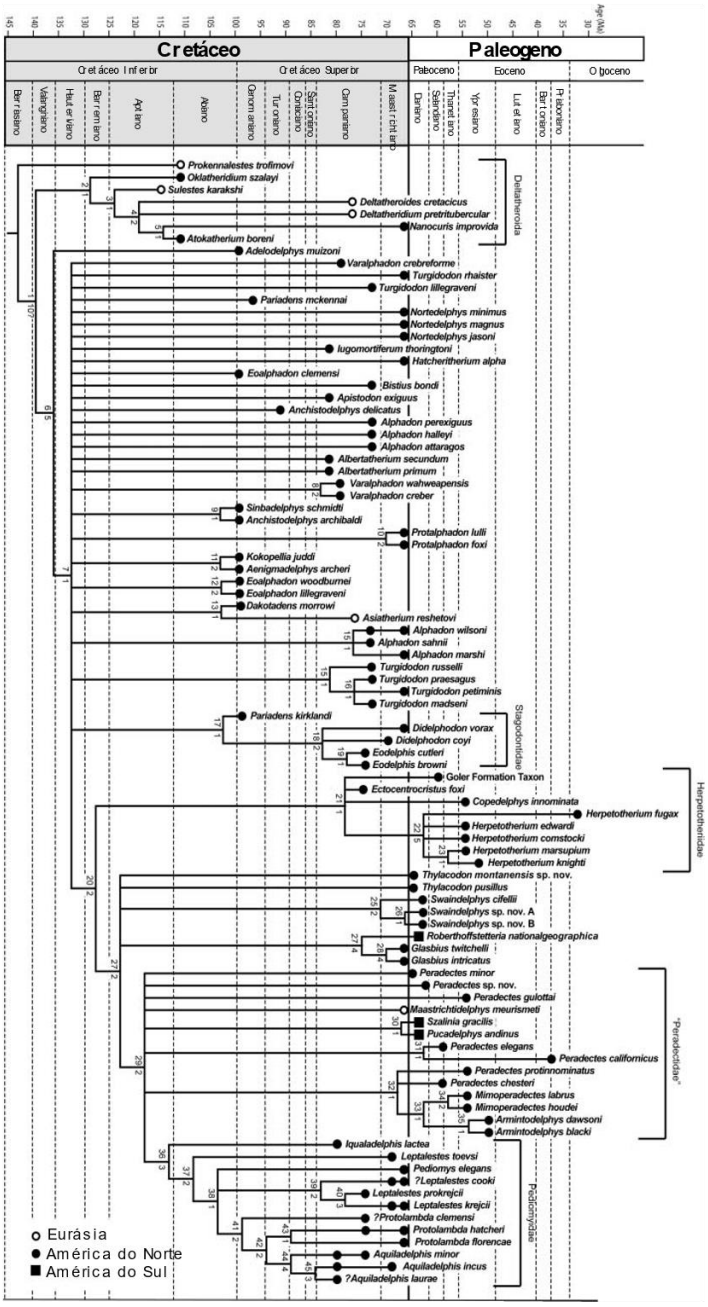


Figura 10. Árvore filogenética dos táxons de Metatheria do Cretáceo e Paleógeno. Modificado de Williamson *et al*. (2012).

No entanto, Chornogubsky & Goin (2015) consideram Glasbiidae uma família basal de Polydolopimorphia, composta por outros táxons, enquanto que

Roberthoffstetteria compõe, juntamente com *Sillustania*, de Laguna Umayo (Peru), a família Sillustanidae, sendo considerados Polydolopiformes basais. Estes autores recuperam a ordem Polydolopimorphia como monofilética, incluindo as subordens Polydolopiformes e Bonapartheriiformes, esta última compreendendo Argyrolagoidea (Figura 11). Os gêneros *Hatcheritherium* e *Ectocentrocristus*, da América do Norte, também já foram considerados basais à ordem Polydolopimorphia e/ou aos Polydolopiformes, tendo sido sugerido que Polydolpimorphia teria, portanto, se originado e se desenvolvido no sul da América do Norte e, em seguida, migrado para a América do Sul no final do Cretáceo. (Case *et al*., 2005; Goin *et al*., 2016).

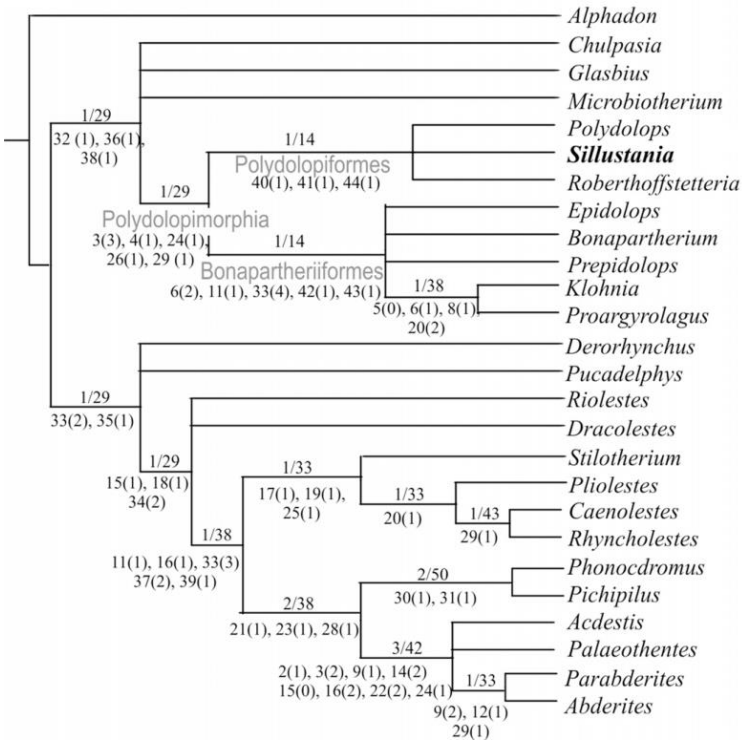


Figura 11. Árvore filogenética de Metatheria obtida por Chornogubsky & Goin (2015). Os números acima dos ramos correspondem ao suporte de Bremer absoluto/relativo. Os números sob os ramos correspondem às sinapomorfias listadas por Goin *et al*. (2009), com adições de Chornogubsky & Goin (2015).

As controvérsias com relação a ordem Polydolopimorphia vão ainda além. Segundo Goin *et al*. (2016), Polydolopimorphia, incluindo a superfamília Argyrolagoidea, está contida em Marsupialia e dentro de Australidelphia, pois teria surgido a partir de Microbiotheria. Já Beck (2017), utilizando uma extensa matriz,

incluindo caracteres morfológicos e moleculares, propõe que Polydolopimorphia (ao menos Epidolopinae, Bonapartheriidae e Polydolopidae) não estão compreendidos dentro de Marsupialia, e, portanto, não são igualmente membros de Australidelphia. Beck (2017) também sugere que Polydolopirmophia não contém Argyrolagoidea, os quais fariam parte da ordem Paucituberculata (Figura 12).

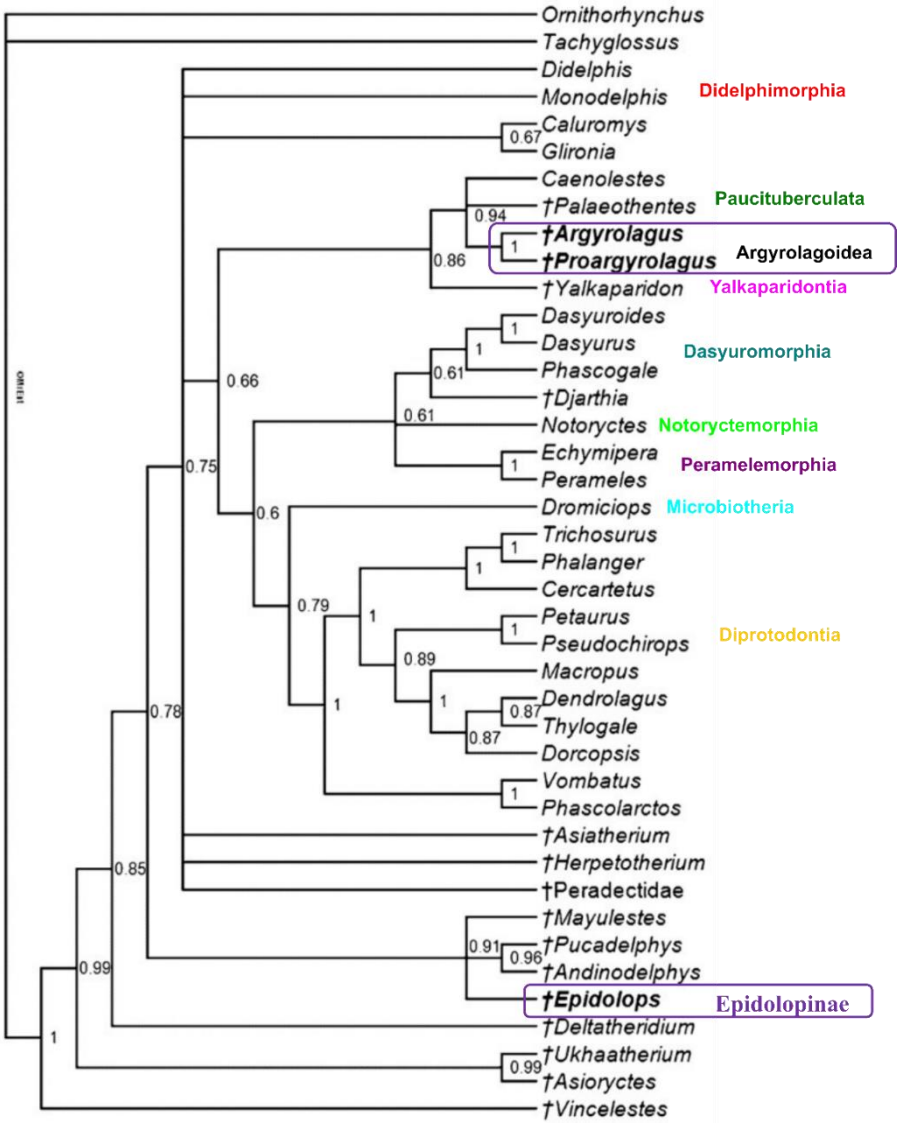


Figura 12. Relações filogenéticas de Metatheria segundo Beck (2017). Os valores presentes nos nós indicam as probabilidades posteriores bayesianas.

Assim, nota-se que, no que se refere ao grupo-coroa de Metatheria, Marsupialia, a posição de sua base e quais táxons de fato pertence ao clado permanecem motivo de debate. Marsupialia é tradicionalmente dividida entre “Ameridelphia” (não-monofilético) e Australidelphia. Estudos recentes (e.g., Horovitz *et al*., 2009) sugerem

que Marsupialia teria como grupo-irmão Herpetotheriidae, enquanto que Peradectidae seria o grupo-irmão de Didelphidae, ambos constituindo a ordem Didelphimorphia, a qual seria grupo irmão dos outros clados de Marsupialia (Figura 13).

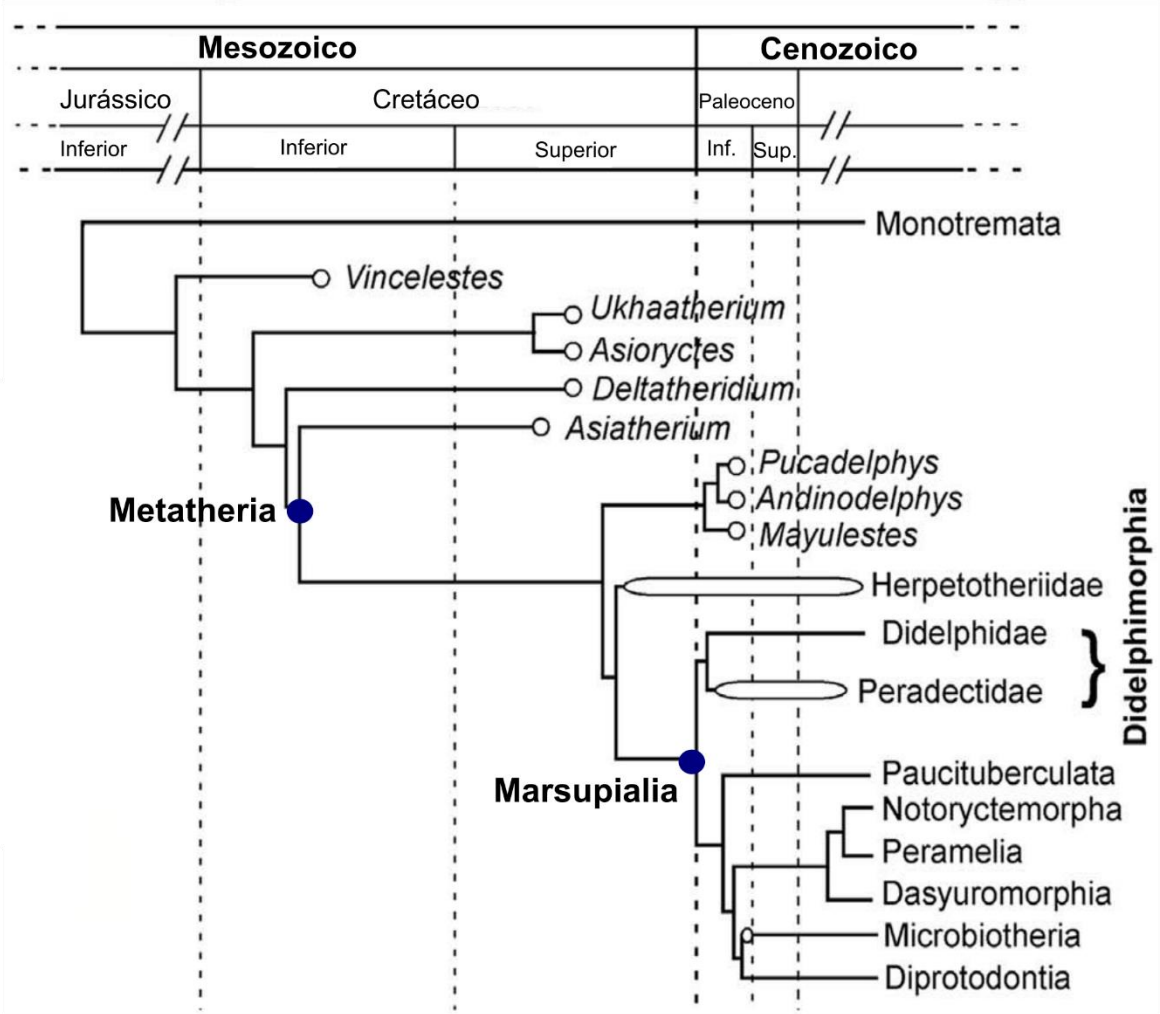


Figura 13. Diagrama representando cladograma mais parcimonioso de Metatheria obtido através de dados morfológicos por Horovitz *et al*. (2009).

Considerando estas diferentes problemáticas com relação a definição de Marsupialia, ressalta-se ainda que as relações entre os táxons que o compõem também são parcamente compreendidas. Um ponto atualmente de bastante consenso é a existência do clado Australidelphia, o qual seria monofilético e incluiria Microbiotheria e todas as quatro ordens viventes de marsupiais da Australásia. Tal hipótese foi primeiramente levantada com base em estudos de morfologia do tarso dos marsupiais (Szalay, 1982, 1994) e subsequentemente corroborada por características moleculares (hibridização de DNA, genes nucleares e mitocondriais) e

de morfologia do esperma, sendo Australidelphia um grupo natural em diversas análises filogenéticas. No entanto, o posicionamento de Microbiotheria dentro de Australidelphia já muito variou, tendo sido apontado como grupo-irmão de todas as demais ordens, ou situado entre estas em diversas posições (Cardillo *et al*., 2004; May-Collado *et al*., 2015). Em filogenias mais recentes vêm se encontrando Microbiotheria como grupo-irmão de Diprotodontia (Figuras 12, 13 e 14). Quanto às ordens australianas atuais, Peramelemorphia, Dasyuromorphia, Notoryctemorphia e Diprotodontia, seu posicionamento e relações filogenéticas também permanecem incertos, visto que diferentes análises recuperam resultados topológicos distintos. Sugere-se que a divergência dos clados teria acontecido rapidamente, o que gera informações filogenéticas conflituosas nas análises moleculares. As relações filogenéticas entre as ordens Peramelemorphia, Dasyuromorphia e Notoryctemorphia, por exemplo, são mais bem compreendidas como uma rede evolutiva, do que como simples bifurcações da árvore filogenética de Australidelphia (Gallus *et al*., 2015).

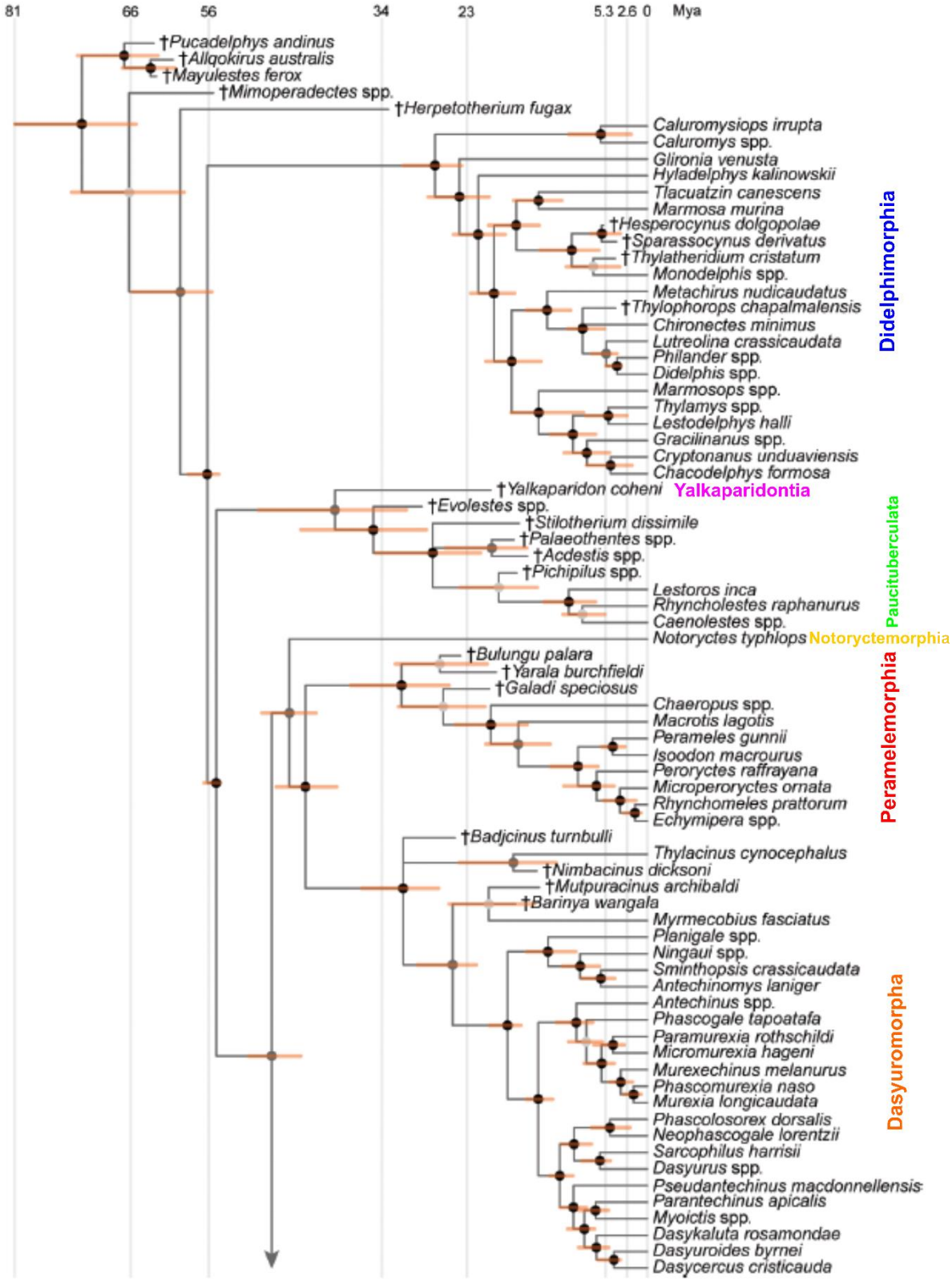
Já “Ameridelphia” não constitui um grupo natural, sendo polifilético, e as relações entre os clados atualmente nele inseridos também não são bem compreendidas. Táxons do Paleógeno da América do Sul raramente estão extensivamente representados nas análises filogenéticas, por seus restos serem muito escassos e fragmentados, dificultando a compreensão de sua posição filogenética. Diferentes análises, usando distintos agrupamentos de táxons e bases de caracteres diferentes, recuperam topologias diversas e, portanto, não se chega a um consenso. Por exemplo, diversos táxons tais como Pucadelphyidae, Protodidelphidae, *Derorhynchus*, *Carolopaulacoutoia* e *Gaylordia*, hoje considerados “Ameridelphia” *incertae sedis*, já foram previamente inseridos em Didelphimorphia (Goin *et al*., 2016). Isto se deve certamente à morfologia conservadora dos membros de fato de Didelphimorphia, a qual muito deve se assemelhar às características “primitivas” de Metatheria e de seus primeiros representantes.

Outra observação importante a ser relevada é o agrupamento por muito tempo considerado válido das ordens sul-americanas Paucituberculata e Polydolopimorphia, chamados de “pseudodiprotodontes”, o qual também era utilizado para relacioná-los com formas australianas da ordem Diprotodontia. Contudo, estudos indicam que o típico incisivo procumbente destes grupos desenvolveu-se convergentemente, sendo

que, por exemplo, em Caenolestidae o incisivo procumbente é o i1 ou i2 e em Diprotodontia o i3 ou i4 (Goin *et al*., 2009) e Polydolopimorphia talvez sequer faça parte de Marsupialia (Beck, 2017). Observa-se com isto, além dos problemas citados acima, que há pouco consenso filogenético no que toca a ordem Polydolopimorphia.

Em um recente esforço buscando a compreensão da filogenia de Marsupialia, e dos clados que a compõem, Beck *et al*. (2022) realizaram análises filogenéticas utilizando ampla amostragem de táxons recentes e fósseis de metatérios, através de dados moleculares e morfológicos, com a utilização de diversas metodologias (Figura 14). Foi observado que Herpetotheriidae novamente foi encontrado como grupo-irmão de Marsupialia. Ademais, as sete ordens com representantes viventes (Didelphimorphia, Paucituberculata, Notoryctemorphia, Peramelemorphia, Dasyuromorphia, Microbiotheria e Diprotodontia), além da ordem fóssil Yalkaparidontia foram recuperadas como monofiléticas.

Em suma, apesar de numerosos e laboriosos esforços buscando uma melhor compreensão das relações filogenéticas dos Metatheria, muitas questões permanecem em aberto. Muitas das problemáticas estão relacionadas ao fato de que grande parte das análises realizadas se baseiam em caracteres moleculares e, portanto, unicamente em táxons viventes (e.g., Beck, 2008, 2022; Nilsson *et al*., 2010; Gallus *et al*., 2015; May-Collado *et al*., 2015). Algumas análises filogenéticas inserem fósseis em suas bases de dados, mas incluem apenas uma quantidade limitada de táxons (e.g., Horovitz *et al*., 2009; Chornogubsky & Goin, 2015), dificultando a compreensão da definição e conteúdo de Metatheria e de seu grupo-coroa Marsupialia.


81
66
56
34
23
5.3 2.6 0
Mya
†Pucadelphys andinus
†Allqokirus australis
†Mayulestes ferox
†Mimoperadectes spp.
†Herpetotherium fugax
Caluromysiops irrupta
Caluromys spp.
Glironia venusta
Hyladelphys kalinowskii
Tlacuatzin canescens
Marmosa murina
†Hesperocynus dolgopolae
†Sparassocynus derivatus
†Thylatheridium cristatum
Monodelphis spp.
Metachirus nudicaudatus
†Thylophorops chapalmalensis
Chironectes minimus
Lutreolina crassicaudata
Philander spp.
Didelphis spp.
Marmosops spp.
Thylamys spp.
Lestodelphys halli
Gracilinanus spp.
Cryptonanus unduaviensis
Chacodelphys formosa
Didelphimorphia
†Yalkaparidon coheni
Yalkaparidontia
†Evolestes spp.
†Stilotherium dissimile
†Palaeothentes spp.
†Acdestis spp.
†Pichipilus spp.
Lestoros inca
Rhyncholestes raphanurus
Caenolestes spp.
Paucituberculata
Notoryctes typhlops
Notoryctemorphia
†Bulungu palara
†Yarala burchfieldi
†Galadi speciosus
Chaeropus spp.
Macrotis lagotis
Perameles gunnii
Isoodon macrourus
Peroryctes raffrayana
Microperoryctes ornata
Rhynchomeles prattorum
Echymipera spp.
Peramelemorphia
†Badjcinus turnbulli
Thylacinus cynocephalus
†Nimbacinus dicksoni
†Mutpuracinus archibaldi
†Barinya wangala
Myrmecobius fasciatus
Planigale spp.
Ningaui spp.
Sminthopsis crassicaudata
Antechinomys laniger
Antechinus spp.
Phascogale tapoatafa
Paramurexia rothschildi
Micromurexia hageni
Murexechinus melanurus
Phascomurexia naso
Murexia longicaudata
Phascolosorex dorsalis
Neophascogale lorentzii
Sarcophilus harrisii
Dasyurus spp.
Pseudantechinus macdonnellensis
Parantechinus apicalis
Myoictis spp.
Dasykaluta rosamondae
Dasyuroides byrnei
Dasycercus cristicauda
Dasyuromorpha

(Figura 14 continuação)

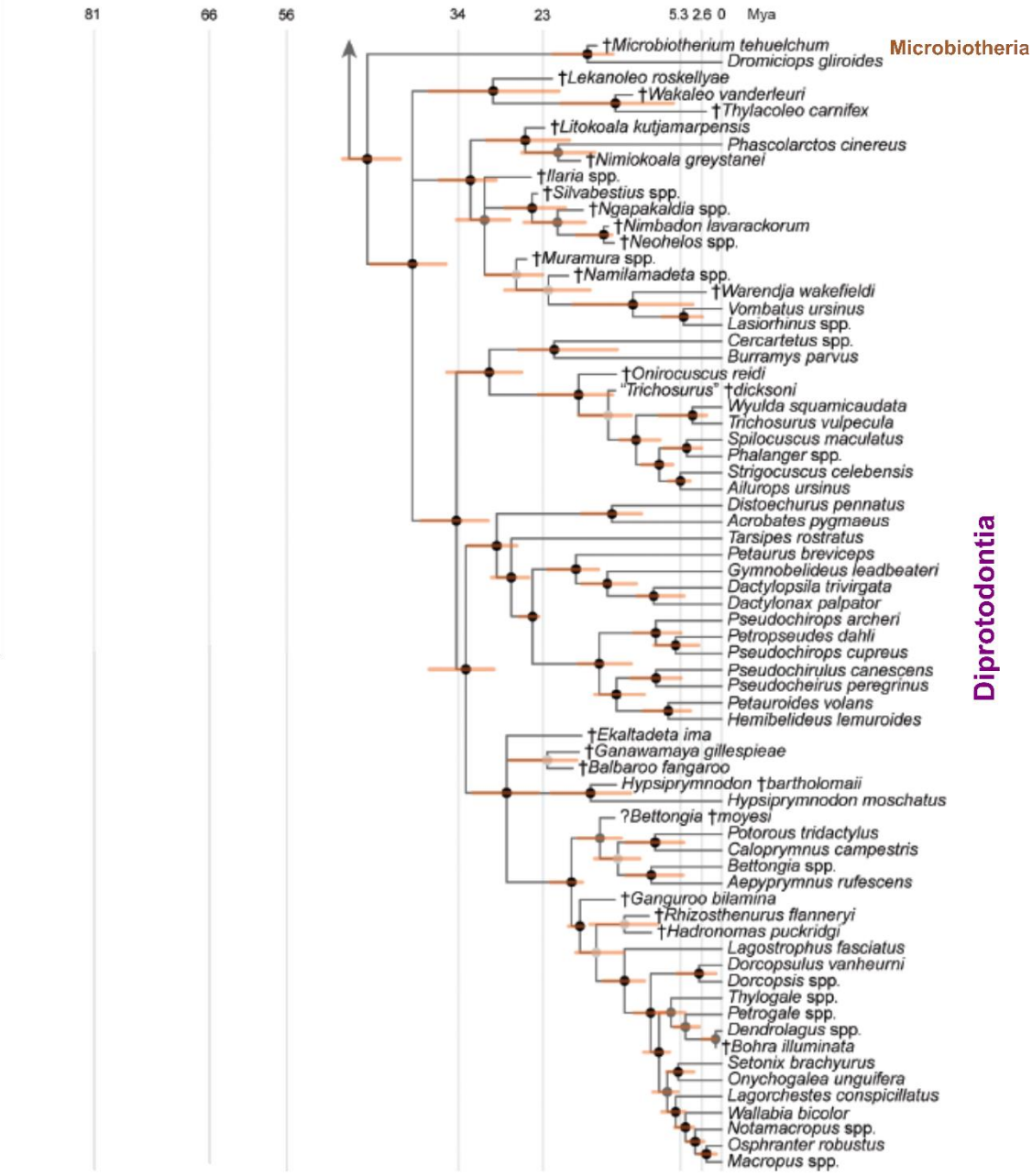


Figura 14. Árvore filogenética gerada com 50% de consenso através de análises Bayesianas datadas realizada por Beck *et al*. (2022). Pontos negros indicando nós com ≥0.95 de probabilidade Bayesiana (forte suporte); pontos cinza escuro indicam 0,75-0,94 de probabilidade Bayesiana (suporte moderado); pontos cinza claro indicam 0,50-0,74 de probabilidade Bayesiana (suporte fraco). Nodos sem pontos foram constringidos a priori de modo a que suas idades pudessem ser calibradas. As barras laranjas representam 95% dos intervalos de Maior Densidade Posterior (*Highest Posterior Density* – HPD) das idades dos nós. Modificado de Beck *et al*. (2022).

3.4 METATHERIA NA AMÉRICA DO SUL

Atualmente, a América do Sul conta com 22 gêneros e 134 espécies de metatérios, todos pertencentes ao grupo-coroa Marsupialia, classificados em três ordens: i) Paucituberculata, representada atualmente somente pela família Caenolestidae (três gêneros e sete espécies); ii) Microbiotheria, com uma família, Microbiotheriidae (um gênero e duas espécies); e iii) Didelphimorphia, hoje constituída exclusivamente pela família Didelphidae (18 gêneros e 125 espécies) (Mammal Diversity Database, 2022). Tal diversidade perfaz aproximadamente 10% da fauna de mamíferos terrestres da América do Sul (Goin *et al*., 2016).

O registro fóssil mais antigo de Metatheria na América do Sul é o do Polydolopimorphia *Cocatherium lefipanum*, da chamada fauna da localidade de Grenier Farm (anterior à fauna de Tiumpampa), do início do Paleoceno, Formação Lefipán, Patagônia Argentina, o qual é igualmente considerado como o primeiro registro de um mamífero tério na América do Sul (Figura 15; Goin *et al*., 2006). Apesar de tratar-se de apenas um molar isolado, tal resto já apresenta um padrão bastante derivado, o que fortalece as teorias de que os metatérios chegaram à América do Sul no final do Cretáceo, com uma ou mais linhagens de imigrantes, ocasionando a evolução de táxons *in situ* (Goin *et al*., 2016). Diversos autores (e.g., Case *et al*., 2005; Forasiepi, 2009; Goin *et al*., 2016; Carneiro *et al*., 2018) vêm sustentando a hipótese de que os metatérios sul-americanos são fruto de radiações sucessivas de marsupialiformes da América do Norte, que se originaram no sul deste continente e em seguida se dispersaram para a América do Sul. Subsequentemente, a América do Sul tornou-se palco de importantes radiações evolutivas do clado Metatheria, sendo que a diversidade atual de marsupiais sul-americanos não representa a miríade de linhagens que habitaram este continente em tempos passados (Goin *et al*., 2016).

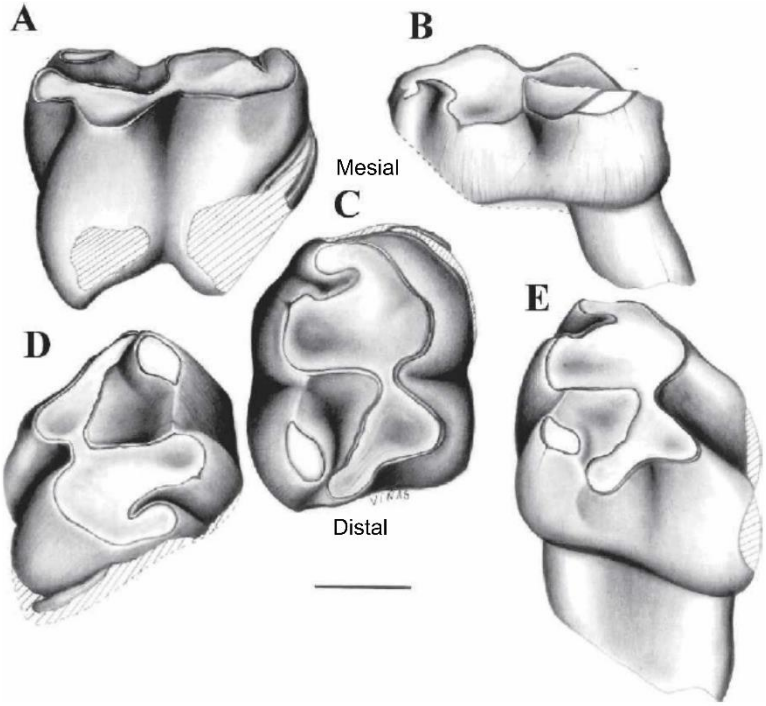


Figura 15. *Cocatherium lefipanum* (Metatheria, Polydolopimorphia), Formação Lefipán, Paleoceno, Argentina, molar inferior em vista: **A**, labial; **B**, lingual; **C**, oclusal; **D**, anterior oclusal; **E**, posterior oclusal. Escala = 1 mm. Modificado de Goin *et al*. (2006).

Dentre os metatérios fósseis encontrados na América do Sul, encontram-se três clados mencionados anteriormente para o Hemisfério Norte: Pediomyidae, Peradectidae e Herpetotheriidae. Supõe-se que o táxon *Khasia*, da fauna de Tiupampa, Bolívia, do início do Paleoceno, teria afinidade com os Pediomyidae, no entanto, trata-se de um táxon enigmático e suas relações filogenéticas necessitam ser melhor exploradas (Goin *et al*., 2016). Por exemplo, de acordo com Muizon & Ladevèze (2020), *Khasia* constituiria um Microbiotheria. Também em relação aos Pediomyidae sul-americanos, Oliveira & Goin (2011) relatam a presença de um táxon inédito pertencente a esta família do início do Eoceno da Bacia de Itaboraí, Brasil, e Sigé (1972) igualmente indica tentativamente a presença de Pediomyidae no Neopaleoceno/Eoeoceno de Laguna Umayo, Peru. Carneiro *et al*. (2018) indicam a presença de Pedimyoidea na Bacia de Itaboraí, Brasil, com o táxon *Austropediomys marshalli*. Quanto aos Peradectidae, registra-se o táxon *Peradectes* também na fauna de Tiupampa (Goin *et al*., 2016). Os Herpetotheriidae, por sua vez, estariam inclusos na coorte “Ameridelphia” segundo Goin *et al*. (2016), dentro dos “Ameridelphia”

incertae sedis, e estariam presentes nos depósitos de Santa Rosa, Peru, Eooligoceno, com o táxon atribuído a cf. Herpetotheriidae, *Rumiodon inti* (Goin & Candela, 2004). Também se cita a presença de restos cf. Herpetotheriidae na Bacia de Itaboraí, Brasil (Oliveira & Goin, 2011).

O restante dos táxons presentes no registro fóssil da América do Sul apresenta distribuição essencialmente restrita a este continente ou ao Hemisfério Sul. A seguir serão apresentados os principais subclados de metatérios sul-americanos, de acordo com a classificação de Goin *et al*. (2016), tendo em vista tratar-se da classificação mais atual e completa dos metatérios da América do Sul, compreendendo: "Ameridelphia" *incertae sedis* (incluindo a ordem Sparassodonta); as ordens com representantes atuais, Didelphimorphia, Paucituberculata e Microbiotheria; e a extinta ordem Polydolopimorphia.

3.4.1 "Ameridelphia" *incertae sedis*

O clado "Ameridelphia" *incertae sedis* é um agrupamento filogeneticamente controverso, reunindo uma série de táxons não inseridos dentro do grupo-coroa Marsupialia, incluindo a ordem Sparassodonta (vide seção 3.4.1.1). Segundo Goin *et al*. (2016), as famílias Pucadelphyidae, Jaskhadelphyidae, Mayulestidae, Protodidelphidae, Derorhynchidae e Sternbergiidae, e os gêneros *Eobrasilia*, *Incadelphys*, *Gaylordia*, *Marmosopsis*, *Monodelphopsis*, *Szalinia* e *Tiulordia*, presentes no registro fóssil da América do Sul, seriam "Ameridelphia" *incertae sedis*, assim como as famílias Pediomyidae e Herpetotheriidae, as quais possuem registros no Hemisfério Norte. Assim, caso venha a ser corroborado que estas últimas duas famílias façam parte de "Ameridelphia" *incertae sedis*, este clado existiria desde o Neocretáceo, estando neste período unicamente presentes no Hemisfério Norte. Do contrário, "Ameridelphia" *incertae sedis* existiria a partir do Paleoceno e somente no Hemisfério Sul. Neste caso, os "Ameridelphia" *incertae sedis* possuem ocorrência limitada ao Paleógeno, entre o Paleoceno (Idade de Mamíferos Terrestres Sul-Americanos – SALMA – Tiupampense) e Eoceno, com registros na Argentina, Bolívia e Brasil (Quadro 1). Foram notavelmente abundantes no início do Eoceno (Itaboraiense), sofrendo grande declínio depois do início do Mesoeoceno (SALMA

Fauna de El Sapo) e continuaram em declínio até se extinguirem no Neoeoceno (Goin *et al*., 2016).

Os “Ameridelphia” *incertae sedis* ocuparam distintos nichos ecológicos, tais como frugívoros de médio/grande porte, pequenos insetívoros e pequenos mesocarnívoros. Na fauna de Tiumpampa, Eopaleceno, Bolívia, foram encontrados diversos Pucadelphyidae, Jaskhadelphyidae e Mayulestidae. Já na fauna de Itaboraí, Brasil, do início do Eoceno, são encontrados Protodidelphidae, Derorhynchidae e Sternbergiidae, considerados táxons mais especializados de ameridélfios basais. Assim, nota-se que desde o início do Paleógeno, os táxons de “Ameridelphia” *incertae sedis* apresentam notável diversidade taxonômica e adaptativa (Figura 16) (Goin *et al*., 2016).

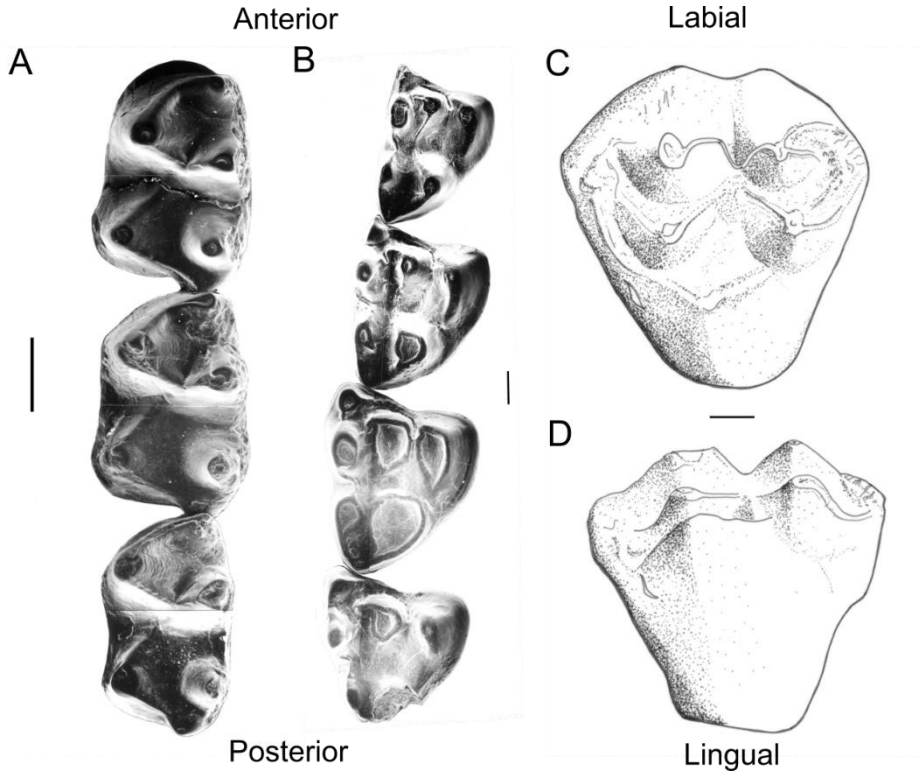


Figura 16. “Ameridelphia” *incertae sedis*: molares inferiores: **A**, *Guggenheimia crocheti* (esquerdos); molares superiores: **B**, *Protodidelphis vanzolinii* (direitos), **C** e **D**, *Carolocoutoia ferigoloi* (esquerdos). Escalas = 1 mm. Modificado de Oliveira & Goin (2011).

Quadro 1. Lista de táxons de “Ameridelphia” *incertae sedis*, de acordo com Goin *et al*. (2016), de ocorrência na América do Sul. Fonte: Paleobiology Database e Goin *et al*. (2016).

Família	Táxon	Ocorrência temporal	Localidades/País
Pediomyidae	*Khasia* Marshall & de Muizon, 1988	Paleoceno	Tiupampa, Bolívia
Pucadelphyidae	*Andinodelphys* Marshall & de Muizon, 1988	Paleoceno	Tiupampa, Bolívia
	Mizquedelphys Marshall & de Muizon, 1988	Paleoceno	Tiupampa, Bolívia
	Pucadelphys Marshall & de Muizon, 1988	Paleoceno	Tiupampa, Bolívia
Jaskhadelphyidae	*Jaskhadelphys* Marshall & de Muizon, 1988	Paleoceno	Tiupampa, Bolívia
	Minusculodelphis Paula Couto, 1962	Eoeoceno	Itaboraí, Brasil
Mayulestidae	*Mayulestes* de Muizon, 1994	Paleoceno	Tiupampa, Bolívia
Protodidelphidae	*Carolocoutoia* Goin *et al*., 1998	Eoeoceno	Itaboraí, Brasil
	Guggenheimia Paula Couto, 1952	Neopaleoceno/ Eoeoceno	Las Flores, Argentina; Itaboraí, Brasil
	Periprotodidelphis Oliveira & Goin, 2011	Eoeoceno	Itaboraí, Brasil
	Protodidelphis Paula Couto, 1952	Paleoceno–Eoceno	Las Flores, Laguna Fría e Paso del Sapo, Argentina; Itaboraí, Brasil
	Zeusdelphys Marshall, 1987	Eoeoceno	Itaboraí, Brasil
Derorhynchidae	*Derorhynchus* Paula Couto, 1952	Paleoceno–Eoceno	Las Flores, Punta Peligro, Laguna Fría, Argentina; Itaboraí, Brasil; Antártica
	Coona Simpson, 1938	Eoceno	Cañadon Hondo e Cerro Negro, Argentina
	Pauladelphys Goin *et al*., 1999	Eoceno	Paso de Sapo e Laguna Fría, Argentina; Antártica
Sternbergiidae	*Carolopaulacoutoia* McKenna & Bell, 1997	Neopaleoceno/ Eoeoceno	Las Flores, Argentina; Itaboraí, Brasil
	Didelphopsis Paula Couto, 1952	Paleoceno/ Eoeoceno	Las Flores e Punta Peligro, Argentina; Itaboraí, Brasil
	Itaboraidelphys Marshall & de Muizon, 1984	Neopaleoceno/ Eoceno	Laguna Fría, Argentina; Itaboraí, Brasil
cf. Herpetotheriidae		Eoceno–Oligoceno	Itaboraí Brasil; Santa Rosa, Peru
Indeterminada	*Eobrasilia* Simpson, 1947	Eoeoceno	Itaboraí, Brasil
	Incadelphys Marshall & de Muizon, 1988	Paleoceno	Tiupampa, Bolívia
	Gaylordia Paula Couto, 1952	Eoeoceno	Itaboraí, Brasil
	Marmosopsis Paula Couto, 1962	Paleoceno–Eoceno	Las Flores e Paso del Sapo, Argentina; Itaboraí, Brasil
	Monodelphopsis Paula Couto, 1952	Neopaleoceno/ Eooceno	Las Flores, Argentina; Itaboraí, Brasil
	Szalinia de Muizon & Cifelli, 2001	Paleoceno	Tiupampa, Bolívia
	Tiulordia Marshall & de Muizon, 1988	Paleoceno	Tiupampa, Bolívia

3.4.1.1 Ordem Sparassodonta

Os Sparassodonta compõem uma ordem extinta de metatérios, atualmente considerada como “Ameridelphia” *incertae sedis*, com registros por quase todo o Cenozoico, exclusivamente na América do Sul. Distribuem-se mais precisamente do Paleoceno ao Plioceno, SALMA Tiupampense ao Chapadmalalense, sendo reportados para Argentina, Bolívia, Brasil, Chile, Colômbia, Uruguai e Peru (Quadro 2). Os Sparassodonta foram pouco diversos até o meio do Neoeoceno (SALMA Barranquense), quando diversos táxons de médio e grande porte, hipercarnívoros, surgiram. Um grande aumento de sua diversidade se deu entre o Neooligoceno/ Eomioceno (Deseadense ao Santacruzense) (Goin *et al*., 2016).

Consistiam nos vertebrados carnívoros de grande parte da fauna da América do Sul do Paleógeno e Neógeno, juntamente com Phorusracoidea (aves do terror), grandes serpentes (Madtsoiidae) e crocodiliformes. Os Sparassodonta possuíam uma grande variedade de morfologias e tamanhos, indo desde formas pequenas semelhantes à didelfídeos até grandes morfótipos semelhantes a ursos, de onívoros a carnívoros extremamente especializados (Forasiepi, 2009). Aproximadamente 60 espécies de Sparassodonta são válidas até o momento, organizadas em: táxons basais, famílias Hondadelphidae e Hathliacynidae e superfamília Borhyaenoidea. Hondadelphidae é registrada para o Mioceno da Colômbia, fauna de La Venta. Os Hathliacynidae possuem registros principalmente para o Neógeno, da Patagônia a Colômbia. Já Borhyaenoidea é constituída pelas famílias Borhyaenidae (amplamente distribuída do Eoceno ao Plioceno), Proborhyaenidae (Eoceno/Oligoceno da Argentina e Bolívia) e Thylacosmilidae (Neógeno da Argentina, Uruguai e Colômbia) (Forasiepi, 2009; Goin *et al*., 2016) (Figura 17).

Diversas características no crânio são partilhadas por grande parte dos Sparassodonta, tais como: crânio achatado em vista lateral; crista sagital pronunciada; rostro curto; nasais estendidos posteriormente até a linha anterior da órbita; contato nasolacrimal frequente; processo orbital discreto e órbitas abertas; constrição póstero-orbital marcada; processos póstero-orbitais desenvolvidos, porém não próximos da órbita; arco zigomático robusto e mais baixo; região occipital expandida para trás; crista nucal bem desenvolvida; forames incisivos e maxilares presentes; palato

posteriormente divergente; dentário dorso-ventralmente baixo e com sínfise ligamentosa. O padrão dos molares dos Sparassodonta evidencia a redução ou ausência das estruturas de trituração do alimento e o desenvolvimento das estruturas de corte. Os molares superiores possuem protocone reduzido; paracone pequeno basalmente fusionado a um grande metacone; pós-metacrista grande; plataforma estilar reduzida ou ausente; e cúspides estilares quase sempre ausentes. Já os molares inferiores possuem grande paracrístida e metacônido e talônido reduzidos ou ausentes. Diversos clados eventualmente desenvolveram modificações deste padrão, de acordo com pressões adaptativas relacionadas às suas dietas (Goin *et al*., 2016).

Os motivos da extinção dos Sparassodonta ainda são alvo de debates. Forasiepi (2009) sugere que não houve sobreposição temporal entre os Sparassodonta e eutérios carnívoros que chegaram a América do Sul com o GIBA, contradizendo a hipótese de que a competição pelos mesmos nichos com os Carnivora teria ocasionado a extinção dos Sparassodonta. Por outro lado, grandes mudanças ambientais ocorridas entre o Mioceno e Plioceno na América do Sul, oriundas do soerguimento dos Andes, assim como competição com outros clados de marsupiais carnívoros, podem estar relacionados ao seu desaparecimento (Forasiepi, 2009).

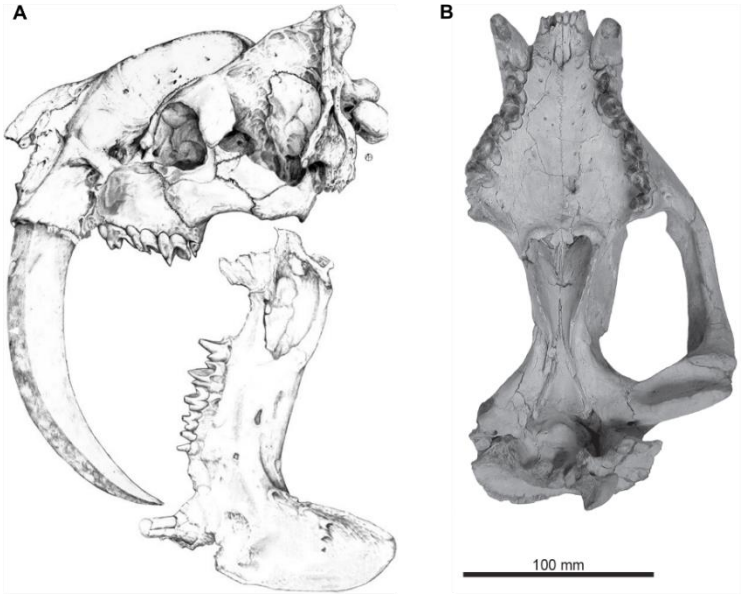


Figura 17. A, Vista lateral do crânio e dentário de *Thylacosmilus atrox* (Thylacosmilidae), de comprimento total 210 mm; **B**, Vista ventral do crânio de *Artodictis sinclari* (Borhyaenidae). Fonte: Forasiepi (2009) e Goin *et al*. (2016).

Quadro 2. Lista de táxons de Sparassodonta, segundo Goin *et al*. (2016), de ocorrência na América do Sul. Fonte: Paleobiology Database e Goin *et al*. (2016).

Família	Táxon	Ocorrência temporal	Localidades/País
	Allqokirus Marshall & de Muizon, 1988	Paleoceno	Tiupampa, Bolívia
	Nemolestes Ameghino, 1902	Eoceno	Bajo de la Palangana, Laguna Fría e Colhué Huapí Norte, Argentina; Guabirotuba, Brasil
	Patene Simpson, 1935	Paleoceno–Oligoceno	Las Flores, Gran Barranca,Cañadón Vaca, Argentina; Itaboraí, Brasil; Santa Rosa, Peru
Hondadelphidae	*Hondadelphys* Marshall, 1976	Mioceno	La Venta, Colômbia
Hathliacynidae	*Acyon* Ameghino, 1887	Mioceno	Gran Barranca, Río Santa Cruz, Monte León e Shehuén, Argentina; Quebrada Honda, Bolívia
	Andinogale Hoffstetter & Petter, 1983	Oligoceno	Salla, Bolívia
	Borhyaenidium Pascual & Bocchino, 1963	Mioceno	Salinas Grandes de Hidalgo, Cantera Relleno Sanitario e Puerta de Corral Quemado, Argentina; Achiri, Bolívia
	Chasicostylus Marshall, 1981	Mioceno	Arroyo Chasicó, Argentina
	Cladosictis Ameghino, 1887	Mioceno	Diversas localidades na Argentina e Chile
	Contrerascynus Mones, 2014	Mioceno	Quebrada Ullum, Argentina
	Notictis Ameghino, 1889	Mioceno	Barrancas del Rio Parana e Pueblo Brugo, Argentina
	Notocynus Mercerat, 1891	Mioceno	Monte Hermoso, Argentina
	Notogale Loomis, 1914	Oligoceno	Argentina; Salla, Bolívia
	Perathereutes Ameghino, 1891	Mioceno	Puesto Estancia La Costa, La Cueva e Cerro Observatorio, Argentina
	Procladosictis Ameghino, 1902	Eoceno	Colhué Huapí Norte, Argentina
	Pseudonotictis Marshall, 1981	Mioceno	Monte León e Cerro Observatorio, Argentina
	Sallacyon Villarroel & Marshall, 1982	Oligoceno	La Flecha, Argentina; Salla, Bolívia
	Sipalocyon Ameghino, 1887	Mioceno	Diversas localidades na Argentina, Chile e Peru
Superfamília Borhyaenoidea			
	Lycopsis Goin, 1997	Mioceno	Estancia La Costa, Arroyo Chasicó e Río Santa Cruz, Argentina; La Venta, Colômbia
	Pharsophorus Ameghino, 1897	Oligoceno	La Cantera, Cabeza Blanca e Gran Barranca, Argentina; Salla, Bolívia
	Prothylacynus Ameghino, 1891	Mioceno	Diversas localides na Argentina e Alto Río Cisnes, Chile
Borhyaenidae	*Arctodictis* Mercerat, 1891	Mioceno	Diversas localidades na Argentina; Monkey Beds, Colômbia
	Australohyaena Forasiepi et al., 2015	Oligoceno	Gran Barraca, Cabeza Blanca, La Flecha e Pico Truncado, Argentina
	Borhyaena Ameghino, 1887	Mioceno	Diversas localides na Argentina e Alto Río Cisnes, Chile
Proborhyaenidae	*Arminiheringia* Ameghino, 1902	Paleoceno–Eoceno	Colhué Huapí Norte, Gran Barranca e Riconada de los López, Argentina; Itaboraí, Brasil
	Callistoe Babot *et al*., 2002	Eoceno	Antofagasta de la Sierra e Estancia Pampa Grande, Argentina
	Paraborhyaena Hoffstetter & Petter, 1983	Oligoceno	Salla, Bolívia
	Proborhyaena Ameghino, 1897	Mioceno	Laguna Payahilé e Rinconada de los Lopez, Argentina; Salla, Bolívia; Paso del Cuello, Uruguai
Thylacosmilidae	*Anachlysictis* Goin, 1997	Mioceno	La Venta, Colômbia
	Patagosmilus Forasiepi & Carlini, 2010	Mioceno	Rio Chico, Argentina
	Thylacosmilus Riggs, 1933	Mioceno–Plioceno	Diversas localidades na Argentina

A ordem Sparassodonta é obtida como um grupo natural em diversas árvores filogenéticas, no entanto, não há consenso sobre com qual táxon teria mais afinidade e hoje é classificada como “Ameridelphia” *incertae sedis*. Sugere-se que a ordem pode ter se originado na América do Norte e em seguida migrado para a América do Sul, apesar de apresentar mais afinidade com formas sul-americanas e australianas do que com táxons norte-americanos (Forasiepi, 2009; Goin *et al*, 2016).

3.4.2 Ordem Didelphimorphia

A ordem Didelphimorphia constitui um táxon complexo, provavelmente parafilético, visto que, como mencionado anteriormente, já incluiu diversos táxons basais e generalistas, com dentição semelhante à dos Didelphidae (*opossum-like*), os quais possuem afinidades incertas. Contudo, análises filogenéticas mais recentes evidenciam que muitos destes táxons extintos não fazem sequer parte de Marsupialia. A comparação com estes táxons basais de Metatheria indica que muitos dos caracteres crânio-dentais diagnósticos de Didelphimorphia seriam na realidade plesiomórficos, tendo os membros desta ordem uma estrutura conservadora, com diversas características “primitivas” e poucas sinapomorfias inequivocadamente definindo a ordem (Kemp, 2005). Assim, mais estudos fazem-se necessários para a compreensão da taxonomia e constituição de Didelphimorphia e de suas famílias, principalmente com relação aos táxons fósseis.

Segundo Goin *et al*. (2016) Didelphimorphia compreende duas superfamílias, a primeira delas, Peradectoidea, é composta pelas famílias Peradectidae, já mencionada anteriormente, com seus táxons do Neocretáceo e início do Paleógeno do Hemisfério Norte e de Tiupampa, Bolívia. Peradectoidea também compreenderia a família Caroloameghiniidae, constituída por *Caroloameghinia* do Eoceno (Casamaiorense) do sul da Argentina; *Procaroloameghinia* de Itaboraí, Brasil e Las Flores, Argentina; e *Canchadelphys*, do Eooligoceno da Patagônia, Argentina (Goin *et al*., 2010, 2016). Por outro lado, a superfamília Didelphoidea é constituída pelas famílias Sparassocynidae e Didelphidae. Sparassocynidae compreende mesocarnívoros com registros para o Mioceno e Plioceno da Argentina (Forasiepi, 2009; Goin *et al*., 2016), enquanto que Didelphidae compreende todos os

Didelphimorphia viventes, seu ancestral comum mais recente e todos os seus descendentes (Voss & Jansa, 2009). Assim, de acordo com Goin *et al*. (2016), com uma definição mais ampla de Didelphimorphia, na América do Sul esta ordem possui registro do Paleoceno (SALMA Tiupampense ou Itaboraiense) ao presente, com restos fósseis reportados para Argentina, Bolívia, Brasil, Colômbia, Peru e Venezuela (Quadro 3).

Diversas análises filogenéticas (e.g., Horovitz *et al*., 2009; Nilsson *et al*., 2010; Gallus *et al*., 2015) sugerem que Didephimorphia teria sido a primeira ordem de Marsupialia a divergir, sendo grupo-irmão de todos os demais marsupiais. Já a radiação de Didelphidae se deu presumidamente bastante recentemente, entre o final do Oligoceno e o início do Mioceno, com a diversificação inicial do grupo ocorrendo em florestas úmidas e perenes (Gardner, 2007; Voss & Jansa, 2009; Jansa *et al*., 2013; Beck *et al*., 2022). Considera-se que os primeiros fósseis indubitavelmente pertencentes à Didelphidae são do início do Mioceno (Castro *et al*., 2021; Stutz *et al*., 2022). É interessante notar este longo ramo entre a divergência dos Didelphimorphia e a origem das linhagens ancestrais dos atuais didelfídeos. Isto caracteriza uma longa linhagem fantasma de *stem* Didelphimorphia, em grande parte ou inteiramente sul-americanos, a qual ainda não foi registrada nos estudos paleontológicos, muito provavelmente devido às dificuldades de distinção de *stem* Didelphimorphia de outros Marsupialia basais bastante plesiomórficos (Beck *et al*., 2022).

A família Didelphidae é o clado mais especioso de marsupiais viventes da América do Sul, constituindo a única linhagem ainda diversa dentre os mamíferos do chamado “Estrato 1” de Simpson (1980), o qual compreende a fauna original do início do Paleógeno da América do Sul, contando com grupos hoje relictuais (Xenarthra) ou extintos (ungulados nativos sul-americanos). Atualmente, Didelphidae está representada por aproximadamente 125 espécies e 18 gêneros, grande parte endêmica da América do Sul. No Brasil, todos os marsupiais com registro atual pertencem à Didelphidae, contando com 15 gêneros e 66 espécies (Abreu *et al*., 2022). A classificação dos Didelphidae reconhece quatro subfamílias: Didelphinae, grupo-irmão de Hyladelphinae, formando um táxon mais proximamente relacionado à Caluromyinae, enquanto que Glironiinae está relacionado a esta última. A subfamília Didelphinae é, por sua vez, dividida em quatro tribos: Marmosini, Metachirini,

Didelphini e Thylamyini (Voss & Jansa, 2009; Goin *et al*., 2016). Os menores (*Chacodelphys* e alguns *Monodelphis*) e maiores (*Didelphis*) marsupiais viventes do Novo Mundo são didelfídeos, sendo que a família abrange formas de menos de 10 a mais de 50 cm de comprimento corporal (Figura 18). Grande parte dos didelfídeos habita florestas tropicais de altitudes moderadas, ocupando diversos nichos ecológicos, de carnívoros aquáticos a arborícolas frugívoros. No entanto, algumas formas são também encontradas em ambientes de maior altitude, áreas temperadas e zonas mais secas.



Figura 18. Representantes de Didelphimorphia, de cima para baixo, fora de escala, *Caluromys derbianus*, *Monodelphis brevicaudata*, *Marmosa robinsoni*, *Chironectes minimus*, *Metachirus nudicaudatus*. Fonte: Voss & Jansa (2009).

A dentição dos Didelphimorphia é considerada bastante semelhante ao padrão primitivo dos marsupiais. Os molares superiores apresentam a condição dilambdodonte, com uma crista em forma de “W” conectando o metacone ao paracone, além de apresentarem plataforma estilar reduzida, apesar de as cúspides estilares não o serem (Kemp, 2005; Goin *et al*., 2016). Ademais, a estrutura do tornozelo dos Didelphimorphia é bastante característica, com a articulação superior modificada, caracterizada pela expansão da faceta astrágalo-fibular, ausência da

faceta calcâneo-fibular e expansão medial da faceta medial astrágalo-tibial, juntamente com a modificação da articulação calcâneo-cuboide (Szalay, 1994).

O crânio dos didelfídeos atuais é alongado anteroposteriormente e possui: caixa craniana e rostro com tamanho semelhante; rostro sem fenestras; nasais longos, se estendendo posteriormente entre os lacrimais; lacrimais com processo facial e dois ou mais forames; forame infraorbital grande; arco zigomático variavelmente robusto e sempre com processo jugal; osso interparietal grande e fusionado ao supraoccipital; região occipital não projetada posteriormente; crista nucal modesta; cristas sagital e frontal ausentes a bem desenvolvidas. O palato possui diversas aberturas; forames incisivos ladeados pela sutura pré-maxilar-maxilar; fenestras maxilo-palatinas presentes; fenestras palatinas às vezes presentes; vômer profundamente dividido; processo timpânico do aliesfenoide bem desenvolvido; ectotimpânico lateralmente exposto; bula auditiva tripartida, conformada por elementos ósseos não fusionados do aliesfenoide, periótico e ectotimpânico; processos mastoide e paraoccipital distintos. O dentário é formado por um corpo alongado anteroposteriormente; processos coronoide e condilar bem desenvolvidos; processo póstero-ventral presente; sínfise mandibular nunca fusionada; crista massetérica sem perfurações e limitada póstero-ventralmente por uma distinta plataforma; côndilo articular transversalmente alongado e relativamente semi-cilíndrico. A fórmula dentária não é reduzida e conta com 50 dentes: incisivos não-gliriformes (poliprotodontes); I1 sempre com coroa mais alta que os demais incisivos e separado do I2 por um diastema; caninos superiores bem desenvolvidos; pré-molares decíduos grandes; terceiro pré-molar pequeno, molariforme, musticuspidado e decíduo; molares superiores trituberculares com plataforma estilar contínua e proeminente; centrocrista contínua; para e metaconulido reduzidos ou ausentes; molares inferiores com cingulido anterior bem desenvolvido e sem cingulido posterior (Gardner, 2007; Voss & Jansa, 2009; Goin *et al*., 2016).

Quadro 3. Lista de táxons de Didelphimorphia, de acordo com Gardner (2007), Forasiepi *et al*. (2009), Voss & Jansa (2009) e Goin *et al*. (2016), de ocorrência na América do Sul. Fonte: Paleobiology Database, Gardner (2007), Forasiepi *et al*. (2009), Voss & Jansa (2009), Goin *et al*. (2016) e Stutz *et al*. (2022).

Família	Táxon	Ocorrência temporal	Localidades/País
Superfamília Peradectoidea			
Peradectidae	*Peradectes* Matthew & Granger, 1921	Paleoceno	Tiupampa, Bolívia
Caroloameghiniidae	*Caroloameghinia* Ameghino, 1901	Eoceno	Diversas localidades no sul da Argentina
	Canchadelphys Goin *et al*., 2010	Oligoceno	La Cancha, Argentina
	Procaroloameghinia Marshall, 1982	Paleoceno-Eoceno	Las Flores, Argentina; Itaboraí, Brasil
Superfamília Didelphoidea			
Didelphidae	*Thylophorops* Reig, 1952	Plioceno	Argentina
	Thylatheridium Reig, 1952	Mioceno–Plioceno	Argentina
	Subfamília Glironiinae		
	Glironia Thomas, 1912	Atual	Bacia do Amazonas (Colômbia, Equador, Peru, Brasil e Bolívia)
	Subfamília Caluromyinae		
	Caluromys Allen, 1900	Quaternário–Atual	Fósseis: Lagoa Santa, Brasil. Atual: norte da América do Sul até o norte da Argentina (Missiones) e ilha de Trinidad
	Caluromysiops Sanborn, 1951	Atual	Colômbia, Peru e Brasil
	Subfamília Hyladephinae		
	Hyladelphys Voss, Lunde & Simmons, 2001	Atual	Guiana Francesa, Guiana, Brasil e Peru
	Subfamília Didelphinae		
	Tribo Marmosini		
	Marmosa Gray, 1821	Mioceno–Atual	Fóssil: La Venta, Colômbia; Monte Hermoso, Punta Martinez de Hoz, Punta Hermengo, Argentina; Guitarrero Cave, Peru; Mato Grosso do Sul, Brasil; Venezuela Atual: América do Sul ao norte do Trópico de Capricórnio, ilhas Trinidad, Tobago e Grenada
	Micoureus Lesson, 1842	Mioceno–Atual	Fóssil: La Venta, Colômbia; MD-67, Peru Atual: por toda a América do Sul até o norte da Argentina
	Monodelphis Burnett, 1830	Quaternário–Atual	Fóssil: Amazonas, Mato Grosso do Sul e Rio Grande do Sul, Brasil Atual: América do Sul tropical e subtropical até leste da Argentina
	Tribo Metachirini		
	Metachirus Burmeister, 1854	Quaternário–Atual	Fóssil: Manaus, Brasil; Guitarrero Cave, Peru Atual: por toda a América do Sul até o norte da Argentina

(Quadro 3. Continuação)

Família	Táxon	Ocorrência	Localidades
	Tribo Didelphini		
	Chironectes Illiger, 1811	Mioceno–Atual	Fóssil: Barrancas Río Paraná, Argentina; São Paulo, Brasil Atual: América do Sul tropical até nordeste da Argentina e Uruguai
	Didelphis Linnaeus, 1758	Mioceno–Atual	Fóssil: Rio Acre, São Paulo, Rio Grande do Sul e Manaus, Brasil; diversas localidades na Argentina. Atual: grande parte da América do Sul até Argentina central
	Hyperdidelphys Ameghino, 1904	Mioceno–Plioceno	Diversas localidades na Argentina
	Lutreolina Thomas, 1910	Mioceno–Atual	Fóssil: diversas localidades na Argentina; Tarija, Bolívia; Rio Grande do Sul, Brasil Atual: Guiana, Venezuela, Colômbia, Bolívia, Brasil, Paraguai, Uruguai e Argentina
	Philander Brisson, 1762	Mioceno–Atual	Fóssil: diversas localidades na Argentina; Rio Grande do Sul e Manaus, Brasil Atual: América do Sul tropical até norte da Argentina
	Tribo Thylamyini		
	Chacodelphys Voss, Gardner & Jansa, 2004	Atual	Norte da Argentina
	Cryptonanus Voss, Lunde & Jansa, 2005	Holoceno? – Atual	Holoceno: possível registro para Rio Grande do Sul, Brasil Atual: biomas ao sul do Rio Amazonas e a leste dos Andes
	Gracilinanus Gardner & Creighton, 1989	Quaternário–Atual	Fóssil: Mato Grosso do Sul e Rio Grande do Sul, Brasil Atual: norte Venezuela a Bolívia, Paraguai, sudeste Brasil, norte da Argentina e Uruguai
	Lestodelphys Tate, 1934	Quaternário–Atual	Fóssil: Diversas localidades na Argentina Atual: Patagônia, Argentina
	Marmosops Matschie, 1916	Atual	Ao longo dos Andes e na Amazônia, até o leste da Bolívia e sudeste do Brasil
	Thylamys Gray, 1843	Mioceno–Atual	Fóssil: Argentina; La Venta, Colômbia; TAR-31, Peru; Mato Grosso do Sul e Rio Grande do Sul, Brasil Atual: Peru, Chile, Bolívia, Paraguai, Argentina, Uruguai e Brasil
Sparassocynidae	*Sparassocynus* Mercerat, 1898	Mioceno–Plioceno	Diversas localidades na Argentina; Bolívia
	Hesperocynus Scott, 1890	Plioceno	Argentina

3.4.3 Ordem Paucituberculata

Os Paucituberculata são registrados do final do Paleoceno (SALMA Itaboraiense) ao presente, com fósseis reportados para a Argentina, Bolívia, Brasil, Chile, Colômbia e Peru (Quadro 4). Os Paucituberculata apresentam baixa diversidade por todo o Paleógeno, tendo seu pico de diversidade somente no Eomioceno (SALMAs Colhuehuapiense e Santacruzense), com a rápida radiação dos Paleothentidae e Abderitidae (Goin *et al*., 2016).

A ordem Paucituberculata é filogeneticamente posicionada mais próxima de Australidelphia do que de Didelphimorphia. Sua divisão nas duas superfamílias Caenolestoidea (com família Caenolestidae) e Paleothentoidea (famílias Pichipilidae, Abderitidae e Paleothentidae, esta última dividida em Paleothentinae e Descastinae) (Quadro 4) também é corroborada por análises filogenéticas recentes (Abello, 2007; Goin *et al*., 2016).

Aproximadamente 50 espécies fósseis de Paucituberculata são hoje reconhecidas, as quais se distribuíam amplamente pelo continente sul-americano, além de possuir variados tamanhos, tipos de locomoção e hábitos alimentares, ocupando principalmente o nicho de pequenos a médios insetívoros e frugívoros. Contudo, atualmente apenas três gêneros e sete espécies, todas pertencentes à família Caenolestidae, persistem na América do Sul, as quais possuem uma distribuição geográfica disjunta do norte da Colômbia e oeste da Venezuela em direção ao sul ao longo dos Andes, até o centro sul do Chile. Os membros atuais de Paucituberculata são pequenos e se assemelham aos insetívoros eutérios da família Soricidae (Abello, 2007; Gardner, 2007; Goin *et al*., 2016).

Os caracteres diagnósticos dos Paucituberculata incluem: vacuidade anterorbital normalmente aberta; dentários não fusionados, cada um contendo um incisivo gliriforme grande e procumbente; molares com aspecto quadrangular em vista oclusal, devido à expansão do metacônulo; série molar com redução pronunciada de tamanho do M1 ao M3, com M4 reduzido; cúspides estilares B e D grandes, aproximadamente do mesmo tamanho e maiores do que o para- e metacone; cúspides estilares C e D fusionadas; paracone e metacone fusionados às bases das cúspides estilares B e C+D, respectivamente; centrocrista aberta; M1–M3 com hipocone não cuspidado. Os molares inferiores tendem a possuir o paracônido e metacônido fusionados e cristas acentuadas anteriores ao entocônido; m2-m3 com hipocônido bem desenvolvido, saliente e não comprimido anteroposteriormente; entocônido comprimido

lateralmente. Ademais, os Abderitidae possuem um primeiro molar plagiaulacoide, característica bastante derivada para a ordem (Abello, 2007; Gardner, 2007; Goin *et al*., 2016). Os Caenolestidae, Paleothentidae e Abderitidae (Figura 19) possuem um primeiro incisivo procumbente e hipertrofiado, sendo por esta razão chamados de “pseudodiprotodontes”, assim como membros da ordem Polydolopimorphia (Goin *et al*., 2009).

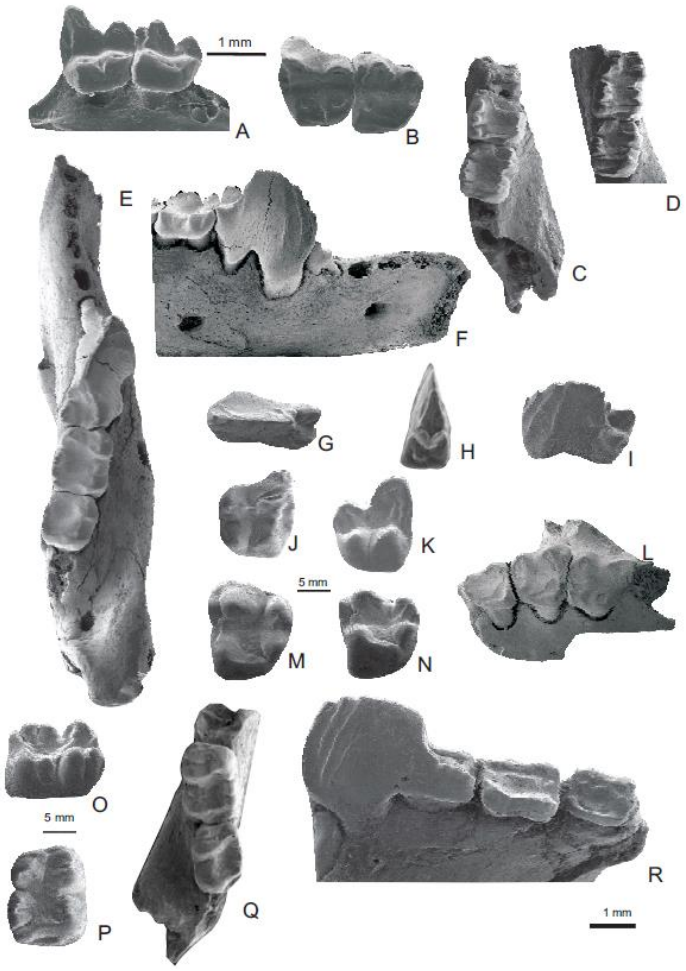


Figura 19. Representantes da ordem Paucituberculata, família Abderitidae: **A-P***, Pitheculites minimus*; **Q**, *P*. *rothi*; **R**, *P*. *chenche*. Figuras A-B, O-P, J-K, M-N com escalas próprias, o restante com a escala presente na parte inferior da figura. Fonte: Abello (2007).

Quanto ao crânio dos Paucituberculata, este é mais conhecido através dos atuais Caenolestidae, que contam com: crânio alongado e comprimido lateralmente; órbitas pequenas; arco zigomático reduzido e expandido lateralmente; região interorbital ampla; caixa craniana bulbosa; dentário grácil e com margem ventral reta; processo coronoide grande e amplo com margem anterior curva; fossa massetérica ampla com pequenos forames; processo angular moderadamente refletido (Goin *et al*., 2016).

Quadro 4. Lista de táxons de Paucituberculata, de acordo com Abello (2007), Rincón *et al*. (2015), Goin *et al*. (2016) e Stutz *et al*. (2022), de ocorrência na América do Sul. Fonte: Paleobiology Database, Abello (2007), Goin *et al*. (2016) e Stutz *et al*. (2022).

Família	Táxon	Ocorrência temporal	Localidades/País
	Bardalestes Goin *et al*., 2009	Paleoceno/Eoceno	Las Flores e Paso del Sapo, Argentina
	Dracolestes Goin *et al*., 2009	Paleoceno/Eoceno	Gran Barranca e La Barda, Argentina
	Evolestes Goin *et al*., 2007	Neooligoceno	Salla, Bolívia
	Riolestes Goin *et al*., 2009	Eoeoceno	Itaboraí, Brasil
Superfamília Caenolestoidea			
Caenolestidae	*Caenolestes* Thomas, 1895	Atual	oeste dos Andes: sul do Equador e norte do Peru
	Lestoros Trouessart, 1898	Atual	sul do Peru e área adjacente da Bolívia
	Rhyncholestes Osgood, 1924	Atual	Chile e Argentina
	Stilotherium Ameghino, 1887	Eo–Mesomioceno	Patagônia, Argentina
	Pliolestes Reig, 1955	Neomioceno/ Eoplioceno	Argentina central
	Gaimanlestes Abello, 2007	Eomioceno	Patagônia central, Argentina
	Caenolestoides Abello, 2007	Eomioceno	Patagônia central, Argentina
Superfamília Palaeothentoidea			
	Pilchenia Ameghino, 1904	Oligoceno	Cabeza Blanca e Gran Barranca, Argentina; Salla, Bolivia
	Perulestes Goin & Candela, 2004	Oligoceno	Santa Rosa, Peru
	Sasawatsu Goin & Candela, 2004	Oligoceno	Contamana e Santa Rosa, Peru
Pichipilidae	*Pichipilus* Ameghino, 1890	Mioceno	sul da Argentina e Chile
	Phonocdromus Ameghino, 1894	Mioceno	Patagônia central, Argentina
	Quirogalestes Goin & Candela, 1998	Eoceno	Patagônia central, Argentina
Palaeothentidae	*Carlothentes* Bown & Feagle, 1993	Oligoceno	Patagônia, Argentina
	Antawallathentes Rincón *et al*., 2015	Oligoceno	Salla, Bolívia
	Hondathentes Dumont & Brown, 1997	Mioceno	La Venta, Colômbia
Subfamília Palaeothentinae Sinclair, 1906			
	Palaeothentes Ameghino, 1887	Mioceno	Diversas localidades na Argentina; TAR-31, Peru
	Palaepanorthus Ameghino, 1902	Mioceno	Patagônia central, Argentina
Subfamília Decastinae Ameghino, 1893			
	Acdestis Ameghino, 1887	Mioceno	Diversas localidades na Argentina; Quebrada Honda, Bolívia
	Trelewthentes Bown & Feagle, 1993	Mioceno	Patagônia central, Argentina
	Titanothentes Rae *et al*., 1996	Mioceno	Diversas localidades na Argentina
Abderitidae	*Abderites* Ameghino, 1887	Oligoceno–Mioceno	sul da Argentina; Alto Río Cisnes, Chile; Contamana, Peru
	Pitheculites Ameghino, 1901	Mioceno	Patagônia, Argentina; Alto Río Cisnes, Chile; La Venta, Colômbia; TAR-31, Peru
	Parabderites Ameghino, 1902	Oligoceno–Mioceno	Patagônia central, Argentina

3.4.4 Ordem Microbiotheria

Os Microbiotheria são registrados do Eoceno (SALMA Itaboraiense) ao presente, com fósseis na Argentina, Brasil, Chile, Colômbia e Peru (Quadro 5). Os microbiotérios possuíram diversidade estável e baixa durante o Paleógeno, tendo atingido seu pico de diversidade no Eomioceno (Goin *et al*., 2016).

A ordem Microbiotheria é formada atualmente por somente uma família (Microbiotheriidae), um gênero e três espécies viventes, *Dromiciops gliroides*, *D*. *mondaca* e *D*. *bozinovici* (Figura 20), as quais se restringem às florestas temperadas patagônicas do sul dos Andes chamadas “bosques valdivianos”, no centro do Chile e áreas adjacentes da Argentina, não se estendendo mais ao sul em regiões mais frias da Patagônia (Gardner, 2007; D’Elía *et al*., 2016). Os Microbiotheria foram, no entanto, mais diversos e amplamente distribuídos no passado, sendo considerados, portanto, elementos relictuais nas faunas modernas (Voss & Jansa, 2009). Aproximadamente 15 espécies de microbiotérios são reconhecidas, sendo que grande parte das formas extintas também ocupava a porção sul do continente sul-americano, assim como a Antártica. Os Microbiotheria são classificados em duas famílias: Microbiotheriidae, na qual se insere a maior parte das espécies, sendo, no geral, pequenos e insetívoros-frugívoros; e Woodburnodontidae, família com representantes de maior porte, frugívoros, com fósseis na Argentina e Antártica (Quadro 5, Hershkovitz, 1999; Goin *et al*., 2007c, 2016).

Os microbiotérios se caracterizam por não possuírem, dentre os incisivos inferiores, um i3 procumbente (“*staggered*”, *sensu* Hershkovitz, 1982). Ademais, possuem molares superiores com protocone amplo e marcado; plataforma estilar reduzida, praticamente sem cúspides estilares; paracone e metacone com praticamente o mesmo tamanho e altura; e centrocrista reta. Os molares inferiores possuem paracônido reduzido; talônido amplo; m1 e m2 com hipoconulido posicionado centralmente na pós-hipocristida (Goin *et al*., 2016).

A articulação inferior do tornozelo dos microbiotérios, a qual possui um padrão contínuo, com as facetas calcâneo-astragalar e sustentacular confluentes (CLAJP, *sensu* Szalay, 1994), é diferente do padrão descontínuo dos marsupiais não-Australidelphia e outros sinápsidos. Ademais, a faceta de articulação calcâneo-cuboide é extremamente modificada, com uma morfologia tripartida, que teria se originado da morfologia bipartida semelhante à dos Didelphimorphia. Estas e outras características do calcâneo, cuboide, astrágalo e articulação ectocuneiforme-primeiro

metatarsal, se assemelham às características encontradas nos marsupiais australianos e basearam a proposição do táxon Australidelphia (Szalay, 1994). Em seguida, características adicionais (e.g., serologia, taxas metabólicas, pareamento dos espermatozoides) foram encontradas, indicando a monofilia da Coorte Australidelphia, que compreende Microbiotheria (Goin *et al*., 2016).

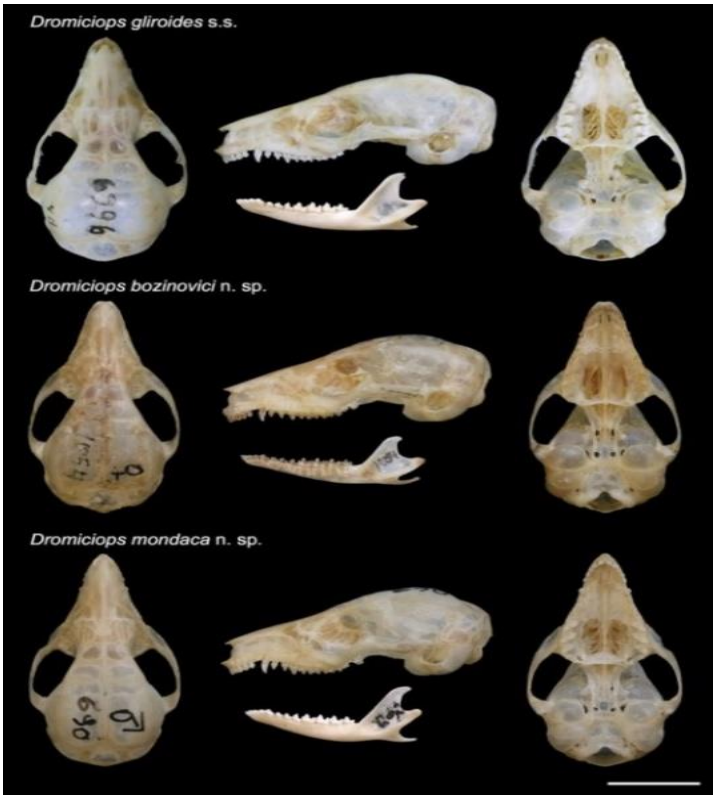


Figura 20. *Dromiciops gliroides*, *D. bozinovici* e *D. mondaca*. Escala = 10 mm. Fonte: D'Elía *et al*. (2016).

Dentre as espécies viventes, *Dromiciops gliroides* possui tamanho semelhante ao de um camundongo, é predominantemente escansorial e animalívora, habitando principalmente ambientes mais abertos. Possui crânio oval em vista dorsal e rostro relativamente curto; nasais não se estendem além da linha orbital; processo pós-orbital ausente; arco zigomático grácil e marcadamente inflexionado ao nível da sutura maxilo-jugal; bula timpânica e caixa craniana grandes e infladas; crista esfenoidal presente; palato posteriormente divergente; forames incisivos e maxilares grandes; dentário grácil, com inflexão ventral pouco desenvolvida. Já a família Microbiotheriidae se caracteriza por possuir: incisivos superiores em forma de espátula, relativamente grandes e formando uma série completa, sem diastemas; quarto ou últimos molares notavelmente reduzidos; molares superiores com centrocrista reta conectando o paracone ao metacone; M4 subtriangular; m1-m3 com talônido mais largo do que o

trigônido; molares inferiores com paracônido bem desenvolvido, principalmente no m1. Ademais, *Dromiciops* é o único dentre os marsupiais sul-americanos atuais a possuir espermatozoides não-pareados (Gardner, 2007; Goin *et al*., 2016).

Quadro 5. Lista de táxons de Microbiotheria, de acordo com Goin *et al*. (2016) e D'Elía *et al*. (2016), de ocorrência na América do Sul e Antártica. Fonte: Paleobiology Database, Hershkovitz (1999), Goin *et al*. (2016) e D'Elía *et al*. (2016).

Família	Táxon	Ocorrência temporal	Localidades/País
Microbiotheria ou Polydolopimorphia			
	Mirandatherium Paula Couto, 1952	Eoceno	Las Flores, Argentina; Itaboraí, Brasil
Woodburnodontiidae	*Woodburnodon* Goin et al., 2007	Paleoceno–Eoceno	Las Flores, Argentina; La Meseta Formation, Antártica
Microbiotheriidae	*Kirutherium* Goin & Candela, 2004	Oligoceno	Santa Rosa, Peru
	Marambiotherium Goin et al., 1999	Eoceno	Formação La Meseta, Antártica
	Subfamília Microbiotheriinae		
	Dromiciops Thomas, 1894	Atual	Chile e Argentina
	Microbiotherium Ameghino, 1887	Oligoceno–Mioceno	Diversas localidades na Argentina; Alto Río Cisnes, Chile
	Subfamília Pachybiotheriinae		
	Clenia Ameghino, 1904	Oligoceno–Mioceno	La Cancha e Gran Barranca, Argentina
	Eomicrobiotherium Marshall, 1982	Eoceno–Mioceno	Diversas localidades na Argentina
	Pachybiotherium Ameghino, 1902	Mioceno	Gran Barranca e Lago Buenos Aires, Argentina; La Venta, Colômbia

3.4.5 Ordem Polydolopimorphia

A ordem Polydolopimorphia, por sua vez, é reportada do início do Paleoceno ao Pleistoceno (SALMA Chapadmalalense) para a Argentina, Brasil, Bolívia, Chile e Peru e Antártica (Quadro 6), além de possíveis restos da Austrália e América do Norte (Goin *et al*., 2016; Beck, 2017). No entanto, se os Argyrolagidae de fato não pertecerem aos Polydolopimorphia, como defendem certos autores (e.g., Beck, 2017), a distribuição da ordem é mais curta, se extinguindo no Oligoceno.

Em sua concepção original, Polydolopimorphia compreenderia apenas o gênero *Polydolops* e formas relacionadas, porém, numerosas descobertas realizadas desde o século XX permitiram maior conhecimento dos polidolopimórfios e a inclusão de diversos táxons nesta ordem (Goin *et al*., 2009). Segundo Goin *et al*. (2016), Polydolopimorphia compreende duas grandes linhagens: a subordem

Bonapartheriiformes, que inclui os Bonapartherioidea (famílias Prepidolopidae, Bonapartheriidae, Gashterniidae e Rosendolopidae), mais antigos, além dos mais recentes Argyrolagoidea (famílias Groeberiidae, Patagoniidae e Argyrolagidae); e a subordem Polydolopiformes, com as famílias Sillustaniidae, que seria uma linhagem basal, e Polydolopidae, considerados como os metatérios mais derivados do Novo Mundo (Figura 21). Além destas duas linhagens, em Polydolopimorphia também se inclui a família Glasbiidae, já mencionada anteriormente, a qual compreenderia as duas espécies do gênero *Glasbius* do Cretáceo da América do Norte, além de táxons do início do Paleógeno da América do Sul (*Palangania*, *Chulpasia*, *Bobbschaefferia* e *Periakros*). No entanto, segundo Williamson *et al*. (2014), as relações de *Glasbius* com formas sul-americanas devem ser tomadas com cautela. Segundo estes autores, Glasbiidae se restringiria ao gênero *Glasbius* e teria como grupo-irmão *Roberthoffstetteria*, este sim um polidolopimórfio basal da fauna de Tiumpampa, Bolívia. Os polidolopimórfios ocuparam diversos nichos ecológicos, de frugívoros e onívoros até herbívoros especializados (Case *et al*., 2005; Goin *et al*., 2016).

Os Polydolopiformes apresentam episódios de diversificação no início do Eoceno (Itaboraiense), atingindo seu pico de diversidade no início do Mesoeoceno (SALMA Fauna de El Sapo) e continuaram com diversidade estável por todo o Mesoeoceno, porém entram em declínio no Neoeoceno, sendo registrados pela última vez na fauna de La Cantera, Argentina. Dentre os Bonapartheriiformes, os Bonapartheriioidea registram importante radiação no início do Eoceno (Itaboraiense), seguido de intervalo com diversidade estável do Meso a Neoeoceno, sendo registrados pela última vez no início do Oligoceno. Já os Argyrolagoidea são pela primeira vez registrados no Mesoeoceno (SALMA Vaquense), e permanecem pouco diversos durante todo o Paleógeno e Neógeno, se extinguindo no Plioceno/Pleistoceno (Goin *et al*., 2016). Os primeiros Polydolopiformes eram principalmente de pequeno e médio porte, frugívoros e insetívoros, passando depois a principalmente frugívoros-folívoros de grande porte. Já dentre os Bonapartheriiformes, os primeiros Bonapartheriidae eram folívoros e insetívoros-frugívoros de tamanho médio, tendo depois do meio do Neoeoceno passado a formas granívoras de menores tamanhos. Os Argyrolagoidea eram principalmente formas pequenas granívoras e folívoras (Goin *et al*., 2016).

O crânio dos representantes da ordem Polydolopimorphia se caracteriza por possuir: caixa craniana globular; nasais expandidos posteriormente até o nível das órbitas; arco zigomático robusto; palato mais amplo ao nível da série molar; forames

incisivos sempre presentes sob diferentes tamanhos, assim como os forames maxilares e palatais. Com relação aos Polydolopiformes, há pouco material craniano preservado, mas o rostro seria alongado e estreito, o palato amplo ao longo da série molar e a caixa craniana expandida e globular (Goin *et al*., 2016).

Os Bonapartherioidea possuem: rostro curto e amplo; órbitas totalmente abertas; constrição póstero-orbital discreta; processos póstero-orbitais pequenos ou ausentes; arco zigomático deslocado para baixo; palato suboval ou em formato de diamante; forames incisivos pequenos; fenestras maxilares aparentemente grandes; dentário robusto e curto; fossa massetérica profunda e com uma crista marcada em sua margem anterior; crista massetérica bem desenvolvida e posteriormente ampla; processo coronoide alto e amplo; côndilo robusto e levemente mais alto que a série molar; processo angular marcado e inflexionado, com extremidade posterior direcionada pra cima. Os Argyrolagoidea possuem rostro delgado; cavidade nasal sobressaindo acima da linha dos incisivos; arco zigomático baixo e com processo jugal desenvolvido; forame infraorbital grande; órbitas anteriormente fechadas e abertas posteriormente; região temporal reduzida; palato oval; forames incisivos grandes; bula auditiva proporcionalmente muito grande e inflada; dentário grácil; incisivos grandes implantados ao nível do m3 (Goin *et al*., 2016).

Grande parte dos polidolopimórfios possui molares bunodontes de coroa relativamente baixa. Representantes da ordem foram os primeiros a desenvolver um padrão molar quadrangular, o qual é apropriado para a ingestão de diversas plantas, de variáveis formas, tamanhos e rigidez. Os molares superiores possuem paracone e metacone associados às cúspides estilares B e C, respectivamente, as quais possuem tamanho semelhante ao paracone e metacone; na margem lingual o metacônulo é expandido e forma a margem póstero-lingual. Nos molares superiores, o paracônido e metacônido são reduzidos e próximos um do outro; o hipocônido é grande, porém não muito saliente (Goin *et al*., 2016; Beck, 2017).

Não obstante, enfatiza-se as problemáticas já mencionadas anteriormente neste texto com relação a monofilia e composição de Polydolopimorphia, questões ainda a ser extensamente trabalhadas e discutidas.

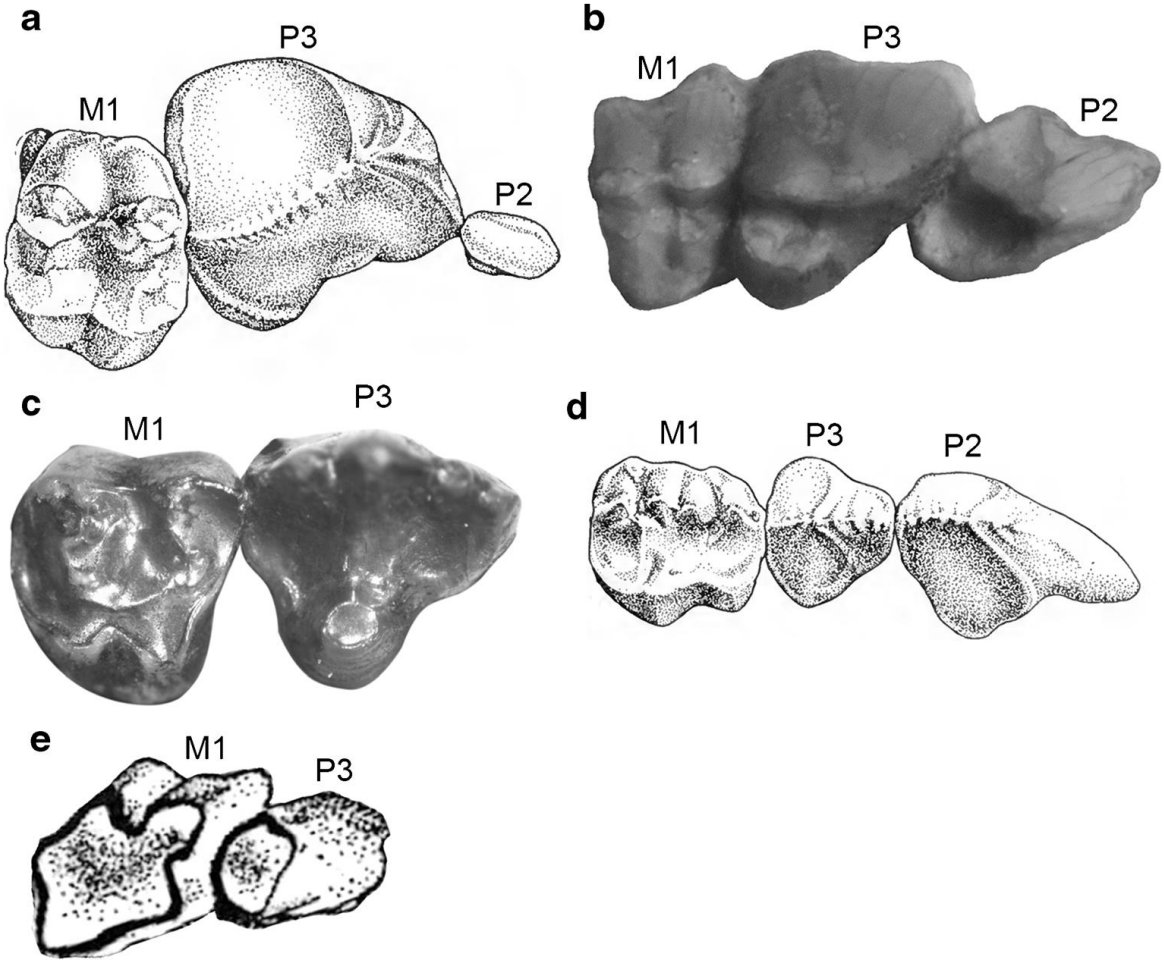


Figura 21. Pré-molares superiores e M1 de: **a**, *Epidolops ameghinoi*; **b**, *Bonapartherium hinakusijum*; **c**, *Gashternia carioca*; **d**, *Polydolops thomasi*; **e**, *Anargyrolagus primus*. Fonte: Beck (2017).

Quadro 6. Lista de táxons de Polydolopimorphia, de acordo com Goin & Candela (2004) e Goin *et al*. (2016), de ocorrência no Hemisfério Sul. Fonte: Paleobiology Database, Goin & Candela (2004) e Goin *et al*. (2016).

Subordem	Superfamília	Família	Táxon	Ocorrência temporal	Localidades/País
Bonapartheriiformes	Bonapartherioidea	Indeterminada	*Wamradolops tsullodon* Goin & Candela, 2004	Eoceno-Oligoceno	Contamana e Santa Rosa, Peru
		Glasbiidae	*Palangania brandmayri* Goin *et al*., 1998	Paleoceno	Patagônia, Argentina
			Palangania cf. *P. brandmayri*	Eoeoceno	Patagônia, Argentina
			Chulpasia mattaueri Crochet & Sigé, 1993	Paleoceno/Eoceno	Chulpas, Peru
			Chulpasia jimthorselli Sigé *et al*., 2009	Paleoceno/Eoceno	Tingamarra, Austrália
			Bobbschaefferia fluminensis Paula Couto, 1970	Paleoceno/Eoceno	Itaboraí, Brasil
			Periakros ambiguus Goin *et al*., 2010	Eooligoceno	Patagônia, Argentina
		Prepidolopidae	*Prepidolops didelphoides* Pascual, 1980	Eoeoceno	Salta, Argentina
			Prepidolops molinai Pascual, 1980	Eoeoceno	Salta, Argentina
			Punadolops alonsoi Pascual, 1983	Mesoeoceno	Antofagasta de la Sierra, Argentina
			Incadolops ucayali Goin & Candela, 2004	Oligoceno	Santa Rosa, Peru
			Coloradolops cardonensis Chornogubsky *et al*., 2019	Mesoeoceno	Salta, Argentina
			Perrodelphys coquinense Goin *et al*. (1999)	Mesoeoceno	Ilha Seymor, Antártica
		Bonapartheriidae	<u>Subfamília Bonapartheriinae</u>		
			Bonapartherium hinakusijum Pascual, 1980	Eoeoceno	Salta, Argentina
			<u>Subfamília Epidolopinae</u>		
			Epidolops ameghinoi Paula Couto, 1952	Eoeoceno	Itaboraí, Brasil
		Gashterniidae	*Gashternia ctalehor* Simpson, 1935	Paleoceno/Eoceno	Cañadón Hondo, Argentina
			Gashternia carioca Goin & Oliveira, 2007	Eoeoceno	Itaboraí, Brasil
			Gashternia sp.	Eoeoceno	Las Flores, Argentina
		Rosendolopiidae	*Rosendolops primigenium* Goin & Candela, 1996	Eoeoceno	Patagônia, Argentina
			Rosendolops ebaios Goin *et al*., 2010	Eooligoceno	La Cancha e La Cantera, Argentina
			Hondonadia feruglioi Goin & Candela, 1998	Mesoeoceno	Gran Hondonada, Argentina
			Hondonadia fierroensis (Flynn & Wyss, 1999)	Eooligoceno	Tinguiririca, Chile
			Hondonadia pittmanae Goin & Candela, 2004	Oligoceno	Santa Rosa, Peru
			Hondonadia praecipitia Goin *et al*., 2010	Eooligoceno	La Cancha, Argentina
			Hondonadia pumila Goin *et al*., 2010	Eooligoceno	La Cancha, Argentina
			Hondonadia parca Goin *et al*., 2010	Eooligoceno	La Cancha, Argentina
	Argyrolagoidea		*Praedens aberrans* Goin *et al*., 2010	Eooligoceno	La Cancha, Argentina
			Klohnia charrieri Flynn & Wyss, 1999	Eooligoceno	Tinguiririca, Chile
			Klohnia major Goin *et al*., 2010	Eooligoceno	La Cancha, Argentina

(Quadro 6. Continuação)

Subordem	Superfamília	Família	Táxon	Ocorrência temporal	Localidades/País
			Epiklohnia verticalis Goin *et al*., 2010	Eooligoceno	La Cantera, Argentina
	Argyrolagoidea	Groeberiidae	*Groeberia minoprioi* Patterson, 1952	Eoceno/Oligoceno	Mendoza, Argentina
			Groeberia pattersoni Simpson, 1970	Eoceno /Oligoceno	Mendoza, Argentina
		Patagoniidae	*Patagonia peregrina* Pascual & Carlini, 1987	final do Oligoceno	Patagônia, Argentina
Bonapartheriiformes	Bonapartherioidea	Argyrolagidae	*Argyrolagus scagliai* Simpson, 1970	Plioceno	Buenos Aires, Argentina
			Argyrolagus rusconi Goin *et al*., 2000	Neomioceno	Cerro Azul, Argentina
			Argyrolagus parodii Ameghino, 1904	?Plioceno	Miramar?, Argentina
			Argyrolagus palmeri Ameghino, 1904	Eoplioceno	Monte Hermoso, Argentina
			Argyrolagus sp.	Eoplioceno	Río Quequén Salado, Argentina
			Argyrolagus sp.	?Neomioceno	Caleufú, Argentina
			Proargyrolagus bolivianus Wolff, 1984	Neooligoceno	Salla, Bolívia
			Proargyrolagus argentinus Goin & Abello, 2013	Eomioceno	Gran Barranca, Argentina
			Proargyrolagus sp. A Antoine e*t al*., 2021	Neoeoceno	Shapaja, Peru
			Proargyrolagus sp. B Antoine e*t al*., 2021	Eooligoceno	Shapaja, Peru
			Anargyrolagus primus Carlini *et al*., 2007	Eomioceno	Patagônia, Argentina
			Microtragulus argentinus Ameghino, 1904	Eoplioceno	Monte Hermoso, Argentina.
			Microtragulus reigi Simpson, 1970	Plioceno/Pleistoceno	Buenos Aires, Argentina
			Microtragulus catamarcensis Kraglievich, 1931	Neomioceno	Andalhuala, Argentina
			Microtragulus bolivianus Hoffstetter & Villarroel, 1974	?Plioceno–Pleistoceno	Vizcachani, Bolívia; San Roque e Jujuy, Argentina
			Microtragulus sp.	?Neomioceno	Tucumán, Argentina
			Hondalagus altiplanensis Villarroel & Marshall, 1988	Mesomioceno	Quebrada Honda, Bolívia
Polydolopiformes			*Cocatherium lefipanum* Goin *et al*., 2006	início do Paleoceno	Patagônia, Argentina
		Sillustaniidae	*Roberthoffstetteria nationalgeographica* Marshall *et al*., 1983	Eopaleoceno	Tiupampa, Bolívia
			Sillustania quechuense Crochet & Sigé, 1996	Paleoceno/Eoceno	Laguna Umayo, Peru
		Polydolopidae	*Amphidolops serrula* Ameghino, 1902	Neoeoceno	Patagônia, Argentina
			Amphidolops yapa Simpson, 1935	Eopaleoceno	Patagônia, Argentina
			Archaeodolops clavulus (Ameghino, 1902)	Neoeoceno	Patagônia, Argentina
			Kramadolops mayoi (Odreman Rivas, 1976)	Eoceno/Oligoceno	Patagônia, Argentina
			Kramadolops abanicoi (Flynn & Wyss, 1999)	Eooligoceno	Tinguiririca, Chile
			Kramadolops fissuratus Goin *et al*., 2010	Início do Oligoceno	La Cancha, Argentina
			Kramadolops hernandezi (Marshall, 1982)	Neoeoceno	Patagônia, Argentina
			Kramadolops maximus Goin *et al*., 2010	Eooligoceno	La Cantera, Argentina
			Kramadolops mckennai (Flynn & Wyss., 2004)	início do Oligoceno	Cachapoal Locality, Chile
			Pliodolops serra (Ameghino, 1902)	Neoeoceno	Patagônia, Argentina
			Pliodolops kamektsen (Simpson, 1935)	Eoeoceno	Patagônia, Argentina
			Pliodolops rothi (Simpson, 1936)	Eo–Mesoeoceno	Patagônia, Argentina
			Pliodolops unicus (Tejedor *et al*., 2009)	Eo–Mesoeoceno	Patagônia, Argentina

(Quadro 6. Continuação)

Subordem	Superfamília	Família	Táxon	Ocorrência temporal	Localidades/País
Polydolopiformes		Polydolopidae	*Pliodolops winecage* (Simpson, 1935)	Eoeoceno	Patagônia, Argentina
			Polydolops thomasi (Ameghino, 1897)	Neoeoceno	Patagônia, Argentina
			Pseudolops princeps (Ameghino, 1902)	Neoeoceno	Patagônia, Argentina
			Eudolops tetragonus Ameghino, 1897	Neoeoceno	Patagônia, Argentina
			Eudolops caroliameghinoi (Simpson, 1948)	Neoeoceno	Patagônia, Argentina
			Antarctodolops dailyi Woodburne & Zinsmeister, 1984	Eoceno/Oligoceno	Formação La Meseta, Antártica
			Antarctodolops mesetaense Chornogubsky *et al*., 2009	Eoceno /Oligoceno	Formação La Meseta, Antártica

3.5 METATHERIA NA ANTÁRTICA E AUSTRALÁSIA

Supõe-se que antes do Eoceno, uma ou mais linhagens de metatérios tenha migrado da América do Sul em direção à Austrália, passando pela Antártica. Estudos recentes sugerem que esta dispersão provavelmente ocorreu do Eo ao Mesopaleoceno (Goin *et al*., 2016).

No Neocretáceo, as condições climáticas presentes no continente antártico eram quentes e proporcionavam a existência de uma flora subtropical a tropical. No Paleoceno o clima passou a ser mais frio, porém ainda sem congelamento no inverno e neve nas montanhas, com a presença de florestas compostas por coníferas e outras formas decíduas. Por volta do início do Eoceno, o clima era frio e úmido, com temperaturas médias entre 8–13°C. A Formação La Meseta, de idade Mesoeoceno, localizada nas ilhas Seymour, Península Antártica, é a única unidade fossilífera na qual se encontram registros dos mamíferos do Paleógeno, incluindo metatérios. Dentre estes últimos, distingue-se a presença das ordens Microbiotheria e Polydolopimorphia e da família Derorhynchidae (Quadros 1, 5 e 6; Figura 22). Além dos metatérios, também foram encontrados restos de gondwanatérios, xenartros, astrapotérios e litopternas, sendo alguns destes endêmicos de La Meseta e outros possivelmente derivados de faunas do início do Eoceno da América do Sul. Os elementos faunísticos de La Meseta possuem mais afinidade com os mamíferos sul-americanos do que com os australianos. Tratam-se de táxons já significativamente derivados, filogeneticamente próximos de clados sul-americanos também considerados derivados. Em La Meseta foram igualmente encontrados restos paleobotânicos de diversidade considerável, os quais sugerem condições climáticas sazonais, frias/temperadas e úmidas, se assemelhando às atuais florestas da Nova Zelândia e bosques valdivianos do Chile e Argentina (Goin *et al*., 2007c, 2016; Chornogubsky *et al*., 2009).

Subsequentemente, ao longo do Eoceno, as condições climáticas progressivamente tornaram-se mais frias na Antártica, com congelamento durante o inverno e montanhas nevadas, dificultando a dispersão de mamíferos da América do Sul para a Austrália, que provavelmente já não ocorria mais, apesar de rotas por regiões de baixas altitudes e litorâneas ainda existirem. Progressivamente, a Austrália

e Antártica foram se separando ao longo da zona de ruptura Tasmânia-Antártica, sendo que há 50 Ma ocorreu a separação total do Mar de Tasman e, a partir de 45 Ma, já havia uma linha de costa contínua no sul da Austrália, inviabilizando qualquer dispersão terrestre vinda da Antártica. As condições climáticas mais frias na Antártica se acentuaram com a abertura da Passagem de Drake e estabelecimento da Corrente Circumpolar Antártica por volta do limite Eoceno/Oligoceno, isolando este continente e inviabilizando a persistência dos metatérios e outros vertebrados terrestres (Goin *et al*., 2007c, 2016; Chornogubsky *et al*., 2009).

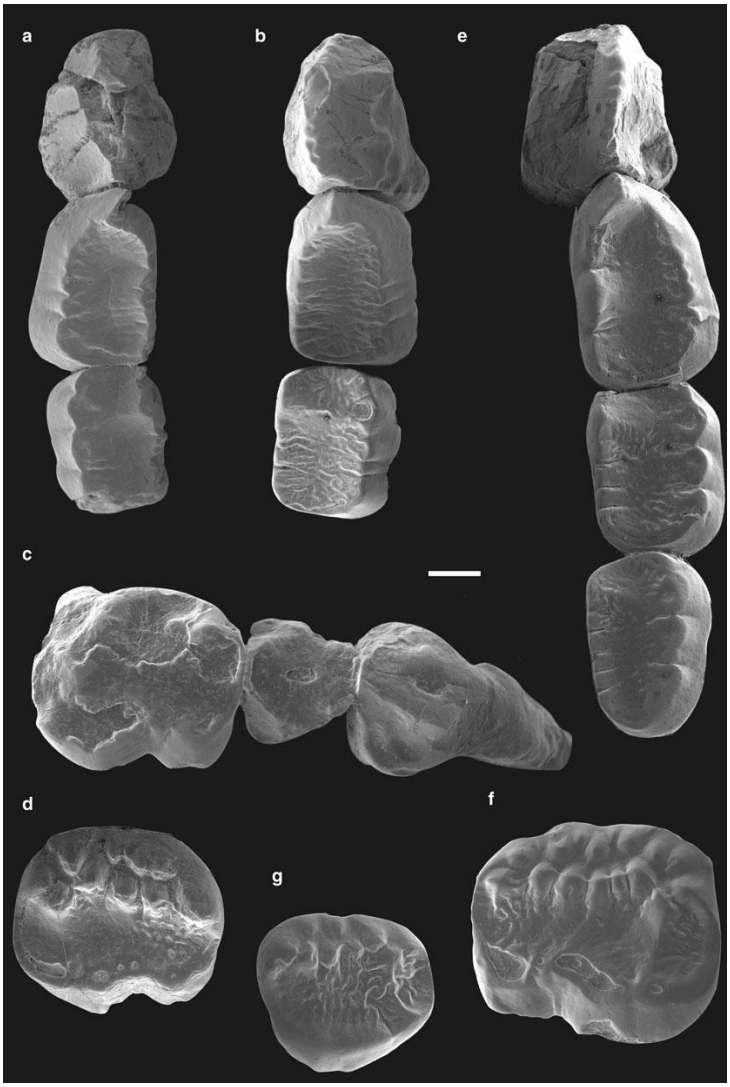


Figura 22. Molares superiores e inferiores de Polydolopidae da Antártica: **a–d**, *Antarctodolops dailyi*; **e-f**, *A*. *mesetaense*; **g**, *Antarctodolops* sp. Escala = 1 mm. Fonte: Chornogubsky *et al*. (2009).

O continente australiano e algumas ilhas em seu entorno são atualmente conhecidos por abrigar notável diversidade taxonômica e ecológica de marsupiais, ocupando os mais diversos nichos ecológicos, os quais são associados a mamíferos placentários em outros lugares do planeta. Atualmente, quatro ordens distribuem-se na Australásia: i) Dasyuromorphia, com três famílias, 19 gêneros e 77 espécies (Figura 23); ii) Peramelemorphia, com três famílias, oito gêneros e 22 espécies (Figura 24); iii) Diprotodontia, com três subordens, 11 familias, 41 gêneros e 150 espécies (Figura 25); e iv) Notoryctemorphia, com apenas uma família, um gênero e duas espécies (Figura 26) (Mammal Diversity Database, 2022). Também se reporta a extinta ordem Yalkaparidontia, do Mioceno da Austrália, com uma família e duas espécies (Black *et al*., 2012).



Figura 23. Representantes das famílias de Dasyuromorphia: Dasyuridae **A**, *Planigale subtilíssima*, **B**, *Dasyurus maculatus*; **C**, Thylacinidae, *Thylacinus cynocephalus*†; **D**, Myrmecobiidae, *Myrmecobius fasciatus*. Fonte: Black *et al*. (2012).

Os restos mais antigos de marsupiais na Austrália são os da fauna local de Tingamarra, em Murgon, do início do Eoceno, a qual é a única anterior ao Neooligoceno. Os elementos da fauna de Tingamarra são ainda bastante plesiomórficos e possivelmente representam o resultado de migrações ocorridas no

Paleoceno, sendo, portanto, posteriores aos eventos dispersivos. A ausência de formas derivadas, como as de La Meseta, na Austrália, assim como a ausência de grupos sul-americanos derivados neste continente, principalmente placentários, também suportam a hipótese de que os eventos dispersivos em direção à Austrália teriam ocorrido antes do Eoceno. Os elementos da fauna de Tingamarra são comparáveis aos elementos do Paleoceno da América do Sul, como os da fauna de Tiupampa. Porém, nenhum elemento da fauna de Itaboraí, já do final do início do Eoceno, apresenta afinidade com formas australianas. Alguns restos da fauna de Tingamarra foram descritos como pertencentes a uma nova espécie do gênero sul-americano *Chulpasia*, de ocorrência em Laguna Umayo, Peru, no entanto, outros autores discordam desta hipótese (Goin *et al*., 2016).

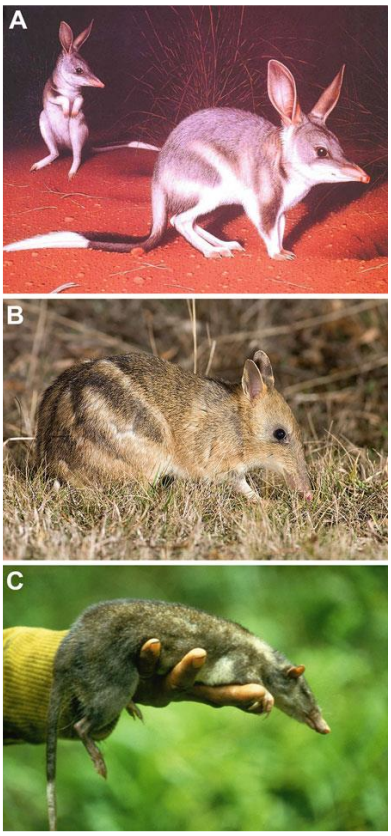


Figura 24. Representantes das famílias da ordem Peramelemorphia: **A**, Thylacomyidae, *Macrotis lagotis*; **B**, Peramelidae, *Perameles gunni*; **C**, Peroryctidae, *Microperoryctes longicaudata*. Fonte: Black *et al*. (2012).



Figura 25. Representantes das famílias da ordem Diprotodontia: **A**, Phascolarctidae, *Phascolarctos cinereus*; **B**, Vombatidae, *Vombatus ursinus*; **C**, Pseudocheiridae, *Pseudocheirus archeri*; **D**, Macropodidae, *Macropus parryi*; **E**, Phalangeridae, *Spilocuscus maculatus*; **F**, Acrobatidae, *Acrobates pygmaeus*; **G**, Burramyidae, *Cercartetus nanus*. Fonte: Black *et al*. (2012).

As ordens atuais de ocorrência na Australásia possuem seus primeiros registros fósseis no Neooligoceno, exceto Notoryctemorphia, a qual é conhecida desde o Eomioceno. Alguns autores sugerem que as ordens Dasyuromorphia e Peramelemorphia teriam seus primeiros registros na fauna de Tingamarra. Contudo, não está clara a relação das formas de Tingamarra com os táxons encontrados em depósitos do Neooligoceno até o Recente. Supõe-se que 17 linhagens fósseis de marsupiais australianos não perduraram até o presente (Black *et al*., 2012; Goin *et al*., 2016).



Figura 26. Representante da ordem Notoryctemorphia, família Notoryctidae, *Notoryctes typhlops*. Fonte: Black *et al*. (2012).

3.6 REGISTRO FÓSSIL DE METATHERIA NA AMÉRICA DO SUL

3.6.1 História evolutiva dos Metatheria na América do Sul

A história evolutiva dos metatérios na América do Sul parece ter sido especialmente impactada pela temperatura e precipitação durante o Paleógeno e muito provavelmente durante todo o Cenozoico (Goin *et al*., 2016).

As SALMAs são um esquema estratigráfico baseado em unidades portadoras de associações de mamíferos, com as denominadas “Idades Mamíferos Terrestres Sul-Americanos”, do inglês *South American Land Mammal Age*/SALMA. As SALMAs não são unidades estatigráficas formais, pois são pobremente definidas em termos de datações absolutas, tendo suas idades baseadas principalmente em biocronologia, estratigrafia e correlação com escalas paleomagnéticas (Woodburne *et al*., 2014). Elas são baseadas na evolução das associações faunísticas de mamíferos, sobretudo em assembleias presentes em afloramentos na porção sul do continente, e têm sido elaboradas há várias décadas e comparadas principalmente a um esquema bioestratigráfico semelhante estabelecido na América do Norte, as “Idades Mamíferos Terrestres Norte-Americanos” (NALMAs) (Pascual & Ortiz Jaureguizar, 1990). Focando no registro fóssil de metatérios, dentre as SALMAs, destacam-se os registros

de metários na SALMA Tiupampense, os quais são principalmente descritos para a fauna de Tiupampa, localizada no departamento de Cochabamba, centro-oeste da Bolívia, do Eopaleoceno. A fauna de Tiupampa é totalmente nova quando comparada às formas do Neocretáceo, SALMA Alamitense, da Argentina, sendo provavelmente fruto da imigração de táxons da América do Norte no final do Cretáceo/início do Paleoceno. Há uma dezena de táxons de metatérios já descritos para Tiupampa, os quais são majoritariamente insetívoro-onívoros e de pequeno tamanho, assim como formas de tamanho médio, carnívoros, insetívoros-frugívoros, principalmente de "Ameridelphia" *incertae sedis*, como também de Sparassodonta, Polydolopimorphia e possivelmente Didelphimorphia. Trata-se de táxons que antecipam as linhagens mais derivadas que atingiriam seu clímax no Eoeoceno (Goin *et al*., 2016). Outra SALMA com importantes registros de metatérios fósseis é o Itaboraiense, registrada nos afloramentos de Las Flores, sul do lago Colhué Huapi, Patagônia argentina, Neopaleoceno, e na Bacia de Itaboraí, estado do Rio de Janeiro, Brasil, do início do Eoceno. O Itaboraiense destaca-se como tendo um padrão faunístico totalmente diferente daquele das faunas precedentes, com uma grande diversificação de mamíferos placentários. É no Itaboraiense que ocorreu a maior radiação dos metatérios e na qual eles atingiram um pico de sua diversidade, não somente taxonômica, como também de tipos ecológicos. Em contrapartida, os cingulados, astrapotérios e notoungulados aparecem pela primeira vez, e litopternas, ocorrentes em SALMAs prévios, são mais numerosos, além dos "Condylarthra", que registram a diversificação significativa dos endêmicos Didolodontidae. Ademais, no Itaboraiense ocorreu o primeiro passo em direção ao aumento do tamanho dos metatérios (Woodburne *et al*., 2014; Goin *et al*., 2016). Na Bacia de Itaboraí, por exemplo, estão presentes metatérios "Ameridelphia" *incertae sedis* como Sternbergiidae, Derorhynchidae, Protodidelphidae, além de Sparassodonta (e.g., Hathliacynidae), Didelphimorphia (e.g., Caroloameghiniidae), Paucituberculata (*Riolestes capricornicus*), Microbiotheria (*Mirandatherium*) e Polydolopimorphia (*Bobbschaefferia fluminensis*, Bonapartheriidae e Gashterniidae) (Oliveira & Goin, 2011). No entanto, no Itaboraiense os metatérios, ainda que numerosos, perderam parte de sua diversidade original e subsequentemente também não a recuperam, estando

presentes nas assembleias fósseis mamalianas das distintas SALMAS subsequentes, porém não como membros com grande riqueza e diversidade.

Segundo Goin *et al*. (2012, 2016), distinguem-se seis fases da evolução dos mamíferos na América do Sul, sendo que os metatérios estariam compreendidos nas últimas quatro fases.

I. Fase sul-americana inicial

Do final do Cretáceo até o limite Eoceno-Oligoceno, marcada pelo declínio das linhagens não-térias e pela chegada dos mamíferos térios provavelmente provenientes da América do Norte (Primeiro Intercâmbio Biótico das Américas – FABI). Os primeiros Metatheria chegaram à America do Sul e rapidamente se diversificaram no Neopaleoceno e Eoeoceno, sendo a maior radiação de metatérios não somente do Paleógeno, como de todo o Cenozoico. Os metatérios foram os mamíferos térios mais diversos na América do Sul até o Mesoeoceno e grande parte das formas eram frugívoras. Tiveram seu pico de diversidade com o máximo térmico do final do Paleoceno e o ótimo climático do Eoeoceno, os quais propiciaram o desenvolvimento de paisagens tropicais na América do Sul. Após o Eoeoceno, as temperaturas globais começaram a baixar e o regime de precipitação também diminuiu, o que levou a rearranjos taxonômicos e ecológicos nas comunidades de mamíferos e ao surgimento de diversas linhagens de eutérios. Supõe-se que esta progressiva degradação climática a partir do Mesoeoceno afetou a diversidade de metatérios, culminando com a importante extinção ocorrida na fase subsequente. Sugere-se que, no final da fase I, no Mesoeoceno, os roedores Caviomorpha e possivelmente os primatas Platyrrhini chegaram à América do Sul.

II. Fase sul-americana tardia

Do limite Eoceno–Oligoceno ao Neomioceno, assinalada por grandes mudanças bióticas causadas por um importante episódio de resfriamento global. O limite Eoceno–Oligoceno representa o episódio mais radical da história evolutiva dos metatérios sul-americanos. Tal evento faz parte de um episódio global de extinção, registrado em diversas regiões e continentes, tendo sido chamado de *Bisagra Patagónica*/*Patagonian hinge* na América do Sul por Goin *et al*. (2010). A degradação

climática afetou a diversidade dos metatérios, suas associações registram diminuição da riqueza e abundância e extinção de diversas linhagens, passando a representar apenas 30% das faunas de mamíferos da América do Sul. Os Sparassodonta, Paucituberculata, Argyrolagoidea, Didelphimorphia e Microbiotheria foram os únicos sobreviventes deste evento de extinção e passaram por mudanças em sua composição taxonômica e ecológica, fundamentando uma nova e distinta etapa da história dos metatérios na América do Sul durante o Neógeno, com a radiação de formas carnívoras e granívoras e desaparecimento dos frugívoros. Durante esta fase os “Ameridelphia” basais são registrados pela última vez (e.g., Sternbergiidae), assim como os Caroloameghiniidae, Glasbiidae, Bonapartherioidea, Polydolopidae, Proborhyaenidade e todos os Sparassodonta basais. Já os Argyrolagoidea são registrados pela primeira vez, tem-se a origem de Thylacosmilidae e Didelphidae, e Paleothentoidea, Borhyaenidae e Microbiotheriidae rapidamente se desenvolveram. Os Argyrolagoidea e Borhyaenoidea inclusive atingiram seus clímaces nesta fase, com as mais extremas formas adaptativas *Argyrolagus* e *Thylacosmilus*, respectivamente. Por volta do início do Mioceno, todas as linhagens modernas de marsupiais já se encontravam estabelecidas. Na SALMA Tinguiririquense aparecem as primeiras associações de eutérios dominados por herbívoros hipsodontes, principalmente notoungulados, evidenciando que nesta época passam a prevalecer ambientes mais abertos, com menos florestas, levando a diversificação de formas de ambientes abertos e declínio e extinção das linhagens não adaptadas a essas novas condições climáticas e ambientais.

III. Fase interamericana

Do Neomioceno até o Ultimo Máximo Glacial, esta fase é marcada por outro pulso climático frio, assim como pelo fechamento do istmo do Panamá, o qual possibilitou o GIBA. Tal rota de migração possibilitou que diversas linhagens norte-americanas de mamíferos placentários adentrassem a América do Sul e que alguns táxons sul-americanos também chegassem à América Central e do Norte. Nesta fase diversas linhagens de mamíferos se extinguem, incluindo metatérios, com o desaparecimento das últimas formas altamente especializadas, como os Argyrolagidae, Paleothentidae e Abderitidae. Os Metatheria foram, durante este

período, influenciados pelo ajuste às condições climáticas mais frias e a chegada dos imigrantes eutérios norte-americanos. O impacto da chegada destes imigrantes sobre a fauna de metatérios ainda não é totalmente compreendido, porém considera-se que não teria sido particularmente devastador. A competição entre os metatérios e imigrantes eutérios pelos mesmos nichos ecológicos pode ter ocorrido, no entanto, novos estudos demonstram que houve um hiato de tempo entre o desaparecimento de certas linhagens de metatérios e o aparecimento de seus correspondentes ecológicos eutérios (Forasiepi *et al*., 2007). As comunidades mamalianas da América do Sul adquiriram sua composição atual nesta fase. No caso de Metatheria, apenas os Caenolestidae, Didelphidae e Microbiotheriidae generalistas persistiram até o presente. Ademais, por volta de 0,8 Ma AP ocorreu a dispersão dos didelfídeos para a América do Norte.

IV. Fase hipoamericana

Esta fase se inicia com o fim do Último Máximo Glacial e a chegada dos *Homo sapiens* na América do Sul e é marcada pela extinção de diversas linhagens de mamíferos. Neste evento, conhecido como “Extinção da Megafauna”, todos os grandes herbívoros sul-americanos e muitos outros mamíferos de médio e grande porte desapareceram, sendo suas causas ainda extensivamente debatidas. No entanto, tal evento de extinção não teria afetado os metatérios, os quais já estão nesta época empobrecidos em termos de diversidade, representando apenas 10% das comunidades mamalianas sul-americanas. Apenas Didelphidae, Caeneolestidae e um gênero de Microbiotheriidae encontram-se presentes e os paucituberculados e microbiotérios já possuem distribuição restrita à Cordilheira dos Andes. Os marsupiais deste período sofreram alterações em sua distribuição geográfica de acordo com mudanças climáticas, tais como o último período interglacial, especialmente os táxons de regiões temperadas.

3.6.2 O registro fóssil de Metatheria na Região Amazônica

Aproximadamente 40% do território da América do Sul é recoberto pelas planícies e terras baixas amazônicas, maior sub-região florestada do Neotrópico. A

Região Amazônica abriga grande riqueza de espécies, com alto grau de endemismo, sendo uma das faunas mais ricas em mamíferos do planeta, com aproximadamente 140 gêneros e 430 espécies, representando cerca de 30% da diversidade total de mamíferos sul-americanos. A porção oeste da Região Amazônica, em especial, destaca-se por possuir os maiores níveis de biodiversidade do Neotrópico, com aproximadamente 215 espécies por área (Patterson & Costa, 2012; Meseguer *et al*., 2022), contando com 12 ordens, 37 famílias e 286 espécies de mamíferos. Todavia, esta diversidade atual compreende quatro ordens de origem norte-americana (vindas durante o GIBA) e apenas três ordens originalmente sul-americanas, destoando da diversidade amazônica anterior ao GIBA (Antoine *et al*., 2017).

Diversas hipóteses evolutivas e ecológicas já foram propostas para explicar a grande biodiversidade hoje presente na Amazônia. Os rios amazônicos constituiriam barreiras à dispersão das espécies e, possivelmente, agentes levando à especiação. Os Arcos de Iquitos e de Purus tiveram igualmente o papel de barreiras físicas no passado. Por outro lado, as flutuações climáticas ocorridas no Quaternário fundamentam a teoria dos refúgios, na qual sucessivas retrações e expansões das florestas durante o Pleistoceno teriam levado ao isolamento de populações nos períodos frios e dispersão nos períodos interglaciais (Patterson & Costa, 2012).

Ademais, processos geotectônicos também tiveram um papel importante na história da Região Amazônica. A Amazônia atual representa apenas uma parte de uma grande região pretérita denominada pan-Amazônia, a qual compreendia as bacias de drenagem dos rios Amazonas, Orinoco e Magdalena, se estendendo por vezes até a região norte da bacia do Rio Paraná. No Paleógeno, as porções noroeste e oeste desta pan-Amazônia oscilavam entre condições fluviais e incursões marinhas marginais. Grande riqueza de mamíferos já se encontrava presente na região centro-oeste da pan-Amazônia no Paleógeno, como atesta a fauna de Santa Rosa detalhada adiante neste texto. O sistema fluvial Paleo-Orinoco predominava na drenagem do noroeste da Amazônia e nas bacias dianteiras andinas do final do Cretáceo ao final do Oligoceno, com rios drenando a periferia do cráton amazônico e correndo em direção noroeste (Hoorn *et al*., 2010; Patterson & Costa, 2012).

A estrutura atual do grande sistema fluvial da bacia do Rio Amazonas se originou a partir do Mioceno, através de importantes eventos tectônicos, com a intensificação

do processo de soerguimento da porção norte dos Andes. A orogenia andina gerou maior carga tectônica e alterou os espaços de acomodação de sedimentos nas bacias dianteiras adjacentes, além de ter impactado o clima, causando, por exemplo, alterações no regime de precipitação. Estes fenômenos levaram a importantes alterações no sistema fluvial amazônico. Por exemplo, desenvolveu-se no oeste da Amazônia, no início do Mioceno, o Sistema Pebas (*Pebas Mega-Wetland System*), formado por grandes áreas úmidas de lagos e canais rasos, planícies de inundação e pântanos, que perdurou de 18 a 10 Ma AP. Tal sistema era alimentado por água e sedimentos provindos dos Andes, e diversos indícios de influência marinha também foram detectados na região, sugerindo a ocorrência de incursões marinhas. As florestas ombrófilas já existentes previamente na Amazônia foram fragmentadas pelo Sistema Pebas, persistindo às margens dos corpos d'água, porém já possuíam riqueza considerável e se assemelhavam, em termos de composição florística, às florestas atuais. Por volta de 9 Ma AP, o Sistema Pebas deu lugar a um sistema fluvial/fluviotidal no oeste amazônico. Neste mesmo período, os sedimentos andinos atingem a costa atlântica pela primeira vez, através do sistema de drenagem, e o Rio Amazonas se estabeleceu por completo. Processos de neotectônica modelaram desde então a paisagem amazônica, levando ao soerguimento de depósitos do Neógeno, desenvolvimento de sistemas de terraços aluviais e ao reajuste dos padrões dos rios, originando a paisagem em mosaico presente atualmente (Hoorn *et al*., 2010, 2017; Patterson & Costa, 2012; Boonstra *et al*., 2015).

Diversos autores (e.g., Antoine *et al*., 2016, 2017; Goin *et al*., 2016) salientam que grande parte do que se conhece do registro fóssil da América do Sul provém de áreas localizadas entre médias e altas latitudes (até 50º N), sendo que as regiões ao norte e ao sul destas permanecem escassamente exploradas, em especial a porção tropical amazônica do continente sul-americano. Como visto acima, por exemplo, grande parte das SALMAs foram reconhecidas e descritas baseando-se em afloramentos da porção sul do continente. Ademais, dentre os registros já relatados para a Região Amazônica, observa-se uma predominância de mamíferos eutérios de grande porte, principalmente nos depósitos fluviais do Plioceno e Quaternário, o que só recentemente mudou, com a aplicação de técnicas de coleta mais apropriadas à descoberta de restos de pequeno tamanho (e.g., *screen-washing*). No que se refere

ao registro fóssil de Metatheria, os fatores citados anteriormente são particularmente problemáticos, visto que, atualmente, os marsupiais se distribuem principalmente em áreas tropicais e subtropicais do continente, além de terem sido, e ainda o serem, majoritariamente de pequeno porte. Estima-se que aproximadamente 60 espécies de pelo menos 14 gêneros de didelfídeos estejam hoje distribuídas na Região Amazônica (Voss, 2022). A Amazônia ocidental, por exemplo, abriga atualmente 29 espécies de Didelphidae (Goin *et al*., 2007b, 2016; Antoine *et al*., 2017).

Muitos consideram que regiões tropicais são desprovidas de fósseis, pela sua difícil preservação nestes ambientes. No entanto, restos fósseis são relativamente comuns, por exemplo, na Amazônia, sob sua espessa cobertura vegetal, sendo encontrados principalmente nas margens dos rios e nos poucos bons afloramentos rochosos. No caso do oeste amazônico, a tectônica andina causou dobramentos e falhas no relevo, possibilitando o acesso a depósitos do Neógeno e, em algumas áreas, depósitos mais antigos (Campbell, 2004). Esforços de campo realizados na Região Amazônica nas últimas décadas, principalmente em sua porção ocidental, demonstram que esta região abrigou, durante o Cenozoico (Mesoeoceno–Holoceno), grande diversidade de mamíferos, com aproximadamente 23 ordens, 89 famílias e 320 espécies, incluindo Allotheria, Metatheria e Eutheria (Antoine *et al*., 2017).

Um importante passo para o conhecimento dos metatérios fósseis tropicais do Paleógeno da América do Sul foi o estudo da fauna local de Santa Rosa, Província de Atalaya, Departamento de Ucayali, Peru, localizada nas margens do Rio Yuruá (Juruá no Brasil), próximo à fronteira Peru-Brasil. Nela foram encontrados poucos grandes vertebrados, mas uma grande riqueza e abundância de organismos de pequeno porte, tais como mamíferos, peixes, anfíbios, répteis e aves, majoritariamente representados sob a forma de dentes isolados de poucos milímetros. Com base no grau evolutivo desta fauna, em especial metatérios e roedores, sugeriu-se uma idade Meso-Eoeoceno/Oligoceno para os depósitos, próximo a SALMA Mustersense (Campbell, 2004). No entanto, datações radiométricas feitas mais recentemente sugerem que a fauna de Santa Rosa seria provavelmente Eooligoceno (Campbell *et al*., 2021). A associação de metatérios de Santa Rosa é composta por 79 fragmentos, sendo, quando de sua descrição, oito novos gêneros e 11 novas espécies (Quadro 7) (Goin & Candela, 2004).

Os depósitos da região de Contamana, Amazônia peruana, da Formação Pozo, Mesoeoceno, proveram os primeiros restos fósseis de roedores na América do Sul, com uma rica assembleia de Caviomorpha, juntamente com os quais foram encontrados restos do Polydolopimorphia *Punadolops* no afloramento CTA-27 (Antoine *et al*., 2012). Posteriormente, Antoine *et al*. (2016), na descrição de diversos afloramentos da região de Contamana, citam a presença de metatérios preliminarmente identificados para o intervalo Mesoeoceno–Neomioceno, das formações Pozo (Didelphimorphia, Sparassodonta, Polydolopimophia Bonaparthe rioidea e Paucituberculata Paleothentoidea); Chambira (metatéria basal ?Herpetotheriidae, Paucituberculata ?Paleothentidae e Abderitidae e Miocrobiotheriidae); e Pebas (Didelphimorphia, Sparassodonta e Polydolopimorphia Argyrolagidae).

Quadro 7. Metatérios fósseis da fauna de Santa Rosa, Peru segundo Goin & Candela (2004).

"Ameridelphia" *incertae sedis*	cf. Herpetotheriidae	*Rumiodon inti*
Sparassodonta	Hathliacynidae	*Patene campbelli*
Polydolopimorphia	Prepidolopidae	*Incadolops ucayali*
	indet.	*Wamradolops tsullodon*
		Hondonadia pittmae
Paucituberculata	Caenolestidae*	*Perulestes cardichi*
		Perulestes fraileyi
	cf. Paleothentidae*	*Sasawatsu mahaynaq*
Microbiotheria	Microbiotheriidae	*Kirutherium paititiensis*
Indet.	indet.	*Wirunodon chanku*
		Kiruwamaq chisu

*Posteriormente tais táxons foram revisados por Abello (2007) e considerados como Palaeothentoidea basais.

Igualmente para o Peru, Antoine *et al*. (2013) registram a presença de Sparassodonta Hathliacynidae *Sipalocyon* sp. e Didelphimorphia Didelphidae tribo Marmosini *Marmosa* (*Micoureus*) cf. *laventica* para a Região Amazônica subandina do Rio Madre de Dios, localidade MD-67, próximo a cidade de Cusco, de idade Mioceno médio (SALMA Colloncurense/início do Laventense). Tejada-Lara *et al*. (2015), na descrição da fauna de Fitzcarrald, uma nova fauna local do Mesomioceno, situada no flanco noroeste do Arco de Fitzcarrald, Amazônia peruana, relatam o achado de um dente caniniforme, tentativamente assignado a um Sparassodonta Borhyaenoidea.

Mais recentemente, Antoine *et al*. (2021), ao descrever novos afloramentos para a Região Amazônica peruana, Seção Paleógena de Shapaja, intervalo final do Eoceno ao início do Oligoceno, reportaram uma vasta fauna, composta, dentre outros, por metatérios, com o registro de 19 táxons: Marsupialiformes *incertae sedis*, Polydolopimorphia das famílias Prepidolopidae e Argyrolagidae, além de Paucituberculata, com Palaeothentoidea basais e as famílias Palaeothentidae e Abderitidae. Também para a Região Amazônica peruana, Stutz *et al*. (2022) registram para a localidade TAR-31, final do Mesomioceno, os táxons: '*Thylamys*' cf. '*T*'. *colombianus* (Didelphimorphia, Didelphidae), *Palaeothentes* sp. (Paucituberculata, Palaeothentidae) e uma nova espécie de Paucituberculata Abderitidae *Pitheculites ipururensis* sp. nov. (vide Parte II, 1 ARTIGO 1).

Na Região Amazônica brasileira, principalmente sua porção ocidental, adjacente à Região Amazônica peruana, também se encontraram importantes depósitos fossilíferos. Diversos grupos de vertebrados são registrados no Estado do Acre, como peixes, aves, além de numerosos répteis e mamíferos (Rodentia, Xenarthra, Notogungulata, Litopterna, Astrapotheria, Proboscidea, Cetartiodactyla, Primates e Chiroptera) (vide Seção 5.1 BRASIL). Ademais, também são reportados alguns restos de metatérios, como Didelphidae não identificados e *Didelphis solimoensis* (Czaplewski, 1996; Cozzuol *et al*., 2006). A espécie *D*. *solimoensis* (Figura 27) foi descrita por Cozzuol *et al*. (2006) com base em restos encontrados nas margens do Rio Acre, localidade de Patos, em afloramentos da Formação Solimões. Segundo os mesmos autores, tal localidade seria de idade Neomioceno (SALMA Huayqueriense), de acordo com sua fauna e *D*. *solimoensis* seria a menor e mais antiga espécie de *Didelphis*. A fauna da Formação Solimões é frequentemente considerada bastante semelhante à fauna de Urumaco (Venezuela) e estima-se que seria do Neomioceno (Huayqueriense). Contudo, diversos elementos, principalmente provindos da região do alto Rio Juruá, sugerem a presença de outra unidade estratigráfica, mais antiga, com fósseis semelhantes a formas da fauna de Santa Rosa, Fitzcarrald (Peru), La Cancha (Argentina) e Salla (Bolívia) (Ribeiro et al., 2013; Hsiou et al., 2022).

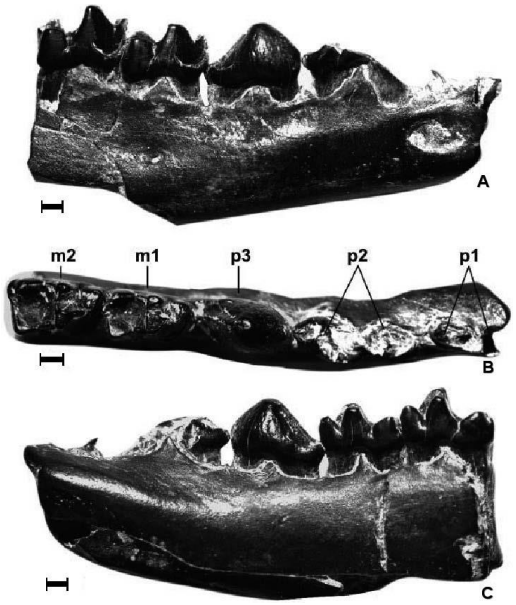


Figura 27. Holótipo de *Didelphis solimoensis*, em vista: **A**, labial; **B**, oclusal; **C**, lingual. Escalas = 1 mm. Fonte: Cozzuol *et al*. (2006).

A associação de metatérios tropicais sul-americanos fósseis melhor conhecida é a de La Venta, Colômbia, a qual, serviu como base para a descrição da SALMA Laventense, Mesomioceno. Embora hoje a região tenha clima semi-árido e vegetação predominantemente arbustiva, no Mesomioceno era recoberta por uma floresta tropical (Kay *et al*., 1997). Dentre os abundantes fósseis de La Venta, os metatérios encontram-se representados por ?“Ameridelphia” *incertae sedis*, Sparassodonta, Paucituberculata, Microbiotheria e Didelphimorphia (Quadro 8). Os metatérios de La Venta possuem diversos tamanhos corporais e hábitos ecológicos e muitos representam novas radiações do Neógeno (Goin, 1997). Dentre os táxons de Sparassodonta, notou-se que as formas de La Venta eram mais generalizadas quando comparadas às formas patagônicas, até mesmo de faunas mais antigas. Esta persistência de formas mais generalistas nos trópicos pode ter ocorrido com outros táxons e em outras idades, no entanto, não é tão conhecida devido à escassez de dados sobre fósseis desta região, o que dificulta o entendimento das relações filogenéticas e paleobiogeográficas de Metatheria (Goin *et al*., 2016). Também para a Colômbia, foi descrita uma nova espécie de Sparassodonta Borhyaenoidea (*Lycopsis*

padillai) para uma localidade da Formação Castilletes, de idade Eo a Mesomioceno (Suárez *et al*., 2015).

Quadro 8. Metatérios fósseis da fauna de La Venta, Colômbia, segundo Goin (1997) e Suárez Gómez (2019).

"Ameridelphia" *incertae sedis*	?Sternbergiidae	*Kiotomops lopezi*
		?Sternbergiidae gen. et sp. indet
Sparassodonta	Hondadelphidae	*Hondadelphys fieldsi* Marshall, 1976
		Hondadelphys sp. 1
		Hondadelphys sp. 2
		Hondadelphys sp. indet.
		?*Hondadelphys*
	Borhyaenoidea	*Dukecynus magnus* Goin, 1997
		?*Dukecynus magnus*
		Lycopsis torresi Cabrera, 1927
		cf. *Lycopsis*
	Thylacosmilidae	*Anachlysictis gracilis* Goin, 1997
		Thylacosmilidae gen. 1 sp. 1
		Thylacosmilidae gen. 1 sp. indet.
Paucituberculata	Paleothentidae	*Hondathentes cazador* Dumont & Brown, 1997
		Hondathentes sp. indet.
		?*Hondathentes*
	Abderitidae	*Pitheculites chenche* (Dumont & Bown, 1997)
Didelphimorphia	Didelphidae	tribo Marmosini
		Marmosa laventica Marshall, 1976
		Marmosa sp. 1
		Marmosini cf. *Tlacuatzin*
		tribo Thylamyini
		Thylamys minutus Goin, 1997
		Thylamys colombianus Goin, 1997
	Incertae sedis	Gênero A sp. 1
		Gênero A sp. 2
Microbiotheria	Microbiotheriidae	*Pachybiotherium minor* Goin, 1997
		?*Pachybiotherium*

Outra fauna bem documentada da porção norte do continente sul-americano provém da Sequência Urumaco (formações Socorro, Urumaco, Codore e San Gregorio), Mesomioceno ao Plioceno, norte da Venezuela. Nesta e em outras formações venezuelanas, de idade semelhante, foram escavados numerosos restos fósseis de notável riqueza, com peixes ósseos e cartilaginosos, aves, crocodilomorfos, quelônios, serpentes, além de mamíferos tais como cetáceos, xenartros, sirênios, litopternas, notoungulados, astrapotérios e roedores. Prevalecem na fauna de

Urumaco restos de táxons de grande porte e supõe-se que se tratava de um ambiente de alta energia, não favorável à preservação de restos de pequenos vertebrados (Sánchez-Villagra *et al*., 2010; Horovitz & Sánchez-Villagra, 2012). Isto poderia explicar a quase ausência de restos de metatérios nessas localidades, de onde apenas se reporta um possível metatério Sparassodonta da família Borhyaenidae, possivelmente do gênero *Stylocynus*, para a Formação Urumaco, Neomioceno (Linares, 2004).

Além destes registros, o conhecimento de fósseis amazônicos persiste limitado. Não se conhece, por exemplo, fósseis anteriores ao Pleistoceno para a atual Região Amazônica do Equador e Colômbia (Antoine *et al*., 2017).

3.6.3 O registro fóssil de Metatheria no Brasil e Peru

O registro fóssil de Metatheria no Peru, fora os registros citados na seção precedente para a Região Amazônica, permanece pouco explorado. No sudeste do Peru, na margem noroeste da Laguna Umayo, encontram-se afloramentos de caráter único na América do Sul, um dos poucos com registros bióticos continentais da crise do limite K–Pg. Dois níveis fossilíferos (LU-3 e nível Chulpas) estão presentes na unidade de argilas vermelhas de Laguna Umayo (*Lower Muñani Formation*), a qual está localizada na região andina do Peru, próximo à cidade de Puno e do lago Titicaca. Nestes depósitos foram encontrados indícios sugerindo idade Neocretáceo, a qual foi utilizada por certo tempo nos estudos da fauna da região. No entanto, mais recentemente se observou que os restos fósseis de eutérios e metatérios, com padrões molares derivados, sugerem a idade Paleógeno inferior, a qual também é apoiada por outras informações geológicas. Em LU-3 foram encontrados restos de carófitas, fragmentos de casca de ovo, peixes, anfíbios, répteis, mamíferos e, possivelmente, aves. Os restos de metatérios descritos para LU-3 incluem: ?Pediomyidae ou ?Microbiotheriidae indeterminado; Peradectidae, *Peradectes* (nec *Alphadon*) *austrinum*; e Didelphimorphia Didelphidae indeterminado. Já os restos do nível Chulpas foram identificados como: pelo menos três formas distintas de Didelphidae indeterminados; Polydolopimorphia, família indeterminada, *Chulpasia mattaueri* (Figura 28), aff. *Chulpasia* e *Sillustania quechuense*. Os Peradectidae e

possivelmente Pediomyidae apresentam afinidade com formas do Neocretáceo da América do Norte e *P*. *austrinum* se assemelha a restos encontrados na fauna de Tiupampa (*P*. cf. *austrinum*) (Sigé *et al*., 2004). Ademais, uma espécie também do gênero *Chulpasia*, *C*. *jimthorselli*, foi descrita para a fauna de Tingamarra, Austrália, como mencionado acima, estabelecendo certa proximidade entre as formas de Laguna Umayo e os marsupiais da Austrália, mas tal denominação necessita maior comprovação (Sigé *et al*., 2009).

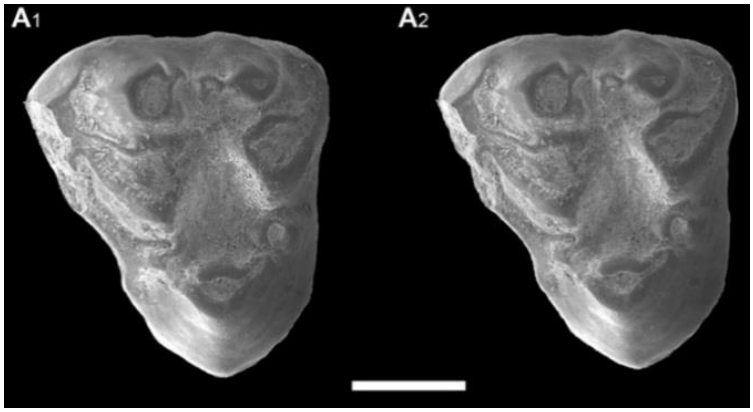


Figura 28. *Chulpasia mattaueri*, holótipo, M1 ou M2 esquerdo, par estéreo. Escala = 1 mm. Fonte: Sigé *et al*. (2009).

Além de Laguna Umayo, no Peru somente se registram fósseis de metatérios para o Quaternário, na chamada *Guitarrero cave*, um sítio arqueológico holocênico na Cordilheira dos Andes, de onde se reportam restos dos Didelphimorphia Didelphidae *Metachirus* e *Marmosa* (Lynch, 1980).

Já no Brasil, o registro fóssil de Metatheria conta com a importante fauna da Bacia de Itaboraí (RJ), assim como os restos relatados para a Amazônia brasileira, Estado do Acre, ambos mencionados precedentemente. Além destes, os únicos registros anteriores ao Quaternário são os da Formação Tremembé da Bacia de Taubaté e da Formação Guabirotuba da Bacia de Curitiba. As bacias Taubaté (São Paulo – SP) e Curitiba (Paraná – PR), assim como as bacias de São Paulo, Resende, Volta Redonda, Depressão da Guanabara e as bacias menores de Itaboraí e Barra de São João, situadas em uma faixa alongada e deprimida de aproximadamente 800 km entre as cidades de Curitiba (PR) e Barra de São João (RJ), formam o chamado Rift Continental do Sudeste do Brasil (RCSB). A região sofreu influência de atividades tectônicas no final do Mesozoico e Cenozoico, as quais causaram subsidência e

soerguimentos de terrenos, levando à implantação do RCSB. A sedimentação nas bacias do RCSB se iniciou no Paleógeno e é exclusivamente de origem continental, principalmente ligada a ambientes fluvial e lacustre (Riccomini, 1989; Fernandes & Chang, 2001).

A Formação Tremembé da Bacia de Taubaté se depositou no Paleógeno e é formada por depósitos lacustres, sendo estes explorados por empresas mineradoras. O registro fóssil encontrado na formação indica idades oscilando entre Neooligoceno e Eomioceno, e compreende peixes, anfíbios, réptil, aves e mamíferos (Eutheria: Cingulata, Chiroptera, Rodentia, Litopterna, Astrapotheria, Notoungulata e Pyrotheria). Os metatérios da Formação Tremembé foram até hoje apenas preliminarmente estudados (Quadro 9, Soria & Alvarenga, 1989; Couto-Ribeiro, 2010).

Em afloramentos da Formação Guabirotuba, Bacia de Curitiba, foi recentemente encontrada uma rica fauna fóssil, ainda somente preliminarmente analisada. Os restos incluem invertebrados e vertebrados, tais como mamíferos Metatheria, Cingulata, Notoungulata e Astrapotheria, os quais sugerem idade final do Mesoeoceno (SALMA Barranquense). Dentre os metatérios foram identificados Sparassodonta, Paucituberculata e Polydolopimorphia (Quadro 9; Figura 29) (Sedor *et al*., 2017).

Tanto a Formação Tremembé quando a Formação Guabirotuba foram depositadas sob condições climáticas úmidas, intercaladas por períodos secos (Couto-Ribeiro, 2010; Sedor *et al*., 2017), e já foi observada certa afinidade entre táxons fósseis de eutérios provenientes de ambas as localidades com formas de níveis de distintas idades aflorantes na região de Contamana, Amazônia peruana (Antoine *et al*., 2016).

Quadro 9. Metatérios fósseis das formações Tremembé (Bacia de Taubaté) e Guabirotuba (Bacia de Curitiba), segundo Couto-Ribeiro (2010) e Sedor *et al*. (2017).

Localidade	Ordem	(Super)Família	Táxon
Formação Tremembé, Bacia de Taubaté	Sparassodonta	Borhyaenidae	Borhyaeninae indet.
		Proborhyaenidae	gen. et sp. indet.
		Hathliacynidae	gen. et sp. indet.
	Indet.	indet.	gen. et sp. indet.
Formação Guabirotuba, Bacia de Curitiba	Sparassodonta	indet.	*Nemolestes* sp.
	Paucituberculata	Paleothentoidea	gen. et sp. indet.
	Polydolopimorphia	Argyrolagoidea	gen. et sp. indet.

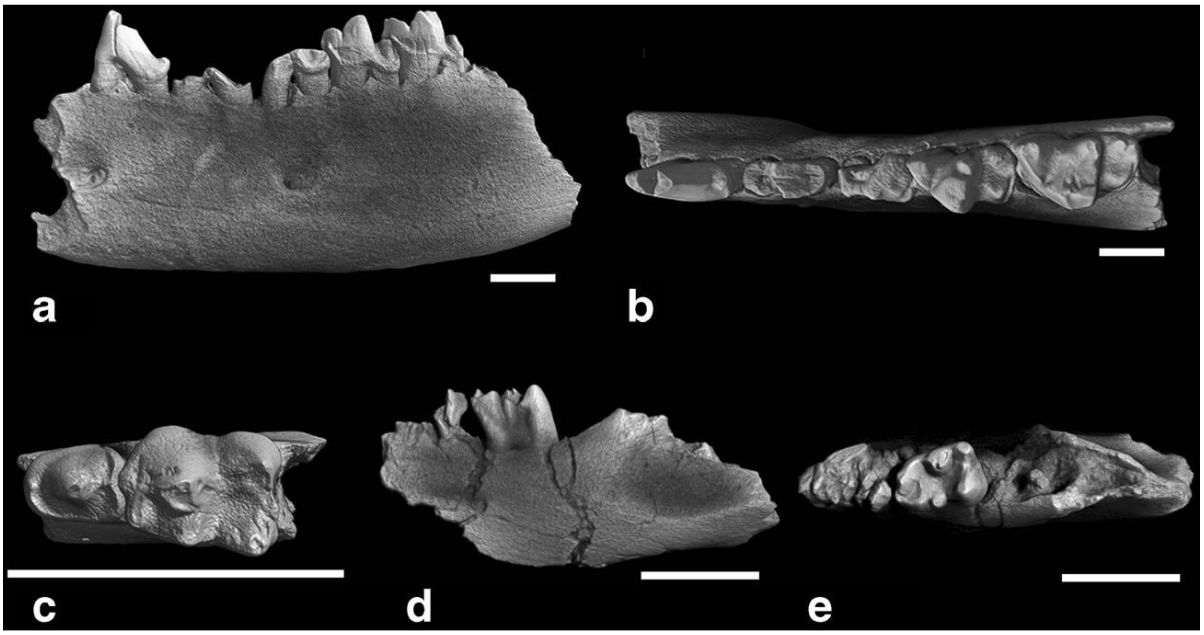


Figura 29. Metatérios fósseis da Formação Guabirotuba, Bacia de Curitiba: *Nemolestes* sp., dentário esquerdo, **a**, vista lateral, **b**, vista oclusal; Paleothentoidea gen. et sp. indet., p3 e m1, **c**, vista oclusal; Argyrolagoidea gen. et sp. indet., dentário esquerdo, **d**, vista lateral, **e**, vista oclusal. Escalas = 5 mm. Fonte: Sedor *et al*. (2017).

O restante dos estudos com fósseis de metatérios brasileiros foram realizados com restos do Quaternário, com registros para os estados de Ceará, Goiás, Mato Grosso do Sul, Minas Gerais, Pará, Piauí, Rio Grande do Sul, São Paulo e Tocantins. Estes registros encontram-se no Quadro 10 e são uma atualização das Tabelas 1 e 3 de Hadler *et al*. (2009), com a adição dos registros: Pleistoceno/Holoceno do Parque Nacional de Ubajara, estado do Ceará (Oliveira, 2010); novos registros para o Quaternário da Serra da Capivara, estado do Piauí (Motta *et al*., 2019); novos registros para o Holoceno do estado do Rio Grande do Sul (Hadler *et al*., 2016); registros do Quaternário do Abismo Iguatemi, estado de São Paulo (Castro & Langer, 2011); e registros do final do Pleistoceno da Gruta dos Moura, estado do Tocantins (Nova *et al*., 2015). A nomenclatura dos táxons segue os trabalhos originais, não foi realizada nenhuma atualização.

Quadro 10. Registros de Didelphimorphia, família Didelphidae, para o Quaternário dos estados brasileiros. Fonte: Hadler *et al*. (2009, 2016); Oliveira (2010); Castro & Langer (2011); Nova *et al*. (2015) e Motta *et al*. (2019).

Estado	Táxon
Ceará	cf. *Didelphis albiventris*
	Monodelphis sp.
Goiás	*Gracilinanus* sp.
	Micoureus demerarae (Thomas, 1905)
	Monodelphis domestica (Wagner, 1842)
	Monodelphis kunsi Pine, 1975
	Thylamys sp.
Mato Grosso do Sul	*Marmosa* sp.
	Gracilinanus sp.
	Monodelphis domestica
	Thylamys macrura (Olfers, 1818)
	Thylamys sp.
Minas Gerais	*Marmosa grisea* Desmarest, 1827
	Marmosa cinerea (Temminck, 1824)
	Marmosa microtarsus (Wagner, 1842)
	Marmosa pusilla Desmarest, 1804
	Marmosa velutina Wagner, 1842
	Marmosa sp.
	Caluromys sp.
	Phylander laniger Winge (1893)
	Metachirops opossum (Linnaeus, 1758)
	cf. *Metachirus* sp.
	Lutreolina crassicaudata (Desmarest, 1804)
	Didelphis marsupialis Linnaeus, 1758
	Didelphis sp.
	Monodelphis domestica
	Monodelphis americana (Müller, 1776)
	Monodelphis sp.
Piauí	*Monodelphis americana*
	Monodelphis domestica
	Marmosa sp.
	Marmosa cf. *M. cinerae*
	Didelphis albiventris Lund, 1840
	Cryptonanus agricolai (Moojen, 1943)
	Gracilinanus agilis (Burmeister, 1854)
	Thylamys karimii (Petter, 1968)

(Quadro 10. Continuação)

Estado	Táxon
Rio Grande do Sul	*Gracilinanus agilis*
	Gracilinanus microtarsus (Wagner, 1842)
	Monodelphis americana
	Thylamys velutinus (Wagner, 1842)
	Philander opossum (Linnaeus, 1758)
	Didelphis sp.
	cf. *Cryptonanus*
	cf. *Marmosa*
	Lutreolina crassicaudata
	Cryptonanus sp.
São Paulo	*Didelphis aurita* Wied-Neuwied, 1826
	Gracilinanus sp.
	Metachirus nudicaudatus (Geoffroy Saint-Hilaire, 1803)
	Metachirus sp.
	Monodelphis sp.
	Philander sp.
	Didelphis albiventris
	Didelphis aurita
	Didelphis sp.
	Chironectes minimus (Zimmermann, 1780)
	Marmosa sp.
Tocantins	*Didelphis aurita*
	Gracilinanus agilis
	Gracilinanus microtarsus
	Marmosa murina (Linnaeus, 1758)
	Monodelphis brevicaudata (Erxleben, 1777)
	Monodelphis domestica
	Sairadelphys tocantinensis Oliveira *et al*., 2011

4 MATERIAIS E MÉTODOS

4.1 MATERIAL

O material estudado constitui-se de dentes isolados e fragmentos de crânio, maxilares e dentários com ou sem dentes incluídos. O material procedente do Estado do Acre (AC), Brasil, constitui-se de 11 dentes isolados das ordens Dildephimorphia e Paucituberculata, sendo: i) afloramento PRJ 25, um fragmento de molar superior (fora de contexto estratigráfico); ii) afloramento PRJ 33, fragmentos de um molar superior e de um molar inferior encontrados *in situ* e um fragmento de molar superior encontrado fora de contexto estratigráfico; iii) afloramento PRE 06, fragmentos de um pré-molar superior, dois pré-molares inferiores, um pré-molar superior decíduo, um pré-molar inferior decíduo, um fragmento de molar superior, um fragmento de molar inferior. Os fósseis provenientes do AC encontram-se depositados na coleção do Laboratório de Paleontologia da Universidade Federal do Acre, campus Floresta (UFAC-CS).

Já o material procedente do Peru constitui-se de 171 restos de Polydolopimorphia das localidades de Contamana (Quadro 11), 100 espécimes da Bacia do Huallaga (Quadro 12) e cinco espécimes provenientes de Atalaya (sendo quatro de TMB-01 e um de URU-210), totalizando 276 fragmentos de metatérios da ordem Polydolopimorphia. Nas mesmas localidades onde foram encontrados os restos de Polydolopimorphia, também foram encontrados restos de outros clados de Metatheria, no entanto, enfatizou-se nesta tese apenas os polidolopimorfios. Ademais, também foram estudados sete fragmentos de metatérios das ordens Didelphimorphia e Paucituberculata, provenientes da localidade TAR-31, Bacia do Huallaga (Quadro 12). Todos estes espécimes estão depositados na coleção do *Museo de Historia Natural, Universidad Nacional Mayor de San Marcos*, Lima, Peru (MUSM).

Quadro 11. Quantidade de restos fósseis de metatérios por afloramento da região de Contamana, Peru, com as respectivas idades sugeridas dos afloramentos.

Localidade	Idade	Restos de metatérios			
		Polydolopimorphia	Didelphimorphia	Paucituberculata	Indet.
CTA-43	Início Neomioceno	1	1	0	1
CTA-66	Final Mesoeoceno	1	0	0	0
CTA-29	Final Mesoeoceno	13	0	2	0
CTA-27	Final Mesoeoceno	149	0	20	80
CTA-51	Final Mesoeoceno	4	0	0	7
CTA-47	Mesoeoceno	3	0	0	0

Quadro 12. Quantidade de restos fósseis de metatérios por afloramento da Bacia do Huallaga, Peru e as respectivas idades dos afloramentos.

Localidade	Idade	Restos de metatérios			
		Polydolopimorphia	Didelphimorphia	Paucituberculata	Indet.
TAR-31	Mesomioceno	0	1	6	0
TAR-14	Neooligoceno	2	0	0	2
TAR-01	Eooligoceno	2	0	18	11
TAR-21	Final do Neoeoceno	46	0	7	26
TAR-47	Neoeoceno	9	0	8	7
TAR-74	Início Neoeoceno	1	0	1	2
TAR-72	Neoeoceno	2	0	3	2
TAR-20	Neoeoceno	3	0	0	3
TAR-45	Meso-Neoeoceno	1	0	0	0
TAR-44	Meso-Neoeoceno	2	0	0	0
TAR-55	Final Mesoeoceno	29	0	8	1
TAR-76	Final Mesoeoceno	2	0	0	0
TAR-56	?Final Mesoeoceno	1	0	0	0

4.2 COLETA

A coleta dos fragmentos fósseis estudados neste projeto se deu pelo método de *wet-screening* dos sedimentos oriundos de camadas fossilíferas previamente reconhecidas, principalmente lentes de microconglomerados. Tal método permite uma coleta mais eficaz de restos de pequeno tamanho de microvertebrados, artrópodes, moluscos e carófitas, dentre outros, através da lavagem dos sedimentos utilizando-se peneiras de 2, 1 e 0,7 mm, seguida da triagem (com e sem uso de microscópio estereoscópio) dos resíduos que permanecem nas peneiras para reconhecimento e separação dos fósseis. A quantidade de sedimento coletado em cada localidade variou de 200 g (para testes preliminares) a 850 kg.

4.3 ANÁLISE

Após a coleta, os fósseis são limpos, com o auxílio de pincéis e agulhas, e, se necessário, consolidados e/ou colados com supercola. Em seguida, os fragmentos fósseis são analisados sob microscópio estereoscópio, para o reconhecimento e estudo das estruturas presentes nos dentes e ossos encontrados, com o objetivo de descrever e identificar taxonomicamente os mesmos, além de observar caracteres úteis para análises filogenéticas e/ou para registro de variabilidade inter/intra-táxons. A identificação dos restos se deu por comparação com espécimes depositados em coleções científicas (e.g., LACM, *Natural History Museum of Los Angeles County*, California, Estados Unidos; MLP, *Departamento Paleontología Vertebrados*, *Museo de La Plata*, La Plata, Argentina; UFSC, Coleção de Fragmentos Ósseos do Laboratório de Paleontologia e Coleção de Mamíferos do Departamento de Ecologia e Zoologia, Universidade Federal de Santa Catarina, Florianópolis, Brasil; MUSM) e com bibliografia especializada (e.g., Pascual, 1980; Goin & Candela, 2004; Abello, 2007, 2013; Cozzuol *et al*., 2006; Goin & Abello, 2013; Suárez Gómez, 2019). A nomenclatura das estruturas dentárias (Figura 30), assim como sistemática de Metatheria a ser utilizada neste projeto segue, no geral, Goin *et al*. (2016), exceto para determinados grupos, nos quais se assinala a referência utilizada (Figuras 31 e 32). Já a nomenclatura das estruturas cranianas segue Beck (2017). Visto que se objetivou

a redação dos trabalhos em inglês, não houve necessidade de se utilizar nomenclatura traduzida para o português. As medidas dos materiais foram realizadas com paquímetro manual de marca *Mitutoyo* de precisão 0,02 mm e com microscópio de medição *Nikon Measurescope 10* conectado a um monitor *Nikon SC 112*.

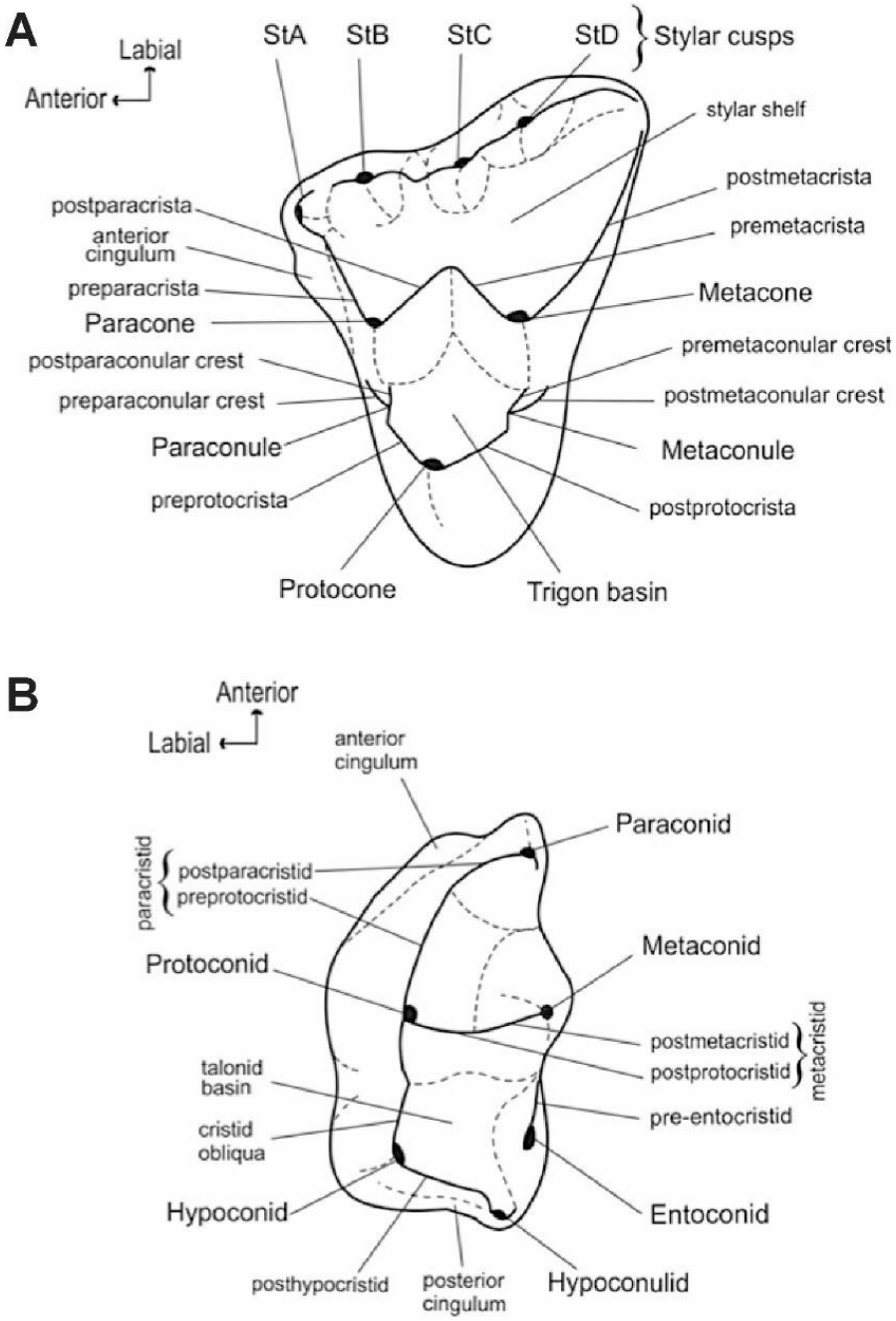


Figura 30. Nomenclatura das estruturas dentárias dos molares de metatérios de acordo com Goin *et al*. (2016): **A**, Molar superior esquerdo, **B**, molar inferior esquerdo.

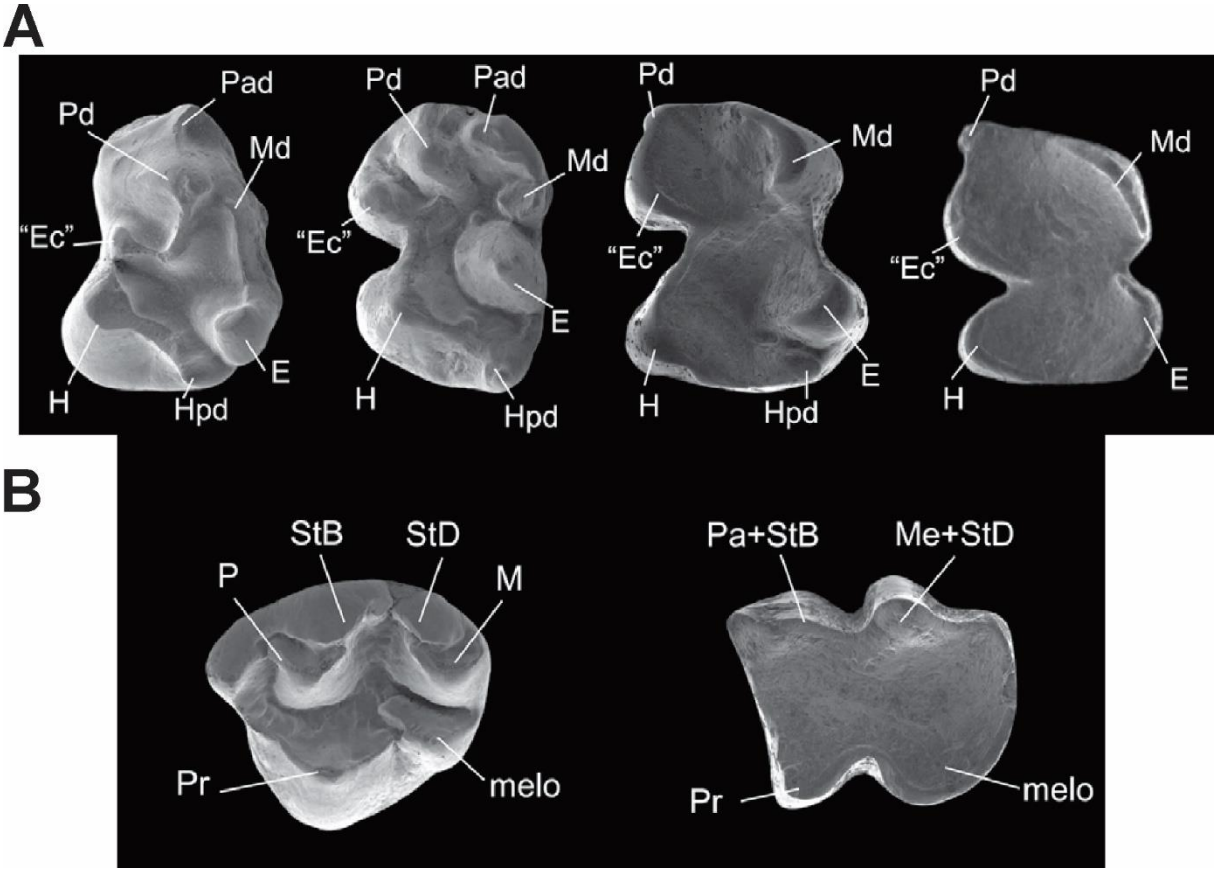


Figura 31. Representação dos padrões dos molares de Argyrolagoidea e a respectiva nomenclatura das estruturas dentárias: **A**, vista oclusal de m2s esquerdos, da esquerda para direita: *Praedens aberrans*, *Klohnia major*, *Proargyrolagus bolivianus* e *Anargyrolagus primus*; **B**, vista oclusal de M2s esquerdos, a esquerda *Klohnia major* e a direita *Proargyrolagus bolivianus*. Abreviações: **cab**, anterobasal cingulum; **cant**, anterior cingulum; **co**, cristid obliqua; **cpme**, premetaconular crest; **cpome**, postmetaconular crest; **E**, entoconid; "**Ec**", ectostylid; **H**, hypoconid; **Hpd**, hypoconulid; **Md**, metaconid; **M**, metacone; *melo*, metaconule; **pc**, postcristid; **P**, paracone; **Pad**, paraconid; **palo**, paraconule; **Pd**, protoconid; **pda**, paracristid; **peda**, pre–entocristid; **pmda**, postmetacristid; **ppa**, postparacrista; **Pr**, protocone; **prda**, postprotocristid; **prep**, preprotocrista; **prepa**, preparacrista; **prme**, premetacrista; **pome**, postmetacrista; **popr**, postprotocrista; **St**, stylar cusp. Adaptado de Goin & Abello (2013).

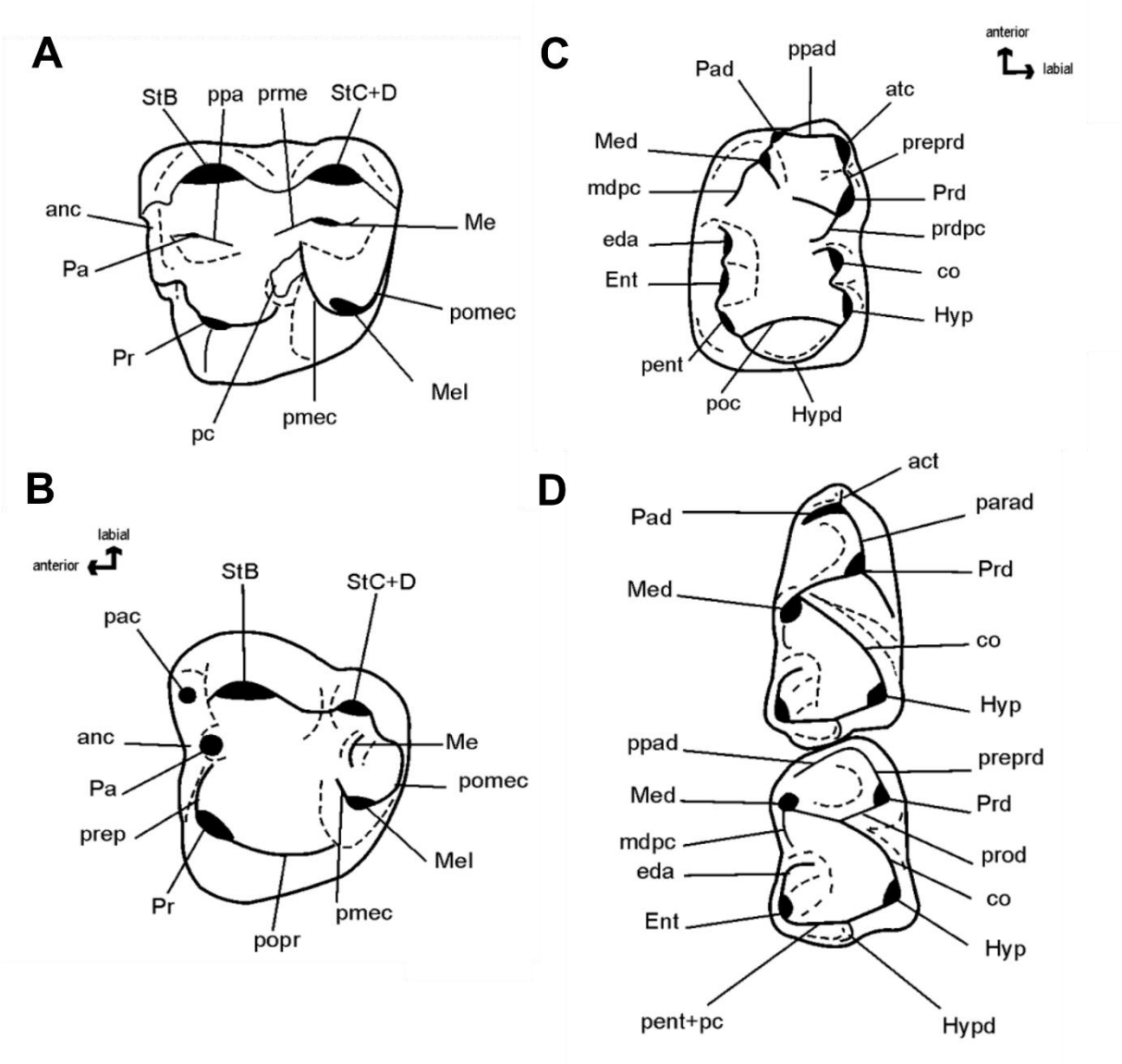


Figura 32. Desenhos esquemáticos da morfologia oclusal e nomenclatura das estruturas dos molares superiores e inferiores de Palaeothentidae e Abderitidae. **A**, *Palaeothentes primus,* M1 esquerdo; **B–C**, *Pitheculithes minimus*, **B**, M2 esquerdo, **C**, m2 direito; **D**, *Palaeothentes minutus*, m1–2 direitos. Abreviações: **abc**, anterobasal cingulum; **act**, anterior crest of m1 trigonid; **anc**, anterior cingulum; **atc**, anterolabial trigonid cusp; **co**, cristid obliqua; **eda**, entocristid; **Ent**, entoconid; **Hyp**, hypoconid; **Hypd**, hypoconulid; **mdpc**, metaconid posterior crest; **Me**, metacone; **Med**, metaconid; **mel**, metaconule; **Pa**, paracone; **pac**, parastylar cusp; **Pad**, paraconid; **pal**, paraconule; **parad**, paracristid; **pc**, premetaconular cusp; **pent**, postentocristid; **pmd**, postmetacristid; **pmec**, premetaconular crest; **poc**, postcristid; **pomec**, post- metaconular crest; **popr**, postprotocrista; **ppa**, postparacrista; **ppad**, postparacristid; **P**r, protocone; **Prd**, protoconid; **prdpc**, protoconid posterior crest; **prep**, preprotocrist; **preprd**, preprotocristid; **prme**, premetacrista; **prod**, protocristid; **prpc**, preparaconular crest; **StA**, stylar cusp A; **StB**, stylar cusp B; **StC**, stylar cusp C; **StC+D**, fused stylar cusps C and D; **StD**, stylar cusp D.

4.4 IMAGEAMENTO

Após a identificação e descrição do material, selecionou-se determinados espécimes, representantes únicos ou bastante característicos de seus respectivos táxons, para serem fotografados e/ou escaneados para melhor visualização de sua morfologia e para fins de publicação. Os espécimes procedentes dos afloramentos do AC foram fotografados no microscópio eletrônico de varredura (MEV) *JEOL* JSM 6060 do Centro de Microscopia e Microanálise (CMM) da Universidade Federal do Rio Grande do Sul (UFRGS) e MEV *FEI* Inspect F50 do Laboratório Central de Microscopia e Microanálise (LabCEMM) da Pontifícia Universidade Católica do Rio Grande do Sul (PUCRS). Já os espécimes provenientes dos afloramentos peruanos foram imageados no MEV *Hitachi* S4000 do *Institut des Neurosciences de Montpellier* (INM) e escaneados no microtomógrafo *RX EasyTom* 150 multiescala multiresolução, o qual possui uma fonte RX de 40-150 kV e resolução de até 5µm, do *Montpellier RIO Imaging* (MRI), *Institut des Sciences de l'Évolution de Montpellier*, Montpellier, França. Os espécimes escaneados foram virtualmente preparados por segmentação manual utilizando-se o *software* AVIZO 7.1 (Visualization Sciences Group). Também foram realizadas fotografias para fins de estudo em estereomicroscópio *Leica* M 205C, acoplado com câmera fotográfica *Leica* DFC 420C, o qual gera imagens resultantes da fusão de diversas fotografias multifocais.

5 CONTEXTO GEOLÓGICO DA ÁREA DE ESTUDO

O material fóssil estudado é proveniente da Amazônia Ocidental, mais precisamente do Estado do Acre, Brasil, regiões do alto Rio Juruá e Rio Envira (Seção 5.1), assim como do Peru, das localidades de Contamana (Departamento de Loreto), Bacia do Huallaga (Departamento de San Martín) e de Atalaya (Departamento de Ucayali) (Seção 5.2). Os depósitos presentes nestas localidades e dos quais provêm os restos fósseis estudados integram o sistema da Bacia Dianteira Amazônica (*Amazonian foreland basin system*). Tal sistema é resultado e fortemente controlado pela tectônica andina e processos de subducção relacionados. A sobrecarga advinda da orogenia andina teria ocasionado um deslocamento do depocentro dos sedimentos cenozoicos, favorecendo sua sedimentação em bacias dianteiras sub-andinas, as quais são denominadas, em conjunto, sistema da Bacia Dianteira Amazônica (ou sinclinal neogênica). Assim, um novo ciclo sedimentar foi estabelecido, o qual foi caracterizado pela deposição de sedimentos de ambiente marinho raso e lacustre, intercalados por camadas arenosas e *red beds*. No Plioceno (~4 Ma), ocorre a elevação do Arco de Fitzcarrald, o qual resulta na separação entre os sistemas da Bacia Dianteira Amazônica do Norte (Colômbia, Equador e norte do Peru) e da Bacia Dianteira Amazônica do Sul (sul do Peru e norte da Bolívia). No Peru, as formações Yahuarango, Huayabamba, Pozo (membros inferior e superior), Chambira (Inferior e Superior), Pebas, Ipururo, Marañon e Juanjui integram o sistema da Bacia Dianteira Amazônica do Norte, abrangendo o intervalo Paleoceno–Plioceno. Já as formações Huayabamba, Bala, Quendeque, Charqui, Ipururo/Madre de Dios integram o sistema da Bacia Dianteira Amazônica do Sul no Peru, abrangendo o intervalo Paleoceno–Mioceno. No Brasil, a Bacia do Acre constitui uma extensão leste da Bacia Dianteira Amazônica, sendo que o novo ciclo de sedimentação iniciado pela orogenia andina está representado nesta bacia pela Formação Solimões (Roddaz *et al*., 2010; Wanderley-Filho *et al*., 2010).

5.1 BRASIL

O material fóssil de metatérios proveniente do Brasil aqui estudado foi coletado em trabalhos de campo realizados nas regiões do Alto Rio Juruá e do Rio Envira, Estado do Acre, entre 2008 e 2022. Ambas as regiões compreendem afloramentos da Formação Solimões, Bacia do Acre.

A Bacia do Acre está situada no noroeste brasileiro, entre os paralelos de 6ºS e 9ºS e meridianos 72º30'O e 74ºO. Está limitada geologicamente na parte leste pelo Arco de Iquitos, que a separa da Bacia do Solimões. A Bacia do Acre é, de acordo com as classificações de depozonas de bacias dianteiras (*foreland*), uma bacia de fosso dianteiro (*foredeep*), ou seja, zona com maior capacidade de receber sedimentos numa bacia *foreland*, com maior espessura. Foi depositada sobre uma litosfera rígida e seu registro do Fanerozoico é composto por 1.500 m de sedimentos paleozoicos, recobertos por sedimentos mesozoicos e cenozoicos, os quais podem atingir até 4.000 m e 2.000 m em espessura. No total, a Bacia do Acre cobre uma área de aproximadamente 150.000 km² e está presente no Acre e no Estado do Amazonas, na Bacia do Solimões. A porção inferior da Formação Solimões corresponde às formações peruanas Pozo e Chambira. Já a porção superior da Formação Solimões corresponde às formações Pebas e Ipururo, do norte do Peru, e à Formação Madre de Dios, do sul do Peru (Figura 33) (Cunha, 2007; Wanderley-Filho *et al*., 2010).

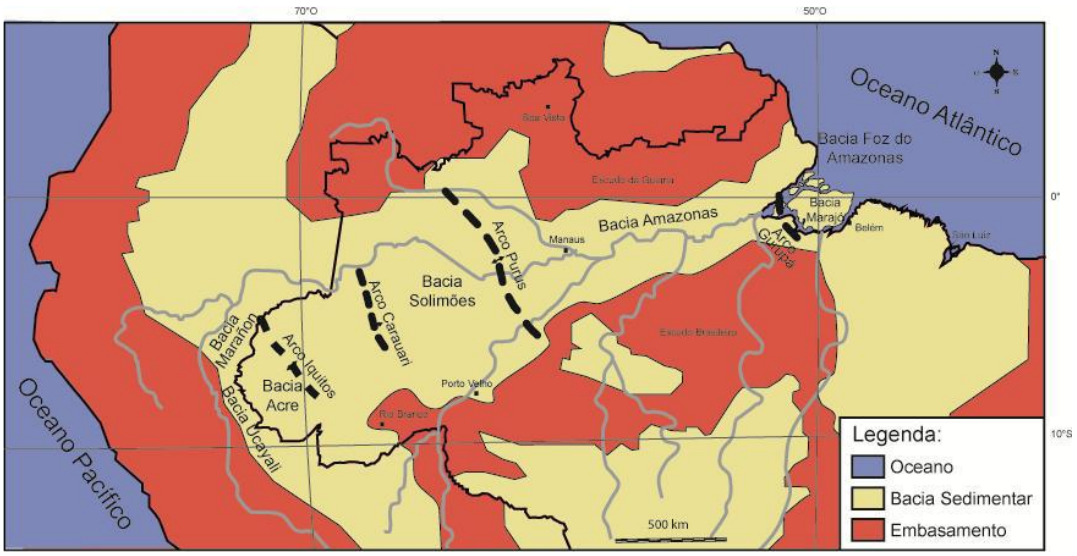


Figura 33. Parte do norte da América do Sul, com as principais bacias sedimentares brasileiras assinaladas, dentre elas a Bacia do Acre. Fonte: Rodrigues *et al*. (2016).

A Formação Solimões corresponde ao último ciclo deposicional da Bacia do Acre, com a sequência Eoceno inferior–Plioceno, representada por sedimentos finos flúvio-lacustres (Figura 34). Trata-se do ciclo de sedimentação estabelecido após as primeiras fases da orogenia andina, tendo sido principalmente afetada por esta durante o Mioceno–Plioceno (Fase Quéchua), constituindo a única bacia do território brasileiro efetivamente submetida à tectônica andina (Cunha, 2007). Os níveis mais superiores da Formação Solimões afloram principalmente nas margens dos rios que a cortam (rios Purus, Juruá, Moa, Caeté, Acre, Iaco, dentre outros) e em cortes de estrada (Lacerda *et al*., 2020). Recentemente foram obtidas as primeiras datações máximas numéricas para afloramentos da Formação Solimões, utilizando-se o método de datação U-Pb em zircões detríticos, os quais foram coletados em dois pontos, uma nas margens do Rio Purus e o outro no Rio Acre, obtendo-se 8.9 ± 0.13 Ma e 8.5 ± 0.5 Ma (i.e., Tortoniano, Neomioceno), respectivamente (Bissaro Júnior *et al*., 2019). Tais idades concordam com idades sugeridas por dados biocronológicos baseados na fauna fóssil registrada para o sudeste do AC, posicionada na SALMA Huayqueriense, o que também foi sugerido através da análise de palinormorfos provenientes do afloramento Patos, no Rio Acre (Negri *et al*., 2010; Ribeiro *et al*., 2013; Kerber *et al*., 2017; Leite *et al*., 2020; Hsiou *et al*., 2022). Análises palinoestratigráficas realizadas com material coletado próximo à cidade de Cruzeiro do Sul também indicam uma idade miocênica para a Formação Solimões, além de indicar que esta se correlaciona com as formações peruanas Pebas e Ipururo (Silva-Caminha *et al*., 2020). Os mesmos autores também sugerem que uma incursão marinha ocorreu na região entre o final do Mesomioceno e o Neomioceno, estendendo em 400 km ao sul a amplitude previamente reportada para esta incursão marinha na Amazônia Ocidental (Silva-Caminha *et al*., 2020). No entanto, mais datações radiométricas fazem-se necessárias para a Formação Solimões, principalmente no Alto Rio Juruá, onde alguns registros fossilíferos vêm indicando idades mais antigas (Ribeiro *et al*., 2013 e referências aí citadas; Haag, 2019).

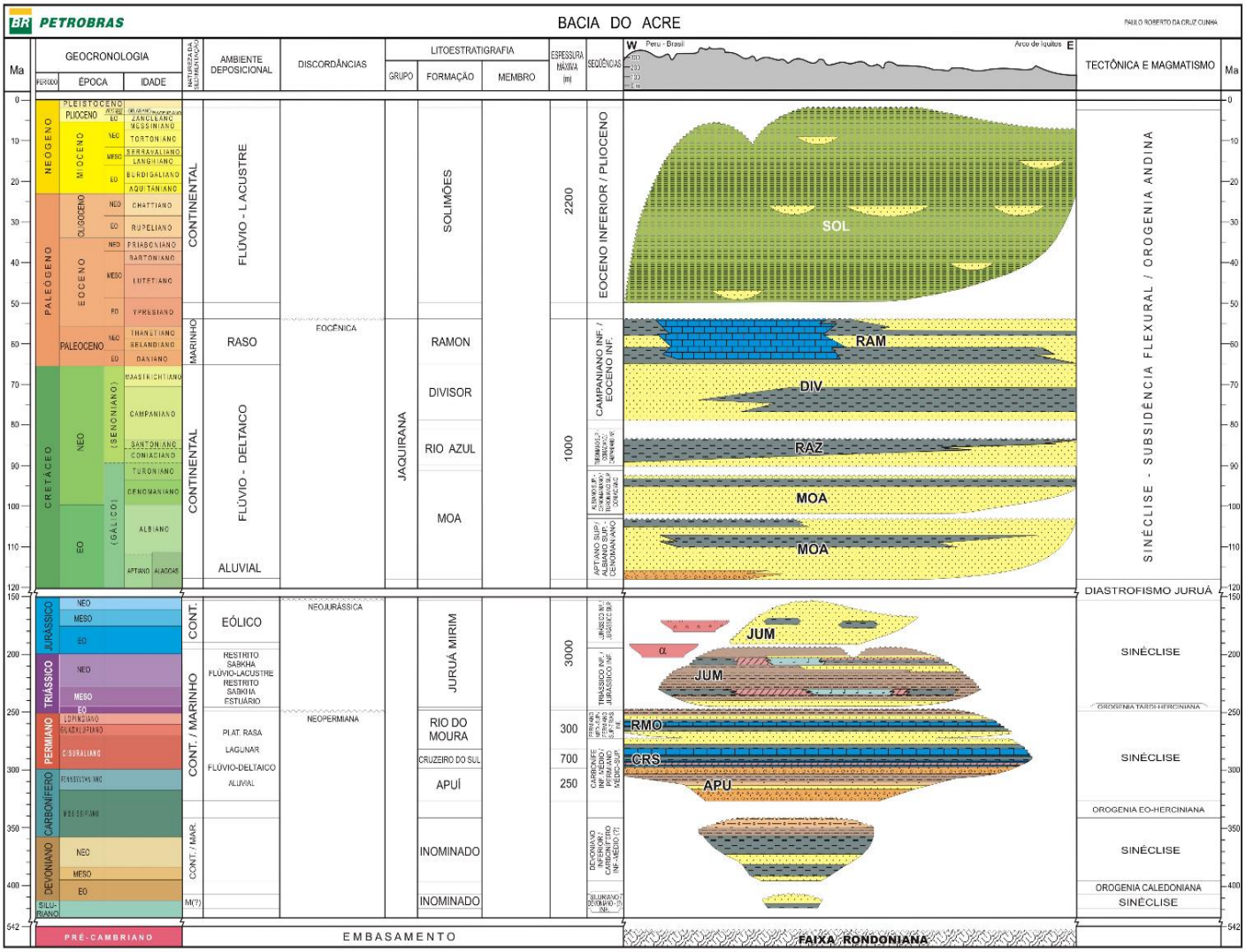


Figura 34. Carta estratigráfica da Bacia do Acre. Fonte: Cunha (2007).

Segundo Rancy (1985), os primeiros fósseis reportados para o atual Estado do Acre foram coletados em 1886 pelo geólogo inglês William Chandless, em localidades do Rio Acre. O potencial e registro fossilífero da Formação Solimões são reconhecidos há décadas (e.g., projeto RADAMBRASIL (Radambrasil, 1977). No final do século XIX e durante o século XX, foram realizadas numerosas coletas e registros de fósseis em expedições de campo no Acre (e.g., Simpson & Paula-Couto, 1981; Paula-Couto, 1982, 1983a, b). Os trabalhos de campo na região são preferencialmente durante o período de estiagem amazônica (maio a outubro), quando o nível das águas está baixo e as barrancas dos rios se tornam visíveis e acessíveis (Souza-Filho & Guilherme, 2015). Também se encontram afloramentos ao longo da BR-364, no trecho que liga as cidades de Rio Branco e Cruzeiro do Sul (Lacerda *et al*., 2020).

Diversos grupos de vertebrados fósseis já foram reportados para a Formação Solimões. No que se refere aos mamíferos, dentre os mais frequentes estão Rodentia (e.g., Negri & Ferigolo, 2004; Kerber *et al*., 2016, 2017, 2018, 2019a, b, 2022; Fontoura *et al*., 2022), Xenarthra (e.g., Paula-Couto, 1983a, b; Mones, 1986; Bocquentin & Guilherme, 1999; Negri, 2004) e Notoungulata (e.g., Paula-Couto, 1944, 1982; Frailey, 1986; Bocquentin & Silva, 1994; Bayá & Bocquentin, 1997; Bergqvist *et al*., 2002; Ribeiro *et al*., 2005). Também foram encontrados restos de outros táxons de mamíferos tais como Litopterna, Astrapotheria, Proboscidea, Cetartiodactyla, Primates e Chiroptera (e.g., Bergqvist *et al*., 2002; Negri *et al*., 2010; Ribeiro *et al*., 2013; Hsiou *et al*., 2022). Quanto aos metatérios, somente um táxon foi registrado para a Formação Solimões, sendo a mais antiga espécie de *Didelphis* - *D*. *solimoensis*, descrita por Cozzuol *et al*. (2006) para um afloramento no Rio Acre. Já quanto aos répteis, seu registro na Formação Solimões é bastante conspícuo, com uma grande diversidade de formas extintas de crocodilomorfos e quelônios. Os crocodilomorfos registrados pertencem às famílias Alligatoridae (*Acresuchus*, *Caiman*, *Mourasuchus* e *Purussaurus*) e Gavialidae (*Brasilosuchus*, *Gryposuchus* e *Hesperogavialis*), além do suposto crocodiloide *Charactosuchus* (e.g., Rodrigues, 1892; Price, 1964; Bocquentin & Souza-Filho, 1990; Souza-Filho, 1998; Souza-Filho *et al*., 1993, 2019; Cidade *et al*., 2019). Os quelônios pertencem a três famílias: Podocnemididae (*Podocnemys* e *Stupendemys*), Chelidae (*Chelus*) e Testudinidae (*Chelonoidis*) (Rodrigues, 1892; Campos, 1977; Campos & Broin, 1981; Broin *et al*., 1993; Gaffney *et al*., 1998; Bocquentin *et al*., 2001; Carvalho *et al*., 2002; Bocquentin & Melo, 2006). Os Squamata também estão presentes no registro fóssil da Formação Solimões, tendo sido mencionados por Bocquentin *et al*. (1996), Latrubesse *et al*. (1997), Souza-Filho (1998) e Negri (2004). Em seguida, se confirmou a presença de largartos Teiidae (Hsiou *et al*., 2009) e serpentes Boidae, “Colubridae” e prováveis serpentes basais do gênero *Colombophis* (Hsiou & Albino, 2009, 2010; Hsiou *et al*., 2010). Já quanto aos registros de aves para Formação Solimões, estes são raros, sendo todos da família Anhingidae (*Macranhinga* e *Anhinga*) (Alvarenga & Guilherme, 2003). Os peixes, por sua vez, estão representados, por exemplo, pelos caracídeos do gênero *Colossoma*, eritrinídeos do gênero extinto *Paleohoplias* (Gayet *et al*., 2003) e pelos pimelodídeos *Phractocephalus* (Aguilera *et al*., 2008).

O registro fóssil de invertebrados, palinomorfos, assim como da paleoflora da Formação Solimões é menos conhecido. Foram registrados moluscos, tais como o bivalve *Pachydon acreanus* e o gastrópode *Ampullaria*, na região entre os municípios de Feijó e Mâncio Lima (Maury, 1937). Também foram reportados para afloramentos nos rios Purus e Acre gastrópodes das famílias Ampullaridae, Thiaridae e Cochliopidae (Souza *et al*., 2021). Folhas fósseis e fragmentos de madeiras (carbonizados e/ou piritizados) foram assinalados pela expedição de Pedro de Moura em 1936 (Rodrigues *et al*., 2016). Lenhos silicificados foram reportados para os rios Acre, Juruá, Purus, Riozinho, Santa Rosa e no Vale do Rio Moa (Machado *et al*., 2006, 2012; Kloster *et al*., 2015). Recentemente também foi realizada uma análise palinoestratigráfica para o Vale do Juruá, a qual atribui uma idade Oligoceno superior–Mioceno superior/Plioceno inferior para os depósitos, com o registro de elementos marinhos (acritarcas, dinoflagelados e escolecodontes), grande quantidade de algas e esporos e palinoflora dominada por plantas aquáticas, pteridófitas, epífitas, lianas, gramíneas, arbustos e algumas ilhas de floresta (com espécies arbóreas das famílias Poaceae, Fabaceae, Cheirolepidiaceae, Arcaceae, Podocarpaceae, Bombacaceae, Ulmaceae, Euphorbiaceae, dentre outras), sugerindo um clima quente e úmido para a região (Haag, 2019).

Como mencionado anteriormente, os restos de metatérios provenientes da Formação Solimões aqui estudados provêm dos afloramentos PRJ 25 e PRJ 33, região do alto Rio Juruá, e PRE 06 nas margens do Rio Envira (Figura 35).

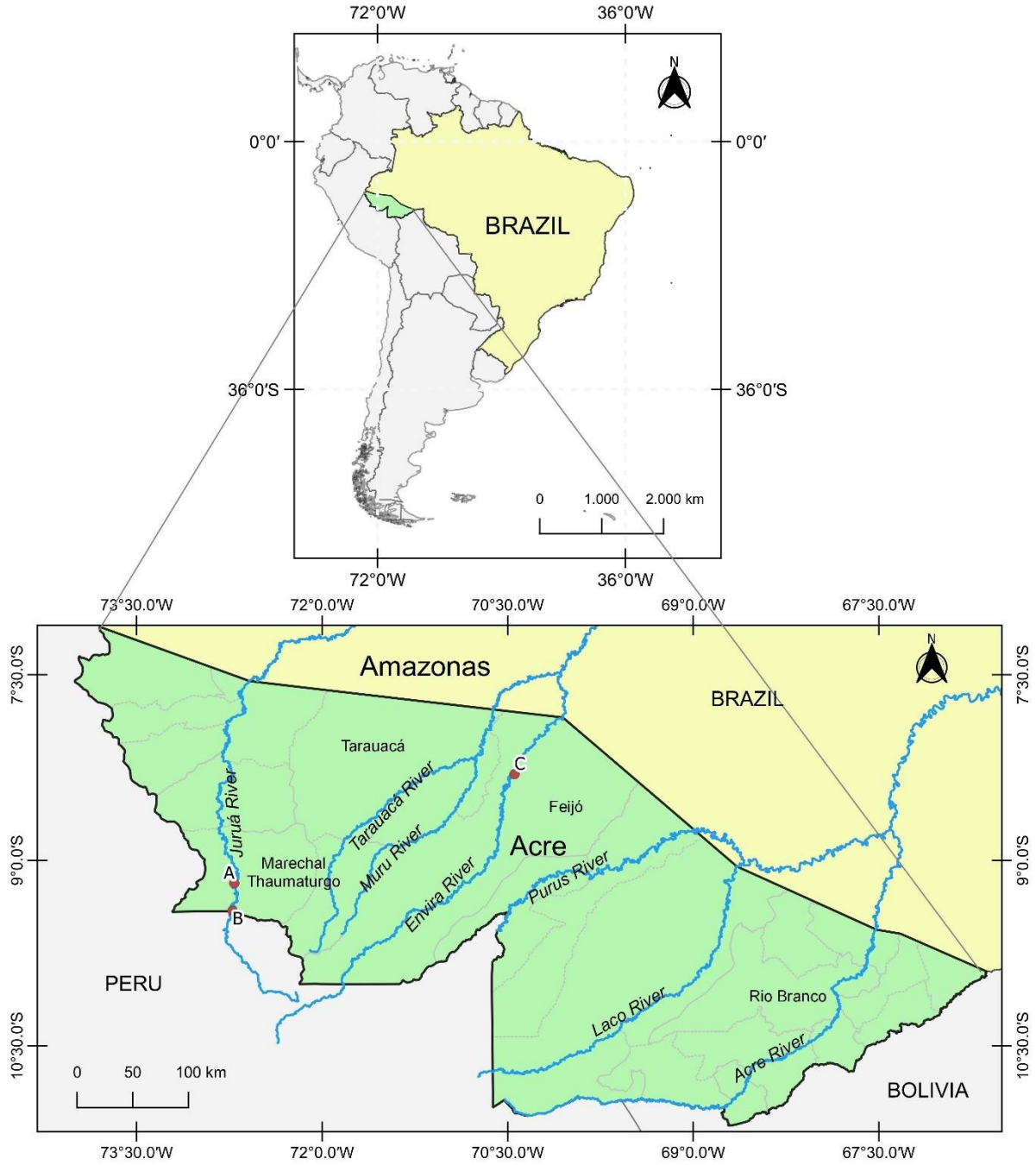


Figura 35. Mapa com a localização dos afloramentos onde foram os espécimes fósseis de metatérios na Formação Solimões, Estado do Acre, Brasil. Alto Rio Juruá: **A**, PRJ 25, **B**, PRJ 33. Rio Envira: **C**, PRE 06.

5.1.1 Alto Rio Juruá

Os trabalhos de campo na região do Alto Rio Juruá durante os quais foram coletados os fragmentos fósseis de metatérios aqui estudados foram efetuados no trecho do rio que se estende do município de Marechal Thaumaturgo até a comunidade de Foz do Breu, divisa com o Peru, entre 2008 e 2022. Foram estudados em detalhe aproximadamente 30 localidades, as quais foram designadas como PRJ (Ponto Rio Juruá). A escolha dos pontos de estudo foi determinada pelos dados publicados por Simpson & Paula Couto (1981), confirmando e localizando outras localidades durante a expedição realizada no ano de 2008 (Figura 36).

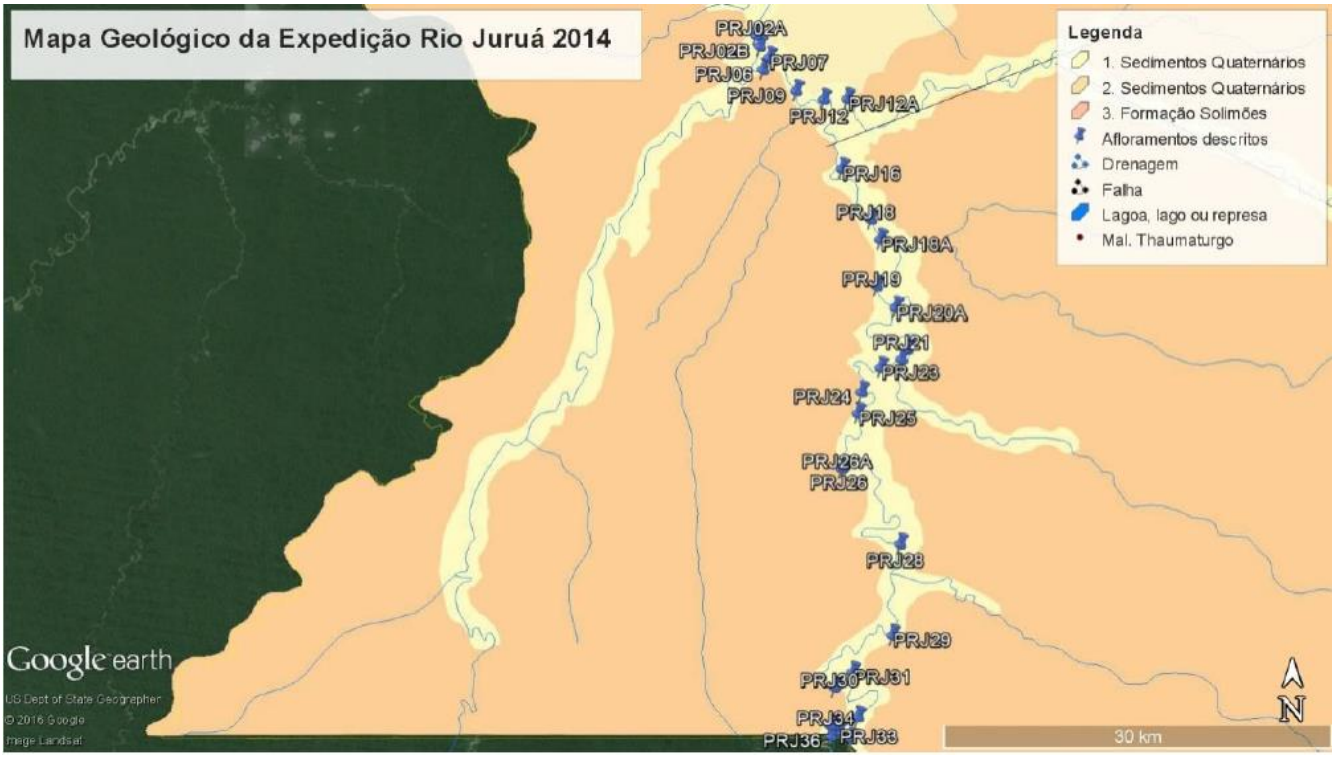


Figura 36. Mapa dos das localidades visitadas e amostradas nas expedições de campo no rio Juruá, Acre, Brasil. Fonte: Rodrigues *et al*. (2016).

Durantes as expedições, foram encontrados restos de metatérios em duas localidades no alto Rio Juruá, PRJ 25 e PRJ 33.

A localidade PRJ 25 (9°11’06.8”S 72°42’37.2”O) está situada perto da propriedade de Belford, na margem esquerda do Rio Juruá. Inclui uma porção horizontal e uma vertical, identificadas como H e V, respectivamente, na Figura 37. A

parte horizontal corresponde às litologias entre 0 e 0,45 m no perfil estratigráfico. Ela é formada pela intercalação de siltito vermelho e arenito fino amarelado, ambos com matriz carbonática e acamamento suavemente inclinado (25–30º). Já a parte vertical corresponde às litologias entre 0,5 e 1,6 m do perfil e é constituída pela mesma sequência sedimentar da parte horizontal. No entanto nota-se que há quatro níveis de concreções carbonáticas contínuas ao longo dos intervalos de siltito e as camadas são menos inclinadas que as da outra parte do afloramento (10–15º). A parte horizontal do afloramento é extensivamente coberta por areias e seixos fluviais holocênicos ricos em fósseis, claramente fora de contexto. Estes depósitos alóctones estão relacionados com a erosão dos estratos a montante do rio, os quais foram transportados pelas correntes e depositados neste afloramento (Figura 37C). Os fragmentos fósseis incluem madeira silicificada e restos de vertebrados. Estes últimos indicam diferentes idades, com, por exemplo, restos de *Astrapotheria* e de *Purussaurus*. Todos os espécimes fósseis encontrados no PRJ 25 provêm destes sedimentos fora de contexto estratigráfico, incluindo o único resto dentário de metatério. Kerber *et al*. (2017) também reportaram para o PRJ 25 restos de roedores caviomorfos, provavelmente de idade Mioceno (Potamarchinae e Erethizontidae não identificados).

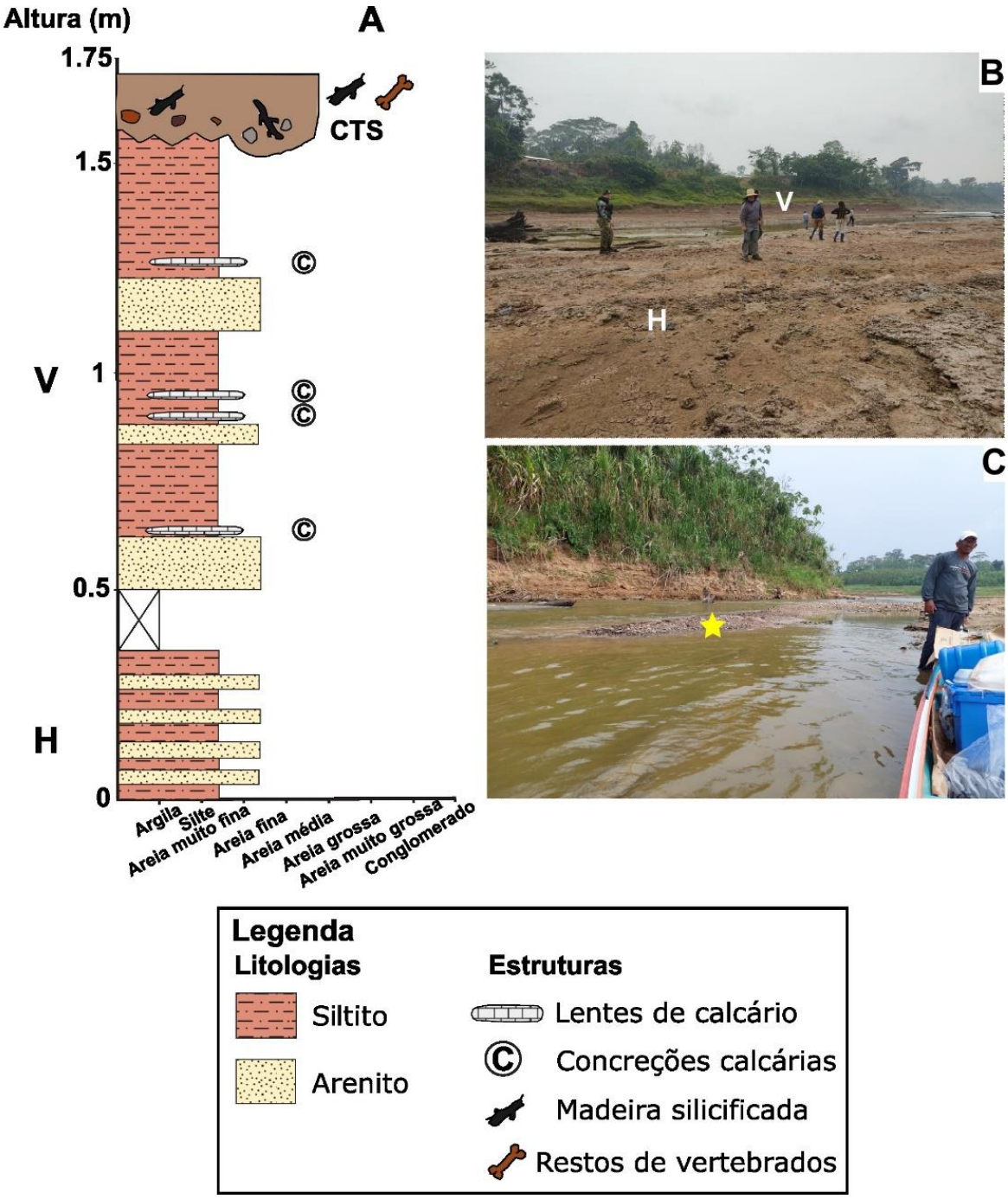


Figura 37. A, Seção estratigráfica e **B-C** fotografias da localidade PRJ 25, com a Formação Solimões como substrato, localizada na margem esquerda do Rio Juruá, Estado do Acre, Brasil. **CTS** = conglomerado holocênico, com uma mistura de seixos e restos fossilizados Mioceno–Holoceno (na sua maioria madeira silicificada e vertebrados), que podem cobrir indiferentemente quaisquer camadas miocênicas. Os fósseis de vertebrados foram encontrados no CTS como na imagem C (estrela amarela). Abreviações: **H**, horizontal; **V**, vertical.

A localidade PRJ 33 (9°24’24.6”S 72°43”27.6”O) está situada na margem esquerda do Rio Juruá e tem 2–3 m de altura aproximadamente (Figura 38). Está conformada por uma camada de siltito avermelhado maciço com fraturas horizontais (e algumas falhas de pequeno porte) preenchidas por concreções carbonáticas. Essas fraturas tendem a ser descontínuas lateralmente no afloramento. O siltito está em contato erosivo com um nível centimétrico (10–15 cm) de microconglomerado fossilífero. Este nível de microconglomerado é composto por concreções carbonáticas e raros clastos de quartzo suportados por uma matriz síltica-arenosa avermelhada. Esse conglomerado está em contato abrupto com uma camada de arenito fino acinzentado maciço no topo da seção. Nesta localidade, dois espécimes de Metatheria foram coletados no nível conglomerático (i.e., *in situ*) e um terceiro espécime foi coletado em uma acumulação de areia com restos fossilizados retrabalhados, a qual se encontrava na base do afloramento, próximo ao rio. O resto fóssil coletado neste ponto, chamado doravante de PRJ 33’, não possui, portanto, contexto estratigráfico. Ribeiro *et al*. (2013) e Kerber *et al*. (2017) reportaram para PRJ 33’ restos fósseis do roedor caviomorfo *Eoincamys*, típico do Paleógeno.

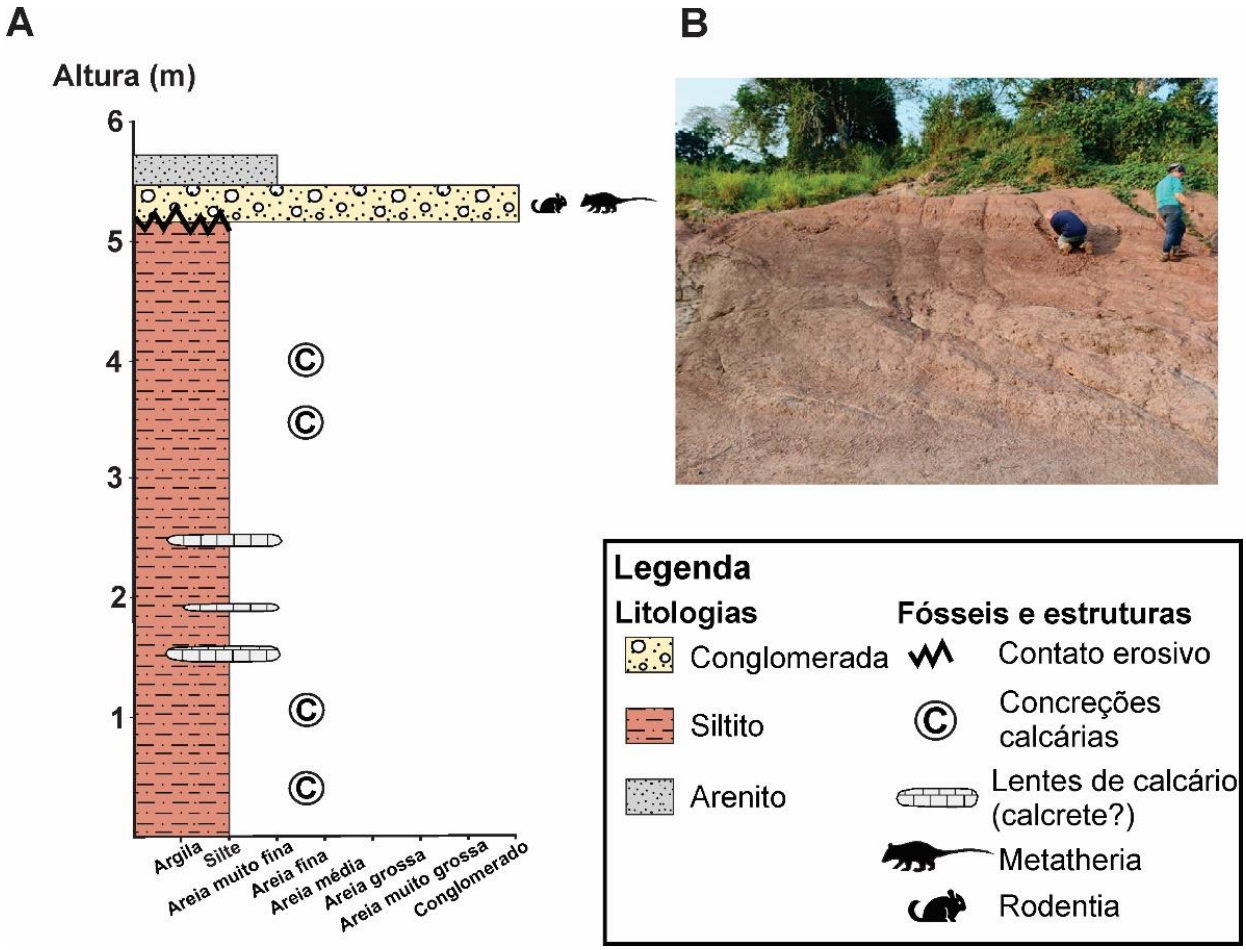


Figura 38. A, Seção estratigráfica e **B**, foto da localidade PRJ 33, Mioceno, Formação Solimões, localizada na margem esquerda do Rio Juruá, Estado do Acre, Brasil.

5.1.2 Rio Envira

No que se refere ao Rio Envira, foram realizados trabalhos de campo nos anos de 2008, 2010, 2019 e 2022. As expedições partiram do município de Feijó e não se distanciaram muito desta cidade (cerca de duas horas de barco). As localidades foram registradas sob a sigla PRE (Ponto Rio Envira). Os restos de metatérios foram coletados no ponto de estudo PRE 06 (Figura 39), também denominado localidade “Coqueiros”, situado sob as coordenadas 08°18’12.6”S 70°26’39.9”O. Nesta localidade, foram prospectados quatro pontos lateralmente equivalentes: A, B, C e D. Somente no ponto C foram encontrados restos de metatérios. A sequência sedimentar nos pontos de amostragem A a C é composta por camadas de argilitos verde acinzentados e vermelhos em contato erosivo com um nível conglomerático muito

fossilífero. O conglomerado é composto por concreções carbonáticas e numerosos fragmentos fósseis (tais como de peixes, répteis e mamíferos) suportados por matriz síltica-arenosa. Esse conglomerado está em contato brusco com camadas intercaladas de argila marrom e areia muito fina a fina amarelada (ritmito). Os pontos A, B e C pertencem ao mesmo horizonte estratigráfico. No entanto, o ponto de amostragem D está fora de contexto estratigráfico, representando uma acumulação de fragmentos de fósseis encontrados na planície de inundação do Rio Envira.

O conteúdo fossilífero do PRE 06, já descrito na literatura, constitui-se de madeira silificada, com uma rica flora semelhante à encontrada atualmente na região (Kloster *et al*., 2017), além de grande diversidade de roedores caviomorfos encontrados nos pontos A–C (*Cardiatherium* sp., Caviidae, Hydrochoerinae; *Potamarchus* sp. e cf. *Pseudopotamarchus*, Dinomyidae, Potamarchinae; e *Neoepiblema* sp., Neoepiblemidae; Fontoura *et al*., 2022), os quais sugerem uma idade Neomioceno.

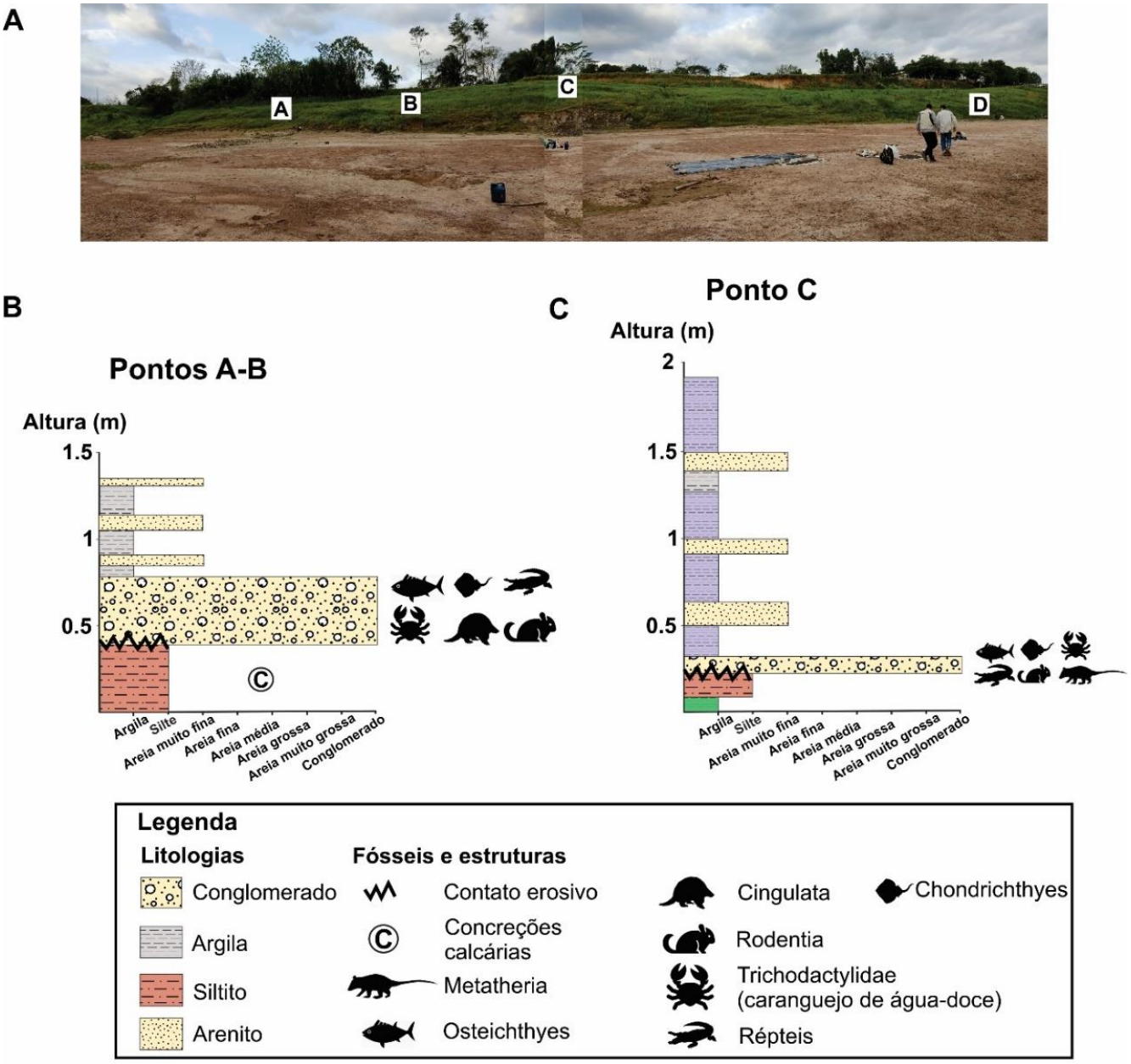


Figura 39. A, Foto e **B–C**, seções estratigráficas da localidade PRE 06, Neomioceno, Formação Solimões, localizada na margem direita do Rio Envira, Estado do Acre, Brasil.

5.2 PERU

Os restos de metatérios estudados no presente projeto provêm do centro-leste do Peru, Região Amazônica. As três regiões estudadas – Contamana, Bacia do Rio Huallaga e Atalaya – integram a porção norte da Bacia Dianteira Amazônica (*North Amazonian foreland basin*).

5.2.1 Contamana

A região de Contamana, Departamento de Loreto, está localizada na bacia do Rio Ucayali, a noroeste do Arco de Fitzcarrald (Figura 40). Estão presentes na área dobramentos de estrutura noroeste-sudeste causados pela tectônica andina, os quais permitem o acesso a uma espessa seção estratigráfica, com um registro sedimentar longo e contínuo do Jurássico ao Holoceno. No total, ao menos 34 localidades fossilíferas foram identificadas na região, com numerosos restos fósseis dos mais diversos grupos: moluscos, artrópodes (ostracodes e crustáceos), microorganismos (foraminíferos, poríferos, algas, dinoflagelados), plantas (palinomorfos, carófitas, sementes, frutos e madeira silicificada), além de vertebrados como peixes, anfíbios, répteis e mamíferos (Antoine *et al*., 2016).

Mais especificamente, ao longo do rio Cachiyacu, na chamada *Quebrada Cachiyacu*, assim como em uma nova estrada para *Quebrada Agua Caliente*, estão localizados depósitos cenozoicos, com idades indo do início do Paleoceno ao Neomioceno–?Plioceno, os quais foram explorados em trabalhos de campo realizados anualmente de 2008 a 2014 (Antoine *et al*., 2016).

As localidades foram nomeadas CTA, seguido de número de acordo com a ordem em que foram encontradas. Os níveis fossilíferos possuem em média de 10 a 50 cm de espessura, sendo que nenhum ultrapassa 1 m. Devido a taxa hipotética de sedimentação calculada para a região ser de 1 mm por ano (Roddaz *et al*., 2010), considera-se que a mistura temporal dos restos nos níveis fossilíferos é praticamente inexistente. Da base ao topo da série cenozoica, foi reconhecida a base da Formação Huchpayacu (Eopaleoceno); Formação Pozo (Mesoeoceno + ?Neoeoceno); seções completas da Formação Chambira (Eooligoceno–final do Eomioceno); Formação Pebas (final do Eomioceno ao início do Neomioceno); e Formação Ipururo (Eomioceno–?Plioceno) (Figuras 41 e 42) (Antoine *et al*., 2016).



Figura 40. A, Mapa da América do Sul apontando a localização de Contamana, Peru. **B**, Localização dos perfis cenozoicos na região de Contamana. Modificado de Antoine *et al*. (2016).

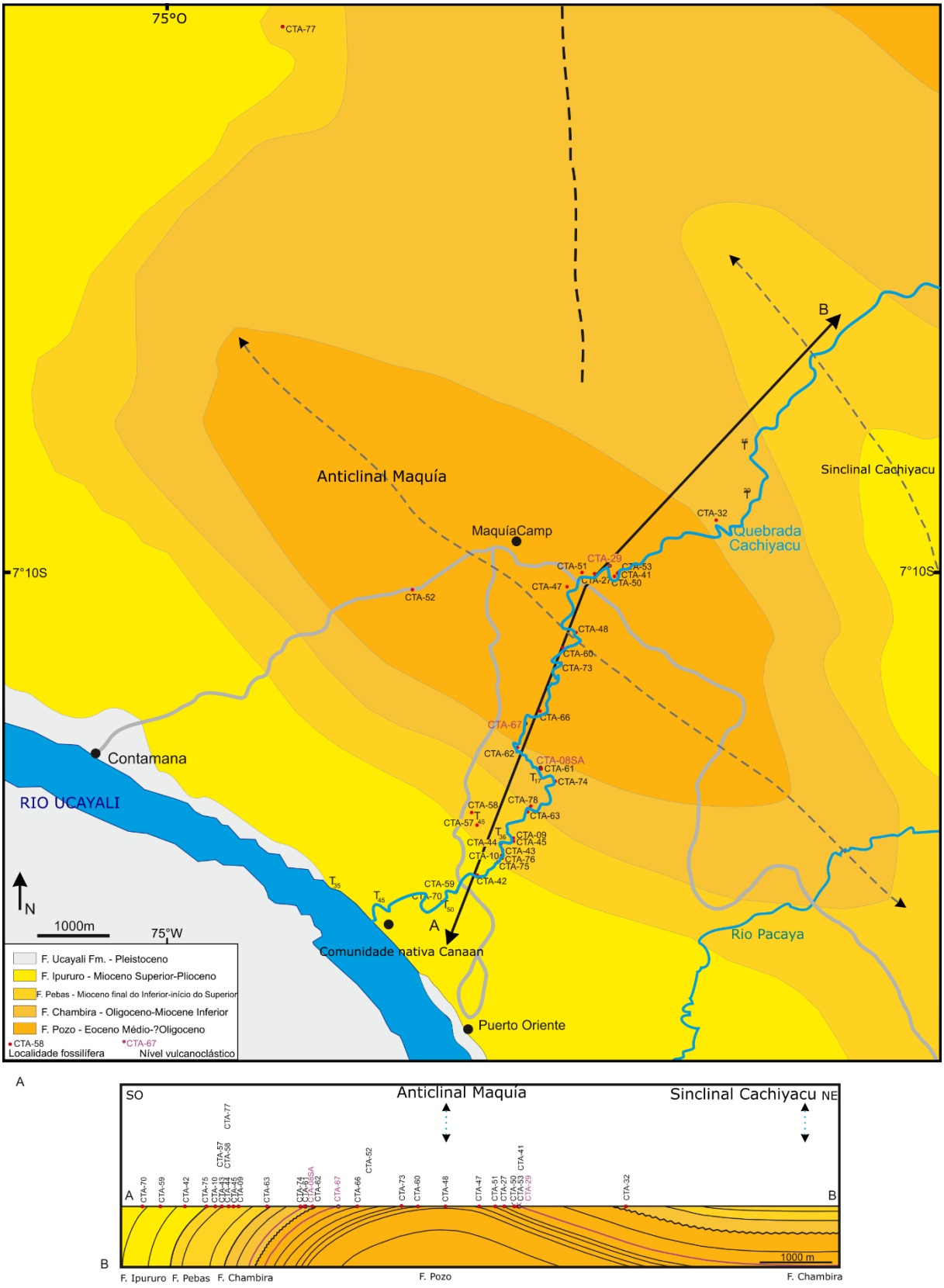


Figura 41. Mapa geológico da região de Contamana, Peru. Modificado de Antoine *et al*. (2016).

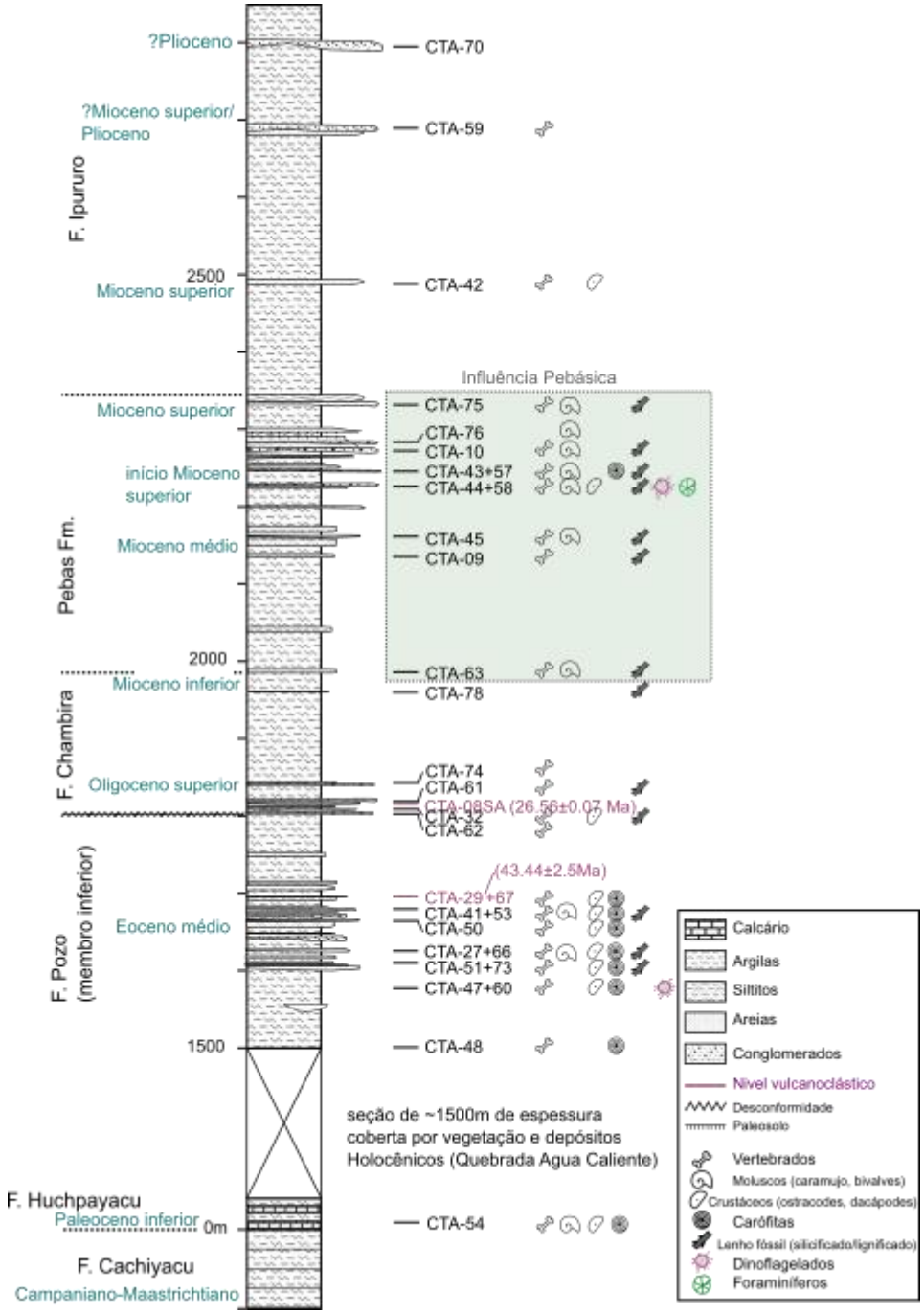


Figura 42. Seção sintética dos depósitos cenozoicos na região de Contamana, Peru. Modificado de Antoine *et al*. (2016).

A cronoestratigrafia dos depósitos de Contamana foi realizada a partir de dados bioestratigráficos (com o uso de fósseis de dinoflagelados, esporos, pólen, carófitas, foraminíferos, ostracodes, moluscos e vertebrados), assim como de dados radioisotópicos. Foram realizadas datações $^{40}Ar/^{39}Ar$ em grãos de feldspato provenientes da turfa CTA-29, obtendo-se a idade de 43,44 ± 2,5 Ma. Também foram

datados zircões detríticos provenientes de CTA-08SA, obtendo-se a idade 26,56 ± 0,07 Ma (Antoine *et al*., 2016).

Com relação ao vasto registro fóssil das localidades em Contamana, em Antoine *et al*. (2016) os autores apresentam um levantamento geológico e paleontológico dos afloramentos da região de Contamana, incluindo listas faunísticas com identificações taxonômicas preliminares do material fóssil descoberto. Foram estudados em detalhe restos fósseis de caranguejos de água doce oriundos de Contamana, das formações Pozo e Chambira, com a identificação de três táxons provavelmente pertencentes à família Trichodactylidae, registrando pela primeira vez caranguejos de água doce no Eoceno, o que seria o registro mais antigo deste grupo (Klaus *et al*., 2017). Fragmentos fósseis de raias de água doce (família Potamotrygonidae) provenientes de Contamana também foram objeto de estudos taxonômicos detalhados, com o registro de quatro espécies, dentre elas *Potamotrygon ucayalensis* do Mesoeoceno, a qual constitui o registro mais antigo da família na América do Sul (Adnet *et al*., 2014; Chabain *et al*., 2017). Dentre os mamíferos, os depósitos de Contamana revelaram fósseis dos primeiros roedores histricognatos da América do Sul, *Cachiyacuy contamanensis*, *Cachiyacuy kummeli* e *Canaanimys maquiensis*, descritos para o afloramento CTA-27 (Antoine *et al*., 2012). De fato, as localidades de Contamana revelaram notável diversidade de fósseis de roedores caviomorfos, com 20 táxons (superfamílias Cavioidea e Octodontoidea) descritos para a Formação Pozo, localidades CTA-27, CTA-47, CTA-51, CTA-73, CTA-66 e CTA-29 (Boivin *et al*., 2017a). Também foram registrados 14 táxons das superfamílias Erethizontoidea, Octodontoidea e Chinchilloidea para a Formação Chambira (CTA-61 e CTA-32) (Boivin *et al*., 2017b). Ademais, foram encontrados restos fósseis de primatas, com a descrição de dois táxons do início do Neomioceno da Formação Pebas (Marivaux e*t al*., 2016a) e uma nova espécie do Neooligoceno da Formação Chambira (*Canaanimico amazonensis*, Marivaux *et al*., 2016b).

Os fragmentos fósseis de metatérios da ordem Polydolopimorphia encontrados na região de Contamana provêm das localidades: CTA-27, CTA-29, CTA-43, CTA-47, CTA-51 e CTA-66 (Quadro 13).

Quadro 13. Afloramentos da região de Contamana, Peru, contendo fósseis de metatérios da ordem Polydolopimorphia.

Localidade	Coordenadas	Idade	Formação	Ambiente deposicional
CTA-43	07º36.497'S 74º95.793'O	Início do Neomioceno	Pebas	Interface de maré
CTA-66	07º34.876'S 74º95.431'O	Final do Mesoeoceno	Pozo, Membro Inferior	Fluvial
CTA-29	07º32.859'S 74º94.556'O	Final do Mesoeoceno	Pozo, Membro Inferior	Fluvial
CTA-27	07º33.011'S 74º94.733'O	Final do Mesoeoceno	Pozo, Membro Inferior	Fluvial
CTA-51	07º32.948'S 74º94.92'O	Final do Mesoeoceno	Pozo, Membro Inferior	Fluvial
CTA-47	07º33.113'S 74º95.127'O	Mesoeoceno	Pozo, Membro Inferior	Fluvial com influência marinha

As localidades CTA-47, CTA-51, CTA-27, CTA-29 e CTA-66 (Figuras 43, 44 e 45; Quadro 13) constituem afloramentos do Membro Inferior da Formação Pozo, o qual seria o único membro desta formação aflorante na *Quebrada Cachiyacu*. Consistem em argilitos vermelhos e paleossolos variegados com esparsas veias de anidrita, alternados com lentes de arenito. Particularmente nas localidades CTA-51, CTA-27, CTA-29 e CTA-66, estes níveis de arenito são acinzentados a amarelados, massivos e não consolidados, com nódulos calcários milimétricos de origem diagenética, os quais contêm restos fósseis incorporados. A localidade CTA-27 é considerada como final do Mesoeoceno, ~41.6–40.94 Ma (início do Barranquense). Trata-se de uma localidade excepcionalmente rica em conteúdo fossilífero, com restos de moluscos, crustáceos e 49 táxons de vertebrados, incluindo: peixes cartilaginosos, peixes ósseos, anfíbios, lagartos, serpentes, quelônios, crocodilomorfos e mamíferos, dentre os quais roedores, ungulados nativos sul-americanos, xenartros, quirópteros e numerosos restos de metatérios. Em CTA-27 também foram encontrados restos de plantas (palinomorfos, madeira silicificada, carófitas, *charcoal*, sementes), sendo que os palinomorfos recuperados possuíam grande diversidade, indicando um paleoambiente de floresta tropical, sem evidências de savanas. As localidades CTA-47 e CTA-51 encontram-se estratigraficamente abaixo de CTA-27, enquanto que CTA-

29 e CTA-66 encontram-se estratigraficamente acima de CTA-27. Em todos estes afloramentos a associação fossilífera encontrada é bastante similar, todas exibindo notável riqueza fóssil, sendo seu conteúdo majoritariamente de origem continental (aquático ou terrestre). A única evidência de influência marinha na formação é a ocorrência, no nível mais inferior (CTA-47), dos dinoflagelados *Cleitosphaeridium*, *Leiosphaeridia* e *Spiniferites* (Antoine *et al*., 2016).



Figura 43. Afloramentos do Membro Inferior da Formação Pozo, final do Mesoeoceno, na região de Contamana, Peru. **A**, CTA-27 e **B**, CTA-47.



Figura 44. Afloramentos do Membro Inferior da Formação Pozo, final do Mesoeoceno, na região de Contamana, Peru. **A**, CTA-29 e **B**, CTA-51.



Figura 45. Afloramento CTA-66, Formação Pozo, final do Mesoeoceno, região de Contamana, Peru.

Já CTA-43 (Figura 46; Quadro 13) é um afloramento da Formação Pebas. A Formação Pebas aflora em alguns pontos a sudeste da Anticlinal Maquia em Contamana, os afloramentos compreendem principalmente siltitos azuis de planície de inundação e paleossolos vermelhos, esparsamente intercalados com canais conglomeráticos, ricos em lenho lignificado e/ou piritizado. Além de restos de metatérios Polydolopimorhia, uma rica fauna de vertebrados foi encontrada em CTA-43, com peixes, répteis e diversos mamíferos [Xenartha, Rodentia (grupo mais abundante e diverso), Primates]. A idade sugerida para CTA-43 é de início do Neomioceno (Mayoense), baseado nos táxons de metatérios e roedores encontrados. Considerando os demais afloramentos da Formação Pebas na região de Contamana, obteve-se um excelente registro de esporos e pólen, o que revelou uma ampla variedade de representantes de florestas tropicais, com grande abundância de táxons que habitavam nas proximidades de corpos d'água, especialmente de água doce. Este contexto fluvial era ocasionalmente perturbado por alagamentos marinhos, indicados por palinomorfos típicos deste ambiente (Antoine *et al*., 2016). A Formação Pebas correlaciona-se com o Sistema Pebas (*Pebas Mega-Wetland System*), citado anteriormente neste texto (Seção 3.6.2 O registro fóssil de Metatheria na Região Amazônica).



Figura 46. Afloramento CTA-43, Formação Pebas, final do Neomioceno, na região de Contamana, Peru.

5.2.2 Bacia do Huallaga

Os afloramentos estudados na região da Bacia do Huallaga, a qual também integra a porção norte da Bacia Dianteira Amazônica (*North Amazonian foreland basin*), estão localizadas no Departamento de San Martín, mais precisamente na zona sub-andina do Rio Huallaga. Partindo-se da capital do Departamento, Tarapoto, em direção sul, os sítios estão localizados em barrancas expostas às margens de estradas e dos rios Huallaga e Mayo, nas proximidades das cidades/vilarejos de Shapaja, Machungo, Juanjui e Balsayacu. A região foi prospectada anualmente entre 2012 e 2019. No total, 77 afloramentos fossilíferos foram reconhecidos, os quais foram nomeados TAR (de Tarapoto), seguido de um número de acordo com a ordem em que foram encontrados. As formações Yahuarango, Chambira, Pozo e Ipururo são aflorantes na região, com idades aproximadas indo do Neocretáceo (Maastrichtiano) ao Neomioceno. Os fósseis de metatérios Polydolopimorphia da região da Bacia do Huallaga, são provenientes de 14 localidades: TAR-01, TAR-14, TAR-20, TAR-21, TAR-44, TAR-45, TAR-47, TAR-55, TAR-56, TAR-72, TAR-74 e TAR-76 (Quadro 14). Estas localidades podem ser divididas de acordo com a seção estratigráfica onde estão localizadas, sendo elas: Balsayacu, Juanjui, Shapaja e Abra de Machungo. Ademais, também foram estudados restos de metatérios das ordens Didelphimorphia

e Paucituberculata da localidade TAR-31, também localizada na Bacia do Huallaga (Quadro 14).

As seções de Balsayacu e de Juanjui são afloramentos do Membro Inferior da Formação Pozo (*Pozo Sands*; Figura 47). As localidades TAR-44, TAR-45 e TAR-47 (Figura 48) integram a seção paleógena de Juanjui. Tal seção possui espessura de aproximadamente 1000 m e é recoberta pelos conglomerados fluviais sub-horizontais da Formação Juanjui (Plioceno/Pleistoceno). A 25 km desta seção situa-se a seção paleógena de Balsayacu (TAR-55, TAR-56, TAR-76, Figura 49 e 50), a qual é menor do que a de Juanjui. Ambas as seções são constituídas de microconglomerados pouco consolidados, com nódulos calcários, seixos e restos vegetais, organizados em canais lenticulares com espessuras indo de aproximadamente 10 cm a alguns metros, os quais teriam origem flúvio-deltaica. Ambas as seções, Juanjui e Balsayacu, possuem aproximadamente a mesma idade, Eoceno. As localidades de Balsayacu parecem preceder a seção de Juanjui, sendo do Mesoeoceno, visto a similaridade encontrada desta com o topo da sequência fossilífera do Membro Inferior da Formação Pozo aflorante em Contamana (CTA-27 e CTA-29). Por exemplo, na seção de Balsayacu estão presentes restos de raias de água doce, antes restritos à Formação Pozo aflorante em Contamana, o que também demonstra a ausência de influência marinha nestes níveis. A seção de Juanjui seria do Neoeoceno e possui táxons com afinidades marinhas (gênero *Pristis*, Chondrichthyes), o que é característico da Formação Pozo, a qual possui um pico de influência marinha em níveis superiores (Assemat *et al*., 2019). Em ambas as seções foram encontrados, além dos metatérios, restos de crustáceos, peixes, crocodilomorfos, roedores, ungulados nativos sul-americanos, dentre outros. Foram estudados em detalhe os restos de roedores provenientes de ambas as seções (Juanjui: TAR-45, TAR-46 e TAR-47; Balsayacu: TAR-55/TAR-55bis e TAR-56), com a descrição de 11 táxons para o intervalo Mesoeoceno a início do Eooligoceno (Assemat *et al*., 2019), os quais teriam uma morfologia intermediária entre os fósseis descritos para os afloramentos mais antigos de Contamana (e.g., CTA-27) e os da seção de Shapaja (Boivin *et al*., 2018) e Santa Rosa (Frailey & Campbell, 2004). E mais, recentemente, Boivin *et al*. (2021) reportaram quatro táxons adicionais de roedores caviomorfos para seção de Balsayacu (TAR-55/TAR-55bis, TAR-76 e TAR-77), os quais sugerem que estas

localidades seriam um pouco mais recentes que CTA-27 e mais antigas que a seção de Shapaja.

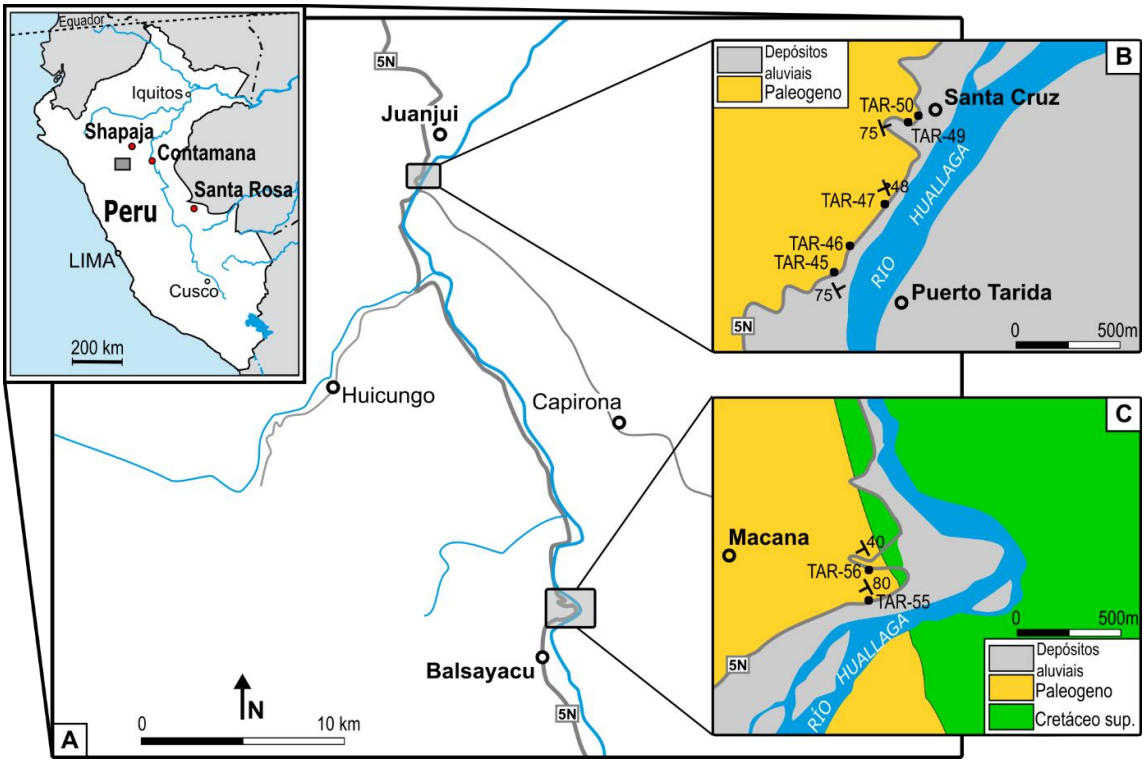


Figura 47. A, Mapa mostrando a localização das seções estratigráficas de Juanjui e Balsayacu, próximas às cidades de Juanjui e Balsayacu, respectivamente. **B–C**, mapas aproximados com a localização dos afloramentos das seções estratigráficas paleógenas de Juanjui e Balsayacu, Bacia do Huallaga, Peru.

Quadro 14. Localidades da Bacia do Huallaga, Peru, contendo fósseis de metatérios.

Localidade	Coordenadas	Seção estratigráfica	Idade	Formação	Descrição
TAR-31	06°35.261'S 76°18.347'O	-	Mesomioceno	Ipururo	Lente microconglomerática argilosa amarelada com folhas oxidadas, em um espesso canal de conglomerado com seixos argilosos
TAR-14	06º42.520'S 76º17.336'O	Abra de Machungo	Neooligoceno	Chambira	Siltito vermelho
TAR-01	06º34.902'S 76º16.903'O	Shapaja	Eooligoceno	Pozo, Membro Superior	Argilas azuis com nódulos calcários
TAR-21	06°34.982'S 76°16.886'O	Shapaja	Final do Neoeoceno	Pozo, Membro Superior	Conglomerado azul/amarelo rico em gipsita e nódulos, intercalado com canais de arenitos de granulometria grosseira e depósitos de planície de inundação
TAR-72	06°34.986'S 76°16.887'O	Shapaja	Neoeoceno	Pozo, Membro Superior	Microconglomerado amarelo a azulado com gipsita e argilas
TAR-20	06°34.901'S 76°16.783'O	Shapaja	Neoeoceno	Pozo, Membro Superior	Microconglomerado amarelo-esverdeado com gipsita e restos de plantas
TAR-74	06°34.910'S 76°16.723'O	Shapaja	Neoeoceno	Pozo, Membro Superior	Conglomerado inconsolidado azul a amarelado, rico em nódulos, abaixo de canais de arenitos beges de granulometria grossa, com fragmentos oxidados de folhas
TAR-47	07°12.840'S 76°44.412'O	Juanjui	?Neoeoceno	Pozo, Membro Inferior	Argilas esverdeadas ricas em nódulos
TAR-45	07°13.067'S 76°44.550'O	Juanjui	Meso-Neooceno	Pozo, Membro Inferior	Siltitos azuis laminados ricos em nódulos
TAR-44	07°13.067'S 76°44.577'O	Juanjui	Meso-Neoeoceno	Pozo, Membro Inferior	Argilas azuis ricas em nódulos com restos de peixes
TAR-55	07°25.809'S 76°39.804'O	Balsayacu	Final do Mesoeoceno	Pozo, Membro Inferior	Microconglomerado marrom rico em nódulos
TAR-76	07°25.807'S 76°39.756'O	Balsayacu	Final do Mesoeoceno	Pozo, Membro Inferior	Microconglomerado azul-acinzentado com fragmentos de caranguejos e lenho
TAR-56	07°25.675'S 76°39.806'O	Balsayacu	?Mesoeoceno	Pozo, Membro Inferior	Microconglomerado azulado rico em nódulos, abaixo de um canal de arenito

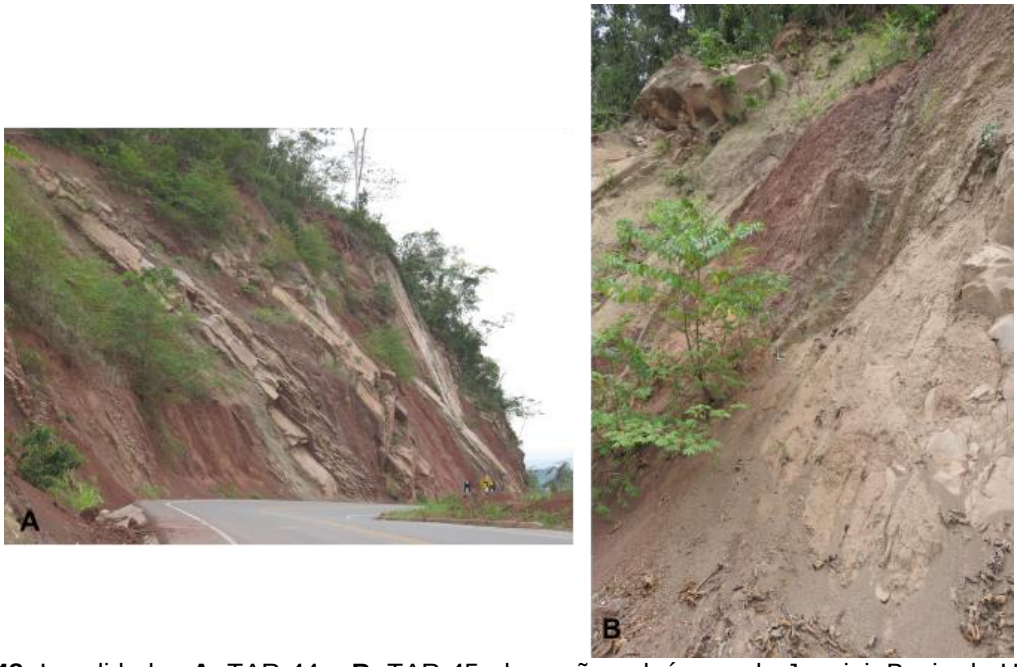


Figura 48. Localidades **A**, TAR-44 e **B**, TAR-45, da seção paleógena de Juanjui, Bacia do Huallaga, Peru.

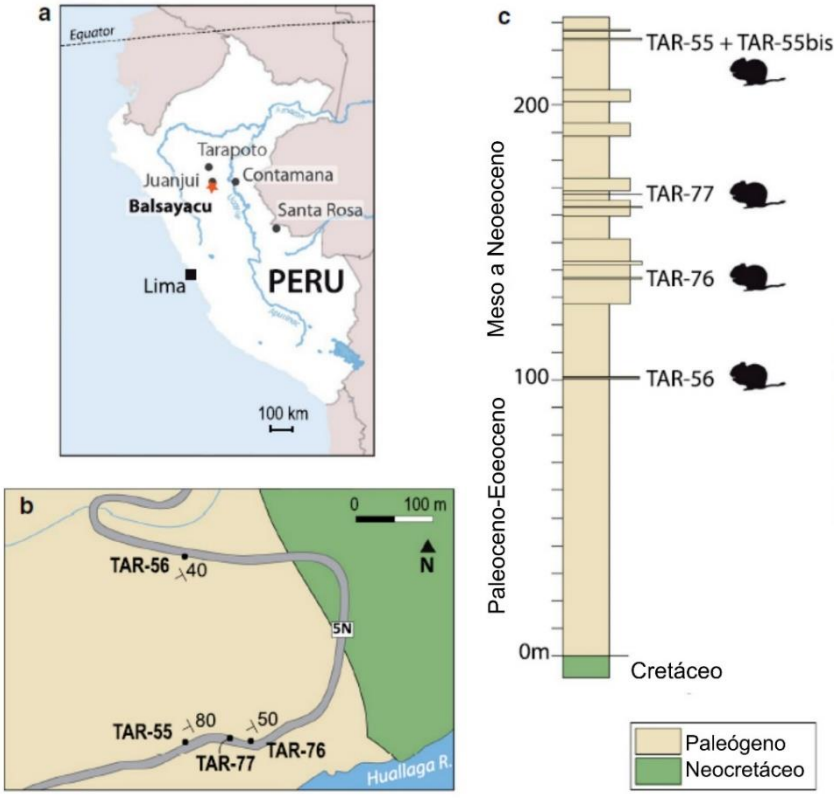


Figura 49. A, Mapa com a localização das cidades prospectadas na região da Bacia do Huallaga, Peru, com destaque para Balsayacu. **B**, mapa da região da seção de Balsayacu, indicando a localização dos afloramentos. **C**, seção estratigráfica sintética dos afloramentos da seção de Balsayacu, com a indicação dos níveis fossilíferos onde foram encontrados restos de roedores caviomorfos.

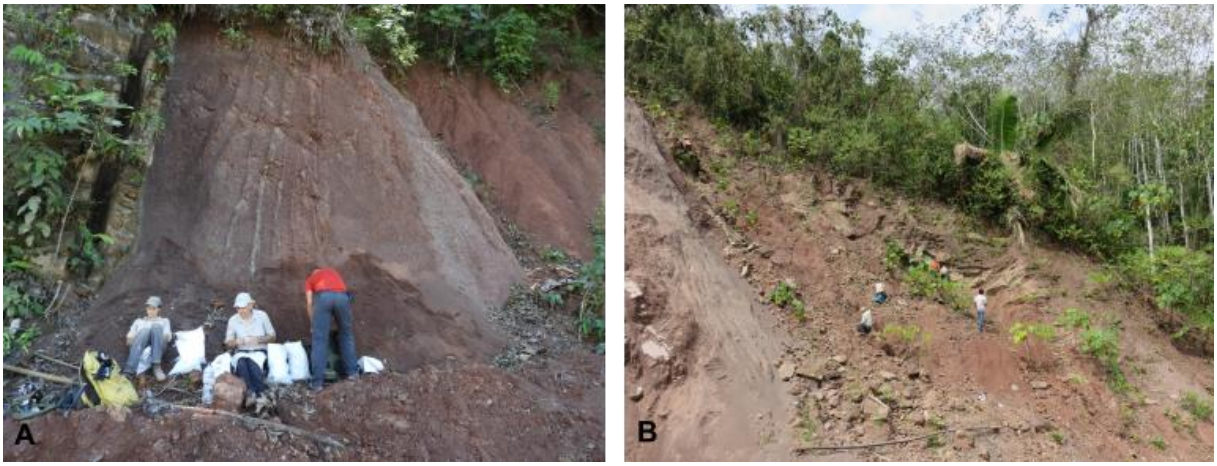


Figura 50. Localidades **A**, TAR-55 e **B**, TAR-56, da seção paleógena de Balsayacu, Bacia do Huallaga, Peru.

Já os afloramentos TAR-74, TAR-20, TAR-72, TAR-21 e TAR-01 integram a seção de Shapaja, próxima a cidade de Shapaja, 12 km a sudeste de Tarapoto (Figuras 51, 52 e 53), acima da confluência entre os rios Mayo e Huallaga. Consistem em depósitos de granulometria fina, de planície de inundação do Membro Superior da Formação Pozo. A sequência estratigráfica é dominada por folhelhos vermelhos e siltitos, com veios de gesso, intercalados com arenitos amarelados finos a grossos, contendo resíduos de folhas oxidadas, e camas de microconglomerados acinzentados e argilosos, ricos em seixos. Também foram observados dois níveis de argilas azuis ricos em nódulos carbonáticos. Não foi observada nenhuma desconformidade na sequência, com nove níveis fossilíferos distribuídos sucessivamente na sequência dentre os níveis de maior granulometria. Foi possível observar em parte dos níveis da seção indícios de influência marinha (ambiente marinho raso/litoral com forte influência de maré), com o achado de restos de raias Myliobatidae marinhas/estuarinas. Nota-se uma mudança gradativa de um ambiente influenciado por maré, com arenitos finos, até lentes microconglomeráticas fluviais intercaladas por depósitos de planície de inundação. O conteúdo fossilífero presentes nos depósitos da seção de Shapaja inclui plantas (madeira silicificada, folhas, frutos, sementes, palinomorfos, carófitas), gastrópodes, caranguejos (um táxon de Trichodactylidae, TAR-01), condrictes, osteíctes, anuros, quelônios, lagartos, crocodilomorfos e mamíferos (incluindo, além dos metatérios, xenartros, ungulados nativos sul-americanos, quirópteros, primatas e roedores caviomorfos) (Klaus *et al*., 2017; Boivin

et al., 2018; Antoine *et al*., 2021). Dentre os roedores caviomorfos, foram registrados 17 táxons para a seção estratigráfica de Shapaja (TAR-21, TAR-13, TAR-22 e TAR-24, superfamílias Erethizontoidea, Octodontoidea e Chinchilloidea (Boivin *et al*., 2018). Os restos de metatérios foram preliminarmente identificados, reportando-se 19 táxons, conforme mencionado anteriormente neste texto (Seção 3.6.2 O registro fóssil de Metatheria na Região Amazônica). De acordo com análises de quimioestratigrafia realizadas em amostras dos diferentes níveis da seção de Shapaja, observou-se que esta registra o intervalo entre o final do Eoceno e o início do Oligoceno, sendo i) TAR-20, TAR-72 e TAR-74 Neoeoceno; ii) TAR-21 no início da transição Eoceno-Oligoceno (final do Neoeoceno); iii) TAR-22, TAR-13, TAR-73 e TAR-01 seriam Eooligoceno. Tais intervalos de tempo puderam ser inclusive correlacionados com marcadas mudanças na composição das assembleias fossilíferas da Seção de Shapaja (Figura 53; Antoine *et al*., 2021).



Figura 51. Mapa com a localização das cidades de Tarapoto e Shapaja, Bacia do Huallaga, Peru.

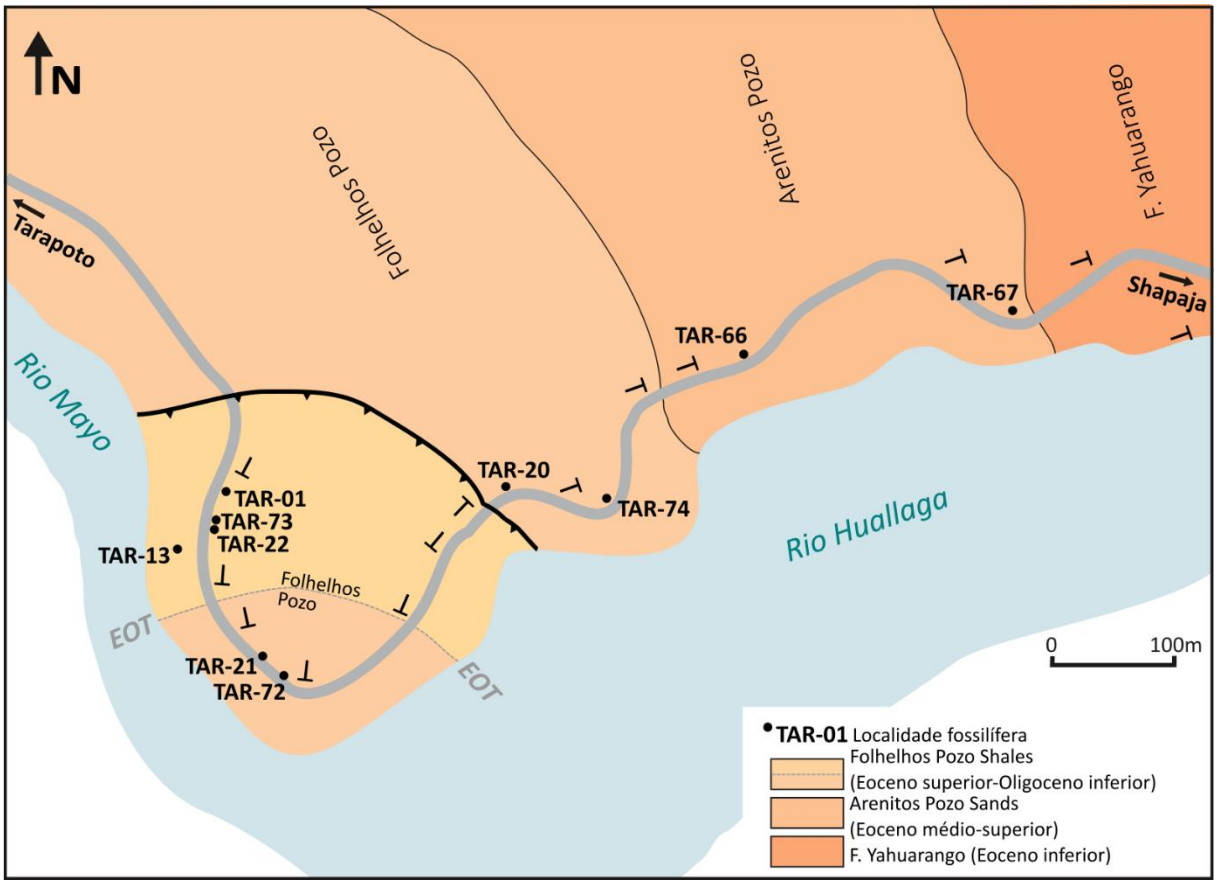


Figura 52. Mapa das localidades da seção paleógena de Shapaja, Bacia do Huallaga, Peru.

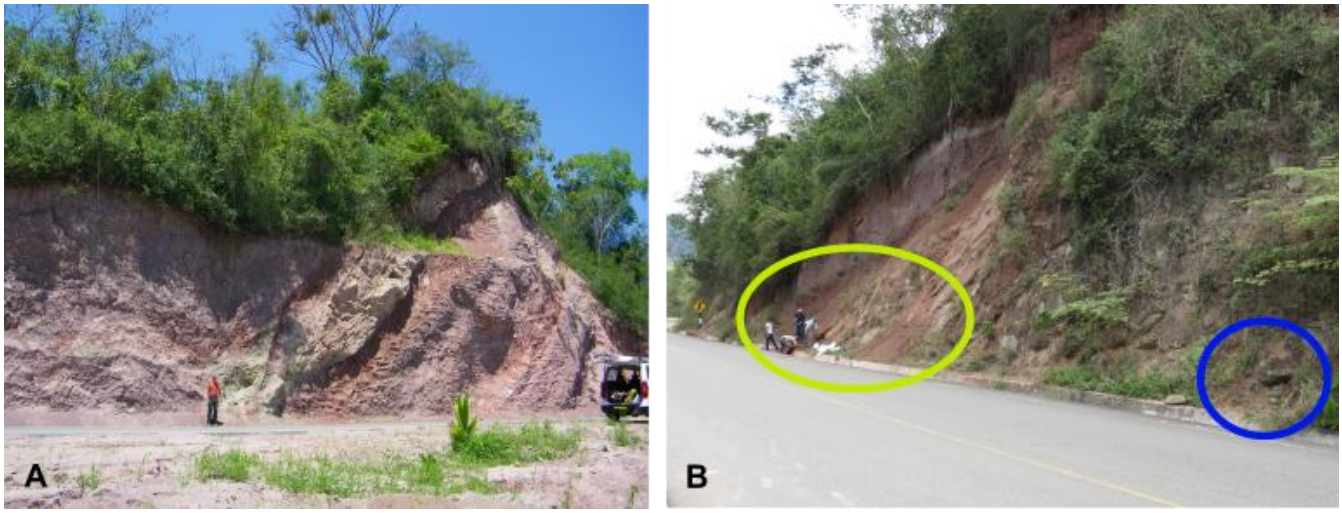


Figura 53. Localidades **A**, TAR-01 e **B**, TAR-21, círculo amarelo e TAR-72, círculo azul, seção paleógena de Shapaja, Bacia do Huallaga, Peru

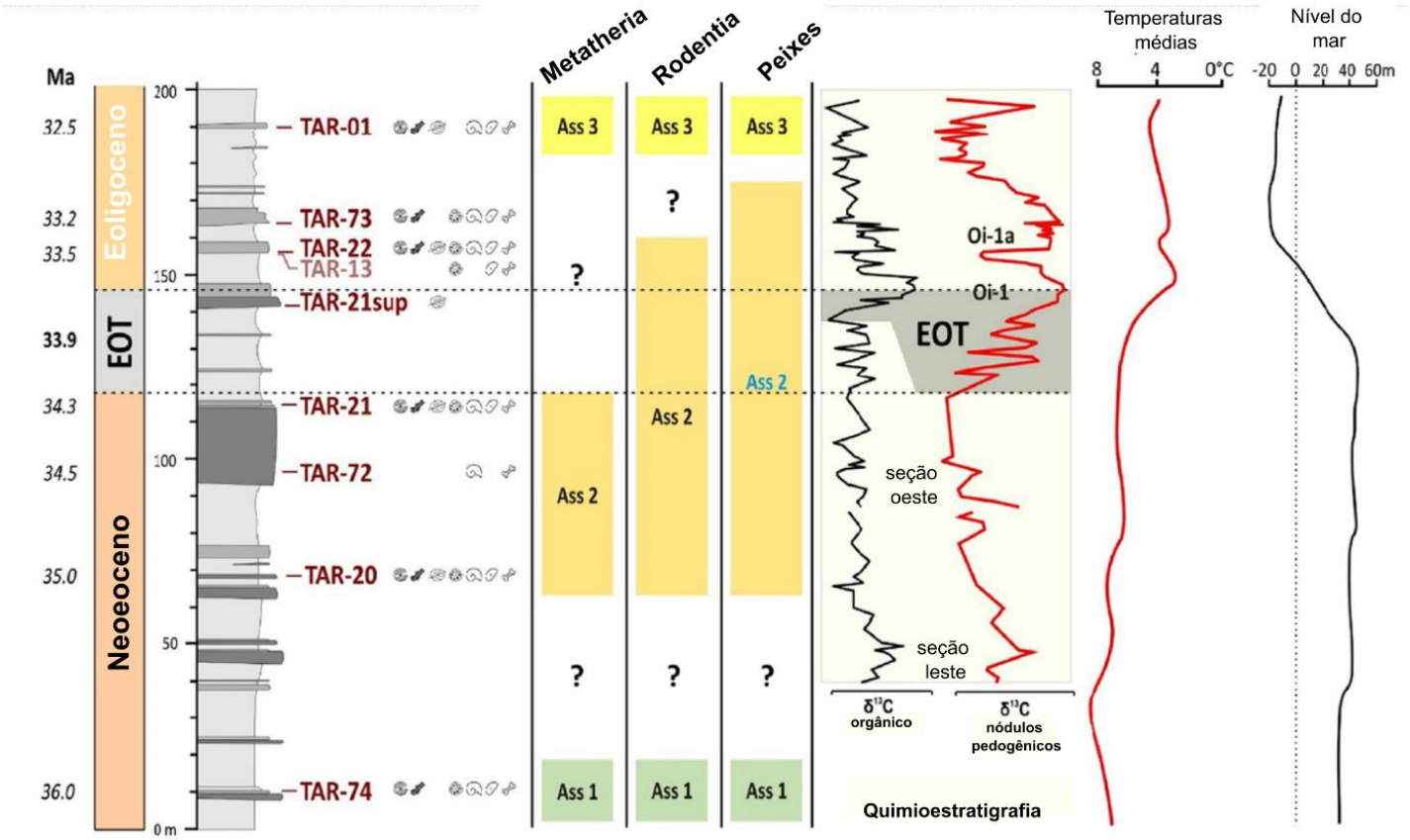


Figura 54. Diagrama crono e bioestratigráfico sintético das assembleias fossilíferas da Seção de Shapaja, Neoeoceno-Eooligoceno, Departamento de San Martín, Peru, representando os dados paleontológicos e de análises de quimioestratigrafia apresentados em Antoine *et al*. (2021), com curva de paleotemperaturas adaptadas de Westerhold *et al*. (2020) e de nível do mar adaptadas de Miller *et al*. (2020).

Analisando-se estratigraficamente as diferentes seções presentes na Bacia do Huallaga (Balsayacu, Juanjui e Shapaja) e comparando-as com os afloramentos da Formação Pozo na região de Contamana, assim como com a fauna local de Santa Rosa (Campbell, 2004) (Figura 55), com base em seu conteúdo fossilífero e datações radiométricas disponíveis, nota-se que existe certa sobreposição temporal entre estas, sendo o Mesoeoceno representado em Contamana, Balsayacu e Juanjui, enquanto o Neoeoceno estaria presente os afloramentos das seções de Juanjui e Shapaja. Já o início do Oligoceno pode ser observado nas seções de Juanjui, Shapaja e em Santa Rosa.

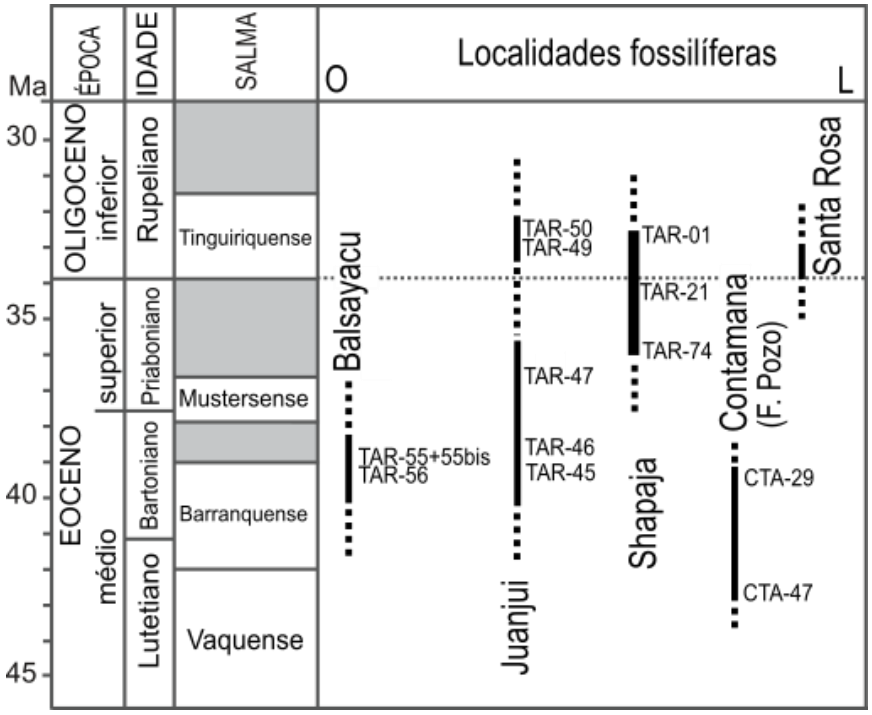


Figura 55. Hipótese de atribuição temporal das seções de Shapaja, Balsayacu e Juanjui em relação às principais faunas já descritas para o Eoceno e Oligoceno da Amazônia peruana. Abreviaturas: L, leste; Ma, milhões de anos; O, oeste; SALMA, South American Land Mammal Age.

TAR-14 é a única localidade de seção estratigráfica de Abra de Machungo onde se encontraram restos de metatérios Polydolopimorphia (Figura 56). Trata-se de um afloramento da Formação Chambira, Neooligoceno (Deseadense). Encontra-se a 50 cm de um arenito contendo zircões detríticos datados pelo método de U/Pb em 25.67 ± 0.64 Ma. Neste afloramento também foram encontrados restos de crustáceos, quelônios, ungulados nativos sul-americanos e roedores.



Figura 56. Localidade TAR-14, afloramento da Formação Chambira, Bacia do Huallaga, Peru.

Por fim, a localidade TAR-31 (Figura 57) localiza-se próximo a Shapaja, distrito de Juan Guerra, porém consiste em um afloramento da Formação Ipururo, final do Mesomioceno. Foram realizadas datações U-Pb em zircões detríticos provenientes de TAR-31, os quais indicaram uma idade máxima de deposição de 17.4 ± 0.12 Ma (Stutz *et al*., 2022). Nesta localidade foi encontrada uma fauna bastante semelhante à de La Venta (Colômbia) com restos de crustáceos, peixes, anfíbios, répteis, aves e mamíferos tais como ungulados nativos sul americanos, roedores e primatas (Marivaux *et al*., 2021; Boivin *et al*., 2021).

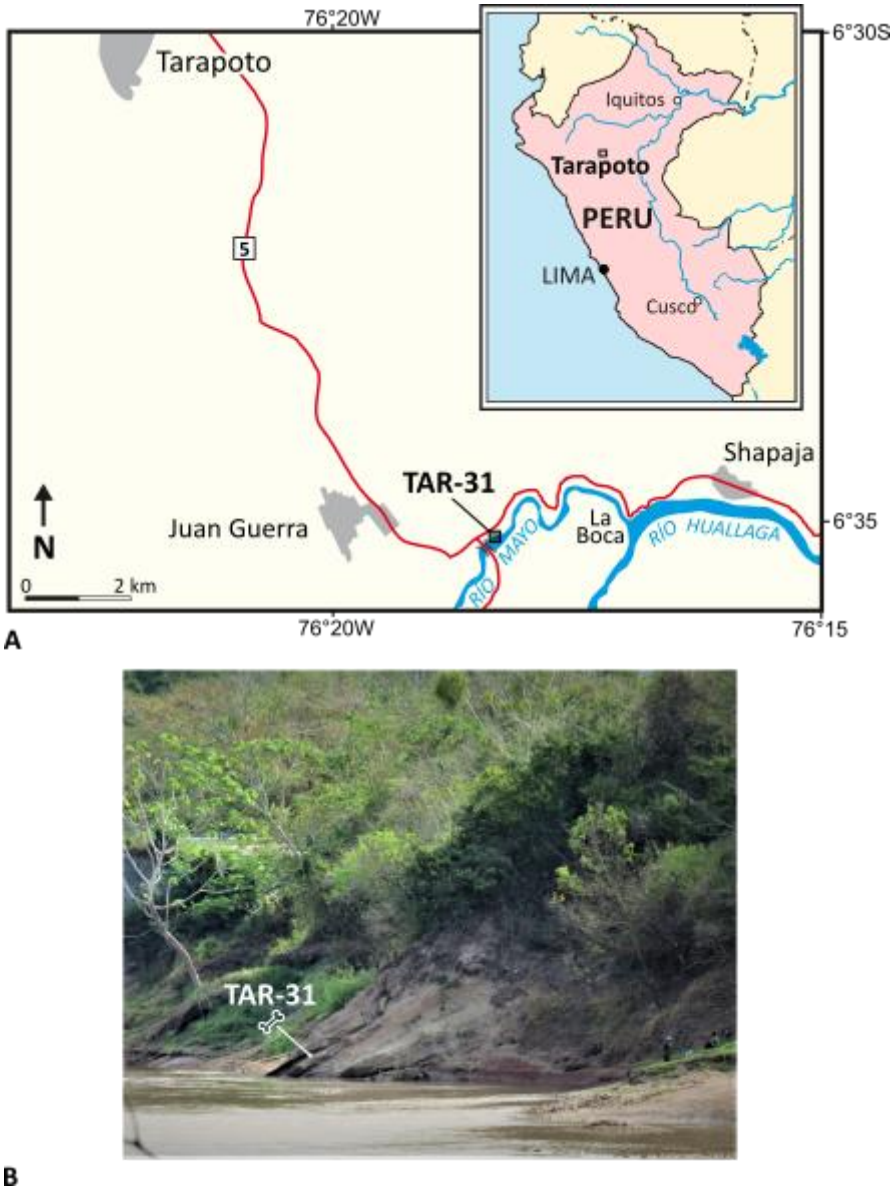


Figure 57. A, Mapa da localização da localidade TAR-31, Formação Ipururo, próximo a cidade de Tarapoto, distrito de Juan Guerra, Departamento de San Martín, Peru. **B**, fotografia do afloramento, situado na margem esquerda do Rio Mayo, indicando a posição do nível fossilífero. Fonte: Stutz *et al*. (2022).

5.2.3 Atalaya

Com relação à região de Atalaya, Departamento de Ucayali, Peru, os trabalhos de campo foram até o momento preliminares, com a realização de uma missão de reconhecimento em 2017. Foram localizados 14 afloramentos fossilíferos, sendo quatro ao longo do rio Tambo (nomeados TMB, seguido de número de acordo com a

ordem de sua descoberta) e 10 ao longo do rio Urubamba (nomeados URU, seguido de número de acordo com a ordem de sua descoberta). As formações Pozo, Chambira e Ipururo são aflorantes na região, designando idades indo do Neoeoceno ao Mesomioceno. Fósseis de metatérios foram encontrados em dois afloramentos em Atalaya: TMB-01 e URU-210 (Figura 58). A localidade TMB-01 (10°45.488'S 73°45.143'O) consiste em argilas vermelho-azuladas com estruturas de canal e nódulos calcários plurimilimétricos, sendo um afloramento do Membro Superior (folhelhos) da Formação Pozo, de idade Neoeoceno, com ambiente deposicional interpretado como sendo flúvio-litoral. Nesta localidade foram também encontrados restos fósseis de peixes Characiformes, anfíbios, quelônios, crocodilomorfos, xenartros, ungulados nativos sul-americanos e roedores, dentre outros. Já URU-210 (10°41.661'S 73°47.490'O) consiste em um microconglomerado marrom com seixos argilosos e fragmentos de folhas, sendo um afloramento da Formação Chambira, de idade ?Eoceno-Oligoceno, onde foram também encontrados restos fósseis de crustáceos, peixes actinopterígeos, quelônios, crocodilomorfos, roedores, dentre outros.



Figura 58. Localidades **A**, TMB-01, afloramento da Formação Pozo, e **B**, URU-210, afloramento da Formação Chambira, Atalaya, Peru.

6 DISCUSSÃO INTEGRADORA E CONCLUSÕES

6.1 SÍNTESE DOS ARTIGOS

Os resultados da presente tese são apresentados abaixo nos Artigos 1 e 2, os quais encontram-se publicados ou em vias de publicação, e no Artigo 3, o qual será formalizado como publicação posteriormente. No caso do Artigo 3, a pandemia de SARS-CoV-2 impactou profundamente o desenvolvimento do trabalho, visto a impossibilidade de visitas às coleções científicas para comparação com material já descrito na literatura, imprescindível para a realização das análises.

No Artigo 1, o qual trata da localidade TAR-31, Amazônia peruana, afloramento da Formação Ipururo, de idade final do Mesomioceno (SALMA Laventense), foi descrita a associação de metatérios composta pelas ordens: Didelphimorphia, família Didelphidae, '*Thylamys*' cf. '*T*.' *colombianus*; e Paucituberculata, subordem Palaeothentoidea, família Palaeothentidae, com *Palaeothentes* sp., e família Abderitidae, com a descrição da nova espécie *Pitheculites ipururensis*. Esta associação de metatérios, assim como a presença registrada de um primata Cebidae em TAR-31, sugerem para esta região, durante aquele período, condições tropicais predominantemente úmidas e quentes, com a ocorrência tanto de florestas como de habitats mais secos. Foi também abordado neste artigo a questão da datação dos depósitos de TAR-31, com a apresentação de datações U-Pb, as quais indicam uma idade máxima de deposição para a camada fossilífera de TAR-31 de 17.4 ± 0.12 Ma. Demonstrou-se a semelhança entre esta assembleia de metatérios com outras faunas temporalmente correlatas, em especial com a de La Venta, Mesomioceno da Colômbia (Goin, 1997; Suárez Gómez, 2019), assim como com fósseis encontrados no Acre, Brasil e em outros afloramentos na Região Amazônica no Peru (Czaplewski, 1996; Cozzuol *et al*., 2006; Antoine *et al*., 2013). Também foi observado a ausência de determinados táxons, como representantes das ordens Sparassodonta e Microbiotheria, os quais já foram reportados para afloramentos do Mesomioceno de baixas latitudes da América do Sul. Estes resultados suportam a hipótese de que a Amazónia Ocidental era uma região biogeográfica única e consistente para os

mamíferos terrestres durante o Mesomioceno, no extremo ocidental do Sistema Pebas, além de salientar o papel da Região Amazônica com relação à radiação dos metatérios no Neógeno.

Já no Artigo 2, são abordadas localidades situadas no Rio Envira (PRE 06) e Alto Rio Juruá (PRJ 25 e 33), Formação Solimões, Bacia do Acre, Estado do Acre, Amazônia Brasileira, com a observação de diferenças na composição taxonômica da assembleia de metatérios entre os diferentes rios. Tais diferenças estariam ligadas às distintas idades destes depósitos. Os afloramentos da região do Alto Rio Juruá, onde foram encontrados metatérios, são sugeridos como de idade Mesomioceno, com base no restante da fauna fóssil encontrada nestas localidades, em particular com base nos roedores caviomorfos. Apesar de alguns restos de metatérios terem sido encontrados fora de contexto estratigráfico nos afloramentos da região do Alto Rio Juruá, os mesmos também sugerem uma idade anterior a do afloramento PRE 06, no Rio Envira, concordando com a fauna encontrada *in situ*. Nas localidades PRJ 25 e PRJ 33 foram identificados os táxons: ordem Paucituberculata, superfamília Palaeothentoidea, família Abderitidae, *Abderites* sp. (PRJ 33, *in situ*) e família Palaeothentidae, Palaeothentinae indet. (PRJ 25 e PRJ 33', em ambas as localidades o material foi encontrado fora de contexto estratigráfico). Tais registros de Paucituberculata são os primeiros para o Mioceno do Acre e também se trata do primeiro registro do gênero *Abderites* para baixas latitudes na América do Sul. Já a assembleia de metatérios da localidade PRE 06, Rio Envira, é composta exclusivamente por membros da ordem Didelphimorphia, família Didelphidae, com os táxons Marmosini cf. *Marmosa*, *Didelphis* cf. *D*. *solimoensis*, '*Thylamys*' *colombianus* e didelfídeos não identificados. Tal associação, em conjunto com os demais restos fósseis encontrados no PRE 06, sobretudo roedores caviomorfos, sugerem uma idade Neomioceno para este afloramento. No geral, a fauna encontrada nos afloramentos de ambos os rios é mais próxima em termos de composição taxonômica à fauna da localidade de TAR-31 (Artigo 1), dentre as demais faunas registradas para o Mioceno de baixas latitudes na América do Sul. Ademais, estes registros incrementam a diversidade de didelfídeos registrados para o Mioceno do Acre, antes restrita à *Didelphis solimoensis* e didelfídeos não identificados (Czaplewski, 1996; Cozzuol *et al*., 2006).

Em contrapartida, o Artigo 3 apresenta dados sobre metatérios coletados em localidades paleógenas e neógenas da Amazônia peruana, nas regiões de Contamana, Bacia do Huallaga e Atalaya. Foram analisados apenas os representantes da ordem Polydolopimorphia, através do estudo de um total de 276 espécimes, com a identificação de 15 táxons. Optou-se por abordar apenas a ordem Polydolopimorphia, apesar da presença de outros clados de metatérios nestes afloramentos, visto o ineditismo e grande abundância e diversidade de polidolopimórfios nestas localidades. Observou-se que a riqueza de polidolopimórfios das localidades estudadas abrange unicamente membros da subordem Bonapartheriiformes, não havendo representantes dos Polydolopiformes. Dentro de Bonapartheriiformes, tanto a superfamília Bonapartherioidea foi registrada, com a presença de representantes da família Prepidolopidae, sendo todos táxons inéditos (seis novos gêneros e seis novas espécies + um táxon indeterminado), assim como a superfamília Argyrolagoidea, com membros da família Argyrolagidae, sendo duas novas espécies do gênero *Proargyrolagus* e outros dois argirolagídeos, aos quais não foi possível atribuir uma identificação taxonômica mais precisa. Ademais, também se registra o gênero *Wamradolops*, de relações filogenéticas incertas dentro de Polydolopimorphia, com a espécie já conhecida para a fauna de Santa Rosa, Eooligoceno do Peru, *W*. *tsullodon* e uma nova espécie de *Wamradolops* de maior tamanho, além de um novo gênero e nova espécie também de relações filogenéticas incertas e polidolopimórfios indeterminados. Observou-se que as assembleias de Polydolopimorphia nas distintas regiões estudadas no Peru se assemelham em termos de composição taxonômica quando se trata de localidades temporalmente correlatas. No entanto, com relação a localidades representando diferentes períodos, mesmo que próximas geograficamente, a composição taxonômica dos polidolopimórfios é distinta, com o aparecimento e/ou desaparecimento, ou diminuição/aumento da diversidade e abundância de determinados grupos.

6.2 EVOLUÇÃO E COMPARAÇÃO DA PALEODIVERSIDADE DE METATÉRIOS

Até o presente momento, poucos foram os estudos que buscaram retratar as assembleias de metatérios fósseis de baixas latitudes da América do Sul, em especial

na região hoje ocupada pelo bioma Amazônia (vide Seção 3.6.2 O registro fóssil de Metatheria na Região Amazônica). Além de registros pontuais de determinados fósseis (e.g., *Didelphis solimoensis*, Formação Solimões, Neomioceno, Brasil, Cozzuol *et al*., 2006; *Lycopsis padillai*, Formação Castilletes, Mesomioceno, Colômbia, Suárez *et al*., 2016; e alguns registros preliminares na Amazônia peruana, Antoine *et al*., 2013, 2016, 2021), apenas duas associações de metatérios fósseis, em maior quantidade e diversidade, foram extensivamente estudadas na Região Amazônica, sendo elas a da fauna local de Santa Rosa, Peru, Eooligoceno (Goin & Candela, 2004) e La Venta, Mesomioceno, Colômbia (Goin, 1997; Suárez Gómez, 2019). Comparando-se estas duas faunas, é possível observar grande dissimilaridade entre suas composições. Tal fenômeno também pode ser agora mais extensamente visualizado comparando-se com os dados apresentados nesta tese. Os Artigos 1 e 2, que tratam de localidades miocênicas, revelam uma assembleia de metatérios de pequena abundância, porém de relativamente grande diversidade. Tais assembleias são compostas somente por membros das ordens Didelphimorphia e Paucituberculata e se assemelham em termos de composição taxonômica sobretudo entre si e com as assembleias de metatérios registrados para Mesomioceno da Região Amazônica, em especial com La Venta. Com relação às comunidades de metatérios do Mioceno de outros locais da América do Sul, estas mostram-se bastante distintas daquelas registradas em baixas latitudes, com a presença, por exemplo, de outros clados de Paucituberculata, como as famílias Caenolestidae e Pichipilidae, apesar de também registrarem a presença de Palaeothentidae e Abderitidae, além do registro relativamente mais abundante de membros da ordem Microbiotheria (vide Quadros 4 e 5).

Já o Artigo 3, o qual trata principalmente de localidades paleógenas, registra comunidades de metatérios bastante distintas daquelas reportadas para o Mioceno, com grande abundância e diversidade de polidolopimorfios, ausência de membros da Ordem Didelphimorphia e aparecimento e diversificação de Paucituberculata no Oligoceno e Mioceno, se assemelhando mais com a fauna local de Santa Rosa.

A ausência de Didelphimorphia, em afloramentos mais antigos (Paleógeno), está diretamente relacionada a radiação tardia de seu grupo-coroa Didelphidae, que teria ocorrido no final do Mioceno. Inclusive, os registros de didelfídeos apresentados nos

Artigos 1 e 2 integram os mais antigos registros de Didelphidae já reportados, os quais só se tornam abundantes por volta do final do Mioceno e início do Plioceno (Castro *et al*., 2021). Por outro lado, o desaparecimento de grande parte dos Polydolopimorphia dos afloramentos miocênicos estudados pode estar correlacionado à extinção de diversos clados desta ordem na transição Eoceno–Oligoceno. Os Polydolopimorphia, a partir deste momento, passaram a ser representados unicamente pelos Argyrolagidae em médias e altas latitudes da América do Sul (Goin *et al*., 2016). Na Região Amazônica, no entanto, já havia o registro de *Wamradolops* e do prepidolopídeo *Incadolops* no Eooligoceno, demonstrando a sobrevivência destes grupos em idades mais recentes nesta região. Com os registros mencionados no Artigo 3, estende-se a distribuição temporal de *Wamradolops* e de Prepidolopidae até o Neooligoceno. Quanto aos Argyrolagidae, seu único registro no Mioceno da Região Amazônica vem a ser o da localidade CTA-43 (Artigo 3), que também seria o seu último nesta região. Posteriormente, os Argyrolagidae se extinguem no Plioceno-Pleistoceno, sendo os seus últimos registros restritos a porções mais ao sul do continente (Bolívia e Argentina; vide Quadro 6).

Tratando-se de correlacionar as localidades paleógenas peruanas estudadas com outras faunas temporalmente correlatas na América do Sul, nota-se que há certa semelhança com a fauna de Santa Rosa, através, por exemplo, da presença de *Wamradolops*, que, nos afloramentos nos quais este é encontrado, é sempre reportado em grande abundância, tanto na fauna local de Santa Rosa, como nos afloramentos aqui estudados. Em Santa Rosa também há um representante de Prepidolopidae, *Incadolops ucayali*, porém, este táxon não é encontrado nos afloramentos de Contamana, Bacia do Huallaga e Atalaya. Outro táxon de Polydolopimorphia encontrado em Santa Rosa é *Hondonadia pittmanae*, família Rosendolopiidae, o qual também não é registrado nos afloramentos estudados das regiões de Contamana, Bacia do Huallaga e Atalaya. Ademais, em Santa Rosa registra-se também diversos táxons de Paucituberculata Palaeothentoidea, clado que começa a aparecer nos afloramentos aqui investigados por volta do final do Eoceno. Porém, os Palaeothentoidea só se tornam diversos e abundantes nas localidades de Contamana e Bacia do Huallaga a partir do Oligoceno. Assim, observa-se que, apesar de certas semelhanças entre a fauna de metatérios de Santa Rosa com as das

localidades de Contamana, Bacia do Huallaga e Atalaya, estas não apresentam a mesma composição taxonômica, especialmente quando se compara Santa Rosa, de idade Eooligoceno, com as localidades Mesoeoceno–Neoeoceno de Contamana, Mesoeoceno–Eooligoceno da Bacia do Huallaga e Neoeoceno/Oligoceno de Atalaya.

Ainda com relação ao Artigo 3, observa-se também certa semelhança entre as faunas paleógenas do Peru aqui estudadas com as do Eo- e Mesoeoceno do noroeste Argentino (províncias de Salta e Catamarca; formações Lumbrera, Quebrada de los Colorados, Geste e Pozuelos; Pascual, 1980; Goin *et al*., 1998; Chornogubsky *et al*., 2019). Aliás, em afloramentos desta região da Argentina foram descobertos os primeiros prepidolopídeos, que basearam a descrição da família (Pascual, 1980) e, além dos registros de *Perrodelphys coquinense* para a Península Antártica e *Incadolops ucayali* na fauna local de Santa Rosa, esta é a única área para onde se reportavam fósseis de prepidolopídeos. Ademais, também são registrados táxons de Argyrolagoidea no noroeste argentino, outro ponto de semelhança com os afloramentos peruanos aqui estudados. De fato, sugere-se que as faunas do Eoceno do noroeste argentino apresentam mais semelhança com às das baixas latitudes da América do Sul do que com as faunas da Patagônia e Antártica (Chornogubsky *et al*., 2019). Outra assembleia de metatérios que apresenta alguma semelhança com as associações paleógenas dos afloramentos peruanos tratados no Artigo 3 é a da Formação Guabirotuba, do final do Mesoeoceno, Bacia de Curitiba, Brasil, a qual também conta com representantes de Argyrolagoidea e Palaeothentoidea (Sedor *et al*., 2017). No entanto, a associação de metatérios de Guabirotuba foi até o momento apenas preliminarmente identificada, pendendo informações mais detalhadas para comparações mais aprofundadas. Ressalta-se a grande diferença em composição taxonômica das comunidades de metatérios das localidades paleógenas aqui estudadas com relação aos táxons registrados em afloramentos mais antigos, do Paleoceno e Eoeoceno, como por exemplo de Tiupampa (Bolívia), Itaboraí (Brasil) e Las Flores e Laguna Fría (Argentina). Já com relação a localidades temporalmente correlatas (Mesoeoceno–Neooligoceno) de outras partes do continente sul-americano, nota-se que as assembleias de polidolopimórfios do sul do continente eram compostas por outros clados, como, por exemplo, as famílias Rosendolopidae, Groeberiidae e Patagoniidae dentre os Bonapartheriiformes, além de diversos táxons

de Polydolopiformes, grupo até o presente nunca registrado nos afloramentos paleógenos da Região Amazônica (vide Quadro 6).

6.3 CONCLUSÕES E PERSPECTIVAS

Assim, nota-se que, através dos resultados obtidos na presente tese, em comparação com a literatura, grandes mudanças (*turnovers*) na composição das comunidades de metatérios da Região Amazônica ocorreram ao longo do intervalo Eoceno–Mioceno (Figura 59). Infelizmente não se dispõe até o momento de dados acerca de metatérios do Paleoceno da Região Amazônica, não sendo possível, portanto, incluir este período no presente estudo. A transição Eoceno–Oligoceno é reconhecida como um momento de grandes mudanças climáticas e ambientais, sendo considerada uma rápida mudança do planeta do "modo estufa" (*greenhouse*) do Paleoceno e Eoceno, para o "modo geladeira" (*icehouse*) no início do Oligoceno. Tal mudança é atrelada, dentre outros mecanismos, a uma diminuição da concentração de CO_2 atmosférico e ao estabelecimento da corrente circumpolar antártica com a abertura do Mar de Tasman e da Passagem de Drake (Zachos *et al*., 2001; Antoine *et al*., 2021). Estas mudanças climáticas afetaram a flora e fauna, o que já foi registrado em diversos locais do planeta (e.g., Sudeste asiático, Marivaux *et al*., 2005; África, Marivaux *et al*., 2017), e, na América do Sul, foi chamada de *Bisagra Patagónica* (Goin *et al*., 2010; 2016). No caso da fauna terrestre, são registradas marcadas extinções em determinados grupos no final do Eoceno, seguidas pela diversificação de outros clados já no início do Oligoceno. Tratando-se de metatérios, após o Eoceno, estes não recobram mais os níveis de diversidade que tinham registrado anteriormente na América do Sul (Goin *et al*., 2016). No entanto, até o presente, este fenômeno vinha sendo retratado sobretudo em faunas fósseis encontradas na porção sul do continente, carecendo de dados sobre como as comunidades de metatérios de baixas latitudes da América do Sul haviam sido impactadas na transição Eoceno–Oligoceno. Observando-se os dados do Artigo 3, assim como com as informações acerca da fauna local de Santa Rosa, nota-se que as associações de metatérios no Mesoeoceno eram predominantemente compostas por membros da ordem Polydolopimorphia, com grande diversidade e abundância, registrando-se nas localidades da Amazônia

Peruana membros de afinidades incertas desta ordem, além da subordem Bonapartheriiformes, com as superfamílias Bonapartherioidea (família Prepidolopidae) e Argyrolagoidea (família Argyrolagidae). Estas assembleias de metatérios passam por um primeiro *turnover* na transição Eoceno–Oligoceno. Este se caracteriza pela diminuição da abundância e diversidade de polidolopimorfios nas assembleias, com o quase desaparecimento dos Prepidolopidae, mas continuação dos Argyrolagidae, assim como pelo aumento dos membros da ordem Paucituberculata, representados unicamente pela superfamília Palaeothentoidea, os quais passam a ter grande abundância e riqueza, tanto de táxons com caracteres mais primitivos, quanto táxons mais derivados à partir do início do Oligoceno.

Contata-se também que, já a partir do Mesoeoceno, os metatérios passam a ser, no geral, cada vez menos abundantes nos afloramentos, enquanto que os restos de roedores caviomorfos tornam-se cada vez mais profusos. Os roedores Caviomorpha chegaram a América do Sul provindos da África, provavelmente no final do Eoceno ou próximo a transição Eoceno–Oligoceno, e rapidamente experimentaram notável diversificação (Boivin *et al*., 2017a, 2018, 2021). As causas desta disparidade entre a quantidade de restos fósseis de metatérios e de roedores caviomorfos permanece a ser mais bem explorada. Pode se tratar de vieses tafonômicos, como a amostragem, predadores, preferência por presas específicas, abundância de presas e habitats preferidos, o que afetaria a abundância e riqueza dos distintos grupos nas amostras coletadas. No entanto, a competição crescente entre roedores e metatérios, assim como com outros grupos de nichos ecológicos similares também poderia levar a um declínio de determinados clados e à ascensão de outros. Porém, este desequilíbrio pode estar relacionado justamente com os impactos drásticos registrados nas faunas de metatérios na transição Eoceno–Oligoceno, que ocasionaram a extinção de diversos grupos, conforme mencionado anteriormente.

A partir do início do Oligoceno até o Mesomioceno, os Palaeothentoidea apresentam grande diversidade e abundância nas comunidades de metatérios da Região Amazônica, isto considerando tanto as localidades na Amazônia peruana quanto brasileira, com as famílias Palaeothentidae e Abderitidae. Porém, já nesta época aparecem os primeiros registros de membros da ordem Didelphimorphia, primeiramente com caracteres mais primitivos (como em TAR-31, Artigo 1).

Por fim, no Neomioceno, as comunidades de metatérios registradas são constituídas praticamente unicamente por didelfídeos, os quais são representados por táxons já derivados e bastante semelhantes aos grupos atuais (segundo *turnover*). Não se registram mais membros da ordem Paucituberculata, o que poderia estar relacionado com a extinção dos Palaeothentoidea no final do Mioceno, tendo em vista que a outra superfamília de paucituberculados, Caenolestoidea, não possui nenhum registro fóssil para o norte da América do Sul, apenas em altas latitudes, além de possuir, até o presente, distribuição bastante restrita (vide Quadro 4). Além dos didelfídeos, no Artigo 3 também se apresenta um registro para o Neomioceno de um Argyrolagidae, único e último representante da grande diversidade de Polydolopimorphia que existiu anteriormente na Região Amazônica. Assim, nota-se que a composição taxonômica das assembleias de metatérios do Neomioceno já muito se assemelhavam a diversidade de metatérios encontrada hoje na região Amazônica, composta unicamente por didelfídeos.

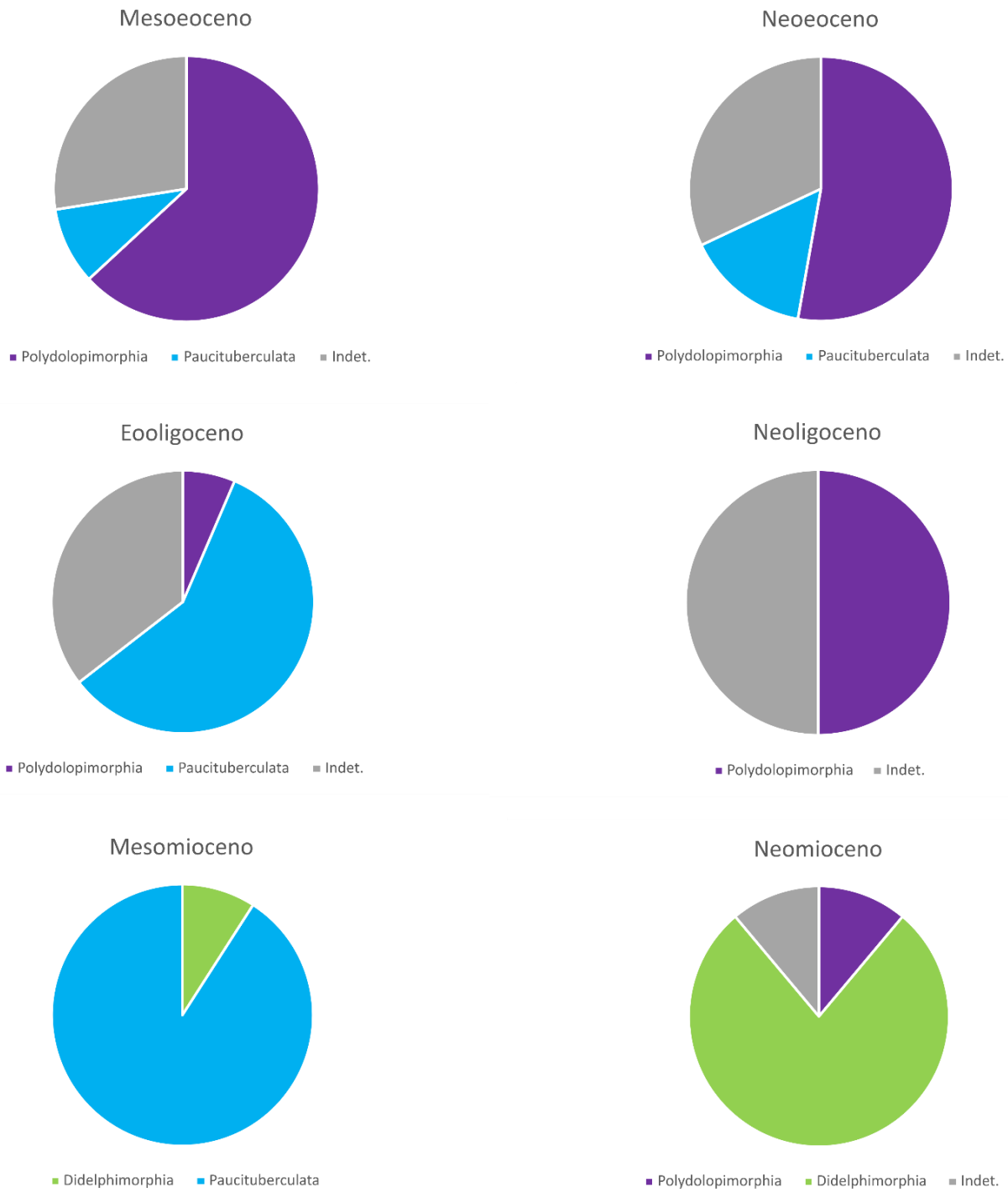


Figura 59. Gráficos representando a quantidade relativa de metatérios, por ordem, presentes nos afloramentos estudados do Mesoeoceno ao Neomioceno das regiões de Contamana, Bacia do Huallaga e Atalaya, Peru, e Acre, Brasil.

Com relação às perspectivas pós-doutoramento, primeiramente os esforços se concentrarão na finalização do Artigo 3, com a realização de análises filogenéticas e publicação do artigo. Espera-se com isso contribuir para o entendimento da família Prepidolopidae, a qual não vem sendo inserida em filogenias publicadas e não passou por revisões taxonômicas, além de contribuir para a conhecimento da ordem Polydolopimorphia como um todo, visto os problemas salientados quanto à sua composição e afinidades filogenéticas. Ademais, como tratado em texto, apenas os restos pertencentes a ordem Polydolopimorphia foram estudados nesta tese. No entanto, os afloramentos tanto do Paleógeno quanto do Neógeno da Amazônia Peruana também proveram fósseis pertencentes a outras ordens de Metatheria, os quais se buscará trabalhar em projetos de pós-doutorado. Ademais, com relação à Região Amazônica Brasileira, os projetos em andamento também podem prover materiais adicionais em futuras expedições de campo, além do material que já se encontra em laboratório aguardando preparação.

Espera-se também que, com a continuidade dos campos na Região Amazônica, tratando-se de localidades já conhecidas quanto de afloramentos inéditos, novos restos de metatérios possam ser descobertos e continuem a contribuir para o conhecimento dos Metatheria da América do Sul. Por exemplo, a localidade de Atalaya, onde foram encontrados restos de polidolopimórfios tratados no Artigo 3, foi somente preliminarmente explorada e novos trabalhos de campo nesta região estão previstos para o ano de 2023.

Ademais, tratar de Metatheria da América do Sul também instiga a curiosidade de se estudar os metatérios da Australásia, o que certamente será uma perspectiva a ser considerada no futuro.

7 REFERÊNCIAS BIBLIOGRÁFICAS

Abello, M. A. 2007. *Sistemática y bioestratigrafía de los Paucituberculata (Mammalia, Marsupialia) del Cenozoico de América del Sur*. Volumen 1. La Plata, 381 p. Tese de Doutorado, Universidad Nacional de La Plata.

Abello, M.A. 2013. Analysis of dental homologies and phylogeny of Paucituberculata (Mammalia: Marsupialia). *Biological Journal of the Linnean Society*, 109(2): 441–465.

Abreu, E.F., Casali, D., Costa-Araújo, R., Garbino, G.S.T., Libardi, G.S., Loretto, D., Loss, A.C., Marmontel, M., Moras, L.M., Nascimento, M.C., Oliveira, M.L., Pavan, S.E. & Tirelli, F.P. 2022. *Lista de Mamíferos do Brasil (2022-1) [Data set]. Zenodo*. Disponível em: https://sbmz.org/mamiferos-do-brasil/. Acesso em: 17 fev. 2023.

Adnet, S., Salas Gismondi, R. & Antoine, P.O. 2014. Comparisons of dental morphology in river stingrays (Chondrichthyes: Potamotrygonidae) with new fossils from the middle Eocene of Peruvian Amazonia rekindle debate on their evolution. *Naturwissenschaften*, 101: 33–45.

Aguilera, O.A., Bocquentin, J., Lundberg, J.G. & Maciente, A. 2008. A new cajaro catfish (Siluriformes: Pimelodidae: *Phractocephalus*) from the Late Miocene of Southwestern Amazonia and its relationship to *Phractocephalus nassi* of the Urumaco Formation. *Paläontologische Zeitschrift*, 82(2): 230–244.

Alvarenga, H.M.F. & Guilherme, E. 2003. The Anhingas (Aves: Anhingidae) from the Upper Tertiary (Miocene-Pliocene) of Southwestern Amazonia. *Journal of Vertebrate Paleontology*, 23(3): 614–621.

Antoine, P.O., Salas-Gismondi, R., Pujos, F., Ganerød, M. & Marivaux, L. 2017. Western Amazonia as a hotspot of mammalian biodiversity throughout the Cenozoic. *Journal of Mammalian Evolution*, 24(1): 5–17.

Antoine, P.O., Roddaz, M., Brichau, S., Tejada-Lara, J., Salas-Gismondi, R., Altamirano, A., Louterbach, M., Lambs, L., Otto, T. & Brusset, S. 2013. Middle Miocene vertebrates from the Amazonian Madre de Dios Subandean Zone, Perú. *Journal of South American Earth Sciences*, 42: 91–102.

Antoine, P.O., Marivaux, L., Croft, D.A., Billet, G., Ganerød, M., Jaramillo, C., Martin, T., Orliac, M.J. Tejada, L., Altamiro, A.J., Duranthon, F., Fanjat, G., Rousse, S. & Salas Gismondi, R. 2012. Middle Eocene rodents from Peruvian Amazonia reveal the pattern and timing of caviomorph origins and biogeography. *Proceedings of The Royal Society B: Biological Sciences*, 279(1732): 1319–1326.

Antoine, P.-O., Yans, J., Aliaga Castillo, A., Stutz, N., Abello, M.A., Adnet, S., Andriolli Custódio, M., Benites-Palomino, A., Billet, G., Boivin, M., Herrera, F., Jaramillo, C., Mártinez, C., Moreno, F., Navarrete, R.E., Negri, F.R., Parra, F., Pujos, F., Rage, J.-C., Ribeiro, A.M., Robinet, C., Roddaz, M., Tejada-Lara, J.V., Varas-Malca, R., Ventura Santos, R., Salas-Gismondi, R. & Marivaux L. 2021. Biotic community and landscape changes around the Eocene–Oligocene transition at Shapaja, Peruvian Amazonia: regional or global drivers? *Global and Planetary Change*, 202: 103512.

Antoine, P.-O., Abello, M.A., Adnet, S., Altamiro Sierra, A.J., Baby, P.; Billet, G., Boivin, M., Calderón, Y., Candela, A., Chabain, J., Corfu, F., Croft, D.A., Ganerød, M., Jaramillo, C., Klaus, S., Marivaux, L., Navarrete, R.E., Orliac, M.J., Parra, F., Pérez, M.E., Pujos, F., Rage, J.C., Ravel, A., Robinet, C., Roddaz, M., Tejada-Lara, J.V., Vélez-Juarbe, J., Wesselingh, F.P. & Salas-Gismondi, R. 2016. A 60-million-year Cenozoic history of western Amazonian ecosystems in Contamana, Eastern Peru. *Gondwana Research*, 31: 30–59.

Assemat, A., Boivin, M., Marivaux, L., Pujos, F., Benites-Palomino, A., Salas-Gismondi, R., Tejada-Lara, J., Varas-Malca, R., Negri, F.R., Ribeiro, A.M. & Antoine, P.O. 2019. Restes inédits de rongeurs caviomorphes du Paléogène de la région de Juanjui (Amazonie péruvienne): systématique, implications macro-évolutives et biostratigraphiques. *Geodiversitas*, 21(20): 699–730.

Bayá, E.M.F. & Bocquentin, J.V. 1997. Uma mandíbula de *Trigodon* sp. (Mammalia, Notoungulata, Toxodontidae) no Neógeno do Alto Rio Acre, fronteira Brasil-Peru. *Revista Geociências*, 2(6): 39–43.

Beck, R.M.D. 2008. A dated phylogeny of marsupials using a molecular supermatrix and multiple fossil constraints. *Journal of Mammalogy*, 89(1): 178–189.

Beck, R.M.D. 2017. The skull of *Epidolops ameghinoi* from the Early Eocene Itaboraí fauna, Southeastern Brazil, and the affinities of the extinct marsupialiform order Polydolopimorphia. *Journal of Mammalian Evolution*, 24(4): 373–414.

Beck, R.M.D., Voss, R.S. & Jansa, S.A. 2022. Craniodental morphology and phylogeny of marsupials. *Bulletin of the American Museum of Natural History*, 457: 1–355.

Bennett, C., Upchurch, P., Goin, F. & Goswami, A. 2018. Deep time diversity of metatherian mammals: Implications for evolutionary history and fossil-record quality. *Paleobiology*, 44(2): 171–198.

Bergqvist, L.P., Ribeiro, A.M. & Bocquentin, J. 2002. Primatas, roedores e liptoternas do Mio/Plioceno da Amazônia Sul-Ocidental (Formação Solimões, Bacia do Acre), Brasil. *Geologia Colombiana*, 23: 19–29.

Bi, S., Zheng, X., Wang, X., Cignetti, N.E., Yang, S. & Wible, J.R. 2018. An Early Cretaceous eutherian and the placental–marsupial dichotomy. *Nature*, 558: 390–395.

Bissaro Júnior, M.C., Kerber, L., Crowley, J.L., Ribeiro, A.M., Guilardi, R.P., Guilherme, E., Negri, F.P., Souza-Filho, J.P. & Hsiou, A.S. 2019. Detrital zircon U-Pb geochronology constrains the age of Brazilian Neogene deposits from Western Amazonia. *Palaeogeography, Palaeoclimatology, Palaeoecology*, 516: 64–70.

Black, K.H., Archer, M., Hand, S.J. & Godthelp, H. 2012. The rise of Australian marsupials: a synopsis of biostratigraphic, phylogenetic, palaeoecologic and palaeobiogeographic understanding. In: Talent, J.A. (ed.). *Earth and life: international year of planet Earth*. Dordrecht, Springer, p. 983–1078.

Bocquentin, J. & Guilherme, E. 1999. As preguiças Mylodontinae (Mammalia, Xenarthra, Mylodontidae) do Neógeno do Sítio Niterói, Acre, Brasil. *Acta Geológica Leopoldensia*, 22(48): 57–67.

Bocquentin, J. & Melo, J. 2006. *Stupendemys souzai* sp. nov. (Pleurodira, Podocnemididae) from the Miocene-Pliocene of the Solimões Formation, Brazil. *Revista Brasileira de Paleontologia*, 9(2): 18–192.

Bocquentin, J. & Silva, W. 1994. Cf. *Gyrinodon* sp. (Notoungulata. Toxodontidae) proveniente do Mioceno Superior da localidade de Cavalcante, Acre, Brasil. *Acta Geológica Leopoldensia*, 39(1): 391–398.

Bocquentin, J.V. & Souza-Filho, J.P. 1990. O crocodiliano sul-americano *Carandaisuchus* como sinonímia de *Mourasuchus* (Nettosuchidae). *Revista Brasileira de Geociências*, 20: 230–233.

Bocquentin, J., Guilherme, E. & Negri, F.R. 2001. Duas espécies do gênero *Chelus* (Pleurodira, Chelidae) no Mioceno Superior - Plioceno Inferior da Amazônia Sul-Ocidental. *Revista Geociências*, 6(6): 50–55.

Bocquentin, J., Souza-Filho, J.P., Rodrigues, A. & Silva, G. 1996. A coleção de vertebrados fósseis do Laboratório de Paleontologia da Universidade Federal do Acre, Brasil. In: Latrubesse, E.M. (ed.). *Paleo e Neoclimas da Amazônia Sul-Ocidental*. Rio Branco, UFAC, p. 76–89.

Boivin, M., Marivaux, L., Orliac, M.J., Pujos, F., Salas-Gismondi, R., Tejada-Lara, J.V. & Antoine, P.-O. 2017a. Late middle Eocene caviomorph rodents from Contamana, Peruvian Amazonia. *Palaeontologia Electronica*, 20.1.19A: 1–50.

Boivin, M., Marivaux, L., Pujos, F., Salas-Gismondi, R., Tejada-Lara, J.V., Varas-Malca, R. & Antoine, P.-O. 2018. Early Oligocene rodents from Shapaja, Peruvian Amazonia. *Palaeontrographica*, 311(1–6): 87–156.

Boivin, M., Marivaux, L., Candela, A.M., Orliac, M.J., Pujos, F., Salas-Gismondi, R., Tejada-Lara, J.V. & Antoine, P.-O. 2017b. Late Oligocene Caviomorph rodents from Contamana, Peruvian Amazonia. *Papers in Paleontology*, 3(1): 69–109.

Boivin, M., Marivaux, L., Aguirre-Díaz, W., Andriolli Custódio, M., Benites-Palomino, A., Pujos, F., Roddaz, M., Salas-Gismondi, R., Stutz, N., Tejada-Lara, J.V., Yans, J. & Antoine, P.-O. 2021. Eocene caviomorph rodents from Balsayacu (PeruvianAmazonia). *Paläontologische Zeitschrift*, 96: 135–160.

Boonstra, M., Troelstra, S.R., Lammertsma, E.I., Ramos, M.I.F., Antoine, P.-O. & Hoorn, C. 2015. Marine connections of Amazonia: Evidence from foraminifera and dinoflagellate cysts (early to middle Miocene, Colombia/Peru). *Palaeogeography, Palaeoclimatology, Palaeoecology*, 417: 176–194.

Broin, F., Bocquentin, J. & Negri, F.R. 1993. Gigant turtles (Pleurodira, Podocnemididae) from the late Miocene-early Pliocene of South Western Amazon. *Bulletin de l'Institut Français d'Études Andines*, 22(3): 657–670.

Brusatte, S., Luo, Z.-X. 2016. The ascent of mammals. *Scientific American*, 314: 28–35.

Cáceres, N.C. (org.). 2012. *Os marsupiais do Brasil: biologia, ecologia e conservação*. 2ª ed. Campo Grande, Editora UFMS, 498 p.

Cáceres, N.C. & Cherem, J.J. 2012. Introdução. In: Cáceres, N.C. (org.). *Os marsupiais do Brasil: biologia, ecologia e conservação*. 2ª ed. Campo Grande, Editora UFMS, p. 9–16.

Campbell, K.E. (Ed.). 2004. *The Paleogene mammalian fauna of Santa Rosa, Amazonian Peru*. Los Angeles, Science Series, Natural History Museum of Los Angeles County, 163 p.

Campbell, K.E., O'Sullivan, P.B., Fleagle, J.G., de Vries, D. & Seiffert, E.R. 2021. An early Oligocene age for the oldest known monkeys and rodents of South America. *PNAS*, 118(37): e2105956118.

Campos, D.A. 1977. *Tartarugas fósseis do Brasil*. Rio de Janeiro, 101 p. Dissertação de Mestrado, Universidade Federal do Rio de Janeiro.

Campos, D.A. & Broin, F. 1981. Tartarugas fósseis do Brasil. *Anais da Academia Brasileira de Ciências*, 53(1): 210–211.

Cardillo, M., Bininda-Emonds, O.R.P., Boakes, E. & Purvis, A. 2004. A species-level phylogenetic supertree of marsupials. *Journal of Zoology*, 264(1): 11–31.

Carneiro, L.M., Oliveira, E.V. & Goin, F.J. 2018. *Austropediomys marshalli* gen. et sp. nov., a new Pediomyoidea (Mammalia, Metatheria) from the Paleogene of Brazil: paleobiogeographic implications. *Revista Brasileira de Paleontologia*, 21(2): 120–131.

Carvalho, P., Bocquentin, J. & Broin, F.L. 2002. Une nouvelle espèce de *Podocnemis* (Pleurodira, Podocnemididae) provenant du Néogène de la Formação Solimões, Acre, Brésil. *Geobios*, 35: 677–686.

Case, J.A., Goin, F.J. & Woodburne, M.O. 2005. “South American” marsupials from the Late Cretaceous of North America and the origin of marsupial cohorts. *Journal of Mammalian Evolution*, 12: 461–494.

Castro, M. & Langer, M. 2011. The mammalian fauna of Abismo Iguatemi, Southeastern Brazil. *Journal of Cave and Karst Studies*, 73(2): 83–92.

Castro, M.C., Dahur, M.J. & Ferreira, G.S. 2021. Amazonia as the origin and diversification area of Didelphidae (Mammalia: Metatheria), and a review of the fossil record of the clade. *Journal of Mammalian Evolution*, 28: 583–598.

Chabain, J., Antoine, P.-O., Altamiro-Sierra, A.J., Marivaux, L., Pujos, F., Salas Gismondi, R. & Adnet, S. 2017. Cenozoic batoids from Contamana (Peruvian Amazonia) with focus on freshwater potamotrygonins and their paleoenvironmental significance. *Geobios*, 50(5–6): 389–400.

Chornogubsky, L. & Goin, F.J. 2015. A review of the molar morphology and phylogenetic affinities of *Sillustania quechuense* (Metatheria, Polydolopimorphia, Sillustaniidae), from the early Paleogene of Laguna Umayo, Southeastern Peru. *Journal of Vertebrate Paleontology*, 35(6): e983238.

Chornogubsky, L., Goin, F.J. & Reguero, M.A. 2009. A reassessment of Antarctic polydolopid marsupials (Middle Eocene, La Meseta Formation). *Antarctic Science*, 21(3): 285–297.

Chornogubsky, L., Zimicz, N., Goin, F.J., Fernicola, J.C., Payrola P. & Cárdenas, M. 2019. New Palaeogene metatherians from the Quebrada de Los Colorados Formation at Los Cardones National Park (Salta Province, Argentina). *Journal of Systematic Palaeontology*, 17(7): 539–555.

Cidade, G.M., Souza-Filho, J.P., Hsiou, A.S., Brochu, C.A. & Riff, D. 2019. New specimens of *Mourasuchus* (Alligatorioidea, Caimaninae) from the Miocene of Brazil and Bolivia and their taxonomic and morphological implications. *Alcheringa*, 43(4): 1–18.

Cifelli, R.L. & Davis, B.M. 2003. Marsupial origins. *Science*, 302: 1899–1900.

Couto-Ribeiro, G.C. 2010. *Avaliação morfológica, taxonômica e cronológica dos mamíferos fósseis da Formação Tremembé (Bacia de Taubaté), estado de São Paulo, Brasil*. 2010. São Paulo, 112 p. Dissertação de Mestrado, Universidade de São Paulo.

Cozzuol, M.A., Goin, F., De Los Reyes, M. & Ranzi, A. 2006. The oldest species of *Didelphis* (Mammalia, Marsupialia, Didelphidae), from the Late Miocene of Amazonia. *Journal of Mammalogy*, 87(4): 663–667.

Crochet, J.-Y., Antoine, P.-O., Benammi, M., Iqbal, N. & Marivaux, L. 2007. A herpetotheriid marsupial from the Oligocene of Bugti Hills, Balochistan, Pakistan. *Acta Palaeontologica Polonica*, 52(3): 633–637.

Cunha, P.R.C. 2007. Bacia do Acre. *Boletim de Geociências da Petrobrás*, 15(2): 207–215.

D'Elía, G., Hurtado, N. & D'Anatro, A. 2016. Alpha taxonomy of *Dromiciops* (Microbiotheriidae) with the description of 2 new species of monito del monte. *Journal of Mammalogy*, 97(4): 1136–1152.

Fernandes, F.L. & Chang, H.K. 2001. Modelagem gravimétrica da Bacia de Taubaté - Vale do rio Paraíba do Sul, leste do estado de São Paulo. *Revista Brasileira de Geofísica*, 19(2): 131–144.

Flynn, J.J., Wyss, A.R., Croft, D.A. & Charrier, R. 2003. The Tinguiririca fauna, Chile: biochronology, paleoecology, biogeography, and a new earliest Oligocene South American Land Mammal 'Age'. *Palaeogeography, Palaeoclimatology, Palaeoecology*, 195(3–4): 229–259.

Fonseca, G.A.B., Paglia, A.P., Sanderson, J. & Mittermeier, R.A. 2003. Marsupials of the new world: status and conservation. In: Jones, M., Dickman, C., Archer, M. (eds.). *Predators with pouches: the biology of carnivorous marsupials*. Collingwood, CSIRO Publishing, p. 399–406.

Fontoura, E., Negri, F.R., Ribeiro, A.M. & Kerber, L. 2022. A new Late Miocene hystricognath rodent assemblage (Caviidae, Dinomyidae, and Neoepiblemidae) from northern Brazil and its biostratigraphic relevance. *Historical Biology*: aop.

Forasiepi, A.M. 2009. Osteology of *Arctodictis sinclairi* (Mammalia, Metatheria, Sparassodonta) and phylogeny of Cenozoic metatherian carnivores from South America. *Monografías del Museo Argentino de Ciencias Naturales "Bernardino Rivadavia"*, 6: 1–174.

Forasiepi, A.M., Goin, F.J. & Martinelli, A.G. 2009. Contribution to the knowledge of the Sparassocynidae (Mammalia, Metatheria, Didelphoidea), with comments on the age of the Aisol Formation (Neogene), Mendoza Province, Argentina. *Journal of Vertebrate Paleontology*, 29(4): 1252–1263.

Forasiepi, A.M., Martinelli, A.G. & Goin, F.J. 2007. Revisión taxonómica de *Parahyaenodon argentinus* Ameghino y sus implicancias en el conocimiento de los grandes mamíferos carnívoros del Mio-Plioceno de América de Sur. *Ameghiniana*, 44(1): 143–159.

Frailey, C.D. 1986. Late Miocene and Holocene mammals, exclusive of the Notoungulata, of the Río Acre region, western Amazonia. *Natural History Museum of Los Angeles County Contributions in Science*, 374: 1–46.

Frailey, C.D. & Campbell, K.E. 2004. Paleogene rodents from Amazonian Peru: the Santa Rosa local fauna. In: Campbell, K.E. (ed). *The Paleogene mammalian fauna of Santa Rosa, Amazonian Peru*. Los Angeles, Natural History Museum of Los Angeles County, Science Series 40, p. 71–130.

Furió, M., Ruiz-Sánchez, F.J., Crespo, V.D., Freudenthal, M. & Montoya, P. 2012. The southernmost Miocene occurrence of the last European herpetotheriid *Amphiperatherium frequens* (Metatheria, Mammalia). *Comptes Rendus Palevol*, 11(5): 371–377.

Gaffney, E.S., Campbel, K.E. & Wood, R.C. 1998. Pelomedusoid side-necked turtles from Late Miocene sediments in Southwestern Amazonia. *American Museum Novitates*, 3245: 1–11.

Gallus, S., Janke, A., Kumar, V. & Nilsson, M.A. 2015. Disentangling the relationship of the Australian marsupial orders using retrotransposon and evolutionary network analyses. *Genome Biology and Evolution*, 7(4): 985–992.

Gardner, A.L. (Ed.). 2007. *Mammals of South America*. Vol. 1. Chicago, The University Of Chicago Press, 669 p.

Gayet, M., Jégu, M., Bocquentin, J. & Negri, F.R. 2003. New characoids from the upper Cretaceous and Paleocene of Bolivia and the Mio-Pliocene of Brazil: phylogenetic position and palaeobiogeographic implications. *Journal of Vertebrate Paleontology*, 23(1): 28–46.

Goin, F.J. 1997. New clues for understanding Neogene marsupial radiations. In: Kay, R.F., Madden, R.H., Cifelli, R.L. & Flynn, J.J. (eds.). *Vertebrate paleontology in the Neotropics: the Miocene fauna of La Venta, Colombia*. Washington, Smithsonian Institution Press, p. 187–206.

Goin, F.J. & Abello, A. 2013. Los Metatheria sudamericanos de comienzos del Neógeno (Mioceno temprano, Edad Mamífero Colhuehuapense): Microbiotheria y Polydolopimorphia. *Ameghiniana*, 50(1): 51–78.

Goin, F.J. & Candela, A.M. 2004. New Palaeogene marsupials from the Amazon Basin of Eastern Peru. In: Campbell, K.E. (ed). *The Paleogene mammalian fauna of Santa Rosa, Amazonian Peru*. Los Angeles, Natural History Museum of Los Angeles County, Science Series 40, p. 15–60.

Goin, F.J., Abello, M.A. & Chornogubsky, L. 2010. Middle Tertiary marsupials from central Patagonia (early Oligocene of Gran Barranca): understanding South America's Grande Coupure. In: Madden, R.H., Carlini, A.A., Vucetich, M.G., Kay, R.F. (eds.). *The Paleontology of Gran Barranca*. Cambridge, Cambridge University Press, p. 69–105.

Goin, F.J., Candela, A.M. & López, G. 1998. Middle Eocene marsupials from Antofagasta de la Sierra, Northwestern Argentina. *Geobios*, 31(1): 75–85.

Goin, F.J., Candela, A., Abello, M.A.; Oliveira, E.V. 2009. Earliest South American paucituberculatans and their significance in the understanding of 'pseudodiprotodont' marsupial radiations. *Zoological Journal of the Linnean Society*, 155: 867–884.

Goin, F.J., Sánchez-Villagra, M., Abello, M.A. & Kay, R.F. 2007a. A new generalized paucituberculatan marsupial from the Oligocene of Bolivia and the origin of the 'shrew-like' opossums. *Palaeontology*, 50(5): 1267–1276.

Goin, F.J., Gelfo, J.N., Chornogubsky, L., Woodburne, M.O. & Martin, T. 2012. Origins, radiations, and distribution of South American mammals: from greenhouse to icehouse worlds. In: Patterson, B.D. & Costa, L.P. (eds.). *Bones, clones, and biomes: an 80-million year history of recent Neotropical mammals*. Chicago, The University of Chicago Press, p. 20–50.

Goin, F.J., Woodburne, M.O., Zimicz, A.N., Martin, G.M. & Chornogubsky, L. 2016. *A brief history of South American metatherians*. New York, Springer Earth System Sciences, 237 p.

Goin, F.J., Abello, A., Bellosi, E., Kay, R., Madden, R. & Carlini, A. 2007b. Los Metatheria sudamericanos de comienzos del Neógeno (Mioceno Temprano, Edad-mamífero Colhuehuapense). Parte I: Introducción, Didelphimorphia y Sparassodonta. *Ameghiniana*, 44(1): 29–71.

Goin, F.J., Zimicz, N., Reguero, M.A., Santillana, S.N., Marenssi, S.A. & Moly, J.J. 2007c. New marsupial (Mammalia) from the Eocene of Antarctica, and the origins and affinities of the Microbiotheria. *Revista de la Asociación Geológica Argentina*, 62(4): 597–603.

Goin, F.J., Pascual, R., Tejedor, M.F., Gelfo, J.N., Woodburne, M.O., Case, J.A, Reguero, M.A., Bond, M., Lopez, G.M., Cione, A.L. *et al*. 2006. The earliest Tertiary therian mammal from South America. *Journal of Vertebrate Paleontology*, 26(2): 505–510.

Haag, N.A. 2019. *Palinostratigrafia do Meso-Cenozoico da Bacia Do Acre (Amazônia sul ocidental, Brasil)*. Coimbra, 424 p. Tese de Doutorado Universidade de Coimbra.

Hadler, P., Ferigolo, J. & Goin, F.J. 2009. Mamíferos de pequeno porte (Didelphimophia, Chiroptera e Rodentia) do Pleistoceno Final/Holoceno do Brasil, com ênfase no Rio Grande do Sul. In: Ribeiro, A.M., Bauermann, S.G. & Scherer, C.S. (orgs.) *Quaternário do Rio Grande do Sul: integrando conhecimentos*. Porto Alegre, Sociedade Brasileira de Paleontologia, p. 155–170.

Hadler, P., Cherem, J.J., Turbay, R., Alberti, A. & Pardiñas, U.F.J. 2016. Diversidade de pequenos mamíferos (Didelphimorphia e Rodentia) do Holoceno do Nordeste do Estado do Rio Grande do Sul, Brasil: implicações taxonômicas e paleoambientais. *Revista Brasileira de Paleontologia*, 19(1): 126–144.

Hershkovitz, P. 1982. The staggered marsupial lower third incisor (i3). *Geobios*, 15(1): 191–200.

Hershkovitz, P. 1999. *Dromiciops gliroides* Thomas, 1894, last of the Microbiotheria (Marsupialia), with a review of the family Microbiotheriidae. *Fieldiana, Zoology*, 93: 1–60.

Hoorn, C., Bogotá-A, G.R., Romero-Baez, M., Lammertsma, E.I., Flantua, S.G., Dantas, E. L., Dino, R., do Carmo, D.A. & Chemale Jr, F. 2017. The Amazon at sea: Onset and stages of the Amazon River from a marine record, with special reference to Neogene plant turnover in the drainage basin. *Global and Planetary Change*, 153: 51–65.

Hoorn, C., Wesselingh, F.P., Ter Steege, H., Bermudez, M.A., Mora, A., Sevink, J., Sanmartín, I., Sanchez-Meseguer, A., Anderson, C.L., Figueiredo, J.P., Jaramillo, C., Riff, D., Negri, F.R., Hooghiemstra, H., Lundberg, J., Stadler, T., Särkinen, T. & Antonelli, A. 2010. Amazonia through time: Andean uplift, climate change, landscape evolution, and biodiversity. *Science*, 330: 927–931.

Horovitz, I. & Sánchez-Villagra, M.R. 2012. El registro fóssil del Cenozoico. In: Sánchez-Villagra, M.R. (ed.). *Venezuela paleontológica*.Zürich, Universität Zürich, p. 133–156.

Horovitz, I., Martin, T., Bloch, J., Ladevèze, S., Kurz, C. & Sánchez-Villagra, M.R. 2009. Cranial anatomy of the earliest marsupials and the origin of opossums. *PLOS ONE*, 4(12): e8278.

Hsiou, A.S. & Albino, A.M. 2009. Presence of the Genus *Eunectes* (Serpentes, Boidae) in the Neogene of Southwestern Amazonia, Brazil. *Journal of Herpetology*, 43(4): 612–619.

Hsiou, A.S. & Albino, A.M. 2010. New snake remains from the Miocene of Northern South America. *Herpetological Journal*, 20: 249–259.

Hsiou, A.S., Albino, A.M. & Ferigolo, J. 2009. First lizard remains (Teiidae) from the Miocene of Brazil (Solimões Formation). *Revista Brasileira de Paleontologia*, 12(3): 225–230.

Hsiou, A.S., Albino, A.M. & Ferigolo, J. 2010. Reappraisal of the South American Miocene snakes of the genus *Colombophis,* with description of a new species. *Acta Palaeontologica Polonica*, 55: 365–379.

Hsiou, A.S., Bissaro-Júnior, M.C., Muniz, F.P., Negri, F.R., Ribeiro, A.M. & Kerber, L. 2022. Bacia do Acre: Evidências das paisagens da proto- Amazônia há 10 milhões de anos, com base em vertebrados fósseis da Formação Solimões. In: Corecco, L. (ed.). *Paleontologia do Brasil: paleoecologia e Paleoambientes*. Rio de Janeiro, Interciência, p. 29–64.

Jansa, S.A., Barker, F.K. & Voss, R.S. 2013. The early diversification history of didelphid marsupials: a window into South America's “splendid isolation”. *Evolution*, 68: 684–695.

Jones, M., Dickman, C. & Archer, M. (eds.). 2003. *Predators with pouches: the biology of carnivorous marsupials*. Collingwood, CSIRO Publishing, 486 p.

Kay, R.F., Madden, R.H., Cifelli, R.L. & Flynn, J.J. (Eds.). 1997. *Vertebrate paleontology in the Neotropics: the Miocene fauna of La Venta, Colombia*. Washington, Smithsonian Institution Press, xvi + 592 p.

Kemp, T. S. 2005. *The origin and evolution of mammals*. Oxford, Oxford University Press, 331 p.

Kerber, L., Ferreira, J.D. & Negri, F.R. 2019a. A reassessment of the cranial morphology of *Neoepiblema acreensis* (Rodentia: Chinchilloidea), a Miocene rodent from South America. *Journal of Morphology*, 280(12): 1821–1838.

Kerber, L., Negri, F.R. & Sanfelice, D. 2019b. Morphology of cheek teeth and dental replacement in the extinct rodent *Neoepiblema* Ameghino, 1889 (Caviomorpha, Chinchilloidea, Neoepiblemidae). *Journal of Vertebrate Paleontology*, 38(6): e1549061.

Kerber, L., Negri, F.R., Ribeiro, A.M., Vucetich, M.G. & Souza-Filho, J.P. 2016. Late Miocene potamarchine rodents from southwestern Amazonia, Brazil—with description of new taxa. *Acta Palaeontologica Polonica*, 61(1): 191–203.

Kerber, L., Bissaro Júnior, M.C., Negri, F.R., Souza-Filho, J.P., Guilherme, E. & Hsiou, A.S. 2018. A new rodent (Caviomorpha: Dinomyidae) from the upper Miocene of southwestern Brazilian Amazonia. *Historical Biology*, 30(7): 985–993.

Kerber, L., Candela, A.M., Ferreira, J.D., Pretto, F.A., Bubadué, J. & Negri, F.R. 2022. Postcranial Morphology of the extinct rodent *Neoepiblema* (Rodentia: Chinchilloidea): insights into the paleobiology of neoepiblemids. *Journal of Mammalian Evolution*, 29(1): 207–235.

Kerber, L., Negri, F.R., Ribeiro, A.M., Nasif, N., Souza-Filho, J. & Ferigolo, J. 2017. Tropical fossil caviomorph rodents from the Southwestern Brazilian Amazonia in the context of the South American faunas: systematics, biochronology, and paleobiogeography. *Journal of Mammalian Evolution*, 24: 57–70.

Kielan-Jaworowska, Z., Cifelli, R. & Luo, Z. 2004. *Mammals from the age of dinosaurs: origins, evolution, and structure*. New York, Columbia University Press, 630 p.

Klaus, S., Magalhães, C., Salas-Gismondi, R., Gross, M. & Antoine, P.-O. 2017. Palaeogene and Neogene brachyurans of the Amazon basin: a revised first appearance date for primary freshwater crabs (Brachyura, Trichodactylidae). *Crustaceana*, 90(7–10): 953–967.

Kloster, A., Gnaedinger, S. & Adami-Rodrigues, K. 2017. Nuevos registros de maderas del Mioceno de la Formación Solimões, cuenca de Acre, Amazonia, Brasil. *Revista Brasileira de Paleontologia*, 20(3): 383–404.

Kloster, A., Gnaedinger, S., Adami-Rodrigues, K. & Urban, C. 2015. New record of Fabaceae fossil woods from the Solimões Formation (Miocene), Acre Basin, Amazon, Brazil. *Revista Brasileira de Paleontologia*, 18(3): 391–492.

Lacerda, M.B.S., De Souza, L.G., Lobo, L.S., Schaefer, C.E.G.R. & Romano, P.S.R. 2020. New outcrop with vertebrate remains from Solimões Formation (Eocene–Pliocene), Southern Solimões Basin, Acre State, Northern Brazil. *Journal of South American Earth Sciences*, 101: 102588.

Latrubesse, E.M., Bocquentin, J., Santos, C.R. & Ramonell, C.G. 1997. Paleoenvironmental model for the late Cenozoic Southwestern Amazonia: paleontology and geology. *Acta Amazonica*, 27(2): 103–118.

Leite, F.P.R.; Silva-Caminha, S.A.F. & D'Apolito, C. 2021. New Neogene index pollen and spore taxa from the Solimões Basin (Western Amazonia), Brazil. *Palynology*, 45(1): 115–141.

Linares, O.J. 2004. Bioestratigrafia de la fauna de mamiferos de las Formaciones Socorro, Urumaco y Codore (Mioceno Medio-Plioceno Temprano) de la region de Urumaco, Falcon, Venezuela. *Paleobiologia Neotropical*, 1: 1–26.

Lynch, T.F. (Ed.). 1980. *Guitarrero Cave: early man in the Andes*. New York, Academic Press INC, 350 p.

Luo, Z.X., Ji, Q., Wible, J.R. & Yuan, C.X. 2003. An Early Cretaceous tribosphenic mammal and metatherian evolution. *Science*, 302(5652): 1934–1940.

Machado, L.G., Bolzon, R.T., Carvalho, M.A. & Carvalho, I.S. 2006. Lenhos silicificados do Neógeno da Amazônia Sul-Ocidental (Estado do Acre), Brasil: um estudo preliminar. *Boletim da Sociedade Brasileira de Paleontologia*, 21(53): 20.

Machado, L.G., Scheel-Ybert, R., Bolzon, R.T., Carvalho, M.A. & Carvalho, I.S. 2012. Lenhos fósseis do Neógeno da Bacia do Acre, Formação Solimões: contexto paleoambiental. *Revista Brasileira de Geociências*, 42(1): 67–80.

Maga, A.M. & Beck, R.M.D. 2017. Skeleton of an unusual, cat-sized marsupial relative (Metatheria: Marsupialiformes) from the middle Eocene (Lutetian: 44-43 million years ago) of Turkey. *PLOS ONE*, 12(11): e0188132.

Mammal Diversity Database. (2022). *Mammal Diversity Database (Version 1.10) [Data set]. Zenodo*. Disponível em: https://www.mammaldiversity.org/taxa.html. Acesso em: 06 fev. 2023.

Marivaux, L., Adnet, S., Benammi, M., Tabuce, R., Yans, J. & Bennammi, M. 2017. Earliest Oligocene hystricognathous rodents from the Atlantic margin of northwestern Saharan Africa (Dakhla, Morocco): systematic, paleobiogeographical, and paleoenvironmental implications. *Journal of Vertebrate Paleontology*, 37: e1357567.

Marivaux, L., Adnet, S., Altamiro-Sierra, A.J., Ramdarshan, A., Salas-Gismondi, R., Tejada-Lara, J.V. & Antoine, P.-O. 2016a. Dental remains of cebid platyrrhines from the earliest late Miocene of Western Amazonia, Peru: macroevolutionary implications on the extant capuchin and marmoset lineages. *American Journal of Physical Anthropology*, 161: 478–493.

Marivaux, L., Adnet, S., Altamiro-Sierra, A.J., Boivin, M., Pujos, F., Ramdarshan, A., Salas-Gismondi, R., Tejada-Lara, J.V. & Antoine, P.-O. 2016b. Neotropics provide insights into the emergence of New World monkeys: new dental evidence from the late Oligocene of Peruvian Amazonia. *Journal of Human Evolution*, 97: 159–175.

Marivaux, L., Antoine, P.-O., Baqri, S.R.H., Benammi, M., Chaimanee, Y., Crochet, J.-Y., de Francheschi, D., Iqbal, N., Jaeger, J.-J., Métais, G., Roohi, G. & Welcomme, J.-L. 2005. Anthropoid primates from the Oligocene of Pakistan (Bugti Hills): Data on early anthropoid evolution and biogeography. *PNAS*, 102(24): 8436–8441.

May-Collado, L.J., Kilpratrick, C.W. & Agnarsson, I. 2015. Mammals from 'down under': a multi-gene species-level phylogeny of marsupial mammals (Mammalia, Metatheria). *PeerJ*, 3: e805.

Maury, C.J. 1937. Argilas fossilíferas do Plioceno do território do Acre. *Boletim do Serviço Geológico e Mineralógico*, 77: 29.

Meseguer, A., Michel A. J., Fabre, P.-H., Pérez-Escobar, O.A., Chomicki, G., Riina, R., Antonelli, A., Antoine, P.-O., Delsuc, F. & Condamine, F.L. 2022. Diversification dynamics in the Neotropics through time, clades, and biogeographic regions. *Elife* 11: e74503.

Miller, K.G. *et al*. 2020. Cenozoic sea-level and cryospheric evolution from deep-sea geochemical and continental margin records. *Science Advances*, 6(20): eaaz1346.

Mones, A. 1986. *Acremylodon* a new name for *Stenodon* Frailey, 1986 (Mammalia: Edentata: Mylodontidae). *Comunicaciones Paleontologicas del Museo de Historia Natural de Montevideo*, 16(1): 229.

Motta, F.A., Hadler, P., Cherem, J.J. & Ribeiro, A.M. 2019. A marsupial assemblage (Mammalia, Didelphimorphia) from the Quaternary of the Serra da Capivara, State of Piauí, Brazil. *Revista Brasileira de Paleontologia*, 22(3): 225–239.

Muizon, C. de & Ladevèze, S. 2020. Cranial anatomy of *Andinodelphys cochabambensis*, a stem metatherian from the early Palaeocene of Bolivia. *Geodiversitas*, 42(30): 597–739.

Negri, F. 2004. R. *Os Tardigrada (Mammalia, Xenarthra) do Neógeno, Amazônia Sul-Ocidental, Brasil*. 2004. Porto Alegre, 156 p. Tese de Doutorado, Pontifícia Universidade Católica do Rio Grande do Sul.

Negri, F.R. & Ferigolo, J. 1999. Anatomia craniana de *Neoepiblema ambrosettianus* (Ameghino, 1889; Rodentia, Caviomorpha, Neoepiblemidae) do Mioceno superior-Plioceno, Estado do Acre, Brasil, e revisão das espécies do gênero. *Boletim do Museu Paraense Emílio Goeldi*, 11: 1–80.

Negri, F.R., Bocquentin-Villanueva, J., Ferigolo, J. & Antoine, P.-O. 2010. A review of Tertiary mammal faunas and birds from Western Amazonia. In: Hoorn, C. & Wesselingh, F.P. (eds.). *Amazonia: Landscape and Species Evolution: A look into the past*. London, Wiley-Blackwell Publishing Ltd, p. 243–258.

Nilsson, M.M., Churakov, G., Sommer, M., Tran, N.V., Zemann, A., Brosius, J. & Schmitz, J. 2010. Tracking marsupial evolution using archaic genomic retroposon insertions. *PLoS Biology*, 8(7): e1000436.

Nova, P.V., Avilla, L.S. & Oliveira, E.V. 2015. Didelphidae marsupials (Mammalia, Didelphimorphia) from the Late Pleistocene deposit of the Gruta dos Moura Cave, northern Brazil. *Anais da Academia Brasileira de Ciências*, 87(1): 193–208.

Oliveira, E.V. & Goin, F.J. 2011. A reassessment of bunodont metatherians from the Paleogene of Itaboraí (Brazil): systematics and age of the Itaboraian SALMA. *Revista Brasileira de Paleontologia*, 14(2): 105–136.

Oliveira, P.V. 2010. *Mamíferos do Neopleistoceno - Holoceno do Parque Nacional de Ubajara, Ceará*. 2010. Porto Alegre, 166 p. Dissertação de Mestrado, Universidade Federal do Rio Grande do Sul.

OpossumBase. *OpossumBase: The Monodelphis domestica Genomic Resources Database*. Disponível em: http://opossumbase.org/. Acesso em: 05 mar. 2020.

Paleobiology Database. *Fossilworks*. Disponível em: http://fossilworks.org/bridge.pl?a=home. Acesso em: abril/maio 2020.

Pascual, R. 1980. Prepidolopidae, nueva familia de Marsupialia Didelphoidea del Eoceno Sudamericano. *Ameghiniana*, XVII(3):216–242.

Pascual, R. & Ortiz Jaureguizar, E. 1990. Evolving climates and mammal faunas in cenozoic South America. *Journal of Human Evolution*, 19(1-2): 23–60.

Patterson, B. & Costa, L. 2012. *Bones, clones, and biomes: the history and geography of recent neotropical mammals*. Chicago, The University of Chicago Press, 432 p.

Paula-Couto, C. 1944. Notícia preliminar sobre um novo Toxodonte do território do Acre: *Abothrodon pricei*. n. g., n. sp. *Boletim do Museu Nacional, Geologia*, 3: 1–4.

Paula-Couto, C. 1982. Fosil Mammals from the Cenozoic of Acre, Brazil. V – Notoungulata Nesodontinae (II), Toxodontinae and Haplodontheriinae, and Litopterna, Pyrotheria and Astrapotheria (II). *Iheringia, Série Geologia*, 7: 5–43.

Paula-Couto, C. 1983a. Fossil mammals from the Cenozoic of Acre, Brazil. VI – Edentata Cingulata. *Iheringia, Série Geologia*, 8: 33–49.

Paula-Couto, C. 1983b. Fossil mammals from the Cenozoic of Acre, Brazil. VII – Miscellanea. *Iheringia, Série Geologia*, 8: 101–120.

Price, L.I. 1964. Sobre o crânio de um grande crocodilideo extinto do alto rio Juruá, Estado do acre. *Anais da Academia Brasileira de Ciências*, 36: 59–66.

Radambrasil. 1977. *Levantamento de recursos naturais. Folha SC. 18 Rio Branco. Volume 12; Javari/Contamana, v. 13.* Rio de Janeiro, Departamento Nacional de Produção Mineral, 413 p.

Rancy, A. 1985. Estudos de paleovertebrados na Amazônia ocidental. *Série Geologia DNPM*, 27: 99–103.

Ribeiro, A.M., Madden, R. & Villanueva, J.B. 2005. Preliminary review of the systematics of the family Toxodontidae (Mammalia, Notoungulata, Toxodonta) from the Tertiary of

Acre State, Western Amazonian Brazil. *In*: 2º CONGRESSO LATINOAMERICANO DE PALEONTOLOGIA DE VERTEBRADOS, Rio de Janeiro, 2005. Boletim de Resumos, Rio de Janeiro, p. 220–221.

Ribeiro, A.M., Madden, R.H., Negri, F.R., Kerber, L., Hsiou, A.S. & Rodrigues, K.A. 2013. Mamíferos fósiles y biocronología en el suroeste de la Amazonia, Brasil. In: Brandoni, D., Noriega, J.I. (eds.). *El Neógeno de la Mesopotamia argentina*. Buenos Aires, Asociación Paleontológica Argentina, p. 207–221.

Riccomini, C. 1989. *O rift continental do sudeste do Brasil*. 1989. São Paulo, 256 p. Tese de Doutorado, Universidade de São Paulo.

Rincón, A.D., Shockey, B.J., Anaya, F. & Solórzano, A. 2015. Palaeothentid marsupials of the Salla Beds of Bolivia (Late Oligocene): two new species and insights into the post-Eocene radiation of palaeothentoids. *Journal of Mammalian Evolution*, 22: 455–471.

Roddaz, M., Hermoza, W., Mora, A., Baby, P., Parra, M., Christophoul, F., Brusset, S. & Espurt, N. 2010, Cenozoic sedimentary evolution of the Amazonian Foreland Basin System. In: Hoorn, C. & Wesselingh, F.P. (eds.). *Amazonia: Landscape and species evolution: A look into the past*. New York, Blackwell Publishing Ltd., p. 61–88.

Rodrigues, J.B. 1892. Les reptiles de la vallée de l'Amazone. *Vellosia*, 2: 41–60.

Rodrigues, K.A., Negri, F.R., Haag, N.A., Scomazzon, A.K., Urban, C., Ribeiro, A.M., Koester, E., Hsiou, A.S., Cardoso, N., Kerber, L. *et al*. 2016. *Relatório Científico Final: Projeto "Biocronoestratigrafia e paleoecologia com base no potencial fossilífero do Cretáceo - Neógeno da Bacia do Acre, vale do Juruá, Amazônia sul ocidental"*. Cruzeiro do Sul, Universidade Federal do Acre Campus Floresta, 89 p.

Rowe, T. 1988. Definition, diagnosis, and origin of Mammalia. *Journal of Vertebrate Paleontology*, 8(3): 241–264.

Sánchez-Villagra, M.R., Aguilera, O.A., Sánchez, R. & Carlini, A.A. 2010. The fossil vertebrate record of Venezuela of the last 65 million years. In: Sánchez-Villagra, M.R., Aguilera, O.A. & Carlini, A.A. (eds.). *Urumaco & Venezuelan Paleontology*. Bloomington, Indiana University Press, p. 19–51.

Sedor, F.A., Oliveira, E.V., Silva, D.D., Fernandes, L.A., Cunha, R.F., Ribeiro, A.M. & Dias, E.V. 2017. A new South American Paleogene land mammal fauna, Guabirotuba Formation (Southern Brazil). *Journal of Mammalian Evolution*, 24: 39–55.

Sigé, B. 1972. La faunule de mammifères du Crétacé supérieur de Laguna Umayo (Andes péruviennes). *Bulletin du Muséum National d'Histoire Naturelle*, 19: 375–405.

Sigé, B., Sempere, T., Butler, R.F., Marshall, L.G. & Crochet, J.-Y. 2004. Age and stratigraphic reassessment of the fossil-bearing Laguna Umayo red mudstone unit, SE Peru, from regional stratigraphy, fossil record, and paleomagnetism. *Geobios*, 37(6): 771–794.

Sigé, B., Archer, M., Crochet, J.-Y., Godthelp, H., Hand, S. & Beck, R. 2009. *Chulpasia* and *Thylacotinga*, late Paleocene-earliest Eocene trans-Antarctic Gondwanan bunodont marsupials: new data from Australia. *Geobios*, 42(6): 813–823.

Silva-Caminha, S.A.F, D'apolito, C., Jaramillo, C., Espinosa, B.S. & Rueda, M. 2020. Palynostratigraphy of the Ramon and Solimões formations in the Acre Basin, Brazil. *Journal of South American Earth Sciences*, 103: 102720.

Simpson, G.G. 1980. *Splendid isolation: the curious history of South American mammals*. New Haven, Yale Univesity Press, 266 p.

Simpson, G.G. & Paula-Couto, C. 1981. Fossil mammals from the Cenozoic of Acre, Brazil. III. Pleistocene Edentata Pilosa, Proboscidea, Sirenia, Perissodactyla and Artiodactyla. *Iheringia, Série Geologia*, 6: 11–73.

Soria, M.F. & Alvarenga, H.M.F. 1989. Nuevos restos de mamíferos de la Cuenca de Taubate, estado de São Paulo, Brasil. *Anais da Academia. Brasileira de Ciências*, 61(2): 157–175.

Sousa, F.N., Marques, R.C., Ribeiro, V.R., Gaia, G.A., Guilherme, E., Maciente, A., Souza-Filho, J.P., Hsiou, A.S. & Ghilardi, R.P. 2021. Gastropods from the Solimões Formation (Upper Miocene), Acre Basin, Brazil. *Revista Brasileira de Paleontologia*, 24(3): 195–204.

Souza-Filho, J.P. 1998. *Novas formas fósseis de Crocodylia (Alligatoridae e Gavialidae) da Formação Solimões, Cenozóico do Estado do Acre-Brasil, representadas por*

materiais cranianos e mandibulares. Porto Alegre, 194 p. Tese de Doutorado, Universidade Federal do Rio Grande do Sul.

Souza-Filho, J.P. & Guilherme, E. 2015. A paleontologia no Estado do Acre. In: Adamy, A. (org.). *Geodiversidade do Estado do Acre: programa geologia do Brasil levantamento da geodiversidade*. Porto Velho, CPRM, p. 145–158.

Souza-Filho, J.P., Bocquentin, J. & Negri, F.R. 1993. Um crânio de *Hesperogavialis* sp. (Crocodylia, Gavialidade), Mioceno superior-Plioceno do estado do Acre, Brasil. *Ameghiniana*, 30: 341–342.

Souza-Filho, J.P., Souza, R.G., Hsiou, A.S., Riff, D., Guilherme, E., Negri, F.R. & Cidade, G.M. 2019. A new caimanine (Crocodylia, Alligatoroidea) species from the Solimões Formation of Brazil and the phylogeny of Caimaninae. *Journal of Vertebrate Paleontology*, 38(5): e1528450.

Springer, M.S., Kirsch, J.A.W. & Case, J.A. 1997. The chronicle of marsupial evolution. In: Givnish, T. & Sytsma, K. (eds.). *Molecular evolution and adaptive radiation*. New York, Cambridge University, p. 129–61.

Stutz, N.S., Abello, M.A., Marivaux, L., Boivin, M., Pujos, F., Benites-Palomino, A.M., Salas-Gismondi, R., Tejada-Lara, J.V., Custódio, M.A., Roddaz, M., Santos, R.V., Ribeiro, A.M. & Antoine, P.-O. 2022. Late middle Miocene Metatheria (Mammalia: Didelphimorphia and Paucituberculata) from Juan Guerra, San Martín Department, Peruvian Amazonia. *Journal of South American Earth Sciences*, 118: 103902.

Suárez, C., Forasiepi, A., Goin, F.J. & Jaramillo, C. 2016. Insights into the Neotropics prior to the Great American Biotic Interchange: new evidence of mammalian predators from the Miocene of Northern Colombia. *Jounal of Vertebrate Paleontology*, 36(1): e1029581.

Suárez Gómez, C. 2019. *Estudios Taxonómicos y Paleobiológicos sobre los Metatheria (Mammalia) del Mioceno Medio de La Venta, Colombia*. La Plata, 292 p. Tese de Doutorado, Universidad Nacional de la Plata.

Szalay, F.S. 1982. A new appraisal of marsupial phylogeny and classification. In: Archer, M. (ed.). *Carnivorous marsupials*. Vol. 2. Mosman, Royal Zoological Society of New South Wales, p. 621–640.

Szalay, F.S. 1994. *Evolutionary history of the marsupials and an analysis of osteological characters*. New York, Cambridge University Press, xii + 481 p.

Tejada-Lara, J., Salas-Gismondi, R., Pujos, F., Baby, P., Benammi, M., Brusset, S., Franceschi, D., Espurt, N., Urbina, M. & Antoine, P.-O. 2015. Life in Proto-Amazonia: Middle Miocene mammals from the Fitzcarrald Arch (Peruvian Amazonia). *Palaeontology*, 58(2): 341–378.

Tejedor, M.F., Goin, F.J., Gelfo, J.N., López, G., Bond, M., Carlini, A.A., Scillato-Yané, G.J., Woodburne, M.O., Chornogubsky, L., Aragón, E. *et al*. 2009. New Early Eocene mammalian fauna from Western Patagonia, Argentina. *American Museum Novitates*, 3638: 1–43.

Upham, N.S., Esselstyn, J.A. & Jetz, W. 2021. Molecules and fossils tell distinct yet complementary stories of mammal diversification. *Current Biology*, 31(19): 4195–4206.e3.

Upham, N.S., Esselstyn, J.A. & Jetz, W. 2019. Inferring the mammal tree: Species-level sets of phylogenies for questions in ecology, evolution, and conservation. *PLoS Biol*, 17(12): e3000494.

Voss, R.S. 2022. An annotated checklist of recent opossums (Mammalia: Didelphidae). *Bulletin of the American Museum of Natural History*, 455(1): 1–76.

Voss, R.S. & Jansa, S.A. 2009. Phylogenetic relationships and classification of didelphid marsupials, an extant radiation of New World metatherian mammals. *Bulletin of the American Museum of Natural History*, 322: 1–177.

Wanderley-Filho, J.R., Eiras, J.E., Cunha, P.R.C. & Van Der Ven, P.H. 2010. The Paleozoic Solimões and Amazonas basins and the Acre foreland basin of Brazil. Hoorn, C. & Wesselingh, F.P. (eds.). *Amazonia: landscape and species evolution. A look into the past*. London, Wiley-Blackwell Publishing Ltd, p. 29–37.

Weaver, L.N., Fulghum, H.Z., Grossnickle, D.M., Brightly, W.H., Kulik, Z.T., Wilson Mantilla, G.P. & Whitney, M.R. 2022. Multituberculate mammals show evidence of a life history strategy similar to that of placentals, not marsupials. *The American Naturalist*, 200(3): 383–400.

Westerhold, T. *et al*. 2020. An astronomically dated record of Earth's climate and its predictability over the last 66 million years. *Science*, 369, 1383–1387.

Williamson, T.E., Brusatte, S.L. & Wilson, G.P. 2014. The origin and early evolution of metatherian mammals: the Cretaceous record. *Zookeys*, 465: 1–76.

Williamson, T.E., Brusatte, S.L., Carr, T.D., Weil, A. & Standhardt, B.R. 2012. The phylogeny and evolution of Cretaceous–Palaeogene metatherians: cladistic analysis and description of new early Palaeocene specimens from the Nacimiento Formation, New Mexico. *Journal of Systematic Palaeontology*, 10(4): 625–651.

Woodburne, M.O., Goin, F.J., Bond, M., Carlini, A.A., Gelfo, J.N., López, G.M., Iglesias, A. & Zimicz, A.N. 2014. Paleogene land mammal faunas of South America; a response to global climatic changes and indigenous floral diversity. *Journal of Mammalian Evolution*, 21: 1–73.

Zachos, J., Pagani, M., Sloan, L., Thomas, E. & Billups, K. 2001. Trends, Rhythms, and Aberrations in Global Climate 65 Ma to Present. *Science*, 292(5517): 686–693.

PARTE II – ARTIGOS

1 ARTIGO 1 – LATE MIDDLE MIOCENE METATHERIA (MAMMALIA: DIDELPHIMORPHIA AND PAUCITUBERCULATA) FROM JUAN GUERRA, SAN MARTÍN DEPARTMENT, PERUVIAN AMAZONIA

Artigo publicado no periódico *Journal of South American Earth Sciences* (Conceito CAPES A3), volume 118, artigo 103902, DOI: 10.1016/j.jsames.2022.103902.

Narla S. Stutz[1,2*]; María Alejandra Abello[3]; Laurent Marivaux[2]; Myriam Boivin[4]; François Pujos[5]; Aldo M. Benites-Palomino[6,7]; Rodolfo Salas-Gismondi[7,8]; Julia V. Tejada-Lara[9]; Michele Andriolli Custódio[10,11,12]; Martin Roddaz[11,12]; Roberto Ventura Santos[11]; Ana Maria Ribeiro[1,13]; Pierre-Olivier Antoine[2]

[1]Programa de Pós-Graduação em Geociências, Universidade Federal do Rio Grande do Sul (PPGGEO UFRGS), Avenida Bento Gonçalves, 9500, 91501-970, Porto Alegre, Brazil

[2]Laboratoire de Paléontologie, Institut des Sciences de l'Évolution de Montpellier (ISEM, UMR 5554, UM/CNRS/IRD/EPHE), Université de Montpellier, Place Eugène Bataillon, 34095, Montpellier, France

[3]Unidades de Investigación Anexo Museo, Facultad de Ciencias Naturales y Museo (UNLP), Avenida 60 y 122, B1900FWA, La Plata, Argentina

[4]Instituto de Ecorregiones Andinas (INECOA), Universidad Nacional de Jujuy, CONICET, IdGyM, Avenida Bolivia 1661, 4600, San Salvador de Jujuy, Argentina

[5]Instituto Argentino de Nivología, Glaciología y Ciencias Ambientales (IANIGLA), CCT–CONICET–Mendoza, Avenida Ruiz Leal s/n, Parque Gral. San Martín, 5500, Mendoza, Argentina

[6]Paläontologisches Institut und Museum, Universität Zürich, Karl-Schmid-Strasse 4, 8006, Zürich, Switzerland

[7]Departamento de Paleontología de Vertebrados, Museo de Historia Natural - Universidad Nacional Mayor San Marcos (UNMSM, DPV-MUSM), Avenida Arenales 1256, Lima 14, Peru

[8]BioGeoCiencias Lab, Facultad de Ciencias y Filosofía/CIDIS, Laboratorios de Investigacion y Desarrollo (LID), Centro de Investigación para el Desarrollo Integral y Sostenible (CIDIS), Universidad Peruana Cayetano Heredia, Avenida Honorio Delgado 430, Lima 31, Peru

[9]Department of Archaeology, University of Cambridge, Downing Street, CB2 3DZ, Cambridge, England.

[10]Instituto de Ciências Exatas, Departamento de Geociências, Universidade Federal do Amazonas (UFAM), Avenida General Rodrigo Octavio Jordão Ramos, 1200, Coroado I, 69067-005, Manaus, Brazil

[11]Laboratório de Geocronologia, Instituto de Geociências, Universidade de Brasília (UnB), Campus Universitário Darcy Ribeiro ICC - Ala Central, 70910-000, Brasília, Brazil

[12]Géosciences-Environnement Toulouse, Université de Toulouse (UPS (SVT-OMP)/CNRS/IRD), 14 Avenue Édouard Belin, F-31400, Toulouse, France

[13]Seção de Paleontologia, Museu de Ciências Naturais, Secretaria do Meio Ambiente e Infraestrutura, Avenida Dr. Salvador França, 1427, 90690-000, Porto Alegre, Brazil

*Corresponding author. *Email address*: narlasstutz@gmail.com (N. Stutz).

Abstract

Currently, marsupials (modern members of the Metatheria clade) are widely distributed in tropical and subtropical areas of South America, but poorly represented in the fossil record of these regions. Except for the species-rich fossiliferous localities of La Venta in Colombia, additional Miocene metatherians from tropical, equatorial South America are sparsely reported in Bolivia, Brazil, Peru, and Venezuela. Here, we introduce new metatherian remains recovered from the late middle Miocene locality of TAR-31, San Martín Department, Peru, which has been assigned to the Laventan South American Land Mammal Age (~13 Ma) by mammalian biostratigraphy. Three metatherian taxa are recognized at TAR-31: the didelphid didelphimorph '*Thylamys*' cf. '*T*.' *colombianus*, and the paucituberculatans aff. *Palaeothentes* and *Pitheculites ipururensis* sp. nov. This assemblage and the presence of a cebid primate at TAR-31 suggests predominantly humid and warm tropical conditions, with the occurrence of both forests

and drier habitats in the surroundings. Comparisons with other Miocene metatherian assemblages at low and mid latitudes of South America clearly confirm close relationships between TAR-31 and La Venta (agreeing with observations based on monkeys and rodents), as well as, to a lesser extent, with Acre River local faunas and Madre de Dios (MD-67) in Brazil and Peru, respectively. The current results support the hypothesis that Western Amazonia was a single and consistent biogeographical region for land mammals over middle Miocene times, at the western edge of the Pebas Mega-Wetland System, and highlight the role of the Amazonian region concerning marsupial Neogene radiation. U-Pb analysis made on detrital zircon grains from TAR-31 gave a maximum depositional age of 17.4 ± 0.12 Ma (*i.e.*, 4 Ma older than the biostratigraphical age), with a mixed detrital source likely comprising Precambrian (Western Amazon Craton), Neoproterozoic (Neoproterozoic mobile belts), and Phanerozoic rocks (Andes).

Keywords: Paucituberculata, Didelphimorphia, Laventan, Paleobiogeography, Pebas Mega-Wetland System.

1. Introduction

Western Amazonia has been regarded as an epicenter of biodiversity across the entire Cenozoic era (*e.g.*, Hoorn *et al*., 2010; Antoine *et al*., 2016, 2021; Carvalho *et al*., 2021). In particular, this area hosted a great mammalian diversity during the middle to late Miocene interval (with up to 14 orders and 40 families documented; Antoine *et al*., 2017). This large diversity in northern South America coincides with a series of geomorphological processes related to the Andean orogeny (Hoorn *et al*., 2010; Moreno *et al*., 2020), and with the Miocene Climatic Optimum (**MCO**; Hoorn *et al*., 2010; Westerhold *et al*., 2020), which would have promoted the growth of tropical forests (probably present in the area since the Paleocene; Wing *et al*., 2009; Jaramillo *et al*., 2010, 2017; Carvalho *et al.*, 2021). Furthermore, between 18 to 10 Ma, Western Amazonia was heavily influenced by the Pebas Mega-Wetland System (**PMWS**), an unparalleled landscape complex with wetlands, swamps, lakes, floodplains, and fluvial systems covering a broad area, fed by water and sediments coming from the Andes, and sporadic marine influence (Hoorn *et al*., 2010; Boonstra *et al*., 2015; Antoine *et al*.,

2016; Alvim *et al*., 2021). This system probably resembled the South American Pantanal in some ways, but differing from it in being considerably larger (Marivaux *et al.*, 2020).

Only a few Miocene fossil mammal-bearing localities are known to depict Miocene faunas at tropical latitudes of South America. These include the Castillo, Querales, Socorro, and Urumaco formations in Venezuela (various localities, early, middle and late Miocene in age; Quiroz and Jaramillo, 2010; Sánchez-Villagra *et al*., 2010; Rincón *et al*., 2014; Moreno *et al*., 2015); Acre basin in Brazil (various localities, late Miocene in age; Negri *et al*., 2010; Bissaro-Júnior *et al*., 2019); Madre de Dios (MD-67 locality, early middle Miocene in age; Antoine *et al*., 2013), Fitzcarrald local fauna (various localities, late middle Miocene in age; Tejada-Lara *et al*., 2015), Tamshiyacu (late middle Miocene; Salas-Gismondi *et al*., 2015), Contamana (various localities spanning the early–early late Miocene; Antoine *et al*., 2016), and Juan Guerra area (locality of TAR-31; Marivaux *et al*., 2020; Boivin *et al*., 2021) in Peru; as well as in Colombia with the Castilletes Formation and the outstanding La Venta fauna (Kay *et al*., 1997; Suárez *et al*., 2016). The best studied of these fossil communities is La Venta, which is represented by dozens of fossil-bearing localities of the Honda Group at the Magdalena Valley, spanning 13.5–11.6 Ma (*e.g*., Montes *et al*., 2021). The La Venta fauna is currently considered the most-diverse and best-documented fossil vertebrate assemblage from the Neotropics (Kay *et al*., 1997; Croft, 2016; Defler, 2019) and typifies the Laventan South American Land Mammal Age (**SALMA**). The Laventan fauna points to significant differences between the fossil record at low and mid+high latitudes of South America, including at composition and abundance level (*e.g*., Kay *et al*., 1997; Engelman *et al*., 2015, 2017; Suárez Gómez, 2019).

Nevertheless, several authors (*e.g*., Flynn *et al*., 2012; Antoine *et al*., 2016, 2017; Goin *et al*., 2016) have noted the poverty of the fossil record of northern South America when compared to that of mid to high latitudes (up to 50° S) of the landmass. Furthermore, among the records already reported for the Amazon region, most of these remains pertain to large eutherian mammals. These biases have long hampered the record and understanding of the paleodiversity and evolution of small mammals, which are the most speciose in Amazonian mammalian guilds (*i.e*., Metatheria, Chiroptera, Primates, and Rodentia; Antoine *et al*., 2017; Defler, 2019). The situation has recently

changed thanks to new collecting techniques (screen-washing; *e.g.*, Antoine *et al.*, 2016, 2017), allowing for sampling microvertebrates and, among them, micromammals.

Metatheria, whose living representatives are the marsupials (*e.g.*, opossums, shrew opossums, and *monito del monte* in the Americas; kangaroos, koalas, and others in Australasia), are currently distributed in South America mainly in tropical and subtropical areas, but poorly represented in the fossil record of these regions (Goin *et al.*, 2007, 2016; Antoine *et al.*, 2017; Voss and Jansa, 2021). During the Miocene epoch, South American fossil metatherians from low and mid-latitudes are solely reported at Cerdas (a new Borhyaenoidea still to be described, Croft *et al.*, 2016), Quebrada Honda (seven species of three families of three orders; Engelman *et al.*, 2017, 2020), and Achiri (Altiplano, with the sparassodontan *Borhyaenidium altiplanicum*, Villarroel and Marshal, 1983) in Bolivia; Acre, in Brazil (sparse records of didelphids; Czaplewski, 1996; Cozzuol *et al.*, 2006), Urumaco, in Venezuela (one possible record; Linares, 2004); and in Peruvian Amazonia, with didelphids from the Río Acre (Czaplewski, 1996; Goin and de los Reyes, 2011), and new sites recently discovered (up to four species, three families, and three orders; *e.g.*, Madre de Dios, Fitzcarrald local fauna, Contamana, and Tarapoto/Juan Guerra vicinity; Antoine *et al.*, 2013, 2016; Tejada-Lara *et al.*, 2015; Marivaux *et al.*, 2020). Furthermore, in Colombia there are records for the Castilletes Formation (the sparassodontan *Lycopsis padillai*, Suárez *et al.*, 2016) and the La Venta local fauna, in Colombia, which is a striking exception, including 11 species documenting four orders and eight families (Suárez Gómez, 2019).

The present study aims at reporting fossil metatherians recovered from the locality of TAR-31, in Peruvian Amazonia, dated as late middle Miocene (Laventan) in age by mammalian biostratigraphy (Marivaux *et al.*, 2020; Boivin *et al.*, 2021), in order to i) part address the regional gap of knowledge regarding metatherians, ii) depict local paleoenvironments, and iii) provide paleobiogeographic insights in northern South America during the middle Miocene. Additionally, U-Pb on zircon grains ages were obtained to independently constrain the age and further reveal the provenance of the concerned sediments at a Panamazonian scale.

2. Paleontological background and geological setting

The locality of TAR-31 (6°35.261S, 76°18.347W) is situated at the vicinity of Juan Guerra, near Tarapoto, in the San Martín Department, Peruvian Amazonia. It is located next to the bridge called "*Puente Colombia*", on the left bank of the *Río Mayo* (Figure 1). The fossil-bearing layer is a microconglomerate lens 10 to 15 cm-thick, which was completely mined out, assigned to the lower member of the Ipururo Formation (**Fm**.) (Figure 2; Marivaux *et al*., 2020; Boivin *et al.*, 2021). Fossil specimens documenting a wide array of organisms have been recovered from this locality, such as seeds, silicified wood, amber clasts (with no organic inclusions so far), decapod crustaceans, fishes (Chondrichthyes and Actinopterygii), anurans, turtles, crocodylomorphs, an unidentified bird, and several mammal orders. Among those mammals, the cebid primate *Neosairimi* cf. *fieldsi*, nine rodent taxa, including the octodontoid *Ricardomys longidens*, the chinchilloids *Microscleromys paradoxalis* and *M*. *cribriphilus*, and the erethizontoid *Nuyuyomys chinqaska* (Marivaux *et al*., 2020; Boivin *et al*., 2021) have already been described in detail. Additionally, the interatheriine notoungulate *Miocochilius* sp., the didolodontid litoptern *Megadolodus* sp., as well as chiropterans, sirenians and xenarthrans have been preliminarily identified. Based on its fauna, TAR-31 was dated as late middle Miocene in age (Laventan; Marivaux *et al*., 2020; Boivin *et al*., 2021) (Figure 2). TAR-31 is further situated stratigraphically ~110 m above another vertebrate locality in the same section (TAR-16, Fig. 2). This latter locality has notably yielded teeth of the giant caimanine *Purussaurus* sp. and dermal scutes of the pampatheriid xenarthran *Scirrotherium* sp., pointing to an early middle–late Miocene age (Jiménez-Lara, 2020), in good agreement with the hypothesized age for TAR-31.

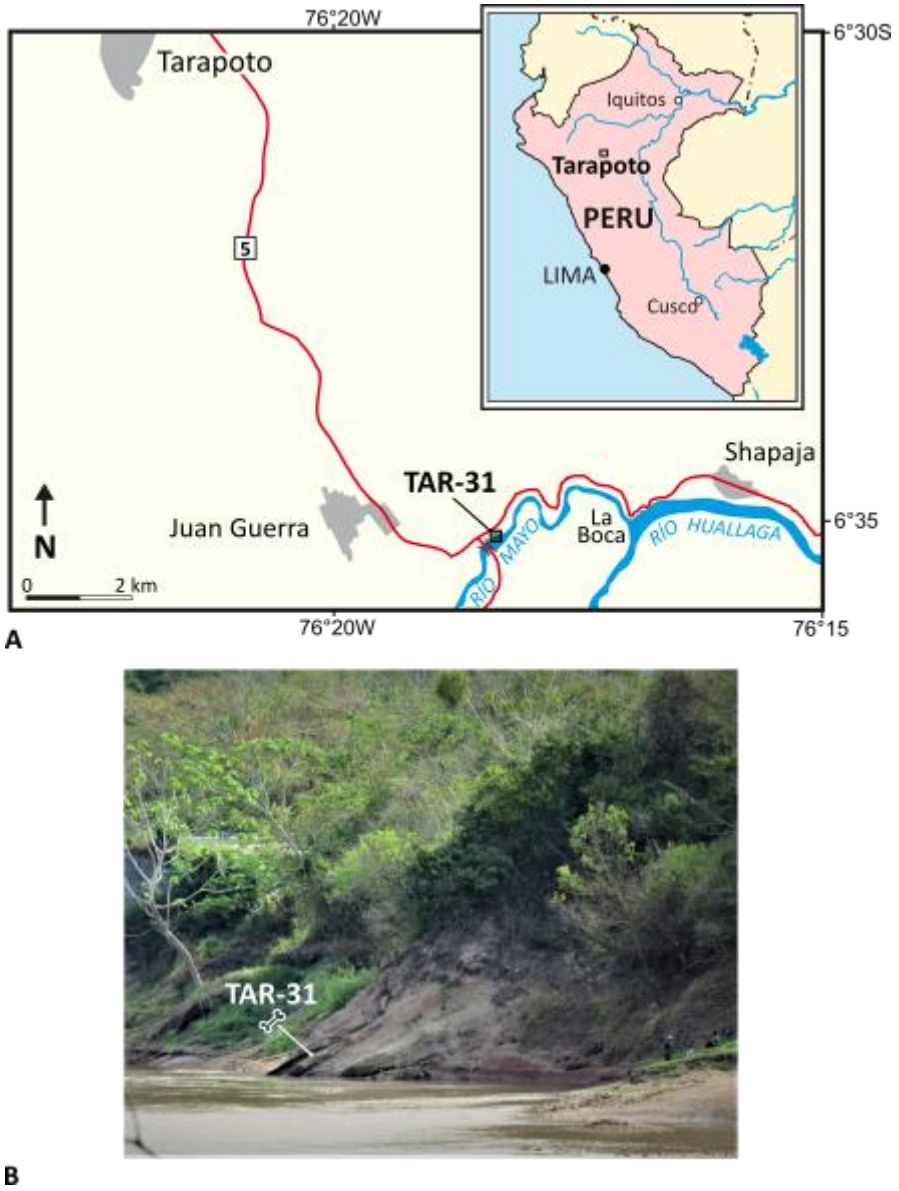


Figure 1. A. Location map of the TAR-31 fossil locality in the Tarapoto/Juan Guerra area, San Martín Department, Peru. **B**. Exposures of the Ipururo Formation along the left bank of the *Río Mayo* during the dry season, with mention of the fossil-yielding level, TAR-31.

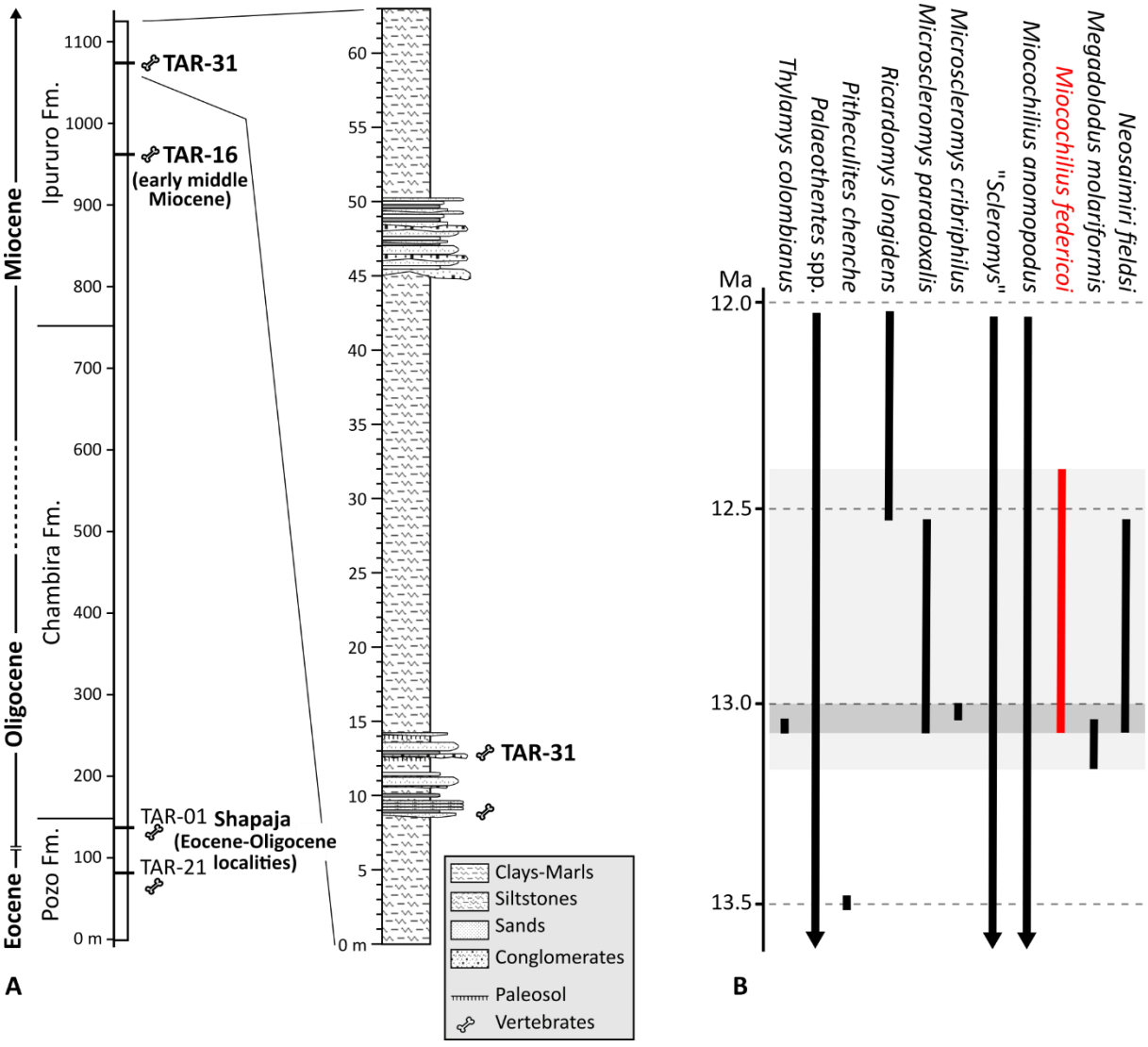


Figure 2. A, Stratigraphic log of the deposits at Juan Guerra, San Martín Department, Peru, including the localities of TAR-31 and TAR-16 and the Shapaja section (see Antoine *et al*., 2021). **B**, Hypothesized age of TAR-31 (dark grey horizontal area), based on biostratigraphical ranges of mammalian taxa of interest (see Marivaux *et al*., 2020, Boivin *et al*., 2021, and references therein). The light grey area encompasses all stratigraphic ranges previously documented for TAR-31 mammals. Abbreviations: Fm., Formation; Lit., Litopterna; Not., Notoungulata; Pr., Primates.

3. Material and Methods

3.1 Material

All the specimens were collected during yearly paleontological field campaigns in 2015–2018, using the screen-washing technique, with meshes of 2 and 1 mm, totaling approximately 550 kg of sediments treated. The residues of the sieves were then examined under stereomicroscopes for microfossil picking.

The specimens are permanently housed at the Vertebrate Paleontology Department of the *Museo de Historia Natural* of the *Universidad Nacional Mayor San Marcos* (**MUSM**) in Lima, Peru. They were photographed using a Hitachi S 4000 Scanning Electron Microscope (**SEM**) at the *Institut des Neurosciences de Montpellier* (**INM**), France. Dental measurements (*i.e*., maximum anteroposterior length and maximum labiolingual width) were made using a microscope fitted with a calibrated reticle (Nikon Measuroscope, 1/100 mm).

3.2 Methods

Systematics and description

The systematics follows Goin *et al*. (2016). The taxonomic identifications were made based on Marshall (1976), Dumont and Bown (1997), Goin (1997), Abello (2007), and Engelman *et al*. (2017). Molars were described based on the dental nomenclature and homologies proposed by Abello (2013), Goin *et al*. (2016), and Engelman *et al*. (2017).

Anatomical abbreviations

M, upper molar; **m**, lower molar; **P**, upper premolar; **p**, lower premolar; **StA**–**D**, stylar cusps (from anterior to posterior).

U-Pb dating methods

Sample TAR-31 was prepared and analyzed for U-Pb analyses at the *Laboratório de Estudos Geodinâmicos, Geocronológicos e Ambientais*, *Universidade de Brasília* (LEGGA/UnB). Zircon grains were obtained from the fossil bearing conglomerate of TAR-31 outcrop. Sample processing included crushing followed by heavy minerals concentration by panning and using a Frantz Isodynamic Magnetic Separator to eliminate magnetic mineral grains. Next, the zircon grains were randomly handpicked (~120 grains) under a stereomicroscope microscope and mounted on adhesive tape,

enclosed in a 9 mm diameter plastic ring placed on the tape around the zircons. Afterwards, the plastic ring was filled with epoxy resin and once polymerized, it was polished to expose the zircon grains (Gehrels *et al*., 2008; Bühn *et al*., 2009; Gehrels, 2014). After this stage, zircon grains were imaged by SEM back-scattered electron (**BSE**) to identify morphological features, internal structures, and the best area for laser ablation. The U-Pb isotopic analyses on zircon by laser ablation mass spectrometry (**LA-MC-ICP-MS**) followed the procedures of Bühn *et al*. (2009). The effective U-Pb ages were $^{206}Pb/^{238}U$ ages for zircon grains with ages < 1.0 Ga and $^{207}Pb/2^{06}Pb$ ages for grains with ages > 1.0 Ga.

Based on U-Pb results, we calculated the oldest possible age of the sedimentary deposit, *i.e*., the maximum depositional age (**MDA**; Dickinson and Gehrels, 2009; Sharman *et al*., 2018; Sharman and Malkowski, 2020). This is a statistic method that aims to date individual particles of sediment, most notably detrital zircon U-Pb dating via laser ablation mass spectrometry. The application of this method assumes that detrital sedimentary rocks cannot be deposited before their constituent particles are formed, so the youngest particles in a given deposit constrain the MDA (Sharman and Malkowski, 2020). We reported the MDA for the detrital sample selecting at least three analyses in the youngest cluster of ages and, the YC2σ [3+] was defined as the weighted mean average of the three youngest overlapped analyses and associated 2σ uncertainty of this cluster (Dickinson and Gehrels, 2009; Sharman *et al*., 2018; Sharman and Malkowski, 2020).

4. Results

4.1 U-Pb dating results

Results from the detrital zircon U-Pb analyses of the sample TAR-31 sample are summarized in Figure 3. Analytical results of the 126 dated grains are presented in the Supplementary Data.

The MDA, calculated as the weighted mean of the YC2σ (+3) following Sharman and Malkowski (2020), yielded an age of 17.4 ± 0.12 Ma, which is older than the presumed biostratigraphic age of the sample (see 5.2).

Potential source of the detrital sample includes Precambrian rocks of the Western Amazon Craton, the Neoproterozoic rocks of the Neoproterozoic mobile belts and Andean rocks including Famatinian and Paleozoic magmatic rocks, Permian volcanic rocks (Mitu), and Meso-Cenozoic volcanic rocks of the Andean Arc (Figure 3).

Based on zircon grains U-Pb geochronological ages distribution (Figure 3), the main source areas of the analyzed sedimentary rock were the Rio Negro-Jurena (1.82–1.54 Ga) (7.9%), Rondonia-San Ignácio (1.54–1.3 Ga) (31%), Greenville Sunsás (1.3–0.9 Ga) (14.3%), Brazilian (0.7–0.5 Ga) (11.1%), Paleozoic-Magmatic Arc (0.4–0.26 Ga) (9.5%), and Cenozoic Andean Arc (< 0.065 Ga) (9.5%) terrains. The grains yielded minor peaks of Central Amazon (> 2.2 Ga) (1.6%), Maroni-Itacaiunas (2.2–2 Ga) (2.4%), Ventuari-Tapajós (2–1.82 Ga) (3.2%), Undefined deposits (0.9–0.7 Ga) (3.2%), Famatinian (0.5–0.4 Ga) (3.2%), Triassic-Jurassic (0.145–0.25 Ga) (1.6%), and Cretaceous Andean Arc (< 0.145 Ga) (1.6%).

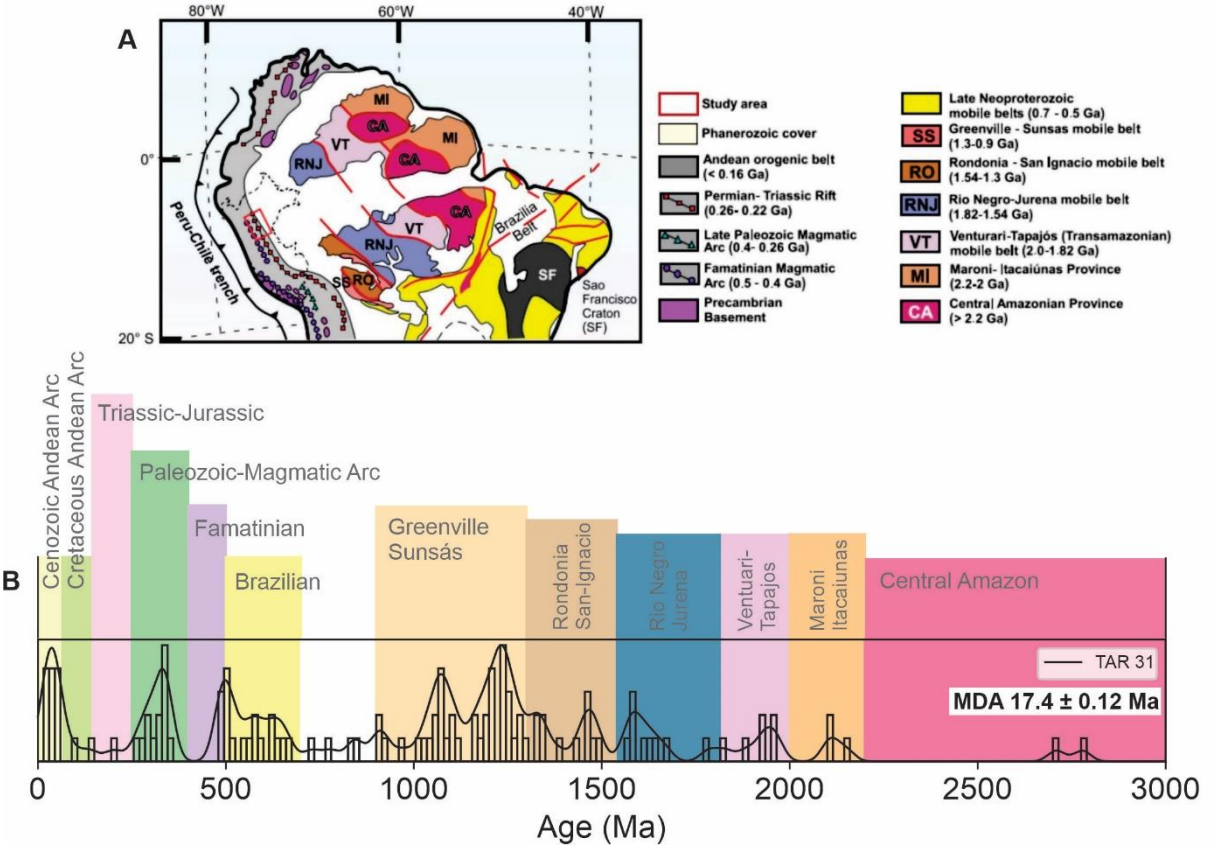


Figure 3. **A**, Sketch map of the northern part of South America illustrating the major tectonic provinces and the ages of their more recent metamorphic events. Modified and adapted from Sato *et al*. (2000), Chew *et al*. (2007, 2008), Bahlburg *et al*. (2009, 2011), Spikings *et al*. (2016), and Hurtado *et al*. (2018). The red rectangle indicates the location of the study area. **B**, Detrital zircon age spectra for the TAR-31 sample and potential corresponding sedimentary sources (identified by colored rectangles, except for undefined deposits).

4.2 Systematic Paleontology

Class Mammalia Linnaeus, 1758

Infraclass Metatheria Huxley, 1880

Supercohort Marsupialia Gill, 1872

Order Didelphimorphia Gill, 1872

Family Didelphidae Gray, 1821

Subfamily Didelphinae Gray, 1821

Tribe Thylamyini Hershkovitz, 1992

Genus ‘*Thylamys*’ Gray, 1843

‘*Thylamys*’ cf. ‘*T.*’ *colombianus* Goin, 1997

(Figure 4A–C)

Referred material. MUSM 4018, left m1 (Figure 4A–C).

Locality. TAR-31, Juan Guerra, Tarapoto Province, San Martín Department, Peru.

Formation and age. Ipururo Fm., lower member, late middle Miocene (see Marivaux *et al*., 2020).

Measurements. See Table 1.

Description. The trigonid of MUSM 4018 is slightly longer and narrower than the talonid, but generally both parts are subequal in dimensions. The paraconid is located slightly labially to the metaconid. Despite the broken tip, the paraconid seems to have been the lowest trigonid cuspid, much lower than the protoconid and slightly lower than the metaconid, but is still conspicuous. The postparacristid is well-developed and obliquely oriented. A subtle anterior cingulid is present, with a protruding anteriormost portion and an inconspicuous basal portion, but it is worn and partially broken. The protoconid is the highest cuspid of the trigonid and of the molar in general. The preprotocristid is well developed and obliquely oriented towards the notch where it joins the postparacristid, forming a wide obtuse angle. The postprotocristid is shorter than the preprotocristid. It is obliquely and dorso-ventrally oriented and linked to the postmetacristid at a slightly lingual position. The postmetacristid is short, even shorter than the postprotocristid. It is also transversal to the anteroposterior molar axis and dorso-ventrally oriented. The metaconid is slightly posterior to the protoconid and lower than it. There is a short cristid located at the posterior base of the well-developed and salient metaconid. The talonid is much lower than the trigonid, and the talonid basin is very deep. The hypoconid is partially worn and located at the posteriormost labial portion of the talonid. The cristid obliqua and the postcristid form an angle of less than 90° at the hypoconid. The cristid obliqua is almost parallel to the anteroposterior molar axis. Its anterior border is located just below the protoconid, at the labial end of the postprotocristid. Most of the entoconid is broken, but from its base it can be inferred that it is a large and robust cuspid, antero-posteriorly elongated and labio-lingually

compressed. The entocristid is very short. The hypoconulid is well developed, triangular-shaped in occlusal view, and situated posterior and slightly labial to the entoconid. There is a small labial cingulid below the cristid obliqua and a marked posterior cingulid, running from the hypoconid to almost the labial tip of the hypoconulid. A large posterior root is preserved; the anterior one is broken at its base.

Comments. The following characteristics allowed the assignment of this material to Didelphidae, according to Voss and Jansa (2009): tribosphenic lower molars, with a developed anterior cingulid (notch for the hypoconulid of the preceding tooth), as well as notched paracristids. However, it is important to mention that some authors consider that there are no synapomorphies on the lower molars that undoubtedly characterize the family Didelphidae (Beck *et al*., 2021). Compared to other Miocene didelphids, the TAR-31 specimen is much smaller than *Didelphis solimoensis* Cozzuol, Goin, de los Reyes, and Ranzi, 2006 from Acre (Cozzuol *et al*., 2006), besides having less developed anterior cingulid and more compressed entoconid. Compared to the didelphids from La Venta, Colombia, and according to the measurements reported by Goin (1997) and Suárez Gómez (2019), this material is smaller than the few reported specimens of *Marmosa laventica* Marshall, 1976, and larger than the specimens of *Thylamys minutus* Goin, 1997, but is approximately the same size as *Thylamys colombianus*. *Marmosa laventica* and MUSM 4018 possess a weak cingular shelf present on the labial side between the proto- and hypoconid; in terms of height, protoconid > metaconid > paraconid; trigonid and talonid making up (almost) the same proportion of the crown area; paraconid antero-lingual to protoconid, while the metaconid is slightly posterior to the protoconid (Marshall, 1976). Conversely, MUSM 4018 differs from m1 of *M*. *laventica* in being smaller, in having a protoconid much larger than the paraconid, and a weak development of the anterobasal cingulid (Goin, 1997). Regarding the species of *Thylamys*, MUSM 4018 is larger than the m1s of *T*. *minutus* and does not have a cristid obliqua ending anteriorly below the postprotocristid-postmetacristid notch as in this taxon (Goin, 1997). However, MUSM 4018 is similar to *T*. *colombianus*, in both size and morphology, sharing with this taxon several diagnostic features: comparatively longer and wider talonids; laterally compressed entoconids; less-developed anterior cingulid; paraconid more labially positioned on the trigonid; open preprotocristid not merged with the postparacristid,

forming a sharp and open angle with it; preprotocristid oriented approximately along the longitudinal axis of the molar, but not completely parallel to it; cristid obliqua directed towards the protoconid (Goin, 1997; Suárez Gómez, 2019). Nonetheless, MUSM 4018 has a posterior cingulid and a slightly larger paraconid compared to specimens of *T*. *colombianus* described in the literature. According to Suárez Gómez (2019), a paraconid slightly labial to the metaconid is present on the m1 of *T*. *colombianus* (almost indistinguishable on m2) and a cristid obliqua forming a right angle with the postcristid further occurs on m1 (narrower on m2). Accordingly, we considered MUSM 4018 to be an m1. Based on the described morphology, which mostly fits the diagnostic characters of *T*. *colombianus*. We left the genus in open nomenclature as '*Thylamys*', since recent phylogenetic studies have considered the genus *Thylamys* to have diverged from other didelphids much later than the age of the deposits of TAR-31 (not until the Pliocene, and, for the last common ancestor of *Thylamys* and *Gracilinanus* + *Cryptonanus*, not until ~10 Ma) (Jansa *et al*., 2014; Beck and Taglioretti, 2020). Thus, it is possible that this taxon and other Miocene allegedly *Thylamys* representatives might not pertain to the *Thylamys* clade, but represent some kind of stem Thylamyini instead.

The presence of a well-developed posterior cingulid in MUSM 4018 is a striking feature, since this structure was until recently considered to be absent in all didelphids, and also in paucituberculatans and microbiotheriids (Beck *et al*., 2021). A posterior cingulid is now described for two didelphids, as well as in basal ameridelphians (Beck *et al*., 2021) and caenolestid paucituberculatans (Abello *et al*., 2021).

MUSM 4018 was previously reported by Antoine as *Marmosa* (*Micoureus*) sp. in Marivaux *et al*. (2020), however, as we argue above, we assign it to '*Thylamys*' cf. '*T*.' *colombianus* instead.

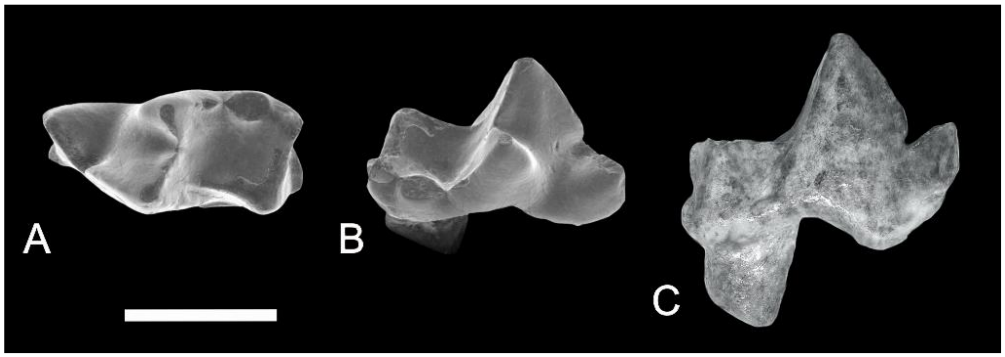


Figure 4. Didelphimorph metatherian from TAR-31, Juan Guerra, San Martín Department, Peru (late middle Miocene). **A**, **B**, and **C**, MUSM 4018, '*Thylamys*' cf. '*T*.' *colombianus*, left m1. **A**, occlusal; **B**, oblique lingual; and **C**, labial views. Scale bar = 1 mm.

Order Paucituberculata Ameghino, 1894

Superfamily Palaeothentoidea Sinclair, 1906

Family Palaeothentidae Sinclair, 1906

Subfamily Palaeothentinae Sinclair, 1906

Genus *Palaeothentes* Ameghino, 1887

aff. *Palaeothentes*

(Figure 5A–F)

Referred material. MUSM 4019, left M1 (Figure 5A–C); MUSM 4020, left broken ?M2 (without paracone, metacone, and stylar shelf); MUSM 4021, right broken m1 (talonid only; Figure 5D–F).

Locality. TAR-31, Juan Guerra, Tarapoto Province, San Martín Department, Peru.

Formation and age. Ipururo Fm., lower member, late middle Miocene (see Marivaux *et al*., 2020).

Measurements. See Table 1.

Description. Upper molars are relatively large and robust. The M1 is subquadrangular in occlusal view. Anteriorly, it has a wide and long anterior cingulum, which extends from a distinct StA, situated on the labial side of the molar, next to the StB, to the cervix, at a point slightly anterior to the preprotocrista mid-portion. The StB is large, high, and situated just in front of the protocone. The posterior crest of StB is long and conspicuous, with first a slightly oblique direction; towards the contact with the StC+D

it changes its course, to become ventrally directed. There is a small protuberance on the anterior lingual face of the StB, at almost half its height, that can be interpreted as the reminiscence of the paracone, with its very subtle crests. The protocone has an open L outline in occlusal view. It is wide, low and slightly more protuberant lingually than the metaconule. The postprotocrista is first linguo-labially directed, before to abruptly rotate labially. There is a deep sulcus separating the postprotocrista from the metaconule. At its labial end, there is a well-developed premetaconular cusp. Below this sulcus, on the lingual side of the molar, a marked protuberance is surrounded by an anterior sulcus and a posterior sulcus. The metaconule is situated at the same level of the StC+D, and is large, with pre- and post-metaconular with rounded margins. A well-developed metacone is present on the anterior portion of the StC+D, although being much shorter than the latter. The StC+D is large and subequal to StB in height. The labial side of the M1 is marked by a well-developed cingulum located at the base of the stylar cusps, less developed on the labial side of the StB and mostly noticeable anteriorly and posteriorly to the StC+D and below the ectoflexus, where a small cuspule is present. Although sharing a very similar morphological pattern, MUSM 4020 was identified as a M2 due to its smaller size in comparison with MUSM 4019 (M1), its narrower occlusal proportions and the presence of a less protruding metaconule. The labial portion of the molar (including stylar cusps) is not preserved, and morphological discrepancies with MUSM 4019 are: shorter anterior cingulum; protocone and metaconule narrower, with a more triangular shape; a more discrete protuberance at the lingual base of the sulcus separating the protocone and metaconule; trigon basin more deeply excavated, with more difference in height between it and the metaconule; and premetaconular cusp less developed. These characters are compatible with the interlocus variation between M1 and M2 of a same taxon.

MUSM 4021 is a broken m1, lacking the trigonid. The talonid is wide and robust. The talonid basin is deep at its central part, but not wide. The metaconid is the highest cuspid preserved. It is conical shaped and has a distinct metaconid posterior crest *sensu* Abello (2013). A long, marked and curved cristid obliqua runs from the hypoconid to the metaconid. The hypoconid is relatively low and triangular shaped. The postentocristid and postcristid are merged, forming a prominent posterior cristid. Below this structure, on the posterior side of the molar, there is a protuberance, the

hypoconulid, starting at a central position and continuing to a point below the entoconid, but it is partly broken. The entoconid is wide and just slightly shorter than the metaconid. A well-developed entocristid is obliquely oriented towards the metaconid posterior crest, but it does not contact it.

Comments. According to the diagnostic characters listed by Abello (2007) for Palaeothentidae, the upper molars from TAR-31 can be assigned to this family by possessing metacone located anteriorly to the apex StC+D and a premetaconular cusp. Compared to *Hondathentes cazador* Dumont and Bown, 1997, a low-latitude palaeothentid of uncertain affinities (see Abello, 2007), the TAR-31 taxon differs in that the postprotocrista is not confluent with the hypocone platform (metaconule *sensu* Abello, 2013) on M1, in lacking the metacone on M1-2, in the presence of a premetaconular cusp on M2 (in *Hondathentes* it is absent), and in m1 lacking the entoconid notch (Dumont and Bown, 1997; Abello, 2007). The M1 from TAR-31 has a wide and long anterior cingulum, and the metaconule and StC+D are aligned as in Decastinae; but, in contrast to the latter, it does not have a protocone posterior to the StB (the protocone is labiolingually aligned with the StB in TAR-31 specimen), which is another diagnostic characteristic of decastines. Furthermore, TAR-31 taxon is smaller than all decastine species, and the lower molar possesses a small cristid posterior to the metaconid, which is considered absent in representatives of this subfamily. As of diagnostic features of Palaeothentinae, specimens from TAR-31 also have StB and StC+D aligned transversally to the protocone and metaconule, respectively; in addition, the lower m1 from TAR-31 has a cristid posterior to the metaconid, as is common among palaeothentines. However, palaeothentines possess a short anterior cingulum on upper molars (Abello, 2007), whereas it is long in MUSM 4019 and MUSM 4020. Accordingly, the TAR-31 palaeothentid has closer affinities with Palaeothentinae.

Among palaeothentines, in *Palaepanorthus* the M1 has a short anterior cingulum and StB larger than StC+D (Abello, 2007); both features are lacking on the M1 from TAR-31. In addition, the TAR-31 taxon differs from *Carlothentes chubutensis* (Ameghino, 1897) in having m1 without cristid obliqua bent in its midline (Abello, 2007). Bown and Fleagle (1993) reported that the species of *Palaeothentes* do not have lower molars with a cristid obliqua bent in its midline, as observed on the m1 from TAR-31.

However, since most of the diagnostic features of this *Palaeothentes* are located on lower molars, they cannot be observed on TAR-31 specimens. According to that, we assign the palaeothentinae from TAR-31 to aff. *Palaeothentes*, which is our favored hypothesis, pending the discovery of more material and associated teeth.

Palaeothentes includes nine species: *P*. *aratae* Ameghino, 1887 (type species), *P*. *intermedius* Ameghino, 1887, *P*. *lemoinei* Ameghino, 1887, *P*. *minutus* Ameghino, 1887, *P*. *marshalli* Bown and Fleagle, 1993, *P*. *migueli* Bown and Fleagle, 1993, *P*. *pascuali* Bown and Fleagle, 1993, *P*. *relictus* Engelman, Anaya and Croft, 2017, and *P*. *serratus* Engelman, Anaya and Croft, 2017 (Abello, 2007; Engelman *et al*., 2017). According to Abello (2007), “Among the species of *Palaeothentes* the paracone on M1 is present uniquely on *P*. *aratae*, *P*. *marshalli* and *P*. *migueli*”, and, according to Engelman *et al*. (2017), M1-2 of *P*. *serratus* also have a paracone. As the M1 from TAR-31 displays a very small paracone on the anterior part of the StB, it would be close to the latter species bearing a paracone on M1. However, Engelman *et al*. (2017) also noted the absence of a crestid-like structure posterior to the metaconid on *P*. *serratus*, differentiating it from the TAR-31 taxon. Concerning other species of *Palaeothentes* bearing a paracone on M1, *P*. *migueli* is smaller than the TAR-31 taxon, and in addition it displays molars appearing more gracile, with smaller general proportions and more delicate occlusal structures; *P*. *marshalli* has well-developed paracone and metacone, but upper molars from TAR-31 have an incipient paracone, in addition to be slightly larger than those of *P*. *marshalli*; and finally, M2s of *P*. *aratae* do not have a paracone, their anterior cingulum is short, their metacone and premetaconular cusp are small (Bown and Fleagle, 1993; Abello, 2007), and this species is larger than the TAR-31 palaeothentid.

Upper molars from TAR-31 have therefore several palaeothentine features, but the anterior cingulum on M1 is more similar to that observed in Decastinae. The lower molar has few characteristics preserved because it is broken and lacks its anterior part (trigonid), but seems to be more related to Palaeothentinae than to Decastinae. Among palaeothentines, the TAR-31 taxon appears particularly close to *Palaeothentes*, and more particularly to *P*. *marshalli* and *P*. *migueli*, plus *P*. *aratae* and *P*. *serratus*, to a lesser extent. However, there are differences between TAR-31 specimens and all the previously described species of *Palaeothentes*. The great taxonomic diversity of

Palaeothentes, plus the small number of fragments retrieved at TAR-31, in addition to their fragmentary state, hamper a more precise alpha taxonomic assignment for the specimens from TAR-31.

Among palaeothentoids from La Venta, the size of the TAR-31 *Palaeothentes* is consistent with that of the “Palaeothentoidea fam., gen. et sp. indet.” mentioned by Suárez Gómez (2019) at La Venta. Nevertheless, the only specimen reported is a dentary with m2, so the comparisons with the molars from TAR-31 are limited. Suárez Gómez (2019) points out that the specimen is morphologically close to those assigned to Palaeothentidae, but it does not possess the diagnostic characteristics of this family. Therefore, it might document a non-palaeothentid palaeothentoid. Since Palaeothentidae features are clearly present on the TAR-31 taxon, most probably the latter does not coincide with this unnamed palaeothentoid taxon from La Venta.

Family Abderitidae Ameghino, 1889

Genus *Pitheculites* Ameghino, 1902

Type species. *Pitheculites minimus* Ameghino, 1902.

Referred species. *Pitheculites rothi* Marshall, 1990 and *Pitheculites chenche* Dumont and Bown, 1997.

Stratigraphical range. Early to late middle Miocene (Colhuehuapian to Laventan SALMAs).

Geographical range. Chubut Province, Argentina (Barranca Sur del Lago Colhué-Huapí locality); Aisén, Chile (Alto Río Cisnes locality); La Venta, Colombia (La Victoria Fm.); Juan Guerra, Peru (locality of TAR-31).

Diagnosis. *Pitheculites* is characterized by the presence of hypertrophied P3 with labial ridges; M1 with wide and long anterior cingulum ending lingually at the occlusal surface, and antero-posteriorly compressed anterolabial root; presence of parastylar cusp on M2; reduced p3 without anterobasal cuspid; antero-posteriorly compressed hypoconids; m2-3 with short cristid obliqua, which has rounded occlusal margins; anterior end of the dentary dorsally projected; molar series obliquely oriented with respect to the antemolar series (Abello, 2007).

Pitheculites ipururensis nov. sp.
(Figure 5G–M)

Holotype. MUSM 4024, right m2 (Figure 5I–J).

Referred specimens. MUSM 4022, right broken m1 (Figure 5G–H); MUSM 4023, left broken m1 (Figure 5K–M).

Etymology. The specific name, *ipururensis*, derives from Ipururo Fm., which crops out at TAR-31.

Type locality. TAR-31, Juan Guerra, Tarapoto Province, San Martín Department, Peru.

Type formation and age. Ipururo Fm., lower member, late middle Miocene (see Marivaux *et al*., 2020).

Measurements. See Table 1.

Diagnosis. *Pitheculites* of intermediate size, being closer to the size of *P*. *rothi*. It differs from other representatives of *Pitheculites* in having longer cristid posterior to the metaconid and a wider hypoconulid shelf on the m2. It differs from *P*. *rothi* in having a narrower and less quadrangular m2, with short and narrow trigonid, paraconid present (as in *P*. *minimus*), postentocristid more posteriorly positioned and merged with the postcristid, and postcristid oblique. It differs from *P*. *chenche* in having a crestid-like postentocristid in m1. It differs from *P*. *minimus* in having m1 with a cuspid-like entocristid (as in *P*. *chenche*), while in *P*. *minimus* it is crested-like.

Description. Both m1s are broken in front of the metaconid. Despite that, the typical plagiaulacoid m1 of Abderitidae can be recognized, with a blade-like trigonid, small and basined talonid, and considerable crown height. The lateral cristids and denticles normally present on this locus are not preserved, and MUSM 4022 is slightly larger and higher than MUSM 4023. The labial side of the preserved trigonid portion is labiolingually compressed, making the trigonid much narrower than the talonid at this point. Both specimens preserve a small posterior protuberance on the occlusal surface of the shearing blade, that according to Abello (2013: figures 4DA, D-E), is homologous to the metaconid, which is joined to the anterior extremity of a long vertical cristid obliqua. On the less-worn MUSM 4021, the cristid obliqua is composed of one anterior long, vertical labially-oriented segment, followed by a small, lingually-oriented one,

both forming an angle of ~90°. On the other hand, both segments are completely merged, forming one long, curved labial cristid on MUSM 4022. The entoconid is small and it has a short and cuspid-like entocristid; the postentocristid is joined with the postcristid forming a complete cristid. The hypoconid is located at the posteriormost portion of the talonid, forming an angle of almost 90° with the postcristid. A small hypoconulid is visible posterior to and below the postcristid.

The m2 has a rectangular shape and it is wider than the m1 at its base. The trigonid is narrower and much shorter than the talonid. The labial margin is higher than the lingual one. There is a well-developed anterolabial trigonid cusp *sensu* Abello (2013: fig 4B), positioned anterior to the protoconid and much higher and larger than the paraconid. Between the trigonid anterior cuspid and the paraconid and metaconid there is a deep narrow basin. A well-developed hypoconulid notch is present just below the anterolabial trigonid cuspid. The paraconid is not very well developed, restricted to a small triangular protuberance at the base of the premetacristid, slightly labial to the metaconid. The metaconid is well developed, but smaller and shorter than the protoconid, being much more anteriorly positioned than the latter. There is a short postmetacristid, and a distinct metaconid posterior crest *sensu* Abello (2013) is present, lingual and posterior to the metaconid, directed towards the entocristid. The protoconid is the largest and tallest cuspid of the molar. The protocristid is incipient, being visible almost only at its base. A well-developed and protuberant protoconid posterior crest *sensu* Abello and Rubilar-Rogers (2012) is present, posterior and labial to the protoconid. At the posterior extremity of this protoconid posterior crest, a deeply excavated sulcus separates it from the cristid obliqua, and the posterior wall of this sulcus is S-shaped. The cristid obliqua is very short and almost sagittal. Besides, it has a rounded occlusal outline and a deep circular excavation at its lingual side. The hypoconid is small and antero-posteriorly compressed, located slightly posterior to the entoconid. A well-marked postcristid is present; it is oblique, connecting to the postentocristid posteriorly to the midline of the teeth. The postentocristid is very well developed, posterolabially directed, forming a small cuspid at the posterolingual extremity of the molar. This cuspid formed by the postentocristid is separated from the entoconid by a deep sulcus. Below the postcristid and postentocristid, a pronounced hypoconulid forms a posterior and ventral shelf covering most of the molar posterior

surface. The entoconid is high and wide at its base. Anterior to the entoconid, a very well-developed entocristid forms a well-defined cuspid. The latter is separated from the metaconid by the conspicuous metaconid posterior crest. The postentocristid plus the entoconid and the entocristid form a set of three marked cuspids on the lingual side of the talonid. The talonid basin is deep, but narrow, due to the widening of the basal portion of the talonid cuspids.

Comments. The assignment of these specimens to Abderitidae is based on the following characters: presence of anterolabial cuspid on the trigonid of m2, and protocristid notch not developed on m2 (Abello, 2007). Among abderitid genera, these remains can be referred to *Pitheculites* by having a small and anteroposteriorly-compressed hypoconid and a short cristid obliqua with rounded occlusal margin on m2 (Abello, 2007). Three species of *Pitheculites* are currently recognized: *P*. *minimus* Ameghino, 1902, *P*. *rothi* Marshall, 1990, and *P*. *chenche* Dumont and Bown, 1997. *Pitheculites ipururensis* nov. sp. from TAR-31 is slightly larger than *P*. *minimus*, with narrower m2, but, as this species, it has a paraconid on m2, and the postentocristid of m1 is sharp (not rounded as in *P*. *chenche*). *Pitheculites ipururensis* nov. sp. differs from *P*. *rothi* in having a much shorter trigonid on m2, the postcristid not merged with the entoconid, but with the postentocristid, and a postcristid less transversally oriented (in *P*. *rothi* the postcristid is more transversally oriented on m2, and rather oblique on m3). The unique specimen of *P*. *chenche*, a partial right dentary preserving p3–m3 (IGM 250941), has much worn teeth. Nevertheless *P*. *ipururensis* nov. sp. is clearly smaller and it has sharp postentocristid on m1. The m2 of *P*. *ipururensis* nov. sp. is also less quadrangular than in *P*. *chenche,* with a labiolingually narrower trigonid, a longer cristid posterior to the metaconid, a more posterior postentocristid, and a wider hypoconulid shelf.

Concerning body mass, according to the equation of Dumont *et al*. (2000), but adding the SE (see Abello *et al*., 2020, SM5):

x = m2 area; log y = 2.419 +1.727 (log x); SE = 1.16

the body mass of *P*. *ipururensis* nov. sp. is estimated at 44.62 g, while that of *P*. *chenche* is at 108.67 g, *P*. *rothi* 61.45 g, and *P*. *minimus* 35.82 g.

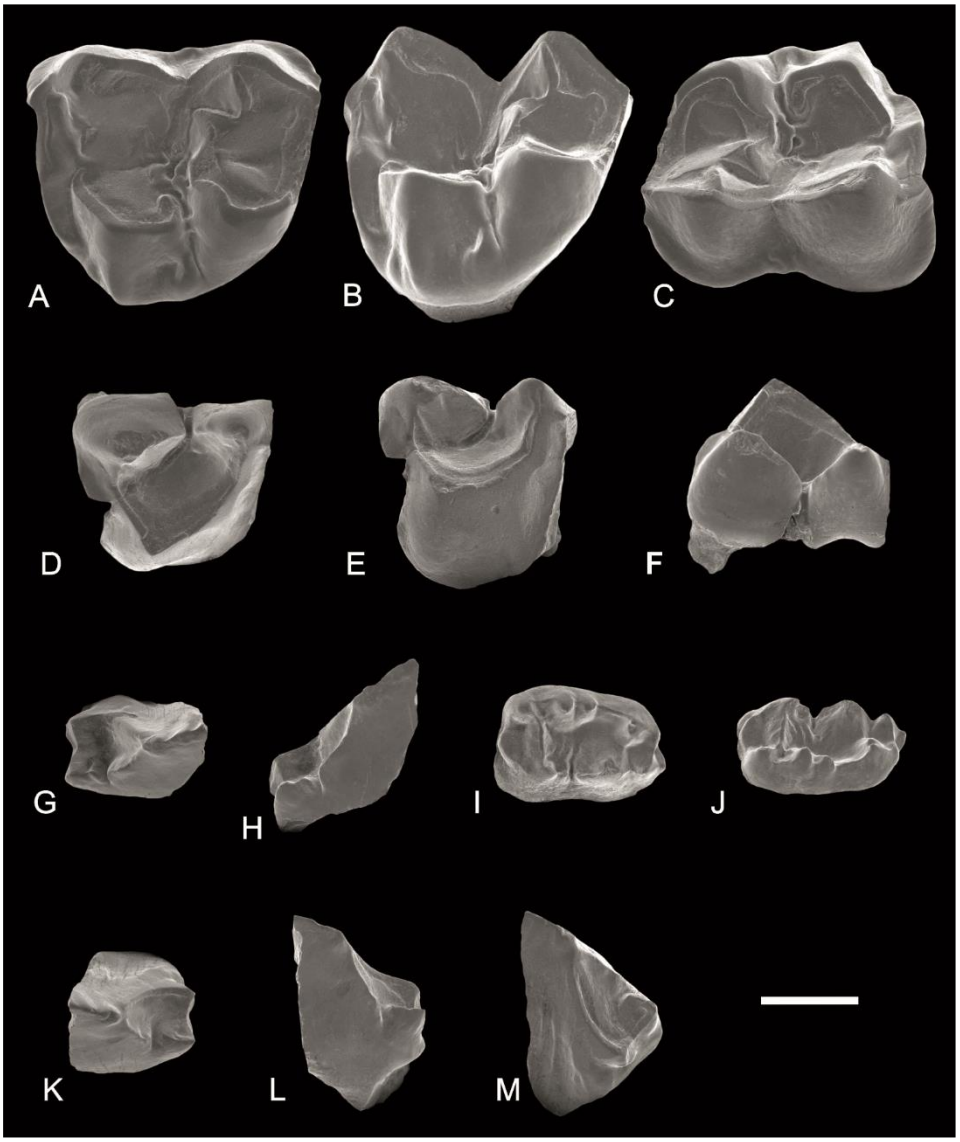


Figure 5. Paucituberculatan metatherians from TAR-31, Juan Guerra, San Martín Department, Peru (late middle Miocene). **A**–**F**, aff. *Palaeothentes*, **A**–**C**, MUSM 4019, left M1; **D**–**F**, MUSM 4021, right m1. **G**–**M**, *Pitheculites ipururensis* nov. sp., **G**–**H**, MUSM 4022, left m1; **I**–**J**, MUSM 4024, right m2 (**holotype**); **K**–**M**, MUSM 4023, right m1. **A**, **D**, **G**, **I**, and **K**, occlusal; **B**, **E**, **H**, **J**, and **L**, lingual; and **C**, **F**, and **M**, partially labial views. Scale bar = 1 mm.

Table 1. Dental measurements (in mm) of molars of '*Thylamys*' cf. '*T*.' *colombianus* (Didelphimorphia), aff. *Palaeothentes*, and *Pitheculites ipururensis* nov. sp. (Paucituberculata) from TAR-31, Juan Guerra, San Martin Department, Peruvian Amazonia (late middle Miocene).

Taxon	Specimen	Length	Width
'*Thylamys*' cf. '*T*.' *colombianus*	MUSM 4018 (m1)	1.73	0.89
aff. *Palaeothentes*	MUSM 4019 (M1)	3.07	2.77
	MUSM 4020 (broken ?M2)	2.76	1.92
	MUSM 4021 (m1, talonid only)	2.10	1.88
Pitheculites ipururensis sp. nov.	MUSM 4022 (broken m1)	Total = 1.83 Talonid = 1.17	Trigonid = 1.33 Talonid = 1.18
	MUSM 4023 (broken m1)	Total = 1.85 Talonid = 1.16	Trigonid = 1.02 Talonid = 1.09
	MUSM 4024 (**holotype**, m2)	Total = 1.80 Trigonid = 0.66 Talonid = 1.13	Trigonid = 1.15 Talonid = 1.29

5. Discussion and Conclusions

5.1 Taxonomy, paleobiology and paleoecology of the metatherians from TAR-31

Despite the low number of fossil specimens (only seven teeth or tooth fragments) and the limited extension of the outcrop (5 m^2, *i.e*., strongly contrasting with La Venta), the metatherian assemblage recorded at TAR-31 can be considered fairly diverse with three taxa belonging to three distinct families and two orders. It can be hypothesized that more marsupial taxa could have been recovered through a wider sampling effort (Magurran, 2004), but the fossil-yielding lens has been fully analyzed in TAR-31 (Marivaux *et al.*, 2020).

Thylamys, probably represented at TAR-31 by '*T*.' cf. '*T*.' *colombianus*, is a genus recovered as monophyletic in recent phylogenetic analyses, which typifies the

Thylamyini, and includes at least nine small-sized living species (Voss and Jansa, 2009). As reported by Suárez Gómez (2019), the estimated body mass of *T*. *colombianus* is approximately 52 g, being larger than *T*. *minutus* (~13 g), also reported at La Venta. Suárez Gómez (2019) additionally suggested that, according to its dental morphology, *T*. *colombianus* would have had insectivorous/faunivorous habits.

As to the paucituberculatans from TAR-31, *Palaeothentes* was recently recovered as a monophyletic genus, when *Palaepanorthus* (*Palaeothentes*) *primus* is excluded (Abello, 2013; Engelman *et al*., 2017). Nevertheless, the species with which aff. *Palaeothentes* from TAR-31 seems to have stronger affinities, *i*.*e*., *P*. *aratae*, *P*. *marshalli*, *P*. *migueli*, and *P*. *serratus*, are not closely related in that same phylogeny (Engelman *et al*., 2017; see also Abello *et al*., 2020), the retention of the paracone seeming to be a plesiomorphic trait. Based on the protocol proposed by Dumont *et al*. (2000), only *P*. *serratus* is hypothesized to have been insectivorous, whereas all three other species were unambiguously interpreted as frugivorous (Engelman *et al*., 2017). Unfortunately, because no m2 has been recovered for aff. *Palaeothentes* at TAR-31 it is not possible to perform a dietary reconstruction for this taxon. The aff. *Palaeothentes* from TAR-31 had an intermediate size, far from larger species of palaeothentids, such as *P*. *aratae* and *Titanothentes simpsoni* Rae, Bown, and Fleagle 1996, with an estimated weight over 500 g, and larger than the small species of the genus (*e*.*g*., *P*. *marshalli* and *P*. *migueli*, with less than 250 g; Abello *et al*., 2020: SM5). In fact, when compared with the coeval species of *Palaeothentes* from Quebrada Honda, aff. *Palaeothentes* from TAR-31 is larger than *P*. *serratus*, which has estimated body mass of approximately 100 g, being closer in size to that of *P*. *relictus*, estimated to have weighted around 150 g (Engelman *et al*., 2017). Palaeothentids were particularly diverse in high-latitude early Miocene localities, with, for instance, six species reported in the Santa Cruz Fm. (Abello and Candela, 2010), plus four other ones in the Pinturas Fm. (Abello, 2007), with body masses ranging from 44 g to 980 g. Some authors suggest that they were abundant in somewhat dry and open habitats, with mixed vegetational cover and seasonal aridity (Engelman *et al*., 2017). Nevertheless, they still favored habitats with relatively high rainfall, explaining their diversity in the Santa Cruz and Pinturas formations, which were not particularly dry (Kramarz and Bellosi, 2005; Spradley *et al*., 2019). Furthermore, the abundance of palaeothentids in lower

Oligocene layers of the Shapaja section, located few km away from TAR-31, presumably supports this hypothesis, since this region went through a drier period by the Eocene–Oligocene transition (Antoine *et al.*, 2021; Stutz *et al*., 2021).

Among Abderitidae, *Pitheculites* is closely related to *Abderites*, a genus spanning the early–middle Miocene interval in Argentina and Chile (Abello and Rubilar-Rogers, 2012). Both genera are more distantly related to *Parabderites*, which has a more plesiomorphic morphology and is recorded in the Oligocene–early Miocene of central Patagonia and Chile (Abello, 2007, 2013). The representatives of *Pitheculites* are among the smallest non-pichipilid palaeothentoids (with a body mass ranging from ~30 to 100 g), differing from representatives of *Abderites* (~280–600 g; Abello *et al*., 2020: SM5). Abderitid dental morphology is interpreted as having allowed the consumption of a wide array of food items, even those with hard covers, making them dietary generalists (Dumont *et al*., 2000). Abderitids would have been more frugivorous than palaeothentids, and a positive correlation between high precipitation rates and the abundance of fruit/frugivores has been recorded (Kay and Madden, 1997). In contrast with palaeothentids, the great abundance of abderitids seems to be a signature of forested areas under wet humid climates, where there would be more fruit and frugivores (Engelman *et al*., 2017).

When detailing the preliminary identifications of the marsupial fauna of TAR-31, Marivaux *et al*. (2020) mentioned the occurrence of “an argyrolagid marsupial” based on a fragmentary high-crowned molar. According to our current evidence, we cannot confirm this assignment, as the tooth in question likely pertains to a pristine deciduous molar of a tiny hegetotheriid instead. Despite not being present in TAR-31, argyrolagids have already been identified in Peruvian Amazonia: one tooth of an indeterminate taxon, being reported from the lowermost late Miocene levels near Contamana (CTA-43 locality, Pebas Fm.; Antoine *et al*., 2016), and dozens of isolated teeth recovered in various latest Eocene–early Oligocene vertebrate assemblages from the Shapaja section, San Martín (*Proargyrolagus* spp.; Antoine *et al*., 2021), thereby suggesting a long-lasting presence for this singular and elusive family in Western Amazonia.

Strikingly, flesh-eating Sparassodonta are not recorded at TAR-31, whereas they are often present in Miocene deposits at mid- and low latitudes of South America, with great diversity. In particular, sparassodonts are remarkably diverse at La Venta,

In Colombia, with four species of at least three families already described (Hathliacynidae, Hondadelphidae, and Thylacosmilidae; Suárez Gómez, 2019). In addition to the taxa from La Venta, one taxon is reported for the Castilletes Formation in Colombia (the sparassodontan *Lycopsis padillai*, Suárez *et al*., 2016); in Bolivia, three taxa of at least one family in Quebrada Honda (Hathliacynidae; Engelman *et al*., 2020), one taxon in Cerdas (a new Borhyaenoidea still to be described, Croft *et al*., 2016), and Achiri (*Borhyaenidium altiplanicum*, Villarroel and Marshal, 1983) in Bolivia; one possible taxon in Urumaco, Venezuela (Linares, 2004); and a hathliacynid at Madre de Dios (MD-67 locality; Antoine *et al*., 2013), a premolar of uncertain affinities at CTA-44 (Contamana, earliest late Miocene, Pebas Fm.; Antoine *et al*., 2016), and one possible record at the Fitzcarrald local fauna (Tejada-Lara *et al*., 2015) in Peru. This absence could be due to specific taphonomic biases (*i*.*e*., size sorting), such as the small size of sediment grains and fossil specimens trapped in TAR-31, thus not favoring the preservation of large-sized fossil taxa, and that sparassodonts are generally rare in South American fossil faunas. Meso- and macrovertebrates are scarce at TAR-31 and documented only by few fragments of teeth (not complete specimens). Ecological reasons (*e*.*g*., low ecomorphological disparity) may further explain this unbalanced metatherian sample (see Croft *et al*., 2018).

Microbiotheria are absent from TAR-31, but also from Quebrada Honda and other Miocene localities at low latitudes (Goin, 1997; Suárez Gómez, 2019). The single known record from La Venta is the northernmost occurrence of the order. The origin, radiation and dispersal of microbiotheres are thought to have occurred in the Austral Kingdom, *i*.*e*., southernmost South America and Antarctica (Goin *et al*., 2016). They are especially recorded in lower Miocene deposits of Patagonian Argentina, a period and an area where they should have reached their peak diversity (Chornogubsky and Kramarz, 2012; Goin and Abello, 2013; Goin *et al*., 2016), being also recorded in the Antarctica Peninsula (Goin *et al*., 1999). Microbiotherian diversity remained low and stable throughout the entire Paleogene, and they are represented today by a sole taxon, *Dromiciops*, with very limited distribution in southern South America (Quintero-Galvis *et al*., 2021).

In addition, among micromammals, it is also worth noting the low metatherian *vs*. rodent remains ratio at TAR-31 (0.018), with ~400 rodent specimens and seven

metatherian remains. However, in terms of taxonomic richness, the discrepancies between rodent and metatherian assemblages are not as extensive, since despite the small sample size, three different metatherians belonging to two superfamilies are so far documented at TAR-31, whereas rodents are represented by nine taxa pertaining to four superfamilies (Boivin *et al*., 2021). In general, it should be added that fossil remains of rodents are considerably more abundant than metatherian specimens in the Eocene–Miocene vertebrate localities of Western Amazonia, being the most species-rich mammalian group in Santa Rosa, Contamana (Pozo, Chambira, and Pebas formations) and the Shapaja section, for example (Frailey and Campbell, 2004; Antoine *et al*., 2016, 2021; Boivin *et al*., 2017a, b, 2018; Arnal *et al*., 2020, 2022). The causes of this disparity remain to be better explored. There might be taphonomic biases, such as sampling biases, predator preference towards specific prey, prey's abundance and preferred habitats, affecting the taxa abundance and richness in the available samples. Nevertheless, this unbalanced pattern could also be related to the consequences of the climatic and environmental shift triggered around the Eocene–Oligocene transition, with drastic impacts recorded on metatherian faunas, at least in the Southern cone of South America (Goin *et al*., 2010, 2016), impacts remaining to be better assessed at low latitudes (Antoine *et al*., 2021).

5.2 Biostratigraphical and chronostratigraphical implications

The age of the TAR-31 fossil assemblage has been proposed to be ranging from 13.1 to 12.5 Ma, as inferred through mammalian biostratigraphy (Figure 2) (Marivaux *et al.*, 2020; Boivin *et al*., 2021). Two metatherian taxa documented here are similar to species recovered at the La Venta deposits thus far, which do not have overlapping stratigraphic ranges ('*Thylamys*' cf. '*T*.' *colombianus* at *ca*. 13.0 Ma and *Pitheculites chenche* at *ca*. 13.5 Ma), according to the magnetostratigraphical age estimates of Madden *et al.* (1997), as revised by Raffi *et al*. (2020). However, these small discrepancies are most likely due to sampling biases with such a poor record, as very few localities were screen-washed at La Venta (Madden *et al*., 1997).

Recently, Castro *et al*. (2021), when revising the fossil record of Didelphidae from South America, considered that the middle Miocene didelphids from Madre de Dios (MD-67), La Venta, and now also TAR-31, could be considered one of the first reliable

occurrences of crown representatives of the family, along with the records presented by Goin *et al*. (2007) for Argentine Patagonia. The records of two species of *Thylamys* in La Venta (*ca*. 13.0 Ma; see above) are the earliest occurrences for the genus, and the recognition of '*T*.' cf. '*T*.' *colombianus* at TAR-31 substantiates this statement as a result (13.1–12.5 Ma, and more probably 13.1–13.0 Ma; Marivaux *et al.*, 2020; Boivin *et al.*, 2021). Conversely, the record of *Pitheculites ipururensis* nov. sp. from TAR-31 (13.1–12.5 Ma) might slightly postdate the former last appearance of Abderitidae, previously documented by *P*. *chenche* in La Venta (*ca*. 13.5 Ma; see above). Following the Oligocene radiation of palaeothentoids, the early–early middle Miocene is considered as the climax of paucituberculatans' evolutionary history, with a high taxonomic diversity of abderitids and palaeothentids (Abello *et al*., 2020). After Laventan times, Palaeothentoidea became extinct and only the Caenolestoidea have persisted until today among paucituberculatans (Engelman *et al*., 2017; Abello *et al*., 2021). Surprisingly, palaeothentoids were still very diverse and abundant in several Laventan localities *i.e*., La Venta, Quebrada Honda and now TAR-31, suggesting that their extinction did not occur as a long decline, and more like an abrupt event triggered by reasons still poorly understood (Engelman *et al*., 2017). Nevertheless, the early late Miocene interval is particularly underrepresented (and perhaps under-sampled) at low latitudes and especially in Western Amazonia (Antoine *et al.*, 2017), which prevents further discussion on this issue at the time being.

The calculated MDA of 17.4 ± 0.12 Ma is ~4 My older than the biostratigraphical age of the sample. Hence, we interpret this MDA as a detrital provenance age. This temporal hiatus might be related to the low volcanic activity during late early and early Miocene times upstream in the corresponding drainage basin, contrary to what occurs in the adjacent Bagua Basin (Moreno *et al*., 2020). Potential source for these early Miocene zircons may include the Callipuy volcanic arc located in the Peruvian Western Cordillera (Navarro *et al*., 2010) or the Saraguro Fm. located in the Inter-Andean region of Southern Ecuador (see Hungerbühler *et al*., 2002 and references therein).

Overall, we interpret TAR-31 to be mainly sourced by Andean terrains, because 25.3% of the analyzed zircons are younger than 500 Ma and hence derived from Andean magmatic rocks (see Hurtado *et al*., 2018 and references therein). Older Meso-Proterozoic zircon grains related to the Amazon Craton provinces of Rio Negro-

Jurena (1.82–1.54 Ga), Rondonia San Ignacio (2.0–1.82 Ga), and Greenville Sunsás (1.3–0.9 Ga) and to the Brazilian Neoproterozoic mobile belts (0.7–0.5 Ga), are interpreted as reworked ancient sedimentary rocks, likely Cretaceous sedimentary rocks that are cratonic in provenance (Erlich *et al*., 2018; Hurtado *et al*., 2018; Louterbach *et al*., 2018). However, despite the large number of older grains, the presence of younger zircons grains strongly suggests an Andean orogenic source during the early middle Miocene that conditioned the provenance and filling of this part of the Huallaga basin at that time, at the western edge of the PMWS.

The Cretaceous Andean Arc zircon age population could be sourced by granites of the Coastal Batholith (100–50 Ma) located in the Western Cordillera (Litty *et al*., 2017). The Permo-Triassic zircon grains could be sourced by the acid volcanics of the Lavasen Fm. (Upper Paleozoic) and the Triassic Rift Mitu (Lower Mesozoic), which were preserved in the northern part of the Eastern Cordillera (Eude *et al*., 2015). Those sequences were affected by an eastward propagation of the Eastern Cordillera (Eude *et al*., 2015), which could be exposed and eroded at that time. However, despite the Miocene uplift of the Eastern Cordillera (Eude *et al*., 2015), we suspect that the Eastern Cordillera was not high enough to act as a topographic barrier because of the presence of the potential zircons from Callipuy volcanic arc (Western Cordillera; Navarro *et al*., 2010) and from Saraguro Fm. (Inter-Andean; Hungerbühler *et al*., 2002) and of the lowest elevation of Eastern Cordillera around 17.6 Ma (Eude *et al*., 2015).

5.3 Paleoenvironmental inferences

The presence of abderitids, along with a cebid primate at TAR-31, suggests predominantly humid and warm tropical conditions, with the occurrence of surrounding forests (Marivaux *et al.*, 2020; see subsection 5.1). Taxonomy, paleobiology and paleoecology of the marsupials from TAR-31). Palaeothentids seemingly preferred drier habitats, but still relatively humid, with mixed vegetational cover (Engelman *et al*., 2017), which would point, to some extent, to a landscape heterogeneity in the concerned area at that time. Aquatic faunal components retrieved at TAR-31 are primarily related to freshwater environments (ichthyofauna, turtles, caimans and gharials, and decapods; Marivaux *et al*., 2020). However, isotopic analyses made on crab claws and fish teeth from TAR-31 (Alvim *et al*., 2021) point to potential oligohaline

conditions, suggesting marine influence, consistent with the hypothesized landscapes as reconstructed at the western margin of the Pebas Mega-Wetland System (Hoorn *et al.*, 2010; Roddaz *et al.*, 2010; Boonstra *et al.*, 2015; Antoine et al., 2016; Marivaux *et al.*, 2020; Alvim *et al*., 2021).

5.4 Paleobiogeographical implications

The Amazonian region has been regarded as a key area concerning the Neogene marsupial radiations (Goin, 1997; Antoine *et al*., 2017; Suárez Gómez, 2019; Castro *et al*., 2021). The records from La Venta, for instance, suggest that this area was both a “cradle”, *i.e*., a high-diversification rate area, as well as a “museum”, with low extinction rates (Suárez Gómez, 2019).

All three marsupial genera recognized at TAR-31 have broad temporal and geographical ranges. *Thylamys* has extant representatives inhabiting subtropical South America, with records from Peru southwards along the Andes and Chilean Pacific coast, as well as eastwards across Argentina, Bolivia, Brazil, Paraguay, and Uruguay, inhabiting almost exclusively arid to semiarid environments and being especially diverse in the region between the Altiplano and northern Patagonia (Gardner, 2007; Voss and Jansa, 2009). Other species of *Thylamys*, either extinct or extant, neither occur in Amazonia nor in the lowermost latitudes. Accordingly, the La Venta and TAR-31 records suggest a distinct and much broader past geographical range for this genus. Besides, other fossil species of *Thylamys* are recorded in the late Miocene of the Pampean Argentina (Buenos Aires and La Pampa provinces, *T*. *pinei* Goin, Montalvo and Visconti, 2000 and *T*. *zetti* Goin, 1997; Huayquerian SALMA; Goin, 1997; Goin *et al*., 2000; Verzi *et al*., 2008), as well as in lower Pliocene deposits of the Buenos Aires Province (*T*. *contrerasi*; Montehermosan SALMA; Goin, 1997; Prevosti *et al*., 2021), and Pleistocene/Holocene localities of Argentina and Brazil (Deschamps and Tonni, 1992; Hadler *et al*., 2009; Motta *et al*., 2019). However, as mentioned above, further analyses are needed to confirm if these Miocene *Thylamys* representatives indeed pertain to *Thylamys sensu stricto* or to some kind of stem Thylamyini instead.

Palaeothentes is a speciose genus with several species recorded in early and middle Miocene deposits of Argentina and Chile (Río Frías Fm., Chile; Sarmiento,

Santa Cruz, and Pinturas formations, Argentina; Colhuehuapian to Friasian SALMAs; Abello, 2007), as well as in Quebrada Honda, Bolivia (Honda Group, late middle Miocene; Engelman *et al*., 2017). Aside from *Pitheculites ipururensis* nov. sp., *Pitheculites* includes the early Miocene *P*. *minimus* from Argentinean Patagonia (Sarmiento Fm., Colhuehuapian SALMA), the early middle Miocene *P*. *rothi* from Chile (Río Frías Fm., "Friasian" age), and the late middle Miocene *P*. *chenche* from La Venta, Colombia (Honda Group, La Victoria Fm., Duke 113 locality; *ca*. 13.5 Ma) (Abello, 2007). *Pitheculites* stands out among abderitids due to its remarkably broad temporal and geographical distribution, spanning around 8 My (21–13.0 Ma) and 50° in terms of latitude, with records from Patagonian Argentina (*ca.* 45°S; the oldest and southernmost ones) to equatorial Colombia (*ca.* 5°N; Abello, 2007) and Peruvian Amazonia (TAR-31; *ca*. 13.0 Ma, 6°30'S). The general pattern is that of a northern shift or northward contraction of the distribution range, strikingly recalling that of astrapotheres and South American monkeys, in the very same time interval (Fleagle *et al*., 1997; Hartwig and Meldrum, 2002; Goillot *et al.*, 2011; Rosenberger and Hartwig, 2013; Kay, 2015; Marivaux *et al*., 2016a, b, 2020).

The palaeothentoid record in Western Amazonia has been widely expanded in the two last decades, through the middle Eocene–Miocene assemblages from Contamana (Pozo, Chambira, and Pebas formations; Antoine *et al*., 2016), the mid-Paleogene Santa Rosa fauna (Goin and Candela, 2004), the upper Eocene–lower Oligocene Shapaja section (Pozo Fm.; Antoine *et al.*, 2021), and the late middle Miocene La Venta fauna (Suárez Gómez, 2019). This long and diverse presence of palaeothentoids in northern South America may represent a key chapter of their evolutionary history, which remains open.

Comparisons with other Miocene metatherian assemblages at low and mid latitudes of South America find that TAR-31 shows the closest relationship to La Venta, as was already noticed for other mammalian groups (Marivaux *et al.*, 2020; Boivin *et al.*, 2021). In general, TAR-31 shows still closer affinities with the mammalian assemblage from the lower part of the Villavieja Fm. at La Venta (13.1–12.5 Ma; Madden *et al.*, 1997), in sharing a cebid primate (*Neosaimiri*; Marivaux *et al*., 2020), three rodent species (Boivin *et al*., 2021), the medium-sized notoungulate *Miocochilius*, and the proterotheriid litoptern *Megadolodus* (Marivaux *et al*., 2020; Boivin *et al*.,

2021). This strong similarity is further supported by metatherians, as all three families of marsupials recorded at TAR-31 (Didelphidae, Abderitidae, and Palaeothentidae) are also documented at La Venta, with one species (‘*Thylamys*’ cf. ‘*T*.’ *colombianus*) and one genus (*Pitheculites*) in common, despite the fact that the latter comes from a single level of the slightly older La Victoria Fm. (Goin, 1997; Madden *et al*., 1997; Suárez Gómez, 2019). The La Venta fauna contains two additional metatherian orders (Sparassodonta and Microbiotheria) and five extra families (Hondadelphidae, Hathliacynidae, Thylacosmilidae, ?Sternbergiidae, and Microbiotheriidae; Suárez Gómez, 2019), which are not recorded at TAR-31. The localities of Madre de Dios (MD-67; Antoine *et al.*, 2013) and Acre in Brazil and Peru (Río Acre, Czaplewski, 1996; Cozzuol *et al*., 2006) also have close affinities with TAR-31 by recording didelphids as well. The other species-rich metatherian assemblage from the Laventan SALMA is Quebrada Honda (13.1–12.4 Ma; Gibert *et al*., 2020), which is mostly distinct from TAR-31, by sharing one single taxon (*Palaeothentes*, family Palaeothentidae). Abderitids and didelphids, occurring at TAR-31, are not recorded in Quebrada Honda. Conversely, sparassodonts are species-rich, but fairly rare, at Quebrada Honda and absent from TAR-31. Argyrolagid polydolopimorphians and decastine palaeothentids are also present in Quebrada Honda deposits and absent at TAR-31 (Engelman *et al*., 2015, 2017, 2020). Therefore, these similarities between the metatherian fauna from TAR-31 and the ones from mid and high latitudes of South America further support the hypothesis that Western Amazonia represented a single and consistent biogeographical region for land mammals over middle Miocene times, probably due to the region's strong relationship within the PMWS (Figure 6). On low latitudes of South America, during the Miocene (from ~16,5 Ma), the orogeny of the Andes started to have a great influence on the climate, by preventing humid air from the southern Pacific to reach eastern forelands, leading to an increase in aridity and cooler temperatures, and thus to the disappearance of tropical and subtropical climates in the southern part of the continent (Blisniuk *et al*., 2005). Until today, the Andean Cordillera is considered a major factor disrupting atmospheric circulation, generating several local and also broad phenomena, such as differences between climatic conditions on its eastern and western slopes and adjacent areas (Garreaud, 2009).

In the present contribution we have described the records of '*Thylamys*' cf. '*T.*' *colombianus*, aff. *Palaeothentes* and *Pitheculites ipururensis* nov. sp. for the late middle Miocene locality of TAR-31, Peruvian Amazonia. These records expand our knowledge of the metatherian diversity during the Miocene in Western Amazonia, partly fulfilling the gap in the knowledge of fossil metatherians from northern South America. Additionally, the data presented here strengthen the idea that Western Amazonia formed a significant unit in terms of paleobiogeography under the influence of the PMWS during middle Miocene.

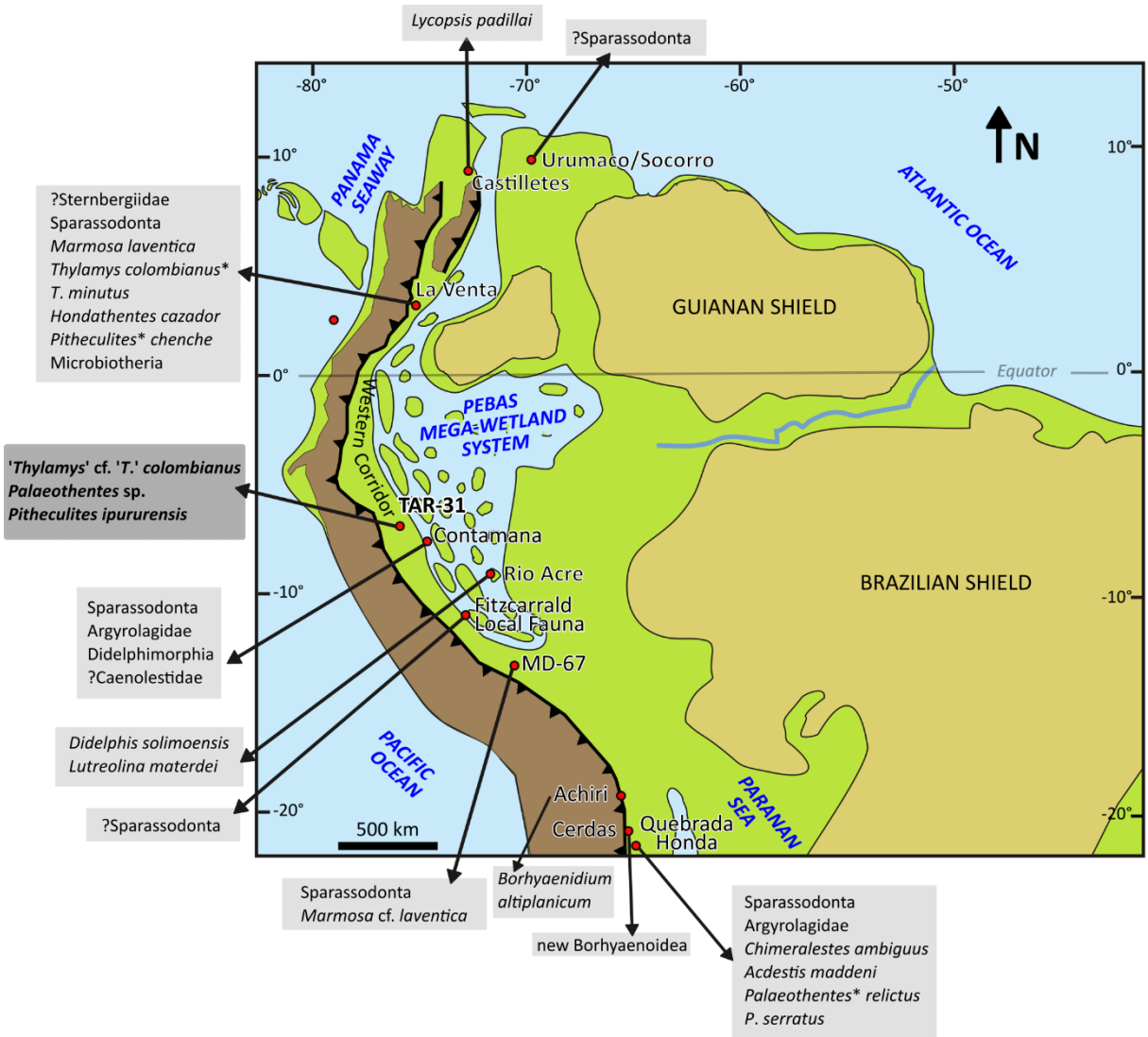


Figure 6. Late middle Miocene (*ca*. 13 Ma) paleogeographic map of Northern South America with the Metatheria taxa recorded in each one of the fossiliferous localities mentioned in the text (red dots). Light green shows low-elevation terra firma forests. Shape and size of emerged landmasses within the Pebas Mega-Wetland System

(PMWS) are tentative. Modified from Hoorn *et al*. (2010), Antoine *et al*. (2013), Boonstra *et al*. (2015), Anderson *et al*. (2016), and Marivaux *et al*. (2020). Paleoecological data from Croft (2007), Cadena *et al*. (2015), Tejada-Lara *et al*. (2015), and Antoine *et al*. (2016, 2017). Faunal lists according to Villarroel and Marshal (1983), Czaplewski (1996), Linares (2004), Cozzuol *et al*. (2006), Antoine *et al*. (2013, 2016), Tejada-Lara *et al*. (2015), Croft *et al*. (2016), Suárez *et al.* (2016), Engelman *et al*. (2017, 2020), and Suárez Gómez (2019). * indicates taxa in common with TAR-31.

Acknowledgments

We thank all the people who participated during the fieldwork campaigns and C. Cazeveille (INM, France) for the access to the SEM facilities. We are highly indebted to Russell K. Engelman and an anonymous reviewer for their constructive and in-depth comments of a former version of this manuscript. This work was supported *by Conselho Nacional de Desenvolvimento Científico e Tecnológico* (CNPq, 140773/2019-3, 312941/2018-8, 306951/2017-7), *Coordenação de Aperfeiçoamento de Pessoal de Nível Superior* (CAPES, COFECUB program Te 924/18 “Paléo-Amazone: evolution Néogène de l’Amazonie Brésilienne”, 88881.143095/2017-01), the National Geographic Society (nº 9679-15), the Campus France program of the French Ministry of Foreign Affairs, the *Institut des Sciences de l’Évolution de Montpellier* (ISEM), The Leakey Foundation, the French *Agence Nationale de la Recherche* (“*Investissements d’Avenir*” grant LabEx CEBA, ANR-10-LABX-25-01), and the international programs of cooperation ECOS-FonCyT (A14- U01), and CoopIntEER CNRS-CONICET (nº 252540). The paleontological investigations in Peru occur in the framework of the cooperation agreement between the ISEM and MUSM. This is ISEM publication n°: 2022-XXX Sud.

References

Abello, M.A. 2007. Sistemática y Bioestratigrafía de los Paucituberculata (Mammalia, Marsupialia) del Cenozoico de América del Sur. Ph.D. Thesis (Unpublished), Universidad Nacional de La Plata: 381 p.

Abello, M.A. 2013. Analysis of dental homologies and phylogeny of Paucituberculata (Mammalia: Marsupialia). Biological Journal of the Linnean Society 109(2): 441–465. doi:10.1111/bij.12048

Abello, M.A.; Candela, A.M. 2010. Postcranial skeleton of the Miocene marsupial *Palaeothentes* (Paucituberculata, Palaeothentidae): paleobiology and phylogeny. Journal of Vertebrate Paleontology 30(5): 1515–1527. doi:10.1080/02724634.2010.501437

Abello, M.A.; Rubilar-Rogers, D. 2012. Revisión del género *Abderites* Ameghino, 1887 (Marsupialia, Paucituberculata). Ameghiniana 49(2): 164–184.

Abello, M.A.; Martin, G.M.; Cardoso, Y. 2021. Review of the extinct 'shrew-opossums' (Marsupialia: Caenolestidae), with descriptions of two new genera and three new species from the Early Miocene of southern South America. Zoological Journal of the Linnean Society 193(2): 464–498. doi:10.1093/zoolinnean/zlaa165

Abello, M.A.; Toledo, N.; Ortiz-Jaureguizar, E. 2020. Evolution of South American Paucituberculata (Metatheria: Marsupialia): adaptive radiation and climate changes at the Eocene- Oligocene boundary. Historical Biology, doi:10.1080/08912963.2018.1502286

Alvim, A.M.V.; Santos, R.V.; Roddaz, M.; Antoine, P.-O.; Ramos, M.I.F.; do Carmo, D.A.; Linhas, A.P.; Negri, F.R. 2021. Fossil isotopic constraints (C, O and 87Sr/86Sr) on Miocene shallow-marine incursions in Amazonia. Palaeogeography, Palaeoclimatology, Palaeoecology 573(1): 110422. doi:10.1016/j.palaeo.2021.110422

Anderson, V.J.; Horton, B.K.; Saylor, J.E.; Mora, A.; Tesón, E.; Breecker, D.O.; Ketcham, R.A. 2016. Andean topographic growth and basement uplift in southern Colombia: Implications for the evolution of the Magdalena, Orinoco, and Amazon river systems. Geosphere 12(4): 1235–1256. doi:10.1130/GES01294.1

Antoine, P.-O.; Salas-Gismondi, R.; Pujos, F.; Ganerød, M.; Marivaux, L. 2017. Western Amazonia as a hotspot of mammalian biodiversity throughout the Cenozoic. Journal of Mammalian Evolution 24(1): 5–17. doi:10.1007/s10914-016-9333-1

Antoine, P.-O.; Roddaz, M.; Brichau, S.; Tejada-Lara, J.; Salas-Gismondi, R.; Altamirano, A.; Louterbach, M.; Lambs, L.; Otto, T.; Brusset, S. 2013. Middle Miocene vertebrates from the Amazonian Madre de Dios Subandean Zone, Perú. Journal of South American Earth Sciences 42: 91–102. doi:10.1016/j.jsames.2012.07.008

Antoine, P.-O.; *et al*. 2016. A 60-million-year Cenozoic history of western Amazonian ecosystems in Contamana, Eastern Peru. Gondwana Research 31: 30–59. doi:10.1016/j.gr.2015.11.001

Antoine, P.-O.; *et al*. 2021. Biotic community and landscape changes around the Eocene–Oligocene transition at Shapaja, Peruvian Amazonia: regional or global drivers? Global and Planetary Change 202: 103512. doi:10.1016/j.gloplacha.2021.103512

Arnal, M.; Pérez, M.E.; Medina, L.T.; Campbell, K.E. 2022. The high taxonomic diversity of the Palaeogene hystricognath rodents (Caviomorpha) from Santa Rosa (Peru, South America) framed within a new geochronological context, Historical Biology aop. doi:10.1080/08912963.2021.2017916

Arnal, M.; Kramarz, A.G.; Vucetich, M.G.; Frailey, C.D.; Campbell, K.E. 2020. New Palaeogene caviomorphs (Rodentia, Hystricognathi) from Santa Rosa, Peru: systematics, biochronology, biogeography and early evolutionary trends. Papers in Palaeontology 6: 193–216. doi:10.1002/spp2.1264

Bahlburg, H.; Vervoort, J.D.; Du Frane, S.A.; Bock, B.; Augustsson, C.; Reimann, C. 2009. Timing of crust formation and recycling in accretionary orogens: insights learned from the western margin of South America. Earth Science Reviews 97(1–4): 215–241. doi:10.1016/j.earscirev.2009.10.006.

Bahlburg, H.; Vervoort, J.D.; DuFrane, A.; Carlotto, V.; Reimann, C.; Cárdenas, J. 2011. The U-Pb and Hf isotope evidence of detrital zircons of the Ordovician Ollantaytambo Formation, southern Peru, and the Ordovician provenance and paleogeography of southern Peru and northern Bolivia. Journal of South American Earth Sciences 32: 196–209. doi:10.1016/j.jsames.2011.07.002.

Beck, R.M.D.; Taglioretti, M.L. 2020. A nearly complete juvenile skull of the marsupial *Sparassocynus derivatus* from the Pliocene of Argentina, the affinities of Sparassocynids", and the diversification of opossums (Marsupialia; Didelphimorphia; Didelphidae). Journal of Mammalian Evolution 27: 385–417. doi:10.1007/s10914-019-09471-y

Beck, R.M.D.; Voss, R.S.; Jansa, S.A. 2021. Craniodental morphology and phylogeny of marsupials. Bulletin of the American Museum of Natural History: preprint.

Bissaro-Júnior, M.C.; Kerber, L.; Crowley, J.L.; Ribeiro, A.M.; Ghilardi, R.P.; Guilherme, E.; Negri, F.R.; Souza Filho, J.P.; Hsiou, A.S. 2019. Detrital zircon U–Pb

geochronology constrains the age of Brazilian Neogene deposits from Western Amazonia. Palaeogeography, Palaeoclimatology, Palaeoecology 516: 64–70. doi:10.1016/j.palaeo.2018.11.032.

Blisniuk, P.M.; Stern, L.A.; Page Chamberlain, C.; Idleman, B.; Zeitler, P.K. 2005. Climatic and ecologic changes during Miocene surface uplift in the Southern Patagonian Andes. Earth and Planetary Science Letters 230(1–2): 125–142. doi:10.1016/j.epsl.2004.11.015.

Boivin, M.; Marivaux, L.; Orliac, M.J.; Pujos, F.; Salas-Gismondi, R.; Tejada-Lara, J.V.; Antoine, P.-O. 2017a. Late middle eocene caviomorph rodents from Contamana, Peruvian Amazonia. Palaeontologia Electronica 20.1.19A: 1–50. doi:10.26879/742

Boivin, M.; Marivaux, L.; Candela, A.M.; Orliac, M.J.; Pujos, F.; Salas-Gismondi, R.; Tejada-Lara, J.V.; Antoine P.-O. 2017b. Late Oligocene caviomorph rodents from Contamana, Peruvian Amazonia. Papers in Palaeontology 3(1): 69–109. doi:10.1002/spp2.1068

Boivin, M.; Marivaux, L.; Pujos, F.; Salas-Gismondi, R.; Tejada-Lara, J.V.; Varas-Malca, R. M.; Antoine, P.-O. 2018. Early Oligocene caviomorph rodents from Shapaja, Peruvian Amazonia. Palaeontographica 311(1–6): 87–156. doi:10.1127/pala/2018/0075

Boivin, M.; *et al*. 2021. Late middle Miocene caviomorph rodents from Tarapoto, Peruvian Amazonia. PLoS ONE 16(11): e0258455. doi:10.1371/journal.pone.0258455

Boonstra, M.; Ramos, M.I.F.; Lammertsma, E.I.; Antoine, P.-O.; Hoorn, C. 2015. Marine connections of Amazonia: evidence from foraminifera and dinoflagellate cysts (early to middle Miocene, Colombia/Peru). Palaeogeography, Palaeoclimatology, Palaeoecology 417: 176–194. doi:10.1016/j.palaeo.2014.10.032

Bown, T.M.; Fleagle, J.G. 1993. Systematics, biostratigraphy, and dental evolution of the Palaeothentidae, later Oligocene to early-middle Miocene (Deseadan-Santacrucian) caenolestoid marsupials of South America. Journal of Paleontology 67(29): 1–76. doi:10.1017/S0022336000062107

Bühn, B.; Pimentel, M.M.; Matteini, M.; Dantas, E.L. 2009. High spatial resolution analysis of Pb and U isotopes for geochronology by laser ablation multi-collector inductively coupled plasma mass spectrometry (LA-MC-ICP-MS). Anais da Academia Brasileira de Ciências 81(1): 99–114. doi:10.1590/S0001-37652009000100011

Cadena, E.A.; Anaya, F.; Croft, D.A. 2015. Giant fossil tortoise and freshwater chelid turtle remains from the middle Miocene, Quebrada Honda, Bolivia: evidence for lower paleoelevations for the southern Altiplano. Journal of South American Earth Sciences 64(1): 190–198. doi:10.1016/j.jsames.2015.10.013

Carvalho, M.R.; *et al*. 2021. Extinction at the end-Cretaceous and the origin of modern Neotropical rainforests. Science 372(6537): 63–68. doi:10.1126/science.abf1969

Castro, M.C.; Dahur, M.J.; Ferreira, G.S. 2021. Amazonia as the origin and diversification area of Didelphidae (Mammalia: Metatheria), and a review of the fossil record of the clade. Journal of Mammalian Evolution 28: 583–598. doi:10.1007/s10914-021-09548-7

Chew, D.M.; Schaltegger, U.; Košler, J.; Whitehouse, M.J.; Gutjahr, M.; Spikings, R.A.; Miškovic, A. 2007. U-Pb geochronologic evidence for the evolution of the Gondwanan margin of the north-central Andes. Geological Society of America Bulletin 119(5–6): 697–711. doi:10.1130/B26080.1

Chew, D.M.; Magna, T.; Kirkland, C.L.; Mišković, A.; Cardona, A.; Spikings, R.; Schaltegger, U. 2008. Detrital zircon fingerprint of the Proto-Andes: evidence for a Neoproterozoic active margin? Precambrian Research 167(1): 186–200. doi:10.1016/j.precamres.2008.08.002.

Chornogubsky, L.; Kramarz, A.G. 2012. Nuevos hallazgos de Microbiotheriidae (Mammalia,

Marsupialia) en la Formación Pinturas (Mioceno temprano, Argentina). Ameghiniana 49(4): 442–450.

Cozzuol, M.A.; Goin, F.; de los Reyes, M.; Ranzi, A. 2006. The oldest species of *Didelphis* (Mammalia, Marsupialia, Didelphidae), from the late Miocene of Amazonia. Journal of Mammalogy 87(4): 663–667. doi:10.1644/05-MAMM-A-282R2.1

Croft, D.A. 2007. The middle Miocene (Laventan) Quebrada Honda fauna, southern Bolivia and a description of its notoungulates. Palaeontology 50(1): 277–303. doi:10.1111/j.1475-4983.2006.00610.x

Croft, D.A. 2016. Horned armadillos and rafting monkeys. Indiana University Press: 304 p. Bloomington and Indianopolis.

Croft, D.A.; Engelman, R.K.; Dolgushina, T.; Wesley, G. 2018. Diversity and disparity of sparassodonts (Metatheria) reveal non-analogue nature of ancient South American

mammalian carnivore guilds. Proceedings of the Royal Society B 285: 20172012. doi:10.1098/rspb.2017.2012

Croft, D.A.; Carlini, A.A.; Ciancio, M.R.; Brandoni, D.; Drew, N.E.; Engelman, R.K.; Anaya, F. 2016. New mammal faunal data from Cerdas, Bolivia, a middle-latitude Neotropical site that chronicles the end of the Middle Miocene Climatic Optimum in South America. Journal of Vertebrate Paleontology 36(5): e1163574. doi:10.1080/02724634.2016.1163574

Czaplewski, N.J. 1996. Opossums (Didelphidae) and bats (Noctilionidae and Molossidae) from the late Miocene of the Amazon Basin. Journal of Mammalogy 77(1): 84–94. doi:10.2307/1382711

Defler, T. 2019. History of Terrestrial Mammals in South America. Springer: 372 p. Cham.

Deschamps, C.M.; Tonni, E.P. 1992. Los vertebrados del Pleistoceno tardío-Holoceno del Arroyo Naposta Grande, Provincia de Buenos Aires: aspectos paleoambientales. Ameghiniana 29(3): 201–210.

Dickinson, W.R.; Gehrels, G.E. 2009. Use of U-Pb ages of detrital zircons to infer maximum depositional ages of strata: a test against a Colorado Plateau Mesozoic database. Earth and Planetary Science Letters 288(1–2): 115–125. doi:10.1016/j.epsl.2009.09.013

Dumont, E.R.; Bown, T.M. 1997. New caenolestoid marsupials. *In* Vertebrate Paleontology in the Neotropics. The Miocene fauna of La Venta, Colombia (Kay, R.F.; Madden, R.H.; Cifelli, R.L.; Flynn, J.J.; editors). Smithsonian Institution Press: 207–212. Washington and London.

Dumont, E.; Strait, S.; Friscia, A. 2000. Abderitid marsupials from the Miocene of Patagonia: an assessment of form, function, and evolution. Journal of Paleontology 74(6): 1161–1172. doi:10.1666/0022-3360(2000)0742.0.CO;2

Engelman, R.K.; Anaya, F.; Croft, D.A. 2015. New specimens of *Acyon myctoderos* (Metatheria, Sparassodonta) from Quebrada Honda, Bolivia. Ameghiniana 52: 204–225. doi:10.5710/AMGH.19.11.2014.2803

Engelman, R.K.; Anaya, F.; Croft, D.A. 2017. New palaeothentid marsupials (Paucituberculata) from the middle Miocene of Quebrada Honda, Bolivia, and their implications for the palaeocology, decline and extinction of the Palaeothentoidea.

Journal of Systematic Palaeontology 15(10): 787–820. doi:10.1080/14772019.2016.1240112

Engelman, R.K.; Anaya, F.; Croft, D.A. 2020. *Australogale leptognathus*, gen. et sp. nov., a second species of small sparassodont (Mammalia: Metatheria) from the Middle Miocene locality of Quebrada Honda, Bolivia. Journal of Mammalian Evolution 27(1): 37–54. doi:10.1007/s10914-018-9443-z

Erlich, R.N.; Fallon, J.; O'Sullivan, P. 2018. Stratigraphy and LA-ICP-MS zircon U-Pb provenance of middle Permian to Maastrichtian sandstones from outcrop and subsurface control in the sub-Andean basins of Peru. *In* Petroleum basins and hydrocarbon potential of the Andes of Peru and Bolivia (Zamora, G.; McClay, K.R.; Ramos, V.A.; editors). AAPG Memoir 117: 175–222.

Eude, A.; Roddaz, M.; Brichau, S.; Brusset, S.; Calderon, Y.; Baby, P.; Soula, J.-C. 2015. Controls on timing of exhumation and deformation in the northern Peruvian eastern Andean wedge as inferred from low-temperature thermochronology and balanced cross section. Tectonics 34(4): 715–730. doi:10.1002/2014TC003641

Fleagle, J.G.; Kay, R.F.; Anthony, M.R.L. 1997. Fossil New World Monkeys. *In* Vertebrate Paleontology in the Neotropics. The Miocene fauna of La Venta, Colombia (Kay, R.F.; Madden, R.H.; Cifelli, R.L.; Flynn, J.J.; editors). Smithsonian Institution Press: 473–495. Washington and London.

Flynn, J.J.; Charrier, R.; Croft, D.A.; Wyss, A.R. 2012. Cenozoic Andean faunas: shedding new light on South American mammal evolution, biogeography, environments, and tectonics. *In* Bones, clones, and biomes: the history and geography of recent neotropical

mammals (Patterson, B.D.; Costa, L.P.; editors). The University of Chicago Press: 51–75. Chicago and London.

Frailey, C.D.; Campbell, K.E. 2004. Paleogene rodents from Amazonian Peru: the Santa Rosa local fauna. *In* The Paleogene mammalian fauna of Santa Rosa, Amazonian Peru (Campbell, K.E.; editor). Natural History Museum of Los Angeles County, Science Series 40: 71–130. Los Angeles.

Gardner, A.L. 2007. Mammals of South America. Vol. 1. The University of Chicago Press: 669 p. Chicago.

Garreaud, R.D. 2009. The Andes climate and weather. Advances in Geosciences 22: 3–11. doi:10.5194/adgeo-22-3-2009, 2009.

Gehrels, G. 2014. Detrital zircon U-Pb geochronology applied to tectonics. Annual Review of Earth and Planetary Sciences 42: 127–149. doi:10.1146/annurev-earth-050212-124012

Gehrels, G.E.; Valencia, V.A.; Ruiz, J. 2008. Enhanced precision, accuracy, efficiency, and spatial resolution of U-Pb ages by laser ablation-multicollector-inductively coupled plasma-mass spectrometry. Geochemistry, Geophysics, Geosystems 9(3): 1–13. doi:10.1029/2007GC001805

Gibert, L.; Deino, A.; Valero, L.; Anaya, F.; Lería, M.; Saylor, B.; Croft, D.A. 2020. Chronology of Miocene terrestrial deposits and fossil vertebrates from Quebrada Honda (Bolivia). Palaeogeography, Palaeoclimatology, Palaeoecology 560: 110013. doi:10.1016/j.palaeo.2020.110013

Goillot, C.; Antoine, P.-O.; Tejada, J.; Pujos, F.; Salas Gismondi, R. 2011. Middle Miocene Uruguaytheriinae (Mammalia, Astrapotheria) from Peruvian Amazonia and a review of the astrapotheriid fossil record in northern South America. Geodiversitas 33(2): 331–345. doi:10.5252/g2011n2a8

Goin, F.J. 1997. New clues for understanding Neogene marsupial radiations. *In* Vertebrate Paleontology in the Neotropics. The Miocene fauna of La Venta, Colombia (Kay, R.F.; Madden, R.H.; Cifelli, R.L.; Flynn, J.J.; editors). Smithsonian Institution Press: 187–206. Washington and London.

Goin, F.J.; Abello, M.A. 2013. Los Metatheria sudamericanos de comienzos del Neógeno (Mioceno Temprano, Edad–Mamífero Colhuehuapense). Parte II: Microbiotheria y Polydolopimorphia. Ameghiniana 50(1): 51–78.

Goin, F.J.; Candela, A.M. 2004. New Palaeogene marsupials from the Amazon Basin of Eastern Peru. *In* The Paleogene mammalian fauna of Santa Rosa, Amazonian Peru (Campbell, K.E.; editor). Natural History Museum of Los Angeles County, Science Series 40: 15–60. Los Angeles.

Goin, F.J.; de los Reyes, M. 2011. Contribución al conocimiento de los representantes extintos de *Lutreolina* Thomas, 1910 (Mammalia, Marsupialia, Didelphidae). Historia Natural 1(2): 15–25.

Goin, F.J.; Abello, M.A.; Chornogubsky, L. 2010. Middle Tertiary marsupials from central Patagonia (early Oligocene of Gran Barranca): understanding South America's Grande Coupure. *In* The paleontology of Gran Barranca: evolution and environmental change through the Middle Cenozoic of Patagonia (Madden, R.H.; Carlini, A.A.; Vucetich, M.G.; Kay, R.F.; editors). Cambridge University Press: 71–107. New York.

Goin, F.J.; Montalvo, C.I.; Visconti, G. 2000. Los marsupiales (Mammalia) del Mioceno Superior de la Formación Cerro Azul (Provincia de La Pampa, Argentina). Estudios Geológicos 56(1–2): 101–126.

Goin, F.J.; Case, J.A.; Woodburne, M.O. Vizcaíno, S.F.; Reguero, M.A. 1999. New discoveries of "oppossum-like" marsupials from Antarctica (Seymour Island, Medial Eocene). Journal of Mammalian Evolution 6: 335–365. doi:10.1017/S0954102094000027

Goin, F.J.; Woodburne, M.O.; Zimicz, A.N.; Martin, G.M.; Chornogubsky, L. 2016. A Brief History of South American Metatherians. Evolutionary Contexts and Intercontinental Dispersals. Springer Earth System Sciences: 237 p. New York.

Goin, F.J.; Abello, A.; Bellosi, E.; Kay, R.; Madden, R.; Carlini, A. 2007. Los Metatheria sudamericanos de comienzos del Neógeno (Mioceno Temprano, Edad-mamífero Colhuehuapense). Parte I: Introducción, Didelphimorphia y Sparassodonta. Ameghiniana 44(1): 29–71.

Hadler, P.; Ferigolo, J.; Goin, F.J. 2009. Mamíferos de pequeno porte (Didelphimophia, Chiroptera e Rodentia) do Pleistoceno Final/Holoceno do Brasil, com ênfase no Rio Grande do Sul. *In* Quaternário do Rio Grande do Sul: integrando conhecimentos (Ribeiro, A.M.; Bauermann, S.G.; Scherer, C.S.; editors). Sociedade Brasileira de Paleontologia: 155–170. Porto Alegre.

Hartwig, W.C.; Meldrum, D.J. 2002. Miocene platyrrhines of the northern Neotropics. *In* The Primate Fossil Record (Hartwig, W.C.; editor). Cambridge University Press: 175–188. Cambridge.

Hoorn, C.; *et al*. 2010. Amazonia through time: Andean uplift, climate change, landscape evolution, and biodiversity. Science 330(6006): 927–931. doi:10.1126/science.1194585

Hungerbühler, D.; Steinmann, M.; Winkler, W.; Seward, D.; Egüez, A.; Peterson, D.E.; Helg, U.; Hammer, C. 2002. Neogene stratigraphy and Andean geodynamics of

southern Ecuador. Earth-Science Reviews 57(1): 75–124. doi:10.1016/S0012-8252(01)00071-X

Hurtado, C.; Roddaz, M.; Santos, R.V.; Baby, P.; Antoine, P.-O.; Dantas, E.L. 2018. Cretaceous-early Paleocene drainage shift of Amazonian rivers driven by Equatorial Atlantic Ocean opening and Andean uplift as deduced from the provenance of northern Peruvian sedimentary rocks (Huallaga basin). Gondwana Research 63: 152–168. doi:10.1016/j.gr.2018.05.012

Jansa, S.A.; Barker, F.K.; Voss, R.S. 2014. The early diversification history of didelphid marsupials: a window into South America's "splendid isolation." Evolution 68: 684–695. doi:10.1111/Evo.12290

Jaramillo, C.; Hoorn, C.; Silva, S.A.F.; Leite, F.; Herrera, F.; Quiroz, L.; Dino, R.; Antonioli, L. 2010. The origin of the modern Amazon rainforest: implications of the palynological and palaeobotanical record. *In* Amazonia: landscape and species evolution (Hoorn, C.; Wesselingh, F.P.; editors). Wiley-Blackwell Publishing Ltd: 317–334. London.

Jaramillo, C.; *et al*. 2017. Miocene flooding events of western Amazonia. Science Advances 3: e1601693. doi:10.1126/sciadv.1601693

Jiménez-Lara, K. 2020. Systematic revision and redefinition of the genus *Scirrotherium* Edmund and Theodor, 1997 (Cingulata, Pampatheriidae): Implications for the origin of pampatheriids and the evolution of the South American lineage including *Holmesina*. Geobios 62: 1–21. doi:10.1016/j.geobios.2020.07.002.

Kay, R.F. 2015. Biogeography in deep time - What do phylogenetics, geology, and paleoclimate tell us about early platyrrhine evolution? Molecular Phylogenetics and Evolution 82: 358–374. doi:10.1016/j.ympev.2013.12.002

Kay, R.F.; Madden, R.H. 1997. Mammals and rainfall: Paleoecology of the middle Miocene at la Venta (Colombia, South America). Journal of Human Evolution 32(2–3): 161–199. doi:10.1006/jhev.1996.0104

Kay, R.F.; Madden, R.H.; Cifelli, R.L.; Flynn, J.J. 1997. Vertebrate Paleontology in the Neotropics: The Miocene Fauna of La Venta, Colombia. Smithsonian Institution Press: 592 p. Washington.

Kramarz, A.G.; Bellosi, E.S. 2005. Hystricognath rodents from the Pinturas Formation, Early–Middle Miocene of Patagonia, biostratigraphic and paleoenvironmental

implications. Journal of South American Earth Sciences 18(2): 199–212. doi:10.1016/j.jsames.2004.10.005

Linares, O.J. 2004. Bioestratigrafía de la fauna de mamíferos de las formaciones Socorro, Urumaco y Codore (Mioceno Medio-Plioceno Temprano) de la región de Urumaco, Falcon, Venezuela. Paleobiologia Neotropical 1: 1–26.

Litty, C.; Lanari, P.; Burn, M.; Schlunegger, F. 2017. Climate-controlled shifts in sediment provenance inferred from detrital zircon ages, western Peruvian Andes. Geology 45(1): 59–62. doi:10.1130/G38371.1

Louterbach, M.; *et al*. 2018. Provenance record of late Maastrichtian–late Palaeocene Andean Mountain building in the Amazonian retroarc foreland basin (Madre de Dios basin, Peru). Terra Nova 30(1): 17–23. doi:10.1111/ter.12303

Madden, R.H.; Guerrero, J.; Kay, R.F.; Flynn, J.J.; Swisher III, C.C.; Walton, A.H. 1997. The Laventan stage and age. *In* Vertebrate Paleontology in the Neotropics. The Miocene fauna of La Venta, Colombia (Kay, R.F.; Madden, R.H.; Cifelli, R.L.; Flynn, J.J.; editors). Smithsonian Institution Press: 499–519. Washington and London.

Magurran, A.E. 2004. Measuring biological diversity. Blackwell Publishing: 256 p. Oxford.

Marivaux, L.; Adnet, S.; Altamirano-Sierra, A.J.; Pujos, F.; Ramdarshan, A.; Salas-Gismondi, R.; Tejada-Lara, J.V.; Antoine, P.-O. 2016a. Dental remains of cebid platyrrhines from the earliest late Miocene of Western Amazonia, Peru: macroevolutionary implications on the extant capuchin and marmoset lineages. American Journal of Physical Anthropology 161(3): 478–493. doi:10.1002/ajpa.23052

Marivaux, L.; Adnet, S.; Altamirano-Sierra, A.J.; Boivin, M.; Pujos, F.; Ramdarshan, A.; Salas-Gismondi, R.; Tejada-Lara, J.V.; Antoine, P.-O. 2016b. Neotropics provide insights into the emergence of New World monkeys: new dental evidence from the late Oligocene of Peruvian Amazonia. Journal of Human Evolution 97: 159–175. *doi:10.1016/j.jhevol.2016.05.011*

Marivaux, L.; Aguirre-Dias, W.; Benites-Palomino, A.; Billet, G.; Boivin, M.; Pujos, F.; Salas-Gismondi, R.; Tejada-Lara, J.V.; Varas-Malca, R.M.; Antoine, P.-O. 2020. New record of *Neosairimi* (Cebidae, Platyrrhini) from the late Middle Miocene of Peruvian Amazonia. Journal of Human Evolution 146: 102835. doi:10.1016/j.jhevol.2020.102835

Marshall, L.G. 1976. New Didelphine marsupials from the La Venta fauna (Miocene) of Colombia, South America. Journal of Paleontology 50(3): 402–418.

Montes, C.; *et al*. 2021. A Middle to Late Miocene trans-andean portal: geologic record in the Tatacoa Desert. Frontiers in Earth Science 8: 587022. doi:10.3389/feart.2020.587022

Moreno, F.; Garzione, C.N.; George, S.W.M.; Horton, B.K.; Williams, L.; Jackson, L.J.; Carlotto, V.; Richter, F.; Bandeian, A. 2020. Coupled Andean growth and foreland basin evolution, Campanian–Cenozoic Bagua Basin, northern Peru. Tectonics 39(7): e2019TC005967. doi:10.1029/2019TC005967

Moreno, F.; *et al*. 2015. Revised stratigraphy of Neogene strata in the Cocinetas Basin, La Guajira, Colombia. Swiss J Palaeontol 134: 5–43. doi:10.1007/s13358-015-0071-4

Motta, F.A.; Hadler, P.; Cherem, J.J.; Ribeiro, A.M. 2019. A marsupial assemblage (Mammalia, Didelphimorphia) from the Quaternary of the Serra da Capivara, State of Piauí, Brazil. Revista Brasileira de Paleontologia 22(3): 225–239. doi:10.4072/rbp.2019.3.05

Navarro, P.; Rivera, M.; Monge, R. 2010. Geología y metalogenia del Grupo Calipuy (volcanismo Cenozoico) segmento Santiago de Chuco, norte del Perú. INGEMMET, Boletín, Serie D, Estudios Regionales, 28: 202 p. Lima.

Negri, F.R.; Bocquentin-Villanueva, J.; Ferigolo, J.; Antoine, P.-O. 2010. A review of Tertiary mammal faunas and birds from Western Amazonia. *In* Amazonia: landscape and species evolution: a look into the past (Hoorn, C.; Wesselingh, F.P; editors). Wiley-Blackwell Publishing Ltd: 243–258. London.

Prevosti, F.J.; *et al*. 2021. New radiometric 40Ar–39Ar dates and faunistic analyses refine evolutionary dynamics of Neogene vertebrate assemblages in Southern South America. Scientific Reports 11: 9830. doi:10.1038/s41598-021-89135-1

Quintero-Galvis, J.F.; Saenz-Agudelo, P.; Celis-Diez, J.L.; Amico, G.C.; Vazquez, S.; Shafer, A.B.; Nespolo, R.F. 2021. The biogeography of *Dromiciops* in Southern South America: middle Miocene transgressions, speciation and associations with *Nothofagus*. Molecular Phylogenetics and Evolution 163: 107234. doi:10.1016/j.ympev.2021.107234

Quiroz, L.; Jaramillo, C. 2010. Stratigraphy and sedimentary environments of Miocene shallow to marginal marine deposits in the Urumaco Through, Falcón Basin, western

Venezuela. *In* Urumaco and Venezuelan Paleontology: The Fossil Record of the Northern Neotropics (Sánchez-Villagra, M.R.; Aguilera, O.; Carlini, A.A.; editors). Indiana University Press: 153–172. Bloomington.

Raffi, I.; Wade, B.S.; Pälike, H.; Beu, A.G.; Cooper, R.; Crundwell, M.P. *et al*. 2020. Chapter 29 – The Neogene Period. *In* Geologic Time Scale 2020. Vol. 2. (Gradstein, F.M.; Ogg, J.G.; Schmitz, M.D.; Ogg, G.M.; editors). Elsevier: 1141–1215. Amsterdam.

Rincón, A.D.; Solórzano, A.; Benammi, M.; Vignaud, P.; McDonald, H.G. 2014. Chronology and geology of an Early Miocene mammalian assemblage in North of South America, from Cerro La Cruz (Castillo Formation), Lara state, Venezuela: implications in the 'changing course of Orinoco River' hypothesis. Andean Geology 41(3): 507–528. doi:10.5027/andgeoV41n3-a02

Roddaz, M.; Hermoza, W.; Mora, A.; Baby, P.; Parra, M.; Christophoul, F.; Brusset, S.; Espurt, N. 2010. Cenozoic Sedimentary Evolution of the Amazonian Foreland Basin System. *In* Amazonia: Landscape and Species Evolution: a Look into the Past (Hoorn, C.; Wesselingh, F.P; editors). Wiley Blackwell Publishing Ltd: 61–88. London.

Rosenberger, A.L.; Hartwig, W.C. 2013. New World Monkeys. *In* eLS. John Wiley & Sons, Ltd (editor). doi:10.1002/9780470015902.a0001562.pub3

Salas-Gismondi, R.; Flynn, J.J.; Baby, P.; Tejada-Lara, J.; Wesselingh, F.P.; Antoine, P.-O. 2015. A Miocene hyperdiverse crocodylian community reveals peculiar trophic dynamics in proto-Amazonian megawetlands. Proceedings of the Royal Society B: Biological Sciences 282(1804): 20142490. doi:10.1098/rspb.2014.2490

Sánchez-Villagra, M.R.; Aguilera, O.A.; Sánchez, R.; Carlini, A.A. 2010. The fossil vertebrate record of Venezuela of the last 65 million years. *In* Urumaco and Venezuelan Paleontology: The Fossil Record of the Northern Neotropics (Life of the Past) (Sánchez-Villagra, M.R.; Aguilera, O.A.; Carlini, A.A.; editors). Indiana University Press: 19–51. Bloomington.

Sato, K.; Teixeira, W.; Tassinari, C.; Basei, M. 2000. Crustal evolution of the South American platform. *In* Tectonic Evolution of South America (Cordani, U.; Milani, E.J.; Tomaz Filho, A.; Campos, D.A.; editors). 31st International Geological Congress: 19–40. Rio de Janeiro.

Sharman, G.R.; Malkowski, M.A. 2020. Needles in a haystack: detrital zircon U-Pb ages and the maximum depositional age of modern global sediment. Earth-Science Reviews 203: 103109. doi:10.1016/j.earscirev.2020.103109

Sharman, G.R.; Sharman, J.P.; Sylvester, Z. 2018. detritalPy: a Python-based toolset for visualizing and analyzing detrital geo-thermochronologic data. The Depositional Record 4(2): 202–215. doi:10.1002/dep2.45

Spikings, R.; Reitsma, M.J.; Boekhout, F.; Mišković, A.; Ulianov, A.; Chiaradia, M.; Gerdes, A.; Schaltegger, U. 2016. Characterization of Triassic rifting in Peru and implications for the early disassembly of western Pangaea. Gondwana Research 35:124–143. doi:10.1016/j.gr.2016.02.008.

Spradley, J.P.; Glazer, B.J.; Kay, R.F. 2019. Mammalian faunas, ecological indices, and machine-learning regression for the purpose of paleoenvironment reconstruction in the Miocene of South America. Palaeogeography, Palaeoclimatology, Palaeoecology 518: 155–171. doi:10.1016/j.palaeo.2019.01.014

Stutz, N.S.; *et al*. 2021. Neotropical metatherian diversity around the Eocene-Oligocene transition: the Shapaja section, Peruvian Amazonia. Libro de Resúmenes – 14 CAPA, Symposium Mamíferos del Paleógeno de América del Sur: 123.

Suárez, C.; Forasiepi, A.; Goin, F.J.; Jaramillo, C. 2016. Insights into the Neotropics prior to the Great American Biotic Interchange: new evidence of mammalian predators from the Miocene of Northern Colombia. Jounal of Vertebrate Paleontology 36(1): e1029581. doi:10.1080/02724634.2015.1029581

Suárez Gómez, C. 2019. Estudios Taxonómicos y Paleobiológicos sobre los Metatheria (Mammalia) del Mioceno Medio de La Venta, Colombia. Ph.D. thesis (Unpublished), Universidad Nacional de la Plata: 292 p.

Tejada-Lara, J.; Salas-Gismondi, R.; Pujos, F.; Baby, P.; Benammi, M.; Brusset, S.; Franceschi, D.; Espurt, N.; Urbina, M.; Antoine, P.-O. 2015. Life in Proto-Amazonia: Middle Miocene mammals from the Fitzcarrald Arch (Peruvian Amazonia). Palaeontology 58(2): 341–378. doi:10.1111/pala.12147

Verzi, D.H.; Montalvo, C.I.; Deschamps, C.M. 2008. Biostratigraphy and biochronology of the Late Miocene of central Argentina: evidence from rodents and taphonomy. Geobios 41(1): 145–155. doi:10.1016/j.geobios.2006.09.005

Villarroel, C.; Marshall, L.G. 1983. Two New Late Tertiary Marsupials (Hathlyacyninae and Sparassocyninae) from the Bolivian Altiplano. Journal of Paleontology 57(5): 1061-1066.

Voss, R.S.; Jansa, S.A. 2009. Phylogenetic relationships and classification of didelphid marsupials, an extant radiation of New World metatherian mammals. Bulletin of the American Museum of Natural History 322: 1–177.

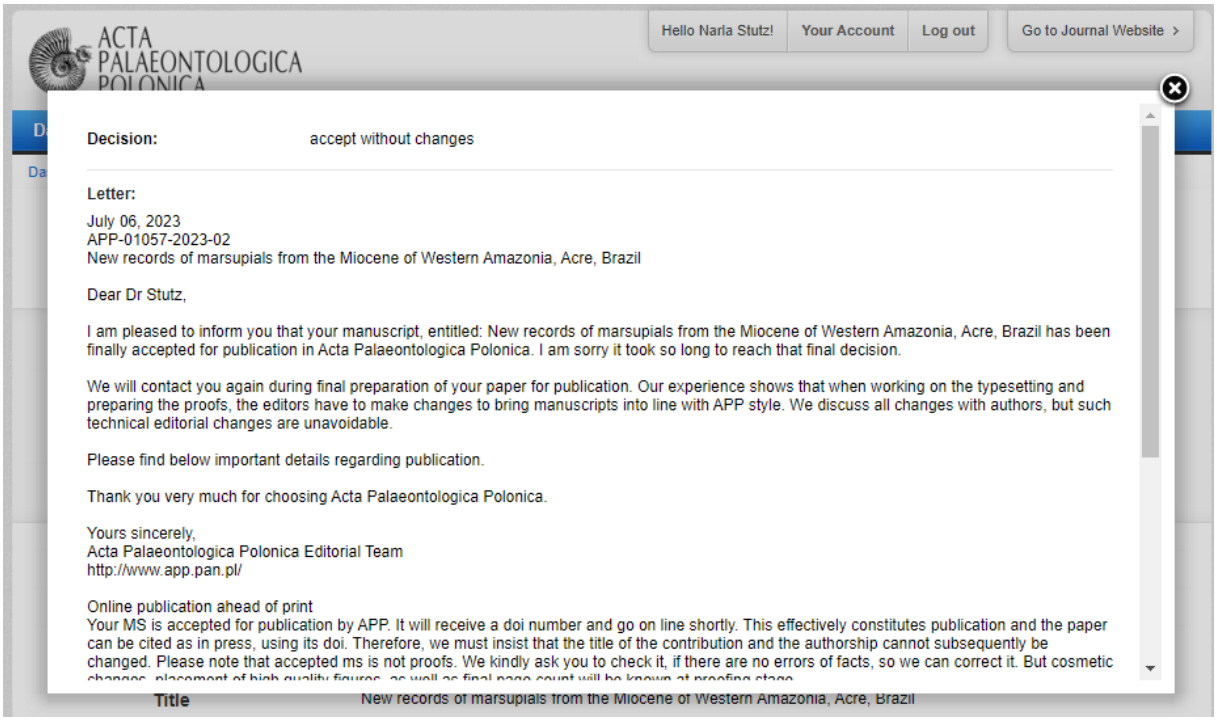
Voss, R.S.; Jansa, S.A. 2021. Opossums: an Adaptive Radiation of New World Marsupials. John Hopkins University Press: 328 p. Baltimore.

Westerhold, T.; *et al*. 2020. An astronomically dated record of Earth's climate and its predictability over the last 66 million years. Science 369(6509): 1383–1388. doi:10.1126/science.aba6853

Wing, S.L.; Herrera, F.; Jaramillo, C.A.; Gómez-Navarro, C.; Wilf, P.; Labandeira, C.C. 2009. Late Paleocene fossils from the Cerrejón Formation, Colombia, are the earliest record of neotropical rainforest. Proceedings of the National Academy of Sciences 106(44): 18627–18632. doi: 10.1073/pnas.0905130106

2 ARTIGO 2 – NEW RECORDS OF MARSUPIALS FROM THE MIOCENE OF WESTERN AMAZONIA, ACRE, BRAZIL

Artigo submetido ao periódico *Acta Palaeontologica Polonica* em 21/01/2023, status: *accepted*.



NARLA S. STUTZ, PATRICIA HADLER, FRANCISCO R. NEGRI, LAURENT MARIVAUX, PIERRE-OLIVIER ANTOINE, FRANÇOIS PUJOS, TIAGO R. JACÓ, EMMANUELLE M. FONTOURA, LEONARDO KERBER, ANNIE S. HSIOU, ROBERTO VENTURA SANTOS, ANDRÉ M. V. ALVIM, and ANA MARIA RIBEIRO

Narla S. Stutz [narlasstutz@gmail.com; ORCID: https://orcid.org/0000-0002-1937-3902] (corresponding author), Programa de Pós-Graduação em Geociências, Universidade Federal do Rio Grande do Sul, Av. Bento Gonçalves 9500, 91501-970, Porto Alegre, Rio Grande do Sul, Brazil, and Laboratoire de Paléontologie, Institut des Sciences de l'Évolution de Montpellier (ISE-M, UMR 5554, CNRS/IRD), Université de Montpellier, Place Eugène Bataillon, 34095, Montpellier, France.

Patricia Hadler [patricia.hadler@ufsc.br; ORCID: https://orcid.org/0000-0003-4897-3111], Laboratório de Paleontologia, Universidade Federal de Santa Catarina, Campus Universitário s/n, 88040-900, Florianópolis, Santa Catarina, Brazil.

Francisco R. Negri [frnegriufac@gmail.com; ORCID: https://orcid.org/0000-0001-7396-0334], Laboratório de Paleontologia, Campus Floresta, Universidade Federal do Acre, Estrada do Canela Fina, Km 12, 69980-000, Cruzeiro do Sul, Acre, Brazil.

Laurent Marivaux [laurent.marivaux@umontpellier.fr; ORCID: https://orcid.org/0000-0002-2882-0874] and Pierre-Olivier Antoine [pierre-olivier.antoine@umontpellier.fr; ORCID: https://orcid.org/0000-0001-9122-1818], Laboratoire de Paléontologie, Institut des Sciences de l'Évolution de Montpellier (ISE-M, UMR 5554, CNRS/IRD), Université de Montpellier, Place Eugène Bataillon, 34095, Montpellier, France.

François Pujos [fpujos@mendoza-conicet.gob.ar; ORCID: https://orcid.org/0000-0002-6267-3927], Consejo Nacional de Investigaciones Científicas y Técnicas (CONICET), and Instituto Argentino de Nivología, Glaciología y Ciencias Ambientales (IANIGLA), CONICET–UNCUYO-Mendoza, Av. Ruiz Leal s/n, Parque Gral. San Martín, 5500, Mendoza, Argentina.

Tiago R. Jacó [jaco.tiago@gmail.com; ORCID: https://orcid.org/0000-0002-5903-4673], Programa de Pós-Graduação em Sistemática e Conservação da Diversidade Biológica (PPGSCBIO), Secretaria do Meio Ambiente e Infraestrutura do Rio Grande do Sul, Universidade Estadual do Rio Grande do Sul, R. Dr. Salvador França 1427, 90690-000, Porto Alegre, Rio Grande do Sul, Brazil.

Emmanuelle M. Fontoura [emmanuelle.fontoura@acad.ufsm.br; ORCID: https://orcid.org/0000-0002-3907-618X], Programa de Pós-Graduação em Biodiversidade Animal (PPGBA), Universidade Federal de Santa Maria, Av. Roraima, 1000, 97105-900, Santa Maria, Rio Grande do Sul, and Centro de Apoio à Pesquisa Paleontológica da Quarta Colônia (CAPPA), Universidade Federal de Santa Maria, R. Maximiliano Vizzotto 598, 97230-000, São João do Polêsine, Rio Grande do Sul, Brazil.

Leonardo Kerber [leonardokerber@gmail.com; ORCID: https://orcid.org/0000-0001-8139-1493], Centro de Apoio à Pesquisa Paleontológica da Quarta Colônia (CAPPA), Universidade Federal de Santa Maria, R. Maximiliano Vizzotto 598, 97230-000, São João do Polêsine, Rio Grande do Sul, Brazil.

Annie S. Hsiou [anniehsiou@ffclrp.usp.br; ORCID: https://orcid.org/0000-0003-2392-6191], Laboratório de Paleontologia, Universidade de São Paulo, Av. Bandeirantes 3900, 14040-901, Ribeirão Preto, São Paulo, Brazil.
Roberto Ventura Santos [robertoventurasantos@gmail.com; ORCID: https://orcid.org/0000-0001-6071-8100] and André M. V. Alvim [andre.mavaal@gmail.com; ORCID: https://orcid.org/0000-0001-5050-4977], Laboratório de Geocronologia, Instituto de Geociências, Universidade de Brasília (UnB), Campus Universitário Darcy Ribeiro ICC - Ala Central, 70910-900, Brasília, Distrito Federal, Brazil.
Ana Maria Ribeiro [ana-ribeiro@sema.rs.gov.br; ORCID: https://orcid.org/0000-0003-4167-8558], Seção de Paleontologia, Museu de Ciências Naturais, Secretaria do Meio Ambiente e Infraestrutura, R. Dr. Salvador França 1427, 90690-000, Porto Alegre, Rio Grande do Sul, and Programa de Pós-Graduação em Geociências, Universidade Federal do Rio Grande do Sul, Av. Bento Gonçalves 9500, 91501-970, Porto Alegre, Rio Grande do Sul, Brazil

ABSTRACT. The Amazonian region covers a significant part of the South American continent and harbors outstanding biodiversity. However, much of its history is still unknown. This situation has begun to change with paleontological field efforts over the last decades, which have been proving that fossils can be common in this region. Despite their great current species richness and abundance in the area today, marsupials have a sparse fossil record, restricted to a few specimens from handful Cenozoic Amazonian localities. Here we present new records of fossil marsupial teeth from the Solimões Formation (lower Eocene–Pliocene), on the Juruá and Envira riverbanks (Acre, Northwestern Brazil). The localities investigated yield at least four distinct didelphid didelphimorphians at PRE 06 (Ponto Rio Envira: Marmosini cf. *Marmosa*, *Didelphis* cf. *D*. *solimoensis*, *Thylamys*? *colombianus*, plus unidentified didelphids), and two paucituberculatans from the Juruá river localities (Ponto Rio Juruá: the palaeothentid Palaeothinae indet. at PRJ 25 and PRJ 33', and Abderitidae indet. from PRJ 33). In agreement with the associated mammalian faunas, most of the didelphids except for *Thylamys*? *colombianus*) from PRE 06 (indicate an (?early) Late Miocene age for this locality. Conversely, the abderitid specimens found in situ at PRJ

33 would match a Middle Miocene age. The palaeothentids found at PRJ 25 and PRJ 33' cannot be considered for biostratigraphic inferences, since they were found outside a stratigraphic context. Nevertheless, these paucituberculatans considerably add to our knowledge, as they are the first ever recorded in Brazilian Amazonia.

Keywords: Middle–Late Miocene, Metatheria, systematics, Didelphimorphia, Paucituberculata, historical biogeography.

1. Introduction

The Amazon plains and lowlands cover approximately 40% of South America, being the largest forested subregion of the Neotropics. It harbors an outstanding biodiversity, with a high degree of endemism, encompassing one of the richest mammal faunas on the planet, especially in its western part (Patterson and Costa, 2012; Meseguer et al., 2022). Nevertheless, the configuration of Amazonia substantially changed throughout the Cenozoic. For example, during the Miocene, but before the Late Miocene, a much larger region, the pan-Amazonia, comprised the drainage basins of the Amazon, Orinoco, and Magdalena rivers, which were all connected, sometimes extending even to the northern part of the Paraná River basin (Hoorn et al., 2010). The Middle Miocene, particularly, was marked by the existence of the Pebas Mega-Wetland System (PMWS), formed by wetlands, shallow lakes, floodplains, and swamps, which covered a broad area of Western Amazonia from 18 to 10 Ma (Hoorn et al., 2010; Boonstra et al., 2015). Around 9 Ma ago, the PMWS gave way to a fluvial/fluviotidal system in Western Amazonia. At about the same time, Andean sediments reached the Atlantic coast for the first time via the drainage system, originating the Amazon River fluvial system as it exists today. These events were influenced by important tectonic activity related to the intensification of the uplifting process in the Northern Andes (Hoorn et al., 2010, 2017).

Tropical regions have long been considered devoid of fossils. However, in Amazonia, for example, fossil remains have proven to be relatively common, being found mainly on riverbanks during the dry seasons (Stutz et al., 2022 and references therein). Indeed, increased field efforts and intensive wet-screening of potentially fossil-bearing sediments, mainly in Western Amazonia, have demonstrated that this

region harbored a great mammal diversity over middle Eocene–Holocene times, with approximately 23 orders, 89 families, and 320 species, including Allotheria, Metatheria, and Eutheria (Antoine et al., 2017). Nonetheless, there may be some biases in our current knowledge about the fossil record from the low and middle latitudes of South America, due to taphonomic factors and surface collecting approaches, with, for instance, a greater representation of large mammals in historical findings (Antoine et al., 2017). Metatheria, despite currently possessing great richness and abundance in the area, with didelphid didelphimorphians (Gardner, 2007), are known as fossils only by a few samples from a handful of localities, such as Santa Rosa, Río Acre, Madre de Dios, Fitzcarrald local fauna, Contamana, and Tarapoto/Juan Guerra vicinity in Peru (Czaplewski, 1996; Goin and Candela, 2004; Goin and de los Reyes, 2011; Antoine et al., 2013; 2016; 2021; Tejada-Lara et al., 2015; Marivaux et al., 2020; Stutz et al., 2022); Cerdas (Croft et al., 2016) and Quebrada Honda (Engelman et al., 2017, 2020) in Bolivia; Urumaco, in Venezuela (Linares, 2004); Castilletes Formation (Suárez et al., 2016) and the La Venta local fauna in Colombia (Goin, 1997; Suárez Gómez, 2019); and Acre, in Brazil (Czaplewski, 1996; Cozzuol et al., 2006). Thus, this study aims to partly address this knowledge gap by describing new records of fossil marsupials from the upper Juruá and Envira riverbanks in the Western Amazonian Acre Basin (State of Acre, Brazil). Once described, compared, and taxonomically assigned, these remains provide valuable information on South American marsupials' biostratigraphy and historical biogeography.

2. Study area

Several field campaigns along the upper Juruá and Envira rivers occurred between 2008 and 2022. The Juruá and Envira river areas are located in the Acre Basin within the State of Acre (AC), Brazil (Figure 1). They comprise outcrops of the Solimões Formation (Fm.), part of the eastern extension of the Amazonian Foreland Basin. The Solimões Fm. corresponds to the last depositional cycle of the Acre Basin, with thin fluvial-lacustrine sediments spanning a Lower Eocene–Pliocene time interval (Cunha, 2007), with its upper levels (Neogene) cropping out mostly on riverbanks and road cuts (Lacerda et al., 2021). U-Pb dating on detrital zircons collected at two fossil-yielding sites of the Solimões Fm. indicate a Tortonian age, Late Miocene (Bissaro

Júnior et al., 2019): one on the banks of the Purus River (8.9 ± 0.13 Ma) and the other on the Acre River (8.5 ± 0.5 Ma). Those ages agree with previous estimations using biochronological data from fossil faunas recovered in Southeastern AC, which mostly placed it in the Huayquerian South American Land Mammal Age (SALMA; e.g., Negri et al., 2010; Ribeiro et al., 2013; Kerber et al., 2017; Hsiou et al., 2022). Palynostratigraphic analyses on samples collected near the city of Cruzeiro do Sul (Northwestern AC) indicate a Miocene age for the Solimões Fm. and point to a correlation with Pebas and Ipururo formations exposed in Peru (Silva-Caminha et al., 2020). The same authors also suggested a late Middle Miocene marine incursion in the region, thereby extending by 400 km to the south the extend of this previously reported incursion event in Western Amazonia (Silva-Caminha et al., 2020).

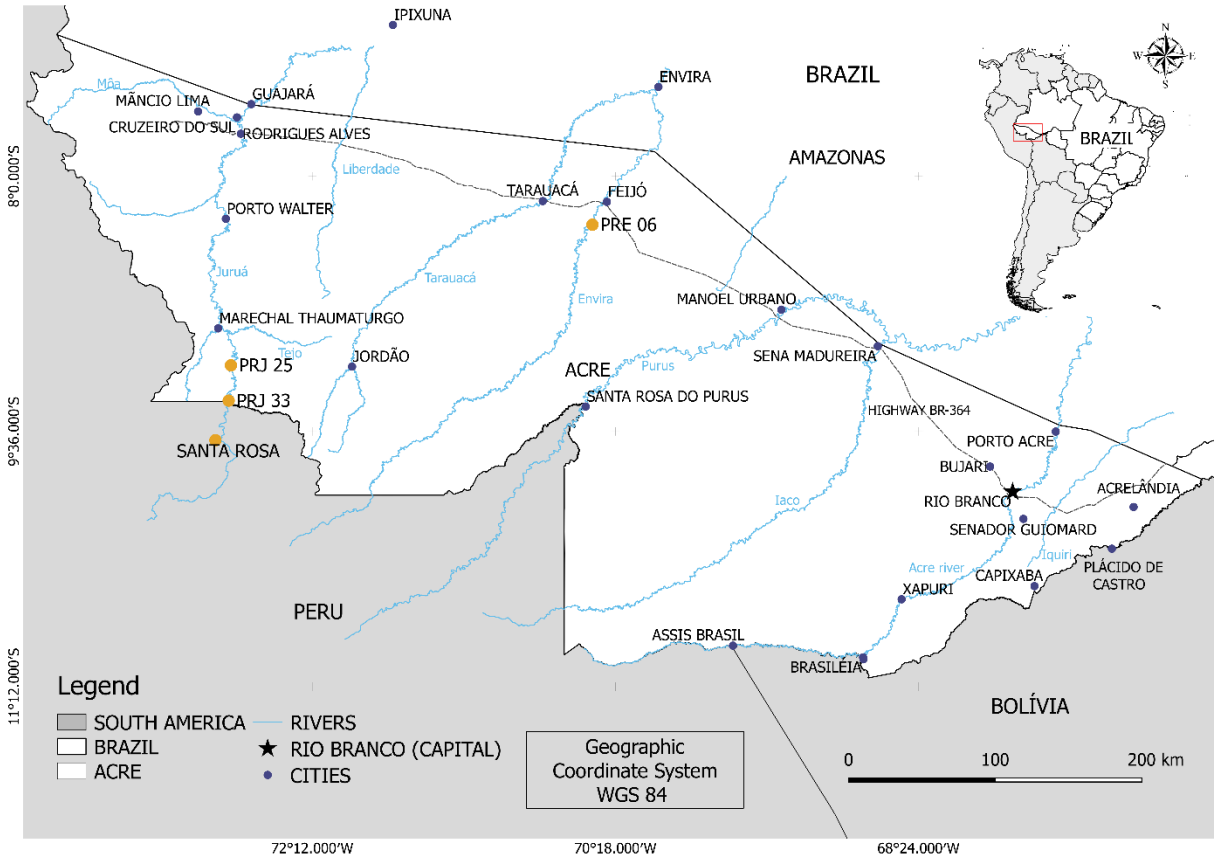


Figure 1. Location map of the studied outcrops PRJ 25, PRJ 33, on the banks of the upper Juruá River, and PRE 06 on the banks of the Envira River, State of Acre, Brazil.

Numerous taxa of fossil vertebrates have already been reported for the Solimões Fm., such as diverse extinct forms of crocodylomorphs, chelonians, squamates, birds, and fishes (Ribeiro et al., 2013; Hsiou et al., 2022). Regarding mammals, among the most frequent taxa are rodents (e.g., Kerber et al., 2016, 2017, 2018, 2019a, b, 2022; Fontoura et al., 2022), xenarthrans (e.g., Negri, 2004) and notoungulates (e.g., Bergqvist et al., 2002). Remains of other mammalian taxa such as litopterns, astrapotheres, sirenians, cetaceans, primates, and chiropterans have also been reported (see Negri et al., 2010; Ribeiro et al., 2013; Hsiou et al., 2022 for a comprehensive review). As for marsupials, very few studies have been published, limited to unidentified didelphids reported for the Acre River by Czaplewski (1996) and the oldest species of the extant genus *Didelphis* Linnaeus, 1758 - *D*. *solimoensis* Cozzuol et al. 2006, also from a locality on the Acre River (Cozzuol et al., 2006).

The fieldwork along the Juruá River was carried out in a segment bracketed between the city of Marechal Thaumaturgo and the community of Foz do Breu, at the border with Peru (upper Juruá River). Approximately 30 outcrops were surveyed and designated as PRJ (Ponto Rio Juruá). Two localities on the upper Juruá riverbanks provided marsupial fossils, namely PRJ 25 (Figures 1, 2, and 3; 9°11’06.8”S 72°42’37.2”W) and PRJ 33 (Figures 1 and 4, 9°24’24.6”S 72°43”27.6”W).

The outcrop PRJ 25 is located near the Belford property, at the left margins of the Juruá River. The outcrop is composed of two parts: a horizontal surface identified as “H”, and a vertical outcrop identified as “V” (Figure 2A-B). The horizontal surface corresponds to the lithologies between 0 and 0.45 m in the stratigraphic profile (Figure 2A). It consists of the intercalation of fractured red siltstone and fine-grained yellowish sandstone dipping 15–18º South. The siltstones and sandstones were cemented by carbonates. The vertical outcrop corresponds to the interval lithologies between 0.5 and 1.6 m in the profile and consisted of the same sedimentary sequence as the horizontal surface. In this part occurs four levels of continuous carbonate concretions within the siltstones. The strata were less inclined than the horizontal part of the outcrop (10–15º). The horizontal part of the outcrop is covered by fossil-rich Miocene–Holocene fluvial sands and gravels as shown in Figure 2. These allochthonous deposits are related to the erosion of upstream strata transported by the river stream and deposited recently in this outcrop (Figure 2C). The corresponding fossil fragments

include silicified wood and vertebrate remains. The latter specimens provide markers of different epochs (e.g., Astrapotheria and *Purussaurus* remains). All the fossil specimens from PRJ 25 originate from these out-of-sequence sands and gravels, including the only dental fragment of marsupial retrieved (UFAC-CS 418). From this ensemble, Kerber et al. (2017) also reported fossil caviomorphs, likely of Miocene affinities (unidentified potamarchine and erethizontid).

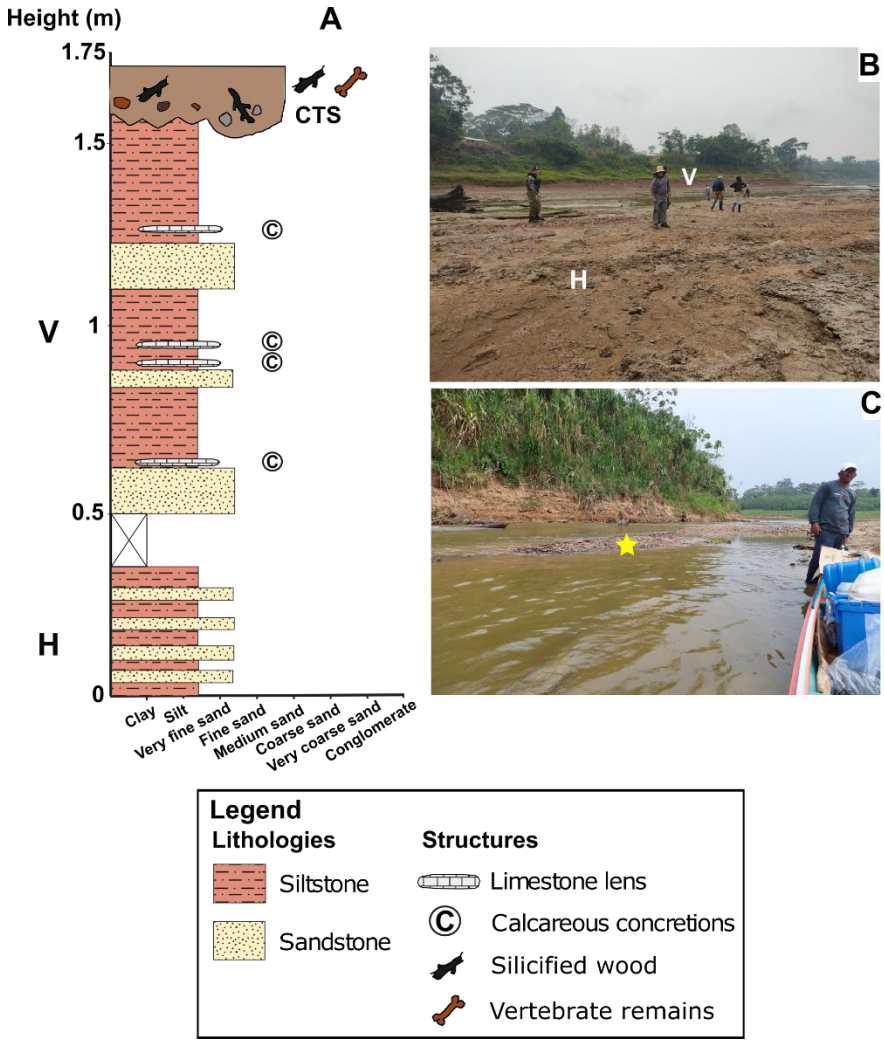


Figure 2. Stratigraphic section (A) and photos (B and C) of the outcrop PRJ 25, with the Solimões Formation as a substratum, located on the left margin of the Juruá River, State of Acre, Brazil. CTS = Holocene conglomerate, with a mixture of Miocene–Holocene pebbles and fossils (mostly silicified wood and vertebrates), which may cover indifferently any Miocene layers. Vertebrate fossils originate from the sands and gravels emerging on B (yellow star). Abbreviations: H, horizontal; V, vertical.

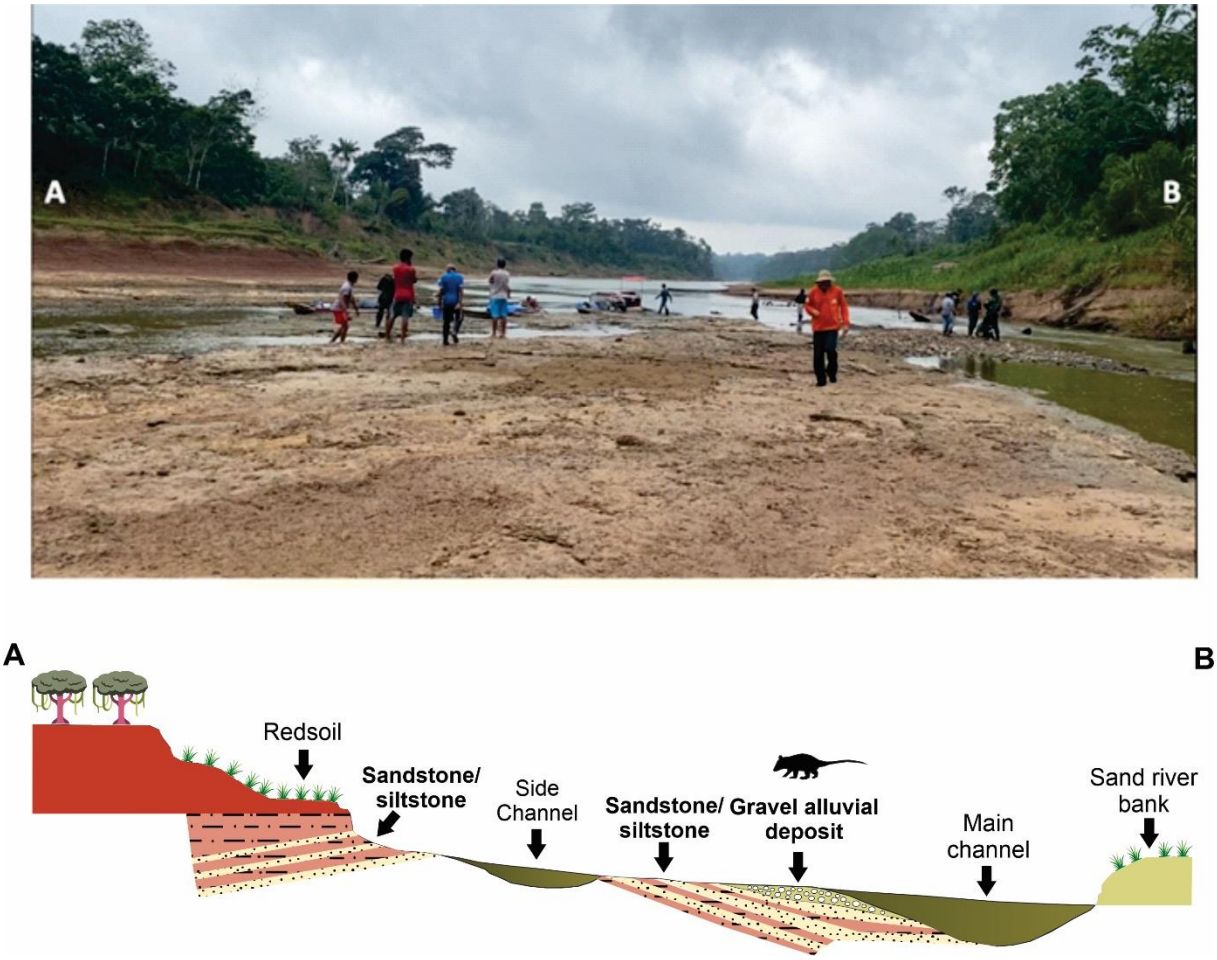


Figure 3. Detailed horizontal profile of the outcrop PRJ 25, on the left margin of the Juruá River, State of Acre, Brazil. The fossil remains were found in the gravel alluvial deposit and lateral sandstone/siltstone.

The outcrop PRJ 33 is situated on the left bank of the Juruá River and has about 2–3 m height (Figure 4A). In this outcrop, occurs a layer of massive reddish siltstone with horizontal fractures and local faults filled by carbonate concretions. These fractures tend to be laterally discontinuous along the outcrop. The siltstone is in erosional contact with the 10–15 cm-thick level of fossiliferous conglomerate composed by clasts of carbonate concretions and rare quartz supported by a reddish sandy-siltstone matrix. The conglomerate level is in direct contact with a layer of massive fine grayish sandstone at the top of the section. At PRJ 33, three specimens were collected: i) *in situ* within the conglomerate layer (UFAC-CS 101 and 109); ii) in the Holocene mixed sediments that comprise reworked bones (PRJ 33', UFAC-CS 65).

These last sediments are placed at the bottom of the outcrop, close to the river, and have fossil specimens outside of their stratigraphic context. Ribeiro et al. (2013) and Kerber et al. (2017) have reported dental remains of the Paleogene caviomorph rodent *Eoincamys* extracted from the mixed sediments.

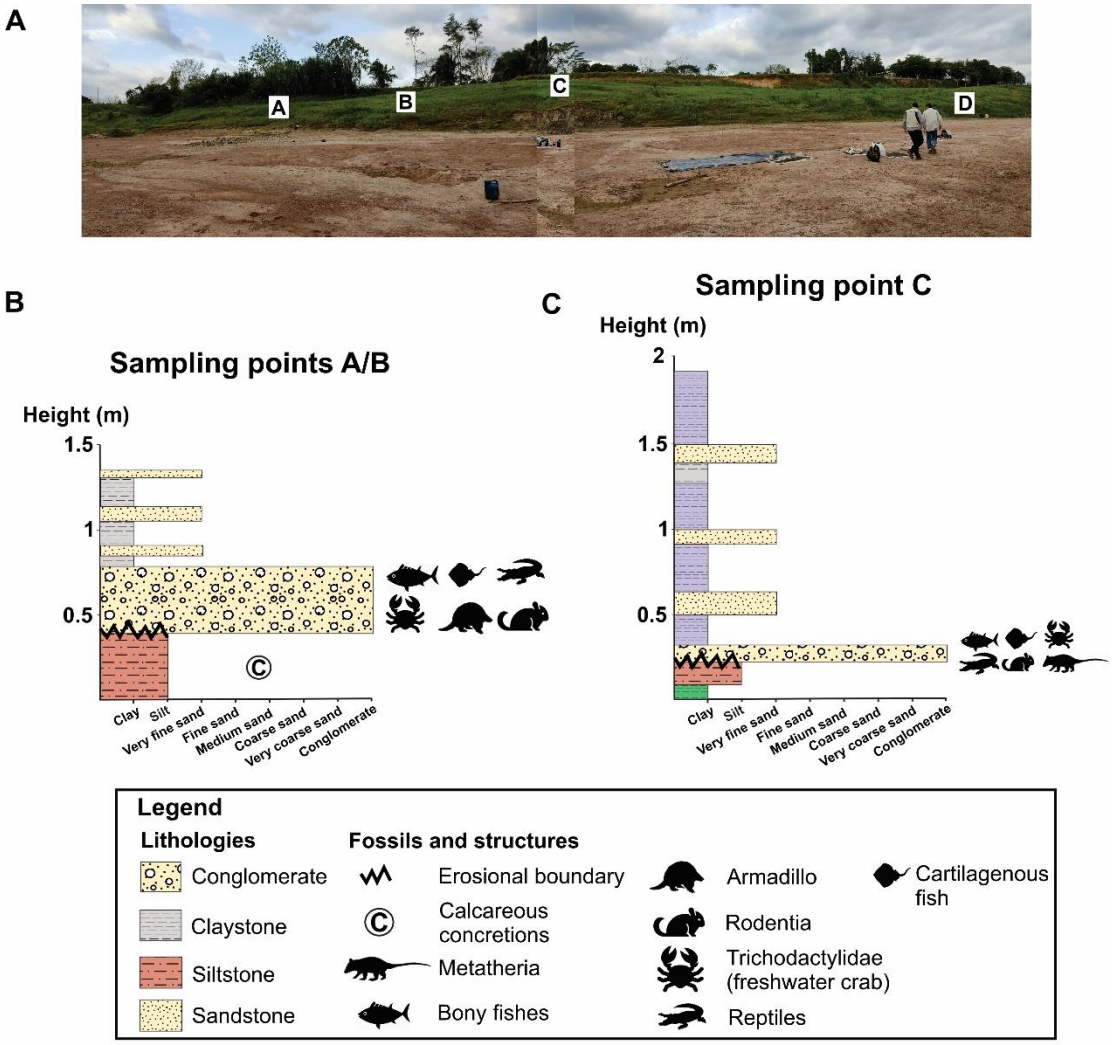


Figure 4. Stratigraphic section (A) and photo (B) of the Miocene outcrop PRJ 33, Solimões Formation, located on the left bank of the Juruá River, State of Acre, Brazil.

In the Envira River area, the outcrops were designated as PRE (Ponto Rio Envira). Six marsupial teeth were retrieved at the outcrop PRE 06, also called locality “Coqueiros” (Figures 1 and 5; 08°18’12.6”S 70°26’39.9”W). Four laterally equivalent sampling points were surveyed (A, B, C, and D; Figure 5A), but only one (C) yielded

fossil marsupials after wet-screening of the sediments. Briefly, the sedimentary sequence at sampling points A to C (Figure 5B-C) comprises layers of grayish-green and red argillites, which are in erosive contact with the conglomeratic level very rich in fossil content. The conglomerate is composed of carbonate concretions and numerous fossil fragments (such as remains of fishes, reptiles, and mammals, currently under study) supported by a silty-sandy matrix. This conglomerate is in direct contact with intercalated layers of brown clay and very fine to fine yellowish sand (rhythmite). Sampling points A, B, and C in section belong to a same stratigraphic horizon, while sampling point D consists of an accumulation of fossil fragments found on the Envira River floodplain and, hence, out of stratigraphical context. Regarding the fossil content from PRE 06, there is fossil wood, with a diverse flora reported by Kloster et al. (2017) that resembles the one currently present in the region. Furthermore, recent studies revealed a diverse record of caviomorph rodents from PRE 06A–C (*Cardiatherium* sp., Caviidae, Hydrochoerinae; *Potamarchus* sp. and cf. *Pseudopotamarchus*, Dinomyidae, Potamarchinae; and *Neoepiblema* sp., Neoepiblemidae; Fontoura et al., 2022), which suggest a Late Miocene age.

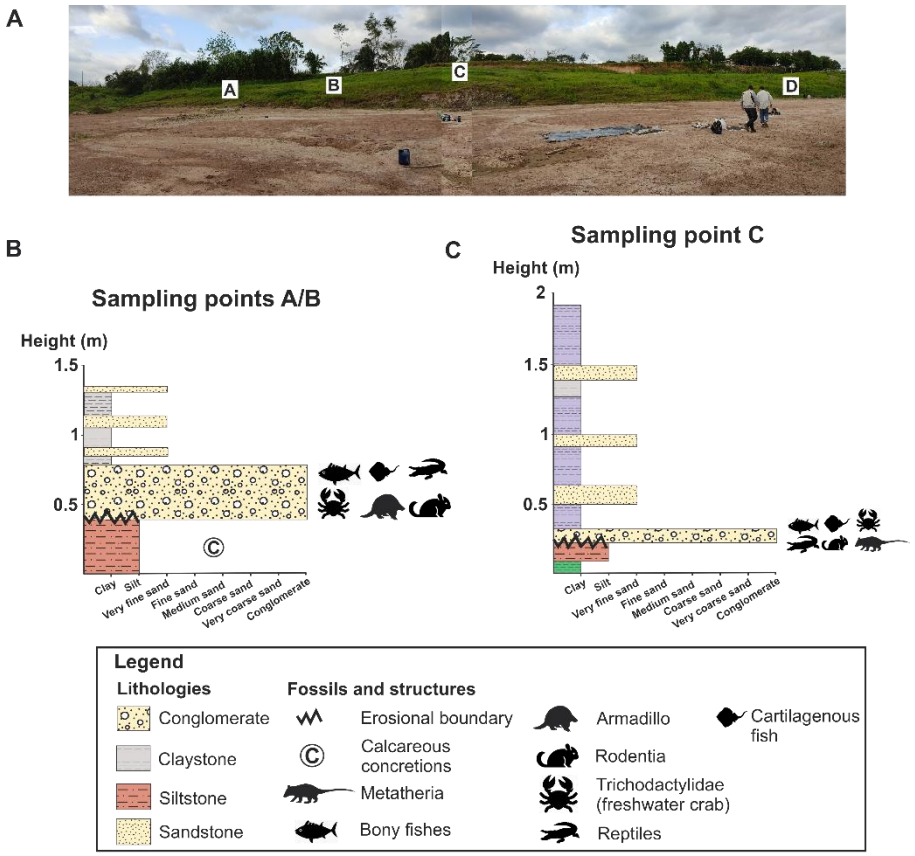


Figure 5. Stratigraphic section (B and C) and photo (A) of the Late Miocene outcrop PRE 06, Solimões Formation, located on the right bank of the Envira River, State of Acre, Brazil.

3. Material and methods

The fossil specimens were collected through wet-screening of the sediments from previously recognized fossil-bearing layers (sands and conglomerates), using sieves of 0.6, 1 and 2 mm, and then sorted out using a stereomicroscope. The specimens are permanently housed in the collection of the Paleontology Laboratory of the Universidade Federal do Acre, Floresta campus, Cruzeiro do Sul, AC (UFAC-CS). The fossils were photographed with Scanning Electron Microscope (SEM) facilities of the Centro de Microscopia e Microanálise (CMM, UFRGS, JEOL JSM 6060) and at the Laboratório Central de Microscopia e Microanálise (LabCEMM, PUCRS, FEI Inspect F50). The measurements of maximum anteroposterior length and maximum labiolingual width were made using a manual Mitutoyo caliper, with a precision of 0.02 mm. The nomenclature of the molar structures and the Marsupialia systematics follow Goin et al. (2016). Taxonomic identifications were made according to Abello (2007), Voss and Jansa (2009), Abello and Rubilar-Rogers (2012). They were directly compared with fossil metatherians from the locality TAR-31 (Juan Guerra, San Martín, Peru) deposited at the Vertebrate Paleontology Department of the Museo de Historia Natural of the Universidad Nacional Mayor San Marcos (MUSM) in Lima, Peru, and with specimens of modern didelphids deposited in the Coleção de Fragmentos Ósseos do Laboratório de Paleontologia and Coleção de Mamíferos do Departamento de Ecologia e Zoologia, Universidade Federal de Santa Catarina (UFSC), Florianópolis, Brazil, and at the Mammal Collection of the MUSM.

3.1 Anatomical abbreviations

D/d, deciduous; L, length; M, upper molar; m, lower molar; P, upper premolar; p, lower premolar; StA-D, stylar cusps A to D (from anterior to posterior); tal, talonid; tri, trigonid; W, width.

4. Systematic paleontology

Class Mammalia Linnaeus, 1758
Infraclass Metatheria Huxley, 1880
Supercohort Marsupialia Gill, 1872
Order Didelphimorphia Gill, 1872
Family Didelphidae Gray, 1821
Subfamily Didelphinae Gray, 1821
Tribe Marmosini Hershkovitz, 1992
Marmosini, cf. *Marmosa*
(Figure 6A1–3)

Referred material. UFAC-CS 413, part of the stylar shelf (StC, StD, and StE) of a right ?M2.

Locality. PRE 06, sampling point C, Envira River, State of Acre, Brazil.

Formation and age. Solimões Fm., Acre Basin, (?early) Late Miocene.

Measurements. StE–ectoflexus = 1.8 mm; Metacone–labial margin = 2.36 mm; Metacone–StE = 2.68 mm.

Description. The specimen is worn and broken at the level of the StC and the trigon basin. It includes part of the stylar shelf with the StC, StD, and StE, and the metacone. The metacone is opposite to StD, relatively far from the latter, and lingually oriented. There is a subtle basin between the metacone and the StC and StD. The premetacrista is short and slightly labiolingually curved. The postmetacrista is longer, extending until the StE with an oblique orientation. There is a crest-like structure at the base of the posterior wall of the metacone, however, it is not possible to state to which crest it corresponds, it could also be a product of the fragmentary and worn state of the molar. There is a small crest-like structure lingually to the StC. The labial margin has a steep oblique orientation from the StC to the StE. The StC and StD are subequal in size; both poorly developed but still visible. The StC and StD are not twinned or close to each other. The StE is posteriorly broken, but it is still possible to observe a small and narrow cusp.

Remarks. Morphological comparisons with similarly sized didelphids indicate that UFAC-CS 413 is smaller than species of *Didelphis*, the latter having more rounded stylar cusps. UFAC-CS 413 is approximately the same size as *Lutreolina* but has a smaller StC. In the species of *Philander*, the StC is more developed and morphologically different. UFAC-CS 413 shows closer affinities with the species of *Marmosa* in morphology, such as the presence of StE, StD and StC (Rossi et al., 2010). UFAC-CS 413 is larger than the teeth of the recent species *M*. *demerarae* (Thomas, 1905). Fossil representatives of the genus include *Marmosa laventica*, the oldest record of *Marmosa*, which was described for the Middle Miocene deposits of La Venta, Colombia (Marshall, 1976a). *Marmosa laventica* is larger than the living species of *Marmosa*, among other diagnostic characteristics. However, it was described based only on lower dentition. Later, Goin (1997), when revisiting the diagnosis of *M*. *laventica*, assigned it to *Micoureus laventicus* and added upper molars in its hypodigm. However, recent molecular analyses considered *Micoureus* as a synonym of *Marmosa*, being now recognized as a subgenus of the latter (Voss and Jansa, 2009). UFAC-CS 413 is larger than the specimens reported by Goin (1997), and, because of its incomplete state, the diagnostic characteristics of *M*. *laventica* could not be observed on it. Marshall (1976a) also reported specimens of *Marmosa* sp. from La Venta, which are smaller than *M*. *laventica*, and thus not compatible in size with UFAC-CS 413. The size of UFAC-CS 413 also distinguishes it from *Marmosa* sp. 1 of Suárez Gómez (2019), which is reported as being ~40% smaller than *M*. *laventica*. Antoine et al. (2013) reported a partial M2 of *Marmosa* (*Micoureus*) cf. *laventica* for the early Middle Miocene locality MD-67 in Peru, which differs from UFAC-CS 413 in being smaller and not possessing StE. Yet, both specimens show a large stylar shelf and StC and StD. Compared to *Hesperocynus*, *Sparassocynus*, and *Thylatheridium*, UFAC-413 does not possess a very long postmetacrista and the metacone does not seem to be a tall cusp, but the latter could be due to the great wear (Goin et al., 2000; Forasiepi et al., 2009; Abello et al., 2015).

Therefore, UFAC-CS 413 was assigned to Marmosini, cf. *Marmosa* due to the morphological resemblance of it with *Marmosa*. Nevertheless, the incomplete state of the specimen hampers a more precise taxonomical identification.

Tribe Didelphini Gray, 1821

Didelphis cf. *D*. *solimoensis*

(Figure 6B1–3)

Referred material. UFAC-CS 415, left DP3.

Locality. PRE 06, sampling point C, Envira River, State of Acre, Brazil.

Formation and age. Solimões Fm., Acre Basin, (?early) Late Miocene.

Measurements. L = 3.08 mm; W = 3.22 mm.

Description. This DP3 is anteroposteriorly elongated in its labial portion and relatively narrow. The protocone is slightly anterior to the paracone, forming a small, triangular-shaped trigon basin, which is deep and anteroposteriorly compressed. The metacone is conic and posteriorly oriented. It is high and well-developed. At its dorsolingual base, there is a small metaconule. The centrocrista is well-developed and U-shaped. The preparacrista is almost vertical and does not reach the anterior cingulum/StA. There is a very long postmetacrista, which is obliquely oriented towards the StE. The pre- and postprotocrista are well-developed, short, and oblique. There is a well-developed anterior cingulum passing along the base of the paracone and joining a small paraconule. At its labial extremity, there is a small StA. A well-marked labial cingulum is present, extending from StA up to StC. The StB is high and fused with the paracone. Next to StB there is a small and rounded StC, which is closer to StD. The StD is wide and slightly shorter than StB, it is located labial to the metacone and followed by a marked crest, which is oriented parallel to the anteroposterior dental axis. At its end, a small StE forms a rounded posteriormost tip.

Remarks. Based on its morphological characteristics and dimensions, UFAC-CS 415 belongs to a didelphid smaller than species of *Didelphis*, *Lutreolina*, *Philander*, and *Chironectes* but larger than *Marmosa murina* (Linnaeus, 1758). Compared with UFAC-CS 413, UFAC-CS 415 is morphologically different from it, and it resembles the DP3 morphology of *Didelphis*, such as the development and position of the cusps, trigon basin, and stylar cusps, and well-developed anterior cingulum and by being anteroposteriorly elongated. However, UFAC-CS 415 has smaller dimensions than what it is observed in the living species of *Didelphis*. *Didelphis solimoensis*, from the Late Miocene of Acre, is considered the smallest known species of the genus (Cozzuol

et al., 2006). UFAC-CS 415 might be slightly smaller than *D*. *solimoensis* however, it should be noted that *D*. *solimoensis* is only known from an isolated dentary with p3–m2. Still, given that the occlusal morphology of UFAC-CS 415 resembles the one of *Didelphis* DP3s and that *D*. *solimoensis* is the smallest *Didelphis* species described in the literature, UFAC-CS 415 was assigned to *Didelphis* cf. *D*. *solimoensis*, pending the discovery of additional specimens of the former, especially preserving the upper dentition.

Tribe Thylamyini Hershkovitz, 1992

Thylamys? colombianus Goin, 1997

(Figure 6C1–3)

Referred material. UFAC-CS 202, left ?m4.

Locality. PRE 06, sampling point C, Envira River, State of Acre, Brazil.

Formation and age. Solimões Fm., Acre Basin, (?early) Late Miocene.

Measurements. L = 1.91 mm; W = 0.9 mm.

Description. UFAC-CS 202 is a small lower molar with high, well-developed trigonid cuspids and a talonid much lower than the trigonid, with scarcely developed cuspids. The paraconid is conspicuous, lower than the metaconid, and slightly labial and distant from it, with a sharp anterior and occlusal tip. The protoconid is large and prominent, being the highest and largest cuspid of the whole molar. The metaconid is opposite to and much lower than the protoconid. The talonid is narrower than the trigonid but is well-developed compared to the small didelphids' condition. The entoconid is laterally compressed and inconspicuous, possibly due to the molar wear, and it seems to be situated more anteriorly than the hypoconid. The hypoconid is short and inconspicuous, being positioned lingual to the protoconid. The hypoconulid is well-developed, triangular-shaped, and lingually located, connected to the posthypocristid via a subtle postcristid. The mesiolingual vestical crest of the paraconid forms a keel on the anteriormost part of the molar. The postparacristid is well-developed and obliquely oriented, meeting a conspicuous preprotocristid. The postprotocristid is almost transversally oriented, meeting a shorter premetacristid and forming a shallow sulcus. The pre- and post- entocristids are poorly developed, the preentocristid having

a labial orientation. The postentocristid connects the entoconid to the hypoconulid. The cristid obliqua is small and almost parallel to the anteroposterior dental axis. A narrow anterobasal cingulid is visible from the base of the paraconid to the base of the protoconid. There is a faint posterior cingulid on the posteriormost wall of the molar. Two roots are preserved, an anterior rounded one and a posterior one, which is larger and ovoid.

Remarks. We interpret UFAC-CS 202 as being a ?m4 due to the presence of a slender and long talonid, a more lingual position of the hypoconid than what is commonly observed on m3, and the absence of a wear-facet on the distal side of the tooth. The posterior cingulid present on this specimen is a plesiomorphic characteristic since the absence of this structure is considered the single unambiguous synapomorphy of Didelphidae. However, some taxa have already been reported to possess this feature (Beck et al., 2021). Compared to basal metatherians that possess a posterior cingulid, UFAC-CS 202 differs from *Marmosopsis* by having longer talonid and hypoconulid; it differs from *Monodelphopsis* by showing high trigonid, which is wider than the talonid and entoconid subequal to hypoconid in size and height (Marshall, 1987). UFAC-CS 202 is smaller than m4 of the species of *Chironectes*, *Didelphis*, *Caluromys*, *Lutreolina* and *Philander*, but larger than those of *Chacodelphys* and the extinct didelphid *Sairadelphys* Oliveira et al., 2011. UFAC-CS 202 differs from the species of *Monodelphis* in having a longer and narrower talonid. UFAC-CS 202 is smaller than m4 of most species of *Marmosa*. Morphological differences with the species of Marmosa are an anterolabial cingulid and entoconid less developed and the absence of a labial cingulid. The m4 of the species of *Gracilinanus* have a larger entoconid and no posterior cingulid, and those of *Cryptonanus* have m4 with a marked labial cingulid. In the species of *Marmosops*, the hypoconulid is more posterior, the hypoconid has a more labial position, the metaconid and protoconid are closer and the entoconid is basally larger concerning the condition observed on UFAC-CS 202. UFAC-CS 202 has the same size as m4s of the species of *Thylamys*; the position of the trigonid cuspids and the entoconid and hypoconulid is also similar. Regarding other fossil species of *Thylamys*, UFAC-CS 202 is larger than m4 of *T*. *minutus* Goin, 1997 from the Middle Miocene of La Venta, Colombia (Goin, 1997). Nevertheless, it has approximately the same size as *T*. *colombianus*, also from La Venta, which has m3 with W = 1.55 mm

and m1? with L = 1.9 mm and W = 0.9 mm (only a partially preserved m4 for this taxon was found; Suárez Gómez, 2019). Besides, UFAC-CS 202 also resembles lower molars of T. colombianus in having: i) a paraconid more mesio-labially displaced, being more distant from other cuspids, ii) a labio-lingually compressed entoconid, iii) a long talonid, and iv) a similar relative entoconid/hypoconulid position. Nevertheless, no well-preserved m4 has been described until now for *Thylamys colombianus*, hampering a more precise comparison. The m1 of *Thylamys* cf. *T*. *colombianus* from TAR-31, (late Middle Miocene, Peru; Stutz et al., 2022) has a paraconid and a hypoconid more anteriorly and more labially placed, respectively, but with a position of the entoconid/hypoconulid similar to that in UFAC-CS 202. Based on living species, recent gene-based phylogenies suggested that *Thylamys* diverged from other didelphids later than the presumed age of the PRE 06 deposits (not until the Pliocene, and, for the last common ancestor of *Thylamys* and *Gracilinanus* + *Cryptonanus*, not until ~10 Ma) (Jansa et al., 2014; Beck and Taglioretti, 2020). Thus, we chose to consider *Thylamys*? as a generic assignment, pending a better assessment of the concerned Miocene specimens, whether they belonged to this genus or a stem representative of Thylamyini.

Stratigraphic and geographic range. Middle Miocene of La Venta, Colombia; and (?early) Late Miocene of the Envira River, Acre, Brazil.

Didelphidae indet.

(Figure 7)

Referred material. UFAC-CS 412, right p1; UFAC-CS 414, right ?p2; UFAC-CS 416, right ?P3; UFAC-CS 427, left dp3.

Locality. PRE 06, sampling point C, Envira River, State of Acre, Brazil.

Formation and age. Solimões Fm., Acre Basin, (?early) Late Miocene.

Measurements. UFSC-CS 412 L = 2.27 mm, W = 1.18 mm; UFAC-CS 414 L = 3.36 mm, W = 1.54 mm; UFAC-CS 416 L = 3.24 mm, L = 1.95 mm; UFAC-CS 427 L = 2,3 mm, W tal = 1.42 mm, W tri = 1,32 mm.

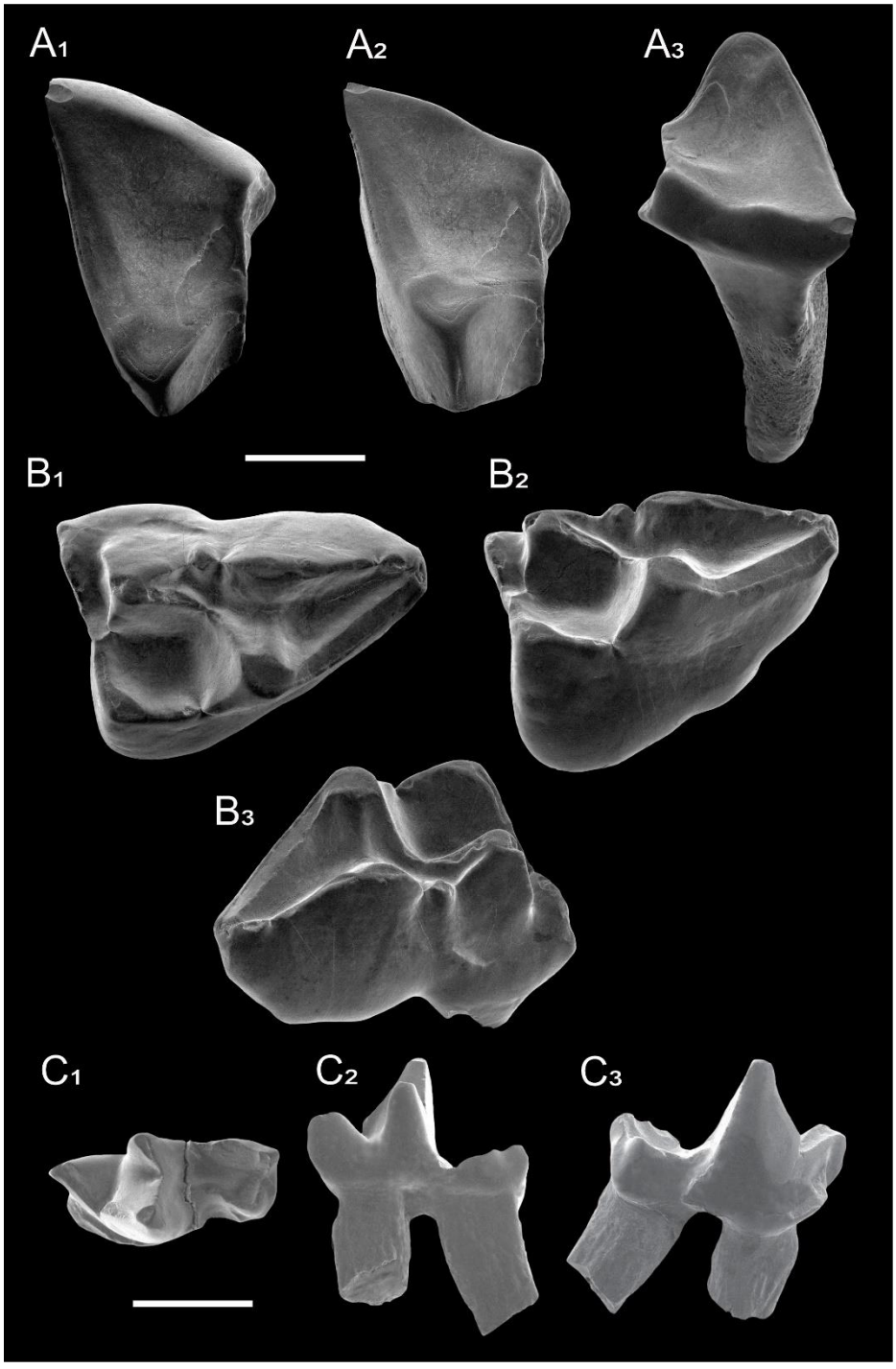


Figure 6. Didelphids from the locality of PRE 06, Envira River, Acre State, Brazil, (?early) Late Miocene: A1–3, Marmosini, cf. *Marmosa*, UFAC-CS 413, partial right ?M2; B1–3, *Didelphis* cf. *D*. *solimoensis*, UFAC-CS 415, left DP3; C1–3, *Thylamys*? *colombianus*, UFAC-CS 202, left ?m4. A1, B1, C1, occlusal; A2, B2, C2, partially lingual; and A3, B3, C3, partially labial views. Scale bars = 1 mm.

Description. UFAC-CS 412 (Figure 5A1-2): small and slender p1 displaying two roots. The crown consists of one single central cuspid, rounded and short (*i.e.*, stocky). It is followed by a subtle cristid running postero-labially. A small cingulid is present posterior to the cuspid, with a minute labially situated accessory cuspid.

UFAC-CS 414 (Figure 5B1-2): this specimen is larger than UFAC-CS 412. It is robust, with one single cuspid, which is broken and abraded. Posteriorly to this cuspid, there is a tenuous cristid labially oriented. A posterior cingulid is present, with a marked accessory cuspid.

UFAC-CS 416 (Figure 5C1-2): this specimen is a large upper premolar with two roots. A subtle anterior cingulum is present. There is only one cusp, which is high, robust, and posteriorly oriented. The anterior margin of the cusp is rounded and at the posterior one is a marked, sharp, and centrally oriented crest. There is a posterior cingulum, which is particularly developed in its labial margin. A small accessory cusp is present, occupying a posterior labial position.

UFAC-CS 427 (Figure 5D1-3): this specimen does not possess any signs of roots in its ventral side, which is open, exposing a broad portion of the tooth's interior. It presents an oval crown outline and robust molariform pattern, being anteroposteriorly compressed and with a rounded labial margin. The trigonid is much higher than the talonid, especially the proto- and metaconids. Proto-, meta-, hypo-, and entoconid are large and blunt. A small, but individualized paraconid is present, which is labially displaced. The protoconid is a large and high cuspid, connected to the paraconid by a short preprotocristid. The protoconid and metaconid are closely positioned, without an evident postprotocristid. The protoconid is higher than the metaconid, but the latter is also a large cuspid. The talonid is short. The hypoconid appears slightly broken on its dorsal tip and labially displaced, evincing a wide talonid basin. The entoconid is robust and anteroposteriorly long, with marked, but short pre- and postentocristids. A minute hypoconulid can be observed, which is twinned with the entoconid and situated at its posterolabial base. The premetacristid is not visible, but the postmetacristid is strongly developed. The cristid obliqua is marked and obliquely oriented, but short. The posthypocristid is marked, short and slightly oblique in relation to the anteroposterior axis of the tooth. A discrete and short anterolabial cingulid is present.

Remarks. We identify UFAC-CS 412 as a lower p1 due to its size, and inconspicuous posterior cingulid and accessory cuspid. UFAC-CS 414 is tentatively identified as a p2 because of its size and the development of the posterior cingulid and posterior accessory cuspid. UFAC-CS 416 is likely considered to be an upper P3 based on its rounded anterior and cutting posterior margins, as observed in didelphids, except for *Caluromys* Allen, 1900, *Caluromysiops* Sanborn, 1951, *Glironia* Thomas, 1912, and *Hyladelphys* Voss, Lunde, and Simmons, 2001 (Voss and Jansa, 2009). According to Voss and Jansa (2009), didelphids, together with other marsupials that display plesiomorphic dental traits (such as microbiotheres), have standard lower premolars with only one dominant cuspid, and a distal cingulid frequently producing a posterior accessory cuspid. The P3 of paucituberculatans has a posterior portion higher than the anterior one and palaeothentoids generally have uniradicular and morphologically indistinct p1 and p2 (Abello, 2007). Members of the clade Argyrolagidae have reduced premolars nearly styliform (Simpson, 1970). Therefore, we preferred to classify the three specimens mentioned above as unidentified Didelphidae due to i) the lack of diagnostic characteristics on didelphid premolars; ii) and Didelphidae being the only metatherian family already recognized at the outcrop PRE 06.

UFAC-CS 427 is identified as a left dp3 due to the absence of robust roots and very closely positioned protoconid and metaconid. Compared to other Miocene didelphids, UFAC-CS 427 does not have a compatible size with *Thylamys*? *colombianus* and *Didelphis* cf. *D*. *solimoensis*, also found at PRE 06 (see below) or with the two *Thylamys* spp. from the La Venta deposits (Suárez Gómez, 2019). Besides, it is smaller than dp3s of *Marmosa laventica* Marshall, 1976 also from La Venta, which possess very different occlusal morphology, with, for instance, well-developed anterolabial cingulid and hypoconulid (Suárez Gómez, 2019). UFAC-CS 427 is also different from *Lutreolina materdei*, Goin and de los Reyes, 2011 from the Late Miocene of Acre River, in Peru, which has large anterolabial cingulid and paraconid and hypoconid not labially displaced, among other distinctive characteristics. However, UFAC-CS 427 and *Lutreolina materdei* bear a minute hypoconulid (Goin and de los Reyes, 2011). When compared to modern didelphids, UFAC-CS 427 stands out by its molariform morphology, with a complete trigonid, differing from the species of *Lestodelphys* Tate, 1934, *Marmosa* Gray, 1821, and

Thylamys Gray, 1843, which possess a blade-like trigonid on the dp3, and from those of *Caluromys*, *Caluromysiops*, and *Tlacuatzin* Voss and Jansa, 2003, which have a very small paraconid or no paraconid at all. *Hyladelphys* is another didelphid with a peculiar dp3, which is significantly reduced (Voss and Jansa, 2009). Besides, UFAC-CS 427 shows a very discrete anterolabial cingulid, which is a more developed structure in the species of *Chironectes* Illiger, 1811, *Lutreolina* Thomas, 1910, *Metachirus* Burmeister, 1854, *Monodelphis* Burnett, 1830, and *Philander* Brisson, 1762. UFAC-CS 427 also possesses labially displaced paraconid and hypoconid, differing from the species of *Chironectes*, *Glironia*, and *Lutreolina*. The protoconid and metaconid are very close in UFAC-CS 427, distinguishing it from the species of *Hyperdidelphys* Ameghino, 1904, *Lutreolina*, *Metachirus* and *Philander*. Other distinctive features of UFAC-CS 427 are a short preprotocristid, distinguishing it from the species of *Metachirus*, which have a long and oblique preprotocristid, a short talonid (long in *Didelphis*), and a large entoconid (small in *Marmosops* Matschie, 1916). The most outstanding distinctive feature of UFAC-CS 427 is its extremely reduced hypoconulid compared to the species of *Chironectes*, *Didelphis*, *Glironia*, *Lutreolina*, *Marmosops*, *Monodelphis*, *Philander* and *Thylophorops* Reig, 1952. The species of *Cryptonanus* Voss, Lunde, and Jansa, 2005, *Gracilinanus* Gardner and Creighton, 1989 and *Chacodelphys* Voss, Gardner, and Jansa, 2004 have much smaller teeth than UFAC-CS 427. The corresponding didelphid was approximately *Marmosa*-sized. Thus, the scarcity of the material and the set of characteristics found in UFAC-CS 427 do not allow its attribution to any of the described didelphid genera, pending the discovery of more specimens.

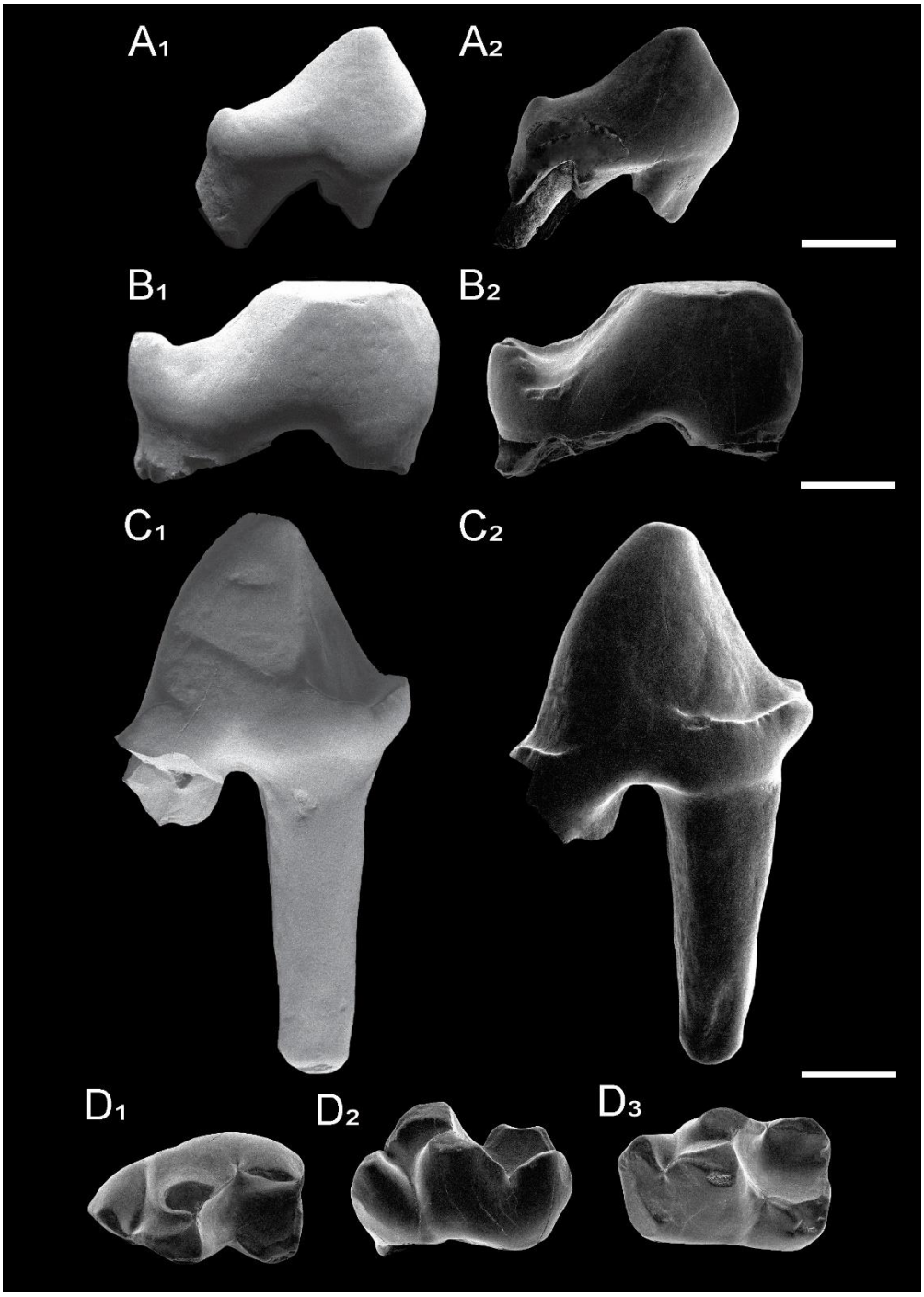


Figure 7. Didelphidae indet. from the locality of PRE 06, Envira River, Acre State, Brazil, (?early) Late Miocene: A1-2, UFAC-CS 412, right p1; B1-2, UFAC-CS 414, right ?p2; C1-2, UFAC-CS 416, right ?P3; D1-3, UFAC-CS 427, left dp3. A1, B1, C1, D2, labial; A2, B2, C2, D3, lingual; and D1, occlusal views. Scale bars = 1 mm.

Order Paucituberculata Ameghino, 1894

Superfamily Palaeothentoidea Sinclair, 1906

Family Palaeothentidae Sinclair, 1906

Subfamily Palaeothentinae Sinclair, 1906

Palaeothentinae indet.

(Figure 8A1–3 and B1–3)

Referred material. UFAC-CS 65, left M2; UFAC-CS 418 right ?M2.

Locality. PRJ 33' (UFAC-CS 65); PRJ 25 (UFAC-CS 418), Juruá River, State of Acre, Brazil.

Formation and age. Solimões Fm., Acre Basin, ?Middle Miocene.

Measurements. UFAC-CS 65 L = 1.91 mm, W = 2.2 mm; UFAC-CS 418 L = 1.98, W = 1.91.

Description. UFAC-CS 65 (Figure 8A1–3) is an upper molar, quadrangular in occlusal outline, with a much broader base compared to the crown in lateral perspective. Antero-lingually to the StB, at its base, there is a smaller cusp, the paracone, that is poorly- developed. The protocone is wide but short and is placed opposite to StB. The metacone is a well-developed cusp, slightly smaller than StC+D, and placed on the anterior portion of the latter. The trigon basin is deep. The metaconule is well-developed and wide but not much higher than the talon basin, having approximately the same height as the protocone. It is located opposite to StC+D. At the base of the metacone, there is a sulcus separating it from the metaconule. The postprotocrista is subequal in length to the preprotocrista (Fig. 7A3); dorsal to it there is a shallow entoflexus. The postmetaconular crest is moderately wide and labially oriented, the molar having a shorter outline, thereby differing from the condition that characterizes M1s of other palaeothentids. A narrow anterior cingulum extends from a point immediately anterior to the StB converging toward the preprotocrista, but oblique and dorsally to the latter. The StA is vestigial or absent. The StB is conical-shaped and represents the highest cusp. The StC+D is well developed but smaller than the StB, from which it is separated by a deeply excavated ectoflexus, with a small style at its base.

UFAC-CS 418 (Figure 8B1–3) is also a quadrangular-shaped upper molar, appearing worn and abraded due to transport, the labial and lingual sides of the molar having a thicker enamel layer compared to the structures on the occlusal surface. The paracone is small and twinned with the StB, being placed at the antero-lingual slope of the latter. The protocone is well-developed, but short. The metacone is twinned with the StC+D, but shorter than the latter and located on its anterior portion. The trigon basin is deep, small, and narrow. Opposite to StC+D there is a well-developed metaconule, preceded by a short premetaconular crest, with a small premetaconular cuspule, and followed posteriorly by a longer postmetaconular crest that runs parallel to the lingual side of the tooth. Both the preprotocrista and postprotocrista are short. A broad but short anterior cingulum is present, running from a well-developed StA to almost the dorsolingual base of the protocone. Beneath the metaconule and protocone, there is a deep entoflexus on the lingual margin of the tooth. There is a deep U-shaped ectoflexus on the labial margin of the tooth. The StB is larger and longer than the StC+D. The StC+D is well-developed and the highest cusp of the molar.

Remarks. UFAC-CS 65: the presence of a premetaconular cusp and the metacone situated in the first half of the StC+D allow us to assign this specimen to the family Palaeothentidae according to Abello (2007). Also, according to this same author, the protocone and metaconule directly opposite to StB and StC+D, regarding an axis perpendicular to the anteroposterior one, unambiguously point to Palaeothentinae affinities for UFAC-CS 65. Conversely, decastine palaeothentids are characterized by a protocone posterior to the StB on M1-2, differing from UFAC-CS 65 (Abello, 2007). Among Palaeothentinae, *Carlothentes* Bown and Fleagle, 1993 is solely known through lower molars, precluding further comparison with UFAC-CS 65. The upper molars of *Palaeopanorthus primus* Ameghino, 1902, although having conspicuous paracone and metacone, have a sizeable premetaconular cusp and a moderately developed to large metaconule, differing from UFAC-CS 65 (Abello, 2007). In the species of *Palaeothentes* Ameghino, 1887, a paracone on M2 is only registered in *P*. *marshalli* Bown and Fleagle, 1993, *P*. *migueli* Bown and Fleagle, 1993 and *P*. *serratus* Engelman et al., 2017 (Abello, 2007; Engelman et al., 2017). *Palaeothentes serratus*, from Quebrada Honda (Middle Miocene of Bolivia), differs from UFAC-CS 65 in possessing a highly reduced metacone. The other species of *Palaeothentes* from

Quebrada Honda, *P*. *relictus* Engelman et al., 2017, is not represented by upper molars (Engelman et al., 2017), hampering comparison with UFAC-CS 65. As for *P*. *migueli* and *P*. *marshalli*, the molars of *P*. *migueli* are smaller than UFAC-CS 65, while those of *P*. *marshalli* are closer in size to UFAC-CS 65. Besides, *P*. *marshalli* has well-developed metacone and teeth that are more triangular-shaped in occlusal view, as UFAC-CS 65. Nevertheless, the M1-M2 of the species of *Palaeothentes* do not present many significative differences with the ones of *Palaeopanorthus primus* (*i*.*e*., differences in the proportional size of the paracone, metacone and premetaconular crest; Bown and Fleagle, 1993; Abello, 2007). Therefore, considering that UFAC-CS 65 is an isolated specimen and that the M2 is not a very distinctive tooth among some Palaeothentinae taxa, we chose an open taxonomic identification, highlighting the closer affinities of UFAC-CS 65 especially with *P*. *marshalli*, but also to *P*. *migueli* and *Palaeopanorthus primus*.

UFAC-CS 418 can be considered as belonging to Palaeothentoidea due to the differences in the enamel thickness observed between the lateral and occlusal sides of the molar, and as a representative of Palaeothentidae due to i) the metacone located on the anterior half of the StC+D, and ii) the presence of a premetaconular cusp on upper molars (Abello, 2007). As mentioned above, for UFAC-CS 65, the M2 of palaeothentines is not very diagnostic; therefore, an open taxonomic identification is again favored. As with UFAC-CS 65, UFAC-CS 418 also has closer affinities with *P*. *marshalli*, *P*. *migueli* and *Palaeopanorthus primus*.

Compared to UFAC-CS 418, UFAC-CS 65 has a less developed anterior cingulum, StA and paracone; a more developed metacone; a more defined triangular outline; and it is larger. Because both are here considered as M2s, these differences would not be related to distinct dental loci but possibly to different taxa. Thus, both UFAC-CS 65 and UFAC-CS 418 are considered to belong to palaeothentines. Yet, a more precise taxonomic assignment would require more associated specimens (especially of other dental loci) and a better knowledge of the morphology of the already described Palaeothentinae.

Family Abderitidae Ameghino, 1889

Abderitidae indet.

(Figure 8C1–4)

Referred material. UFAC-CS 101, right M2; UFAC-CS 109, left ?m2.

Locality. PRJ 33, stratified conglomerate level, Juruá River, State of Acre, Brazil.

Formation and age. Solimões Fm., Acre Basin, Middle Miocene.

Measurements. UFAC-CS 101, L = 1.58 mm, W = 1.9 mm; UFAC-CS 109, W = 1.41, L = 1,08.

Description. UFAC-CS 101 (Figure 8C1–3) is a small upper molar, quadrangular in occlusal view, strongly recalling the morphology and outline of an M2. It is wide at its base, especially labio-lingually, with a conspicuous labial slope at the base of the StB. The protocone is robust but relatively short. The metaconule is smaller than the protocone. The postprotocrista meets a crest that runs anterolingually to the metaconule, lingually delimitating a small trigon basin, which is separated from the talon basin. There is a wide anterior cingulum, with a conspicuous parastylar cusp *sensu* Abello and Rubilar-Rogers (2012) present at its labial margin, which presents a small projection/style at its labial base. The StB is large and high, being the tallest cusp of the molar. The posterior StB crest presents a small cusp-like structure. This crest and the anterior StC+D crest do not form a V-shaped sulcus but run more parallel to the anteroposterior molar axis. The StC+D is small and is placed quite posteriorly. Posterolingual to the StC+D, there is a short wide basin formed by the postmetaconular crest. Crest-like structures run from the stylar cusps towards the protocone and metaconule.

The UFAC-CS 109 specimen (Figure 8C4) is a fragment of a lower molar, with only the talonid preserved. None of the trigonid cuspids are preserved, and the talonid displays two lingual cuspids and one labial. The two lingual ones correspond to an anterior cuspid-like entocristid, which has a blunt tip, and a posterior entoconid, both labio-lingually compressed. The hypoconid occupies a posterior position, with a cristid-like structure running antero-lingually from its tip to the talonid basin. The talonid basin is relatively narrow. Posteriorly to the entoconid, a postentocristid runs almost perpendicular to the anteroposterior molar axis, joining a postcristid towards the molar

midline. Basal to them there is a small hypoconulid. The cristid obliqua is slightly oblique and has a sharp occlusal margin.

Remarks. The presence of lophodont molars is considered a diagnostic characteristic of the family Abderitidae. Besides, the presence of a parastylar cusp on the M2 is also common among abderitids (Abello, 2007). The latter and the absence of both paracone and metacone on the tooth, as well as a cristid obliqua with sharp occlusal margin on the m2–m3 and a hypoconid not anteroposteriorly compressed are characteristics present in UFAC-CS 101 and UFAC-CS 109 which are diagnostic of the genus *Abderites* Ameghino, 1887, according to Abello and Rubilar-Rogers (2012). Three species of *Abderites* are currently recognized, *A*. *meridionalis* Ameghino, 1887, *A*. *crispus* Ameghino, 1902 and *A*. *aisenense* Abello and Rubilar-Rogers, 2012. The size of UFAC-CS 101 and UFAC-CS 109 is much smaller than the specimens assigned to any known species of *Abderites*, the closer of them in size being *A*. *crispus* (Abello and Rubilar-Rogers, 2012). Several of the characteristics that define each of the species of Abderites are located on other molar loci or regions not preserved in the specimens from Acre. Several synonymies were already considered among the referred species, the differences among them being somewhat subtle (Abello and Rubilar-Rogers, 2012). The labial slope seen in UFAC-CS 101 is a peculiar characteristic not found in none of the previously known species of *Abderites*, which have a sub-vertical labial wall on M1–M3. Besides, compared to another abderitid, *Pitheculites* Ameghino, 1902, the specimens from Acre are slightly larger than *P*. *minimus* Ameghino, 1902, slightly smaller than *P*. *rothi* Marshall, 1990 and *P*. *ipururensis* Stutz et al., 2022 and much smaller than *P*. *chenche* (Dumont and Bown, 1997) (Marshall, 1976b; Suárez Gómez, 2019; Stutz et al., 2022). Furthermore, *Pitheculites* is characterized by a metacone on M2 and a short cristid obliqua with a rounded occlusal margin (Abello, 2007).

Therefore, due to their scarcity and fragmentary state, the open taxonomic assignation Abderitidae indet. is considered more conservative for the specimens UFAC-CS 101 and UFAC-CS 109.

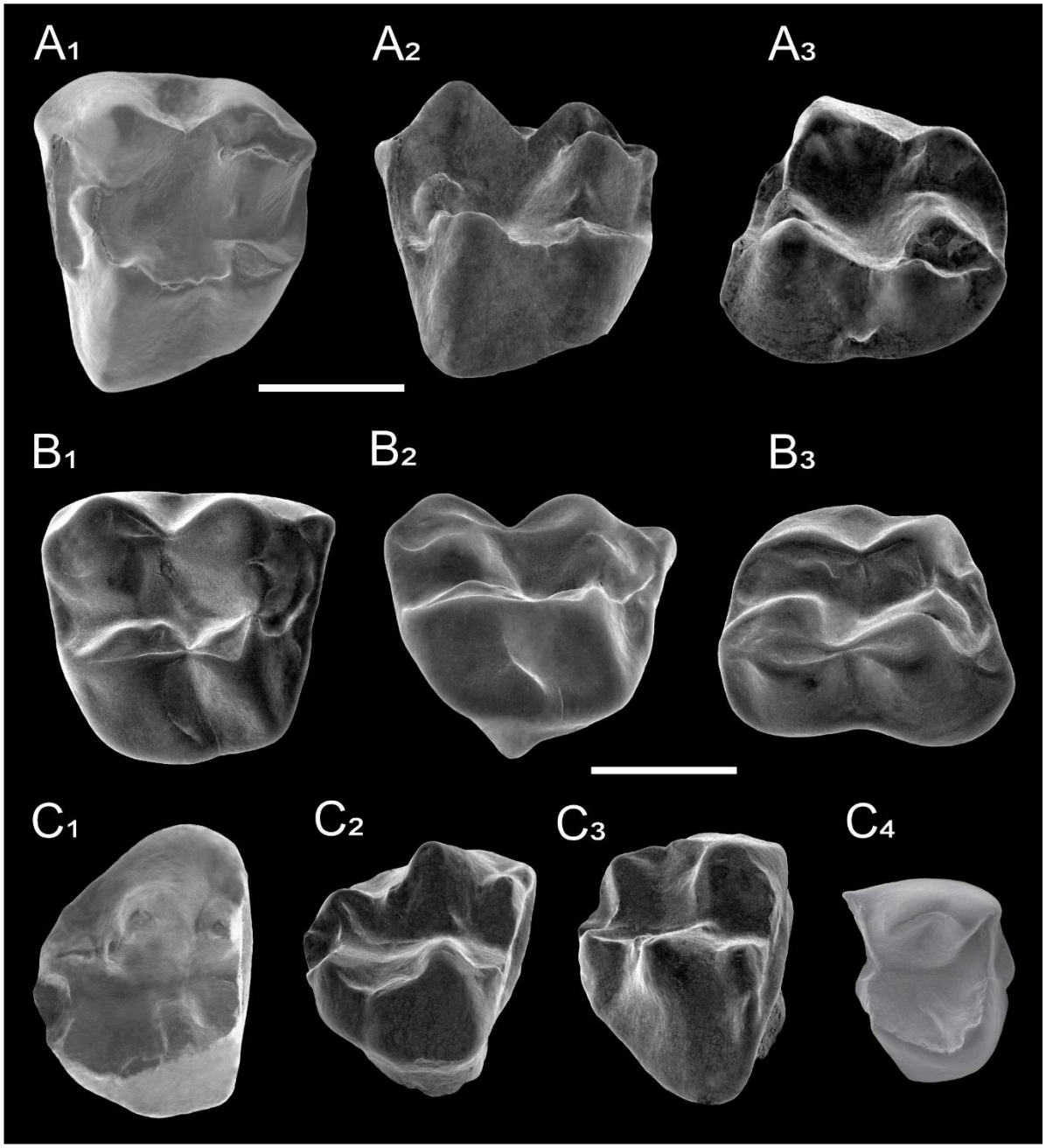


Figure 8. Paucituberculatans from the upper Juruá River, State of Acre, Brazil. A1–3, Palaeothentinae indet., UFAC-CS 65, left M2, PRJ 33', out of stratigraphic context, allochthonous sediments; B1–3, Palaeothentinae indet., UFAC-CS 418, right ?M2, PRJ 25, out of stratigraphic context, allochthonous sediments; C1–4, Abderitidae indet., C1–3: UFAC-CS 101, right M2, and C4: UFAC-CS 109, left fragmentary ?m2, PRJ 33, conglomerate level, in situ sediments. A1, B1, C1, C4, occlusal views; A2, B2, C2, partially lingual views; A3, B3, C3, partially labial views. Scale bars = 1 mm.

5. Discussion

5.1 Miocene Acre diachronous deposits in the upper Juruá and Envira rivers

The fossil record of Amazonian metatherians remains scarce, especially when compared to the high latitudes of the South American landmass, and the marsupial faunas are quite distinct in their composition between both areas (Goin et al., 2016). Such a disparity does not allow for a precise taxonomic assignment in most cases for newly-found fossil remains, mainly when they consist of isolated tooth specimens. A review of the Middle–Late Miocene metatherian record from Northern South America was recently proposed by Stutz et al. (2022). In Brazilian Amazonia, only didelphids had so far been described, also from Miocene deposits of Acre (unidentified specimens and *D. solimoensis*; Czaplewski, 1996; Cozzuol et al., 2006). Thus, the new records reported here from the Solimões Fm. add three didelphid taxa and another order (Paucituberculata), with two new families documented (Palaeothentidae and Abderitidae) to the marsupial paleodiversity of Acre. Although notable, the absence of the orders Sparassodonta and Microbiotheria is likely related primarily to the low number of specimens recovered, despite the field efforts. Nevertheless, these orders are recorded in other coeval localities in northern South America, sometimes in association (*e.g.*, La Venta, Colombia; Suárez Gómez, 2019), and sparassodontans are present and diverse in Quebrada Honda (Bolivia; Engelman et al., 2020). Comparatively, with one didelphid, one palaeothentid, and one abderitid but no sparassodontan or microbiothere, the Middle Miocene (Laventan) TAR-31 locality from Peruvian Amazonia (Stutz et al., 2022) yields the taxonomically-closest marsupial community with the three assemblages described here. The presence of Abderitidae indet., found in the PRJ 33 conglomerate level, suggests a Middle Miocene age for this fossil-bearing locality, an age estimate that would agree with that deriving from chinchilloid (*e.g.*, *Microscleromys* sp.) and erethizontoid (*Nuyuyomys* sp.) rodent specimens found on the same level (preliminary identifications made by L. Marivaux and L. Kerber, material under analysis).

Traditionally, the vertebrate fauna of the Solimões Fm. is often estimated to be Late Miocene in age (Tortonian, Huayquerian SALMA, see Hsiou et al., 2022 for a recent review) and similar in age to the Urumaco fauna (Venezuela) and Ituzaingó

Formation (Argentina) (Cozzuol, 2006; Carrillo et al., 2015; Kerber et al., 2017). However, some faunal elements from the Solimões Fm. present similarities with La Venta, Fitzcarrald and Quebrada Honda faunas, which are considered as Middle Miocene in age (after the native ungulates and rodents; Goillot et al., 2011; Ribeiro et al., 2013; Tejada-Lara et al., 2015). Furthermore, a Middle to Late Miocene interval is recorded through palynostratigraphy in the Solimões Fm. (near Cruzeiro do Sul, AC; Silva-Caminha et al., 2020). Several elements of the upper Juruá River region suggest the presence of still older stratigraphic units, with taxa closely related to those from the Oligocene Santa Rosa, La Cancha (Argentina), and Salla (Bolivia) faunas (Ribeiro et al., 2013; Kerber et al., 2017).

The distinct marsupial assemblages in the two rivers studied here, upper Juruá and Envira (Table 1), indicate that the concerned deposits do not document the same age and/or environmental context. At PRE 06 (Envira River), considered to be (?early) Late Miocene in age (according to the rodent fauna; Fontoura et al., 2022), solely didelphids were recorded, as in classical Acre localities. Late Miocene records of didelphids are much more abundant than Middle Miocene ones. Besides, it is considered as a period of significant diversification and colonization of new areas by this family (Castro et al., 2021). Conversely, only Palaeothentoidea paucituberculatans were found at PRJ 25 and PRJ 33. This superfamily became extinct by the end of the Miocene (Abello et al., 2020). Nevertheless, there is no Late Miocene record of palaeothentoids in Northern South America. However, this group had great abundance and diversity, as well as a broad geographical range in Early–Middle Miocene low-latitude localities (*e.g.*, Quebrada Honda, MD-61, MD-67, CTA-45, TAR-31, and La Venta localities; e.g., Antoine et al., 2013, 2016, 2017; Engelman et al., 2017; Stutz et al., 2022). Based on these recorded occurrences, the extinction of Palaeothentoidea was hypothesized not to have happened as a long, gradual decline but as an abrupt event (Engelman et al., 2017), or perhaps two events instead (Middle-Late Miocene transition at low latitudes; Late Miocene at mid- and high latitudes). Consequently, the presence of palaeothentoids at PRJ 25 and PRJ 33 furthers the hypothesis of the upper Juruá River fossil-bearing localities being older than their Envira River (and classical Acre) counterparts, and most likely Middle Miocene in age. On the other hand, the species-rich didelphid assemblage at PRE 06, with no paucituberculatan specimens,

further matches the (?early) Late Miocene age as recently proposed based on rodent biostratigraphy (Fontoura et al., 2022), more in line with the classical Huayquerian Acre faunas. Unfortunately, the lack of a precise geological context for the PRJ 25 specimens and part of the material from PRJ 33 does not help in this context.

Table 1. Marsupial assemblages by the upper Juruá (PRJ 25 and PRJ 33 localities, Middle Miocene) and Envira rivers (PRE 06 locality, [?early] Late Miocene), Acre, Brazil.

	Localities		
	PRJ 25	**PRJ 33**	**PRE 06**
Taxa			
Paucituberculata			
Palaeothentidae			
Palaeothentinae indet.	X	X	
Abderitidae			
Abderitidae indet.		X	
Didelphimorphia			
Didelphidae			
Marmosini, cf. *Marmosa*			X
Didelphis cf. *D. solimoensis*			X
Thylamys? *colombianus*			X
Didelphidae indet.			X
	middle Miocene		(?early) late Miocene

5.2 Miocene metatherian diversity, ecology, and paleobiogeography in the Acre region

Marmosini is a monophyletic tribe of didelphids, which includes *Marmosa*, *Tlacuatzin*, and *Monodelphis*. *Marmosa* is a complex genus with five subgenera and 25 living species, broadly distributed in Central and South America and occurring in many tropical and subtropical habitats (Rossi et al., 2010; Voss, 2022). The phylogenetic pattern of *Marmosa* was shown to be closely related to the Andes and its orogeny, with a trans-Andean clade of species (mostly in Central America and Western South America) and a cis-Andean group (Patterson et al., 2012). As mentioned above, fossils documenting *Marmosa* are reported from the La Venta deposits, Middle Miocene of Colombia, with *M. laventica*, *Marmosa* sp., and *Marmosa* sp. 1 (Marshall, 1976; Goin, 1997; Suárez Gómez, 2019). Besides, Antoine et al. (2013) mentioned the

presence of *Marmosa* (*Micoureus*) cf. *laventica* at MD-67, Middle Miocene of Peru. Additional fossil specimens of *Marmosa* have been reported only from the Chapadmalal Fm. (Pliocene) in Argentina (Marshall, 1976a). The new possible record of Marmosini, cf. *Marmosa* from PRE 06 highlights the broad presence of close allies of this taxon in the Western Amazonian region during the Miocene.

The genus *Didelphis* today comprises six species, which occur from North to South America, occupying almost all the tropical and subtropical biomes (except deserts) of the Americas. Nevertheless, its species-level taxonomy is puzzling (Voss and Jansa, 2009; Voss, 2022). *Didelphis* was previously recognized in the Late Miocene of Acre, with *D*. *solimoensis* at the Patos locality, on the Acre River (Cozzuol et al., 2006). Moreover, two extinct species of *Didelphis* were described from the late Pliocene-early Pleistocene of Argentina (Goin and Pardiñas, 1996; Cozzuol et al., 2006). The record of *Didelphis* cf. *D*. *solimoensis* at PRE 06 possibly adds new specimens of this taxon, which is known solely for its holotype thus far (only lower dentition).

Thylamys is considered a monophyletic genus, with two subgenera and nine species, occurring solely in South America. It is considered a marker of open vegetation environments (Giarla and Jansa, 2014). Fossil occurrences of the genus include the extinct *T*. *minutus* and *T*. *colombianus* from La Venta, Colombia (Goin, 1997), and '*Thylamys*' cf. '*T*.' *colombianus* from Peruvian Amazonia (TAR-31; Stutz et al., 2022), both Middle Miocene in age, as well as Late Miocene and Pliocene records in Argentina (Gardner, 2007). The record of *Thylamys*? *colombianus* at PRE 06 expands the range of this taxon east and southwards and allow for considering its survival in Late Miocene times in Western Amazonia.

Thus, the record of these three didelphid taxa from PRE 06 highlights the diversity and distribution of the Didelphidae during the (?early) Late Miocene in Western Amazonia. As pointed out by Goin (1997) and Suárez Gómez (2019) for the La Venta deposits, this area would have functioned both as a high-diversification rate region, as well as a place with low extinction rates (see also Meseguer et al., 2022). Castro et al. (2021) emphasized the importance of Amazonia for the early diversification of didelphids, with the La Venta and Madre de Dios records (MD-67,

Peru), as well as the records in Argentinean Patagonia (Goin et al., 2007) as the first reliable ones of crown representatives of Didelphidae.

Since a more precise taxonomic attribution could not be achieved for Marmosini, cf. *Marmosa* from PRE 06, it is impossible to correlate this taxon to specific paleoenvironmental conditions. Indeed, species of *Marmosa* inhabit a wide range of habitats. Most species, however, occur in lowland rainforests, and marmosines are generally associated with a more insectivorous-carnivorous niche (Goin, 1997; Voss and Jansa, 2009). *Didelphis* species are also distributed in almost all types of habitats, and are considered to have omnivorous and opportunistic behavior, thus, not a helpful indicator for paleoenvironmental considerations either (Cozzuol et al., 2006; Gardner, 2008; Voss, 2022). On the other hand, species of *Thylamys* occur today in open environments of subequatorial South America (none in low latitudes), having insectivorous-omnivorous habits (Gardner, 2008; Cáceres, 2012). As to the fossil *Thylamys*, Suárez Gómez (2019) suggested that *T*. *colombianus* would have had insectivorous/faunivorous habits. Besides, this *Thylamys* diversity recorded in Amazonia would suggest a much widespread geographical distribution in the past, but the question remains as to whether these Miocene specimens belong to stem Thylamyini or to *Thylamys* sensu stricto. Interestingly, the ancestral area of Thylamyini was suggested to be Amazonia, with stem thylamyin inhabiting closed-canopy forests and later diversifying and colonizing open habitats east of the Andes, prior to the Late Miocene (Jansa et al., 2014; Castro et al., 2021)

Palaeothentes is a speciose genus that was recovered as monophyletic in the most recent phylogenies considering a comprehensive taxonomic sampling of paucituberculatans, but excluding '*Palaeothentes*' *primus*, reassigned to *Palaepanorthus* (Abello, 2007; Engelman et al., 2017). The unidentified palaeothentine(s) from the upper Juruá (PRJ 25 and PRJ 33') have the closest affinities with *P*. *marshalli* and *P*. *migueli* (both being closely related) and with *Palaeopanorthus primus* (phylogenetically remote) (Engelman et al., 2017; Abello et al., 2020). *Palaepanorthus primus* is known from the early Miocene of Argentinean Patagonia, it had a medium size compared to other palaeothentines, and its dietary habits are not known (Bown and Fleagle, 1993; Abello, 2007). *Palaeothentes* is widespread in Miocene localities all over South America, and Northern Amazonia seems to have

played a significant role in the evolutionary history of its superfamily, which needs to be more investigated (Stutz et al., 2022 and references therein).

Regarding body size, Palaeothentinae indet. from the upper Juruá (PRJ 25 and PRJ 33') can be considered to have been small to medium-sized when compared to other palaeothentines, being much smaller than the very large *P*. *aratae* and *Titanothentes simpsoni* (>500 g; Abello et al., 2020), and slightly smaller than *P*. *serratus* (~100 g) and *P*. *relictus* (~150 g; Engelman et al., 2017). The absence of m2 in the studied material hinders the dietary reconstruction of the unidentified palaeothentine(s), following Dumont et al.' (2000) protocol. Nonetheless, *P*. *marshalli* and *P*. *migueli* were unambiguously interpreted as frugivorous (Engelman et al., 2017). Palaeothentids have been related to various feeding habits and different kinds of habitats (mixed vegetational cover and seasonal aridity at Quebrada Honda, Bolivia, Engelman et al., 2017; at Santa Cruz and Pinturas formations, Argentina, markedly seasonal, not dry reconstructed paleoenvironment, Kramarz and Bellosi, 2005; Spradley et al., 2019). In Western Amazonia, palaeothentids were abundantly recorded at the Shapaja section in early Oligocene deposits, which do record a drier period after the Eocene-Oligocene transition (Antoine et al., 2021; Stutz et al., 2021, work in progress) as well as in La Venta, which is suggested as having hosted a tropical rainforest by the Middle Miocene (Spradley et al., 2019) and at TAR-31, where the paleoenvironmental conditions are suggested to have been humid, warm, with heterogenous landscape (Stutz et al., 2022).

The record of Abderitidae indet. at PRJ 33 broadens the geographical range of this family and adds a new occurrence of it in South American low latitudes. The only abderitid recognized in Northern South America is Pitheculites, with *P*. *chenche* in La Venta and *P*. *ipururensis* in TAR-31, Peru (Middle Miocene; Suárez Gómez, 2019; Stutz et al., 2022), whereas *Parabderites* and *Abderites* are classically restricted to the southern part of South America (Argentina and Chile) and spanning the Early–Middle Miocene interval (Colhuehuapian–Colloncuran SALMAs; Abello and Rubilar-Rogers, 2012). Since a more precise taxonomic assignment could not be achieved, it is not possible to state if these specimens represent the occurrence of another abderitid genus in the Amazon region. Abderitids are considered to have been dietary generalists, with a derived dental complexity allowing them to process a wide range of

food items (Abello et al., 2020). They thrive in wet and humid paleoenvironments (Ortiz Jaureguizar, 2003; Engelman et al., 2017).

6. Conclusions

The upper Juruá and Envira marsupials described here highlight the role of Western Amazonia regarding Middle and Late Miocene didelphids and palaeothentoids, especially for palaeothentines and abderitids, which were previously unknown in Brazilian Amazonia. Strong affinities are revealed with Middle-early Late Miocene localities of Peruvian Amazonia (MD-67 in Madre de Dios; TAR-31 near Tarapoto; CTA-44 and CTA-43 near Contamana), Colombia (La Venta) and Quebrada Honda (Bolivia). Hence, it reinforces the hypothesis of a unique and homogeneous biogeographical province for land mammals in Western Amazonia over the Middle Miocene times, and probably slightly before and after, possibly in close relation with the Pebas Mega-Wetland System (Stutz et al., 2022). However, the upper Juruá and Envira river outcrops need to be better constrained stratigraphically and in terms of geochronological data. Furthermore, much remains to be investigated in terms of fossil marsupials from Northern South America: no pre-Pleistocene fossils are known for the current Amazon region of Ecuador and Colombia (Antoine et al., 2017). As pointed out by Goin et al., (2016), this scarcity of fossil data makes it challenging to understand the South American marsupials' phylogenetic and paleobiogeographic relationships, not only at tropical latitudes but also from the whole continent.

Acknowledgments

The authors would like to thank all the people who participated in the field campaigns and the staff of the CMM-UFRGS and LabCEMM-PUCRS for access to SEM facilities. We would also like to thank Paulo Simões Lopes, Jorge J. Cherem, Maurício Graipel (UFSC), and Victor Pacheco (MUSM) for the access to the scientific collections. This work was supported by Conselho Nacional de Desenvolvimento Científico e Tecnológico (CNPq) and Coordenação de Aperfeiçoamento de Pessoal de Nível Superior (CAPES) PhD grants (CNPq 140773/2019-3, CAPES-COFECUB nº 88881.143095/2017-01) (NSS); Fundação de Amparo à Pesquisa do Estado do Rio Grande do Sul (FAPERGS, 21/2551-0000781-8) and CNPq grants (PQ 310023/2021-

1 and CNPq/MCTI/CONFAP-FAPS PROTAX 22/2020 441626/2020-3 to AMR; PQ 309414/2019-9 to LK; and PQ 310948/2021-5 to ASH); Fundação de Amparo à Pesquisa do Estado de São Paulo (FAPESP 2011/14080-0 and 2019/14153-0) (ASH); Ministério de Ciência e Tecnologia e Inovação (01200.001631/2010-32 and 01200.001631/2010-32); and the French Agence Nationale de la Recherche (ANR) in the framework of the LabEx CEBA (ANR-10-LABX-25-01), through the EMERGENCE project (NSS, LM, POA, FP). This is ISEM publication n°: 2022-XXX Sud.

References

Abello, M.A. 2007. Sistemática y Bioestratigrafía de los Paucituberculata (Mammalia, Marsupialia) del Cenozoico de América del Sur. 381 pp. Unpublished Ph.D. Thesis, Universidad Nacional de La Plata, La Plata. [in Spanish, with English abstract]

Abello, M.A. and Candela, A.M. 2010. Postcranial skeleton of the Miocene marsupial *Palaeothentes* (Paucituberculata, Palaeothentidae): paleobiology and phylogeny. Journal of Vertebrate Paleontology 30(5): 1515–1527.

Abello, M.A. and Rubilar-Rogers, D. 2012. Revisión del género *Abderites* Ameghino, 1887 (Marsupialia, Paucituberculata). Ameghiniana 49(2): 164–184. [in Spanish]

Abello, M.A., Toledo, N., and Ortiz-Jaureguizar, E. 2020. Evolution of South American Paucituberculata (Metatheria: Marsupialia): adaptive radiation and climate changes at the Eocene-Oligocene boundary. Historical Biology 22(4): 476–493.

Abello, M.A., De Los Reyes, M., Candela, A.M., Pujos, F., Voglino, D. and Quispe, B.M. 2015. Description of a new species of *Sparassocynus* (Marsupialia: Didelphoidea: Sparassocynidae) from the late Miocene of Jujuy (Argentina) and taxonomic review of *Sparassocynus heterotopicus* from the Pliocene of Bolivia. Zootaxa 3937(1): 147–160.

Antoine, P.O., Salas-Gismondi, R., Pujos, F., Ganerød, M., and Marivaux, L. 2017. Western Amazonia as a hotspot of mammalian biodiversity throughout the Cenozoic. Journal of Mammalian Evolution 24(1): 5–17.

Antoine, P.-O., Roddaz, M., Brichau, S., Tejada-Lara, J., Salas-Gismondi, R., Altamirano, A., Louterbach, M., Lambs, L., Otto, T., and Brusset, S. 2013. Middle Miocene vertebrates from the Amazonian Madre de Dios Subandean Zone, Perú. Journal of South American Earth Sciences 42: 91–102.

Antoine, P.-O., Abello, M.A., Adnet, S., Altamiro Sierra, A.J., Baby, P.; Billet, G., Boivin, M., Calderón, Y., Candela, A., Chabain, J., Corfu, F., Croft, D.A., Ganerød, M., Jaramillo, C., Klaus, S., Marivaux, L., Navarrete, R.E., Orliac, M.J., Parra, F., Pérez, M.E., Pujos, F., Rage, J.C., Ravel, A., Robinet, C., Roddaz, M., Tejada-Lara, J.V., Vélez-Juarbe, J., Wesselingh, F.P., and Salas-Gismondi, R. 2016. A 60-million-year Cenozoic history of western Amazonian ecosystems in Contamana, Eastern Peru. Gondwana Research 31: 30–59.

Antoine, P.-O., Yans, J., Aliaga Castillo, A., Stutz, N., Abello, M.A., Adnet, S., Andriolli Custódio, M., Benites-Palomino, A., Billet, G., Boivin, M., Herrera, F., Jaramillo, C., Mártinez, C., Moreno, F., Navarrete, R.E., Negri, F.R., Parra, F., Pujos, F., Rage, J.-C., Ribeiro, A.M., Robinet, C., Roddaz, M., Tejada-Lara, J.V., Varas-Malca, R., Ventura Santos, R., Salas-Gismondi, R., and Marivaux L. 2021. Biotic community and landscape changes around the Eocene–Oligocene transition at Shapaja, Peruvian Amazonia: regional or global drivers? Global and Planetary Change 202: 103512.

Assemat, A., Boivin, M., Marivaux, L., Pujos, F., Benites-Palomino, A., Salas-Gismondi, R., Tejada-Lara, J.V., Varas-Malca, R.M., Negri, F.R., Riveiro, A.M., and Antoine, P.-O. 2019. Restes inédits de rongeurs caviomorphes du Paléogène de la région de Juanjui (Amazonie péruvienne) : systématique, implications macro-évolutives et biostratigraphiques. Geodiversitas 41(20): 699–730. [in French]

Beck, R.M.D. and Taglioretti, M.L. 2020. A Nearly Complete Juvenile Skull of the Marsupial *Sparassocynus derivatus* from the Pliocene of Argentina, the Affinities of *Sparassocynids*, and the Diversification of Opossums (Marsupialia; Didelphimorphia; Didelphidae). Journal of Mammalian Evolution 27: 385–417.

Bergqvist, L.P., Ribeiro, A.M., and Bocquentin, J. 2002. Primatas, roedores e liptoternas do Mio/Plioceno da Amazônia Sul-Ocidental (Formação Solimões, Bacia do Acre), Brasil. Geologia Colombiana 23: 19–29. [in Portuguese]

Bissaro Júnior, M.C., Kerber, L., Crowley, J.L., Ribeiro, A.M., Guilardi, R.P., Guilherme, E., Negri, F.P., Souza-Filho, J.P., and Hsiou, A.S. 2019. Detrital zircon U-Pb geochronology constrains the age of Brazilian Neogene deposits from Western Amazonia. Palaeogeography, Palaeoclimatology, Palaeoecology 516: 64–70.

Boivin, M., Marivaux, L., Pujos, F., Salas-Gismondi, R., Tejada-Lara, J.V., Varas-Malca, R. M., and Antoine, P.O. 2018. Early Oligocene caviomorph rodents from Shapaja, Peruvian Amazonia. Palaeontographica 311(1–6): 87–156.

Boonstra, M., Troelstra, S.R., Lammertsma, E.I., Ramos, M.I.F., Antoine, P.-O., and Hoorn, C. 2015. Marine connections of Amazonia: Evidence from foraminifera and dinoflagellate cysts (early to middle Miocene, Colombia/Peru). Palaeogeography, Palaeoclimatology, Palaeoecology 417: 176–194.

Bown, T.M. and Fleagle, J.G. 1993. Systematics, biostratigraphy, and dental evolution of the Palaeothentidae, later Oligocene to early-middle Miocene (Deseadan-Santacrucian) caenolestoid marsupials of South America. Journal of Paleontology 67(Suppl. 2): 1–76.

Cáceres, N.C. (org). 2012. Os marsupiais do Brasil. 2ª ed. 498 pp. Editora UFMS, Campo Grande. [in Portuguese]

Campbell, K.E. (ed.). 2004. The Paleogene mammalian fauna of Santa Rosa, Amazonian Peru. 163 pp. Science Series, Natural History Museum of Los Angeles County, Los Angeles.

Campbell, K.E., O'Sullivan, P.B., Fleagle, J.G., de Vries, D., and Seiffert, E.R. 2021. An early Oligocene age for the oldest known monkeys and rodents of South America. PNAS 118(37): e2105956118.

Carrillo, J.D., Forasiepi, A., Jaramillo, C., and Sánchez-Villagra, M.R. 2015. Neotropical mammal diversity and the Great American Biotic Interchange: spatial and temporal variation in South America's fossil record. Frontiers in Genetics 5: 451.

Castro, M.C., Dahur, M.J., and Ferreira, G.S. 2021. Amazonia as the origin and diversification area of Didelphidae (Mammalia: Metatheria), and a review of the fossil record of the clade. Journal of Mammalian Evolution 28: 583–598.

Cozzuol, M.A., Goin, F., de los Reyes, M., and Ranzi, A. 2006. The oldest species of *Didelphis* (Mammalia, Marsupialia, Didelphidae), from the late Miocene of Amazonia. Journal of Mammalogy 87(4): 663–667.

Croft, D.A., Carlini, A.A., Ciancio, M.R., Brandoni, D., Drew, N.E., Engelman, R.K., and Anaya, F. 2016. New mammal faunal data from Cerdas, Bolivia, a middle-latitude Neotropical site that chronicles the end of the Middle Miocene Climatic Optimum in South America. Journal of Vertebrate Paleontology 36(5): e1163574.

Cunha, P.R.C. 2007. Bacia do Acre. Boletim de Geociências da Petrobrás 15(2): 207–215. [in Portuguese]

Czaplewski, N.J. 1996. Opossums (Didelphidae) and bats (Noctilionidae and Molossidae) from the late Miocene of the Amazon Basin. Journal of Mammalogy 77(1): 84–94.

Dumont, E., Strait, S., and Friscia, A. 2000. Abderitid marsupials from the Miocene of Patagonia: an assessment of form, function, and evolution. Journal of Paleontology 74(6): 1161–1172.

Engelman, R.K., Anaya, F., and Croft, D.A. 2017. New palaeothentid marsupials (Paucituberculata) from the middle Miocene of Quebrada Honda, Bolivia, and their implications for the palaeocology, decline and extinction of the Palaeothentoidea. Journal of Systematic Palaeontology 15(10): 787–820.

Engelman, R.K., Anaya, F., and Croft, D.A. 2020. *Australogale leptognathus*, gen. et sp. nov., a second species of small sparassodont (Mammalia: Metatheria) from the Middle Miocene locality of Quebrada Honda, Bolivia. Journal of Mammalian Evolution 27(1): 37–54.

Fontoura, E., Negri, F.R., Ribeiro, A.M., and Kerber, L. 2022. A new Late Miocene hystricognath rodent assemblage (Caviidae, Dinomyidae, and Neoepiblemidae) from northern Brazil and its biostratigraphic relevance. Historical Biology: aop.

Forasiepi, A.M., Goin, F. and Martinelli, A.G. 2009. Contribution to the knowledge of the Sparassocynidae (Mammalia, Metatheria, Didelphoidea), with comments on the age of the Aisol Formation (Neogene), Mendoza Province, Argentina. Journal of Vertebrate Paleontology 29(4): 1252–1263.

Frailey, C.D. and Campbell, K.E. 2004. Paleogene rodents from Amazonian Peru: the Santa Rosa local fauna. In: K.E. Campbell (ed.), The Paleogene mammalian fauna of Santa Rosa, Amazonian Peru. Natural History Museum of Los Angeles County, Science Series 40: 71–130.

Gardner, A.L. 2007. Mammals of South America. Vol. 1. 669 pp. The University of Chicago Press, Chicago.

Giarla, T.C. and Jansa, S.A. 2014. The role of physical geography and habitat type in shaping the biogeographical history of a recent radiation of Neotropical marsupials (*Thylamys*: Didelphidae). Journal of Biogeography 41: 1547–1558.

Goillot, C., Antoine, P.-O., Tejada Lara, J., Pujos, F., and Salas-Gismondi, R. 2011. Middle Miocene Uruguaytheriinae (Mammalia, Astrapotheria) from Peruvian Amazonia and a review of the astrapotheriid fossil record in northern South America. Geodiversitas 33: 331–345.

Goin, F.J. 1997. New clues for understanding Neogene marsupial radiations. In: R.F. Kay, R.H. Madden, R.L. Cifelli, and J.J. Flynn (eds.), Vertebrate Paleontology in the Neotropics. The Miocene fauna of La Venta, Colombia. Smithsonian Institution Press: 187–206.

Goin, F.J. and Candela, A.M. 2004. New Palaeogene marsupials from the Amazon Basin of Eastern Peru. In: K.E. Campbell (ed.), The Paleogene mammalian fauna of Santa Rosa, Amazonian Peru. Natural History Museum of Los Angeles County, Science Series 40: 15–60.

Goin, F.J. and de los Reyes, M. 2011. Contribución al conocimiento de los representantes extintos de *Lutreolina* Thomas, 1910 (Mammalia, Marsupialia, Didelphidae). Historia Natural 1(2): 15–25. [in Spanish]

Goin, F.J. and Pardiñas, U.F.J. 1996. Revisión de las especies del género *Hyperdidelphys* Ameghino, 1904 (Mammalia, Marsupialia, Didelphidae). Su significación filogenética, estratigráfica y adaptative en el Neógeno del cono sur sudamericano. Estudios Geológicos 52: 327–359. [in Spanish]

Goin, F.J., Montalvo, C.I. and Visconti, G. 2000. Los marsupiales (Mammalia) del Mioceno Superior de la Formación Cerro Azul (Provincia de La Pampa, Argentina). Estudios Geológicos 56: 101–126. [in Spanish]

Goin, F.J., Woodburne, M.O., Zimicz, A.N., Martin, G.M., and Chornogubsky, L. 2016. A brief history of South American metatherians. 237 pp. Springer Earth System Sciences, New York.

Hoorn, C., Wesselingh, F.P.; Hovikoski, J., and Guerrero, J. 2010. The development of the Amazonian mega-wetland (Miocene; Brazil, Colombia, Peru, Bolivia). In: C. Hoorn and F.P. Wesselingh (eds.), Amazonia, Landscape and Species Evolution: A Look into the Past. Blackwell-Wiley: 123–142.

Hoorn, C., Wesselingh, F.P., Ter Steege, H., Bermudez, M.A., Mora, A., Sevink, J., Sanmartín, I., Sanchez-Meseguer, A., Anderson, C.L., Figueiredo, J.P., Jaramillo, C., Riff, D., Negri, F.R., Hooghiemstra, H., Lundberg, J., Stadler, T., Särkinen, T., and

Antonelli, A. 2010. Amazonia through time: Andean uplift, climate change, landscape evolution, and biodiversity. Science 330: 927–931.

Hoorn, C., Bogotá-A, G.R., Romero-Baez, M., Lammertsma, E.I., Flantua, S.G., Dantas, E. L., Dino, R., do Carmo, D.A., and Chemale Jr, F. 2017. The Amazon at sea: Onset and stages of the Amazon River from a marine record, with special reference to Neogene plant turnover in the drainage basin. Global and Planetary Change 153: 51–65.

Horovitz, I. and Sánchez-Villagra, M.R. 2012. El registro fósil del Cenozoico. In: M.R. Sánchez-Villagra (ed.) Venezuela paleontológica. Universität Zürich: 133–156. [in Spanish]

Hsiou, A.S., Bissaro-Júnior, M.C., Muniz, F.P., Negri, F.R., Ribeiro, A.M., and Kerber, L. 2022. Bacia do Acre: Evidências das paisagens da proto- Amazônia há 10 milhões de anos, com base em vertebrados fósseis da Formação Solimões. In: L. Corecco (ed.), Paleontologia do Brasil: paleoecologia e paleoambientes. Interciência: 29–64.

Jansa, S.A., Barker, F.K., and Voss, R.S. 2014. The early diversification history of didelphid marsupials: a window into South America's "splendid isolation". Evolution 68: 684–695.

Kay, R.F., Madden, R.H., Cifelli, R.L., and Flynn, J.J. 1997. Vertebrate paleontology in the Neotropics: the Miocene fauna of La Venta, Colombia. xvi + 592 pp. Smithsonian Institution Press, Washington.

Kerber, L., Ferreira, J.D., and Negri, F.R. 2019b. A reassessment of the cranial morphology of *Neoepiblema acreensis* (Rodentia: Chinchilloidea), a Miocene rodent from South America. Journal of Morphology 280(12): 1821–1838.

Kerber, L., Negri, F.R., and Sanfelice, D. 2019a. Morphology of cheek teeth and dental replacement in the extinct rodent *Neoepiblema* Ameghino, 1889 (Caviomorpha, Chinchilloidea, Neoepiblemidae). Journal of Vertebrate Paleontology 38(6): e1549061.

Kerber, L., Negri, F.R., Ribeiro, A.M., Vucetich, M.G., and Souza-Filho, J.P. 2016. Late Miocene potamarchine rodents from southwestern Amazonia, Brazil—with description of new taxa. Acta Palaeontologica Polonica 61(1): 191–203.

Kerber, L., Bissaro Júnior, M.C., Negri, F.R., Souza-Filho, J.P., Guilherme, E., and Hsiou, A.S. 2018. A new rodent (Caviomorpha: Dinomyidae) from the upper Miocene of southwestern Brazilian Amazonia. Historical Biology 30(7): 985–993.

Kerber, L., Candela, A.M., Ferreira, J.D., Pretto, F.A., Bubadué, J., and Negri, F.R. 2022. Postcranial Morphology of the extinct rodent *Neoepiblema* (Rodentia: Chinchilloidea): insights into the paleobiology of neoepiblemids. Journal of Mammalian Evolution 29(1): 207–235.

Kerber, L., Negri, F.R., Ribeiro, A.M., Nasif, N., Souza-Filho, J., and Ferigolo, J. 2017. Tropical fossil caviomorph rodents from the Southwestern Brazilian Amazonia in the context of the South American faunas: systematics, biochronology, and paleobiogeography. Journal of Mammalian Evolution 24: 57–70.

Kloster, A., Gnaedinger, S., and Adami-Rodrigues, K. 2017. Nuevos registros de maderas del Mioceno de la Formación Solimões, cuenca de Acre, Amazonia, Brasil. Revista Brasileira de Paleontologia 20(3): 383–404. [in Spanish]

Kramarz, A.G. and Bellosi, E.S. 2005. Hystricognath rodents from the Pinturas Formation, Early–Middle Miocene of Patagonia, biostratigraphic and paleoenvironmental implications. Journal of South American Earth Sciences 18(2): 199-212.

Lacerda, M.B.S., Romano, P.S.R., Bandeira, K.L.N., and Souza, L.G. 2021. Georeferencing fossiliferous localities from Solimões and Acre Basins (Brazil) - what we know so far about Solimões Formation and future perspectives. Anais da Academia Brasileira de Ciências 93(Suppl. 2): e20201642.

Linares, O.J. 2004. Bioestratigrafia de la fauna de mamiferos de las Formaciones Socorro, Urumaco y Codore (Mioceno Medio-Plioceno Temprano) de la region de Urumaco, Falcon, Venezuela. Paleobiologia Neotropical 1: 1–26. [in Spanish]

Marshall, L.G. 1976a. New Didelphine marsupials from the La Venta fauna (Miocene) of Colombia, South America. Journal of Paleontology 50(3): 402–418.

Marshall, L.G. 1976b. Revision of the South American subfamily Abderitinae (Mammalia, Caenolestidae). Publicaciones del Museo Municipal de Ciencias Naturales de Mar del Plata Lorenzo Scaglia 2(3): 57–90.

Marshall, L.G. 1987. Systematics of Itaboraian (middle Paleocene) age opossum-like marsupials from the limestone quarry at São José de Itaboraí, Brazil. In: M. Archer (ed.), Possums and opossums: studies in evolution. Surrey Beatty and Sons and the Royal Zoological Society of New South Wales: 91–160.

Meseguer, A., Michel A. J., Fabre, P.-H., Pérez-Escobar, O.A., Chomicki, G., Riina, R., Antonelli, A., Antoine, P.-O., Delsuc, F. and Condamine, F.L. 2022. Diversification

dynamics in the Neotropics through time, clades, and biogeographic regions. Elife 11: e74503.

Negri, F.R. 2004. Os Tardigrada (Mammalia, Xenarthra) do Neógeno, Amazônia Sul-Ocidental, Brasil. 156 pp. Unpublished. Ph.D. Thesis, Pontifícia Universidade Católica do Rio Grande do Sul, Porto Alegre.

Negri, F.R., Bocquentin Villanueva, J., Ferigolo, J., and Antoine, P.-O., 2010. 16. A review of Tertiary mammal faunas and birds from western Amazonia. In: C. Hoorn and F.P. Wesselingh (eds.), Amazonia, Landscape and Species Evolution: A Look into the Past. Blackwell-Wiley: 245–258.

Ortiz-Jaureguizar, E. 2003. Relaciones de similitud, paleoecología y extinción de los Abderitidae (Marsupialia, Paucituberculata). Coloquios de Paleontología, Extra Volume 1: 475–498. [in Spanish]

Patterson, B. and Costa, L. 2012. Bones, clones, and biomes: the history and geography of recent neotropical mammals. 432 pp. The University of Chicago Press, Chicago.

Patterson, B.D., Solari, S., and Velazco, P.M. 2012. The Role of the Andes in the Diversification and Biogeography of Neotropical Mammals. In: B.D. Patterson and L. Costa (eds.), Bones, clones, and biomes: the history and geography of recent neotropical mammals. The University of Chicago Press: 351–378.

Paula-Couto, C. 1982. Fosil Mammals from the Cenozoic of Acre, Brazil. Nesodontinae (II), Toxodontinae and Haplodontheriinae, and Litopterna, Pyrotheria and V – Notoungulata Astrapotheria (II). Iheringia, Série Geologia 7: 5–43.

Ribeiro, A.M., Madden, R.H., Negri, F.R., Kerber, L., Hsiou, A.S., and Rodrigues, K.A. 2013. Mamíferos fósiles y biocronología en el suroeste de la Amazonia, Brasil. In: D. Brandoni and J.I. Noriega (eds.), El Neógeno de la Mesopotamia argentina. Asociación Paleontológica Argentina: 207–221. [in Spanish]

Rossi, R.V., Voss, R.S., and Lunde, D.P. 2010. A revision of the didelphid marsupial genus *Marmosa*. Part 1. The species in Tate's '*mexicana*' and '*mitis*' sections and other closely related forms. Bulletin of the American Museum of Natural History 334: 1–83.

Sánchez-Villagra, M.R., Aguilera, O.A., Sánchez, R., and Carlini, A.A. 2010. The fossil vertebrate record of Venezuela of the last 65 million years. In: M.R. Sánchez-Villagra, O.A. Aguilera, and A.A. Carlini (eds.), Urumaco & Venezuelan Paleontology. Indiana University Press: 19–51.

Silva-Caminha, S.A.F., D'apolito, C., Jaramillo, C., Espinosa, B.S., and Rueda, M. 2020. Palynostratigraphy of the Ramon and Solimões formations in the Acre Basin, Brazil. Journal of South American Earth Sciences 103: 102720.

Simpson, G.G. 1970. The Argyrolagidae, extinct South American marsupials. Bulletin of the Museum of Comparative Zoology 139(1): 1–86.

Spradley, J.P., Glazer, B.J., and Kay, R.F. 2019. Mammalian faunas, ecological indices, and machine-learning regression for the purpose of paleoenvironment reconstruction in the Miocene of South America. Palaeogeography, Palaeoclimatology, Palaeoecology 518: 155–171.

Stutz, N.S., Abello, M.A., Marivaux, L., Boivin, M., Custódio, M.A., Benites-Palomino, A.M., Salas-Gismondi, R., Pujos, F., Tejada-Lara, J.V., Ribeiro, A.M., and Antoine, P.-O. 2021. Neotropical metatherian diversity around the Eocene-Oligocene transition: the Shapaja section, Peruvian Amazonia. Libro de Resúmenes – 14 CAPA, Symposium Mamíferos del Paleógeno de América del Sur: 123.

Stutz, N.S., Abello, M.A., Marivaux, L., Boivin, M., Pujos, F., Benites-Palomino, A.M., Salas-Gismondi, R., Tejada-Lara, J.V., Custódio, M.A., Roddaz, M., Santos, R.V., Ribeiro, A.M., and Antoine, P.-O. 2022. Late middle Miocene Metatheria (Mammalia: Didelphimorphia and Paucituberculata) from Juan Guerra, San Martín Department, Peruvian Amazonia. Journal of South American Earth Sciences 118: 103902.

Suárez, C., Forasiepi, A., Goin, F.J., and Jaramillo, C. 2016. Insights into the Neotropics prior to the Great American Biotic Interchange: new evidence of mammalian predators from the Miocene of Northern Colombia. Jounal of Vertebrate Paleontology 36(1): e1029581.

Suárez Gómez, S.C. 2019. Estudios taxonómicos y paleobiológicos sobre los Metatheria (Mammalia) del Mioceno medio de La Venta, Colombia. 292 pp. Unpublished Ph.D. thesis, Universidad Nacional de la Plata, La Plata. [in Spanish]

Tejada-Lara, J., Salas-Gismondi, R., Pujos, F., Baby, P., Benammi, M., Brusset, S., Franceschi, D., Espurt, N., Urbina, M., and Antoine, P.-O. 2015. Life in Proto-Amazonia: Middle Miocene mammals from the Fitzcarrald Arch (Peruvian Amazonia). Palaeontology 58(2): 341–378.

Villarroel, C. and Marshall, L.G. 1983. Two New Late Tertiary Marsupials (Hathlyacyninae and Sparassocyninae) from the Bolivian Altiplano. Journal of Paleontology 57(5): 1061–1066.

Voss, R.S. 2022. An annotated checklist of recent opossums (Mammalia: Didelphidae). Bulletin of the American Museum of Natural History 455(1): 1–76.

Voss, R.S. and Jansa, S.A. 2009. Phylogenetic relationships and classification of didelphid marsupials, an extant radiation of New World metatherian mammals. Bulletin of the American Museum of Natural History 322: 1–177.

3 ARTIGO 3 – NEW RECORDS OF POLYDOLOPIMORPHIAN METATHERIA FROM THE PALEOGENE OF PERUVIAN AMAZONIA

Artigo em preparação, a ser concluído e submetido para publicação após a defesa.

Stutz, N.S.[1,2]; Ribeiro, A.M.[1,3]; Abello, M.A.[4]; Marivaux, L.[2]; Pujos, F.[5,6]; Salas-Gismondi, R.[7,8]; Tejada-Lara, J.V.[9]; Benites-Palomino, A.M.[7,10]; Negri, F.R.[11]; Boivin, M.[12]; Antoine, P.-O.[2]

[1]Programa de Pós-Graduação em Geociências, Universidade Federal do Rio Grande do Sul (PPGGEO UFRGS), Avenida Bento Gonçalves, 9500, 91501-970, Porto Alegre, Brazil
[2]Laboratoire de Paléontologie, Institut des Sciences de l'Évolution de Montpellier (ISEM, UMR 5554, UM/CNRS/IRD/EPHE), Université de Montpellier, Place Eugène Bataillon, 34095, Montpellier, France
[3]Seção de Paleontologia, Museu de Ciências Naturais, Secretaria do Meio Ambiente e Infraestrutura, Avenida Dr. Salvador França, 1427, 90690-000, Porto Alegre, Brazil
[4]Unidades de Investigación Anexo Museo, Facultad de Ciencias Naturales y Museo (UNLP), Avenida 60 y 122, B1900FWA, La Plata, Argentina
[5]Consejo Nacional de Investigaciones Científicas y Técnicas (CONICET), Argentina.
[6]Instituto Argentino de Nivología, Glaciología y Ciencias Ambientales (IANIGLA), CCT–CONICET–Mendoza, Avenida Ruiz Leal s/n, Parque Gral. San Martín, 5500, Mendoza, Argentina
[7]Departamento de Paleontología de Vertebrados, Museo de Historia Natural - Universidad Nacional Mayor San Marcos (UNMSM, DPV-MUSM), Avenida Arenales 1256, Lima 14, Peru
[8]BioGeoCiencias Lab, Facultad de Ciencias y Filosofía/CIDIS, Laboratorios de Investigacion y Desarrollo (LID), Centro de Investigación para el Desarrollo Integral y Sostenible (CIDIS), Universidad Peruana Cayetano Heredia, Avenida Honorio Delgado 430, Lima 31, Peru
[9]Department of Archaeology, University of Cambridge, Downing Street, CB2 3DZ, Cambridge, England.

[10]Paläontologisches Institut und Museum, Universität Zürich, Karl-Schmid-Strasse 4, 8006, Zürich, Switzerland
[11]Laboratório de Paleontologia, Campus Floresta, Universidade Federal do Acre, Estrada do Canela Fina, Km 12, 69980-000, Cruzeiro do Sul, Acre, Brazil.
[12]Instituto de Ecorregiones Andinas (INECOA), Universidad Nacional de Jujuy, CONICET, IdGyM, Avenida Bolivia 1661, 4600, San Salvador de Jujuy, Argentina

*Corresponding author. Email address: narlasstutz@gmail.com (N. Stutz).

1. Introduction

Metatheria constitutes an infraclass of Mammalia, encompassing the mammalian stem metatherians that are closer to living marsupials than to Eutheria (placental mammals), including basal taxa (stem metatherians), the Deltatheroidea and Marsupialiformes. Marsupialiformes, in turn, contains the Marsupialia (crown group, which comprehends the living marsupials) and basal metatherians closer to Marsupialia than to Deltatheroidea (Kemp, 2005; Williamson *et al*., 2014). The earliest records of metatherians are Deltatheroidea and Marsupialiformes taxa from the Aptian-Albian of North America (Bi *et al*., 2018; Beck *et al*., 2022).

It is considered that one or more lineages of North American metatherians migrated towards South America most probably in the Late Cretaceous. Several authors (e.g., Case *et al*., 2005; Forasiepi, 2009; Goin *et al*., 2016; Carneiro *et al*., 2018) have supported the hypothesis that South American metatherians are the result of successive radiations of marsupialiforms from North America, which originated in the south of this continent and then dispersed southwards. The oldest fossil record of Metatheria in South America is that of the Polydolopimorphia *Cocatherium lefipanum*, from the early Paleocene, Lefipán Formation, Argentinean Patagonia, which is also considered to be the first record of a therian mammal in South America (Goin *et al*., 2006). Subsequently, the Metatheria clade went through significant radiation and diversification processes in South America, with, for example, the origin of the closest ancestors of the Marsupialia crown-group during the Paleogene (Goin *et al*., 2016).

Currently, all living marsupials belong to the Marsupialia crown-group and are classified into seven orders and approximately 91 genera and 385 species, distributed across North America, Central America, South America, and Australasia (Mammal Diversity Database, 2022). In South America, marsupials represent approximately 10% of the terrestrial mammal fauna (Goin *et al*., 2016), being, together with bats and rodents, the main components of small mammal communities (Fonseca *et al*, 2003), counting approximately 22 genera and 134 species, belonging to three orders: i) Paucituberculata, currently represented only by the family Caenolestidae (three genera and seven species); ii) Microbiotheria, with one family, Microbiotheriidae (one genus and two species); and iii) Didelphimorphia, today consisting exclusively of the family Didelphidae (18 genera and 125 species), which comprises most of the living marsupials in South America (Mammal Diversity Database, 2022). However, this current diversity of South American marsupials does not represent the myriad of lineages that once inhabited this continent (Goin *et al*., 2016).

Among the extinct Metatheria clades that once inhabited South American lands is the order Polydolopimorphia. This order is recorded from the early Paleocene to the Pleistocene (South American Land Mammal Age – **SALMA** – Chapadmalalan) in Argentina, Brazil, Bolivia, Chile, Peru, and Antarctica, in addition to possible remains from Australia and North America (Goin *et al*., 2016; Beck, 2017). Polydolopimorphians have occupied diverse ecological niches, from frugivores and omnivores to specialized herbivores (Case *et al*., 2005; Goin *et al*., 2016). In its original conception, Polydolopimorphia included only the genus *Polydolops* and its related forms. However, numerous discoveries have allowed a greater knowledge about the polydolopimorphians and the inclusion of several taxa in this order (Goin *et al*., 2009). According to Goin *et al*. (2016), Polydolopimorphia comprises two major lineages: the suborder Bonapartheriiformes, which includes the superfamily Bonapartherioidea (families Prepidolopidae, Bonapartheriidae, Gashterniidae, and Rosendolopidae), as well as the more recent Argyrolagoidea (families Groeberiidae, Patagoniidae, and Argyrolagidae); and the suborder Polydolopiformes, with the families Sillustaniidae, which would be a basal lineage, and Polydolopidae, considered to be the most derived metatherians of the New World. In addition to these two lineages, Polydolopimorphia also includes the family Glasbiidae, which, in this classification, encompasses the two

species of the genus *Glasbius* from the Cretaceous of North America, in addition to taxa from the early Paleogene of South America (*Palangania*, *Chulpasia*, *Bobbschaefferia*, and *Periakros*). Nevertheless, according to Williamson *et al*. (2014), the relationships of *Glasbius* with South American forms should be taken cautiously. According to these authors, Glasbiidae would be restricted to the genus *Glasbius* and have as a sister group *Roberthoffstetteria*, the latter being a basal polydolopimorphian from the Tiumpampa fauna, Bolivia. Moreover, some hypotheses consider that the Argyrolagidae do not belong to Polydolopimorphia (e.g., Beck, 2017). Thus, the Polydolopimorphia monophyly and composition remain issues to still be extensively studied and discussed, with implications on the geographic and temporal distribution of the order.

Many authors (e.g., Antoine *et al*., 2016, 2017; Goin *et al*., 2016) point out that much of what is known of the fossil record of South America comes from areas located between middle and high latitudes (up to 50º N), with the regions north and south of these remaining sparsely explored, especially the tropical Amazonian portion of the South American continent. Furthermore, among the records already reported for the Amazon Region, a predominance of large eutherian mammals is observed, mainly in Pliocene and Quaternary fluvial deposits. In the last decades this started to change, with the application of collection techniques more appropriate for the discovery of small-sized remains (e.g., screen washing) (Goin *et al*., 2007a, 2016; Antoine *et al*., 2017). As far as the Metatheria fossil record is concerned, the aforementioned factors are particularly problematic, since metatherians are currently distributed mainly in tropical and subtropical areas of the continent, with, for example, 60 species of at least 14 genera of didelphids inhabiting today the Amazon Region. Besides, metatherians have been, and still are, mostly small-sized (Voss, 2022).

Thus, this work aims at partly fulfilling the gap in the knowledge of low latitude fossil metatherians, emphasizing on remains of the order Polydolopimorphia found at several localities in the Peruvian Amazonia (Contamana, Huallaga Basin and Atalaya regions), encompassing the latest middle Eocene to early Late Miocene interval. We expect to contribute for the understanding of the diversity and composition of Polydolopimorphia, further adding new taxa and new occurrences for the group.

2. Paleontological background and geological setting

The localities of Contamana (Loreto Department), Huallaga Basin (San Martín Department) and Atalaya (Ucayali Department) are located in Peruvian Amazonia (Figure 1). The studied deposits that yielded the Polydolopimorphia remains are part of the Northern Amazonian foreland basin system, which spans the Paleocene–Pliocene interval (Roddaz *et al*., 2010; Wanderley-Filho *et al*., 2010).



Figure 1. Map showing the location of the regions of the studied outcrops in the Peruvian Amazonia (bold), as well as other significant fossiliferous localities in the Western Amazon.

2.1 Contamana region

The Contamana region is located in the Ucayali River basin, northwest of the Fitzcarrald Arch. Northwest-southeast structural folds caused by Andean tectonics are present in the area, which allow access to a thick stratigraphic section with a long and continuous sedimentary record from the Jurassic to the Holocene. In total, at least 34 fossil localities have been identified in the region, which were named **CTA** (after

Contamana), followed by a number according to the order they were found. Numerous fossil remains were found in the Contamana region outcrops, such as mollusks, arthropods (ostracods and crustaceans), microorganisms (foraminifera, porifera, algae, dinoflagellates), plants (palynomorphs, carophytes, seeds, fruits, and silicified wood), as well as vertebrates such as fishes, amphibians, reptiles, and mammals. Antoine *et al*. (2016) presented an extensive study of the geological and paleontological aspects of outcrops in the Contamana region.

The fossil remains of metatherians belonging to the order Polydolopimorphia were found in the following localities in the Contamana region: CTA-27, CTA-29, CTA-43, CTA-47, CTA-51, and CTA-66 (Table 1; Figures 2, 3 and 4).

Table 1. Outcrops from the Contamana region, Peru, containing fossil remains of metatherians of the order Polydolopimorphia.

Locality	Coordinates	Age	Geological Formation	Depositional environment
CTA-43	07º36.497'S 74º95.793'W	early Late Miocene	Pebas	Tidal interface
CTA-66	07º34.876'S 74º95.431'W	late middle Eocene	Pozo, Lower Member	Fluvial
CTA-29	07º32.859'S 74º94.556'W	late middle Eocene	Pozo, Lower Member	Fluvial
CTA-27	07º33.011'S 74º94.733'W	late middle Eocene	Pozo, Lower Member	Fluvial
CTA-51	07º32.948'S 74º94.92'W	late middle Eocene	Pozo, Lower Member	Fluvial
CTA-47	07º33.113'S 74º95.127'W	middle Eocene	Pozo, Lower Member	Fluvial with marine influence

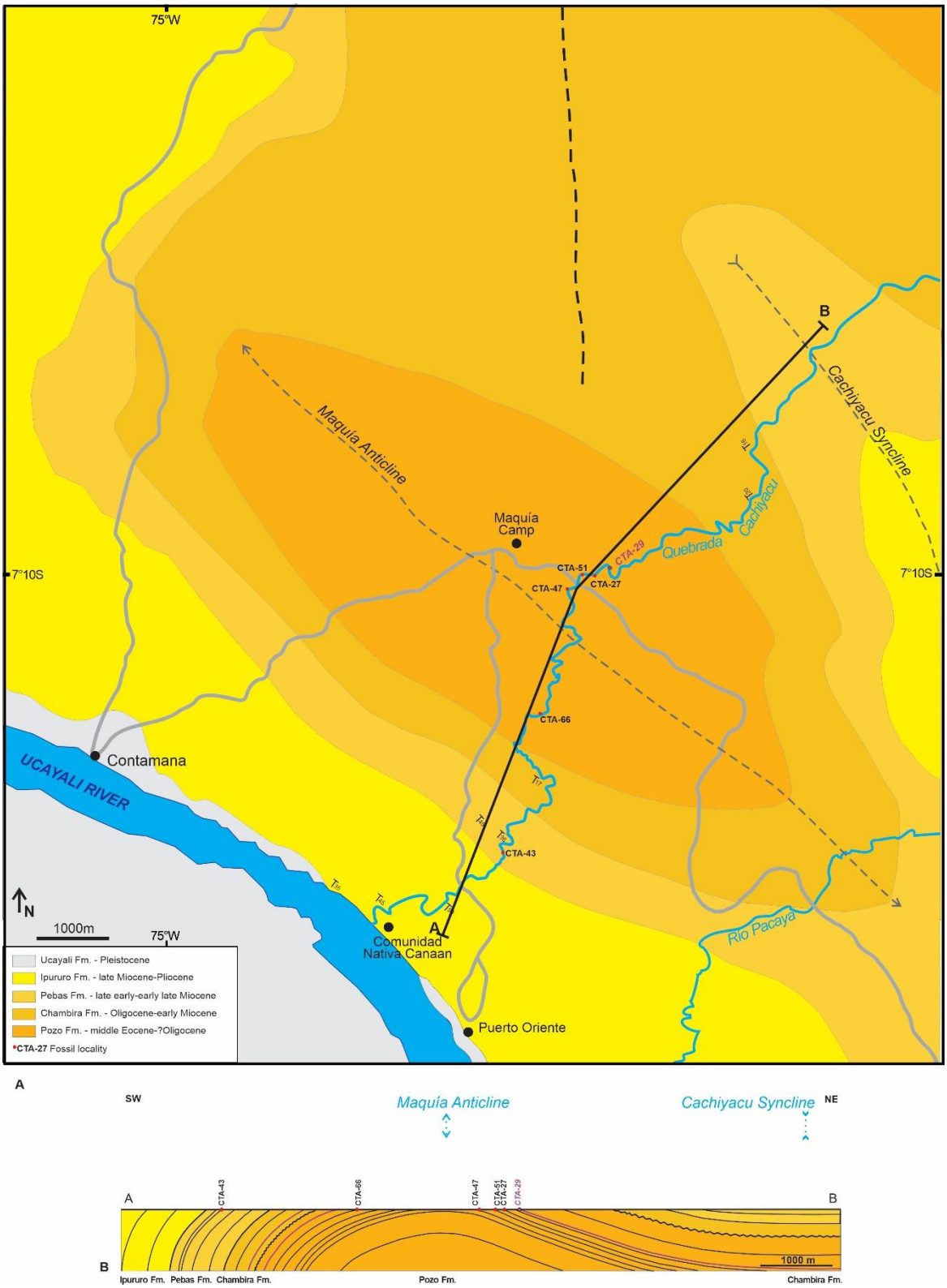


Figure 2. Geological map of the Contamana region showing the location of the outcrops where fossil remains of Metatheria of the order Polydolopimorphia have been found. Modified from Antoine *et al*. (2016).

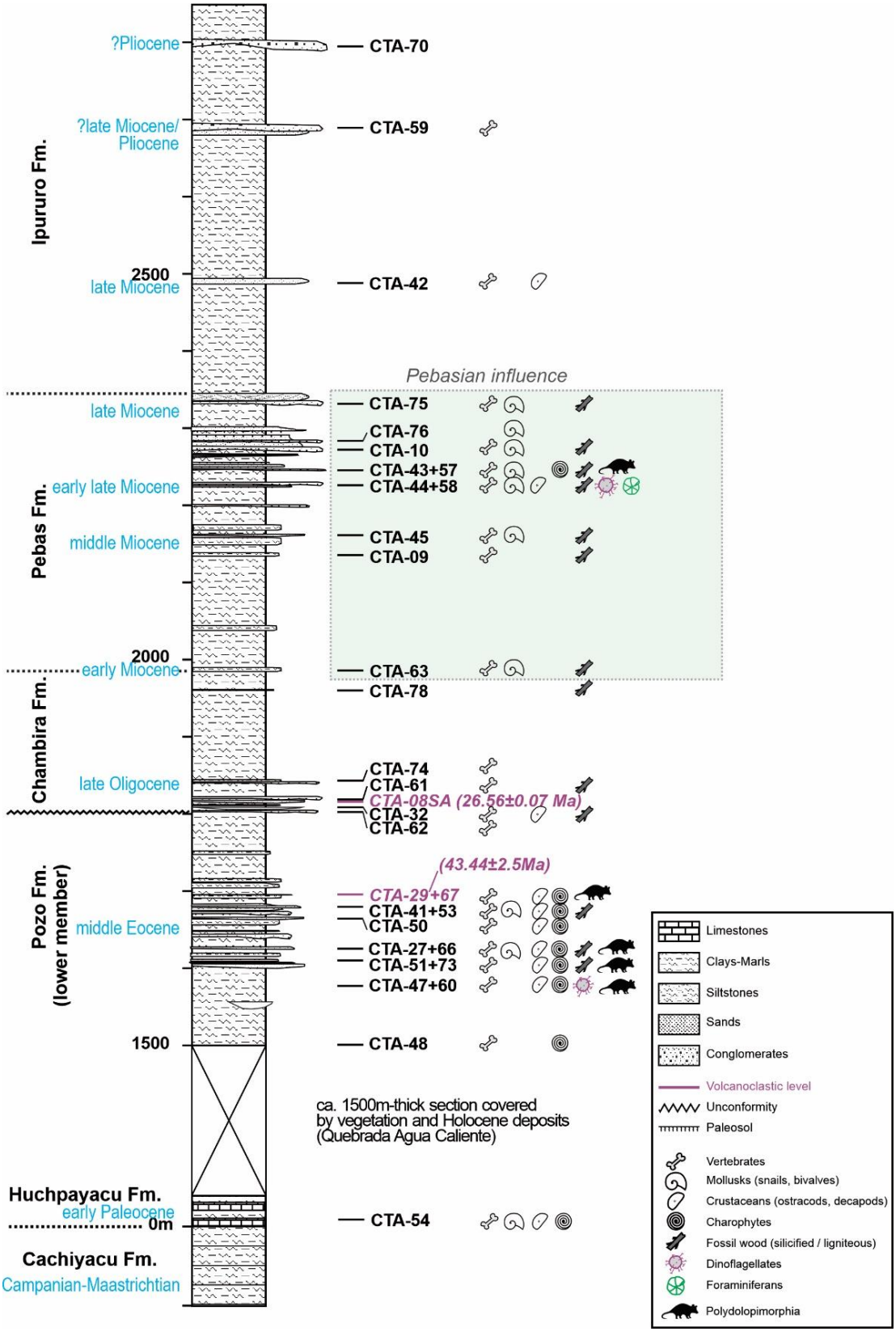


Figure 3. Synthetic stratigraphic section of the Cenozoic deposits in the Contamana region, Peru, with the indication of the outcrops where remains of metatherians of the order Polydolopimorphia were retrieved. Modified from Antoine *et al*. (2016).



Figure 4. Outcrops in the Contamana region, Peru, that yielded fossil remains of metatherians of the order Polydolopimorphia. Pozo Formation, Lower Member, late middle Eocene: **A**, CTA-51; **B**, CTA-29; **C**, CTA-66; **E**, CTA-27; **F**, CTA-47. Pebas Formation, early late Miocene: **D**, CTA-43.

2.2 Huallaga Basin

The outcrops that were surveyed in region of the Huallaga Basin are located in the sub-Andean zone of the Huallaga River. From Tarapoto (capital of the San Martín Department) heading southwards, the sites are located in roadcuts and along the banks of the Huallaga and Mayo rivers, in the vicinity of the towns/villages of Shapaja, Machungo, Juanjui, and Balsayacu. The region was prospected annually between 2012 and 2019. A total of 77 fossiliferous outcrops were recognized, which were named **TAR** (from Tarapoto), followed by a number according to the order in which they were found. The Yahuarango, Chambira, Pozo and Ipururo formations are outcropping in the region, with approximate ages ranging from the Late Cretaceous (Maastrichtian) to the Late Miocene. The Polydolopimorphia remains were found in 14 localities in the Huallaga Basin region: TAR-01, TAR-14, TAR-20, TAR-21, TAR-44, TAR-45, TAR-47, TAR-55, TAR-56, TAR-72, TAR-74, and TAR-76 (Table 2). These localities can be divided according to the stratigraphic section where they are located: Balsayacu (Figures 5, 6 and 7), Juanjui (Figures 5 and 8), Shapaja and Abra de Machungo.

Rodent remains from the Juanjui and Balsayacu Paleogene sections (Figure 5, Juanjui: TAR-45, 46 and 47; Balsayacu: TAR-55/TAR-55bis and TAR-56) were studied in detail, with the description of 11 taxa for the middle Eocene to early Oligocene interval (Assemat *et al*., 2019), which would have an intermediate morphology between the fossils described for the oldest outcrops of Contamana (e.g., CTA-27) and those from the Shapaja section (Boivin *et al*., 2018) and Santa Rosa (Frailey & Campbell, 2004). Plus, recently, Boivin *et al*. (2021) reported four additional caviomorph rodent taxa for the Balsayacu section (TAR-55/TAR-55bis, TAR-76, and TAR-77), which suggest that these localities would be somewhat more recent than CTA-27 and older than the Shapaja section.

Table 2. Localities in the Huallaga Basin, Peru, which yielded remains of metatherians of the order Polydolopimorphia.

Locality	Coordinates	Stratigraphic section	Age	Geological Formation	Description
TAR-14	06º42.520'S 76º17.336'W	Abra de Machungo	late Oligocene	Chambira	Red siltites
TAR-01	06º34.902'S 76º16.903'W	Shapaja	earliest Oligocene	Pozo, Upper Member	Blue clays with calcareous nodules
TAR-21	06°34.982'S 76°16.886'W	Shapaja	latest late Eocene	Pozo, Upper Member	Blue/yellowish conglomerate rich in gypsum and nodules, interspersed with coarse-grained sandstone channels and floodplain deposits
TAR-72	06°34.986'S 76°16.887'W	Shapaja	latest Eocene	Pozo, Upper Member	Yellow-bluish microconglomerate with gypsum and clay
TAR-20	06°34.901'S 76°16.783'W	Shapaja	late Eocene	Pozo, Upper Member	Yellow-greenish microconglomerate with gypsum and plant remains
TAR-74	06°34.910'S 76°16.723'W	Shapaja	late Eocene	Pozo, Upper Member	Blue to yellowish, nodule-rich, unconsolidated conglomerate below coarse-grained beige sandstone channels, with oxidized fragments of leaves
TAR-47	07°12.840'S 76°44.412'W	Juanjui	?late Eocene	Pozo, Lower Member	Greenish clays rich in nodules
TAR-45	07°13.067'S 76°44.550'W	Juanjui	middle-late Eocene	Pozo, Lower Member	Blue laminated nodule-rich siltstones
TAR-44	07°13.067'S 76°44.577'W	Juanjui	middle-late Eocene	Pozo, Lower Member	Blue nodule-rich clays with fish remains
TAR-55	07°25.809'S 76°39.804'W	Balsayacu	late middle Eocene	Pozo, Lower Member	Brown, nodule-rich microconglomerate
TAR-76	07°25.807'S 76°39.756'W	Balsayacu	late middle Eocene	Pozo, Lower Member	Blue-gray microconglomerate with fragments of crabs and wood
TAR-56	07°25.675'S 76°39.806'W	Balsayacu	?middle Eocene	Pozo, Lower Member	Bluish nodule-rich microconglomerate below a sandstone channel

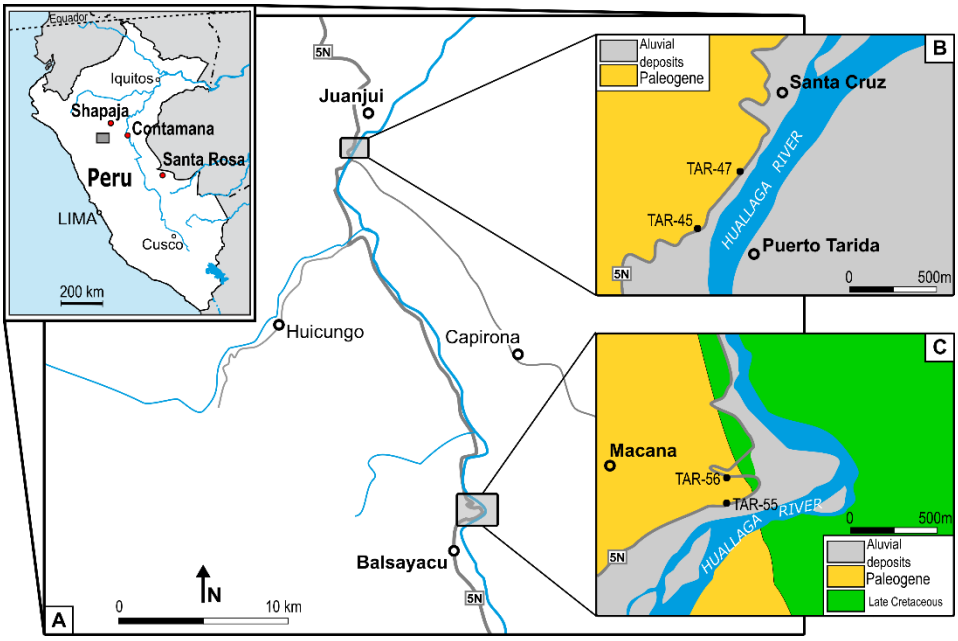


Figure 5. A, map showing the location of the stratigraphic Paleogene sections of Juanjui and Balsayacu, which are close to the cities of Juanjui and Balsayacu, Peru, respectively. **B–C**, maps zooming in the location of the outcrops of the Juanjui and Balsayacu stratigraphic sections, Huallaga Basin, Peru.

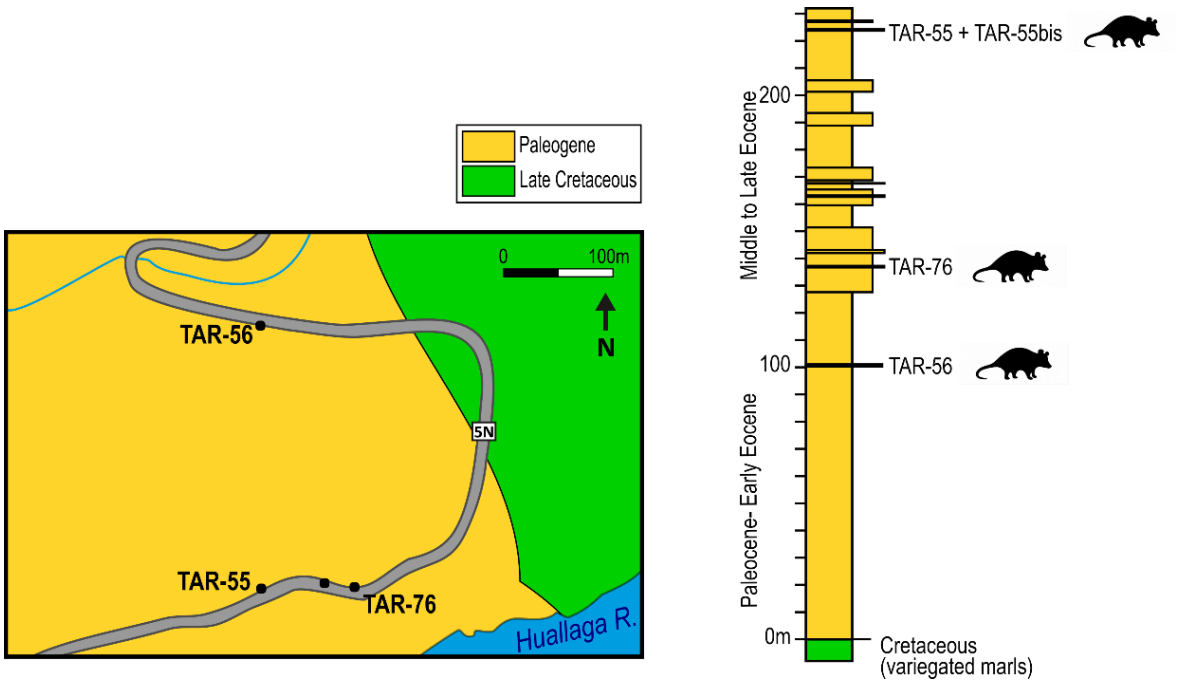


Figure 6. On the left, map of the location of the Balsayacu Paleogene stratigraphic section, Peru, indicating the outcrops where the remains of metatherians of the order Polydolopimorphia were found. On the right, synthetic stratigraphic section of the Basayacu outcrops, with the indication of the ones that yielded the polydolopimorphian remains.

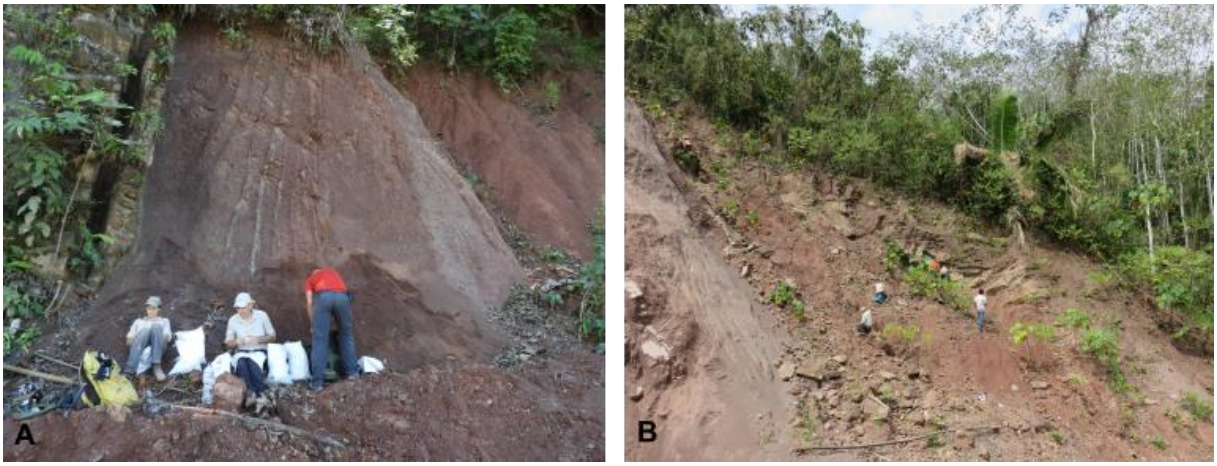


Figure 7. Localities **A**, TAR-55 and **B**, TAR-56, Balsayacu Paleogene stratigraphic section, Huallaga Basin, Peru.



Figure 8. Localities **A**, TAR-44 and **B**, TAR-45, Juanjui Paleogene stratigraphic section, Huallaga Basin, Peru.

The Shapaja section is located near the town of Shapaja, 12 km southeast of Tarapoto, above the confluence of the Mayo and Huallaga rivers (Figures 9, 10, and 11). In total, it yields nine fossiliferous levels distributed successively in the sequence, and polydolopimorphian remains were found in the levels TAR-74, TAR-20, TAR-72,

TAR-21 and TAR-01. It was possible to observe in part of the levels of the section indications of marine influence (shallow marine/seaboard environment with strong tidal influence), with a gradual change from a tidally influenced environment to fluvial and floodplain deposits. The fossiliferous content present in the Shapaja section deposits includes plants (silicified wood, leaves, fruits, seeds, palynomorphs, carophytes), gastropods, crabs, chondrichthyans, osteichthyans, anurans, chelonians, lizards, crocodilomorphs, and mammals (including, in addition to metatherians, xenarthans, South American native ungulates, chiropterans, primates, and caviomorph rodents) (Klaus *et al*., 2017; Boivin *et al*., 2018; Antoine *et al*., 2021). Among the caviomorph rodents, 17 taxa were recorded for the Shapaja stratigraphic section (TAR-21, TAR-13, TAR-22 and TAR-24), with the superfamilies Erethizontoidea, Octodontoidea and Chinchilloidea (Boivin *et al*., 2018). Metatheria remains from the Shapaja section were preliminarily identified, with the record of 19 taxa (Antoine *et al*., 2021). According to chemostratigraphic analyses carried out on samples from the different levels of the Shapaja section, it most likely records the interval between the late Eocene and early Oligocene, being i) TAR-20, TAR-72 and TAR-74 late Eocene; ii) TAR-21 at the beginning of the Eocene-Oligocene transition (latest late Eocene); iii) TAR-22, TAR-13, TAR-73 and TAR-01 would be early Oligocene (Figure 12). Such time intervals coincide with marked changes in the composition of the fossil assemblages of the Shapaja Section (Antoine *et al*., 2021).

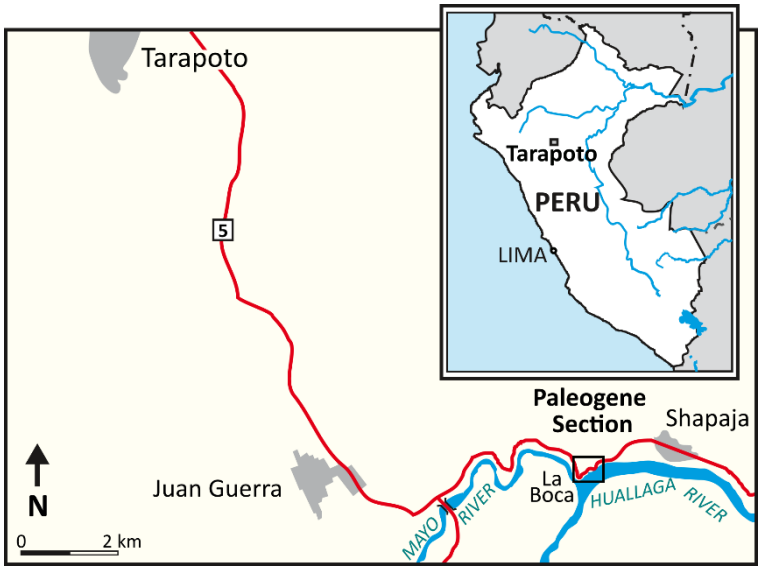


Figure 9. Location map of the cities of Tarapoto and Shapaja, with the indication of the location of the Shapaja Paleogene stratigraphic section, Huallaga Basin, Peru.

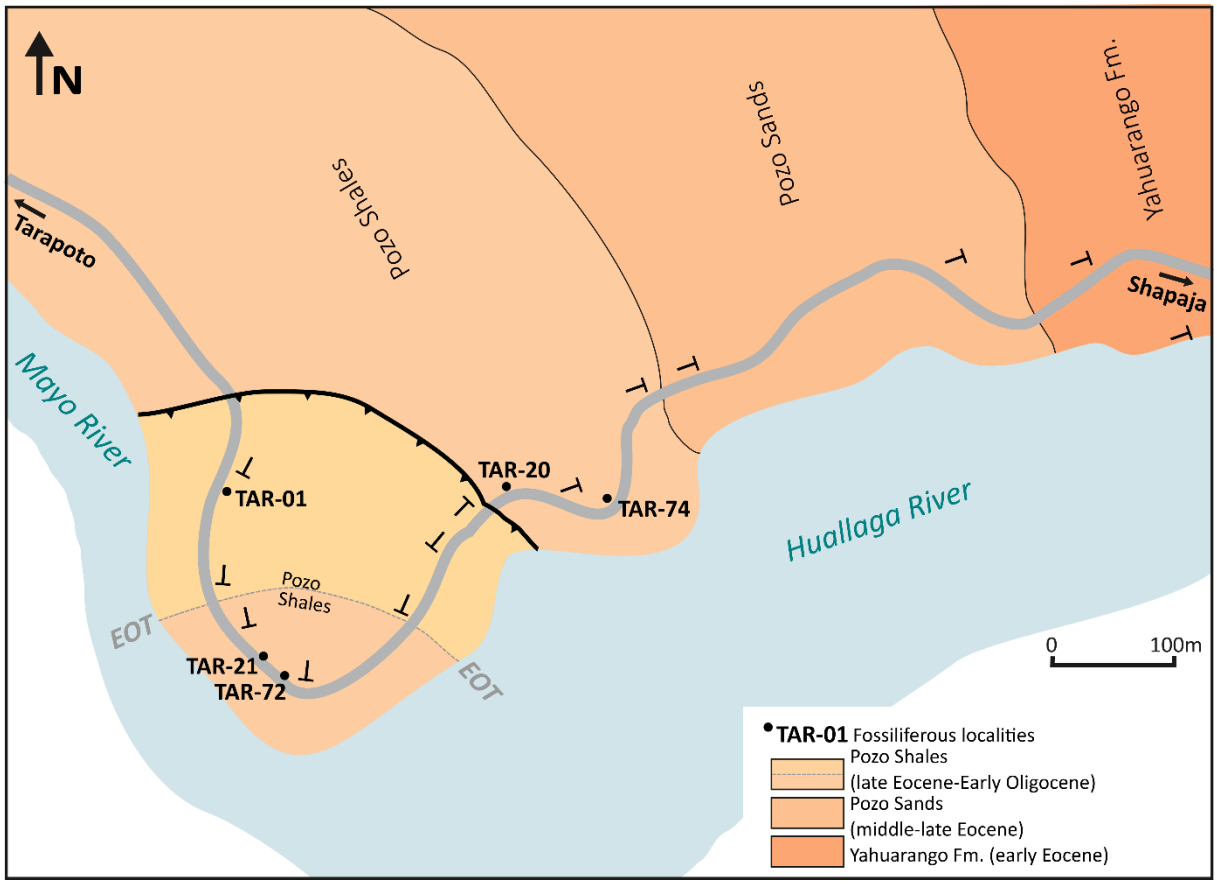


Figure 10. Location map of the outcrops of the Shapaja Paleogene stratigraphic section, Peru, that yielded fossil remains of metatherians of the order Polydolopimorphia.

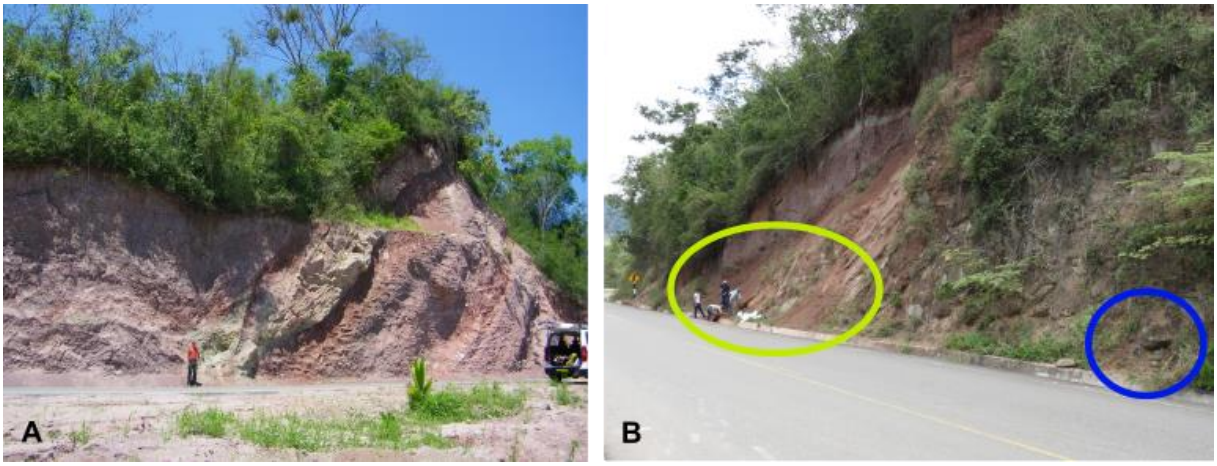


Figure 11. Localities **A**, TAR-01 and **B**, TAR-21, yellow circle and TAR-72, blue circle, Shapaja Paleogene stratigraphic section, Huallaga Basin, Peru.

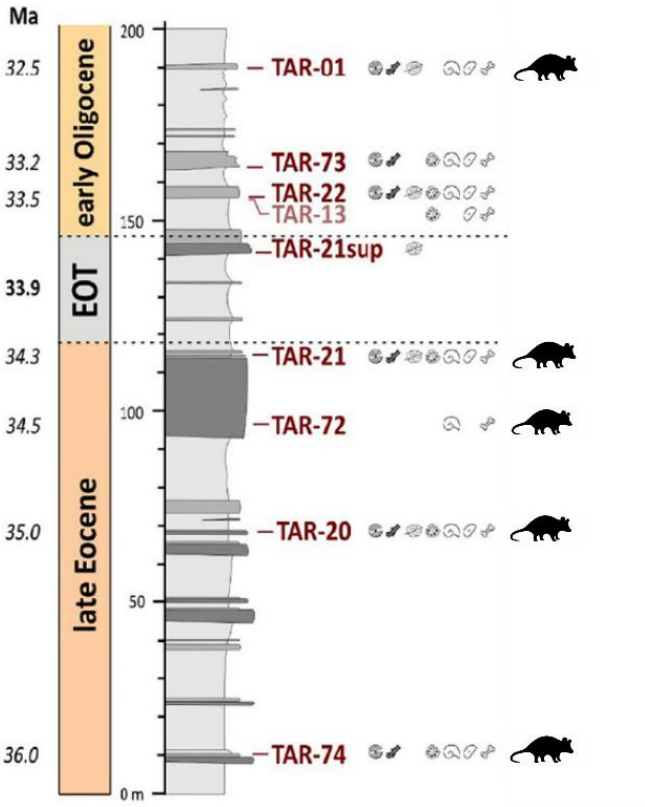


Figure 12. Synthetic stratigraphic section of the Shapaja Paleogene outcrops, Peru, with the indication of the ones that yielded fossil remains of metatherians of the order Polydolopimorphia. Modified Antoine *et al*. (2021).

The comparison between the different sections present in the Huallaga Basin (Balsayacu, Juanjui and Shapaja), the outcrops of the Pozo Formation in the Contamana region and the Santa Rosa local fauna (Campbell, 2004), based on their fossiliferous content and available radiosotopic datings, allows for considering some temporal overlap between these localities, with the late middle Eocene being represented in Contamana, Balsayacu and Juanjui, while the late Eocene would be present in the outcrops of the Juanjui and Shapaja sections. The early Oligocene is observed in the Juanjui, Shapaja and Santa Rosa sections (Figure 13).

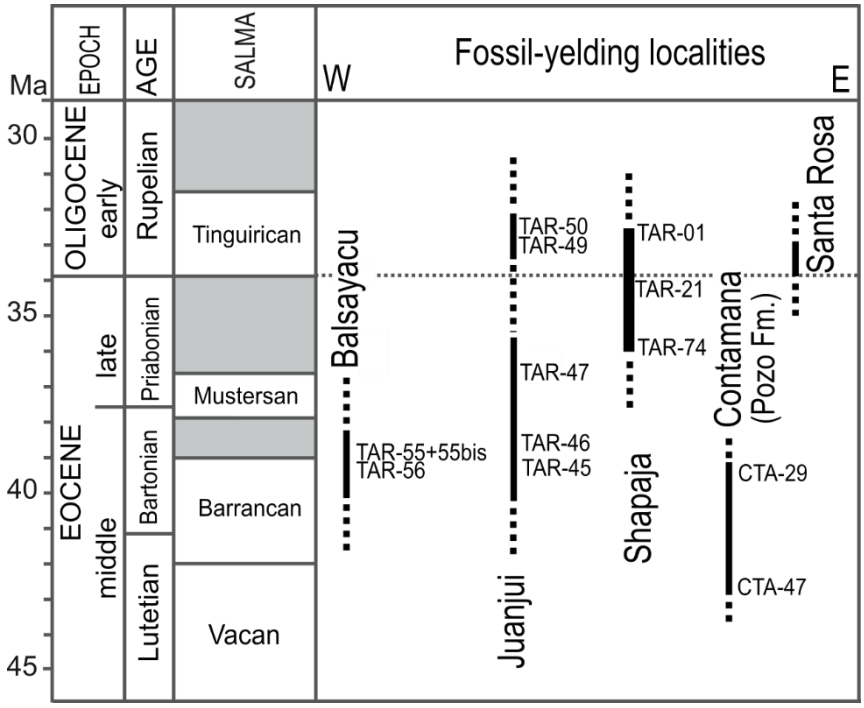


Figure 13. Suggested temporal correlations between the Shapaja, Balsayacu and Juanjui stratigraphic sections, in comparison with the main Paleogene faunas already described for the Amazon Region. Abbreviations: E, east; Ma, millions of years ago; W, west; SALMA, South American Land Mammal Age. Modified from Assemat *et al*. (2019)

The locality TAR-14 (Figure 14) is the only one located in the Abra de Machungo stratigraphic section where remains of Polydolopimorphia metatherians were found. It consists of an outcrop of the Chambira Formation, late Oligocene (Deseadean). It is located 50 cm from a sandstone containing detrital zircons dated by the U-Pb method as 25.67 ± 0.64 Ma (Martin Roddaz, pers. comm.). Remains of crustaceans, chelonians, South American native ungulates (a new uruguaytheriine astrapotheriid and a representative of the notoungulate *Taubatherium*), and rodents were also found in this outcrop.

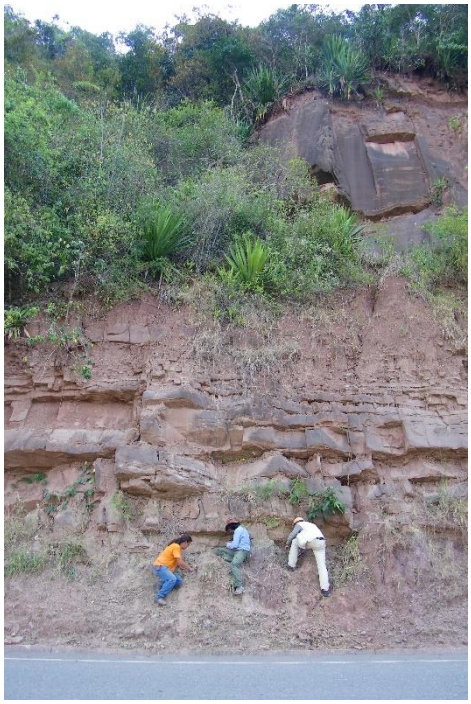


Figure 14. Locality TAR-14, Chambira Formation, Huallaga Basin, Peru.

2.3 Atalaya region

Regarding the Atalaya region, fieldwork has so far been preliminary, with a single fieldtrip carried out for recognition of the area in 2017. Fourteen fossiliferous outcrops were found, four along the Tambo River (named **TMB**, followed by number according to the order of their discovery) and 10 along the Urubamba River (named **URU**, followed by a number according to the order of their discovery). Metatherian fossils were found in two outcrops in Atalaya: TMB-01 and URU-210 (Figure 15). The locality TMB-01 (10°45.488'S 73°45.143'W) consists of red-blue clays with channel structures and plurimillimetric calcareous nodules and is an outcrop of the Upper Member (shales) of the Pozo Formation, late Eocene in age, with a depositional environment interpreted to be fluvial-littoral. Fossil remains of Characiform fish, amphibians, chelonians, crocodilomorphs, xenarthrans, South American native ungulates and rodents, among others, were also found in this locality. The locality URU-210 (10°41.661'S 73°47.490'W) is a brown microconglomerate with clay pebbles and leaf fragments, constituting an outcrop of the Chambira Formation, of Eocene-Oligocene

age, where fossil remains of crustaceans, actinopterygian fish, chelonians, crocodilomorphs, rodents, and others have been found.



Figure 15. Outcrops in the Atalaya region, Peru, where fossil remains of metatherians of the order Polydolopimorphia were found: **A**, TMB-01, Pozo Formation; **B**, URU-210, Chambira Formation.

3. Material and Methods

The studied material consists of a total of 276 Polydolopimorphia remains, being 171 from the localities of Contamana (Table 3), 100 specimens from the localities of the Huallaga Basin (Table 4), and five specimens from Atalaya (four from TMB-01 and one from URU-210). All the specimens are deposited in the collection of the Museo de Historia Natural, Universidad Nacional Mayor de San Marcos, Lima, Peru (**MUSM**).

Table 3. The amount of remains of Polydolopimorphia metatherians retrieved in each locality in the Contamana region, Peru, with the suggested ages of the outcrops.

Locality	Age	Polydolopimorphia remains
CTA-43	early Late Miocene	1
CTA-66	late middle Eocene	1
CTA-29	late middle Eocene	13
CTA-27	late middle Eocene	149
CTA-51	late middle Eocene	4
CTA-47	middle Eocene	3

The fossil remains were collected by the wet screening of sediments from previously-recognized fossiliferous layers, mainly microconglomerate lenses. This method allows for a more efficient collection of small-sized remains of microvertebrates, arthropods, mollusks and carophytes, among others, by washing the sediments using 2, 1 and 0.7 mm sieves, followed by fossil hand-picking (with and without the use of a stereomicroscope) of the sieves' residues. The amount of sediment collected at each site ranged from 200 g (for preliminary tests) to 850 kg.

Table 4. The amount of remains of Polydolopimorphia metatherians retrieved in each locality in the Huallaga Basin region, Peru, with the suggested ages of the outcrops.

Locality	Age	Polydolopimorphia remains
TAR-14	late Oligocene	2
TAR-01	early Oligocene	2
TAR-21	latest late Eocene	46
TAR-72	late Eocene	2
TAR-20	late Eocene	3
TAR-74	late Eocene	1
TAR-47	?late Eocene	9
TAR-45	middle-late Eocene	1
TAR-44	middle-late Eocene	2
TAR-55	middle late Eocene	29
TAR-76	middle late Eocene	2
TAR-56	?middle Eocene	1

The fossils were then cleaned, with the help of brushes and needles, and, if necessary, consolidated and/or glued with superglue. The remains were then analyzed under a stereomicroscope, in order to describe and taxonomically identify them. Identification of the remains was made by comparison with specimens deposited in scientific collections (e.g., **MLP**, Departamento Paleontología Vertebrados, Museo de La Plata, La Plata, Argentina; MUSM) and with specialized litterature (e.g., Pascual, 1980a, b; Goin *et al*., 1998; Goin & Candela, 2004; Chornogubsky *et al*., 2019). The

nomenclature of the dental structures, as well as Metatheria systematics follow, in general, Goin *et al*. (2016), except for certain groups, in which the reference used is marked. The nomenclature of the cranial structures follows Beck (2017). Measurements of the materials were made with a Nikon Measurescope 10 measuring microscope connected to a Nikon SC 112 monitor.

After the identification and description of the specimens, some representatives of each recognized taxon were selected to be photographed and/or scanned. The photographs were made at the scanning electron microscope (**SEM**) Hitachi S4000 of the *Institut des Neurosciences de Montpellier* (**INM**) and the scans on the EasyTom 150 multiscale multiresolution RX microtomograph, which has a 40-150 kV RX source and resolution up to 5µm, of the *Montpellier RIO Imaging* (**MRI**), *Institut des Sciences de l'Évolution de Montpellier*, Montpellier, France. The scanned specimens were virtually prepared by manual segmentation using AVIZO 7.1 software (Visualization Sciences Group).

Anatomical abbreviations

C, upper canine; **c**, lower canine; **D/d**, deciduous; **L**, length; **M**, upper molar; **m**, lower molar; **P**, upper premolar; **p**, lower premolar; **StA-D**, stylar cusps A to D (from anterior to posterior); **tal**, talonid; **tri**, trigonid; **W**, width.

4. Systematic Paleontology

Order Polydolopimorphia Archer, 1984

Indet.

Referred material. TAR-56: MUSM 4026, one left P3. TAR-20: MUSM 4061, one right p2. TAR-72: MUSM 4073, one right P3. TAR-01: MUSM 4119, one left P3. CTA-51: MUSM 4126, one left p3.

Locality. Contamana region, Loreto Department, Peru: CTA-51, Pozo Formation, Lower Member, late middle Eocene. Huallaga Basin, San Martín Department, Peru: TAR-56, Balsayacu Paleoegene section, Pozo Formation, Lower Member, ?middle

Eocene; TAR-20, TAR-72 and TAR-01, Shapaja section, Pozo Formation, Upper Member, late Eocene to earliest Oligocene.

Description and comments. MUSM 4026 is a medium-sized plagiaulacoid P3 with a relatively high crown and two roots. Its base is wide, much more than the ventral portion. The occlusal surface is worn, but three cusps can be observed, one anterior, which is slightly higher than the two posterior ones (one labial and one lingual, the labial one being higher than the lingual one). There are marked sulci separating the anterior cusp from the posterior ones, both on the labial and on the lingual surfaces of the tooth. On the lingual side this sulcus is deeper and wider. Below the posterior lingual cusp there is a platform-like structure, which could be a posterior lingual cingulid.

MUSM 4073 is a small and very worn plagiaulacoid P3, with two roots. Its occlusal surface is almost flat due to the wear. But it is still possible to observe a separation of the anterior portion from the posterior one, through shallow sulci on the labial and lingual surfaces. The anterior portion is wider than the posterior one.

MUSM 4119 is also a plagiaulacoid P3, with two roots, being slightly larger than MUSM 4026 and much larger than MUSM 4073. It resembles morphologically MUSM 4026, but it is less worn. The anteriormost portion is marked by a high cusp followed by a much smaller cusp on the labial side. Deep sulci on the labial and lingual surfaces of the tooth separate this anterior portion form the posterior one, the lingual sulcus being deeper and wider. Two low but long cusps are present on the posterior portion, as well as a subtle hypoconule. There is a platform-like structure below the posterior lingual cusp, but it is less-developed than in MUSM 4026.

MUSM 4126 is a medium-sized worn p3, with only the anterior root preserved. Compared to the aforementioned P3s, it much wider and has a lower crown. It has an ovoid shape, and, on the occlusal surface, an anterior cuspid, followed by a long crest, without serrated margins, going almost until the posterior margin of the tooth. The labial surface is lingually inclined and much less curved than the lingual surface. The lingual surface is marked by two sulci, one anterior, which starts at the base of the anterior cuspid and goes dorsally until the base of the tooth, and one posterior, shallower, going from the base of the molar until the posterior portion of the occlusal cristid.

MUSM 4061 is a medium-sized simplified p2, with a low crown, its roots are not preserved. It is long and narrow, with a crest-like structure running through the anteriormost portion of the tooth until almost its posterior margin. This crest-like structure is closer to the labial surface of the tooth.

Lower and upper premolars are teeth that do not possess many diagnostic features. Compared to the literature (e.g., Pascual, 1980a; b; Beck, 2017), the specimens cited above do resemble Polydolopimorphia premolars. However, even among the Polydolopimorphia, a very similar morphology of the premolars is shared between the two suborders Bonapartheriiformes and Polydolopiformes. Also, other metatherian clades, such as paucituberculatans, possess premolars that resemble morphologically the ones of polydolopimorphians. Thus, we preferred to assign these specimens to Polydolopimorphia indet, pending a detailed analysis on Polydolopimorphia premolars to clarify their diagnostic characteristics.

Measurements. MUSM 4026, left P3, L = 1.625; W = 1.3605.

Family Indeterminate

Wamradolops Goin & Candela, 2004

Wamradolops tsullodon Goin & Candela, 2004

(Figures 16 and 17)

Referred material. TAR-55: MUSM 4030, one left maxillary with M1–M2; MUSM 4031, one right P3; MUSM 4032, one right dentary with m1–m2; MUSM 4033, one right p3; MUSM 4034, one right m2; MUSM 4035, one left dentary with m2. TAR-14: MUSM 4120, one left m2. URU-210: MUSM 4122, one right maxillary with M1–M2. CTA-47: MUSM 4123, one left M3; MUSM, 4124, one right m1; MUSM 4125, one right m2. CTA-51: MUSM 4127, one right dentary with m2. CTA-29: MUSM 4130, 4131, 4132, three right maxillaries with P3; MUSM 4133, one left maxillary with P3–M1; MUSM 4134, one left M1; MUSM 4135, one right M2; MUSM 4136, one right dentary with p3–m3; MUSM 4137, one right dentary with root fragments of two molars; MUSM 4138, one left dentary with p3; MUSM 4139, one left m1; MUSM 4140, 4141, two left m2. CTA-66: MUSM 4142, one left P3. CTA-27: MUSM 4179, one partial skull; MUSM 4180, one right maxillary with P3–M1; MUSM 4181, one right maxillary with M2; MUSM 4182,

4183, two right P3; MUSM 4184, 4185, 4186, three left P3; MUSM 4187, 4188, 4189, 4190, 4191, 4192, 4193, seven right M1; MUSM 4194, 4195, 4196, 4197, four left M1; MUSM 4198, 4199, 4200, 4201, 4202, five right M2; MUSM 4203, 4204, 4205, 4206, 4207, 4208, six left M2; MUSM 4209, 4210, 4211, 4212, 4213, 4214, six right M3; MUSM 4215, 4216, 4217, 4218, four left M3; MUSM 4219, one right dentary with p3–m2; MUSM 4220, one right dentary with m1–2; MUSM 4221, one right dentary with p3–m2; MUSM 4222, one left dentary with p3; MUSM 4223, 4224, 4225, three left dentaries without teeth; MUSM 4226, 4227, two right p2; MUSM 4228, 4229, 4230, 4231, 4232, 4233, 4234, seven right p3; MUSM 4233, 4234, 4235, 4236, 4237, 4238, 4239, 4240, 4241, 4242, 4243, 4244, 4245, 13 left p3; MUSM 4246, 4247, 4248, 4249, 4250, 4251, 4252, 4253, eight right m1; MUSM 4254, 4255, 4256, 4257, 4258, 4259, 4260, 4261, eight left m1; MUSM 4262, 4263, 4264, 4265, 4266, 4267, eight right m2. Without collection numbers: CTA-27: nine left m2; three right m3; three left m3; TMB-01: one right dentary with m1–2; one left m1; one left m2.

Geographic and stratigraphic distribution. Santa Rosa, early Oligocene, Peru and from this work: i) Contamana region, Peru, CTA-47, middle Eocene (Barrancan); CTA-27 late middle Eocene (early Barrancan, ~41.6-40.94 Ma); CTA-51, CTA-66 and CTA-29, late middle Eocene (early Barrancan), Pozo Formation, Lower Member; ii) Huallaga Basin, Peru: TAR-55, Balsayacu Paleogene section, San Martín Department, Pozo Formation, Lower Member, late middle Eocene; TAR-14, Abra de Machungo, San Martín Department, Chambira Formation, late Oligocene (Deseadan SALMA); iii) Atalaya region, Peru: URU-210, Atalaya, Ucayali Department, Chambira Formation, ?Eocene-Oligocene; TMB-01, Atalaya, Ucayali Department, Pozo Formation, Upper Member, late Eocene (Mustersan SALMA?).

Description. MUSM 4179 is a partial cranium without the associated dentaries. It probably belonged to an adult individual, since all teeth are erupted, and sutures are not visible. MUSM 4179 is laterally compressed, with its right side dislocated antero-dorsally, the nasals ventrally displaced, and the posterior portion of the right maxillary also ventrally displaced. It is very small and has a short rostrum. Some fragments of teeth and bone are *ex situ* and concentrated in a portion next to the anterior left teeth, attached among themselves and to the cranium by sediment. Only the anterior portion of the cranium is preserved, with parts of the premaxillaries, most of the maxillaries

and most of the nasals, but these are broken mainly on the right side. The anteriormost portion of the cranium is missing, as are the jugals, palatines and the complete postero-ventral portion of the cranium. Some bone fragments on the dorsal view could be parts of the frontals, but these are largely missing. The infraorbital foramen is quite large. The anterior portion of the right maxillary is slightly displaced anteriorly (infraorbital foramen farther forward). The left maxillary and pre-maxillary are close to their anatomical position, slightly displaced dorsally. In ventral view, the palate is not visible, since the medio-lateral crushing changed the position of the bones and dislocated the palate. Maxillary foramen not in its anatomical position due to its dorsal exposure. There is a foramen-like structure at the P3-M1 intersection, what could be a foramen or the exposure on the orbital floor of some tooth root. The zygomatic arches are not entirely preserved, represented only by their anterior root on left and right sides. The anterior root of the zygomatic arches is broad dorsoventrally, like in *Proargyrolagus* and *Epidolops* and more than in *Bonapartherium*. The lacrimals are not visible, in the left side, in the place where it should be, there is a hole, much like the one that would be left by a bite. Antorbital vacuities are not visible since this portion of the cranium is broken. The orbital region is not entirely preserved, but from the orbital region of the maxillaries, which are broad dorso-ventrally and medio-laterally and orientated laterally, we could say that the individual had relatively big lateral orbits (and eye sockets). The orbital rim is visible in its antero-inferior portion, composed by the maxilla. It is quite large and developed, laterally displaced (eyes would be more lateral and not so much in front of the cranium). The roots of the teeth, especially the molars, end up protruding on the surface of the orbital rim, which does not have a thick lower wall, indicating that the eyes were probably large. The maxillo-jugal suture is significantly oblique. The labio-lingual thickness of the maxilla starts from P2, but mainly from P3. The auditory region is not preserved. On the left side, I4-M3 are preserved completely, the M4 is missing and the I1-I3 are broken. On the right side the P2-M4 are preserved, while the biradiculate C1 is broken, with only its roots visible. A big incisor, resembling the left I1, is preserved in the central accumulation of bone+teeth+sediments. Dental formula: 4I (being the I1 very big and gliriform) + 1C (not caniniform, with two roots) + 2P (being P2 very small and P3 very big) + 4M (being M4 very atrophied).

The comparative description of MUSM 4179 is as it follows:

On dorsal view: the pre-maxillaries are broken on the right side. On the left side the posterior portion of the pre-maxillaries is visible, with the pre-maxillary-maxillary suture slightly visible. The nasals are crushed in the middle of the specimen, slightly displaced to the right. The sutures between them and the nasals-maxillary sutures are full of sediment. The anterior portion of the nasals are missing, mainly on the right side. The posterior portion is also missing, also mostly on the right side. As their posterior portion is mostly broken, it is difficult to analyze their morphology and sutures. However, we can say that they extend at least to the level of the posterior portion of P2/anterior portion of the P3 and that they seem to be wider in their posterior portion, not as much as in *Proargyrolagus*, but more than in *Bonapartherium*. The maxilla-frontal suture is oblique, with a latero-posterior direction, similar to *Bonapartherium*. The frontals are situated posteriorly to the nasals, presented as some bone fragments, mainly on the left side, but it is difficult to distinguish their morphology and the sutures. There is contact between the frontals and the maxillaries. The maxillaries are visible both on the right and left side, as well as their dorsomedial portion, the internal part of the maxillary portion of the zygomatic arch. Maxillary-nasal suture is visible mostly on the left side (on the right side it looks sunken and full of sediment), appearing straight and practically parallel to the anteroposterior axis of the skull. Infraorbital foramen visible, just before the suture with the pre-maxillary on the left side, slightly posterior and dorsal to the diastema between P2-C1. On the right side, the infraorbital foramen is totally exposed, since the suture with the nasal is displaced. The portion of the maxillary which forms the orbital rim is well developed and robust, with orbits directed laterally. The roots of the teeth, mainly from M2 on, can be observed emerging in the orbital rim.

The ventral view of MUSM 4179 is obstructed by the medio-lateral crushing of the skull. The palatine portion of the left maxillary is preserved and exposed in what would be its anatomical position. The right maxillary is completely displaced and not visible. The palatine foramen cannot be seen. The right premaxillary is not visible and the left premaxillary is below what can be seen of the incisors but obscured by the mixture of teeth+bone+sediments in the middle of the cranium. Palatal foramina and vacuities not visible.

On the left lateral view, MUSM 4179 is flattened dorso-ventrally, but not as much as *Epidolops* and *Bonapartherium*, possibly due to the compression and displacement of the bones. The large size of the I1 and P3 are remarkable features. Rostrum much shorter compared to *Epidolops*, without diastema between the premolars and the canine. The cranium is shorter like the one of *Bonapartherium*, but without the huge canines that the latter possess. The premaxillary is observed, but it is broken in its anterior portion. The premaxillary-maxillary suture is hardly visualized, probably due to the fractures. It seems to have the shape of an arch, heading antero-ventrally, from the level of the posterior root of the C1, with its ventral portion ending above the root of I4. It was not possible to observe whether it has serrated or smooth margins. A large infra-orbital foramen located above P2 can be observed. The portion of the maxilla that integrates the orbital rim is quite developed and robust in its anterior portion, mainly above the P3. Posteriorly (from M2 on), the thickness of the maxilla, i.e. the ventral portion of the orbital rim, is much smaller. The maxillo-jugal suture, which is not very well preserved, has a pronounced inclination. It seems that there is no contact between the premaxillary and the frontal, but that there was a contact between the maxillary and the nasal. The maxillary extends up to the C1, composing the alveoli of this tooth, but the preservation is not very good, and it could be the premaxillary that composes the anterior alveolus of C1. The maxillary foramen (posterior extremity of the infraorbital foramen) is observed, with a sulcus on its ventro-medially portion. On the right lateral view, it is possible to clearly observe the medio-lateral compression of the cranium, which has disfigured it. It is not possible to access the details of the morphology since the bones are not in their anatomical position. The maxillary has its lateral margin seemingly eroded, and the roots of the M1 are visible. The maxillary-jugal suture is markedly oblique.

The P3 is plagiaulacoid, with two roots and no serrated margins. There is an anterior portion, which is higher and with one cusp, and a posterior portion, much lower, with a labial and a lingual cusp separated by a narrow basin. The anterior and posterior portions are separated by deep sulci on the labial and lingual surfaces, the lingual one being deeper. The lingual surface is concave and the labial one is straight but lingually inclined.

The M1 has an ovoid shape. The paracone and StB are fused, but ventrally there is a small basin separating their tips. Anteriorly to them there is a developed crest-like structure. The ectoflexus is very deep and wide, with, below it, a very well-developed cusp-like structure, almost at the base of the teeth. The centrocrista is V-shaped and directed anteriorly. A mesially positioned well developed stylar cusp (St?C) is present. The metacone is fused with the StD. The postmetacrest and the StD posterior crest form a style-like structure on their posterior margin. A narrow but relatively long posterior cingulum is present, reaching the metaconule, which is antero-posteriorly compressed and low. It is separated from the protocone by a wide sulcus on the labial margin of the teeth. The protocone is higher than the metaconule and is more centrally positioned. A well-developed ?pretocononal cingulum *sensu* Goin & Candela (2004) is present anteriorly and below the protocone.

The M2 also possess the paracone fused to the StB and anteriorly and labially to them there are two developed cinguli/sulci (depending on the wear). The centrocrista is more open than in the M1 and turned to the center of the trigon basin. The ectoflexus is much less deep and wide than in the M1. No St?C could be distinguished. The metacone is merged with the StD and a small style is located posteriorly to them. The posterior cingulum is much wider than in the M1, with lingual to it a labio-lingually elongated and antero-posteriorly compressed metaconule. Between the metaconule and the protocone there is a lingual sulcus, which is deeper than in the M1. The protocone is a well-defined, high, and large cusp, anteriorly positioned. A much smaller ?preprotoconal cingulum is present.

The M3 has few diagnostic characteristics. It is a small triangular-shaped tooth, with paracone fused to the StB, very open centrocrista, shallow ectoflexus, metacone fused to the StD, but both are not very developed and well-defined structures, becoming, with increasing wear, an oblique crest-like structure. A well-developed posterior cingulum is present, with a metaconule at its lingual extremity. These two structures seem like merged, forming a wide posterior cingulum in specimens with more wear.

The m1 has unilateral hyposontia, with a much higher labial margin, which is inclined lingually. It is labio-lingually compressed, with a wider base. The paraconid is an incipient structure, with an antero-labial position. Below and lingually to the

paraconid there is a conspicuous rounded hypoconulid notch. The postparacristid is short and almost straight, connected to a high and large protoconid. The postprotocristid is short, labially, and ventrally directed, meeting a short and oblique postmetacristid at a level below the trigonid, forming an angle of approximately 45º. The metaconid is a small structure. A short prehypocristid connects the hypoconid to a crest that starts below the postprotcristid and postmetacrist junction. The hypoconid is much smaller than the entoconid, the latter being a high, large, and rounded cusp. A conspicuous hypoconulid is present, situated slightly labial to or the base of the entoconid, depending on the specimen. The talonid basin is very narrow but deep. A pronounced vertical sulcus is present of the posterior margin of the teeth, below the hypoconid.

The m2 is brachydont but shows a slightly unilateral hypsodonty. The trigonid is shorter and narrower than the talonid. Protoconid and metaconid are subequal in height, and the paraconid, the smaller cusp of the trigonid, is quite reduced and anteroposteriorly compressed. The postparacristid is transversally oriented and joins the straight, and anteroposteriorly oriented preprotocristid. The entoconid is low, conical-shaped and more anteriorly set than the hypoconid. The hypoconulid is well developed and a slight posterior cingulid runs along the posterior wall of the molar.

The m3 has a very similar morphology compared to the m2, but it is smaller and comparatively wider, with a lower crown. The paraconid is almost undistinguishable, only the protoconid and metaconid being visible on the trigonid, which are connected by an oblique crest. An anterobasal is present in some specimens. The hypoconid and entoconid are both large, and a small hypoconulid is present, situated posteriorly to the entoconid. The talonid basin is wide and deep.

Comments. The general morphology of these specimens is very close to that of *W. tsullodon* (Goin & Candela, 2004) from the Santa Rosa local fauna, early Oligocene of Peru. The slightly unilateral hypsodonty in the lower molars is found in *Wamradolops tsullodon* and in other polydolopimorphians such as prepidolopids and bonapartheriids (Goin & Candela, 2004; Goin *et al*., 2010). The position and morphology of the entoconid also resembles the one found in polydolopimorphians. The size and arrangement of trigonid cusps, the orientation of trigonid cristids, and the relative size proportions among trigonid and talonid are similar to what is described for *W*. *tsullodon*.

The type and referred material from Santa Rosa differs from that of *W*. *tsullodon* from Contamana in having, for example, a m2 with a very robust hypoconulid and by having narrower and shorter trigonid.

Differing from other Polydolopimorphia craniums already described in the literature, which are said to be flattened dorsoventrally (*Kramadolops*, *Bonapartherium* and *Epidolops*), MUSM 4173 is compressed laterally compressed. It is very small when compared to other Polydolopimorphia craniums (*Kradadolops*, *Bonapartherium*, *Epidolops*) and has a short rostrum. Other Polydolopimorphia craniums described in the literature also lack their posterior portions, like *Kramadolops*, *Epidolops* and *Bonapartherium*, which could be a characteristic of post-mortem taphonomic processes and/or traces of the typical damages done on mammals' skulls by predatory birds (Pascual, 1981; Flynn & Wyss, 2004; Beck, 2017). The absence of antorbital fossa and protruded and expanded nasals and not so big infraorbital foramen suggests that *Wamradolops* did not have a proboscis, as in *Proargyrolagus* (Sánchez-Villagra & Kay, 1997). Also differing from this genus, which had small eyes, *Wamradolops* was a visually oriented animal, possibly to detect and avoid predators (Sánchez-Villagra & Kay, 1997). The infraorbital foramen seems to be quite large, but smaller than in *Proargyrolagus* (Sánchez-Villagra & Kay, 1997), similar to that of *Kramadolops* and *Bonapartherium* and in *Epidolops* it is not visible (Pascual, 1981; Flynn & Wyss, 2004; Beck, 2017), which indicates many barbs on the worm. The orbital region is not entirely preserved, but from the orbital region of the maxillaries, which are broad dorsoventrally and medio-laterally and orientated laterally, we could say that the individual had relatively big lateral orbits (and eyes), differing from the small convergent orbits of *Proargyrolagus*, and more similar to the *Epidolops* (big orbits) and *Bonapartherium*, somewhat similar to *Caluromys*, but smaller (Pascual, 1981; Flynn & Wyss, 2004; Flores *et al*., 2010; Beck, 2017). Differing from *Epidolops* and more similar to *Kramadolops* and *Bonapartherium*, the P3 axis is in line with the molar series. As in *Bonapartherium*, *Epidolops* and *Proargyrolagus* it possesses a M4, differing from *Kramadolops* in which this tooth is absent (Pascual, 1981; Sánchez-Villagra & Kay, 1997; Flynn & Wyss, 2004; Beck, 2017). Differing from *Kramadolops*, *Epidolops* and *Bonapartherium*, there is no diastema between the C1 and the P2 (Pascual, 1981; Flynn & Wyss, 2004; Beck, 2017). Compared with the *Epidolops* skull, the opening

angle of the jaw (between rostrum and cheek) is much less marked; the diastema between P2-C1 is much smaller; the P2 is more developed; and P3 is less developed and without serrated margins (Beck, 2017).

Measurements. See Table 5.

Table 5. Measurements, in mm, of the teeth of *Warmradolops tsullodon* specimens from Contamana, Huallaga Basin and Atalaya regions, Peruvian Amazonia.

Locality	Specimen	Locus	Length	Width
CTA-27	MUSM 4179	Right P2	0.888	0.655
		Left P2	0.793	0.665
TAR-55	MUSM 4031	Right P3	1.448	1.106
CTA-29	MUSM 4130	Right P3	1.165	1.047
	MUSM 4131	Right P3	1.319	1.091
	MUSM 4132	Right P3	1.479	1.268
CTA-27	MUSM 4179	Right P3	1.494	1.416
	MUSM 4180	Right P3	1.567	1.334
	MUSM 4182	Right P3	1.427	1.359
	MUSM 4183	Right P3	1.563	1.35
CTA-66	MUSM 4142	Left P3	1.553	1.15
CTA-27	MUSM 4179	Left P3	1.403	1.328
	MUSM 4184	Left P3	1.657	1.421
	MUSM 4185	Left P3	1.5	1.347
	MUSM 4179	Right M1	1.1	1.557
	MUSM 4187	Right M1	1.11	1.59
	MUSM 4188	Right M1	1.087	1.439
	MUSM 4189	Right M1	1.096	1.374
	MUSM 4190	Right M1	1.018	1.28
TAR-55	MUSM 4030	Left M1	0.829	1.172
CTA-29	MUSM 4134	Left M1	0.9105	1.409
CTA-27	MUSM 4179	Left M1	1.166	1.254
	MUSM 4194	Left M1	1.071	1.56
	MUSM 4194	Left M1	1.082	1.518

Table 5. Continuation.

Locality	Specimen	Locus	Length	Width
CTA-29	MUSM 4135	Right M2	1.058	1.256
CTA-27	MUSM 4179	Right M2	0.974	1.223
	MUSM 4181	Right M2	0.906	1.091
	MUSM 4198	Right M2	0.97	1.176
	MUSM 4199	Right M2	0.955	1.2
	MUSM 4200	Right M2	0.965	1.15
	MUSM 4201	Right M2	1.049	1.117
TAR-55	MUSM 4030	Left M2	0.739	0.966
CTA-27	MUSM 4179	Left M2	1.045	1.28
	MUSM 4203	Left M2	0.98	1.41
	MUSM 4204	Left M2	0.929	1.258
	MUSM 4205	Left M2	0.955	1.373
	MUSM 4206	Left M2	0.961	1.221
	MUSM 4207	Left M2	0.887	1.123
	MUSM 4179	Right M3	0.855	0.929
	MUSM 4209	Right M3	1.043	0.846
	MUSM 4210	Right M3	1.094	0.938
	MUSM 4211	Right M3	1.015	0.749
	MUSM 4212	Right M3	1.079	0.861
	MUSM 4213	Right M3	0.968	0.774
	MUSM 4214	Right M3	0.948	0.791
CTA-47	MUSM 4123	Left M3	0.781	0.8625
CTA-27	MUSM 4179	Left M3	0.918	0.946
	MUSM 4215	Left M3	1.013	0.885
	MUSM 4216	Left M3	0.985	0.851
	MUSM 4217	Left M3	1.025	0.895
	MUSM 4218	Left M3	0.993	0.843
	MUSM 4226	Right p2	1.312	0.657
	MUSM 4227	Right p2	1.346	0.587
TAR-55	MUSM 4033	Right p3	1.477	1.17
CTA-29	MUSM 4136	Right p3	1.192	0.749
CTA-27	MUSM 4129	Right p3	1.299	1.29
	MUSM 4221	Right p3	1.357	1.208
	MUSM 4222	Left p3	1.466	1.324
	MUSM 4233	Left p3	1.324	1.054

Table 5. Continuation.

Locality	Specimen	Locus	Length	Width
TAR-55	MUSM 4032	Right m1	0.937	0.966
CTA-47	MUSM 4124	Right m1	1.134	0.892
CTA-29	MUSM 4136	Right m1	0.122	0.991
CTA-27	MUSM 4149	Right m1	1.132	1.173
	MUSM 4220	Right m1	1.105	0.977
	MUSM 4221	Right m1	1.127	1.053
	MUSM 4246	Right m1	1.19	1.008
	MUSM 4247	Right m1	1.214	0.967
CTA-27	MUSM 4248	Right m1	1.143	1.062
	MUSM 4249	Right m1	1.115	1.188
	MUSM 4250	Right m1	1.063	1.041
	MUSM 4251	Right m1	1.259	1.221
TMB-01		Right m1	1.068	0.855
CTA-29	MUSM 4139	Left m1	1.358	1.211
CTA-27	MUSM 4254	Left m1	1.264	0.962
	MUSM 4255	Left m1	1.029	0.881
	MUSM 4256	Left m1	1.29	1.014
	MUSM 4257	Left m1	1.195	1.075
	MUSM 4258	Left m1	1.262	1.147
	MUSM 4259	Left m1	1.287	1.227
	MUSM 4260	Left m1	1.167	1.219
TMB-01		Left m1	1.183	1.107
TAR-55	MUSM 4032	Right m2	0.856	0.953
	MUSM 4034	Right m2	0.967	0.966
CTA-47	MUSM 4125	Right m2	0.865	0.7
CTA-51	MUSM 4127	Right m2	1.094	1.052
CTA-29	MUSM 4136	Right m2	0.926	0.778
CTA-27	MUSM 4129	Right m2	1.1	1.039
	MUSM 4220	Right m2	1.021	0.988
	MUSM 4221	Right m2	1.066	1.086
	MUSM 4262	Right m2	1.037	1.017
	MUSM 4263	Right m2	1.059	1.009
	MUSM 4264	Right m2	0.922	1.048
	MUSM 4265	Right m2	0.966	1.077
	MUSM 4266	Right m2	1.122	1.088

Table 5. Continuation.

Locality	Specimen	Locus	Length	Width
CTA-27	MUSM 4267	Right m2	1.069	1.038
TMB-01		Right m2	1.002	0.929
TAR-55	MUSM 4035	Left m2	0.856	0.752
TAR-14	MUSM 4120	Left m2	1.189	0.95
CTA-27		Left m2	1.037	0.954
		Left m2	1.049	0.942
		Left m2	1.104	0.929
		Left m2	1.007	0.844
CTA-27		Left m2	1.101	0.91
		Left m2	1.166	0.991
		Left m2	1.063	0.905
		Left m2	1.088	0.854
		Left m2	1.066	0.931
TMB-01		Left m2	1.047	0.902
CTA-27		Right m3	0.996	0.868
		Right m3	0.876	0.903
		Right m3	0.959	0.835
		Left m3	1.067	0.842
		Left m3	0.976	0.845

sp. nov. (large)

(Figure 18)

Holotype. MUSM 4036, one right maxillary with M1.

Referred material. TAR-55: MUSM 4037, one left M1; MUSM 4038, one right M2; MUSM 4039, 4040, two left M3; MUSM 4041, one right dentary with m1; MUSM 4042, one right dentary without teeth; MUSM 4043, one left p3; MUSM 4044, one right m1; MUSM 4045, 4046, 4047, 4048, 4049, five left m1; MUSM 4050, 4051, 4052, three left m2; MUSM 4053, 4054, two right m3; MUSM 4055, 4056, 4057, three left m3. TAR-44: MUSM 4058, one left P3; MUSM 4059, one right M3. TAR-45: MUSM 4060, one right m1. Without collection number: TMB-01: one right p2.

Etymology. To be done.

Type locality. TAR-55, Balsayacu Paleogene section, San Martín Department, Peru.

Type horizon and age. Pozo Formation, Lower Member, late middle Eocene.

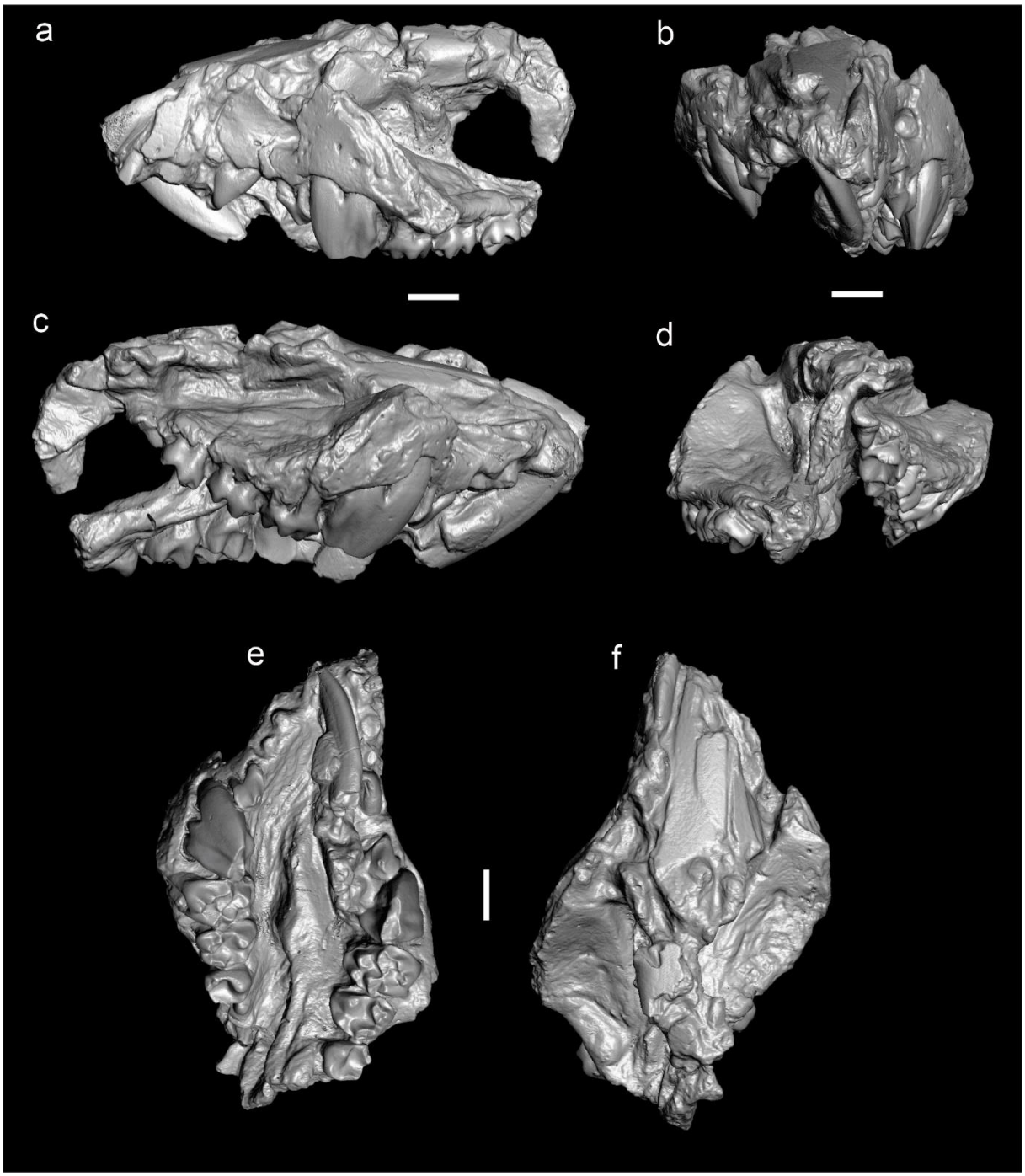


Figure 16. MUSM 4179, *Wamradolops tsullodon* fragmentary cranium from CTA-27, late middle Eocene, Contamana, Peru, on: **a**, left slightly lateral view; **b**, right slightly lateral view; **c**, anterior view; **d**, posterior view; **e**, slightly ventral view; **f**, slightly dorsal view. Scale bars = 1 mm.

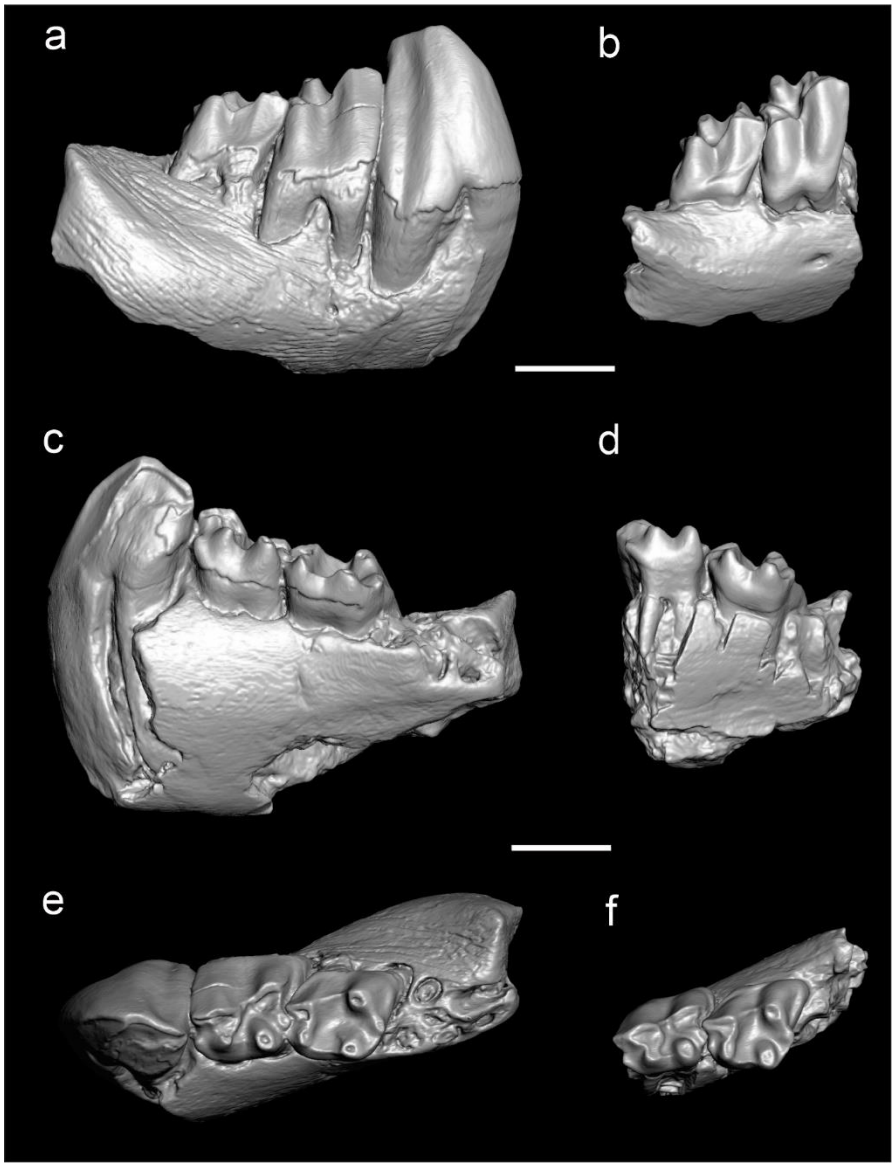


Figure 17. *Wamradolops tsullodon* fragmentary dentaries: **a, c, e,** MUSM 4221, right dentary with p3–m2, CTA-27, late middle Eocene, Contamana, Peru; **b, d, f**, MUSM 4032, right dentary with m1–m2, TAR-55, late middle Eocene, Balsayacu Paleogene section, Huallaga Basin, Peru. **a, b**, labial views; **c, d**, lingual views; **e, f**, occlusal views. Scale bars = 1 mm.

Other localities. TAR-44 and TAR-45, Juanjui Paleogene section, San Martín Department, Pozo Formation, Lower Member, middle-late Eocene. TMB-01, Atalaya, Ucayali Department, Pozo Formation, Upper Member, late Eocene.

Diagnosis. *Wamradolops* sp. nov. (large) is characterized by a larger size compared to *W*. *tsullodon*, as well as the presence of marked cristae anterior and posteriorly to the crest-like structure below the ectoflexus on the M1, absence of cinguli/sulci anterior and posteriorly to the paracone+StB on the M2, postprotocristid and postmetacristid junction forming an wider angle (45º in *W*. *tsullodon* and 90º in *W*. sp. nov. [large]) on the m1, hypoconulid smaller and at the base of the entoconid on the m1, the hypoconulid notch on the m2 is larger and more dorsally positioned.

Description. MUSM 4058 is the single P3 recorded for this taxon, it is plagiaulacoid without preserved roots, of relatively large size. It has an anterior cusp, the highest one, followed by two crests, one labial, well-developed, and one lingual, more subtle. These crests connect the anterior cusp to two posterior ones, one labial and one lingual, the lingual one being larger. Between these two cusps there is a small shallow basin. Two sulci separate the anterior portion from the posterior one, the labial sulcus is shallow and the lingual one is deeper and wider. There is a posterior crest running dorsally from the base of the posterior lingual cusp, with a notch at its dorsal end.

The M1 is quadrangular-shaped and with two visible roots, one lingual and one labial. The paracone is fused to the StB, being slightly higher than the latter. Anteriorly to the paracone, there is a short but marked crest. The StB posterior crest and the postparacrest are short, running parallel until joining at the ectoflexus. The ectoflexus is wide and relatively deep, with below a cuspid-like structure with pre and postcrista at the base of the tooth. The St?C is antero-posteriorly compressed and located just after the ectoflexus. It is connected by short crests to the metacone and the StD, which are fused. The metacone is higher than the StD and shorter than the St?C. Below the StD there is a posterior cingulum, very narrow, that goes until the base of the metaconule. The metaconule is long and lingually salient, but it is shorter than the protocone. Between the metaconule and the protocone there is a lingual sulcus. The protocone is antero-posteriorly compressed and occupies a more anterior position. Anteriorly and below the protocone there is a well-developed ?preprotoconal cingulum *sensu* Goin & Candela (2004). The trigon basin is almost non-existent, being antero-posteriorly and labio-lingually compressed. The centrocrista is V-shaped.

The M2 is smaller than the M1 and with a simplified morphology. It has an intermediate shape between the quadrangular one of the M1 and the triangular one of

the M3. The paracone is fused with the StB and anterior to it there is a short subtle crest. The StB posterior crest has a cusp-like aspect, forming a small tip just before the ectoflexus. The ectoflexus is incipient and with no structures below it as in the M1. An antero-posteriorly compressed St?C is present just after the ectoflexus, connected by cristae to the metacone+StD. Below the metacone there is a well-developed posterior cingulum, wider than in the M1, with, at its lingual extremity, a small and rounded metaconule. Between the metaconule and the protocone there is a lingual sulcus, but it is much more subtle than in the M1. The protocone is a high and well-defined cusp, slightly more centrally positioned than in the M1. Below the protocone there is a well-developed ?preprotoconal cingulum, but it is narrower than in the M1. The trigon basin is not compressed as in the M1, being wide and deep. The centrocrista is not V-shaped as in the M1, but less open than in the M3.

The M3 is triangular-shaped. The StB is merged with the paracone, forming a single rounded tip. The postparacrista is short, ending at an almost non-visible ectoflexus. The metacone is short and not very well-defined as a cusp, possibly due to wear. It was not possible to observe a St?C or StD. The metacone is followed by a postmetacrista, which connects it to a well-developed posterior cingulum. The protocone is high, rounded and centrally positioned. The pre- and postprocrista have almost the same length, but the postprotocrista is more oblique. The trigon basin is wide and very deep, the centrocrista is U-shaped.

The p2 is long, narrow, and low-crowned. It is worn, relatively large, with a rounded labial surface and a crest running antero-posteriorly on the occlusal surface.

The m1 is labio-lingually compressed and with unilateral hypsodontia. The trigonid is narrower than the talonid. A small, very anteriorly positioned paraconid is present, below which, on the lingual side, there is a small, rounded hypoconulid notch. The paraconid is followed by a marked postparacristid, which connects it to a high protoconid. The protoconid is followed by an oblique postprotocristid which runs ventrally, meeting the postmetacristid, which also has an oblique and dorsal direction. The angle formed by the connection of the postprotcristid and the postmetacristid is very narrow, being much less than 90º in specimens with no/few wear, and about 90º in worn specimens. A marked and very oblique cristid obliqua goes from below the connection of the postprotcristid-postmetacristid until a long but narrow hypoconid. The

hypoconulid is small and situated at the base of the entoconid. The entoconid is high and rounded. No preentocristid could be observed. The talonid basin is narrow but deep.

The m2 is almost of the same length of the m1, but it is not labio-lingually compressed, having a quadrangular shape. On the trigonid, the paraconid is smaller than in the m1, and it also has a hypoconulid notch below and lingual to it, but in this case this it is closer to the occlusal surface. In specimens with more wear, the notch is visible on the same level as the paraconid, letting the m2 with a quadrangular-shaped trigonid. The postparacristid is, as in the m1, marked. The protoconid is a high cuspid, with a more labial position than in the m1. It is connected to the metaconid by a single crest, perpendicular to the molar axis. The metacone is not very high and well-defined as a cupid. In specimens with more wear, the metaconid and the cristid connecting it to the protoconid form a single horizontal perpendicular structure. The cristid obliqua is less developed and shorter than in the m1. The hypoconid is a high and large cuspid. The hypoconulid is a wide but not high structure, starting at the middle of the posterior margin of the tooth and going just below the entoconid. The entoconid is also a high cuspid, but narrower than the hypoconid. It is preceded by a well-developed preentocristid. The talonid basin is deep and much wider than the one present on the m1.

The m3 is smaller than the m2, both in length as in width. But morphologically, it resembles a lot to the m2, being just more simplified. The trigonid is shorter, the paraconid being an incipient structure only visible in specimens with no/few wear. The protoconid and metaconid have subequal height and are connected by a single crest, as in the m2, but in the m3 this crest has a more oblique direction. The cristid obliqua is even less marked than in the m2. The hypocone is a large high cuspid and the entoconid a high narrow cuspid, as in the m2. The hypoconulid is smaller and less posteriorly salient than in the m2. The talonid basin is wide and deep and a preentocristid is present, as in the m2.

Comments. The presence of a large, posterolingual metaconule on the upper molars; very reduced trigon basin, especially on the M1; presence of a ?StC; and a strong ?pretoconal cingulum anterolingual to the paracone, especially on the M1, are characteristics present on these specimens and on the diagnosis of *Wamradolops*

tsullodon, which was the type and only known species of the genus *Wamradolops* until today (Goin & Candela, 2004). However, through the analysis of all the specimens belonging to *Wamradolops* present in the Contamana, Huallaga Basin and Atalaya regions, it was possible to observe that more than one taxon was present. Thus, *Wamradolops* sp. nov. (large) is as a new species of *Wamradolops*, which differentiates from *W*. *tsullodon* in having larger size (~40%), presence of marked anterior and posterior cristae around the crest-like structure below the ectoflexus on the M1, absence of cinguli/sulci anterior and posterior to the paracone+StB on the M2, larger ?preprotoconal cingulum on the M2, postprotocristid and postmetacristid junction forming an angle of ~90º (45º in *W*. *tsullodon*) in the m1, less developed hypoconulid on the m1, larger entoconid on the m2, among others. *Wamradolops* sp. nov. (large) occurs in the same outcrops as *W*. *tsullodon* in the Contamana, Huallaga Basin and Atalaya regions. Because of its larger size, it is possible to suggest that both species were not direct trophic/ecological competitors.

This new species of *Wamradolops* adds information to this enigmatic genus of uncertain phylogenetic affinities. *Wamradolops* was described as being morphologically closer to prepidolopids and bonapartheriids, as well as sharing some features with groeberiids and polydolopines, for example. Indeed, *Wamradolops* has a mixture of derived and “primitive” characters (Goin & Candela, 2004), and its addition to phylogenetic analyses will help to understand its position among polydolopimorphians, and to test its monophyly. Such a phylogenetic analysis could not be achieved for the current work, but it is planned for the next months.

Measurements. See Table 6.

Table 6. Measurements, in mm, of the teeth of *Wamradolops* sp. nov. (large) specimens from Huallaga Basin and Atalaya regions, Peruvian Amazonia.

Locality	Specimen	Locus	Length	Width
TAR-44	MUSM 4058	Left P3	1.84	1.412
TAR-55	MUSM 4036	Right M1	1.53	2.098
	MUSM 4038	Right M2	1.404	1.615
	MUSM 4039	Left M3	1.249	1.271
	MUSM 4040	Left M3	1.125	1.397
TMB-01		Right p2	1.846	0.932
TAR-55	MUSM 4043	Left p3	2.005	1.626
	MUSM 4041	Right m1	1.546	1.6
TAR-45	MUSM 4060	Right m1	1.624	1.275
TAR-55	MUSM 4045	Left m1	1.681	1.469
	MUSM 4046	Left m1	1.605	1.427
	MUSM 4047	Left m1	1.64	1.538
	MUSM 4048	Left m1	1.65	1.555
	MUSM 4050	Left m2	1.589	1.285
	MUSM 4051	Left m2	1.434	1.334
	MUSM 4052	Left m2	1.569	1.307
	MUSM 4053	Right m3	1.307	1.198
	MUSM 4054	Right m3	1.23	1.137
	MUSM 4055	Left m3	1.306	1.185
	MUSM 4056	Left m3	1.249	1.076
	MUSM 4057	Left m3	1.279	1.058

Polydolopimorphia indet.

gen. nov. A

Type species. Polydolopimorphia indet. gen. nov. A sp. nov.

Diagnosis. As for the type and only known species.

Etymology. To be done.

gen. nov. A sp. nov.

(Figure 19)

Holotype. MUSM 4150, one right M1.

Referred material. CTA-51: MUSM 4128, one right M2. CTA-27: MUSM 4148, one right maxillary with P2–M2; MUSM 4149, one left maxillary with M2–M3; MUSM 4151, one right M1; MUSM 4152, MUSM 4153, MUSM 4154, three left M2; MUSM 4155, one left M3; MUSM 4156, one left dentary with m2–m3; MUSM 4157, one left dentary with m2; MUSM 4158, one left dentary without teeth; MUSM 4159, 4160, two right p2; MUSM 4161, 4162, 4163, 4164, 4165, five left p3; MUSM 4166, 4167, 4168, 4169, four right m1; MUSM 4170, 4171, two left m1; MUSM 4172, one right m2; MUSM 4173, 4174, two left m2; MUSM 4175, 4176, two right m3; MUSM 4177, 4178, two left m3.

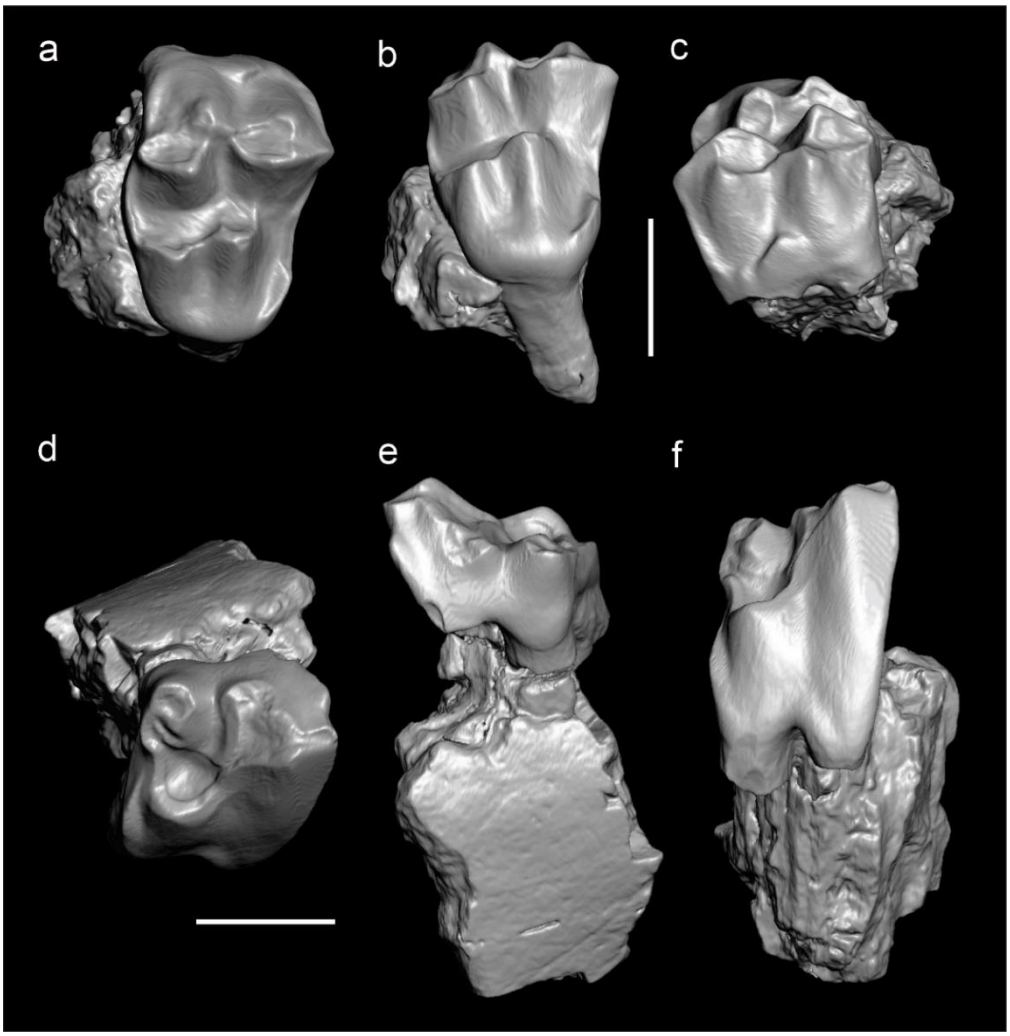


Figure 18. *Wamradolops* sp. nov. (large) from TAR-55, late middle Eocene, Balsayacu Paleogene section, Huallaga Basin, Peru: **a–c,** MUSM 4036, fragmentary right maxillary with M1; **d–f**, MUSM 4041, right dentary with m1. **a, d**, occlusal views; **b, e**, lingual views; **c, f**, labial views. Scale bars = 1 mm.

Etymology. To be done.

Type locality. CTA-27, Contamana, Loreto Department, Peru.

Type horizon and age. Pozo Formation, Lower Member, late middle Eocene (early Barrancan, ~41.6-40.94 Ma).

Other localities. CTA-51, Pozo Formation, Lower Member, late middle Eocene (early Barrancan), Contamana, Loreto Department, Peru.

Diagnosis. Polydolopimorphia indet. gen. nov. A sp. nov. is characterized by: on the M1, fused StB and paracone, but with a large basin separating their tips, long ?preprotocononal cingulum *sensu* Goin & Candela (2004) running from the crest anterior to the paracone until the lingual sulcus separating the metaconule from the protocone, StB posterior crest not reaching the ectoflexus, quadrangular-shaped open centrocrista, short posterior cingulum; M2: quandrangular outline, quadrangular-shaped centrocrista; M3: no distinguishable metaconule; m1: short and not ventrally-directed posprotocristid and postmetacristid, very low hypoconid, relatively wider talonid basin, small hypoconulid situated labially to the entoconid; m2: more developed hypoconulid.

Description. The only preserved P2 and P3 (MUSM 4148) are almost completely broken, with only the basal portion and the roots preserved. Their identity was established based on their position on the maxilla.

The M1 resembles morphologically the ones of *Wamradolops* spp. The paracone and StB are fused, but their tips are more apart than in *Wamradolops*. The paracone has a marked crest anterior to it, which is connected dorsally to a conspicuous ?preprotoconal cingulum that runs through the entire anterior margin of the tooth, and also on the lingual surface, reaching the sulcus that separates the metaconule from the protocone. The StB posterior crest does not reach the ectoflexus. The postparacrest reaches the ectoflexus and is connected to a St?C anterior crest that is parallel to the antero-posterior molar axis. This gives a quadrangular shape to the centrocrista, which is open. The ectoflexus is wide but not very deep. Below it, there is a marked crest, with anterior and posterior cinguli. The St?C is the highest cusp, but antero-posteriorly compressed. It is connected to the metacone+StD, which are subequal in size. Below the StD starts a posterior cingulum, which is very narrow, ending before reaching the metaconule. The metaconule is not high, and it is antero-

posteriorly compressed. The protocone is slightly wider and higher than the metaconule, situated in front of the ectoflexus. The trigon basin is narrow.

The M2 is smaller and narrower than the M1, and with a simplified morphology and quadrangular shape. The paracone is fused to the StB. There is a crest-like structure anterior to the StB+paracone. The ?preprotoconal cingulum is much more reduced than in the M1. The ectoflexus is incipient and followed by a small St?C. The centrocrista also has a quadrangular shape. The metacone+StD are much less developed than in the M1, labially to it there is a well-developed posterior cingulum, which reaches the metaconule. The metaconule is less prominent than in the M1, being separated from the protocone by a sulcus. The protocone is a high and well-defined cusp, with an anterior position. The trigon basin is deep and wide.

The M3 is much smaller than the M1 and M2, and with a very simplified morphology. It has a more anteriorly positioned protocone, paracone merged with the StB, and incipient StD+metacone. A well-developed posterior cingulum is present, but no metaconule could be distinguished.

The p2 are long and narrow teeth with one single root, rounded labial and lingual margins and a crest running antero-posteriorly on the occlusal surface.

The p3 has a blade-like aspect, the roots are not preserved. One central cuspid is present and one anterior crest and a posterior one. Two striae run on the labial margin of the teeth from this cuspid to the base of the teeth. The labial side is concave.

The m1 is labio-lingually compressed and has unilateral hypsodontia, with a much higher labial side. The paraconid is a small and low structure, followed by a short postparacritid, which runs parallel to the antero-posterior molar axis. It connects to a high and wide protocone, which is followed by a short postprotocristid, which is slightly oblique and does not have a ventral direction. The protocristid connects to the postmetacristid, which is short and oblique, their connection forming an angle of more than 90º, even in specimens with more wear. The cristid obliqua is relatively long and connected to a wide but very low hypoconid. The hypoconulid is small and located just labially to the entoconid. The entoconid is high and rounded. The talonid basin is deep and relatively wide.

The m2 is smaller, more simplified and with much less pronounced unilateral hypsodontia. It has a quadrangular shape, with shorter but wider trigonid. The

paraconid is incipient and with a hypoconulid notch just lingual to it. The protoconid is not well-developed, being less high than the metaconid and connected to it by a single oblique crest. The hypoconid is larger than in the m1, but still smaller than the entoconid. A hypoconulid is also present and it is wider and more salient than in the m1. The entoconid is also a large cuspid.

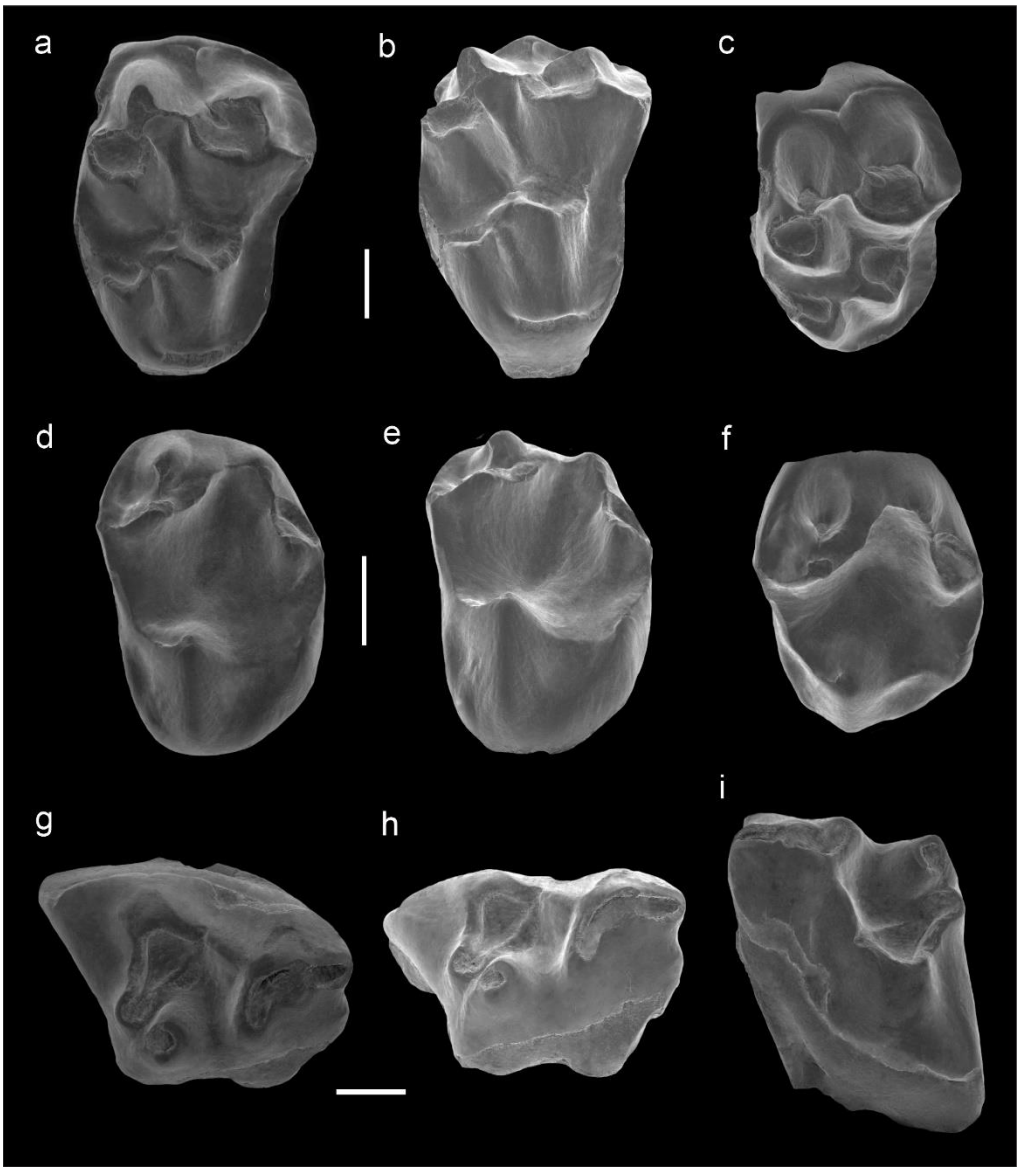


Figure 19. Polydolopimorphia indet. gen. nov. A sp. nov. from CTA-27, late middle Eocene, Contamana, Peru: **a–c,** MUSM 4150, right M1; **d–f**, MUSM 4152, left M3; **g–i**, MUSM 4171, one left m1. **a, d, g**, occlusal views; **b, e, h**, lingual views; **c, f, i**, labial views. Scale bars = a–c and g–i = 400 µm and d–f = 500 µm.

The m3 is morphologically a simplified version of the m2, being smaller than the latter and with a quadrangular shape. The paraconid is indistinguishable, the trigonid being even shorter than in the m2. The talonid basin is also deep and wide, and a hypoconulid is present, but much smaller than in the m2.

Comments. Large-sized polydolopimorphian, with the largest measurements regarding upper teeth among the taxa from the Contamana, Huallaga Basin and Atalaya regions. The presence of a developed metaconule, which gives a quadrangular outline to the molars, as well as other characteristics, such as M1 with a posterolabial "shifting" of the protocone, well-developed ?preprotoconal cingulum, reduced trigon basin are common between Polydolopimorphia indet. gen. nov. A sp. nov. and *Wamradolops* spp. However, Polydolopimorphia indet. gen. nov. A sp. nov. differentiates from *Wamradolops* spp. by having M1 with a quadrangular, more open centrocrista, the St?C is absent and the cusp-like structure below the ectoflexus is much less developed (Goin & Candela, 2004). Polydolopimorphia indet. gen. nov. A sp. nov. resembles the prepidolopids, but the latter have triangular-shaped upper molars, and lower molars with trigonid and talonid of subequal height, which are characteristics not found in Polydolopimorphia indet. gen. nov. A sp. nov. (Pascual, 1980a, b). Thus, we chose to assign this new taxon to none of the known Polydolopimorphia families, pending detailed phylogenetic analyses to explore its affinities.

Measurements. See Table 7.

Table 7. Measurements, in mm, of the teeth of Polydolopimorphia indet. gen. nov. A sp. nov. specimens from the Contamana region, Peruvian Amazonia.

Locality	Specimen	Locus	Length	Width
CTA-27	MUSM 4148	Left M1	1,491	2,018
CTA-51	MUSM 4128	Right M2	1,263	1,461
CTA-27	MUSM 4148	Left M2	1,351	1,769
	MUSM 4149	Left M2	1,35	1,745
	MUSM 4148	Left M3	1,103	1,627
	MUSM 4149	Left M3	1,156	1,297
	MUSM 4161	Left p3	2,188	1,588
	MUSM 4162	Left p3	1,839	1,143
	MUSM 4166	Right m1	1,428	1,276

Table 7. Continuation.

Locality	Specimen	Locus	Length	Width
CTA-27	MUSM 4167	Right m1	1,43	1,133
	MUSM 4170	Left m1	1,403	-
	MUSM 4172	Right m2	1,04	0,971
	MUSM 4173	Left m2	1,183	1,136
	MUSM 4157	Left m2	1,206	1,207
	MUSM 4174	Left m2	1,178	1,138
	MUSM 4175	Right m3	0,997	1,001
	MUSM 4174	Left m3	1,397	1,275
	MUSM 4177	Left m3	1,178	1,138

Superfamily Bonaparthérioidea Pascual, 1980

Family Prepidolopidae Pascual, 1980

gen nov. 1

Type species. Prepidolopidae gen. nov. 1 sp. nov. 1.

Diagnosis. As for the type and only known species.

Etymology. To be done.

gen. nov. 1 sp. nov. 1

(Figure 20)

Holotype. MUSM 4027, one right M2.

Referred material. MUSM 4028, one right p3.

Etymology. To be done.

Type locality. TAR-76, Balsayacu Paleogene section, San Martín Department, Peru.

Type horizon and age. Pozo Formation, Lower Member, late middle Eocene.

Diagnosis. Prepidolopidae gen. nov. 1 sp. nov. is a medium-sized prepidolopid, characterized by the presence of well-developed metaconule and postcingulum, two stylar cusps (StB + neomorphic cusp) anterior to the ectoflexus, high protocone, anterior cingulum and StA, wide and deep trigon basin, shallow ectoflexus, and open centrocrista.

Description. MUSM 4027 is a right upper molar, most probably an M2 due to its size and morphology (anterior portion of the stylar shelf is narrow, differing from the M1 where it is broad). It is somewhat bunoid, subtrapezoidal-shaped and relatively large. There is a marked precingulum anterior and below the protocone. The protocone is anteriorly positioned and high. The trigon basin is wide and deep. The preprotocrista is connected to a short and narrow anterior cingulum, with a parastyle at its labial tip. This parastyle is connected to a broad and high paracone by a short but marked preparacrista. The paracone is fused to the StB, the latter being slightly higher and posteriorly positioned. Antero-lingually to the paracone + StB and lingually to the parastyle there is a subtle cingulum. Posteriorly to the StB and anterior to the centrocrista, there is another stylar cusp, which could be the St?C or a neomorphic feature, and it is also fused with the paracone and StB. The postparacrista is long and connected to this neomorphic stylar cusp and not to the premetacrista, the centrocrista being thus open. The ectoflexus is shallow. The StD is slightly higher than the metacone, but shorter than the StB and subequal to the neomorphic stylar cusp. It is fused to the metacone, which is slightly smaller than the paracone. Posterolingually to the StD + metacone, there is a subtle cingulum. A well-developed metaconule connected to a wide posterior cingulum is present. The posterior cingulum extends itself until below the posterior tip of the postmetacrista. The metaconule is separated from the protocone by a lingual sulcus, the postprotocrista not being well-developed.

MUSM 4028 is a right p3, with the roots, base and part of the lingual side broken. It is trenchant, triangular shaped, with one higher anterior portion, followed by a straight cristid that goes posterior and ventrally. The lingual side lacks an enamel covering, but the labial side is covered by a thick enamel layer. Also, the labial side is curved and no flexi, cristid or striae are visible, nor a posterior platform is present on occlusal view.

Comments. The presence of, on, the upper molars, of developed StB and StD fused with the para- and metacone, respectively, a triangular shape, and absence of stylar platform, as well as a hypertrophied p3 without serrated margins allow to assign this new taxon to the family Prepidolopidae, according to Pascual (1980a, b).

The attribution of MUSM 4028 to Prepidolopidae gen. nov. 1 sp. nov. 1 is based on its size and the fact that it resembles in morphology Bonapartherioidea p3s. However, p3s possess few diagnostic features to distinguish different

bonapartherioids. On the other hand, MUSM 4027 possess several diagnostic characteristics. Regarding the other polydolopimorphians from Contamana, Huallaga Basin and Atalaya, it is different of *Wamradolops* spp. by being larger, having smaller anterior cingulum and precingulum, higher StB and StD compared to para- and metacone and by the absence of postcingulum. Prepidolopidae gen. nov. 1 sp. nov. 1 differentiates from Polydolopimorphia indet. gen. nov. A sp. nov. by being smaller, having less developed anterior labial cingulum, metacone almost with the same high as the paracone, and the absence of postcingulum. Prepidolopidae gen. nov. 1 sp. nov. 1 is different from Prepidolopidae gen. nov. 3 sp. nov. 3 by being larger and quadrangular-shaped, having higher protocone, pre and anterior cingulum, metaconule, wide and long posterior cingulum and trigon basin, the presence of a labial anterior cingulum, two stylar cusps anterior to the ectoflexus, open centrocrista and paracone higher than metacone, but both have a large posterior cingulum. Regarding Prepidolopidae gen. nov. 4 sp. nov. 4, Prepidolopidae gen. nov. 1 sp. nov. 1 differentiates by having more subtrapezoidal shape, anterior high protocone, precingulum, metaconule, more developed posterior cingulum, deep trigon basin, anterior labial cingulum, shallower ectoflexus, and open centrocrista. Regarding Prepidolopidae gen. nov. 5 sp. nov. 5, Prepidolopidae gen. nov. 1 sp. nov. 1 is much larger and do not possess sulci on the labial margin of the p3. Prepidolopidae gen. nov. 1 sp. nov. 1 is also very different from the ?Prepidolopidae gen. et sp. indet. from TAR-21, the latter being triangular-shaped and much smaller, having lower protocone, smaller posterior cingulum, narrower trigon basin, much higher StB and StD compared to para-and metacone, deeper ectoflexus, V-shaped centrocrista, metacone higher than paracond, and by not having precingulum, anterior labial cingulum, two stylar cusps anterior to the ectoflexus.

Regarding the prepidolopids already described in the literature, Prepidolopidae gen. nov. 1 sp. nov. 1 is different from *Prepidolops* spp. by possessing M2 with shallower ectoflexus, more bunoid molars with higher protocone, and it is more quadrangular-shaped (and not triangular) and smaller (Pascual, 1980a, b). It differs from *Punadolops alonsoi* M2s by possessing metaconule, para- and metacone closer to the stylar cusps B and D, respectively, and less open ectoflexus, despite having approximately the same size, more bunoid molars with larger protocone, and

metacone postero-lingually placed in relation to the StD as in this taxon (Pascual, 1983; Goin *et al*., 1998). Prepidolopidae gen. nov. 1 sp. nov. 1 differs from *Incadolops ucayali* in having a more open centrocrista, premetaconular crest meeting the base of the metacone, metacone smaller than paracone, and absence of long and sharp cristae connecting the stylar cusps. However, MUSM 4027 do resembles *I*. *ucayali* by also having a metaconule with a post-cingulum at its base, which in this case is even bigger, presence of an anterobasal cingulum, which is less developed than in *I*. *ucayali*, and large trigon basin (even larger) (Goin & Candela, 2004). Another prepidolopid, the only one that was described for outside the South American continent, at the Antartic Peninsula, is *Perrodelphys coquinense*, but it is known uniquely by lower molars, hampering direct comparisons with Prepidolopidae gen. nov. 1 sp. nov. 1. However, its size is much larger than the one of Prepidolopidae gen. nov. 1 sp. nov. 1 (Goin *et al*., 1999). It differs from *Coloradolops* by having M2 with StB and StD more distant situated, protocone less robust and pre- and postprotocrista much less marked (Chornogubsky *et al*., 2019). Thus, among Prepidolopidae, Prepidolopidae gen. nov. 1 sp. nov. 1 is morphologically closer to *Punadolops*, from the middle Eocene of northwestern Argentina, and *Incadolops*, from the Santa Rosa local fauna, early Oligocene of Peruvian Amazonia.

Measurements. Medium-sized Bonapartherioidea taxon (see Table 8).

Table 8. Measurements, in mm, of the teeth of Prepidolopidae gen. nov. 1 sp. nov. 1 sp. nov. specimens from the Contamana region, Peruvian Amazonia.

Locality	Specimen	Locus	Length	Width
TAR-76	MUSM 4028	Right ?M2	1.338	1.7763
		Right p3	1.5875	0.92

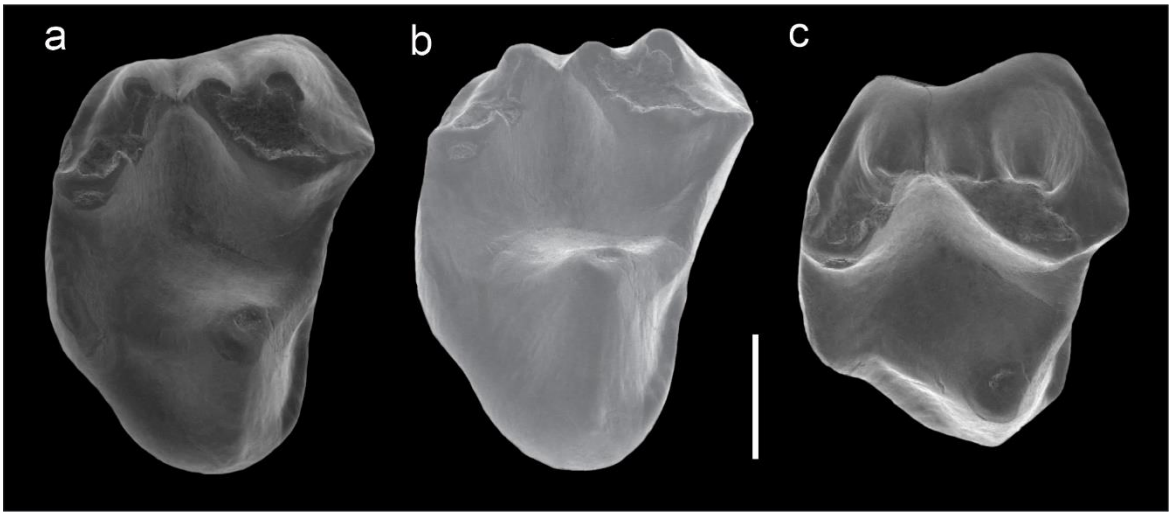


Figure 20. Prepidolopidae gen. nov. 1 sp. nov. 1 from TAR-76, late middle Eocene, Balsayacu Paleogene section, Huallaga Basin, Peru: **a–c,** MUSM 4027, right M2. **a**, occlusal, **b**, slightly lingual, **c**, slightly labial views. Scale bars = 500 µm.

gen. nov. 2

Type species. Prepidolopidae gen. nov. 2 sp. nov. 2

Diagnosis. As for the type and only known species.

Etymology. To be done.

gen. nov. 2 sp. nov. 2

(Figure 21)

Holotype. MUSM 4029, one left dentary with p3–m1.

Etymology. To be done.

Type locality. TAR-55, Balsayacu Paleogene section, San Martín Department, Peru.

Type horizon and age. Pozo Formation, Lower Member, late middle Eocene.

Diagnosis. Large-sized prepidolopid with m1 antero-posteriorly compressed, with postprotocristid and postmetacristid junction forming an angle of slightly less than 90°, metaconid and entoconid close to each other, no entocristid, rounded and low entoconid, narrow and low hypoconid, almost absent postcingulid, wide and not protuberant hypoconulid, narrow and shallow talonid basin.

Description. Fragment of a right dentary, broken behind the m1, but could be reconstructed with a posterior portion encompassing four molar roots. The p3 and m1

are preserved and they are large when compared to the other polydolopimorphians from Contamana, Huallaga Basin and Atalaya regions. The p3 is a large, robust, with two roots, one anterior portion higher and cuspidated, followed by a straight cristid that goes posteriorly and ventrally. It has a crown height of 2.86 mm on its lingual side and 4.534 mm on the labial one. Both the labial and lingual surfaces are curved, and only the labial side is covered by an enamel layer, the lingual side lacks this structure. There are no cristids on the labial and lingual surfaces of the p3, but subtle sulci are present on the labial side. The m1 is shorter in length and height when compared to the p3. It has unilateral hypsodontia, the labial side being much higher than the lingual one, and it is quadrangular shaped, larger at the base. The trigonid is higher and narrower than the talonid. The protoconid is the highest cuspid of the molar, it is located anteriorly to the metaconid. The pre- and postprotocristids are anteroposteriorly aligned, the preprotocristid being short and with a small paraconid at its anterior tip. The postprotocristid is ventrally directed, meeting the postmetacristid in a much lower positioned in relation to the trigonid cuspids. The postmetacristid is slightly oblique, and this arrangement of proto- and metaconids resembles a triangle in occlusal view, the postprotocristid and postmetacristid forming an angle of little less than 90° at this junction. Also, on the lingual side but below to the paraconid, there is a well-developed hypoconulid notch. The entoconid is by far the highest cusp of the talonid and it is rounded. There is no visible entocristid and the entoconid is not situated far from the metaconid, being separated from it by a sulcus. The hypoconulid is located just labially to the base of the entoconid and it is labio-lingually wide and antero-posteriorly short. The hypoconid is narrow antero-posteriorly and very low. A very incipient postcingulid is visible below and posteriorly to the hypoconid. The cristid obliqua is short and obliquely oriented, and a deep sulcus is present of the labial side of the molar between the trigonid and the talonid. The talonid basin is very narrow antero-posteriorly and labio-lingually and not very deep.

Comments. The presence of hypertrophied p3 without serrated margins and lower molars with labiolingually compressed trigonid and high proto- and entoconid allow to assign this new taxon to the family Prepidolopidae, according to Pascual (1980a, b).

Compared to the other polydolopimorphians from Contamana, Huallaga Basin and Atalaya regions, represented by the same dental loci, Prepidolopidae gen. nov. 2

sp. nov. 2 resembles most *Wamradolops* sp. nov. (large) but it differentiates from *Wamradolops* spp. by having more developed hypoconulid notch, lower hypoconid and entoconid, and less developed postcingulid, besides being much larger than *Wamradolops tsullodon*. Compared to Polydolopimorphia indet. gen. nov. A sp. nov., Prepidolopidae gen. nov. 2 sp. nov. 2 has more developed hypoconulid notch, shorter cristid obliqua, anteroposteriorly compressed hypoconid, less developed postcingulid, narrower talonid basin, postprotocristid and postmetacristid junction lower and meta- and entoconid more closely situated. Finally, when compared to Prepidolopidae gen. nov. 5 sp. nov. 5, Prepidolopidae gen. nov. 2 sp. nov. 2 is much larger, has a less antero-posteriorly compressed m1, smaller hypoconulid notch, lower hypoconid and entoconid, less developed hypoconulid and postcingulid, and no entocristid and by having a lingual sulcus separating the trigonid from the talonid. Prepidolopidae gen. nov. 2 sp. nov. 2 distinguishes itself from Prepidolopidae gen. nov. 1 sp. nov. 1 by being larger and having subtle sulci on the labial surface of the p3. Prepidolopidae gen. nov. 3 sp. nov. 3 is represented solely by one upper molar, hampering detailed comparisons with Prepidolopidae gen. nov. 2 sp. nov. 2, however the latter seems to be larger. Regarding Prepidolopidae gen. nov. 4 sp. nov. 4, this one has m1 with proto- and metacone more distantly situated, the junction of the preprotocristid and the postprotocristid more dorsally positioned and forming an angle larger than 90°, long cristid obliqua, longer and wider talonid basin, and narrower hypoconulid. Prepidolopidae gen. nov. 2 sp. nov. 2 differs from Prepidolopidae gen. nov. 6 sp. nov. 6 by being smaller and not having a developed posterior portion of the p3, which has no cusps.

Regarding the remaining prepidolopids already described in the literature, Prepidolopidae gen. nov. 2 sp. nov. 2 differentiates from *Prepidolops didelphoides* by not having well-developed cristid obliqua and entocristid, besides being slightly smaller. Prepidolopidae gen. nov. 2 sp. nov. *2* is also different from *P*. *molinai* by not having a low cristid obliqua, thus not allowing the “entoflexid” to join the “hypoflexid” creating a deep transversal labio-lingual sulcus between the talonid and trigonid (Pascual, 1980a; b). Prepidolopidae gen. nov. 2 sp. nov. 2 m1 is larger than the one of *Punadolops*, and, differing from this one, does not have the metaconid anteriorly positioned in relation to the protoconid and as the highest cuspid of the trigonid,

besides it does not have wide and more rounded hypoconid and wide talonid basin (Goin *et al*., 1998). *Perrodelphys coquinense* is much larger than Prepidolopidae gen. nov. 2 sp. nov. 2, and, differing from the latter, has high laterally compressed entoconid, wide talonid basin and a peculiar configuration of the trigonid, with para- and metaconid oriented anterolingually (Goin *et al*., 1999). Concerning *Coloradolops*, Prepidolopidae gen. nov. 2 sp. nov. 2 differentiates itself by being larger, having p3 with only two roots, and m1 with narrower hypoconid. However, the only m1 reported for this taxon is not figured, hampering the comparisons with Prepidolopidae gen. nov. 2 sp. nov. 2 (Chornogubsky *et al*., 2019). As for *Incadolops*, it is not represented by lower dentition, preventing further comparisons with Prepidolopidae gen. nov. 2 sp. nov. 2 (Goin & Candela, 2004).

Measurements. Large-sized Bonapartherioidea taxon, one of the largest regarding lower teeth (see Table 9).

Table 9. Measurements, in mm, of the teeth of Prepidolopidae gen. nov. 2 sp. nov. 2 specimens from the Huallaga Basin, Peruvian Amazonia.

Locality	MUSM 4029	Length	Width
TAR-55	Left p3	2.112	1.654
	Left m1	1,5133	1.4253

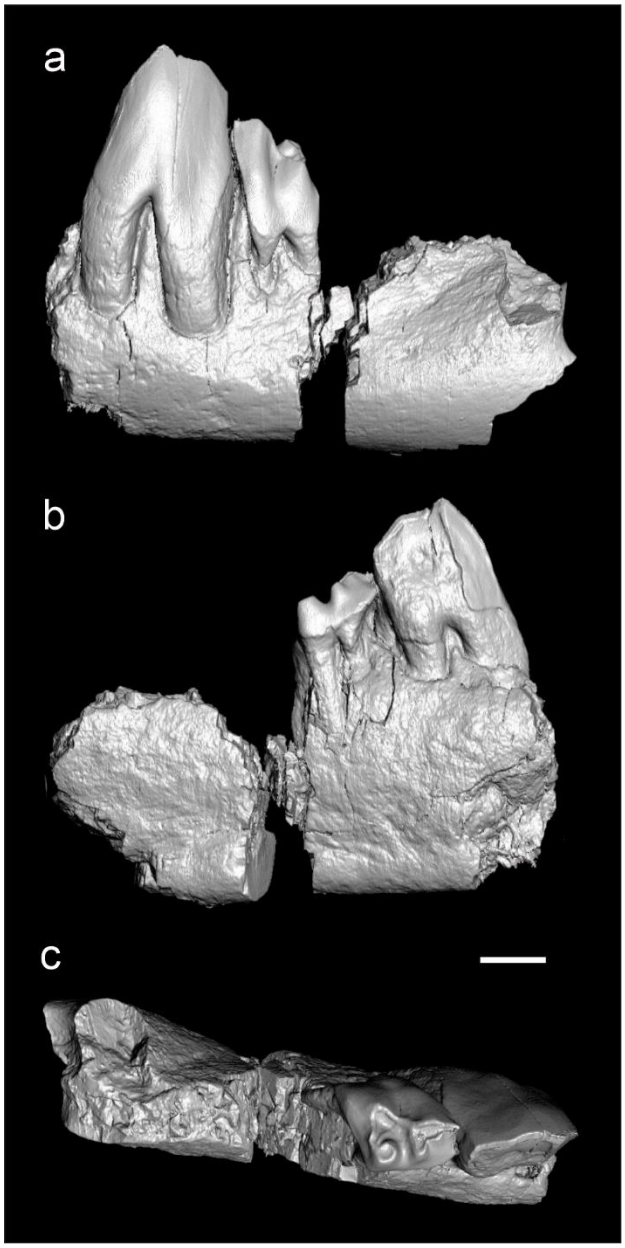


Figure 21. Prepidolopidae gen. nov. 2 sp. nov. 2 from TAR-55, late middle Eocene, Balsayacu Paleogene section, Huallaga Basin, Peru: **a–c,** MUSM 4029, one left dentary with p3–m1. **a**, labial, **b**, lingual, and **c**, occlusal views. Scale bar = 1 mm.

gen. nov. 3

Type species. Prepidolopidae gen. nov. 3 sp. nov. 3.

Diagnosis. As for the type and only known species.

Etymology. To be done.

gen. nov. 3 sp. nov. 3

(Figure 22)

Holotype. MUSM 3959, one right ?M1.

Etymology. To be done.

Type locality. TAR-74, Shapaja Paleogene section, San Martín Department, Peru.

Type horizon and age. Pozo Formation, Upper Member, late Eocene.

Diagnosis. Medium-sized prepidolopid with triangular upper molar with small paracone fused to the StB, well-developed metacone higher than the paracone and located posteriorly to the StC, narrow trigon basin, wide and short posterior cingulum and open narrow centrocrista.

Description. Triangular-shaped upper right molar of medium size among Contamana, Huallaga Basin and Atalaya bonapartherioids. It is most probably a M1 due to its broad anterior portion of the stylar shelf, differing from the M2 where this portion is narrower. The lingual margin is worn/broken. The anterior surface is slightly concave, and no anterior cingulum is present. The protocone is broken, but it has an antero-lingual position and is low and rounded. The preprotocrista is shorter that the postprotocrista. The paracone is fused to the StB, being positioned just lingually to it and much smaller in height. The metacone is fused to the StC and StD, being slightly posterior to the StC, but it is very large and high. The StC is the highest cusp of the molar, followed by the StD. The large metacone occupies a great amount of the trigon basin, which is labio-lingually narrow and not very deep. The centrocrista is open but narrow, the postparacrista is long and almost reaches the ectoflexus, but the premetacrista goes directly to the StC, not at the level of the ectoflexus. The ectoflexus is shallow. A wide but short posterior cingulum is present, extending lingually until the level of the metacone base.

Comments. The presence of triangular-shaped upper molars, with developed StB and StD fused with the para- and metacone, respectively, and absence of stylar platform allow to assign this new taxon to the family Prepidolopidae, according to Pascual (1980a, b).

Prepidolopidae gen. nov. 3 sp. nov. 3 differs from all the remaining prepidolopids already described in the literature by having a large posterior cingulum (Pascual,

1980a, b; Goin *et al*., 1998, 1999; Goin & Candela, 2004; Chornogubsky *et al*., 2019). However, it is morphologically closer to *Incadolops* and *Prepidolops* than to *Punadolops*. Regarding the other Contamana, Huallaga Basin and Atalaya bonapartherioids M1s, it differs from the *Wamradolops* spp. and Polydolopimorphia indet. gen. nov. A sp. nov. by its size (smaller than *Wamradolops* sp. nov. (large) and Polydolopimorphia indet. gen. nov. A sp. nov., and larger than *Wamradolops tsullodon*), absence of anterior cingulum and parastyle, protocone positioned more anteriorly and lingually, smaller paracone, narrower centrocrista, larger metacone, shallower ectoflexus, larger trigon basin and the absence of metaconule. Prepidolopidae gen. nov. 3 sp. nov. 3 is distinct from Prepidolopidae gen. nov. 1 sp. nov. 1 by having M2 with marked cingulum anterior and below the protocone, more developed parastyle and cinguli anterior and posterior to the paracone+StB, paracone+StB higher than metacone+stD, presence of a StC, wider and deeper trigon basin, V-shaped centrocrista, and narrower and shorter posterior cingulum. Prepidolopidae gen. nov. 3 sp. nov. 3 differentiates from Prepidolopidae gen. nov. 4 sp. nov. 4 by having a narrower centrocrista, higher metacone+StD, smaller protocone, more developed and long posterior cingulum, and the absence of an anterior cingulum below the protocone, and of a StC. It is also different from ?Prepidolopidae gen. et sp. indet. due to its larger size, concave anterior surface, smaller paracone, larger metacone, smaller stylar cusps, shallower ectoflexus and trigon basin, and posterior cingulum, and by the absence of anterior cingulum, parastyle and metaconule.

Measurements. Length = 1.3595 mm; width = 1.625 mm.

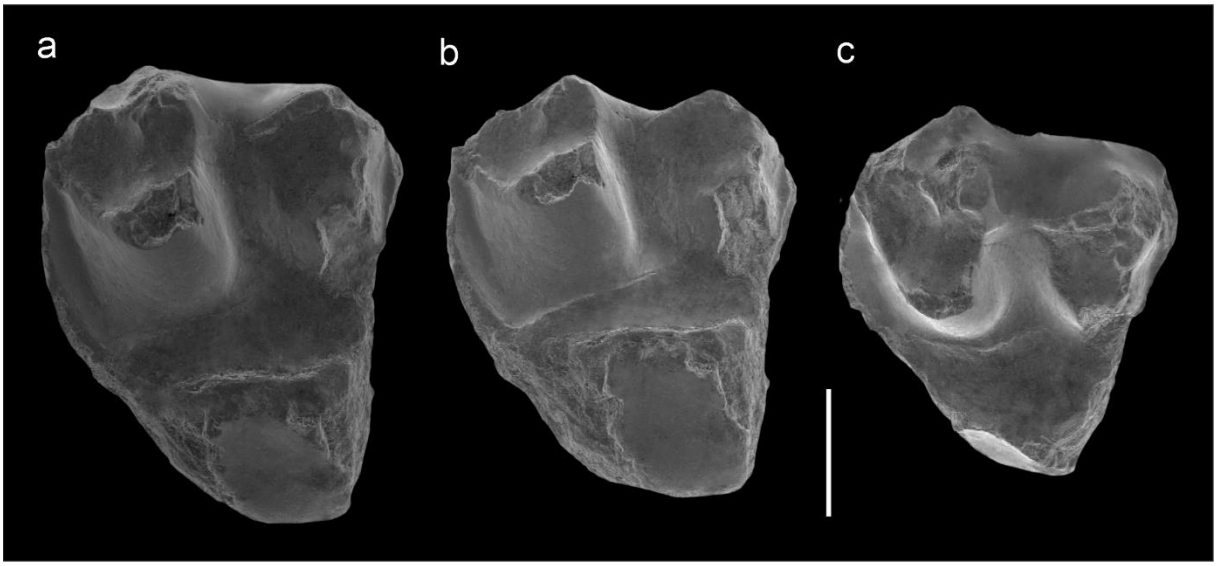


Figure 22. Prepidolopidae gen. nov. 3 sp. nov. 3 from TAR-74, late Eocene, Shapaja Paleogene section, Huallaga Basin, Peru: **a–c,** MUSM 3959, one right ?M1. **a**, occlusal, **b**, slightly lingual, **c**, slightly labial views. Scale bar = 500 µm.

gen. nov. 4

Type species. Prepidolopidae gen. nov. 4 sp. nov. 4.

Diagnosis. As for the type and only known species.

Etymology. To be done.

gen. nov. 4 sp. nov. 4

(Figure 23)

Holotype. MUSM 4068, one right M2.

Referred material. TAR-47: MUSM 4067, one right P3; MUSM 4069, one left M2; MUSM 4070, one left ?M3; MUSM 4071, one right dentary with broken ?m3; MUSM 4072, one right m1.

Etymology. To be done.

Type locality. TAR-47, Juanjui Paleogene section, San Martín Department, Peru.

Type horizon and age. Pozo Formation, Lower Member, ?late Eocene.

Description. MUSM 4067 is a P3 is small, and it is broken at its base and lingual side. An enamel covering is present only on the lingual side of the tooth and it is thick. There are no distinct cusps or sharp tips on it, possibly due to wear. On the labial surface

there is a deep groove, separating the P3 into two lobes, one anterior, which is longer and slightly higher, and one posterior smaller and lower.

The M2s MUSM 4068 and 4069 are triangular-shaped, and MUSM 4068 is broken, without the whole stylar region. Compared to the other bonapartherioids from Contamana, Huallaga Basin and Atalaya, they are considerably large. The protocone occupies a central position in relation to the antero-posterior molar axis and it is low. The preprotocrista is marked and long, almost forming a precingulum. When it reaches the paracone/stylar region it divides into two small cristae, i) one directed antero-labially, towards a cingulum between the parastyle and the anterior margin of the teeth; and ii) another small crest directed posteriorly, meeting lingually a very small and subtle preparacrista, and labially this small crest meets a well-developed parastyle. The paracone is large and high, being slightly higher than the metacone, but lower than the stylar cusps. The paracone is twinned with the parastyle and StB, which are subequal in size and separated occlusally by a deep sulcus running through the labial surface of the tooth. A long, curved and well-marked postparacrista connects the paracone to the tip of the StB. The posterior crest of the StB is short, as is the anterior crest of the StD. The ectoflexus is deep but not ventrally long. The StD has the same size as the parastyle and StB. Postero-lingually to the StD there is a small cingulum. The StD is connected to the metacone by a long premetacrista. The metacone is lower and antero-posteriorly shorter than the paracone, with a short postmetacrista that does not reach the cingulum present between the metacone and the StD. At the base of the metacone there is a small cingulum, which is connected to the postprotocrista. The centrocrista is more V-shaped, but not very narrow, since the postparacrista and the premetacrista do not meet directly. The trigon basin is wide, but shallow.

MUSM 4070 is most probably a M3, being much smaller than the M2 and it is also triangular-shaped. The protocone is also large and centrally positioned but, compared to the M2, it is higher. The preparacrista is also well-developed, forming a sort of cingulum, but the parastyle is much less developed than in the M2. Para- and metacone are also connected to the StB and StD, respectively, being slightly lower than these latter. The ectoflexus is insconspicuous and the centrocrista is much more open compared to the M2. The trigon basin is wider and deeper as well. A conspicuous postcingulum is also present.

MUSM 4071 is a very small fragment of a dentary with a fragment of one molar of intermediate size, with the labial surface and part of the anterior lingual surface. The labial side of the molar is shorter than the lingual one, but the bone is higher on the lingual side, so more of the crown surface is exposed on the labial side, despite the unilateral hypsodontia being less pronounced. The labial side is also marked by a considerable groove, just below the cristid obliqua. It has a much less antero-posteriorly compressed trigonid and no paraconid. The protoconid is large but lower than the metaconid. It is connected to the metaconid by a short dorsally oriented preprotocristid, delimiting a shallow anterior groove. The metaconid is only partially preserved, but it seems to be the higher cusp of the molar. The talonid is also broken, the entoconid and part of the talonid basin not being preserved. The hypoconid is anteroposteriorly large and low. The cristid obliqua is almost parallel to the antero-posterior molar axis.

MUSM 4072 is a rectangular-shaped m1, not as antero-posteriorly compressed as other bonapartherioids from Contamana, Huallaga Basin and Atalaya, and it is intermediate in size. The base of the tooth is wider than the top. It also shows unilateral hypsodontia on the labial side, but not as marked as other bonapartherioids. The trigonid is labio-lingually compressed, with para-, proto- and metaconid centrally and sequentially positioned. Antero-lingually to the paraconid there is a well-developed hypoconulid notch. The paraconid is very small, anterior to the protoconid and connected to the protoconid by a short but marked preprotocristid. The protoconid is large and high, but slightly shorter than the metaconid. It is anteriorly positioned in relation to the metaconid by a short, subtle postprotocristid, which does not go ventrally, but stays more at the same level than the proto- and metaconid. The angle formed by the preprotocristid and the postprotocristid is larger than 90°. The metaconid is slightly higher than the protoconid, but much smaller. The talonid is longer and wider than the trigonid, the talonid basin being deep. The entoconid is high, cuspidate, and slightly posteriorly positioned in relation to the hypoconid. The preencotcristid is not marked and neither is the postentocristid. The hypoconid is antero-posteriorly elongated and of medium high, being smaller than the entoconid. It is situated labio-lingually distant from the entoconid. The hypoconid is connected to the cristid obliqua

by a well-marked prehypocristid. The cristid obliqua is long and transversal. Postero-labially to the entoconid there is a significant and wide hypoconulid.

Comments. The presence of, on the upper molars, developed StB and StD fused with the para- and metacone, respectively, a triangular shape, and absence of stylar platform, as well as a hypertrophied P3, and on the lower molars labiolingually compressed trigonid and high proto- and entoconid allow to assign this new taxon to the family Prepidolopidae, according to Pascual (1980a, b).

Prepidolopidae gen. nov. 4 sp. nov. 4 is characterized by triangular-shaped upper molars of relatively large size among the polydolopimorphians from Contamana, Huallaga Basin and Atalaya. It is larger than Prepidolopidae gen. nov. 5 sp. nov. 5, but smaller than Polydolopimorphia indet. gen. nov. A sp. nov and *Wamradolops* sp. nov. (large). Prepidolopidae gen. nov. 4 sp. nov. 4 differentiates from *Wamradolops* spp. and Polydolopimorphia indet. gen. nov. A sp. nov. by not having upper molars with a metaconule and a quadrangular shape. It differentiates from Prepidolopidae gen. nov. 1 sp. nov. 1 by having M2 with a more triangular and less subtrapezoidal shape, shorter and less developed posterior cingulum, and metacone+StD more developed. Prepidolopidae gen. nov. 3 sp. nov. 3 is different from Prepidolopidae gen. nov. 4 sp. nov. 4 by having M2 with much more developed posterior cingulum and by the absence of a St?C. Prepidolopidae gen. nov. 2 sp. nov. 2 distinguishes itself from Prepidolopidae gen. nov. 4 sp. nov. 4 by labio-lingually compressed m1, with narrower trigonid, protoconid and metaconid being closely positioned, much lower entoconid and smaller trigonid basin. Prepidolopidae gen. nov. 5 sp. nov. 5 possess lower molars much more labio-lingually and antero-posteriorly compressed, narrower talonid basin, more developed hypoconulid and sulcus on the posterior margin of the molar.

Compared to the other prepidolopids, Prepidolopidae gen. nov. 4 sp. nov. 4 differs from *Perrodelphys coquinense* by having a less anteroposterioly compressed trigonid, more developed paraconid, metaconid much more posterior to the protoconid, and entoconid not laterally compressed (Goin *et al*., 1999). The differences among Prepidolopidae gen. nov. 4 sp. nov. 4 and *Coloradolops cardonensis* are that in the first one, on the upper molars, there is an anterior cingulum below the protocone, the trigon basin is narrower, the postparacrista is barely visible, the posterior cingulum is more developed and the small rim below the StB+paracone one the labial margin of

the teeth is absent; and, on the m1, the hypoconulid is positioned more distant from the entoconid (Chornogubsky *et al*., 2019). Compared to *Punadolops alonsoi*, Prepidolopidae gen. nov. 4 sp. nov. 4 does not possess paracone and metacone more separated from the StB and StD on the upper molars, and, on the lower molars, the metacone is not the highest cusp of the trigonid and is not situated anteriorly to the protoconid (Goin *et al*., 1998). *Prepidolops* spp. differ from Prepidolopidae gen. nov. 4 sp. nov. 4 by having on the upper molars a deep ectoflexus, wide tigon basin, triangular shape; lower molars with wider and longer trigonids and conspicuous anterobasal cingulum (Pascual, 1980a, b). Prepidolopidae gen. nov. 4 sp. nov. 4 can be distinguished from *Incadolops ucayali* by having a more open centrocrista, narrower trigon basin, larger posterior cingulum and by the absence of a metaconule (Goin & Candela, 2004).

Measurements. See Table 10.

Table 10. Measurements, in mm, of the teeth of Prepidolopidae gen. nov. 4 sp. nov. 4 specimens from the Huallaga Basin, Peruvian Amazonia.

Locality	Specimen	Locus	Length	Width
TAR-47	MUSM 4067	Right P3	1.043	0.775
	MUSM 4068	Right M2	1.081	1.2845
	MUSM 4069	Left M2	1.372	1.714
	MUSM 4070	Left M3	1.0395	1.0925
	MUSM 4072	right m1	1.354	1.003

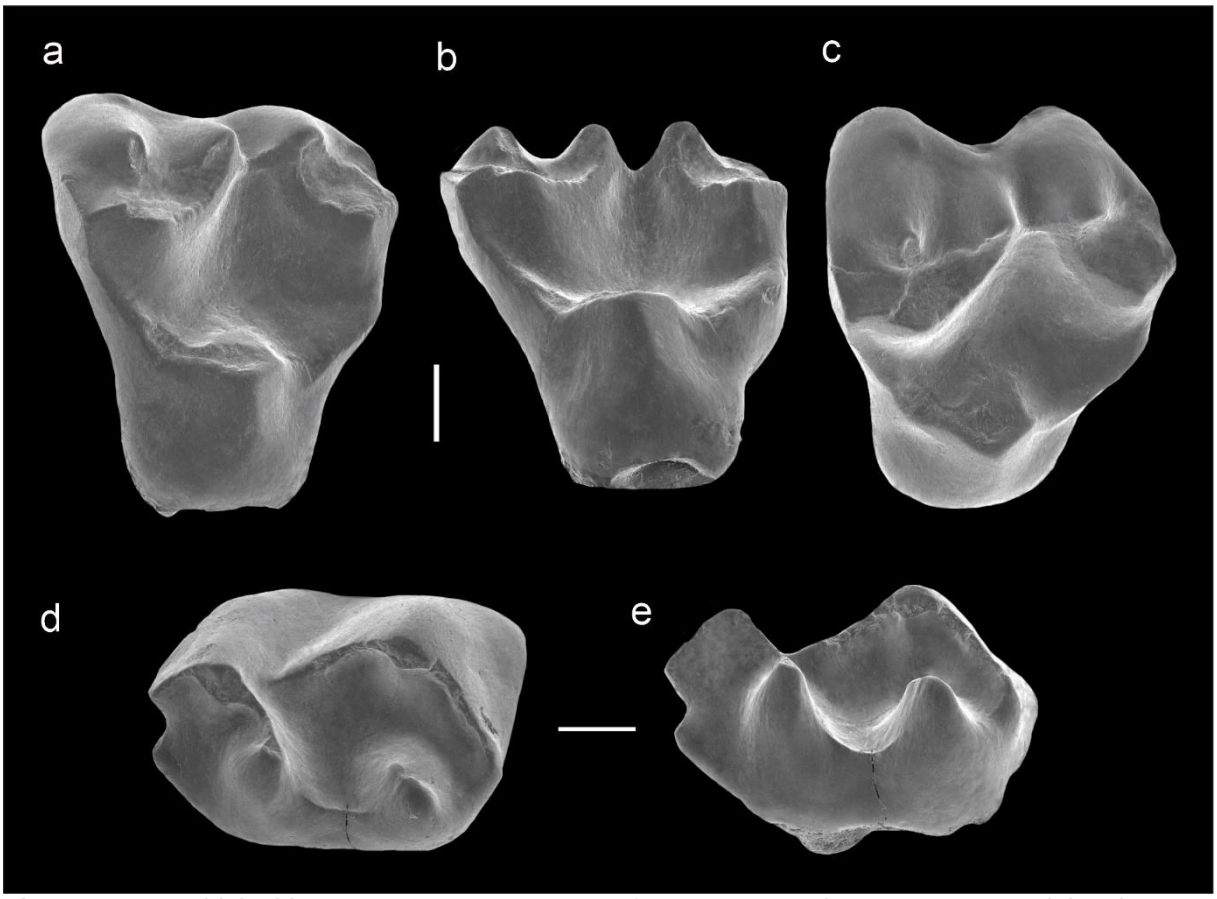


Figure 23. Prepidolopidae gen. nov. 4 sp. nov. 4 from TAR-47, ?late Eocene, Juanjui Paleogene section, Huallaga Basin, Peru: **a–c,** MUSM 4069, one left M2; **d–e,** MUSM 4072, right m1. **a, d**, occlusal, **b, e**, slightly lingual, **c**, slightly labial views. Scale bars = 300 µm.

gen. nov. 5

Type species. Prepidolopidae gen. nov. 5 sp. nov. 5.

Diagnosis. As for the type and only known species.

Etymology. To be done.

gen. nov. 5 sp. nov. 5

(Figure 24)

Holotype. MUSM 4144, one left dentary with p2–m1.

Etymology. To be done.

Referred material. CTA-51: MUSM 4129, one right m2. CTA-27: MUSM 4145, one dentary without teeth; MUSM 4146, one right m1; MUSM 4147, one left m1.

Type locality. CTA-27, Contamana, Loreto Department, Peru.

Type horizon and age. Pozo Formation, Lower Member, late middle Eocene (early Barrancan, ~41.6-40.94 Ma).

Other localities. CTA-51, Pozo Formation, Lower Member, late middle Eocene, Contamana, Loreto Department, Peru.

Diagnosis. Prepidolopidae gen. nov. 5 sp. nov. 5 is characterized by a very small size; m1 with marked postprotocristid and postmetacristid forming an angle of less than 90º, small slightly oblique cristid obliqua, developed hypoconid, well-developed hypoconulid below the entoconid, small and subtle preentocristid; m2 with large and high hypoconid, below which, on the posterior surface of the molar, there is an oblique dorso-ventrally oriented sulcus, hypoconulid situated closer to the hypoconid, entoconid smaller and less high than the hypoconid, and marked, long and parallel to the antero-posterior molar axis entocristid.

Description. The p2 is a very small and low-crowned tooth. Its wide but very short and located under the anterior portion of the p3. It has a very simplified morphology and a triangular shape. It seems to have one central cuspid, the highest portion of the occlusal surface. The p3 has two roots and a blade-like aspect. Compared to the p2 and m1 it is much higher. At the base of its anterior portion there is a V-shaped notch, with a lingual side much shorter, below which is the p2. On the occlusal surface, a posterior high cuspid is present, which is preceded by a marked anterior cingulid and followed by a short cristid, connecting it to another cuspid, much smaller and shorter. There are shallow sulci on the lingual and labial surfaces between these two cuspids. The posterior cuspid is followed by a marked and long cristid, at the end of which there is a notch, where the anterior portion of the m1 is inserted.

The m1 has unilateral hypsodontia, with its labial surface being much higher than the labial one. It is labio-lingually compressed, with a much wider base. Two roots are visible. The trigonid possess three cuspids: a small paraconid which is located under the p3 notch, followed by a small slightly oblique postparacristid, connecting it to a high protoconid; the protoconid is followed by a marked but short postprotocristid, which runs ventrally and is parallel to the antero-posterior molar axis; this postprotocristid is

connected to an also marked postmetacristid, which also runs dorsally but is perpendicular to the anteroposterior molar axis, their junction forms an angle of less than 90º; the postmetacristid is connected lingually to the metaconid, which is a very small cuspid. Below the junction of the postprotocristid and postmetacristid there is a small slightly oblique cristid obliqua, connected to a narrow but notable hypoconid. There is a well-developed hypoconulid below the entoconid. The entoconid is a large and high cuspid, preceded by a small and subtle preentocristid. The trigonid basin is narrow but very deep. There is a wide sulcus on the posterior margin of the molar. MUSM 4146 is slightly more worn m1, its protoconid having become shorter and with a more rounded tip. In MUSM 4146 it is possible to observe the anterior surface of the tooth, where there is a marked rounded hypoconulid notch below the paraconid. MUSM 4147 is very worn m1, with much of the occlusal morphology not visible, the trigonid has a triangular-shape and the trigonid basin is wider and shallower than in MUSM 4144 and MUSM 4146.

The m2 is shorter and smaller than the m1 and with a more quadrangular shape. Its unilateral hypsodontia is less developed and the tooth is less compressed labio-lingually than the m1 as well. The trigonid is more antero-posteriorly compressed than in the m1, with a very small paraconid, below which there is a smaller rounded hypoconulid notch. The protoconid and metaconid have approximately the same height and are connected by a single cristid, which is very marked and perpendicular to the antero-posterior molar axis. This cristid is almost at the same height as the proto- and metaconid, which can be due to wear. The cristid obliqua is almost absent, but the hypoconid is a large and high cuspid, below which, on the posterior surface of the molar, there is an oblique dorso-ventrally oriented sulcus. A large hypoconulid is also present, but it is situated closer to the hypoconid, and not below the entoconid as in the m1. The entoconid is smaller than the hypoconid, but only slightly shorter. It is preceded by a marked entocristid, which is longer than in the m1, and almost parallel to the antero-posterior molar axis.

MUSM 4145 was assigned to this species due to its very small size, which is very characteristic of Prepidolopidae gen. nov. 5 sp. nov. 5.

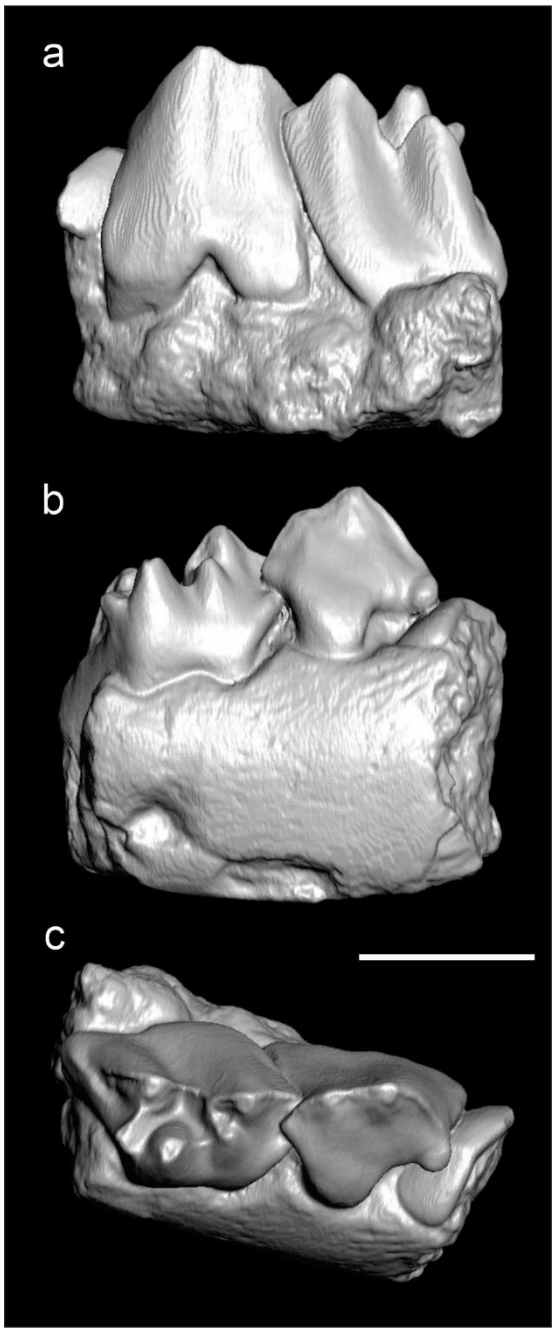


Figure 24. Prepidolopidae gen. nov. 5 sp. nov. 5 from CTA-27, late middle Eocene, Contamana, Peru: **a–c,** MUSM 4144, one left dentary with p2–m1. **a**, labial, **b**, lingual, **c**, occlusal views. Scale bar = 1 mm.

Comments. The presence of hypertrophied p3 without serrated margins, and lower molars with labiolingually compressed trigonid and high proto- and entoconid allow to assign this new taxon to the family Prepidolopidae, according to Pascual (1980a, b).

Prepidolopidae gen. nov. 5 sp. nov. 5 is the smallest Polydolopimorphia taxon from Contamana, Huallaga Basin and Atalaya regions. It is much smaller than the coeval Polydolopimorphia indet. gen. nov. A sp. nov. and the *Wamradolops* spp. and

it is also smaller than Prepidolopidae gen. nov. 2 sp. nov. 2 and Prepidolopidae gen. nov. 4 sp. nov. 4.

Compared to *Punadolops*, the m1 has the protoconid as the highest trigonid cusp and it is anterior to the metaconid; the m1 is not necessarily shorter and wider than m2. The m2 also is smaller than *Prepidolops* and more brachydont, with bunoid cusps, anterobasal cingulum poorly developed, ento- and hypoconid very small, talonid and trigonid with less difference in height, the trigonid is also very compressed, talonid is wide, as is the talonid basin, but it is not shallow, it is deep. The m2 seems to be less elongated than the one of *Punadolops*, the protoconid of *Punadolops* seems to be posterior to the metaconid, and here it is the contrary. In *Punadolops* the postmetacristid is directed anteriorly, meeting the postprotocrisid, which is rounded and anteriorly directed, forming a curve, but in this taxon the postmetacristid and the postprotocristid are straight and cannot be differentiated, both directed towards the center of the molar, forming a unique, straight and shallow crest (Goin *et al*., 1998). Compared to *Prepidolops* the m1 has less difference in height between the trigonid and the talonid, the anterobasal cingulum of m1 is less developed and it is smaller. It has shorter and narrower trigonid. Protoconid has more difference of height with the metaconid and is more anteriorly placed, the postprotocristid and the postmetacristid join more labially and ventrally, forming a smaller angle. The whole molar seems narrower and shorter. Talonid is less wide, paraconid placed more in a continuation of the preprotocristid and not as a cuspid as in *Prepidolops*, the cristid obliqua is shorter and parallel, not oblique, and long as in *Prepidolops*, the entocristid is shorter, metaconid is much lower, hypoconid less developed. The m2 has less oblique preprotocristid, which is moreparallel to the axis, proto and metaconid have less height difference, the postprotocristid is not deep and V-shaped, it is straight and shallow, hypo and entoconids are more bunoids, hypoconulid is shorter, not extending itself to the to the lingual margin but ending in a more mesial position, cristid obliqua is shorter and straight, entocristid is more lingually placed and is more straight, longer and marked, the talonid is slightly wider than in *Prepidolops*, presence of a small protuberance lingual and posterior to the paraconid, less developed anterobasal cingulum (Pascual, 1980a, b). Compared to *Perrodelphys*, this species does not have a preprotocristid long and parallel as in this taxon, the protoconid is not so much

anterior to the metaconid, postmetacristid and postoprotocristid form a much more open angle, the talonid seems to be much lower and without developed cusps, besides it is bigger (Goin *et al*., 1999). Compared to *Coloradolops cardonensis*, Prepidolopidae gen. nov. 5 sp. nov. 5 has on the m1 the paraconid much more distant from the protoconid than the metaconid, narrow hypocone and hypoconulid not twinned with the entoconid, situated slightly labial to the latter (Chornogubsky *et al*., 2019).

Measurements. See Table 11.

Table 11. Measurements, in mm, of the teeth of Prepidolopidae gen. nov. 5 sp. nov. 5 specimens from the Contamana region, Peruvian Amazonia.

Locality	Specimen	Locus	Length	Width
CTA-27	MUSM 4144	Left p3	1.116	0.9585
	MUSM 4146	Right m1	1.008	0.92
	MUSM 4144	Left m1	1.065	0.9835
	MUSM 4147	Left m1	0.8183	0.744
CTA-51	MUSM 4129	Right m2	0.9515	0.8075

gen. nov. 6

Type species. Prepidolopidae gen. nov. 6 sp. nov. 6.

Diagnosis. As for the type and only known species.

Etymology. To be done.

gen. nov. 6 sp. nov. 6

(Figure 25)

Holotype. MUSM 4121, one left p3.

Etimology. To be done.

Type locality. TAR-14, Abra de Machungo, San Martín Department, Peru.

Type horizon and age. Chambira Formation, late Oligocene (Deseadan SALMA).

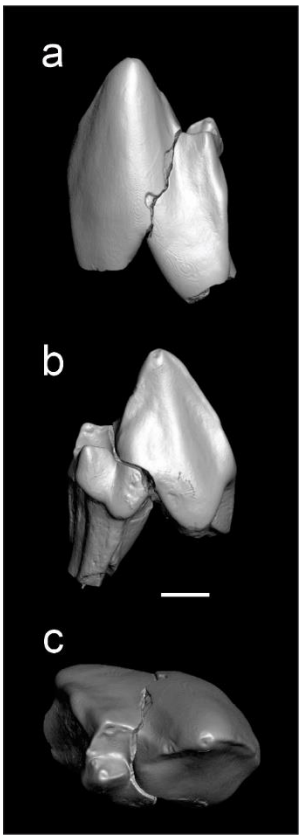


Figure 25. Prepidolopidae gen. nov. 6 sp. nov. 6 from TAR-14, late Oligocene, Abra de Machungo, Huallaga Basin, Peru: **a–c,** MUSM 4121, one left p3. **a**, labial, **b**, lingual, **c**, occlusal views. Scale bar = 1 mm.

Description. Large, tall, trenchant, double-rooted p3, lacking serrated edge. One anterior cusp is present in the anterior half of the tooth, very big, tall and robust. From this high cusp there is a robust anterior crest going antero-lingually, and a more delicate crest going posterolabially, which is shorter and ends above a well-developed posterior platform, much narrower and lower than the anterior portion of the tooth, with two “cusps”: one labial and one lingual, which have approximately the same height. The labial and lingual surfaces are rounded. In the labial surface, between the anterior and posterior portions, there is a marked vertical groove. On the posterobasal surface, the distinction between the crown and the root is very marked, with a sharp groove, signaling the contact surface with the m1.

Comments. Large sized prepidolopid, much bigger than the p3 of Prepidolopidae gen. nov. 2 sp. nov. 2. According to Pascual (1980a, b), Prepidolopidae p3 are hypertrophied, sharp, but with straight crests, not serrated. Both *Prepidolops* spp. have

almost similar p3 and in the descriptions of *Punadolops*, *Perrodelphys* and *Incadolops* there are no diagnostic features for p3. It is much larger than the largest p3 of a Prepidolopidae described until the present, the one of *Coloradolops*, since the specimens of *Perrodelplys* do not present p3. It differentiaties from Polydolopidae and *Epidolops* by not having a p3 with serrated margins, from Rosendolopidae by its much greater size, and by being more complex and bigger than Argyrolagoidea p3 (Pascual, 1980a, b; Goin *et al*., 1998, 1999; Goin & Candela, 2004; Beck, 2017; Chornogubsky *et al*., 2019).

Measurements. Total length = 3.27; trigonid length = 2.23; trigonid width = 2.41; talonid length = 1.02; talonid width = 2.36.

?Prepidolopidae

gen. et sp. indet.

(Figure 26)

Referred material. MUSM 4075, one left ?M1 (if *Evolestes* it would be a M3).

Locality. TAR-21, Shapaja Paleogene section, San Martín Department, Peru.

Formation and age. Pozo Formation, Upper Member, latest late Eocene.

Description. Left upper molar triangular-shaped of diminute size and gracile morphology. The protocone is low and very lingually projected, with a sharp tip. The preprotocristid is very marked and long, meeting the paracone anterolingually. The paracone is low, but anteroposteriorly developed, and it is twinned with the StB. The preparacrista is short, but clearly visible, joining anterolingually the StB. There is a well-developed and wide anterobasal cingulum, with a small StA at its lingual end. But this cingulum is not long and does not reach the lingual side of the tooth. Instead, it goes ventrally and ends up at below the meeting point of the preprotocrista and the paracone. The StB is very well-developed, being the largest and highest cusp of the molar, and it is not labio-lingually compressed. It is slightly posterior to the paracone. The posterior crest of the StB is very marked and longer than the anterior crest of the StD, but both are deep, as is the ectoflexus. The StD is smaller and lower than the StB, and, as the latter, it is not labio-lingually compressed. The metacone is twinned with the StD and slightly posterior to it. It is big, but lower than the StD. The premetacrista

is not very long and meets the StD basally at the center of it. Postparacrista and premetacrista do not contact each other directly and the centrocrista is very open. The postmetacrista is long, curved and postero-lingually directed, almost perpendicular to the molar axis, reaching the labial side of the teeth, forming a small cuspid there (StE?). Below the metacone there is a small metaconule. The trigon basin is narrow antero-posteriorly, but deep labio-lingually. On the posterior side of the molar, its surface is excavated just below the metaconule.

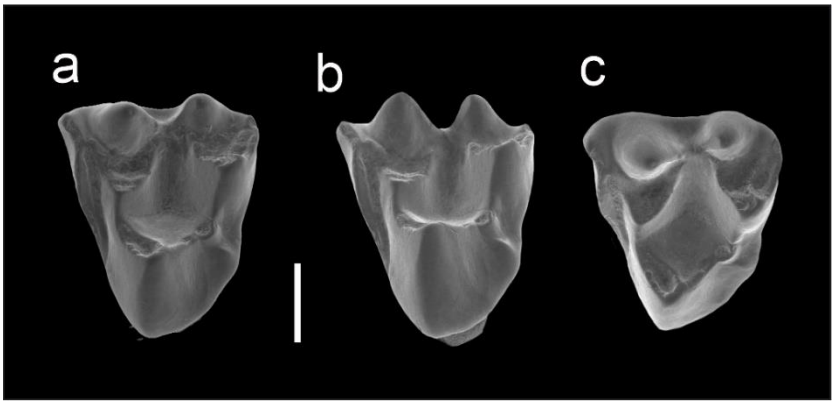


Figure 26. ?Prepidolopidae gen. et sp. indet. from TAR-21, latest late Eocene, Shapaja Paleogene section, Huallaga Basin, Peru: **a–c,** MUSM 4075, one left ?M1. **a**, occlusal, **b**, slightly lingual, **c**, slightly labial views. Scale bar = 500 µm.

Comments. MUSM 4075 resembles *Evolestes* by being triangular shaped, without well-developed metaconule also having the StB as the highest cusp, small paracone, deep ectoflexus, short preparacrista, shorter and more perpendicular postmetacrista, but the latter still ends at the labial side of the teeth, with a small StE?. However, it differentiates from *E*. *hadrommatos* by seemingly having a less lingually salient protocone, much smaller StE?, more open centrocrista, StB and StD more distant from one another, smaller metacone, the premetaconular crest is not visible, trigon basin antero-posteriorly longer, and there is no deep sulcus separating the metacone and the metaconule.

MUSM 4075 differentiates from Polydolopimorphia, in general, by having a large difference in the size between the stylar cusps (small StD, not common among polydolopimorphians). It differentiates from Prepidolopidae by having a large anterior cingulum, that is not present or poorly developed in prepidolopids. Also, according to the diagnosis of Pascual (1980a, b), prepidolopids are characterized by almost

coalescent StB and StD with paracone and metacone, respectively, which is not the case in this specimen.

Thus, we assign this specimen to ?Prepidolopidae gen. et sp. indet., pending further comparisons with *Evolestes* and close allies, as well as with prepidolopids.

Measurements. Length = 1.2543; width = 1.473.

Superfamily Argyrolagoidea Ameghino, 1904

Family Argyrolagidae Ameghino, 1904

Proargyrolagus Wolff, 1984

sp. nov. 1 (small)

(Figure 27)

Holotype. MUSM 4083 one right M2.

Referred material. TAR-21: MUSM 3060, one left M2; MUSM, 3061, one left m1; MUSM 4076, 4077, 4078, three right M1; MUSM 4079, 4080, 4081, 4082, four left M1; MUSM 4084, one right M2; MUSM 4085, 4086, 4087, 4088, 4089, 4090, six left M2; MUSM 4091, one right m1; MUSM 4092, 4093, two left m1; MUSM 4094, 4095, 4096, 4097, 4098, 4099, 4100, seven right m2; MUSM 4101, 4102, 4103, three left m2; MUSM 4104, one right m3; MUSM 4105, 4106, 4107, 4108, 4109, 4110, 4111, 4112, eight ?m3; MUSM 4113, 4114, 4115, 4116, 4117, 4118, six very fragmentary molars. CTA-29: MUSM 4141, one left M2.

Etimology. To be done.

Type locality. TAR-21, Shapaja Paleogene section, San Martín Department, Peru.

Type horizon and age. Pozo Formation, Upper Member, latest late Eocene.

Other localities. CTA-29, Pozo Formation, Lower Member, late middle Eocene Contamana, Loreto Department, Peru.

Diagnosis. Small argyrolagid with protohypsodont molars; M2 with long but not large parastyle, well-developed and long posterior cingulum, and deep lingual sulcus; m1 with more lingually positioned metaconid and well-developed “ectostyle” and hyponoculid.

Description. The upper and lower molars are prismatic and “protohypsodont” (i.e., high-crowned) and complete specimens retain closed roots. The M1 and M2 are very

similar morphologically, both being quadrangular-shaped, relatively high-crowned and resembling in occlusal morphology. The M1 is just slightly longer than the M2. On the M1, on the antero-labial margin, only one cusp is present, the paracone completely fused to the StB. A parastyle is present antero-labially to the paracone. The postparacrista is long and directed dorsally towards the trigon basin. The ectoflexus is deep and narrow. After the ectoflexus there is the StD and the metacone, which are fused, the metacone being small (and not visible in specimens with more wear). There is a well-developed premetacrista going from the metacone towards the trigon basin. A StD posterior crest is connected to a well-developed posterior cingulum, running along the entire posterior margin of the teeth, connected to the metaconule on the lingual margin. The metaconule is wide but not very salient. Between the metaconule and the protocone there is a deep and wide lingual sulcus. The protocone is a high cusp, antero-posteriorly compressed and lingually salient.

On the M2 a much larger and more salient parastyle is present next to the paracone. The ectoflexus is narrower, and the structure formed by it and the postparacrista and the StD is V-shaped. No metacone is present, only a high and large StD. Just below and lingually to the StD there is a fossa, this part of the trigon basin being much deeper than the portion between the protocone and the paracone. In specimens with more wear, this fossa becomes shallower, being surrounded by two cristae, which form a drop-shaped structure, going from the ectoflexus until the trigon basin, lingual to the StD. The posterior cingulum is also well-developed, as in the M1, but the metaconule is antero-posteriorly compressed. There is a deep sulcus separating the metaconule from the protocone. The protocone is less anteroposteriorly compressed than in the M1, having a more rounded shape. Both in the M1 and in the M2, with the increasing wear, most of the occlusal structures disappear, the labial and lingual cusps and a wide flat trigon basin remaining.

The lower molars have a weak labiolingual constriction among trigonid and talonid, and small protoconid, entoconid and hypoconulid. The m1 is triangular-shaped and has unilateral hypsodontia, with the lingual margin being higher. The protoconid is very high, and labio-lingually compressed, forming a thin anterior tip. Antero-labially to the protoconid there is a well-developed crest running ventrally. Postero-labially to the protoconid, a conspicuous “ectostyle” *sensu* Goin & Abello (2013) is present. It is

followed by a long and oblique cristid obliqua, ending at a low, labially salient, and relatively wide hypoconid. The hypoconulid is developed and situated behind the entoconid. The entoconid is a very tall cuspid, but not lingually salient. It is preceded by a short preentocristid, connected to a long and straight crest, that goes until the postparacristid. The talonid basin is relatively wide, the posterior portion of the m1 being much wider than the anterior one in general.

The m2 is quadrangular-shaped. It is high crowned with less difference between the labial and lingual margins, the lingual one being slightly higher. The paraconid is a very incipient structure present only in some molars with few wear just anteriorly to the metaconid. This structure is connected by a crest to the protoconid, which is very small and antero-labially positioned. Posteriorly to the protoconid there is a very well-developed “ectostyle”, which is rounded and as labially salient as the hypoconid. Behind and below the “ectostyle”, a long and straight cristid obliqua is present, connected posteriorly to a low hypoconid, but this one is higher than in the M1. A well-developed hypoconulid is present, but it is positioned more labially to the entoconid than in the m1. The entoconid is a very high cusp, situated much more anteriorly than the hypoconid. The talonid basin is not very wide neither very deep.

The m3 is very similar morphologically to the m2, being quadrangular-shaped, but with a lower crown and smaller size. On the anterior portion, only the metaconid and the “ectostyle” are present, the metaconid being much higher than the latter. The cristid obliqua is shorter and with an oblique direction, differing from the one in the m2. The hypoconid is low and slightly antero-posteriorly compressed. The hypoconulid is present, but it is smaller than in the m1-m2 and is situated labially to the entoconid. The entoconid is a high and large cusp, preceded by a marked oblique preentocristid. The talonid basin is not very wide neither very deep. As with the upper molars, the lower molars also lose much of its occlusal structures with increasing wear, when it is possible to see only the main cuspids and flat basins between them. This hampers the taxonomic identification of the specimens, as well as the identification of the locus to which they belong.

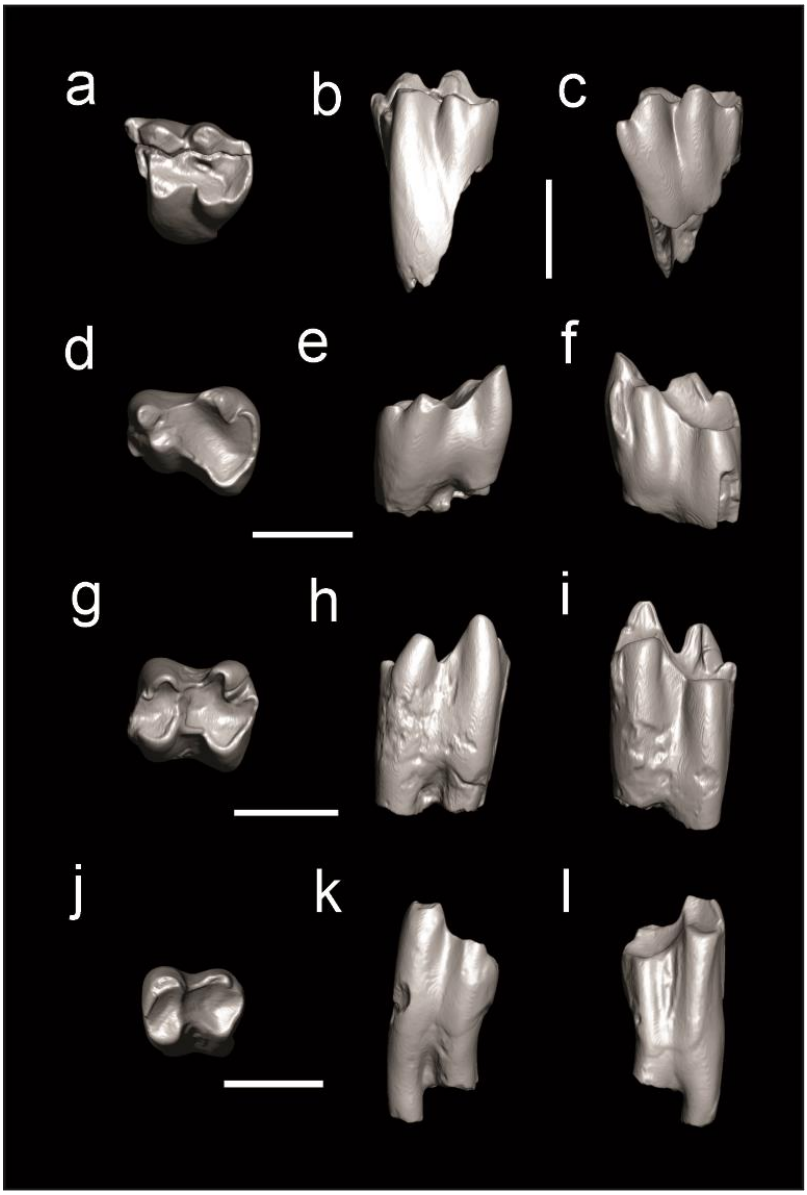


Figure 27. *Proargyrolagus* sp. nov. 1 (small) from TAR-21, latest late Eocene, Shapaja Paleogene section, Huallaga Basin, Peru: **a–c**, MUSM 4083, right M2; **d–e**, MUSM 3061, left m1; **g–i**, MUSM 4101, left m2; **j–l**, MUSM 4104, right m3. **a, d, g, j**, occlusal, **b, e, h, k**, lingual, **c, f, l, l**, labial views. Scale bars = 1 mm.

Comments. Small species of Argyrolagidae. These tiny taxa are mostly documented by millimetric molars showing the molar pattern of argyrolagid *Proargyrolagus* (see Goin & Abello 2013) and can be assigned to this genus by the presence of closed-roots hypsodont molars with anterior and posterior lobes of about the same size (Wolff, 1984). Molar cusps of argyrolagids such as *Proargyrolagus*, are well identified on fresh teeth (Sanchez Villagra & Kay, 1997, fig.6; Goin & Abello, 2013, fig. 4:1-12), but they

disappear as wear progresses. However, wear degree of some of *Proargyrolagus* sp. nov. 1 (small) is not so strong allowing comparisons with the remaining species of this genus: *P. bolivianus* (late Oligocene, Bolivia; Wolff 1984) and *P. argentinus* (early Miocene, Patagonia; Goin & Abello 2013). *Proargyrolagus* sp. nov. 1 (small) differs from *P*. *bolivianus* by not having a strong posterolingually directed postparacrista, by having a marked premetacrista on the upper molars; and, on the lower molars, the labial sulcus is deeper and the lingual one is shallower, and the molars are more labiolingually compressed (Wolff, 1984; Sánchez-Villagra & Kay, 1997). It differentiates from *P*. *argentinus* by having shorter trigonid on m2-m3, parastylar corner more developed on M2-M3, M1 with more lingually salient protocone and higher paracone+StB (Goin & Abello, 2013).

Based on comparisons of m1, *Proargyrolagus* sp. nov. 1 (small) and *P*. *magnus* sp. nov. share the same general morphology, but differ in their size, *Proargyrolagus* sp. nov. 1 (small) being 30% smaller than *P*. *magnus* sp. nov.

Measurements. See Table 12.

sp. nov. 2 (large)

(Figure 28)

Holotype. MUSM 4064, one right M2.

Referred material. TAR-47: MUSM 4065, one right M2; MUSM 4066, one right P3; TAR-01: MUSM 3991, one left m1.

Type locality. TAR-01, Shapaja Paleogene section, San Martín Department, Peru.

Type horizon and age. Pozo Formation, Upper Member, earliest Oligocene.

Other localities. TAR-47, Juanjui Paleogene section, Pozo Formation, Lower Member, ?late Eocene, San Martín Department, Peru.

Diagnosis. Medium-sized argyrolagid with protohypsodont and slender molars. Centrally positioned metaconid and not very well-developed “ectostyle” on m1; M2 with conspicuous but not long parastyle, moderate posterior cingulum and shallow lingual sulcus.

Table 12. Measurements, in mm, of *Proargyrolagus* sp. nov. 1 (small) from the Contamana and Huallaga Basin regions, Peruvian Amazonia.

Locality	Specimen	Locus	Length	Width
TAR-21	MUSM 4076	Right M1	1.333	1.1235
	MUSM 4077	Right M1	1.296	1.152
	MUSM 4079	Left M1	1.2093	1.0735
	MUSM 4080	Left M1	1.3523	1.088
	MUSM 4081	Left M1	1.291	1.0835
	MUSM 4082	Left M1	1.3615	1.087
	MUSM 4083	Right M2	1.129	1.092
	MUSM 4084	Right M2	1.136	1.092
	MUSM 3060	Left M2	1.102	1.2365
	MUSM 4085	Left M2	1.1075	1.1055
	MUSM 4086	Left M2	1.054	1.126
CTA-29	MUSM 4141	Left M2	1.2155	1.24
TAR-21	MUSM 4091	Right m1	1.2015	0.845
	MUSM 3061	Left m1	1.1875	0.9265
	MUSM 4092	Left m1	1.3215	1.0195
	MUSM 4093	Left m1	1.2115	0.9285
	MUSM 4094	Right m2	1.235	1.144
	MUSM 4101	Left m2	1.235	1.084
	MUSM 4102	Left m2	1.258	1.0945
	MUSM 4104	Right m3	1.094	0.998

Description. MUSM 4066 is a high-crowned P3 with two roots, it is worn, with very few characteristics of the occlusal surface preserved. The labial surface is rounded and the labial one is concave. It is still possible to observe a sulcus on the lingual side, separating the anterior portion from the posterior one. The occlusal surface is like a flat basin, with an anterior portion slightly higher.

MUSM 4064 and 4065 are two large, quadrangular-shaped M2, MUSM 4064 is not very worn and 4065 is more worn. They are both relatively high-crowned, especially the labial margin. On the anterior labial margin, only one cusp is present, which could be the paracone or the paracone fused with the StB, in this latter case the StB would be completely undistinguishable from the paracone. Anteriorly to the paracone there is a conspicuous parastyle, but it is not wide labio-lingually. The paracone is followed by a short posparacrista, connecting it to a deep but narrow ectoflexus. The metacone is

incipient, and connected to a large StD, which is higher than the paracone. Below the paracone, starting on the ectoflexus, until the trigon basin, there is a crest, connected posteriorly to the premetacrest, forming a V-shaped centrocrista, which is oblique, directed posteriorly. This centrocrista also delimitates a deep fossa on the trigon basin, going until the posterior margin of the metacone+StD. The StD posterior crest is long and connects the StD to a well-developed posterior cingulum, which is rounded. The posterior cingulum is connected lingually to a wide but not high metaconule. Between the metaconule and the protocone there is a deep sulcus on the labial margin of the teeth. The protocone is a wide and high cusp, situated just in front of the paracone. On MUSM 4065, due to wear, much of this occlusal morphology is not visible. It is still possible to observe the paracone, the deep ectoflexus, the high StD, the well-developed posterior cingulum and metaconule, the labial sulcus and the protocone. But between the structures located on the margins of the tooth, there is a flat basin, with no structures.

MUSM 3991 is a triangular-shaped m1, with a relatively high crown, especially the lingual margin. The trigonid is much narrower than the talonid. The paraconid is more lingually positioned, being a rounded cusp. Anterior to it, on the anterior surface of the molar, there is crest-like structure, very conspicuous, that goes almost until the base of the molar. Just below the paraconid, labial and posteriorly to it, there is an “ectosyle” *sensu* Goin & Abello (2013), but it is not very well-defined, possibly because of the wear. This “ectostyle” is connected to a long and oblique cristid obliqua, which is straight and not rounded. The hypoconid is somewhat antero-posteriorly compressed, forming a small tip labially salient. The posthypocristid is long and connected to a small, not very posteriorly salient hypoconulid, situated behind the entoconid. The entoconid is a high cuspid, and has an inclined position, towards the centro-anterior portion of the tooth. The preentocristid goes straight and ventrally, meeting an also straight and dorsally-directed postmetacristid.

Comments. *Proargyrolagus* sp. nov. 2 (large) comes from TAR 01 and TAR-47. Similarly, to known species of this genus, M2 of *P*. sp. nov. 2 (large) have the anterior labial cusp (StB+paracone, Goin & Abello, 2013) smaller than the posterior one (StD+metacone, Goin & Abello, 2013) and protocone and metaconule equally salient. In contrast to *Proargyrolagus* sp. nov. 1 (small), *P*. sp. nov. 2 (large) has shallower

labial sulcus and ectoflexus, and larger parastilar corner. It differentiates from *Proargyrolagus argentinus* by having less labio-lingually compressed upper and lower molars, parastylar corner on M2 more developed, and metaconule on M2 less lingually salient (Goin & Abello, 2013). *Proargyrolagus* sp. nov. 2 (large) differs from *P. bolivianus* by not having a posterolingually directed postparacrista and by having a marked premetacrista on the upper molars, and by having on the m1 a smaller "ectostyle".

Measurements. See Table 13.

Table 13. Measurements in mm of *Proargyrolagus* sp. nov. 2 (large) teeth from the Huallaga Basin, Peruvian Amazonia.

Locality	Specimen	Locus	Length	Width
TAR-47	MUSM 4066	Right P3	1.693	1.255
	MUSM 4064	Right M2	1.595	1.52
	MUSM 4065	Right M3	1.357	1.356
TAR-01	MUSM 3991	Left m1	1.667	1.196

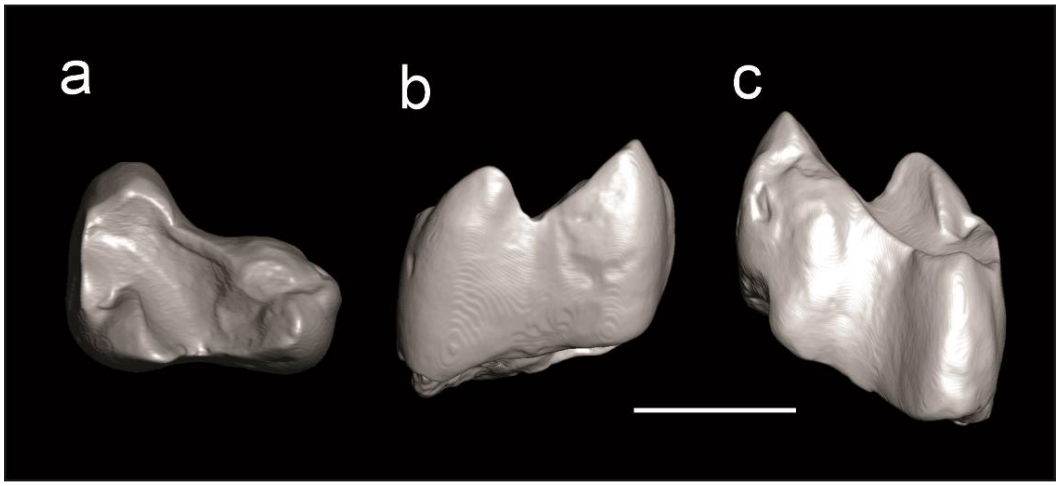


Figure 28. *Proargyrolagus* sp. nov. 2 (large) from TAR-01, early Oligocene, Shapaja Paleogene section, Huallaga Basin, Peru: **a–c,** MUSM 3991, one left m1. **a**, occlusal, **b**, slightly lingual, **c**, slightly labial views. Scale bar = 1 mm.

cf. *Proargyrolagus* sp.

Referred material. TAR-20: MUSM 4062, 4063, two left m2. TAR-72: MUSM 4074, one right M2.

Locality. Shapaja Paleogene section, San Martín Department, Peru.

Formation and age. Pozo Formation, Upper Member, late Eocene.

Description. MUSM 4072 is a partial upper molar, with the labial cusps and the part of the protocone preserved, but without much of the posterior portion. It is possible to observe a developed parastyle, the paracone, a very small metacone connected to a high StD. There is a deep and relatively wide ectoflexus. MUSM 4062 and 4063 are two left m2 broken and very worn. On MUSM 4062, the anterior portion of the tooth is preserved, with two cuspid-like structures ("ectostylid" and metaconid), which are rounded and low. The posterior portion is lower, it is possible to observe a hypoconid and part of the hypoconulid, the entoconid portion is broken. On MUSM 4063 only the anterior portion is preserved, with the protoconid, metaconid and the "ectostyle".

Comments. MUSM 4062 and MUSM 4063 approximately the same size as *Proargyrolagus* sp. nov. 1 (small) and MUSM 4074 has the same size as specimens of *Proargyrolagus* sp. nov. 2 (large). However, due to the incomplete and worn state of these specimens, a more open taxonomic assignment was preferred, given the difficulties to distinguish *Proargyrolagus* spp. species and even the molar locus based on broken and worn material.

Measurements. See table 14.

Table 14. Measurements in mm of cf. *Proargyrolagus* sp. teeth from the Huallaga Basin, Peruvian Amazonia.

Locality	Specimen	Locus	Length	Width
TAR-72	MUSM 4074	right M2	1,694	1,601
TAR-20	MUSM 4062	Left m2	1,0573	0,9335
	MUSM 4063	Left m2	0,818	1,112

Argyrolagidae indet.

(Figure 29)

Referred material. MUSM 4143, 1 left ?m2.

Locality. CTA-43, Contamana, Loreto Department, Peru.

Formation and age. Pebas Formation, earliest Late Miocene (Mayoan SALMA).

Description. Very high-crowned lower molar, with open root. One labial and one lingual sulci are present, dividing the molar into two lobes, one anterior, which is wider and longer, and one posterior, anteroposteriorly compressed, both lobes have rounded margins. The labial sulcus is deeper than the lingual one. The lingual cusps are much higher than the labial ones. Between the cusps, there is a wide shallow basin, with no preserved occlusal structures. On the anterior portion, one small very labially displaced protoconid is present. The anterior portion also possesses a large metaconid and a smaller "ectostyle" *sensu* Goin & Candela (2013). On the posterior portion, an anteroposteriorly compressed hypoconid is present, as well as a labio-lingually compressed entoconid. No hypoconulid is visible.

Comments. This specimen is very different from the *Proargyrolagus* spp. and cf. *Proargyrolagus* sp. from the Contamana and Huallaga Basin regions, both in morphology and in size. The crown height is remarkable, as well as the complete open root. The occlusal morphology is much more simplified, lacking most of the structures present on the other cited taxa. Compared to the other argyrolagids, this specimen resembles *Anagyrolagus* by having euhypsodont bilobed lower molars, with deep opposite vertical sulci on the labial and lingual surfaces of the molar, and a subtriangular shape in cross-section (Carlini *et al*., 2007). It differs from *Hondalagus* in having an anterior lobe wider than the posterior one, since in *Hondalagus* both lobes have the same width (Sánchez-Villagra e*t al*., 2000). It differs from *Microtragulus* in having a well-developed lingual sulcus, which in *Microtragulus* is incipient or absent (Simpson, 1970). *Argyrolagus* spp. differentiate from MUSM 4143 in possessing subquadrangular-shaped lower molars in cross section and, in general, longer anterior lobes (Simpson, 1970; Carlini *et al*., 2007).

Measurements. Length = 2.217 mm; width = 1.192 mm; crown height = 6.498 mm.

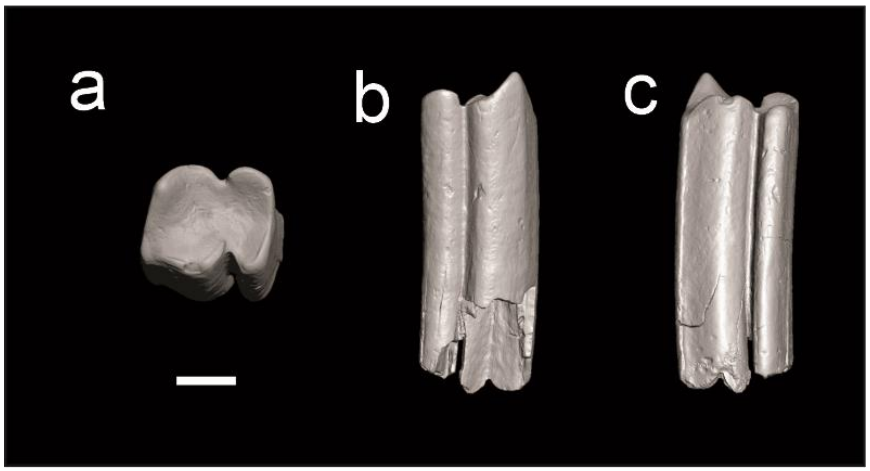


Figure 29. Argyrolagidae indet. from CTA-43, early Late Miocene, Contamana, Peru: **a–c,** MUSM 4143, 1 left ?m2. **a**, occlusal, **b**, lingual, **c**, labial views. Scale bar = 1 mm.

5. Discussion and Conclusions

5.1 Order Polydolopimorphia?

The phylogenetic relationships, the monophyly and taxonomic composition of the order Polydolopimorphia are far from being settled.

Molecular clocks estimations point out that the origin of the crown-group of Metatheria, Marsupialia, would have happened in the Late Cretaceous (Upham *et al*., 2019), or more recently between the late Paleocene-early Eocene (Beck *et al*., 2022). Taxa arguably considered to belong to Marsupialia are known only for the Cenozoic and with an exclusive distribution in Gondwana, with the exception of didelphids, which subsequently dispersed from South America to North America during the Great American Biotic Interchange (**GABI**). The only craniodental character considered as a synapomorphy of Marsupialia would be the absence of a posterior cingulid on the lower molars. However, a posterior cingulid has already been reported for lower molars of some marsupial taxa, including didelphids (Beck *et al*., 2022).

The members of the Marsupialia are traditionally divided into two large cohorts "Ameridelphia" and Australidelphia. “Ameridelphia” used to encompass the South American orders Didelphimorphia, Paucituberculata, Sparassodonta and several basal fossil taxa, mostly of South American occurrence. However, it has been shown that it is an artificial clade, with no phylogenetic support. On the other hand, Australidelphia

has been shown to be a phylogenetically well-supported clade, including four orders with a current distribution in Australasia (Dasyuromorphia, Peramelemorphia, Notoryctemorphia, and Diprotodontia), the South American order Miocrobiotheria (with current and fossil representatives), and a fossil order from the Miocene of Australia, Yalkaparidontia (Black *et al*., 2012; Goin *et al*., 2016).

Some authors (Goin *et al*., 2016) argue that the fossil order Polydolopimorphia, which has records in South America, Antarctica, and Australia, would also belong to Australidelphia. However, this remains uncertain, since according to other authors Polydolopimorphia cannot be safely considered as belonging to Marsupialia, as well as all the Mesozoic metatherian forms such as †*Asiatherium*, Deltatheroidea, "Alphadontidae," "Pediomyidae," Stagodontidae, †Herpetotheriidae, and †Peradectidae and basal South American taxa such as Pucadelphyidae, Protodidelphidae, Caroloameghinidae, Derorhynchidae, and Sparassodonta (Beck *et al*., 2022). Since there is no agreement regarding which clades do belong to Marsupialia, it is not reliable to consider polydolopimorphians as marsupials.

According to Muizon & Ladevèze (2020) interpretation of the metatherians from the fauna of Tiupampa, early Paleocene of Bolivia, it encompasses taxa of Sparassodonta and other basal "Ameridelphia" *incertae sedis*, as well as of the orders Polydolopimorphia and Microbiotheria. For Beck (2017), in the Itaboraí fauna (early Eocene, Brazil) no definite Marsupialia taxa are found. However, according to Oliveira & Goin (2011), the Itaboraí fauna would already include several representatives of Marsupialia, with the orders Didelphimorphia, Paucituberculata, Microbiotheria and Polydolopimorphia. In the Santa Rosa local fauna (early Olligocene, Peru) remains of Paucituberculata and Microbiotheria are present (Goin & Candela, 2004). Thus, due to the divergent conceptions about which groups belong or not to Marsupialia, the first records of this clade in South America remain uncertain.

With respect to basal non-Marsupialia metatherians, Williamson *et al*. (2012, 2014) have provided phylogenetic analyses with Cretaceous and early Paleogene metatherian taxa, mainly from North America and included three South American taxa: *Roberthoffstetteria nationalgeographica*, *Szalinia gracilis* and *Pucadelphys andinus*, all from Tiupampa, Bolivia. According to their analysis, *Roberthoffstetteria* is a

polydolopimorphian, and it is phylogenetically close to the North American genus *Glasbius* (family Glasbiidae).

However, Chornogubsky & Goin (2015) consider Glasbiidae as a basal family of Polydolopimorphia, being composed of other taxa, while *Roberthoffstetteria* would compose, together with *Sillustania*, from Laguna Umayo (Peru), the family Sillustanidae, considered basal Polydolopiformes. These authors recover the order Polydolopimorphia as monophyletic, including the suborders Polydolopiformes and Bonapartheriiformes, the latter comprising Argyrolagoidea. The genera *Hatcheritherium* and *Ectocentrocristus* from North America have also previously been considered basal to the order Polydolopimorphia and/or the Polydolopiformes, and it has been suggested that Polydolpimorphia would therefore have originated and developed in southern North America and then migrated to South America in the late Cretaceous (Case *et al*., 2005; Goin *et al*., 2016).

The controversies regarding the order Polydolopimorphia go even further. According to Goin *et al*. (2016), Polydolopimorphia, including the superfamily Argyrolagoidea, can be considered as belonging to Marsupialia and within Australidelphia, as it would have arisen from Microbiotheria. Beck (2017), meanwhile, proposes that Polydolopimorphia (at least Epidolopinae, Bonapartheriidae, and Polydolopidae) are not comprised within Marsupialia, and thus are not members of Australidelphia either. Beck (2017) also suggests that Polydolopimorphia do not contain Argyrolagoidea, which would be part of the order Paucituberculata.

The skull of the representatives of the order Polydolopimorphia is characterized by: globular braincase; posteriorly expanded nasals, up to the level of the orbits; robust zygomatic arch; broader palate at the level of the molar series; incisive foramina always present under different sizes, as well as maxillary and palatal foramina. Regarding the Polydolopiformes, there is little cranial material preserved, but the rostrum would be elongated and narrow, the palate broad along the molar series, and the braincase expanded and globular (Goin *et al*., 2016).

The Bonapartherioidea possess: short, broad rostrum; fully open orbits; inconspicuous posterorbital constriction; small or absent posterorbital processes; downwardly displaced zygomatic arch; suboval or diamond-shaped palate; small incisor foramina; apparently large maxillary fenestra; short, robust deep dentary

masseteric fossa, with a marked ridge on its anterior margin; masseteric ridge well developed and posteriorly wide; coronoid process high and wide; condyle robust and slightly higher than the molar series; angular process marked and inflexed, with the posterior end directed upwards (Goin *et al*., 2016).

Argyrolagoidea have slender rostrum; nasal cavity protruding above the incisor line; low zygomatic arch with developed jugal process; large infraorbital foramen; orbits anteriorly closed and open posteriorly; reduced temporal region; oval palate; large incisor foramen; proportionately very large and inflated auditory bulla; slender dentary; large incisors implanted at the level of the m3 (Goin *et al*., 2016).

Most polydolopimorphians have relatively low-crowned bunodont molars. Representatives of the order were the first to develop a quadrangular molar pattern, which is suitable for ingesting diverse plants of varying shapes, sizes, and rigidity. The upper molars have a paracone and metacone associated with the stylar cusps B and C, respectively, which are similar in size to the paracone and metacone; at the lingual margin the metacone is expanded and forms the posterolingual margin. In the upper molars, the paracone and metacone are reduced and close to each other; the metaconule is large but not very prominent (Goin *et al*., 2016; Beck, 2017).

5.2 Polydolopimorphians from Contamana, Huallaga Basin and Atalaya: general aspects

The abundance and diversity of polydolopimorphians found in the studied outcrops in the Contamana, Huallaga Basin and Atalaya are remarkable (Table 15). No members of the suborder Polydolopiformes were found, only Bonapartheriiformes. But the latter are represented by its two superfamilies, Bonapartherioidea and Argyrolagoidea. Among the Bonapartherioidea, all the six reported taxa belong to the family Prepidolopidae, with Prepidolopidae gen. nov. 1 sp. nov., Prepidolopidae gen. nov. 2 sp. nov. 2, Prepidolopidae ge. nov. 3 sp. nov. 3, Prepidolopidae gen. nov. 4 sp. nov. 4, Prepidolopidae gen. nov. 5 sp. nov. 5, and Prepidolopidae gen. nov. 6 sp. nov. 6. Until today, this family was known by five genera and six species: *Prepidolops didelphoides* Pascual, 1980a; b (early Eocene, Lumbrera Formation, Salta, Argentina), *Prepidolops molinai* Pascual, 1980a (early Eocene, Lumbrera Formation, Salta Province, Argentina), *Punadolops alonsoi* (Pascual, 1983) (middle Eocene, Pozuelo,

Geste and Quebrada de los Colorados formations, Salta and Catamarca provinces, Argentina), *Incadolops ucayali* Goin & Candela, 2004 (early Oligocene, Santa Rosa local Fauna, Peru), *Coloradolops cardonensis* Chornogubsky *et al*., 2019 (middle Eocene, Quebrada de los Colorados Formation, Argentina), and *Perrodelphys coquinense* Goin *et al*., 1999 (middle Eocene, La Meseta Formation, Seymor Island, Antarctica). Thus, the prepidolopids here reported, which all represent new genera and new species, more than double the previously-known diversity of Prepidolopidae, and considerably widen their geographical and temporal distribution. Indeed, until today, *Incadolops* was the only representative of Prepidolopidae described for the Amazon Region. Before, Prepidolopidae was considered to be a clade exclusively represented in mid-high latitudes. Now, with the new taxa here reported, the diversity of prepidolopids in the Amazon Region outweighs that from the middle-high latitudes of South America. Additionally, Prepidolopidae was recorded from the early Eocene to the early Oligocene, and now TAR-14, late Oligocene, is the last record of prepidolopids, a hypothesis to be furthered by a formal phylogenetic analysis.

Interestingly, *Incadolops* possesses some peculiar characteristics when compared to other members of the family Prepidolopidae. According to the description of the family, made by Pascual (1980a, b), the upper molars of this family would be triangular- shaped. However, *Incadolops* has a metaconule on the upper molars, a structure that modifies this typical triangular pattern of prepidolopid upper molars and that is not present in the prepidolopids from Argentina (Pascual, 1980a, b; Chornogubsky *et al*., 2019). Some of the prepidolopids here described also possess a metaconule on their upper molars, which are more subtrapezoidal-shaped. Thus, the presence of metaconule and more quadrangular upper molars seem to be a recurrent and exclusive characteristic of Amazonian prepidolopids.

The specimens of Argyrolagidae here reported represent both the earliest and the northernmost occurrence of the family, suggesting a long-termed and unsuspected presence of argyrolagids throughout the Eocene–Miocene interval in the Proto-Amazonia. Indeed, until today, the family was known from abundant rests, but all from middle and high latitudes of South America and the oldest records of the family were reported for the late Oligocene of Salla, Bolivia (Babot & Garcia-López, 2016). With

the records presented here, their oldest record would be from CTA-29, late middle Eocene.

Wamradolops was solely known for the lower Oligocene levels of Santa Rosa, Peru (Goin & Candela, 2004), and preliminary identifications for the Contamana specimens (*Wamradolops* sp., middle Eocene; Antoine *et al*., 2016). The specimens described here add knowledge about this polydolopimorphian confirming that its temporal distribution ranges from late middle Eocene (CTA-27 and CTA-29, Contamana locality) to the late Oligocene (TAR 14, Abra de Machungo). Together with Polydolopimorphia indet. gen. nov. A sp. nov. both taxa represent polydolopimorphians of peculiar characteristics, making their attribution to any of the known families of Polydolopimorphia very difficult, and showing the presence of basal polydopimorphians also in the low latitudes of South America.

Table 15. Polydolopimorphian assemblages in the Contamana and Huallaga Basin localities. The localities are ordered, from left to right, from the oldest to the newest (see Tables 1–4 for age information).

Taxa	CTA-47	CTA-51	CTA-27	CTA-29	CTA-66	TAR-56	TAR-76	TAR-55	TAR-44	TAR-45	TAR-20	TAR-72	TAR-74	TAR-47	TAR-21	TAR-01	TAR-14	CTA-43
Indet.		X				X					X	X				X		
Wamradolops tsullodon	X	X	X	X	X			X									X	
Wamradolops sp. nov. (large)								X	X	X								
Polydolopimorphia indet. gen. nov. A sp. nov.		X	X															
Bonapartherioidea																		
Prepidolopidae																		
Prepidolopidae gen. nov. 1 sp. nov. 1							X											
Prepidolopidae gen. nov. 2 sp. nov. 2								X										
Prepidolopidae gen. nov. 3 sp. nov. 3													X					
Prepidolopidae gen. nov. 4 sp. nov. 4														X				
Prepidolopidae gen. nov. 5 sp. nov. 5		X	X															
Prepidolopidae gen. nov. 6 sp. nov. 6																	X	
?Prepidolopidae gen. et sp. indet.															X			
Argyrolagoidea																		
Argyrolagidae																		
Indet.																		x
Proargyrolagus sp. nov. 1 (small)				X											X			
Proargyrolagus sp. nov. 2 (large)																X		
cf. *Proargyrolagus* sp.											X	X						

Interestingly, while still abundant and diverse in the studied localities during the late middle Eocene to early Oligocene, polydolopimorphians become rarer from the late Oligocene, with a unique and last record in the early Late Miocene. The persistence of only arygolagids until the Miocene is in agreement with the record of polydolopimorphians from the mid-high latitudes of South America, where other Bonapartheriiformes disappear from the early Oligocene on and solely the Argyrolagoidea persist in the Neogene. The Amazon Region shows an increase in the diversity of metatherians belonging to the order Paucituberculata after the early Oligocene, which reach a great diversity in the middle Miocene, as well as the presence of sparassodontans in the Miocene deposits. According to recent reviews (Castro *et al*., 2012), the order Didelphimorphia has its first records in the Early-Middle Miocene and become the single metatherian order present in the region from the Late Miocene until today (Goin, 1997; Antoine *et al*., 2016, 2017, 2021; Stutz *et al*., 2022).

5.3 Polydolopimorphian fossil record

As mentioned before, the first record of a therian mammal in South America is that of *Cocatherium lefipanum*, which is a metatherian of the order Polydolopimorphia, and was recorded for early Paleocene deposits in the Argentinean Patagonia (Goin *et al*., 2006).

However, the first record of a vast metatherian community comes from the Tiupampa fauna in Bolivia, considered to be of early Paleocene age. The fauna of Tiupampa is entirely new compared to the late Cretaceous taxa, Alamitan SALMA, of Argentina, and is probably the result of immigration of taxa from North America in the late Cretaceous/early Paleocene. There are a dozen metatherian taxa already described for Tiupampa, which are mostly insectivorous and small-sized, as well as medium-sized, carnivorous, insectivorous-frugivorous forms, mainly of "Ameridelphia" *incertae sedis*, as well as Sparassodonta, Polydolopimorphia and possibly Didelphimorphia (however see discussion above about the phylogenetic affinities of the basal taxa from South America). These are taxa that anticipate the more derived lineages that would reach their climax in the early Eocene (Goin *et al*., 2016).

Another early Paleogene records of polydolopimorphias come from the Chulpas level, in southeastern Peru, on the northwestern margin of Laguna

Umayo. Two fossiliferous levels (LU-3 and Chulpas level) are present in the Laguna Umayo red clay unit (Lower Muñani Formation), which is located in the Andean region of Peru. The fossil remains of eutherians and metatherians, with derived molar patterns, suggest an early Paleogene age for these levels, which is also supported by other geological information. In the Chulpas level the following metatherians were recorded: Didelphidae indeterminate; Polydolopimorphia, *Chulpasia mattaueri*, aff. Chulpasia and *Sillustania quechuense* (Sigé *et al*., 2004; however see discussion above about the phylogenetic affinities of the basal taxa from South America). Another species also of the genus *Chulpasia*, *C*. *jimthorselli*, was described for the fauna of Tingamarra, early Eocene of Australia, establishing some proximity between the forms from Laguna Umayo and Australian metatherians, and suggesting that the polydolopimorphians would have reached Australasia, but these taxonomic affinities still need further substantiation (Sigé *et al*., 2009).

Subsequently, other important metatherian assemblages come from the late Paleocene-early Eocene (Itaboraian Salma) of the localities Las Flores, southern Lake Colhué Huapi, Argentinean Patagonia, and the Itaboraí Basin, Rio de Janeiro State, Brazil. The Itaboraian stands out as having a faunal pattern totally different from that of the preceding faunas, with a great diversification of placental mammals. It is in the Itaboraian that the greatest radiation of metatherians occurred and in which they reached a peak of their diversity, not only taxonomically, but also in ecological types. In contrast, cingulates, astrapotheres and notoungulates appear for the first time, and litopterns, occurring in previous SALMAs, are more numerous, in addition to the "Condylarthra", which record the significant diversification of the endemic Didolodontidae. Furthermore, in the Itaboraian is the first step towards increasing size among metatherians (Woodburne *et al*., 2014; Goin *et al*., 2016). In the Itaboraí Basin, for example, "Ameridelphia" *incertae sedis* such as Sternbergiidae, Derorhynchidae, Protodidelphidae, as well as Sparassodonta (e.g., Hathliacynidae), Didelphimorphia (e.g., Caroloameghiniidae), Paucituberculata (*Riolestes capricornicus*), Microbiotheria (*Mirandatherium*) and Polydolopimorphia (*Bobbschaefferia fluminensis*, Bonapartheriidae and Gashterniidae) are recorded (Oliveira & Goin, 2011, however see discussion above about the phylogenetic affinities of the basal taxa from South America).

Nevertheless, in the Itaboraian the metatherians, although numerous, already lost part of their original diversity and subsequently do not recover it either, being present in the mammalian fossil assemblages of the subsequent distinct SALMAs, but not as members with high richness and diversity.

In the outrcrops of the La Meseta Formation, middle Eocene in age, located on the Seymour Islands, Antarctic Peninsula of the beginning of the Eocene, the polydolopymorphians Polydolopidae *Antarctodolops dailyi* Woodburne & Zinsmeister, 1984 and *Antarctodolops mesetaense* Chornogubsky *et al*., 2009 were recorded, as well as the prepidolopid *Perrodelphys coquinense* cited above, along with microbiotheres and derorhynchids, and other mammals. This is the only fossiliferous unit in which records of Paleogene mammals are found in Antarctica. The faunal elements of La Meseta have more affinity with South American mammals than with Australian ones. These are already significantly derived taxa, phylogenetically close to South American clades also considered derived. Paleobotanical remains of considerable diversity have also been found in La Meseta, which suggest seasonal, cool/temperate and humid climatic conditions, resembling the present-day forests of New Zealand and Valdivian woodlands of Chile and Argentina (Goin *et al*., 2007b, 2016; Chornogubsky *et al*., 2009).

In outcrops of the Guabirotuba Formation, Curitiba Basin, Southern Brazil, a rich fossil fauna was recently found, still only preliminarily analyzed. The remains include invertebrates and vertebrates, such as Metatheria, Cingulata, Notoungulata and Astrapotheria mammals, which suggest a late middle Eocene age (Barrancan SALMA). Among the Metatheria, Sparassodonta, Paucituberculata and Polydolopimorphia Argyrolagoidea gen. et sp. indet. were identified (Sedor *et al*., 2017).

Regarding the deposits from Northern South American, Amazon Region, the Santa Rosa local fauna, early Oligocene, Peru, located on the banks of the Yuruá River, close to the Peru-Brazil border, also yielded remains of metatherians, including polydolopimorphians. The Santa Rosa metatherian association is composed of 79 fragments, with, at the time of its description, eight new genera and 11 new species (Goin & Candela, 2004), including the polydolopimorphians: *Incadolops ucayali* (family Prepidolopidae), *Wamradolops tsullodon* of uncertain affinities, and *Hondonadia pittmae* (later considered to

belong to the family Rosendolopidae). Also in Peru, deposits from the Contamana region, of the Pozo Formation, middle Eocene, provided the first rodent fossil remains in South America, with a rich assemblage of Caviomorpha, along with the remains of the prepidolopid *Punadolops* (CTA-27 outcrop; Antoine *et al*., 2012). Subsequently, Antoine *et al*. (2016), in describing several outcrops from the Contamana region, cite the presence of preliminarily identified metatherians for the middle Eocene to late Miocene interval, among them the polydolopimorphians *Wamradolops* sp., Bonapartherioidea indeterminate, Prepidolopidae indeterminate, and Argyrolagidae, as well as remains of Sparassodonta (Borhyaenidae), Didelphimorphia (?Marmosini and indeterminate), Paucituberculata (*Sasawatsu* sp., cf. *Perulestes*, *Abderites* sp., Palaeothentidae indet. and ?Caenolestidae) and Microbiotheria (indeterminate), in addition to ?Herpetotheriidae (Antoine *et al*., 2016). More recently, Antoine *et al*. (2021), when describing new outcrops for the Peruvian Amazon, the Paleogene Shapaja Section, late Eocene to early Oligocene interval, reported a vast fauna, composed, among others, of metatherians, with the record of 19 taxa: Marsupialiformes *incertae sedis*, Polydolopimorphia of the families Prepidolopidae and Argyrolagidae, and Paucituberculata, with basal Palaeothentoidea and the families Palaeothentidae and Abderitidae.

In sum, the Polydolopiformes show episodes of diversification in the early Eocene (Itaboraian), reaching their peak diversity in the early middle Eocene (El Sapo fauna) and continued with stable diversity throughout the middle Eocene, but enter into decline in the late Eocene, being recorded for the last time in the fauna of La Cantera, Argentina. Among the Bonapartheriiformes, the Bonapartheriioidea record important radiation at the beginning of the Eocene (Itaboraian), followed by an interval with stable diversity from the middle to late Eocene. Until today, the last records of bonapartherioids were for the early Oligocene, but with the additional records presented here, their last record would be in the late Oligocene (TAR-14). Prepidolopids are recorded from the early Eocene to the late Oligocene. With the occurrences in the Santa Rosa local fauna and the taxa here described, the last occurrences of the Prepidolopidae would be in the Amazon Region, suggesting that eventually the family persisted for long in the tropical latitudes of South America, after disappearing from the locations on south. The Argyrolagoidea, on the other hand, are first recorded in the middle

Eocene (Vacan SALMA), and remain sparsely diverse throughout the Paleogene and Neogene, being recorded until the Pliocene-Pleistocene (Goin *et al*., 2016).

The first Polydolopiformes were mainly small- to medium-sized, frugivorous and insectivorous, later changing to mainly large frugivorous-pholivorous. Among the Bonapartheriiformes, on the other hand, the first Bonapartheriidae were large medium-sized folivores and insectivores-frugivores, and, after the middle late Eocene, they changed to smaller granivorous forms. The Argyrolagoidea were mainly small granivorous and folivorous forms (Goin *et al*., 2016).

6. Conclusions

In this article we present new metatherian assemblages from the regions of Contamana, Huallaga Basin and Atalaya, Peruvian Amazonia, ranging from the middle Eocene to the late Miocene. One new species of the phylogenetically enigmatic genus *Wamradolops* and the new genus and species Polydolopimorphia indet. gen. nov. sp. nov. are described as belonging to an indeterminate family of Polydolopimorphia. Six new genera and species of the family Prepidolopidae are described: Prepidolopidae gen. nov. 1 sp. nov. 1, Prepidolopidae gen. nov. 2 sp. nov. 2, Prepidolopidae gen. nov. sp. nov. 3, Prepidolopidae gen. nov. 4 sp. nov. Prepidolopidae gen. nov. 5 sp. nov. 5, and Prepidolopidae gen. nov. 6 sp. nov. 6. Two new species of the genus *Proargyrolagus*, family Argyrolagidae, are described, *P*. sp. nov. 1 (small) and *P*. sp. nov. 2 (large), as well as cf. *Proargyrolagus* sp. and an indeterminate argyrolagid. These represent important additions to the temporal and geographical knowledge of polydolopimorphians: i) extending the record of *Wamradolops* to the late Oligocene and adding new localities where this taxon is found, with the description of a new species of the genus; ii) extending the temporal distribution of Prepidolopidae to the late Oligocene and considerably enlarging the known diversity and geographical distribution of this family, previously known mostly for middle latitudes in South America; and iii) recording the first and northernmost argyrolagids, the family was before restricted to the mid-high latitudes of South America and from the late Oligocene on, showing their presence from the late Eocene until the Late Miocene in the Amazon Region. This highlights the importance and need for more paleontological investigations

in the tropical latitudes of the South American continent, to unravel the patterns of diversity of many fossil groups in this region, which seemingly still holds many surprises.

7. References

Antoine, P.O., Salas-Gismondi, R., Pujos, F., Ganerød, M. & Marivaux, L. 2017. Western Amazonia as a hotspot of mammalian biodiversity throughout the Cenozoic. *Journal of Mammalian Evolution*, 24(1): 5–17.

Antoine, P.O., Marivaux, L., Croft, D.A., Billet, G., Ganerød, M., Jaramillo, C., Martin, T., Orliac, M.J. Tejada, L., Altamiro, A.J., Duranthon, F., Fanjat, G., Rousse, S. & Salas Gismondi, R. 2012. Middle Eocene rodents from Peruvian Amazonia reveal the pattern and timing of caviomorph origins and biogeography. *Proceedings of The Royal Society B: Biological Sciences*, 279(1732): 1319–1326.

Antoine, P.-O., Yans, J., Aliaga Castillo, A., Stutz, N., Abello, M.A., Adnet, S., Andriolli Custódio, M., Benites-Palomino, A., Billet, G., Boivin, M., Herrera, F., Jaramillo, C., Mártinez, C., Moreno, F., Navarrete, R.E., Negri, F.R., Parra, F., Pujos, F., Rage, J.-C., Ribeiro, A.M., Robinet, C., Roddaz, M., Tejada-Lara, J.V., Varas-Malca, R., Ventura Santos, R., Salas-Gismondi, R. & Marivaux L. 2021. Biotic community and landscape changes around the Eocene–Oligocene transition at Shapaja, Peruvian Amazonia: regional or global drivers? *Global and Planetary Change*, 202: 103512.

Antoine, P.-O., Abello, M.A., Adnet, S., Altamiro Sierra, A.J., Baby, P.; Billet, G., Boivin, M., Calderón, Y., Candela, A., Chabain, J., Corfu, F., Croft, D.A., Ganerød, M., Jaramillo, C., Klaus, S., Marivaux, L., Navarrete, R.E., Orliac, M.J., Parra, F., Pérez, M.E., Pujos, F., Rage, J.C., Ravel, A., Robinet, C., Roddaz, M., Tejada-Lara, J.V., Vélez-Juarbe, J., Wesselingh, F.P. & Salas-Gismondi, R. 2016. A 60-million-year Cenozoic history of western Amazonian ecosystems in Contamana, Eastern Peru. *Gondwana Research*, 31: 30–59.

Assemat, A., Boivin, M., Marivaux, L., Pujos, F., Benites-Palomino, A., Salas-Gismondi, R., Tejada-Lara, J., Varas-Malca, R., Negri, F.R., Ribeiro, A.M. & Antoine, P.O. 2019. Restes inédits de rongeurs caviomorphes du Paléogène de

la région de Juanjui (Amazonie péruvienne): systématique, implications macro-évolutives et biostratigraphiques. *Geodiversitas*, 21(20): 699–730.

Babot, M.J. & García-López, D.A. 2016. Redescription of the argyrolagid *Microtragulus bolivianus* (Metatheria, Polydolopimorphia, Bonapartheriiformes) based on new remains from Northwestern Argentina. *Palaeontologia Electronica*, 19.2.23A: 1–23.

Beck, R.M.D. 2017. The skull of *Epidolops ameghinoi* from the Early Eocene Itaboraí fauna, Southeastern Brazil, and the affinities of the extinct marsupialiform order Polydolopimorphia. *Journal of Mammalian Evolution*, 24(4): 373–414.

Beck, R.M.D., Voss, R.S. & Jansa, S.A. 2022. Craniodental morphology and phylogeny of marsupials. *Bulletin of the American Museum of Natural History*, 457: 1–355.

Bi, S., Zheng, X., Wang, X., Cignetti, N.E., Yang, S. & Wible, J.R. 2018. An Early Cretaceous eutherian and the placental–marsupial dichotomy. *Nature*, 558: 390–395.

Black, K.H., Archer, M., Hand, S.J. & Godthelp, H. 2012. The rise of Australian marsupials: a synopsis of biostratigraphic, phylogenetic, palaeoecologic and palaeobiogeographic understanding. In: Talent, J.A. (ed.). *Earth and life: international year of planet Earth*. Dordrecht, Springer, p. 983–1078.

Boivin, M., Marivaux, L., Pujos, F., Salas-Gismondi, R., Tejada-Lara, J.V., Varas-Malca, R. & Antoine, P.-O. 2018. Early Oligocene rodents from Shapaja, Peruvian Amazonia. *Palaeontrographica*, 311(1–6): 87–156.

Boivin, M., Marivaux, L., Aguirre-Díaz, W., Andriolli Custódio, M., Benites-Palomino, A., Pujos, F., Roddaz, M., Salas-Gismondi, R., Stutz, N., Tejada-Lara, J.V., Yans, J. & Antoine, P.-O. 2021. Eocene caviomorph rodents from Balsayacu (PeruvianAmazonia). *Paläontologische Zeitschrift*, 96: 135–160.

Campbell, K.E. (Ed.). 2004. *The Paleogene mammalian fauna of Santa Rosa, Amazonian Peru*. Los Angeles, Science Series, Natural History Museum of Los Angeles County, 163 p.

Carlini, A.A., Pascual, R. & Goin, F.J. 2007. A new argyrolagid marsupial from the Early Miocene of Patagonia (Argentina). *Neues Jahrbuch für Geologie und Paläontologie*, 245(3): 323–330.

Carneiro, L.M., Oliveira, E.V. & Goin, F.J. 2018. *Austropediomys marshalli* gen. et sp. nov., a new Pediomyoidea (Mammalia, Metatheria) from the Paleogene of Brazil: paleobiogeographic implications. *Revista Brasileira de Paleontologia*, 21(2): 120–131.

Case, J.A., Goin, F.J. & Woodburne, M.O. 2005. “South American” marsupials from the Late Cretaceous of North America and the origin of marsupial cohorts. *Journal of Mammalian Evolution*, 12: 461–494.

Castro, M.C., Dahur, M.J. & Ferreira, G.S. 2021. Amazonia as the origin and diversification area of Didelphidae (Mammalia: Metatheria), and a review of the fossil record of the clade. *Journal of Mammalian Evolution*, 28: 583–598.

Chornogubsky, L. & Goin, F.J. 2015. A review of the molar morphology and phylogenetic affinities of *Sillustania quechuense* (Metatheria, Polydolopimorphia, Sillustaniidae), from the early Paleogene of Laguna Umayo, Southeastern Peru. *Journal of Vertebrate Paleontology*, 35(6): e983238.

Chornogubsky, L., Goin, F.J. & Reguero, M.A. 2009. A reassessment of Antarctic polydolopid marsupials (Middle Eocene, La Meseta Formation). *Antarctic Science*, 21(3): 285–297.

Chornogubsky, L., Zimicz, N., Goin, F.J., Fernicola, J.C., Payrola P. & Cárdenas, M. 2019. New Palaeogene metatherians from the Quebrada de Los Colorados Formation at Los Cardones National Park (Salta Province, Argentina), *Journal of Systematic Palaeontology*, 17(7): 539–555.

Flores, D.A., Abdala, F. & Giannini, N. 2010. Cranial ontogeny of *Caluromys philander* (Didelphidae: Caluromyinae): a qualitative and quantitative approach. *Journal of Mammalogy*, 91(3): 539–550.

Flynn, J.J. & Wyss, A.R. 2004. Chapter 6: A polydolopine marsupial skull from the Cachapoal Valley, Andean main range, Chile. *Bulletin of the American Museum of Natural History*, 285: 80–92.

Fonseca, G.A.B., Paglia, A.P., Sanderson, J. & Mittermeier, R.A. 2003. Marsupials of the new world: status and conservation. In: Jones, M., Dickman, C., Archer, M. (eds.). *Predators with pouches: the biology of carnivorous marsupials*. Collingwood, CSIRO Publishing, p. 399–406.

Forasiepi, A.M. 2009. Osteology of *Arctodictis sinclairi* (Mammalia, Metatheria, Sparassodonta) and phylogeny of Cenozoic metatherian carnivores from South America. *Monografías del Museo Argentino de Ciencias Naturales "Bernardino Rivadavia"*, 6: 1–174.

Frailey, C.D. & Campbell, K.E. 2004. Paleogene rodents from Amazonian Peru: the Santa Rosa local fauna. In: Campbell, K.E. (ed). *The Paleogene mammalian fauna of Santa Rosa, Amazonian Peru*. Los Angeles, Natural History Museum of Los Angeles County, Science Series 40, p. 71–130.

Goin, F.J. 1997. New clues for understanding Neogene marsupial radiations. In: Kay, R.F., Madden, R.H., Cifelli, R.L. & Flynn, J.J. (eds.). *Vertebrate paleontology in the Neotropics: the Miocene fauna of La Venta, Colombia*. Washington, Smithsonian Institution Press, p. 187–206.

Goin, F.J. & Abello, A. 2013. Los Metatheria sudamericanos de comienzos del Neógeno (Mioceno temprano, Edad Mamífero Colhuehuapense): Microbiotheria y Polydolopimorphia. *Ameghiniana*, 50(1): 51–78.

Goin, F.J. & Candela, A.M. 2004. New Palaeogene marsupials from the Amazon Basin of Eastern Peru. In: Campbell, K.E. (ed). *The Paleogene mammalian fauna of Santa Rosa, Amazonian Peru*. Los Angeles, Natural History Museum of Los Angeles County, Science Series 40, p. 15–60.

Goin, F.J., Abello, M.A. & Chornogubsky, L. 2010. Middle Tertiary marsupials from central Patagonia (early Oligocene of Gran Barranca): understanding South America's Grande Coupure. In: Madden, R.H., Carlini, A.A., Vucetich, M.G., Kay, R.F. (eds.). *The Paleontology of Gran Barranca*. Cambridge, Cambridge University Press, p. 69–105.

Goin, F.J., Candela, A.M. & López, G. 1998. Middle Eocene marsupials from Antofagasta de la Sierra, Northwestern Argentina. *Geobios*, 31(1): 75–85.

Goin, F.J., Candela, A., Abello, M.A.; Oliveira, E.V. 2009. Earliest South American paucituberculatans and their significance in the understanding of ‘pseudodiprotodont’ marsupial radiations. *Zoological Journal of the Linnean Society*, 155: 867–884.

Goin, F.J., Case, J.A., Woodburne, M.O., Vizcaíno, S.F. & Reguero, M. 1999. New discoveries of "opposum-like" marsupials from Antarctica (Seymour Island, Medial Eocene). *Journal of Mammalian Evolution*, 6(4): 335–365.

Goin, F.J., Woodburne, M.O., Zimicz, A.N., Martin, G.M. & Chornogubsky, L. 2016. *A brief history of South American metatherians*. New York, Springer Earth System Sciences, 237 p.

Goin, F.J., Abello, A., Bellosi, E., Kay, R., Madden, R. & Carlini, A. 2007. Los Metatheria sudamericanos de comienzos del Neógeno (Mioceno Temprano, Edad-mamífero Colhuehuapense). Parte I: Introducción, Didelphimorphia y Sparassodonta. *Ameghiniana*, 44(1): 29–71.

Goin, F.J., Zimicz, N., Reguero, M., Santillana, S.N., Marenssi, S.A. & Moly, J.J. 2007b. New marsupial (Mammalia) from the Eocene of Antarctica, and the origins and affinities of the Microbiotheria. *Revista de la Asociación Geológica Argentina*, 62(4): 597–603.

Goin, F.J., Pascual, R., Tejedor, M.F., Gelfo, J.N., Woodburne, M.O., Case, J.A, Reguero, M.A., Bond, M., Lopez, G.M., Cione, A.L. *et al*. 2006. The earliest Tertiary therian mammal from South America. *Journal of Vertebrate Paleontology*, 26(2): 505–510.

Kemp, T. S. 2005. *The origin and evolution of mammals*. Oxford, Oxford University Press, 331 p.

Klaus, S., Magalhães, C., Salas-Gismondi, R., Gross, M. & Antoine, P.-O. 2017. Palaeogene and Neogene brachyurans of the Amazon basin: a revised first appearance date for primary freshwater crabs (Brachyura, Trichodactylidae). *Crustaceana*, 90(7–10): 953–967.

Mammal Diversity Database. (2022). *Mammal Diversity Database (Version 1.10) [Data set]. Zenodo*. Disponível em: https://www.mammaldiversity.org/taxa.html. Acesso em: 06 fev. 2023.

Muizon, C. de & Ladevèze, S. 2020. Cranial anatomy of *Andinodelphys cochabambensis*, a stem metatherian from the early Palaeocene of Bolivia. *Geodiversitas*, 42(30): 597–739.

Oliveira, E.V. & Goin, F.J. 2011. A reassessment of bunodont metatherians from the Paleogene of Itaboraí (Brazil): systematics and age of the Itaboraian SALMA. *Revista Brasileira de Paleontologia*, 14(2): 105–136.

Pascual, R. 1980a. Nuevos y singulares tipos ecológicos de marsupiales extinguidos de America del Sur (Paleoceno tardio o Eoceno temprano) del noroeste argentino. In: *Actas I Congreso Lationoamericano de Paleontologia and II Congreso Argentino de Palentologia y Bioestratigrafia*, Buenos Aires, 1978, vol. 2, p. 151–173.

Pascual, R. 1980b. Prepidolopidae, nueva familia de Marsupialia Didelphoidea del Eoceno Sudamericano. *Ameghiniana*, XVII(3):216–242.

Pascual, R. 1981. Adiciones al conocimiento de *Bonapartherium hinakusijum* (Marsupialia, Bonapartheriidae) del Eoceno temprano del noroeste argentino. In: *Anais II Congresso Latinoamericano de Paleontologia*, Porto Alegre, 1981, p. 507–520.

Pascual, R. 1983. Novedosos marsupials paleogenos de la Formación Pozuelos (Grupo Pastos Grandes) de la Puna, Salta, Argentina. *Ameghiniana*, XX(3-4): 265–280.

Roddaz, M., Hermoza, W., Mora, A., Baby, P., Parra, M., Christophoul, F., Brusset, S. & Espurt, N. 2010, Cenozoic sedimentary evolution of the Amazonian Foreland Basin System. In: Hoorn, C. & Wesselingh, F.P. (eds.). *Amazonia: Landscape and species evolution: A look into the past*. New York, Blackwell Publishing Ltd., p. 61–88.

Sánchez-Villagra, M.R. & Kay, R.F. 1997. A skull of *Proargyrolagus*, the oldest argyrolagid (Late Oligocene Salla Beds, Bolivia), with brief comments concerning its paleobiology. *Journal of Vertebrate Paleontology*, 17(4): 717–724.

Sánchez-Villagra, M.R., Kay, R.F. & Anaya-Daza, F. 2000. Cranial anatomy and palaeobiology of the Miocene marsupial *Hondalagus altiplanensis* and a phylogeny of argyrolagids. *Palaeontology*, 43: 287–301.

Sedor, F.A., Oliveira, E.V., Silva, D.D., Fernandes, L.A., Cunha, R.F., Ribeiro, A.M. & Dias, E.V. 2017. A new South American Paleogene land mammal fauna, Guabirotuba Formation (Southern Brazil). *Journal of Mammalian Evolution*, 24: 39–55.

Sigé, B., Sempere, T., Butler, R.F., Marshall, L.G. & Crochet, J.-Y. 2004. Age and stratigraphic reassessment of the fossil-bearing Laguna Umayo red mudstone unit, SE Peru, from regional stratigraphy, fossil record, and paleomagnetism. *Geobios*, 37(6): 771–794.

Sigé, B., Archer, M., Crochet, J.-Y., Godthelp, H., Hand, S. & Beck, R. 2009. *Chulpasia* and *Thylacotinga*, late Paleocene-earliest Eocene trans-Antarctic Gondwanan bunodont marsupials: new data from Australia. *Geobios*, 42(6): 813–823.

Simpson, G.G. 1970. The Argyrolagidae, extinct South American marsupials. *Bulletin of the Museum of Comparative Zoology*, 139 :1–86.

Stutz, N.S., Abello, M.A., Marivaux, L., Boivin, M., Pujos, F., Benites-Palomino, A.M., Salas-Gismondi, R., Tejada-Lara, J.V., Custódio, M.A., Roddaz, M., Santos, R.V., Ribeiro, A.M. & Antoine, P.-O. 2022. Late middle Miocene Metatheria (Mammalia: Didelphimorphia and Paucituberculata) from Juan Guerra, San Martín Department, Peruvian Amazonia. *Journal of South American Earth Sciences*, 118: 103902.

Upham, N.S., Esselstyn, J.A. & Jetz, W. 2019. Inferring the mammal tree: Species-level sets of phylogenies for questions in ecology, evolution, and conservation. *PLoS Biol*, 17(12): e3000494.

Voss, R.S. 2022. An annotated checklist of recent opossums (Mammalia: Didelphidae). *Bulletin of the American Museum of Natural History*, 455(1): 1–76.

Wanderley-Filho, J.R., Eiras, J.E., Cunha, P.R.C. & Van Der Ven, P.H. 2010. The Paleozoic Solimões and Amazonas basins and the Acre foreland basin of Brazil. Hoorn, C. & Wesselingh, F.P. (eds.). *Amazonia: landscape and species evolution. A look into the past*. London, Wiley-Blackwell Publishing Ltd, p. 29–37.

Williamson, T.E., Brusatte, S.L. & Wilson, G.P. 2014. The origin and early evolution of metatherian mammals: the Cretaceous record. *Zookeys*, 465: 1–76.

Williamson, T.E., Brusatte, S.L., Carr, T.D., Weil, A. & Standhardt, B.R. 2012. The phylogeny and evolution of Cretaceous–Palaeogene metatherians: cladistic analysis and description of new early Palaeocene specimens from the Nacimiento Formation, New Mexico. *Journal of Systematic Palaeontology*, 10(4): 625–651.

Wolff, R.G. 1984. A New Early Oligocene Argyrolagid (Mammalia: Marsupialia) from Salla, Bolivia. *Journal of Vertebrate Paleontology*, 4(1): 108–113.

Woodburne, M.O., Goin, F.J., Bond, M., Carlini, A.A., Gelfo, J.N., López, G.M., Iglesias, A. & Zimicz, A.N. 2014. Paleogene land mammal faunas of South America; a response to global climatic changes and indigenous floral diversity. *Journal of Mammalian Evolution*, 21: 1–73.

UNIVERSIDADE FEDERAL DO RIO GRANDE DO SUL
INSTITUTO DE GEOCIÊNCIAS
PROGRAMA DE PÓS-GRADUAÇÃO EM GEOCIÊNCIAS

METATÉRIOS PALEÓGENOS E NEÓGENOS DA AMAZÔNIA OCIDENTAL: SISTEMÁTICA E HISTÓRIA EVOLUTIVA

NARLA SHANNAY STUTZ

ORIENTADORA – Profª. Drª. Ana Maria Ribeiro

ORIENTADOR – Prof. Dr. Pierre-Olivier Antoine

Volume 2

Porto Alegre, 2023

UNIVERSIDADE FEDERAL DO RIO GRANDE DO SUL
INSTITUTO DE GEOCIÊNCIAS
PROGRAMA DE PÓS-GRADUAÇÃO EM GEOCIÊNCIAS

METATÉRIOS PALEÓGENOS E NEÓGENOS DA AMAZÔNIA OCIDENTAL: SISTEMÁTICA E HISTÓRIA EVOLUTIVA

NARLA SHANNAY STUTZ

ORIENTADORA – Profª. Drª. Ana Maria Ribeiro
ORIENTADOR – Prof. Dr. Pierre-Olivier Antoine
BANCA EXAMINADORA
Dra. Analia M. Forasiepi – Instituto Argentino de Nivología, Glaciología y Ciencias Ambientales, Centro de Investigaciones Científicas y Técnicas (CCT CONICET Mendoza), Mendoza, Argentina - *revisora*
Prof. Dr. César L. Schultz – Departamento de Paleontologia e Estratigrafia, Instituto de Geociências, Universidade Federal do Rio Grande do Sul, Porto Alegre, Brasil - *examinador*
Prof. Dr. Darin Croft – Department of Anatomy, Case Western Reserve University School of Medicine, Cleveland, OH, Estados Unidos - *revisor*
Profa. Dra. Silane A. F. da Silva-Caminha – Faculdade de Geociências, Universidade Federal de Mato Grosso, Cuiabá, Mato Grosso, Brasil – *examinador*
Dra. Marie-Pierre Ledru – Institut de Recherche pour le Développement, Montpellier, França - *examinadora*

Volume 2

Tese de Doutorado apresentada como requisito parcial para a obtenção do Título de Doutora em Ciências.

Porto Alegre, 2023

CIP - Catalogação na Publicação

Stutz, Narla Shannay
METATÉRIOS PALEÓGENOS E NEÓGENOS DA AMAZÔNIA OCIDENTAL: SISTEMÁTICA E HISTÓRIA EVOLUTIVA / Narla Shannay Stutz. -- 2023.
756 f.
Orientadora: Ana Maria Ribeiro.

Coorientador: Pierre-Olivier Antoine.

Tese (Doutorado) -- Universidade Federal do Rio Grande do Sul, Instituto de Geociências, Programa de Pós-Graduação em Geociências, Porto Alegre, BR-RS, 2023.

1. Marsupial. 2. Eoceno. 3. Oligoceno. 4. Mioceno. 5. Polydolopimorphia. I. Ribeiro, Ana Maria, orient. II. Antoine, Pierre-Olivier, coorient. III. Título.

Elaborada pelo Sistema de Geração Automática de Ficha Catalográfica da UFRGS com os dados fornecidos pelo(a) autor(a).

SUMÁRIO

PARTE III – COMPLEMENTOS..... 3
1 HISTÓRICO ESCOLAR..... 3
1.1 UNIVERSITÉ DE MONTPELLIER..... 3
1.2 PPGGEO UFRGS..... 4
2 CERTIFICADOS..... 5
2.1 Curso De Língua Inglesa..... 5
2.2 Membra Do Corpo Editorial Revista Brasileira De Paleontologia..... 6
3 RESUMOS PUBLICADOS EM ANAIS DE EVENTOS CIENTÍFICOS..... 7
3.1 REUNIÓN DE COMUNICACIONES DE LA ASOCIACIÓN PALEONTOLÓGICA ARGENTINA, 2019, LA PLATA..... 7
3.2 PALEO RS, 2020, PORTO ALEGRE..... 10
3.3 PALEONTOLOGICAL VIRTUAL CONGRESS, 2021..... 12
3.4 PALEO RS, 2021, PORTO ALEGRE..... 14
3.5 PALEO RS, 2021, PORTO ALEGRE..... 16
3.6 REUNIÓN DE COMUNICACIONES DE LA ASOCIACIÓN PALEONTOLÓGICA ARGENTINA, 2021..... 18
3.7 XIX ANNUAL CONFERENCE OF THE EUROPEAN ASSOCIATION OF VERTEBRATE PALAEONTOLOGISTS, 2022, BENEVENTO/PIETRAROJA. 21
3.8 REUNIÓN DE COMUNICACIONES DE LA ASOCIACIÓN PALEONTOLÓGICA ARGENTINA, 2022, SALTA..... 24
3.9 CONGRÈS DE L'ASSOCIATION PALÉONTOLOGIQUE FRANÇAISE, 2022, MONTPELLIER..... 27
4 OUTROS ARTIGOS CIENTÍFICOS..... 29
4.1 ROEDORES MUROIDEOS (MAMMALIA, CRICETIDAE E MURIDAE) DA TOCA DOS OSSOS, OUROLÂNDIA, CAATINGA DO ESTADO DA BAHIA, BRASIL..... 29
4.2 SMALL MAMMAL DIVERSITY IN SEMI-DECIDUOUS SEASONAL FOREST OF THE SOUTHERNMOST BRAZILIAN PAMPA: THE IMPORTANCE OF OWL PELLETS FOR RAPID INVENTORIES IN HUMAN-CHANGING ECOSYSTEMS 57
4.3 EOCENE CAVIOMORPH RODENTS FROM BALSAYACU (PERUVIAN AMAZONIA)..... 82

4.4 LATE MIDDLE MIOCENE CAVIOMORPH RODENTS FROM TARAPOTO, PERUVIAN AMAZONIA..... 127
4.5 BIOTIC COMMUNITY AND LANDSCAPE CHANGES AROUND THE EOCENE–OLIGOCENE TRANSITION AT SHAPAJA, PERUVIAN AMAZONIA: REGIONAL OR GLOBAL DRIVERS?..... 241
4.6 INCISOR ENAMEL MICROSTRUCTURE OF WEST INDIAN CAVIOMORPH HYSTRICOGNATHOUS RODENTS (OCTODONTOIDEA AND CHINCHILLOIDEA)..... 290
4.7 NEW STRATIGRAPHIC AND PALEOENVIRONMENTAL CONSTRAINTS ON THE PALEOGENE PALEOGEOGRAPHY OF WESTERN AMAZONIA..... 332

PARTE III – COMPLEMENTOS

1 HISTÓRICO ESCOLAR

1.1 UNIVERSITÉ DE MONTPELLIER

RÉCAPITULATIF DE PARTICIPATION AUX FORMATIONS
NARLA STUTZ

Doctorat : Paléobiologie
Ecole Doctorale : GAIA - Biodiversité, Agriculture, Alimentation, Environnement, Terre, Eau
Etablissement : Université de Montpellier
Date de la 1ere inscription en thèse : 1 mars 2019 (4 A en 2022)
Direction de thèse : Pierre-Olivier ANTOINE
Sujet de thèse : Metathériens paléogènes et neogènes d'Amazonie Occidentale: systématique et histoire évolutive

Formations suivies

Catégorie : Communication

☛ Cérémonie solennelle 2020 de rentrée des doctorants du Collège Doctoral de l'Université de Montpellier (16 janvier 2020 - 16 janvier 2020) Université de Montpellier Site Nord Triolet Amphi Dumontet
3 heures

☛ Journée de rentrée des doctorants de l'ED Gaia (16 janvier 2020) Amphi DUMONTET, Bâtiment 7, Université de Montpellier
2 heures enregistrées par : GAIA - Biodiversité, Agriculture, Alimentation, Environnement, Terre, Eau.

Total du nombre d'heures pour la catégorie Communication : *5 h*

Catégorie : Enseignement à distance

☛ Éthique de la recherche (07 avril 2020 - 11 mai 2020) proposé par Université de Lyon et diffusé sur la plate-forme FUN
15 heures enregistrées par : GAIA - Biodiversité, Agriculture, Alimentation, Environnement, Terre, Eau.

Total du nombre d'heures pour la catégorie Enseignement à distance : *15 h*

Catégorie : Formations scientifiques

☛ 'PERSPECTIVAS DA PESQUISA PALEONTOLÓGICA ANTÁRTICA' (20 juillet 2020 - 23 juillet 2020) Sociedade Brasileira de Paleontologia - Brésil
8 heures enregistrées par : GAIA - Biodiversité, Agriculture, Alimentation, Environnement, Terre, Eau.

☛ COVID-19: TACKLING THE NOVEL CORONAVIRUS (23 mars 2020) LONDON SCHOOL OF HYGIENE & TROPICAL MEDICINE AND UK PUBLIC HEALTH RAPID SUPPORT TEAM; Londres
12 heures enregistrées par : GAIA - Biodiversité, Agriculture, Alimentation, Environnement, Terre, Eau.

Total du nombre d'heures pour la catégorie Formations scientifiques : *20 h*

Catégorie : Langues vivantes

☛ Renforcer ses compétences orthographiques (10 février 2020 - 30 avril 2020) proposé par Université de Caen et diffusé sur la plate-forme FUN
16 heures enregistrées par : GAIA - Biodiversité, Agriculture, Alimentation, Environnement, Terre, Eau.

Total du nombre d'heures pour la catégorie Langues vivantes : *16 h*

Catégorie : Outils et méthodes

☛ Datação U-Pb in situ em zircões: conceitos básicos, rocedimentos analíticos e interpretação de dados (09 novembre 2022 - 16 décembre 2022) Programa de Pós-Graduação em Geociências, Universidade Federal do Rio Grande do Sul, Porto Alegre
25 heures enregistrées par : GAIA - Biodiversité, Agriculture, Alimentation, Environnement, Terre, Eau.

Total du nombre d'heures pour la catégorie Outils et méthodes : *25 h*

Catégorie : Outils transverses

☛ MOOC Travailler en France - niveau A2 à B1 (31 mars 2019 - 1 avril 2022) En ligne
20 heures

Total du nombre d'heures pour la catégorie : *20 h*

Total participation : 101 heures / 8 modules

1.2 PPGGEO UFRGS

Universidade Federal do Rio Grande do Sul
Programa de Pós-Graduação em Geociências

Histórico Curso

Nome: Narla Shannay Stutz
Identidade: 99756985
Curso: GEOCIÊNCIAS - Doutorado
Área de Concentração: PALEONTOLOGIA
Orientador: ANA MARIA RIBEIRO
Coorientador: Pierre-olivier Antoine
Cotutela: Université de Montpellier I **País:** França
Orientação Cotutela: Pierre-olivier Antoine
Proficiência no(s) Idioma(s): Francês, Inglês

Cartão: 291875
CPF: 05903481914

Situação: ATIVO
Data de Nascimento: 31/07/1992

Período	Código	Atividade de Ensino/Professor	Créditos	Carga Horária	Conceito	Frequência (%)	Situação	Instituição
21/12/2020		Exame de Qualificação	-	-	-	-	Aprovado	UFRGS
2022/02	GEB0158	Datação U-Pb in situ em zircões: conceitos básicos, procedimentos analíticos e interpretação de dados - Professor: Palestrante: Gabriel Bertolini Titulação: Doutorado Professor: Professor: JULIANA CHARAO MARQUES Titulação: Doutorado	4	60	A	100.00	Aprovado	UFRGS
2019/01	GEB00107	Geologia Isotópica, geocronologia e estratigrafia quí. das bacias sedi. Professor: Professor: ANA MARIA PIMENTEL MIZUSAKI Titulação: Doutorado	5	75	A	90.00	Aprovado	UFRGS
2019/01	GEB41-47	T. E. em Paleontologia: Ilustração Científica de Materiais Biológicos Ap Professor: Palestrante: BIANCA MARTINS MASTRANTONIO Titulação: Doutorado Professor: Professor: CESAR LEANDRO SCHULTZ Titulação: Doutorado	2	30	A	90.00	Aprovado	UFRGS
2019/01	GEB41-53	T.E. EM PALEONTOLOGIA: Icnologia de vertebrados fósseis e recentes Professor: Professor: CESAR LEANDRO SCHULTZ Titulação: Doutorado	2	30	A	100.00	Aprovado	UFRGS
		Aproveitamento de Crédito neste Ingresso	24	-	-	-	Aprov. neste ingresso	
		Aproveitamento de Francês	-	-	-	-		
		Aproveitamento de Inglês	-	-	-	-		

Conceitos
A - Conceito Ótimo
B - Conceito Bom
C - Conceito Regular
D - Conceito Insatisfatório
FF - Falta de Frequência

Totais	
Créditos Cursados com Aprovação neste Curso:	13
Aproveitamento de Créditos neste Ingresso:	24
Total:	37

Documento gerado sob autenticação Nº RUS.784.718.0QV
Podendo ser constatada em até 45 dias a partir da data de emissão, na Internet, pelo endereço http://www.ufrgs.br/autenticacao, tendo validade sem carimbo e assinatura.

2 CERTIFICADOS

2.1 CURSO DE LÍNGUA INGLESA



IDIOMAS SEM FRONTEIRAS

UFRGS
UNIVERSIDADE FEDERAL DO RIO GRANDE DO SUL

Certificado

Certificamos que **NARLA SHANNAY STUTZ** concluiu o curso Desenvolvimento de habilidades orais e pronúncia da Língua Inglesa nível B2, com carga horária de 48 horas, Número do Registro 649369, com nota 10.00, oferecido pelo Núcleo de Línguas da UNIVERSIDADE FEDERAL DO RIO GRANDE DO SUL no âmbito do Programa Idiomas sem Fronteiras - Inglês no período de 26/03/2019 a 11/06/2019.

Denise Martins de Abreu e Lima
Presidente do Programa IsF

Utilize um leitor de QR Code no código acima para validar este certificado ou use o código validador **BC080C36** em http://isfaluno.mec.gov.br/validador

CAPES

Ministério da Educação

2.2 MEMBRA DO CORPO EDITORIAL REVISTA BRASILEIRA DE PALEONTOLOGIA

REVISTA BRASILEIRA
DE PALEONTOLOGIA

Porto Alegre, 01 de fevereiro de 2023.

DECLARAÇÃO

Declaro para os devidos fins, que **Narla Shannay Stutz** é Editora-técnica da Revista Brasileira de Paleontologia desde junho de 2020.

MATIAS DO NASCIMENTO RITTER:00907874045

Assinado de forma digital por MATIAS DO NASCIMENTO RITTER:00907874045
DN: cn=MATIAS DO NASCIMENTO RITTER:00907874045, ou=UFRGS - Universidade Federal do Rio Grande do Sul, o=ICPEdu, c=BR
Dados: 2023.02.01 12:49:16 -03'00'

Matias do Nascimento Ritter
Editor-Chefe
Revista Brasileira de Paleontologia

3 RESUMOS PUBLICADOS EM ANAIS DE EVENTOS CIENTÍFICOS

3.1 REUNIÓN DE COMUNICACIONES DE LA ASOCIACIÓN PALEONTOLÓGICA ARGENTINA, 2019, LA PLATA.

EL EOCENO DE LOS ROEDORES CAVIOMORFOS: ENTRE LA RADIACIÓN INICIAL Y APARICIÓN DE LAS SUPERFAMILIAS, FALENCIAS EN EL REGISTRO FÓSIL Y DESCUBRIMIENTOS RECIENTES

M. BOIVIN[1,2], A. ASSEMAT[3], L. MARIVAUX[3], F. PUJOS[4], A. BENITES-PALOMINO[5], R. SALAS-GISMONDI[5,6], **N. STUTZ[7]**, J.V. TEJADA-LARA[5,8], F.R. NEGRI[9], A.M. RIBEIRO[7] y P.-O. ANTOINE[3]

[1]Instituto de Ecorregiones Andinas (INECOA), Universidad Nacional de Jujuy-Consejo Nacional de Investigaciones Científicas y Técnicas (CONICET), Instituto de Geología y Minería. Av. Bolivia 1661, Y4600GNE San Salvador de Jujuy, Jujuy, Argentina. boivin.myriam63@gmail.com

[2]Laboratoire de Planétologie et Géodynamique (LPG), Unité Mixte de Recherche 6112, Centre National de la Recherche Scientifique (CNRS), Université de Nantes. Bât. 4, 2 Chemin de la Houssinière, F-44300 Nantes Cedex 3, France.

[3]Laboratoire de Paléontologie, Institut des Sciences de l'Evolution de Montpellier (ISEM), UMR 5554 CNRS, Institut de Recherche pour le Développement (IRD), École Pratique des Hautes Etudes (EPHE), Université de Montpellier. Place Eugène Bataillon, F-34095 Montpellier Cedex 5, France. alexandre.assemat@gmail.com; laurent.marivaux@umontpellier.fr; pierre-olivier.antoine@umontpellier.fr

[4]Instituto Argentino de Nivología, Glaciología y Ciencias Ambientales (IANIGLA), Centro Científico y Tecnológico del Consejo Nacional de Investigaciones Científicas y Técnicas (CCT CONICET Mendoza). Av. A. Ruiz Leal s/n, M5502IRA Mendoza, Argentina. fpujos@mendoza-conicet.gob.ar

[5]Departamento de Paleontología de Vertebrados, Museo de Historia Natural, Universidad Nacional Mayor San Marcos (UNMSM). Av. Arenales 1256, 15072 Lima, Perú. aldomar1955@gmail.com

[6]BioGeoCiencias Lab, Facultad de Ciencias y Filosofía/CIDIS, Universidad Peruana Cayetano Heredia. Av. Honorio Delgado 430, Urb Ingeniería, Lima, Perú. rodolfo.salas@upch.pe
[7]Seção de Paleontologia, Museu de Ciências Naturais, Fundação Zoobotânica do Rio Grande do Sul. Av. Salvador França 1427, 90690-000 Porto Alegre, RS, Brazil. narla_stutz@yahoo.com.br; ana-ribeiro@fzb.rs.gov.br
[8]Columbia University and Division of Vertebrate Paleontology, American Museum of Natural History. Central Park West at 79th Street, New York, USA. julia.tejada@columbia.edu
[9]Laboratório de Paleontologia, Campus Floresta, Universidade Federal do Acre, Campus Floresta/Cruzeiro do Sul. Rua Paraná, 860, 69980-000 Cruzeiro do Sul, Brazil. frnegri@ufac.br

Investigaciones en la Amazonía peruana han permitido el descubrimiento de yacimientos paleógenos (Santa Rosa y áreas de Contamana y Tarapoto) portadores de varias especies de caviomorfos, documentando las primeras etapas de la historia evolutiva del grupo. Se realizó un análisis cladístico detallado a gran escala (107 taxones; 513 caracteres morfológicos) incluyendo algunas de las especies amazónicas. Por primera vez, distintos caviomorfos basales son reconocidos (*Cachiyacuy*, *Canaanimys*, *Eobranisamys*, *Eoespina*-*Eosachacui*, *Pozomys*, *Shapajamys*, *Tarapotomys*). El estatus supragenérico de varios taxones es comprobado. Las bajas latitudes de América del Sur son vistas como la cuna de la primera radiación de los caviomorfos. Una segunda diversificación de este grupo ocurrió durante el Eoceno Tardío–Oligoceno Temprano, y correspondería a la aparición de las cuatro superfamilias, un resultado obtenido ya en precedentes estudios. Estas fases de diversificación parecen coincidir con eventos climáticos globales y periodos de intensa elevación de los Andes. Los resultados obtenidos sugieren la existencia de linajes fantasmas, algunos de ellos vinculados a ausencias en el registro fósil, e.g., la del Eoceno Medio–Eoceno Tardío al nivel de la divergencia de las superfamilias. El descubrimiento de yacimientos inéditos en las áreas de Balsayacu-Juanjui y Tarapoto (Perú) permitió documentar este intervalo de tiempo poco conocido hasta la fecha. En efecto, los análisis de la morfología de los molariformes y de la microestructura del esmalte de los incisivos indican la presencia de taxones basales, como *Cachiyacuy*, en los niveles inferiores de Balsayacu-Juanjui, a los que suceden taxones más derivados como Eoincamys. En Tarapoto, las nuevas

faunas fueron encontradas en niveles inferiores a los de las faunas previamente conocidas (e.g., TAR-01) y parecen documentar taxones con caracteres más primitivos.

3.2 PALEO RS, 2020, PORTO ALEGRE.

NEOGENE METATHERIA (MAMMALIA) FROM BRAZILIAN AMAZONIA

N. S. Stutz[1,2]; P.-O. Antoine[2]; F. R. Negri[3]; L. Kerber[4,5]; A. S. Hsiou[6]; A. M. Ribeiro[1,7]

[1]Programa de Pós-Graduação em Geociências, Universidade Federal do Rio Grande do Sul, Avenida Bento Gonçalves, 9500, Porto Alegre, RS. [2]Institut des Sciences de l'Évolution, Université de Montpellier, campus Triolet, Montpellier, França. [3]Laboratório de Paleontologia, Campus Floresta, Universidade Federal do Acre, Cruzeiro do Sul, Acre. [4]Centro de Apoio à Pesquisa Paleontológica da Quarta Colônia, Universidade Federal de Santa Maria, São João do Polêsine, RS. [5]Museu Paraense Emílio Goeldi, Coordenação de Ciências da Terra e Ecologia, Belém, PA. [6]Laboratório de Paleontologia, Departamento de Biologia, FFCLRP, Universidade de São Paulo, Ribeirão Preto, SP. [7]Museu de Ciências Naturais/SEMA, Rua Dr. Salvador França, 1427, Porto Alegre, RS.

Metatheria, whose current representatives are known as marsupials, currently comprise seven orders distributed in North, Central and South America, and Australasia. It is's considered that the group originated in Asia in the Late Jurassic. In the Late Cretaceous, metatherians dispersed from North to South America, with its oldest record in this continent in the lower Paleocene of Argentina. Today, South American marsupials are represented by 23 genera and 104 species, belonging to three orders and families: Paucituberculata, Caenolestidae; Microbiotheria, Microbiotheriidae; and Didelphimorphia, Didelphidae. Although being today conspicuous elements in South American small mammals' communities, the peak of Metatheria diversity in this continent occurred in the Paleogene, with great abundance and taxonomic and ecological diversity. Nevertheless, Metatheria's fossil record in South America remains full of gaps, especially for the northern part of the continent, mainly in the region occupied today by the Amazonian rainforest. In this regard, the present work aims to study fossil metatherian remains from two outcrops of the Solimões Formation, Acre Basin, state of Acre, northwestern Brazil. The screen-washing method was employed to collect micromammals' remains, which were subsequently prepared and analyzed under stereomicroscope. The recognition of dental structures and taxonomic identification were made by comparison with

specialized literature. The PRJ-33 outcrop, located on the banks of the Juruá River, near the Peruvian border, is middle Miocene in age. Two distinct taxa of Paucituberculata were found in PRJ-33: one left upper molar of the family Caenolestidae or Pichipilidae; and one right M2 of the superfamily Palaeothentoidea, family Abderitidae. The second outcrop, PRE-06 (Coqueiros), located on the banks of the Envira River and late Miocene in age, delivered one lower left molar of the order Dildephimorphia, family Didelphidae. These taxa indicate similarities with the late middle Miocene La Venta fauna, Colombia, as previously suggested by some other fossil mammals of the Solimões Formation (e.g., rodents, notoungulates, astrapotheres), and with the early middle Miocene MD-67 fauna, Madre de Dios, Peru. Further analysies underway will provide more detailed information on the taxonomic and systematic identity of these Metatheria remains, as well as on the Solimões Formation geological context in Acre. [CNPq 140773/2019-3, 306951/2017-7; CAPES 88887.462070/2019-00]

3.3 PALEONTOLOGICAL VIRTUAL CONGRESS, 2021.

A NEW FOSSIL RODENT ASSEMBLAGE FROM THE SOLIMÕES FORMATION (LATE MIOCENE), ACRE, BRAZIL

E. Fontoura[1,2]*, A. M. Ribeiro[3,4], **N. Stutz[4,5]**, A. S. Hsiou[6], F. R. Negri[7], P.-O. Antoine[5], L. Marivaux[5] and L. Kerber[1,2,8]

[1]Programa de Pós-Graduação em Biodiversidade Animal (PPGBA), Universidade Federal de Santa Maria (UFSM), Santa Maria, Brazil
[2]CAPPA - Centro de Apoio à Pesquisa Paleontológica da Quarta Colônia, São João do Polêsine, Brazil
[3]Museu de Ciências Naturais, Secretaria do Meio Ambiente e Infraestrutura, RS, Brazil
[4]Programa de Pós-Graduação em Geociências, Universidade Federal do Rio Grande do Sul (UFRGS), Porto Alegre, Brazil
[5]Institut des Sciences de l'Evolution de Montpellier (ISEM), France
[6]Universidade de São Paulo (USP), São Paulo, Brazil
[7]Universidade Federal do Acre (UFAC), Acre, Brazil
[8]Museu Paraense Emílio Goeldi, (MPEG), Brazil
*emmanuelle.fontoura@acad.ufsm.br

Keywords: Rodentia, Caviomorpha, Neogene, Acre region, Brazilian Amazon

Caviomorpha is a clade of South American hystricognath clade rodents with great taxonomic and phenotypic diversity. Their stratigraphic distribution ranges from the middle Eocene to the present times. In the Solimões Formation, northwest Brazil, a rich Neogene fossil record has been documented over the last years. Here, we report preliminary data about a new fossiliferous assemblage from the Solimões Formation recovered in recent fieldwork in the Envira River, State of Acre. The specimens were collected in 2010 and 2019 from Neogene sedimentary strata exposed in this river and are housed at the paleontological collection of the Universidade Federal do Acre, Campus Floresta, Cruzeiro do Sul (UFAC-CS). The fossils were found using screen-washing with an aqueous hydrogen peroxide solution and subsequent fossil-handpicking under stereomicroscope. After these procedures, the specimens are being scanned with a micro-CT. The preliminary analysis identified a mandible with

premolar and molars and many isolated molariform teeth. Our results suggest the presence of Octodontoidea (including *Acarechimys*-like), Erethizontoidea, Chinchilloidea (*Scleromys*-like dinomyids, Potamarchinae and Neoepiblemidae), and Cavioidea (Hydrochoerinae). Based on previous records of Solimões Formation, the presence of potamarchines, neoepiblemids, and hydrochoerines is in accordance with a Late Miocene age for these strata (typical Acre fauna). Although fossils have not yet been identified at a less inclusive level, it is possible to observe that this is the most diverse assemblage of Neogene rodents from the Brazilian Amazon.

3.4 PALEO RS, 2021, PORTO ALEGRE.

PRELIMINARY RECORDS ON NEW MARSUPIALS FROM THE LATE MIDDLE MIOCENE TAR-31 LOCALITY, SAN MARTÍN DEPARTMENT, PERUVIAN AMAZONIA

NARLA S. STUTZ[1,2]; MARÍA ALEJANDRA ABELLO[3]; LAURENT MARIVAUX[2]; MYRIAM BOIVIN[4]; FRANÇOIS PUJOS[5]; ALDO M. BENITES-PALOMINO[6,7]; RODOLFO SALAS-GISMONDI[7,8]; JULIA V. TEJADA-LARA[2]; ANA MARIA RIBEIRO[1,9]; PIERRE-OLIVIER ANTOINE[2]

Marsupials, common name of the members of the infraclass Metatheria, are mammals currently distributed in South America mainly in tropical and subtropical areas, but poorly represented in the fossil record of these regions. Except for the species-rich record of La Venta, Colombia, Miocene metatherians from tropical-equatorial South America are sparsely reported in Bolivia, Brazil, Peru, and Venezuela. The present study aims at reporting preliminary data on marsupials recovered from the TAR-31 locality, San Martín Department, Peru. Mammalian biostratigraphy provided a late middle Miocene (Laventan) age for these findings. At TAR-31, the fossil-yielding layer is a 10 to 15 cm-thick microconglomerate lens, assigned to the lower member of the Ipururo Formation, which documents the diverse biota of the time, such as seeds, silicified wood, amber clasts, decapod crustaceans, fishes, anurans, turtles, crocodylomorphs, bird, and several mammals. The material was collected using the screen-washing technique (2–1 mm meshes) and is permanently housed at the Vertebrate Paleontology Department of the Museo de Historia Natural, Universidad Nacional Mayor San Marcos. Our concerned specimens were photographed with scanning electron microscope at the Institut des Neurosciences de Montpellier, France. Preliminary identifications allowed the recognition of one tooth of *Thylamys* cf. *colombianus* among didelphid didelphimorphs; and three teeth of the palaeothentid *Palaeothentes* sp. and a new abderitid taxon among paucituberculatans. The presence of abderitids, as well as that of cebid primates at TAR-31, suggests predominantly wet and warm tropical conditions, with the occurrence of forests in the surroundings. Palaeothentids seemingly preferred drier habitats, with mixed vegetational cover, which would point, to some extent, to a landscape heterogeneity in the concerned area at that time. Comparisons with other Miocene metatherian assemblages at low and

mid latitudes of South America clearly point to a close relationship between TAR-31 and La Venta, as already noticed for other mammalian groups, as well as with Acre River local fauna and Madre de Dios (MD-67) in Brazil and Peru. The current results further the hypothesis of Western Amazonia as a single and consistent biogeographical region for land mammals over middle Miocene times, at the edge of the Pebas Mega-Wetland System. [CNPq 140773/2019-3; CAPES 88887.462070/2019-00; National Geographic Society 9679-15; LabEx CEBA, ANR-10-LABX-25-01; ECOS-FonCyT A14- U01; CoopIntEER CNRS-CONICET nº 252540]

[1]Programa de Pós-Graduação em Geociências, Universidade Federal do Rio Grande do Sul, Porto Alegre, RS. [2]ISEM, Univ Montpellier, CNRS, IRD, Montpellier, France. [3]Unidades de Investigación Anexo Museo, Facultad de Ciencias Naturales y Museo, La Plata, Argentina. [4]Instituto de Ecorregiones Andinas, Universidad Nacional de Jujuy, CONICET, IdGyM, San Salvador de Jujuy, Argentina. [5]Instituto Argentino de Nivología, Glaciología y Ciencias Ambientales, CCT–CONICET–Mendoza, Mendoza, Argentina. [6]Paläontologisches Institut und Museum, Universität Zürich, Zürich, Switzerland. [7]Departamento de Paleontología de Vertebrados, Museo de Historia Natural - Universidad Nacional Mayor San Marcos, Lima, Peru. [8]BioGeoCiencias Lab, Facultad de Ciencias y Filosofía/CIDIS, Laboratorios de Investigacion y Desarrollo (LID), Centro de Investigación para el Desarrollo Integral y Sostenible (CIDIS), Universidad Peruana Cayetano Heredia, Lima, Peru. [9]Seção de Paleontologia, Museu de Ciências Naturais, Secretaria do Meio Ambiente e Infraestrutura, Porto Alegre, Brazil.

3.5 PALEO RS, 2021, PORTO ALEGRE.

NOVA ASSEMBLEIA FOSSILÍFERA DE ROEDORES DA FORMAÇÃO SOLIMÕES (MIOCENO SUPERIOR) ACRE, BRASIL.

E. FONTOURA[1,2]; A.M. RIBEIRO[3,4]; **N. STUTZ[4,7]**; A.S. HSIOU[5]; F.R. NEGRI[6]; P.O. ANTOINE[7]; L. MARIVAUX[7]; L. KERBER[1,2,8]

[1]Programa de Pós-Graduação em Biodiversidade Animal, Universidade Federal de Santa Maria, Santa Maria, RS. [2]CAPPA - Centro de Apoio à Pesquisa Paleontológica da Quarta Colônia, São João do Polêsine, RS. [3]Museu de Ciências Naturais, Secretaria do Meio Ambiente e Infraestrutura, Porto Alegre, RS. [4]Programa de Pós-Graduação em Geociências, Universidade Federal do Rio Grande do Sul, Porto Alegre, RS. [5]Universidade de São Paulo, São Paulo, Brasil. [6]Universidade Federal do Acre, Rio Branco, AC. [7]Institut des Sciences de l'Evolution de Montpellier. [8]Museu Paraense Emílio Goeldi, Belém, PA.

Caviomorpha é um clado de roedores histricognatos sul-americanos com grande diversidade taxonômica e fenotípica. Sua distribuição estratigráfica varia do Eoceno médio até o recente. Na Formação Solimões, localizada no noroeste do Brasil, um rico registro fóssil do Neógeno foi documentado nos últimos anos, sendo encontrados marsupiais, roedores, xenartros, primatas, aves, cobras, invertebrados, plantas, entre outros. Aqui, relatamos dados preliminares sobre uma nova assembleia fossilífera de roedores da Formação Solimões recuperada em trabalhos de campo no Rio Envira (Acre). Os espécimes foram coletados nos anos de 2010 e 2019 em estratos sedimentares do Neógeno expostos nas margens deste rio e estão depositados no acervo paleontológico da Universidade Federal do Acre, Campus Floresta, Cruzeiro do Sul (UFAC-CS). Os fósseis foram encontrados utilizando o método screen-washing com solução aquosa de peróxido de hidrogênio e subsequente triagem manual sob estereomicroscópio. Após esses procedimentos, as amostras estão sendo digitalizadas com um micro-CT. A análise preliminar identificou uma mandíbula com pré-molares e molares e vários dentes molariformes isolados. Nossos resultados sugerem a presença de Octodontoidea (semelhantes a *Acarechimys*), Erethizontoidea, Chinchilloidea (semelhante a *Scleromys*, Dinomydae, Potamarchinae e Neoepiblemidae) e Cavioidea (Hydrochoerinae). Com base em registros anteriores

da Formação Solimões, a presença de potamarquíneos, neoepiblemídeos e hidrochoerineos indicam uma idade do Mioceno Superior para esses estratos. Embora esses fósseis ainda não tenham sido identificados em um nível menos inclusivo, é possível observar que esta é a mais diversa assembleia de roedores do Neógeno da Amazônia brasileira. [CNPq 140639/2021-7]

3.6 REUNIÓN DE COMUNICACIONES DE LA ASOCIACIÓN PALEONTOLÓGICA ARGENTINA, 2021.

NEOTROPICAL METATHERIAN DIVERSITY AROUND THE EOCENE-OLIGOCENE TRANSITION: THE SHAPAJA SECTION, PERUVIAN AMAZONIA

N.S. STUTZ[1,2], M.A. ABELLO[3], L. MARIVAUX[1], M. BOIVIN[4], M.A. CUSTÓDIO[5,6,7], A. BENITES-PALOMINO[8,9], R. SALAS-GISMONDI[9,10], F. PUJOS[11], J.V. TEJADA-LARA[1], A.M. RIBEIRO[2,12], P.-O. ANTOINE[1]

[1]Laboratoire de Paléontologie, Institut des Sciences de l'Évolution de Montpellier (ISEM, UMR 5554, CNRS/UM/IRD/EPHE), Université de Montpellier, Place Eugène Bataillon, F-34095, Montpellier Cedex 5, France.
[2]Programa de Pós-Graduação em Geociências, Universidade Federal do Rio Grande do Sul (PPGGEO UFRGS). Av. Bento Gonçalves, 9500, 91501-970, Porto Alegre, Rio Grande do Sul, Brazil.
[3]Facultad de Ciencias Naturales y Museo (UNLP), Laboratorio de Sistemática y Biología Evolutiva (LASBE), Unidades de investigación Anexo Museo, Av. 60 y 122, B1900FWA La Plata, Argentina.
[4]Instituto de Ecorregiones Andinas (INECOA), Universidad Nacional de Jujuy, CONICET, IdGyM, Av. Bolivia 1661, 4600 San Salvador de Jujuy, Jujuy, Argentina.
[5]Departamento de Geociências, Universidade Federal do Amazonas, CEP: 69.077-000, Manaus, AM, Brazil.
[6]Instituto de Geociências, Universidade de Brasília (UnB), Campus Universitário Darcy Ribeiro ICC - Ala Central, 70910-000, Brasília, Brazil.
[7]Géosciences-Environnement Toulouse, Université de Toulouse, 14 Avenue Édouard Belin, F-31400 Toulouse, France.
[8]Paläontologisches Institut und Museum, Universität Zürich, Karl-Schmid-Strasse 4, 8006 Zürich, Switzerland.
[9]Departamento de Paleontología de Vertebrados, Museo de Historia Natural - Universidad Nacional Mayor San Marcos (UNMSM, DPV-MUSM). Av. Arenales 1256, Lima 14, Peru.
[10]BioGeoCiencias Lab, Facultad de Ciencias y Filosofía/CIDIS, Laboratorios de Investigacion y Desarrollo (LID), Centro de Investigación para el Desarrollo Integral y

Sostenible (CIDIS), Universidad Peruana Cayetano Heredia, Avenida Honorio Delgado 430, Lima 31, Peru.
[11]Instituto Argentino de Nivología, Glaciología y Ciencias Ambientales (IANIGLA), CCT–CONICET–Mendoza. Av. Ruiz Leal s/n, Parque Gral. San Martín, 5500 Mendoza, Argentina.
[12]Seção de Paleontologia, Museu de Ciências Naturais, Secretaria do Meio Ambiente e Infraestrutura, Av. Dr. Salvador França, 1427, 90690-000, Porto Alegre, Brazil.

Metatheria (Mammalia) were remarkable faunal components of South American Cenozoic history. Now represented solely by the marsupials (e.g., opossums, kangaroos), metatherians evolved multiple adaptive types with greater past diversity and abundance than today. One important chapter of this history is the Eocene-Oligocene transition (EOT), a period of considerable changes worldwide, with marked extinctions, diversity changes and drastic climatic processes (i.e., transition from the early Cenozoic “Greenhouse World” to the post-Eocene “Icehouse World”). For Metatheria, the EOT is considered the major turnover point in their evolutionary history in South America, an assumption mainly based on the fossil record from Argentinian Patagonia. However, the EOT is scarcely known at tropical latitudes of South America, so are other time intervals, since this region is still poorly understood through a paleontological and geological standpoint. This study aims at partly filling this gap of knowledge, by reporting preliminary identifications of metatherians from the late Eocene-early Oligocene Shapaja section, near Tarapoto, Peruvian Amazonia. Nine fossiliferous localities of the Pozo Formation were dated by chemostratigraphy and explored through wet screening (1–2 mm meshes), which allowed recovering small-sized fossils (plants, mollusks, decapods, fishes, amphibians, reptiles, and many mammals). Metatherians were found in most localities and, according to their taxonomic composition, three assemblages could be recognized throughout the section, a pattern also observed in rodents and fishes. The oldest assemblage (TAR-74, early late Eocene) is composed by only one new prepidolopid polydolopimorphian. The second assemblage (TAR-20, 72, 21), latest Eocene, encompasses scarce and fragmentary remains of another probable prepidolopid, numerous remains of a small gerbil-like argyrolagid, and teeth of palaeothentoids, an extinct clade of paucituberculatans, with two basal forms plus two palaeothentines. These records represent the oldest occurrences of Palaeothentinae and Argyrolagidae, and also the northernmost record of the latter clade. The earliest Oligocene localities yielded none

(TAR-22) or few fragmented metatherian remains (TAR-13), possibly due to taphonomic biases, being considered transitional. Finally, the third assemblage (TAR-01, early Oligocene) includes one larger, rarer argyrolagid and several palaeothentoids (three basal taxa, three palaeothentids, and one abderitid). Thus, the Shapaja section does not attest to a smaller diversity around the EOT. However, the changes in the taxonomic composition of the assemblages, as well as other geological and paleontological data, point to two biotic turnovers. The first one, during the late Eocene, has probably been driven by regional processes related to the Andean orogeny, which led to an episodic marine incursion in this area. The later biotic turnover, by contrast, seems to be related to the EOT global processes, namely the great drop in sea level and the onset of drier and cooler climates worldwide, with decreased precipitation and increased seasonality. Indeed, fossil plants from Shapaja indicate the occurrence of multi-stratified rainforests during the latest Eocene and more open, deciduous forests in the earliest Oligocene. Finally, the Shapaja section highlights the importance of fieldwork and research efforts in northern South America, to get better correlations with middle and high latitudes localities, and thus a refined paleobiodiversity picture in the whole continent.

*Project supported by: National Geographic Society (9679-15), The Leakey Foundation, “Investissements d’Avenir” grant by the Agence Nationale de la Recherche LabEx CEBA (ANR-10-LABX-25-01), ECOS-FonCyT (A14-U01), CoopIntEER CNRS-CONICET (252540), ISEM, and Campus France program of the French Ministry of Foreign Affairs.

3.7 XIX ANNUAL CONFERENCE OF THE EUROPEAN ASSOCIATION OF VERTEBRATE PALAEONTOLOGISTS, 2022, BENEVENTO/PIETRAROJA.

MIDDLE MIOCENE METATHERIANS FROM JUAN GUERRA (SAN MARTIN, PERU) EXPAND THE RECORD OF SMALL MAMMALS IN THE PROTO AMAZONIA

N.S. Stutz[1,2], M.A. Abello[3], L. Marivaux[2], M. Boivin[4]; F. Pujos[5]; A.M. Benites-Palomino[6,7], R. Salas-Gismondi[7,8], J.V. Tejada-Lara[9]; M.A. Custódio[10,11,12], M. Roddaz[11], R.V. Santos[12], A.M. Ribeiro[1,13], P.-O. Antoine[2]

[1]Programa de Pós-Graduação em Geociências, Universidade Federal do Rio Grande do Sul (PPGGEO UFRGS), Avenida Bento Gonçalves, 9500, 91501-970, Porto Alegre, Brazil.

[2]Laboratoire de Paléontologie, Institut des Sciences de l'Évolution de Montpellier (ISEM, UMR 5554, UM/CNRS/IRD/EPHE), Université de Montpellier, Place Eugène Bataillon, 34095, Montpellier, France.

[3]Unidades de Investigación Anexo Museo, Facultad de Ciencias Naturales y Museo (UNLP), Avenida 60 y 122, B1900FWA, La Plata, Argentina.

[4]Instituto de Ecorregiones Andinas (INECOA), Universidad Nacional de Jujuy, CONICET, IdGyM, Avenida Bolivia 1661, 4600, San Salvador de Jujuy, Argentina.

[5]Instituto Argentino de Nivología, Glaciología y Ciencias Ambientales (IANIGLA), CCT–CONICET–Mendoza, Avenida Ruiz Leal s/n, Parque Gral. San Martín, 5500, Mendoza, Argentina.

[6]Paläontologisches Institut und Museum, Universität Zürich, Karl-Schmid-Strasse 4, 8006, Zürich, Switzerland.

[7]Departamento de Paleontología de Vertebrados, Museo de Historia Natural - Universidad Nacional Mayor San Marcos (UNMSM, DPV-MUSM), Avenida Arenales 1256, Lima 14, Peru.

[8]BioGeoCiencias Lab, Facultad de Ciencias y Filosofía/CIDIS, Laboratorios de Investigacion y Desarrollo (LID), Centro de Investigación para el Desarrollo Integral y Sostenible (CIDIS), Universidad Peruana Cayetano Heredia, Avenida Honorio Delgado 430, Lima 31, Peru.

[9]Department of Archaeology, University of Cambridge, Downing Street, CB2 3DZ, Cambridge England.

[10]Instituto de Ciências Exatas, Departamento de Geociências, Universidade Federal do Amazonas (UFAM), Avenida General Rodrigo Octavio Jordão Ramos, 1200, Coroado I, 69067-005, Manaus, Brazil.
[11]Laboratório de Geocronologia, Instituto de Geociências, Universidade de Brasília (UnB), Campus Universitário Darcy Ribeiro ICC - Ala Central, 70910-000, Brasília, Brazil.
[12]Géosciences-Environnement Toulouse, Université de Toulouse (UPS (SVT-OMP)/CNRS/IRD), 14 Avenue Édouard Belin, F-31400, Toulouse, France.
[13]Seção de Paleontologia, Museu de Ciências Naturais, Secretaria do Meio Ambiente e Infraestrutura, Avenida Dr. Salvador França, 1427, 90690-000, Porto Alegre, Brazil.

Keywords: Paucituberculata, Didelphimorphia, Laventan, Paleobiogeography, Pebas Mega-Wetland System.

Currently, marsupials (modern members of Metatheria), are widely distributed in tropical and subtropical areas of South America, but poorly represented in their fossil record. Except for the species-rich fossiliferous localities of La Venta (Colombia), additional Miocene metatherians from tropical-equatorial South America are sparsely reported in Bolivia, Brazil, Peru, and Venezuela. Here, we introduce new metatherian remains recovered in the late middle Miocene TAR-31 locality, Peru, assigned to the early Laventan South American Land Mammal Age (~13 Ma) by mammalian biostratigraphy. U-Pb analysis made on detrital zircon grains from TAR-31 gave a maximum depositional age of 17.4 ± 0.12 Ma. Three metatherian taxa are recognized at TAR-31: the didelphid *Thylamys* cf. *T. colombianus*, plus the paucituberculatans *Palaeothentes* sp. (palaeothentid) and the new abderitid *Pitheculites ipururensis* nov. sp. This assemblage, along with a cebid primate at TAR-31, suggests predominantly humid and warm tropical conditions, with the occurrence of both forests and drier habitats in the surroundings. Comparisons with other Miocene metatherian assemblages at low and mid latitudes of South America clearly confirm closest relationships between TAR-31 and La Venta (previously observed on monkeys and rodents), as well as, to a lesser extent, with Acre River local fauna and Madre de Dios (MD-67) and in Brazil and Peru, respectively. The current results further the hypothesis of Western Amazonia as a single and consistent biogeographical region for land mammals over middle Miocene times, at the western edge of the Pebas Mega-Wetland

System, and highlight the role of the Amazonian region concerning marsupial Neogene radiation.

3.8 REUNIÓN DE COMUNICACIONES DE LA ASOCIACIÓN PALEONTOLÓGICA ARGENTINA, 2022, SALTA.

NEW RECORDS OF NEOGENE METATHERIA (MAMMALIA) FROM WESTERN AMAZONIA (ACRE, BRAZIL)

Narla S. STUTZ[1,2], Patrícia HADLER[3], Francisco R. NEGRI[4], Laurent MARIVAUX[2], François PUJOS[5,6], Tiago R. JACÓ[7], Emmanuelle M. FONTOURA[8], Roberto VENTURA SANTOS[9], André M. V. ALVIM[9], Pierre-Olivier ANTOINE[2] y Ana M. RIBEIRO[1,10]

[1]Programa de Pós-Graduação em Geociências (PPGGEO), Universidade Federal do Rio Grande do Sul, Avenida Bento Gonçalves, 9500, 91501-970, Porto Alegre, Rio Grande do Sul, Brazil.
[2]Institut des Sciences de l'Évolution (ISE-M), Université de Montpellier, CNRS, IRD, Place Eugène Bataillon, 34095, Montpellier, France.
[3]Laboratório de Paleontologia, Programa de Pós-Graduação em Geologia, Universidade Federal de Santa Catarina, Campus Universitário s/n, 88040-900, Florianópolis, Santa Catarina, Brazil.
[4]Laboratório de Paleontologia, Campus Floresta, Universidade Federal do Acre, Estrada do Canela Fina, Km 12, 69980-000, Cruzeiro do Sul, Acre, Brazil.
[5]Consejo Nacional de Investigaciones Científicas y Técnicas (CONICET), Argentine.
[6]Instituto Argentino de Nivología, Glaciología y Ciencias Ambientales (IANIGLA), CONICET–UNCUYO-Mendoza, Avenida Ruiz Leal s/n, Parque Gral. San Martín, 5500, Mendoza, Argentine.
[7]Programa de Pós-Graduação em Sistemática e Conservação da Diversidade Biológica (PPGSCBIO), Secretaria do Meio Ambiente e Infraestrutura do Rio Grande do Sul, Universidade Estadual do Rio Grande do Sul, Rua Dr. Salvador França, 1427, 90690-000, Porto Alegre, Rio Grande do Sul, Brazil.
[8]Programa de Pós-Graduação em Biodiversidade Animal (PPGBA), Universidade Federal de Santa Maria, Avenida Roraima, 1000, 97105-900, Santa Maria, Rio Grande do Sul, Brazil.
[9]Laboratório de Geocronologia, Instituto de Geociências, Universidade de Brasília (UnB), Campus Universitário Darcy Ribeiro ICC - Ala Central, 70910-000, Brasília, Distrito Federal, Brazil.

[10]Seção de Paleontologia, Museu de Ciências Naturais, Secretaria do Meio Ambiente e Infraestrutura do Rio Grande do Sul, Rua Dr. Salvador França, 1427, 90690-000, Porto Alegre, Rio Grande do Sul, Brazil.

Almost 40% of South America is covered by the plains and lowlands of the Amazon River and its tributaries, the largest low-latitude subregion of the Neotropics. The forests of the great Amazonian Basin harbor an outstanding biological diversity, encompassing one of the richest mammal faunas on the planet, especially in its western part. The fossil record in tropical regions may appear as particularly poor, due to the unfavorable preservation conditions, but also, as in Amazonia, due to the densely forested environments, and somewhat difficult paleontological field conditions. In Amazonia, paleontological field efforts over the past few decades have proven that fossils can be relatively common. Although still fragmentary, fossils of large reptiles and placental mammals have been substantially documented. Despite their great current species richness and abundance in the area, the fossil record of Metatheria, whose recent representatives are grouped into marsupials, is known only from few Cenozoic localities. Here we present new records of fossil metatherians from the PRE-06 locality (Coqueiros, 8°18'08.5"S 70°26'40.8"W), situated on the banks of the Rio Envira (Acre Basin, state of Acre, northwestern Brazil), where the Solimões Formation (lower Eocene–Pliocene) crops out. This locality, which consists of a 30 cm-thick fossil-bearing microconglomerate of detrital origin, was recently extensively exploited, including using wet-screening to collect remains of micromammals. A preliminary faunal list for PRE-06 includes mollusks (bivalves and gastropods), crabs, fishes (selachians, characiforms, siluriforms, and dipnoans), amphibians, reptiles, bird, and mammals (metatherians, xenarthrans, notoungulates, litopterns, cetaceans, and rodents). The specimens are permanently housed at the collection of the Laboratório de Paleontologia of the Universidade Federal do Acre, Floresta campus (UFAC-CS), Cruzeiro do Sul, Acre, Brazil. Previously, fossil wood fragments were reported for PRE-06, with a diverse flora, which resembles in many aspect that occurring in the region today, thereby suggesting that similar equatorial climatic conditions were already present at the time of the PRE-06 deposition. Only seven metatherian dental specimens have been found at PRE-06, exclusively representing didelphid Didelphimorphia, with cf. *Marmosa*, *Didelphis* cf. *D*. *solimoensis*, *Thylamys colombianus*, and unidentified didelphids. These speciments, along with the associated mammals, indicate an early late Miocene age for PRE-06. The relative low

abundance of metatherian remains with respect to those of rodents, and the absence of sparassodonts, paucituberculatans and microbiotheres, found in other tropical-equatorial areas of South America at the same epoch, are striking features to be further investigated, in addition to detailed taxonomic analysis.

*This work was supported by: CNPq 140773/2019-3; 310023/2021-1; CNPq/MCTI/CONFAP-FAPS 441626/2020-3; CAPES 88887.462070/2019-00; ANR LabEx CEBA, ANR-10-LABX-25-01.

3.9 CONGRÈS DE L'ASSOCIATION PALÉONTOLOGIQUE FRANÇAISE, 2022, MONTPELLIER.

MESACERATHERIUM GAIMERSHEIMENSE HEISSIG, 1969 (MAMMALIA, RHINOCEROTIDAE) DE LA JAVIE (OLIGOCÈNE SUPÉRIEUR, SE FRANCE)

Pierre-Olivier ANTOINE[1], **Narla Shannay STUTZ[1,2]**, Julia TEJADA[1,3,4], Laurent MARIVAUX[1], Myette GUIOMAR[5]

1. ISEM, Univ Montpellier, CNRS, IRD, Montpellier, France
2. Programa de Pós-Graduação em Geociências, UFRGS, Porto Alegre, Brésil
3. Department of Archaeology, University of Cambridge, Angleterre
4. DPV, Museo de Historia Natural - UNMSM, Lima, Pérou
5. Réserve Naturelle géologique de Haute Provence, Conseil Départemental des Alpes de Haute-Provence, Digne-les-Bains, France

Le Ravin du Rousset (commune de La Javie), situé dans la Réserve Naturelle Géologique de Haute-Provence, voit affleurer largement la Molasse rouge gréseuse oligocène. Cette formation continentale aux alternances de grès et de marnes présente localement, dans sa partie inférieure, des argilites de couleur rouge à débit en plaquettes auxquelles succèdent des niveaux plus carbonatés terminés par une barre calcaire formant une corniche. La découverte de fragments dentaires de rhinocérotidé en surface par l'une d'entre nous (MG) lors d'une ronde de veille sous la corniche carbonatée a conduit à l'organisation d'une fouille de sauvetage en juin 2021, à laquelle ont participé tous les présents auteurs. Les restes appartiennent à un seul individu et correspondent à un squelette partiel. Plusieurs éléments du squelette postcrânien sont encore enchâssés dans la matrice sur place, mais le basicrâne, les deux séries molaires supérieures, la mandibule (avec les deux séries p3-m3 et la symphyse), l'atlas, un unciforme, trois vertèbres et des côtes ont pu être extraits. Les caractéristiques morpho-anatomiques (notamment sur M3 et la symphyse mandibulaire) et les dimensions des restes déjà préparés correspondent en tous points à celles observées chez *Mesaceratherium gaimersheimense* Heissig, 1969, un rhinocérotiné basal connu dans l'Oligocène supérieur d'Europe occidentale (MP28-MP30 ; Blanchon et al. 2018 ; Tissier et al. 2020). Cette attribution taxinomique taxonomique est conforme à l'âge préalablement attribué à la partie médiane de la

formation par biostratigraphie mammalienne (MP28), grâce à la présence du rongeur Issiodoromys limognensis dans une argile ligniteuse latéralement équivalente au niveau à Mesaceratherium (Tortosa 2005). Quelques dents de cette espèce ont d'ailleurs été découvertes par lavage-tamisage de cette même argile au cours de l'opération de fouille en juin 2021.

Blanchon M., Antoine P.-O., Blondel C. & Bonis L. de 2018. Rhinocerotidae (Mammalia, Perissodactyla) from the latest Oligocene Thézels locality, SW France, with a special emphasis on *Mesaceratherium gaimersheimense* Heissig, 1969. Annales de Paléontologie 104, 217-229.

Heissig K. 1969. Die Rhinocerotidae (Mammalia) aus der oberoligozänen Spaltenfüllung von Gaimersheim bei Ingolstadt in Bayern und ihre phylogenetische Stellung. Abhandlungen der Bayer. Akad. der Wissenschaften, Math. Klasse 138.

Tissier J., Antoine P.-O. & Becker, D. 2020. New material of *Epiaceratherium* and a new species of *Mesaceratherium* clear up the phylogeny of early Rhinocerotidae (Perissodactyla). Royal Society Open Science 7, 200633.

Tortosa T. 2005. La Lignée évolutive d'*Issiodoromys* (Rodentia, Theridomyidae) : un outil pour la datation de nouveaux gisements. Rapport DEA, Université Montpellier II, 25 pp. (inédit)

4 OUTROS ARTIGOS CIENTÍFICOS

4.1 ROEDORES MUROIDEOS (MAMMALIA, CRICETIDAE E MURIDAE) DA TOCA DOS OSSOS, OUROLÂNDIA, CAATINGA DO ESTADO DA BAHIA, BRASIL

Artigo publicado no periódico Boletim do Museu Paraense Emilio Goeldi, Ciencias Naturais, volume 15, p. 777-794, 2020, DOI: 10.46357/bcnaturais.v15i3.215.

Anny Caroliny Gomes[I] | Carolina Saldanha Scherer[I] | Patrícia Hadler[II] | Jorge José Cherem[II] | Téo Veiga de Oliveira[III] | **Narla Shannay Stutz[IV]**

[I]Universidade Federal do Recôncavo da Bahia, Cruz das Almas, Bahia, Brasil
[II]Universidade Federal de Santa Catarina, Florianópolis, Santa Catarina, Brasil
[III]Universidade Estadual de Feira de Santana, Feira de Santana, Bahia, Brasil
[IV]Universidade Federal do Rio Grande do Sul, Porto Alegre, Rio Grande do Sul, Brasil

Resumo: Roedores muroideos incluem as duas famílias mais diversas de mamíferos do mundo, Cricetidae e Muridae. Apesar disso, são ainda pouco estudados em muitas regiões, como a Caatinga. O presente estudo dá a conhecer os roedores muroideos da Toca dos Ossos, situada em Ourolândia, centro-norte da Bahia. A Toca dos Ossos é uma cavidade natural escavada em maciço calcário da Formação Caatinga, destacando-se por ser um importante sítio paleontológico. O material estudado é constituído por fragmentos cranianos e mandibulares coletados em duas áreas da caverna. Em uma delas, egagropilos de *Tyto furcata* foram coletados em uma dolina e, na outra, o material foi coletado no sedimento de superfície em salões e condutos internos da caverna. Sete espécies foram registradas: *Necromys lasiurus*, a mais frequente na amostra, *Cerradomys* sp., *Holochilus sciureus*, *Oligoryzomys* sp., *Calomys* sp., *Wiedomys pyrrhorhinos* e *Rattus rattus*, este exclusivo nas amostras de egagropilos. Apesar das diferenças nas frequências dos táxons, as amostras em ambas as áreas da caverna apresentam grande similaridade taxonômica e são compostas por espécies de ocorrência atual na Caatinga, incluindo a espécie exótica *R*. *rattus*, o que sugere uma idade recente para o material, posterior à expansão desse bioma, que ocorreu há cerca de 4.000 anos.

Palavras-chave: Caverna. Egagropilo de coruja. Floresta tropical sazonal seca. Sigmodontinae.

Abstract: Muroid rodents include the two most diversified mammalian families of the world, Cricetidae and Muridae. Despite this, muroids are still poorly addressed in many regions, such as the Caatinga biome. This study reports the muroid rodents from the 'Toca dos Ossos', municipality of Ourolândia, central-northern Bahia state. The 'Toca dos Ossos' is a natural cavity excavated in the limestone massif of the Caatinga Formation, standing out as an important paleontological site. The studied material consists of cranial and mandibular fragments retrieved in two cave areas. One of them represent *Tyto furcata* pellets collected at a sinkhole, and the other is from material collected in the surface sediment of cave halls and internal conduits. The following species were recorded: *Necromys lasiurus*, the most frequent in the samples, *Cerradomys* sp., *Holochilus sciureus*, *Oligoryzomys* sp., *Calomys* sp., *Wiedomys pyrrhorhinos*, and *Rattus rattus*, the latter exclusively found in the owl pellets samples. Even though there are differences in the frequencies of the taxa, the communities from both of the cave areas possess great taxonomic similarity and include species currently found in the Caatinga, including the exotic species *R*. *rattus*, suggesting a recent age for the material, subsequent to the expansion of this biome, which happened 4,000 years ago.
Keywords: Cave. Owl pellet. Seasonally dry tropical forest. Sigmodontinae.

INTRODUÇÃO

Os muroideos compreendem um grupo de roedores miomorfos caracterizados por sua fórmula dentária simplificada (ausência de pré-molares nas mandíbulas e maxilas) e pela presença de anterocone/ídeo bem desenvolvido no primeiro molar (Flynn *et al.*, 1985). Eles compõem uma parte significativa das assembleias de mamíferos na maioria dos continentes, ocorrem nos mais variados ambientes, perfazendo, aproximadamente, 28% do total de espécies de mamíferos, e incluem as duas famílias mais diversas de mamíferos, Cricetidae (792 espécies) e Muridae (834 espécies) (Jansa & Weksler, 2004; Honeycutt *et al*., 2007; Fabre *et al*., 2012; Burgin *et al*., 2018).

Na América do Sul, a família Cricetidae é representada pela subfamília Sigmodontinae, que inclui mais de 430 espécies viventes e ilustra um dos mais extraordinários eventos de radiação explosiva, considerando que sua história evolutiva no continente pode se estender por um período inferior a 4 milhões de anos (Pardiñas *et al*., 2017; Barbière *et al*., 2019). Por outro lado, as três espécies de

Muridae distribuídas amplamente na América do Sul são invasoras recentes, tendo sido introduzidas acidentalmente pelos exploradores do Novo Mundo (Catzeflis, 2018).

A Caatinga é um bioma típico do semiárido do Nordeste brasileiro, formada por um mosaico de ambientes arbustivos e florestais (Leal *et al*., 2005). Atualmente considerada uma das maiores áreas de floresta tropical sazonalmente seca do Novo Mundo, a Caatinga abriga uma biodiversidade considerável para uma região semiárida, composta por, pelo menos, 3.150 espécies de plantas, 98 de anfíbios, 79 de répteis e 548 de aves (Silva *et al*., 2017). Em relação aos mamíferos, Carmignotto & Astúa (2017) registraram 183 espécies autóctones, 11 das quais são endêmicas do bioma. Rodentia é a segunda ordem em riqueza, com 41 espécies, sendo que 23 delas pertencem à família Cricetidae (Carmignotto & Astúa, 2017). Além disso, as três espécies de murídeos invasores também estão presentes na Caatinga (Moojen, 1952).

Nesse bioma, destaca-se a Reserva Particular do Patrimônio Natural (RPPN) Toca dos Ossos, criada em 27 de dezembro de 2016 (INEMA, 2016), a qual tem, entre outros aspectos, elevada relevância paleontológica (*e.g*., Cartelle & Lessa, 1988, 1989; Cartelle & Abuhid, 1994; Czaplewski & Cartelle, 1998; Lessa *et al*., 1998; Lobo *et al*., 2017; Gomes *et al*., 2019). Por outro lado, poucos estudos foram realizados sobre a fauna atual de mamíferos da Toca dos Ossos e região do entorno (*e.g*., Sbragia & Cardoso, 2008; Jesus & Oliveira, 2017). Entre os roedores da Toca dos Ossos, foram conduzidos apenas estudos sobre variação em caracteres cranianos do caviomorfo *Kerodon rupestris* (Wied-Neuwied, 1820) (Lessa & Pessôa, 2005; Lessa *et al.*, 2005).

Apesar da elevada riqueza dos roedores no estado da Bahia como um todo, levantamentos abordando esse grupo têm sido conduzidos principalmente na Mata Atlântica (*e.g*., Vaz, 2005; Geise & Pereira, 2008; Carvalho & Oliveira, 2015), havendo, entretanto, poucos na Caatinga (Oliveira *et al*., 2003; Freitas *et al*., 2005; Oliveira &

Pessôa, 2005; Pereira & Geise, 2009). Devido à escassez de registros de roedores neste bioma, é de fundamental importância o estudo da fauna da Toca dos Ossos. Neste sentido, este trabalho tem como objetivos fornecer uma lista comentada de roedores muroideos dessa localidade, bem como apontar o provável intervalo temporal de depósito do material.

MATERIAL E MÉTODOS

ÁREA DE ESTUDO

A Toca dos Ossos está localizada na bacia do rio Salitre, município de Ourolândia, estado da Bahia, região Nordeste do Brasil. Sua entrada principal situa-se 560 m acima do nível do mar (10º 55’ 51,25” S, 41º 3’ 27,10” O) (Figuras 1ª e 1B). A Toca dos Ossos representa uma cavidade natural escavada em um maciço calcário da Formação Caatinga, situada na porção norte da Chapada Diamantina, com grande concentração de fósseis (*e.g*., Lessa *et al*., 1998; Gomes *et al*., 2019).

A Toca dos Ossos possui 14.200 m de projeção horizontal mapeados (Rubbioli *et al*., 2019). Apresenta padrões morfológicos peculiares que a diferem de outras cavernas brasileiras, com galerias meandrantes interconectadas em vários pontos. Entre as galerias maiores, pode ser observada uma complexa rede labiríntica, responsável pela ligação de áreas distintas da caverna (Figura 1C) (Auler *et al*., 2006; Rubbioli *et al*., 2019). Esse aspecto espongiforme, sem padrões definidos, fica evidente no período chuvoso, quando o alagamento da galeria principal escoa água para as áreas mais baixas da caverna, enquanto as áreas posicionadas em um nível superior permanecem com seu sedimento seco (Auler *et al*., 2006).

A bacia do rio Salitre, na qual se situa a Toca dos Ossos, está inserida no bioma Caatinga e é caracterizada predominantemente por duas fitofisionomias, Caatinga Arbustiva (esparsa ou densa, formada por arbustos de 2 a 3 metros de altura e arvoretas de 5 a 6 metros) e Caatinga Arbórea (composta predominantemente por árvores de 8 a 10 metros) (Rizzini, 1997; CBHS, 2017). No entanto, grande parte da vegetação nessa região encontra-se atualmente alterada por ação antrópica, com a conversão de quase 50% da cobertura vegetal natural em áreas de cultivo agrícola e pastagem. As estações seca e chuvosa são bem definidas, e a estação chuvosa está concentrada nos meses de novembro a março. A precipitação total anual varia de 300 a 600 mm (CBHS, 2017). O clima, segundo a classificação de Köppen, é do tipo BSh, semiárido, de baixas latitude e altitude, caracterizado pela baixa pluviosidade e temperatura média anual de cerca de 25 °C (Alvares *et al*., 2013).

AMOSTRAGEM

O material estudado consiste de 210 fragmentos cranianos e mandibulares, coletados em 03 de julho de 2011, 10-11 de agosto de 2012 e 09 de junho de 2013, em duas áreas da Toca dos Ossos (doravante denominadas TO), distantes 500 metros uma da outra, aproximadamente. A primeira compreende uma dolina, denominada TO-I (Figuras 1C e 1D), onde o material foi obtido a partir da triagem de

egagropilos inteiros ou desagregados de corujas-das-igrejas – *Tyto furcata* (Temminck, 1827) – (Figura 1E). A segunda área, denominada TO-II, localiza-se na parte mais interna da caverna e está composta por vários salões e condutos (Figuras 1C e 1F), onde o material foi coletado diretamente do sedimento de superfície (Figura 1G). A coleta dos espécimes na caverna foi autorizada pelo Instituto Chico Mendes de Conservação da Biodiversidade (ICMBio), por meio das licenças números 27530 e 35904.

TRIAGEM E IDENTIFICAÇÃO

Em laboratório, o material foi limpo sob estereomicroscópio binocular, com o auxílio de pincel e agulha. Posteriormente, os espécimes da TO-I foram depositados na Coleção de Mamíferos do Museu de Zoologia da Universidade Estadual de Feira de Santana (MZFS-DM) e da TO-II nas coleções Paleontologia de Vertebrados do Museu de Zoologia e Paleontologia da Universidade Federal do Recôncavo da Bahia (UFRB-PV).

A identificação das espécies foi realizada a partir de fontes bibliográficas (Pardiñas & Teta, 2011; Bonvicino, 2015; Brandão & Nascimento, 2015; Salazar-Bravo, 2015; Weksler & Bonvicino, 2015; Catzeflis, 2018; Cherem *et al*., 2018; Stutz *et al*., 2018) e da comparação com espécimes depositados nas coleções de mamíferos do Museu de Zoologia da Universidade Estadual de Feira de Santana (MZFS-DM) e do Departamento de Ecologia e Zoologia da Universidade Federal de Santa Catarina (UFSC) (Apêndice 1). Quando necessário, foram tomadas medidas utilizando-se paquímetro digital com precisão de 0,02 mm: largura do forâmen incisivo (LFI); comprimento da série molar superior (CM1-M3); comprimento da série molar inferior (Cm1-m3); comprimento do primeiro molar inferior (Cm1).

A nomenclatura dentária seguiu Reig (1977) e Percequillo (2006). A nomenclatura e o ordenamento taxonômicos seguiram Patton *et al*. (2015) para Sigmodontinae e Wilson & Reeder (2005) para Muridae. O número mínimo de indivíduos (NMI) por espécie foi determinado segundo Beisaw (2013).

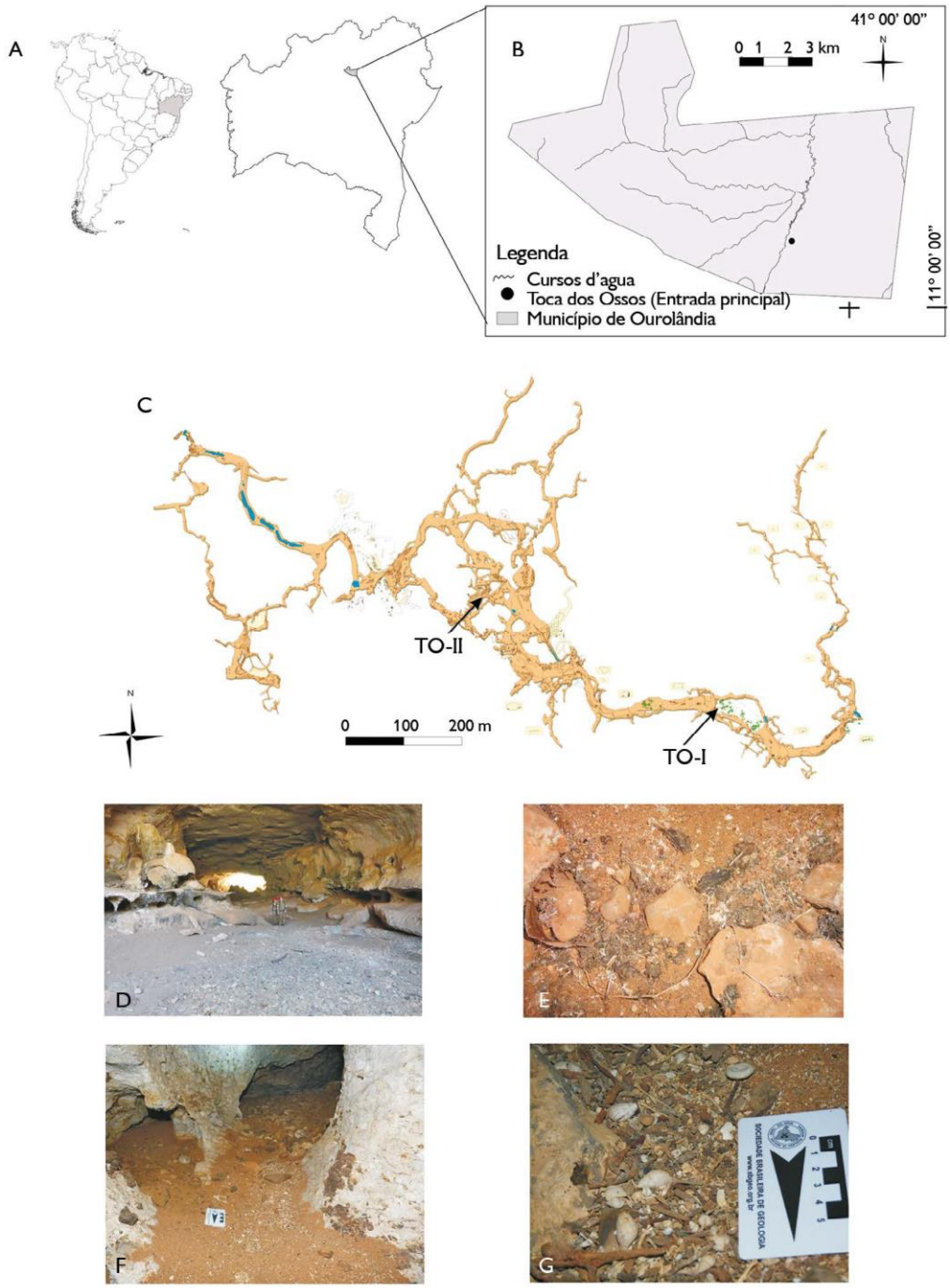


Figura 1. Localização e imagens da Toca dos Ossos: A) mapa da América do Sul, com destaque para o estado da Bahia, no Brasil; B) município de Ourolândia; C) mapa da caverna Toca dos Ossos, indicando os pontos de coleta do material (modificado de Rubbioli *et al*., 2019); D) dolina da Toca dos Ossos-I; E) egagropilos de *Tyto furcata* coletados na Toca dos Ossos-I; F) porção interna da caverna, denominada Toca dos Ossos-II; G) detalhe do material coletado no sedimento de superfície da Toca dos Ossos-II. Mapas: modificados de Rubbioli *et al*. (2019). Fotos: C. S. Scherer (2013).

RESULTADOS

COMPOSIÇÃO DAS AMOSTRAS

A amostra total de roedores muroideos da Toca dos Ossos foi composta por duas famílias e sete espécies, com NMI = 99 (Tabela 1; Apêndice 2). Entre os cricetídeos, foram registrados táxons pertencentes a quatro tribos: Akodontini (33,3% dos indivíduos), que apresentou a maior abundância relativa, e Phyllotini (22,2%), Wiedomyini (21,2%) e Oryzomyini (21,3%), com abundâncias similares. Apesar de menos frequente na amostra, a tribo Oryzomyini apresentou maior riqueza, com três táxons (*Cerradomys* sp., *Holochilus sciureus* Wagner, 1842 e *Oligoryzomys* sp.). *Rattus rattus* (2%) foi o único representante da família Muridae identificado na área de estudo. A amostra TO-I apresentou NMI = 39 e foi representada por seis espécies de Cricetidae e uma de Muridae. A amostra TO-II, com NMI = 60, incluiu as mesmas seis espécies de Cricetidae. Apesar da composição taxonômica semelhante, as duas amostras apresentaram diferenças nas frequências dos táxons. *Necromys lasiurus* (Lund, 1840) foi o táxon dominante (56,4%) em TO-I, seguido por *Wiedomys pyrrhorhinos* (Wied-Neuwied, 1821) (18%) e *Calomys* sp. (10,4%). Por outro lado, *Calomys* sp. predominou na TO-II, com 30%, seguido por *W. pyrrhorhinos*, com 23,3%, *N. lasiurus* e *H. sciureus*, ambos com 18,3% (Tabela 1).

IDENTIFICAÇÃO DOS TÁXONS

Família Cricetidae Fischer, 1817

Subfamília Sigmodontinae Wagner, 1843

Tribo Akodontini Vorontsov, 1959

Necromys lasiurus (Lund, 1840)

Figuras 2A, 2B, 3A, 4A e 5ª

Material: 18 crânios, 21 maxilares e 39 dentários (Apêndice 2).

Descrição: material de médio porte. Crânio alto com rostro curto e forâmen incisivo longo, estendendo-se posteriormente até o nível do protocone do M1; crista supraorbital presente, mas pouco marcada. Dentário baixo e robusto, com projeção capsular desenvolvida.

Tabela 1. Número mínimo de indivíduos (NMI) e percentual de indivíduos por táxon registrado nas duas áreas de amostragem (TO-I e TO-II) na Toca dos Ossos, Ourolândia, estado da Bahia, Brasil.

Táxon	TO-I		TO-II		Total	
	NMI	%	NMI	%	NMI	%
Família Cricetidae						
Tribo Akodontini						
Necromys lasiurus (Lund, 1840)	22	56,4	11	18,3	33	33,3
Tribo Oryzomyini						
Cerradomys sp.	1	2,5	5	8,4	6	6,1
Holochilus sciureus Wagner, 1842	2	5,1	11	18,3	13	13,2
Oligoryzomys sp.	1	2,5	1	1,7	2	2,0
Tribo Phyllotini						
Calomys sp.	4	10,4	18	30	22	22,2
Tribo Wiedomyini						
Wiedomys pyrrhorhinos (Wied-Neuwied, 1821)	7	18	14	23,3	21	21,2
Família Muridae						
Rattus rattus (Linnaeus, 1758)	2	5,1	0	0	2	2,0
Total	39	100	60	100	99	100

Molares com cúspides alternadas; flexo anteromediano ausente; mesolofo ausente, exceto em UFRB-PV 2857, 2975 e MZFS-DM 0820, 0864; flexídeo anteromediano presente apenas em espécimes jovens (UFRB-PV 2998, 3002, 3031, 3119; MZFS-DM 0841, 0843, 0847, 0848, 0855, 0861, 0862, 0863, 0874 e 0875); mesolofídeo ausente.

Comentários: as características apresentadas, em particular sobre seu porte, desenvolvimento do rostro, extensão do forâmen incisivo, presença de crista supraorbital e morfologia dos molares, permitiram atribuir esses espécimes a *N. lasiurus*, de acordo com Anderson & Olds (1989), Pardiñas *et al*. (2015b) e Stutz *et al*. (2018). *Necromys lasiurus* foi o roedor mais frequente na Toca dos Ossos e único representante da tribo Akodontini registrado nas amostras. Carmignotto & Astúa (2017) relacionaram uma segunda espécie da tribo para a Caatinga, *Akodon cursor* (Winge, 1887), que se diferencia de *N. lasiurus* principalmente por seu crânio mais baixo e crista supraorbital ausente (Geise, 2012). Além disso, *Akodon* Meyen, 1833 apresenta flexo/ídeo anteromediano e mesolofo/ídeo (exceto em espécimes mais velhos, com molares muito gastos) (Stutz *et al*., 2018).

Tribo Oryzomyini Vorontsov, 1959

Cerradomys sp.

Figuras 3B, 4B e 5B

Material: um crânio fragmentado, seis maxilares e seis dentários (Apêndice 2).

Descrição: material de médio porte. Forâmen incisivo, geralmente se estende posteriormente até a margem anterior do M1; palato longo, estendendo-se posteriormente à margem posterior do M3, exceto em espécimes jovens (UFRB-PV 959, 2820 e 2990). Dentário alto e robusto, com projeção capsular bem desenvolvida; processo coronoide pequeno; crista massetérica inferior pouco marcada. Molares pentalofodontes; M2 com paracone e protocone opostos; flexo/ídeo anteromediano ausente; cíngulo anterolabial presente nos molares inferiores; procíngulo no m1 curto; mesolofídeo bem desenvolvido.

Comentários: o tamanho e a morfologia dos molares, conforme descrito, são caracteres diagnósticos do gênero *Cerradomys* Weksler, Percequillo & Voss, 2006, de acordo com Weksler *et al*. (2006) e Percequillo *et al*. (2008). Em relação ao material utilizado para comparação (Apêndice 1), *Cerradomys* apresenta forâmen incisivo mais longo, projeção capsular mais desenvolvida e hipoflexídeo menos profundo do que *Hylaeamys* Weksler, Percequillo & Voss, 2006; palato mais longo do que *Rhipidomys* Coues, 1884, o qual apresenta flexo/ídeo anteromediano; crista massetérica inferior menos marcada e molares pouco maiores do que em *Euryoryzomys* Weksler, Percequillo & Voss, 2006; forâmen incisivo mais longo, dentário mais alto e diastema mais longo do que em *Oecomys* Thomas, 1906. O dentário mais robusto, mas com processo coronoide mais baixo, a posição relativa do protocone e paracone no M2 e a presença de mesolofídeo nos molares inferiores permitem diferenciar *Cerradomys* de *Wiedomys* Hershkovitz, 1959.

Cerradomys inclui oito espécies, duas das quais estão presentes atualmente na Caatinga, *Cerradomys langguthi* Percequillo, Hingst-Zaher & Bonvicino, 2008 e *Cerradomys vivoi* Percequillo, Hingst-Zaher & Bonvicino, 2008 (Bonvicino *et al*., 2014; Carmignotto & Astúa, 2017). Dentre essas duas, apenas *C. vivoi* possui registro recente para o estado da Bahia (Percequillo *et al*., 2008). Os espécimes registrados na Toca dos Ossos foram referidos como *Cerradomys* sp. Por não haver caracteres morfológicos que permitam distinguir confiavelmente essas duas espécies (Percequillo *et al*., 2008; Caccavo & Oliveira, 2016).

Holochilus sciureus Wagner, 1842

Figuras 2C, 2D, 3C, 4C e 5C

Material: quatro crânios, 11 maxilares e nove dentários (Apêndice 2).

Descrição: material de grande porte, o maior entre os cricetídeos nas amostras da Toca dos Ossos. Palato longo, estendendo-se além da margem posterior do M3; forâmen incisivo muito curto, não alcançando a margem anterior do M1. Dentário robusto e crista massetérica inferior bem marcada. Molares com cúspides alternadas e lofídeos com margem prismática; fossetídeo anteromediano pequeno; borda posterior do proto e hipoconídeo orientado transversalmente.

Comentários: as características listadas e a ausência de mesolofídeo permitiram identificar o material como *H. sciureus*, conforme Pardiñas & Teta (2011) e Brandão & Nascimento (2015). Esta é a única espécie do gênero com ocorrência atual na Caatinga (Carmignotto & Astúa, 2017).

Oligoryzomys sp.

Figuras 2E, 2F, 3D, 4D e 5D

Material: um crânio, um maxilar e dois dentários (Apêndice 2).

Descrição: material de tamanho diminuto. Forâmen incisivo estendendo-se posteriormente até o nível da borda anterior do M1. Dentário alto, com dois alvéolos para as raízes do m2 e m3. Molares baquiodontes; mesolofo presente no M1 e M2; flexo/ídeo anteromediano presente, mas pouco marcado (MZFS-DM 0825) ou perdido pelo desgaste (UFRB-PV 2735, MZFS-DM 0856); mesoestilídeo presente no m2, mas mesolofídeo ausente.

Comentários: entre os espécimes da Toca dos Ossos, *Oligoryzomys* sp. Bangs, 1900 apresenta porte similar a *Calomys* sp., diferenciando-se pela menor extensão posterior do forâmen incisivo, menor número de alvéolos no M2/m2 e M3/m3 (três nesses molares de *Calomys*), e presença de mesolofo.

Quatro espécies de *Oligoryzomys* Bangs, 1900 ocorrem atualmente na Caatinga (Carmignotto & Astúa, 2017). Entre elas, *O. rupestris* Weksler & Bonvicino, 2005 apresenta o anterocone não dividido por um flexo anteromediano (Weksler & Bonvicino, 2015), diferindo do material da Toca dos Ossos. *Oligoryzomys nigripes* (Olfers, 1818) e *O. stramineus* Bonvicino & Weksler, 1998 apresentam porte relativamente grande para o gênero, enquanto *O. mattogrossae* (Allen, 1916) é comparativamente menor (Weksler *et al*., 2017), mas há sobreposição nas medidas dentárias entre essas espécies (Tabela 2). Desta forma, considerando o pequeno tamanho da amostra da Toca dos Ossos, sua natureza fragmentária e a ausência de

caracteres claramente diagnósticos, esses espécimes foram identificados apenas em nível de gênero.

Tribo Phyllotini Vorontsov, 1959

Calomys sp.

Figuras 2G, 2H, 3E, 4E e 5E

Material: seis crânios, nove maxilares e 36 dentários (Apêndice 2).

Descrição: espécimes de tamanho diminuto. Crânio com crista supraorbital desenvolvida e forâmen incisivo longo, alcançando o protocone do M1. Dentário delicado, mas alto; projeção capsular medianamente desenvolvida; três alvéolos para as raízes do M2/m2 e M3/m3. Molares tetralofodontes e braquiodontes; M1 com flexo anteromediano muito profundo, dividindo o anterocone em dois cônulos, sendo um menor, anterolingual, e outro maior, anterolabial. No espécime UFRB-PV 2991, o flexo anteromediano não está visível, em razão do desgaste.

Comentários: o material foi atribuído ao gênero *Calomys* pelo conjunto de características descritas, conforme Salazar-Bravo (2015). *Calomys* foi o único representante da tribo Phyllotini registrado nas amostras. Revisões recentes têm apontado *C. expulsus* (Lund, 1840) como a única espécie do gênero presente na Caatinga (Salazar-Bravo, 2015; Carmignotto & Astúa, 2017). No entanto, considerando a natureza fragmentária dos espécimes da Toca dos Ossos e a ausência de caracteres diagnósticos que permitam a identificação da espécie, optou-se por tratar o material como *Calomys* sp.

Tabela 2. Comparação entre as medidas dentárias (em milímetros) dos espécimes de *Oligoryzomys* sp. registrados na Toca dos Ossos (MZFS-DM 0825 e UFRB-PV 2735) e das espécies do gênero presentes na Caatinga: 1 = espécimes de *O. mattogrossae* do Nordeste do Brasil (Weksler *et al*., 2017); 2 = espécimes de *O. mattogrossae* ao longo de toda a distribuição (Weksler *et al*., 2017); 3 = espécimes de *O. rupestris*, *O. stramineus* e *O. nigripes* ao longo de suas distribuições (Weksler & Bonvicino, 2005); 4 = espécimes de *O. nigripes* do estado do Espírito Santo ao estado do Rio Grande do Sul (Machado *et al*., 2011); n = número de espécimes.

Espécimes/Espécies	Comprimento M1-M3	Largura M1
MZFS-DM 0825	3,37	1,05
UFRB-PV 2735	-	1,00
O. mattogrossae[1]	2,94-3,15 (n = 4)	0,86-0,96 (n = 4)
O. mattogrossae[2]	2,84-3,64 (n = 39)	0,81-1,20 (n = 39)
O. rupestris[3]	3,2-3,5 (n = 8)	1,0-1,1 (n = 8)
O. stramineus[3]	3,3-4,2 (n = 36)	1,0-1,3 (n = 36)
O. nigripes[3]	3,5-4,0 (n = 35)	1,0-1,2 (n = 35)
O. nigripes[4]	3,06-4,28 (n = 153)	0,84-1,12 (n = 155)

Tribo Wiedomyini Reig, 1980

Wiedomys pyrrhorhinos (Wied-Neuwied, 1821)

Figuras 2I, 2J, 3F, 4F e 5F

Material: 14 crânios, 12 maxilares e 12 dentários (Apêndice 2).

Descrição: material de tamanho mediano nas amostras da Toca dos Ossos. Palato curto, não se estendendo além da margem posterior do M3, exceto em três espécimes (MZFS-DM 0956, 0965 e 2907), nos quais o palato é longo; forâmen incisivo longo, com sua borda posterior ultrapassando a margem anterior do M1. Dentário comparativamente delicado e processo coronoide baixo. M2 com paracone e protocone alternados; flexo/ídeo anteromediano conspícuo, exceto em indivíduos com maior desgaste (MZFS-DM 0905, 0955, 0956, 0965; UFRB-PV 906, 2819, 2897, 2956, 2957, 2983, 3121 e 3176); mesolofo presente; mesolofídeo ausente; m1 com procíngulo longo.

Comentários: o comprimento do forâmen incisivo, a alternância das cúspides, a presença de mesolofo e a ausência de mesolofídeo estão entre os caracteres diagnósticos de *Wiedomys*, assim como o palato curto (Bonvicino, 2015). No entanto, alguns espécimes podem apresentar palato longo, como observado em três casos da Toca dos Ossos e no espécime ilustrado por Bezerra *et al*. (2013, fig. 2). *Wiedomys* foi o único representante da tribo Wiedomyini registrado para a Toca dos Ossos. O gênero inclui duas espécies, *W. pyrrhorhinos* e *W. cerradensis* Gonçalves, Almeida & Bonvicino, 2005, ambas com ocorrência atual na Caatinga (Carmignotto & Astúa, 2017). De acordo com Bonvicino (2015), *W. pyrrhorhinos* apresenta forâmen incisivo mais largo (> 2,22 mm) e série molar superior mais longa (> 4,6 mm) do que *W. cerradensis*. Desta maneira, as medidas do material da Toca dos Ossos – LFI = 2,30-2,57 mm (n = 12); CM1-M3 = 4,56-4,81 mm (n = 17) – indicam se tratar de *W. pyrrhorhinos*.

Família Muridae Illiger, 1811

Rattus rattus (Linnaeus, 1758)

Figura 3G

Material: dois dentários (Apêndice 2).

Descrição: espécimes de grande porte. Dentários grandes e robustos, com projeção capsular pouco marcada e processo coronoide desenvolvido.

Comentários: a família Muridae está representada no continente americano por dois gêneros: *Mus* inclui apenas uma espécie, *M. musculus* (Linnaeus, 1758), de pequeno porte, enquanto *Rattus* Fischer de Waldheim, 1830 inclui duas espécies de maior tamanho (Catzeflis, 2018). Dentre eles, *Rattus* foi o único gênero registrado na Toca dos Ossos. O material inclui os dois maiores dentários presentes nas amostras. O comprimento da série molar inferior (Cm1-m3 = 5,94 mm, MZFS-DM 0924) e o comprimento do m1 (Cm1 = 2,43 mm, MZFS-DM 0839; Cm1 = 2,63 mm, MZFS-DM 0924) desses espécimes estão dentro da variação registrada para *R. rattus* (Cm1-m3 = 5,8-6,7 mm; Cm1 = 2,5-2,9 mm) e abaixo dos valores para *R. norvegicus* (Berkenhout, 1769) (Cm1-m3 = 6,7-7,5 mm; Cm1 = 3,0-3,2 mm) (Catzeflis, 2018).

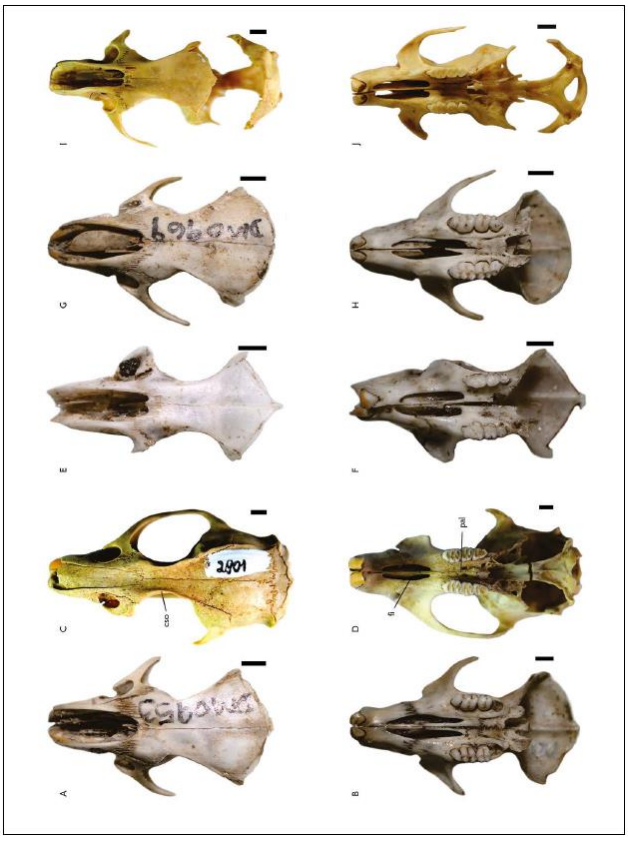


Figura 2. Vista dorsal e ventral dos crânios de: A, B) *Necromys lasiurus*, MZFS-DM 0953; C, D) *Holochilus sciureus*, UFRB-PV 2901; E, F) *Oligoryzomys* sp., MZFS-DM

0825; G, H) *Calomys* sp., MZFS-DM 0969; I, J) *Wiedomys pyrrhorhinos*, UFRB-PV 2898. Escala = 2 mm. Abreviaturas: cso = crista supraorbital; fi = forâmen incisivo; pal = palato.

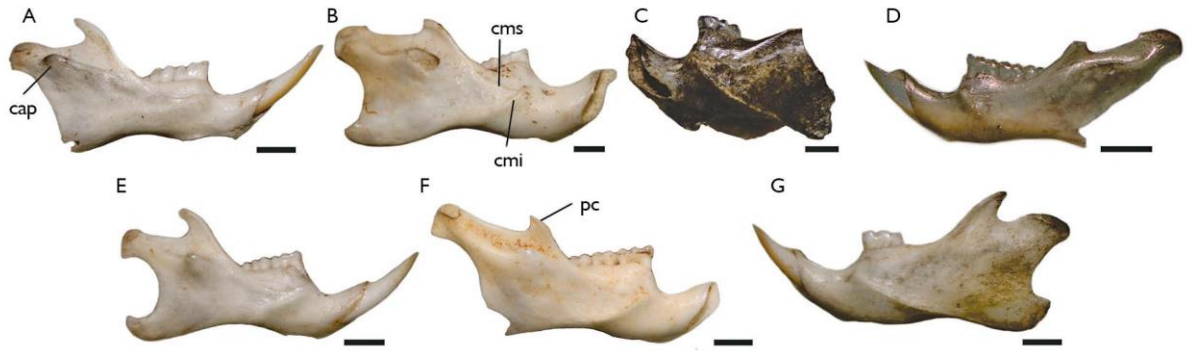


Figura 3. Vista lateral do dentário de: A) *Necromys lasiurus*, MZFS-DM 0831, direito; B) *Cerradomys* sp., MZFS-DM 0826, direito; C) *Holochilus sciureus*, UFRB-PV 908, esquerdo; D) *Oligoryzomys* sp., MZFS-DM 0867, esquerdo; E) *Calomys* sp., MZFS-DM 0835, direito; F) *Wiedomys pyrrhorhinos*, MZFS-DM 0838, direito; G) *Rattus rattus*, MZFS-DM 0839, esquerdo. Escala = 2 mm. Abreviaturas: cap = projeção capsular; cmi = crista massetérica inferior; cms = crista massetérica superior; pc = processo coronoide.



Figura 4. Vista oclusal dos molares superiores de: A) *Necromys lasiurus*, UFRB-PV 2748, M1-M3 esquerdos; B) *Cerradomys* sp., UFRB-PV 2861, M1-M3 esquerdos; C) *Holochilus sciureus*, UFRB-PV 2992, M1-M3 direitos; D) *Oligoryzomys* sp., UFRB-PV 2735, M1-M2 esquerdos; E) *Calomys* sp., UFRB-PV 2745, M1-M3 esquerdos; F)

Wiedomys pyrrhorhinos, UFRB-PV 2823, M1-M3 esquerdos. Escala = 1 mm. Notar que o flexo anteromediano é indistinto devido ao desgaste dos molares em *Oligoryzomys* sp. e *Calomys* sp. Escala A, B, C, E, F = 1 mm; D = 0,5 mm. Abreviaturas: fam = flexo anteromediano; la = cônulo anterolabial; li = cônulo anterolingual; mes = mesolofo; Pa = paracone; Pr = protocone.

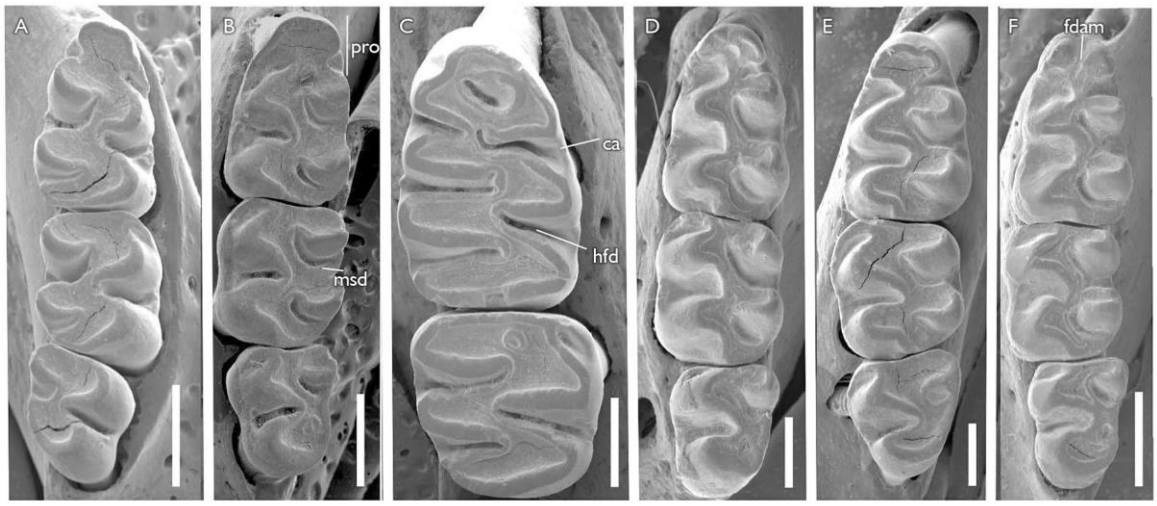


Figura 5. Vista oclusal dos molares inferiores de: A) *Necromys lasiurus*, MZFS-DM 0840, m1-m3 direitos; B) *Cerradomys* sp., MZFS-DM 0828, m1-m3 esquerdos; C) *Holochilus sciureus*, UFRB-PV 907, m1-m2 direitos; D) *Oligoryzomys* sp., MZFS-DM 0867, m1-m3 esquerdos; E) *Calomys* sp., MZFS-DM 0833, m1-m3 esquerdos; F) *Wiedomys pyrrhorhinos*, MZFS-DM 0836, m1-m3 esquerdos. Escala = 1 mm. Notar que o flexídeo anteromediano está pouco marcado devido ao desgaste dos molares em *Oligoryzomys* sp. e *Calomys* sp. Escala A, B, C, F = 1 mm; D, E = 0,5 mm. Abreviaturas: ca = cíngulo anterolabial; fdam = flexídeo anteromediano; hfd = hipoflexídeo; msd = mesolofídeo; pro = procíngulo.

DISCUSSÃO

Todos os táxons registrados neste trabalho possuem ocorrência atual na Caatinga e nas florestas estacionais associadas a este bioma, sendo *Wiedomys pyrrhorhinos* o único endêmico da Caatinga (Carmignotto & Astúa, 2017). A riqueza registrada na Toca dos Ossos (sete espécies) representou 26,9% dos roedores muroideos conhecidos para a Caatinga, que abriga 23 espécies de cricetídeos e três espécies de murídeos (Moojen, 1952; Carmignotto & Astúa, 2017). Em comparação com outros levantamentos conduzidos nesse bioma, a maior parte dos estudos cuja amostragem se baseou na captura com armadilhas registrou riquezas menores, como

no Parque Nacional de Ubajara, no Ceará (Guedes *et al*., 2000; três espécies); no Morro do Chapéu, Chapada Diamantina (Oliveira & Pessôa, 2005; quatro espécies); em cinco localidades dos estados da Bahia e de Sergipe (Bezerra *et al*., 2014; quatro espécies); em Ouricuri, Pernambuco (Delciellos, 2016; quatro espécies); e no Parque Nacional do Catimbau, município de Buíque, Pernambuco (Geise *et al*., 2010; cinco espécies). Por outro lado, Souza, M. *et al*. (2004) registraram 12 espécies de muroideos nos brejos de altitude nos estados da Paraíba e de Pernambuco. Assim, a análise dos egagropilos de corujas, dos quais provêm pelo menos parte do material da Toca dos Ossos (TO-I), demonstra ser uma importante ferramenta de amostragem de pequenos mamíferos, como já apontado em estudos prévios (*e.g*., Massoia, 1984; Bonvicino & Bezerra, 2003; Formoso *et al*., 2016; Heisler *et al*., 2016).

A riqueza de roedores muroideos na Toca dos Ossos (sete espécies) foi intermediária àquelas obtidas em estudos com pelotas de *Tyto furcata* conduzidos em outros biomas. Por exemplo, três espécies foram registradas em uma área urbana e quatro em uma área rural na Mata Atlântica do estado de Pernambuco (Souza, D. *et al*., 2010); sete espécies em duas localidades no ecótono entre Amazônia e Cerrado do médio Araguaia (Rocha *et al*., 2011); oito espécies em uma restinga do estado do Rio de Janeiro (Lemos *et al*., 2015); dez espécies no Cerrado do estado da Bahia (Bonvicino & Bezerra, 2003); e 13 espécies em duas localidades em Floresta Ombrófila Mista na Mata Atlântica do estado de Santa Catarina (Cherem *et al*., 2018).

A diversidade encontrada nos egagropilos de coruja da TO-I foi semelhante à de outras cavernas estudadas na região Nordeste. Mancini *et al*. (2018) conduziram um levantamento de mamíferos recentes de pequeno porte através da análise de egagropilos de corujas em sete cavernas nos estados da Bahia e Sergipe. Esses autores obtiveram sete espécies de cricetídeos e duas de murídeos, e uma riqueza total variando de duas a nove espécies entre as cavernas, o que corresponde a uma espécie a mais para cada família, em comparação com os dados obtidos na Toca dos Ossos. Além disso, Mancini *et al*. (2018) registraram *Calomys* cf. *expulsus* como o táxon mais frequente entre os roedores muroideos, seguido por *Necromys lasiurus*, enquanto, na Toca dos Ossos, *N. lasiurus* foi a espécie mais abundante na TO-I e *Calomys* sp., a mais abundante na TO-II. *Holochilus sciureus* foi o único táxon aqui registrado que não foi encontrado na amostra analisada por Mancini *et al*. (2018).

Dados sobre roedores muroideos do Quaternário do Nordeste do Brasil são muito escassos. Castro *et al*. (2014) estudaram a assembleia de vertebrados da Gruta do Ioiô, no município de Palmeiras, Bahia, e reportaram apenas uma espécie de

Sigmodontinae, *Holochilus sciureus*. Neves *et al*. (2017) analisaram a assembleia de sigmodontíneos da Serra da Capivara, estado do Piauí, e registraram sete táxons. Entre estes, *Pseudoryzomys simplex* (Winge, 1887) e *Bibimys* sp., gênero atualmente ausente na região Nordeste (Pardiñas *et al*., 2015a), não estiveram presentes na TO-II. O único táxon registrado em TO-II e que não estava entre os espécimes analisados por Neves *et al*. (2017) foi *Oligoryzomys* sp. Na amostra da Serra da Capivara, *Calomys* sp. foi o táxon mais frequente.

A amostra de TO-I representa material recente, visto que a espécie exótica *Rattus rattus* foi encontrada nos egagropilos de *Tyto furcata*. Por outro lado, o material proveniente da TO-II foi encontrado no sedimento de superfície da caverna e pode representar um intervalo de tempo maior. Auler *et al*. (2003) demonstraram que há considerável variação no tipo e na intensidade dos processos de acúmulo de material nas cavernas brasileiras, tanto na escala de regiões cársticas quanto de condutos dentro de uma mesma caverna, resultando em sítios fossilíferos complexos. Auler *et al*. (2006) analisaram a tafonomia relacionada a 19 espécies de megafauna da Toca dos Ossos e concluíram que esses fósseis foram transportados para o interior da caverna pelo escoamento de corpos d'água durante um ou vários momentos de maior precipitação. Os autores também demonstraram, através de datação de espeleotemas, que o período de deposição de fósseis nas cavernas brasileiras é bastante amplo, variando do Pleistoceno Médio ao Holoceno. Entretanto, não foi possível obter datas para a Toca dos Ossos no referido trabalho. Considerando a ausência de datações e de análise tafonômica detalhada do material de pequeno porte, não é possível indicar a idade do material da TO-II. No entanto, a ocorrência dos mesmos táxons na TO-I e na TO-II e sua similaridade com o registro atual na Caatinga (Carmignotto & Astúa, 2017) podem sugerir que o material analisado proveniente da TO-II seja recente, tendo sido depositado após o estabelecimento local da Caatinga.

Os dados paleopalinológicos para a região noroeste da Bahia, onde se insere a Toca dos Ossos, indicam clima mais frio e úmido no início do Holoceno e a ocorrência de florestas úmidas de galeria, sendo que o estabelecimento das condições áridas teria ocorrido nos últimos 4.000 anos, levando a uma expansão da Caatinga (De Oliveira *et al*., 1997). A partir do registro de *Myocastor coypus* (Molina, 1782), Cartelle & Lessa (1989) sugeriram clima mais úmido e frio durante o fim do Pleistoceno e início do Holoceno, com vegetação provavelmente composta por matas ciliares e cerrado. Lessa *et al*. (1998) também registraram espécies de hábitos florestais – *e.g*., *Eira*

barbara (Linnaeus, 1758) – e semiaquáticos – *e.g*., *Lontra longicaudis* (Olfers, 1818) – entre os carnívoros fósseis coletados na Toca dos Ossos.

A análise e a identificação de fragmentos pertencentes a outros grupos de pequenos mamíferos coletados na Toca dos Ossos, como marsupiais e roedores caviomorfos, constituem importante etapa subsequente do estudo dessa caverna do Nordeste brasileiro. Além disso, a análise tafonômica do material de pequenos mamíferos da Toca dos Ossos também deverá ser objeto dos próximos estudos e poderá auxiliar no entendimento da assembleia dessa caverna. Esses dados serão importantes para a compreensão dos pequenos mamíferos em uma região ainda pouco amostrada, como a Caatinga.

CONCLUSÃO

A análise de 210 fragmentos cranianos e mandibulares de roedores muroideos provenientes da Toca dos Ossos, no bioma Caatinga, resultou no registro de 99 indivíduos, pertencentes a duas famílias, Cricetidae e Muridae, e sete espécies (*Necromys lasiurus*, *Cerradomys* sp., *Holochilus sciureus*, *Oligoryzomys* sp., *Calomys* sp., *Wiedomys pyrrhorhinos* e *Rattus rattus*). Essa riqueza é considerável e relevante, comparada a outros trabalhos sobre a mastofauna deste bioma. Apesar de muito semelhantes taxonomicamente, as amostras dos dois pontos de coleta (TO-I e TO-II) apresentaram diferenças nas frequências dos táxons. No entanto, ambas as áreas da Toca dos Ossos incluíram somente táxons de ocorrência atual na Caatinga, o que sugere que o material de TO-II também é bastante recente, tendo sido depositado após o estabelecimento deste bioma na região, o qual ocorreu há cerca de 4.000 anos.

AGRADECIMENTOS

Agradecemos à Universidade Federal do Recôncavo da Bahia (UFRB), pela infraestrutura concedida; ao Laboratório Central de Microscopia Eletrônica da UFSC, pelas fotografias em MEV. Ao Sr. Admir Brunelli, pelo apoio aos trabalhos de campo. À editora Alexandra Bezerra e a três revisores anônimos, por suas correções e sugestões nas versões preliminares do texto. Ao Conselho Nacional de Desenvolvimento Científico e Tecnológico (CNPq), através dos editais MCT/CNPq 14/2010 - Universal (475291/2010-7) e MCT/CNPq 14/2011 - Universal (475287/2011-8).

REFERÊNCIAS

ALVARES, C. A., J. L. STAPE, P. C. SENTELHAS, G. MORAES, J. LEONARDO & G. SPAROVEK, 2013. Köppen's climate classification map for Brazil. **Meteorologische Zeitschrift** 22(6): 711-728. DOI: https://doi.org/10.1127/0941-2948/2013/0507

ANDERSON, S. & N. OLDS, 1989. Notes on Bolivian mammals. 5. Taxonomy and distribution of *Bolomys* (Muridae, Rodentia). **American Museum Novitates** (2935): 1-22.

AULER, A. S., L. B. PILÓ, P. L. SMART, X. WANG, W. A. NEVES & R. L. EDWARDS, 2003. Cronologia e processos de deposição da megafauna quaternária em cavernas brasileiras. **Anais do Congresso sobre Planejamento e Gestão das Zonas Costeiras dos Países de Expressão Portuguesa/Congresso da Associação Brasileira de Estudos do Quaternário/Congresso do Quaternário dos Países de Língua Ibérica** 2/9/2: 1 CD-ROM.

AULER, A. S., L. B. PILÓ, P. L. SMART, X. WANG, D. HOFFMANN, D. A. RICHARDS, R. L. EDWARDS, W. A. NEVES & H. CHENG, 2006. U-series dating and taphonomy of Quaternary vertebrates from Brazilian caves. **Palaeogeography, Palaeoclimatology, Palaeoecology** 240: 508-522.

BARBIÈRE, F., P. E. ORTIZ & U. F. J. PARDIÑAS, 2019. The oldest sigmodontine rodent revisited and the age of the first South American cricetids. **Journal of Paleontology** 93(2): 368-384. DOI: https://doi.org/10.1017/jpa.2018.74

BEISAW, A. M., 2013. **Identifying and interpreting animal bones**: a manual: 1-214. Texas A & M University Press, College Station.

BEZERRA, A. M. R., A. LAZAR, C. R. BONVICINO & J. MARINHO FILHO, 2013. *Wiedomys cerradensis* Gonçalves, Almeida and Bonvicino, 2005 (Mammalia: Rodentia: Cricetidae) in Tocantins and Goiás states, central- northern Brazil. **Check List** 9(3): 680-83. DOI:https://doi.org/10.15560/9.3.680

BEZERRA, A M. R., A. LAZAR, C. R. BONVICINO & A. S. CUNHA, 2014. Subsidies for a poorly known endemic semiarid biome of Brazil: non-volant mammals of an eastern region of Caatinga. **Zoological Studies** 53: 16. DOI: https://doi.org/10.1186/1810-522X-53-16

BONVICINO, C. R., 2015. Tribe Wiedomyini Reig, 1980. In: J. L. PATTON, U. F. J. PARDIÑAS & G. D'ELÍA (Ed.): **Mammals of South America**: vol. 2: Rodents: 682-685. University of Chicago Press, Chicago.

BONVICINO, C. R. & A. M. R. BEZERRA, 2003. Use of regurgitated pellets of Barn Owl (*Tyto alba*) for inventorying small mammals in the cerrado of Central Brazil. **Studies**

on Neotropical Fauna and Environment 38(1): 1-5. DOI: http://doi.org/10.1076/snfe.38.1.1.14030

BONVICINO, C. R., F. CASADO & M. WEKSLER, 2014. A new species of *Cerradomys* (Mammalia: Rodentia: Cricetidae) from Central Brazil, with remarks on the taxonomy of the genus. **Zoologia** 31(6): 525-540. DOI: http://dx.doi.org/10.1590/S1984-46702014000600002

BRANDÃO, M. V. & F. O. NASCIMENTO, 2015. On the occurrence of *Holochilus chacarius* (Cricetidae: Sigmodontinae) in Brazil, with taxonomic notes on *Holochilus* species. **Papéis Avulsos de Zoologia** 55(3): 47-67. DOI: http://dx.doi.org/10.1590/0031-1049.2015.55.03

BURGIN, C. J., J. P. COLELLA, P. L. KAHN & N. S. UPHAM, 2018. How many species of mammals are there? **Journal of Mammalogy** 99(1): 1-14. DOI: https://10.1093/jmammal/gyx147

CACCAVO, A. & J. A. OLIVEIRA, 2016. Detecting morphological limits between parapatric species: cranial variation in *Cerradomys* (Cricetidae: Sigmodontinae) from northeastern Brazil. **Journal of Mammalogy** 97(6): 1602-1616. DOI: https://doi.org/10.1093/jmammal/gyw124

CARMIGNOTTO, A. P. & D. ASTÚA, 2017. Mammals of the Caatinga: diversity, ecology, biogeography, and conservation. In: J. M. C. SILVA, I. R. LEAL & M. TABARELLI (Ed.): **Caatinga**: 211-254. Springer, Cham.

CARTELLE, C. & G. LESSA, 1988. Descrição de um novo gênero e espécie de Macraucheniidae (Mammalia, Litopterna) do Pleistoceno do Brasil. **Paulacoutiana** 3: 3-26.

CARTELLE, C. & G. LESSA, 1989. Presença de *Myocastor coypus* (Molina, 1782), Rodentia, Myocastoridae, do Pleistoceno Final e Holoceno, no centro-oeste da Bahia. **Anais do Congresso Brasileiro de Paleontologia** 11: 583-591.

CARTELLE, C. & V. S. ABUHID, 1994. Chiroptera do Pleistoceno final-Holoceno da Bahia. **Acta Geológica Leopoldensia** 39: 429-440.

CARVALHO, M. S. & T. V. OLIVEIRA, 2015. Small non-volant mammals (Didelphimorphia and Rodentia) from the RPPN Guarirú, an Atlantic Forest fragment in northeastern Brazil. **Check List** 11(6): 1-9. DOI: http://dx.doi.org/10.15560/11.6.1782

CASTRO, M. C., F. C. MONTEFELTRO & M. C. LANGER, 2014. The Quaternary vertebrate fauna of the limestone cave Gruta do Ioiô, northeastern Brazil. **Quaternary International** 352: 164-175. DOI: http://dx.doi.org/10.1016/j.quaint.2014.06.038

CATZEFLIS, F., 2018. Invasive rodents in French Guiana: an overview for *Mus musculus, Rattus norvegicus,* and *R. rattus* (Murinae: Muridae). **Boletim da Sociedade Brasileira de Mastozoologia** 81: 1-9.

CHEREM, J. J., P. HADLER, N. S. STUTZ & U. F. J. PARDIÑAS, 2018. Pequenos mamíferos (Didelphimorphia, Chiroptera e Rodentia) em egagropilos de *Tyto furcata* (coruja-das-igrejas) (Aves, Tytonidae) do sul do Brasil. **Biotemas** 31(3): 43-58. DOI: http://dx.doi.org/10.5007/2175-7925.2018v31n3p43

COMITÊ DA BACIA HIDROGRÁFICA DO RIO SALITRE (CBHS), 2017. **Plano de recursos hídricos e proposta de enquadramento dos corpos de água da Bacia Hidrográfica do Rio Salitre**: síntese executiva: 1-242. Instituto do Meio Ambiente e Recursos Hídricos, Salvador.

CZAPLEWSKI, N. J. & C. CARTELLE, 1998. Pleistocene bats from cave deposits in Bahia, Brazil. **Journal of Mammalogy** 79(3): 784-803.

DELCIELLOS, A. C., 2016. Mammals of four Caatinga areas in northeastern Brazil: inventory, species biology, and community structure. **Check List** 12(3): 1-15. DOI: http://dx.doi.org/10.15560/12.3.1916

DE OLIVEIRA, P. E., A. M. F. BARRETO & K. SUGUIO, 1997. Paleovegetação e paleoclima do Quaternário tardio da caatinga brasileira: o campo de dunas do médio rio São Francisco, Bahia. **Resumos Expandidos do Congresso da Associação Brasileira de Estudos do Quaternário** 6: 171-175.

FABRE, P. H., L. HAUTIER, D. DIMITROV & E. DOUZERY, 2012. A glimpse on the pattern of rodent diversification: a phylogenetical approach. **BMC Evolutionary Biology** 12: 88. DOI: https://doi.org/10.1186/1471-2148-12-88

FLYNN, L. J., L. L. JACOBS & E. H. LINDSAY, 1985. Problems in muroid phylogeny: relationship to other rodents and origin of major groups. In: W. P. LUCKETT & J. L. HARTENBERGER (Ed.): **Evolutionary relationships among rodents**: 589-616. Springer, Boston. DOI: https://doi.org/10.1007/978-1-4899-0539-0_22

FORMOSO, A. E., P. TETA, A. E. CARBAJO & U. F. J. PARDIÑAS, 2016. Unraveling the patterns of small mammal species richness in the southernmost aridlands of South America. **Journal of Arid Environments** 134: 136-144. DOI: https://doi.org/10.1016/j.jaridenv.2016.07.007

FREITAS, R. R., P. L. B. ROCHA & P. C. SIMÕES-LOPES, 2005. Habitat structure and small mammals abundances in one semiarid landscape in the Brazilian Caatinga. **Revista Brasileira de Zoologia** 22(1): 119-129. DOI: http://dx.doi.org/10.1590/S0101-81752005000100015

GEISE, L., 2012. *Akodon cursor*. **Mammalian Species** 44(893): 33-43.

GEISE, L. & L. G. PEREIRA, 2008. Rodents (Rodentia) and marsupials (Didelphimorphia) in the municipalities of Ilhéus and Pau Brasil, state of Bahia, Brazil. **Check List** 4(2): 174-177. DOI: http://dx.doi.org/10.15560/4.2.174

GEISE, L., R. PARESQUE, H. SEBASTIÃO, L. T. SHIRAI, D. ASTÚA & G. MARROIG, 2010. Non-volant mammals, Parque Nacional do Catimbau, Vale do Catimbau, Buíque, state of Pernambuco, Brazil, with karyologic data. **Check List** 6(1): 180-186. DOI: http://dx.doi.org/10.15560/6.1.180

GOMES, A. C. F., G. LESSA, C. CARTELLE & L. KERBER, 2019. New fossil remains of Quaternary capybaras (Rodentia: Caviomorpha: Caviidae) from the intertropical region of Brazil: morphology and taxonomy. **Journal of South American Earth Sciences** 91: 36-46. DOI: https://doi.org/10.1016/j.jsames.2019.01.006

GUEDES, P. G., S. S. P. SILVA, A. R. CAMARDELLA, M. F. G. ABREU, D. M. BORGES-NOJOSA, J. A. G. SILVA & A. A. SILVA, 2000. Diversidade de mamíferos do Parque Nacional de Ubajara (Ceará, Brasil). **Mastozoología Neotropical** 7(2): 95-100.

HEISLER, L. M., C. M. SOMERS & R. G. POULIN, 2016. Owl pellets: a more effective alternative to conventional trapping for broad-scale studies of small mammal communities. **Methods in Ecology and Evolution** 7(1): 96-103. DOI: https://doi.org/10.1111/2041-210X.12454

HONEYCUTT, R. L., L. J. FRABOTTA & D. L. ROWE, 2007. Rodent evolution, phylogenetics and biogeography. In: J. O. WOLFF & P. W. SHERMAN (Ed.): **Rodent societies**: an ecological & evolutionary perspective: 8-23. The University of Chicago Press, Chicago.

INSTITUTO DO MEIO AMBIENTE E RECURSOS HÍDRICOS (INEMA), 2016. Portaria n° 13.203, de 27 de dezembro de 2016. **Diário Oficial do Estado da Bahia** 22084: 44-45.

JANSA, S. A. & M. WEKSLER, 2004. Phylogeny of muroid rodents: relationships within and among major lineages as determined by IRBP gene sequences. **Molecular Phylogenetics and Evolution** 31(1): 256-276. DOI: https://doi.org/10.1016/j.ympev.2003.07.002

JESUS, D. S. & T. V. OLIVEIRA, 2017. Morcegos (Mamalia, Chiroptera) em egagrópilas da coruja-das-torres (*Tyto furcata*) em uma caverna do Nordeste brasileiro. **Boletim do Museu de Biologia Mello Leitão, Nova Série** 39(1): 69-93.

LEAL, I. R., J. M. C. SILVA, M. TABARELLI & T. E. LACHER, 2005. Mudando o curso da conservação da biodiversidade na Caatinga do Nordeste do Brasil. **Megadiversidade** 1(1): 139-146.

LEMOS, H. M., C. A. O. SILVA, F. M. PATIU & P. R. GONÇALVES, 2015. Barn Owl pellets (Aves: *Tyto furcata*) reveal a higher mammalian richness in the Restinga de Jurubatiba National Park, Southeastern Brazil. **Biota Neotropica** 15(2): e20140121. DOI: http://dx.doi.org/10.1590/1676-06032015012114

LESSA, G., C. CARTELLE, H. D. FARIA & P. R. GONÇALVES, 1998. Novos achados de mamíferos carnívoros do Pleistoceno Final-Holoceno em grutas calcárias do estado da Bahia. **Acta Geologica Leopoldensia** 21(46-47): 157-169.

LESSA, G., P. R. GONÇALVES & L. M. PESSÔA, 2005. Variação geográfica em caracteres cranianos quantitativos de *Kerodon rupestris* (Wied, 1820) (Rodentia, Caviidae). **Arquivos do Museu Nacional** 63(1): 75-88.

LESSA, G. & L. M. PESSÔA, 2005. Variação ontogenética e sexual em caracteres cranianos de *Kerodon rupestris* Wied, 1820, (Rodentia: Caviidae). **Arquivos do Museu Nacional** 63(3): 599-618.

LOBO, L. S., G. LESSA, C. CARTELLE & P. S. R. ROMANO, 2017. Dental eruption sequence and hypsodonty index of a Pleistocene macraucheniid from the Brazilian Intertropical Region. **Journal of Paleontology** 91(5): 1083-1090. DOI: https://doi.org/10.1017/jpa.2017.54

MACHADO, L. F., R. PARESQUE & A. U. CHRISTOFF, 2011. Anatomia comparada e morfometria de *Oligoryzomys nigripes* e *O. flavescens* (Rodentia, Sigmodontinae) no Rio Grande do Sul, Brasil. **Papéis Avulsos de Zoologia** 51(3): 29-47. DOI: http:// dx.doi.org/10.1590/S0031-10492011000300001

MANCINI, M. C. S., P. R. O. ROTH, P. G. G. BRENNAND, J. M. R. E. AGUILAR & P. A. ROCHA, 2018. *Tyto furcata* (Tytonidae: Strigiformes) pellets: tools to access the richness of small mammals of a poorly known Caatinga area in northeast Brazil. **Mammalia** 83(4): 390-398. DOI: http://dx.doi.org/10.1515/mammalia-2018-0017

MASSOIA, E., 1984. La importancia de los análisis de regurgitados de aves estrigiformes. **ACINTACNIA, Asociación Cooperadora INTA** 1(11): 38-39.

MOOJEN, J., 1952. **Os roedores do Brasil**: 1-214. Instituto Nacional do Livro, Rio de Janeiro.

NEVES, S. B., E. L. MAYER, P. HADLER & A. M. RIBEIRO, 2017. Sigmodontine rodents (Rodentia, Cricetidae) from Quaternary cave deposits of Serra da Capivara,

northeastern Brazil. **Revista Brasileira de Paleontologia** 20(2): 163-178. DOI: http://dx.doi.org/10.4072/rbp.2017.2.02

OLIVEIRA, J. A., P. R. GONÇALVES & C. R. BONVICINO, 2003. Mamíferos da Caatinga. In: J. A. LEAL, M. TABARELLI & J. M. C. SILVA (Ed.): **Ecologia e conservação da Caatinga**: 275-334. Editora Universitária da UFPE, Recife.

OLIVEIRA, J. A. & L. M. PESSÔA, 2005. Mamíferos. In: F. A. JUNCÁ, L. FUNCH & W. ROCHA (Ed.): **Biodiversidade e conservação da Chapada Diamantina**: 377-405. Ministério do Meio Ambiente, Brasília.

PARDIÑAS, U. F. J. & P. TETA, 2011. Fossil history of the marsh rats of the genus *Holochilus* and *Lundomys* (Cricetidae, Sigmodontinae) in southern South America. **Estudios Geológicos** 67(1): 111-129. DOI: https://doi.org/10.3989/egeol.40347.136

PARDIÑAS, U. F. J., G. D'ELÍA & P. TETA. 2015a. Genus *Bibimys* Massoia, 1979. In: J. L. PATTON, U. F. J. PARDIÑAS & G. D'ELÍA (Ed.): **Mammals of South America**: vol. 2: Rodents: 204-208. University of Chicago Press, Chicago.

PARDIÑAS, U. F. J., P. TETA, P. E. ORTIZ, J. P. JAYAT & J. SALAZARBRAVO, 2015b. Genus *Necromys* Ameghino, 1889. In: J. L. PATTON, U. F. J. PARDIÑAS & G. D'ELÍA (Ed.): **Mammals of South America**: vol. 2: Rodents: 232-247. University of Chicago Press, Chicago.

PARDIÑAS, U. F. J., P. MYERS, L. LEÓN-PANIAGUA, N. O. GARZA, J. COOK, B. KRYŠTUFEK, R. HASLAUER, R. BRADLEY, G. SHENBROT & J. L. PATTON, 2017. Family Cricetidae. In: D. E. WILSON, T. E. LACHER & R. A. MITTERMEIER (Ed.): **Handbook of the mammals of the world**: vol. 7: Rodents II: 204-279. Lynx Ediciones, Barcelona.

PATTON, J., U. F. J. PARDIÑAS & G. D'ELÍA, 2015. **Mammals of South America**: vol. 2: Rodents: 1-1336. The University of Chicago Press, Chicago.

PERCEQUILLO, A. R., 2006. Guia para a nomenclatura e padronização da descrição da dentição nos roedores sigmodontíneos. **Boletim da Sociedade Brasileira de Mastozoologia** (47): 5-11.

PERCEQUILLO, A. R., E. HINGST-ZAHER & C. R. BONVICINO, 2008. Systematic review of genus *Cerradomys* Weksler, Percequillo and Voss, 2006 (Rodentia: Cricetidae: Sigmodontinae: Oryzomyini), with description of two new species from eastern Brazil. **American Museum Novitates** (3622): 1-46. DOI: https://doi.org/10.1206/495.1

PEREIRA, L. G. & L. GEISE, 2009. Non-flying mammals of Chapada Diamantina (Bahia, Brazil). **Biota Neotropica** 9(3): 185-196. DOI: http://dx.doi.org/10.1590/S1676-06032009000300019

REIG, O. A., 1977. A proposed unified nomenclature for the enamelled components of the molar teeth of the Cricetidae (Rodentia). **Journal of Zoology** 181(2): 227-241. DOI: http://doi.org/10.1111/j.1469-7998.1977.tb03238.x

RIZZINI, C. T., 1997. **Tratado de fitogeografia do Brasil**: 1-747. Âmbito Cultural Edições Ltda., Rio de Janeiro.

ROCHA, R. G., E. FERREIRA, Y. L. LEITE, C. FONSECA & L. P. COSTA, 2011. Small mammals in the diet of barn owls, *Tyto alba* (Aves: Strigiformes) along the mid-Araguaia river in central Brazil. **Zoologia** 28(6): 709-716. DOI: https://doi.org/10.1590/S1984-46702011000600003

RUBBIOLI, E., A. AULER, D. MENIN & R. BRANDI, 2019. **Cavernas – Atlas do Brasil subterrâneo**: 1-340. Instituto Chico Mendes de Conservação da Biodiversidade, Brasília.

SALAZAR-BRAVO, J., 2015. Genus *Calomys* Waterhouse, 1837. In: J. L. PATTON, U. F. J. PARDIÑAS & G. D'ELÍA (Ed.): **Mammals of South America**: vol. 2: Rodents: 481-507. University of Chicago Press, Chicago.

SBRAGIA, I. A. & A. CARDOSO, 2008. Quiropterofauna (Mammalia: Chiroptera) cavernícola da Chapada Diamantina, Bahia, Brasil. **Chiroptera Neotropical** 14(1): 360-365.

SILVA, J. M. C., I. R. LEAL & M. TABARELLI, 2017. Preface. In: J. M. C. SILVA, I. R. LEAL & M. TABARELLI (Ed.): **Caatinga**: vii-x. Springer, Cham.

SOUZA, M. A. N., A. LANGGUTH & E. A. GIMENEZ, 2004. Mamíferos dos brejos de altitude em Paraíba e Pernambuco. In: K. C. PORTO, J. J. P. CABRAL & M. TABARELLI (Org.): **Brejos de altitude em Pernambuco e Paraíba**: história natural, ecologia e conservação: 229-254. Ministério do Meio Ambiente, Brasília.

SOUZA, D. P., P. H. ASFORA, T. C. LIRA & D. ASTÚA, 2010. Small mammals in Barn Owl (*Tyto alba* – Aves, Strigiformes) pellets from northeastern Brazil, with new records of *Gracilinanus* and *Cryptonanus* (Didelphimorphia, Didelphidae). **Mammalian Biology** 75(4): 370-374. DOI: http://doi.org/10.1016/j.mambio.2009.08.003

STUTZ, N. S., P. HADLER, J. J. CHEREM, F. J. FERNÁNDEZ, U. F. J. PARDIÑAS & A. M. RIBEIRO, 2018. Noteworthy sigmodontine (Rodentia: Cricetidae) diversity in southern Brazil as an indication of environmental change during the Holocene. **Historical Biology** 32(5): 649-670. DOI: https://doi.org/10.1080/08912963.2018.15

VAZ, S. M., 2005. Mamíferos colecionados pelo serviço de estudos e pesquisas sobre a febre amarela nos municípios de Ilhéus e Buerarema, estado da Bahia, Brasil. **Arquivos do Museu Nacional** 63(1): 21-28.

WEKSLER, M. & C. R. BONVICINO, 2005. Taxonomy of pigmy rice rats (genus *Oligoryzomys*, Rodentia: Sigmodontinae) of the Brazilian Cerrado, with the description of two new species. **Arquivos do Museu Nacional** 63(1): 113-130.

WEKSLER, M., A. R. PERCEQUILLO & R. S. VOSS, 2006. Ten new genera of oryzomyine rodents. **American Museum Novitates** 3537: 1-29.

WEKSLER, M. & C. R. BONVICINO, 2015. Genus *Oligoryzomys* Bangs, 1900. In: J. L. PATTON, U. F. J. PARDIÑAS & G. D'ELÍA (Ed.): **Mammals of South America**: vol. 2: Rodents: 417-437. University of Chicago Press, Chicago.

WEKSLER, M., E. M. S. LEMOS, P. S. D'ANDREA & C. R. BONVICINO, 2017. The taxonomic status of *Oligoryzomys mattogrossae* (Allen 1916) (Rodentia: Cricetidae: Sigmodontinae), reservoir of Anajatuba Hantavirus. **American Museum Novitates** (3880): 1-32. DOI: https://doi.org/10.1206/3880.1

WILSON, D. E. & D. M. REEDER, 2005. **Mammal species of the world**: a taxonomic and geographic reference: 3. ed.: 1-2142. The Johns Hopkins University Press, Baltimore.

Apêndice 1. Lista dos espécimes depositados na Coleção de Mamíferos do Museu de Zoologia da Universidade Estadual de Feira de Santana (MZFS-DM) e do Departamento de Ecologia e Zoologia da Universidade Federal de Santa Catarina (UFSC) utilizados para a comparação com os fragmentos amostrados na Toca dos Ossos.

Akodon cursor – UFSC 4712, 4785.

Calomys tener – UFSC 5166, 5490.

Cerradomys subflavus – MZFS-DM 0202; UFSC 2248, 2251, 2254, 2257, 2258, 2260, 2280.

Cerradomys vivoi – MZFS-DM 0109, 0111; UFSC 5222, 5223.

Euryoryzomys russatus – UFSC 3940, 3944, 4891, 5689.

Holochilus grupo *brasiliensis* – UFSC 5074, 5890.

Holochilus sciureus – UFSC 2754, 2755.

Hylaeamys laticeps – MZFS-DM 0003, 0004, 0010, 0020.

Necromys lasiurus – MZFS-DM 0033; UFSC 3599, 3600, 3876, 4714, 4815, 5212.

Oecomys catherinae – UFSC 2277, 2278, 2279.

Oligoryzomys sp. – UFSC 2525, 2527, 2530, 3707, 3950, 3951, 4399, 4717, 4791, 4792, 6025.

Rhipidomys sp. – MZFS-DM 0651.

Rhipidomys mastacalis – MZFS-DM 0025.

Wiedomys cerradensis – UFSC 6191.
Wiedomys pyrrhorhinos – UFSC 2822, 2823, 2827, 2828, 2829, 5224.

Apêndice 2. Lista do material estudado da TO-I depositado na Coleção de Mamíferos do Museu de Zoologia da Universidade Estadual de Feira de Santana (MZFS-DM) e da TO-II na Coleção de Paleovertebrados da Universidade Federal do Recôncavo da Bahia (UFRB-PV). Os dentes, se presentes, são indicados entre parênteses. Abreviaturas: Cr: crânio; dir = direito; Dn = dentário; esq = esquerdo; M = molar superior; m = molar inferior; Mx = maxilar.

TO-I

Calomys* sp.:** Cr: MZFS-DM 0876, 0968 (M1-M3 dir e M1-M3 esq); 0964 (M2-M3 dir e M1-M3 esq); 0966 (M1-M3 dir e M1 esq); Dn dir: MZFS-DM 0835, 0846, 0877 (m1-m3); Dn esq: MZFS-DM 0829, 0833 (m1-m3). ***Cerradomys* sp.:** Mx dir: MZFS-DM 0815 (M1-M2); Dn dir: MZFS-DM 0826 (m1-m3); Dn esq: MZFS-DM 0828 (m1-m3). ***Holochilus sciureus*:** Cr: MZFS-DM 0950 (M1-M3 dir e M1-M3 esq); Mx dir: MZFS-DM 0913 (M1). ***Necromys lasiurus*:** Cr: MZFS-DM 0857, 0948, 0949, 0951, 0952, 0953, 0959, 0967, 0969 (M1-M3 dir e M1-M3 esq); 0957 (M1-M2 dir e M1-M3 esq); 0954, 0958, 0963 (M1-M2 dir e M1-M2 esq); 0983 (M1-M2 dir); 0960 (M1 e M3 dir e M1 esq); 0961 (M1 dir e M1 esq); Mx dir: MZFS-DM 0821, 0823, 0866 (M1-M2); 0824, 0864 (M1); Mx esq: MZFS-DM 0818, 0820, 0821, 0823, 0824 (M1-M3); 0816, 0865 (M1-M2); 0817 (M1); Dn dir: MZFS-DM 0840, 0843 (m1-m3); 0841, 0844 (m1-m2); 0842, 0863 (m1); Dn esq: MZFS-DM 0847, 0848, 0852, 0858, 0859 (m1-m3); 0849, 0853, 0860 (m1-m2); 0831, 0834, 0837, 0845, 0854, 0855, 0861, 0862, 0874, 0875 (m1). ***Oligoryzomys* sp.:** Cr: MZFS-DM 0825 (M1-M3 dir e M1-M3 esq); Dn dir: MZFS-DM 0856 (m1); Dn esq: MZFS-DM 0867 (m1-m3). ***Wiedomys pyrrhorhinos: Cr: MZFS-DM 0691, 0905, 0946, 0956, 0965, 2907 (M1-M3 dir e M1-M3 esq); 0955 (M2-M3 dir e M1-M3 esq); Mx esq: MZFS-DM 0822 (M1-M2); 0819 (M1); Dn dir: MZFS-DM 0832 (m1-m3), 0850 (m1-m2); Dn esq: MZFS-DM 0836, 0838 (m1-m3). ***Rattus rattus*:** Dn esq: MZFS-DM 0924 (m1-m3); 0839 (m1).

TO-II

***Calomys* sp.:** Cr: UFRB-PV 2862 (M1-M3 dir e M1-M3 esq); UFRB-PV 2960 (M1-M3 dir e M3 esq); Mx dir: UFRBPV 3132 (M1-M3); 2746 (M1-M2); 951 (M1); Mx esq: UFRB-PV 2738, 2745, 2863, 2955 (M1-M3); 2991, 3157 (M1-M2); Dn dir: UFRB-PV

2714; 2873, 2874, 2935, 2937, 2939, 2994, 3007; 3017, 3113 (m1-m3); 2707, 2713, 2715, 2825, 3114 (m1-m2); 2712, 2993, 3022 (m1); Dn esq: UFRB-PV 2872, 2997 (m1-m3); 2709, 2716, 2824, 2954, 3018 (m1-m2); 949, 2705, 2711, 2718, 2869, 2876 (m1). ***Cerradomys* sp.:** Cr: UFRB-PV 2861 (M1-M3 dir e M1-M3 esq); Mx dir: UFRB-PV 2820 (M1-M3); Mx esq: UFRB-PV 959, 2818, 2990 (M1-M3); 2987 (M1-M2); Dn dir: UFRB-PV 3019, 3020, 3028 (m1); Dn esq: UFRB-PV 2934 (m1-m2). ***Holochilus sciureus*:** Cr: UFRB-PV 2901, 2919, 2969 (M1 dir e M1-M3 esq); Mx esq: UFRB-PV 2911, 2918, 2965 (M1-M3); 2992, 3123 (M1-M2); 962, 2988 (M2-M3); 2864, 2989 (M1); 972 (M2); Dn dir: UFRB-PV 907, 2978 (m1-m3); 2852, 2972, 2977 (m1-m2); 936 (m1); Dn esq: UFRB-PV 2956 (m1-m3); 908 (m1-m2), 948 (m2). ***Necromys lasiurus*:** Cr: UFRB-PV 2975 (M1-M3 dir e M1-M2 esq); 2857 (M1 dir e M1-M2 esq), Mx dir: UFRBPV 2733, 2952, 2986, 3012 (M1-M2); Mx esq: UFRB-PV 2748, 2822 (M1-M3); 2737, 2740, 2743, 3131 (M1-M2); 2747, 2953, 2985 (M1); Dn dir: UFRB-PV 947, 2829, 2999, 3109, 3112 (m1-m2); 2998 (m1); Dn esq: UFRB-PV 3001, 3002, 3026 (m1-m3); 2731, 2833, 3031 (m1-m2); 2936, 3030, 3119 (m1). ***Oligoryzomys* sp.:** Mx esq: UFRB-PV 2735 (M1-M2). ***Wiedomys pyrrhorhinos*:** Cr: UFRB-PV 2855, 2858, 2898 (M1-M3 dir e M1-M3 esq); 2859 (M1-M3 dir e M2-M3 esq); 2897 (M1-M3 dir e M1 e M3 esq); 2957 (M1-M2 dir e M1-M2 esq); 906 (M3 dir e M1-M3 esq); Mx dir: UFRB-PV 2819, 3108, 3134, 3176 (M1-M3); Mx esq: UFRB-PV 2823, 3121, 3130 (M1-M3); 956 (M2-M3), 973, 2983 (M1); Dn dir: UFRBPV 2826, 3023 (m1-m3); 3006 (m1-m2); Dn esq: UFRB-PV 2690 (m1-m3); 3021, 3024 (m1-m2); 2710, 2877 (m1).

4.2 SMALL MAMMAL DIVERSITY IN SEMI-DECIDUOUS SEASONAL FOREST OF THE SOUTHERNMOST BRAZILIAN PAMPA: THE IMPORTANCE OF OWL PELLETS FOR RAPID INVENTORIES IN HUMAN-CHANGING ECOSYSTEMS

Artigo publicado no periódico Papeis Avulsos de Zoologia, volume 60, artigo e20206025, 2020, DOI: 10.11606/1807-0205/2020.60.25.

Narla Shannay Stutz[1], Patrícia Hadler[2], Jorge José Cherem[3] & Ulyses Francisco José Pardiñas[4]

[1] Universidade Federal do Rio Grande do Sul, Programa de Pós-Graduação em Geociências. Porto Alegre, RS, Brasil.
[2] Universidade Federal de Santa Catarina, Departamento de Geologia, Laboratório de Paleontologia, Programa de Pós-Graduação em Geologia. Florianópolis, SC, Brasil.
[3] Caipora Cooperativa. Florianópolis, SC, Brasil.
[4] Instituto de Diversidad y Evolución Austral (IDEAus-CONICET). Puerto Madryn, Chubut, Argentina. Associate Researcher, Instituto Nacional de Biodiversidad (INABIO). Quito, Ecuador.

Abstract

The Pampa biogeographic province covers a mere 2% of the Brazilian territory (176,496 km^2). However, it stands out as a complex and diverse ecosystem, although its mammal communities are still scarcely understood. Human activities are transforming the territory into a mosaic of agroecosystems, native and exotic forest fragments, and grasslands. Here we conducted the first investigation to determine the richness of small mammal assemblages in the region based on extensive analyses of owl pellets (*Tyto furcata*). Craniodental remains were studied from samples collected from 12 Semi-deciduous Seasonal Forest sites in the municipality of São Lourenço do Sul, State of Rio Grande do Sul, Southern Brazil. A total of 2,617 individuals belonging to 19 taxa were recorded, including 2 marsupials (Didelphidae; 0.42%), 2 chiropterans (Molossidae, Phyllostomidae; 0.12%), and 15 rodents (Cricetidae, Muridae, Caviidae; 99.46%). The rodent genera *Oligoryzomys*, *Mus*, *Calomys*, and *Akodon* were the most common taxa. Large samples also included poorly known taxa, such as the cricetids *Bibimys*, *Juliomys* (recording here its southernmost occurrence), *Lundomys*, and *Wilfredomys*. From a biogeographical point of view, the recorded assemblage

embraces a mixture of Platan, Pampean, and Atlantic Forest elements, highlighting the role of the southernmost Brazilian hills as a wedge favoring the penetration of forest micromammals to higher latitudes. Our findings testify to the great diversity of the Pampa, but also point to a growing homogeneity and dominance of rodent species that are widespread in agroecosystems. Rapid inventories based on owl pellets emerge as a suitable, economic, non-invasive tool to document these community changes.

Keywords: *Bibimys*; *Juliomys*; *Lundomys*; *Tyto furcata*; *Wilfredomys*

INTRODUCTION

The Pampa biogeographic province extends from the southern half of the State of Rio Grande do Sul (RS, hereafter) in Brazil across the whole of Uruguay to Central Argentina (Morrone, 2001). In Brazil, the Pampa is one of the smallest biomes, covering an area of 176,496 km², which corresponds to 2.07% of the national territory (IBGE, 2004a). Although dominated by grasslands and largely treated as a non-forest ecosystem (Overbeck *et al*., 2015), the Brazilian Pampa also encompasses the southernmost expression of Semi-deciduous Seasonal Forest (Belton, 1984). The latter is arranged into two blocks: The larger Southern Block (10,137.73 km²) is located on the eastern slope of the Serra do Sudeste, flanking the Patos lagoon, and the Northern Block (3,159.03 km²) is located on the southeastern Meridional Plateau. These forest environments have been almost totally converted to agroecosystems (IBGE, 2004b; Cordeiro & Hasenack, 2009). Today, the general landscape is constituted by myriad small patches of native and exotic forests and cleared areas supporting pastures or grasslands (Cordeiro & Hasenack, 2009). The few, but important, efforts directed at exploring the non-volant small mammals in these grassland–forest ecotones have revealed diverse communities of rodents and marsupials, while also finding disturbed habitats harbor simplified species assemblages (Luza *et al*., 2016).

The analysis of owl pellet samples has been considered a useful tool to inventory small mammals (*e.g.*, Taylor, 1994; Bonvicino & Bezerra, 2003; Torre *et al*., 2004; Pardiñas *et al*., 2005; Teta *et al*., 2010; Meek *et al*., 2012; Baglan & Catzeflis, 2016; Mancini *et al*., 2018). In addition, it is a relatively easy and low-cost method that generates estimates of species richness that are identical or higher than those obtained by expensive traditional methods (*e.g.*, trapping; Torre *et al*., 2004). Indeed, the fauna contained in owl pellets has been considered a better representation of the

composition of small mammal communities on a broader spatiotemporal scale (Formoso *et al*., 2016; Heisler *et al*., 2016). In southern Brazil, few studies have utilized *Tyto furcata* (Temminck, 1827) pellets. Nonetheless, the potential of the pellets to record small mammal communities has been corroborated by the variety of species recorded and the reports of rare taxa (*e.g*., González *et al*., 1999; Scheibler & Christoff, 2007; Peters *et al*., 2010; Cherem *et al*., 2018).

Here, we studied a large sample of cranial and mandibular fragments of small mammals derived from *Tyto furcata* pellets representing Semi-deciduous Seasonal Forest faunas in the southern Pampa Biome. Our survey focused on the municipality of São Lourenço do Sul in RS, Brazil. This administrative unit is of particular relevance because it encompasses several mammal type-localities (*e.g*., *Wilfredomys oenax* (Thomas, 1928), *Lutreolina crassicaudata lutrilla* Thomas, 1923, *Lasiurus enslenii* Lima, 1926) (Avila-Pires, 1994). In addition, it represents the southernmost expression of forest elements and, as such, the potential limit between the Brazilian and Patagonian mammalian subregions (Hershkovitz, 1958). Our aim is thus to contribute to the knowledge of current Pampa small mammal assemblages, including the record of poorly known taxa. In addition, we emphasize the necessity to conduct extensive and low-cost surveys as a way to explore small mammal assemblages in rapidly changing anthropogenic environments.

MATERIAL AND METHODS

The municipality of São Lourenço do Sul (SLS, hereafter) is located on the eastern slope of the Serra do Sudeste, near the coastal region of RS (Brazil). The climate is mild mesothermal, with average temperatures between 10 and 15°C, super humid, and without periods of drought (IBGE, 1978). On the 2nd and 3rd July 2018, owl pellet samples were collected from inside buildings (sheds, churches, and abandoned houses) that were used as shelters by the owl *Tyto furcata*, totaling 12 sampling sites in SLS (Figure 1). The sites are located at altitudes of between 70 and 280 m and are within the phytoecological region of Semi-deciduous Seasonal Forest, Pampa Biome (Leite, 2002).

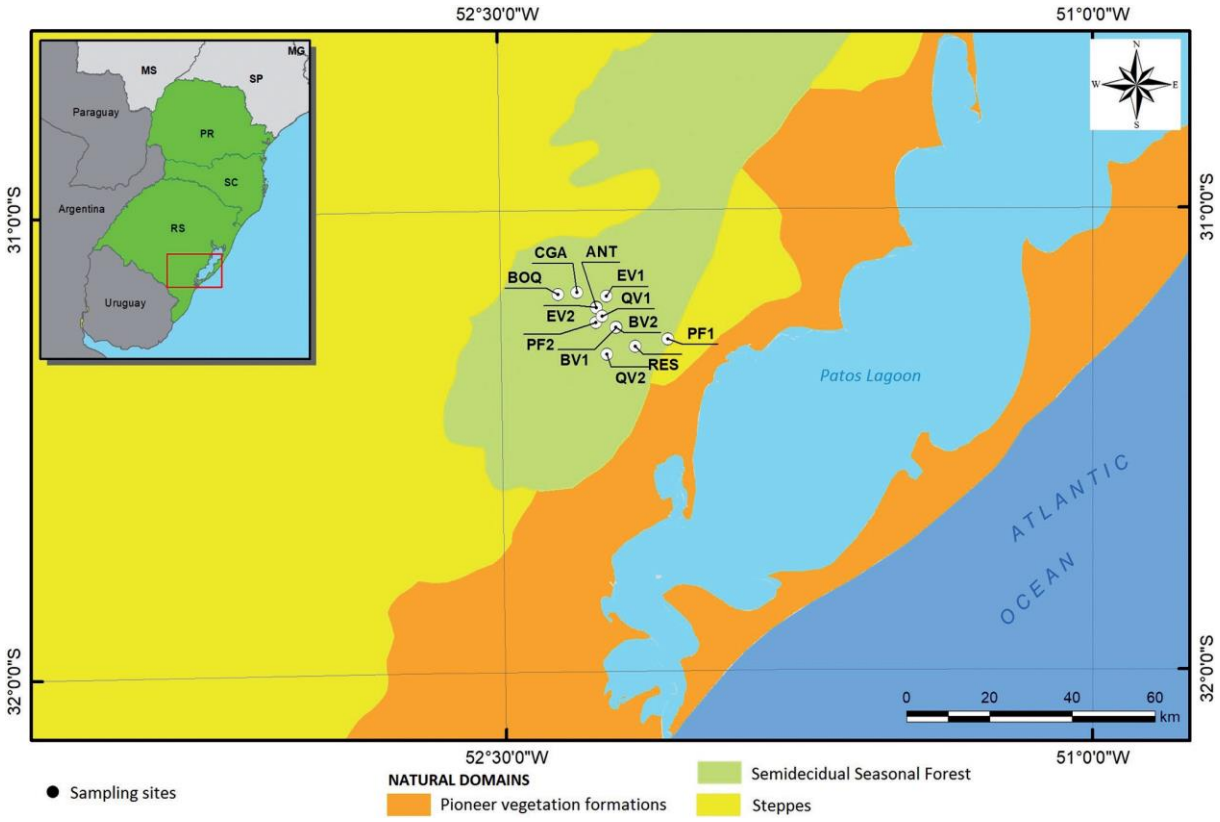


Figure 1. Location of the sampling sites of the *Tyto furcata* pellets at the Municipality of São Lourenço do Sul, State of Rio Grande do Sul, Southern Brazil. BV1 = Boa Vista I; BV2 = Boa Vista II; BOQ = Boqueirão; CGA = Canta Galo; EV1 = Evaristo I; EV2 = Evaristo II; ANT = Picada das Antas; PF1 = Picada Feliz I; PF2 = Picada Feliz II; QV1 = Quevedos I; QV2 = Quevedos II; RES = Reserva. Map modified from MMA (1992).

The owl pellet preparation included maceration in hot water with NaClO 2% (3 ml per liter of water) over 24 hours, followed by washing with running water to remove bristles and then handpicking of the bones. The craniodental material was deposited in the Coleção de Fragmentos Ósseos do Laboratório de Paleontologia, Universidade Federal de Santa Catarina, Florianópolis (UFSC-CF), State of Santa Catarina, Brazil (Table 1). The taxonomic identification of the small mammals was made by comparison with specimens deposited in the Coleção de Mamíferos do Departamento de Ecologia e Zoologia, Universidade Federal de Santa Catarina, Florianópolis (UFSC) (see Appendix 1) and specific literature (Barquez *et al*., 1999; Gonçalves *et al*., 2007; Patton *et al*., 2015; Hadler *et al*., 2016; Stutz *et al*., 2017, 2018; Cherem *et al*., 2018). The taxonomy employed here follows Gardner (2008) for Didelphimorphia and Chiroptera, Wilson & Reeder (2005) for Muridae, and Patton *et al*. (2015) for the other rodents; taxonomic ordination follows Wilson & Reeder (2005). Threatened species at global

(IUCN, 2019), national (ICMBio, 2018), and state (Rio Grande do Sul, 2014) levels are indicated, as are exotic invasive species (Rio Grande do Sul, 2013). The minimum number of individuals (MNI) per species and per sampling site was determined by considering the greatest number of right or left mandibles or maxillaries (Beisaw, 2013). The length of the upper molar series (LM1–M3) of the sigmodontine rodents was measured with a manual caliper with a precision of 0.02 mm. Molar abbreviations are: M1, first upper molar; m1, first lower molar; M2, second upper molar; m2, second lower molar; M3, third upper molar; m3, third lower molar.

Table 1. Sampling sites of *Tyto furcata* pellets at the municipality of São Lourenço do Sul, State of Rio Grande do Sul, Southern Brazil. UFSC-CF = Coleção de Fragmentos Ósseos do Laboratório de Paleontologia, Universidade Federal de Santa Catarina.

Sampling Site	Abbreviation	Coordinates (WGS 84)	Catalog number
Boa Vista I	BV1	31°15′17″S, 52°12′31″W	UFSC-CF 38
Boa Vista II	BV2	31°15′18″S, 52°12′34″W	UFSC-CF 39
Boqueirão	BOQ	31°16′55″S, 52°04′39″W	UFSC-CF 35
Canta Galo	CGA	31°10′58″S, 52°21′19″W	UFSC-CF 41
Evaristo I	EV1	31°11′13″S, 52°13′58″W	UFSC-CF 40
Evaristo II	EV2	31°10′43″S, 52°18′25″W	UFSC-CF 42
Picada das Antas	ANT	31°18′48″S, 52°13′58″W	UFSC-CF 37
Picada Feliz I	PF1	31°12′39″S, 52°15′29″W	UFSC-CF 32
Picada Feliz II	PF2	31°12′46″S, 52°15′29″W	UFSC-CF 33
Quevedos I	QV1	31°14′41″S, 52°15′35″W	UFSC-CF 34
Quevedos II	QV2	31°13′51″S, 52°14′37″W	UFSC-CF 43
Reserva	RES	31°17′47″S, 52°09′38″W	UFSC-CF 36

RESULTS

The *Tyto furcata* pellets from 12 sites in SLS contained 2,617 individuals belonging to 19 small mammal taxa, including two didelphimorphian species (Didelphidae) (Figure 2), two chiropterans (Molossidae and Phyllostomidae) (Figure 3), and 15 rodents (Cricetidae, Muridae, and Caviidae) (Figures 4, 5, and 6) (Table 2). The rodents were dominant in the samples (78.95% of the taxa and 99.46% of the individuals) and, among them, the cricetids prevailed (63.16% and 71.23%, respectively). Marsupials and chiropterans were represented by two taxa each, composing 0.42% and 0.12% of the total individuals, respectively. The greatest

number of taxa was registered at site Picada Feliz I (16 taxa), followed by Evaristo II (11 taxa), Boqueirão (9 taxa), and Quevedos II (8 taxa) (Table 2).

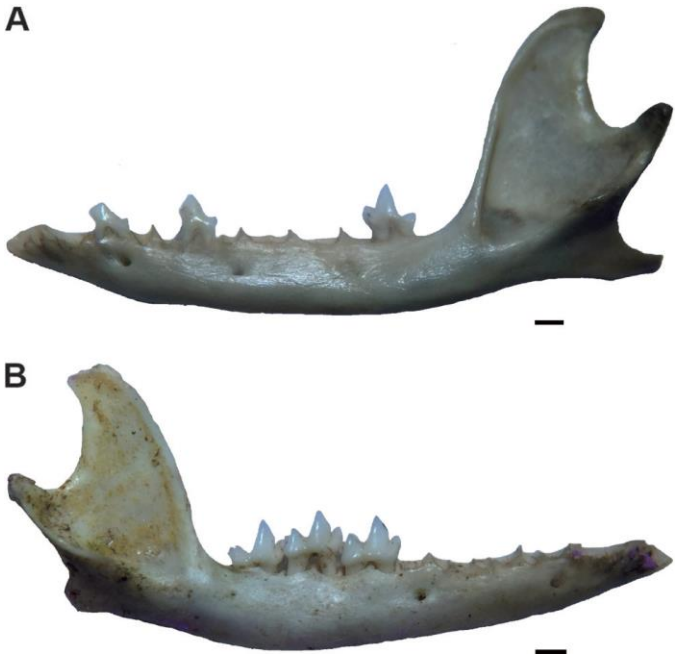


Figure 2. Didelphimorphia specimens from the *Tyto furcata* pellets from the Municipality of São Lourenço do Sul, State of Rio Grande do Sul, Brazil. (A) = labial view of the left dentary of *Cryptonanus guahybae,* UFSC-CF 32-2-1. (B) = labial view of the right dentary of *Gracilinanus microtarsus,* UFSC-CF 42-10-1. Scale bars: 1 mm.

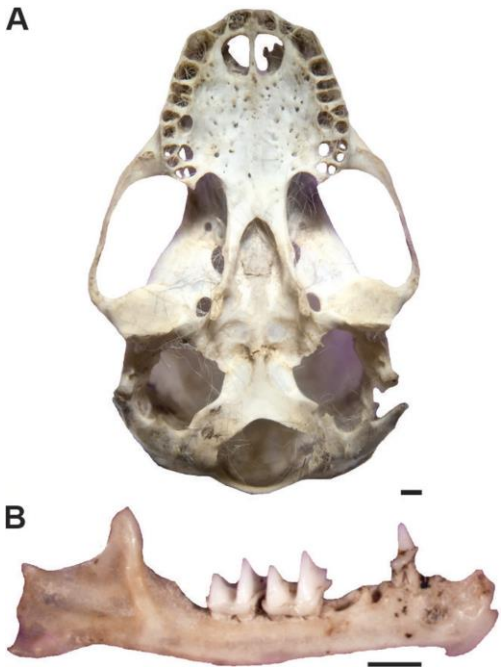


Figure 3. Chiroptera specimens from the *Tyto furcata* pellets from the Municipality of São Lourenço do Sul, State of Rio Grande do Sul, Brazil. (A) = ventral view of the skull of *Sturnira lilium,* UFSC-CF 40-5-1. (B) = labial view of the right dentary of *Tadarida brasiliensis,* UFSC-CF 42-11-1. Scale bars: 1 mm.

Mus musculus, an exotic invasive murine, was registered in all of the sites. Moreover, *Akodon* spp., *Calomys* sp., and *Oligoryzomys* sp. were registered in 11 sites, being absent only in the smaller sample (Reserva). Five taxa (*Tadarida brasiliensis*, *Sturnira lilium*, *Akodon azarae*, *Juliomys* sp., and *Lundomys molitor*) occurred only in one site. *Oligoryzomys* sp. represented 52.5% of the recorded individuals, being the most frequent taxon in ten of the 12 studied sites, followed by *M. musculus* (28.28%; most frequent in Picada das Antas), *Calomys* sp. (7.64%), and *Akodon* spp. (6.07%). The other 12 taxa together represented 5.46% of the individuals. *Wilfredomys oenax*, a threatened species ("endangered" at the global level and "critically endangered" at the national and state levels), was reported for three sites (Evaristo II, Picada Feliz I, and Quevedos I).



Figure 4. Occlusal view of the upper molars of the Sigmodontine rodents from the *Tyto furcata* pellets from the Municipality of São Lourenço do Sul, State of Rio Grande do Sul, Brazil. (A) = *Akodon azarae,* UFSC-CF 43-2-1, left M1-M3. (B) = *Akodon* sp., UFSC-CF 32-4-1, left M1-M3. (C) = *Bibimys* sp., UFSC-CF 32-5-1, left M1-M3. (D) = *Calomys* sp., UFSC-CF 32-6-1, left M1-M3. (E) = *Juliomys* sp., UFSC-CF 32-7-1, left M1-M3. (F) = *Holochilus* sp., UFSC-CF 43-4-1, left M1-M3. (G) = *Oligoryzomys* sp.,

UFSC-CF 32-11-1, left M1-M3. (H) = *Oxymycterus* sp., UFSC-CF 32-12-1, left M1-M3. (I) = *Sooretamys angouya,* UFSC-CF 32-13-1, right M1-M3. (J) = *Wilfredomys oenax,* UFSC-CF 32-14-1, left M1-M3. Scale bars: C = 200 µm; A, B, D, E, F, G, H, I, J = 500 µm.

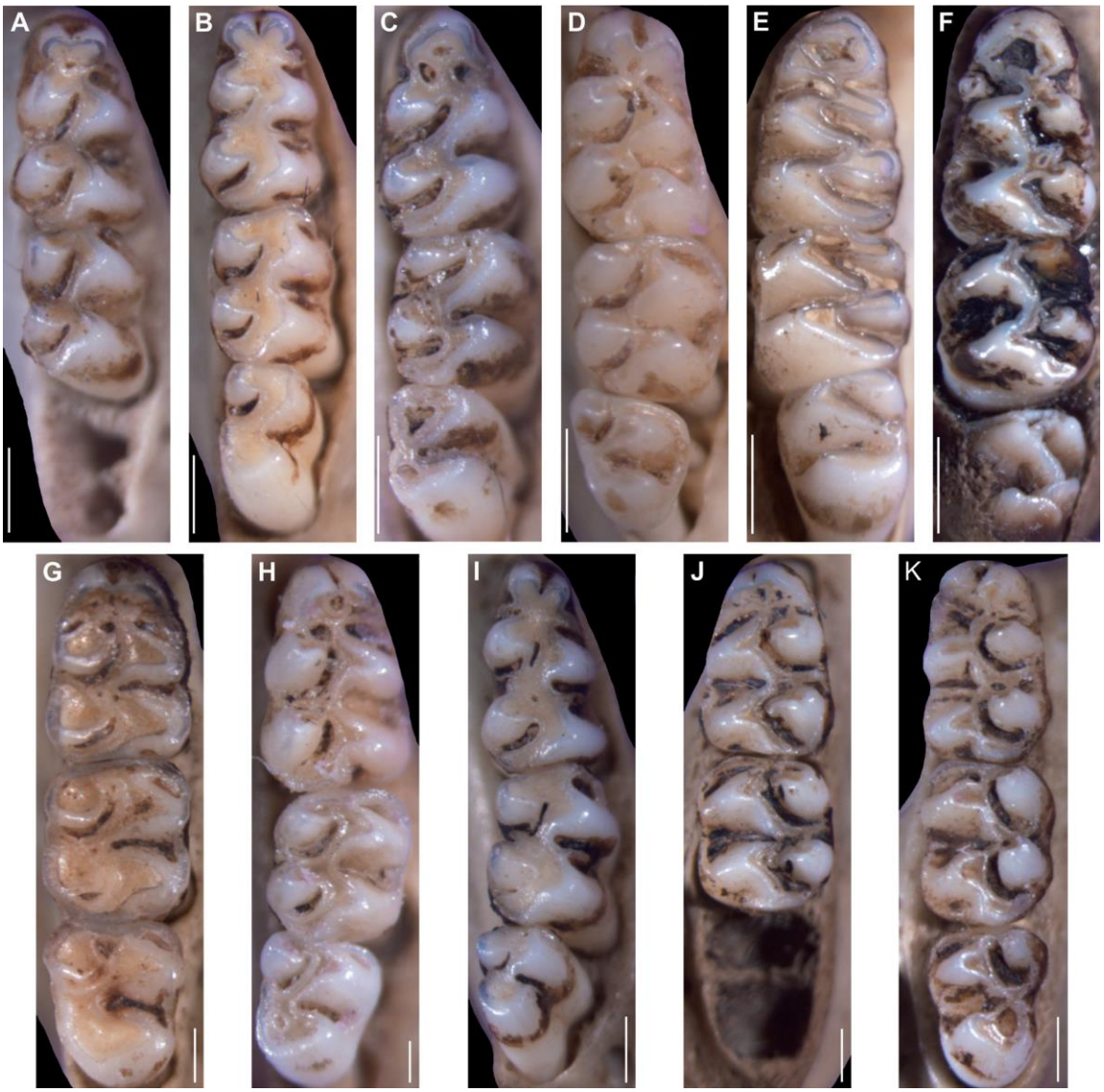


Figure 5. Occlusal view of the lower molars of the Sigmodontine rodents from *Tyto furcata* pellets from the Municipality of São Lourenço do Sul, State of Rio Grande do Sul, Brazil. (A) = *Akodon azarae,* UFSC-CF 43-2-2, right m1-m2. (B) = *Akodon* sp., UFSC-CF 32-4-2, right m1-m3; (C) = *Bibimys* sp., UFSC-CF 32-5-2, right m1-m3. (D) = *Calomys* sp., UFSC-CF 32-6-2, right m1-m3. (E) = *Holochilus* sp., UFSC-CF 43-4-2, left m1-m3. (F) = *Lundomys molitor,* UFSC-CF 32-9-1, left m1-m3. (G) = *Nectomys squamipes,* UFSC-CF 32-10-1, right m1-m3. (H) = *Oligoryzomys* sp., UFSC-CF 32-11-2, right m1-m3. (I) = *Oxymycterus* sp., UFSC-CF 32-12-2, right m1-m3. (J) = *Sooretamys angouya,* UFSC-CF 32-13-2, left m1-m2. (K) = *Wilfredomys oenax,*

UFSC-CF 32-14-2, left m1-m3. Scale bars: H = 200 μm; A, B, C, D, G, I, J, K = 500 μm; E, F = 1 mm.

Akodon azarae, one of the smallest Brazilian species of *Akodon*, was present in the SLS pellets, represented by a skull, one isolated maxillary, and six dentaries from the site Quevedos II. The skull possesses complete upper molar rows, measuring LM1–M3 = 3.98 mm. In addition, the specimens present an alveolar LM1–M3 = 4.04 to 4.1 mm (n = 2) and very deep anteromedian flexi/flexids, allowing their attribution to *A*. *azarae* following Hershkovitz (1990). The other specimens were treated as *Akodon* spp. They included maxillae with longer molar series (n = 53, LM1–M3 = 4.2 to 4.82 mm), which could be referred to *A*. *montensis* Thomas, 1913 (relatively shorter molar series) or *A*. *paranaensis* Christoff *et al*., 2000 or *A*. *reigi* González *et al*., 1998 (relatively longer molar series), following Gonçalves *et al*. (2007). However, the absence of clear diagnostic characters and the fragmentary nature of the studied specimens prevent species determination.

The genus *Bibimys* was represented by a MNI = 13 in three SLS samples (Evaristo II, Picada Feliz I and II). The uncertain taxonomic status and subtle cranial traits of the three species recognized for this genus preclude reliably assigning these specimens to one particular species (Pardiñas *et al*. 2015a, 2017a). Populations recorded in RS are referred to *B*. *labiosus* (Winge, 1887) (*e.g*., Pardiñas *et al*., 2015a; Machado *et al*., 2016), which is a plausible hypothesis for the SLS specimens pending a revision of a more extensive set of traits (*e.g*., molecular data).

Two species of *Calomys* are mentioned for RS: *C*. *tener* (Winge, 1887) and *C*. *laucha* (G. Fischer, 1814) (Haag *et al*., 2007; Quintela *et al*., 2014; González-Ittig *et al*., 2019). The SLS specimens belonging to this genus possess a distinctively prominent supraorbital margin, large sphenopalatine vacuities, and a generally conspicuous capsular projection. These features are commonly attributed to *C*. *tener*. Nevertheless, the studied material also presents an M3 with a shallow hypoflexus and a “W-shaped” m3, which are reported as characteristics of *C*. *laucha* (Salazar-Bravo, 2015). Thus, the specific assignment of the studied material was not possible.

One specimen of the arboreal mouse *Juliomys* was registered in the Picada Feliz I sample. The generic attribution is supported by its short and broad palate and the complex morphology of the brachydont molars, which possess a broad procingulum, well-developed anteromedian flexus, mesoloph, and developed enteroloph in M1; and an anterostyle in M2. The features preserved in this specimen do not allow its

assignment to one of the three species recorded in RS, *J. ossitenuis* Costa *et al*., 2007, *J. pictipes* (Osgood, 1933), and *J. ximenezi* Christoff *et al*., 2016.

Table 2. Minimum number of individuals per taxon of small mammals registered in *Tyto furcata* pellets from the municipality of São Lourenço do Sul, State of Rio Grande do Sul, Brazil. The sites abbreviations follow Table 1.

Taxon	BV1	BV2	BOQ	CGA	EV1	EV2	ANT	PF1	PF2	QV1	QV2	RES	Total	%
Didelphimorphia														
Didelphidae														
Cryptonanus guahybae (Tate, 1931)			1			1		7					9	0,34
Gracilinanus microtarsus (Wagner, 1842)						1		1					2	0,08
Chiroptera														
Molossidae														
Tadarida brasiliensis (I. Geoffroy, 1824)						1							1	0,04
Phyllostomidae														
Sturnira lilium (E. Geoffroy, 1810)					2								2	0,08
Rodentia														
Cricetidae														
Akodon azarae (J. Fischer, 1829)											3		3	0,11
Akodon spp.	9	4	9	2	4	15	2	104	4	3	3		159	6,08
Bibimys sp.						2		10	1				13	0,50
Calomys sp.	5	5	3	5	13	21	10	122	3	3	10		200	7,64
Juliomys sp.								1					1	0,04
Holochilus sp.			1					3			3		7	0,27
Lundomys molitor (Winge, 1887)								1					1	0,04
Nectomys squamipes (Brants, 1827)						1		1					2	0,08
Oligoryzomys sp.	41	21	42	26	26	145	23	949	38	13	50		1374	52,5
Oxymycterus nasutus (Waterhouse, 1837)	1	1	4	1		4	3	51			8	1	74	2,83
Sooretamys angouya (G. Fischer, 1814)		1	1	1			1	3				2	9	0,34
Wilfredomys oenax (Thomas, 1928)						3		7		1			11	0,42
Muridae														
Mus musculus Linnaeus, 1758	15	20	32	4	9	22	33	564	12	2	26	1	740	28,28
Rattus rattus (Linnaeus, 1758)			2					5					7	0,27
Cavilidae														
Cavia aperea Erxleben, 1777								1			1		2	0,08
MNI	71	52	95	39	54	216	72	1830	58	22	104	4	2617	100,00
Richness (small mammals total)	5	6	9	6	5	11	6	16	5	5	8	3	19	

Holochilus and *Lundomys* are semiaquatic rats, and are also present in the SLS pellets, the former registering in three sites (Boqueirão, Picada Feliz I, and Quevedos II) and the latter in only one site (Picada Feliz I). Two species of *Holochilus* occur currently in RS, *H. brasiliensis* (Desmarest, 1819) and *H. vulpinus* (Brants, 1827), both belonging to the *H. brasiliensis* group (Pardiñas *et al*. 2013; D'Elía *et al*. 2015). Dental differences between these species are poorly addressed, precluding the specific assignment of the fragmentary material. The identification of *Lundomys* was based on the following features: a low coronoid process; poorly developed capsular projection (compared to *Holochilus*); masseteric crests which do not join together and which extend farther from the mentonian process than in *Holochilus*; flexi and flexids shallower than in *Holochilus* and non-interpenetrating; an M1/m1 and M2/m2 with a

small and distinct mesoloph/mesolophid; a procingulum divided by a small anteromedian flexus, which is absent in *Holochilus*; and an M2 with a protoflexus (Voss & Carleton, 1993).

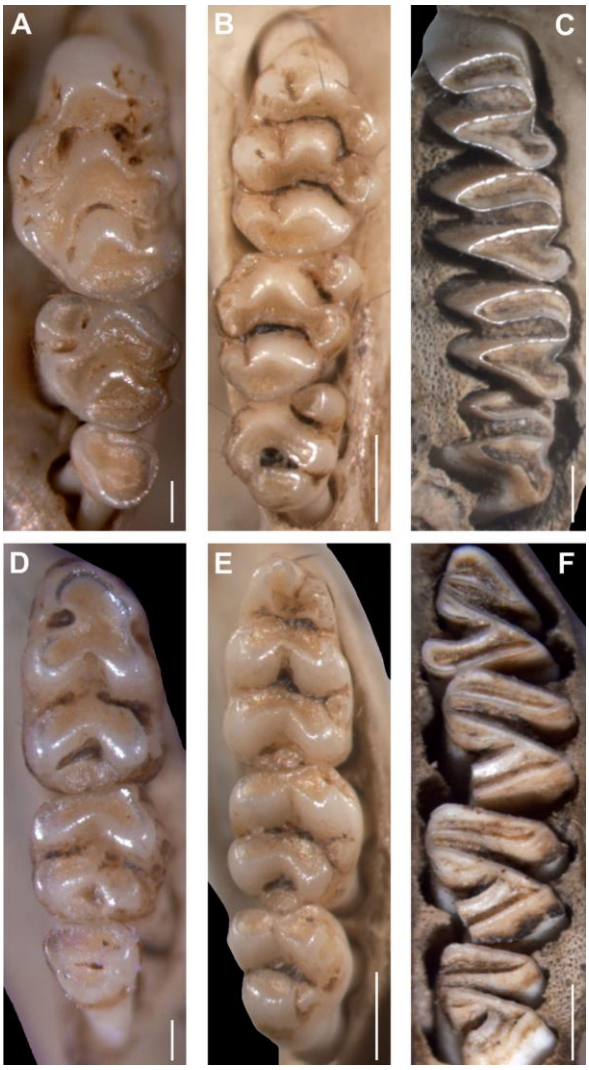


Figure 6. Occlusal view of the upper and lower molars of the Muridae and Caviidae rodents from *Tyto furcata* pellets from the Municipality of São Lourenço do Sul, State of Rio Grande do Sul, Brazil. (A) = *Mus musculus,* UFSC-CF 32-15-1, left M1-M3. (B) = *Rattus rattus,* UFSC-CF 35-9-1, right M1-M3. (C) = *Cavia aperea,* UFSC-CF 43-8-1, left P4-M3. (D) = *M. musculus*, UFSC-CF 32-15-2, right m1-m3. (E) = *R. rattus,* UFSC-CF 35-9-2, right m1-m3. (F) = *C. aperea,* UFSC-CF 43-8-2, right p4-m3. Scale bars A, D = 200 µm; B, C, E, F = 1 mm.

The genus *Oligoryzomys* comprises two species in Southern Brazil, *O. flavescens* (Waterhouse, 1837) and *O. nigripes* (Olfers, 1818), which are reported as being very similar in metrics and cranial morphology (Pardiñas *et al*., 2017b). Some characters, such as the length of the upper molar series, the length of the incisive

foramen, the position of the frontal (or suprafrontal) foramen, and the development of the capsular projection on the dentary, have already been considered diagnostic for these two species (Langguth, 1963; Machado *et al*., 2011; Boroni *et al*., 2015). Nevertheless, these features showed some variation in the material used for comparison (see the discussion in Cherem *et al*., 2018). Thus, the SLS specimens were identified only as *Oligoryzomys* sp.

DISCUSSION

Semi-deciduous Seasonal Forests in the Brazilian Pampa: small mammal taxonomy

Although we uncritically referred the studied *Lundomys* material to the single species today recognized for the genus, *L*. *molitor* (Winge, 1887), it is important to note that the species has its type locality in Lagoa Santa, Minas Gerais, about 1,500 km northeast of SLS, where it became extinct (Voss & Carleton, 1993; Pardiñas & Teta, 2013). Today, *L*. *molitor* is mostly known from populations in the Uruguayan territory and three adjacent Brazilian localities (Silveira *et al*., 2011; Voss, 2015; Brandão & Fegies, 2017). In addition, differences in molar morphology have been highlighted between the Lagoa Santa material and living samples (Pardiñas & Teta, 2011). More important to the focus of the present study, Brandão & Fegies (2017) reported subtle differential traits between individuals from SLS and Uruguay. In this context, the nominal form *Holochilus magnus*, erected by Hershkovitz (1955) with a type locality in eastern Uruguay, deserves attention for its potential value in a much needed revision of *Lundomys*.

The case of the arboreal cricetid *Wilfredomys* seems to have some parallelism with that described above for *Lundomys*. *Wilfredomys oenax*, the type and single species recognized for the genus, was described based on material collected in SLS (Thomas, 1928). This rat has a large geographic range, including most of the Uruguayan territory and also isolated enclaves in the Brazilian states of Santa Catarina, Paraná, and São Paulo (González *et al*., 2015). Vaz Ferreira (1960) highlighted differences between the type material and one specimen from Uruguay, and Pine (1980:198) expanded these comparisons and concluded “further study may show that the Brazilian and Uruguayan populations are worthy of subspecific designation.” Our knowledge about the alpha taxonomy of *Wilfredomys* is poor (Machado *et al*., 2015), and specimens available for study are so scarce and

fragmentary (Brandão, 2015) that non-geographic variation is difficult to assess (González *et al*., 2015:106). However, taking into account that *W*. *oenax* comes from the hilly surroundings of SLS, despite its geographic proximity to Uruguayan localities, environmental differences could be associated with the reported variability.

The alpha taxonomy of *Juliomys*, a small forest dweller, deserves attention, especially regarding its southernmost expressions. With the recent description of *J*. *ximenezi*, a new species was added to the pool of *Juliomys* species reported for the southern portion of the Atlantic Forest, totaling three forms including *J*. *pictipes* and *J*. *ossitenuis* (Christoff *et al*., 2016). This is a striking case of sympatry because they are phenotypically very similar (Pavan & Leite, 2011), suggesting no major niche differences among them. If the diversity of the assemblage is not artifactual (*i.e*., misidentifications), clearly a working hypothesis is needed to explain the recorded sympatry. In sharp contrast, populations of *Juliomys* in Misiones Province, Argentina, are exclusively attributed to a single species, *J*. *pictipes* (Pardiñas *et al*., 2006). The material recovered in SLS, extending the southern limit of the distribution of this genus by around 250 km, could represent an important piece of information to clarify the taxonomy of *Juliomys* in its southern range. Since most of the current understanding of the alpha taxonomy of *Juliomys* is based on genetic data, the growing possibility of extracting DNA from remains retrieved from owl pellets is exciting.

The current alpha taxonomy of the rare akodontine *Bibimys*, which includes three species, is mostly based on subtle cranial and genetic differences (D'Elía *et al*., 2005; Gonçalves *et al*., 2005; Pardiñas *et al*., 2015a). The Brazilian samples are traditionally referred to *B*. *labiosus* (see Grazzini *et al*., 2015; Pardiñas *et al*., 2015a), but the populations from the grasslands of southern Misiones Province (Argentina), not far from SLS, are referred to *B*. *chacoensis* (Pardiñas *et al*., 2017a). The SLS record enlarges the known distribution of this genus by about 450 km to the south in Brazil, but its specific assignment needs to be strengthened; again, the possibility to extract DNA from owl pellet material seems a plausible way to do that. In addition, since SLS is about 200 km from the Uruguayan border, a future record of *Bibimys* in that country is not unlikely, taking into account the environmental continuity between southernmost RS and the Cerro Largo department (Brazeiro *et al*., 2008).

Semi-deciduous Seasonal Forests in the Brazilian Pampa: small mammal biogeography

The SLS small mammal assemblage as revealed by the owl pellet samples studied here is composed of a mixture of species with different ecological affinities. The perceptible dominance of *Oligoryzomys* (possibly including *O*. *flavescens* and *O*. *nigripes*) reflects disturbed environments, since this genus includes opportunistic invasive species in cleared areas of the Atlantic Forest (Fonseca & Kierluff, 1989; Pardini & Umetsu, 2006; Melo *et al*., 2011). The moderate abundance of *Calomys* (possibly including *C*. *laucha* and *C*. *tener*), typically a grassland phyllotine, seems in line with the extensive implementation of agroecosystems (Bilenca *et al*., 1992; Courtalon *et al*., 2003; Castellarini *et al*., 2011). The occurrence of Pampean and high-elevation grassland elements, such as *Akodon azarae* and *Oxymycterus nasutus* (Bilenca *et al*., 1992; Paise & Vieira, 2006; Sponchiado *et al*., 2012; Oliveira & Gonçalves, 2015), reinforces the notion that these species are intruders favored by forest clearance. However, a small group of primarily sylvan (*e.g*., *Gracilinanus microtarsus*, *Juliomys* sp., *Sooretamys angouya*) or scrub and perisylvan grass-associated (*e.g*., *Bibimys* sp., *Wilfredomys oenax*) species (Pardini & Umetsu, 2006; González *et al*., 2015) probably represent the original core of the SLS assemblage. Fragmented populations of these mammals surely survive favored by gallery forests which normally bordered watercourses coupled with occasional patches of forest and scattered trees that covered the top of the hills. Clearly, these marsupials and rodents are penetrating into the area from more densely forested areas in the northeastern part of RS, and some of them reach their southernmost occurrences in or close to SLS (*Juliomys*, *Nectomys*, *Sooretamys*).

The SLS small mammal assemblage reflects a biogeographical mixture. Hershkovitz (1958), in his seminal contribution exploring mammal units within the Neotropics, crossed southernmost RS with the limit between Brazilian (to the east) and Patagonian (to the west) subregions. In a more focused geographical approach, González (2000) argued for the displacement of this boundary to the south, dissecting Uruguay centrally. The latter author also recognized an assemblage of Platan mammals (alluding to the Río de la Plata fluvial system), in which he included several of the rodents recorded in SLS, such as *A*. *azarae*, *Lundomys*, and *Wilfredomys* (González, 2000:fig. 1). In this context, the SLS assemblage could be interpreted as a mixed fauna composed of Pampean and Platan elements interpenetrated by Atlantic Forest invasive species. One of the most comprehensives studies to explore the biogeography of the Atlantic Forest was conducted by Pires *et al*. (2000) based on a cladistic analysis of the distribution of marsupials, rodents, and primates. According to

their results, the southern portion of this biome is retrieved in a polytomy, revealing a poor community structure in sharp contrast to the central and northern portions. These findings suggest that these regions, where SLS and the Semi-deciduous Seasonal Forest of southwestern RS are included, support mixed ecotonal micromammal assemblages mostly infiltrated by those Atlantic Forest elements with greater ecological lability. Corroborating this, *Juliomys* sp., *Nectomys squamipes,* and *Sooretamys angouya*, and perhaps *Akodon montensis*, were recorded in SLS. *Juliomys* and *Sooretamys* were genera hitherto considered endemic to the Atlantic Forest Biome (Paglia *et al*., 2012), while *N*. *squamipes*, a semiaquatic rodent, is strongly associated with this biome and the adjacent Cerrado gallery forests (Bonvicino & Weksler 2015). *Akodon montensis* has a wider distribution, from eastern Paraguay and northeastern Argentina to the coast of Brazil (Pardiñas *et al*., 2015b), but has been associated with a closed and dense microhabitat (*e.g*., a higher percentage of canopy cover or abundance of bamboo) in the Brazilian Atlantic Forest Biome (Geise *et al*., 2004; Dalmagro & Vieira, 2005; Lima *et al*., 2010). Thus, the southeastern extension of the range of these species, penetrating into the Pampa Biome, is due to presence of the Semi-deciduous Seasonal Forest at high latitudes. A similar pattern was reported by Lima *et al*. (2010), who recorded *A*. *montensis*, *Juliomys* sp., and *S*. *angouya* in a deciduous forest area on the austral boundary of the Atlantic Forest in central RS.

Rapid inventories in human-changing ecosystems: owl pellet value

Several studies have stressed the importance of owl pellet analysis in small mammal surveys (*e.g*., Bonvicino & Bezerra, 2003; Formoso *et al*., 2016; Mancini *et al*., 2018), and this was also corroborated by the present work. The data obtained in SLS reveal a rich small mammal community occurring in a forested portion of the Pampa Biome in Southern Brazil, including at least 17 taxa of non-volant small mammals and two chiropterans. This is the richest owl pellet sample studied in RS to date (Cherem *et al*., 2018, 10 taxa; González *et al*., 1999, 11 taxa; Peters *et al*., 2010, 13 taxa; Scheibler & Christoff 2007, 16 taxa), and one of the richest reported in South America (*e.g*., Baglan & Catzeflis, 2016, 12 species in coastal savannas in French Guiana; Fernández *et al*., 2012, 13 species in Quiñihual, Argentinean Pampa; Massoia *et al*., 1990, 14 species in Desaguadero, Argentinean wetlands; Brito *et al*., 2015, 14 species in Los Santiagos, Ecuador; Bonvicino & Bezerra 2003, 16 species in Brazilian Cerrado; Lemos *et al*., 2015, 17 species in coastal Rio de Janeiro, Brazil; Mancini *et al*., 2018, 26 species in caves of the Caatinga, Northeastern Brazil).

Therefore, we highly recommend the analysis of owl pellet samples as an efficient, non-invasive and low-cost method to record small mammals in vast and poorly known Neotropical territories. Despite the material being fragmentary, it is possible to achieve great taxonomic resolution through comparison with specimens housed in scientific collections and the literature. Furthermore, molecular analysis could also be used to elucidate the taxonomic identity of several taxa with poorly resolved taxonomies (Buś *et al*., 2014; Rocha *et al*., 2015). An increase in morphological studies is desirable to help in the identification of the material retrieved from owl pellets.

Acknowledgements

We would like to thank João Pedro Hammes, José Carlos Dilli, Edla da Silva, Gilberto Griep, Renato Schmafiss, Daniele Radtke, Laercio Timm, and Guilherme Renato Schinid for the access to the sampling sites, and, particularly, Carmem Milbrath, for all the support during the fieldwork. We also thank Vitor Zimmermann for the map elaboration; the Laboratório Multiusuário de Estudos em Biologia (LAMEB-UFSC) for the photos; Katarzyna Piper for the English review; and the two anonymous reviewers for their valuable suggestions.

Funding

Financial support for this study was given by the Conselho Nacional de Desenvolvimento Científico e Tecnológico, Brazil (CNPq 444508/2014-7) (PH), and the Agencia Nacional de Promoción Científica y Tecnológica, Argentina (PICT 2014, #1039) (UFJP).

References

Avila-Pires, F.D. 1994. Mamíferos descritos do Estado do Rio Grande do Sul, Brasil. *Revista Brasileira de Zoologia,* 54(3): 367–384.

Baglan, A. & Catzeflis, F. 2016. Barn owl pellets collected in coastal savannas yield two additional species of small mammals for French Guiana. *Mammalia,* 80(1): 91–95.

Barquez, R.M.; Mares, M.A.; Braun, J.K. 1999. *The bats of Argentina*. Special Publications, Museum of Texas Tech University, Lubbock.

Beisaw, A.M. 2013. *Identifying and interpreting animal bones: a manual.* Texas A&M University Press, College Station.

Belton, W. 1984. Birds of Rio Grande do Sul, Brazil. Part 1. Rheidae through Furnariidae. *Bulletin of the American Museum of Natural History,* 178: 369–636.

Bilenca, D.N.; Kravetz, F.O. & Zuleta, G.A. 1992. Food habits of *Akodon azarae* and *Calomys laucha* (Cricetidae, Rodentia) in agroecosystems of central Argentina. *Mammalia,* 56(3): 371–383.

Bonvicino, C.R. & Bezerra, A.M.R. 2003. Use of regurgitated pellets of barn owl (*Tyto alba*) for inventorying small mammals in the Cerrado of Central Brazil. *Studies on Neotropical Fauna and Environment,* 38(1): 1–5.

Bonvicino, C.R. & Weksler, M. 2015. Genus *Nectomys* Peters, 1861. *In:* Patton, J.L.; Pardiñas, U.F.J. & D'Elía, G. (Eds). *Mammals of South America. Vol. 2.* The University of Chicago Press, Chicago, p. 369–377.

Boroni, N.L.; Pardiñas, U.F.J. & Lessa G. 2015. *Oligoryzomys fornesi* (Massoia, 1973), Mammalia, Rodentia, Sigmodontinae: distribution extension. *Boletim do Museu de Biologia Mello Leitão,* 37(3): 301–311.

Brandão, M.V. 2015. The occurrence of *Wilfredomys oenax* (Rodentia: Cricetidae: Sigmodontinae) in São Paulo State, southeastern Brazil: a locally extinct species? *Papeis Avulsos de Zoologia,* 55(4): 69–80.

Brandão, M.V. & Fegies, A.C. 2017. Range extension of *Lundomys molitor* (Winge, 1887) (Mammalia: Rodentia: Cricetidae) to eastern Rio Grande do Sul state, Brazil. *Check List,* 13(2): 2101.

Brazeiro, A.; Achkar, M.; Canavero, A.; Fagúndez, C.; González, E.; Grela, I.; Lezama, F.; Ma-neyro, R.; Barthesagy, L.; Camargo, A.; Carreira, S.; Costa, B.; Núñez, D.; da Rosa, I. & Toranza, C. 2008. *Prioridades Geográficas para la Conservación de la Biodiversidad Terrestre de Uruguay.* Resumen Ejecutivo. Proyecto PDT 32-26.

Brito, J.M.; Orellana-Vásquez, H.; Cadena-Ortiz, H.; Vargas, R.; Pozo-Zamora, G.M. & Curay, J. 2015. Mamíferos pequeños en la dieta de la lechuza *Tyto alba* (Strigiformes: Tytonidae) en dos localidades del occidente de Ecuador, con ampliación distribucional de *Ichthyomys hydrobates* (Rodentia: Cricetidae). *Papeis Avulsos de Zoologia,* 55(19): 261–268.

Buś, M.M.; Żmihorski, M.; Romanowski, J.; Balčiauskienė, L.; Cichocki, J. & Balčiauskas, L. 2014. High efficiency protocol of DNA extraction from *Micromys minutus* mandibles from owl pellets: a tool for molecular research of cryptic mammal species. *Acta Theriologica,* 59(1): 99–109.

Castellarini, F.; Dellafiore, C. & Polop, J. 2003. Feeding habits of small mammals in agroecosystems of central Argentina. *Mammalian biology,* 68(2): 91–101.

Cherem, J.J.; Hadler, P.; Stutz, N.S. & Pardiñas, U.F.J. 2018. Pequenos mamíferos (Didelphimorphia, Chiroptera e Rodentia) em egagropilos de *Tyto furcata* (coruja-das-igrejas) (Aves, Tytonidae) do sul do Brasil. *Biotemas,* 31(3): 43–58.

Christoff, A.U.; Vieira, E.M.; Oliveira, L.R.; Gonçalves, J.W.; Valiati, V.H. & Tomasi, P.S. 2016. A new species of *Juliomys* (Rodentia, Cricetidae, Sigmodontinae) from the Atlantic Forest of Southern Brazil. *Journal of Mammalogy,* 97(5): 1469–1482.

Cordeiro, J.L.P. & Hasenack, H. 2009. Cobertura vegetal atual do Rio Grande do Sul. *In:* Pillar, V.D.; Müller, S.C.; Castilhos, Z.M.S. & Jacques, A.V.A. (Eds). *Campos Sulinos - conservação e uso sustentável da biodiversidade.* Ministério do Meio Ambiente, Brasília, p. 285–299.

Courtalon, P.; Dolcemascolo, A.; Troiano, V.; Álvarez, M.R. & Busch, M. 2003. Inter and intraspecific relationships in *Akodon azarae* and *Calomys laucha* (Rodentia, Sigmodontinae) in pampean agroecosystems. *Mastozoología Neotropical,* 10(1): 27–39.

Dalmagro, A.D. & Vieira, E.M. 2005. Patterns of habitat utilization of small rodents in an area of Araucaria forest in Southern Brazil. *Austral Ecology,* 30(4): 353–362.

D'Elía, G.; Hanson, D.; Mauldin, M.; Teta, P. & Pardiñas, U.F.J. 2015. Molecular systematics of the South American marsh rats of the genus *Holochilus* (Muroidea, Cricetidae, Sigmodontinae). *Journal of Mammalogy,* 96(5): 1081–1094.

Fernández, F.J.; Idoeta, F.; Esponda, C.G.; Carrera, J.D.; Ballejo, F.; De Santis, L.J.M. & Moreira, G.J. 2012. Small mammals (Didelphimorphia, Rodentia and Chiroptera) from pampean region, Argentina. *Check List,* 8(1): 130–134.

Fonseca, G.A.B. & Kierulff, M.C.M. 1989. Biology and natural history of Brazilian Atlantic Forest small mammals. *Bulletin of the Florida State Museum, Biological Sciences,* 34(3): 99–152.

Formoso, A.; Teta, P.; Carbajo, A. & Pardiñas, U.F.J. 2016. Unraveling the patterns of small mammal species richness in the southernmost aridlands of South America. *Journal of Arid Environments,* 134: 136–144.

Gardner, A.L. (Ed). 2008. *Mammals of South America. Vol 1.* University of Chicago Press, Chicago.

Geise, L.; Pereira, L.G.; Bossi, D.E.P. & Bergallo, H.G. 2004. Pattern of elevational distribution and richness of nonvolant mammals in Itatiaia National Park and its surroundings, in southeastern Brazil. *Brazilian Journal of Biology,* 64(3B): 599–612.

Gonçalves, P.R.; Myers, P.; Vilela, J.F. & Oliveira, J.A. 2007. Systematics of species of the genus *Akodon* (Rodentia: Sigmodontinae) in Southeastern Brazil and implications for the biogeography of the campos de altitude. *Miscellaneous Publications, Museum of Zoology, University of Michigan,* 197: 1–24.

Gonçalves, P.R.; Oliveira, J.A.; Corrêa, M.O. & Pessôa, L.M. 2005. Morphological and cytogenetic analyses of *Bibimys labiosus* (Winge, 1887) (Rodentia, Sigmodontinae): implications for its affinities with the Scapteromyine group. *In:* Lacey, E.A. & Myers, P. (Eds). *Mammalian diversifcation: from chromosomes to phylogeography to phylogeography.* University of California Press, Berkeley, p. 175–210.

González, E.M. 2000. Lista sistemática, afinidades biogeográficas, hábitos y hábitats de los mamíferos terrestres autóctonos de Uruguay (Mammalia): una introducción. *In: Jornadas sobre animales silvestres, desarollo sustentable y medio ambiente.* Comisión Ambientalista, Facultad de Veterinaria, Montevideo, p. 58–73.

González, E.M.; Claramunt, S.J. & Saralegui, A.M. 1999. Mamíferos hallados en egagrópilas de *Tyto alba* (Aves, Strigiformes, Tytonidae) en Bagé, Rio Grande do Sul, Brasil. *Iheringia, Série Zoologia,* 86: 117–120.

González, E.M.; Oliveira, J.A. & Pardiñas U.F.J. 2015. Genus *Wilfredomys* Avila-Pires, 1960. *In:* Patton, J.L.; Pardiñas, U.F.J. & D'Elía, G. (Eds). *Mammals of South America. Vol. 2.* The University of Chicago Press, Chicago, p. 105–107.

González-Ittig, R.E.; Narayan, P.K.; Bonvicino, C.R. & Salazar-Bravo, J. 2019. Does the widely distributed rodent *Calomys tener* (Cricetidae: Sigmodontinae) constitute a single evolutionary unit? *Zoologia*, 36: e30354.

Grazzini, G.; Rezini, J.A.; Boraschi dos Santos, B.S.; Venâncio, F.J., Gatto-Almeida, F.; Sbalqueiro, I.J.; Hass, I. & Tiepolo, L.M. 2015. *Bibimys labiosus* Winge, 1887 (Mammalia: Rodentia: Sigmodontinae): new records in Paraná state, southern Brazil, and update of the known geographic distribution. *Check List,* 11(3): 1632.

Haag, T.; Muschner, V.C.; Freitas, L.B.; Oliveira, L.F.B.; Langguth, A.R.; Mattevi, M.S. 2007. Phylogenetic relationships among species of the genus *Calomys* with emphasis on South American lowland taxa. *Journal of Mammalogy,* 88(3): 769–776.

Hadler, P.; Cherem, J.J.; Turbay, R.; Alberti, A. & Pardiñas, U.F.J. 2016. Diversidade de pequenos mamíferos (Didelphimorphia e Rodentia) do Holoceno do nordeste do estado do Rio Grande do Sul, Brasil: implicações taxonômicas e paleoambientais. *Revista Brasileira de Paleontologia,* 19(1): 127–144.

Heisler, L.M.; Somers, C.M. & Poulin, R.G. 2016. Owl pellets: a more effective alternative to conventional trapping for broad-scale studies of small mammal communities. *Methods in Ecology and Evolution,* 7(1): 96–103.

Hershkovitz, P. 1955. South American marsh rats, genus *Holochilus*, with a summary of sigmodont rodents. *Fieldiana Zoology,* 37(24): 639–673.

Hershkovitz, P. 1958. A geographic classification of neotropical mammals. *Fieldiana Zoology*, 36(6): 1–646.

Hershkovitz, P. 1990. Mice of the *Akodon boliviensis* size class (Sigmodontinae, Cricetidae), with the description of two new species from Brazil. *Fieldiana Zoology,* 57: 1–35.

IBGE. 1978. Mapa de clima do Brasil. Available at https://www.ibge.gov.br/geociencias/informacoes-ambientais/climatologia/15817-clima.html?=&t=downloads. Acess in 05/01/2020.

IBGE. 2004a. Mapa de biomas do Brasil. Available at ftp://ftp.ibge.gov.br/Cartas_e_Mapas/Mapas_Murais/. Access in 12/11/2018.

IBGE. 2004b. Mapa de vegetação do Brasil. Available at ftp://geoftp.ibge.gov.br/informacoes_ambientais/vegetacao/mapas/brasil/vegetacao.pdf. Access in 07/24/2019.

ICMBio. 2018. *Livro vermelho da fauna brasileira ameaçada de extinção. Vol. II – Mamíferos*. ICMBio/MMA, Brasília.

IUCN. 2019. The IUCN Red List of Threatened Species. Version 2019–1. Available at http://www.iucnredlist.org. Access 03/21/2019.

Langguth, A. 1963. Las especies uruguayas del genero *Oryzomys* (Rodentia, Cricetidae). *Comunicaciones Zoológicas del Museo de Historia Natural de Montevideo,* 7: 1–19.

Leite, P.F. 2002. Contribuição ao conhecimento fitoecológico do sul do Brasil. *Ciência e Ambiente,* 24: 51–73.

Lemos, H.M.; Silva, C.A.O.; Patiu, F.M. & Gonçalves, P.R. 2015. Barn owl pellets (Aves: *Tyto furcata*) reveal a higher mammalian richness in the Restinga de Jurubatiba National Park, Southeastern Brazil. *Biota Neotropica,* 15(2): e20140121.

Lima, D.O.; Azambuja, B.O.; Camilotti, V.L. & Cáceres, N.C. 2010. Small mammal community structure and microhabitat use in the austral boundary of the Atlantic Forest, Brazil. *Zoologia,* 27(1): 99–105.

Luza, A.L.; Gonçalves, G.L.; Pillar, V.D. & Hartz, S.M. 2016. Processes related to habitat selection, diversity and niche similarity in assemblages of non-volant small mammals at grassland–forest ecotones. *Natureza e Conservação,* 14(2): 88–98.

Machado, F.S.; Lima, I.J.; Lopes, A.P.M.; Moura, A.S. & Abreu, T.C.K. 2016. New occurrences and biological aspects to four species of rodents (Mammalia: Cricetidae) from Brazil. *Revista Agrogeoambiental,* 8(2): 35–51.

Machado, L.F.; Paresque, R. & Christoff, A.U. 2011. Anatomia comparada e morfometria de *Oligoryzomys nigripes* e *O*. *flavescens* (Rodentia, Sigmodontinae) no Rio Grande do Sul, Brasil. *Papeis Avulsos de Zoologia,* 51(3): 29–47.

Machado, L.F.; Passaia, M.H; Rodrigues, F.P.; Peters, F.B.; Sponchiado, J.; Valiati, V.H. & Christoff, A.U. 2015. Molecular phylogenetic position of endangered *Wilfredomys* within Sigmodontinae (Cricetidae) based on mitochondrial and nuclear DNA sequences and comments on Wiedomyini. *Zootaxa,* 3986(4): 421–434.

Mancini, M.C.S.; Roth, P.R.O.; Brennand, P.G.G.; Aguilar, J.M.R.E. & Rocha, P.A. 2018. *Tyto furcata* (Tytonidae: Strigiformes) pellets: tools to access the richness of small mammals of a poorly known Caatinga area in northeast Brazil. *Mammalia,* 83(4): 390–398.

Massoia, E.; Chébez, J.C. & Fortabat, S.H. 1990. Mamíferos depredados por *Tyto alba* tuidara en Desaguadero, departamento capital, provincia de Corrientes. *Boletín Científico APRONA,* 18: 14–17.

Meek, W.R.; Burman, P.J.; Sparks, T.H.; Nowakowski, M. & Burman, N.J. 2012. The use of barn owl *Tyto alba* pellets to assess population change in small mammals. *Bird Study,* 59(2): 66–174.

Melo, G.; Sponchiado, J.; Machado, A. & Cáceres, N. 2011. Small-mammal community structure in a South American deciduous Atlantic Forest. *Community Ecology,* 12(1): 58–66.

MMA. 1992. Shapefile do mapa de vegetação do Brasil. Available at http://mapas.mma.gov.br/i3geo/datadowload.htm. Access in 04/17/2018.

Morrone, J.J. 2001. *Biogeografia de América Latina y el Caribe.* M&T–Manuales & Tesis SEA, Vol. 3, Zaragoza.

Oliveira, J.A. & Gonçalves, P.R. 2015. Genus *Oxymycterus* Waterhouse, 1837. *In:* Patton, J.L.; Pardiñas, U.F.J. & D'Elía, G. (Eds). *Mammals of South America. Vol. 2.* The University of Chicago Press, Chicago, p. 247–268.

Overbeck, G.E.; Vélez-Matin, E.; Scarano, F.R.; Lewinsohn, T.M.; Fonseca, C.R.; Meyer, S.T.; Müller, S.C.; Ceotto, P.; Dadalt, L.; Durigan, G. *et al*. 2015. Conservation in Brazil needs to include non-forest ecosystems. *Diversity and Distributions,* 21: 1455–1460.

Paglia, A.P.; Fonseca, G.A.B.; Rylands, A.B.; Herrmann, G.; Aguiar, L.M.S.; Chiarello, A.G.; Leite Y.L.R.; Costa, L.P.; Siciliano, S.; Kierulff, M.C.M.; *et al*. 2012. *Annotated Checklist of Brazilian Mammals. 2nd ed.* Occasional Papers in Conservation Biology. No 6. Conservation International, Arlington.

Paise, G. & Vieira, E.M. 2006. Daily activity of a Neotropical rodent (*Oxymycterus nasutus*): seasonal changes and influence of environmental factor. *Journal of Mammalogy,* 87(4): 733–739.

Pardiñas, U.F.J. & Teta, P. 2011. Fossil history of the marsh rats of the genus *Holochilus* and *Lundomys* (Cricetidae, Sigmodontinae) in southern South America. *Estudios Geológicos,* 67(1): 111–129.

Pardiñas, U.F.J. & Teta, P. 2013. Taxonomic status of *Mus talpinus* Lund (Rodentia: Sigmodontinae) from the Quaternary deposits of Lagoa Santa, Minas Gerais, Brazil and its paleoenvironmental meaning. *Mammalia,* 77(3): 347–355.

Pardiñas, U.F.J.; D'Elía, G. & Teta, P. 2015. Genus *Bibimys* Massoia, 1979. *In:* Patton, J.L.; Pardiñas, U.F.J. & D'Elía, G. (Eds). *Mammals of South America. Vol. 2.* The University of Chicago Press, Chicago, p. 204–208.

Pardiñas, U.F.J.; Teta, P. & Forbatat, S.H. 2005. Vertebrate prey of the barn owl (*Tyto alba*) in subtropical wetlands of northeastern Argentina and eastern Paraguay. *Journal of Raptor Research,* 39(1): 65–69.

Pardiñas, U.F.J.; Voglino, D. & Galliari, C.A. 2017a. Miscellany on *Bibimys* (Rodentia, Sigmodontinae), a unique akodontine cricetid. *Mastozoología Neotropical,* 24(1): 241–250.

Pardiñas, U.F.J.; Teta, P.; D'Elía, G. & Galliari, C. 2008. Rediscovery of *Juliomys pictipes* (Rodentia: Cricetidae) in Argentina: emended diagnosis, geographic distribution, and insights on genetic structure. *Zootaxa,* 1758: 29–44.

Pardiñas, U.F.J.; Teta, P.; Voglino, D. & Fernández, F.J. 2013. Enlarging rodent diversity in west-central Argentina: a new species of the genus *Holochilus* (Cricetidae, Sigmodontinae). *Journal of Mammalogy,* 94(1): 231–240.

Pardiñas, U.F.J.; Teta, P.; Alvarado-Serrano, D.; Geise, L.; Jayat, J.P.; Ortiz, P.E.; Gonçalves, P.R. & D'Elía, G. 2015. Genus *Akodon* Meyen, 1833. *In:* Patton, J.L.;

Pardiñas, U.F.J. & D'Elía, G. (Eds). *Mammals of South America. Vol. 2.* The University of Chicago Press, Chicago, p. 144–204.

Pardiñas, U.F.J.; Myers, P.; León-Paniagua, L.; Garza, N.O.; Cook, J.; Kryštufek, B.; Haslauer, R.; Bradley, R.; Shenbrot, G. & Patton, J.L. 2017b. Family Cricetidae. *In:* Wilson, D.E.; Lacher, T.E. & Mittermeier, R.A. (Eds). *Handbook of the mammals of the world. Vol. 7, Rodents II.* Lynx Edicions, Barcelona, p. 204–279.

Pardini, R. & Umetsu, F. 2006. Pequenos mamíferos não-voadores da Reserva Florestal do Morro Grande – distribuição das espécies e da diversidade em uma área de Mata Atlântica. *Biota Neotropica*, 6(2): 1–22.

Patton, J.L.; Pardinãs, U.F.J. & D'Elía, G. (Eds). 2015. *Mammals of South America. Vol. 2.* University of Chicago Press, Chicago.

Pavan, S.E. & Leite, Y.L.R. 2011. Morphological diagnosis and geographic distribution of Atlantic Forest red-rumped mice of the genus *Juliomys* (Rodentia: Sigmodontinae). *Zoologia,* 28(5): 663–672.

Peters, F.B.; Roth, P.R.O.; Machado, L.F.; Coelho, E.L.; Jung, D.M.H. & Christoff, A.U. 2010. Assembléia de mamíferos dos agroecossistemas constituintes da bacia hidrográfica do rio da Várzea, Rio Grande do Sul. *Biotemas,* 23(4): 91–107.

Pine, R.H. 1980. Notes on rodents of the genera *Wiedomys* and *Thomasomys* (including Wilfredomys). *Mammalia,* 44(2): 195–202.

Pires, L.; Leite, Y.L.R.; Fonseca, G. & Tavares de Fonseca, M. 2000. Biogeography of South American Forest Mammals: endemism and diversity in the Atlantic Forest. *Biotropica,* 32(4): 872–881.

Quintela, F.M.; Silveira, E.C.; Dellagnese, D.G. & Cademartori, C.V. 2014. *Calomys tener* (Winge, 1887) (Rodentia: Cricetidae: Sigmodontinae): Filling gaps. *Check List,* 10(3): 650–654.

Rio Grande do Sul. 2013. Portaria SEMA Nº 79, de 31 de outubro de 2013. Available at https://www.legisweb.com.br/legislacao/?id=261368. Access in 07/18/2017.

Rio Grande do Sul. 2014. Decreto Nº 51.797, de 8 de setembro de 2014. Diário Oficial.

Rocha, R.G.; Justino, J.; Leite, Y.L.R.; Fonseca, C. & Costa, L.P. 2015. DNA from owl pellet bones uncovers hidden biodiversity. *Systematics and Biodiversity,* 13(4): 403–412.

Salazar-Bravo, J. 2015. Genus *Calomys* Waterhouse, 1837. *In:* Patton, J.L.; Pardiñas, U.F.J. & D'Elía, G. (Eds). *Mammals of South America. Vol. 2.* The University of Chicago Press, Chicago, p. 481–507.

Scheibler, D.R. & Christoff, A.U. 2007. Habitat associations of small mammals in southern Brazil and use of regurgitated pellets of birds of prey for inventorying a local fauna. *Brazilian Journal of Biology,* 67(4): 619–625.

Silveira, E.C.; Cadermatori, C.V. & Kautzmann, R.M. 2011. Avaliação de indicadores ambientais em área úmida na APA do Banhado Grande, Viamão, RS, para uso em processos de mitigação e restauração ambiental. *In: Anais do III Congresso Brasileiro de Carvão Mineral, 2011*. Universidade Federal do Rio Grande do Sul, Porto Alegre.

Sponchiado, J.; Melo, G.L. & Cáceres, N.C. 2012. Habitat selection by small mammals in Brazilian Pampas biome. *Journal of Natural History,* 46(21-22): 1321–1335.

Stutz, N.S.; Cherem, J.J.; Pardiñas, U.F.J. & Hadler, P. 2017. Roedores sigmodontíneos (Mammalia, Rodentia, Cricetidae) holocênicos do Rio Grande do Sul, Brasil – O sítio RS-TQ-58: Afonso Garivaldino Rodrigues. *Revista Brasileira de Paleontologia,* 20(1): 133–148.

Stutz, N.S.; Hadler, P.; Cherem, J.J.; Fernández, F.J.; Pardiñas, U.F.J. & Ribeiro, A.M. 2018. Noteworthy sigmodontine (Rodentia: Cricetidae) diversity in southern Brazil as an indication of environmental change during the Holocene. *Historical Biology,* aop.

Taylor, I. 1994. *Barn Owls*. University Press, Cambridge.

Teta, P.; González-Fischer, C.M.; Codesido, M. & Bilenca, D.N. 2010. A contribution from barn owl pellets analysis to known micromammalian distributions in Buenos Aires province, Argentina. *Mammalia,* 74(1): 97–103.

Thomas, O. 1928. A new *Thomasomys* from Rio Grande do Sul. *Annals & Magazine of Natural History,* 10(2): 409–410.

Torre, I.; Arrizabalaga, A. & Carles, F. 2004. Three methods for assessing richness and composition of small mammal communities. *Journal of Mammalogy,* 85(3): 524–530.

Vaz Ferreira, R. 1960. Nota sobre Cricetinae del Uruguay. *Archivos de la Sociedad de Biología de Montevideo,* 24: 66–75.

Voss, R.S. 2015. Genus *Lundomys* Voss and Carleton, 1993. *In:* Patton, J.L.; Pardiñas, U.F.J. & D'Elía, G. (Eds). *Mammals of South America. Vol. 2.* The University of Chicago Press, Chicago, p. 346–348.

Voss, R.S. & Carleton, M.D. 1993. A new genus for *Hesperomys molitor* Winge and Holochilus magnus Hershkovitz (Rodentia; Muridea) with an analysis of its phylogenetic relationships. *American Museum Novitates,* 3085: 1–39.

Wilson, D.E. & Reeder, D.M. (Eds). 2005. *Mammal species of the world: a taxonomic and geographic reference. 3rd ed*. The Johns Hopkins University Press, Baltimore.

Appendix 1

List of the specimens deposited in the Coleção de Mamíferos do Departamento de Ecologia e Zoologia da Universidade Federal de Santa Catarina (UFSC) which were used for comparison with the SLS owl pellet specimens:

Cryptonanus guahybae: UFSC 4465, 4589, 4854, 5197, 5234, 5434. *Gracilinanus microtarsus*: UFSC 3851, 4857, 5951, 5893. *Marmosa paraguayana*: UFSC 4048, 4374. *Monodelphis dimidiata*: UFSC 3778, 4823, 4861, 5740. *Monodelphis iheringi*: UFSC 3797, 4585, 4607, 5436. *Monodelphis scalops*: UFSC 3780, 3915, 4056. *Akodon montensis*: UFSC 222, 288. *Akodon paranaensis*: UFSC 3628, 3631. *Brucepattersonius iheringi*: UFSC 3425, 4925. *Brucepattersonius soricinus*: UFSC 4692, 4810. *Calomys tener*: UFSC 5166, 5490. *Euryoryzomys russatus*: UFSC 4960, 4961. *Juliomys ossitenuis*: UFSC 950, 4812. *Juliomys pictipes*: UFSC 2960, 2963. *Necromys lasiurus*: UFSC 3599, 3600, 3876, 4714. *Nectomys squamipes*: UFSC 5078, 5494. *Oligoryzomys flavescens*: UFSC 3643, 4400, 4548, 4694. *Oligoryzomys nigripes*: UFSC 498, 501, 3638, 4544. *Oxymycterus dasythrichus*: UFSC 2084, 2085, 2086. *Oxymycterus nasutus*: UFSC 955, 5892, 5934. *Oxymycterus quaestor*: UFSC 4817, 5645, 5787. *Scapteromys meridionalis*: UFSC 2662, 2671, 3597, 3819. *Sooretamys angouya*: UFSC 5927, 6031. *Rattus norvegicus*: UFSC 428, 5456. *Rattus rattus*: UFSC 5565, 5749.

4.3 EOCENE CAVIOMORPH RODENTS FROM BALSAYACU (PERUVIAN AMAZONIA)

Artigo publicado no periódico *Palaeontologische Zeitschrift*, volume 96, p. 135–160, 2022, DOI:10.1007/s12542-021-00551-0.

Myriam Boivin[1], Laurent Marivaux[2], Walter Aguirre-Diaz[3], Michele Andriolli Custódio[4,5,6], Aldo Benites-Palomino[3,7], François Pujos[8], Martin Roddaz[5,6], Rodolfo Salas-Gismondi[3,9], **Narla Stutz[2,10]**, Julia V. Tejada-Lara[2,3], Johan Yans[11], Pierre-Olivier Antoine[2]

[1]Instituto de Ecorregiones Andinas (INECOA), Universidad Nacional de Jujuy, CONICET, IdGyM, Avenida Bolivia 1661, 4600 San Salvador de Jujuy, Jujuy, Argentina.
[2]Laboratoire de Paléontologie, Institut des Sciences de l'Evolution de Montpellier (ISEM, UMR 5554, CNRS/UM/IRD/EPHE), Université de Montpellier, Place Eugène Bataillon, 34095, Montpellier Cedex 5, France.
[3]Departamento de Paleontología de Vertebrados, Museo de Historia Natural, Universidad Nacional Mayor San Marcos (UNMSM, DPV-MUSM), Avenida Arenales 1256, Lima, Lima 14, Peru.
[4]Departamento de Geociências (DEGEO), Universidade Federal do Amazonas (UFAM), Instituto de Ciências Exatas, Avenida Rodrigo Otávio, Japiim, Manaus, Brazil.
[5]Laboratorio de Geocronologia, Instituto de Geociências, Universidade de Brasília, Campus Universitário Darcy Ribeiro ICC, Ala Central, Brasília, 70910-900, Brazil.
[6]Géosciences-Environnement Toulouse (GET), Université de Toulouse, UPS (SVT-OMP), LMTG, CNRS, IRD, 14 Avenue Édouard Belin, 31400, Toulouse, France.
[7]Paläontologisches Institut und Museum, Universität Zürich, Karl-Schmid-Strasse 4, 8006, Zürich, Switzerland
[8]Instituto Argentino de Nivología, Glaciología y Ciencias Ambientales (IANIGLA), CCT–CONICET–Mendoza, Avenida Ruiz Leal s/n, Parque Gral. San Martín, 5500, Mendoza, Argentina
[9]BioGeoCiencias Laboratory, Laboratorios de Investigacion y Desarrollo (LID), Facultad de Ciencias y Filosofía/CIDIS, Centro de Investigación para el Desarrollo Integral y Sostenible (CIDIS), Universidad Peruana Cayetano Heredia, Avenida Honorio Delgado 430, Lima, Lima 31, Peru

[10]Programa de Pós-Graduação em Geociências, Universidade Federal do Rio Grande do Sul, Avenida Bento Gonçalves 9500, Porto Alegre, 91501-970, Brazil
[11]Department of Geology, Institute of Life, Earth and Environment (ILEE), Université of Namur, Rue de Bruxelles 61, 5000, Namur, Belgium

Abstract

The Paleogene record of caviomorph rodents has substantially increased over the last decades, and their evolutionary history better understood by the discovery of their earliest representatives, so far recorded in several pre-Deseadan localities in Peruvian Amazonia. We report here the discovery of new caviomorph fossils from the Balsayacu area in Peru (TAR-55/TAR-55bis, TAR-76 and TAR-77 localities, San Martin Department). The study of this new material reveals the occurrence of four caviomorph taxa in these localities: *Balsayacuy huallagaensis* gen. et sp. nov., *Chachapoyamys kathetos* gen. et sp. nov. and Caviomorpha gen. et sp. indet. 1 and 2. It allows the revision and refinement of taxonomic assignments of previously described specimens. The first three taxa have a primitive dental pattern, as that characterizing stem Caviomorpha recorded in pre-Deseadan localities of Peru (Eocene localities of Contamana and ?late Eocene/early Oligocene Santa Rosa). We support here an Eocene age for the Balsayacu section due to the complete absence of morphologically derived taxa representing modern caviomorph superfamilies. By the presence of derived characters in *Balsayacuy* and *Chachapoyamys* compared to *Canaanimys maquiensis* and *Cachiyacuy contamanensis* from CTA-27 (Contamana, Peru; late middle Eocene), the Balsayacu section may document a time interval slightly younger than CTA-27 (which further yields *Chachapoyamys* cf. *kathetos*) and older than those of Santa Rosa and Tarapoto-Shapaja, likely documenting latest middle or early late Eocene times. These low-latitude stem caviomorph faunas provide new insights into the early evolutionary history and paleodiversity of that group immediately before the rise of modern superfamilies.

Keywords: Rodentia, Systematics, Biostratigraphy, Peru, South America

Introduction

Due to a complex ecological and geological history, Amazonia is one of the regions of the world with the maximum biodiversity of many groups of organisms (Jenkins et al. 2013). Understanding the emergence of such biodiversity raises many questions surrounding its evolution, dynamics, the geographic origin of taxonomic

groups that compose it, and factors that could have constrained and molded it (Stebbins 1974; Hoorn et al. 2010). Paleontological studies are fundamental to understand the evolutionary dynamics of this biodiversity, yet the fossil record of this geographic area had long been elusive. Indeed, owing to the dense vegetation cover, extensive recent alluvial depositions, aggressive alteration and pedogenesis, frequent landslides and seasonal floodings, fossiliferous outcrops are rare and of difficult access most of the time. In addition, field conditions are particularly harsh in such moist and warm climate environment. Since the end of the last century, thanks to field efforts driven by several scientific teams, many mammal-bearing localities were discovered in this region including Santa Rosa (Peru; ?late Eocene/early Oligocene; e.g., Campbell 2004), Cerro Colorado (Peru; late Miocene–Late Pleistocene; Campbell et al. 2000, 2001, 2010), and Acre (Brazil; late Miocene; e.g., Frailey 1986; Campbell et al. 2006; Negri et al. 2010; Kerber et al. 2017). Since 2003, our paleontological surveys in several areas of Peruvian Amazonia (i.e., Bagua, Contamana, Fitzcarrald, Iquitos-Nueva Union, Juanjui, Madre de Dios, and Tarapoto) led to the discovery of numerous fossils providing a better knowledge of the Cenozoic record of many mammalian groups (e.g., Antoine et al. 2007, 2012, 2013, 2016, 2017, in revision; Goillot et al. 2011; Marivaux et al. 2012, 2016a,b, 2020; Bianucci et al. 2013; Pujos et al. 2013; Tejada-Lara et al. 2015; Boivin et al. 2017a, b, 2018a, b, 2019a). The fossil record of caviomorph rodents (Caviomorpha Wood, 1955) significantly increased after these discoveries, and the understanding of their evolutionary history improved, especially for its earliest stages. Indeed, Peruvian Amazonia has yielded the earliest representatives of the group, so far recorded in several pre-Deseadan localities: Contamana (late Middle Eocene [~ 41 Ma]; Antoine et al. 2012; Boivin et al. 2017a, 2019a, b), Balsayacu (late middle Eocene; Assemat et al. 2019), Juanjui (late middle Eocene–early Oligocene; Assemat et al. 2019), Tarapoto-Shapaja (late Eocene–early Oligocene; Boivin et al. 2018a, 2019a, b; Assemat et al. 2019: 723, fig. 7; Antoine et al. in revision), and Santa Rosa (Frailey and Campbell 2004; Arnal et al. 2020). Based on the evolutionary stages of its rodent assemblage (Frailey and Campbell 2004; Arnal et al. 2020), its metatherian fauna (Goin and Candela 2004) and the presence of some primates (Bond et al. 2015), a ?late Eocene age was advocated for the mammal-bearing deposits of Santa Rosa. However, considering the entire mammalian fauna of that locality, and taking into account the fossil data assembled in recent years, notably from (bio)geographically close localities from Peruvian Amazonia, Santa Rosa is most likely earliest Oligocene in age (Shockey et al. 2004; Croft et al. 2008; Vucetich et al.

2010; Antoine et al. 2012, 2017; Kay 2015; De Vries and Seiffert 2017; Assemat et al. 2019; Seiffert et al. 2020).

During our 2018 and 2019 field seasons in Peruvian Amazonia, we returned to the Balsayacu area (San Martin Department, Peru), and collected larger amounts of sediments than previously found in TAR-55 and TAR-55bis fossil- bearing localities. Wet-screening of the sediments has allowed for the recovery of about thirty additional isolated rodent teeth. Additionally, in the same stratigraphic section, about a hundred meters below TAR-55, we discovered two new localities, TAR-76 and TAR-77, the samplings of which have yielded few dental remains of caviomorphs. The primary purpose of this contribution is to: (1) revise the caviomorph fauna from TAR-55 and TAR-55bis (Assemat et al. 2019) in light of the new material, and (2) describe the rodent material from the new localities TAR-76 and TAR-77. The systematic and biostratigraphical implications of these faunas are discussed. This work also includes the description of a new isolated tooth and the revision of two teeth from CTA-27 (Contamana area, Loreto Department, Peru). The study of these caviomorph assemblages, among the oldest known in South America, allows to further our understanding of the early evolutionary history and paleodiversity of the group.

Material and methods

All the caviomorph dental specimens described herein (except MUSM 2785, 2786, and 3943) originate from four localities in the vicinity of the small town of Balsayacu (San Martin Department, Peru; Fig. 1a): TAR-55, TAR-55bis, TAR-76, and TAR-77. These localities plus a fifth locality (TAR-56) belong to the same stratigraphic section along the Huallaga River (Assemat et al. 2019; Fig. 1b, c). This section is assigned to the lower member of the Pozo Formation (“Pozo Sands”; late middle Eocene) based on its fossil content, its stratigraphic position, and its lithological features (Assemat et al. 2019 and see below). TAR-55bis is located 1.5 m above TAR-55 and 121.5 m above TAR-56. TAR-76 and TAR-77 are situated between TAR-56 and TAR-55, TAR-76 is 165 m above TAR-56, and TAR-77 is 195 m above the latter. The fossil-bearing localities of this section consist of poorly-consolidated microconglomerates with limestone nodules, soft pebbles and oxidized plant remains, organized into lenticular channels of decimetric thickness and of fluvial to fluvio-deltaic origin (Fig. 1c).

TAR-55 and TAR-55bis yielded charophytes, fossilized wood, seeds, ostracods, crabs, chondrichthyans, actinopterygians, chelonians, caimanine alligatorids, and

mammals (metatherians and placentals). The biostratigraphic age of the Balsayacu section is supported by its similarity with the top of the fossiliferous sequence of the lower member of the Pozo Formation at Contamana (CTA-27–CTA-29; late middle Eocene; Antoine et al. 2016), notably due to the occurrence at the TAR-55 of the freshwater ray *Potamotrygon ucayalensis* also found at the Contamana sequence, but absent from younger deposits, either at Contamana or at Shapaja (Chabain et al. 2017; Boivin et al. 2018a; Antoine et al. in revision). Moreover, the previous study of its caviomorph fauna revealed taxa close to those of the Eocene localities of Contamana (*Cachiyacuy* and *Canaanimys*; Assemat et al. 2019). Among the rodent taxa previously recorded in TAR-55 and TAR-55bis, none displayed na advanced evolutionary stage of their dental pattern (i.e., oblique loph(-id)s such as the chinchilloid *Eoincamys*) or incisive enamel microstructure (multiserial enamel subtype 2–3), contrary to younger deposits of the region from Juanjui (TAR-49 and TAR-50; Assemat et al. 2019) and Shapaja (Boivin et al. 2018a, 2019a) areas. The biostratigraphic implications of the caviomorph fauna from TAR-55 and TAR-55bis in the context of this present work are discussed in the section 'Age of TAR-55/TAR-55bis, TAR-76 and TAR-77' of the Discussion section. In addition to caviomorph teeth, crab and actinopterygian remains were found in TAR-76 and TAR-77. Finally, TAR-76 also yielded rests of wood, chelonians, metatherians and notungulates.

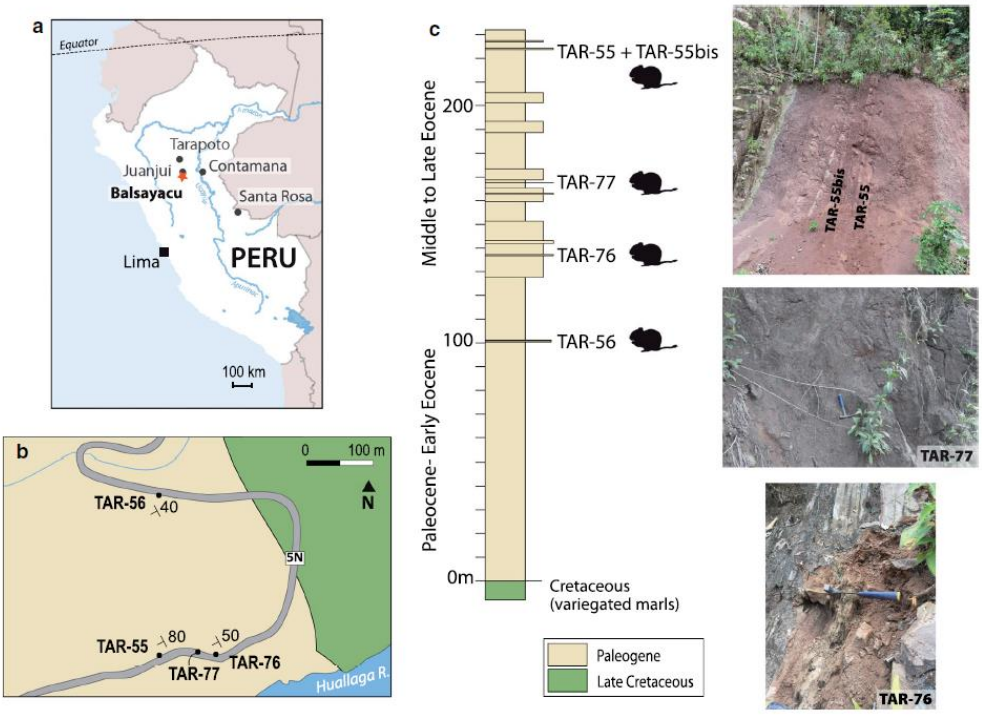


Fig. 1 Geographic location and stratigraphy of TAR-76, TAR-77, TAR-55 and TAR-55bis localities (Balsayacu, Peru; late middle or early late Eocene). **a** General map of

Peru with the Balsayacu area (San Martin Department; star symbol) and the other pre-Deseadan localities yielding caviomorphs in Amazonia (circle symbols): Contamana area (Loreto Department; late middle Eocene; Antoine et al. 2012; Boivin et al. 2017a, b), Juanjui area (late middle Eocene–early Oligocene; Assemat et al. 2019), Tarapoto area (Shapaja section; San Martin Department; late Eocene–early Oligocene; Boivin et al. 2018a, b) and Santa Rosa (Ucayali Department; ?late Eocene/early Oligocene; Frailey and Campbell 2004; Arnal et al. 2020). Scale bar: 100 km. **b** Simplified geological map of the Balsayacu area. Scale bar: 100 m. **c** synthetic stratigraphic section of Balsayacu with the position of the rodent-bearing localities TAR-56, TAR-76, TAR-77, TAR-55 and TAR-55bis, and photos of the last four localities. Modified from Assemat et al. (2019)

Since 2015, the material from TAR-55 and TAR-55bis was collected by excavating and screen-washing (1 mm mesh) a total of 610 kg of sediment. The caviomorph fossils from TAR-55 and TAR-55bis, collected in 2015 and 2016, as a result of the processing of 133 kg of sediments, corresponds to nine isolated teeth, which were previously studied and figured in Assemat et al. (2019). In 2018 and 2019, 465 kg of additional sediments were processed, allowing the discovery of 33 caviomorph teeth. As TAR-55 and TAR-55bis are levels with same geological characteristics, very close in position in the same outcrop, and yielding similar fossil contents, we chose to study the caviomorph material of these localities together. The localities TAR-76 and TAR-77 were discovered in 2019. In total, 75 kg of sediments for TAR-76 and 25 kg for TAR-77 were processed by screen-washing the same year.

The three isolated teeth from Contamana that we are describing/revisiting here (MUSM 2785, 2786, and 3943) come from the CTA-27 locality (late middle Eocene; Antoine et al. 2012, 2016). CTA-27 is located on the northeastern flank of the Maquia Anticline and belongs to the lower member of the Pozo Formation (Antoine et al. 2016). It corresponds to inframetric channelized and unconsolidated sandstones, which include millimetric calcareous nodules of diagenetic origin locally encrusting fossil elements (Antoine et al. 2016). The fossil material from CTA-27 was collected by wet-screening (2 and 1 mm-mesh) during previous field seasons (2008–2010). MUSM 3943 was recently found in unprocessed sediments and thus was neither included in the original description of the fauna (Antoine et al. 2012) nor in its revision (Boivin et al. 2017a). MUSM 2785 and 2786 were attributed to *Cachiyacuy kummeli* by Boivin et

al. (2017a: fig. 4.12, 4.13). We revised here these teeth in light of the new material from Balsayacu.

All teeth described in this contribution are permanently stored in the Vertebrate Paleontological collection of the “Museo de Historia Natural, Universidad Nacional Mayor de San Marcos” (MUSM), Lima, Peru. The terminology for rodent dentition follows Boivin and Marivaux (2020) and the literature cited therein. Uppercase letters are used for Upper dentition (dP, for decidual premolar; P, for premolar; M, for molar) and lowercase letters are used for lower dentition (dp, for decidual premolar; p, for premolar; m, for molar). Working on isolated teeth requires the consideration of distinct levels of morphological variation: i. variation depending on the dental locus; ii. variation owing to the occlusal wear; iii. intraspecific or intrataxonomic variation; and iv. Interspecific or intertaxonomic variation. In this study, several taxa are described. The association of the material attributed to these taxa is based on several points: i. a similar size; ii. a similar proportion of the maximum mesiodistal length and the maximum linguolabial width; iii. a similar occlusal outline; iv. a similar occlusal pattern (taeniodonty/non-taeniodonty; development, position of cusp[-id]s; presence/absence, continuity/discontinuity, length and height of loph[-id]s; absence/presence and intensity of connections between dental structures; and position of the opening of flexi[-ds]); and v. a compatible occlusal pattern between upper and lower teeth. For teeth at advanced stages of wear, we took into account the potential impact of occlusal wear on characters aforementioned. Based on a wide array of closely or distantly related rodent taxa, our comparisons led to preferentially used a size criterion for the recognition of m1s vs m2s and M1s vs M2s: we considered the m1/M1s to be smaller than the m2/M2s. The recognition of other loci is based on the occlusal shape of teeth (for more details, see descriptions in the Systematic Paleontology section) and on the presence of mesial/distal vertical contact facets due to next teeth. The M3s are characterized by a smaller and more labial hypocone with respect to the protocone than on M1–2 s, characters further constraining the occlusal shape. The argumentation for assigning the teeth to either *Balsayacuy huallagaensis* or *Chachapoyamys kathetos*, which are similar in size, is provided in Online Resource 1 (for upper teeth) and 2 (for lower teeth). From a taeniodont to a non-taeniodont condition, two patterns of pseudo-taeniodonty can be recognized on the studied material: i. pattern I: incomplete posterior arm of the protocone/cristulid from the hypolophid-ectolophid junction and/or crestule from the labial protoloph-mure junction/anterior arm of the hypoconid (if both are present, They are disconnected); and ii. pattern II: posterior arm of the protocone/cristulid from the

hypolophid-ectolophid junction and crestule from the labial protoloph-mure junction/anterior arm of the hypoconid linked at their base but not at their top. We restricted our diagnoses and comparisons to the taxa showing a closer morphology. The caviomorph taxa cited in the text and used for comparisons in this study are listed in Table 1. The list of the studied specimens from TAR-55/TAR-55bis, TAR-76 and TAR-77 is available in Table 2, which also includes the measurements made on this material (i.e., maximum mesiodistal length and maximum linguolabial width). For the material from TAR-55/TAR-55bis collected in 2015–2016, we used the measurements made by A. Assemat with a measuroscope Nikon 10 (Assemat et al. 2019). The rest of material was measured by M. Boivin from photos (SEM and optical) using Adobe Photoshop CS4 (2008 Adobe Systems Incorporated). We used Adobe Illustrator CS4 (2008 Adobe Systems Incorporated) and Inkscape 0.92.4 (2020) to design the figures.

Institutional abbreviations. LACM, Los Angeles County Museum, Los Angeles, USA; MUSM, Museo de Historia Natural de la Universidad Nacional Mayor San Marcos, Lima, Peru.

Other abbreviations. max length, maximum mesiodistal length; max width, maximum labiolingual width; SALMA, South American Land Mammal Age.

Systematic paleontology

Nomenclatural remark. The new species and genus described below shall be referred to Boivin, 2021, following the article 50.1 and the “recommendation 50A concerning multiple authors” of the International Code of Zoological Nomenclature (ICZN 1999: 182).

Order **Rodentia** Bowdich, 1821

Suborder **Ctenohystrica** Huchon, Catzeflis and Douzery, 2000

Infraorder **Hystricognathi** Tullberg, 1899

Parvorder **Caviomorpha** Wood, 1955

Genus ***Balsayacuy*** gen. nov.

Etymology. From “Balsayacu”, the Sub-Andean Peruvian village in the vicinity of which the type locality was discovered, and “cuy”, which means guinea pig in Quechua language. The name Balsayacu refers to the balsa wood, *Ochroma*, with which the rafts are built and used to navigate the Huallaga River and other Amazonian rivers. As

the new rodent *Balsayacuy* being probably one of the early stem Caviomorpha, its name is also in reference to the “raft” hypothesis to explain the trans-Atlantic dispersal and arrival of hystricognathous rodents in South America from Africa.

Type species. *Balsayacuy huallagaensis* sp. nov.

Species content. Only the type species.

Geographic and stratigraphic distribution. Balsayacu (TAR-55/TAR-55bis and TAR-77 localities), San Martin Department, Pozo Formation, lower member (late middle or early late Eocene), Peru.

Generic diagnosis. As for the type and only known species.

Table 1. Paleogene caviomorph taxa used for comparisons in this study and cited in the text. The suprageneric assignment of the taxa follows the phylogenetic results of Boivin et al. (2019b).

Genus	Species	Locality and/or Formation (Fm.)	Age	Observed material (original or cast)	Primary references
Cachiyacuy	*C. contamanensis*	Contamana CTA-27 (lower Mb., Pozo Fm.), Peru	late Middle Eocene	MUSM & UM (original & cast)	Antoine et al., 2012; Boivin et al., 2017
	C. sp. cf. *C. contamanensis*	Santa Rosa (Yahuarango Fm.), Peru	?Late Eocene / Early Oligocene		Arnal et al., 2019
	C. kummeli	Contamana CTA-27 (lower Mb., Pozo Fm.) and Santa Rosa (Yahuarango Fm.), Peru	late Middle Eocene–Early Oligocene	MUSM & UM (original & cast)	Antoine et al., 2012; Boivin et al., 2017
Canaanimys	*C. maquiensis*	Contamana CTA-27 (lower Mb., Pozo Fm.), Peru	late Middle Eocene	MUSM & UM (original & cast)	Antoine et al., 2012; Boivin et al., 2017
	C. sp. cf. *C. maquiensis*	Santa Rosa (Yahuarango Fm.), Peru	late Middle Eocene	MUSM & UM (original & cast)	Arnal et al., 2019
Eobranisamys	*E. javierpradoi*	Contamana CTA-27 (lower Mb., Pozo Fm.), Peru	late Middle Eocene		Antoine et al., 2012; Boivin et al., 2017
Pozomys	*P. ucayaliensis*	Contamana CTA-29 (lower Mb., Pozo Fm.) and Santa Rosa (Yahuarango Fm.), Peru	late Middle Eocene–Early Oligocene	MUSM & UM (original & cast)	Boivin et al., 2017; Arnal et al., 2019
Eosallamys	*E. paulacoutoi*	Santa Rosa (Yahuarango Fm.), Peru	?Late Eocene / Early Oligocene	INGEMMET (holotype)	Frailey & Campbell, 2004; Arnal et al., 2019
Eoespina	*E. woodi*	Santa Rosa (Yahuarango Fm.), Peru	?Late Eocene / Early Oligocene	INGEMMET (holotype)	Frailey & Campbell, 2004; Arnal et al., 2019
Eosachacui	*E. lavocati*	Santa Rosa (Yahuarango Fm.), Peru	?Late Eocene / Early Oligocene	INGEMMET (holotype)	Frailey & Campbell, 2004
Chinchilloidea					
Eoincamys	*E. ameghinoi*	Santa Rosa (Yahuarango Fm.), Peru	?Late Eocene / Early Oligocene	INGEMMET (holotype)	Frailey & Campbell, 2004
	E. pascuali	Santa Rosa (Yahuarango Fm.), Peru	?Late Eocene / Early Oligocene	INGEMMET (holotype)	Frailey & Campbell, 2004
	E. aff. *pascuali*	Juanjui TAR-50, Peru	Early Oligocene	MUSM & UM (original & cast)	Assémat et al., 2019
	E. cf. *pascuali*	Tarapoto-Shapaja TAR-01 (upper Mb., Pozo Fm.), Peru	Early Oligocene	MUSM & UM (original & cast)	Boivin et al., 2018
	E. valverdei	Tarapoto-Shapaja TAR-20, 21, 13, 22 (upper Mb., Pozo Fm.), Peru	Late Eocene–Early Oligocene	MUSM & UM (original & cast)	Boivin et al., 2018
	E. parvus	Tarapoto-Shapaja TAR-20, 21, 22 (upper Mb., Pozo Fm.), Peru	Late Eocene–Early Oligocene	MUSM & UM (original & cast)	Boivin et al., 2018
	Eoincamys sp.	Juanjui TAR-49, Peru	Early Oligocene	MUSM & UM (original & cast)	Assémat et al., 2019
Octodontoidea					
Eodelphomys	*E. almeidacomposi*	Santa Rosa (Yahuarango Fm.), Peru	?Late Eocene / Early Oligocene	INGEMMET (holotype)	Frailey & Campbell, 2004
Erethizontoidea					
Eopululo	*E. wigmorei*	Santa Rosa (Yahuarango Fm.), Peru	?Late Eocene / Early Oligocene	INGEMMET (holotype)	Frailey & Campbell, 2004

Fm., Formation; INGEMMET, Instituto Geológico Minero y Metalúrgico, Lima; Mb, Member; MUSM, Museo de Historia Natural de la Universidad Nacional Mayor San Marcos, Lima; UM, Université de Montpellier.

Balsayacuy huallagaensis sp. nov.

Figures 2a–v, Table 2

2019 *Cachiyacuy* cf. *kummeli*—Assemat et al.: 707, fig. 3C–E.

2019 *Canaanimys* aff. *maquiensis*—Assemat et al.: 711, fig. 4O, P.

Etymology. From the Peruvian Huallaga River, which flows near the type locality.

Holotype. MUSM 3935, left M2 (Fig. 2p).

Referred material. MUSM 3373 (Assemat et al. 2019: 707, fig. 3E; Fig. 2g), 3908 (Fig. 2i), 3921 (Fig. 2d), left m1s; MUSM 3922 (Fig. 2a), 3923 (Fig. 2e), right m1s; MUSM 3924 (Fig. 2j), 3925, left m2s; MUSM 3910 (Fig. 2h), 3926 (Fig. 2b), 3927 (Fig. 2f), right m2s; MUSM 3928 (Fig. 2c), left m3; MUSM 3929 (Fig. 2n), right fragmentary P4; MUSM 3930 (Fig. 2m), right fragmentary upper molar; MUSM 3934, left fragmentary M1; MUSM 3931–3933 (Fig. 2o, s, t), left M1s; MUSM 3377 (Assemat et al. 2019: 707, fig. 3C; Fig. 2r), right fragmentary M1; MUSM 3378 (Assemat et al. 2019: 707, fig. 3D; Fig. 2k), 3936 (Fig. 2l), left M2s; MUSM 3379 (Assemat et al. 2019: 711, fig. 4P; Fig. 2v), left fragmentary M3; MUSM 3371 (Assemat et al. 2019: 711, fig. 4O; Fig. 2q), left M3; MUSM 3938 (Fig. 2u), right M3.

Type locality. TAR-55/TAR-55bis, Balsayacu, San Martin Department, Western Amazonia, Peru.

Other locality. TAR-77 (only for MUSM 3921), Balsayacu, San Martin Department, Western Amazonia, Peru.

Formation and age. Pozo Formation, lower member, late middle Eocene to early late Eocene (i.e., Barrancan or Mustersan SALMAs).

Diagnosis. Small-sized rodent characterized by brachydont and bunolophodont teeth. Lower molars with a pseudo-taeniodont pattern at early stages of wear. Upper teeth with a variable morphology of the lingual protoloph, which can be either complete, reduced to one or two connected or disconnected crestules (i.e., posterior arm of the protocone or crestule from the labial protoloph-mure junction), or absent, but the pseudo-taeniodont pattern is more frequently present. Round P4s with a transverse lingual protoloph, and with a connection of its labial structures (i.e., anteroloph, paracone, mesostyle, and posteroloph) at a moderate stage of wear. P4s and upper molars with a frequently incomplete third transverse crest. P4s and M1–2s without metaloph. If it is present, the metaloph is strongly reduced and lingually free on M3s at early stage of wear. M1–2s frequently with a long mesoloph faintly linked to the mesolophular spur or lingually free (the mesophular spur being absent). Accessory, thin and short enamel structures (posteroloph spur included) may be present between the third crest and the posteroloph, and connected to either or both transverse crests on upper molars. Differs from *Cachiyacuy contamanensis*, *Eobranisamys*, *Eosallamys paulacoutoi*, and ‘*Eosallamys*’ *simpsoni* in having a smaller size. Differs from *Canaanimys maquiensis* in having more square-shaped M1–2s and from *Eobranisamys*, *Es*. *paulacoutoi*, ‘*Es*.’ *simpsoni*, *Eoespina*, and *Pozomys* in having

more transverse M1–2s. Differs from *Cc*. *contamanensis*, *Cachiyacuy kummeli*, *Es*. *paulacoutoi*, '*Es*.' *simpsoni*, *Eoespina*, and *Eosachacui* in having a higher tendency toward the taeniodonty; and from *Eobranisamys* and *Pozomys* in having a lower tendency toward the taeniodonty. The metaloph is absent on M1–2s of *Balsayacuy*, differing from the most frequent morphology of this crest in *Cc*. *contamanensis*, *Canaanimys*, *Eobranisamys*, and *Es*. *paulacoutoi*, in which the metaloph is present. Differs from *Cc*. *contamanensis*, *Cc*. *kummeli*, *Cn*. *maquiensis*, *Eobranisamys*, *Es*. *paulacoutoi*, '*Es*.' *simpsoni*, *Eoespina*, and *Eosachacui* in having a mesoloph more frequently faintly linked to the mesolophular spur or lingually free on M1–2s. It further differs from *Cc*. *kummeli*, *Eobranisamys*, *Eoespina*, and *Pozomys* in having more important developed accessory structures between the third crest and the posteroloph on some upper molars; from *Cc*. *contamanensis*, *Eobranisamys*, *Eoespina*, and *Es*. *paulacoutoi* in having more rounded P4s; from *Cc*. *contamanensis* in having a connection of the labial structures (i.e., anteroloph, paracone, mesostyle, and posteroloph) on P4s at an earlier stage of wear; from *Eoespina* and '*Es*.' *simpsoni* in having a transverse lingual protoloph on P4s; from *Eoespina* in having a stronger connection of the labial structures on P4s at moderate stage of wear; from *Eobranisamys* and *Eosachacui* in having a complete mure on P4s; from *Eosachacui*, *Es*. *paulacoutoi*, and '*Es*.' *simpsoni* in having a reduced third crest; and from *Pozomys* in having a third crest on P4s.

Description. The lower molars (m1–3s) share the same dental structure (Fig. 2a–j). They are rectangular- or squareshaped. The m1s are clearly smaller than m2s. The unique identified m3 (MUSM 3928; Fig. 2c) has a similar width to that of m1s, but it is longer than m1s and m2s. MUSM 3928 is distinguished by a lingual margin of the entoconid that is more labial in position to the mesiolingual corner of the tooth, and by showing a distal expansion and a labiolingual shortness of the posterolophid (Fig. 2c). The m2s have a trigonid and talonid with an equal width, as well as the m1s, but the latter can also show a shorter labiolingual trigonid (MUSM 3922; Fig. 2a). Mesially, there is no trace of anterocingulid at the base of the crown. The protoconid is distally located with respect to the metaconid, and both are linked by a straight metalophulid I. The latter is high and continuous on MUSM 3921 (Fig. 2d). The other lower molars at early stages of wear (MUSM 3910, 3923, 3926, and 3927; Fig. 2b, e, f, h) show a discontinuous metalophulid I, with an anterior arm of the metaconid separate from the anterior arm of the protoconid by a tiny notch, much thinner and shallower on MUSM 3927. On MUSM 3910, 3923, and 3926 (Fig. 2b, e, h), the anterior arm of the

protoconid is lower and shorter than the anterior arm of the metaconid, whereas both are rather similar in size and height on MUSM 3927 (Fig. 2f). On MUSM 3373 (Fig. 2g), the anterior arm of the protoconid is slightly linked to the anterior arm of the metaconid. On MUSM 3922 (Fig. 2a) and the lower molars at more advanced stages of wear (MUSM 3924 and 3928; Fig. 2c, j), the metalophulid I is continuous, but is thinner in its middle part. They had probably a discontinuity of this lophid at an earlier stage of wear. On MUSM 3373, the metaconid bears a very tiny cristulid, distally free on the anteroflexid (i.e., metaconid cristid; Fig. 2g). MUSM 3910 (Fig. 2h) has a cuspid-shaped structure on the anteroflexid and a cristilid on the distal part of the second cristid. The lower molars show a strong and long posterior arm of the metaconid, which is well connected to a mesostylid or to its anterior arm. In contrast, a deep and narrow furrow separates the mesostylid from the entoconid on m1–2s. On the MUSM 3928 m3 (Fig. 2c), the mesostylid has a short, but strong posterior arm, which reaches the anterior arm of the entoconid, thus closing the mesoflexid lingually. The second transverse cristid can be straigth or sinuous (S-shaped). It is somewhat difficult to describe it in some cases inasmuch as it appears continuous and without interruption or irregularities. However, on some teeth (MUSM 3373, 3908, 3910, 3921, and 3928; Fig. 2c, d, g, h, i), this cristid is formed by a long posterior arm of the protoconid, which is connected to a shorter neomesolophid. On MUSM 3923 (Fig. 2e), the neomesolophid is dominant and the posterior arm of the protoconid is short and thin. The ectolophid is continuous and strongly mesiolabially directed, except on some specimens (MUSM 3924, 3925, and 3927, in which it is more longitudinal (i.e., parallel to the mesiodistal axis of the tooth; Fig. 2f, j). The hypoconid and entoconid are labiolingually opposed on MUSM 3910, 3921 and 3927 (Fig. 2d, f, h), whereas the entoconid is more mesially situated than the hypoconid on other lower molars. These two cuspids are linked by a long and straight or slightly oblique hypolophid, which usually connects labially to a short anterior arm of the hypoconid (i.e., absence of taeniodont pattern). On MUSM 3923, 3910, 3921 and 3927 (Fig. 2d–f, h), there are two very short cristulids, one on the distolabial margin of the hypolophid and the other stemming from the hypoconid (its anterior arm), both are clearly spaced, but are joined by the base. Due to the non-connection of these cristulids at their top, the hypoflexid is partly confluent with the metaflexid on this tooth (i.e., pattern II of pseudo-taeniodont). Two lower molars at moderate stages of wear (MUSM 3922 and 3926; Fig. 2a, b) are non-taeniodont, but have a cristulid from the hypolophid + anterior arm of the hypoconid that is thin in its middle or showing difference of height of its anterior

and posterior parts. Hence, they were probably pseudo-taeniodont at an earlier stage of wear. The entoconid can display anterior and posterior arms. When it is present, the anterior arm of the entoconid is thin and faintly visible (except on MUSM 3910 and 3921; Fig. 2d, h), contrary to the posterior arm, which is usually stronger. It connects to the posteroloph (MUSM 3373, 3921, and 3926; Fig. 2b, d, g) or remains separated from the latter by a thin and shallow furrow (MUSM 3908, 3910, 3922, 3925, and 3927; Fig. 2a, f, h, i) or by a larger and deeper one (MUSM 3923 and 3928; Fig. 2c, e). The hypoconid is mesiolingually-distolabially compressed and develops a strong and curved posterolophid. There is no hypoconulid. The anteroflexid and metaflexid are mesiodistally wide.

The MUSM 3929 P4 is moderately worn and mesiolabially broken (Fig. 2n). In occlusal view, its crown outline is round with a continuous surrounding crest, which forms the complete margin of the tooth. This surrounding crest is composed of a crestiform protocone, its posterior outgrowth, a minute hypocone, the anteroloph, and the posteroloph. It could also include a mesiolingual crestule stemming from the hypocone, a mesostyle, and a metacone. The labial protoloph is strong and distolingually oriented. Contrary to the straight and complete lingual protoloph, the mure is discontinuous and longitudinal. The anterior arm of the hypocone is more oblique than the labial protoloph and is connected to a mesolophule. The latter shows a transverse and high lingual part and a lower and slightly longer labial part, directed distolabially. Due to its characteristic, its labial part could be a relic of a connection of the third crest with the posteroloph. The two other fossettes of the tooth are one small and mesiolabially-distolingually elongated parafossette and one expanded hypofossette.

M1–3s referred to *Balsayacuy huallagaensis* gen. Et sp. nov. are brachydont (Fig. 2k–m, o–v). The M1s are the smallest upper molars, while the M2–3s are quite similar in size. The M3s (MUSM 3371, 3379, and 3938; Fig. 2q, u, v) exhibit a smaller and more labial located hypocone with respect to the protocone than on M1–2 s (Fig. 2k, l, o, p, r–t). On the less worn upper molars (MUSM 3371, 3377, and 3379; Fig. 2q, r, v), the main cusps are usually well defined, especially the cuspate paracone and mesostyle. The metacone can be well defined (MUSM 3371, 3935, and 3938; Fig. 2p, q, u) or crestiform and poorly recognisable from the posteroloph (MUSM 3379 and 3931; Fig. 2o, v). The lingual protoloph is either elevated and complete (MUSM 3371; i.e., non-taeniodont pattern; Fig. 2q), reduced and limited to a tiny posterior arm of the protocone and/or crestule from the labial protoloph-mure junction (MUSM 3377, 3379,

3930, 3931, 3933, 3935, and 3938; i.e., pseudo-taeniodont pattern; Fig. 2m, o, p, r, s, u, v) or absent (MUSM 3932; i.e., taeniodont pattern; Fig. 2t). MUSM 3377 has a posterior arm of the protocone and crestule from the labial protoloph-mure junction linked at their base, but not at their top (i.e., pattern II of pseudo-taeniodonty; Fig. 2r). The other pseudo-taeniodont upper molars (i.e., pattern I of pseudo-taeniodonty) have either a posterior arm of the protocone, a crestule from the labial protoloph-mure junction, or both. In the latter case, these two crestules remain disconnected. Two upper molars at a moderate stage of wear (MUSM 3378 and 3936; Fig. 2k, l) are non-taeniodont, but they have a thin lingual protoloph. They may have been pseudo-taeniodont when pristine and at earlier stages of wear. The protocone is mesiolinguallydistolabially pinched and connected to a strong anteroloph. This mesial transverse crest runs labially and is separated from the paracone by a medium-sized furrow (MUSM 3371, 3379, 3933, and 3935; Fig. 2p, q, s, v) or connected to the mesial base of this cusp (MUSM 3378, 3931, 3932, and 3938; Fig. 2k, o, t, u). The labial protoloph is slightly oblique, whereas the mure is longitudinal (i.e., parallel to the mesiodistal axis of the tooth; except on MUSM 3932; Fig. 2t). The mesostyle is mesially and distally isolated from the paracone and metacone, respectively. The third transverse crest is straight and strongly linked to the mesostyle in most of cases. This crest is usually formed by either a long mesoloph connected to a mesolophular spur (MUSM 3371, 3378, 3933, and 3935; Fig. 2k, p, q, s) or only by a long mesoloph lingually free (MUSM 3377 and 3930; Fig. 2m, r). On MUSM 3931 and 3938, the configuration of the third crest is different: a long and straight mesolophule runs labially and remains isolated from the mesostyle (MUSM 3931; Fig. 2o) or tightly connected to a tiny mesoloph spur (MUSM 3938; Fig. 2u). The metaloph is absent except on the MUSM 3938 M3, in which it is tiny but clearly distinct (Fig. 2u). On that tooth, there are two very short crestules originate from the posteroloph more lingually. The more lingually located crestule is recognized as a posteroloph spur. A posteroloph spur is also recognized on MUSM 3371 (Fig. 2q) and MUSM 3378 (Fig. 2k). MUSM 3371, 3378, and 3935 have accessory structures (i.e., crestule(s) and/or cusp-shaped structures; Fig. 2k, p, q) between the third crest and the posteroloph, which are not interpreted as remnants of metaloph. These structures can be associated to a posteroloph spur (MUSM 3371 and 3378). They can be either isolated (MUSM 3371; Fig. 2q) or linked to the third crest (MUSM 3935; Fig. 2p) or to the third crest and posteroloph spur (MUSM 3378; Fig. 2k). The two worn upper molars, MUSM 3932 (Fig. 2t) and MUSM 3936 (Fig. 2l), show a small and rounded enlargement of the

anterolingual enamel margin, which may correspond to a posteroloph spur or/and accessory structures. The hypocone bears a low posterior arm, which faintly connects to the longer posteroloph.

Comparisons. By its brachydonty, bunolophodonty, thin and roughly transverse loph(-id)s, tetralophodont lower molars, with a strong posterior arm of the metaconid, mesostylid and complete second transverse cristid, the presence of a mesostyle and third transverse crest on upper teeth, and the presence of a metacone on upper molars, the morphology of *Balsayacuy* is strongly reminiscent of that found in several Paleogene caviomorphs. By its upper molars with a Strong reduction or absence of the metaloph, *Balsayacuy* recalls *Cachiyacuy* cf. *contamanensis* 2 and *Pozomys ucayalensis* (CTA-29 and Santa Rosa; Boivin et al. 2017a; Arnal et al. 2020), *Eoespina woodi*, *Eosachacui lavocati*, and '*Eosallamys*' *simpsoni* (Santa Rosa; Frailey and Campbell 2004; Arnal et al. 2020). On MUSM 2832 attributed to *Cc*. cf. *contamanensis* 2 from CTA-29, the metaloph is longer than MUSM 3938, the unique upper molar of *Balsayacuy* with a metaloph. On LACM 143374 and 143398 of '*Es*.' *simpsoni*, the metaloph is connected to the posteroloph or very close to the posteroloph spur, respectively, contrary to MUSM 3938. The morphology of the MUSM 3936 P4 attributed to *Balsayacuy* is closer to that of *Eoespina*. Particularly, the LACM 143459 P4 of *Eoespina* is characterized by an incomplete third crest disconnected to the mesostyle, and by a thin lingual protoloph as in *Balsayacuy*. Moreover, no metaloph is distinct on LACM 143459, like on MUSM 3936, but the posteroloph is thicker and may be fused with a metaloph contrary to MUSM 3936. Some upper molars of *Cc*. cf. *contamanensis* 2 from CTA-29, *Eosachacui* and *Pozomys* can have a long mesoloph, more or less connected to a very short mesolophule, as some M1–2s from TAR-55/TAR-55bis assigned to *Balsayacuy*. Particularly, the LACM 159207 M1 or M2 of *P*. *ucayalensis* (Arnal et al. 2020: 203, fig. 4C) displays the mesoloph less connected to the mesolophule, and in addition with a tiny crestule on its distolingual extremity directed towards (but not linked to) a posteroloph spur, a configuration close to the morphology of some upper molars of *Balsayacuy*. The lower and Upper molars of *Balsayacuy* shows a tendency toward the taeniodonty (particularly on its upper molars), a character found in *P*. *ucayalensis*, as well as in *Eobranisamys* (CTA-27 and Santa Rosa; Frailey and Campbell 2004; Boivin et al. 2017a). Nevertheless, the latters usually show a taeniodont pattern much more achieved. Moreover, lower molars of *Balsayacuy* strongly differ from those of *P*. *ucayalensis* in having a very thin discontinuity of the metalophulid I, which is connected to the protoconid. *Balsayacuy*

also differs from *Pozomys* in having a third crest on P4s; from *Eoespina* and '*Es*.' *simpsoni* in having P4s with transverse lingual protoloph; from *Eoespina* in having a stronger connection of the labial structures at moderate stage of wear; from *Eobranisamys* and *Eoespina* in having rounded P4s; from *Eobranisamys* and *Eosachacui* with a complete mure on P4s; from *Eosachacui* and '*Es*.' *simpsoni* in having a reduced third crest on P4s; and from *Eobranisamys* in displaying upper molars with either a reduced metaloph, or devoid of this crest. The presence of accessory crestules between the third transverse crest and the posteroloph on upper molars is a character also found in two basal caviomorphs from Peru: *Cachiyacuy* and *Eosallamys* (Eocene localities of Contamana, Balsayacu-Juanjui, and Santa Rosa; Frailey and Campbell 2004; Antoine et al. 2012; Boivin et al. 2017a; Assemat et al. 2019; Arnal et al. 2020). Besides, *Cachiyacuy* and *Eosallamys* can exhibit a long mesoloph faintly connected to a mesolophular spur, as well as a reduction of the metaloph. Although the more frequent configuration in *Cachiyacuy contamanensis* is a long metaloph terminating very close to the crestules between the third crest to the posteroloph (it can be connected to both crests or only to the posteroloph), some upper molars of this species have a more or less reduced metaloph, and the latter can be absent (MUSM 2744; Boivin et al. 2017a) as in *Balsayacuy*. Upper molars of *Cachiyacuy* cf. *contamanensis* from Santa Rosa (Arnal et al. 2020) have a reduced metaloph, but the latter is always more developed than on molars of *Balsayacuy*. In *Eosallamys paulacoutoi* (Santa Rosa; Frailey and Campbell 2004; Arnal et al. 2020), the metaloph can be more reduced as on MUSM 3938 from TAR-55/TAR-55bis. However, the upper molars of *Cachiyacuy* cf. *contamanensis* and *Es*. *paulacoutoi* always have a metaloph, and the latter is rarely lingually free. *Balsayacuy* differs from *Cc*. *Contamanensis* and *Eosallamys* in having more rounded P4s; from *Cc*. *contamanensis* in having a connection of the labial structures (i.e., anteroloph, paracone, mesostyle, and posteroloph) on P4s at an earlier stage of wear; and from *Eosallamys* in having a reduced third crest on P4s. *Cachiyacuy kummeli* (CTA-27 and Santa Rosa; Antoine et al. 2012; Boivin et al. 2017a; Arnal et al. 2020; this work) has upper molars with a metaloph lingually free, well-marked (MUSM 1882 and 1884 [Antoine et al. 2012: fig. 2m, o], LACM 159246 [Arnal et al. 2020: fig. 2T]), reduced (MUSM 1883 [Antoine et al., 2012: fig. 2n], LACM 159244 [Arnal et al. 2020: fig. 2V], and LACM 159250 [Arnal et al. 2020: fig. 2W]) or absent (MUSM 2785 [Boivin et al. 2017a: fig. 4.12]; Fig. 3q). On MUSM 1882, 1884, and LACM 159246, the metaloph is

longer than that in *Balsayacuy* (when it is present). Teeth of *Balsayacuy* are smaller than those of *Cc*. *contamanensis*, *Cc*. cf. *contamanensis* 2 from CTA-29, *Cc*. cf. *contamanensis* from Santa Rosa, *Eobranisamys*, *Es*. *paulacoutoi* and '*Es*.' *simpsoni*. Their size is similar to that of *Cc*. *kummeli* and *Canaanimys maquiensis* (CTA-27; Antoine et al. 2012; Boivin et al. 2017a). *Balsayacuy* differs from *Cc*. *contamanensis*, *Cc*. cf. *contamanensis* 2 from CTA-29,*Cc*. cf. *contamanensis* from Santa Rosa, *Cc*. *kummeli*, and *Es*. *paulacoutoi* in having a stronger tendency toward the taeniodonty on molars at early stages of wear, which can develop a pseudo-taeniodont (the more frequent case) or a taeniodont pattern. Some M3s of *Cn*. *maquiensis* and the LACM 159351 M1 of *Canaanimys* cf. *maquiensis* from Santa Rosa (Arnal et al. 2020: 201, fig. 3A) have a very short metaloph lingually free, but on their Other upper molars, this crest turns forward and terminates close to the third crest and can connect to the latter unlike in *Balsayacuy*. Contrary to *Balsayacuy*, *Canaanimys* cf. *maquiensis* has some lower molars with an incomplete second cristid; and P4s with a metaloph, a complete transverse third crest and a slightly oblique lingual protoloph. Finally, *Balsayacuy* differs from *Cachiyacuy* cf. *contamanensis*, *Canaanimys* cf. *maquiensis*, *Eobranisamys*, *Es*. *paulacoutoi*, *Ep*. *woodi*, and *P*. *ucayalensis* in having M1–2s more transverse and from *Cn*. *maquiensis* in having M1–2s more square-shaped. Some teeth from TAR-55/TAR-55 attributed here to *Balsayacuy* were formerly considered as *Cachiyacuy* cf. *kummeli* (MUSM 3373, 3377, and 3378) or *Canaanimys* aff. *maquiensis* (MUSM 3371 and 3379; Assemat et al. 2019). The discovery of new dental material from TAR-55/TAR-55bis and TAR-77 including new loci has allowed us to refine these attributions. The material defining *Balsayacuy* is characterized by a mosaic of traits principally shared with *Cachiyacuy*, *Canaanimys*, *Eosallamys*, *Eoespina*, and *Pozomys*. This combination of characters and the morphological tendencies of this taxon are somewhat singular, which leads us to propose here a new taxon: *Balsayacuy huallagaensis* gen. et sp. nov.

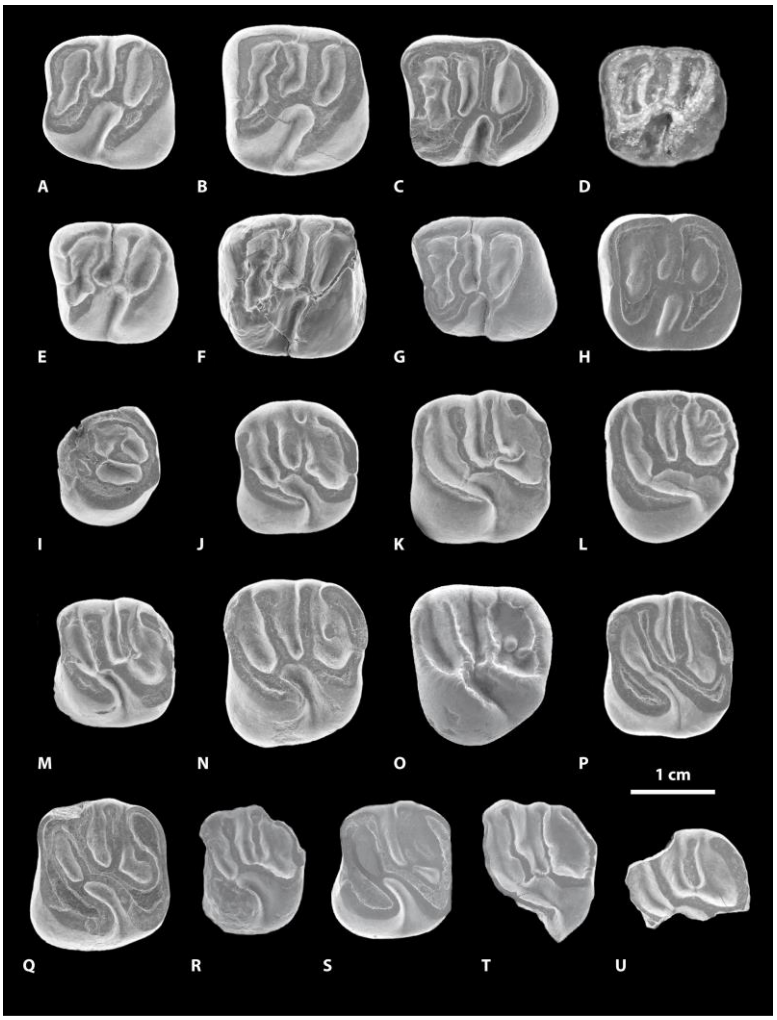


Fig. 2. Scanning electron microscope images (in occlusal view) of *Balsayacuy huallagaensis* gen. et sp. nov. from TAR-55/TAR-55bis and TAR-77 (Balsayacu, San Martín Department, Peru; late Middle or early Late Eocene). (A–C, E–P) from TAR-55/TAR-55bis and (D) from TAR-77. (A) MUSM 3922, right m1 (reversed); (B) MUSM 3926, right m2 (reversed); (C) MUSM 3928, left m3; (D) MUSM 3921, left m1; (E) MUSM 3923, right m1 (reversed); (F) MUSM 3927, right m2 (reversed); (G) MUSM 3373, left m1; (H) MUSM 3924, left m2; (I) MUSM 3929, right P4 (reversed); (J) MUSM 3931, left M1; (K) MUSM 3935, left M2; (L) MUSM 3938, right M3 (reversed); (M) MUSM 3933, left M1; (N) MUSM 3937, right M2 (reversed); (O) MUSM 3371, left M3; (P) MUSM 3932, left M1; (Q) MUSM 3936, left M2; (R) MUSM 3371, right M1 (reversed); (S) MUSM 3378, left M2; (T) MUSM 3379, left M3; (U) MUSM 3930, labial fragment of right M (reversed).

Genus ***Chachapoyamys*** gen. nov.

Etymology. From the Andean-Amazonian Chachapoya culture, once developed in the Balsayacu area, and -mys (Greek for mouse).
Type species. *Chachapoyamys kathetos* sp. nov.
Species content. Only the type species.
Geographic and stratigraphic distribution. Contamana (CTA-27), Loreto Department and Balsayacu (TAR-55/TAR-55bis), San Martin Department, Pozo Formation, lower member (late middle–early late Eocene), Peru.
Generic diagnosis. As for the type and only known species.

Chachapoyamys kathetos sp. nov.

Figure 3a–n, Table 2

2019 *Cachiyacuy* cf. *kummeli*—Assemat et al.: 707, fig. 3A, B, F, G.
Etymology. From κάθετος (kathetos, Greek for vertical, upraised), referring to the vertical layers in which the holotype and referred specimens were found, at TAR-55/TAR-55bis locality.
Holotype. MUSM 3918, right M2 (Fig. 3h).

Table 2. Dental measurements (in millimeters) of rodent material from TAR-55/TAR-55bis, TAR-76 and TAR-77 (Peru; late Middle Eocene). The holotype of *Balsayacuy huallagaensis* gen. et sp. nov. is marked with an asterisk.

Inventory number	Taxon	Specimen	State	Locality	References and figuration	Previous identification	Max. lenght	Max. width
MUSM 3907	*Cachlyacuy* aff. *kummeli*	right p4	strongly worn	TAR-55/TAR-55bis	this work: Fig. 3C		1.51	1.53
MUSM 3908	*Cachlyacuy* aff. *kummeli*	left m1	strongly worn, slightly anteriorly broken	TAR-55/TAR-55bis	this work: Fig. 3E		1.58	1.52
MUSM 3909	*Cachlyacuy* aff. *kummeli*	left m1	eroded	TAR-55/TAR-55bis	this work		1.59	1.72
MUSM 3374	*Cachlyacuy* aff. *kummeli*	right m1	pristine tooth	TAR-55/TAR-55bis	Assémat et al., 2019: fig. 3G; this work: Fig. 3B	*Cachlyacuy* cf. *kummeli*	1.731	1.848
MUSM 3375	*Cachlyacuy* aff. *kummeli*	right m1	anterolingually broken	TAR-55/TAR-55bis	Assémat et al., 2019: fig. 3F; this work: Fig. 3D	*Cachlyacuy* cf. *kummeli*	1.37	1.58
MUSM 3910	*Cachlyacuy* aff. *kummeli*	right m2	pristine tooth	TAR-55/TAR-55bis	this work: Fig. 3A		1.82	1.93
MUSM 3911	*Cachlyacuy* aff. *kummeli*	left dP4	anterolabially broken	TAR-55/TAR-55bis	this work: Fig. 3J		1.41	1.32
MUSM 3372	*Cachlyacuy* aff. *kummeli*	left P4	pristine tooth, broken in its middle	TAR-55/TAR-55bis	Assémat et al., 2019: fig. 3A; this work: Fig. 3O	*Cachlyacuy* cf. *kummeli*	1.307	1.806
MUSM 3912	*Cachlyacuy* aff. *kummeli*	right P4	pristine tooth, lingually and labially broken	TAR-55/TAR-55bis	this work		-	-
MUSM 3913	*Cachlyacuy* aff. *kummeli*	right P4	slightly labially broken	TAR-55/TAR-55bis	this work: Fig. 3I		1.44	1.58
MUSM 3376	*Cachlyacuy* aff. *kummeli*	left M1		TAR-55/TAR-55bis	Assémat et al., 2019: fig. 3B; this work: Fig. 3N	*Cachlyacuy* cf. *kummeli*	1.17	1.62
MUSM 3915	*Cachlyacuy* aff. *kummeli*	right M1	strongly worn, slightly labially and posterolingually broken	TAR-55/TAR-55bis	this work: Fig. 3H		1.62	1.80
MUSM 3916	*Cachlyacuy* aff. *kummeli*	left M2	nearly a pristine tooth	TAR-55/TAR-55bis	this work: Fig. 3M		1.61	2.10
MUSM 3917	*Cachlyacuy* aff. *kummeli*	right M2		TAR-55/TAR-55bis	this work: Fig. 3G		1.87	2.19
MUSM 3918	*Cachlyacuy* aff. *kummeli*	right M2		TAR-55/TAR-55bis	this work: Fig. 3K		1.79	2.19
MUSM 3919	*Cachlyacuy* aff. *kummeli*	right M3		TAR-55/TAR-55bis	this work: Fig. 3F		1.71	2.04
MUSM 3920	*Cachlyacuy* aff. *kummeli*	right M3	strongly worn	TAR-55/TAR-55bis	this work: Fig. 3L		1.69	2.06
MUSM 3373	*Balsayacuy huallagaensis*	left m1		TAR-55/TAR-55bis	Assémat et al., 2019: fig. 3E; this work: Fig. 2G	*Cachlyacuy* cf. *kummeli*	1.62	1.681
MUSM 3921	*Balsayacuy huallagaensis*	left m1		TAR-77	this work: Fig. 2D		1.51	1.44
MUSM 3922	*Balsayacuy huallagaensis*	right m1		TAR-55/TAR-55bis	this work: Fig. 2A		1.57	1.60
MUSM 3923	*Balsayacuy huallagaensis*	right m1		TAR-55/TAR-55bis	this work: Fig. 2E		1.51	1.62
MUSM 3924	*Balsayacuy huallagaensis*	left m2	strongly worn	TAR-55/TAR-55bis	this work: Fig. 2H		1.70	1.67
MUSM 3925	*Balsayacuy huallagaensis*	left m2	slightly anterolingually broken	TAR-55/TAR-55bis	this work		1.76	1.72
MUSM 3926	*Balsayacuy huallagaensis*	right m2		TAR-55/TAR-55bis	this work: Fig. 2B		1.71	1.79
MUSM 3927	*Balsayacuy huallagaensis*	right m2		TAR-55/TAR-55bis	this work: Fig. 2F		1.73	1.75
MUSM 3928	*Balsayacuy huallagaensis*	left m3		TAR-55/TAR-55bis	this work: Fig. 2C		1.88	1.58
MUSM 3929	*Balsayacuy huallagaensis*	right P4	anterolabially broken	TAR-55/TAR-55bis	this work: Fig. 2I		1.21	1.30
MUSM 3930	*Balsayacuy huallagaensis*	right M	lingual fragment, slightly anterolabially broken	TAR-55/TAR-55bis	this work: Fig. 2U		-	-
MUSM 3931	*Balsayacuy huallagaensis*	left M1		TAR-55/TAR-55bis	this work: Fig. 2J		1.47	1.71
MUSM 3932	*Balsayacuy huallagaensis*	left M1		TAR-55/TAR-55bis	this work: Fig. 2P		1.53	1.79
MUSM 3933	*Balsayacuy huallagaensis*	left M1		TAR-55/TAR-55bis	this work: Fig. 2M		1.41	1.72
MUSM 3934	*Balsayacuy huallagaensis*	left M1	labially broken	TAR-55/TAR-55bis	this work		1.55	1.64
MUSM 3377	*Balsayacuy huallagaensis*	right M1	slighly posterolabially and anterolabially broken	TAR-55/TAR-55bis	Assémat et al., 2019: fig. 3C; this work: Fig. 2R	*Cachlyacuy* cf. *kummeli*	1.28	1.53
MUSM 3378	*Balsayacuy huallagaensis*	left M2	slighly posteriorly broken	TAR-55/TAR-55bis	Assémat et al., 2019: fig. 3D; this work: Fig. 2S	*Cachlyacuy* cf. *kummeli*	1.69	1.782
MUSM 3935*	*Balsayacuy huallagaensis*	left M2		TAR-55/TAR-55bis	this work: Fig. 2K		1.64	1.84
MUSM 3936	*Balsayacuy huallagaensis*	left M2	strongly worn	TAR-55/TAR-55bis	this work: Fig. 2Q		1.65	1.83
MUSM 3937	*Balsayacuy huallagaensis*	right M2		TAR-55/TAR-55bis	this work: Fig. 2N		1.70	1.93
MUSM 3371	*Balsayacuy huallagaensis*	left M3	pristine tooth	TAR-55/TAR-55bis	Assémat et al., 2019: fig. 4O; this work: Fig. 2O	*Canaanimys* aff. *maquiensis*	1.684	1.806
MUSM 3379	*Balsayacuy huallagaensis*	left M3	anteriorly broken	TAR-55/TAR-55bis	Assémat et al., 2019: fig. 4P; this work: Fig. 2T	*Canaanimys* aff. *maquiensis*	1.35	1.74
MUSM 3938	*Balsayacuy huallagaensis*	right M3		TAR-55/TAR-55bis	this work: Fig. 2L		1.59	1.84
MUSM 3939	Caviomorpha gen. et sp. indet. 1	right m	labial fragment	TAR-55/TAR-55bis	this work: Fig. 3Q		-	-
MUSM 3940	Caviomorpha gen. et sp. indet. 1	left P4	eroded, labially broken	TAR-55/TAR-55bis	this work: Fig. 3R		1.80	2.31
MUSM 3941	Caviomorpha gen. et sp. indet. 2	left p4	poorly worn, posterior fragment	TAR-76	this work: Fig. 3S		1.35	1.79
MUSM 3942	Caviomorpha gen. et sp. indet. 2	right m1 or m2	strongly worn	TAR-76	this work: Fig. 3T		1.45	1.46

Max.lenght, maximum anteroposterior length; Max. width, maximum linguolabial width.

Referred material. MUSM 3907 (Fig. 3n), right p4; MUSM 3909, left m1; MUSM 3375 (Assemat et al. 2019: 707, fig. 3F; Fig. 3l), right fragmentary m1; MUSM 3374 (Assemat et al. 2019: 707, fig. 3G; Fig. 3m), right m1; MUSM 3911 (Fig. 3e), left fragmentary dP4; MUSM 3372 (Assemat et al. 2019: 707, fig. 3A; Fig. 3j), left fragmentary P4; MUSM 3912, 3913 (Fig. 3d), right fragmentary P4s; MUSM 3915 (Fig. 3f), 3937 (Fig.

3i), right M1s; MUSM 3916 (Fig. 3c), left M2; MUSM 3917 (Fig. 3b), right M2; MUSM 3919 (Fig. 3a), 3920 (Fig. 3g), right M3s.

Tentatively referred material. MUSM 3376 (Assemat et al. 2019: 707, fig. 3B; Fig. 3k), left fragmentary M1.

Type locality. TAR-55/TAR-55bis, Balsayacu, San Martin Department, Western Amazonia, Peru.

Formation and age. Pozo Formation, lower member, late middle Eocene to early late Eocene (i.e., Barrancan or Mustersan SALMAs).

Diagnosis. Small-sized rodent characterized by brachydont, bunolophodont and non-taeniodont teeth. p4s and lower molars with a short posterior arm of the metaconid and a discontinuity of the metalophulid I, which can generate a wide notch. Oval P4s with a third crest connected to the mesostyle and anterior arm of the hypocone, and the presence of a metaloph. Transverse lower and upper molars. M1–2s with an absent or strongly reduced metaloph lingually free or completely isolated on the posterior flexus. M3s with an absent or short metaloph lingually free. Accessory, thin and short enamel structures (posteroloph spur included) almost always present between the third crest and the posteroloph on dP4s and upper molars, and connected to either or both transverse crests on upper molars. Differs from *Cachiyacuy contamanensis*, *Eobranisamys*, *Eosallamys paulacoutoi*, and '*Eosallamys*' *simpsoni* in having a smaller size; from *Balsayacuy*, *Cachiyacuy*, *Canaanimys*, *Eobranisamys*, *Eoespina*, *Eosachacui*, *Es*. *paulacoutoi*, '*Es*.' *simpsoni*, and *Pozomys* in having more transverse lower molars; and from *Balsayacuy*, *Cachiyacuy*, *Eobranisamys*, *Eoespina*, *Eosachacui*, *Es*. *paulacoutoi*, '*Es*.' *simpsoni*, and *Pozomys* in having more transverse upper molars. Differs from *Balsayacuy*, *Eobranisamys*, *Canaanimys*, and *Pozomys* in having teeth always non-taeniodont. Differs from *Pozomys* in having a curved (i.e., mesially concave) second cristid on p4s; from *Eoespina*, *Eosachacui*, *Es*. *paulacoutoi*, and some p4s of *Cc*. *contamanensis* in being devoid of accessory cristulids (mesolophid included) on the anteroflexid and/or mesoflexid on p4s; from *Cachiyacuy*, *Eoespina*, *Es*. *paulacoutoi*, and '*Es*.' *simpsoni* in having a more important discontinuity of the metalophulid I on p4s; from *Balsayacuy*, *Cachiyacuy*, *Canaanimys*, *Eobranisamys*, *Eoespina*, *Eosachacui*, *Es*. *paulacoutoi*, and '*Es*.' *simpsoni* in having lower molars, which can have a more important discontinuity of the metalophulid I; from *Balsayacuy* in having a shorter anterior arm of the metaconid on lower molars, and oval P4s with a third crest connected to the mesostyle and the presence of a metaloph; from *Balsayacuy* and *Es*. *paulacoutoi* in having P4s with a oblique lingual protoloph;

from *Balsayacuy* and *Eobranisamys* in having P4s with a paracone, which remains separate from the mesostyle at a moderate stage of wear; from *Eosachacui* and '*Es*.' *simpsoni* in having a metaloph on P4s; from *Eosachacui* in having non-taeniodont P4s; from *Eobranisamys* and *Eosachacui* in having P4s with a complete mure; from *Eoespina* in having P4s with always a third crest connected to the mesostyle; from *Eobranisamys* and '*Es*.' *simpsoni* in having a reduced metaloph disconnected to the posteroloph on dP4s; from *Eosachacui* in having a relictual metaloph on the posterior flexus on dP4s; and from *Balsayacuy*, *Cachiyacuy kummeli*, *Eobranisamys*, *Eoespina*, and *Pozomys* in having some upper molars with more important developed accessory structures between the third crest and the posteroloph, which connect both crests. The metaloph is absent or reduced to a very short crest lingually free on M1–2s of *Chachapoyamys*, differing from the most frequent morphology of this crest in *Cachiyacuy contamanensis*, *Canaanimys*, and *Eobranisamys*, in which the metaloph is longer. Differs from *Es*. *paulacoutoi* in having a metaloph (when present) more reduced and isolated on the posterior flexus on M1s, a shorter metaloph lingually free on M2s and lingually free (when present) on M3s.

Description. The MUSM 3907 p4 is moderately eroded and shows digestion marks (Fig. 3n). It has rounded corners. Although being narrower than the talonid, the trigonid is wide, its width being about 77% of that of the talonid. With wear, the four main cuspids (i.e., metaconid, entoconid, protoconid, and hypoconid) are not discernable from the lophids, especially the protoconid and hypoconid areas, which correspond to large dentine platforms. The metaconid and protoconid areas are well separate. The metaconid develops mesiolabially a transverse and short anterior arm being separate from the protoconid by a wide and deep notch. Besides, the metaconid distally bears a very short, but strong posterior arm. There is no anterocingulid. The posterior arm of the metaconid slightly joins a mesostylid, which corresponds with wear to a small and rather round structure of dentine, surrounded by enamel. Stemming from the protoconid area, the second transverse cristid is mostly mesially concave, being distalolingually directed toward the metaconid and mesostylid. The eroded condition of the p4 does not allow to state if a connection is present between these structures. The ectolophid is strong and longitudinal, linking the protoconid to the long and roughly transverse hypolophid. The ectolophid being labially located, it delimits, with the protoconid, the hypoconid, and its anterior outgrowth, a small hypoflexid, poorly extended labiolingually. A very short anterior arm of the hypoconid seems to be faintly connected to the hypolophid (i.e., non taeniodont pattern). The distal cristid formed by

the fusion of the hypoconid, its anterior outgrowth and a strong and curved posterolophid, runs lingually and reaches the posterior arm of the entoconid. Moreover, a short cristulid on the metaflexid links the anterior margin of the posterolophid to the hypolophid. As a result of this double connection of the posterolophid with the entoconid-hypolophid, the metaflexid is lingually closed and divided into two subfossettids, a small and round lingual one and a labial one, more labiolingually extended.

The lower molars are brachydont and rectangular, being wider than long (Fig. 3l, m). Contrary to the p4s, the trigonid and talonid are roughly similar in width, although the trigonid can be slightly narrower than the talonid (MUSM 3374; Fig. 3m). All lower molars are tetralophodont and non-taeniodont. The metaconid, protoconid and hypoconid are crestiform, whereas the entoconid and mesostylid are in contrast highly cuspate. On the unworn MUSM 3374 m1 (Fig. 3m), the protoconid, distolabially-mesiolingually pinched, is the highest cuspid of the tooth. The lower and smaller metaconid is positioned on the mesial margin of the tooth, and is mesiodistally compressed. This cuspid bears a strong, short and curved posterior arm faintly linked to a small mesostylid. On MUSM 3909, the protoconid and metaconid are linked by a strong and complete metalophulid I. On MUSM 3375 (Fig. 3l), the latter is formed by two cristids, a lingual long anterior arm of the metaconid connecting to a shorter labial anterior arm of the protoconid. On MUSM 3374 (Fig. 3m), the protoconid is well separated from the anterior arm of the metaconid by a large and deep notch. The anterior arm of the protoconid seems to be absent, but it is possible that it would appears on the labial slope of the anterior arm of the metaconid at a more advanced stage of wear. At the junction between the two anterior arms, a short cristid runs distolingually on the anteroflexid and then ends close to the base of a spur on the mesial margin of the second transverse cristid. MUSM 3375 also shows a very short spur on the mesial margin of the second transverse cristid (Fig. 3l). The second cristid, connecting the mesostylid to the protoconid, is quite thin and S-shaped on MUSM 3374 (Fig. 3m), and distolingually directed on MUSM 3375 (Fig. 3l). The ectolophid can be roughly longitudinal (i.e., parallel to the mesiodistal axis of the tooth; MUSM 3374 and 3375; Fig. 3l, m) or more oblique (MUSM 3909). The hypolophid is strong and transverse (MUSM 3375 and 3909; Fig. 3l) or slightly curved (MUSM 3374; Fig. 3m). It is connected labially to a thin but high and complete anterior arm of the hypoconid. The hypoconid has a long and mesiolabially oriented outgrowth. The entoconid is more mesially positioned with respect to the hypoconid, and bears a strong and short

posterior arm on MUSM 3374 (Fig. 3m). The posterolophid reaches the posterior arm of the entoconid and thus the metaflexid is closed lingually, forming a broad metafossettid.

The dP4 (MUSM 3911; Fig. 3e) is damaged and moderately worn. The paracone, labial protoloph, and most of the anteroloph are missing. Although damaged, the distal margin of this tooth and the preserved lingual part of its mesial margin suggest that this tooth would have been trapezoidal. Among the present cusps/styles, only the mesostyle on the labial margin is clearly visible. The mesostyle is mesially and distally separate from the paracone and the labial extremity of the posteroloph. The protocone corresponds to a large dentine platform due to wear. A lingual protoloph is strong and links the protocone to the mure (i.e., non-taeniodont pattern). The latter is complete and oblique, but not aligned with the anterior arm of the hypocone. The probable third transverse crest is straight and continuous. The metacone is not discernable, entirely subsumed within the posteroloph. The latter is long and curved. On the posterior flexus (i.e., confluence of the distal mesoflexus with the metaflexus), there is a wide structure corresponding to a thin dentine line, surrounded by massive enamel layer. It is mesiolabially directed, contiguous to the distal part of the third crest and to the mesial slope of the metacone. This structure is probably a part of the metaloph and/or relictual connections of this loph with the third crest and the posteroloph.

Three specimens are fragmented P4s (MUSM 3372, 3912, and 3913; Fig. 3d, j). Being slightly broken on its labial margin, MUSM 3913 is the most complete of the three (Fig. 3d). MUSM 3912 is damaged labially and lingually and the central part of MUSM 3372 is missing (Fig. 3j). MUSM 3372 and 3913 are oval in occlusal outline. With its paracone more lingually situated than the mesostyle and metacone, MUSM 3372 (Fig. 3j) shows a mesial part narrower than its distal part. The labial cusps/styles are well defined, whereas the protocone and hypocone are strongly crestiform. Via its long and curved posterior outgrowth, the protocone is twinned with the hypocone, forming a protocone-hypocone complex that closes the hypoflexus lingually. The anteroloph, low and short, remains separate from the paracone (MUSM 3372 and 3913) or reaches the base of this cusp (MUSM 3912). The paracone is clearly the largest cusp and displays a strong and oblique labial protoloph. The lingual extremity of the labial protoloph is mesially connected to a complete and distolabially directed lingual protoloph and distally to a high and longitudinal mure. On MUSM 3372 (Fig. 3j), the mesostyle and metacone are equal-sized. The mesostyle is separate from the paracone by a very thin furrow and it is faintly connected to the labial extremity of the

posteroloph. The metacone, slightly less distinct, is subsumed within the long posteroloph. Due to the advanced stage of wear of MUSM 3913 (Fig. 3d), the mesostyle, metacone and their potential associated lophs (i.e., mesoloph and metaloph, respectively) are fused on this tooth. They are probably subsumed within the posteroloph, forming a posterior broad dentine platform. On this P4, there are two short crestules on the anterior arm of the hypocone: anteriorly a mesolophule and posteriorly a neocrestule lingually free. The mesolophule appears to have two connections with the posterior platform, which could be with a mesoloph stemming from the mesostyle and a metaloph from the metacone. Despite of its fragmentary state, MUSM 3372 (Fig. 3j) shows a third transverse crest, connected to the mesostyle and the anterior arm of the hypocone, a metaloph, and a tiny damaged crest on the anterior arm of the hypocone backward to the third crest. This damaged crest being aligned with the metaloph, which seems to be unconnected to the posteroloph, might be a rest of a connection of the metaloph with the anterior arm of the hypocone. Another hypothesis is that it could be a neocrest lingually free as on MUSM 3913 (Fig. 3d).

The upper molars referred here to *Chachapoyamys kathetos* are brachydont, transverse and non-taeniodont (Fig. 3a–c, f–i, k). M2s are larger than M1s and M3s, and M1s are the smallest upper molars. The M3s differ from other Upper molars in having a hypocone clearly displaced much more labially. On the nearly pristine M2 (MUSM 3916; Fig. 3c), the protocone, strongly mesiolingually-distolabially pinched, is not discernable from its anterior arm and its posterior outgrowth, forming a high curved crest on the mesiolingual corner of the tooth. This crest, as well as the hypocone and its anterior and posterior arms, are the highest structures of the tooth. The anterior arm of the protocone and posterior arm of the hypocone are connected to a low and long anteroloph and posteroloph, respectively. The anteroloph can remain separate from the paracone by a tiny and shallow furrow (MUSM 3376, 3916–3918 and 3937; Fig. 3b, c, h, I, k) or can be faintly connected to this cusp (MUSM 3919; Fig. 3a). On MUSM 3917 (Fig. 3b), the labial extremity of the anteroloph is enlarged and could correspond to a parastyle. With wear, the posterior outgrowth of the protocone becomes longer especially on M2s and M3s. As a result of the development of a long posterior outgrowth of the protocone on these molars, the hypoflexus is more mesiodistally constricted. The lingual protoloph is always strong and complete. The labial protoloph is slightly oblique (i.e., mesiolabially directed) and the third transverse crest can be straight or parallel to the labial protoloph (MUSM 3919; Fig. 3a). The third crest is

composed of a long mesoloph stemming from the mesostyle associated with a mesolophular spur originating on the anterior arm of the hypocone. The mure is usually roughly longitudinal, but it can be more oblique as on M3s (Fig. 3a, g) and MUSM 3916 (Fig. 3c). On MUSM 3376 (Fig. 3k) and 3916 (Fig. 3c), the mure is incomplete because disconnected to the labial protoloph. On the labial margin, the mesostyle and the paracone are well defined and bulbous, the latter cusp being very large and protruding. These two cusps remain separate on all upper molars by a tiny furrow. On MUSM 3916 (Fig. 3c), there is an additional cusp-shaped structure between the labial protoloph and the third crest. On MUSM 3917 (Fig. 3b), a metacone is presente on the distolabial corner of the tooth and displays thin anterior and posterior arms as well as a short metaloph lingually free. On other upper molars, there is no distinct metacone, the latter being probably subsumed within the posteroloph. On MUSM 3918 (Fig. 3h) and 3920 (Fig. 3g), a thin metaloph lingually free is anteriorly oriented. MUSM 3937 displays a rounded structure on the posterior flexus, which probably corresponds to a residual metaloph (Fig. 3b). There is no metaconule. The posteroloph bears a posteroloph spur, almost incipient (MUSM 3916; Fig. 3c) or more developed (MUSM 3917, 3918, and 3919; Fig. 3a, b, h). It can reach an accessory crestule or a net of accessory crestules connected to the mesoloph-mesolophule junction (MUSM 3917 and 3918; Fig. 3b, h) or can be free (MUSM 3916 and 3919; Fig. 3a, c). In the latter case, it can end close to the accessory crestule stemming from the mesoloph-mesolophule junction (MUSM 3916; Fig. 3c).

Remarks. Although the MUSM 3376 M1 (Fig. 3k) is fragmentary, it has a smaller size with respect to the other M1s assigned to *Chachapoyamys kathetos*. Owing its characters similar to the other upper molars of *Ch*. *kathetos* (i.e., brachydonty, transversality, non-taeniodonty, third crest corresponding to a long mesoloph associated with a mesolophular spur, and accessory crestules between the third crest and the posteroloph), we consider that MUSM 3376 would have documented a small individual of this taxon.

Comparisons. By its brachydonty, bunolophodonty, thin and roughly transverse loph(-id)s, tetralophodont p4s and lower molars, with a posterior arm of the metaconid, mesostylid and complete second transverse cristid, the presence of a mesostyle, metacone and complete third transverse crest on upper teeth, and the presence of the metaloph (although strongly reduced) on some upper teeth, the morphology of *Chachapoyamys* from TAR-55/TAR-55bis is strongly reminiscente of that found in several Paleogene caviomorphs, particularly five basal caviomorph representatives:

Cachiyacuy, *Canaanimys*, *Eoespina*, *Eosachacui*, and *Eosallamys* from Peru (Eocene localities of Contamana, Balsayacu-Juanjui, and Santa Rosa; Frailey and Campbell 2004; Antoine et al. 2012; Boivin et al. 2017a; Assemat et al. 2019; Arnal et al. 2020), as well as *Balsayacuy huallagaensis* gen. et sp. nov. described above. By its non-taeniodonty, an important development of crestules (crestule from the third crest and posteroloph spur included) between the third transverse crest and the posteroloph on dP4s and upper molars, which can connect these two transverse crests on some Upper molars, this species from TAR-55/TAR-55bis is close to *Cachiyacuy contamanensis* from CTA-27 (Contamana, Peru; late middle Eocene; Antoine et al. 2012; Boivin et al. 2017a), *Cachiyacuy* cf. *contamanensis* and *Eosallamys paulacoutoi* from Santa Rosa (Peru, ?late Eocene/early Oligocene; Frailey and Campbell 2004; Arnal et al. 2020). The M1–2 s of *Cc*. *contamanensis* usually have a well-marked metaloph longer than on MUSM 3917, the unique upper molar of *Chachapoyamys* that distinctly bears this crest. In most cases, *Cc*. *contamanensis* has upper molars bearing a metaloph that ends very close to the crestules linking the third crest to the posteroloph (it can be connected to them), or that is only connected to the posteroloph (via crestules or not). Conversely, the short metaloph, which remains lingually free on MUSM 3917, is remote from these crestules. However, in *Cc*. *contamanensis*, the M3s show more frequently a reduction of the metaloph, whereas its M1–2s exhibit a high morphological variation of this crest in terms of development and connections. Indeed, on some M1–2s, the metaloph can be reduced to a short crest or a very short spur, or absent (MUSM 2744), and can be lingually free and far from the crestules between the third crest and the posteroloph (MUSM 2742), as in *Chachapoyamys*. The length of the metaloph of M1–2s of *Cachiyacuy* cf. *contamanensis* from Santa Rosa is shorter than the most frequent configuration of this crest in *Cc*. *contamanensis* but usually longer than in *Chachapoyamys*, in which the metaloph has a development more similar to the configuration of *Es*. *paulacoutoi*. The LACM 159241 M1 or M2 of *Cachiyacuy* cf. *contamanensis* and several upper molars of *Es*. *paulacoutoi* (LACM 143267, 144302, 149494, and 160206) show a similar morphology to that of MUSM 3917 from TAR-55/TAR-55bis and MUSM 2742 from CTA-27 in having a reduced metaloph remote from the crestules between the third crest and the posteroloph. Nevertheless, neither *Cachiyacuy* cf. *contamanensis* nor *Es*. *paulacoutoi* have an upper molar without metaloph, contrary to MUSM 3916 and 3919 from TAR-55/TAR-55bis. Unlike *Chachapoyamys*, the other upper molars of *Cachiyacuy* cf. *contamanensis* and *Es*. *paulacoutoi* have a metaloph connected to both the third crest and the posteroloph

(LACM 143376, 143380, 159245 and the LACM 143422 M2–3), or only to the third crest (LACM 159243, 159240, 143363 and the LACM 143422 M1). *Chachapoyamys* differs from *Cc*. *contamanensis*, *Cachiyacuy* cf. *contamanensis*, *Es*. *paulacoutoi*, as well as from *Eobranisamys* (CTA-27 and Santa Rosa) and '*Eosallamys*' *simpsoni* (Santa Rosa; Frailey and Campbell 2004; Boivin et al. 2017a; Arnal et al. 2020), in having a smaller size, similar to that of *Cc*. *kummeli*, *Canaanimys maquiensis* from CTA-27 (Antoine et al. 2012; Boivin et al. 2017a) and *B*. *huallagaensis*. The metaloph of *Cc*. *kummeli* is reduced or almost absent and lingually free on M2s, and more developed and tends to connect to the posteroloph (via a potential very short posteroloph spur) on M1s and M3s (Antoine et al. 2012; Boivin et al. 2017a; Arnal et al. 2020; this work). On upper molars of this species, there is no crestule that tend to link the third crest to the posteroloph. On M1–2s of *Cn*. *maquiensis*, the metaloph is long, turned forward and ends close to the third crest, and can connect to the latter. *Chachapoyamys* differs from *Es*. *paulacoutoi* and some p4s of *Cc*. *contamanensis* in having no accessory cristulid on the anteroflexid and/or mesoflexid (mesolophid included) on p4s; from *Es*. *paulacoutoi* in having P4s with a oblique lingual protoloph; and from *Canaanimys* cf. *maquiensis* from CTA-27 (Arnal et al. 2020) in having P4s with a more oblique lingual protoloph and lower molars with always a complete second cristid. In comparison to *Ch*. *kathetos*, *B*. *huallagaensis* from the same locality show a tendency toward a taeniodont pattern in having a pattern II of pseudo-taeniodonty on lower molars and a more frequent pattern I of pseudo-taeniodonty on Upper molars; a rounded P4 with a transverse lingual protoloph, a connection of its labial structures at a moderate stage of wear, a third crest disconnected to the mesostyle and without metaloph; a longer posterior arm of the metaconid on lower molars; a tendency to have a mesoloph disconnected to the anterior arm with the reduction/absence of the mesolophule on M1–2s; and a reduction or more frequent absence of the crestules between the third crest and the posteroloph By its upper molars with a strong reduction or absence of the metaloph, *Chachapoyamys* recalls *Eoespina woodi*, *Eosachacui lavocati*, and '*Es*.' *simpsoni* (Santa Rosa; Frailey and Campbell 2004; Arnal et al. 2020), as well as *Pozomys ucayalensis* (CTA-29 and Santa Rosa; Boivin et al. 2017a; Arnal et al. 2020), *Chachapoyamys* differs from all taxa mentioned above in having more transverse lower molars; from all taxa mentioned above (except *Cc*. *maquiensis*) in having more transverse upper molars; from *Cn*. *maquiensis*, *Eobranisamys*, and *P*. *ucayalensis* in having non-taeniodont teeth; from *P*. *ucayalensis* in having a curved (i.e., mesially concave) second cristid on p4s; from *Eoespina* and *Eosachacui* in having

no accessory cristulids on the anteroflexid and/or mesoflexid (mesolophid included) on p4s; from *Cachiyacuy*, *Eoespina*, *Es*. *paulacoutoi*, and '*Es*.' *simpsoni* in having a more important discontinuity of the metalophulid I on p4s; from all taxa mentioned above (except *P*. *ucayalensis*) in having lower molars, which can have a more importante discontinuity of the metalophulid I close to the protoconid; from *Eobranisamys* and '*Es*.' *simpsoni* in having a reduced metaloph disconnected to the posteroloph on dP4s; from *Eosachacui* in having a rest of metaloph on the posterior flexus on dP4s; from *Eoespina* in having always a third crest connected to the mesostyle on P4s; from *Eosachacui* and '*Es*.' *simpsoni* in having a metaloph on P4s; from *Eobranisamys* and *Eosachacui* in having P4s with a complete mure; from *Eosachacui* in having non-taeniodont P4s; from *Eobranisamys* in having P4s with paracone, which remains separate the mesostyle at a moderate stage of wear, and a shorter or absent metaloph on upper molars; and from *Eobranisamys*, *Ep*. *woodi* and *P*. *ucayalensis* in having some upper molars with a connection between the third crest and the posteroloph. Some teeth from TAR-55/TAR-55 attributed here to *Chachapoyamys kathetos* were previously referred to *Cachiyacuy* cf. *kummeli* (MUSM 3372 and 3374–3376; Assemat et al. 2019). The discovery of new dental material from TAR-55/TAR-55bis including new loci has allowed us to refine the former attributions. The Upper molars of *Chachapoyamys* are included in the morphological variation of *Cc*. *contamanensis*, *Cachiyacuy* cf. *contamanensis*, and *Es*. *paulacoutoi*. Owing an absent or more reduced metaloph than the most frequent morphology of this crest in these taxa, its transverse molars, the discontinuity of the metalophulid I on p4s and lower molars with a short posterior arm of the protoconid, we attribute this material from TAR-55/TAR-55bis to a new taxon: *Chachapoyamys kathetos* gen. et sp. nov.

Chachapoyamys cf. ***kathetos***

Figure 3o, p

2017a *Cachiyacuy kummeli*—Boivin et al.: 8, fig. 4.13.

Referred material. MUSM 2786 (Boivin et al. 2017a: fig. 4.13; Fig. 3o), 3943 (Fig. 3p), left M1 or M2.

Locality. CTA-27, Contamana, Loreto Department, Western Amazonia, Peru.

Formation and age. Pozo Formation, lower member, late middle Eocene (i.e., Barrancan or Mustersan SALMAs).

Description. MUSM 2786 and 3943 are brachydont and transverse-shaped (Fig. 3o, p). The transverse crests (anteroloph, protoloph, mesolophule/mesoloph, and posteroloph) are thin. There is no metaconule. Lingually, the protocone is massive and distolabially-mesiolingually compressed. On MUSM 2786 (Fig. 3o), the protocone displays a short distolabially directed posterior arm, which reaches a longer crestule from the labial protoloph-mure junction. These two crestules are joined at their base, but remain separate at their top by a very tiny and shallow notch (i.e., pattern II of pseudo-taeniodont). MUSM 3943 (Fig. 3p) shows a complete posterior arm of the protocone (i.e., non-taeniodont pattern). However, the latter is slightly connected to the labial protoloph-mure junction. Hence, it is possible that MUSM 3943 had a pseudo-taeniodont pattern at earlier stages of wear (Fig. 3p). The anteroloph is long and barely curved. From the protocone, the anteroloph runs labially and reaches the paracone. The parafossette is labiolingually well extended. The labial protoloph is long and slightly oblique. The mure connects the anterior arm of the hypocone to the protoloph lingually. The mure is thin and longitudinal on MUSM 3943 (Fig. 3p), whereas it is thicker and oblique on MUSM 2786 (Fig. 3o). The third transverse crest, strongly developed, links the anterior arm of the hypocone to a strong mesostyle, centrally situated in the labialmost margin of the crown. This crest is formed by the union of a long and straight mesoloph with a short and slightly distolabially oblique mesolophule. The mesostyle is mesially isolated from the paracone (or from its posterior arm). This style is clearly disconnected to the metacone on MUSM 3943 (Fig. 3p), while its posterior arm links to the metacone on MUSM 2786 (Fig. 3o). Due to the moderate stage of wear of the teeth, the metacone is not visible and seems to be fused with the posteroloph. At the level of the metacone area, MUSM 2786 has a thickening of the posteroloph, without metaloph (Fig. 3o). On MUSM 3943, a tiny spur, stemming from the metacone and interpreted as a relic of the metaloph, is present on the mesial slope of the posteroloph (Fig. 3p). Both upper molars are characterized by a connection between the third crest and the posteroloph on the posterior flexus (i.e., confluence of the distal mesoflexus with the metaflexus). On MUSM 2786, this connection is formed by two accessory crestules: a mesial crestule from the third crest joining a posteroloph spur (Fig. 3o). On MUSM 3943, these two accessory crestules appear to be present, as well as a third accessory crestule, which would be longer, stronger and mesiolingually directed (Fig. 3p). It is faintly connected mesially to the crestule from the third transverse crest, and distally to the posteroloph and its spur. This crestule

may be a part of relictual connections of the metaloph (and a part of this loph?) to the third transverse crest and posteroloph.

Comparisons. By their brachydonty, bunolophodonty, thin and roughly transverse lophs, the presence of a mesostyle, metacone and complete third transverse crest, the morphology of MUSM 2786 and 3943 is strongly reminiscent of that found in several Paleogene caviomorphs. By the presence of a long lingual protoloph, and a connection, via crestule(s) between the third transverse crest and the posteroloph, MUSM 2786 and 3943 recall upper molars of the basal caviomorphs from Peru, *Cachiyacuy* and *Eosallamys* (Eocene localities of Contamana and Balsayacu-Juanjui, and Santa Rosa; Frailey and Campbell 2004; Antoine et al. 2012; Boivin et al. 2017a; Assemat et al. 2019; Arnal et al. 2020), as well as upper molars of *Chachapoyamys kathetos* gen. et sp. nov. from TAR-55/55-bis. MUSM 2786 and 3943 are closer to *Chachapoyamys kathetos* in being transverse and in having a very minute or absent metaloph. The size of MUSM 2786 and 3943 is similar to that of the M1s of *Chachapoyamys kathetos*. However, MUSM 2786 and 3943 are more transverse than the upper molars of *Chachapoyamys kathetos*. Moreover, these two specimens from CTA-27 have mesiodistally thinner flexi, a stronger connection between the anteroloph and the paracone, and a slight reduction of the lingual protoloph (pattern II of pseudo-taeniodonty, at least for MUSM 2786). MUSM 2786 and 3943 differ from the upper molars of *Cachiyacuy contamanensis* and *Eosallamys* in being more transverse; from the upper molars of *Eosallamys* and the most of upper molars of *Cc*. *Contamanensis* in having a much shorter metaloph or an absence of this loph. MUSM 2786 and 3943 recall the M2s of *Cachiyacuy kummeli* from CTA-27 and Santa Rosa (Antoine et al. 2012; Boivin et al. 2017a; Arnal et al. 2020; Fig. 3u) in having a similar size and in bearing an incipient or absent metaloph (see below). However, the upper molars of Cc. kummeli have a paracone strongly separate from the anteroloph and do not show similar crestules located between the third transverse crest and the posteroloph. The upper molars of *Balsayacuy huallagaensis* gen. et sp. nov. can have crestules located between the third transverse crest and the posteroloph, but they are shorter. Unlike MUSM 2786 and 3943, the M1–2s of *Balsayacuy* are square-shaped with mesiodistally well-expanded flexi. Owing to the differences between MUSM 2786 and 3943 and the upper molars of *Chachapoyamys kathetos* and the low quantity of this material from CTA-27, we prefer keeping it in open nomenclature, as *Chachapoyamys* cf. *kathetos*.

Genus ***Cachiyacuy*** Antoine, Marivaux, Croft, Billet, Ganerod, Jaramillo, Martin, Orliac, Tejada, Altamirano, Duranthon, Fanjat, Rousse, and Salas-Gismondi, 2012

Type species. *Cachiyacuy contamanensis* Antoine, Marivaux, Croft, Billet, Ganerod, Jaramillo, Martin, Orliac, Tejada, Altamirano, Duranthon, Fanjat, Rousse, and Salas-Gismondi, 2012.

Species content. The type species and *Cachiyacuy kummeli* Antoine, Marivaux, Croft, Billet, Ganerod, Jaramillo, Martin, Orliac, Tejada, Altamirano, Duranthon, Fanjat, Rousse, and Salas-Gismondi, 2012.

Cachiyacuy kummeli Antoine, Marivaux, Croft, Billet, Ganerod, Jaramillo, Martin, Orliac, Tejada, Altamirano, Duranthon, Fanjat, Rousse, and Salas-Gismondi, 2012
Figure 3q

Holotype. MUSM 1882, left M1 (in Antoine et al. 2012: 1322, fig. 2m).

Referred material. MUSM 2785 (Boivin et al. 2017a: fig. 4.12; Fig. 3q), left M2.

Locality. CTA-27, Contamana, Loreto Department, Western Amazonia, Peru.

Formation and age. Pozo Formation, lower member, late middle Eocene (i.e., Barrancan SALMA).

Description. MUSM 2785 is a pristine M2, labially broken at the level of the mesostyle (Fig. 3q). It is brachydont, transverse-shaped, fully tetralophodont and characterized by a pattern II of pseudo-taeniodonty. The protocone is the most massive cusp. The latter, as well as the hypocone and the metacone (see below), are crestiform, whereas the paracone is more bulbous. There is no metaconule. The transverse crests (anteroloph, protoloph, mesolophule/mesoloph, and posteroloph) are thin. The first loph and posteroloph are long and curved, anteriorly convex or concave, respectively. Conservely, the labial protoloph and the third crest are straight, roughly parallel and slightly oblique (i.e., mesiolabially directed). The protocone has a long anterior arm, which is separate from the anteroloph by a very tiny and shallow notch. The labial part of the anteroloph is isolated from the paracone and enlarged, thus it probably corresponds to a parastyle. The mure is rather longitudinal and divided into two equal-sized crestules: a mesial crestule stemming from the labial protoloph and a distal one from the third crestanterior arm of the hypocone junction. The third crest, strongly developed, links the mesostyle to the anterior arm of the hypocone. This crest is formed

by a long mesoloph and a shorter and distolabially oblique mesolophule. There is neither metaloph nor distinct metacone. However, considering the other upper molar attributed to this taxon (Antoine et al. 2012; Arnal et al. 2020), this cusp is probably fused with the posteroloph. The hypocone has a short, but strong, posterior arm slightly connected to the posteroloph. Labially, the paraflexus and probably the mesial mesoflexus are opened, whereas the posterior flexus (i.e., confluence of the distal mesoflexus and metaflexus) is closed and forms a well-extended fossette.

Remarks. MUSM 2785 has a size and general morphology similar to that the other upper molars attributed to this taxon (Antoine et al. 2012; Arnal et al. 2020). MUSM 2785 was originally described as a M1 by Boivin et al. (2017a). However, other M1s of *Cachiyacuy kummeli* (MUSM 1882 [Antoine et al. 2012: fig. 2m] and LACM 159246 [Arnal et al. 2020: fig. 2T]) are characterized bu a well-marked metaloph, a loph absent on MUSM 2785. The metaloph is almost absent on M2s of *Cc*. *kummeli* (MUSM 1883 [Antoine et al. 2012: fig. 2n], LACM 159244 [Arnal et al. 2020: fig. 2V], and LACM 159250 [Arnal et al. 2020: fig. 2W]), reduced to a minute cups-shaped structure on the posterior flexus. Furthermore, the rectangular shape of MUSM 2785 is more similar to that of the MUSM 1883 M2 than the holotype (the MUSM 1882 M1). Based on these two characters (i.e., absence of metaloph and rectangular shape), we consider MUSM 2785 as being a M2 instead of a M1.

Caviomorpha gen. et sp. indet. 1

Figure 3r, s, Table 2

Referred material. MUSM 3939 (Fig. 3r), right labial fragment of lower molar or left lingual fragment of upper molar; MUSM 3940 (Fig. 3s), left P4.

Locality. TAR-55/TAR-55bis, Balsayacu, San Martin Department, Western Amazonia, Peru.

Formation and age. Pozo Formation, lower member, late middle Eocene to early late Eocene (i.e., Barrancan or Mustersan SALMAs).

Description. MUSM 3939 is a right labial fragment of a moderately worn lower or upper molar, in which only the protoconid/hypocone area, the parts of the hypoflexid/hypoflexus and the anterior outgrowth of the hypoconid/posterior outgrowth of the protocone are preserved (Fig. 3r). The anterior outgrowth of the hypocone/posterior outgrowth of the protocone seems to be mostly labially/lingually directed and the hypoflexid/hypoflexus does not show any mesiodistal constriction.

These characters suggest that this damaged tooth could be a labial fragment of lower molar instead of a lingual fragment of upper molar.

MUSM 3940 is an eroded, labially broken and moderately worn P4 (Fig. 3s). The anteroloph, paracone, and the labial part of the labial protoloph are missing. MUSM 3940 is non-taeniodont and could be tetralophodont. The protocone displays a strong posterior arm (or lingual protoloph) connected to the labial protoloph and a long and curved posterior outgrowth. The latter reaches the anterior arm of a minute hypocone. As it is not confluent with the paraflexus and given it is lingually closed, the hypoflexus forms a fossette mesiodistally extended. The mure is long, longitudinal, and composed of two linked crests, a strong mesial one stemming from the labial protoloph and a thinner distal one that runs from the oblique anterior arm of the hypocone. The third transverse crest is straight and distally situated, close to the posteroloph. Because of the position of the third crest, the mesial mesoflexus is well expanded. Conversely, the posterior flexus is strongly reduced (i.e., confluence of the distal mesoflexus with the metaflexus). All the preserved labial structures are connected, and thus, the mesial mesoflexus and the posterior flexus form two fossettes.

Comparisons. Despite their very fragmentary nature, these two specimens document the presence of a medium-sized species, which is the largest taxon to be recorded at TAR-55/TAR-55bis. The MUSM 3939 and 3940 are comparable in size to the material attributed to *Eobranisamys javierpradoi* from CTA-27 (Contamana, Peru; late middle Eocene; Boivin et al. 2017a). By its characters (i.e., possible tetralophodont pattern, transverse crest distally positioned, and a labial link between the labial protoloph, the third crest and the posteroloph), the MUSM 3940 P4 has a morphological pattern close to that of the P4s of *Eb*. *javierpradoi* (Antoine et al. 2012: 1322, fig. 2a'; Boivin et al. 2017a) in having a similar oval occlusal outline, and a mesial mesoflexus mesiodistally well-extended and labially closed in moderate stage of wear. However, a typical character of *Eb*. *javierpradoi*, the taeniodonty of its upper molars, is not present on MUSM 3940. In addition, the P4s of *Eb*. *javierpradoi* are characterized by an incomplete mure, while it is complete on MUSM 3940. Some taxa can show tetralophodont and non-taeniodont P4s as MUSM 3940: *Balsayacuy huallagaensis* gen. et sp. nov. (MUSM 3936), *Cachiyacuy contamanensis* (MUSM 2725), *Cachiyacuy* aff. *kummeli* from TAR-47 (Juanjui; MUSM 3523), *Eoespina woodi* (LACM 143459), *Eosallamys paulacoutoi* (LACM 143415), and '*Eosallamys*' *simpsoni* (LACM 149451; Frailey and Campbell 2004; Boivin et al. 2017a; Assemat et al. 2019; Arnal et al. 2020). MUSM 3940 differs from P4s of all these taxa in having a more mesiodistally extended

mesial hypoflexus; all these taxa except to *Cc*. aff. *kummeli* from TAR-47 in having a more mesiodistally extended mesial mesoflexus; of *Cc*. aff. *kummeli* from TAR-47 and *Ep*. *woodi* in having a complete third crest; from other P4s of *Es*. *paulacoutoi* (LACM 143422 and 159214) in having no metaloph. Owing to the fragmentary state of these teeth and the poor quantity of material, we provisionally refer the material of TAR-55/TAR-55bis to as Caviomorpha gen. et sp. indet. 1.

Caviomorpha gen. et sp. indet. 2

Figure 3t, Table 2

Referred material. MUSM 3941 (Fig. 3t), left posterior fragmente of dp4 or p4.
Locality. TAR-76, Balsayacu, San Martin Department, Western Amazonia, Peru.
Formation and age. Pozo Formation, lower member, late middle Eocene to early late Eocene (i.e., Barrancan or Mustersan SALMAs).
Description. MUSM 3941 is a fragment corresponding to the posterior part of a p4, bearing digestion marks (Fig. 3t). Only the entoconid, hypolophid, hypoconid, its anterior arm and outgrowth, and the posterolophid are preserved. Mesially, the tooth shows a rest of a transverse cristid, probably of a neomesolophid or posterior arm of the protoconid. The area of the mesostylid is broken. The entoconid is bulbous and bears a roughly straight hypolophid. The anterior arm of the crestiform hypoconid and the labial extremity of the hypolophid are separate at their top, but connected at their base (i.e., pattern II of pseudo-taeniodonty). The anterior outgrowth of the hypoconid is very short, strong, with a strong labially-directed component. MUSM 3941 is characterized by a posterolophid strongly curved and connected to the posterior slope of the entoconid. The latter characters (i.e., short anterior outgrowth of the hypoconid, labially directed, and posterolophid strongly curved) suggest that this damaged tooth would be a distal fragment of right dp4 or p4. *Comparisons*. By its brachydonty, bunolophodonty, thin and roughly transverse lophids, the presence of a posterior arm of the metaconid, mesostylid and complete second transverse cristid, the morphology of MUSM 3941 is strongly reminiscent of that found in several Paleogene caviomorphs. MUSM 3941 shows a pattern II of pseudo-taeniodonty as *Balsayacuy huallagaensis* gen. et sp. nov. In the case of that specimen would be a p4, its size would be similar to that of *B*. *huallagaensis* and *Chachapoyamys kathetos* gen. et sp. nov. from TAR-55/TAR-55bis. However, in the case of that specimen would be a dp4, its size would be clearly larger than that of these taxa, and perhaps could be similar to that of

Caviomorpha gen. et sp. indet. 1 described above. The fragmentary nature of MUSM 3941 does not allow to conclude regarding the determination of this material as *B. huallagaensis*, *Chachapoyamys kathetos*, Caviomorpha gen. et sp. indet. 1, or another early caviomorph.

Discussion

A single caviomorph assemblage at TAR-55/TAR-55bis, TAR-76 and TAR-77

Two taxa were previously described at TAR-55/TAR-55bis: *Cachiyacuy* cf. *kummeli* and *Canaanimys* aff. *Maquiensis* (Assemat et al. 2019). The study of the new material from these localities has allowed for a taxonomic revision of the rodent fauna from TAR-55/TAR-55bis. Three taxa are currently recognized: *Balsayacuy huallagaensis* gen. et sp. nov. (coinciding fully with *Canaanimys* aff. *maquiensis* sensu Assemat et al. 2019 and partly with *Cachiyacuy* cf. *kummeli* sensu Assemat et al. 2019), *Chachapoyamys kathetos* gen. et sp. nov. (partly synonymous with *Cachiyacuy* cf. *kummeli* sensu Assemat et al. 2019) and Caviomorpha gen. Et sp. indet. 1. *Balsayacuy huallagaensis* also occurs at TAR-77. The material from TAR-76, here referred to as Caviomorpha gen. et sp. indet. 2, could be attributed to both *B. huallagaensis* and *Chachapoyamys kathetos*. Nevertheless, this material could also document other early caviomorphs and its fragmentary nature and advanced stage of wear do not allow us to conclude on their taxonomic determination. This taxonomic uniformity is compatible with the existence of short time interval between all the localities from the upper part of the stratigraphic section (within a 90 m-thick section), as suggested by similar conditions, based on lithology (see Assemat et al. 2019). Hence, the concerned assemblages caviomorph samples are likely to document a single local faunal assemblage. *Balsayacuy huallagaensis*, *Chachapoyamys kathetos* and Caviomorpha gen. et sp. indet. 1. share dental characters, considered as plesiomorphic in caviomorphs: small size; brachydonty; bunolophodonty; thin and transverse loph(-id)s; tetralophodont p4s and lower molars with a posterior arm of metaconid, mesostylid and complete second transverse cristid; presence of a mesostylid and third transverse crest on upper teeth; presence of a metacone on upper molars; and presence of a metaloph, although very reduced, on some upper molars (Antoine et al. 2012; Boivin et al. 2017a, 2019b; Boivin and Marivaux 2020). These three taxa show strong morphological affinities with basal caviomorphs found in pre-Deseadan localities of Peru, especially in CTA-27 (Contamana, late Middle Eocene; Antoine et al. 2012; Boivin et al. 2017a) and, to a lesser extent, Santa Rosa (Frailey

and Campbell 2004; Arnal et al. 2020). By having some upper molars bearing accessory structures between the third transverse crest and the posteroloph, and which tend to connect to both transverse crests, *Balsayacuy* and *Chachapoyamys* are particularly close to *Cachiyacuy* and *Eosallamys* from CTA-27 and Santa Rosa. However, contrary to *Balsayacuy* and *Chachapoyamys*, in which the metaloph is absent or strongly reduced and lingually free, *Cachiyacuy contamanensis* and *Eosallamys paulacoutoi* have a longer metaloph, which ends very close to these accesory structures or that is connected to them in most cases. Within caviomorphs, a connection between the third crest and the metaloph is unusual, and otherwise found only in *Canaanimys maquiensis* from CTA-27, *Canaanimys* cf. *maquiensis* from Santa Rosa and on one upper molar of *Eosachacui* from Santa Rosa (LACM 143292; Frailey and Campbell 2004; Antoine et al. 2012; Boivin et al. 2017a; Arnal et al. 2020). As previously noted (Antoine et al. 2012; Boivin et al. 2017a), in non-caviomorph hystricognathous rodents, some earliest African–Asian hystricognaths ("protophiomyines", "baluchimyines", and "bugtimyids"; Marivaux and Boivin 2019) are characterized by this connection (e.g., *Baluchimys*, *Hodsahibia*, *Bugtimys*, *Protophiomys*, *Walsamys*), but some others "phiomyids" also have a double connection of the metaloph with the third crest and the posteroloph (e.g., *Acritophiomys*, *Phiomys*, *Phenacophiomys*). As a result, these species from CTA-27 (i.e., *Cn*. *Maquiensis* and *Cc*. *contamanensis*) and to a lesser extent some taxa from Santa Rosa (i.e., *Canaanimys* cf. *maquiensis*, *Cachiyacuy* cf. *contamanensis*, and *E*. *paulacoutoi*; because they have M1–2 s with a more reduced metaloph than in species from CTA-27) appear to be the caviomorph taxa so far known with a strongly reminiscent occlusal morphology with these African-Asian basal hystricognaths. Moreover, *Balsayacuy* and *Chachapoyamys* share some characters with other taxa from CTA-29 (another Eocene locality from Contamana) and Santa Rosa: *Eoespina woodi*, *Eosachacui lavocati*, '*Eosallamys*' *simpsoni* and *Pozomys ucayalensis* (Frailey and Campbell 2004; Boivin et al. 2017a; Arnal et al. 2020). According to the recent phylogenetic analyses of Boivin et al. (2019b), these species are resolved as basal representatives of caviomorphs (early stem Caviomorpha). Finally, Caviomorpha gen. et sp. indet. 1 from TAR-55/TAR-55bis exhibits some affinities with *Cc*. *contamanensis*, *Cachiyacuy* aff. *kummeli* from TAR-47 (Juanjui: Assemat et al. 2019), *Ep*. *woodi*, *Es*. *paulacoutoi*, and '*Es*.' *simpsoni*, as well as with *Eobranisamys javierpradoi* from CTA-27 (Boivin et al. 2017a), a species also recently recognized as a stem caviomorph (Boivin et al. 2019b). In conclusion, all three rodent taxa from TAR-55/TAR-55bis would

likely be basal representatives of caviomorphs. *Balsayacuy* and *Chachapoyamys* seem to have slightly more advanced morphology of their M1–2 s over *Cn*. *maquiensis*, *Cc*. *contamanensis* and *E*. *paulacoutoi* by showing a metaloph that is either absent or strongly reduced and lingually free.

Age of TAR-55/TAR-55bis, TAR-76 and TAR-77

Although three taxa are henceforth recognized at TAR-55/TAR-55bis and they have different names from those described before (see Assemat et al. 2019), they are strongly similar with some basal caviomorph representatives, suggesting an old age for these localities, as proposed by Assemat et al. (2019). According to these authors, these localities would be late middle Eocene in age owing to their species resemblance with the late middle Eocene localities of Contamana (in particular with CTA-27), and in the absence of taxa with more derived dental characters and representatives of modern superfamilies of caviomorphs, even as dental fragments (Boivin et al. 2019b). The younger deposits of the region (TAR-49 and TAR-50, Juanjui area) record taxa evolutionarily more advanced, with an occlusal morphology characterized by a marked obliquity of loph(-id)s (the chinchilloid *Eoincamys*), and some with incisors having already achieved a derived multiserial enamel subtype 2–3 (Assemat et al. 2019). *Eoincamys* was originally described in Santa Rosa (Frailey and Campbell 2004) and subsequently in the localities of the Shapaja section near Tarapoto (Peru; Boivin et al. 2018a; Antoine et al. in revision). The latter section ranges the late Eocene–early Oligocene time interval, based on mammalian biostratigraphy, depositional environment sequence, stratigraphic correlation in the northern Peruvian foreland (Boivin et al. 2018a; Assemat et al. 2019), and chemostratigraphy (Antoine et al. in revision). The age of Santa Rosa is less constrained. Santa Rosa has yielded caviomorph taxa related to those of the Eocene localities of Contamana, as recognized through newly described specimens (Arnal et al. 2020). Santa Rosa unambiguously has a younger signature, however, as suggested by the conspicuous occurrence of at least three of the four modern superfamilies of caviomorphs, such as *Eoincamys* (Chinchilloidea), *Eodelphomys* (Octodontoidea) or *Eopululo* (Erethizontoidea; Frailey and Campbell 2004; De Vries and Seiffert 2017; Boivin et al. 2019b). These genera, or closely related taxa, further occur around the Eocene–Oligocene transition at Shapaja-Tarapoto (Antoine et al. in revision). In accordance with the results of Assemat et al. (2019), the Balsayacu caviomorph record (from TAR-56, TAR-76, TAR-77, and TAR-55/TAR-55bis) attests to the full absence of taxa with such an advanced occlusal

morphology in these localities, as well as in TAR-76 and TAR-77 (and TAR-56; see Assemat et al. 2019), even through dental fragments. In addition, we could assign two upper molars from CTA-27 to *Chachapoyamys* cf. *kathetos* (one of them had previously been referred to as *Cc*. *kummeli*; Boivin et al. 2017a). The presence of somewhat derived characters observed in *Balsayacuy* and *Chachapoyamys* with respect to *Canaanimys maquiensis* and *Cachiyacuy contamanensis* (i.e., a metaloph absent or strongly reduced and lingually free) suggests that TAR-55/TAR-55bis, TAR-76 and TAR-77 document a time interval posterior to CTA-27, i.e., documenting latest middle or early late Eocene.

Conclusion

The study of new caviomorph material from TAR-55/TAR-55bis, TAR-76 and TAR-77 (Balsayacu) reveals the presence of four caviomorph taxa in these localities: *Balsayacuy huallagaensis* gen. et sp. nov., *Chachapoyamys kathetos* gen. et sp. nov. and Caviomorpha gen. et sp. indet. 1 and 2. The first three taxa show strong affinities with stem Caviomorpha recorded in pre-Deseadan localities in Peru (Eocene localities of Contamana plus Santa Rosa), and thus providing additional information regarding the paleodiversity of early low latitude caviomorphs of South America. In accordance with the results of a previous study (Assemat et al. 2019), we propose an Eocene age for the Balsayacu section, based on the absence of morphologically derived taxa, and notably the absence of representatives of the four modern superfamilies of Caviomorpha (contrary to younger localities such as TAR-49, TAR-50, those of the Shapaja section, and Santa Rosa). In other words, the Balsayacu section may document intermediate between CTA-27 (late middle Eocene) and Santa Rosa/Shapaja/Juanjui assemblages (latest Eocene–early Oligocene. Continuing field efforts in this Amazonian region of the Andean foothills should provide new critical insights into the early evolutionary history and paleodiversity of small South American mammals. Taxonomic-free age constraints such as provided by U/Pb datings on detrital zircon grains or chemostratigraphy would considerably add to the knowledge of the evolutionary dynamics of such puzzling African-Asian Paleogene incomers.

Acknowledgements Many thanks to all the people that helped us in the field and in the lab. We are particularly grateful to our drivers Giancarlo, Manuel, and Percy, for their long-standing help during the yearly field seasons in the San Martin Department of Peruvian Amazonia. We warmly thank A. Assemat (ISEM, Montpellier, France) for

taking SEM photographs of the original specimens from TAR-55/TAR-55bis collected in 2015–2016; C. Cazeveille (Montpellier RIO Imaging, Institut des Neurosciences de Montpellier, France) for access to a scanning electron microscope facility; and C. Girard (ISEM) for access to her optical stereomicroscope facility. We are indebted to A.-L. Charruault and S. Jiquel (ISEM) for the cast preparation of the rodent material from the Balsayacu section and from other Peruvian localities. We also thank the Editors of the PalZ. Palaontologische Zeitschrift, Thomas Mors and Mike Reich, as well as M. Arnal (MLP, La Plata, Argentina) and A. Kramarz (MACN, Buenos Aires, Argentina), who provided formal reviews of this manuscript that enhanced the final version. This work was supported by The Leakey Foundation, the National Geographic Society, the “Investissements d’Avenir” grant managed by the “Agence Nationale de la Recherche” (CEBA, ANR-10-LABX-25-01), and by the COOPINTEER CNRS/CONICET (n° 252540) and the ECOS-SUD/FONCyT (n° A-14U01) international collaboration programs. This work was carried out in the frame of the ongoing cooperation agreement between the “Museo de Historia Natural de la Universidad Nacional Mayor San Marcos” (Lima, Peru) and the “Institut des Sciences de l’Evolution de Montpellier-Universite de Montpellier” (France). This is ISEM publication 2021-032-Sud.

References

Antoine, P.-O., R. Salas-Gismondi, P. Baby, M. Benammi, S. Brusset, D. De Franceschi, N. Espurt, C. Goillot, F. Pujos, J. Tejada, and M. Urbina. 2007. The middle Miocene (Laventan) Fitzcarrald fauna, Amazonian Peru. In Proceedings of the 4th EMPSLA, eds. E. Diaz-Martinez, and I. Rabano. *Cuadernos del Museo Geominero* 8: 19–24.

Antoine, P.-O., L. Marivaux, D.A. Croft, G. Billet, M. Ganerod, C. Jaramillo, T. Martin, M.J. Orliac, J. Tejada, A. J. Altamirano, F. Duranthon, G. Fanjat, S. Rousse, and R. Salas-Gismondi. 2012. Middle Eocene rodents from Peruvian Amazonia reveal the pattern and timing of caviomorph origins and biogeography. *Proceedings of the Royal Society of London (B: Biological Sciences)* 279: 1319–1326.

Antoine, P.-O., M. Roddaz, S. Brichau, J. Tejada-Lara, R. Salas-Gismondi, A. Altamirano, M. Louterbach, L. Lambs, T. Otto, and S. Brusset. 2013. Middle Miocene vertebrates from the Amazonian Madre de Dios Subandean Zone, Peru. *Journal of South American Earth Sciences* 42: 91–102.

Antoine, P.-O., M.A. Abello, S. Adnet, A.J. Altamirano Sierra, P. Baby, G. Billet, M. Boivin, Y. Calderon, A. Candela, J. Chabain, F. Corfu, D.A. Croft, M. Ganerod, C. Jaramillo,

S. Klaus, L. Marivaux, R.E. Navarrete, M.J. Orliac, F. Parra, M.E. Perez, F. Pujos, J.-C. Rage, A. Ravel, C. Robinet, M. Roddaz, J.V. Tejada-Lara, J. Velez-Juarbe, F.P. Wesselingh, and R. Salas-Gismondi. 2016. A 60-million-year Cenozoic history of western Amazonian ecosystems in Contamana, eastern Peru. *Gondwana Research* 31: 30–59.

Antoine, P.-O., R. Salas-Gismondi, F. Pujos, M. Ganerod, and L. Marivaux. 2017. Western Amazonia as a hotspot of mammalian biodiversity throughout the Cenozoic. In Proceedings of the Symposium Cenozoic Evolution of TRopical-Equatorial Mammals (IPC4), eds. P.-O. Antoine, and F. Pujos. *Journal of Mammalian Evolution* 24: 5–17.

Antoine, P.-O., J. Yans, A. Aliaga Castillo, N. Stutz, M.A. Abello, S. Adnet, M. Andriolli Custodio, A. Benites-Palomino, G. Billet, M. Boivin, F. Herrera, C. Jaramillo, C. Martinez, F. Moreno, R.E. Navarrete, F.R. Negri, F.J. Parra, F. Pujos, J.-C. Rage, A.M. Ribeiro, C. Robinet, M. Roddaz, J. Tejada Lara, R. Varas-Malca, R. Ventura Santos, R. Salas-Gismondi, and L. Marivaux. 2021, in revision. Biotic community and landscape changes around the Eocene–Oligocene transition at Shapaja, Peruvian Amazonia: regional or global drivers? *Global and Planetary Change.*

Arnal, M., A.G. Kramarz, M.G. Vucetich, C.D. Frailey, and K.E. Campbell. 2020. New Palaeogene caviomorphs (Rodentia, Hystricognathi) from Santa Rosa, Peru: systematics, biochronology, biogeography and early evolutionary trends. *Papers in Palaeontology* 6: 193–216.

Assemat, A., M. Boivin, L. Marivaux, F. Pujos, A. Benites-Palomino, R. Salas-Gismondi, J.V. Tejada-Lara, R.M. Varas-Malca, F.R. Negri, A.M. Ribeiro, and P.-O. Antoine. 2019. Restes inedits de rongeurs caviomorphes du Paleogene de la region de Juanjui (Amazonie peruvienne): systematique, implications macroevolutives et biostratigraphiques. *Geodiversitas* 41: 699–730.

Bianucci, G., O. Lambert, R. Salas-Gismondi, J. Tejada, F. Pujos, M. Urbina, and P.-O. Antoine. 2013. A Miocene relative of the Ganges River dolphin (Odontoceti, Platanistidae) from the Amazonian basin. *Journal of Vertebrate Paleontology* 33: 741–745.

Boivin, M., and L. Marivaux. 2020. Dental homologies and evolutionary transformations in Caviomorpha (Hystricognathi, Rodentia): new data from the Paleogene of Peruvian Amazonia. *Historical Biology* 32: 528–554.

Boivin, M., L. Marivaux, M.J. Orliac, F. Pujos, R. Salas-Gismondi, J. V. Tejada-Lara, and P.-O. Antoine. 2017a. Late middle Eocene caviomorph rodents from Contamana, Peruvian Amazonia. *Palaeontologia Electronica* 20.1.19A: 1–50.

Boivin, M., L. Marivaux, A.M. Candela, M.J. Orliac, F. Pujos, R. Salas-Gismondi, J.V. Tejada-Lara, and P.-O. Antoine. 2017b. Late Oligocene caviomorph rodents from Contamana, Peruvian Amazonia. *Papers in Palaeontology* 3: 69–109.

Boivin, M., L. Marivaux, F. Pujos, R. Salas-Gismondi, J.V. Tejada-Lara, R.M. Varas-Malca, and P.-O. Antoine. 2018a. Early Oligocene caviomorph rodents from Shapaja, Peruvian Amazonia. *Palaeontographica (A: Paläozoologie und Stratigraphie)* 311: 87–156.

Boivin, M., S. Ginot, L. Marivaux, A.J. Altamirano-Sierra, F. Pujos, R. Salas-Gismondi, J.V. Tejada-Lara, and P.-O. Antoine. 2018b. Tarsal morphology and locomotor adaptation of some late Middle Eocene caviomorph rodents from Peruvian Amazonia reveal early ecological diversity. *Journal of Vertebrate Paleontology* 38: e1555164.

Boivin, M., L. Marivaux, R. Salas-Gismondi, E.C. Vieytes, and P.-O. Antoine. 2019a. Incisor enamel microstructure of Paleogene caviomorph rodents from Contamana and Shapaja (Peruvian Amazonia). *Journal of Mammalian Evolution* 26: 389–406.

Boivin, M., L. Marivaux, and P.-O. Antoine. 2019b. L'apport du registre paleogene d'Amazonie sur la diversification initiale des Caviomorpha (Hystricognathi, Rodentia): implications phylogenetiques, macroevolutives et paleobiogeographiques. *Geodiversitas* 41: 143–245.

Bond, M., M.F. Tejedor, K.E. Campbell, L. Chornogubsky, N. Novo, and F. Goin. 2015. Eocene primates of South America and the African origins of New World monkeys. *Nature* 520: 538–541.

Bowdich, T.E. 1821. *An analysis of the natural classifications of Mammalia: for the use of students and travellers*. Paris: J. Smith.

Campbell, K.E. 2004. The Paleogene mammalian fauna of Santa Rosa, Amazonian Peru. *Natural History Museum of Los Angeles County, Science Series* 40: 1–163.

Campbell, K.E., C.D. Frailey, and L. Romero-Pittman. 2000. The Late Miocene gomphothere *Amahuacatherium peruvium* (Proboscidea: Gomphotheriidae) from Amazonian Peru: implications for the Great American Faunal Interchange. *Boletín del Ingemmet* 23: 1–152.

Campbell, K.E., M. Heizler, C.D. Frailey, L. Romero-Pittman, and D.R. Prothero. 2001. Upper Cenozoic chronostratigraphy of the southwestern Amazon Basin. *Geology* 297: 595–598.

Campbell, K.E., C.D. Frailey, and L. Romero-Pittman. 2006. The Pan-Amazonian Ucayali Peneplain, Late Neogene sedimentation in Amazonia, and the birth of the modern

Amazon River system. *Palaeogeography Palaeoclimatology Palaeoecology* 239: 166–219.

Campbell, K.E., D.R. Prothero, L. Romero-Pittman, F. Hertel, and N. Rivera. 2010. Amazonian magnetostratigraphy: dating the first pulse of the Great American Faunal Interchange. *Journal of South American Earth Sciences* 29: 619–626.

Chabain, J., P.-O. Antoine, A.J. Altamirano-Sierra, L. Marivaux, F. Pujos, R. Salas Gismondi, and S. Adnet. 2017. Cenozoic batoids from Contamana (Peruvian Amazonia) with focus on freshwater potamotrygonins and their paleoenvironmental significance. *Geobios* 50: 389–400.

Croft, D.A., J.J. Flynn, and A.R. Wyss. 2008. The Tinguiririca Fauna of Chile and the early stages of “modernization” of South American mammal faunas. *Arquivos do Museu Nacional* 66: 191–211.

De Vries, D., and E.R. Seiffert. 2017. Bayesian Tip-dating of Caviomorph Rodent Phylogenies provides New Age Estimates for South America’s oldest Platyrrhines. Program of the 86th Annual Meeting of the American Association of Physical Anthropologists (New Orleans, Unites States). *American Journal of Physical Anthropologists* 162: 161–162.

Frailey, C.D. 1986. Late Miocene and Holocene mammals, exclusive of the Notoungulata, of the Rio Acre region, Western Amazonia. *Natural History Museum of Los Angeles County Contribution in Science* 374: 1–46.

Frailey, C.D., and K.E. Campbell. 2004. Paleogene rodents from Amazonian Peru: the Santa Rosa local fauna. In *The Paleogene Mammalian Fauna of Santa Rosa*, Amazonian Peru, ed. K.E. Campbell. *Natural History Museum of Los Angeles County, Science Series* 40: 71–130.

Goillot, C., P.-O. Antoine, J. Tejada, F. Pujos, and R. Salas-Gismondi. 2011. Middle Miocene Uruguaytheriinae (Mammalia, Astrapotheria) from Peruvian Amazonia and a review of the astrapotheriid fossil record in northern South America. *Geodiversitas* 33: 331–345.

Goin, F.J., and A.M. Candela. 2004. New Paleogene marsupials from the Amazon Basin of Eastern Peru. In *The Paleogene Mammalian Fauna of Santa Rosa*, Amazonian Peru, ed. K.E. Campbell. *Natural History Museum of Los Angeles County, Science Series* 40: 15–60.

Hoorn, C., F.P. Wesselingh, H. Ter Steege, M.A. Bermudez, A. Mora, J. Sevink, I. Sanmartin, A. Sanchez-Meseguer, C.L. Anderson, J.P. Figueiredo, C. Jaramillo, D. Riff, F.R. Negri, H. Hooghiemstra, J. Lundberg, T. Stadler, T. Sarkinen, and A.

Antonelli. 2010. Amazonia through time: Andean uplift, climate change, landscape evolution, and biodiversity. *Science* 330: 927–931.

Huchon, D., F.M. Catzeflis, and E.J.P. Douzery. 2000. Variance of molecular datings, evolution of rodents, and the phylogenetic affinities between Ctenodactylidae and Hystricognathi. *Proceedings of the Royal Society of London (B: Biological Sciences)* 267: 393–402.

Jenkins, C.N., P.L. Stuart, and L.N. Joppa. 2013. Global patterns of terrestrial vertebrate diversity and conservation. *Proceedings of the National Academy of Sciences* 110: E2602–E2610.

Kay, R.F. 2015. New World monkey origins. *Science* 347: 1068–1069.

Kerber, L., F.R. Negri, A.M. Ribeiro, N. Nasif, J.P. Souza-Filho, and J. Ferigolo. 2017. Tropical fossil caviomorph rodents from the southwestern Brazilian Amazonia in the context of the South American faunas: systematics, biochronology, and paleobiogeography. *Journal of Mammalian Evolution* 24: 57–70.

Marivaux, L., and M. Boivin. 2019. Emergence of hystricognathous rodents: Palaeogene fossil record, phylogeny, dental evolution and historical biogeography. *Zoological Journal of the Linnean Society* 187: 929–964.

Marivaux, L., R. Salas-Gismondi, J. Tejada, G. Billet, M. Louterbach, J. Vink, J. Bailleul, M. Roddaz, and P.-O. Antoine. 2012. A platyrrhine talus from the early Miocene of Peru (Amazonian Madre de Dios Sub-Andean Zone). *Journal of Human Evolution* 63: 696–703.

Marivaux, L., S. Adnet, A.J. Altamirano-Sierra, M. Boivin, F. Pujos, A. Ramdarshan, R. Salas-Gismondi, J.V. Tejada-Lara, and P.-O. Antoine. 2016a. Neotropics provide insights into the emergence of New World monkeys: new dental evidence from the late Oligocene of Peruvian Amazonia. *Journal of Human Evolution* 97: 159–175.

Marivaux, L., S. Adnet, A.J. Altamirano-Sierra, F. Pujos, A. Ramdarshan, R. Salas-Gismondi, J.V. Tejada-Lara, and P.-O. Antoine. 2016b. Dental remains of cebid platyrrhines from the earliest late Miocene of Western Amazonia, Peru: macroevolutionary implications on the extant capuchin and marmoset lineages. *American Journal of Physical Anthropology* 161: 478–493.

Marivaux, L., W. Aguirre-Diaz, A. Benites-Palomino, G. Billet, M. Boivin, F. Pujos, R. Salas-Gismondi, J.V. Tejada-Lara, R.M. Varas-Malca, and P.-O. Antoine. 2020. New record of *Neosaimiri* (Cebidae, Platyrrhini) from the late Middle Miocene of Peruvian Amazonia. *Journal of Human Evolution* 146: 102835.

Negri, F.R., J. Bocquentin-Villanueva, J. Ferigolo, and P.-O. Antoine. 2010. A review of Tertiary mammal faunas and birds from western Amazonia. In *Amazonia, landscape and species evolution: a look into the past*, eds. C. Hoorn and F.P. Wesselingh, 245–258. Hoboken: Blackwell-Wiley.

Pujos, F., R. Salas-Gismondi, G. Baby, P. Baby, C. Goillot, J. Tejada, and P.-O. Antoine. 2013. Implication of the presence of *Megathericulus* (Xenarthra: Tardigrada: Megatheriidae) in the Laventan of Peruvian Amazonia. *Journal of Systematic Palaeontology* 11: 973–991.

Seiffert, E.R., M.F. Tejedor, J.G. Fleagle, N.M. Novo, F.M. Cornejo, M. Bond, D. De Vries, and K.E. Campbell. 2020. A parapithecid stem anthropoid of African origin in the Paleogene of South America. *Science* 368: 194–197.

Shockey, B.J., R. Hitz, and M. Bond. 2004. Paleogene notoungulates from the Amazon Basin of Peru. In *The Paleogene Mammalian Fauna of Santa Rosa*, *Amazonian Peru*, ed. K.E. Campbell. *Natural History Museum of Los Angeles County, Science Series* 40: 61–70.

Stebbins, G.L. 1974. *Flowering plants: evolution above the species level*. Cambridge: The Belknap Press of Harvard University Press.

Tejada-Lara, J.V., R. Salas-Gismondi, F. Pujos, P. Baby, M. Benammi, S. Brusset, D. De Franceschi, N. Espurt, M. Urbina, and P.-O. Antoine. 2015. Life in protoamazonia: Middle Miocene mammals from the Fitzcarrald Arch (Peruvian Amazonia). *Palaeontology* 58: 341–378.

Tullberg, T. 1899. Ueber das System der Nagethiere: eine phylogenetische Studie. *Nova Acta Regiae Societatis Scientiarum Upsaliensis* 18: 1–514.

Vucetich, M.G., E.C. Vieytes, M.E. Perez, and A.A. Carlini. 2010. The rodents from La Cantera and the early evolution of caviomorphs in South America. In *The Paleontology of Gran Barranca, Evolution and Environmental Change through the Middle Cenozoic of Patagonia*, eds. R.H. Madden, A.A. Carlini, M.G. Vucetich, and R.F. Kay, 189–201. Cambridge: Cambridge University Press.

Wood, A.E. 1955. A revised classification of the rodents. *Journal of Mammalogy* 36: 165–187.

4.4 LATE MIDDLE MIOCENE CAVIOMORPH RODENTS FROM TARAPOTO, PERUVIAN AMAZONIA

Artigo publicado no periódico *PLoS ONE*, volume 16, número 11, artigo e0258455, 2021, DOI: 10.1371/journal.pone.0258455

Myriam Boivin[1], Laurent Marivaux[2], Walter Aguirre-Diaz[3], Aldo Benites-Palomino[3,4], Guillaume Billet[5], François Pujos[6], Rodolfo Salas-Gismondi[3,7], **Narla S. Stutz[2,8]**, Julia V. Tejada-Lara[2,3], Rafael M. Varas-Malca[3], Anne H. Walton[9], Pierre-Olivier Antoine[2]

[1]Laboratorio de Paleontologia de Vertebrados, Instituto de Ecorregiones Andinas (INECOA), Universidad Nacional de Jujuy, CONICET, San Salvador de Jujuy, Jujuy, Argentina, [2]Laboratoire de Paléontologie, Institut des Sciences de l'Evolution de Montpellier (ISEM, UMR 5554, CNRS/UM/IRD/EPHE), Université de Montpellier, Montpellier, France, [3]Departamento de Paleontologia de Vertebrados, Museo de Historia Natural—Universidad Nacional Mayor San Marcos (UNMSM, DPV-MUSM), Lima, Peru, 4 Paläontologisches Institut und Museum, Universität Zürich, Zürich, Switzerland, [5]Département Origine et Evolution, Muséum national d'Histoire naturelle (MNHN, CR2P-UMR 7207 CNRS/MNHN/Sorbonne Université), Paris, France, [6]Laboratorio de Paleontologia, Instituto Argentino de Nivologia, Glaciologia y Ciencias Ambientales (IANIGLA), CCT–CONICET–Mendoza, Mendoza, Argentina, [7]BioGeoCiencias Lab, Facultad de Ciencias y Filosofia/CIDIS, Laboratorios de Investigacion y Desarrollo (LID), Centro de Investigación para el Desarrollo Integral y Sostenible (CIDIS), Universidad Peruana Cayetano Heredia, Lima, Peru, [8]Programa de Pós-Graduac¸ão em Geociências, Universidade Federal do Rio Grande do Sul, Porto Alegre, Rio Grande do Sul, Brazil, [9]Springfield Technical Community College, Springfield, Massachusset, United States of America.

Abstract

Miocene deposits of South America have yielded several species-rich assemblages of caviomorph rodents. They are mostly situated at high and mid- latitudes of the continent, except for the exceptional Honda Group of La Venta, Colombia, the faunal composition of which allowed to describe the late middle Miocene Laventan South American Land Mammal Age (SALMA). In this paper, we describe a new caviomorph assemblage from TAR-31 locality, recently discovered near Tarapoto in Peruvian

Amazonia (San Martı´n Department). Based on mammalian biostratigraphy, this single-phased locality is unambiguously considered to fall within the Laventan SALMA. TAR-31 yielded rodent species found in La Venta, such as the octodontoid *Ricardomys longidens* Walton, 1990 (*nom*. *nud*.), the chinchilloids *Microscleromys paradoxalis* Walton, 1990 (*nom*. *nud*.) and *M*. *cribriphilus* Walton, 1990 (*nom*. *nud*.), or closely-related taxa. Given these strong taxonomic affinities, we further seize the opportunity to review the rodent dental material from La Venta described in the Ph.D. volume of Walton in 1990 but referred to as *nomina nuda*. Here we validate the recognition of these former taxa and provide their formal description. TAR-31 documents nine distinct rodent species documenting the four extant superfamilies of Caviomorpha, including a new erethizontoid: *Nuyuyomys chinqaska* gen. et sp. nov. These fossils document the most diverse caviomorph fauna for the middle Miocene interval of Peruvian Amazonia to date. This rodent discovery from Peru extends the geographical ranges of *Ricardomys longidens*, *Microscleromys paradoxalis*, and*M*. *cribriphilus*, 1,100 km to the south. Only one postcranial element of rodent was unearthed in TAR-31 (astragalus). This tiny tarsal bone most likely documents one of the two species of *Microscleromys* and its morphology indicates terrestrial generalist adaptations for this minute chinchilloid.

Introduction

Caviomorphs (Caviomorpha Wood, 1955) are hystricognathous rodents originating from South America, such as guinea pig, New World porcupines, chinchillas, and spiny rats. Nowadays, they show a great taxonomical diversity and a large array of lifestyles (arboreal, fossorial, semi-aquatic, and terrestrial) [1]. Among caviomorphs, two main clades, each divided into two superfamilies, are recognised [2–4]: Erethicavioi Boivin, 2019 (comprising Cavioidea Fischer, 1817 + Erethizontoidea Bonaparte, 1845 + stem-groups) and Octochinchilloi Boivin, 2019 (comprising Chinchilloidea Bennett, 1833 + Octodontoidea Waterhouse, 1839 + stemgroups). Their evolutionary history extends back to the late middle Eocene, with the earliest representatives of the group so far recorded in Peruvian Amazonia [5–8].

The Miocene record of caviomorphs is particularly well documented. Numerous fossilbearing localities yielded abundant specimens and species-rich assemblages of rodents [9]. Most of them are situated at high and middle latitudes, notably in Argentina (e.g., Pinturas, Sarmiento, Santa Cruz, Collo´n Cura, Cerro Azul and Ituzaingo formations) [9–15] and Chile (e.g., Laguna del Laja and Pampa Castillo) [16, 17]. At

low latitudes of South America, two remarkable and very species-rich caviomorph faunas are known, La Venta in Colombia (Honda Group; late middle Miocene) [18] and Acre in Brazil (Solimoes Fm. [Formation]; late Miocene; see [19]). Since the early discoveries of fossil-bearing localities in the Honda Group of the upper Magdalena valley in 1923, considerable field efforts led by petroleum companies and several scientific teams were performed in this region of Colombia, and notably in the La Venta area, until 1992 [20, 21]. As a result, 140 localities over 52 different stratigraphic levels, yielding thousands of fossils of many vertebrate groups were discovered in the Honda Group dating from the late middle Miocene [22]. In particular, the recognition in 1945 of the first fossil remains of primates in the Magdalena valley [23, 24] has been one of the most significant discoveries that motivated numerous subsequent field expeditions [20]. The mammal fauna from La Venta encompasses at least 77 species and 80 genera, representing 29 families [25, 26]. Concerning rodents, around 20 taxa documenting the four main caviomorph superfamilies have so far been reported (excluding the indeterminate genera and species) [18, 27–30]. In addition to La Venta, the Peruvian faunas from MD-67 (Madre de Dios) [31], the Fitzcarrald local fauna (near Atalaya, Ucayali) [32, 33], and CTA-45 (near Contamana, Loreto) [34], also middle Miocene in age, document representatives of the four caviomorph superfamilies (4, 8, and 2 taxa, respectively). Finally, a fourth late middle Miocene caviomorph-bearing locality also occurs in low latitudes, from the Socorro Formation in Venezuela, but so far it has only yielded a fragmented distal femur of a giant caviomorph [35].

Over the last decade, our yearly paleontological surveys in the Tarapoto area (San Martín Department, Peruvian Amazonia), have allowed the discovery of a new fossil-bearing locality, TAR-31, in the vicinity of the Juan Guerra village. This locality is considered to be late middle Miocene in age (Laventan SALMA) based on mammalian biostratigraphy (see [36]; see Material and Methods section of this paper). TAR-31 yielded a diverse assemblage of aquatic and terrestrial vertebrates, including numerous caviomorph specimens that are the subject of this paper. The primary purpose of the present work is to describe the new caviomorph materials found in TAR-31. This locality shares taxa or closely related taxa with La Venta fauna described by one of us (AHW) in the framework of her PhD [37]: *Microsteiromys*, *Ricardomys*, and *Microscleromys*. Because *Microsteiromys*, *Ricardomys*, *Microscleromys*, and the species included within these genera were not formally described (*nomina nuda*) [18, 37, 38], here we also revise the material from La Venta attributed to these taxa, in order to clarify their systematics.

Material and methods

TAR-31, Tarapoto, Peru

The rodent fossil material from Peruvian Amazonia described in the present work originates from the TAR-31 locality, situated in the vicinity of the small town Juan Guerra, along the Mayo River (Tarapoto area, San Martı´n Department, Peru; Fig 1A and 1B). TAR-31 consists of a 10–15 cm-thick yellow microconglomerate interbedded within a grey cross-stratified and sandstone-dominated fluvial unit (Fig 2A [36]). The latter is intercalated between thick violingrey variegated paleosols pointing to the existence of a meandering river with sustainable floodplain [36]. These levels were originally mapped as belonging to the lower member of Ipururo Formation (middle Miocene in age in the Huallaga basin) [39–42], an assignation in agreement with the nature of their facies and depositional environment sequence.

The fossil content of the TAR-31 encompasses plants, amber clasts, crabs, chondrichthyans, osteichthyans, anurans, chelonians, crocodylomorphs, birds, and mammals (including metatherians, xenarthrans, liptoterns, notungulates, sirenians, chiropterans, primates, and caviomorph rodents). The TAR-31 mammal assemblage includes a didelphid marsupial (currently under study by one of us, NSS), the interatheriine notoungulate *Miocochilius* sp., the didolodontid *Megadolodus* sp., the platyrrhine primate *Neosaimiri* aff. *fieldsi* [36], and the caviomorph fauna described here (see ‘Age of TAR-31’ section of this present work). This assemblage recalls some of the Laventan SALMA localities: Quebrada Honda in Bolivia (13.1–12.2 Ma) [43–46], the Fitzcarrald local fauna in SE Peru [33], and especially the lower part of the Villavieja Formation in the La Venta area in Colombia (13.8–11.6 Ma; [47] and see above). Accordingly, the TAR-31 locality most likely documents the late middle Miocene Laventan SALMA [36].

The material from TAR-31 was collected by excavating and wet screening (2 and 1 mm meshes) about 550 kg of sediment during our yearly field expeditions (August 2015, 2016, and 2018). The caviomorph material corresponds to about 400 isolated teeth (complete or fragmentary), one fragment of mandible (MUSM 4643), one fragment of maxilla (MUSM 4375), and one astragalus (MUSM 4658). No permits were required for the described study, which complied with all relevant regulations. The field work on TAR-31 was carried out in the framework of the ongoing cooperation agreement between the ‘Museo de Historia Natural de la Universidad Nacional Mayor San Marcos’ (Lima, Peru) and the ‘Institut des Sciences de l’Evolution de Montpellier-

Université de Montpellier' (France). The TAR-31 fossil specimens are permanently stored in the palaeontological collection of the 'Museo de Historia Natural, Universidad Nacional Mayor de San Marcos', Lima, Peru (MUSM).

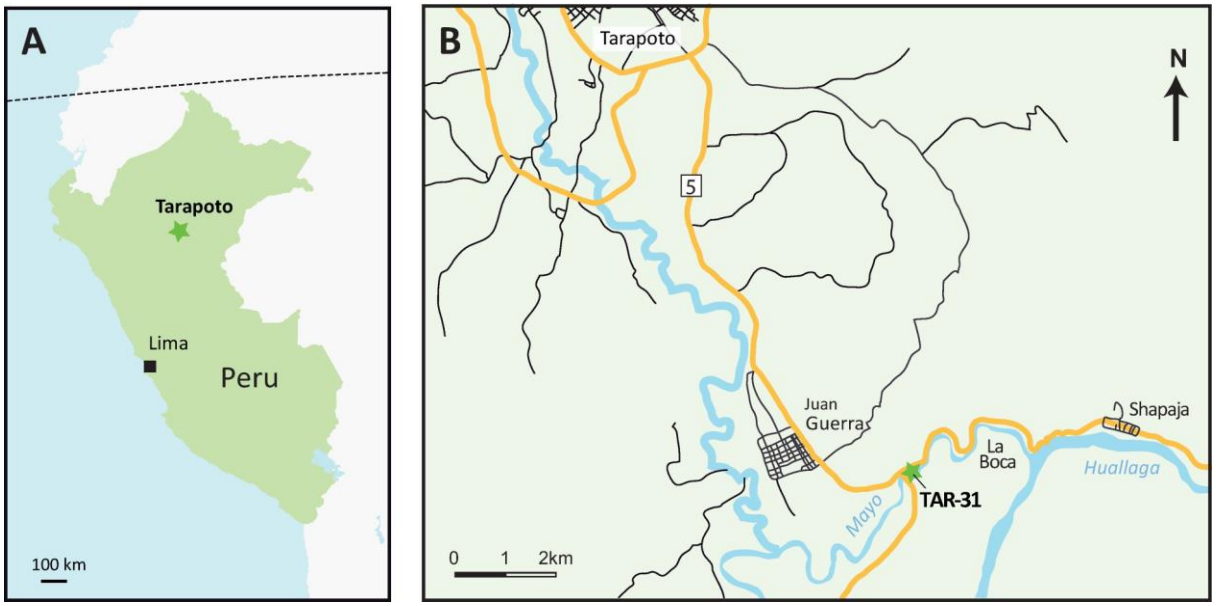


Fig 1. Geographic location of TAR-31 (San Martín Department, Peru; late middle Miocene, Laventan SALMA). (A) Location map of the Tarapoto area (star symbol) in Peru. (B) Location map of the TAR-31 (star symbol) in the Tarapoto area. SALMA, South American Land Mammal Age.

La Venta area, Colombia

The fossil rodent material from La Venta re-analysed here (originally studied in the framework of the Ph.D. of Anne H. Walton) [18, 37] originates from the badland exposures located in the vicinities of the Villavieja and La Victoria villages, in the upper valley of the Magdalena River (Huila Department, Colombia). Numerous fossil-bearing localities are known in the La Venta area (and the Magdalena upper valley in general) [26]. These are assigned to two successive formations of the Honda Group: La Victoria and Villavieja formations [48]. The studied material from this area was found in: (i) one locality from La Victoria Formation (IGM-DU loc. 075, between the Chunchullo Beds and the Tatcoa Sandstone Beds), and (ii) distinct localities from the Villavieja Formation, including several localities in the Fish Bed (CVP 5, 8, 9, 10, 10A, and 13B), two localities in the Monkey Bed (IGM-DU loc. 006–1 and IGM-DU loc. 022 or UCMP loc. V4536), and one in the El Cardo´n Red Beds (IGM-DU loc. 032 and its screenwashed locality 032–5). The Unit between the Chunchullo and Tatacoa Sandstone Beds is 149.3 m-thick, and is composed of very fine sandstones and

mudstones alternating with metric medium-grained sandstone lenses [48]. The Villavieja Formation is divided into the Baraya Member, including the Fish and Monkey beds, and the Cerro Colorado Member, including the El Cardón Red Beds [48]. The Baraya Member is very fossiliferous and is composed mainly of gray mudstones and sandstones with minor layers of red mudstones, while the Cerro Colorado Member is less fossiliferous and consists of thick horizons of red mudstones with a very small amount of volcanic litharenites and chert litharenites [48]. The La Venta fauna is late middle Miocene in age (13.8–12.05 Ma) based on 40Ar/39Ar datings realised on volcanic units from different localities of the Honda Group (on biotites, hornblendes, and plagioclases; 13.8–12.2 Ma) and magnetostratigraphic correlations of the Honda Group (13.61 [base of C5ABn chron] –12.05 Ma [top of C5An.1n]) [26, 47, 49]. The La Venta area yielded a very rich vertebrate fauna including chondrichthyans, osteichthyans, amphibians, squamates, chelonians, crocodylomorphs, birds and mammals (metatherians, xenarthrans, astrapotheres, litopterns, notoungulates, cetaceans, chiropterans, sirenians, primates and caviomorph rodents) [21, 22].

The caviomorph remains from La Venta included in this work were formerly studied by one of us [18, 37]. In a doctoral thesis manuscript, Walton [37] described several new genera and species such as *Microsteiromys jacobsi*, *Ricardomys longidens*, *Microscleromys paradoxalis*, and *Microscleromys cribriphilus*. As the latter taxa were not formally described, they should be considered as not available following the articles 8, 9, 11, 13 of the International Code of Zoological Nomenclature (i.e., *nomen nudum*; p. 132–143, 246 [38]). As formally recognised for *nomina nuda* (“A *nomen nudum* is not an available name, and therefore the same name may be made available later for the same or a different concept; in such a case it would take authorship and date [Arts. 21, 50] from that act of establishment, not from any earlier publication as a nomen nudum” [38], we chose to keep the taxonomic names proposed by Walton [37]. For reasons related to the covid pandemic and confinement, the original material from La Venta could not be directly observed. The description and comparison of this material in the present work is based on published photos and drawings [18, 37]. Most of these specimens were collected by surface collecting and wet screening (2 and 0.6 or 0.25 mm meshes) in the years 1985 through 1989. This material is stored in the ‘Museo Geológico José Royo y Gómez, Servio Geológico Colombiano’ (IGM; formerly, ‘Instituto Nacional de Investigaciones en Geociencias, Mineria y Química’) and the ‘Departamento de Geociencias, Universidad Nacional de Colombia’ (UNC), Bogotá, Colombia, as well as in the Field Museum of Natural History,

Chicago (FMNH), USA. Some specimens do not have collection number (unnumbered specimens). We used their field number to refer to them (S1 Table).

Imaging

For the largest specimens (mandibular and maxillary fragments) and high-crowned teeth found at TAR-31, we used X-ray microtomography (μCT-scan) for obtaining three-dimensional digital models (3D surface renderings). The dental/jaw specimens and the astragalus were scanned with a resolution of 6 μm and 5 μm, respectively, using a μCT-scanning station EasyTom 150/Rx Solutions (Montpellier RIO Imaging [MRI], ISEM, Montpellier, France). They have been virtually delimited by manual segmentation under AVIZO 7.1 software (Visualization Sciences Group). The specimens were prepared within a 'Label Field' module of AVIZO, using the segmentation threshold selection tool. The other teeth figured in this paper were photographed with a Scanning Electron Microscope (SEM) HITACHI S 4000 (Institut des Neurosciences de Montpellier [INM], France). Some of the pictures of the astragalus are photographs of the original specimen, which are the result of the fusion of multifocus images obtained with an optical stereomicroscope (LeicaM205C) connected to a camera (Leica DFC 420C; ISEM).

Nomenclature and comparisons

The main terminology for the rodent dentition follows Boivin & Marivaux [50], and the literature cited therein. Some extant caviomorphs and related extinct forms show a highly derived/specialised dental pattern with respect to that of the oldest representatives of this group (for which the aforementioned nomenclature was based on). This is the case of two taxa described below: (i) Caviidae indet. gen. et sp., for which nomenclatures proposed by several authors [51–55] were followed (Fig 2A); and (ii) the adelphomyine *Ricardomys longidens*, for which we partly followed the nomenclature proposed by Patterson & Pascual [56] (Fig 2B and 2C). Lower case letters are used for lower dentition (dp, for decidious premolar; p, for premolar; m, for molars) and upper case letters for upper dentition (dP, for decidious premolar; P, for premolar; M, for molars). The astragalar nomenclature is based on Ginot et al. [57], Rose & Chinnery [58], and Wible & Hughes [59]. The caviomorph taxa cited in the text and used for dental comparisons are listed in S2 Table. Three isolated teeth from MD-67 locality in Peru (MUSM 1974, 1975, and 4298; early middle Miocene) were originally attributed to cf. *Microsteiromys* sp [31]. They are reassigned here in light of the new

material from Tarapoto. For the MUSM 4658 astragalus, we used the same comparative sampling as Boivin et al. [60]. In addition, we consulted supplementary astragalar material attributed to the erethizontid *Steiromys duplicatus* (MACN A 10055–78, 10081 and 10082; see [61]), the caviids *Dolicavia minuscula* (MMP 10055–78) and *Galea leucoblephara* (INBIAL-CV 00290), the neoepiblemid *Neoepiblema* sp. (probably *N*. *acreensis*; UFAC 5249 and 61840), the octodontids *Abalosia castellanosi* (MMP 1439-M) and *Pithanotomys columnaris* (MACN-Pv 7429–7431), the echimyid *Eumysops chapalmalensis* (MACN-Pv 17868), and the ctenomyid *Actenomys priscus* (MMP 367-S and 395-S). When the fossils described in this paper are compared with several taxa, they are primarily listed according to their chronostratigraphic order (from the oldest to the most recent) and then alphabetically.

Nomenclatural acts

The electronic edition of this article conforms to the requirements of the amended International Code of Zoological Nomenclature, and hence the new names contained herein are available under that Code from the electronic edition of this article. This published work and the nomenclatural acts it contains have been registered in ZooBank, the online registration system for the ICZN. The ZooBank LSIDs (Life Science Identifiers) can be resolved and the associated information viewed through any standard web browser by appending the LSID to the prefix “http://zoobank.org/”. The LSID for this publication is: urn:lsid:zoobank.org:pub:ECE79D67-9203-4929-9CCF-7C8D51C8326E. The electronic edition of this work was published in a jornal with an ISSN, and has been archived and is available from the following digital repositories: LOCKSS.

Dental associations

Working on isolated teeth requires the consideration of distinct levels of morphological variation: (i) variation depending on the dental locus; (ii) variation owing to the occlusal wear; (iii) intra-specific or intra-taxonomic variation or polymorphism; and (iv) inter-specific or intertaxonomic variation. In this study, several taxa from TAR-31 are described. The association of the material attributed to these taxa is based on several complementary criteria: (i) a similar occlusal size; (ii) a similar crown height (for a given occlusal size and stage of wear); (iii) a similar proportion of the maximum mesiodistal length and the maximum linguolabial width; (iv) a similar occlusal outline; (v) a similar occlusal pattern (bunolophodonty/lophodonty; taeniodonty/non-

taeniodonty; presence/absence, development, position of cusp[-id]s/styl[e/id]s; presence/absence, continuity/discontinuity, length, height and obliquity of loph[-id]s; and presence/absence and types of fusion of dental structures); and (vi) a compatible occlusal pattern between upper and lower teeth. For teeth at advanced stages of wear, we took into account the potential impact of occlusal wear on characters aforementioned. Based on a wide array of closely- or distantly-related rodent taxa, we prefered to use a size criterion for the recognition of m1s vs m2s and M1s vs M2s (i.e., m1/M1s to be smaller than the m2/M2s in a given species). The recognition of other loci is based on the occlusal shape of teeth (for more details, see descriptions in the Systematic Palaeontology section) and on the presence and/or absence of mesial/distal vertical contact facets due to contiguous teeth. The occlusal shape of M3s is further characterised by a smaller and more labial hypocone with respect to the protocone than on M1–2s. However, the recognition of molar loci is quite ambiguous for several taxa, especially for the first two upper molars. In that case, we determined these loci with uncertainty (e.g., lower molar, m1?, m2?, m3?, upper molar, M1 or M2, M1 or M2?, M3?).

Measurements and statistics

For each dental specimen of TAR-31, we measured both the maximum mesiodistal length (len) and linguolabial width (wid), as well as the maximum lingual crown height (Hg) and labial crown height (Hb; S1 Table). These measurements were made by M. Boivin with a measuroscope Nikon 10 and a Keyence Digital Microscope VHX-2000F. For *Microsteiromys jacobsi* and *Ricardomys longidens* from La Venta, we used the measurements available in Walton [37] (S1 Table). However, we noted some inconsistencies regarding the m3 of the type of *Ricardomys*, IGM 183847, between the measurements reported in Table 2, p. 33 [37] and the scaled photo of the specimen in Fig 9A, p. 31 [37]. Similarly, the measurements of the type of *M*. *jacobsi* (FMNH PM 54672 in Table 6, p. 58 [37]) do not match with its scaled representation (in Fig 16A, p. 56 [37]). For these two specimens, we chose to use the measurements made from their figuration in the Figs 9A and 16A [37]. For the Laventan material attributed to *Microscleromys*, the measurements made from the figures of the specimens in Walton (Figs 11–13 [37]) and those from Walton (Fig 24.2 [18]) are different. We extracted the measurements from the first study (Ph.D.) because the specimens were photographed (instead of drawn) with a larger scale and more material is represented. The hypsodonty index of a tooth (HI) [62] equals its crown height divided by its

anteroposterior length (H/ML); teeth with a HI < 1 are considered as brachydont, those with a HI = 1 are considered as mesodont, and those with a HI > 1 are considered as hypsodont. The latter are either protohypsodont When they still have roots, or euhypsodont if they lack roots [51]. Two hypsodonty indexes were calculated in function to the side of the crown considered: from Hb (HIb) and from Hg (HIg). The HI values mentioned in the descriptions were measured on specimens at the early stages of wear. The MUSM 4658 astragalus from TAR-31 was measured following the protocol of Ginot et al. [57] (Table 1).

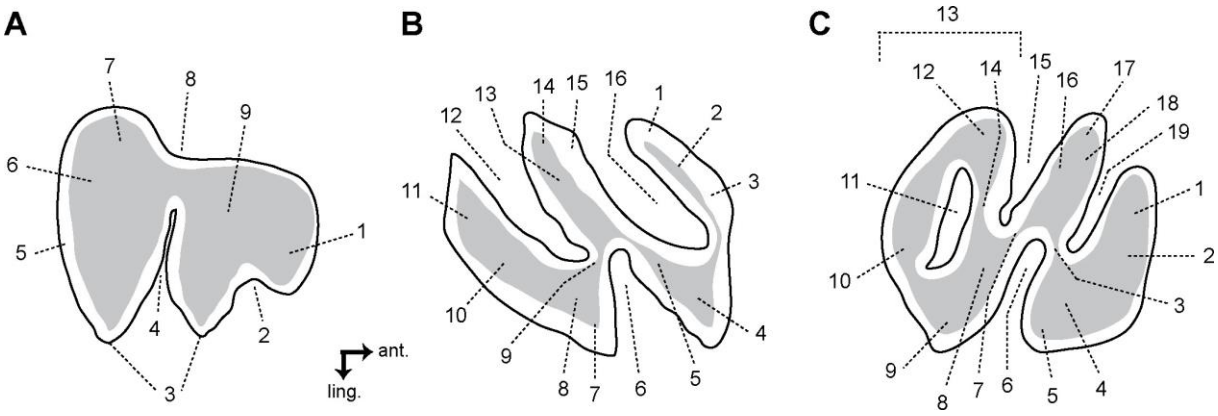


Fig 2. Dental nomenclature for cavioid (A) and adelphomyine (B, C) rodent teeth in occlusal view. (A) p4; 1, anterior projection of the anterior lobe; 2, interprismatic furrow; 3, apexes; 4, hypoflexid; 5, enamel; 6, dentine; 7, posterior lobe; 8, longitudinal furrow opposite to the hypoflexid (= primary internal flexid); 9, anterior lobe. (B) Lower molar; 1, metaconid (+ its posterior arm?); 2, first lamella; 3, metalophulid I; 4, protoconid; 5, ectolophid; 6, hypoflexid; 7, anterior outgrowth of the hypoconid; 8, hypoconid; 9, anterior arm of the hypoconid; 10, posterolophid; 11, third lamella; 12, metaflexid; 13, second lamella; 14, entoconid; 15, hypolophid; 16, confluence between the anteroflexid and the mesoflexid. (C) Upper molar; 1, first lamella; 2, anteroloph; 3, posterior arm of the protocone (= lingual protoloph); 4, protocone; 5, posterior outgrowth of the protocone; 6 hypoflexus; 7, mure; 8, anterior arm of the hypocone; 9, hypocone; 10, posteroloph; 11, confluence of the distal mesoflexus with the metaflexus; 12, mesostyle; 13, third lamella; 14, third transverse crest (= mesoloph and/or mesolophule); 15, mesial mesoflexus; 16, second lamella; 17, paracone; 18, labial protoloph; 19, paraflexus; ant., anterior; ling., lingual. (B, C) Note that the position of the fused structures is speculative. The dental terminology is modified after several authors [50–56]. Not to scale.

Table 1. Measurements (mm) of the astragalus from TAR-31, MUSM 4658.

ABW	AmTL	ATL	ATW	EL	EW	HH	HW	LBH
2.265	~1.220	3.088	2.649	1.447	1.231	0.954	1.316	1.069
LTL	MBH	MTL	NL	SL	SW	TW	mTAH	
1.860	1.682	2.015	1.382	1.211	1.035	1.832	0.725	

ABW, Astragalus Body Width; AmTL, Astragalar-medial Tarsal facet Length; ATL, Astragalus Total Length; ATW, Astragalus Total Width; EL, Ectal facet Length; EW, Ectal facet Width; HH, Head Height; HW, Head Width; LBH, Lateral Body Height; LTL, Lateral Trochlear Length; MBH, Medial Body Height; MTL, Medial Trochlear Length; NL, Neck Length; SL, Sustentacular Facet Length; SW, Sustentacular Facet Width; TW, Trochlear Width; mTAH, medial Trochlear Arc Height.

In order to help identifying the number of species and discriminating which species of *Microscleromys* are present in TAR-31 and La Venta, we performed three types of statistical analyses on the maximum mesiodistal length and linguolabial width by locus (i.e., dp4, p4, m1–2(?), m3(?), dP4, P4, M1–2(?), M3(?)) with R v.4.0.3. [63] (S1 and S2 Files). First, we tested statistical differences between potential taxonomic groups mentioned by Walton (*M*. *paradoxalis nom*. *nud*., *M*. *cribriphilus nom*. *nud*., *M*. ?*paradoxalis*, and *Microscleromys* sp.) [37] and *Microscleromys* from TAR-31 using Kruskal-Wallis, Permutation Analysis of Variance, Student and Wilcoxon tests, depending to what preconditions were satisfied, with the 'dunn.test', 'RVAide-Memoire', 'stats' and 'trend' packages [63–66]. Second, partitioning analyses were conducted until five (dp4), nine (m3) or fifteen (other loci) groups depending the number specimens for each loci with the 'cluster' package [67]. Finally, we performed several Bayesian models on the most numerous loci including several specimens previously attributed to *M*. *cribriphilus* and *M*. *paradoxalis* (i.e., p4, m1–2(?), and M1–2(?)) in order to obtain the most probable partioning with the 'glm' function of 'MASS' and 'stats' packages [63, 68]. We tested 39 models for the M1–2(?) and 51 models for the p4 and m1–2(?) including the partionings following the previous systematic hypotheses and those obtained with the partitioning analyses (see S1 File).

Abbreviations

Institutional abbreviations. FMNH, Field Museum of Natural History, Chicago, USA; **IGM,** Servicio Geológico Colombiano (before Instituto Nacional de Investigaciones en Geociencias, Mineria y Química [INGEOMINAS]), Museo Geológico José Royo y Gómez, Bogotá, Colombia; **IGM-DU,** Field numbers from expeditions by the INGEOMINAS in cooperation with Duke University. Specimens deposited at the Museo Geológico José Royo y Go´mez, Bogotá, Colombia; **INBIAL-CV,** Instituto de Biologı´a de la Altura, San Salvador de Jujuy, Argentina; **ING-KU,** Field

numbers from expeditions by the INGEOMINAS in cooperation with Kyoto University. Specimens deposited at the Museo Geológico José Royo y Gómez, Bogotá, Colombia; **LACM,** Los Angeles County Museum, Los Angeles, USA; **MCZ,** Museum of Comparative Zoology, Cambridge, USA; **MACN,** Museo Bernardino Rivadavia, Buenos Aires, Argentina; **MLP,** Museo de La Plata, La Plata, Argentina; **MMP,** Museo Municipal De Ciencias Naturales Lorenzo Scaglia, Mar del Plata, Argentina; **MNHN,** Museum National d'Histoire Naturelle, Paris, France; **MPEF-PV,** Museo Paleontológico Egidio Feruglio, Trelew, Argentina; **MUSM,** Museo de Historia Natural de la Universidad Nacional Mayor San Marcos, Lima, Peru; **UCMP,** University of California Museum of Paleontology, Berkeley, USA; **UFAC,** Colecção de Paleovertebrados do Laboratório de Pesquisas Paleontológicas, Universidade Federal do Acre, Rio Branco-AC, Brazil; **UNC,** Departamento de Geociencias, Universidad Nacional de Colombia, Bogotá, Colombia.

Other abbreviations. CVP, locality belongs to the Fish Bed in La Venta area collected by screenwashing during the expeditions by the INGEOMINAS in cooperation with Duke University; **IGM-DU loc.,** fossiliferous locality found during the expeditions by the INGEOMINAS in cooperation with Duke University in La Venta area; **UCMP loc.,** fossiliferous locality found during the expeditions by the University of California in La Venta area.

Systematic paleontology

Nomenclatural Remark: The new species and genera described below must be referred to Boivin & Walton, 2021, following the article 50.1 and the "recommendation 50A concerning multiple authors" of the International Code of Zoological Nomenclature (p. 182 [38]). This is of particular interest for *nomina nuda* that were previously used by Walton [18, 37] and made available here, following the International Code of Zoological Nomenclature [38].

Rodentia Bowdich, 1821

Ctenohystrica Huchon, Catzeflis & Douzery, 2000

Hystricognathi Tullberg, 1899

Caviomorpha Wood, 1955

Erethicavioi Boivin, 2019 in Boivin, Marivaux & Antoine, 2019

Erethizontoidea Bonaparte, 1845

Microsteiromys Boivin & Walton gen. nov. urn:lsid:zoobank.org:act:70F9B9F7-51EB-4FFF-913C-2E89EBF5F9DB

Type species

Microsteiromys jacobsi gen. et sp. nov.

Species content

Only the type species.

Derivation of name

Based on the original description of the species [37]: 'In reference to its small size and general resemblance to the erethizontoid *Steiromys* Ameghino, 1887'.

Geographical and stratigraphical distribution

La Venta, Baraya and Cerro Colorado members, Villavieja Fm. (Laventan SALMA, late middle Miocene), Huila Department, Colombia.

Generic diagnosis

As for the type and only known species.

Microsteiromys jacobsi Boivin & Walton sp. nov. urn:lsid:zoobank.org:act:1DF51272-C949-4105-BC5C-299F88252206

Fig 3 and S1 Table

Nom. *nud*. *Microsteiromys jacobsi* Walton, 1990, Fig 16A–16C, p. 56.

Nom. *nud*. *Microsteiromys jacobsi* Walton, 1997, Figs 24.1B and 24.2B, p. 394, 395.

Holotype

FMNH PM 54672, right mandibular fragment bearing dp4–m3 (Walton, 1990: Fig 16A; Walton, 1997: Figs 24.1B and 24.2B; Fig 3A).

Referred material

IGM-DU 89–249, left mandibular fragment bearing p4–m1 (Walton, 1990: Fig 16C; Fig 3B); IGM-DU 88–034, right posterior fragment of lower tooth (Walton, 1990: Fig 16B; Fig 3C).

Derivation of name

Based on the original description of the species [37]: 'In honour to Dr. Louis L. Jacobs, palaeontologist and educator'.

Type locality

IGM-DU loc. 022 or UCMP loc. V4536 (only for the type), Monkey Beds, La Venta Badlands, upper Magdalena Valley, Huila Department, Colombia.

Other localities

CVP 10 (for IGM-DU 88–034), Fish Bed and screewashed locality 032–5 (for IGM-DU 89–249), El Cardón Red Bed, La Venta Badlands, upper Magdalena Valley, Huila Department, Colombia.

Formation and age

Baraya and Cerro Colorado members, Villavieja Fm., late middle Miocene (i.e., Laventan SALMA).

Diagnosis

Rodent characterised by a small size and brachydont teeth. Lower teeth with a tetralophodont and non-taeniodont pattern, complete metalophulid I, and oblique and complete ectolophid. dp4s with a mesiodistally short and linguolabially wide trigonid and a curved metalophulid I. Large p4s with a linguolabially wide trigonid. Mesiodistally elongated lower molars with a narrow mesoflexid and well-extended metaflexid. Differs from *Eopululo*, *Protosteiromys*, *Branisamyopsis*, *Hypsosteiromys*, *Parasteiromys*, *Eosteiromys*, *Steiromys*, and *Neosteiromys* in having a smaller size; from *Eosteiromys annectens* and *Steiromys duplicatus* in having non-taeniodont lower teeth; from *Hypsosteiromys* in having brachydont lower teeth with transverse lophids and a complete metalophulid I, and less elongated dp4s; from *Shapajamys*, *Branisamyopsis*, *Eosteiromys homogidens*, *Steiromys*, and *Coendou insidiosus* in having tetralophodont dp4s; from *Eosteiromys segregatus* in having a longer p4 with a long anterior arm of the entonconid; from *Shapajamys*, *Palaeosteiromys*, *Protosteiromys*, *Branisamyopsis*, *Eosteiromys annectens*, *Steiromys*, and *Neosteiromys* in having more rectangular lower molars; from *Palaeosteiromys*, *Branisamyopsis australis*, *Branisamyopsis praesigmoides*, *Steiromys duplicatus*, and *Neosteiromys* in having always tetralopodont lower molars; from *Shapajamys*, *Branisamyopsis praesigmoides* and *Steiromys duplicatus* in having an ectolophid always complete and oblique on lower molars; from *Shapajamys* in having an ectolophid always oblique on lower molars; from *Palaeosteiromys* in having lower molars with a metaflexid more extended; from *Protosteiromys*, *Branisamyopsis*, *Eosteiromys homogidens*, *Steiromys detentus*, and *Neosteiromys* in having a narrower mesoflexid on lower molars.

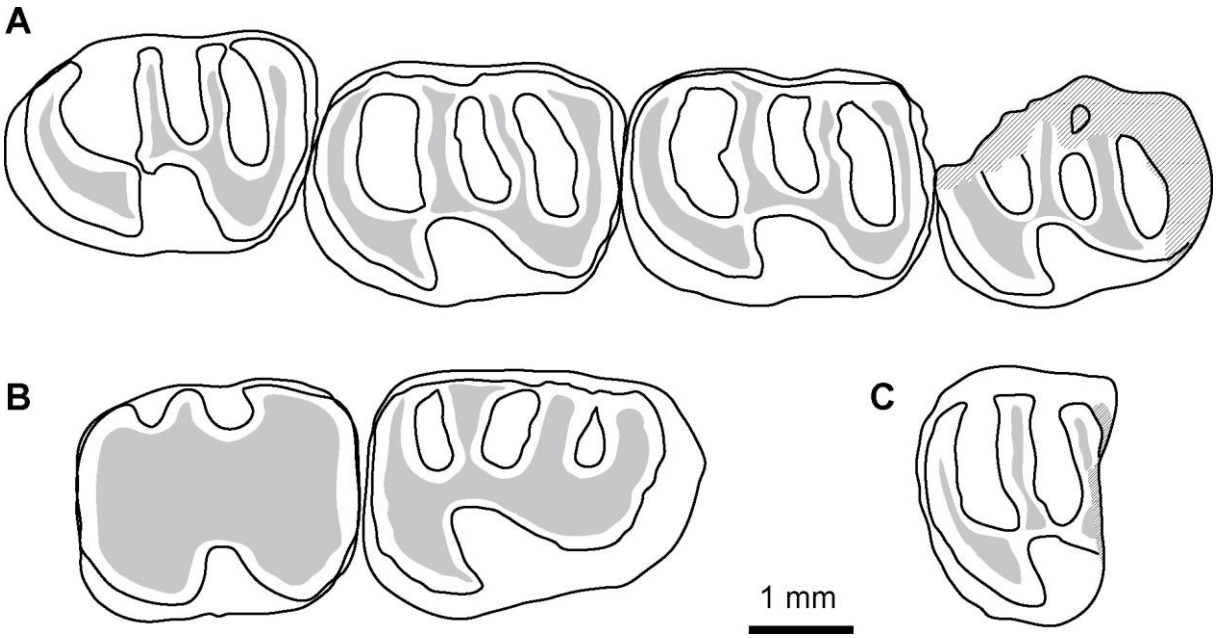


Fig 3. *Microsteiromys jacobsi* gen. et sp. nov. from La Venta, Colombia (late middle Miocene, Laventan SALMA). (A) FMNH PM 54672***, right mandibular fragment bearing dp4–m3. (B) IGM-DU 89–249, left mandibular fragment bearing p4–m1 (reversed), (C) IGM-DU 88–034, right posterior fragment of m1 or m2. Occlusal views. The asterisks appoint the holotype material. Based on Walton (Fig 16A-16C [37]). The illustrations of the fossil specimens are computerised schematic line drawings.

Description

FMNH PM 54672 (Fig 3A) and IGM-DU 89–249 (Fig 3B) are two mandibular fragments bearing dp4–m3 and p4–m1, respectively. The body of the FMNH PM 54672 mandible is anteriorly broken at the level of the anterior part of the lower diastema, which makes visible the lower incisor alveola. Posteriorly, the angular apophysis and most of the ascending ramus, including the mandibular condyle, are missing. The coronoid process is broken at its base. Labially, a mental foramen is located at the midpoint of the body of the mandible height (i.e., dorsoventrally). The notch for the insertion of the tendon of the *zygomatico-mandibularis pars infraorbitalis* is medium-sized, below dp4–m1, and centrally situated on the labial edge of the mandible. The anterior tip of the masseteric crest ends below the m1, and links the notch for the insertion of the tendon of the *zygomatico-mandibularis pars infraorbitalis*, at the level of its posteroventral region. The masseteric crest is posteriorly broken. It is posteroventrally directed and prominent in its anterior part.

The dp4 of the FMNH PM 54672 mandibular fragment (Fig 3A) is mesially and distolingually broken at the level of the metaconid, metalophulid I, mesostylid, entoconid, and posterolophid. This tooth is more worn and shorter than the molars (m1–3) beared by FMNH PM 54672. It is characterised by a short trigonid, which has an equal width with the talonid. This dp4 is brachydont and non-taeniodont. Despite its damaged state, no supplementary lophids are visible in addition to the metalophulid I, second transverse cristid, hypolophid and posterolophid, which suggests that the FMNH PM 54672 dp4 was tetralophodont. As this tooth is at an advanced stage of wear, the cuspids are not well defined to the lophids. On the lingual margin of the tooth, the anteroflexid and mesoflexid are closed, thereby suggesting that the mesostylid (or its arms) was connected to the metaconid (or its posterior arm) and its posterior arm reaches the entoconid (or its anterior arm). The metalophulid I, mesially convex, seems to be complete and strongly connected to the protoconid labially (hypothesis 1 on Fig 4A1; see the remark below). This cuspid is crestiform and faintly linked to the second cristid. The latter is slightly oblique (i.e., mesiodistally directed). It bears posteriorly a tiny and horrizontal cristulid, which joins the mesial margin of the hypolophid, dividing the mesoflexid into two small and round fossettids. The labiodistal aspect of the second cristid links to a transverse hypolophid via a very short and oblique ectolophid. The hypoconid is mesiolingually-distolabially compressed. It displays strong anterior arm, anterior outgrowth and posterolophid. The anterior outgrowth is mesiolabially oriented and delimits with the anterior arm of the hypoconid, hypolophid, ectolophid, second transverse cristid and protoconid, a triangular-shaped hypoflexid, oriented distolingually, and showing a wide labial opening. Although the lingual part of the posterolophid is missing, the metaflexid appears lingually closed as is the case as well for the anteroflexid and the mesoflexid.

The p4 of the IGM-DU 89–249 mandibular fragment (Fig 3B) is much longer and moderately worn with respect to the associated m1, which shows a very advanced state of wear characterised by a fusion all lophids and cuspids/stylids. As the FMNH PM 54672 dp4, it is brachydont, tetralophodont and non-taeniodont. However, it is much longer than the dp4 and has a mesial margin more straight. The protoconid corresponds to a large dentine plateform on the mesiolabial corner of the tooth. It is mesially connected to a metalophulid I, reaching the metaconid on the lingual margin, and distally to the second cristid and to na oblique and long ectolophid. The labial part of the metalophulid I is mesiolingually directed, while its lingual part is slightly directed distolingually. The metaconid is faintly linked to the mesostylid, which appears to have

an equal size to the former. Due to the moderate state of wear of the tooth, the presence of a posterior arm of the metaconid cannot be assessed, but if it would be present, the latter would be short. The mesostylid bears short anterior and posterior arms. Comparatively, the entoconid has longer arms, especially its anterior arm, reaching the posterior arm of the mesostylid. The second cristid is complete and slightly mesiolingually directed, whereas the hypolophid and the posterolophid are transverse. There is a connection between the latter and the posterior arm of the entoconid, which lingually closes the metaflexid. Thus, all the lingual flexids are closed and form round-oval fossettids. The anterior arm of the hypoconid is strong and mesiolingually oriented, whereas its anterior outgrowth is long and mesiolabially oriented. These cristids, with the ectolophid and protoconid, delimit a widely open and retroverse hypoflexid (triangular-shaped and distolingually directed).

The m1–3 of the FMNH PM 54672 specimen (Fig 3A) have a similar/compatible size with the unique and very worn molar (m1) borne by the IGM-DU 89–249 mandibular fragment (Fig 3B). On FMNH PM 54672, all molars are roughly equal in length. The m1 and m2 have a similar width, whereas m3 is narrower. The latter is characterised by a shorter posterolophid due to a linguolabial compression of its posterior part. The morphology of lower molars has the same pattern than that of dp4 and p4. As dp4 and p4, molars are brachydont, tetralophodont, non-taeniodont with a strong anterior arm of the hypoconid, and they have an oblique ectolophid and a triangular-shaped hypoflexid showing a wide labial opening. This flexid has a general distolingual direction, but the latter varies depending on the locus: it is slight on m3, more oblique on dp4 and m1, and the most oblique on p4 and m2. As dp4 and p4, m1–2 display all their lingual flexids closed, whereas m3 has a mesoflexid opened by a shallow and thin furrow, and a posterolophid well-separated from the entoconid. On m1–2, this cuspid appears to have a long posterior arm On m1–3, the metalophulid I is complete, transverse to slightly arched. The metaconid bears a long posterior arm strongly connected to the mesostylid (or its anterior arm). The second cristid and hypolophid are close and separated by a narrow mesoflexid (i.e., furrow-like flexid). These two transverse cristids are straight and roughly parallel on m1 and m3. On m2, most part of the second cristid (i.e., lingual part) is slightly distolingually directed. Because of a thinning on its central part on m1 and its orientation change on m2, the second cristid may be composed of two cristids on these lower molars: a neomesolophid lingually and a posterior arm of the protoconid labially. On all molars,

the posterolophid is curved, especially on m3. The metaflexid/metafossettid is mesiodistally well extended.

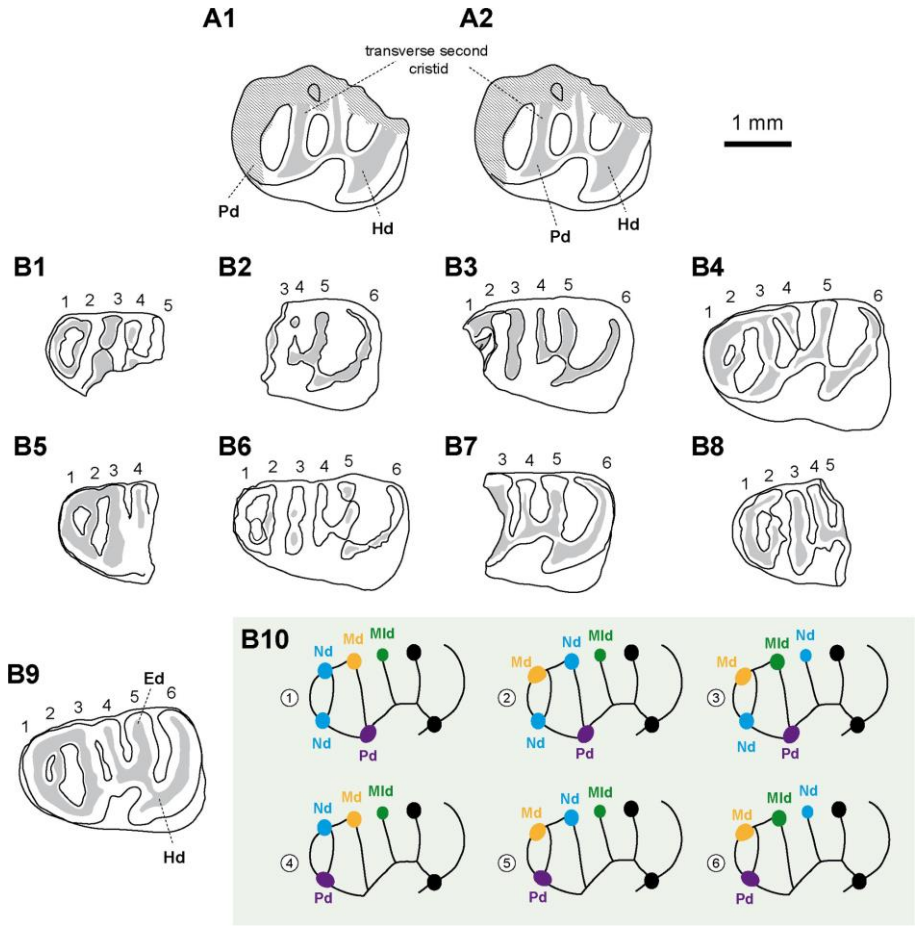


Fig 4. Hypotheses regarding the homology of structures on dp4 of the erethizontoid *Microsteiromys jacobsi* (A) and *Nuyuyomys chinqaska* (B). (A1) Hypothesis 1: protoconid in anterior position, aligned with the metalophulid I (followed here). (A2) Hypothesis 2: protoconid in posterior position, aligned with the second transverse cristid. (B1–9) Equivalent transversal cristids (and their associated cuspids/stylids) indicated by numbers (1–6) on all dp4s of *N*. *chinqaska*. (B10) Different hypotheses regarding the position of the anterior cuspids/stylids based on the morphology of MUSM 4333. For the transversal cristids 1 and 2, the position and number of the structures can slightly vary depending the considering specimen (e.g., MUSM 4332). In the case of the hypotheses 1–4, the neoconid(s) can be present on the cristid 1 or not (correspond solely to thickenings of this cristid). The hypotheses 1 and 3 are the most consistent with the morphology and development of the dental structures. (A) IGM-DU 89–249, (B1) MUSM 4326, (B2) MUSM 4327, (B3) MUSM 4328, (B4) MUSM 4329, (B5) MUSM 4325, (B6) MUSM 4332, (B7) MUSM 4331, (B8) MUSM 4330, and (B9) MUSM 4333. Ed, entoconid; Hd, hypoconid; Md, metaconid; Mld, mesostylid; Nd,

neoconid; Pd, protoconid. The illustrations of the specimens are computerised schematic line drawings.

Remark

Considering the pattern of dp4s of some erethizontoids (*Steiromys detentus*, MLP 15−339; *Erethizon dorsatum*, MCZ 51367) [69], another hypothesis can be proposed with respect to the position of the protoconid on the FMNH PM 54672 dp4 (hypothesis 2 on Fig 4A2): this cuspid could be situated more posterolingually than in hypothesis 1 and aligned with the second transverse cristid. The discovery of a pristine dp4 of this species would make it possible to decide between these two proposed hypotheses.

Comparisons

Brachydonty, non-taeniodonty, extended and moderately narrow flexids, weak obliquity of lophids, and p4 with a wide trigonid suggest erethizontoid affinities for these specimens from La Venta. They are markedly smaller than most of erethizontoid species, except for *Kichkasteiromys raimondii*, *Shapajamys labocensis* [70], *Palaeosteiromys amazonensis* [71], *Noamys hypsodonta* [72] and the material from the early middle Miocene of Madre de Dios, Peru formerly attributed to cf. *Microsteiromys* sp. (MD-67; [31] and see below). *Kichkasteiromys raimondii*, *N*. *hypsodonta* and the taxon from MD-67 being documented only by upper teeth, direct morphological comparisons with the material of La Venta cannot be made. The lower molars from La Venta differ from those of *Shapajamys* and *Palaeosteiromys* in being more rectangular. They are characterised by an ectolophid always complete and oblique, contrary to *Shapajamys*, and by a metaflexid more extended than in *Palaeosteiromys*. These specimens from La Venta are always tetralophodont, contrary to those of *Palaeosteiromys*, *Branisamyopsis australis*, *Branisamyopsis praesigmoides*, *Steiromys duplicatus* and *Neosteiromys*, which can exhibit a pentalophodont pattern by the addition of a mesial neolophid [71, 73–77]. By its rounded shape as well as its short and wide trigonid, the FMNH PM 54672 dp4 is close to the dp4s of the extant species *Coendou insidiosus*. The FMNH PM 54672 dp4 is tetralophodont, as dp4s of *Hypsoteiromys* [74, 78], but the latter are clearly more elongated, with a longer trigonid and more extended lingual flexids. Contrary to FMNH PM 54672, dp4s of other erethizontoids are elongated with a pentalophodont (*Eosteiromys homogidens*, *Eosteiromys annectens* and *C*. *insidiosus*) or hexalophodont (*Shapajamys*, *Branisamyopsis*, ?*Eosteiromys* sp. nov. *sensu* Candela

[69], and *Steiromys*) pattern. MNHN 1903-3-18 (Fig 32 [79]) was originally determined as a m3 of *Protosteiromys asmodeophilus*. However, its trigonid is clearly narrower than its talonid, a feature better characterising a premolar (p4 or dp4). MNHN 1903-3-18 is tetralophodont and non-taeniodont as p4s and dp4s from La Venta, but has lingual flexids much more extended. The material from La Venta differs from *Eopululo*, *Protosteiromys*, *Branisamyopsis*, *Hypsosteiromys*, *Parasteiromys*, *Eosteiromys*, *Steiromys* and *Neosteiromys* [73–76, 78–82] in having a smaller size; from *Hypsosteiromys* in having brachydont lower teeth with transverse lophids and a complete metalophulid I; from *E*. *annectens* and *S*. *duplicatus* in having non-taeniodont lower teeth; from *Branisamyopsis*, *S*. *duplicatus*, *Steiromys verzii sensu* Candela [74], and some p4s of *S*. *detentus* in having a p4s with tetralophodont pattern; and from *Eosteiromys segregatus* in having a longer p4 with a long anterior arm of the entonconid; from *Protosteiromys*, *Branisamyopsis*, *E*. *annectens*, *Steiromys* and *Neosteiromys* in having more rectangular lower molars; from *Protosteiromys*, *Branisamyopsis*, *E*. *homogidens*, *Steiromys detentus* and *Neosteiromys* in having a narrower mesoflexid on lower molars; from *B*. *praesigmoides* and *S*. *duplicatus* in having an ectolophid always complete on lower molars. To sum up, these few specimens from La Venta show a set of distinctions (i.e., small size; brachydonty; tetralophodont and non-taeniodont lower teeth; a complete metalophulid I, and an oblique and complete ectolophid on lower teeth; round dp4s with a short and wide trigonid; mesiodistally elongated lower molars with narrow mesoflexid and well-extended metaflexid) that allows us to refer them to a new genus and new species. Thus, we validate *Microsteiromys jacobsi* Walton, 1990, which had remained until now as a *nomen nudum*. *Nuyuyomys* Boivin & Walton gen. nov. urn:lsid:zoobank.org:act:360EBF95-C067-4C81-81F4-8FAD41067E7E

Type species

Nuyuyomys chinqaska gen. et sp. nov.

Species content

Only the type species.

Derivation of name

From *Nuyuy*, flooding in Quechua language, referring to the location of both fossil localities yielding this genus (at the water level only during the driest season and below it most of the year) and *-mys*, mouse in Greek, a classical suffix for rodents.

Geographical and stratigraphical distribution

Pilcopata (MD-67), unnamed Fm. (Colloncuran-Laventan, middle Miocene), Madre de Dios Department, Peru; Tarapoto/Juan Guerra (TAR-31), lower member, Ipururo Fm. (Laventan, late middle Miocene), San Martı´n Department, Peru.

Generic diagnosis

As for the type and only known species.

Nuyuyomys chinqaska Boivin & Walton sp. nov. urn:lsid:zoobank.org:act:353264FD-EB4C-428F-9F6D-EFC6DC1D7A04

Fig 5 and S1 Table

2013 cf. *Microsteiromys* sp. Antoine et al., Fig 3M, 3N, p. 94.

Holotype

MUSM 4308 (Fig 5R), right M1?.

Referred material

MUSM 4325–4329 (Fig 5F), left dp4s; MUSM 4330–4333 (Fig 5A), right dp4s; MUSM 4334 (Fig 5B), left p4; MUSM 4335–4339, left lower molars; MUSM 4340–4342, right lower molars; MUSM 4343, 4344, left m1s; MUSM 4345–4348 (Fig 5C and 5G), right m1s; MUSM 4349–4357 (Fig 5H, 5J and 5K), left m2s; MUSM 4358–4363 (Fig 5D and 5L–5N), right m2s; MUSM 4364 (Fig 5I), left m3; MUSM 4365, 4366 (Fig 5E and 5O), right m3s; MUSM 4284–4288 (Fig 5Z), left dP4s; MUSM 4289–4294 (Fig 5P, 5U, 5C' and 5D'), right dP4s; MUSM 4295 (Fig 5Q), left P4; MUSM 4296, 4297, right upper molars; MUSM 4299, right M1 or M2?; MUSM 4300–4306, left M1?s; MUSM 4307–4314 (Fig 5A' and 5B'), right M1?s; MUSM 4315, right M2 (or M3)?; MUSM 4316–4320 (Fig 5S and 5W), left M2?s; MUSM 4321, 4322, right M2?s; MUSM 4323 (Fig 5X), left M3; MUSM 4324 (Fig 5T), right M3.

Tentitavely referred material

MUSM 1974 (Antoine et al., 2013: Fig 3M, p. 94), left P4; MUSM 1975 (Antoine et al., 2013: Fig 3N, p. 94), right upper molar; MUSM 4298 (Fig 5E'), left M1 or M2?.

Derivation of name

From *chinqaska*, vanished in Quechua language, referring to the disappearance of both MD-67 and TAR-31 outcrops since their discovery, due to water erosion and paleontological exploitation, respectively.

Type locality

TAR-31, Tarapoto/Juan Guerra, Mayo River, Shapaja road, San Martı´n Department, Western Amazonia, Peru.

Other locality

MD-67, Pilcopata, Rinconadera and Madre de Dios rivers, Madre de Dios Department, Western Amazonia, Peru.

Formation and age

Unnamed Fm., middle Miocene (i.e., Colloncuran-Laventan SALMA); lower member, Ipururo Fm., late middle Miocene (i.e., Laventan SALMA).

Diagnosis

Rodent characterised by small size, brachydont lower teeth and dP4s, brachydont-mesodont P4s and upper molars, and a weak obliquity of loph(-id)s. dp4s, p4s and upper teeth with a non-taeniodont pattern. Lower molars with a non-taeniodont or pseudo-taeniodont pattern at early stages of wear, the former pattern being the most frequent. Elongated dp4s with a hexalophodont pattern. p4s are longer than wide, with a large trigonid and tetralophodont pattern. Lower molars with a tetralophodont or pentalophodont pattern, the latter corresponding to the addition of a neolophid between the metalophulid I and the second transverse cristid. dP4s with a pentalophodont or tetralophodont pattern, the former pattern being the most frequent. The metaloph (when present) can be lingually free or connected to the posteroloph or to both the third crest and posteroloph on dP4s. Round and tetralophodont P4s with an anterior arm of the protocone thicker and mesiolabially directed connected to an anteroloph lower, thinner and roughly transverse, and without endoloph. Pentalophodont upper molars with a metaloph always long and joining the metacone to the posteroloph on M2?s and complete or reduced on M1?s and M3?s. *Nuyuyomys* is markedly smaller than all erethizontoid species except *Kichkasteiromys*, *Shapajamys*, *Palaeosteiromys*, *Microsteiromys* and *Noamys*. Differs from *Eosteiromys homogidens*, *Eosteiromys annectens*, *Hypsosteiromys*, *Microsteiromys* and *Coendou insidiosus* in having hexalophodont dp4s; from *Shapajamys*, *Protosteiromys*, *Eosteiromys* and *Microsteiromys* in having no neolophid on the anteroflexid on lower molars; from *Shapajamys*, *Branisamyopsis praesigmoides* and *Steiromys duplicatus* in having an ectolophid always complete. Differs from *Kichkasteiromys*, *Shapajamys* and *Palaeosteiromys* in having a metaloph disconnected labially to the metacone on some upper molars; from *Shapajamys* in having no distinct metaloph on P4s, metaloph more developed on ?M2s and an ectolophid always oblique on lower molars; from *Kichkasteiromys* in having a lingual protoloph less lingually situated and a posterior

outgrowth of the protocone more oblique on upper molars; from *Palaeosteiromys* in having a mesoflexid more extended on m3s; from *Microsteiromys* in having more elongated dp4s with a narrower trigonid, the mesoflexid still lingually open at advanced stage of wear on m1–2s and less rectangular lower molars. Differs from *Hypsosteiromys* in having loph(-id)s more transverse, round P4s, pentalophodont M1–2s, and a complete metalophulid I on lower teeth; from *Noamys* in having pentalophodont and sligthly smaller dP4 and M1 without oval-shaped occlusal contour and flexi less extended. Differs from *Eosteiromys annectens* and *Steiromys duplicatus* in having non-taeniodont lower teeth; from *Neosteiromys* and *Parasteiromys* in having always a complete mure on dP4s and upper molars; from *Eopululo*, *Protosteiromys pattersoni* and *Neosteiromys* in having a P4 without endoloph; from *Eosteiromys homogidens* in having a mesial mesoflexus less mesiodistally extended on P4s; from *Eosteiromys annectens*, *Branisamyopsis* and *Neosteiromys* in having non-taeniodont dP4s and Upper molars; from *Eopululo* and *Protosteiromys pattersoni* in having upper molars always with a metaloph (which is not reduced, far from being a relictual structure); from *Protosteiromys*, *Parasteiromys*, *Branisamyopsis*, *Eosteiromys*, *Steiromys* and *Neosteiromys* in having some elongated upper molars (potential M1s) and an incomplete metaloph on some upper molars; from *Protosteiromys medianus* in having a complete third crest on M3s.

Description

dp4s are brachydont and much longer than wide, with a talonid slightly wider than the trigonid. They are non-taeniodont and hexalophodont. In addition to six complete transverse lophids, one dp4 (MUSM 4332; Fig 5A) has a tiny low cristulid stemming from the metalophulid I on the anteroflexid. Owing to its low elevation and shortness, it is interpreted here as a neolophid. The entoconid and hypoconid and their associated lophids (i.e., hypolophid [cristid 5 in Fig 4B1–4B9], anterior outgrowth of the hypoconid, anterior arm of the hypoconid, and posterior arm of hypoconid/posterolophid [cristid 6 in Fig 4B1–4B9]), distally positioned on the tooth, are well recognisable. The entoconid is the largest lingual cuspid. It is clearly isolated on almost all dp4s. On MUSM 4331, its isolation is less important because it is separated from the posterolophid by a thinner and shallower notch. The hypolophid is transverse or slightly arcuate (i.e., mesially concave). The crestiform hypoconid displays an anterior arm, which is mesiolingually oriented, thin and linked to the labiodistal extremity of the hypolophid. On MUSM 4332 (Fig 5A), the mesialmost part of the anterior arm of the hypoconid is lower than its distal part, but it is connected to the hypolophid and clearly separates the hypoflexid from

the metaflexid (i.e., non-taeniodont pattern). The hypoconid exhibits a strong and short anterior outgrowth. The posterolophid is particularly long and curved, notably in its lingual part. On the less worn dp4s, it is composed of two (MUSM 4329; Fig 5F) or three (MUSM 4327 and 4332; Fig 5A) interconnected parts, a posterior arm of the hypoconid and posterolophid included. Mesially, the recognition of the main cuspids (i.e., protoconid, metaconid, and mesostylid) and cristids (i.e., posterior arm of the protoconid, metaconid cristid, mesolophid, and neomesolophid) is ambiguous by the addition of some neostructures (i.e., neoconids and neolophids). Several hypotheses of homology can be proposed (Fig 4B10). The mesialmost cristid (cristid 1 in Fig 4B1–4B9) is curved. It (mainly) corresponds to the metalophulid I. It shows one or several cuspate thickenings in its central part and/or extremities (MUSM 4325, 4326, 4329, and 4330, 4332, 4333; Figs 4B1, 4B4–4B6, 4B8, 4B9 and 5A and 5F). They can correspond to the main cuspids (i.e., protoconid, metaconid, mesostylid) and/or neoconids (Fig 4B10). The second cristid (cristid 2 in Fig 4B1–4B9) is highly variable. It can be constituted of one or two linked cristulids, which can be associated to the thickenings of the metalophulid I. They can be connected to the central part of the cristid 1 (MUSM 4329 and 4333; Fig 4B4 and 4B9) and/or to one (MUSM 4325; Fig 4B5) or two of its extremities (MUSM 4326, 4330, and 4332; Fig 4B1, 4B6 and 4B8). The next transverse cristid (cristid 3 in Fig 4B1–4B9) is thick and long, stemming from a cuspate structure on the lingual margin of the tooth to connect to a large another cuspid-shaped structure on the labial margin. These cuspid-like structures are clearly isolated at early stages of wear (MUSM 4326, 4330, and 4332; Figs 4B1, 4B6, 4B8 and 5A) and can link the structures located mesially (metalophulid I and annexes) at more advanced staged of wear (MUSM 4329 and 4333; Figs 4B4, 4B9 and 5F). On MUSM 4326 and 4329, this transverse cristid has two parts: a lingual cristid connected to a labial one, equally sized (MUSM 4326; Fig 4B1) or shorter (MUSM 4329; Figs 4B4 and 5F). Owing to the important development of this cristid and of its cuspate structures on all dp4s, they are probably not neostructures (hypotheses 1 and 3 in Fig 4B10). The transverse cristid appearing in fourth position (cristid 4 in Fig 4B1–4B9) is labially connected to the hypolophid via the distal ectolophid on all dp4s. This cristid can be continuous (MUSM 4327, 4328, and 4330–4333; Fig 4B2, 4B3, 4B6–4B9) or divided into two parts, which are joined (4326 and 4329; Fig 4B1 and 4B4). In addition, it can be high (MUSM 4326 and 4330–4333; Fig 4B1, 4B6–4B9), entirely low (MUSM 4327; Fig 4B2) or only its labial part can be low (MUSM 4329; Figs 4B4 and 5F). On MUSM 4327 (Fig 4B2), it is slightly connected to a bulbous cuspid clearly distinct on the lingual

margin of the tooth. MUSM 4334 is an almost pristine p4 (Fig 5B). It is longer than wide, with a trigonid narrower than the talonid. It is brachydont and tetralophodont. On its mesiolingual corner, the crestiform metaconid is convex forward. Distally, this cuspid displays a very short posterior arm. There is a tiny spur-like cristulid on the anteroflexid, labially free and stemming from the distal extremity of the posterior arm of the metaconid. Mesially, the metaconid has a transverse and long anterior arm. From its central part, a short cristulid runs distally on the anteroflexid. The anterior arm of the metaconid is linked to a faintly curved anterior arm of the protoconid. The latter cristid is clearly sloped with a high distal part stemming from the triangular-shaped protoconid. The second transverse cristid is essentially composed of a long neomesolophid joining a very short posterior arm of the protoconid. The ectolophid is mainly oblique and Sshaped. It reaches the distal slope of the protoconid. The entoconid is high and it has a sharp posterior arm. Labially, this cuspid is connected to a hypolophid, strong and distolingually oblique. On the labiodistal margin of the ectolophid-hypolophid junction, a tiny cristulid is present. Its top is separate from the anterior arm of the hypoconid by a very shallow notch. However, the contact between these structures remains high despite the presence of this notch (i.e., non-taeniodont pattern). The anterior outgrowth of the hypoconid is short and directed mesiolabially. The posterolophid is transverse with curved lingual and labial extremities. On the lingual margin, all structures (i.e., metaconid, mesostylid, entoconid and lingual extremity of the posterolophid) are merged together at their base, but they remain disconnected at their apex. The mesostylid is discreet and isolated from the posterior arm of the metaconid and the entoconid by wide and deep furrows. The notch separating the entoconid from the lingual extremity of the posterolophid is thinner and shallower. The anteroflexid and metaflexid are more expanded than the mesoflexid. The hypoflexid is triangular-shaped with a wider labial openning. The lower molars are brachydont and rectangular-shaped. m3s (MUSM 4364–4366; Fig 5E, 5I and 5O) show a talonid slightly narrower than the trigonid, notably lingually. m1s and m2s usually have a trigonid and a talonid roughly of same width and m2s are larger than m1s and m3s. On all lower molars, the metaconid, protoconid and hypoconid are crestiform, whereas the mesostylid and entoconid are more bulbous. The metalophulid I is transverse and complete, joining the metaconid to the protoconid. On the lower molars at the earliest stage of wear (MUSM 4342, 4347, and 4359; Fig 5C and 5D), this cristid corresponds to a long anterior arm of the metaconid, whose lingual extremity is low and linked a short anterior arm of the protoconid. On most lower molars, the mesostylid is linked to the posterior

arm of the metaconid, this connection can be slight or tight. These two structures can be separated by a wide furrow (e.g., MUSM 4336, 4357, and 4365; Fig 5O) or a thin notch (e.g., MUSM 4356, 4347, and 4348; Fig 5C, 5G and 5J). Several lower molars exhibit two short cristulids on their mesiolingual area: the first cristulid is situated on the distolingual part of the metalophulid I, and the second is located distally to the metaconid, on its posterior arm (MUSM 4344, 4352, 4355, 4364, and 4362; Fig 5H, 5I, 5K and 5L). On MUSM 4344, 4364 and 4362 (Fig 5I and 5L), these two cristulids are joined, and form a mesial neolophid on the anteroflexid (i.e., pentalophodont pattern). On MUSM 4352 and 4355, they remain separate (Fig 5H and 5K). On MUSM 4351, there is only the cristulid of the metalophulid I, whereas on MUSM 4348 (Fig 5G), there is only the cristulid distally to the metaconid. The second transverse cristid is a long neomesolophid directly connected to the protoconid or via its very short posterior arm. It can be slightly oblique, transverse, or sometimes sinuous (S-shaped). The ectolophid is always oblique, either aligned with the protoconid or a little more longitudinal. The entoconid can display strong anterior and posterior arms. On MUSM 4336 and 4351, the posterior arm is particularly long. The latter can be connected (e.g., MUSM 4336, 4352, 4364, and 4359; Fig 5D, 5I and 5K) or disconnected (e.g., MUSM 4351, 4354, 4356, 4357, 4347, and 4365; Fig 5C, 5J and 5O) to the posterolophid. The hypolophid is well marked and often parallel to the second transverse cristid. The anterior arm of the hypoconid is complete and high in most cases (i.e., nontaeniodont pattern). Two lower molars, MUSM 4356 and 4347 (Fig 5C and 5J), show a pseudo-taeniodont pattern. On MUSM 4356 (Fig 5J), the anterior arm of the hypoconid is complete, but moderately low. On MUSM 4347 (Fig 5C), there is a very low cristulid stemming from the hypolophid-ectolophid junction and joining the mesial slope of the hypoconid, thereby involving a partial confluence between the metaflexid and the hypoflexid. dP4s are longer than wide with a rectangular or slightly trapezoidal occlusal outline. On all dP4s (except on MUSM 4293; Fig 5C'; see below), the protocone is somewhat bulbous, a morphology accentuated by a thinning at the level of its connection with the anteroloph. In addition, the lingual extremity of the latter is sometimes thickened (MUSM 4284, 4287, and 4289–4292; Fig 5P and 5U). The anteroloph is mesially convex, and can have an enamel thickening on its labial part, that we interpret as a parastyle, associated with a spur-like crestule (MUSM 4285, 4287, 4289, 4290, and 4292; Fig 5P, 5U and 5Z). This crestule remains lingually free on the paraflexus. On the labial margin of dP4s, the paracone is the largest cusp. It is clearly separated mesially from the labial extremity of the anteroloph and distally from the mesostyle by

wide and deep furrows in most cases. On MUSM 4290 (Fig 5P), the paracone is separate from the anteroloph by a shallower notch. The labial protoloph can be transverse (MUSM 4291), oblique (i.e., mesiolabially directed; MUSM 4293; Fig 5C') or with an oblique lingual part and a labial part more transverse (on the other dP4s). On MUSM 4287, in its middle, the labial protoloph displays a tiny crestule on its mesial part. Its ends close to the distal extremity of the crestule stemming from the parastyle, but does not connect to it. The mure is oblique (e.g., MUSM 4290 and 4293; Fig 5P and 5C') or more longitudinal (i.e., parallel to the mesiodistal long axis of the tooth; e.g., MUSM 4291 and 4292; Fig 5U). Its junction with the labial protoloph is linked to the protocone via its thin anterior arm (i.e., non-taeniodont pattern). Labially, the mesostyle is large, whereas the metacone is faintly visible from the posteroloph. On MUSM 4290–4292 and 4294 (Fig 5P, 5U and 5D'), the mesostyle shows a long posterior arm. The mesostyle or its posterior arm is either linked to the metacone-posteroloph complex (MUSM 4287, 4290, 4291, and 4293; Fig 5P and 5C') or is separated from this cusp by a thin and shallow notch (MUSM 4285, 4286, 4292, and 4294; Fig 5U, 5Z and 5D'). The third crest is complete and S-shaped. On MUSM 4285 and 4292 (Fig 5U and 5Z), this crest consists of a long mesoloph stemming from the mesostyle and joining lingually the mure-anterior arm of the hypocone junction directly (MUSM 4292; Fig 5U) or via a short mesolophule (MUSM 4285; Fig 5Z). The posteroloph is mesially concave and links the metacone to the hypocone. The metaloph shows a variable length, direction and lingual connection. On MUSM 4285, 4290 and 4292 (Fig 5P, 5U and 5Z), the metaloph is long, turned backwardly (either curved or L-shaped), and linked to the posteroloph via (or not) a posteroloph spur. On MUSM 4286, the metaloph is short, mesiolingually directed and lingually free. On that tooth, there is also a crestule, close to the metaloph and connected lingually to the posteroloph spur and labially to the posteroloph. Due to its position and configuration, it is probably a rest of metaloph. On some worn dP4s (MUSM 4287, 4291, and 4293; Fig 5C'), the metacone and metaloph are likely subsumed within the posteroloph (+ its spur), thereby forming a thick platform distally. Neocrestules connect the third transverse crest to the metacone or to the distal platform on MUSM 4289–4291 (Fig 5P). On MUSM 4294 (Fig 5D'), there is no metaloph or distinct metacone (which is probably fused with the posteroloph). On that tooth, the thin posteroloph bears a long spur, which runs mesiolabially on the posterior flexus and remains free. The hypoflexus forms a U-shaped structure, mesiolabially directed. P4s are round, MUSM 4295 shows an oval outline (Fig 5Q), whereas MUSM 1974 is longer and more circular-shaped (Fig

3M [31]). MUSM 4295 is higher-crowned with respect of the other teeth attributed to *Nuyuyomys chinqaska* (Hling = 0.89; Hlab = 0.62; Fig 5Q). On MUSM 4295, the area of the protocone and that of the hypocone are large and conical, corresponding to oval regions of dentine delimited by a very thick exterior enamel layer (Fig 5Q). On the two P4s, the mesialmost crest is divided into two parts, which are connected together. Its lingual part, the anterior arm of the protocone, is thicker, mesiolabially directed, longer on MUSM 4295 (Fig 5Q), but shorter on MUSM 1974 (Fig 3M [31]). This crest is in the continuity with the protocone and its short posterior outgrowth. The labial part of the mesialmost crest, the anteroloph, is thinner, roughly transverse, shorter on MUSM 4295, but longer on MUSM 1974. It should be lower than the anterior arm of the protocone (and the other occlusal structures) at early stage of wear, because it is barely worn contrary to all other structures of the occlusal surface. The anteroloph is separate from a strong paracone (or the mesial extremity of its sloped anterior arm on MUSM 4295) by a thin furrow. The labial protoloph is oblique. It is connected, with the mure, to a strong and complete posterior arm of the protocone. On MUSM 4295 (Fig 5Q), the mure is very short and longitudinal (i.e., parallel to the mesiodistal axis of the tooth). On MUSM 1974 (Fig 3M [31]), the mure is absent or reduced to a very tiny crestule from the third crest-anterior arm of the hypocone jonction that remains mesially free. The third crest is almost parallel to the oblique labial protoloph, and is composed of a long mesolophule sligthly linked to a short mesoloph. The mesostyle is strongly connected to a curved and thick posteroloph. There is no clear distinct metacone or metaloph. Hence, the posterior flexus is fully closed. However, the posteroloph appears to have a thickenning, which could correspond to a relictual metaloph, on MUSM 4295 (Fig 5Q). The latter and paraflexus are long, narrow mesiolabially-distolingually extended and oriented on MUSM 4295 (Fig 5Q), whereas they are more mesiodistally expanded on MUSM 1974 (Fig 3M [31]), due to the higher length of that tooth. The mesial mesoflexus and hypoflexus are clearly open. M3s of *Nuyuyomys chinqaska* (MUSM 4323 and 4324; Fig 5T and 5X) are well recognisable by their distal part, which is labiolingually pinched (notably labially), and their hypocone, being clearly smaller and with a lingual margin occupying a more labial position than the protocone. Among other upper molars attributed to this taxon, some are small-sized and subsquare or slightly mesiodistally elongated, and other larger can be also subsquare but they are usually more transverse, being wider than long. We interpret them as possibly M1s and M2s, respectively (i.e., M1? and M2?). The height of crown is widely variable. Some upper molars at early stages of wear have a higher crown (e.g., the

MUSM 4303 M1? and 4320 M2?; Hling = 0.74–0.89) than other, which are less worn (e.g., the MUSM 4313 and 4314 M2?s; Hling = 0.60–0.69). Because there are teeth with intermediary crown height between these two extremes and no morphological character allowing to differentiate them, we consider that all the material reported here documents a single taxon. On all upper molars, the crests are thin. The paracone and the mesostyle are well differentiated, whereas the protocone and hypocone are more crestiform, as the metacone in most cases. The latter is more cuspate on two Upper molars (MUSM 4309 and 4320; Fig 5W and 5A'). The protocone and hypocone are mesiolingually-distolabially and mesiodistally compressed, respectively. As on the MUSM 4295 P4, the anterior arm of the protocone is mesiolabially directed and in continuity with the protocone, its posterior outgrowth and sometimes a part of the anteroloph, like on MUSM 4314 (Fig 5B'). The anteroloph (or its labial part) is more transverse. At early stages of wear, labially the paraflexus can be either closed (MUSM 4298 and 4303; Fig 5Y and 5E') or opened (e.g., MUSM 1975, 4306, 4308, 4309, 4311, and 4320; Fig 3N [31]; Fig 5R, 5V, 5W and 5A'), separate from the paracone by a thin notch (e.g., MUSM 4308, 4309, and 4320; Fig 5R, 5W and 5A') or a wider furrow (MUSM 1975, 4306 and 4311; Fig 3N [31]; Fig 5V). The posterior outgrowth of the protocone can be very short, particularly on M1?s, or moderately longer. The posterior arm of the protocone is complete and thin. On MUSM 4303, 4307 and 4314 (Fig 5Y and 5B'), this crest is slightly lower than the protocone, but remains high (i.e., non-taeniodont pattern). Although the paracone and mesostyle are close in position, they do not share connection in most cases. On MUSM 4298, 4320 and 4323 (Fig 5W, 5X and 5E'), however they are linked via their arms (i.e., posterior arm of the paracone and anterior arm of the mesostyle). The labial protoloph is usually straight and mesiolabially directed, but it can have a lingual part oblique, whereas its labial part is more transverse such as on MUSM 4298, 4318 and 4322 (Fig 5E'). Two upper molars (MUSM 4311 and 4317) have one crestule on the mesial margin of the labial protoloph, which is mesially free. MUSM 4323 does not have that crestule, but it shows a tiny enamel swelling on the labial part of the paraflexus (Fig 5X). The third crest is often parallel to the labial protoloph, and is usually composed of a long mesoloph linked to a mesolophular spur. The mure is short but complete, oblique and linked to a strong and long anterior arm of the hypocone. As dP4s, some upper molars have a long posterior arm of the mesostyle (MUSM 4303, 4307, 4319, and 4323; Fig 5S, 5X and 5Y). On other upper molars, this arm is usually short, but it can also be undeveloped (MUSM 1975 and 4314; Fig 3N [31]; Fig 5B'). The metacone can be connected to the

mesostyle or its posterior arm (e.g., MUSM 4303, 4308, and 4319; Fig 3N [31]; Fig 5R, 5S and 5Y), or separated from these structures by a very tiny notch (e.g., MUSM 4306, 4307 and 4320; Fig 5V and 5W), except on MUSM 1975 and 4314, where the notch is thicker (Fig 3N [31] and Fig 5B'). On all upper molars, a metaloph is present, either long or short. It is often connected lingually to the posteroloph (via a posteroloph spur on MUSM 4315 and 4320; Fig 5W), but it can also be lingually free (MUSM 4298, 4303, and 4312; Fig 5Y and 5E'). On MUSM 1975, 4308 and 4307 (Fig 3N [31] and Fig 5R), it is reduced to a crestule labially disconnected to the metacone, and lingually linked to the posteroloph spur. Specifically, the metaloph is always long and joining the metacone to the posteroloph on teeth identified as M2?s, whereas it is complete or reduced on M1?s and M3?s. The MUSM 4323 M3 displays a neocrest stemming from the anterior arm of the metacone, and connecting lingually to the third crest (Fig 5X). The hypocone has a short posterior arm slightly connected to the posteroloph (MUSM 4308, 4309, 4311, 4315, 4318, 4319, and 4324; Fig 5R, 5S, 5T and 5A') or separate from it by a minute and shallow notch (MUSM 4298, 4303, 4306, 4313, 4320, and 4323; Fig 5V, 5W, 5X, 5Y and 5E'). This notch is wider on MUSM 4314 (Fig 5B'). Some upper molars have a mesiodistal constriction at the base of the hypoflexus (MUSM 4303, 4307, 4312, 4319, and 4324; Fig 5S, 5T and 5Y).

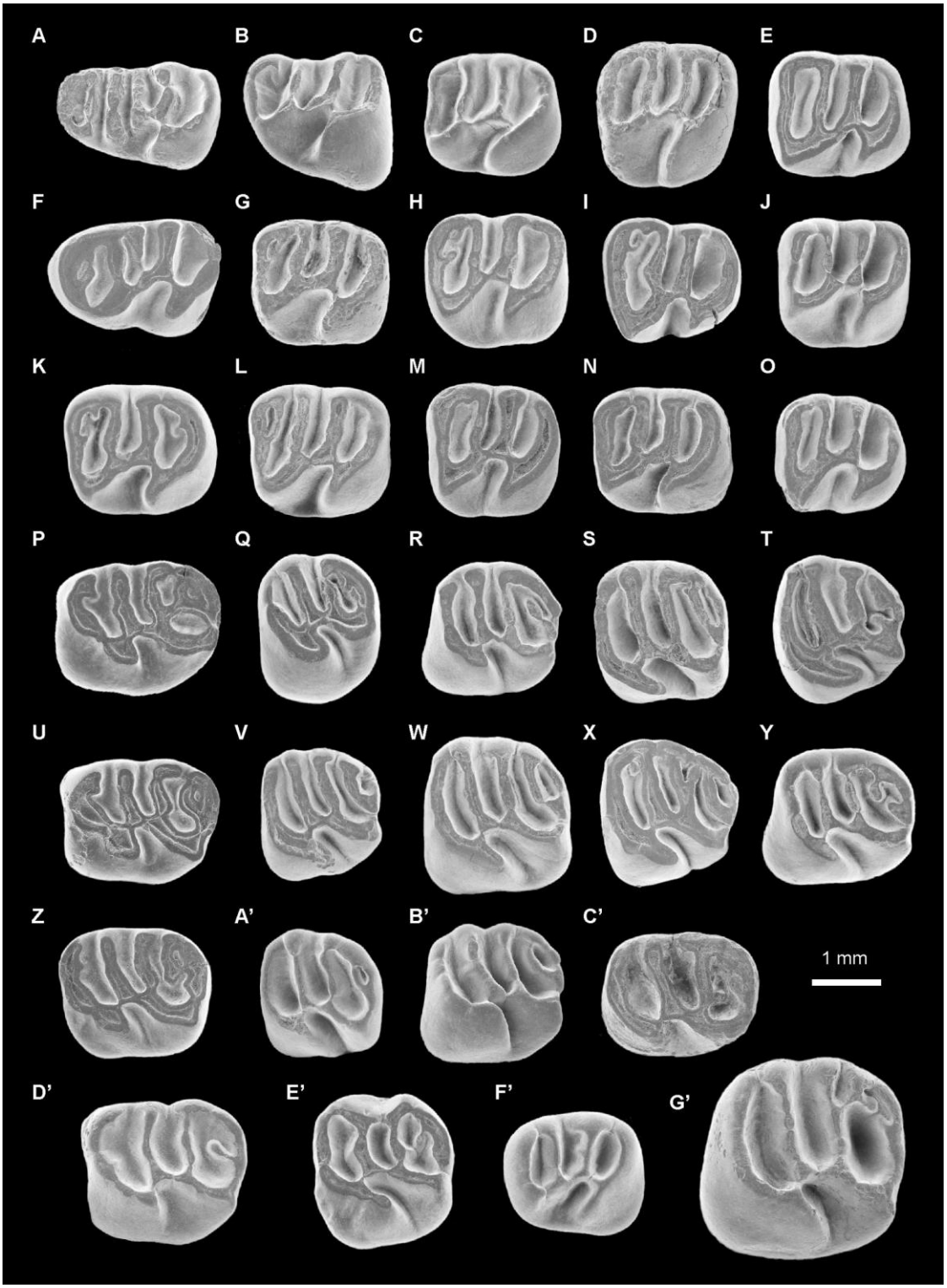


Fig 5. Erethizontoid rodents from TAR-31, Peru (late middle Miocene, Laventan SALMA). (A-E') *Nuyuyomys chinqaska* gen. et sp. nov. (F') Erethizontoidea gen. et sp. indet. 1. (G') Erethizontoidea gen. et sp. indet. 2. (A) MUSM 4332, right dp4 (reversed). (B) MUSM 4334, left p4. (C) MUSM 4347, right m1 (reversed). (D) MUSM 4359, right m2 (reversed). (E) MUSM 4366, right m3 (reversed). (F) MUSM 4329, left dp4. (G) MUSM 4348, right m1 (reversed). (H) MUSM 4355, left m2. (I) MUSM 4364, left m3.

(J) MUSM 4356, left m2. (K) MUSM 4352, left m2. (L) MUSM 4362, right m2 (reversed). (M) MUSM 4363, right m2 (reversed). (N) MUSM 4360, right m2 (reversed). (O) MUSM 4365, right m3 (reversed). (P) MUSM 4290, right dP4 (reversed). (Q) MUSM 4295, left P4. (R) MUSM 4308***, right M1? (reversed). (S) MUSM 4319, left M2?. (T) MUSM 4324, right M3 (reversed). (U) MUSM 4292, right dP4 (reversed). (V) MUSM 4306, left M1?. (W) MUSM 4320, left M2?. (X) MUSM 4323, left M3. (Y) MUSM 4303, left M1?. (Z) MUSM 4285, left dP4. (A') MUSM 4309, right M1? (reversed). (B') MUSM 4314, right M1? (reversed). (C') MUSM 4293, right dP4 (reversed). (D') MUSM 4294, right dP4 (reversed). (E') MUSM 4298, M1 or 2?. (F') MUSM 4367, left p4. (G') MUSM 4368, right M1 or M2 (reversed). The asterisks appoint the holotype material. The illustrations of the fossil specimens are scanning electron photomicrographs.

Remark 1

The MUSM 4293 and 4294 (Fig 5C' and 5D') dP4s have size, a crown height and global occlusal morphology similar than the rest of dP4s attributed to *Nuyuyomys chinqaska* (i.e., rectangular or slightly trapezoidal occlusal outline, pentalophodonty-tetralophodonty, nontaeniodonty, and U-shaped hypoflexus). Nevertheless, they differ from other dP4s attributed to this taxon in some characters. MUSM 4293 (Fig 5C') has a protocone strongly linked with the anteroloph without any thinning of this crest. On MUSM 4294 (Fig 5D'), the protocone is less bulbous than on other dP4s of *N*. *chinqaska*, and the anteroloph shows a more sligthly thinning. Finally, there is no distinct metacone and metaloph on MUSM 4294 (Fig 5D'). We interpret all these differences between MUSM 4293, 4294, and the rest of dP4s attributed to *N*. *chinqaska* as documenting intra-specific variation.

Remark 2

We tentatively assigned the MUSM 4298 upper molar (Fig 5E') to *Nuyuyomys chinqaska* because it shows a particular pattern, not really shared with other upper molars attributed to *N*. *chinqaska*. On that tooth, the apices of the paracone and mesostyle appear to be lingually displaced and they bear very long arms with unusual orientations due to a kind of unusual invagination of the labial crown margin: the anterior arm of the paracone is mesiolabially directed, its posterior arm is very slightly distolabially directed, and the anterior arm of the mesostyle is mesiolingually directed. Owing to the orientation of these arms and the connections anteroloph-anterior arm of the paracone, posterior arm of the paracone-anterior arm of the mesostyle, and

mesostyle-metacone, the dental structures of the tooth labially form a “M”. In addition, the extremity of the posterior outgrowth of the protocone is bulged appearing as a cusp-like structure. Nevertheless, MUSM 4298 matches with the morphology of the Other upper molars of *N*. *chinqaska* by other characters (i.e., size, crown-height, pentalophodonty, non-taeniodonty, crestules on the paraflexus, oblique mure, long mesoloph connected to a mesolophular spur, and tiny and shallow furrow separating the posterior arm of the hypocone from the posteroloph). As far we know, such M-shaped pattern for the labial dental structures on upper molars is not found in caviomorphs or very rare. Consequently, the peculiar characters of MUSM 4298 may result to some abnomalies or extreme intra-specific variation of this taxon.

Remark 3

In addition, the specimens of TAR-31 have a small size and general pattern (i.e., non-taeniodonty; complete mure on upper teeth; presence of a metaloph on dP4s and upper molars) similar to those of the material from the early middle Miocene of Madre de Dios formerly attributed to cf. *Microsteiromys* sp. (MD-67, Peru) [31]. The latter is documented by only two upper teeth: MUSM 1974 P4 and MUSM 1975 upper molar (Fig 3M and 3N, p. 94 [31]). By their mesiodistally-elongated shape, ?M1s from TAR-31 are close to MUSM 1975. Particularly, MUSM 4307 and 4308 (Fig 5R) from TAR-31 show a labial protoloph and a third crest slightly oblique and a short metaloph labially unconnected to the metacone and lingually linked to the posteroloph spur, as on MUSM 1975. Due to the absence of lower teeth attributed to the táxon from MD-67 and differences on P4 (i.e., longer; absence or strong reduction of the mure; flexus shape), we prefer to tentatively refer this material (MUSM 1974 and 1975) to as *Nuyuyomys chinqaska* for the time being.

Comparisons

By its non-taeniodonty, extended flexi(-ds), weak obliquity of loph(-id)s, p4 with a large trigonid, rounded P4, pentalophodont upper molars, and a well-defined, and slightly oblique (faintly backwardly oriented) metaloph on upper molars, the material from TAR-31 exhibits strong erethizontoid affinities. Moreover, like on some lower molars from TAR-31, a subpentalophodont pattern (i.e., presence of a short neolophid in the anteroflexid) is otherwise found in some erethizontoids (e.g., *Palaeosteiromys amazonensis*, *Branisamyopsis australis*, *Branisamyopsis praesigmoides*, *Steiromys duplicatus* and *Neosteiromys pattoni*) [71, 74–77]. The material from TAR-31 shows

brachydont lower teeth and submesodont-mesodont upper teeth, a rather rare crown condition found among the erethizontoids, which are usually brachydont. The only extinct erethizontoids so far showing high tooth crowns are *Hypsosteiromys* (Sarmiento Fm., Argentina; early Miocene) [74, 78, 83] and *Noamys* (site 3 of Rı´o Chico Locality, Guanaco Fm., Argentina; late Miocene and/or early Pliocene) [72]. However, *Nuyuyomys* is clearly distinct from the latter taxa. *Hypsosteiromys* has a larger size, loph(-id)s more oblique, square P4s, tetralophodont M1–2s, tetralophodont-pentalophodont dp4s, and a metalophulid I reduced to an anterior arm of the metaconid disconnected to the protoconid on lower teeth. *Noamys* has tetralophodont and sligthly longer dP4 and M1 with oval-shaped occlusal contour and flexi more extended, especially anteroposteriorly. The specimens from TAR-31 are markedly smaller than all erethizontoid species except *Kichkasteiromys raimondii*, *Shapajamys labocensis*, *Palaeosteiromys amazonensis*, *Microsteiromys jacobsi* gen. et sp. nov., and *Noamys* [18, 37, 70–72] (this work). Contrary to *Shapajamys*, the P4s from TAR-31 and MD-67 (MUSM 4295 and MUSM 1974) do not have any distinct metaloph. Unlike the material from MD-67 and TAR-31, *Kichkasteiromys*, *Shapajamys* and *Palaeosteiromys* do not display a metaloph disconnected labially to the metacone on upper molars. One M1 of *Shapajamys* (MUSM 2993) has a reduced metaloph that is lingually free, as on some M1?s from TAR-31. However, ?M2s from TAR-31 have a metaloph more developed than in *Shapajamys*. Upper molars from TAR-31 differ from the MUSM 2925 M1 or M2 of *Kichkasteiromys* (Fig 2D, p. 92 [70]) in having a lingual protoloph less lingually situated and a posterior outgrowth of the protocone more oblique. For lower teeth, like on the material from TAR-31, some erethizontoids (*Shapajamys*, *Branisamyopsis*, *?Eosteiromys* sp. nov. *sensu* Candela [69], and *Steiromys*) show hexalophodont dp4s with accessory structures. By its elongated shape and tetralophodont pattern, the MUSM 4334 p4 is particularly close to the p4 of*M*. *jacobsi* (IGM-DU 89–249 in Fig 16C, p. 56 [37]; Fig 3B), whereas dp4s from TAR-31 are much more elongated, and with a narrower trigonid than in*M*. *jacobsi* (FMNH PM 54672 in Fig 24.2B, p. 395 [18]; Fig 3A). In addition, dp4s from TAR-31 are hexalophodont, while the FMNH PM 54672 dp4 appears tetralophodont. The lower molars of*M*. *jacobsi* (FMNH PM 54672) and of *Shapajamys* do not have any neolophid on their anteroflexid, contrary to several specimens from TAR-31 and *Palaeosteiromys*. The material from TAR-31 differs from *M*. *jacobsi* in having the mesoflexid still lingually open at advanced stage of wear on m1–2s and less rectangular lower molars; and from *Shapajamys* in having an ectolophid always

complete and oblique on lower molars. Compared to the MUSM 2861 m3 of *Palaeosteiromys* (Fig 4L, p. 77 [71]), m3s from TAR-31 have no neolophid or have a shorter one, and show a mesoflexid more extended. The material from TAR-31 differs from *Eosteiromys annectens* and *Steiromys duplicatus* in having non-taeniodont lower teeth; *Eosteiromys homogidens*, *Eosteiromys annectens*, and *Coendou insidiosus* in having hexalophodont dp4s; from *Protosteiromys* and *Eosteiromys* in having no neolophid on the anteroflexid on lower molars; from *Branisamyopsis praesigmoides* and *Steiromys duplicatus* in having an ectolophid always complete; from *Neosteiromys* and *Parasteiromys* in always having a complete mure on dP4s and upper molars; from *Eopululo*, *Protosteiromys pattersoni* and *Neosteiromys* in having a P4 without endoloph; from *Eosteiromys homogidens* in having a mesial mesoflexus less mesiodistally extended on P4s; from *Eosteiromys annectens*, *Eosteiromys kramarzi sensu* Candela [74], *Branisamyopsis* and *Neosteiromys* in having non-taeniodont dP4s and Upper molars; from *Eopululo*, *Protosteiromys pattersoni* and the three Erethizonthoidea indet. From Acre region (Brazil; Late Miocene) [84, 85] in having upper molars always with a metaloph (which is not reduced, far from being a relictual structure); from *Protosteiromys*, *Parasteiromys*, *Branisamyopsis*, *Eosteiromys*, *Steiromys* and *Neosteiromys* in having some elongated upper molars (potential M1s) and an incomplete metaloph on some upper molars; from *Branisamyopsis pardinas sensu* Candela [74] in having a complete third crest on M1–2s; from *Protosteiromys medianus* in having a complete third crest on M3s [74–77, 80–83]. To summarise, the erethizontoid teeth from TAR-31 are morphologically close to those of *Kichkasteiromys*, *Shapajamys laboensis*, *Palaeosteiromys*, and*M*. *jacobsi*. In having elongated dp4s, with a hexalophodont pattern, the material from TAR-31 clearly differs from that of*M*. *jacobsi*. Hence, we consider the dental material from TAR-31 as documenting a new genus and species: *Nuyuyomys chinqaska*.

Erethizontoidea gen. et sp. indet. 1
Fig 5F’ and S1 Table

Referred material

MUSM 4367, left p4 (Fig 5F’).

Locality

TAR-31, Tarapoto/Juan Guerra, Mayo River, Shapaja road, San Martín Department, Western Amazonia, Peru.

Formation and age

Lower member, Ipururo Fm., late middle Miocene (i.e., Laventan SALMA).

Description

MUSM 4367 is a pristine p4, with rounded corners and trigonid slightly narrower than the talonid (Fig 5F'). It is brachydont, tetralophodont and non-taeniodont. The entoconid is the highest and largest cuspid. The metaconid and hypoconid are mesiodistally compressed, whereas the mesostylid is more bulbous. On the mesiolabial corner of MUSM 4367, the metalophulid I is connected to a cuspate structure with a size similar to the mesostylid, that we interpret as the protoconid due to its position and connection with the metalophulid I. The latter is complete and continuous. It has a transverse and long lingual part connecting to the poorly distinct metaconid, whereas its labial one is shorter and curved. On its distal slope, the metaconid has a short and quite transverse posterior arm, which is disconnected to the mesostylid. The second transverse cristid is straight and well-marked. It appears to be formed by a long neomesolophid, connecting the mesostylid to a shorter and sloping posterior arm of the protoconid. The latter is labially linked to a labial cuspid-shaped structure. This structure is elongated, mesiolabially directed. It is aligned with a cristid stemming from the hypolophidanterior arm of the hypoconid junction (= the ectolophid or a part of the ectolophid), but remains separate from it, as well as from the protoconid mesiolabially, by notches. This elongated cuspid-shaped structure could correspond to a part of the ectolophid fused with the protoconid cristid (see [4]). The entoconid is somewhat bulbous and displays thick, but faintly defined, arms. Its anterior arm is clearly separate from the mesostylid, whereas its posterior arm almost connects to the lingual extremity of the posterolophid, a very thin and shallow notch separating both cristids. The hypolophid is slightly oblique and delimits, with the entoconid, the curved posterolophid and the strong and high anterior arm of the hypoconid, a well-extended and oval metafossettid. The anteroflexid and mesoflexid are rectangular-oval and have a similar extension, smaller than that of the metafossettid. The U-shaped hypoflexid with a distolingual direction is linguolabially well-expanded.

Comparisons

MUSM 4367 is brachydont with a large trigonid, non-taeniodont pattern, extended flexi(-ds), and a weak obliquity of loph(-id)s, which are characters found in erethizontoids. In addition to its size, which is similar to that of p4s of *Microsteiromys jacobsi* (IGM-DU 89–249) and *Nuyuyomys chinqaska* (MUSM 4334), MUSM 4367 has

a similar morphology (i.e., brachydonty, tetralophodonty, non-taeniodonty, and oblique ectolophid). However, contrary to p4s of*M*. *jacobsi* and *N*. *chinqaska*, as well as the MNHN 1903-3-18 premolar of *Protosteiromys asmodeophilus* (Fig 32 [79] and see above), MUSM 4367 is more round shaped and less elongated, with a shorter trigonid and a straight mesial crown margin. In particular, MUSM 4367 differs from MUSM 4334 of *N*. *chinqaska* in having a wider trigonid comparing to the width of the talonid, a higher labial part of the metalophulid I, and a protoconid more mesially canted; from MNHN 1903-3-18 of *P*. *asmodeophilus* in having smaller lingual flexid/fossettids and a larger hypoflexid. Unlike p4s of *Hypsosteiromys*, MUSM 4367 has more straight lophids and a complete metalophulid I connected to the protoconid [74, 83]. The MLP 93-XI-18-1 p4 of *Eosteiromys homogenidens* [74] appears to have a similar mesiolabial morphology to MUSM 4367 in having a second cristid labially connected to an elongated and oblique structure, which may correspond to a part of the ectolophid + protoconid cristid, disconnected to the rest of the ectolophid. This structure is slightly connected to the protoconid on MLP 93-XI-18-1, contrary to MUSM 4367, but it was probably disconnected to this cuspid at an earlier stage of wear. MUSM 4367 differs from p4s of *E*. *homogenidens*, *Eosteiromys annectens* [77], *Branisamyopsis australis* [74, 75], *Branisamyopsis praesigmoides* [77], and *Steiromys detentus* [74] in being more square-shaped; of *E*. *homogenidens* in having a straight metalophulid I and less extended anteroflexid; of *E*. *annectens* in having a non-taeniodont pattern and a less oblique hypolophid and posterolophid; of *Eosteiromys segregatus* [74] in having no posterior arm of the mesostylid and a more extended metaflexid; of *Branisamyopsis*, *Steiromys duplicatus* [74], *Steiromys verzii sensu* Candela [74], and some p4s of *S*. *detentus* in having a tetralophodont pattern; of *S*. *detentus* in having a less extended anteroflexid and more oblique ectolophid; and of *S*. *duplicatus* in having a straight metalophulid I. MUSM 4367 is smaller than *Hypsosteiromys*, *Branisamyopsis*, *Eosteiromys* and *Steiromys*. Given the paucity of the material, we provisionally assign MUSM 4367 to Erethizontoidea gen. et sp. indet. 1.

Erethizontoidea gen. et sp. indet. 2

Fig 5G’ and S1 Table

Referred material

MUSM 4368, left M1 or M2 (Fig 5G’).

Locality

TAR-31, Tarapoto/Juan Guerra, Mayo River, Shapaja road, San Martín Department, Western Amazonia, Peru.

Formation and age

Lower member, Ipururo Fm., late middle Miocene (i.e., Laventan SALMA).

Description

The unique M1 or 2 (MUSM 4368; Fig 5G') documenting this taxon is large, brachydont, and non-taeniodont. It has a subsquare to rounded occlusal outline. The main cusps/styles (paracone, mesostyle, protocone, and hypocone) are large and well defined. The labial cusps/styles are also well defined, whereas the lingual ones are somewhat compressed labiodistally-linguomesially, especially the protocone, which has a strongly crestiform aspect. The worn part of the posterior outgrowth of the protocone is very short at this early stage of wear of the tooth. The anteroloph is long and curved. It is lingually connected to the protocone and labially separated from the paracone by a thin notch. The lingual protoloph, stemming from the protocone, is high and reaches the labial protoloph–mure junction (i.e., non-taeniodont pattern). The labial protoloph and the third crest are faintly oblique. The mure, linking these two transverse crests lingually, is longitudinal (i.e., on the mesiodistal axis of the tooth). Labially, a large furrow separates the mesostyle from the paracone. The metacone is visible because it does not display tight connections with the other labial dental structures. A thin and shallow groove separates it from the mesostyle, and a very slight connection is present between the tiny posterior arm of the metacone and the posteroloph. The third transverse crest is complete, but labially thinner and shorter, thereby indicating that it could be formed primarily by a long mesolophule and a short labial mesoloph. The metacone displays a straight and very short metaloph. At the level of this lingual part, the metaloph exhibits: (i) a very short crestule mesially, which connects to the labial extremity of the mesolophule via a longer crestule; and (ii) an alignement of crestules distally, which remain free. This connection between the metaloph and the third crest generates a small and narrow flexus labially located. The hypocone has mesially a long anterior arm, which is strongly linked to the mure-third crest junction, and distally a posterior arm slightly curved and connected to the straight posteroloph. In addition, a third short crest runs distolingually stemming from the hypocone, and can be recognised as a posterior outgrowth of this cusp. In its middle part, the posteroloph bears a spur, labially directed towards the distal crestules of the metaloph but without connection with them. All the main flexi are well extended and deep.

Comparisons

Among the four superfamilies of caviomorphs, MUSM 4368 exhibits strong erethizontoid affinities in being brachydont, non-taeniodont, pentalophodont, and in showing extended flexi and straight lophs. Erethizontoid molars have usually a better-defined metaloph than MUSM 4368, but some species can also be characterised by a reduced metaloph (e.g., *Protosteiromys pattersoni*, *Eosteiromys kramarzi*, *Parasteiromys uniformis*, and *Steiromys detentus*) or the absence of this crest (e.g., *Eopululo wigmorei*, *P*. *pattersoni*, *Hypsosteiromys*, *Eosteiromys segregatus*, *Steiromys detentus*, and *Noamys hypsodonta* [72, 74, 78, 80–83, 86]. However, these species with a reduced metaloph do not show a configuration similar to that of MUSM 4368, with crestules on the lingual extremity of the metaloph, some of which are connected to the third transverse crest. MUSM 4368 is smaller than the upper molars of *P*. *pattersoni*, *Hypsosteiromys*, *P*. *uniformis*, *E*. *kramarzi*, *E*. *segregatus*, and *Steiromys*. Moreover, MUSM 4368 differs from the upper molar attributed to *E*. *wigmorei* (LACM 143269 in p. 111 [81]) in having a more quadrate shape; from upper molars of *Hypsosteiromys* in having lower crown and lophs less oblique; of *P*. *uniformis* in having a complete mure; and of *E*. *kramarzi* in having a lingual protoloph. By its size larger than MUSM 4367 and the material attributed to *N*. *chinqaska*, MUSM 4368 probably documents another erethizontoid at TAR-31, provisionally identified as Erethizontoidea gen. et sp. indet. 2.

Cavioidea Fischer, 1817

Caviidae Fischer, 1817

Caviidae gen. et sp. indet.

Fig 6 and S1 Table

Referred material

MUSM 4283, right p4 (Fig 6).

Locality

TAR-31, Tarapoto/Juan Guerra, Mayo River, Shapaja road, San Martín Department, Western Amazonia, Peru.

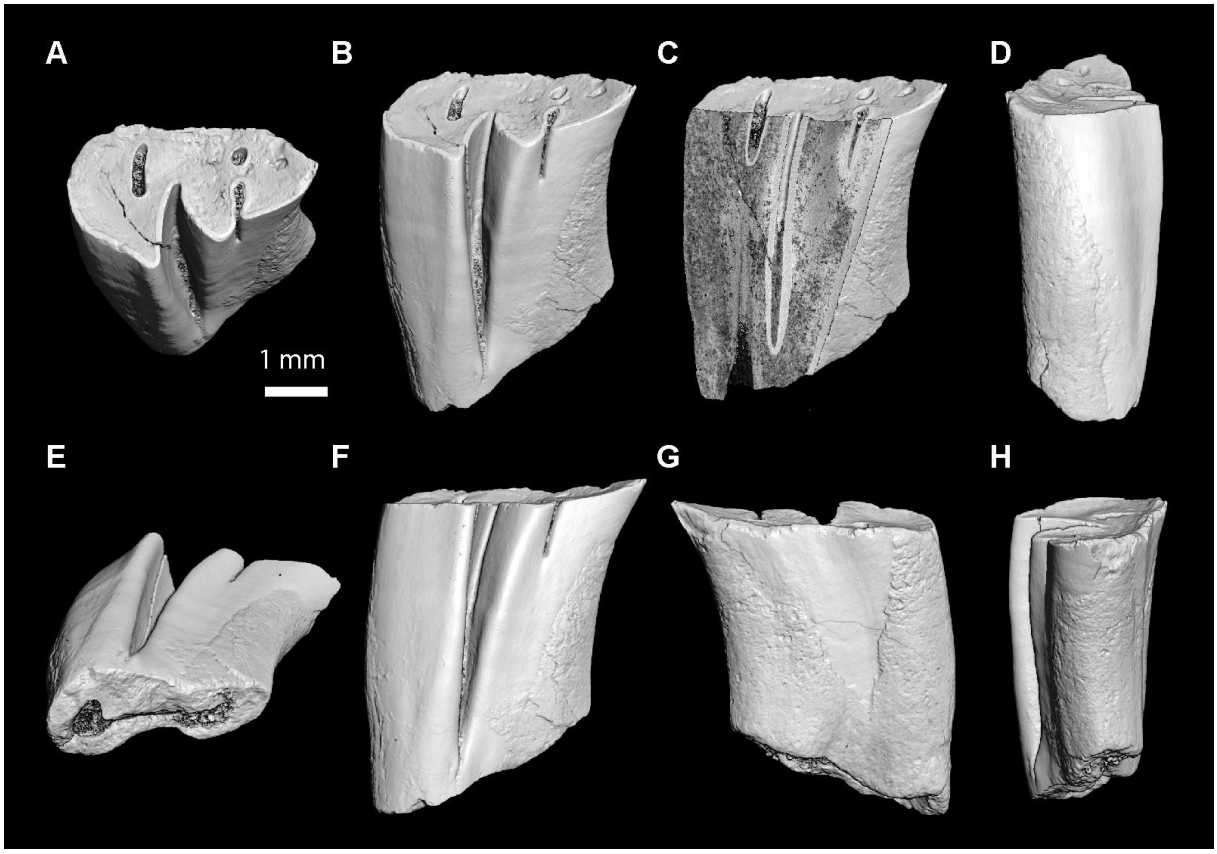


Fig 6. Caviidae gen. et sp. indet. from TAR-31, Peru, MUSM 4283, right p4. (A) Occlusal, (B) occluso-labial, (C) crosssectional, (D) posterior, (E) ventral, (F) labial, (G) lingual, (H) anterior views. The illustrations of the fossil specimen are 3D digital models obtained by X-ray μCT surface reconstruction. The image in C is a 2D orthoslice of the tooth (crosssection).

Formation and age

Lower member, Ipururo Fm., late middle Miocene (i.e., Laventan SALMA).

Description

The MUSM 4283 p4 is slightly damaged at the level of its mesiolingual margin (Fig 6A, 6G and 6H). It also shows a crack on its labiodistal part. The enamel and dentine are damaged and eroded in several regions of the crown and occlusal surface. MUSM 4283 is clearly high crowned (Hling = 1.15; Hlab = 1.27; Fig 6B, 6D, 6F and 6G) and, although the presence of roots is not directly visible, the closing of the hypostriid suggests the closing of the crown too (Fig 6E and 6F). Hence, the tooth was seemingly protohypsodont. The cuspids/stylids and lophids are not visible because they are subsumed within three enlarged lobes, corresponding (from anterior to posterior) to

the anterior projection, anterior lobe and posterior lobe. The dentine is predominating, surrounded by a continuous and thin enamel layer. The tooth has a triangular mesial margin. The anterior projection is narrower than the anterior lobe, which itself is narrower than the posterior lobe. The anterior projection is roughly tear-drop shaped, with a labial extremity short and distolabially directed. In its lingual part, the projection has na oval structure, which is hollow and shallow (Fig 6A and 6B). Nevertheless, it is not a fossettid because it is not surrounded by enamel layer. It is probably a dentine scar owing to an external impact during the mastication or a taphonomic process. The limit between the anterior projection of p4 and the anterior lobe is marked by the presence of: (i) labially, a flexid almost labially closed; and (ii) lingually, an isolated fossettid (Fig 6A). This fossettid is small, round and shallow. It has a thinner enamel layer than that of the margins of the tooth. As the mesialmost lobe of the tooth is determined as the anterior projection, the flexid almost closed would be the homologous of the interprismatic furrow *sensu* Pe´rez [51] separating the anterior projection from the anterior lobe in some stem-Caviidae (*Guiomys* and "*Prodolichotis pridiana"*) [51, 87–90], and which is variably present in Caviidae [1, 55, 91–98]. The enamel layer of the distal margin of this flexid is thinner than that of its mesial margin and of the rest of the exterior enamel layer of the tooth. On the labial margin, the striid corresponding to the opening of the interprismatic furrow is mesiodistally very thin. Its depth represents less than 20% of the crown height (Fig 6B and 6C). Due to their position, the fossettid and/or the interprismatic furrow could be rests of the anteroflexid. The anterior lobe is quite oval and labially separated from the posterior lobe by a triangular hypoflexid. This flexid is linguolabially extended and its lingual extremity reaches more than the half of the width of the tooth. It displays a continuous and homogenous enamel layer. The hypostriid is mesiodistally large and almost reaches the neck of MUSM 4283. On the lingual margin of the tooth, there is an inward fold faintly developed at the transition between the anterior and posterior lobes. It could correspond to a very slight longitudinal furrow opposite to the hypoflexid (= primary internal flexid [hpi]). The posterior lobe is tear-drop shaped, with its labial apex short and mesiolabially directed. In its mesiolingual part, there is a fossettid linguolabially extended, with a thin enamel layer. Its depth is slightly shallower than the striid corresponding to the opening of the interprismatic furrow (Fig 6C). This fossettid probably corresponds to the metafossettid. Because the hypoflexid and metafossettid are not confluent, the tooth is non-taeniodont. The lingual fossettids and the hypoflexid

(at its base) show a white deposit, which by its aspect, does not seem to be coronary cement, but more probably sediments that filled them after the death of the animal.

Comparisons

The protohypsodonty, formation of lobes, linguolabial extension of the hypoflexid, and nontaeniodonty primarily suggest caviid affinities. The very slight development of a possible longitudinal furrow opposite to the hypoflexid (= hpi), a slight development of the interprismatic furrow (= secondary external flexid [hse]), and a relatively narrow anterior projection exclude hydrochoerine affinities for this material from TAR-31. Moreover, MUSM 4283 does not have any additional flexids as observed in capybaras (i.e., internal flexids, including secondary internal flexids and supernumerary internal flexid; see [99]). MUSM 4283 shares characters, which would be ancestral during the evolution of the caviid family [89, 100], with stem-Caviidae: protohypsodonty (*Chubutomys*, *Luantus minor*, *Luantus propheticus*, *Luantus toldensis*, *Phanomys*, and *Eocardia*), presence of lingual fossettids on worn teeth (*Asteromys*, *Chubutomys*, *Luantus*, *Phanomys*, *Eocardia fissa*, and *Schistomys erro*), and a hypoflexid that does not reach the lingual margin of the tooth (*Asteromys*, *Chubutomys*, and *Luantus*) [52, 73, 79, 86, 100–104]. The presence of an anterior projection, which can be associated with an interprismatic furrow, is otherwise found in some derived stem-Caviidae (*Guiomys* and "*Prodolichotis" pridiana*) [51, 87–90] and crown-Caviidae [1, 55, 91–98]. However, *Guiomys*, "*Prodolichotis"* and the crown caviids do not have any lingual fossettids on worn teeth contrary to MUSM 4283. p4s of *L*. *toldensis* (MACN Pv SC4033 in Fig 5F [101]) and *Phanomys* [100] have a lingual thickening of the metalophulid I/their mesial margin, which could correspond to an incipient anterior projection. If the latter is really present in these taxa, it is less developed than on MUSM 4283. In all Caviidea with an interprismatic furrow associated with an anterior projection on p4s, the interprismatic furrow is never almost labially close, unlike on MUSM 4283. This tooth differs from p4s of *Asteromys* in having a hypoflexid more linguolabially extended; of *Asteromys* and *Luantus initialis* in having a higher crown; of *Asteromys*, *Chubutomys*, *Eocardia*, and *L*. *propheticus* in having an anterior projection; of *Phanomys* in having a thinner enamel; and of *Eocardia* in having a hypoflexid less linguolabially extended. The stemcaviid *Guiomys* is euhypsodont unlike MUSM 4283, and shows a p4 with a hypoflexid more linguolabially extended, a more developed anterior projection and longitudinal furrow opposite to the hypoflexid [51, 105]. MUSM 4283 differs from p4s of *Schistomys erro* and *Microcardiodon* in being protohypsodont,

and in having an anterior projection and a well-marked hypoflexid; of *Microcardiodon* in having fossettids; and of *Schistomys erro* in having two persistente lobes [52, 87]. The size of MUSM 4283 is similar with that of *Chubutomys simpsoni*, *Chubutomys leucoreios*, *Luantus minor*, and *Guimoys unica*. As Dolichotinae gen. 2 large from La Venta (IGM 183425 in Fig 24.7A, p. 401 [18]), MUSM 4283 shows a very slight longitudinal furrow opposite to the hypoflexid, and a lingual extremity of the hypoflexid exceeding the half of the width of the tooth, but without reaching its lingual margin. However, MUSM 4283 is characterised by the presence of fossettids and an anterior projection, contrary to Dolichotinae gen. 2 large from La Venta. MUSM 4283 differs from p4s of "*P*." *pridiana*, *Neocavia*, *Prodolichotis prisca*, *Dolicavia*, *Orthomyctera*, and *Dolichotis* in having a less developed longitudinal furrow opposite to the hypoflexid; of *Paleocavia*, *Cavia*, *Galea* and *Microcavia* in having a clearly less developed longitudinal furrow, which is opposite to the hypoflexid; of *Cavia*, *Galea* and *Microcavia* in having a hypoflexid without cement; of "*P*." *pridiana*, *Neocavia*, *Paleocavia*? *mawka*, *Paleocavia impar*, *P. prisca*, *Dolicavia*, *Orthomyctera*, *Cavia*, *Dolichotis*, and *Galea* in having a linguolabially narrower hypoflexid; of *Cavia* in having a more developed anterior projection [28, 54, 55, 90, 94, 95, 106–113]. In conclusion, the morphology of MUSM 4283 appears particular by a mosaic association of characters, combining primitive characters (i.e., protohypsodonty, presence of fossettids on worn teeth, and a hypoflexid, which do not reach the lingual margin of the tooth) and more derived ones (i.e., development of a relatively large anterior projection); and also by an unique configuration of the fossettids and the interprismatic furrow. Thus, it is possible that MUSM 4283 documents a new species among the stem-Caviidae, but given the scarce available material, we provisionally identified it as Caviidea gen. et sp. indet.

Octochinchilloi Boivin, 2019 in Boivin, Marivaux & Antoine, 2019
Octodontoidea Waterhouse, 1839
Adelphomyidae Patterson & Pascual, 1968, nov. stat.
Ricardomys Boivin & Walton gen. nov. urn:lsid:zoobank.org:act:46B7B00E-E14D-4123-BF6D-9AB7AFF4AAD4

Type species
Ricardomys longidens gen. et sp. nov.
Species content
Only the type species.

Derivation of name

Based on the original description of the species [37]: ‘In honor of Richard Kay, professor of Evolutionary Anthropology at Duke University, who discovered the holotype of this species’.

Geographic and stratigraphic distribution

La Venta (IGM-DU loc. 032), Cerro Colorado Member, Villavieja Fm. (Laventan, late Middle Miocene), Huila Department, Colombia; Tarapoto/Juan Guerra (TAR-31), lower member, Ipururo Fm. (Laventan, late middle Miocene), San Martı´n Department, Peru.

Generic diagnosis

As for the type and only known species.

Ricardomys longidens Boivn & Walton sp. nov. urn:lsid:zoobank.org:act:83062BD3-9006-4C73-BB02-37BF66BF6663

Fig 7 and S1 Table

Nom. *nud*. *Ricardomys longidens* Walton, 1990, Fig 9A, 9B, p. 31.

Nom. *nud*. *Ricardomys longidens* Walton, 1997, Figs 24.1C and 24.2D, p. 394, 395.

Holotype

IGM 183847, left mandibular fragment bearing dp4–m2 (Walton, 1990: Fig 9A, 9B; Walton, 1997: Figs 24.1C and 24.2D; Fig 7A).

Referred material

MUSM 4397–4401 (Fig 7B and 7F), left dp4s; MUSM 4402–4406 (Fig 7J), right dp4s; MUSM 4407, right lower molar; MUSM 4408, left m1 or m2?; MUSM 4409 (Fig 7C), left m1?; MUSM 4410 (Fig 7G), right m1?; MUSM 4411–4413 (Fig 7D and 7H), left m2?s; MUSM 4414, 4415 (Fig 7K), right m2?s; MUSM 4416–4419 (Fig 7E and 7I), left m3?s; MUSM 4370–4373, 4391–4394 (Fig 7U and 7V), left upper teeth; MUSM 4374, 4395, 4396 right upper teeth; MUSM 4375 (Fig 7P–7R), left fragment of maxillary bearing dP4 (or M1)? and M1 (or M2)?; MUSM 4376, 4377 (Fig 7L and 7N), left dP4s (or M1s)?; MUSM 4378–4380 (Fig 7M), right dP4s (or M1s)?; MUSM 4381, right dP4?; MUSM 4382–4384 (Fig 7O), left M1 or M2?s; MUSM 4385–4388 (Fig 7S), right M1 or M2?s; MUSM 4389, left M2?; MUSM 4390 (Fig 7T), right M3?.

Derivation of name

Based on the original description of the species [37]: ‘from the latin *longidens*, in reference to the length and slenderness of the tooth row of the holotype of this species’.

Type locality

IGM-DU loc. 032 (only for the holotype), El Cardo´n Red Bed, La Venta Badlands, upper Magdalena Valley, Huila Department, Colombia.

Other locality

TAR-31, Tarapoto/Juan Guerra, Rı´o Mayo, Shapaja road, San Martı´n Department, Western Amazonia, Peru.

Formation and age

Cerro Colorado Member, Villavieja Fm.; lower member, Ipururo Fm.; late middle Miocene (i.e., Laventan SALMA).

Diagnosis

Octodontoid rodent characterised by a small size and non-taeniodont teeth with thick and oblique lamellae. Lower teeth with a trilophodont pattern characterised by the absence of metaconid cristid, posterior arm of the protoconid, neomesolophid and mesolophid. Thick lingual parts of the first and second lamellae on lower teeth, and a first lamella divided into two parts by a thin and shallow furrow on lower molars. Upper teeth with a transversal extension of the hypoflexus, prompt loss of the third transverse crest with wear and the absence of metaloph. Differs from *Eodelphomys* in being smaller and in having lower molars with a thinner furrow dividing the first lamella, more expanded lingual flexids, metaflexid always open at a more advanced stage of wear, less transversely extended hypoflexid, an entoconid area with thickening and without discernable entoconid arms. Differs from *Xylechimys* in having less transversely extended hypoflexid, an ectolophid which is not discernable because fused with the hypolophid, hypoconid and the protoconid, an indistinct posterior arm of the metaconid, and no posterior arm of the protoconid on lower molars. Differs from *Ethelomys*, *Paradelphomys*, *Quebradahondomys*, *Deseadomys*, *Adelphomys*, *Prostichomys*, *Stichomys*, *Prospaniomys*, and *Spaniomys* in having a thickening of the lingual parts of the two first lamellae on lower teeth; from *Ethelomys* in having thicker cristids and a less-transversely extended hypoflexid on lower molars; from *Paradelphomys* in having a non-taeniodont and trilophodont dp4s with a lingual part of the first lamella less distally extended and the first and second lamellae very close in position, and no furrow-shaped flexids on lower teeth; from *Quebradahondomys* in having more oblique cristids on lower molars; from *Deseadomys*, *Adelphomys*, *Prostichomys*, *Stichomys*, *Prospaniomys*, and *Spaniomys* in always having trilophodont dp4s, m1s, and m2s; from *Deseadomys* and *Prospaniomys* in having no recognisable cusp(-id)s and more oblique and thicker lamellae; from *Deseadomys* and *Spaniomys* in having a less

transversely extended hypoflexid on lower teeth; from *Prospaniomys* in having a more transversely extended hypoflexus on upper teeth; from *Adelphomys* in having posterior fossette probably less persistent on upper teeth, a metaflexid always open at a more advanced stage of wear on lower teeth, and a first lamella which can be divided into two parts on lower molars; from *Spaniomys* in having more oblique lamellae, and a straight and distolingually directed second lamella on m3s; and from *Prostichomys* in having thicker lamellae, posterior fossette less persistente on upper teeth, and no mesostylid and an indistinct posterior arm of the metaconid on lower molars.

Description

IGM 183847 is a left mandibular fragment preserving dp4–m2 (Fig 7A). The body of the mandible is anteriorly broken at the level of the anterior root of the dp4. Posteriorly, the angular apophysis and all the ascending ramus, including the mandibular condyle, are missing. The coronoid process is broken at its base. Labially, the notch for the insertion of the tendon of the *zygomatico-mandibularis pars infraorbitalis* is small, below m1, and situated ventrally on the labial edge of the mandible. The anterior tip of the masseteric crest and that of the lateral crest end below the m1, and they appear to be not linked to the notch for the insertion of the tendon of the *zygomatico-mandibularis pars infraorbitalis*, at the level of its posteroventral and posterodorsal regions, respectively. The masseteric crest is posteriorly broken. It is posteroventrally directed and poorly prominent in its anterior part. The lateral crest is posterodorsally directed and almost undistinct. The teeth referred to this taxon are brachydont. The less worn tooth from TAR-31 (MUSM 4377) presents a fairly high crown, but its hypsodonty indexes stay below 1 (Hling = 0.62; Hlab = 0.63). This tooth was probably submesodont at earlier wear stages. All lower and Upper teeth are non-taeniodont. The cusp(-id)s and styles (stylids) are not visible even on the tooth at the earliest stage of wear (MUSM 4377). They are subsumed within loph(-id)s, thereby forming flat-topped and thick crestiform structures (lamellae *sensu* Patterson & Pascual [56]). Each lamella displays a continuous enamel layer, coating a dentine layer, which is increasingly thicker with the dental wear. The dp4s are longer than wide (Fig 7A, 7B, 7F and 7J). Their trigonid is wide but narrower than the talonid. These teeth are characterised by two roots and a trilophodont pattern with oblique lamellae. Mesiolabially, the area of the protoconid is well expanded and usually triangular-shaped. From this area, emerge mesially the first lamella and distally the second lamella. The first lamella is mesially convex. Its lingual part is short and would correspond to the metaconid area (without its posterior arm?). It can be thick with respect of the thin central part of the first lamella

(metalophulid I; IGM 183847, MUSM 4400, 4401, 4405, and 4406; Fig 7A, 7B, 7F and 7J). On the worn MUSM 4397 dp4, the protoconid area is not recognisable from the rest of the first lamella, these structures are fully fused, forming a round and large structure of dentine at the mesial part of the tooth. On all dp4s, the second lamella is a central cristid distolingually directed. It would result of the fusion between the entoconid + the hypolophid + the mesial and distal ectolophids + a part of the protoconid. As the lingual part of the first lamella on some specimens, the lingual part of the second lamella (the entoconid area), by its thickness, is well discernable from the other structures. There would be neither metaconid cristid, neomesolophid, posterior arm of the protoconid, nor mesolophid. The third lamella is cristiform on the dp4 at the earliest stage of wear (MUSM 4401; Fig 7B) and diamond/parallelogram-shaped on other dp4s. It would include the hypoconid + its anterior outgrowth + the posterolophid. On MUSM 4400 and 4401, it bears a small spur in its mesiolabial aspect (i.e., anterior outgrowth; Fig 7B and 7F). It is linked to the second lamella by a complete and thin anterior arm of the hypoconid. On IGM 183847, the anterior arm of the hypoconid reaches a short cristulid stemming from the second lamella (Fig 7A). The anterior arm of the hypoconid is mesiolingually directed, strongly oblique on IGM 183847 and MUSM 4399–4401 (Fig 7B and 7F), and more longitudinal on MUSM 4404–4406 (Fig 7J). Owing to the absence of the metaconid cristid, posterior arm of the protoconid, neomesolophid and mesolophid, the anterolingual flexid corresponds to the confluence of the anteroflexid with the mesial and distal mesoflexids. This flexid and the metaflexid are widely open lingually and more extended than the U-shaped hypoflexid. Lower molars have a pattern similar to that characterising dp4s (i.e., non-taeniodonty, trilophodonty, and obliquity, global shape and composition of lamellae; Fig 7A, 7C–7E, 7G–7I and 7K). Comparatively to dp4s, lower molars have three roots (i.e., two mesial and one distal) and a more rectangular shape with a transverse mesial margin. Four lower molars (MUSM 4416–4419; Fig 7E and 7I) show a distal part of the talonid labiolingually pinched, and as such They are probably m3s (determined as m3?s). MUSM 4416 (Fig 7E) also has a posterior root directed distally, a character typically found on m3s. Among the isolated lower molars without distal pinch, some are small-sized, and as such could be m1s (determined as m1?s; MUSM 4409, and 4410; Fig 7C and 7G). On IGM 183847 and MUSM 4417, 4419 and 4415 (Fig 7K), the lingual part of the first lamella is separated from the protoconid area by a thin and shallow furrow open on the mesial margin of the tooth (MUSM 4415 is broken at the level of the furrow giving the impression that it is larger and deeper; Fig 7K). On MUSM 4417,

the margins of the furrow are composed of two sloped cristulids, one lingual and one labial. The lingual cristulid stems from the metaconid area (the ?anterior arm of the metaconid), while the labial one stems from the protoconid area (the ?anterior arm of the protoconid). They are connected at the base of the furrow. On molars with a more advanced stage of wear (MUSM 4408–4414 and 4418; Fig 7C–7E and 7G–7I), this furrow is fully closed. The morphology of the second and third lamellae is very similar of that of dp4s, except they are longer. Regarding upper teeth (Fig 7L–7V), the absence of complete tooth row and a documentation of the whole stages of wear make it difficult to recognise the dental intra-specific variation related to the difference of loci, wear, or polymorphism. Four morphs can be distinct. The unique fragment of maxillary found at TAR-31 and attributed to this species, MUSM 4375 (Fig 7P–7R), bears two upper teeth. This specimen and the comparison with upper teeth of other adelphomyines or closely related forms (e.g., *Deseadomys*, *Adelphomys*, *Prostichomys*, and *Spaniomys*) allow us to propose hypotheses regarding the locus determination for these morphs:

• Morph 1: small upper teeth longer than wide or subsquare, and with a quadrangular occlusal outline and three transverse lophs (MUSM 4375–4381; Fig 7L–7N and 7P–7R). MUSM 4381 seems to have three roots (i.e., two labial and one large lingual), whereas other teeth have not conserved their roots. This morph could correspond to the morphology of dP4s (or M1s);

• Morph 2: upper teeth larger than those of the morph 1, either subsquare or rectangular, and with quadrangular occlusal outlines, three transverse lophs and four roots (MUSM 4375 and 4382–4389; Fig 7O–7S). This morph could correspond to the morphology of M1s or M2s. MUSM 4389 has a very short posterior crest as MUSM 4390 (see below morph 3). This shortness may be related to a strong labial displacement of the hypocone. Nevertheless, MUSM 4389 shows typical characters of morph 2: large size, quadrangular occlusal outline with a straight distal margin and four roots. It could correspond to a M2;

• Morph 3: this morph is represented by one small upper tooth (MUSM 4390; Fig 7T) characterised by three roots, a more round outline than teeth of the morphs 1 and 2, distal pinch, and three transverse lophs. This morph could correspond to the morphology of M3s;

• Morph 4: this morph is represented by six mesially-broken upper teeth (MUSM 4391–4396; Fig 7U and 7V). These fragments of teeth have different size, some are small-sized (MUSM 4391 and 4392; Fig 7U), medium-sized (MUSM 4393 and 4395; Fig 7V),

while other are larger (MUSM 4396). They have a more rounded occlusal outline than teeth of morphs 1 and 2, and a distal part slightly labiolingually narrower than the mesial part. They seem to be mesiodistally elongated. Because they are broken, the hypsodonty index cannot be calculated. However, they have thinner crests and deeper flexi than teeth of other morphs, and three (MUSM 4392 and 4395; Fig 7U) or four (MUSM 4391, 4393, 4394, and 4396; Fig 7V) transverse lophs. Owing to the latter characters, this morph likely clusters upper molars at less advanced wear stages than those of morphs 2 and 3. The first lamella is diamond/parallelogram-shaped with a large and rounded apex at the mesiolingual corner of the tooth. Two other apices, the first at the mesiolabial corner of the tooth and the second in the center of its lingual edge, are usually narrower and tapered. This lamella would include the protocone + the posterior outgrowth of the protocone + the anteroloph. The second lamella, which would correspond to the paracone + the labial protoloph, is either transverse or oblique (i.e., mesiolabially directed) or lingually oblique and labially transverse. It is short due to a strong transversal extension of the hypoflexus. The lingual protoloph is thin, distolabially directed and complete, thus linking the first lamella to the second (i.e., non-taeniodont pattern). On the trilophodont upper teeth (MUSM 4373, 4375–4389, 4390, and 4395; Fig 7L–7U), the third lamella is usually bean-shaped, but can be suboval (MUSM 4389 and 4390; Fig 7T). On the tetralophodont MUSM 4394, this third lamella presents a round flexus still distolabially open. On other tetralophodont upper teeth (MUSM 4391–4393 and 4396; Fig 7V), this flexus is fully closed, thereby forming a round fossette. This flexus/fossette separates the third transverse crest from the posteroloph. On all tetralophodont Upper teeth, these two transverse lophs are very thin and short, except on MUSM 4394, in which the third transverse crest is thicker. On MUSM 4391 and 4393 (Fig 7V), the third crest is composed of a very short mesoloph, whose lingual extremity is connected to a mesolophular spur. The third lamella on trilophodont upper teeth would include the mesostyle and/or the metacone (see [50]) + the third transverse crest + the posteroloph + the hypocone + its anterior arm. Near the center of the tooth, the second lamella and the third lamella are connected via a mure mesiolabially directed (strongly oblique).

Comparisons

A small size, non-taeniodont teeth with thick and oblique lamellae, and a transverse extension of the hypoflexus, the prompt loss of the third transverse crest with wear and the absence of metaloph on upper teeth are dental traits found in adelphomyine octodontoids [4, 56], thereby suggesting adelphomyine affinities for this material from

La Venta and TAR-31. By their size and morphology, the lower teeth from TAR-31 are close to those of IGM 183847 from La Venta, previously attributed to *Ricardomys longidens nom*. *nud*. (Figs 24.1C and 24.2D [18]; Fig 9A, 9B [37]; Fig 7A). As lower teeth from TAR-31, the IGM 183847 lower teeth have a trilophodont pattern characterised by the absence of metaconid cristid, posterior arm of the protoconid, neomesolophid and mesolophid. These lower teeth also show oblique lamellae, thick lingual parts of the first and second lamellae, and a first lamella divided into two parts by a thin and shallow furrow on lower molars. However, the lower molars from TAR-31 slightly differ from IGM 183847 in having the first lamella more oblique. A similar pattern to dp4s from La Venta and TAR-31 is also found on the MUSM 2856 dp4 attributed to Adelphomyinae indet. 2 from CTA-61 (Peru, late Oligocene) [71]. Unlike dp4s from La Venta and TAR-31, MUSM 2856 does not have a hypoflexid transversely oriented, but the latter is distolingually oriented. Other adelphomyines or closely related forms have strictly trilophodont lower molars: *Eodelphomys* (Santa Rosa, Peru; ?late Eocene/early Oligocene) [81], *Ethelomys* (Cabeza Blanca, Argentina; late Oligocene) [114], *Paradelphomys* (Sarmiento Fm., Argentina; early Miocene) [56], and *Quebradahondomys* (Quebrada Honda, Bolivia; late middle Miocene) [105]. *Eodelphomys* is only known from a single m3 (LACM 144298 in p. 130 [81]), which shows a first lamella divided into two parts by a furrow. However, the latter is larger than that on lower molars from La Venta and TAR-31 (when the furrow is present). The lower molars from La Venta and TAR-31 also differ from LACM 144298 in having lingual flexids more expanded mesiodistally, always open at a more advanced stage of wear, less transversely extended hypoflexid, and an entoconid area with thickening and without discernable entoconid arms. In comparison with the material form La Venta and TAR-31, *Ethelomys*, *Paradelphomys*, and *Quebradahondomys* do not have any thickening of the lingual parts of the two first lamellae (or at least of the second lamella) on lower teeth; *Ethelomys* has thinner cristids and a more transversely extended hypoflexid on lower molars; *Paradelphomys* has furrowshaped flexids on lower teeth, a taeniodont and tetralophodont dp4 with a lingual part of the first lamella more distally extended (with posterior arm of the metaconid?) and the first and second lamellae very close in position; and *Quebradahondomys* has less oblique lamellae on lower molars. As the lower teeth from La Venta and TAR-31, *Xylechimys* (Laguna de los Machos, Argentina; late Oligocene) [56] appears to develop a lingual thickening of the second lamella on lower molars with the dental wear (visible on the m1 of the holotype). Nevertheless, *Xylechimys* has a trigonid of lower molars clearly different characterised

by: (i) a posterior arm of the protoconid linked to the metaconid area, thus delimiting a small and rounded anterofossettid, (ii) discernable ectolophid and posterior arm of the metaconid, and (iii) a more transversely extended hypoflexid. The general pattern of the upper teeth from TAR-31 is similar to that of adelphomyines (or closely-related forms) documented by upper teeth: *Deseadomys* (Cabeza Blanca and La Flecha, Argentina; late Oligocene) [79], *Adelphomys* (Pinturas Fm. And Santa Cruz Fm., Argentina; early Miocene) [73, 77], *Prostichomys* (Sarmiento Fm. and Pinturas Fm., Argentina; early Miocene) [77, 115, 116], *Stichomys* (Santa Cruz Fm.; late early Miocene) [73], *Prospaniomys* (Sarmiento Fm.; early Miocene) [11, 78, 117], and *Spaniomys* (Pinturas Fm. and Santa Cruz Fm.; Pampa Castillo, Chile; late early Miocene) [16, 73, 77, 118, 119]. Contrary to the material from La Venta and TAR-31, all these taxa display no thickening of the lingual parts of the two first lamellae (or at least of the second lamella) on lower teeth, and can have tetralophodont lower teeth (usually dp4s, m1s or m2s). The tetralophodont pattern of these lower teeth is characterised by the presence of a posterior arm of the protoconid + metaconid cristid and/or neomesolophid (and mesolophid on some dp4 of *Prostichomys*). The material from La Venta and TAR-31 also differs from *Deseadomys* and *Prospaniomys* in having no recognisable cusp(-id)s and more oblique and thicker lamellae; from *Deseadomys* and *Spaniomys* in having a less transversely extended hypoflexid on lower teeth; from *Prospaniomys* in having a more transversely extended hypoflexus on upper teeth; from *Adelphomys* in having a posterior fossette probably less persistent on upper teeth, always open at a more advanced stage of wear on lower teeth, and a first lamella which can be divided into two parts on lower molars; from *Spaniomys* in having more oblique lamellae, and a straight and distolingually directed second lamella on m3s; and from *Prostichomys* in having thicker lamellae, a posterior fossette less persistent on upper teeth, and no mesostylid and no discernable posterior arm of the metaconid on lower molars. To summarize, due to the morphological similarity between the lower teeth from La Venta and TAR-31, we assign them to the same taxon. By its particular set of characters, the entire material from these both areas is determinable as a new species, hence we validate *Ricardomys longidens*.

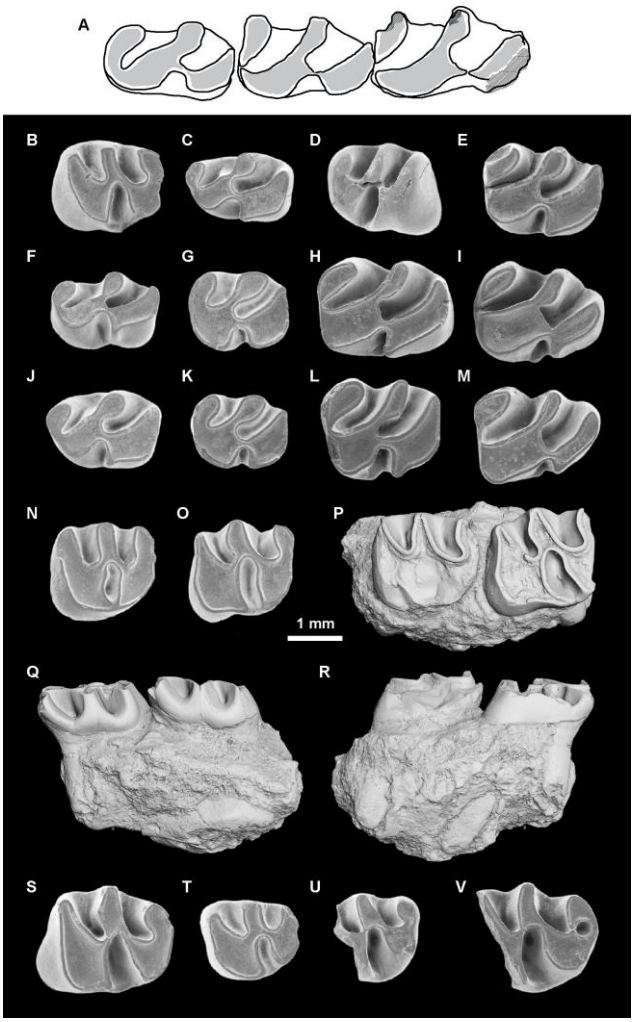


Fig 7. *Ricardomys longidens* gen. et sp. nov. (A) Material from La Venta, Colombia. (B–V) Material from TAR-31, Peru. (A) IGM 183847***, left mandibular fragment bearing dp4–m2. (B) MUSM 4401, left dp4. (C) MUSM 4409, left m1?. (D) MUSM 4411, left m2?. (E) MUSM 4416, left m3?. (F) MUSM 4400, left dp4. (G) MUSM 4410, right m1? (reversed). (H) MUSM 4413, left m2?. (I) MUMS 4418, left m3?. (J) MUSM 4406, right dp4 (reversed). (K) MUSM 4415, right m2? (reversed). (L) MUSM 4377, left dP4 (or M1)?, morph 1. (M) MUSM 4380, right dP4 (or M1)?, morph 1 (reversed). (N) MUSM 4376, left dP4 (or M1)?, morph 1. (O) MUMS 4384, left M1 or M2?, morph 2. (P–R) MUSM 4375, left maxila fragment bearing dP4–M1 (or M1–2)?, morph 1 and 2. (S) MUSM 4388, right M1 or M2?, morph 2 (reversed). (T) MUSM 4390, right M3?, morph 3. (U) MUSM 4392, left fragmentary upper molar, morph 4. (V) MUSM 4393, left fragmentary upper molar, morph 4. (A-P, S-V) Occlusal, (Q) labial, and (R) lingual views. The asterisks appoint the holotype material. The illustrations of the fossil specimens are computerized schematic line drawings based on Walton (Fig 9A [37]). (A), scanning electron photomicrographs (B-O and S-V), and 3D digital models obtained by X-ray μCT surface reconstruction (P-R).

Octodontoidea gen. et sp. indet.

Fig 8 and S1 Table

Referred material

MUSM 4662, left m1 or m2 (Fig 8A); MUSM 4660, left dP4 (Fig 8B); MUSM 4661, right M3 (Fig 8C).

Locality

TAR-31, Tarapoto/Juan Guerra, Mayo River, Shapaja road, San Martín Department, Western Amazonia, Peru.

Formation and age

Lower member, Ipururo Fm., late middle Miocene (i.e., Laventan SALMA).

Description

Due to the very advanced stage of wear of the MUSM 4662 m1 or m2 (Fig 8A), its occlusal pattern is faintly discernable, especially on the mesial area of the tooth, where a broad dentine platform is present. There is a thick, continuous enamel layer on the entire periphery of the crown. It is thinner at the level of the lingual parts of the hypoflexid and of the mesoflexid. Only three transverse lophids are visible, delimited by a very thin enamel layer, which is absent in some regions. The mesialmost lophid is transverse and connects the area of the posterior arm of the metaconid/mesostylid to the junction of the protoconid (or the protoconid cristid) and the ectolophid. This lophid is recognised as a second transverse cristid (i.e., neomesolophid and/or posterior arm of the protoconid). Mesially, it is partially fused with the mesial dentine platform, which probably corresponds to the fusion at least of the metalophulid I with the anteroflexid. The transverse lophid that is second in position, is the hypolophid, running slightly labiomesially from the area of the entoconid to link the posterior part of the ectolophid. The hypolophid is almost parallel to the second cristid. The ectolophid is short and gently oblique. The transverse lophid appearing in third position is a curved posterolophid, lingually connected to a strong posterior arm of the entoconid. The area of the hypoconid is enlarged and oval, formed by the fusion of the hypoconid, its anterior outgrowth and its posterior arm (if present) and/or the labial part of the posterolophid. There is a thick and complete anterior arm of the hypoconid (i.e., non-taeniodont pattern). The mesoflexid and metaflexid are lingually closed, whereas the hypoflexid remains labially open. The metafossettid is oval and smaller than the mesofossettid.

The MUSM 4660 dP4 (Fig 8B) has a trapezoidal crown outline in occlusal view (i.e., labial marging longer than the lingual margin). This tooth shows an advanced stage of wear. Labially, the dental structures have a thick enamel layer, while the lingual structures are surrounded by a clearly thinner enamel layer. The posteroloph area is very enlarged due to the wear, and forms a dentine platform, in which a metacone, a metaloph or a rest of this loph may be included. The hypoflexus is triangular and poorly extended linguolabially. It separates lingually the area of the protocone from that of the hypocone. The areas of the protocone, mure and of the hypocone are also strongly enlarged and broadly merged together, as well as with the platform of the posteroloph, forming a S-shape dentine structure on the distolingual part of the tooth. From this dentine structure, three main lophs run labially: the anteroloph, the labial protoloph and the third transverse crest. The anteroloph is curved with a lingual part thicker than its labial part. The labial protoloph and third crest are transverse and parallel. The paraflexus is still open labially, separating the anteroloph from the labial protoloph. In contrast, the other transverse lophs are connected labially, forming a small oval mesial mesofosette and a more linguolabially extended distal mesofosette.

As MUSM 4662, the MUSM 4661 M3 (Fig 8C) is much worn, but it documents a slightly earlier stage of wear. A thick enamel layer surrounds the tooth as well, but the latter is internal at the level of the mesial mesoflexus, which is still opened labially contrary to MUSM 4662. Moreover, all the transverse lophs and flexi are still discernable. The hypocone is clearly more labially situated than the protocone, which indicates that the specimen would be a M3. MUSM 4661 is tetralophodont and non-taeniodont. The area of the protocone corresponds to a broad dentine platform, including the protocone, its posterior outgrowth and its anterior arm (if present) and/or the lingual part of the anteroloph. From this platform, the anteroloph runs labially and links the paracone. The lingual part of the anteroloph is transverse, whereas its labial part is curved. Due to the connection between the anteroloph and the paracone, a parafossette is formed and reduced to a thin and straight structure. The enamel layer that surrounds it is thick, notably on its mesial margin. On the labial margin of the tooth, the paracone and mesostyle are strong and of similar size. The posterior arm of the protocone is thick and oblique. It connects to the mure, which is linguodistally oriented and in the continuity with the anterior arm of the hypocone. The labial protoloph and the third transverse crest (i.e., mesoloph and/or mesolophule) are roughly straight and parallel. There is neither metaloph nor discernable metacone. A well-curved

posteroloph is labially connected to the mesostyle and lingually to the area of the hypocone, which is triangular-shaped. The mesial mesoflexus is very thin. The posterior fossette (i.e., confluence of the distal mesoflexus and the metaflexus) is reduced to a very small and rounded structure. As the parafossette, the mesial mesoflexus and the posterior fossette are surrounded by a thick enamel layer.

Comparisons

By its small size, weak loph(-id) obliquity, non-taeniodonty, tetralophodont upper molars (i.e., absence of metaloph), and a strong mesostyle on upper molars, these three teeth from TAR-31 likely document a single and distinctive octodontoid. Indeed, many Palaeogene and Neogene octodontoids also display these characters. They are usually characterised by a reduction or the absence of the second transverse cristid, and a reduction of the posterior arm of the metaconid on lower molars, and a metacone more distally positioned on upper molars (e.g., *Acarechimys*, *Deseadomys*, *Dudumus*, and *Caviocricetus*) [30, 79, 120, 121], characters absent on the specimens from TAR-31. However, *Paulacoutomys* and some lower molars of *Platypittamys*, *Sciamys principalis*, *Prostichomys* and *Plesiacarechimys* show a complete second transverse cristid and a well-developed posterior arm of the metaconid [77, 115, 116, 122–126], as it is observed on the material from TAR-31. Among the latter taxa, the material from TAR-31 is closer to *Paulacoutomys* and *Plesiacarechimys* in having transverse loph(-id)s and a similar extension of the flexi(-ds). In addition, these genera can have an ectolophid slightly oblique on lower molars, as it does on MUSM 4662. The material from TAR-31 differs from *Paulacoutomys* and *Plesiacarechimys* in having a smaller size; from *Platypittamys* and *Prostichomys* in having a more longitudinal ectolophid on lower molars; from *Platypittamys* in having M3 with third crest that is not curved, a mesial mesoflexus less extended, a posterior flexus/fossette more extended; from *Prostichomys* and *S*. *principalis* in having a mesostyle less connected to the posteroloph on dP4s and upper molars; from *Prostichomys* in having a more transverse hypolophid on lower molars, a more transverse labial protoloph on dP4s and upper molars, and more transverse M3 with a wider distal part; and from *S*. *principalis* in having a mesial part of the lower molars (= fusion of the metalophulid I with the second cristid) more mesiodistally long at its lingual and labial extremities, a hypoflexid less extended labiolingually, and a mesoflexid which is lingually closed although a metafossettid is still present on lower molars, and a hypoflexus less extended labiolingually and a mesial mesoflexus which is strongly reduced although

the posterior fossette is still present on upper molars. In sum, given the condition and scarcity of the material, we provisionally refer these teeth to an octodontoid indet.

Chinchilloidea Bennett, 1833

Microscleromys Boivin & Walton gen. nov. urn:lsid:zoobank.org:act:785C5F6A-DCCD-4C02-B136-A2B49702E6DA

Type species

Microscleromys paradoxalis gen. et sp. nov.

Species content

The type species and *Microscleromys cribriphilus* gen. et sp. nov.

Derivation of name

Based on the original description of the species [37]: 'In reference to its small size and general resemblance to *Scleromys* Ameghino, 1887'.

Geographic and stratigraphic distribution

La Victoria Fm. and Baraya Member of the Villavieja Fm. (Laventan SALMA, late middle Miocene), Huila Department, Colombia; Tarapoto/Juan Guerra (TAR-31), lower member, Ipururo Fm., (Laventan SALMA, late middle Miocene), San Martín Department, Peru.

Generic diagnosis

Chinchilloid rodent characterised by a small or moderate size. Relative size of m3s/M3s smaller in average than that of m1–2s/M1–2s. Brachyodont to mesodont teeth. P4s and Upper molars with noticeable high crowns. Upper teeth with a higher lingual crown and lower molars with a higher distolabially crown. Absence of cement or in small quantity. Homogeneous thickness of the enamel layer of dental strutures. Poorly distinct cusp(-id)s from the loph(-id)s, which do not form lamina. At early stages of wear, lower teeth with pseudo-taeniodont or taeniodont pattern, lower molars with a pseudo-taeniodont pattern more frequently present, taeniodont P4s, dP4s and upper molars with a taeniodont pattern more frequently present. dp4s with a metalophulid I not connected to the metaconid and protoconid at early stages of wear, a posterolophid well-separated from the entoconid, a mesostylid mesially and distally isolated in most cases, and a tendency to the reduction or absence of the third crisitid. Lower molars with usually a groove on the metalophulid I at early stages of wear. Suboval dP4s, with well-arcuate anteroloph and posteroloph as well as a bulbous protocone slightly or strongly separate from the anteroloph. Round/oval P4s with a connection between the

posterior outgrowth of the protocone and the hypocone. Upper molars with usually a mure oblique and aligned with the anterior arm of the hypocone. Important variation in terms of development, configuration and orientation of the second transverse cristid on p4s and lower molars, and of the third transverse crest and metaloph on upper teeth, but with a tendency to their reduction and absence. Trilophodont lower molars in most cases. Among upper teeth, P4s with stronger reduction of the third crest and metaloph. Upper molars with a third crest more frequently reduced to a mesoloph and without metaloph. Persistent flexids/fossettids on lower molars and flexi/fossettes except the posterior ones (the distal mesoflexus and metaflexus if present) on upper molars. Differs from *Chambiramys* in having slightly higher crowns, and more quadrangular upper molars; from *Eoincamys*, *Incamys* and *Scleromys*/"*Scleromys*" in having more square-shaped upper molars and a more important reduction of the third transverse crest on upper molars (i.e., more frequent trilophodont pattern than in these genera); from *Eoincamys ameghinoi*, *Eoincamys pascuali* and *Incamys* in having a second transverse cristid usually more reduced on lower molars; from *Eoincamys pascuali* in having a thinner furrow (when it is present) on the metalophulid I, which can be situated at the middle of this lophid; from *Saremmys* in having lower-crowned teeth, thinner loph(-id)s, a metaconid postionned more distally and strongly connected to the protoconid by a thick second cristid (metaconid cristid and/or posterior arm of the protoconid) on dp4s, a less oblique hypolophid on p4s and lower molars, a more bulbous protocone and a hypocone mesiolabially-distolingually compressed on dP4s, and some upper molars with a distinct metacone and a long metaloph and mesoloph; from *Saremmys*, *Scleromys*/"*Scleromys*", *Garridomys* and *Drytomomys* in having an anterior arm of the hypoconid, which can be present on p4s and lower molars, and in a more curved posterolophid on lower molars; from *Incamys*, *Saremmys*, *Scleromys*/"*Scleromys*", *Garridomys* and *Drytomomys* in having a smaller size; from *Garridomys* and *Drytomomys* in having a second transverse cristid usually more reduced on lower molars; from *Garridomys* in having a homogeneous thickness of the enamel layer, thinner loph(-id)s, and strong and high protoconid and ectolophid on p4s; from "*Scleromys*" *colombianus* and *Drytomomys aequatorialis* in having a separation between the hypocone and the posteroloph thinner and less persistente at early wear stages on upper molars; and from *Drytomomys* in having a less oblique hypolophid on lower molars.

Microscleromys paradoxalis Boivin & Walton sp. nov.
urn:lsid:zoobank.org:act:38631BE9-32E6-4E5D-B5CE-469C37B98D8C
Fig 9 and S1 Table

Nom. *nud*. *Microscleromys cribriphilus* Walton, 1990, Fig 12F, 12G-12O, p. 45.
Nom. *nud*. *Microscleromys paradoxalis* Walton, 1990, Fig 11A-11J, p. 39.
Nom. *nud*. *Microscleromys ?paradoxalis* Walton, 1990, Fig 13B, 13C p. 49.
Microscleromys sp. Walton, 1990, Fig 13A, p. 49.
Nom. *nud*. *Microscleromys cribriphilus* Walton, 1997, Fig 24.2.N, p. 295.
Nom. *nud*. *Microscleromys paradoxalis* Walton, 1997, Fig 24.2.G-I, p. 295.

Holotype

IGM 250321, right M1 or M2? (Fig 9P).

Referred material

MUSM 4643 (Fig 9A–9E), left fragment of mandible bearing incisor and dp4–m1; ING-KU 8604, right fragment of mandible bearing p4–m2; MUSM 4640–4642 (Fig 9F), left dp4s; IGM 250306 (Fig 9G), left p4; IGM 250305 and 250308 (Fig 9K), right p4s; MUSM 4644, left lower molar; IGM 250265, MUSM 4645, right lower molar; IGM 250288, 250307, IGM-DU 88–814, 89–675, MUSM 4646–4650 (Fig 9H, 9I, 9M and 9N), left m1 or m2; IGM 250319, MUSM 4651–4656 (Fig 9L), right m1 or m2s; IGM 250274, 250285, 250304, MUSM 4657 (Fig 9J), left m3s; IGM 251020 (Fig 9O), right m3; IGM 250302, IGM-DU 88–815 (Fig 9Z), ING-KU unnumbered specimen (Fig 9U), MUSM 4623 (Fig 9Q), left dP4s; MUSM 4624 (Fig 9A'), left P4; MUSM 4625 (Fig 9V), right P4; MUSM 4626, left upper molar; MUSM 4627, right Upper molar; IGM 250283, IGM-DU 89–673, MUSM 4628–4631 (Fig 9X, 9B' and 9C'), left M1 or M2?s; MUSM 4632–4636 (Fig 9R, 9S and 9W), right M1 or M2?s; IGM 250284, MUSM 4637 (Fig 9T), left M3?s; IGM-DU 85–410, MUSM 4638, 4639 (Fig 9Y and 9D'), right M3?s.

Derivation of name

Based on the original description of the species [37]: 'from the latin *paradoxalis*, in reference to the strange and confusing morphology of this species'. In light of the last discoveries of caviomorph faunas in Peru, the morphology of this species does not appear so strange or confusing, but we prefer maintaining this name for the sake of both usage and courtesy.

Type locality

CVP 13B locality, Fish Bed near Casa Cuzco, La Venta Badlands, upper Magdalena Valley, Huila Department, Colombia.

Other localities

localities unknown (for ING-KU unnumbered specimen and ING-KU 8604), IGM-DU loc. 075, between the Chunchullo and the Tatcoa Sandstone Beds (only for IGM 250265), and localities of the Fish Bed (including CVP 5, 8, 9, 10, and 10A) and IGM-DU loc. 006–1, Monkey Beds (only for IGM-DU 88–814), La Venta Badlands, upper Magdalena Valley, Huila Department, Colombia; TAR-31, Tarapoto/Juan Guerra, Río Mayo, Shapaja road, San Martín Department, Western Amazonia, Peru.

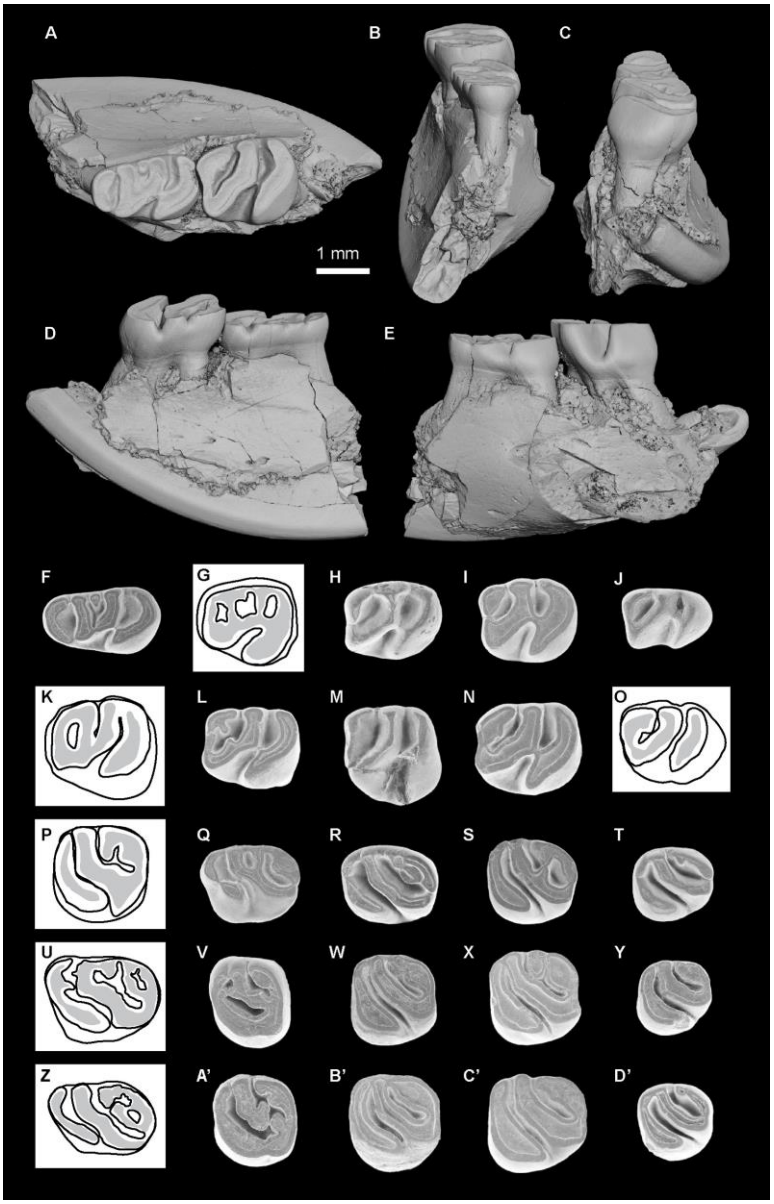


Fig 9. *Microscleromys paradoxalis* gen. et sp. nov. Mateial from TAR-31, Peru (black background) and from La Venta, Colombia (white background). (A–E) MUSM 4643, left mandibular fragment bearing dp4–m1. (F) MUSM 4641, left dp4. (G) IGM

250306, left p4. (H) MUSM 4647, left m1 or m2. (I) MUSM 4648, left m1 or m2. (J) MUSM 4657, m3. (K) IGM 250308, right p4 (reversed). (L) MUSM 4654, right m1 or m2 (reversed). (M) MUSM 4650, left m1 or m2. (N) MUSM 4649, left m1 or m2. (O) IGM 251020, right m3 (reversed). (P) IGM 250321***, right M1 or M2? (reversed). (Q) MUSM 4623, left dP4. (R) MUSM 4634, right M1 or M2? (reversed). (S) MUSM 4633, right M1 or M2? (reversed). (T) MUSM 4637, left M3?. (U) ING-KU unnumbered specimen, left dP4. (V) MUSM 4625, right P4 (reversed). (W) MUSM 4632, right M1 or M2? (reversed). (X) MUSM 4631, left M1 or M2?. (Y) MUSM 4638, right M3? (reversed). (Z) IGM-DU 88–815, left dP4. (A') MUSM 4624, left P4. (B') MUSM 4630, left M1 or M2?. (C') MUSM 4629, left M1 or M2?. (D') MUSM 4639, right M3? (reversed). (A, F-D') Occlusal, (B) anterior, (C) posterior, (D) lingual, and (E) labial views. The asterisks appoint the holotype material. The illustrations of the fossil specimens are 3D digital models obtained by X-ray μCT surface reconstruction (A-E), scanning electron photomicrographs (F, H-J, L-N, Q-T, V-Y, and A'-D'), and computerized schematic line drawings based on Walton (Fig 24.2 [18]; Fig 13 [37]) (G, K, O, P, U, and Z).

Formation and age

La Victoria Fm. and Baraya Member of the Villavieja Fm.; lower member, Ipururo Fm.; late middle Miocene (i.e., Laventan SALMA).

Diagnosis

Species with teeth approximately 25–30 per cent larger than those of*M*. *cribriphilus*. dP4s can have a pseudo-taeniodont or taeniodont pattern.

Description

MUSM 4643 is a right fragment of mandible bearing a part of the lower incisor and dp4–m1 (Fig 9A–9E). The incisor is mesially and distally broken, but the preserved portion testifies to a long radius of curvature of this tooth. The preserved part of the dentary corresponds to the ventrally broken body below the dp4–m1. It is very damaged, showing the base of the roots of the cheek teeth and the entire surface of the preserved fragment of incisor. The anterior root of dp4 is mesiodistally large, perpendicular to the plan of the neck, but clearly oriented mesioventrally in the dentary. Conversely, the posterior root of m1 is slightly oriented distoventrally. The morphology of the notch for the insertion of the tendon of the *zygomatico-mandibularis pars infraorbitalis*, masseteric crest or lateral crest is not accessible. In addition to the dp4 preserved on MUSM 4643 (Fig 9A), three other dp4s are attributed to *Microscleromys*

paradoxalis (Fig 9F). MUSM 4641 is complete (Fig 9F), whereas MUSM 4642 is a posterior fragment of dp4, in which the metaconid and metalophulid I are missing. MUSM 4640 is worn and abraded especially at the level of the metalophulid I, which is reduced to its distal part. The two complete dp4s are longer than wide, with a trigonid narrower than the talonid. The metalophulid I is distally well arcued, forming the mesial edge of the tooth. It is separate from the metaconid and protoconid by narrow notches on the MUSM 4643 dp4 (Fig 9A). On MUSM 4641 (Fig 9F), a similar configuration is present for its lingual extremity, whereas its labial extremity reaches the base of the protoconid. A continuous second cristid links the metaconid to the protoconid. Hence, it would be formed by a metaconid cristid and/or posterior arm of the protoconid. It is mesiolingually directed and faintly curved on MUSM 4641 (Fig 9F) and MUSM 4643 dp4 (Fig 9A). It appears more transverse on MUSM 4640. On the MUSM 4643 dp4, MUSM 4641 and 4642 (Fig 9A and 9F), a mesostylid is present on the lingual margin. It can be mesially and distally isolated (MUSM 4641; Fig 9F), mesially isolated (MUSM 4643 dp4; Fig 9A) or connected to both the metaconid and entoconid (MUSM 4642). From that stylid, a neomesolophid runs labially and connects to a mesolophid reduced to a low spur. The two complete dp4s show neither neomesolophid nor mesolophid. The mesial and distal ectolophids are distolingually directed and aligned. They are not discernable from each other on the MUSM 4640, 4642 and 4643 dp4 (Fig 9A). On MUSM 4641 (Fig 9F), They are constituted of a short and thin mesial part (?mesial ectolophid) connecting to a longer and thicker distal part (?distal ectolophid). The labial part of the hypolophid is slightly oblique (i.e., distolingually directed), whereas its lingual part is more transverse. At early stages of wear (MUSM 4641; Fig 9F), the hypoconid displays a very short anterior outgrowth, which becomes longer with wear (MUSM 4642 and 4643 dp4; Fig 9A). The dp4s at advanced stages of wear have a non-taeniodont pattern, whereas MUSM 4641 shows a low and thin anterior arm of the hypoconid (i.e., pseudo-taeniodont pattern). The posterolophid is strong, well curved and separate from the entoconid by a large furrow. The hypoflexid is V-shaped with an anterior margin longer than the distal one. The p4s are slightly longer than wide with the trigonid smaller than the talonid (Fig 9G and 9K). They are tetralophodont. Due to the moderate-advanced stage of wear of all p4s, the conids and stylids are not discernable from the lophids. The mesial margin of p4s is constituted by a transverse metalophulid I. Although it cannot be confirmed, a mesostylid may be presente because the area of the posterior arm of the metaconid is long, especially on IGM 250306 (Fig 9G) and 250308 (Fig 9K), and could be fused with this stylid distally. The second cristid is

complete on IGM 250306 (Fig 9G) and 250308 (Fig 9K), transverse on the former and mesiolingually directed on the latter. Moreover, IGM 250306 has a tiny spur on its lingual margin between the second cristid and the entonconid (Fig 9G). This spur could be a very short neomesolophid. On IGM 250305, the second cristid is reduced to a lingual cristid, labially free. It woud be a metaconid cristid or a neomesolophid depending on if it is stemming from the metaconid or the mesostylid, respectively. The metaconid area is thick on the mesiolingual corner of the p4 of the mandibular fragment ING-KU 8604, and could include a metaconid cristid. On that tooth, the protoconid has a very short posterior arm, and posteriorly to the metaconid area, there is a spur similar to that of IGM 250306 (Fig 9G), which is probably a rest of neomesolophid. The posterior arm of the metaconid (or mesostylid) is slightly connected to the entoconid on IGM 250305, 250306 (Fig 9G) and 250308 (Fig 9K). It is strongly linked to this cuspid on the most worn p4 (ING-KU 8604 p4). The ectolophid is oblique and connected mesially to the protoconid on all p4s. It connects distally to the hypolophid on IGM 250305, 250306 (Fig 9G) and 250308 (Fig 9K). Contrary to the other specimens, the ING-KU 8604 p4 shows the labial extremity of the hypolophid linked to the posterolophid instead of the ectolophid. The hypolophid is roughly transverse on all p4s. The hypoconid is fused with its anterior outgrowth, and the posterolophid is curved, with its lingual extremity reaching the entoconid. The anterior arm of the hypoconid is strong and complete on all p4s, except on IGM 250308 in which this arm is absent and the hypoflexid is fully confluent with the metaflexid (Fig 9K). Lower molars are brachydont (Hling = 0.47–0.57; Hlab = 0.49–0.72; Fig 9A, 9H–9J and 9L–9O). The talonid of m3s is slightly narrower than the trigonid and with a distal part pinched labiolingually. The cuspids are very cristiform and thus, faintly differentiated from the cristids. At early stages of wear, the lower molars display a groove at the level of the metalophulid I separating it into an anterior arm of the metaconid and an anterior arm of the protoconid. The position of this groove varies: either in the middle part of the metalophulid I (MUSM 4647 and 4648; Fig 9H and 9I), lingual to the protoconid (IGM 250319, IGM-DU 88–814, 89–675, MUSM 4650 and 4655; Fig 9M), or closer to the metaconid (MUSM 4654; Fig 9L). On some other lower molars, the anterior arms of the metaconid and protoconid are slightly linked, either equally-sized (MUSM 4649–4653; Fig 9N) or the anterior arm of the protoconid can be shorter (MUSM 4657; Fig 9J). The posterior arm of the metaconid is strong and long (MUSM 4647, 4650, and 4655; Fig 9H and 9M), except on MUSM 4654 in which it is short (Fig 9L). On that tooth, there is a short posterior arm of the protoconid and metaconid cristid, which are

both labially free. IGM 250304 has a metaconid cristid, which runs distolabially and remains free. On some lower molars at an advanced stage of wear (e.g., IGM 250274, 250319, 251020, IGM-DU 88–814, 89–675, ING-KU 8604, MUSM 4652, and 4653; Fig 9O), there is a dentine plateform at their mesiolingual corner, formed by the fusion of the metaconid, its arms, and possibly a metaconid cristid (+ ?neomesolophid + ?mesostylid). On MUSM 4644 and 4646, the ectolophid shows a small expansion, which could be a relic of the posterior arm of the protoconid.

The ectolophid is oblique, aligned with the crestiform protoconid in most cases, and sometimes with the labial part of the hypolophid, its lingual part being more transverse (IGM-DU 88–814, 89–675, IGM 250319, 251020, and MUSM 4657; Fig 9J and 9O). The entoconid occupies a mesial position with respect to the hypoconid. The former usually has long and thick anterior and posterior arms, which are separated mesially to the posterior arm of the metaconid and distally to the posterolophid by tiny furrows (MUSM 4647, 4652, and 4653; Fig 9H). On MUSM 4650, the entoconid, having shorter and thinner arms, is mesially and distally isolated from these structures by larger notches (Fig 9M). The anterior arm of the hypoconid is either incomplete (MUSM 4654 and 4657; Fig 9J and 9L), notched (MUSM 4651 and 4653) or absent (e.g., IGM 250274, 250285, 251020, ING-KU 8604, MUSM 4643, and 4655; Fig 9ª and 9O). On some lower molars at advanced stage of wear, the anterior arm of the hypoconid is, however, connected to the hypolophid-ectolophid junction (i.e., non-taeniodont pattern). The anterior outgrowth of the hypoconid is thin and becomes longer with wear. In addition, the hypoconid is strongly connected to the posterolophid. The latter is thick and C-shaped or hook-shaped.

The dP4s have a suboval/subtrapezoidal occlusal outline, with rounded corners (Fig 9Q, 9U and 9Z). The cusps are quite bulbous. Mesially, the anteroloph is curved and separate labially from the paracone. Lingually, it is strongly (IGM-DU 88–815 and ING-KU unnumbered specimen; Fig 9U and 9Z) or slightly (IGM 250302 and MUSM 4623; Fig 9Q) connected to a massive protocone or its anterior arm. The posterior outgrowth of the protocone is very short. On IGM 250302 and ING-KU unnumbered specimen (Fig 9U), a short crestule (i.e., neoformation) runs distally from the anteroloph and remains free. On all dP4s, the lingual protoloph is absent (i.e., taeniodont pattern). The labial protoloph is strong and either transverse (IGM 250302, ING-KU unnumbered specimen, and MUSM 4623; Fig 9Q and 9U) or oblique (IGM-DU 88–815; Fig 9Z). The mure is complete, oblique, and tends to be aligned with the anterior arm of the hypocone. On the labial margin, the paracone and mesostyle have

a similar size, whereas the metacone remains poorly distinct (not well-defined) as it is fused with the curved posterolophid. The mesostyle is connected to the metacone solely (or its anterior arm) on IGM-DU 88–815 (Fig 9Z), whereas it joins the paracone and metacone or its anterior arm on ING-KU unnumbered specimen and MUSM 4623 (Fig 9Q and 9U). On IGM 250302, the mesostyle is mesially and distally isolated. The third transverse crest corresponds to a mesoloph, which is lingually free (IGM 250302) or slightly connected to a mesolophular spur stemming from the anterior arm of the hypocone (MUSM 4623; Fig 9Q), or directly to the anterior arm of the hypocone (ING-KU unnumbered specimen and IGM-DU 88–815; Fig 9U and 9Z). Most of dP4s have a short metaloph backwardly connected to the posteroloph via a longer posteroloph spur or not, delimiting a small and oval metafossette. However, it can be more slightly connected to the posteroloph spur (MUSM 4623; Fig 9Q). On IGM-DU 88–815, the metacone does not seem to bear a metaloph (Fig 9Z). On that tooth, a long crest slightly linked to the posteroloph in its lingual part is present, which could be a rest of metaloph and/or the posteroloph spur. In addition, there is a tiny crestule stemming from the labial part of the posteroloph, which connects to the labial extremity of the metaloph/posteroloph spur, thus delimiting a small and oval fossette on IGM-DU 88–815 (Fig 9Z). MUSM 4624 (Fig 9A') and 4625 (Fig 9V) are two complete P4s at moderate stages of wear. They preserve a part of their roots: a lingual one very massive and two labial much smaller, which externally diverge. These two specimens are oval and high-crowned, especially at the level of their lingual margin, their labial margin being lower (Hling = 0.80–0.87; Hlab = 0.62–0.70). On the labial margin, the paracone is large and connected to a strong and oblique labial protoloph. On MUSM 4625 (Fig 9V), the mure strongly links the labial protoloph to the short anterior arm of the hypocone. On that tooth, the mure is aligned with the anterior arm of the hypocone. On MUSM 4624 (Fig 9A'), the mure is slightly connected to the anterior arm of the hypocone by a thin and short crestule. In addition to the paracone, the rest of the occlusal outline is composed of a curved and long crest formed by the fusion of the anteroloph, protocone, its anterior arm and its posterior outgrowth, the mesostyle, posteroloph, and hypocone. On MUSM 4624, the paracone is mesially and distally separated from this long crest by a thin furrow (Fig 9A'), while the anteroloph reaches this cusp on MUSM 4625 (Fig 9V). On MUSM 4625, there are two connected crestules, one stemming from the anteroloph and the Other from the labial protoloph (Fig 9V). The lingual protoloph is absent (i.e., taeniodont pattern). On MUSM 4624, the mesostyle is smaller than the paracone, whithout any mesoloph, and it joins the

posteroloph (Fig 9A'). On that tooth, a metaloph stemming from a metacone entirely subsumed within the posteroloph, runs mesiolingually. Its lingual extremity is distally connected to a spur of the posteroloph, and ends close to a longer mesolophule, without connection to the latter. On MUSM 4625, the posteroloph exhibits a thickening in its labial part, which may correspond to its fusion with the mesostyle/mesoloph and/or metacone/metaloph (Fig 9V).

The upper molars determined as M1 or M2?s are clearly mesiodistally elongated (IGM 250283, MUSM 4633, and 4634; (Fig 9R and 9S) or subsquare (IGM 250321, IGM-DU 89–673, MUSM 4629–4632, and 4635; Fig 9W, 9X, 9B' and 9C'). It seems that these upper molars show a tendency of shape variation, ranging from mesiodistally elongated at early stages of wear to squarer configuration at later stages of wear. On these upper molars, the hypocone is either more labially situated than the protocone, or situated at the same level of this cusp. Other upper molars have a hypocone clearly positioned labially with respect to the protocone, and thus they could be M3s (determined as M3?s). All upper molars have a taeniodont pattern characterised by a paraflexus and hypoflexus fully confluent. On the two upper molars at the earliest stage of wear (MUSM 4634 and 4637; Fig 9R and 9T), there is a short anteroloph (+ parastyle?), which is separate from the long and curved anterior arm of the protocone by a thin (MUSM 4634; Fig 9R) or wider (MUSM 4637; Fig 9T) furrow. The anteroloph is either not connected to the paracone (e.g., IGM-DU 89–673, MUSM 4629, 4632, 4634; Fig 9R, 9W and 9C'), slightly (MUSM 4633, 4638; Fig 9S and 9Y) or more strongly (MUSM 4637, 4639; Fig 9T and 9D') connected to this cuspid. The strong labial protoloph is usually oblique but it can also be transverse (IGM 250321 and MUSM 4629; Fig 9C'). The anterior arm of the hypocone is oriented mesiolabially, except on MUSM 4634, in which it is more longitudinal. It tends to be aligned with a short mure. The labial protoloph can be in continuity to both the mure and anterior arm of the hypocone with roughly the same orientation (MUSM 4632, 4635, 4637, and 4639; Fig 9T, 9W and 9D'). On MUSM 4635, the labial protoloph bears on its mesial part a short crestule, which remains free on the paraflexus. It likely corresponds to a neocrest. Some upper molars have a well-defined mesostyle (MUSM 4626, 4632, 4634, 4637, and 4639; Fig 9R, 9T, 9W and 9D'). At early stages of wear, a thin and shallow notch separates the paracone from the mesostyle. A mesoloph, stemming from this style, is usually presentes with a medium or short length, but it can also be more reduced as on MUSM 4637, in which it is incipient and poorly distinct from the mesostyle (Fig 9T). It can be transverse, either lingually free (IGM 250321 and MUSM

4637; Fig 9T), connected to a short mesolophule (MUSM 4633; Fig 9S), or directly connected to the anterior arm of the hypocone (MUSM 4631; Fig 9X). Some upper molars (IGM 250283, 250284, IGM-DU 89–673, MUSM 4630, and 4634; Fig 9R and 9B') have a mesoloph backarldly directed and linked to the posteroloph (or its spur), thereby delimiting an oval and small posterior fossette. On MUSM 4626, 4632, and 4639 (Fig 9W and 9D'), the third crest is absent (neither mesoloph nor mesolophule). There is no clear metacone on all upper molars, but a metaloph connected lingually to the posteroloph is presente on MUSM 4631 (Fig 9X). It is faintly linked to the posterior arm of the mesostyle on that tooth. One upper molar at an early stage of wear, MUSM 4639 (Fig 9D'), has a trilophodont pattern without neither third crest nor metaloph. At more advanced stages of wear, some molars are trilophodont but with a thick posteroloph, which may include a mesoloph and/or a metaloph and their associated cusps/styles (MUSM 4627–4629, 4632, 4635, and 4638; Fig 9W, 9Y and 9C').

Microscleromys cribriphilus Boivin & Walton sp. nov.
urn:lsid:zoobank.org:act:74B60D5-F-A8B3-4A2C-9483-D22739400EC8
Fig 10 and S1 Table

Nom. *nud*. *Microscleromys cribriphilus* Walton, 1990, Fig 12A-12E, p. 45.
Nom. *nud*. *Microscleromys cribriphilus* Walton, 1997, Fig 24.2.K-M,O, p. 295.
Nom. *nud*. *Microscleromys paradoxalis* Walton, 1997, Fig 24.2.J, p. 295.

Holotype

MUSM 4491, left M1 or M2? (Fig 10H').

Referred material

MUSM 4545, right fragmentary dp4 or p4; MUSM 4532–4541 (Fig 10A, 10F and 10K), left dp4s; MUSM 4542–4544, right dp4s; IGM-DU 88–818, MUSM 4546–4550 (Fig 10G, 10L and 10P), left p4s; IGM 251018 (Fig 10Q), MUSM 4551–4558 (Fig 10B), right p4s; IGM-DU 89–676, left m1 or m2 (or p4); MUSM 4558–4561, left lower molars; MUSM 4562–4565, right lower molars; MUSM 4566, left m1 or m2?; IGM 250309, right m1 or m2?; MUSM 4567–4588 (Fig 10H and 10M), left m1?s; MUSM 4589–4600 (Fig 10C), right m1?s; MUSM 4601–4608 (Fig 10D, 10I, 10N and 10S), left m2?s; IGM 250303 (Fig 10R), MUSM 4609–4615, right m2s; MUSM 4621, left m3?; MUSM 4616–4620 (Fig 10E, 10O and 10T), left m3s; MUSM 4622 (Fig 10J), right m3; MUSM 4420–4433 (Fig 10U and 10E'), left dP4s; IGM 250320 (Fig 10J'), MUSM 4434–4447 (Fig

10Z), right dP4s; MUSM 4469, right P4 or M3?; MUSM 4448–4458 (Fig 10V and 10F'), left P4s; IGM 251040 (Fig 10K'), MUSM 4459–4468 (Fig 10A'), right P4s; MUSM 4470, 4471, left upper molars; MUSM 4472–4478, right upper molars; MUSM 4479–4497 (Fig 10B' and 10H'), left M1 or M2?s; MUSM 4498–4510 (Fig 10W, 10G' and 10L'), right M1 or M2?s; MUSM 4511–4513 (Fig 10C' and 10M'), left M2?s; MUSM 4514–4516 (Fig 10X), right M2?s; MUSM 4517–4524 (Fig 10Y and 10N'), left M3?s; MUSM 4525–4531 (Fig 10D' and 10I'), right M3?s.

Derivation of name

Based on the original description of the species [37]: from the latin *cribri* (sieve) and *philus* (liking to or attracted to) 'because this rodent is so far only known from isolated teeth recovered by screenwashing'.

Type locality

TAR-31, Tarapoto/Juan Guerra, Mayo River, Shapaja road, San Martín Department, Western Amazonia, Peru.

Other localities

Localities of the Fish Bed (including CVP 9, 10A, and 13B), La Venta Badlands, upper Magdalena Valley, Huila Department, Colombia.

Formation and age

Lower member, Ipururo Fm.; Baraya Member of the Villavieja Fm.; late middle Miocene (i.e., Laventan SALMA).

Diagnosis

Species with teeth approximately 25–30 per cent smaller than those of*M*. *paradoxalis*. dP4s can have a non-taeniodont pattern characterised by a complete and high lingual protoloph in continuity with the labial protoloph.

Description

The pattern of teeth usually follows that of*M*. *paradoxalis* described above, with few exceptions, but mostly the smaller size allows for a clear distinction of the two species (see S1 File). dp4s are longer than wide, with a trigonid narrower than the talonid. The protoconid appears to be the largest cuspid. On the dp4 at the earliest stage of wear (MUSM 4532; Fig 10A), the metaconid is the most cristiform cuspid, which is linguolabially pinched. On worn dp4s (MUSM 4539, 4540, and 4544; Fig 10F), the protoconid displays three connections: (i) a mesiolingual one with a curved metalophulid I, which extends lingually to the metaconid; (ii) a distolingual one with the second transverse cristid, which connects labially to the metaconid; and (iii) a distal one with the mesial extremity of the mesial ectolophid. On the dp4s at the earliest stage

of wear (MUSM 4532 and 4536; Fig 10A and 10K), the protoconid is separated from the metalophulid I and from the mesial ectolophid by two notches. The notch between the protoconid and the metalophulid I is the deepest and thus, it closes at a latter stage of wear than that between the protoconid and the mesial ectolophid (MUSM 4534). Conservely to MUSM 4532, the protoconid is also isolated from the second transverse cristid, which is reduced to a medium-sized metaconid cristid, on MUSM 4536 (Fig 10K). However, both structures are connected at their base. On MUSM 4532, 4534, and 4536 (Fig 10K), the metalophulid I is not connected to the metaconid (Fig 10A). On all dp4s, the second transverse cristid is slightly directed mesiolingually. The mesial and distal ectolophids are thin, distolingually directed, aligned and often not discernable from each other. A small mesostylid is often presente (MUSM 4534, 4536, 4539, 4540, and 4541; Fig 10F and 10K). It is isolated from the entoconid on all dp4s. It is connected to the metaconid on MUSM 4534, 4539 and 4540 (Fig 10F). On MUSM 4532 (Fig 10A), a mesostyle may be present, fused with the long posterior arm of the metaconid. On MUSM 4539, a complete third transverse cristid links the mesostylid with the ectolophids. The other dp4s do not show any development of the third cristid. On all dp4s, a well-marked hypolophid links the large entoconid to the distal ectolophid. In most cases, the labial part of the hypolophid is slightly oblique (i.e., distolingually directed), whereas its lingual part is more transverse. The hypoconid always displays a short anterior outgrowth and a low, but complete anterior arm, reaching the hypolophid-distal ectolophid junction (i.e., pseudotaeniodont pattern). Besides, the hypoconid has lingually a very short posterior arm, connecting to a strong and well-curved posterolophid on MUSM 4532 and 4534 (Fig 10A). At early stages of wear, the posterolophid is separate from the entoconid or its posterior arm by a large furrow. The three lingual flexids show a similar large expansion. The hypoflexid is less extended, distolingually oriented and V- or U- shaped. Its anterior margin is longer than its distal one, except on MUSM 4533. p4s are brachydont-submesodont (Hling = 0.45–0.77; Hlab = 0.54–0.81; Fig 10B, 10G, 10L, 10P and 10Q). They are slightly longer than wide, with a talonid clearly wider than the trigonid. By their high elevation and large surface, the protoconid and hypoconid are the most distinct cuspids of the crown at the earliest stage of wear (MUSM 4548; Fig 10G). The protoconid is labiolingually pinched, whereas the hypoconid is mesiodistally compressed. At the mesiolingual corner, the metaconid is well defined during the first stages of wear (MUSM 4548 and 4553; Fig 10B and 10G). It displays a short or moderate posterior arm (MUSM 4548, 4550, and

4553; Fig 10B, 10G and 10P). On MUSM 4548 (Fig 10G), the metalophulid I is continuous and high, joining the protoconid to the metaconid. On MUSM 4546 and 4553 (Fig 10B), the anterior arms of the protoconid and metaconid are short, strongly sloped and separated by a large furrow, which is thinner on MUSM 4547 and 4550 (Fig 10P). The protoconid frequently has a short posterior arm, which can be very short (MUSM 4546–4548; Fig 10G and 10L) or reduced to a spur (IGM-DU 88–818, MUSM 4550, 4551, and 4557; Fig 10P). On IGM-DU 88–818, MUSM 4547 and 4557, it is lingually free. The posterior arm of the protoconid is absent on IGM 251018, MUSM 4553 and 4558 (Fig 10B). A thin and short metaconid cristid can be present (MUSM 4546 and 4548; Fig 10G and 10L). On MUSM 4546 (Fig 10L), it is slightly connected to the posterior arm of the protoconid. On MUSM 4548 (Fig 10G), these two cristids are linked at their base but not connected at their apex. The worn MUSM 4554 p4 shows an oblique second transverse cristid, linking the metaconid to the protoconid. Thus, this cristid may be formed here by the fusion of a metaconid cristid with a posterior arm of the protoconid.

On MUSM 4551, a round and small mesostylid is clearly distinct, separated from the metaconid (or its posterior arm) and entoconid by tiny notches. On that tooth, a cristid, probably a neomesolophid, is faintly connected to the mesostylid and to a very tiny posterior arm of protoconid. In addition, it shares a very slight connection mesially with the mesialmost lophid and distally with the hypolophid. On MUSM 4546, the distal extremity of the posterior arm of the metaconid displays a tiny spur that may be a neomesolophid that would be connected to a mesostylid fused with the posterior arm of the metaconid (Fig 10L). At some advanced stage of wear, the metaconid, its anterior and posterior arms, metaconid cristid, as well as possibly the mesostylid and neomesolophid (if present), fuse and form a small platform of dentine on the mesiolingual corner of the teeth. If the entoconid has anterior and posterior arms, the latter is longer than the former (MUSM 4547, 4548, 4550, and 4556; Fig 10G and 10P), except on IGM 251018 and MUSM 4546, in which they are equally-sized (Fig 10L and 10Q). The entoconid (or its anterior arm) is separated from the mesostylid-posterior arm of the metaconid by a large furrow (MUSM 4548 and 4553; Fig 10B and 10G) or a very thin notch (MUSM 4546, 4547, 4550, and 4556; Fig 10L and 10P). On p4s at a more advanced stage of wear, these structures are connected. Stemming from the entoconid, a hypolophid runs labiomesially (i.e., oblique) and slightly connects to the ectolophid (IGM-DU 88–818, MUSM 4546, and 4548; Fig 10L). The anterior arm of the hypoconid usually reaches the hypolophidectolophid junction (i.e., non-taeniodont

pattern). On p4s at early stages of wear (MUSM 4546, 4548, and 4553; Fig 10B, 10G and 10L), this cristid is more or less notched but remains elevated. However, on MUSM 4550 (Fig 10P), the notch of the anterior arm of the hypoconid is more pronounced, involving a partial confluence between the metaflexid and the retroverse hypoflexid (i.e., pseudo-taeniodont pattern). IGM 251018 appears to have a taeniodont pattern (Fig 10Q). The posterior arm of the hypoconid is fused with the strong and curved posterolophid, the latter extending lingually and ending directly distal to the entoconid, connecting to its base. The hypoconid displays a long and thin anterior outgrowth. Lower molars are brachydont-mesodont (Hling = 0.50–0.79; Hlab = 0.54–0.91; Fig 10C–10E, 10H–10J, 10M–10O and 10R–10T). The m3s have a distal part of the talonid labiolingually pinched, and thus are more recognisable than m1s and m2s. Some lower molars appear smaller, and could be m1s (identified as m1?s). The m3s are either roughly equal in size to the lower molars determined as m1?s or smaller. Lower molars differ from p4s in having a wider trigonid comparatively to the talonid. The cristids are thick and incorporate in their ends the cuspids, which are thus faintly differentiated (except for the entoconid). The metalophulid I can show a thin interruption (groove) either in its middle part, separating equally-sized anterior arms of the metaconid and of the protoconid (MUSM 4611), or directly lingual to the protoconid, separating a long anterior arm of the metaconid from a very short and low anterior arm of the protoconid (MUSM 4588 and 4616; Fig 10O). On some other lower molars, both arms are slightly connected (e.g., IGM 250303, MUSM 4573, 4597, 4599, and 4620; Fig 10C, 10R and 10T). MUSM 4586 shows an additional cristid stemming from the metalophulid I, running distally and ending freely. The metaconid has a strong posterior arm, which can be long (e.g., MUSM 4592) or short (e.g., MUSM 4580, 4588, and 4599; Fig 10C). This cristid connects to a distinct mesostylid on some lower molars (MUSM 4580, 4582, 4584, 4588, 4597, 4599, 4601, and 4605; Fig 10C and 10N). A neomesolophid stemming from the mesostylid can be present (e.g., MUSM 4580, 4588, and 4605; Fig 10N) or absent (e.g., MUSM 4582, 4584, 4597, 4599, and 4601; Fig 10C). The neomesolophid is either limited to a very short enamel spur or short cristulid. It is labially free on all specimens. Two lower molars (MUSM 4597 and 4613) exhibit a short lingual cristulid from the metaconid, recognised as a metaconid cristid, which remains labially free. As p4s, some lower molars at an advanced stage of wear have a mesiolingual dentine platform, formed by the fusion of the metaconid, its arms, and possibly the metaconid cristid and/or neomesolophid + mesostylid. On several lower molars (e.g., MUSM 4560, 4563, 4568, 4571, 4588, 4613, and 4622; Fig 10J), there is

a small lingual expansion on the ectolophid that is likely to be a relic of the posterior arm of the protoconid. With the reduction or absence of the neomesolophid and the posterior arm of the protoconid, the mesoflexid is partly or entirely confluent with the anteroflexid. The ectolophid is oblique, frequently aligned with the crestiform protoconid and the hypolophid, thereby forming a long mesiocentral (diagonal) cristid. Lingually, the entoconid is the most differentiated cuspid. It is frequently mesiodistally elongated by developing strong anterior and posterior arms, which are particularly long on MUSM 4582. They tend to be mesially connected with wear to the mesostylid-posterior arm of the metaconid, and distally to the posterolophid. On lower molars at earliest stages of wear, thin furrows usually isolate the entoconid from these other structures mesially and distally. A short but strong hypolophid extends from the entoconid to the distal extremity of the ectolophid. As on p4s, the hypoconid on lower molars is mesiodistally compressed and displays a thin anterior outgrowth, which becomes long with wear. The hypoconid is distal in position to the entoconid. The anterior arm of the hypoconid can be present or absent (e.g., IGM 250303, MUSM 4600, and 4616; Fig 10O and 10R). When it is present, it is faintly developed and runs to the ectolophid–hypolophid junction. It is grooved (e.g., MUSM 4579, 4605, and 4620; Fig 10N and 10T) or deeply notched (e.g., MUSM 4569 and 4602; Fig 10S), showing a suite of intermediate sizes of the notch. Hence, the metaflexid is more or less confluent with the hypoflexid (i.e., from pseudo-taeniodont pattern to taeniodont pattern). However, many lower molars at an advanced stage of wear show a complete anterior arm of the hypoconid, which can be thick (i.e., non-taeniodont pattern; e.g., MUSM 4581, 4606, and 4622; Fig 10H–10J). A massive and hook-shaped posterolophid strongly connects to the hypoconid, both structures being fused and in perfect continuity. dP4s are longer than wide and with rounded corners (Fig 10U, 10Z, 10E’ and 10J’). They have a suboval occlusal outline, with a well-arcuate anteroloph (i.e., mesially convex) and posteroloph (i.e., distally convex). All dP4s are brachydont. The cusps are usually moderately inflated. The anteroloph is curved, short, and located far mesially. At early stages of wear, two notchs separate the anteroloph labially from the paracone (except on MUSM 4445; Fig 10Z) and lingually from the strong and bulbous protocone or its anterior arm. The first notch is wide, while the second is highly variable in terms of development. It corresponds to a very large notch on some dP4s (MUSM 4425, 4427, 4428, 4431, 4432, and 4435; Fig 10U and 10E’), whereas, on other teeth, it is a thinner and shallower furrow (MUSM 4429, 4439, 4440, and 4443) or a tiny groove (MUSM 4430, 4437, 4442, 4445, and 4446; Fig 10Z). On MUSM 4438,

the protocone is mesiolingually-distolabially pinched, developing a short anterior arm, which is strongly connected to the anteroloph. The posterior outgrowth of the protocone is very short on the whole dP4s. On MUSM 4422 and 4428 (Fig 10E'), a well-cuspate parastyle is discernable on the mesiolabial corner of the tooth. This style bears short, but strong, anterior and posterior arms, separate by deep furrows from the anteroloph and paracone, respectively. On MUSM 4422, a medium-sized loph (i.e., neoformation) runs lingually from the parastyle, slightly directed distolingually, but with its lingual extremity faintly linked to the anteroloph via a very short and thin crestule. On MUSM 4428 (Fig 10E'), this loph is present but reduced to a short spur, whose base is connected to a peculiar anteroloph, short and labially concave. Hence, the parastyle, its anterior arm, its spur and the anteroloph delimit a small and round fossette. On the labial margin, the paracone and mesostyle are equally sized, and the metacone is smaller and usually still visible. The mesostyle is separate mesially from the paracone by a large furrow, that closes with wear. This style can be connected (MUSM 4422, 4431, and 4438) or disconnected (MUSM 4424, 4425, 4427, 4428, 4430, 4439, and 4445; Fig 10U, 10Z and 10E') to the metacone (or its anterior arm). Posteriorly, the metacone is strongly connected to the well-curved posteroloph. On dP4s at early stages of wear, the lingual protoloph can be absent (i.e., taeniodont pattern; e.g., MUSM 4422, 4427, and 4428; Fig 10E') or present, either thin and low (i.e., pseudo-taeniodont pattern; MUSM 4437, 4438, and 4445; Fig 10Z) or high (i.e., non-taeniodont pattern; MUSM 4425, 4431, and 4446; Fig 10U). The labial protoloph is thick and usually straight, but it can also be slightly oblique. On IGM 250320, MUSM 4420, 4427, 4428, 4444, and 4445 (Fig 10Z, 10E' and 10J'), it is particularly strongly oblique. On MUSM 4425, 4429, 4431, 4432, 4439, 4440, 4442 and 4446, the labial and lingual protolophs are aligned and form a transverse crest linking the paracone to the protocone (Fig 10U). The mure is complete and high, except on MUSM 4429 in which it is low, involving a partial confluence of the mesial mesoflexus with the hypoflexus. It is usually longitudinal (i.e., parallel to the mesiodistal axis of the tooth), but can be more oblique, aligned with the anterior arm of the hypocone (IGM 250320, MUSM 4420, 4421, 4422, 4427, and 4443; Fig 10J'), and sometimes with an oblique protoloph (MUSM 4420 and 4427). The third transverse crest is parallel with the labial protoloph. It is composed of two crests: a short and thick mesoloph stemming from the mesostyle and a mesolophular spur stemming from the anterior arm of the hypocone. On some dP4s (MUSM 4425, 4438, and 4446; Fig 10U), the third crest is complete, with the mesoloph linked to a short mesolophule, whereas they can be unconnected or faintly

connected together on other teeth (MUSM 4420, 4427, 4428 and 4443–4445; Fig 10Z and 10E'). On IGM 250320, MUSM 4428 and 4444 (Fig 10E' and 10J'), the mesoloph seems to be absent or strongly reduced. IGM 250320 appears to not have any mesolophule (Fig 10J'). Most of dP4s have a short metaloph backwardly connected to the posteroloph via a longer posteroloph spur or not, delimiting a small and oval metafossette. However, it can be lingually free (MUSM 4427) or absent (MUSM 4425, 4428, and 4431; Fig 10U and 10E'). On MUSM 4442, there is a short posteroloph spur and a cusp-like structure on the distalmost flexus, which is probably a relic of the metaloph. The latter structures are not linked. On dP4s at the earliest stages of wear, the posteroloph displays a shallow (MUSM 4425, 4430, 4431, 4442; Fig 10U) or deep (MUSM 4427, 4428, 4446; Fig 10E') furrow, which separates it from the hypocone. P4s are high-crowned, especially at the level of their lingual crown, their labial crown being lower (Hling = 0.81–0.96; Hlab = 0.45–0.79; Fig 10V, 10A', 10F' and 10K'). In occlusal view, their crown is oval, labiolingually wider than longer. Mesiolingually, the anteroloph, protocone, its anterior arm and its posterior outgrowth form a long crest, which is separate from the large and well-cuspate paracone by a thin furrow. Distally, the paracone remains free and separate from a long distal crest including the mesostyle, posteroloph, hypocone and its long anterior outgrowth. Therefore, a usually wider and persistant furrow occurs distal to the paracone. The mesial extremity of the anterior outgrowth of the hypocone is connected to the posterior outgrowth of the protocone, and to the whole of the aforementioned structures, thereby forming most of the peripheral margin of the tooth. There is no lingual protoloph on the whole specimens. Accordingly, the most anterior flexus is a fossette, corresponding to the confluence of the paraflexus with the hypoflexus (i.e., taeniodont pattern). In mostcases, the mure and the short anterior arm of the hypocone are thin, linked, and aligned, forming a longitudinal or oblique crest. On MUSM 4450 and 4455, these two structures are not aligned, the mure being more longitudinal than the anterior arm of the hypocone. On MUSM 4456, the mure is not linked to the anterior arm of the hypocone or to the posteroloph. The mure is connected to the lingual extremity of the labial protoloph, which is almost transverse (IGM 251040, MUSM 4449, 4455, 4457, 4459, and 4466; Fig 10A' and 10K') or oblique (MUSM 4450–4454, 4456, 4461–4464, 4467, and 4468). The mure is absent on MUSM 4463, in which the labial protoloph is not connected to the anterior arm of the hypocone. On MUSM 4449, a longitudinal crest connects the anteroloph to the labial protoloph. Hence, these strutures and the paracone delimits a very small rounded fossette. The mesostyle is small and

crestiform, poorly distinct from the posteroloph. On MUSM 4452 and 4466 (Fig 10A' and 10F'), it displays a very short mesoloph lingually free, longer on MUSM 4466 (Fig 10A') than on MUSM 4452 (Fig 10F'). On P4s in a more advanced stage of wear (MUSM 4451, 4456, and 4468), the mesoloph is longer. On MUSM 4451, its lingual extremity is slightly connected to the mure-anterior arm of the hypocone and to the posteroloph. One P4, MUSM 4453 (Fig 10V), do not show any mesoloph. MUSM 4466 has a very short metalophular spur labially free, as well as a tiny crestule from the posteroloph, which could be a posteroloph spur or a metaloph (Fig 10A'). With wear, the posteroloph often exhibits a thickening in its labial part, which may correspond to its fusion with the mesostyle/mesoloph, metacone/metaloph and/or posteroloph spur (IGM 251040, MUSM 4450, 4455, 4458, 4459, 4463, and 4467; Fig 10K'). This plateform can be free, joined lingually to a tiny mesolophular spur (MUSM 4450) or directly to the mure (MUSM 4455). The different loci documenting upper molars (i.e., M1 vs M2 vs M3) are not easily recognisable (Fig 10W–10Y, 10B'–10D', 10G'–10I' and 10L'–10N'). Some upper molars are small, with a rounded occlusal outline and a hypocone clearly labially positioned with respect to the protocone, and thus they could be M3s (determined as M3?s; Fig 10Y, 10D', 10I' and 10N'). Other upper molars are square, mesiodistally elongated or transverse. On these upper molars, the hypocone is either more labially situated than the protocone or situated at the level of this cusp (i.e., distal). As for P4s, upper molars are labiolingually asymmetrical with a higher lingual crown (Hling = 0.71–1.07; Hlab = 0.42–0.65). In general, the cusps/styles are crestiform, and not well defined. In most cases (MUSM 4487, 4493, 4502, 4508, 4511, 4525, and 4527; Fig 10C', 10G', 10I' and 10L'), the protocone shows a long and curved anterior arm, which is slightly connected to a shorter and straight anteroloph (+ ?parastyle). These two crests can be also strongly connected (MUSM 4489 and 4520; Fig 10B') or separated by a narrow (MUSM 4491; Fig 10H') or wide (MUSM 4505; Fig 10W) furrow. The anteroloph is connected to the mesial aspect of the paracone on some M1s or M2s (MUSM 4483, 4487, 4489, 4495, and 4502; Fig 10B' and 10G') and all M3?s (MUSM 4520, 4526, and 4527), whereas it remains separate from the paracone by a narrow furrow such as on MUSM 4482, 4486, 4491, 4494, 4499, 4505, 4513, and 4514 (Fig 10W, 10X, 10H' and 10M'). On the MUSM 4525 M3?, the paracone is fully fused with the anteroloph (Fig 10I'). On MUSM 4511, the anteroloph bears a short but well-marked crestule lingually free on the paraflexus (Fig 10C'). The lingual protoloph is absent on all upper molars, thereby the paraflexus and hypoflexus are confluent (i.e., taeniodont pattern). The protocone displays a long and strong

posterior outgrowth that can end close to the hypocone (MUSM 4495, 4498, 4517, 4519, 4520, 4524, and 4527–4530; Fig 10D' and 10N'), or can connect to this cusp with wear (MUSM 4521; Fig 10Y). On all upper molars, the hypocone is usually smaller than the other main cusps. It displays a strong and oblique anterior arm, which connects to the mure and tends to be aligned with it. A labial protoloph, strong, short and slightly (e.g., MUSM 4486 and 4529) or strongly (e.g., MUSM 4483, 4489, and 4520; Fig 10B') oblique, links the paracone to the mure. The anterior arm of the hypocone and the mure are in continuity with the labial protoloph, forming a long and diagonal central crest with a strong obliquity on some upper teeth (e.g., MUSM 4481, 4485, 4489, 4493, 4520; Fig 10B'). The labial protoloph can bear a short crestule mesially free on the paraflexus (MUSM 4498 and 4511; Fig 10C'). Labially, a strong mesostyle is present. It is clearly distinct on some upper molars (MUSM 4482, 4505, 4514, 4516, 4527, and 4530; Fig 10W, 10X and 10D'). It is separated from the paracone by a thin and shallow notch (e.g., MUSM 4483, 4487, 4505, and 4529; Fig 10W) or connected to this cusp (or to the posterior arm of paracone; MUSM 4489, 4516, and 4520; Fig 10B'), thereby forming a labial wall that closes the mesial mesoflexus. Distolabially, a metacone is either well separate from the posterior arm of the mesostyle by a large but shallow notch (MUSM 4505 and 4514; Fig 10W and 10X), faintly connected to the posterior arm of the mesostyle (MUSM 4482, 4487, 4508, and 4522; Fig 10L') or more strongly linked to it (MUSM 4516 and 4521; Fig 10Y). The upper molars show an importante variation in the development, configuration and orientation of the third crest and metaloph. From the mesostyle, a strong but short mesoloph runs either (i) lingually: it is free (MUSM 4510, 4512, 4514, 4516, 4522, and 4525; Fig 10X and 10I') or connects to a short mesolophule (MUSM 4471, 4487, 4494, 4513, 4515, and 4520; Fig 10M'); or (ii) backwardly: it is free (MUSM 4483 and 4499), or connects to the metaloph (MUSM 4508 and 4521; Fig 10Y and 10L'), to the posteroloph (via a spur or not; MUSM 4481, 4489, 4491, 4501, 4504, 4511, and 4528; Fig 10B', 10C' and 10H'), or seemingly to both crests (MUSM 4482). On MUSM 4521, the mesolophule is not connected to the mesoloph (Fig 10Y). On MUSM 4505, the mesoloph is slightly joined to a tiny mesolophule as well as to the metaloph (Fig 10W). Some Upper molars show a distinct metacone, but without metaloph (or almost absent; MUSM 4491; Fig 10H'). If the metaloph is present and not linked to the mesoloph and/or to the posteroloph (via a spur or not; MUSM 4482, 4505, 4508, and 4521; Fig 10W, 10Y and 10L'), it is lingually free (MUSM 4487, 4514, 4516, and 4522; Fig 10X). On MUSM 4502, 4529 and 4530 (Fig 10D' and 10G'), there is neither the third crest

nor the metaloph (i.e., trilophodont pattern). Most of molars at more advanced stages of wear are trilophodont (MUSM 4470, 4476, 4481, 4484, 4492, 4495, 4496, 4498, 4518, 4519, and 4528), but have a enlarged posteroloph, which may include a mesoloph and/or a metaloph and their associated cusps/styles (entirely subsumed within the posteroloph). The flexi are furrow-shaped, especially the anterior flexus (i.e., paraflexus + hypoflexus).

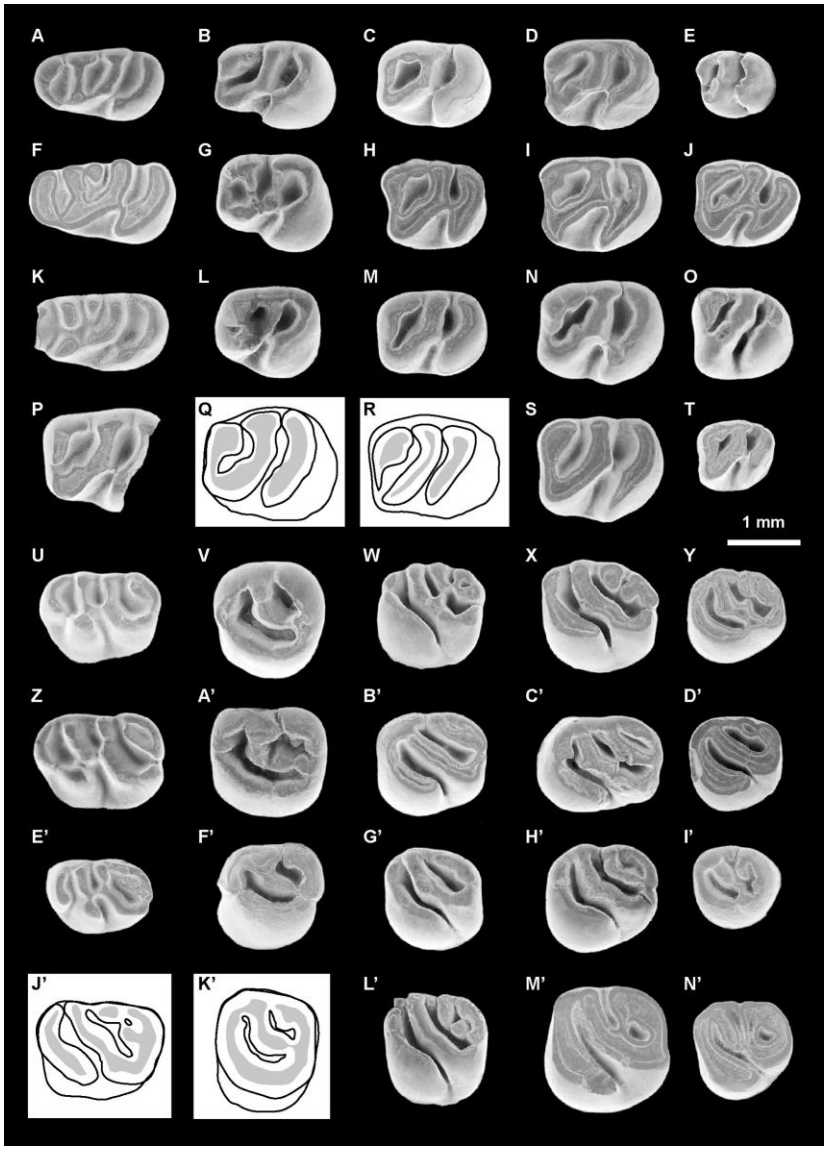


Fig 10. *Microscleromys cribriphilus* gen. et sp. nov. Material from TAR-31, Peru (black background) and from La Venta, Colombia (White background). (A) MUSM 4532, left dp4. (B) MUSM 4553, right p4 (reversed). (C) MUSM 4599, right m1? (reversed). (D) MUSM 4603, left m2?. (E) MUSM 4619, left m3. (F) MUSM 4540, left dp4. (G) MUSM 4548, left p4. (H) MUSM 4581, left m1?. (I) MUSM 4606, left m2?. (J) MUSM 4622, right m3 (reversed). (K) MUSM 4536, left dp4. (L) MUSM 4546, left p4. (M) MUSM 4583, left m1?. (N) MUSM 4605, left m2?. (O) MUSM 4616, left m3. (P) MUSM 4550,

left p4. (Q) IGM 251018, right p4 (reversed). (R) IGM 250303, right m2? (reversed). (S) MUSM 4602, left m2?. (T) MUSM 4620, left m3. (U) MUSM 4425, left dP4. (V) MUSM 4453, left P4. (W) MUSM 4505, right M1 or M2? (reversed). (X) MUSM 4514, right M2? (reversed). (Y) MUSM 4521, left M3?. (Z) MUSM 4445, right dP4 (reversed). (A') MUSM 4466, right P4 (reversed). (B') MUSM 4489, left M1 or M2?. (C') MUSM 4511, left M2?. (D') MUSM 4530, right M3? (reversed). (E') MUSM 4428, left dP4. (F') MUSM 4452, left P4. (G') MUSM 4502, right M1 or M2? (reversed). (H') MUSM 4491***, left M1 or M2?. (I') MUSM 4525, right M3? (reversed). (J') IGM 250320, right dP4 (reversed). (K') IGM 251040, right P4 (reversed). (L') MUSM 4508, right M1 or M2? (reversed). (M') MUSM 4513, left M2?. (N') MUSM 4517, left M3?. Occlusal views. The asterisks appoint the holotype material. The illustrations of the fóssil specimens are scanning electron photomicrographs (A-P, S-I', and L'-N') and computerized schematic line drawings based on Walton (Fig 24.2 [18]; Fig 14 [37]) (Q, R, J', and K').

Remark

The specimens attributed to *Microscleromys cribriphilus* show a great variation of size. For example, the size range of the lower molars extends from 1.08 mm to 1.78 mm for the length, and from 1.01 mm to 1.57 mm for the width. Likewise, the size range of upper molars is 1.17–1.71 mm for the length and 1.07–1.66 mm for the width. Due to the sample size that is distributed quite uniformly for the minimum range and without shape variation, we consider that all the material reported here documents a single taxon. Accordingly, we consider the smaller specimens to document smaller individuals. Moreover, it is worth noting that the smallest specimens are often teeth determined as m3?s and M3?s. We attribute the observed size variation between specimens partly resulting of size variation between loci.

Common comparisons

Basically, among caviomorph rodents, (i) the presence of high-crowned teeth with a taeniodont pattern and oblique loph(-id)s, (ii) the absence or reduction of second transverse cristid on lower molars, and (iii) the absence of metaloph and third transverse crest, or the reduction of the latter (mesoloph) on upper molars, are dental features characterising Chinchilloidea. The specimens described here do not show any heterogeneous thickness of the enamel layer, usually found in most advanced chinchilloid forms (including *Incamys*) [114, 127, 128]. There is also no heterogeneous thickness of the enamel layer in the alleged chinchilloid *Branisamys* (Salla, Bolivia, late early Oligocene–late Oligocene; [129–131], but see [4]), *Saremmys* [132], and in taxa

recognised as stem-Chinchilloidea (*Eoincamys* and *Chambiramys*) [4]. Furthermore, this character is only insinuated in *Scleromys*/"*Scleromys*" [127]. By having highcrowned teeth with a tendency to show oblique loph(-id)s, not forming lamina, and with flexi (-ds) not filled with cement; p4s with a complete tetralophodont pattern or with a more trilophodont pattern; lower molars with a groove on the metalophulid I and without second transverse cristid (or the latter if present, being strongly reduced); upper teeth with a metaloph reduced or absent, a third transverse crest absent or limited usually to a short mesoloph lingually free or backwardly connected to the posteroloph, the concerned dental specimens from TAR-31 have a morphology matching that of *Microscleromys nom*. *nud*. from La Venta (Colombia; late middle Miocene; Fig 24.2G-24.2O, p. 395 [18]; Figs 11–13 [37]). In particular, some specimens from TAR-31 are larger and attribuable to*M*. *paradoxalis*, whereas other, smaller, are determinable as*M*. *cribriphilus* (S1 File) [18, 37]. In addition, *M*. *cribriphilus* differs from *M*. *paradoxalis* in having some dP4s showing a non-taeniodont pattern characterised by a complete and high lingual protoloph in continuity to the labial protoloph (this study). Several other chinchilloid genera (*Eoincamys*, *Chambiramys*, *Incamys*, *Saremmys*, and *Scleromys*/"*Scleromys*") [28, 70, 71, 73, 81, 114, 118, 130–134] have a similar pattern (i.e., highcrowned teeth, homogeneous thickness of the enamel layer; taeniodonty, obliquity of loph(-id) s, no lamina and no cement). Like *Microscleromys*, *Eoincamys*, *Chambiramys*, *Incamys* and *Scleromys*/"*Scleromys*" also show a great variation of the morphology of the second transverse cristid on lower molars, and third transverse crest and metaloph on upper molars in terms of presence/absence, length, orientation and connections. No lower molar from TAR-31 and La Venta has a neomesolophid as long as or longer than on the MUSM 2875 m2 of *Chambiramys sylvaticus* (Fig 5G, p. 80 [71]). *Microscleromys* differs from *Chambiramys* in being slightly higher-crowned, and with more quadrangular upper molars; from *Eoincamys*, *Incamys* and *Scleromys*/"*Scleromys*" in having upper molars more square-shaped and a reduction more important of the third transverse crest on upper molars (i.e., more frequent trilophodont pattern than in these genera); from *Eoincamys ameghinoi*, *Eoincamys pascuali* and *Incamys* in having a second transverse cristid usually more reduced on lower molars; from *Eoincamys pascuali* in having a thinner furrow (when it is present) on the metalophulid I, which can be situated in the middle of this lophid; from *Saremmys* in having lower-crowned teeth, thinner loph (-id)s, a less oblique hypolophid on p4s and lower molars, and some upper molars with a distinct metacone, and long metaloph and mesoloph; from *Saremmys* and

Scleromys/"*Scleromys*" in having an anterior arm of the hypoconid, which can be present on p4s and lower molars, and with a more curved posterolophid on lower molars; and from *Incamys*, *Saremmys*, and *Scleromys*/"*Scleromys*" in having a smaller size. *Saremmys* is documented by two dp4s at early stages of wear (MPEF-PV 11348b and 11349a in Fig 6A and 6B [132]). However, in our opinion, MPEF-PV 11348b would be a dP4 by the proportions between its mesial and distal parts, shape of its outline margin and a pentalophodont pattern closer to an occlusal morphology of a dP4 than dp4. Comparatively to MPEF-PV 11349a, dp4s from La Venta and TAR-31 show a metaconid postionned more distally and strongly connected to the protoconid by a thick second cristid, which corresponds to a metaconid cristid and/or a posterior arm of the protoconid. Unlike dP4s of *Microscleromys*, MPEF-PV 11348b has a hypocone compressed distolabially-mesiolingually. Moreover, MPEF-PV 11348b displays a more crestiform protocone. *Microscleromys* differs from *Garridomys* and *Drytomomys* in having a smaller size, an anterior arm of the hypoconid that can be present on p4s and lower molars, and a second transverse cristid usually more reduced, and a more curved posterolophid on lower molars; from *Garridomys* in having a homogeneous thickness of the enamel layer, thinner loph(-id)s, and strong and high protoconid and ectolophid on p4s; from "*Scleromys*" *colombianus* and *Drytomomys aequatorialis* in having a separation between the hypocone and the posteroloph, which is narrower and less persistent at early wear stages on upper molars [28, 29, 127, 135]; and from *Drytomomys* in having a less oblique hypolophid on lower molars. To sum up, the material from TAR-31 is closer to *Microscleromys*. After revison, we validate *Microscleromys paradoxalis* and*M*. *cribriphilus* described by Walton [37] from La Venta, and identify both species at TAR-31.

Microscleromys sp. 1
Fig 8D and 8E and S1 Table

Nom. *nud*. *Microscleromys* ?*paradoxalis* Walton, 1990, Fig 13E, 13D, p. 49.

Referred material

UNC unnumbered specimen, left P4 (Fig 8D); IGM-DU 85–411, left P4 (Fig 8E).

Localities

Locality unknown (for UNC unnumbered specimen) and CVP locality of the Fish Bed (for IGM-DU 85–411), La Venta Badlands, upper Magdalena Valley, Huila Department,

Colombia.

Formation and age

Baraya Member of the Villavieja Fm.; late middle Miocene (i.e., Laventan SALMA).

Description and comparison

UNC unnumbered specimen (Fig 8D) and IGM-DU 85–411 (Fig 8E) are two P4s at advanced states of wear. They have a morphology very similar to those of *Microscleromys paradoxalis* and*M*. *cribriphilus* characterised by a circular/oval outline, a taeniodont pattern, the reduction/absence of third crest and metaloph, and a hypoflexus lingually close due to a connection between the posterior outgrowth of the protocone and the hypocone. The latter structures, as well as the paracone, anteroloph, protocone, posteroloph and mesostyle (and metacone if present) are fused, and form a circular peripheral wall. The paracone is distally separate from this circular wall by a very thin furrow on UNC unnumbered specimen (Fig 8D), whereas both structures are slightly linked together on IGM-DU 85–411 (Fig 8E). The labial protoloph and the mure are mesiolabially oriented on IGM-DU 85–411 (Fig 8E). On UNC unnumbered specimen, the labial protoloph is transverse and the mure is longitudinal (i.e., parallel to the mesiodistal plan of the tooth; Fig 8D). On that tooth, the anterior arm of the hypocone is tiny, oblique, and links the mure to the hypocone. From the mesostyle area runs a short crest, corresponding to a mesoloph, which remains labially free on UNC unnumbered specimen (Fig 8D). On the two P4s, there is no apparent metaloph. In addition, IGM-DU 85–411 does not have any distinct mesoloph (Fig 8E). However, this tooth shows a more advanced stage of wear and a thick labial part of the posteroloph, which could encorporate a mesostyle, the metacone, and/or the rest of a mesoloph and/or metaloph. These two teeth differ from their counterparts in *M*. *paradoxalis* and*M*. *cribriphilus* in being clearly larger (S1 File). By their taeniodonty, complete and elevated mure, and the connection between the posterior outgrowth of the procone and hypocone, the pattern of these P4s recalls the morphology of P4s of certain stem-caviomorphs (*sensu* Boivin et al. [4]; such as *Cachiyacuy contamanensis*, *Cachiyacuy kummeli*, *Pozomys*, *Eoespina*, and *Tarapotomys*), the chinchilloid *Eoincamys parvus*, and some cavioids (*Australopracta*, *Luantus*, and *Neoreomys*) [6, 11, 16, 70, 81, 86, 101, 136, 137]. The material from La Venta differs from *Cachiyacuy*, *Pozomys*, *E*. *parvus* and *Tarapotomys* in having a larger size; from *C*. *contamanensis* and some P4s of *Tarapotomys subandinus* in having a more reduced third crest; from *C*. *kummeli* in having an anterior arm of the hypocone and third crest (when present) reduced to a mesoloph instead of a

mesolophule; from *Pozomys* in having a complete anteroloph; from *Australoprocta*, *Luantus initialis* and *L*. *propheticus* in having a slightly larger size; from *Australoprocta* in having no (or more reduced) metaloph; from *L*. *initialis* and *L*. *propheticus* in having a curved lingual edge of the hypocone; from *L*. *propheticus* in having a lower crown and a less quick closure of the lingual mesoflexus; from *Neoreomys* in having a lower crown, thinner crests, more expanded flexi, and a mesoloph not connected to the posteroloph. In summary, these two P4s from La Venta are clearly closer to those of *Microscleromys*. Their large size is not compatible with that of two species of the genus. Thus, we attribute them to *Microscleromys* sp. 1.

Microscleromys sp. 2
Fig 11 and Table 1

Referred material
MUSM 4658, left astragalus.

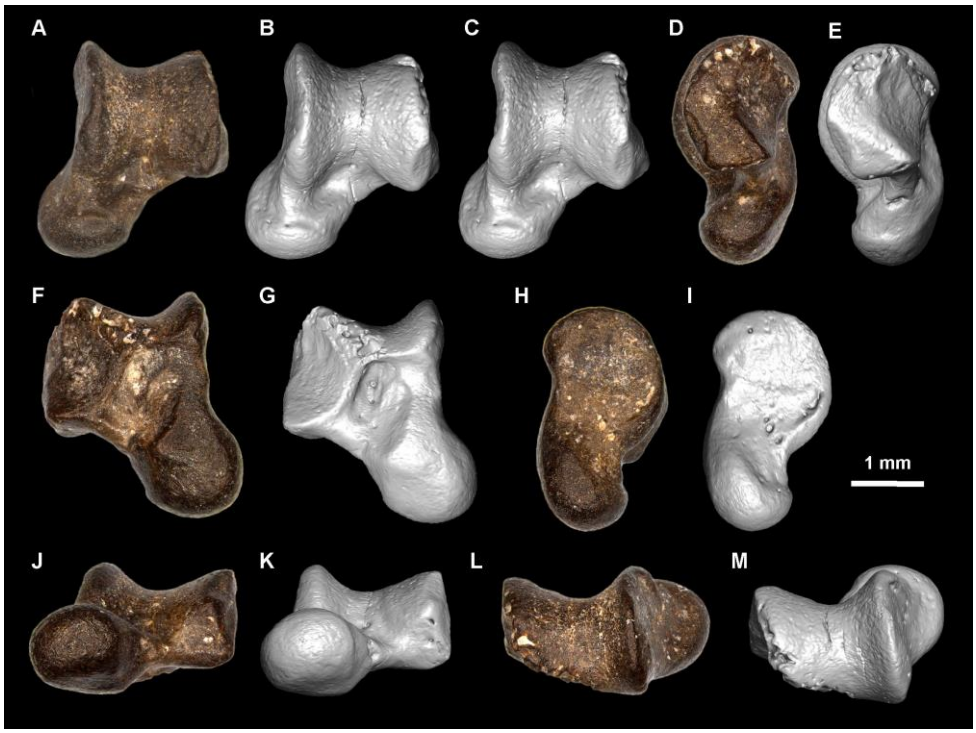


Fig 11. *Microscleromys* sp. 2 from TAR-31, Peru, MUSM 4658, left astragalus. (A-C) Dorsal, (D, E) lateral, (F, G) plantar, (H, I) medial, (J, K) distal, and (L, M) proximal views. (B, C) Stereomicroscopic views. The illustrations of the fossil specimen are the result of the fusion of numerical multi-focus images obtained with na optical stereomicroscope (A, D, F, H, J, and L) and 3D digital models obtained by X-ray μCT surface reconstruction (B-C, E, G, I, K, and M).

Locality

TAR-31, Tarapoto/Juan Guerra, Mayo River, Shapaja road, San Martín Department, Western Amazonia, Peru.

Formation and age

Lower member, Ipururo Fm., late middle Miocene (i.e., Laventan SALMA).

Description

MUSM 4658 from TAR-31 is a well preserved left astragalus (Fig 11). It is slightly damaged at the level of the lateral ridge of the trochlea (= lateral tibial and lateral fibular facets) and the ectal facet. In dorsal view, the astragalar body is slightly longer (proximodistally) than wide (lateromedially; Fig 11A–11C). The combined length of the neck and head is shorter than that of the trochlea. The latter is characterised by steep-sided lateral and medial margins (fibular facet and medial tibial facet, respectively). It is moderately grooved with slightly asymmetric internal facets. The internal lateral facet of the trochlea (= lateral tibial facet) is extensive and slopes gently, whereas the medial one is more inclined, taller, narrower, and barely longer (Fig 11A–11C and 11J–11M). No astragalar foramen (= superior astragalar foramen *sensu* Cifelli [138]) is evident. The neck is thick, short and very deflected medially (36.2˚; Fig 11A–11C). The head is rounded and bears a navicular facet wider than long. In medial view (Fig 11H and 11I), the navicular and medial tarsal facets are slightly proximally distinct, but distally continuous. The medial tarsal facet is particularly extensive proximally on the medial aspect of the neck (Fig 11H and 11I). In lateral and medial views, the rims of the trochlea are circular, with a moderate radius of curvature (Fig 11D, 11E, 11H and 11I). In medial view, seven large foramina are recognisable (Fig 11H and 11I). Three foramina are present distally to the área along which the tendons of *m*. *peroneus longus* and *brevis* slide and ventroproximally situated to the most distalmost rim of the medial ridge of the trochlea. They are ventroproximally aligned, the smallest foramen being the most proximal, whereas the largest is in the middle. There are three other foramina on the dorsodistal part of the area along which the tendons of *m*. *peroneus longus* and *brevis* slide, which are dorsoproximally aligned. The last foramen is located proximally to the area along which the tendons of *m*. *peroneus longus* and *brevis* slide. In plantar view (Fig 11F and 11G), the ectal (= calcaneo-astragalar) facet is oval and faintly curved (very slightly concave; i.e., high radius of curvature). Its distal part is not markedly projected laterally (i.e., absence of a protruding lateral process). It is clearly separated from the sustentacular facet by a deep and wide sulcus calcaneus, which is

oblique (proximomediallydistolaterally) and divergent distally. As the proximolateral side of the sustentacular facet is gently sloping, the sulcus appears particularly wide. Three main foramina are situated on the sulcus, the largest being the most proximal, close to the medial plantar tuberosity. It might correspond to the plantar astragalar foramen (= inferior astragalar foramen *sensu* Cifelli [138]). Another foramen is present at the base of the proximolateral slope of the sustentacular facet. This tuberosity is well marked. The sustentacular facet is triangular-shaped and with a major axis proximodistally oriented. It is well extended distally toward the head, and reaches the navicular facet. The distal extremity of the sustentacular facet is wide and concave, whereas its proximal one is narrower and convex. The sustentacular and ectal facets have similar dimensions (i.e., length and width). The navicular and medial tarsal facets are poorly distinct over their entire contact. In distal view (Fig 11J and 11K), two large foramina are present on the distal extremity of the lateral ridge of the trochlea.

Comparisons

The trochlea of MUSM 4658 is shorter than in *Euryzygomatomys*, narrower than in *Steiromys*, *Neoepiblema* and *Coendou*, and less grooved than in *Cavia*, *Dolichotis* and *Proechimys*. It has a lateral ridge narrower and less distally positioned than *Chinchilla* and *Dactylomys*, and wider (but somewhat sloping) than the medial one, a feature observed on astragali of several Other taxa (*Platypittamys*, *Drytomomys*, *Phoberomys*, *Abalosia*, *Actenomys*, *Dolicavia*, *Eucelophorus*, *Eumysops*, *Pithanotomys*, *Praectenomys*, *Dactylomys*, *Euryzygomatomys*, *Lagostomus*, *Proechimys*, and *Octodon*) and particularly accentuated on astragali of *Steiromys*, *Neoepiblema* and *Coendou*. The neck of MUSM 4658 is well differentiated from the body, and is strongly deflected medially as on astragali of *Steiromys*, *Drytomomys*, *Neoepiblema*, *Phoberomys*, *Abalosia*, *Eumysops*, *Coendou*, *Dactylomys*, *Euryzygomatomys*, *Myocastor* and *Proechimys*. Particularly, the deflection angle of MUSM 4658 is similar to that of astragali of *Abalosia*, *Eumysops*, *Myocastor* and *Proechimys* (35–37˚). Conversely, astragali of *Platypittamys*, *Neoreomys*, "*Scleromys*", *Actenomys*, *Dolicavia*, *Eucelophorus*, *Pithanotomys*, *Praectenomys*, *Cavia*, *Chinchilla*, *Clidomys*, *Ctenomys*, *Dinomys*, *Dolichotis*, *Galea*, *Lagostomus* and *Octodon* have their neck being clearly less or not deflected medially. On MUSM 4658, the head is rounded with the medial tarsal facet strongly developed on the medial aspect of the neck in dorsal view as on astragali of *Steiromys*, *Drytomomys*, *Actenomys*, *Eucelophorus*, *Eumysops*, *Pithanotomys*, *Coendou*, *Dactylomys*, *Octodon*, and *Proechimys*. MUSM 4658 displays an ectal facet narrower than that of astragali of *Neoepiblema*,

Actenomys and *Eumysops*; shorter than in *Pithanotomys*; narrower and longer than in *Coendou*. Contrary to the astragali of *Neoreomys*, "*Scleromys*" *colombianus*, *Drytomomys*, *Neoepiblema*, *Eumysops*, *Pithanotomys*, *Cavia*, *Chinchilla*, *Dinomys*, *Dolichotis*, *Galea*, *Myocastor*, *Octodon* and *Proechimys cuvieri*, there is no well marked lateral process of the ectal facet on MUSM 4658. The ectal facet is less concave than in *Steiromys*, *Neoepiblema*, *Pithanotomys*, *Cavia porcellus*, *Dolichotis* and *Galea*. Several taxa (*Steiromys*, "*Scleromys*", *Drytomomys*, *Neoepiblema*, *Phoberomys*, *Abalosia*, *Actenomys*, *Dolicavia*, *Eucelophorus*, *Eumysops*, *Pithanotomys*, *Cavia*, *Chinchilla*, *Dactylomys*, *Dinomys*, *Dolichotis*, *Euryzygomatomys*, *Galea*, *Lagostomus*, *Myocastor*, *Octodon*, and *Proechimys*) have a wide sulcus calcaneus distally divergent like on MUSM 4658, but none seem to have a similar configuration of this sulcus and the proximolateral side of the sustentacular facet, which is gently sloping. In addition, MUSM 4658 differs from astragali of all aforementioned taxa in having a particular triangular-shaped sustentacular facet; from *Steiromys*, *Neoepiblema*, *Coendou*, *Lagostomus*, and *Myocastor* in having a sustentacular facet oriented proximodistally; from *Dolicavia*, *Cavia*, *Chinchilla*, *Dolichotis*, *Euryzygomatomys*, *Galea* and *Myocastor* in having a sustentacular facet not strongly fused with the navicular facet and/or the medial tarsal facet of the neck; and from *Steiromys*, *Abalosia*, *Eumysops*, *Pithanotomys* and *Dactylomys* in having no clear separation between the sustentacular facet and the navicular and medial tarsal facets. At first order, the MUSM 4658 astragalus matches very small body-sized extant and fossil rodents. Regression of the body mass in function of trochlear width in living mammals [139] shows that MUSM 4658 belonged to a small rodent having a body mass of about 43 g (Table 2). The smallest body-sized species from TAR-31, *Ricardomys longidens*, *Microscleromys paradoxalis* and *M*. *cribriphilus*, could be the best candidates. Considering the least-squares regression equation of [140] based on the m1 area in mammals, the body mass of *R*. *longidens* is estimated to be ~40 g, that of*M*. *paradoxalis* to be ~51 g and that of*M*. *cribriphilus* to be ~21 g (Table 2). The values estimated with equation proposed by the same author for rodents are clearly higher (~132, ~161, and ~76 g; Table 2), which makes it difficult to conclude. Given that the dental material from TAR-31 referred to*M*. *cribriphilus* is more abundant than that of *R*. *longidens* and *M*. *paradoxalis*, referral of MUSM 4658 to*M*. *cribriphilus* could be a plausible taxonomic option. Nevertheless, as the size ranges of two co-occuring species of *Microscleromys* are overlapping, we prefer to keep it in open nomenclature as *Microscleromys* sp. 2.

Table 2. Metric feature of the MUSM 4658 astragalus (mm) and m1s (mm2) from TAR-31 and La Venta and body mass estimates (g).

Material	Trochlear Width (mm)	Mean area m1 (mm^2)	Dental locus used	N	Body mass estimates (g)	Regression equation for:	Reference
MUSM 4658	1.832			1	43.00	mammals	Tsubamoto, 2014
Microsteiromys jacobsi		7.51	m1	1	243.26	mammals	Legendre, 1986
					614.50	rodents	
Nuyuyomys chinqaska		4.36	m1	6	89.98	mammals	
					262.28	rodents	
Ricardomys longidens		2.82	m1?	2	40.49	mammals	
					132.40	rodents	
Microscleromys cribriphilus		1.97	m1?	34	21.15	mammals	
					75.94	rodents	
Microscleromys paradoxalis		3.19	m1*	2	50.90	mammals	
					161.06	rodents	
"*Scleromys*" sp.		14.67	m	2	826.65	mammals	
					1751.02	rodents	

* based on MUSM 4643 from TAR-31 and IGM unnumbered specimen from La Venta.

"*Scleromys*" Ameghino, 1887

"*Scleromys*" sp.

Fig 12 and S1 Table

Referred material

MUSM 4277, left dp4; MUSM 4278, 4279, right fragmentary dp4s; MUSM 4280, left p4; MUSM 4281, 4282, right lower molars; MUSM 4270–4272, left fragmentary upper molars; MUSM 4273, 4274, left upper molars; MUSM 4275, 4276 right upper molars.

Locality

TAR-31, Tarapoto/Juan Guerra, Mayo River, Shapaja road, San Martı´n Department, Western Amazonia, Peru.

Formation and age

Lower member, Ipururo Fm., late middle Miocene (i.e., Laventan SALMA).

Description

MUSM 4278 is a distal fragment of dp4 preserving only the posterolophid, the hypoconid, its anterior outgrowth, and the distal margin of the ectolophid, hypolophid, and of the entoconid. MUSM 4279 is a mesial fragment of dp4, broken at the level of the ectolophids, the hypolophid and the entoconid (Fig 12C). This tooth also shows several damaged areas, especially at the level of the protoconid and the distal part of

the metalophulid I. MUSM 4277 (Fig 12A) is a complete dp4 at a more advanced wear stage than MUSM 4278 and 4279. These three brachydont dp4s are characterised by thick lophids. MUSM 4277 is pentalophodont, probably like MUSM 4279. Despite its degree of wear, MUSM 4279 seemingly displays bulbous lingual cuspids. On this tooth, the metalophulid I is mesially convex and shows a mesiodistal thickening at its centre. The metaconid and protoconid are distally linked by a second cristid, mesially concave, corresponding to a posterior arm of the protoconid and/or a metaconid cristid. The metalophulid I, the second cristid, the metaconid and protoconid delimit a C-shaped anterofossettid. The mesostylid is large and displays a short and strong neomesolophid mesiolabially directed and lingually free. The mesostylid is well separated from the metaconid and entoconid. This cuspid is higher than the mesostylid and metaconid. The hypolophid, distal ectolophid and mesial ectolophid are fused, and form a long cristid stemming from the entoconid and directed toward the protoconid, but without connection to it. This cristid is mesiolabially oriented, but its labial part is more longitudinal than its lingual part. The labial extremity of the neomesolophid is close to the mesial margin of the cristid combining the hypolophid and ectolophids. MUSM 4277 (Fig 12A) shows a similar pattern to that of MUSM 4279 (Fig 12C), but with features deriving from a more advanced stage of wear: loss of relief, lingual closure of the mesial mesoflexid and metaflexid, lingual and labial closure of the distal mesoflexid, and reduction of the anterofossettid and of the mesial mesofossettid to two small and circular fossettids. MUSM 4279 displays a heterogeneous thickness of the enamel layer, which is thicker on the trailing edges and thinner on the leading edges. On MUSM 4277 and 4278, the distalmost cristid (posterolophid + hypoconid + its anterior outgrowth) is curved and there is no anterior arm of the hypoconid, thereby involving the confluence of the metaflexid with the hypoflexid (i.e., taeniodont pattern). The MUSM 4280 p4 (Fig 12E) is slightly damaged at the level of the protoconid, the hypoconid and its anterior outgrowth. MUSM 4280 is hypsodont (Hling = 1.13; Hlab = 1.52; Fig 12F and 12G). Compared to dp4s, MUSM 4280 is tetralophodont, more square-shaped, and with a trigonid clearly narrower than the talonid. The cuspids are crestiform and faintly differentiated from the lophids. On the lingual margin, the metaconid and mesostylid are equally sized and separated by the anterostriid. The metaconid is connected to a metalophulid I, which is very slightly concave and labially free. This crest corresponds to an anterior arm of the metaconid, the anterior arm of the protoconid being absent. Its labial extremity is thin and separated from the protoconid by a narrow and deep furrow, which forms a striid. The second transverse

cristid is reduced to a short neomesolophid stemming from the mesostylid. The neomesolophid is mesiolabially directed and labially free. The protoconid is fused with the ectolophid, forming a cristid distolingually oriented. The hypolophid is parallel to the neomesolophid and in continuity of the cristid composed of the protoconid + ectolophid (but the latter being more longitudinal). The hypoconid has no anterior arm (i.e., taeniodont pattern) and it is not distinct from its anterior outgrowth and the posterolophid. The main direction of the posterolophid is the same that those of the neomesolophid and hypolophid. The flexids are furrow-shaped and form striids. On the labial margin, the hypostriid is deep, but ends far from the neck of the crow. On the lingual margin, the anterostriid and mesostriid have a similar depth, which represents more than the double that of the short metastriid. As for p4, the lower molars, MUSM 4281 and 4282, are high crowned (but retaining roots), tetralophodont and taeniodont, with deep furrow-shaped flexids, forming striids, dental structures that fused with wear, forming thick and oblique cristids, and a second transverse cristid reduced to a neomesolophid (Fig 12B and 12D). Contrary to the MUSM 4280 p4, their trigonid and talonid are equally wide. They present a more advanced stage of wear with respect to MUSM 4280: their crown is lower (Hling = 0.82–0.83; Hlab = 0.82–1.19) and their lingual flexids are closed except the metaflexid on MUSM 4281. The metalophulid I is complete on both molars. On MUSM 4281 (Fig 12B), the neomesolophid is very short and labially free. Consequently, the Y-shaped anterior fossettid corresponds to the confluence between the anteroflexid with the mesoflexid. Conversely, on MUSM 4282 (Fig 12D), the neomesolophid is longer and labially connected to the metalophulid I, thereby delimiting a small and circular anterofossettid. Like on MUSM 4280, the hypolophid, ectolophid and protoconid are in continuity, forming a central cristid. The latter is straight and oblique (i.e., mesiolabially directed) on MUSM 4281. On MUSM 4282, its labial part is mesiolabially directed, while the hypolophid is more transverse. Due to the closure of the anteroflexid and mesoflexus on MUSM 4281 and 4282, the trigonid is delimited by a triangular-shaped structure formed by the metalophulid I, metaconid, mesostylid, entoconid, hypolophid, ectolophid and protoconid. This triangularshaped structure is separate from the distalmost cristid by a very thin furrow-shaped flexid (i.e., confluence of the metaflexid with the hypoflexid). The distalmost cristid, formed by the fusion of the posterolophid, hypoconid and its anterior outgrouwth, is mesially concave. The thickness of the enamel layer is homogenous on MUSM 4282 (Fig 12D). MUSM 4281 displays a homogenous thickness of the enamel layer at the level of the metaflexid but a heterogeneous one (thicker on the trailing

edges and thinner on the leading edges) at the level of its mesial and distal margins and those of the hypoflexid (Fig 12B). The hypostriid has a height similar to that of the MUSM 4280 p4. Upper molars have an occlusal pattern similar to that characterising p4 and lower molars (i.e., tetralophodonty, taeniodonty, deep furrow-shaped flexi, forming stria, and dental structures merging with wear, forming thick and oblique crests), which can contribute to confuse them. They show a unilateral hypsodonty characterised by a lingual crown higher that the labial one (Hling = 1.00–1.69; Hlab = 0.51–0.92), whereas the distolabial crown is the highest part of crown on p4 and lower molars. Upper molars are labiolingually wider than lower molars. Upper molars have three roots: a large lingual one and two small labial ones. The mesial margin of the crown is formed by a curved crest, which corresponds to the fusion of the anteroloph, protocone and its posterior outgrowth. On all complete upper molars, this crest is labially connected to the paracone. The labial protoloph is roughly transverse or slightly oblique and in continuity with the mure and anterior arm of the hypocone, which are more distolingually directed. The mesostyle is faintly isolated from the metacone on MUSM 4273 (Fig 12H). On the other upper molars, it is slightly (MUSM 4270 and 4272; Fig 12J) or strongly (MUSM 4274–4276; Fig 12I and 12K) connected to the this cusp and to the paracone. As for the second transverse cristid on p4 and lower molars, the third transverse crest is reduced to a mesoloph stemming from the mesostyle, either lingually free (MUSM 4270 and 4272) or connected to the posteroloph (MUSM 4273 and 4275; Fig 12H and 12I). On MUSM 4272 (Fig 12J), the posteroloph presents, on its mesial margin, a very short crestule (i.e., posteroloph spur), mesially free. On MUSM 4273 (Fig 12H) and 4275 (Fig 12I), the mesoloph and posteroloph (+ posteroloph spur?) delimit a small and circular fossette. On upper molars at a more advanced stage of wear (MUSM 4274 and 4276; Fig 12K), the small posterior fossette disappears due to the fusion between the mesoloph, mesostyle and posteroloph (+ posteroloph spur?). On MUSM 4270 and 4272 (Fig 12J), a tiny notch separtes the hypocone from the posteroloph. On the other upper molars, which show a more advanced stage of wear, the hypocone is strongly linked to the posteroloph. On the most worn upper molar, MUSM 4274, the two remaining flexi (the mesialmost) are fully closed and divided into two parts. Most upper molars (MUSM 4270, 4272 and 4274–4276; Fig 12J, 12I and 12K) display a homogenous thickness of the enamel layer, while MUSM 4273 (Fig 12H) has a slight heterogeneous thickness of the enamel layer (thicker on the trailing edges and thinner on the leading edges) at the level of its mesial and distal margins, and the mesial and distal margins of the anterior flexus.

Comparisons

These large dental specimens from TAR-31 described here show typical chinchilloid affinities, notably characters documenting *Scleromys*/"*Scleromys*": (i) medium-sized and protohypsodont teeth, (ii) taeniodonty, (iii) dental structures merging with wear, forming thick and oblique crests/cristids, (iv) deep furrow-shaped flexi(-ds), forming striia/striids, (v) upper molars tetralophodont at early stages of wear, becoming trilophodont at more advanced stages of wear, (vi) a metaflexid as being the most persistent lingual flexid on lower teeth, and (vii) an enamel layer with a thickness homogeneous or slightly heterogeneous (i.e., insinuated heterogeneous thickness *sensu* Kramarz, Vucetich & Arnal [127]; see also [128]). The dental remains from TAR-31 are similar in size to those from La Venta (Colombia; late middle Miocene) attributed to either "*Scleromys*" *schurmanni* Stehlin, 1940 [18, 27, 28] or "*Scleromys*" cf. *schurmanni* [18]. By its short and labially-free metalophulid I and neomesolophid, the pattern of the MUSM 4280 p4 is particularly close to that of the p4 borne on the IGM 184233 specimen from La Venta attributed to "*Scleromys*" cf. *schurmanni* (Fig 24.3E, p. 397 [18]). However, it differs from the latter in having no mesiolingual protuberance of crown, and in showing separated metaconid and mesostylid. As for the material from TAR-31, the lower molars of "*Scleromys*" cf. *schurmanni* from La Venta can have a neomesolophid labially free or connected to the metalophulid I. The figured p4 of "*Scleromys*" *schurmanni*, also from La Venta (UCMP 38967 in Fig 24.3D, p. 397 [18]), has a complete second transverse cristid composed of a neomesolophid and a shorter posterior arm of the protoconid, contrary to MUSM 4280. The p4s of "*Scleromys*" *schurmanni* described by Field [28] show a complete second transverse cristid as well (UCMP 38987 in Figs 4A and 5D, p. 285 [28]) or a second cristid reduced to a neomesolophid linked to the metalophulid I (UCMP 37931 in Figs 4D and 5C, p. 285 [28]). The dp4s of "*S*". *schurmanni* (UCMP 39902 and 38974 in Fig 5A and 5B, p. 285 [28]) seem to be hexalophodont, having more anterior flexids than on dp4s from TAR-31. The TAR-31 teeth are smaller than those of *S*. *quadrangulatus* (Pinturas Fm., Argentina; late early Miocene) [133], *S*. *angustus* (Santa Cruz Fm., Argentina; late early Miocene) [73] and *S*. *osbornianus* (Pinturas and Santa Cruz Fm.; late early Miocene) [118, 133]. Comparatively to *S*. *quadrangulatus*, teeth from TAR-31 have a slender closure of the flexi(-ds), a longer metalophulid I on p4, and a paracone area smaller on upper molars at early stages of wear. The MUSM 4280 p4 has a lingual margin more parallel to the mesiodistal axis of the tooth than p4s of *S*. *quadrangulatus*

and *S*. *angustus*. In addition, MUSM 4280 has a neomesolophid, contrary to those species of *Scleromys*. At early stages of wear, molars of *S*. *angustus* and *S*. *osbornianus* display a trilophodont pattern [73, 133], contrary to molars from TAR-31, which remain tetralophodont. The dp4s from TAR-31 share a similar pattern in terms of number, types and morphology of the main cristids with the two dp4s from Madre de Dios, Peru: dp4 referred to *S*. *quadrangulatus* (MD-61, early Miocene) [141] and dp4 referred to "*Scleromys*" sp., gr. *quadrangulatus-schurmanni-colombianus* (MD-67, early middle Miocene) [31]. Nevertheless, they have a metalophulid I connected to the metaconid and protoconid, contrary to dp4s from MD-61 and -67. Unlike dp4s from TAR-31, dp4s from MD-61 and -67 have supernumerary structures on the anteroflexid: a cuspid-shaped structure on the dp4 from MD-67, and a low cristulid connected to the lingual and labial extremity of the metalophulid I on the dp4 from MD-61. The dp4s from TAR-31 display more opened lingual flexids than the dp4 from MD-61. They show Other distinctive characters with respect to the dp4 from MD-67: a metaconid isolated from the mesostylid, and a second cristid and a hypolophid-ectolophid cristid, which are more curved. "*Scleromys*" *colombianus* and *Drytomomys aequatorialis*, both from La Venta (and from Nabo´n region, Ecuador, for *D*. *aequatorialis*; late middle Miocene) [28, 29, 135] are recognisable in having larger-sized teeth and a separation between the hypocone and the posteroloph, wider and more persistent at early stages of wear on upper molars, than on the TAR-31 material. The material from TAR-31 differs from "*S*." *colombianus* [18, 28] and "*Scleromys*" cf. *colombianus* [18] in having p4s with a transverse mesial margin and a shorter neomesolophid labially free, and upper molars with a more persistent posterior fossette. It differs from *Drytomomys* in having a quicker reduction of the anterofossettid on lower molars; from *D*. *aequatorialis* in having shorter neomesolophid on p4s; from *D*. *typicus* (Ituzaingo Fm., Argentina; late Miocene) [29, 106] in having different morphology of dp4s with a third cristid reduced to a short neomesolophid and without neolophid on the anterofossettid. Comparatively to MUSM 4280, "*Drytomomys*" sp. (small) and "*Drytomomys*" sp. (large) from La Venta ("*Olenopsis*" sp. *sensu* Walton [18], but see [29]) show a longer neomesolophid labially connected to the metalophulid I on p4s. Moreover, p4s of "*Drytomomys*" sp. (large) are pentalophodont with a short metaconid cristid, contrary to MUSM 4280. The moderate size, marked hypsodonty and thickness of the crests of these teeth from TAR-31 exclude affinities with *Eoincamys* (Brazil and Peru; ?late Eocene–early Oligocene) [8, 19, 70, 81], *Microscleromys* (La Venta, TAR-31; this study) [18] and with the octodontoid *Protadelphomys* (Sarmiento Fm., Argentina; early Miocene) [142–144].

They are also too high-crowned and slightly larger for *Maquiamys* (CTA-61, Peru; late Oligocene) [4, 71]. To sum up, the material from TAR-31 has the closest affinities with the specimens of "*Scleromys*" found in northern South America (La Venta, Colombia and MD-61 and MD-67, Peru). As it would be necessary to deeply revise *Scleromys* and notably the northern forms (recognized as "*Scleromys*" [18, 71]), we prefer keeping the material from TAR-31 in open nomenclature as "*Scleromys*" sp.

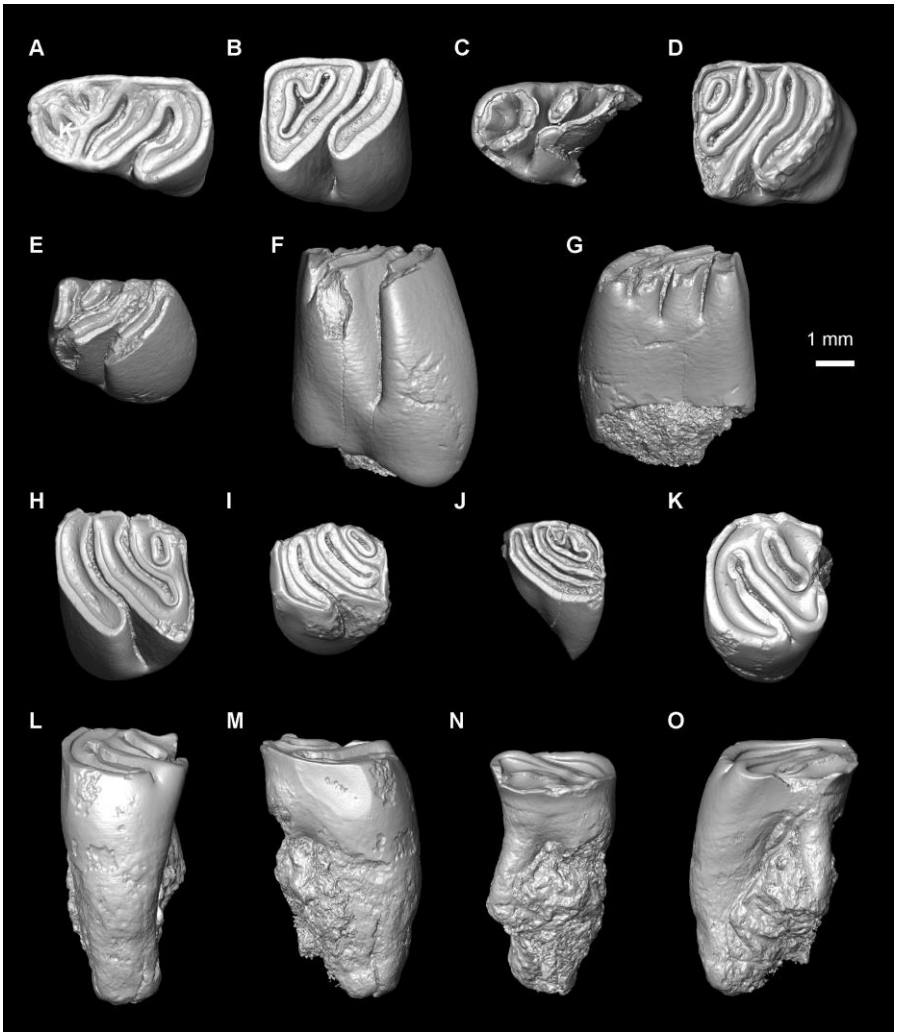


Fig 12. *"Scleromys*" sp. indet. from TAR-31, Peru. (A) MUSM 4277, left dp4. (B) MUSM 4281, right lower molar (reversed). (C) MUSM 4279, fragment of right dp4 (reversed). (D) MUSM 4282, right lower molar (reversed). (E–G) MUSM 4280, left p4. (H) MUSM 4273, left upper molar. (I) MUSM 4275, right upper molar (reversed). (J) MUSM 4272, left upper molar. (K–O) MUSM 4276, right upper molar (reversed). (A-E, H-K) Occlusal, (F, N) labial, (G, L) lingual, (M) anterior, and (O) posterior views. The illustrations of the fossil specimens are 3D digital models obtained by X-ray μCT surface reconstruction.

Discussion

The caviomorph fauna from La Venta: Revision and validation of Walton's *nomina nuda*

Microsteiromys jacobsi, *Ricardomys longidens*, *Microscleromys paradoxalis* and *Microscleromys cribriphilus*, originally described in La Venta in the framework of the Anne H. Walton's Ph.D [37], have remained *nomina nuda* given that they were not formally described so far. According to the International Code of Zoological Nomenclature (p. 246 [38]), a *nomen nudum* is not available but the same name can be made available subsequently for the same concept or for a different concept, in a way meeting the criteria of availability (chapter 4 [38]). Our revision of the original material of these species, combined with the study of the new specimens from TAR-31, allowed us to validate all the concerned taxa. It is worth noting that we have usually not followed the unpublished diagnoses proposed by Walton [37]. In the case of *Microscleromys*, a classical descriptive and comparative approach combined with statistical analyses on dental dimensions (length and width; S1 File) allowed us to test the taxonomic groups proposed by Walton [18, 37]. Our results (i.e., statistical differences) suggest an inappropriate taxonomic delimitation of these potential groups (S1 File). Thus, we propose a new delimitation of the two *Microscleromys* species implying changes in the assignation of some specimens (i.e., from *M*. *cribriphilus* to*M*. *paradoxalis*, and vice versa). In addition, we revised the suprageneric status of this taxon, which was previously assigned to the cavioid family Dasyproctidae [18, 37]. Like *Microscleromys*, other fossil taxa such as *Eoincamys*, *Incamys* and *Scleromys*, were previously attributed to the dasyproctids [81, 130, 131]. However, *Eoincamys*, *Incamys* and *Scleromys* have then been related to the superfamily Chinchilloidea [70, 114, 133]. As noted by Walton [18], *Microscleromys* shows an occlusal pattern similar to *Scleromys*, as well as to chinchilloids in general (i.e., high-crowned teeth with a taeniodont pattern and oblique loph [-id]s, the absence of the second transverse cristid or its reduction on lower molars, and the absence of the metaloph and third transverse crest, or the reduction of the latter to notably a mesoloph on upper molars). According to the recent phylogenetic analyses of Boivin et al. [4], the phylogenetic position of *Microscleromys*, but also those of *Eoincamys*, *Incamys* and *Scleromys* were retrieved as stem representatives of Chinchilloidea (but see [127, 145, 146]). Finally, as noted by Walton [18, 37], *Ricardomys* shows an occlusal morphology similar to *Adelphomys* and other adelphomyine octodontoids. Here, we assign it to the family Adelphomyidae, following the results of Boivin et al. [4].

The caviomorph assemblage from TAR-31

In being restricted to a single 5–20 cm-thick channelised lens in a very small area (~5 square metres in one piece), TAR-31 records a single attritional accumulation [36], which strongly contrasts with La Venta and Fitzcarrald local faunas (several levels from distinct outcrops spanning a long or short interval, respectively) [26, 33]. Nevertheless, TAR-31 yields a total of nine rodent taxa, with the co-occurrence of the four extant superfamilies: Erethizontoidea (three taxa), Cavioidea (one taxon), Octodontoidea (two taxa) and Chinchilloidea (three taxa). Compared with other Laventan caviomorph assemblages from low latitudes of South America, TAR-31 ranks second just in front to the fauna from Fitzcarrald Arch (eight taxa) [32, 33], but far from La Venta, which includes 28 taxa (21 excluding the indeterminate genera and specie; La Victoria and Villavieja formations, Colombia; see [18, 28] and this work). Like TAR-31, the faunas from La Venta and Fitzcarrald Arch, as well as that from MD-67 (Madre de Dios; similar outcrop conditions as in TAR-31) [31], show representatives of the four caviomorph superfamilies. Without considering the validation of the *nomina nuda* from La Venta, TAR-31 records a new erethizontoid (*Nuyuyomys chinqaska* gen. et sp. nov.) and perhaps a new stemcaviid, here described as Caviidae gen. et sp. indet. (see Systematic Palaeontology section). The single specimen assigned to this taxon does not allow for its formal description as a new species. TAR-31 shares two taxa or closely related taxa with MD-67 ("*Scleromys*" sp. and *Nuyuyomys chinqaska*) and one with the assemblages from Fitzcarrald local fauna and La Victoria Fm. of La Venta ("*Scleromys*"). TAR-31 shares with the Villavieja Fm. of La Venta a representative of "*Scleromys*", as well as three species only recorded in La Venta so far: *Microscleromys paradoxalis*,*M*. *cribriphilus* and *Ricardomys longidens*. In striking contrast, there is no taxon in common between TAR-31 and most middle Miocene assemblages at mid- and high latitudes in South America (Argentina, Bolivia; Chile) [10, 30, 51, 87, 105, 123, 126, 147–152]. The Only assemblage showing similarities with TAR-31 is that from the Marino Fm. (Divisadero Largo area, Mendoza, Argentina) [153], in yielding *Scleromys* sp. Nevertheless, *Scleromys* (and "*Scleromys*") had a wide geographic (Argentina, Brazil, Chile, Colombia, and Peru) and a long stratigraphical range (late Oligocene–late middle Miocene) [15–19, 27, 28, 31, 33, 34, 73, 133, 141, 154]. Moreover, some doubts were expressed about the cogeneric afinities between *Scleromys* spp. from northern *versus* southern South America [18, 71].

Astragalus of *Microscleromys* from TAR-31: Morpho-functional implications

The trochlea of MUSM 4658 does not have a mediolateral widening nor a high degree of asymmetry between its medial and lateral rims, thereby suggesting that parasagittal movements would be more favoured during plantar- or dorsi- flexion of the foot [57, 61, 155]. The trochlea is however moderately grooved with shallower and less sharp crests than those of astragali of cursorial-jumping taxa in which lateral movements are strongly restricted (cavioids: *Cavia*, *Dasyprocta*, *Dolichotis*, *Galea*) [61]. The ectal facet is long with a high radius of curvature and not projected laterally, which would give proximodistal and mediolateral mobility with the calcaneus (astragalo-calcaneal joint = sub-astragalar joint) [57]. The narrowing and the proximodistal orientation of the sustentacular facet (here long reaching the navicular facet) would indicate parasagittal movements at the astragalo-calcaneal joint, limiting the inversion of the foot [57, 61]. In addition, the sulcus calcaneus is particularly wide, thereby suggesting the presence of a strong ligament linked to the dorsal side of the calcaneus [57]. This character is found in numerous caviomorphs, but associated with a proximodistal sustentacular facet, it would confer more resistance of the ankle by limiting the general mobility of the foot with respect to the leg [156, 157]. The neck is long and medially deflected with a medial tarsal facet on its dorsal and medial aspects, and a round head, characters typically found in arboreal taxa such as *Coendou* or *Sciurus*, but also in some terrestrial echimyids (*Proechimys*) [57, 61]. In addition to the increase of the articular surface of the sustentacular facet with the calcaneus [57], these featurs would therefore be facilitated lateral and rotator movements of the foot at the astragalo-navicular joint and at the contact between the astragalus and the medial tarsal bone (= first sesamoid) [61, 155]. Moreover, the extension of the medial tarsal facet on the neck would permit to stabilize the astragalus during inversion of the foot [57, 155, 158]. In summary, MUSM 4658 shows an intermediary morphology between morphotypes of the cursorial-jumping and climbing locomotory groups recognised by Ginot et al. [57]. Some of its characters (i.e., ectal facet slightly concave and not projected laterally, neck medially deflected, round head, medial tarsal facet extended on the dorsal and medial aspects of the neck) would enhance mediolateral movements particularly at the level of the distal joints with the navicular and medial tarsal bone, whereas others (i.e., moderately groveed and slightly asymmetric trochlea with no mediolateral widening, narrowing and the proximodistal orientation of the sustentacular facet, wide sulcus calcaneus) would tend to favor parasagittal

movements especially of the astragalo-tibial joint (= cruro-astragalar joint). Such an astragalar morphology matches that of terrestrial generalists with a possible higher trend toward arboreal locomotion.

Age of TAR-31 and biostratigraphical implications

The caviomorph fauna from TAR-31 shares four taxa with the assemblage characterising the lower part of the Villavieja Fm. at La Venta (see above). Similar affinities are observed on their non-rodent mammalian content (e.g., *Miocochilius anomopodus*, *Neosaimiri fieldsi* and *Megadolodus molariformis*; Fig 29.5, p. 508 [26]; see also [36] and the section Material and methods of this paper). An age ranging between 13.18–12.47 Ma can therefore be hypothesised for TAR-31, corresponding with the timespan of the magnetostratigraphically-constrained lower part of the Villavieja Fm. (C5AAn–C5AR.1R chrons) [26, 49]. The MUSM 4283 p4 of Caviidae gen. et sp. indet. from TAR-31 is particular in having more primitive characters (i.e., protohypsodonty, presence of flexids/fossettids, and a hypoflexid not reaching the lingual margin of the tooth) than the caviids found in other caviomorph faunas at low latitudes of South America from Laventan deposits such as *Prodolichotis pridiana* (La Venta and Fitzcarrald Arch), Dolichotinae gen. 2 large and Dolichotinae gen. 2 small (La Venta), and *Guiomys* sp. (MD-67) [18, 31, 33] or from sligthly younger deposits (Mayoan SALMA; CTA-44 Top, CTA-43) [34]. Similarly, it differs from middle Miocene caviids from southern South America (*Cardiomys*? *andinus*, *Cardiomys*? *buemulensis*, *Eocardia robusta*, *Eocardia robertoi*, *Guiomys unica*, *Microcardiodon huemulensis* and *Microcardiodon williensis*) [51, 87, 105]; in having of flexids/fossettids, and a hypoflexid, which does not reach the lingual margin of the tooth, characters otherwise found only in early Miocene stem-caviids such as *Chubutomys* or *Luantus* [52, 101, 103]. Thus, the discovery of a tooth with such characters suggests that this kind of morphotype may have subsisted until the late middle Miocene, at least in some representatives of the superfamily at low latitudes of the continent. Occurring in both MD-67 and TAR-31 localities, *Nuyuyomys chinqaska* likely spans the entire middle Miocene interval.

Palaeobiogeographical implications

The Miocene epoch is marked by important environmental changes, particularly in low-latitude regions of South America [159]. During the latest Oligocene–early Miocene interval, Andean deformations are generalised, in particular by the Eastern

Cordillera of the Northern and Central Andes (beginning of the “Quechua phase” as defined by Steinmann [160]; [161–165]). However, the Eastern Cordillera of Northern Andes had not reached its full elevation at that time, with a major uplift episode during late Miocene–Pliocene times [166–168]. In relation with the uplift of this region, the Solimoes Basin in Brazil is occupied by swamps and shallow lakes [169–173]. These bodies of water belonged to a vast wet system (mega-wetland), which also covered the Andean foreland retroarc basins in Peru and Colombia, and had a north connection with the Caribbean Sea [174]. This system reaches its maximal extension from ~16.0 to 11.3 Ma and forms the Pebas System, which corresponds to a dynamic mosaic of swampy, lake, fluvial and fluvio-marine environments [174, 175]. With our results, the geographical ranges of *Ricardomys longidens*, *Microscleromys paradoxalis* and *M. cribriphilus* are now extended southerly to Peruvian Amazonia for the Laventan interval. More generally, strong taxonomic affinities between the vertebrate assemblages of La Venta (Colombia) and Fitzcarrald, Madre de Dios (MD-67), Iquitos, Contamana, and TAR-31 in Peruvian Amazonia support the existence of a single “Pebasian” biome throughout the middle–earliest late Miocene, and more specifically during the Laventan SALMA, as shown by their terrestrial and aquatic components (crocodylomorphs, chelonians, marsupials, rodents, primates, notoungulates, astrapotheres, litopterns, sirenians, and/or cetaceans; [21, 26, 31–34, 36, 176–178] and see this work). These moderate or strong faunal similarities suggest that the Eastern Cordillera of the North Andes and Pebas System would have not constituted barriers for mammalian dispersals during this interval at least for a region close to the Andes (Western Corridor) [36, 44].

Conclusions

The TAR-31 locality in Tarapoto area, Peru, documents nine caviomorph taxa encompassing all four living superfamilies. This assemblage encompasses: *Microsteiromys jacobsi* gen. et sp. nov., *Nuyuyomys chinqaska* gen. et sp. nov., Erethizontoidea gen. et sp. indet. 1 and 2 (Erethizontoidea), Caviidae gen. et sp. indet. (Cavioidea), *Ricardomys longidens* gen. et sp. nov. and Octodontoidea gen. et sp. indet. (Octodontoidea), plus *Microscleromys paradoxalis* gen. et sp. nov.,*M. cribriphilus* gen. et sp. nov., and “*Scleromys*” sp. (Chinchilloidea). The study of na astragalus suggests that at least a representative of *Microscleromys* was a terrestrial generalista rodent. Although very restricted in terms of area (5 square meters) and volume investigated (~550 kg wet-screened) with respect to other assemblages, this

locality yields the most diverse Middle Miocene caviomorph fauna recorded in Western Amazonia. In addition, it is the second most diverse for this time window in low-latitude regions of South America, well after La Venta. The geographical range of *Ricardomys longidens*, *Microscleromys paradoxalis* and*M*. *Cribriphilus* is now expanded 1,100 km to the south, during the Laventan SALMA, as a further testimony of the extent of the Pebasian biome at those times.

Acknowledgments

Many thanks to M. Roddaz (GET, Toulouse, France), M.A. Custódio and R. Ventura (GEOCRON/IG, Brasília, Brazil) and whoever helped us in the field and in the lab. We are particularly grateful to our drivers Giancarlo and Manuel, for their long standing help during the yearly field seasons. We warmly thank M.R. Ruiz-Monachesi (IBIGEO, Salta, Argentina) for discussing on statistics, his relevant suggestions and aid with respect to the Bayesian models and the osteological preparation of the *Galea*. We are much indebted to M.C. Madozzo-Jaén (Lillo, San Miguel de Tucuma´n, Argentina) and to M.E. Pe´rez (MEF, Trelew, Argentina) for discussing on phylogeny and homology of dental structures in cavioids. Many thanks to A. A. lvarez and M.D. Ercoli (INECOA, San Salvador de Jujuy, Argentina) for providing us fotos of collection material for dental comparisons. Christine Argot (MNHN, Paris, France), M. Reguero (MLP, La Plata, Argentina), L. Chornogubsky and A.G. Kramarz (MACN, Buenos Aires, Argentina), and M. Taglioretti (MMP, Mar del Plata, Argentina) kindly granted access to the collections under their care. We are much indebted to M. Gómez Pérez, the team of Museo Geológico Nacional—Servicio Geológico Colombiano and J.D. Carrillo (MNHN) for the correspondance between the field numbers and the collection numbers for the material from La Venta. We warmly thank B. Rondeau and L. Lena (LPG, Nantes, France) for access to a Keyence Digital Microscope facility; C. Cazeveille (Institut des Neurosciences de Montpellier [INM], France) for access to a electron microscope scanning facility; and A.-L. Charruault and R. Lebrun (ISEM, Montpellier, France) for µCT scan acquisitions and treatments. We thank the MRI and the LabEx CeMEB for access to the electron microscope and µCT scanning facilities (ISEM, Montpellier). We are indebted to A.-L. Charruault (ISEM, Montpellier, France) for the cast preparation of the rodent material from TAR-31. We gratefully thank the E. Beucler and O. Bourgeois (LPG, Nantes, France) in order to have allowed MB realizing a journey in Montpellier. This is ISEM publication 2021-225-Sud.

Author Contributions

Conceptualization: Myriam Boivin, Laurent Marivaux, Pierre-Olivier Antoine.

Formal analysis: Myriam Boivin.

Funding acquisition: Myriam Boivin, Laurent Marivaux, Franc¸ois Pujos, Pierre-Olivier Antoine.

Investigation: Myriam Boivin, Laurent Marivaux, Walter Aguirre-Diaz, Aldo Benites-Palomino, Guillaume Billet, Franc¸ois Pujos, Rodolfo Salas-Gismondi, Narla S. Stutz, Julia V. Tejada-Lara, Rafael M. Varas-Malca, Anne H. Walton, Pierre-Olivier Antoine.

Methodology: Myriam Boivin.

Resources: Laurent Marivaux, Pierre-Olivier Antoine.

Visualization: Myriam Boivin, Laurent Marivaux, Narla S. Stutz.

Writing – original draft: Myriam Boivin.

Writing – review & editing: Myriam Boivin, Laurent Marivaux, Guillaume Billet, Narla S. Stutz, Julia V. Tejada-Lara, Anne H. Walton, Pierre-Olivier Antoine.

References

1. Patton JL, Pardiñas UF, D'Elía G. Mammals of South America. Vol. 2: Rodents. 1st ed. Chicago: University of Chicago Press; 2015.

2. Opazo JC. A molecular timescale for caviomorph rodents (Mammalia, Hystricognathi). Mol Phylogenet Evol 2005; 37: 932–937. https://doi.org/10.1016/j.ympev.2005.05.002 PMID: 16085429

3. Huchon D, Chevret P, Jordan U, Kilpatrick CW, Ranwez V, Jenkins PD, et al. Multiple molecular evidences for a living mammalian fossil. Proc Natl Acad Sci USA. 2007; 104: 7495–7499. https://doi.org/10.1073/pnas.0701289104 PMID: 17452635

4. Boivin M, Marivaux L, Antoine P-O. L'apport du registre paléogène d'Amazonie sur la diversification initiale des Caviomorpha (Hystricognathi, Rodentia): implications phylogénétiques, macroévolutives et paléobiogéographiques. Geodiversitas. 2019; 41: 143–245.

5. Antoine P-O, Marivaux L, Croft DA, Billet G, Ganerød M, Jaramillo C, et al. Middle Eocene rodents from Peruvian Amazonia reveal the pattern and timing of caviomorph origins and biogeography. Proc R Soc Lond B Biol Sci. 2012; 279: 1319–1326. https://doi.org/10.1098/rspb.2011.1732 PMID: 21993503

6. Boivin M, Marivaux L, Orliac MJ, Pujos F, Salas-Gismondi R, Tejada-Lara JV et al. Late middle Eocene caviomorph rodents from Contamana, Peruvian Amazonia. Palaeontol Electron. 2017;20.1.19A: 1–50.

7. Boivin M, Marivaux L, Aguirre-Diaz W, Andriolli Custódio M, Benites-Palomino A, Pujos F. et al. Eocene caviomorph rodents from Balsayacu (Peruvian Amazonia). Paläontol Z. 2021. doi: 210.1007/s12542-021-00551-0.

8. Assemat A, Boivin M, Marivaux L, Pujos F, Benites-Palomino A, Salas-Gismondi R, et al. Restes inédits de rongeurs caviomorphes du Paléogène de la région de Juanjui (Amazonie péruvienne): systématique, implications macro-évolutives et biostratigraphiques. Geodiversitas. 2019; 41: 699–730.

9. Vucetich MG, Arnal M, Deschamps CM, Pérez ME, Vieytes EC. A brief history of caviomorph rodents as told by the fossil record. In: Vassallo AI Antenucci D, editors. Biology of Caviomorph Rodents: Diversity and Evolution. Buenos Aires: Sociedad Argentina para el Estudio de los Maméferos (SAREM); 2015. pp. 11–62.

10. Vucetich MG, Mazzoni MM, Pardiñas UFJ. Los roedores de la Formación Collón Cura (Mioceno Medio), y la ignimbrita Pilcaniyeu. Cañadón del Tordillo, Neuquen. Ameghiniana. 1993; 30: 361–381.

11. Vucetich MG, Kramarz AG, Candela AM. Colhuehuapian rodents from Gran Barranca and other Patagonian localities: the state of the art. In: Madden RH, Carlini AA, Vucetich MG, Kay RF, editors. The Paleontology of Gran Barranca, Evolution and Environmental Change through the Middle Cenozoic of Patagonia. Cambridge: Cambridge University Press; 2010. pp. 206–219.

12. Kramarz AG, Bellosi ES. Hystricognath rodents from the Pinturas Formation, early-middle Miocene of Patagonia, biostratigraphic and paleoenvironmental implications. J South Am Earth Sci. 2005; 18: 199–212.

13. Nasif NL, Candela AM, Rasia L, Madozzo-Jaén MC, Bonini R. Actualización del conocimiento de los roedores del Mioceno Tardío de la Mesopotamia argentina: aspectos sistemáticos, evolutivos y paleobiogeográficos. Publ electrón Asoc Paleontol Argent. 2013; 14: 147–163.

14. Deschamps CM, Tomassini RL. Late Cenozoic vertebrates from the southern Pampean Region: systematic and bio-chronostratigraphic update. In: Martínez M, Olivera D, editors. Palinologı´a del Meso- Cenozoico de Argentina—Volumen en homenaje a Mirta Elena Quattrocchio. Publ electrón Asoc Paleontol Argent. 2016; 16, 202–225.

15. Arnal M, Pérez ME, Deschamps C. Revision of the Miocene caviomorph rodents from the Rio Santa Cruz (Argentinean Patagonia). Publ electrón Asoc Paleontol Argent. 2019; 19: 193–229.

16. Flynn JJ, Novacek MJ, Dodson HE, Frassinetti D, Mckenna MC, Norell MA, et al. A new fossil mammal assemblage from the southern Chilean Andes: implications for geology, geochronology, and tectonics. J South Am Earth Sci. 2002; 15: 285–302.

17. Flynn JJ, Charrier R, Croft DA, Gans PB, Herriott TM, Wertheim JA et al. Chronologic implications of new Miocene mammals from the Cura-Mallín and Trapa Trapa formations, Laguna del Laja area, south central Chile. J South Am Earth Sci. 2008; 26: 412–423.

18. Walton AH. Rodents. In: Kay RF, Madden RH, Cifelli RL, Flynn JJ editors. Vertebrate paleontology in the Neotropics. The Miocene Fauna of La Venta, Colombia. Washington and London: Smithsonian Institution Press; 1997. pp. 392–409.

19. Kerber L, Negri FR, Ribeiro AM, Nasif N, Souza-Filho JP, Ferigolo J. Tropical fossil caviomorph rodents from the southwestern Brazilian Amazonia in the context of the South American faunas: systematics, biochronology, and paleobiogeography. J Mammal Evol. 2017; 24: 57–70.

20. Madden RH, Savage DE, Fields RW. History of Vertebrate Paleontology in the Magdalena Valley. In: Kay RF, Madden RH, Cifelli RL, Flynn JJ editors. Vertebrate paleontology in the Neotropics. The Miocene Fauna of La Venta, Colombia. Washington and London: Smithsonian Institution Press; 1997. pp. 3–11.

21. Benites-Palomino A, Aguirre-Fernández G, Moreno-Bernal JW, Vanegas A, Jaramillo C. Miocene Freshwater Dolphins from La Venta, Huila, Colombia Suggest Independent Invasions of Riverine Environments in Tropical South America. J Vertebr Paleontol. 2020; 40: e1812078.

22. Kay RF, Madden RH, Cifelli RL, Flynn JJ. Vertebrate paleontology in the Neotropics. The Miocene Fauna of La Venta, Colombia. 1st ed. Washington and London: Smithsonian Institution Press; 1997.

23. Stirton RA. Ceboid monkeys from the Miocene of Columbia. Univ Calif Publ Geol Sci. 1951; 28: 315–356.

24. Stirton RA, Savage DE. A new monkey from the La Venta Miocene of Colombia. CEGOC. 1950; 8: 345–356.

25. Kay RF, Madden RH. Paleogeography and Paleoecology. In: Kay RF, Madden RH, Cifelli RL, Flynn JJ editors. Vertebrate paleontology in the Neotropics. The Miocene Fauna of La Venta, Colombia. Washington and London: Smithsonian Institution Press; 1997. pp. 520–550.

26. Madden RH, Guerrero J, Kay RF, Flynn JJ, Swisher III CC, Walton AH. The Laventan Stage and Age. In: Kay RF, Madden RH, Cifelli RL, Flynn JJ editors.

Vertebrate paleontology in the Neotropics. The Miocene Fauna of La Venta, Colombia. Washington and London: Smithsonian Institution Press; 1997. pp. 499–519.

27. Stehlin HG. Ein nager aus dem Miocaen von Columbien. Eclogae Geol Helv. 1940; 32: 179–183.

28. Fields RW. Hystricomorph rodents from the late Miocene of Colombia, South America. Univ Calif Publ Geol Sci. 1957; 32: 273–404.

29. Candela AM, Nasif NL. Systematics and biogeographic significance of *Drytomomys typicus* (Scalabrini in Ameghino, 1889) nov. comb., a Miocene Dinomyidae (Rodentia, Hystricognathi) from Northeast of Argentina. Neues Jahrb Geol Palaontol Abh. 2006; 3: 165–181.

30. Arnal M, Vucetich MG, Croft DA, Bargo MS, Fernicola JC, Vizcaino SF. Systematic revision and evolutionary history of *Acarechimys* Patterson in Kraglievich, 1965 (Rodentia, Caviomorpha, Octodontoidea). Ameghiniana. 2017; 54: 307–330.

31. Antoine P-O, Roddaz M, Brichau S, Tejada-Lara J, Salas Gismondi R, Altamirano A, et al. Middle Miocene vertebrates from the Amazonian Madre de Dios Subandean Zone, Perú. J South Am Earth Sci. 2013; 42: 91–102.

32. Antoine P-O, Salas-Gismondi R, Baby P, Benammi M, Brusset S, De Franceschi D, et al. The Middle Miocene (Laventan) Fitzcarrald fauna, Amazonian Peru. In: Díaz-Martínez E, Rábano I, editors. Proceedings of the 4th EMPSLA. Cuad del Mus Geominero. 2007; 8: 19–24.

33. Tejada-Lara J, Salas-Gismondi R, Pujos F, Baby P, Benammi M, Brusset S, et al. Life in protoamazonia: Middle Miocene mammals from the Fitzcarrald Arch (Peruvian Amazonia). Palaeontology. 2015; 58: 341–378.

34. Antoine P-O, Abello M, Adnet S, Altamirano Sierra AJ, Baby P, Billet G, et al. A 60-million-year Cenozoic history of western Amazonian ecosystems in Contamana, eastern Peru. Gondwana Res. 2016; 31: 30–59.

35. Carrillo JD, Sanchez-Villagra MR. Giant rodents from the Neotropics: diversity and dental variation of late Miocene neoepiblemid remains from Urumaco, Venezuela. Paläontol Z. 2015; 89: 1057–1071.

36. Marivaux L, Aguirre-Diaz W, Benites-Palomino A, Billet G, Boivin M, Pujos F, et al. New record of *Neosaimiri* (Cebidae, Platyrrhini) from the late Middle Miocene of Peruvian Amazonia. J Hum Evol. 2020; 146: 102835. https://doi.org/10.1016/j.jhevol.2020.102835 PMID: 32652341

37. Walton AH. Rodents of the La Venta Fauna, Miocene, Colombia: biostratigraphy and paleoenvironmental implications. Ph.D. Thesis, Southern Methodist University. 1990.

38. Code international de nomenclature zoologique. 4th ed. 1999 [cited 2021 July 01]. In: International Commission on Zoological Nomenclature [Internet]. Available from: iczn.org.

39. Sánchez-Fernández AW. Geología de los cuadrángulos de Tarapoto, Papa Playa, Utcurarca y Yanayacu 13-k, 13-l, 14-k, 14-l. Boletín INGEMMET, Serie A: Carta Geológica Nacional. 1997; 94.

40. Hermoza W, Brusset S, Baby P, Gil W, Roddaz M, Guerrero N, et al. The Huallaga foreland basin evolution: thrust propagation in a deltaic environment, northern Peruvian Andes. J South Am Earth Sci. 2005; 19: 21–34.

41. Feussom Tcheumeleu A, Fauquette S, Aliaga Castilo A, Martinez C, Moreno F, Navarrete RE, et al. Upper Miocene depositional environments and landscapes, Shumanza section, Subandean Zone, Northern Peru. Paleobiodivers Paleoenviron. 2019. https://doi.org/10.1007/s12549-019-00400-8

42. Antoine P-O, Yans J, Aliaga Castillo A, Stutz N, Abello MA, Adnet S, et al. Biotic community and landscape changes around the Eocene–Oligocene transition at Shapaja, Peruvian Amazonia: regional or global drivers? Glob Planet Change. 2021. https://doi.org/10.1016/j.gloplacha.2021.103512.

43. MacFadden BJ. Chronology of Cenozoic primate localities in South America. J Hum Evol. 1990; 19: 7–21.

44. Croft DA. The middle Miocene (Laventan) Quebrada Honda fauna, southern Bolivia and a description of its notoungulates. Palaeontology. 2007; 50: 277–303.

45. Brandoni D, Carlini AA, Anaya F, Gans P, Croft DA. New Remains of *Megathericulus patagonicus* Ameghino, 1904 (Xenarthra, Tardigrada) from the Serravallian (Middle Miocene) of Bolivia; Chronological and Biogeographical Implications. J Mammal Evol. 2018; 25: 327–337.

46. Gibert L, Deino A, Valero L, Anaya F, Lería M, Saylor B, et al. Chronology of Miocene terrestrial deposits and fossil vertebrates from Quebrada Honda (Bolivia). Palaeogeogr Palaeoclimatol Palaeoecol. 2020; 560: 110013.

47. Flynn JJ, Guerrero J, Swisher III CC. Geochronology of the Honda Group, Columbia. In: Kay RF, Madden RH, Cifelli RL, Flynn JJ editors. Vertebrate paleontology in the Neotropics. The Miocene Fauna of La Venta, Colombia. Washington and London: Smithsonian Institution Press; 1997. pp. 44–60.

48. Guerrero J. Stratigraphy, Sedimentary Environments, and the Miocene Uplift of the Colombian Andes. In: Kay RF, Madden RH, Cifelli RL, Flynn JJ editors. Vertebrate paleontology in the Neotropics. The Miocene Fauna of La Venta, Colombia. Washington and London: Smithsonian Institution Press; 1997. pp. 15–43.

49. Raffi I, Wade BS, Pälike H, Beu AG, Cooper R, Crundwell MP, et al. Chapter 29—The Neogene Period. In: Gradstein FM, Ogg JG, Schmitz MD, Ogg GM, editors. Geologic Time Scale 2020. Vol. 2. Amsterdam: Elsevier; 2020. pp.1141–1215.

50. Boivin M., Marivaux L. Dental homologies and evolutionary transformations in Caviomorpha (Hystricognathi, Rodentia): new data from the Paleogene of Peruvian Amazonia. Hist Biol. 2020; 32: 528–554.

51. Pérez ME. A new rodent (Cavioidea, Hystricognathi) from the middle Miocene of Patagonia, mandibular homologies, and the origin of the crown group Cavioidea *sensu stricto*. J Vertebr Paleontol. 2010; 30: 1848–1859.

52. Pérez ME. Sistemática, ecología y bioestratigrafía de Eocardiidae (Rodentia, Hystricognathi, Cavioidea) del Mioceno temprano y medio de Patagonia. Ph.D. Thesis, Universidad Nacional de La Plata. 2010.

53. Pérez ME, Deschamps CM, Vucetich MG. Diversity, phylogeny and biogeography of the South American 'cardiomyine'rodents (Hystricognathi, Cavioidea) with a description of two new species. Pap Palaeontol. 2018; 4: 1–19.

54. Madozzo-Jaén MC. Systematic and phylogeny of Prodolichotis prisca (Caviidae, Dolichotinae) from the Northwest of Argentina (late Miocene-early Pliocene): advances in the knowledge of the evolutionary history of maras. C R Palevol. 2019; 18: 33–50.

55. Madozzo-Jaén MC, Pérez ME, Montalvo C, Tomassini RL. Systematic review of Neocavia from the Neogene of Argentina: Phylogenetic and evolutionary implications. Acta Palaeontol Pol. 2018; 63: 241–260.

56. Patterson B, Pascual R. New echimyid rodents from the Oligocene of Patagonia, and a synopsis of the family. Breviora. 1968; 301: 1–14.

57. Ginot S, Hautier L, Marivaux L, Vianey-Liaud M. Ecomorphological analysis of the astragalo-calcaneal complex in rodents and inferences of locomotor behaviors in extinct rodent species. PeerJ. 2016; 4: e2393. https://doi.org/10.7717/peerj.2393 PMID: 27761303

58. Rose KD, Chinnery BJ. The postcranial skeleton of early Eocene rodents. Bull Carnegie Mus Nat Hist. 2004; 2004, 211–244.

59. Wible JR, Hughes EM. Anatomy of the Pedal Skeleton of the Hispaniolan Solenodon, *Solenodon paradoxos* Brandt, 1833 (Mammalia, Lipotyphla, Solenodontidae). Annls Carnegie Mus. 2016; 83: 167–205.

60. Boivin M, Ginot S, Marivaux L, Altamirano-Sierra AJ, Pujos F, Salas-Gismondi R, et al. Tarsal morphology and locomotor adaptation of some late middle Eocene caviomorph rodents from Peruvian Amazonia reveal early ecological diversity. J Vertebr Paleontol. 2019; 38: e1555164.

61. Candela AM, Picasso MB. Functional anatomy of the limbs of Erethizontidae (Rodentia, Caviomorpha): indicators of locomotor behavior in Miocene porcupines. J Morphol. 2008; 269, 552–593. https://doi.org/10.1002/jmor.10606 PMID: 18157864

62. Janis CM. An estimation of tooth volume and hypsodonty indices in ungulate mammals, and the correlation of these factors with dietary preference. In: Russell DE, Santoro JP, Sigogneau-Russell D, editors. Teeth Revisited. Proceedings of the 7th International Symposium on Dental Morphology (Paris). Mém Mus natl hist nat, Sér C Geól. 1986; 53: 367–387.

63. R Core Team. R: a language and environment for statistical computing v.4.0.3. Vienna: R Foundation for Statistical Computing. 2020. Available from: http://www.r-project.org.

64. Dinno A. 2017. dunn.test: Dunn's Test of Multiple Comparisons Using Rank Sums. R package version 1.3.5. https://CRAN.R-project.org/package=dunn.test.

65. Pohlert T. trend: Non-Parametric Trend Tests and Change-Point Detection. R package version 1.1.4. 2020. Available at: https://CRAN.R-project.org/package=trend.

66. Hervé M. RVAideMemoire: Testing and Plotting Procedures for Biostatistics. R package version 0.9–79. 2021. Available from: https://CRAN.R-project.org/package=RVAideMemoire.

67. Maechler M, Rousseeuw P, Struyf A, Hubert M, Hornik K. cluster: Cluster Analysis Basics and Extensions. R package version 2.1.0. 2019. Available from: https://CRAN.R-project.org/package=cluster.

68. Venables WN, Ripley BD. Modern Applied Statistics with S. 4th Edition. New York: Springer; 2002.

69. Candela AM. Lower deciduous tooth homologies in Erethizontidae [Rodentia, Hystricognathi]: evolutionary significance. Acta Palaeontol Pol. 2002; 47: 717–723.

70. Boivin M, Marivaux L, Pujos F, Salas-Gismondi R, Tejada-Lara J.V, Varas-Malca R, et al. Early Oligocene caviomorph rodents from Shapaja, Peruvian Amazonia. Palaeontogr Abt A. 2018; 311: 87–156.

71. Boivin M, Marivaux L, Candela AM, Orliac MJ, Pujos F, Salas-Gismondi R, et al. Late Oligocene caviomorph rodents from Contamana, Peruvian Amazonia. Pap Palaeontol. 2017; 3: 69–109.

72. Ercoli MD, Á lvarez A, Verzi DH, Ulberich JPV, Quiñones SI, Constantini OE, et al. A new mammalian assemblage for Guanaco Formation (northwestern Argentina), and the description of a new genus of New World porcupine. J South Am Earth Sci. 2021; 110: 103389.

73. Ameghino F. Enumeración sistematica de las especies de mamíferos fósiles coleccionados por Carlos Ameghino en los terrenos eocenos de Patagonia austral y depositados en el museo de La Plata. Bol Mus La Plata. 1887; 1: 1–26.

74. Candela AM. Los Erethizontidae (Rodentia, Hystricognathi) fo´ siles de Argentina. Sistemática e historia evolutiva y biogeográfica. Ph.D. Thesis, Universidad Nacional de La Plata. 2000.

75. Candela AM. A new porcupine (Rodentia, Erethizontidae) from the early and middle Miocene of Patagonia. Ameghiniana. 2003; 40: 483–494.

76. Candela AM. A New Giant Porcupine (Rodentia, Erethizontidae) from the Late Miocene of Argentina. J Vertebr Paleontol. 2004; 24: 732–741.

77. Kramarz AG. Octodontoids and erethizontoids (Rodentia, Hystricognathi) from the Pinturas Formation, Early-Middle Miocene of Patagonia, Argentina. Ameghiniana. 2004; 41: 199–216.

78. Ameghino F. Notices préliminaires sur des mammifères nouveaux des terrains crétacés de Patagonie. Bol acad nac cien, Córdoba. 1902; 17: 1–68.

79. Wood AE, Patterson B. The rodents of the Deseadan Oligocene of Patagonia and the beginnings of South American rodent evolution. Bull Mus Comp Zool. 1959; 120: 281–428.

80. Candela AM. The evolution of the molar pattern of the Erethizontidae (Rodentia, Hystricognathi) and the validity of *Parasteiromys* Ameghino, 1904. Palaeovertebrata. 1999; 28: 53–73.

81. Frailey CD, Campbell KE. Paleogene rodents from Amazonian Peru: the Santa Rosa local fauna. In Campbell KE, editor. The Paleogene Mammalian Fauna of Santa Rosa, Amazonian Peru. Natural History Museum of Los Angeles County, Science Series. 2004; 40: 71–130.

82. Pérez ME, Arnal M, Boivin M, Vucetich MG, Candela A, Busker F, et al. New caviomorph rodents from the late Oligocene of Salla, Bolivia: taxonomic, chronological,

and biogeographic implications in the Deseadan faunas of South America. J Syst Palaeontol. 2019; 17: 821–847.

83. Candela AM, Vucetich MG. *Hypsosteiromys* (Rodentia, Hystricognathi) from the early Miocene of Patagonia (Argentina), the only Erethizontidae with a tendency to hypsodonty. Geobios. 2002; 35: 153–161.

84. Frailey CD. Late Miocene and Holocene mammals, exclusive of the Notoungulata, of the Rio Acre region, western Amazonia. Los Angeles County Mus Contr Sci. 1986; 374: 1–46.

85. Campbell KE, Frailey CD, Romero-Pittman L. The pan-Amazonian Ucayali Peneplain, late Neogene sedimentation in Amazonia, and the birth of the modern Amazon River system. Palaeogeogr Palaeoclimatol Palaeoecol. 2006; 239: 166–219.

86. Candela AM, Rasia LL, Pérez ME. Early Miocene Paleobiology in Patagonia: Paleobiology of Santacrucian caviomorph rodents: a morphofunctional approach. In: Vizcaíno SF, Kay RF, Bargo MS, editors. Early Miocene Paleobiology in Patagonia: High-Latitude Paleocommunities of the Santa Cruz Formation. New York: Cambridge University Press; 2012. pp. 287–305.

87. Pérez ME, Vucetich MG. A new extinct genus of Cavioidea (Rodentia, Hystricognathi) from the Miocene of Patagonia (Argentina), and the evolution of cavioid mandibular morphology. J Mammal Evol. 2011; 18: 163–183.

88. Pérez ME, Pol D. Major radiations in the evolution of caviid rodents: reconciling fossils, ghost lineages, and relaxed molecular clocks. PLoS One. 2012; 7: e48380. https://doi.org/10.1371/journal.pone.0048380 PMID: 23144757

89. Pérez ME, Vucetich MG, Deschamps CM. Mandibular remains of *Procardiomys martinoi* Pascual, 1961 (Hystricognathi, Cavioidea) from the Arroyo Chasicó Formation (early late Miocene) of Argentina: anatomy and the phylogenetic position of the genus within Caviidae. Hist Biol. 2014; 26: 16–25.

90. Madozzo-Jaén MC, Pérez ME. The most ancient caviine rodent (Hystricognathi, Cavioidea) comes from the late Miocene of Northwest Argentina (South America). Hist Biol. 2017; 29: 376–383.

91. Kraglievich L. Diagnosis de nuevos géneros y especies de roedores cávidos y eumegámidos fósiles de la Argentina. Anales Soc. Ci. Argent. 1932; 114: 93–140.

92. Contreras JR. Datos acerca de la variación intrapoblacional de la morfología de los molares de entidades de los géneros *Galea y Microcavia* (Rodentia, Caviidae). Ameghiniana. 1964; 3: 235–255.

93. Pisano JA. Un nuevo y significativo caso de adición prismática observado en el premolar cuarto (p4) inferior de un ejemplar del género *Cavia* (Rodentia, Caviidae). Ameghiniana. 1964; 3:169–172.

94. Quintana C. Diversidad del roedor Microcavia (Caviomorpha, caviidae) de América del sur. Mastozool. neotrop. 1996; 3: 63–86.

95. Quintana C. El roedor *Dolicavia minuscula* (Caviomorpha, Caviidae) del Plioceno superior de la província de Buenos Aires, Argentina. Hist. an. 1997; 3: 55–71.

96. Quintana C. *Galea* (Rodentia, Caviidae) del Pleistoceno Superior y Holoceno de las sierras de Tandilia Oriental, Provincia de Buenos Aires, Argentina. Ameghiniana. 2001; 38: 399–408.

97. Candela AM, Bonini RA. A new guinea pig (Rodentia, Caviomorpha) from northwestern Argentina: implications for the origin of the genus *Cavia*. J Vertebr Paleontol. 2017; 37: e1352591.

98. Teta P, Campo DH. Is *Galea tixiensis* Quintana, 2001 a synonym of *G. leucoblephara* Burmeister, 1861?. Therya. 2017; 8: 209–216.

99. Vucetich MG, Deschamps CM, Olivares AI, Dozo MT. Capybaras, size, shape, and time: a model kit. Acta Palaeontol Pol. 2005; 50: 259–272.

100. Pérez ME, Vucetich MG. A revision of the fossil genus *Phanomys* Ameghino, 1887 (Rodentia, Hystricognathi, Cavioidea) from the early Miocene of Patagonia (Argentina) and the acquisition of euhypsodonty in Cavioidea *sensu stricto*. Paläontol Z. 2012; 86: 187–204.

101. Kramarz AG. Eocardiids (Rodentia, Hystricognathi) from the Pinturas Formation, late early Miocene of Patagonia, Argentina. J Vertebr Paleontol. 2006; 26: 770–778.

102. Pérez ME, Vucetich MG. *Asteromys punctus* Ameghino (Rodentia, Hystricognathi, Cavioidea) from the Late Oligocene of Patagonia (Argentina) and the early evolution of *Cavioidea sensu* stricto. Ameghiniana. 2012; 49: 118–125.

103. Pérez ME, Vucetich MG, Kramarz AG. The first Eocardiidae (Rodentia) in the Colhuehuapian (early Miocene) of Bryn Gwyn (northern Chubut, Argentina) and the early evolution of the peculiar cavioid rodents. J Vertebr Paleontol. 2010; 30: 528–534.

104. Pérez ME, Krause M, Vucetich MG. A new species of *Chubutomys* (Rodentia, Hystricognathi) from the late Oligocene of Patagonia and its implications on the early evolutionary history of Cavioidea *sensu stricto*. Geobios. 2012; 45: 573–580.

105. Croft DA, Chick JM, Anaya F. New Middle Miocene caviomorph rodents from Quebrada Honda, Bolivia. J Mammal Evol. 2011; 18: 245–268.

106. Ameghino F. Contribución al conocimiento de los mamíferos fósiles de la República Argentina. Actas Acad Nac Cienc Repúb Argent. 1889; 6: 1–1027.

107. Rovereto C. Los estratos araucanos y sus fósiles. Anales Mus Nac Hist Nat Buenos Aires. 1914; 25: 1–247.

108. Castellanos A. Nota preliminar sobre nuevos restos de mamíferos fósiles en el Brocherense del Valle de Los Reartes (provincia de Córdoba, Argentina). Separata de: 20˚ Congreso Geológico Internacional, México, 1956. Sección VII. 1958. 217–233.

109. Prado JL, Cerdeño E. Los mamíferos pliocenos de la fauna local Quequén Grande (Provincia de Buenos Aires, Argentina). Estud Geol. 1998; 54: 75–83.

110. Ubilla M, Rinderknecht A. Consideraciones sobre el género '*Galea*' Meyen, 1831 (Rodentia, Caviidae), su registro en el Pleistoceno de Uruguay y descripción de una nueva especie extingida. Bol R Soc Esp Hist Nat Sec Geol. 2001; 96: 111–122.

111. Ubilla M, Rinderknecht A. A late Miocene Dolichotinae (Mammalia, Rodentia, Caviidae) from Uruguay, with comments about the relationships of some related fossil species. Mastozool. neotrop. 2003; 10: 293–302.

112. Ubilla M, Rinderknecht A. Comparative analysis of *Galea* (Rodentia, Caviidae) and expanded diagnosis of *Galea ortodonta* Ubilla and Rinderknecht, 2001 (late Pleistocene, Uruguay). Geobios. 2014; 47: 255–269.

113. Tauber AA. Mamíferos fósiles y edad de la Formación Sálicas (Mioceno tardío) de la sierra de Velasco, La Rioja, Argentina. Ameghiniana. 2005; 42: 443–460.

114. Vucetich MG, Dozo MT, Arnal M, Pérez ME. New rodents (Mammalia) from the Late Oligocene of Cabeza Blanca (Chubut) and the first rodent radiation in Patagonia. Hist Biol. 2015; 27: 236–257.

115. Kramarz AG. Un nuevo roedor Adelphomyinae (Hystricognathi, Echimyidae) del Mioceno Medio-Inferior de Patagonia, Argentina. Ameghiniana. 2001; 38: 163–168.

116. Kramarz AG, Vucetich MG, Carlini AA, Ciancio MR, Abello MA, Deschamps CM et al. A new fauna at the top of the Gran Barranca sequence and its biochronological significance. In: Madden RH, Carlini AA, Vucetich MG, Kay RF, editors. The Paleontology of Gran Barranca, Evolution and Environmental Change through the Middle Cenozoic of Patagonia. Cambridge: Cambridge University Press; 2010. pp. 264–277.

117. Arnal M, Kramarz AG. First complete skull of an octodontoid (Rodentia, Caviomorpha) from the Early Miocene of South America and its bearing in the early evolution of Octodontoidea. Geobios. 2011; 44: 435–444.

118. Ameghino F. Enumération synoptique des espèces de mammifères fossiles des formations éocènes de Patagonie. Bol acad nac cien, Córdoba. 1894; 13: 259–455.

119. Kay R, Vizcaíno S, Bargo M. A review of the paleoenvironment and paleoecology of the Miocene Santa Cruz Formation. In: Vizcaı´no SF, Kay RF, Bargo MS, editors. Early Miocene Paleobiology in Patagonia: High-Latitude Paleocommunities of the Santa Cruz Formation. New York: Cambridge University Press; 2012. pp. 331–365.

120. Vucetich MG, Verzi DH. A peculiar octodontoid (Rodentia, Caviomorpha) with terraced molars from the Lower Miocene of Patagonia (Argentina). J Vertebr Paleontol. 1996; 16: 297–302.

121. Arnal M, Kramarz AG, Vucetich MG, Vieytes EC. A new early Miocene octodontoid rodent (Hystricognathi, Caviomorpha) from Patagonia (Argentina) and a reassessment of the early evolution of Octodontoidea. J Vertebr Paleontol. 2014; 34: 397–406.

122. Wood AE. A new Oligocene rodent genus from Patagonia. Am Mus Novit. 1949; 1435: 1–54.

123. Vucetich MG, Vieytes EC. A middle Miocene primitive octodontoid rodent and its bearing on the early evolutionary history of the Octodontoidea. Palaeontogr Abt A. 2006; 81–91.

124. Vucetich MG, Souza Cunha FL De, Alvarenga HMF de. Un Roedor Caviomorpha de la Formación Tremembé (Cuenca de Taubaté), Estado de Sao Paulo, Brasil. An Acad Bras Ciênc. 1993; 65: 247–251.

125. Arnal M, Vucetich MG. First record of supernumerary teeth in South American fossil rodents. J Vertebr Paleontol. 2011; 31: 925–927.

126. Arnal M, Pérez ME. A new acaremyid rodent (Hystricognathi: Octodontoidea) from the Middle Miocene of Patagonia (South America) and considerations on the early evolution of Octodontoidea. Zootaxa. 2013; 3616: 119–34. https://doi.org/10.11646/zootaxa.3616.2.2 PMID: 24758798

127. Kramarz AG, Vucetich MG, Arnal M. A new early Miocene chinchilloid hystricognath rodent; an approach to the understanding of the early chinchillid dental evolution. J Mammal Evol. 2013; 20: 249–261.

128. Marivaux L, Vélez-Juarbe J, Merzeraud G, Pujos F, Vinola Lopez LW, Boivin M, et al. 2020. Early Oligocene chinchilloid caviomorphs from Puerto Rico and the initial rodent colonization of the West Indies. Proc Royal Soc. B. 2020; 287: 20192806. https://doi.org/10.1098/rspb.2019.2806 PMID: 32075529

129. Hoffstetter R, Lavocat R. Découverte dans le Déséadien de Bolivie des genres pentalophodontes appuyant les affinite´s africaines des rongeurs caviomorphes. C R Acad Sci Paris. 1970; 271: 172–175.

130. Lavocat R. Rongeurs caviomorphes de l'Oligocène de Bolivie. Rongeurs du bassin déséadien de Salla. Palaeovertebrata. 1976; 7: 15–90.

131. Patterson B, Wood AE. Rodents from the Deseadan Oligocene of Bolivia and the relationships of the Caviomorpha. Bull Mus Comp Zool. 1982; 149: 371–543.

132. Busker F, Pérez ME, Dozo MT. A new chinchilloid (Rodentia, Hystricognathi) from the early Miocene of the localities of Bryn Gwyn and Gran Barranca (Patagonia, Argentina). C R Palevol. 2019; 18: 525–540.

133. Kramarz AG. *Neoreomys* and Scleromys (Rodentia, Hystricognathi) from the Pinturas Formation, late Early Miocene of Patagonia, Argentina. Rev. Mus. Argent. Cienc. Nat. 2006; 8: 53–62.

134. Busker F, Dozo MT. First confirmed record of *Incamys bolivianus* (Caviomorpha, Chinchilloidea) in the Deseadan of Patagonia (Argentina). Ameghiniana. 2017; 54: 706–712.

135. Anthony HE. A new fossil rodent from Ecuador. Am Mus Novit. 1922; 35: 1–8.

136. Kramarz AG. Un nuevo dasyproctidae (Rodentia, Caviomorpha) del Mioceno inferior de Patagonia. Ameghiniana. 1998; 35: 181–192.

137. Arnal M, Kramarz AG, Vucetich MG, Frailey CD, Campbell KE. New Palaeogene caviomorphs (Rodentia, Hystricognathi) from Santa Rosa, Peru: systematics, biochronology, biogeography and early evolutionary trends. Pap Palaeontol. 2020; 6: 193–216.

138. Cifelli R. Eutherian tarsals from the late Paleocene of Brazil. Am Mus Novit. 1983; 2761: 1–31.

139. Tsubamoto T. Estimating body mass from the astragalus in mammals. Acta Palaeontol Pol. 2014; 59: 259–265.

140. Legendre S. Analysis of mammalian communities from the Late Eocene and Oligocene of Southern France. Palaeovertebrata. 1986; 16: 191–212.

141. Marivaux L, Salas-Gismondi R, Tejada J, Billet G, Louterbach M, Vink J, et al. A platyrrhine talus from the early Miocene of Peru (Amazonian Madre de Dios Sub-Andean Zone). J Hum Evol. 2012; 63: 696–703. https://doi.org/10.1016/j.jhevol.2012.07.005 PMID: 22974538

142. Vucetich MG, Bond M. Un nuevo Octodontoidea (Rodentia, Caviomorpha) del Oligoceno tardío de la provincia de Chubut (Argentina). Ameghiniana. 1984; 21: 105–114.

143. Vucetich MG, Verzi DH, Dozo MT. El 'status' sistemático de *Gaimanomys alwinea* (Rodentia, Caviomorpha, Echimyidae). Ameghiniana. 1992; 29: 85–86.

144. Vucetich MG, Verzi DH. The presence of *Protadelphomys* (Rodentia, Echimyidae) in the Colhuehuapian of the South Barrancas of Lake Colhue Huapi (Chubut). Ameghiniana. 1994; 31: 93–94.

145. Kerber L, Ferreira JD, Negri FR. A reassessment of the cranial morphology of *Neoepiblema acreensis* (Rodentia: Chinchilloidea), a Miocene rodent from South America. J Morphol. 2019; 280: 1821–1838. https://doi.org/10.1002/jmor.21067 PMID: 31633247

146. Rasia LL, Candela AM, Cañón C. Comprehensive total evidence phylogeny of chinchillids (Rodentia, Caviomorpha): Cheek teeth anatomy and evolution. J. Anat. 2021. https://doi.org/10.1111/joa.13430 PMID: 33721329

147. Kraglievich L. La Formación Friaseana del río Fénix, Laguna Blanca, etc. (Patagonia) y su fauna de mamíferos. Physis. 1930; 10: 127–161.

148. Vucetich MG. Los roedores de la Edad Friasense (Mioceno Medio) de Patagonia. Rev Mus La Plata. 1984; 50: 47–126.

149. Candela AM, Morrone JJ. Biogeografía de puercoespines neotropicales (Rodentia: Hystricognathi): Integrando datos fósiles y actuales a través de un enfoque panbiogeográfico. Ameghiniana. 2003; 40: 361–378.

150. Vucetich MG, Kramarz AG. New Miocene rodents of Patagonia (Argentina) and their bearing in the early radiation of the octodontoids (Hystricognathi). J Vertebr Paleontol. 2003; 23: 435–444.

151. Flynn JJ, Wyss R, Croft DA, Charrier R. The Tinguiririca Fauna, Chile: biochronology, paleoecology, biogeography, and a new earliest Oligocene South American Land Mammal 'Age'. Palaeogeogr Palaeoclimatol Palaeoecol. 2003; 195: 229–259.

152. Vucetich MG, Pérez ME. The putative cardiomyines (Rodentia, Cavioidea) of the middle Miocene of Patagonia (Argentina) and the differentiation of the family Hydrochoeridae. J Vertebr Paleontol. 2011; 31: 1382–1386.

153. Cerdeño E, Vucetich MG. The first rodent from the Mariño Formation (Miocene) at Divisadero Largo (Mendoza, Argentina) and its biochronological implications. Andean Geol. 2007; 34: 199–207.

154. López GM, Vucetich MG, Carlini AA, Bond M, Pérez ME, Ciancio MR, et al. New Miocene mammal assemblages from Neogene Manantiales basin, Cordillera Frontal, San Juan, Argentina. In: Salfity JA, Marquillas RA, editors. Cenozoic Geology of the Central Andes of Argentina. Salta: SCS Publisher; 2011. pp. 211–226.

155. Szalay FS. Rodent and lagomorph morphotype adaptations, origins, and relationships: some postcranial attributes analyzed. In: Luckett WP, Hartenberger JP, editors. Evolutionary Relationships among Rodents. Berlin: Springer; 1985. pp. 83–132.

156. Hildebrand M. Walking and running. In: Hildebrand M, Bramble DM, Liem KF, Wake DB, editors. Functional Vertebrate Morphology. Cambridge: Harvard University Press; 1985. pp. 38–57.

157. Hildebrand M, Goslow GE Jr. Digging, and crawling without appendages. In: Hildebrand M, Hurley GE, editors. Analysis of vertebrate structure. New Jersey: John Wiley and Sons, Inc; 2001. pp. 455–474.

158. Szalay FS. Evolutionary history of the marsupials and an analysis of osteological characters. New York: Cambridge University Press; 1994.

159. Hoorn C, Wesselingh FP, Ter Steege H, Bermudez MA, Mora A, Sevink J, et al. Amazonia through time: Andean uplift, climate change, landscape evolution, and biodiversity. Science. 2010; 330: 927–931. https://doi.org/10.1126/science.1194585 PMID: 21071659

160. Steinmann G. Geologie von Peru. Heidelberg: Karl Winter; 1929.

161. Mégard F. The Andean orogenic period and its major structures in central and northern Peru. J Geol Soc. 1984; 141: 893–900.

162. Jaillard E, Soler P. Cretaceous to early Paleogene tectonic evolution of the northern Central Andes (0–18 degrees S) and its relations to geodynamic. Tectonophysics. 1996; 259: 41–53.

163. Gómez E, Jordan TE, Allmendinger RW, Hegarty K, Kelley S, Heizler M. Controls on architecture of the Late Cretaceous to Cenozoic southern Middle Magdalena Valley Basin, Colombia. Geol Soc Am Bull. 2001; 115: 131–147.

164. Bayona G, Cortés M, Jaramillo C, Ojeda G, Aristizabal JJ, Reyes-Harker A. An integrated analysis of an orogen sedimentary basin pair: Latest Cretaceous-Cenozoic evolution of the linked Eastern Cordillera orogen and the Llanos foreland basin of Colombia. Geol Soc Am Bull. 2008; 120: 1171–1197.

165. Mora A, Baby P, Roddaz M, Parra M, Brusset S, Hermoza W, et al. Tectonic history of the Andes and sub-Andean zones: implications for the development of the

Amazon drainage basin. In: Hoorn C, Wesselingh FP, editors. Amazonia, Landscape and Species Evolution: A Look into the Past. Hoboken: Blackwell Wiley; 2010. pp. 38–60.

166. Lundberg JG, Machado-Allison A, Kay RF. Miocene characid fishes from Colombia: evolutionary stasis and extirpation. Science. 1986; 234: 208e209. https://doi.org/10.1126/science.234.4773.208 PMID: 17746480

167. Hoorn C, Guerrero J, Sarmiento GA, Lorente MA. Andean tectonics as a cause for changing drainage patterns in Miocene northern South America. Geology. 1995; 23: 237–240.

168. Anderson VJ, Horton BK, Saylor JE, Mora A, Tesón E, Breecker DO, Ketcham RA. Andean topographic growth and basement uplift in southern Colombia: Implications for the evolution of the Magdalena, Orinoco, and Amazon river systems. Geosphere. 2016; 12: 1235–1256.

169. Maia RGN, Godoy HK, Yamaguti HS, Moura PAD, Costa FSFD, Holanda MAD et al. Projeto carvão no Alto Solimões: relatório final. CPRM. 1977; 6: 1–267.

170. Hoorn C. Marine incursions and the influence of Andean tectonics on the Miocene depositional history of northwestern Amazonia: results of a palynostratigraphic study. Palaeogeogr Palaeoclimatol Palaeoecol. 1993; 105: 267–309.

171. Hoorn C. Fluvial palaeoenvironments in the intracratonic Amazonas Basin (early Miocene-early Middle Miocene, Colombia). Palaeogeogr Palaeoclimatol Palaeoecol. 1994; 109: 1–54.

172. Wesselingh FP. Miocene long-lived lake Pebas as a stage of mollusc rolution in western Amazonia. Scr Geol. 2006; 133: 1–17.

173. Hoorn C, Roddaz M, Dino R, Soares E, Uba C, Ochoa-Lozano D et al. The Amazonian craton and its influence on past fluvial systems (Mesozoic-Cenozoic, Amazonia). In: Hoorn C, Wesselingh FP, editors. Amazonia, Landscape and Species Evolution: A Look into the Past. Hoboken: Blackwell Wiley; 2010. pp. 103–122.

174. Hoorn C, Wesselingh FP, Hovikoski J, Guerrero J. The development of the Amazonian mega-wetland (Miocene; Brazil, Colombia, Peru, Bolivia). In: Hoorn C, Wesselingh FP, editors. Amazonia, Landscape and Species Evolution: A Look into the Past. Hoboken: Blackwell Wiley; 2010. pp. 123–142.

175. Hovikoski J, Wesselingh FP, Räsänen M, Gingras M, Vonhof HB. Marine influence in Amazonia: evidence from the geological record. In: Hoorn C, Wesselingh FP, editors. Amazonia, Landscape and Species Evolution: A Look into the Past. Hoboken: Blackwell Wiley; 2010. pp. 143–161.

176. Salas-Gismondi R, Flynn JJ, Baby P, Tejada-Lara J, Wesselingh FP, Antoine P-O. A Miocene hyperdiverse crocodylian community reveals peculiar trophic dynamics in proto-Amazonian megawetlands. Proc Royal Soc. B. 2015; 282: 20142490.

177. Salas-Gismondi R, Flynn JJ, Baby P, Tejada-Lara JV, Claude J, Antoine P-O. A new 13 million year old gavialoid crocodylian from proto-Amazonian mega-wetlands reveals parallel evolutionary trends in skull shape linked to longirostry. PLoS One. 2016; 11: e0152453. https://doi.org/10.1371/journal.pone.0152453 PMID: 27097031

178. Salas-Gismondi R, Antoine P-O, Baby P, Brusset S, Benammi M, Espurt N, et al. Middle Miocene crocodiles from the Fitzcarrald Arch, Amazonian Peru. Cuad del Mus Geominero. 2007; 8: 355–360.

4.5 BIOTIC COMMUNITY AND LANDSCAPE CHANGES AROUND THE EOCENE–OLIGOCENE TRANSITION AT SHAPAJA, PERUVIAN AMAZONIA: REGIONAL OR GLOBAL DRIVERS?

Artigo publicado no periódico *Global and Planetary Change*, volume 202, artigo 103512, 2021, DOI: 10.1016/j.gloplacha.2021.103512.

Pierre-Olivier Antoine[a], Johan Yans[b], Angélica Aliaga Castillo[c,d], **Narla Stutz[a,e]**, M. Alejandra Abello[f,g], Sylvain Adnet[a], Michele Andriolli Custódio[h,i], Aldo Benites-Palomino[c,j], Guillaume Billet[k], Myriam Boivin[i], Fabiany Herrera[m], Carlos Jaramillo[a,d,n], Camila Mártinez[d,o], Federico Moreno[d,p], Rosa E. Navarrete[q], Francisco Ricardo Negri[r], Francisco Parra[q,s], François Pujos[g,t], Jean-Claude Rage[k,a], Ana Maria Ribeiro[e,u], Céline Robinet[f], Martin Roddaz[h,i], Julia V. Tejada-Lara[a,c], Rafael Varas-Malca[c,v], Roberto Ventura Santos[h], Rodolfo Salas-Gismondi[c,v], Laurent Marivaux[a]

[a]Institut des Sciences de l'Evolution de Montpellier, Univ Montpellier, CNRS, IRD, EPHE, Montpellier, France

[b]University of Namur, Department of Geology, Institute of Life, Earth and Environment, ILEE, 61 rue de Bruxelles, 5000 Namur, Belgium

[c]Departamento de Paleontología de Vertebrados, Museo de Historia Natural - Universidad Nacional Mayor de San Marcos, Lima, Peru

[d]Smithsonian Tropical Research Institute, Unit 0948, APO AA 34002, Balboa, Ancon 0843-03092, Panama

[e]Programa de Pós-Graduação em Geociências, Universidade Federal do Rio Grande do Sul, Av. Bento Gonçalves, 9500, 91501-970 Porto Alegre, Brazil

[f]Unidades de investigaci´on Anexo Museo, Facultad de Ciencias Naturales y Museo (UNLP), Av. 60 y 122. B1900FWA, La Plata, Argentina

[g]Consejo Nacional de Investigaciones Científicas y Técnicas (CONICET), Argentina

[h]Laboratório de Geocronologia, Instituto de Geociências, Universidade de Brasília, Brasília, DF 70910-000, Brazil

[i]Géosciences-Environnement Toulouse, Université de Toulouse; UPS (SVT-OMP), CNRS, IRD, 14 Avenue ´Edouard Belin, F-31400 Toulouse, France

[j]Paläontologisches Institut und Museum, Universität Zürich, Karl-Schmid-Straße 4, Zürich 8006, Switzerland

[k]Sorbonne Universités, CR2P, MNHN, CNRS, UPMC-Paris 6, Muséum national d'Histoire naturelle, CP 38, 8 rue Buffon, 75231 Paris, cedex 05, France
[l]Instituto de Ecorregiones Andinas (INECOA), Universidad Nacional de Jujuy, CONICET, IdGyM, Av. Bolivia 1661, San Salvador de Jujuy 4600, Jujuy, Argentina
[m]Chicago Botanic Garden, 1000 Lake Cook Rd, Glencoe, IL 60022, USA
[n]Department of Geology, Faculty of Sciences, University of Salamanca, Salamanca, Spain
[o]Departamento de Ciencias Biológicas, Facultad de Ciencias, Universidad EAFIT, Medellín, Colombia
[p]Earth & Environmental Sciences, University of Rochester, 227 Hutchison Hall, Rochester, NY 14627, USA.
[q]Paleosedes E.U, Tv 27 n◦57-49 Campin, Bogotá, Colombia
[r]Laboratório de Paleontologia, Universidade Federal do Acre, Cruzeiro do Sul, Brazil
[s]Laboratorio de Bioquimio-Estratigrafía, Facultad de Geociencias, Universidad Nacional de Colombia, Bogot´a, Colombia
[t]Instituto Argentino de Nivología, Glaciología y Ciencias Ambientales (IANIGLA), CCT-CONICET-Mendoza, Av. Ruiz Leal s/n, Parque Gral, San Martín 5500, Mendoza, Argentina
[u]Museu de Ciências Naturais, Secretaria do Meio Ambiente e Infraestrutura do Rio Grande do Sul, Av. Salvador França, 1427, 90690-000 Porto Algre, Brazil
[v]BioGeoCiencias Lab, Facultad de Ciencias y Filosofía/CIDIS, Universidad Peruana Cayetano Heredia, Lima, Peru

A B S T R A C T

Since 2012, we have investigated a stratigraphic section encompassing the late Eocene–earliest Oligocene interval at Shapaja (Tarapoto area, Peruvian Amazonia, ca. 7◦S), through paleontological and geological fieldwork. The measured sedimentary series (120 m-thick [West] plus 90 m-thick [East]), assigned to the upper member of the Pozo Formation, records fluvial micro-conglomeratic lenses intercalated with floodplain and evaporite-rich fine red deposits, estuarine/coastal-plain tidally-influenced fine sandstones, and oxbow lake nodule-rich blue clays. This sedimentary shift coincides locally with the demise of the large Eocene coastal-plain wetland known as Pozo System. The late Eocene–early Oligocene Shapaja section was extensively sampled for chemostratigraphy (δ13C on dispersed organic matter and pedogenic carbonate nodules), which in turn allowed for refining the location of the Eocene-

Oligocene Transition (EOT) and other climatic events recognized at a global scale (i.e., Oi-1 and Oi-1a). The section has yielded nine fossil localities with plant remains (leaves, wood, charophytes, and palynomorphs), mollusks, decapods, and/or vertebrates (selachians, actinopterygians, lungfishes, amphibians, sauropsids, and mammals), documenting ~130 distinct taxa. Four localities of the upper member of the Pozo Formation at Shapaja predate the EOT, one is clearly within the EOT, while four are earliest/early Oligocene in age. The small leaf impressions found along the Shapaja section could be indicative of dry and/or seasonal conditions for this region throughout and after the EOT. Monkeys, indicative of tropical rainforest environments, are only recorded in a latest Eocene locality (TAR-21). Two biotic turnovers are perceptible in the selachian, metatherian, and rodent communities, well before the EOT [~35–36 Ma] and a few hundred thousand years after the EOT [~33 Ma]. The latter turnover seems to be primarily related to a global sea-level drop (ichthyofauna: marine-littoral elements replaced by obligate freshwater taxa) and/or the onset of a drier and more seasonal climate in early Oligocene times (terrestrial components). Changes in the structure of the Shapaja paleocommunities were mostly driven by the flexural subsidence during the late Eocene, and then globally driven by the earliest Oligocene climatic deterioration.

Keywords: Andes-Amazonia transition, Pozo System demise, Paleontology, Sedimentary geology, Chemostratigraphy, Paleoenvironments

1. Introduction

The Eocene-Oligocene transition (EOT, ca. 33.9 million years ago) was one of the most dramatic episodes of climatic, environmental, and biotic change recorded throughout the Cenozoic era. It corresponds to a phase of oceanic reorganization, global cooling (ca. 4 ◦C), and to onset of semi-permanent ice sheets on Antarctica, which led to a noticeable drop in global sea level (Mudelsee et al., 2014; Miller et al., 2020). Basically, the EOT marks the rapid shift from the Paleocene–Eocene “greenhouse” Earth to the “icehouse” Earth during the earliest Oligocene. The prevailing proposed mechanisms of that climatic deterioration include a decrease in the concentration of atmospheric CO2 (e.g., Zachos et al., 2001, 2008; DeConto and Pollard, 2003; Pagani et al., 2005; Westerhold et al., 2020) and the opening of Southern Ocean gateways (Tasmania Sea and Drake Passage) that established the Antarctic circumpolar current (e.g., Toumoulin et al., 2020). Important changes

occurred in floras and faunas around the world, reflecting the shift from warm to colder/drier climatic regimes (e.g., Miller et al., 1991; Coxall and Pearson, 2007; Dupont-Nivet et al., 2007; Hutchinson et al., 2018). This climatic transition consisted of alternating phases of expansion and contraction of Antarctic ice sheets, reflected in successive episodes of sea level rise and fall (Miller et al., 2020). Accordingly, the EOT was an interval of substantial ecological reorganization, biotic turnovers, dispersals, extinction, provincialism, and speciation in many biological groups, with patterns varying from landmass to landmass and across latitudes (e.g., Stehlin, 1909; Savage and Russell, 1983; Janis, 1993; Meng and McKenna, 1998; Marivaux et al., 2005, 2017a, 2017b; Coxall and Pearson, 2007; Seiffert, 2007; Liu et al., 2009; Goin et al., 2010; Beard et al., 2017; Godfrey et al., 2020).

Continental proxies crossing the EOT, however, are somewhat sparse and they seem to be much blurrier than in the marine records (e.g., Berggren and Prothero, 1992; Coxall and Pearson, 2007; Zachos et al., 2008; Tramoy et al., 2016; Pound and Salzmann, 2017; Westerhold et al., 2020). Furthermore, continental fossil records often lack the accurate time resolution that allows for a precise correlation of biotic events and pulses with the earliest Oligocene glacial maxima, as recorded by marine records. Also, compared with northern continents (e.g., Coxall and Pearson, 2007; Zanazzi et al., 2007), much less is known about the tempo and intensity of biotic and environmental changes that occurred across the EOT in tropical-equatorial areas of Africa (e.g., Seiffert, 2007; Beard et al., 2017; Marivaux et al., 2017a, 2017b; Benammi et al., 2019), South Asia (Marivaux et al., 2002, 2005; Ni et al., 2016), and more markedly, of South America (Jaramillo et al., 2006; Hoorn et al., 2010). Surprisingly, although with regionally heterogeneous floras, no drastic change in paleo-biome distribution, terrestrial isotopes and phytolith assemblages has been detected between the late Eocene and the early Oligocene in the Southern cone of South America (e.g., Dunn et al., 2015; Kohn et al., 2015; Pound and Salzmann, 2017; Barreda and Palazzesi, 2021). In contrast, substantial changes are recorded on palynomorphs at lower latitudes, especially from north-east South America (Colombia and Venezuela), with a rapid phase around the EOT, likely linked to the onset of the Antarctic glaciation (Jaramillo et al., 2006). At tropical-equatorial latitudes, it seems that the global cooling provoked both a sustained drop in precipitation and increased seasonality. So far, based only on vegetation proxies, the aridification resulted in a decrease of plant morpho-diversity and in the opening of terrestrial environments, hitherto dominated by evergreen rainforests (Jaramillo et al., 2006; Hoorn et al., 2010).

Here, we describe nine plurispecific fossil localities originating from Shapaja, San Martín Department, at ca. 7◦ S in Peruvian Amazonia, and distributed along a 120 + 50 m-thick section (Figs. 1, 2; see Geological setting for more details). This stratigraphic interval belongs to the upper member of the Pozo Formation [Fm.] (Pozo Shales) and encompasses the late Eocene–earliest Oligocene interval (Fig. 2). The concerned fossil localities yielded plant remains (leaves, seeds, wood, charophytes, and palynomorphs), mollusks, decapods, and/or vertebrates (selachians, actinopterygians, lungfishes, amphibians, turtles, crocodylomorphs, and mammals. Decapods and rodents originating from some of the concerned localities (TAR-20, TAR-21, TAR-22, TAR-13, and TAR-01) were previously studied by Klaus et al. (2017) and Boivin et al. (2018, 2019a, 2019b), respectively.

In the absence of radioisotopic datings so far available in the Shapaja section (e.g., through Ar/Ar ages on volcaniclastic sediments or U/Pb ages on detrital zircons), this section was extensively sampled for chemostratigraphy (δ13C on dispersed organic matter and pedogenic carbonate nodules) in order to refine the local stratigraphy and to accurately locate the EOT, as well as hypothetic hints of early Oligocene glaciations (Fig. 2; Zachos et al., 2001, 2008; Vandenberghe et al., 2012; Westerhold et al., 2020). Indeed, C-isotopes on both organic matter and pedogenic nodules have been judged as reliable material for chemostratigraphy in many sections and paleoenvironments over the world, including terrestrial settings (e.g., Gr¨ocke et al., 1999; Magioncalda et al., 2004; Noiret et al., 2016 and references therein). Ultimately, we also aim to test the occurrence of biotic turnovers related to the EOT and subsequent climatic events, through the analysis of potential shifts in terrestrial and aquatic communities along the concerned section.

2. Regional setting

Thick Cretaceous–Cenozoic sections crop out continuously along river banks and newly-cut roads in the San Martín Department. Hermoza et al. (2005) and Roddaz et al. (2010) provided a synthetic overview of Cenozoic tectono-sedimentary history of Northern Peruvian foreland basin, recently refined by Eude et al. (2015) and Moreno et al. (2020). The studied section, overhanging the confluence between the Ríos Mayo

and Huallaga (Fig. 1), was considered as documenting the sandstone-dominated Chambira Fm., i.e. allegedly late Oligocene–early Miocene in age, in the Utcurarca geological map, without any chronostratigraphic or biostratigraphic constraints (S´anchez Fern´andez et al., 1997). Nevertheless, given that floodplain and fine-

grained detrital deposits (shales) are fully dominating, the concerned sequence might be referable as a whole to the upper member of the underlying Pozo Fm. instead ("Upper Pozo (shale) member"; see Hermoza et al., 2005; Roddaz et al., 2010). This shale-dominated member, further characterized by shallow marine/littoral components, most probably spans the late Eocene–late Oligocene interval in the northern Peruvian foreland basin (Roddaz et al., 2010; Antoine et al., 2016). Similar deposits assigned to the Upper Pozo Shale member recently yielded various fossil remains near Juanjuí, 80 km further to the SW (TAR-47, TAR-49, and TAR-50 localities; Assemat et al., 2019). In contrast, the base of the Chambira Fm. (late Oligocene) overlies unconformably the sand-dominated lower member of the Pozo Fm. (Pozo Sands, late middle–late Eocene) in the Ucayali Basin, near Contamana (Antoine et al., 2016).

The fossil-yielding stratigraphic subsections at Shapaja are i) 120 m-thick, with a general N80–110 direction and 20–30◦ W dipping for the western part and ii) 90 m-thick, with a general N160 direction and 45◦ W dipping for the eastern part. A reverse fault delimits both sections, with the eastern section overriding the western one (Fig. 1). A ~ 10 m-thick overlap is hypothesized between the eastern and the western sections, on lithostratigraphical grounds. On both sides, the stratigraphic sequence is dominated by fine-grained sediments (red shales and siltites), with gypsum veins distributed obliquely with respect to the general dipping, and alternating with fine- to coarse-grained yellow sandstones, with oxidized leaf litters (TAR-74, TAR-20, TAR-21sup, and TAR-22 localities) and clay pebble-rich grey microconglomerates (TAR-72, TAR-21, and TAR-73 localities). Two lenses of carbonate nodule-rich blue clays further occur in the upper part of the western section (TAR-13 and TAR-01 localities). Given the general geometry of deposits and thrust, all nine successive fossil localities are distributed within these coarse-grained bodies, with the following fossil locality sequence: TAR-74, TAR-20, TAR-72, TAR-21, TAR-21sup, TAR-13, TAR-22, TAR-73, and TAR-01 (Fig. 1C). Lower in the eastern series two more fossil-yielding localities were found, TAR-67 and TAR-66. These two localities are assignable to the lower member of the Pozo Fm. (Pozo Sands) and they document a noticeably-earlier stratigraphic interval (late middle–early late Eocene; Fig. 1). Their detailed analysis falls beyond the scope of the current work.

3. Material and methods

The fossil localities studied here were discovered in 2012–2018 and investigated in 2012–2019 (see SI). Samplings for chemostratigraphical analyses were performed in 2018.

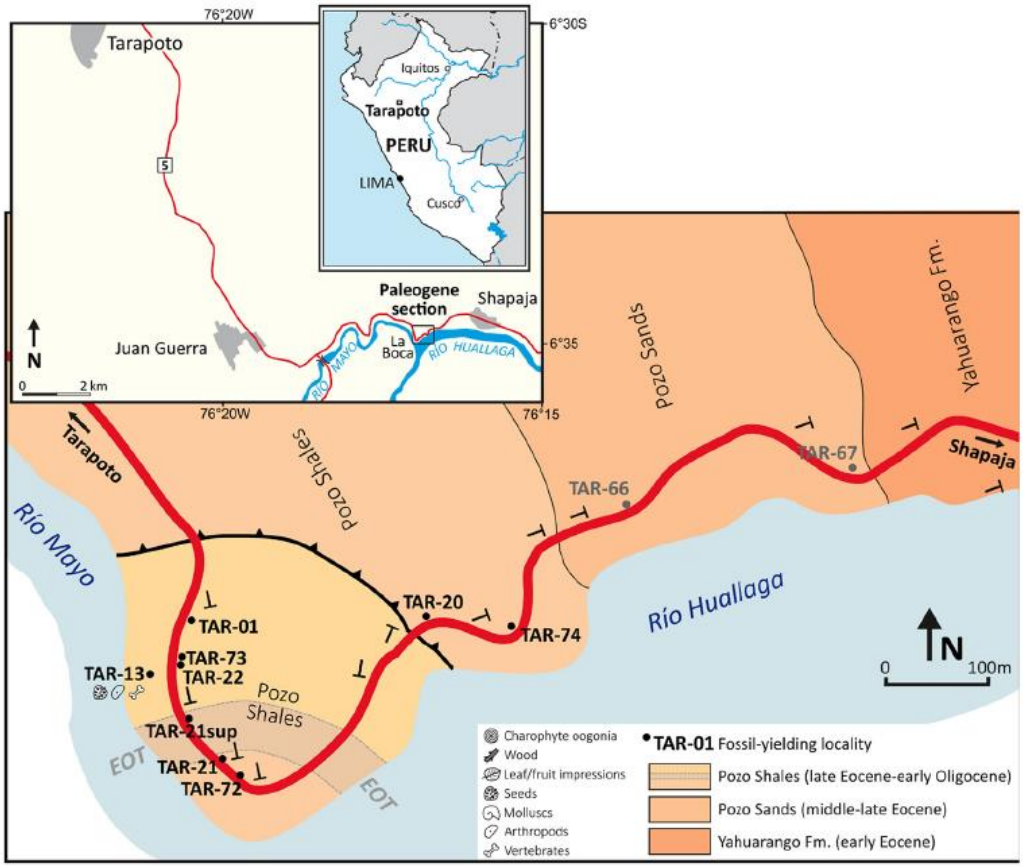


Fig. 1. Location (A) and geological map (B) of the studied area, around the Río Huallaga–Río Mayo confluence, with fossil localities of interest, at Shapaja, San Martín Department, Peruvian Amazonia. TAR-67 and TAR-66 localities (Pozo Sands; late middle–early late Eocene), significantly older than all other TAR- localities (based on stratigraphy, lithology, and distinct mammalian faunas). EOT, Eocene–Oligocene transition. Ideograms denote fossil content for the locality TAR-13, which is situated outside the measured sections illustrated in Fig. 2.

3.1. Chemostratigraphy

A total of 168 samples were collected in both western and eastern sections at Shapaja (137 and 31 samples, respectively). Carbon isotope analyses on dispersed organic matter (δ13Corg) were performed on 121 samples (Table 1). Samples not considered for organics had too low carbon content and/or major traces of roots, deep oxidation/weathering, preventing robust isotopic analyses. Carbon isotope analyses on pedogenic nodules (δ13Cnod) were performed on 92 samples, typically in red/brown

pedogenic marls and siltstones (Table 1). In the Shapaja section, C-isotope analyses on bulk (carbonates) were not performed due to the fact that secondary fluids most likely perturbed the primary signal.

Organic matter of the sediments was isolated, following the procedure described in Yans et al. (2010) refined by Storme et al. (2012). The dispersed organic carbon isotope analyses (δ13Corg) are based on powdered rock samples of about 3 to 10 g, acidified in 25% HCl solution during 2 h in order to remove carbonate. Soluble salts were removed by repetitive (1–6) centrifuging (4000 rpm) with deionized water until a neutral sediment was obtained. Finally, residues were dried at 35 ◦C and powdered again. Analyses were performed with an elemental analyzer (Carlo-Erba 1110) connected online to a ThermoFinnigan Delta V Plus mass spectrometer at the University of Erlangen. Accuracy and reproducibility of the analyses were checked by replicate analyses of international standards USGS40 and USGS41. The reproducibility of analyses is within 0.2‰ (1σ).

Pedogenic nodules (δ13Cnod) were crushed and powders reacted with 100% phosphoric acid at 70 ◦C using a Gasbench II® connected to a ThermoFinnigan V Plus® masspectrometer at the University of Erlangen. Isotopic compositions are calibrated with standards NBS19 for δ13Cnod. Reproducibilities are within +/□ 0.05‰ (1σ). Each sample was analyzed 1 to 3 times. Organic 13C/12C values are normalized to the international VPDB standard (Vienna Pee Dee Belemnite). Total organic content (%TOC) was measured with an elemental analyzer LECO® (CS-200). The CaCO3 (%) content of the samples was measured with a Bernard Calcimeter.

3.2. Fossil plants

The macrofossil plant material of the Shapaja section corresponds to impressions of non-monocot angiosperm leaves and fruits, which were studied and stored at the Paleontological Collection of the Museo de Historia Natural de la Universidad Nacional Mayor de San Marcos Lima, Peru (DPV-MHN-UNMSM; inventory numbers PVMUSM-60 to -83). Fossil leaves were organized and described by morphotypes following the method proposed by Peppe et al. (2008). Each morphotype has a two-letter prefix (PZ) based on the formation name (Pozo Formation) plus a number starting from one.

Fossil seeds were recovered by screenwashing (seed additional details below) from samples TAR-74, TAR-20, TAR-21, TAR-13, TAR-22, TAR-73, and TAR-01. The specimens are mostly preserved as silicified and/or iron-rich locule casts, and less commonly as carbonized remains.

Taxonomic affinities of the leaf, fruit, and seed morphotypes were proposed when possible based on the presence of taxonomicallyinformative characters (shape, size, margin type or venation patterns in leaves), extant material available for comparison, and the level of completeness of the description of each morphotype.

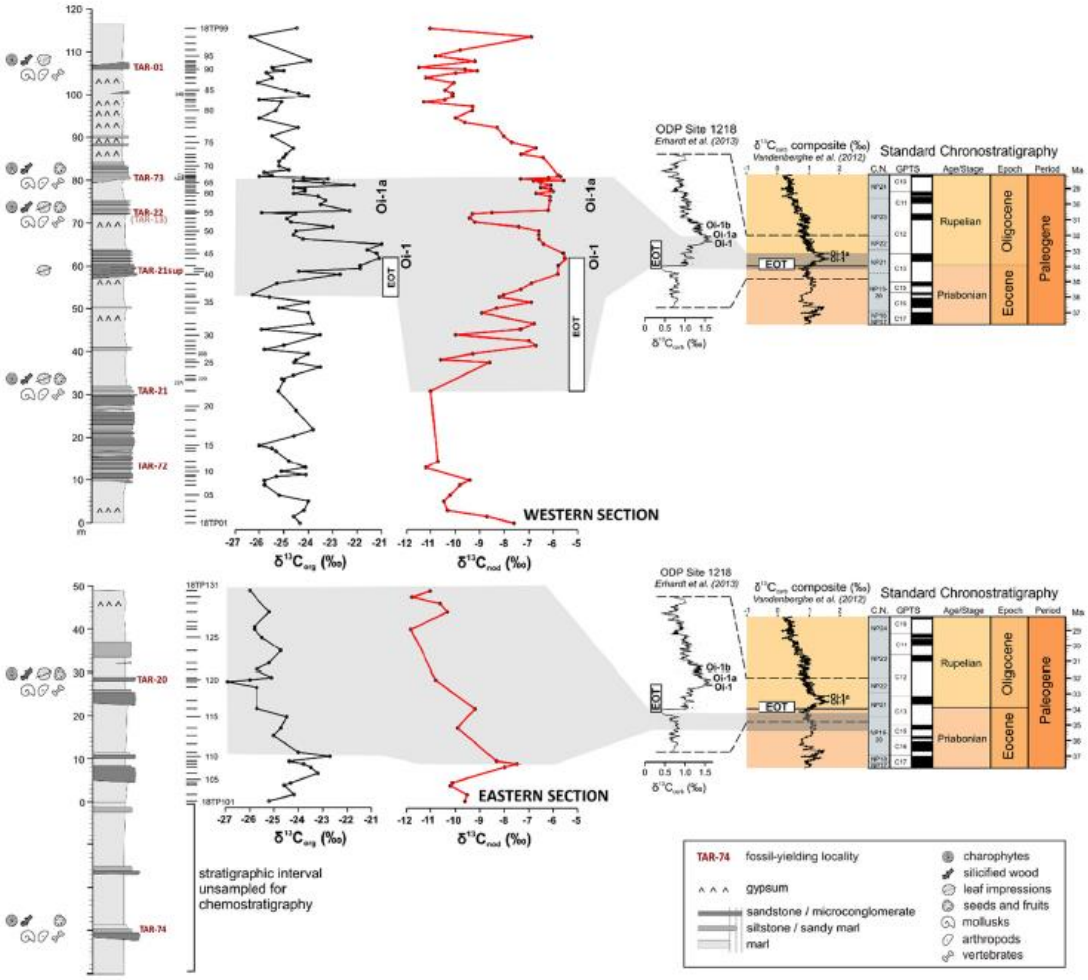


Fig. 2. Stratigraphic sections encompassing the late Eocene–early Oligocene interval at Shapaja, with location of chemostratigraphical samples, resulting δ13C curves (on organic matter [δ13Corg] and pedogenic carbonate nodules [δ13Cnod], in ‰), and chronological interpretations (right) based on δ13C curves around the Eocene-Oligocene transition in ODP Site 1218 (Erhardt et al., 2013) and reference δ13C composite curve (Cramer et al., 2009 modified by Vandenberghe et al., 2012). Top = western section; bottom = eastern section. Ideograms denote fossil content (charophytes, wood, leaf imprints, seeds/fruits, mollusks, crustaceans, and vertebrates, respectively; see Fig. 1). C.N., Calcareous Nannoplankton. EOT, Eocene–Oligocene Transition. GPTS, geomagnetic polarity timescale.

Table 1. Chemostratigraphical data of the Shapaja area, including section, sample labels, heights (m), CaCO3 content (%), δ13Corg values (‰, VPDB) and δ13Cnod values (‰, VPDB)

Section	Sample	Height (m)	$CaCO_3$ (%)	$\delta^{13}C_{org}$ (‰) - organics	$\delta^{13}C_{nod}$ (‰) - nodules	Section	Sample	Height (m)	$CaCO_3$ (%)	$\delta^{13}C_{org}$ (‰) - organics	$\delta^{13}C_{nod}$ (‰) - nodules
Western	18TP99	115.5	11	−24.5	−11	Western	18TP35	51.5	18	−24	−6.9
Western	18TP98	113.5	8	−26.5	−6.9	Western	18TP34	50.1	64	−25.2	−8.3
Western	18TP97	112	6	TOC too low	–	Western	18TP33	49	18	−24.1	−8.9
Western	18TP96	110.5	13	TOC too low	−9.8	Western	18TP32	46.5	25	−23.8	−6.8
Western	18TP95	109	16	TOC too low	−10.7	Western	18TP31	45.2	24	−25.9	−7.4
Western	18TP94	108	18	−23.9	−9.2	Western	18TP30	43.8	15	−23.5	−10.1
Western	18TP93	107.9	49	TOC too low	–	Western	18TP29	42.5	27	TOC too low	−7
Western	18TP92	107.5	17	−24.5	−11.5	Western	18TP28	41.4	29	−25	−6.8
Western	18TP91	106.4	16	TOC too low	–	Western	18TP27	40.8	19	−25.8	–
Western	18TP90	106	8	−25.4	−9.5	Western	18TP26B	39.5	8	−24	−9.3
Western	18TP89	105.6	8	−25	−9.2	Western	18TP26	38.1	18	−24.5	−10.6
Western	18TP88	105.1	8	−25.7	−10	Western	18TP25	37.5	20	−24.6	–
Western	18TP87	104	13	−25.5	−11.2	Western	18TP24	36.4	14	−23.5	–
Western	18TP86	102.8	16	−26.1	−10	Western	18TP23	34.5	19	−24.6	–
Western	18TP85	101.1	17	−24.9	−10.3	Western	18TP22B	33.3	15	−25.1	–
Western	18TP84B	100.3	10	−24.4	−10.1	Western	18TP22A	33.6	13	−25	–
Western	18TP84	99.8	9	−24	−10.1	Western	18TP21	30.8	53	−25.2	−10.8
Western	18TP83	98.8	18	−26	−10.4	Western	18TP20	27.3	32	TOC too low	–
Western	18TP82	98.3	8	−24.1	−11.3	Western	18TP19	26.3	21	−24.5	–
Western	18TP81	97.6	66	TOC too low	−9.3	Western	18TP18	24	30	TOC too low	–
Western	18TP80	96.2	8	−25.4	−9.3	Western	18TP17	21.8	27	−23.8	–
Western	18TP79	94.5	24	−26	−10	Western	18TP16	20.4	15	−24.6	–
Western	18TP78	93.5	25	TOC too low	−9.6	Western	18TP15	18.2	12	−26	–
Western	18TP77	92.2	21	−24.4	−8.3	Western	18TP14	17.5	10	−25.5	–
Western	18TP76	91.2	22	−25.5	−8	Western	18TP13	16.9	14	−25.3	–
Western	18TP75	88.8	12	−22.4	−7.7	Western	18TP12	14.4	34	−24.8	−10.7
Western	18TP74	87.5	23	−24.5	−6.7	Western	18TP11	13	65	−24.1	−11.2
Western	18TP73	86.1	28	−24.9	−7.3	Western	18TP10	12	21	−25.1	–
Western	18TP72	85.3	28	−25	−6.4	Western	18TP09	11.2	19	−24.2	–
Western	18TP71	84.3	26	−25.2	–	Western	18TP08	10.8	10	−25.2	–
Western	18TP70	83.3	27	−25.2	–	Western	18TP07	9.8	32	−25.8	−8.8
Western	18TP69	82.3	26	−24.8	–	Western	18TP06	8.9	27	−25.8	−9.8
Western	18TP68	81.2	23	−25.8	–	Western	18TP05	6.5	10	−25.2	−10.2
Western	18TP67C	81.2	27	−25.5	−5.8	Western	18TP04	5	8	−24	−10.6
Western	18TP67B	80.75	24	−26	−5.7	Western	18TP03	2.9	15	−24.2	−10.3
Western	18TP67NEW	80.3	28	−24.3	−6.2	Western	18TP02	1.5	10	−24.6	−8.7
Western	18TP67	80.3	33	−23.2	−6.5	Western	18TP01	0	5	−24.3	−7.7
Western	18TP66	80	25	−24.6	−6.8	Eastern	18TP131	48.9	24	−26	−11.1
Western	18TP65	79.4	24	−23.4	−6.5	Eastern	18TP130	47.5	13	TOC too low	−11.8
Western	18TP64	78.8	24	−22.1	−6.1	Eastern	18TP129	46	25	TOC too low	−10.8
Western	18TP63	78.3	22	−24.6	−6.6	Eastern	18TP128	43.9	14	−25.2	−10.2
Western	18TP62	77.9	23	−24.1	−6.1	Eastern	18TP127	40.5	9	−25.8	–
Western	18TP61	77.5	21	−24.1	−6	Eastern	18TP126	39.9	11	−25.8	−11.8
Western	18TP60	77	20	−24.6	−6.7	Eastern	18TP125	38.1	8	−25.5	–
Western	18TP59	76.3	24	−23.6	−6.1	Eastern	18TP124	34.9	11	−24.7	–
Western	18TP58	75.3	22	−23.3	−6.1	Eastern	18TP123	32	9	−25.2	–
Western	18TP57	74.3	20	−23.5	–	Eastern	18TP122	30.5	10	−25.7	–
Western	18TP56	73	19	−22.3	−6.2	Eastern	18TP121	28.8	12	−25.1	–
Western	18TP55	72.5	31	−25.9	−8.7	Eastern	18TP120	28.3	13	−26	−10.8
Western	18TP54	72.1	13	−24.5	−9.3	Eastern	18TP119	27.9	32	−26.9	–
Western	18TP53	71.1	15	−24.9	−9.4	Eastern	18TP118	26.6	30	−25.7	–
Western	18TP52	70.2	17	−24.7	−9.2	Eastern	18TP117	23.5	24	TOC too low	–
Western	18TP51	69.2	20	−23	−7.4	Eastern	18TP116	21.7	9	−25.7	−9.2
Western	18TP50	68.2	23	−24.5	−6.6	Eastern	18TP115	19.8	10	−24.5	–
Western	18TP49	67.3	23	−24.6	−6.6	Eastern	18TP114	17.2	10	−24.7	−9.9
Western	18TP48	66.3	21	−24.2	−6.6	Eastern	18TP113	15.4	5	−25	–
Western	18TP47	65.1	20	−21	−6.4	Eastern	18TP112	13.5	5	TOC too low	–
Western	18TP46	63.8	15	−21.6	–	Eastern	18TP111	11.5	6	−24	–
Western	18TP45	63	16	−21.2	−5.6	Eastern	18TP110	10.5	18	−22.7	–
Western	18TP44	61.8	21	−21.1	−5.5	Eastern	18TP109	9.5	13	−24.4	−9.6
Western	18TP43	60.2	22	−21.9	−5.8	Eastern	18TP108	8.9	11	−23.8	−7.5
Western	18TP42	59.5	20	−21.9	–	Eastern	18TP107	8.1	10	−23.5	−8
Western	18TP41	58.8	20	−24.4	–	Eastern	18TP106	6.7	13	−23.2	–
Western	18TP40	58.1	24	−22.7	−5.8	Eastern	18TP105	5.2	11	−25.2	–
Western	18TP39	55.9	9	−25.7	−6.7	Eastern	18TP104	4.5	22	−24.3	−10.1
Western	18TP38	54.5	12	TOC too low	−7.3	Eastern	18TP103	4	12	−24.6	−10.2
Western	18TP37	53.2	16	−26.3	−8	Eastern	18TP102	1.8	19	−24.2	−9.5
Western	18TP36	52.6	20	−25.6	−8.2	Eastern	18TP101	0.2	13	−25.2	−9.6

3.3. Other fossil remains (charophytes, mollusks, decapods, and vertebrates)

Large mollusk and vertebrate specimens uncovered were prepared mechanically in the field and at lab. Small vertebrate specimens, decapod claws, and micromollusks were concentrated by screenwashing ca. 2000 kg of raw sediment, with 2 mm, 1 mm, and 0.7 mm meshes (12–762 kg per locality; see SI for more details), using highly-

diluted hydrogen peroxide, in 2012–2019. This protocol also allowed for obtaining charophyte oogonia and seeds, as well as carbonized and silicified wood chunks. Except when mentioned, all concerned specimens are permanently housed in the DPV-MHN-UNMSM.

The palynological preparation was carried out at the Stratigraphy Research Institute (IIES) at the Universidad de Caldas, Manizales, Colombia, following the Traverse's (2007) standard procedure (37% hydrochloric acid, Hydrofluoric acid at 70% and density separation using Zinc Chloride). Samples were mounted using Canada balsam.

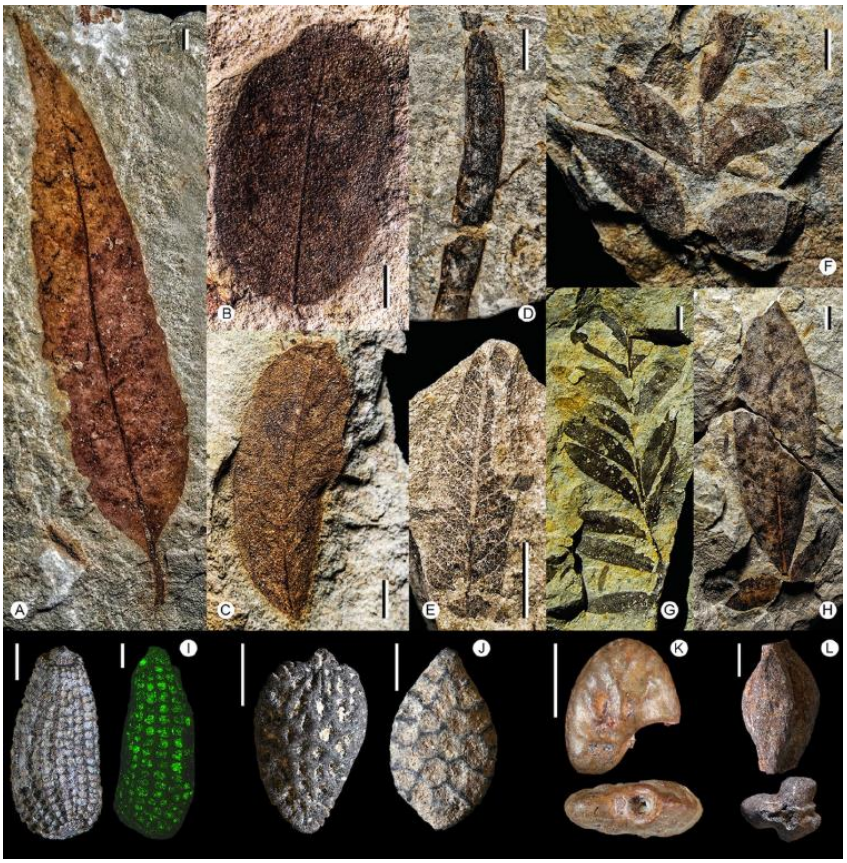


Fig. 3. Plants (leaf and fruit impressions; permineralized seeds and fruit) from the late Eocene-early Oligocene Shapaja section, San Martín, Peruvian Amazonia. A, PZ1, non–monocot of uncertain affinities (PVMUSM-60; TAR-21sup). B, PZ2, non–monocot of uncertain affinities, resembling Fabaceae (PVMUSM-66; TAR-21sup). C, PZ3, non–monocot of uncertain affinities (PVMUSM-68; TAR-21sup). D, PZ4, Fabaceae fruit (PVMUSM-71; TAR-01). E, PZ7, non–monocot of uncertain affinities (PVMUSM-78; TAR-01). F, PZ8, Fabaceae compound leaf (PVMUSM-80; TAR-01). G, PZ9, compound leaf of uncertain affinities (PVMUSM-82; TAR-01). H, PZ10, non–monocot of uncertain affinity (PVMUSM-83; TAR-01). I, cf. Elatine seeds showing reticulate seed coats, left (TAR-74), right (TAR-01) photographed under epifluorescence. J, Two

Passifloroideae seed types showing conspicuously pitted surfaces (TAR-21). K, Araceae (cf. Monstera) seed; top in lateral view, bottom in ventral view, note depressed hilum (TAR-21). L, Loculicidal fruit of euphorbiaceous affinity. Scale bars = 5 mm (A–H), 2 mm (J left, L), 1 mm (J right, K), and 500 μm (I).

4. Results

4.1. Chemostratigraphy

Carbon isotopic values on dispersed organic matter (δ13Corg) range from -26.9 to -21.0‰ (Table 1). These data are in good agreement with the expected δ13C values on organics at the Eocene-Oligocene interval (see Sarkar et al., 2003; Benammi et al., 2019). Carbon isotopic values on pedogenic nodules (δ13Cnod) range from -5.7‰ to -11.8‰ (Table 1).

We provide a detailed description of all the isotopic results in SI. The most relevant chemostratigraphic features are as follows: in the Eastern section, C-isotope values on both organics and pedogenic nodules show (from base to top) a short positive trend followed by a quite long negative trend (Fig. 2; Table 1). In the Western section, two main positive excursions are observed. This pattern is particularly obvious for C-isotope data on pedogenic nodules (Fig. 2; Table 1).

TOC content is very low for all the samples (around 0.05%), whereas the CaCO3 contents much more satisfactorily range from 5% to 66% depending on the samples (Table 1).

4.2. Plant remains

4.2.1. Leaf and fruit impressions (Fig. 3 A-H)

Ten magnoliopsid dicot morphotypes were recognized in the Shapaja section, through leaf and fruit impressions (nine morphotypes and one [PZ4], respectively), recovered from TAR-20 (late Eocene), TAR-21sup (EOT), and TAR-01 (early Oligocene). Most morphotypes are documented by several specimens. These morphotypes are fully described, compared, and illustrated in the SI. TAR-20 yielded a single leaf morphotype (PZ5; Fig. S1M) and TAR-21sup three (PZ1–3; Fig. 3A-C), all of uncertain affinities. TAR-01 provided by far the most diversified macroflora, with a fruit morphotype (PZ4: legume; Fig. 3D) and seven leaf morphotypes (PZ1, PZ3, PZ6–10; Fig. 3E-G). Three of them document Fabaceae Fabales (PZ4, 8, and 9). Leaf morphotypes PZ1 and PZ3 were recognized both at TAR-21sup and TAR-01.

All leaves from the Shapaja section have entire margins and pinnate primary venation. Most have nanophyll and/or microphyll leaflet laminar sizes (dimorphic leaflets in PZ10; Fig. 3F), with petiolate leaf and marginal blade attachments. PZ1 and PZ2 have larger leaflets (mesophyll and notophyll, respectively; Fig. 3A,C). Some leaves are compound pinnae or bipinnate, imparipinnate with opposite (PZ8; Fig. 3F) or alternate (PZ9; Fig. 3G), non-overlapping pinnules. The leaves/leaflets are either oblong, obovate, ovate, or elliptic in shape (PZ9), mostly with an acute apex. Major secondaries are brochidodromous in most morphotypes, except for PZ6 and PZ8 (craspedodromous). PZ2 has affinities with the late Miocene morphotype IP2 from Shumanza (Feussom-Tcheumeleu et al., 2019) and with *Machaerium* (Fabaceae). All four fruit specimens available at TAR-01 are straight and symmetric legumes, with placental and non-placental margins (well-developed, but very narrow and non-winged), seven symmetrical seminal chambers separated by a septum, and a convex apex (Fig. 3D).

4.2.2. Seeds

Approximately forty seeds were identified throughout the Shapaja section. However, most of the specimens came from late Eocene samples, particularly from locality TAR-21. Seeds that were taxonomically identified are briefly described here.

- cf. *Elatine* (TAR-74, TAR-01): two small seeds (~600–700 µm long), slightly curved, operculate, with reticulate coat (Fig. 3I).

- Passifloroideae (TAR-21): two different seed morphotypes of the passion fruit family were identified from TAR-21. Both seeds are bilateral, ellipsoidal to ovoid with a rounded base and a pointed apex, chalaza apical, and a conspicuously pitted surface (>20 depressions) (Fig. 3J).

- Araceae (cf. *Monstera*): The most common seed morphotype from the Shapaja section, with ~30 specimens. The seeds are ~2 mm high and 2.5 mm wide, flattened ventrally and with a dorsal ridge, the micropyle is on the opposite side of the hilum from the chalaza. The hilum appears as a depressed channel (Fig. 3K).

Three other seeds are less understood due to their fragmentary preservation and will require additional study to confirm their affinity, but they can be preliminarily assigned to the families Vitaceae (TAR-20), Poaceae (TAR-20), and Nymphaceae (TAR-73). A single loculicidal fruit of euphorbiaceous affinity is also reported from sample TAR-21 (Fig. 3L).

4.2.3. Charophytes and wood

All localities but TAR-72, TAR-21sup, and TAR-13 have yielded charophyte oogonia and wood chunks (millimetric to centimetric, either silicified or oxidized). They were not identified thus far.

4.2.4. Pollen

Several samples were processed but they were all sterile with the exception of a sample at TAR-72, i.e., 12 stratigraphic meters below TAR-21 (latest Eocene). The TAR-72 sample had a poor recovery of organic matter mostly dominated by coaly matter and a few grains that include the magnoliopsid *Psilatricolporites* sp., Fungi monocellate, and the fern spores *Psilatriletes* sp. and *Baculatriletes* sp. The high level of organic matter degradation suggests a seasonal water-table that oxidized the organic matter.

4.3. Mollusks and decapods

Mollusks are mostly represented by freshwater gastropod inner casts, with two distinct species of small pachychilids (TAR-01; tropical distribution; Fig. 5A), three specimens of a small planorbid (*Helisoma* sp.; one in TAR-20, two in TAR-21), several ampullariids either large or small (TAR-22; Fig. 4C), and small unidentified turriform snails (TAR- 20, TAR-72, and TAR-73), and a bulliform snail of unknown affinities (two specimens in TAR-21; Fig. 4D). An external cast of a pluricentimetric bivalve with paired valves, referred to as a probable corbiculid of freshwater-brackish affinities, was unearthed at TAR-22 (Fig. 4A-B). Decapod claw and carapace fragments were found by hundreds in most localities (TAR-74, TAR-20, TAR-21, TAR-13, TAR-22, TAR-73, and TAR-01). All of them are assigned to Trichodactylidae, a South and Central American family of freshwater crabs of tropical affinities, abundant in Amazonian lowland streams today (Yeo et al., 2007), but with a scarce fossil record ranging the middle Eocene–late Miocene in Western Amazonia (Klaus et al., 2017). None of the specimens from the Shapaja decapod sample, partly studied by Klaus et al. (2017) for the TAR-01 locality, is identifiable at the genus or species level.

4.4. Vertebrates:

4.4.1. Metatherian mammals

Two fragmentary dental remains from TAR-74 and TAR-01, preventing precise taxonomic identification (Fig. 4E), and a 1-mm wide astragalus (Fig. 5B-D) are referred to as Marsupialiformes *incertae sedis*.

The extinct order Polydolopimorphia is represented in Shapaja by five taxa assigned to Bonapartheriiformes. Aside from a new prepidolopid bonapartherioid documented at TAR-74 (Fig. 4F-G), at least two taxa are assigned to argyrolagid argyrolagoids. The affinities of argyrolagids (gerbil-like marsupials) are still under debate. There is evidence supporting Argyrolagidae as representatives of polydolopimorphians (Goin et al., 2009; Chornogubsky and Goin, 2015) and of paucituberculatans (Sánchez-Villagra, 2001; Beck, 2017); in addition, a recent phylogeny indicates that argyrolagids are not paucituberculatans, and that they are phylogenetically close to peramelemorphs (Abello and Candela, 2020). Nonetheless, this discussion is out of the scope of this study, so we will assign here argyrolagids to?Polydolopimorphia. Fragmentary and heavily-worn molars from TAR-20 and TAR-72 (late Eocene) are identified as cf. *Proargyrolagus*. In contrast, specimens from TAR-21 (latest Eocene) and TAR-01 (early Oligocene) are well preserved and abundant (upper and lower cheek teeth). They document two distinct new species of *Proargyrolagus*: a small species in TAR-21 (*P.* nov. sp. A; Fig. 4H-J) and a larger one in TAR-01 (*P.* nov. sp. B; Fig. 5E-F). Accordingly, the Shapaja section attests to the earliest occurrence of i) *Proargyrolagus*, previously from upper Oligocene Salla Beds, Bolivia (Wolff, 1984; S´anchez-Villagra and Kay, 1997), and ii) the earliest and northernmost occurrences of Argyrolagidae, further pointing to the unsuspected and long-termed presence of these unique metatherians throughout the Eocene–Miocene interval in Proto-Amazonia (see Antoine et al., 2016). These teeth are “proto-hypsodont” (i.e., high- crowned) and complete specimens retain closed roots.

Unidentifiable plagiaulacoid premolars are also recognized in TAR- 20, TAR-72 (late Eocene) and TAR-01 (early Oligocene), and assigned to polydolopimorphians of uncertain affinities.

Paucituberculata (shrew opossums) are the most diverse order in Shapaja, with at least 12 taxa, all belonging to the extinct superfamily Palaeothentoidea (Fig. 5G-I). The records from Shapaja encompass two primitive species of Non-Pichipilidae palaeothentoids (NPP) in uppermost Eocene levels (TAR-72 and TAR-21), one of them being close to *Perulestes*, previously described at Santa Rosa (Goin and Candela, 2004) with close allies in early Contamana faunas (Antoine et al., 2016). Representatives of Palaeothentidae and Abderitidae are much more diversified in

TAR-01 (early Oligocene; Fig. 5I). In addition, fragmentary remains from TAR-72 and TAR-21 and referred to Palaeothentinae might document the earliest occurrence of the subfamily, previously recorded in the late Oligocene of Argentina and Bolivia (Abello, 2007; Rinc´on et al., 2015).

Contrary to all other localities, TAR-13 and TAR-22 have yielded a single marsupialiform specimen (a tiny astragalus of an unidentified marsupialiform (Fig. 5B-D) and a palaeothentoid molar, respectively; Table 2). This low abundance is particularly striking with respect to the volume of sediment treated at TAR-22 (214 kg; see SI). No metatherian specimen was recognized at TAR-73.

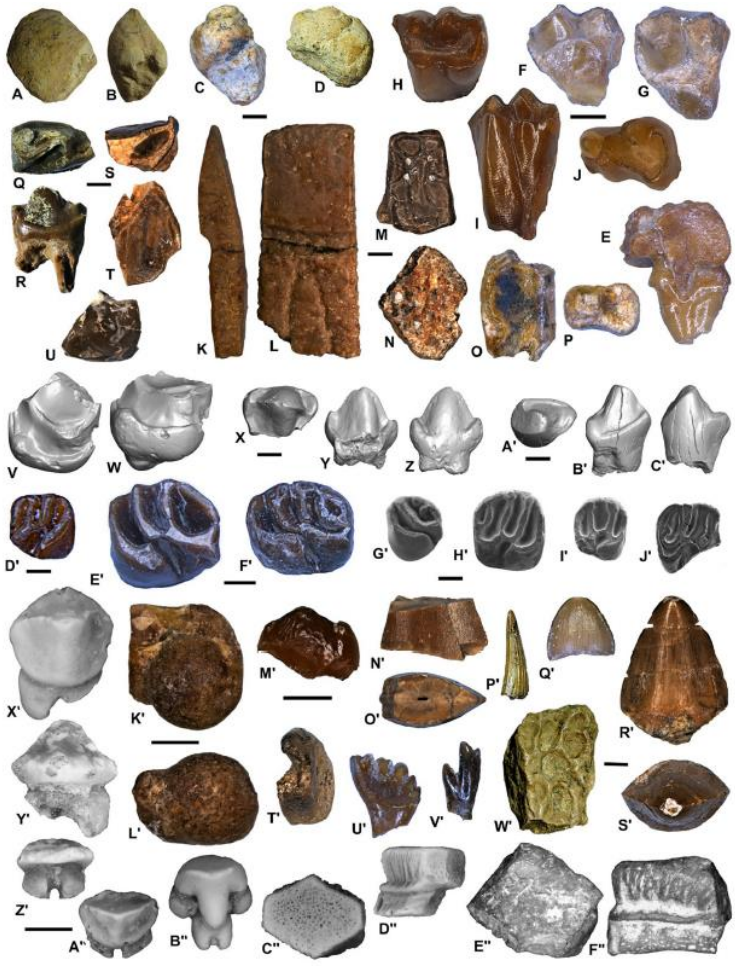


Fig. 4. Representative faunal content of late Eocene–earliest Oligocene paleocommunities near Shapaja, San Martín, Peruvian Amazonia (Assemblages 1 and 2; see Tables 2–4). **A-B**, MUSM 3955, Corbiculidae indet., natural inner cast with joined valves, in lateral (A) and dorsal views (B), TAR-22. **C**, MUSM 3956, Gastropoda indet., natural inner cast in front view, TAR-22. **D**, MUSM 3957, Gastropoda indet., bulliform, natural inner cast in front view, TAR-22. **E**, MUSM 3958, Marsupialiformes *incertae sedis*, left P3 in labial view, TAR-74. **F-G**, MUSM 3959, Prepidolopidae gen. et sp. nov., right Mx in lingual (F) and occlusal views (G), TAR-74. **H-J**, *Proargyrolagus*

nov. sp. A, TAR-21: MUSM 3960, left M2 in occlusal (H) and lingual views (I); MUSM 3961, left m1 in occlusal view (J). **K-M**, *Parastegosimpsonia peruana*: MUSM 3962, mobile osteoderm in cross (K) and lateral views (L), TAR-21; MUSM 3963, fixed osteoderm in external view (M), TAR-22. **N**, MUSM 3964, Peltephilidae indet., fixed osteoderm, TAR-21. **O**–**P**, MUSM 3965, Mylodontidae indet., molariform in lateral (O) and vertical views (P), TAR-22. **Q-R**, MUSM 3966, Leontiniidae indet., right p3 in occlusal (Q) and labial views (R), TAR-74. **S-T**, MUSM 3967, Adianthidae indet., fragmentary right M2–3 in occlusal (S) and lingual views (T), TAR-21. **U**, MUSM 3968, Didolodontidae indet., fragment of a left?m1 in occlusal view, TAR-22. **V**–**W**, MUSM 3969, Anthropoidea indet. 1, right upper molar fragment in occlusal (V) and lingual views (W), TAR-21. **X-C′**, Anthropoidea indet. 2 (small) TAR-21: MUSM 3970, right upper premolar (labial part) in occlusal (X), lingual (Y), and labial views (Z); MUSM 3971, left p2 in occlusal (A'), lingual (B′), and labial views (C′). **D′**, MUSM 3972, *Pozomys* nov. sp., left m1 in occlusal view, TAR-74; **E'-F′**, *Eopululo* cf. *wigmorei*, TAR-74: E', MUSM 3973, left M1/2 in occlusal view; F′ , MUSM 3974, left dP4 in occlusal view. **G'**, MUSM 2965, *Eoincamys parvus*, left M3 in occlusal view, TAR-22. **H′**, MUSM 2925, *Kichkasteiromys raimondii*, right M1/2 (holotype) in occlusal view, TAR-21. **I′**, MUSM 2960, *Selvamys paulus*, right M2 in occlusal view, TAR-22; **J'**, MUSM 3332, *Tarapotomys subandinus*, fragmentary right M1 in occlusal view, TAR-20. **K′-L'**, MUSM 3975, Anura indet., distal humerus in anterior (K′) and distal views (L'), TAR-20. **M'**, MUSM 3976, unidentified?teiid squamate tooth in lateral view, TAR-21. **N′-O′**, MUSM 3977, Sebecidae indet., fragmentary tooth in lingual (N′) and apical views (O′), TAR-74. **P′**, MUSM 3978, Gavialoidea indet., tooth in sagittal view, TAR-22. **Q'**, MUSM 3979, Caimaninae indet., globular tooth in lingual view, TAR-22. **R'-S′**, MUSM 3980, Caimaninae indet., leaf-shaped tooth in lingual (R') and apical views (S′). **T'**, MUSM 3981, Lepidosirenidae indet., large dental plate in apical view, TAR-72. **U′**, MUSM 3982, Anostomidae, cf. *Leporinus* sp., hexacuspid tooth, TAR-21. **V′** , MUSM 3983, Loricariidae indet., muffle-shaped tooth, TAR-21. **W′**, MUSM 3984, cf. *Phractocephalus* sp., fragmentary cranial bone, TAR-22. **X'-Y′**, MUSM 3985, *Paratrygon* nov. sp., female anterior tooth in lingual (X') and labial views (Y′), TAR-22. **Z'-A"**, MUSM 3986, *Potamotrygon* nov. sp., female anterior tooth in lingual (Z') and labial views (A"), TAR-21. **B″** , MUSM 3987, *Pristis* sp., oral tooth in lingual view, TAR-22. **C″ -D″** , MUSM 3988, *Myliobatis* sp., tooth of a neonate/young individual in occlusal (C″) and lateral views (D″), TAR-21. **E"-F″** , MUSM 3989,?*Myliobatis* sp., tooth in occlusal (E") and lateral views (F″), TAR-21. V-C′ are 3D surface renderings. Scale

bars = 500 µm (*E*-J, V-D′ , G’-L’, U′ -V′ , E"-F″), 1 mm (E’-F′ , M’-O′ , X’-D″), 2 mm (C, K–P, S–U, Q’-T’), 5 mm (D, Q-R, P′), and 10 mm (A-B)

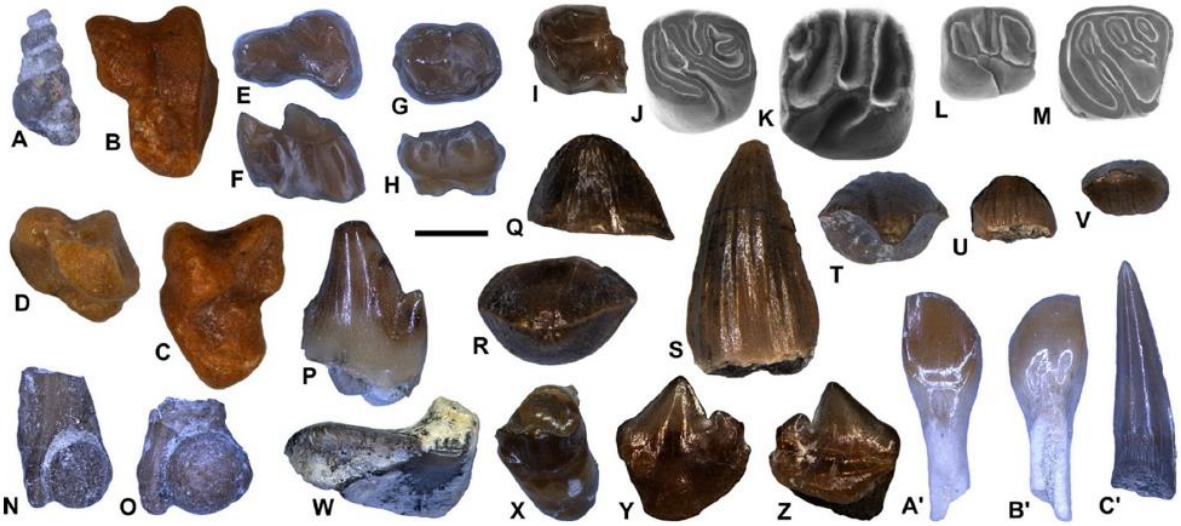


Fig. 5. Representative faunal content of the early Oligocene paleocommunities near Shapaja, San Martín, Peruvian Amazonia (Assemblage 3; see Tables 2–4). All specimens originate from TAR-01, except for MUSM 4018 (B-D: TAR-13). **A**, MUSM 3990, Pachychilidae indet. sp. 2, natural inner cast in front view. **B**–**D**, MUSM 4018, Marsupialiformes *incertae sedis*, right astragalus in dorsal (B), plantar (C) and distal views (D). ***E*-F**, MUSM 3991, *Proargyrolagus* nov. sp. B, left m1 in occlusal (B) and labial views (C). **G-H**, MUSM 3992, Palaeothentoidea indet. 2, right?m4 in occlusal (D) and lingual views (E). **I**, MUSM 3993, Abderitidae indet., fragmentary right m2, in occlusal view. **J**, MUSM 3496, *Tarapotomys mayoensis*, left M2 (holotype) in occlusal view. **K**, MUSM 2995, *Shapajamys labocensis*, right M2 (holotype) in occlusal view. **L**, MUSM 3159, *Mayomys confluens*, left M1 in occlusal view. **M**, MUSM 3492, *Eoincamys* cf. *pascuali*, right m1 in occlusal view. **N**, MUSM 3994, Anura indet., distal humerus fragment in anterior view. **O**, MUSM 3995, Anura indet., non-Pipidae, distal humerus fragment in anterior view. **P**, MUSM 3996, Unidentified squamate tricuspid tooth in lingual view. **Q-R**, MUSM 3997, Caimaninae indet., broken tooth, with irregular enamel in labial (N) and apical views (O). **S-T**, MUSM 3998, Caimaninae indet., tooth with grooved enamel in labial (P) and apical views (Q). **U**–**V**, MUSM 3999, Caimaninae indet., durophagous tooth, in labial (R) and apical views (S). **W**, MUSM 4000, Lepidosirenidae indet., large dental plate. **X**, MUSM 4001, cf. *Colossoma* sp., tooth in apical view. **Y-Z**, MUSM 4002, cf. *Serrasalmus* sp., 4th or 5th tooth of the dentary, in labial (V) and lingual views (W). **A’-B′**, MUSM 4003, *Leporinus* sp., tooth in palatine

(X) and ab-palatine views (Y). **C′**, MUSM 4004, *Hydrolycus* sp., tooth in lingual view. Scale bar = 500 μm (B–D), 1 mm (E-P, U–V, Y-Z) and 2 mm (A, Q-T, W-X, A'-C′).

Table 2 Taxonomic composition of metatherian communities from the late Eocene–early Oligocene Shapaja section, San Martín, Peruvian Amazonia, suggesting the presence of two successive turnovers (Assemblages 1–3), as for rodents (Table 3) and fish assemblies (Table 4, Fig. 6). Ass, Assemblage.

Taxa / Locality - Age	late Eocene				early Oligocene		
	TAR-74	TAR-20	TAR-72	TAR-21	TAR-13	TAR-22	TAR-01
Marsupialiformes *incertae sedis*	X				X		X
Polydolopimorphia							
Prepidolopidae gen. et sp. nov.	X						
?Prepidolopidae				X			
Polydolopimorphia indet.		X	X				X
?Polydolopimorphia							
Argyrolagidae							
cf. *Proargyrolagus*		X	X				
Proargyrolagus nov. sp. A (small)				X			
Proargyrolagus nov. sp. B (large)							X
Paucituberculata							
Palaeothentinae indet. 1			X				
Palaeothentinae indet. 2				X			
Palaeothentidae sp. nov. C							X
Palaeothentidae sp. nov. D							X
Palaeothentidae indet.							X
Abderitidae indet.							X
cf. *Perulestes*				X			
Palaeothentoidea, Abderitidae-Palaeothentidae indet. 1						X	
Palaeothentoidea, Abderitidae-Palaeothentidae indet. 2							X
Palaeothentoidea, non-Pichipilidae indet. 1 (basal)			X				
Palaeothentoidea, non-Pichipilidae indet. 2							X
Palaeothentoidea indet.							X
Co-occurring species	**2**	**2**	**4**	**4**	**1**	**1**	**10**
Weight of sediment sampled (kg)	220	185	119	762	20	214	470
	Ass 1	Assemblage 2			Transitional?		Ass 3

4.4.2. Eutherian mammals

Cingulates (armadillos). Two osteoderms (one movable and one fixed) from TAR-21 and TAR-22 (Fig. 4K-M), are referable to *Parastegosimpsonia peruana*, an astegotheriine dasypodid originally described at Santa Rosa (Ciancio et al., 2013). Two other osteoderms are too eroded/fragmentary for a precise identification but attributable to the Peltephilidae (TAR-21; Fig. 4N) and Dasypodidae (TAR-01) families.

Pilosans (sloths). A molariform belonging to a small mylodontid (under study by FP) was recovered from TAR-22 (Fig. 4O-P). Smaller in size than the smallest known representative of the family (*Brievabradys laventensis*, middle Miocene of Colombia; Villarroel, 2000), this "8"- shaped tooth is somewhat reminiscent to last upper molariforms of the late Oligocene *Octodontotherium* and *Paroctodontotherium* (Deseadan of Argentina and Bolivia, respectively; Hoffstetter, 1956; Shockey and

Anaya, 2011). Excluding *Pseudoglyptodon* (an Oligocene sloth-like xenarthran of dubious affinities; McKenna et al., 2006), this fossil from TAR-22 likely stands as the oldest record of a true sloth (for a review, see Pujos et al., 2017).

As for Astrapotheria (elephant-like native ungulates), the occurrence of unidentified Astrapotheriidae is suspected in TAR-21 and TAR-01, through small fragments of large-sized cheek teeth with apparent vertical and horizontal decussation on enamel (Koenigswald, 1997).

Among Notoungulata, representatives of the suborders Toxodontia (horse- and rhino-like native ungulates) and Typotheria (rabbit-like native ungulates) were recognized throughout the section, on the basis of isolated teeth and tooth fragments. Unfortunately, most remains are fragmentary and not assignable at the family level or below. Toxodontia indet. are documented by fragments of large-sized teeth (TAR-74, TAR- 20, and TAR-01). An early-diverging leontiniid occurs in TAR-74, as recorded by a mesodont lower premolar (p3; length = 16 mm; width = 11 mm; Fig. 4Q-R) with a strong distolabial extension of the protolophid, a bunoid entoconid united to the hypolophid, a short entolophid, an un-isolated fossettid, and a talonid longer than the trigonid. Somewhat reminiscent of p3–4 of *Elmerriggsia* from Deseadan beds of Patagonia (e. g., Shockey et al., 2012), it is much closer morphologically to the p3 of *Scarrittia barranquensis*, from La Cantera (early Oligocene, Patagonia; Ribeiro et al., 2010), from which it only differs in being 30% smaller and 40% narrower. Typotheria may have been more diversified than toxodonts, with two distinct bispecific faunas, in TAR-74 and TAR-22. More precisely, TAR-74 (late Eocene) yields a small hypsodont cheek tooth fragment, with cement, pointing to an unidentified interatheriid or hegetotheriid and low-crowned tooth fragments of a small unidentified typothere (morph 1). This morph 1 also likely occurs in TAR-21. In TAR- 22 (earliest Oligocene), a medium-sized molar fragment, hypsodont, with a closed fossette/fossettid and a wide enamel band, is assignable to a late “archaeohyracid” (*Archaeohyrax*, *Archaeotypotherium*, or *Protarchaeohyrax*), while smaller-sized low-crowned fragmentary teeth (decidual teeth?) may document another typothere referred to as “Archaeohyracidae” indet. A 14 mm-long lower tooth from TAR-73, eroded and heavily worn, has diverging roots. It is assigned to Notoungulata indet.

Litopterna (horse- and camel-like native ungulates) are not abundant in the Shapaja section. At TAR-21, the mesiolabial tip of a right upper molar documents an adianthine adianthid (Fig. 4S-T). The corresponding tooth is low-crowned, with a sharp and labially-protruding parastyle, a shallow oblique fossette, a smooth labial cingulum,

thin enamel, and a saddle-shaped neck both lingually and labially. Its morphological pattern closely resembles that of M2–3s of *Tricoelodus* from Deseadan beds of Argentina and Bolivia (Cifelli and Soria, 1983), but with a size 50% larger than in both species assigned to *Tricoelodus*. This specimen likely fills a stratigraphic gap between the Eocene indalecines and the late Oligocene adianthines, only occurring at mid- and high latitudes (Cifelli and Soria, 1983).

We refer to a tooth fragment as an unidentified didolodontid (TAR- 22; Fig. 4U). This pristine specimen preserves the distolingual part of a left lower molar (probably m1), of brachydont and bunodont condition. It has a prominent and conical entoconid, a much thinner and lower hypoconulid with a low postentocristid joining them, and a marked postentocingulid between both cuspids. Such morphological features closely resemble those of the m1 of *Didolodus* from the late middle Eocene of Patagonia (e.g., Simpson, 1967), the latter being 15% larger than the Shapaja specimen. It is much larger than *Ernestokokenia* and *Saltaodus* (Gelfo et al., 2019). Direct comparison with *Sallalodus deutherotherioides* is not possible, as its original hypodigm is restricted to two associated upper molars, larger sized than the specimen from TAR- 22 (Soria and Hoffstetter, 1983).

Pyrotheria (mastodon-like native ungulates) are documented at Shapaja by tooth fragments with a lophodont Bauplan, thick enamel with vertically-oriented bands (Koenigswald et al., 2015), and a typical sagittally-oblique wear pattern. They are tentatively assigned either to Pyrotheria indet. (TAR-20 and TAR-21; latest Eocene) or to the pyrotheriid cf. *Griphodon* sp. (TAR-13, TAR-22, and TAR-01; earliest Oligocene) when their features and dimensions match closely those of *Griphodon*. *Griphodon peruvianus* was originally described in Paleogene deposits from the vicinity of Shapaja (probably Eocene in age; Anthony and Richards, 1924; Patterson et al., 1942). Other tooth fragments were assigned to unidentified native ungulates (TAR-72).

Chiropterans (bats). Distolabial fragments of two hyperdilambdodont upper molars from TAR-21 and TAR-01 (estimated length < 2 mm) are assignable to unidentified chiropterans (Chiroptera indet.).

Primates (monkeys). In the Shapaja section, primates have so far been found only at TAR-21. Despite the large amount of sediment sampled and treated by wet screening, the fossil material documenting primates is particularly rare compared to that of metatherians or rodents from the same locality (see specific paragraphs). It consists of five dental remains, most of which are fragmentary (a well-preserved trigon region of an upper molar (Fig. 4V-W), an upper molar fragment, the buccal part of an

upper premolar (Fig. 4X-Z), a complete but worn lower second premolar (Fig. 4A'-C′), and a worn lower molar). These fossils attest to the co-occurrence of at least two tiny but size-distinct species. Pending the discovery of new specimens, the paucity and fragmentary nature of the currently available material does not allow evaluating the phylogenetic affinities of these two species. However, despite the scarce morphological information, the lingual part of a half upper molar displays a complete and quite strong lingual cingulum, with a minute but well-defined hypocone, without a pre-hypocrista (Fig. 4W). Such a simple pattern illustrates, to some extent, the degree of primitiveness of that primate, which rather matches that of some basal anthropoids from the Paleogene of Africa and *Perupithecus* from Santa Rosa (early Oligocene; Bond et al., 2015; Seiffert et al., 2020) or even *Parvimico* from Madre de Dios (early Miocene; Kay et al., 2019) than that of most subsequent stem and/or crown platyrrhines of South America (i.e., Homunculidae and extant families; for details, see Marivaux et al., 2016).

Rodents are by far the most conspicuous and species-rich mammalian group in the Shapaja section, with teeth uncovered in all localities, and ca. 500 specimens identified taxonomically. TAR-21 and TAR-01 yielded most rodent material. This material was extensively described in Boivin et al. (2018, 2019a, 2019b) and we only provide here an updated overview, including additional specimens from the last field campaigns (2018–2019). Twenty-two distinct caviomorph taxa document stem Caviomorpha (sensu Boivin et al., 2019a), representatives of three extant superfamilies (i.e., Chinchilloidea [chinchillas], Erethizontoidea [New World porcupines], and Octodontoidea [spiny rats]; Table 3), and caviomorphs of uncertain affinities. Caviomorphs from the Shapaja localities notably display a well-marked disparity regarding crown height, as brachydont, mesodont, and subprotohypsodont / protohypsodont morphs are recognized (Boivin et al., 2018). Although small-sized rodents widely predominate in the Shapaja section, specimens attesting to the presence of larger-sized taxa were found in late Eocene localities such as TAR-74 (*Eopululo* cf. *wigmorei*; Fig. 4E'-F′) and TAR-21 (Caviomorpha gen. et sp. indet. 5), and in the earliest Oligocene TAR-22 locality (Caviomorpha gen. et sp. indet. 2). In terms of taxonomic richness, the most diversified rodent fauna from Shapaja is recorded at TAR-21 (with eight co-occurring species), followed by TAR- 22 (six, including *Selvamys paulus* (Fig. 4I')), TAR-01 and TAR-20 (five), TAR-74 and TAR-13 (four), and lastly TAR-72 (two). The earliest rodent fauna (TAR-74: Assemblage 1) is fully distinct from all younger ones. It includes a new representative of *Pozomys* (Fig.

4D'), a genus originally restricted to late middle Eocene localities of Contamana (Boivin et al., 2017) and recognized at Santa Rosa (Arnal et al., 2020). It also yields *Eopululo* cf. *wigmorei*, i.e. a close ally of a species defined at Santa Rosa (Frailey and Campbell, 2004), a taxon tentatively approximated to *Eoincamys* (a stem chinchilloid, distinct from that of TAR-13), and an unidentified caviomorph. Overlying localities yield quite homogenous rodent faunas over the TAR-20 to TAR-22 interval, with genera and/or species in common, especially among *Eoincamys* and *Tarapotomys* (Assemblage 2; Table 3): *Eoincamys valverdei* occurs in all localities from this interval; *Eoincamys parvus* is recognized at TAR-20, TAR-21, and TAR-22 (Fig. 4G'); *Tarapotomys subandinus* is documented in all localities, except in TAR-13 (Fig. 4J'); Caviomorpha nov. gen. et sp. ranges from TAR-20 to TAR-13, and an unidentified caviomorph (Caviomorpha gen. et sp. indet. 1) occurs at TAR-20 and TAR-21. The early erethizontoid *Kichkasteiromys raimondii* is restricted to TAR-21 (Fig. 4H'). Conversely, the uppermost locality of the section (TAR-01) provides a very distinctive fauna, with *Tarapotomys mayoensis*, *Shapajamys labocensis*, *Mayomys confluens*, *Eoincamys* cf. *pascuali*, and an unidentified chinchilloid (Assemblage 3; Table 3; Fig. 5J-M). Moreover, only five rodent species are recognized at TAR-01, which is a strikingly low taxonomic diversity with respect to the number of specimens uncovered (406 cheek teeth) and to the volume of sediment treated (470 kg; see SI).

Table 3 Taxonomic composition of caviomorph rodent communities from the late Eocene–early Oligocene Shapaja section, San Martín, Peruvian Amazonia, suggesting the presence of two successive turnovers (Assemblages 1–3), as for metatherians (Table 2) and fish assemblies (Table 4, Fig. 6). Ass, Assemblage.

Taxa / Locality - Age	late Eocene				early Oligocene		
	TAR-74	TAR-20	TAR-72	TAR-21	TAR-13	TAR-22	TAR-01
Caviomorpha							
Stem Caviomorpha							
Pozomys sp. nov.	X						
Tarapotomys subandinus		X	X	X		X	
Tarapotomys mayoensis							X
aff. *Tarapotomys* sp.				X			
Caviomorpha gen. et sp. nov.		X		X	X		
Shapajamys labocensis							X
Incertae sedis							
Caviomorpha gen. et sp. indet. 1		X		X			
Caviomorpha gen. et sp. indet. 2						X	
Caviomorpha gen. et sp. indet. 3						X	
Caviomorpha gen. et sp. indet. 4	X						
Caviomorpha gen. et sp. indet. 5				X			
Erethicavioi							
Erethizontoidea							
Eopululo cf. *wigmorei*	X						
Kichkasteiromys raimondii				X			
Octochinchilloi							
Mayomys confluens							X
Octodontoidea							
Adelphomyidae gen. et sp. indet.					X		
Selvamys paulus						X	
Chinchilloidea							
Eoincamys valverdei		X	X	X	X	X	
Eoincamys parvus		X		X		X	
Eoincamys cf. *pascuali*							X
?*Eoincamys* sp. 1 (TAR-74)	X						
?*Eoincamys* sp. 2 (TAR-13)					X		
Chinchilloidea gen. et sp. indet.							X
Co-occurring species	**4**	**5**	**2**	**8**	**4**	**6**	**5**
Weight of sediment sampled (kg)	220	185	119	762	20	214	470
	Ass 1	Assemblage 2					Ass 3

4.4.3. Anurans (frogs)

A dozen of postcranial elements of very small dimensions were recovered in four localities over the studied section. All of them are of uncertain taxonomic affinities. They consist of fragmentary humeri (TAR-74, TAR-20 (Fig. 4K'-L'), and TAR-01 [two morphs, including non- Pipidae; (Fig. 5N-O)), radio-ulnae (TAR-20, TAR-21, and TAR-01), and ilium (TAR-01).

4.4.4. Squamates (lizards)

Isolated millimetric tricuspid teeth document three distinct squamate morphotypes at TAR-21 (morph 1: corrugated enamel; Fig. 4M') and TAR-01 (morph 2: high-crowned and sharp-edged (Fig. 5P); morph 3: bulbous crown), probably assignable to scincomorphan lizards (teiids?). Neither snake remains nor lacertilian osteoderms were unearthed in the concerned localities.

4.4.5. Chelonians (turtles and tortoises)

Chelonian remains occur throughout the section (TAR-20, TAR-21, TAR-22, and TAR-01). The concerned fossil specimens consist of isolated smooth-surfaced scutes, referable to unidentified pelomedusoid pleurodiran turtles, and documenting a wide size range. In particular, they are substantially large sized at TAR-22.

4.4.6. Crocodylomorphs (crocodylians and their stem relatives)

At Shapaja, crocodylomorphs are documented from most localities by basically isolated, small-sized teeth. The Shapaja communities include two (TAR-74, TAR-72, and TAR-22) up to four (TAR-21), and even five co-occurring crocodylomorph taxa (TAR-01).

Sebecosuchians (extinct terrestrial crocs) occur in TAR-74, TAR-72, TAR-22, and TAR-01 (Fig. 4N'-O′). Teeth, easily recognizable thanks to their triangular profile, almond-shaped cross section and serrated edges, are referred to as Sebecidae indet. (sensu Pol and Powell, 2011). The fragmentary state of the available sample and the sparse Paleogene fossil record of sebecosuchians in tropical-equatorial areas of South America discards to refine further their taxonomic assignment or to consider the co-occurrence of several taxa.

Elongated teeth with fluted enamel, typical of longirostrine fish-eating crocodylians are recognized throughout the section (from TAR- 74 up to TAR-01). They are either assignable to unidentified crocodyloids or gavialoids (Fig. 4P') in all localities. Only at TAR-20 a large tooth with a clear S-shaped profile can be referred to as a gryposuchine gavialoid.

The record of caimanine teeth far exceeds that of other crocodylomorph components at Shapaja (TAR-20 to TAR-01; Fig. 4Q'-S′ , 5Q-V). A complete skull (under study by RSG) and an osteoderm referable to this group were also recovered at TAR-20 and TAR-21, respectively. Teeth may document several morphs related to caimans, including globular, blunt with a short crown, leaf-shaped (MUSM 3980; Fig. 4R'- S′) and conical with strongly-fluted enamel morphs, aside from the more "generalized" caiman dental shapes (Fig. 5Q-V; for a review, see Salas- Gismondi et al., 2015).

4.4.7. Ichthyofauna

4.4.7.1. Dipnoi (lungfish).

Dipnoan dental plates of a single morph and dentine/bone structure, but of two distinct sizes, were uncovered in localities of the Shapaja section. Small ones occur throughout the considered section (from TAR-74 to TAR-01). They are mostly documented through tiny fragments (Fig. 3), sometimes as conspicuous elements of the ichthyofaunal community (up to 21 and 24 specimens at TAR-21 and TAR-01, respectively; Fig. 5W). The largest ones only occur in late Eocene localities (TAR-20, TAR-72, TAR-21; Fig. 4T'), which is not primarily linked to stream energy, as a similar

grain size is recorded at TAR-22 and TAR-73 (earliest Oligocene). They are far smaller than tooth plates of *Lepidosiren* recorded in Miocene deposits of Brazil, Colombia, and Peru (Lundberg, 1997; Toledo and Bertini, 2005). All these remains are referred to as Lepidosirenidae indet.

4.4.7.2. Actinopterygians (ray-finned fish).

Characiforms (characins and kin) dominate the actinopterygian record (see SI), with a constant composition throughout the Shapaja section (from TAR-74 to TAR-01). Most if not all localities have yielded isolated teeth referable to serrasalmids (pacu, cf. *Colossoma* sp.; 2230 specimens at TAR-01; Fig. 5X), anostomids (cf. *Leporinus* sp., incisor-like and hexacuspid [rare; Fig. 4U']; *Leporinus* sp., incisor-like and paddle-shaped teeth [629 specimens at TAR-01; Fig. 5A'-B′], and cynodontids (cf. *Hydrolycus* sp., monocuspid, sharp and dagger-like teeth; 359 specimens at TAR-01; Fig. 5C'). Unidentified hook-like, pad-like, and acuminated unicuspid pharyngeal teeth add to the characiform record. TAR-01 yielded three millimetric razor-sharp bicuspid teeth with an interlock furrow, unquestionably referable to as a crown piranha, and closely resembling the 4th or 5th tooth of the dentary of *Serrasalmus* (cf. *Serrasalmus* sp., Fig. 5Y-Z; Shellis and Berkovitz, 1976).

In contrast, siluriforms (catfish) are mostly documented by pectoral and/or dorsal spines at TAR-20, TAR-21, and TAR-01 (Siluriformes indet.). A small muffle-shaped tooth from TAR-21 and a small spine with a typical punctuated ornamentation from TAR-01 are assigned to an unidentified loricariid (armored catfish; Loricariidae indet.). The tooth has a small accessory cusp at the tip of the crown (Fig. 4V'), contrary to the loricariid teeth from Miocene deposits of Contamana (Antoine et al., 2016). A cranial fragment of a large-sized goliath catfish recovered at TAR-22 is recognizable thanks to the ornamented external aspect, with thick ridges and elongated sulci (Fig. 4W'). It is referred to as a pimelodid, cf. *Phractocephalus* sp. (for comparison, see Lundberg and Aguilera, 2003; Aguilera et al., 2008).

4.4.7.3. Selachians (sharks, skates, and rays).

Both the oldest (TAR-74) and the youngest Shapaja localities (TAR-73 and TAR-01) have not yielded a single selachian specimen, whereas all interbedded localities gather one to four co-occurring selachian species. Myliobatiforms are fully dominant over pristiforms (see SI). The most conspicuous elements by far are freshwater stingrays (Potamotrygonidae), with a new species of *Potamotrygon* documented at

TAR-20, TAR-21, and TAR-22 (one to 40 teeth per locality; Fig. 4Z'-A"), *Potamotrygon canaanorum* at TAR-13 (previously restricted to upper Oligocene-upper Miocene deposits from Contamana area; Chabain et al., 2017), and a representative of *Paratrygon* (*Paratrygon* sp.) at TAR-21 and TAR-22 (Fig. 4X'-Y′). To our knowledge, these are the first fossil occurrences of this Recent monotypic genus. Myliobatids occur at TAR-20, TAR-72, and TAR-13 (with a neonate tooth in each locality), and TAR-21 (20 teeth of *Myliobatis* sp. (Fig. 4E"-F″) and a tooth assigned to the bat ray?*Rhinoptera*). Some *Myliobatis* specimens are particularly large (30 mm-long) at TAR-21, whereas unusually small batoid specimens in TAR-20, TAR-72, and TAR-13 are cautiously interpreted as documenting neonate/young specimens of bat rays (?*Myliobatis*; Fig. 4C"-D″). In addition, a single oral tooth of the sawfish *Pristis* sp. was recognized at TAR-22 (Fig. 4B"). To sum up, the Shapaja selachian sample likely attests to the presence of a single and consistent community between TAR-20 and TAR-22, with brackish/coastal plain affinities, as indicated by bat rays and *Pristis*.

Table 4 Taxonomic composition of fish communities from the late Eocene–early Oligocene Shapaja section, San Martín, Peruvian Amazonia, suggesting a turnover pattern similar to that of metatherian and rodent paleocommunities (see Tables 2-3, Fig. 6). Blue-typed occurrences and locality names refer to the marine affinities of Assemblage 2 (mixohaline coastal plain), as hypothesized by the presence of myliobatiform and pristiform selachians. Ass, Assemblage.

Taxa / Locality - Age	late Eocene				early Oligocene			
	TAR-74	TAR-20	TAR-72	TAR-21	TAR-13	TAR-22	TAR-73	TAR-01
Selachii								
Myliobatiformes								
Myliobatidae								
Myliobatis sp.		X	X	X	X			
?*Rhinoptera* sp.				X				
Potamotrygonidae								
Potamotrygon nov. sp.		X		X		X	X	
Potamotrygon canaanorum					X			
Paratrygon sp.				X		X		
Pristiformes								
Pristidae								
Pristis sp.						X		
Actinopterygii								
Characiformes								
Serrasalmidae								
cf. *Colossoma* sp.	X	X	X	X	X	X	X	X
cf. *Serrasalmus* sp.								X
Anostomidae								
cf. *Leporinus* sp.	X	X		X	X	X	X	X
Leporinus sp.	X	X	X	X	X	X	X	X
Cynodontidae								
cf. *Hydrolycus* sp.	X	X	X	X	X	X	X	X
Characiformes indet. 1	X	X		X				X
Characiformes indet. 2		X						X
Characiformes indet. 3		X		X		X	X	X
Siluriformes								
Siluriformes indet.		X		X				X
Loricariidae indet.				X				X
Pimelodidae								
cf. *Phractocephalus* sp.						X		
Sarcopterygii								
Lepidosireniformes								
? *Lepidosiren* sp.	X	X	X	X		X	X	X
Co-occurring species	**6**	**11**	**5**	**13**	**6**	**10**	**7**	**11**
Weight of sediment sampled (kg)	220	185	119	762	20	214	12	470
	Ass 1	Assemblage 2						Ass 3

5. Discussion

5.1. Age

Here we performed, for the first time, chemostratigraphical investigation using carbon isotopes on dispersed organic matter (δ13Corg) and pedogenic nodules (δ13Cnod) at Shapaja (Western and Eastern sections), in order to i) provide a stratigraphic framework of the upper part of the Pozo Fm. in the Tarapoto area (Peruvian Amazonia), ii) refine the position of nine fossil-bearing levels in this stratigraphic framework. Unravelling the age of fossil-bearing levels in terrestrial to proximal marine sections is challenging mainly due to the lack of marine biostratigraphical reference fossils. Moreover, usage of certain terms has changed through time regarding the Eocene/Oligocene boundary (EOB; Premoli-Silva and Jenkins, 1993; Hutchinson et al., 2018). In common practice, the EOB is linked to the Oi-1 event, based on δ18O perturbations (Van Mourik and Brinkhuis, 2005). The late Eocene–early Oligocene interval comprised several isotopic events initially defined by Miller et al. (1991). The oldest of these events are major δ18O and δ13C positive shifts,

starting in the latest Eocene and ending in the earliest Oligocene (e.g., Coxall et al., 2005; Katz et al., 2008; Lear et al., 2008; Vandenberghe et al., 2012; Fig. 2). This isotopic event, called Eocene- Oligocene (climate) transition (EOT), lasting ~500 kyr (Coxall and Pearson, 2007), then encompasses the Eocene-Oligocene boundary. The EOB occurs approximately two thirds of the way through the EOT (Hutchison et al., 2020). Using a high-resolution carbon isotope study of the ODP site 1218, Erhardt et al. (2013) showed that the EOT positive shift is followed by two positive δ13C and δ18O excursions called Oi-1 and Oi-1a, both earliest Oligocene in age. This isotopic pattern was also observed by Zhifei et al. (2004) in ODP Leg 208 Site 1262, 1265 and 522. These trends are followed by another positive excursion (Oi-1b), clearly showing lighter maximal values than Oi-1 and Oi-1a excursions. While diagenesis increasingly alters the oxygen-isotope signature of sediments, C-isotope geochemistry is less influenced by diagenesis (Weissert et al., 2008). Oxygen isotopes (δ18O) on organic matter do not provide primary signals and are therefore not useful for stratigraphy. Conversely, variations in terrestrial organic carbon-isotope composition (δ13Corg) allow for using C-isotope stratigraphy as tool for correlating marine and terrestrial records, as demonstrated in a wide array of sections and time intervals (e.g. Gröcke et al., 1999). These variations have been satisfactorily used for allocating the position of Paleogene fossil-bearing levels in terrestrial sections (e.g. Yans et al., 2014a, 2014b; Noiret et al., 2016), including the EOB and around (Benammi et al., 2019). The Shapaja section was previously assigned an early Oligocene age (Klaus et al., 2017; Boivin et al., 2018, 2019a, 2019b), then a late Eocene–early Oligocene age range, on the basis of paleontological content and lithological correlations (Assemat et al., 2019). In the Western section of Shapaja, our new isotopic data on both organics (δ13Corg) and pedogenic nodules (δ13Cnod) clearly show (Fig. 2): i) a positive shift attributed to the EOT event, ii) followed by quite positive values considered as Oi-1, iii) overlaid by a positive excursion interpreted as Oi- 1a. These isotope trends perfectly match those observed at the global cooling of the Eocene–Oligocene transition described above (Erhardt et al., 2013). During Paleogene to Miocene times, similar C-isotope patterns, showing two successive high-amplitude positive δ13C excursions, are only recorded after the Mid-Eocene Climatic Optimum (MECO, Bartonian) and around the Mid-Miocene Climatic Optimum (MMCO, Langhian; Zachos et al., 2001; Luciani et al., 2010; Vandenberghe et al., 2012). As mentioned above, the MECO and MMCO time intervals are widely at odds with the inferred biostratigraphic age range of Shapaja localities studied here. Moreover, middle Miocene fossils have been collected ~1800

m above TAR-01 (at TAR-31 locality; Marivaux et al., 2020) whereas late Middle Eocene rodents were recognized at TAR-67, i.e., 280 m below the lowermost locality (TAR-74; Fig. 1). The uppermost positive peak at Shapaja (6.9‰ at 113.5 m) may be interpreted as Oi-1b but this remains tentative since i) this peak is based on a single point and ii) δ13Corg does not show the same trend for this sample. The main part of the Eastern section shows a negative trend, interpreted as global negative trend observed below the EOT (Fig. 2), which further matches local lithological sequences and taxonomic affinities of the concerned paleocommunities. In Shapaja, the C-isotope values on organics and pedogenic nodules are globally consistent, showing similar trends (Fig. 2). However, two minor discrepancies are observed in the following intervals: i) hypothetical base of the EOT located in the δ13Corg curve ~20 m above its location in the δ13Cnod curve, and ii) negative trend of the Oi-1a excursion, well-marked in the δ13Cnod curve (from 5.8‰ at 81.2 m to 11.3‰ at 98.3 m) and less marked in the δ13Corg curve. These local inconsistencies may be explained by the poor carbon content of organics (usually <0.05%) in all studied samples. In Shapaja, organic matter most probably experienced intense recent oxidation/weathering, leading to potential biases in the resulting δ13Corg values/trends. We therefore consider the data on pedogenic nodules as more robust (meteoric water-sourced), allowing us to use the δ13Cnod values as the best primary signals where data on both the studied materials (organics vs nodules) are not consistent. Our data in the Western section suggest that the EOT is observed between 53 and 59 m using δ13Corg data, and between 32 and 59 m, using δ13Cnod data. Thus, the EOB is located somewhere in this latter interval (Fig. 6). It is not possible, however, to refine the location of the EOB, at our current stage of knowledge. Based on these new chemostratigraphical data, we conclude that i) TAR-20 and TAR-72 (and TAR- 74, even if this underlying level was not sampled in our study) are late Eocene in age, ii) TAR-21 is located at the earliest EOT (i.e., most probably latest Eocene in age), iii) TAR-21sup is within the EOT (latest Eocene? – earliest Oligocene?), and iv) TAR-22, TAR-13, TAR-73, and TAR-01 are early Oligocene in age. Among metatherians, most new records of palaeothentids and abderitids at Shapaja are consistent with previously-estimated divergence times (i.e., earliest Oligocene; Abello et al., 2018). However, the presence of palaeothentines by the EOT at Shapaja implies an unexpected ghost lineage of the group, and as such, a much earlier divergence, not only of the palaeothentids and abderitids, but also of the major palaeothentid lineages (i.e. Palaeothentinae and

Acdestinae). Further studies (in progress) will allow to test the current taxonomic assignations and to refine diversification timings of non-Pichipilidae Palaeothentoidea.

5.2. Environment

The abundance of pedogenic nodules (calcretes) throughout the latest Eocene–early Oligocene interval points to contrasted seasonal rainfall and water-table oscillation. The poor palynomorph recovery at TAR-72 is compatible with understory vegetation in a tropical rainforest (Fungi monocellate and fern spores) and with seasonal water-table fluctuation. Quantitative paleoclimatic inferences were not performed due to the limited number of leaf and seed fossil material that could be collected in the field. The Shapaja record, however, consists mostly of nanophyll leaflets of compound leaves or microphyll leaves. In addition, most of the fossil leaves recovered came from the early Oligocene section (i.e., TAR-01), which could indicate that the forests at this time likely adapted to longer periods of drought (e.g., strong seasonal precipitation pattern) by becoming deciduous and reducing the leaf lamina (see Peppe et al., 2011). Nevertheless, larger collections are necessary to confirm this hypothesis. Interestingly, recent studies documenting macrofloras throughout the late Eocene to early Oligocene from Neotropical localities also provide evidence to support an increment in seasonal conditions in this region (Calvillo-Canadell and Cevallos-Ferriz, 2005; Woodcock et al., 2017; Martínez et al., 2021), a pattern that has been previously proposed for northern high-latitude localities (Eldrett et al., 2009). Most of the taxonomically identified fossil seeds came from the latest Eocene locality (TAR-21), which includes at least two taxa of Passifloroideae (passion fruit subfamily) and one taxon of the Araceae (cf. *Monstera*). These plants are common vines or epiphytes in extant tropical rainforests in the region. The presence of these plants in the latest part of the Eocene also coincides with the occurrence of primates, indicative of tropical rainforest environment (Fig. 4V-C'). The persistence of vine/epiphytic plants suggests the presence of high-canopy trees in this part of the section near the vicinity of streams (TAR-74 to TAR-73) and ponds (TAR-01) throughout the section. Seeds of Nymphaceae (TAR-73) and cf. *Elatine* (Elatinaceae; TAR-74 and TAR-01; Fig. 3I), a common cosmopolitan plant of aquatic environments (e.g., ponds, freshwater lakes), also indicate the presence of freshwater settings. Moreover, the oldest and youngest localities (TAR-74 and TAR-73 + TAR-01, respectively) testify to the presence of obligate freshwater settings, as revealed by the mollusk, decapod, and fish communities. Conversely, a marine/brackish influence can be hypothesized in the

middle part of the section (between TAR-20 and TAR-22) thanks to the conspicuous presence of myliobatid and pristid selachians (bat rays and sawfish, respectively). These taxa co-occur with a freshwater ichthyofauna dominated by characiform actinopterygians and dipnoans, thus pointing to an estuarine environment. The presence of neonate/young batoid specimens at TAR-20, TAR-13, and TAR-72 might further support brackish conditions for the concerned interval, as many *Myliobatis* females enter estuaries and coastal plains to give birth today (Mianzan et al., 2001). Accordingly, we can hypothesize that the concerned settings were close to such protected environments playing a nursery role for bat rays (even if the occurrence of a minute euryhaline/freshwater myliobatid species of unknown affinities cannot be fully discarded). In the uppermost levels of the section (TAR-73 and TAR-01), the fish community characterizes again a freshwater environment without any marine influence (potamotrygonid selachians, dipnoans, and characiform actinopterygians). Nodule-rich blue clays of TAR-01 may have deposited in an oxbow lake, which would further explain the presence of piranhas (see CTA-32 near Contamana; Antoine et al., 2016).

5.3. Community turnovers

In this section, we provide a short overview of the most prominent taxonomic groups for which changes have been recognized in terms of community composition over the studied section. The faunal components of the different localities were informally grouped into three assemblages based on taxonomic composition of relevant groups. Assemblages 1 and 3 refer to the late Eocene (TAR-74) and early Oligocene (TAR-01) metatherian, rodent, and fish assemblies, respectively, while Assemblage 2 refers to the latest Eocene–earliest Oligocene transitional taxonomic composition (TAR-20, TAR-72, TAR-21, TAR-22, and TAR-73). Charophyte and plant remains (leaves, silicified wood, and seeds) are documented throughout the complete studied section. Changes in the diversity of the leaf macroflora along the section are hard to evaluate as most of the material collected came from only one Oligocene locality (TAR-01). Nevertheless, we found two leaf morphotypes (PZ1 and PZ3, shared between TAR-21sup (EOT) and TAR-01), and also one seed taxon, cf. *Elatine* (shared between TAR-74 and TAR-01), implying that these plants persisted to the EOT and were tolerant of the new climatic conditions of the early Oligocene. Although additional plant fossil material will be required to fully reconstruct the forest types of the Shapaja section, our preliminary data suggests the presence of multistratified rainforests during the latest part of the Eocene (TAR-21) and more open, deciduous forests in the earliest

Oligocene (TAR-21sup to TAR-01). As for mammals, only metatherians and rodents are sufficiently documented in terms of specimen numbers and taxonomic richness to provide evidence related to faunal turnovers (Tables 2–4). Among metatherians, the Assemblage 1 (TAR-74, late Eocene) yields a new prepidolopid and an unidentified marsupialiaform, but neither argyrolagids nor palaeothentoids, which fully dominate latest Eocene assemblages (from TAR-20 to TAR-21; Assemblage 2). Another obvious turnover is observed between TAR-21 and TAR-01 (Assemblages 2 vs. 3: no species in common). Indeed, latest Eocene localities (Assemblage 2) are fully dominated by small argyrolagids, very abundant in TAR-21 and co-occurring with another possible prepidolopid and some early palaeothentoids. By the early Oligocene, however, argyrolagids are much less conspicuous while there is a profusion of derived non-Pichipilidae palaeothentoids, with the presence of new taxa among Palaeothentidae and Abderitidae (TAR-01: Assemblage 3). Unfortunately, the timing of this turnover cannot be refined, due to the lack of marsupial remains in interbedded localities (TAR-13, TAR-22, and TAR-73; Table 2). Even though a sampling bias cannot be fully discarded, the differences between Shapaja Assemblages 2 and 3 might well illustrate a real change in taxonomic composition and diversity. A sharp decline of metatherian diversity by the EOT has already been observed as part of the Patagonian hinge ("*Bisagra patag´onica*"; Goin et al., 2010, 2016): Patagonian faunas reveal the EOT as a major ecologically-induced turnover in the history of Metatheria, with the disappearance of some lineages and the diversification of other ones (Goin et al., 2016). With respect to other Eocene–Oligocene South American metatherian faunas, Shapaja communities are fully distinct from the Tinguiririca fauna, Chile (Flynn et al., 2003) and very dissimilar to those of Argentinean Patagonia (La Cancha and La Cantera) and Southeastern Brazil (Guabirotuba), except for the presence of basal NPPs and argyrolagoids (Goin et al., 2010; Sedor et al., 2017). Strikingly, except for yielding a prepidolopid and basal NPPs (*Perulestes* and *Sasawatsu*), the Santa Rosa fauna does not have strong affinities with Shapaja metatherian assemblages: sparassodontans, microbiotherians, and other Polydolopimorphia (e.g., *Wamradolops* and *Rosendolops*) do not occur at Shapaja; Argyrolagidae, Palaeothentidae (including Palaeothentinae), and Abderitidae have not been found at Santa Rosa. Shapaja and coeval mid- and low-latitude metatherian paleocommunities need to be thoroughly revised and compared with their higher latitude counterparts, in order to unravel their evolutionary dynamics at the South American scale. According to our results, three distinct rodent communities are recognized in the studied Shapaja section

(Assemblages 1–3; Table 3). The Assemblage 1 and 3 are late Eocene and early Oligocene in age, respectively, whilst the Assemblage 2 is well documented in both latest Eocene and earliest Oligocene localities. Four species of this Assemblage 2 survive the EOT locally (*Tarapotomys subandinus*, Caviomorpha gen. et sp. nov., *Eoincamys valverdei*, and *E. parvus*). More generally, chinchilloids and erethizontoids first occur prior to the EOT, whereas octodontoids (as represented by Adelphomyidae indet. Gen. et sp. at TAR-13 and *Selvamys* at TAR-22) appear after the EOT, at least locally. The most prominent turnover occurs between TAR-22 (Assemblage 2) and TAR-01 (Assemblage 3), with species replacements among *Tarapotomys* (*T. subandinus* versus *T. mayoensis*) and *Eoincamys* (*E. valverdei* + *E. parvus* versus *E*. cf. *pascuali*), and the first appearance of both *Shapajamys* and of *Mayomys* at TAR-01. As illustrated by distinct depositional settings, this turnover likely concurs with environmental changes locally, potentially related to the EOT. Nevertheless, the corresponding turnover does not coincide temporally with this event but occurs somewhat later (by Oi-1a times; Figs. 2, 6). Strikingly, all stratigraphically-constrained Shapaja rodent assemblages (1–3), spanning the late Eocene–early Oligocene time interval (ca. 36–32.5 Ma), are equally homotaxic with the Santa Rosa rodent fauna, notably in sharing a stem caviomorph (*Pozomys*; TAR-74), erethizontoids (from TAR-74 upward), chinchilloids (with a strong domination of *Eoincamys* at TAR-20 and younger localities), and adelphomyine octodontoids (at TAR-13; Boivin et al., 2018, 2019a, 2019b). This raises questions about Santa Rosa i) consisting of several successive fossil-yielding levels of distinct ages or ii) being a time-averaged level with reworked specimens, as further suggested by its extreme rodent specific richness (17 co-occurring species; Arnal et al., 2020), recalling that of upper Oligocene Salla Beds, Bolivia (multiple fossil-bearing levels, 29–25 Ma; e.g., P´erez et al., 2019). So far, no primate has been recorded in the early Oligocene TAR-01 locality, which has been sampled as extensively as TAR-21 and has yielded a specimen-rich rodent fauna (868 specimens). Most tiny primates are dependent on dense forest habitats, and can be highly sensitive to environmental changes. Although a taphonomic bias cannot be ruled out for explaining this contrast between TAR-21 and the well-sampled overlying early Oligocene localities (i.e., TAR-22 and TAR- 01), the apparent rarefaction of primates in post-EOT deposits could also be linked to paleoenvironmental changes, at least locally, thereby corresponding to the onset of drier/open terrestrial environments by the EOT or afterwards. Even if it is likely to predate it, the bispecific primate community at TAR-21 strongly recalls that of Santa Rosa (Bond et al., 2015; Seiffert et

al., 2020). Conversely, poorly-documented Shapaja ungulate assemblies seem to be highly distinct, at least for northern South America. The Shapaja fish faunas are strongly reminiscent of the modern Amazonian lowland ichthyofauna, with characiform and siluriform actinopterygians, potamotrygonid selachians, and dipnoans (Brito and Deynat, 2004). They also recall the middle Eocene–late Miocene freshwater-dominated fish communities from Contamana (Adnet et al., 2014; Antoine et al., 2016; Chabain et al., 2017). In more detail, the Shapaja fish communities have distinctive features (Table 4), such as the conspicuous presence of a new species of *Potamotrygon* (in TAR-20, TAR- 21, and TAR-22), the first fossil occurrence of the discus ray *Paratrygon* (TAR-21 and TAR-22), and the earliest occurrence of loricariid siluriforms (TAR-21), of *Potamotrygon canaanorum* (TAR-13; previously restricted to upper Oligocene settings; Chabain et al., 2017), and of piranhas closely allied to *Serrasalmus* (TAR-01; previously recorded from upper Oligocene settings onward; Antoine et al., 2016). TAR-74 and TAR-01 did not yield any selachian specimens, in spite of having been extensively sampled (Table 4; see SI). Despite the large amount of sediment sampled (220 kg), the fish community at TAR-74 only consists of characiforms and lepidosirenid dipnoans, typical of running-water settings, and consistent with those of overlying localities (TAR-20 to TAR-73). However, the localities TAR-20 to TAR-22 yielded selachians of marine/brackish affinities, such as *Myliobatis*, *Rhinoptera*, and/or *Pristis*. The presence of *Myliobatis* neonates (at TAR-20, TAR-72, and TAR-13) may further point to a mixohaline coastal plain environment (bat ray nurseries). In contrast, the distinctiveness of TAR-01 in terms of ichthyofaunal content, without any selachians and further illustrated by the presence of piranhas, may be related to the depositional setting (oxbow lake), contrasting with that of all underlying localities, although the role of other EOT-related drivers cannot be discarded (Table 4). In other words, the discrepancies between Shapaja fish Assemblages 1–3 appear to be mainly related to environmental conditions, with a strict freshwater setting (TAR-74: Assemblage 1), a transgressive lag (brackish interval from TAR-20 to TAR-22: Assemblage 2), and a subsequent regression (TAR-01: Assemblage 3). TAR-73 may correspond to a transitional phase between the Assemblages 2 and 3 (no marine component, but a potamotrygonid).

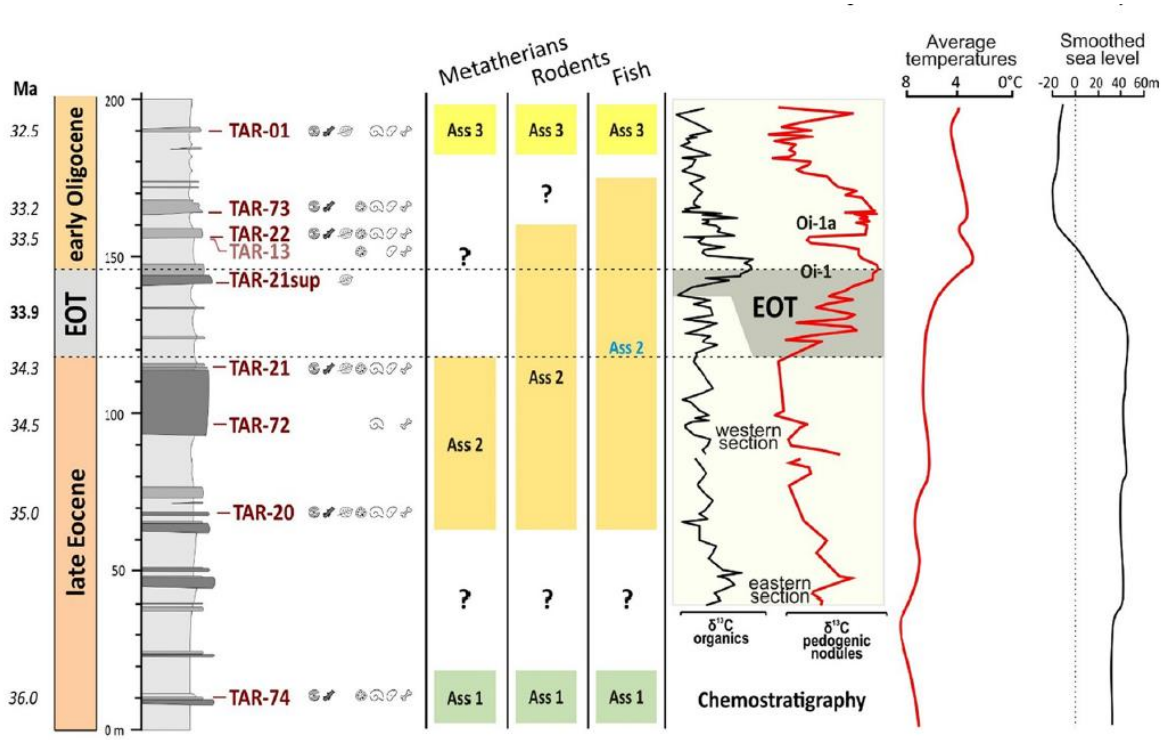


Fig. 6. Synthetic chrono-biostratigraphical chart of late Eocene–early Oligocene paleocommunities from Shapaja, San Martín, Peruvian Amazonia. Timeframe based on Vandenberghe et al. (2012) and current chemostratigraphical analyses. Ages in italics are approximate and tentative. Assemblages 1–3 derive from the present work, based on metatherian, rodent, and fish assemblages (selachians + actinopterygians) (see Tables 2-4). Blue-typed fish component refers to the marine affinities of Assemblage 2 (mixohaline coastal plain). Paleotemperature curve (Westerhold et al., 2020) and smoothed sea level curve (Miller et al., 2020) are adapted to match the timeframe of the section. (For interpretation of the references to colour in this figure legend, the reader is referred to the web version of this article.)

5.4. Regional and/or global drivers

Assessing which drivers have provoked past biotic changes is quite challenging, especially in areas as widely under-investigated paleontologically as tropical-equatorial regions of South America. In the Shapaja section recording and bracketing the EOT, we will nonetheless try to disentangle the potential roles of main regional and global drivers (i.e., vertical movements vs. climatic and sea-level changes, respectively), likely to explain the biotic turnovers observed during the late Eocene–earliest Oligocene interval. From a tectono-sedimentary perspective, the Shapaja area is located in the Sub-Andean Zone today. Recent regional syntheses for the Huallaga

and Bagua basins in the northern Central Andes consistently state that the concerned area only experienced Andean thrust-related deformation much later, i.e., from late Miocene times onward (Hermoza et al., 2005; Roddaz et al., 2010; Eude et al., 2015; Moreno et al., 2020). During the late Eocene–Oligocene interval, this region was steadily part of the foredeep depozone of the foreland basin. This time period coincides with the onset of a tectonic loading stage, leading locally to flexural subsidence (Roddaz et al., 2010). Such downward settling likely forced the late Eocene shift from freshwater to brackish/marine-influenced depositional environments, as recorded locally between TAR-74 and TAR-20 and further illustrated by the first ichthyofaunal turnover (Fig. 6: Assemblage 1 vs. Assemblage 2). In addition, this shift occurred during a time period with no noticeable global sea-level change (Fig. 6; Miller et al., 2020). Thereby, the concerned late Eocene biotic changes might have been fully locally-driven. In contrast, the time interval spanning the EOT and the earliest Oligocene records unstable and deteriorating global conditions: a drastic cooling led to a ca. 80 m drop in sea level between ca. 34 and 33.2 Ma (Fig. 6), provoked a sustained drop in precipitation, and increased seasonality, with a worldwide onset of drier climatic regimes (Hutchinson et al., 2018; Miller et al., 2020; Westerhold et al., 2020). Both the abundance of pedogenic nodules in the concerned interval of the Shapaja section and the concurrent shift from multistratified rainforest to more open deciduous forest consistently point to the strengthening of seasonal contrast, especially regarding rainfall (see previous sections). This global event temporally coincides with the decay of the Assemblage 2, as perceived on metatherians and rodents (Fig. 6). The apparently-delayed response of the ichthyofaunal community (turnover starting ca. 33–32.5 Ma) with respect to that of terrestrial components (plants and mammals: ca. 33.7 Ma) is perhaps related to the persistence of regional flexural subsidence accommodating locally the effect of global sea-level drop. In other words, during the EOT and the earliest Oligocene, Shapaja biotic community turnovers have probably been primarily globally-driven, particularly for their terrestrial components (plants and mammals). TAR-01 probably records new stable environmental conditions, under a drier and more seasonally-contrasted climate, but its highly-distinctive metatherian and rodent assemblages prevent from discussing further their sustainability at any spatiotemporal scale (Assemblage 3; Fig. 6).

6. Conclusion

The Shapaja section ranges the late Eocene–early Oligocene interval (ca. 36–32.5 Ma). As suggested by chemostratigraphical results, this section records both the EOT and positive carbon isotopic incursions interpreted as Oi-1 and Oi1a events. The latest Eocene–earliest Oligocene interval evidences a marine/brackish influence, as indicated by the co-occurrence of several selachians, likely forced by regional flexural subsidence. Obligate freshwater depositional environments of the uppermost part of the section are compatible with the earliest Oligocene global sea level drop. Leaf physiognomy (mainly nanophyll leaflets of compound leaves or microphyll leaves with entire margins) tentatively suggests a warm seasonal climate during the EOT interval, while the seeds of vine/epiphytic plants during the latest Eocene points to the presence of high-canopy trees near the vicinity of streams and/or ponds. Two biotic turnovers are retrieved (metatherians, rodents, and fish): one during the late Eocene (ca. 35-–36 Ma) and another one several thousand years after the EOT (ca. 33 Ma). TAR-21 (latest Eocene) records the first South American primates unquestionably predating the EOT. More broadly, this section documents the earliest occurrences of several genera, families, and/or superfamilies: *Eopululo* and Erethizontoidea (late Eocene); *Paratrygon*, *Proargyrolagus* and Argyrolagidae, Palaeothentidae, *Parastegosimpsonia*, Chinchilloidea, *Eoincamys*, and Loricariidae (latest Eocene); Adelphomyinae, Mylodontidae, Abderitidae, and true piranhas (earliest Oligocene). The paleocommunities from Shapaja exemplify a local response of terrestrial and aquatic organisms to drastic regionally- then globally-driven changes over the late Eocene–early Oligocene interval, at low latitudes in South America.

Declaration of Competing Interest

All authors declare that they do not have any conflict of interest.

Acknowledgments

We are indebted to Adriana Albino (Museo de La Plata, Argentina) for her taxonomic assignment of squamate remains. Fieldwork and post-field analyses in Peru were carried out thanks to the support from the National Geographic Society (grant n◦ 9679-15) and the Campus France program of the French Ministry of Foreign Affairs to POA, from the Doctoral School SIBAGHE/Gaia of the Montpellier University to MB, the Oak Spring Garden Foundation to F. Herrera and from the Institut des Sciences de l’Evolution de Montpellier, and The Leakey Foundation to LM. This work was further supported by an “Investissements d’Avenir” grant managed by the Agence Nationale

de la Recherche (CEBA, ANR- 10-LABX-25-01) and by the cooperative programs ECOS-FonCyT (A14- U01) and CoopIntEER CNRS-CONICET (n◦252540), in the frame of the ongoing cooperation agreement between the Museo de Historia Natural de la Universidad Nacional Mayor San Marcos (Lima, Peru) and the Institut des Sciences de l'Evolution-Universit´e de Montpellier. We are particularly indebted to the invited editor, Carina Hoorn, to Robin M. D. Beck and to an anonymous reviewer for their useful comments and helpful suggestions on a previous version of the manuscript. This is the article ISEM-2021-039 SUD.

References

Abello, M.A., 2007. Sistemática y bioestratigrafía de los Paucituberculata (Mammalia: Marsupialia) del Cenozoico de América del Sur. Doctoral dissertation. Universidad Nacional de La Plata.

Abello, M.A., Candela, A.M., 2020. Paleobiology of *Argyrolagus* (Marsupialia, Argyrolagidae): an astonishing case of bipedalism among South American mammals. J. Mamm. Evol. 27, 419–444.

Abello, M.A., Toledo, N., Ortiz-Jaureguizar, O., 2018. Evolution of South American Paucituberculata (Metatheria: Marsupialia): adaptive radiation and climate changes at the Eocene-Oligocene boundary. Hist. Biol. https://doi.org/10.1080/08912963.2018.1502286.

Adnet, S., Salas Gismondi, R., Antoine, P.-O., 2014. Comparisons of dental morphology in river stingrays (Chondrichthyes: Potamotrygonidae) with new fossils from the middle Eocene of Peruvian Amazonia rekindle debate on their evolution. Naturwissenschaften 101 (1), 33–45.

Aguilera, O.A., Bocquentin, J., Lundberg, J.G., Maciente, A., 2008. A new cajaro catfish (Siluriformes: Pimelodidae: Phractocephalus) from the late Miocene of southwestern Amazonia and its relationship to †*Phractocephalus nassi* of the Urumaco Formation. Paläont Z 82 (2), 231–245.

Anthony, H.E., Richards, J.G., 1924. A new fossil perissodactyl from Peru. Am. Mus. Novit. 111.

Antoine, P.-O., et al., 2016. A 60-million-year Cenozoic history of western Amazonian ecosystems in Contamana, eastern Peru. Gondwana Res. 31, 30–59.

Arnal, M., Kramarz, A.G., Vucetich, M.G., Frailey, C.D., Campbell, K.E., 2020. New Palaeogene caviomorphs (Rodentia, Hystricognathi) from Santa Rosa, Peru:

systematics, biochronology, biogeography and early evolutionary trends. Pap. Palaeontol. 6 (2), 193–216.

Assemat, A., et al., 2019. Restes inédits de rongeurs caviomorphes du Paléogène de la région de Juanjui (Amazonie péruvienne): systématique, implications macro-évolutives et biostratigraphiques. Geodiversitas 41 (20), 699–730.

Barreda, V., Palazzesi, L., 2021. Role of climate and tectonism on the modernization of Patagonian floras: evidence from the fossil record. Glob. Planet. Chang. this issue.

Beard, K.C., Coster, M.C., Salem, M.J., Chaimanee, Y., Jaeger, J.-J., 2017. Biogeographic provincialism shown by Afro-Arabian mammals during the middle Cenozoic: climate change, Red Sea rifting and global eustasy. In: Agius, D.A., Khalil, E., Scerri, E.M.L., Williams, A. (Eds.), Human Interaction with the Environment in the Red Sea - Selected Papers of Red Sea Project VI. Koninklijke Brill NV, Leiden, pp. 48–68.

Beck, R.M.D., 2017. The Skull of *Epidolops ameghinoi* from the early Eocene Itaboraí Fauna, Southeastern Brazil, and the Affinities of the Extinct Marsupialiform Order Polydolopimorphia. J. Mamm. Evol. 24, 373–414.

Benammi, M., et al., 2019. Geology, biostratigraphy and carbon isotope chemostratigraphy of the Paleogene fossil-bearing Dakhla sections, Southwestern Moroccan Sahara. Geol. Mag. 156 (1), 117–132.

Berggren, W.A., Prothero, D.R. (Eds.), 1992. Eocene-Oligocene Climatic and Biotic Evolution: An Overview. Princeton University Press, Princeton, p. 568.

Boivin, M., et al., 2017. Late Oligocene caviomorph rodents from Contamana, Peruvian Amazonia. Pap. Palaeontol. 3 (1), 69–109.

Boivin, M., et al., 2018. Early Oligocene caviomorph rodents from Shapaja, Peruvian Amazonia. Palaeontographica Abt. A 311 (1–6), 87–156.

Boivin, M., Marivaux, L., Antoine, P.-O., 2019a. L'apport du registre paléogène d'Amazonie sur la diversification initiale des Caviomorpha (Hystricognathi, Rodentia): implications phylogénétiques, macroévolutives et paléobiogéographiques. Geodiversitas 41 (4), 143–245.

Boivin, M., Marivaux, L., Salas-Gismondi, R., Vieytes, E.C., Antoine, P.-O., 2019b. Incisor enamel microstructure of Paleogene caviomorph rodents from Contamana and Shapaja (Peruvian Amazonia). J. Mamm. Evol. 26 (3), 389–406.

Bond, M., et al., 2015. Eocene primates of South America and the African origins of New World monkeys. Nature 520, 538–541.

Brito, P.M., Deynat, P.P., 2004. Freshwater stingrays from the Miocene of South America with comments on the rise of potamotrygonids (Batoidea, Myliobatiformes). In: Arratia, G., Wilson, M.V.H., Cloutier, R. (Eds.), Recent Advances in the Origin and Early Radiation of Vertebrates. Dr. Friedrich Pfeil, Munich, pp. 575–582.

Calvillo-Canadell, L., Cevallos-Ferriz, S.R.S., 2005. Diverse assemblage of Eocene and Oligocene Leguminosae from Mexico. Int. J. Plant Sci. 166, 671–692.

Chabain, J., et al., 2017. Cenozoic batoids from Contamana (Peruvian Amazonia) with special focus on freshwater potamotrygonins (Chondrichthyes, Myliobatiformes) and their paleoenvironmental significance. Geobios 50, 389–400.

Chornogubsky, L., Goin, F.J., 2015. A review of the molar morphology and phylogenetic affinities of *Sillustania quechuense* (Metatheria, Polydolopimorphia, Sillustaniidae), from the early Paleogene of Laguna Umayo, southeastern Peru. J. Vertebr. Paleontol. 35 (6), e983238.

Ciancio, M.R., Carlini, A.A., Campbell, K.E., Scillato-Yané, G.J., 2013. New Palaeogene cingulates (Mammalia, Xenarthra) from Santa Rosa, Perú and their importance in the context of South American faunas. J. Syst. Palaeontol. 11 (6), 727–741.

Cifelli, R., Soria, M.F., 1983. Systematics of the Adianthidae (Litopterna, Mammalia). Am. Mus. Novit. 2771, 1–25.

Coxall, H.K., Pearson, P.N., 2007. The Eocene–Oligocene Transition. In: Williams, M., Haywood, A.M., Gregory, F.J., Schmidt, D.N. (Eds.), Deep-Time Perspectives on Climate Change: Marrying the Signal from Computer Models and Biological Proxies. The Micropalaeont. Soc., Spec. Pub. The Geol. Soc., London, pp. 351–387.

Coxall, H.K., Wilson, P., Palike, H., Lear, C., Backman, J., 2005. Rapid stepwise onset of Antarctic glaciation and deeper calcite compensation in the Pacific Ocean. Nature 433, 53–57.

DeConto, R.M., Pollard, D., 2003. Rapid Cenozoic glaciation of Antarctica induced by declining atmospheric CO2. Nature 421, 245–249.

Dunn, R.E., Strömberg, C.A.E., Madden, R.H., Kohn, M.J., Carlini, A.A., 2015. Linked canopy, climate, and faunal change in the Cenozoic of Patagonia. Science 347 (6219), 258–261.

Dupont-Nivet, G., et al., 2007. Tibetean plateau aridification linked to global cooling at the Eocene-Oligocene transition. Nature 445, 635–638.

Eldrett, J.S., Greenwood, D.R., Harding, I.C., Huber, M., 2009. Increased seasonality through the Eocene to Oligocene transition in northern high latitudes. Nature 459 (7249), 969–973.

Erhardt, A.M., Pälike, H., Paytan, A., 2013. High-resolution record of export production in the eastern equatorial Pacific across the Eocene-Oligocene transition and relationships to global climatic records. Paleoceanography 28, 130–142.

Eude, A., Roddaz, M., Brichau, S., Brusset, S., Calderon, Y., Baby, P., Soula, J.-C., 2015. Controls on timing of exhumation and deformation in the northern Peruvian Eastern Andean wedge as inferred from low-temperature thermochronology and balanced cross section. Tectonics 34 (4), 715–730.

Feussom-Tcheumeleu, et al., 2019. Upper Miocene depositional environments and landscapes, Shumanza section, Subandean Zone, Northern Peru. Palaeobiodiver. Palaeoenviron. 100 (3), 719–735.

Flynn, J.J., Wyss, A.R., Croft, D.A., Charrier, R., 2003. The Tinguiririca Fauna, Chile: biochronology, paleoecology, biogeography, and a new earliest Oligocene South American Land Mammal “Age”. Palaeogeogr. Palaeoclimatol. Palaeoecol. 195, 229–259.

Frailey, C.D., Campbell, K.E., 2004. Paleogene rodents from Amazonian Peru: the Santa Rosa local fauna. In: Campbell, K.E. (Ed.), The Paleogene Mammalian Fauna of Santa Rosa, Amazonian Peru. Nat. Hist. Mus. Los Angeles County, Los Angeles, pp. 71–130.

Gelfo, J.N., Alonso, R.N., Madden, R.H., Carlini, A.A., 2019. An Eocene bunodont South American native ungulate (Didolodontidae) from the Lumbrera Formation, Salta Province, Argentina. Ameghiniana 57 (2), 132–145.

Godfrey, L.R., et al., 2020. Mid-Cenozoic climate change, extinction, and faunal turnover in Madagascar, and their bearing on the evolution of lemurs. BMC Evol. Biol. 20 (1-18), 97.

Goin, F.J., Candela, A.M., 2004. New Paleogene marsupials from the Amazon Basin of eastern Peru. In: Campbell, K.E. (Ed.), The Paleogene Mammalian Fauna of Santa Rosa, Amazonian Peru. Nat. Hist. Mus. Los Angeles County, Los Angeles, pp. 15–60.

Goin, F.J., Candela, A.M., Abello, M.A., Oliveira, E.V., 2009. Earliest South American paucituberculatans and their significance in the understanding of ‘pseudodiprotodont’ marsupial radiations. Zool. J. Linnean Soc. 155, 867–884.

Goin, F.J., Abello, M.A., Chornogubsky, L., 2010. Middle Tertiary marsupials from Central Patagonia (early Oligocene of Gran Barranca): understanding South America’s Grande Coupure. In: Madden, R.H., Carlini, A.A., Vucetich, M.G., Kay, R.F. (Eds.), The Paleontology of Gran Barranca. Evolution and Environmental Change through the Middle Cenozoic of Patagonia. Cambridge Univ. Press, Cambridge, pp. 69–105.

Goin, F.J., Woodburne, M.O., Zimicz, A.N., Martin, G.M., Chornogubsky, L., 2016. A Brief History of South American Metatherians. Springer Earth System Sciences, New York, p. 237.

Gröcke, D.R., Hesselbo, S., Jenkyns, H.C., 1999. Carbon-isotope composition of lower cretaceous fossil wood: ocean atmosphere chemistry and relation to sea-level change. Geology 27, 155–158.

Hermoza, W., et al., 2005. The Huallaga foreland basin evolution: thrust propagation in a deltaic environment, northern Peruvian Andes. J. South Am. Earth Sc. 19, 21–34.

Hoffstetter, R., 1956. Contribution `a l´´etude des Orophodontoidea, Gravigrades cuirassés de la Patagonie. Ann. Paléontol. 42, 535–636.

Hoorn, C., et al., 2010. Amazonia through time: Andean uplift, climate change, landscape evolution, and biodiversity. Science 330, 927–931.

Hutchinson, D.K., et al., 2018. The Eocene-Oligocene transition: a review of marine and terrestrial proxy data, models and model-data comparisons. Clim. Past. https://doi. org/10.5194/cp-2020-68.

Janis, C.M., 1993. Tertiary mammal evolution in the context of changing climates, vegetation, and tectonic events. Annu. Rev. Ecol. Syst. 24, 467–500.

Jaramillo, C., Rueda, M.J., Mora, G., 2006. Cenozoic plant diversity in the Neotropics. Science 311, 1893–1896.

Katz, M.E., et al., 2008. Stepwise transition from the Eocene greenhouse to the Oligocene icehouse. Nat. Geosci. 1, 329–334.

Kay, R.F., et al., 2019. Parvimico materdei gen. Et sp. nov.: a new platyrrhine from the early Miocene of the Amazon Basin. Peru. J. Hum. Evol. 134, 102628.

Klaus, S., Magalhães, C., Salas-Gismondi, R., Gross, M., Antoine, P.-O., 2017. Palaeogene and Neogene brachyurans of the Amazon Basin: a revised first appearance date for primary freshwater crabs (Brachyura, Trichodactylidae). Crustaceana 90 (7–10), 953–967.

Koenigswald, W.v., 1997. Brief survey of the enamel diversity at the schmelzmuster level in Cenozoic placental mammals. In: Koenigswald, W.V., Sander, P.M. (Eds.), Tooth Enamel Microstructure. Balkema, Rotterdam, pp. 137–161.

Koenigswald, W.v., Martin, T., Billet, G., 2015. Enamel microstructure and mastication in *Pyrotherium romeroi* (Pyrotheria, Mammalia). Pal¨aontol. Z. 89 (3), 593–609.

Kohn, M.J., et al., 2015. Quasi-static Eocene-Oligocene climate in Patagonia promotes slow faunal evolution and mid-Cenozoic global cooling. Palaeogeogr. Palaeoclimatol. Palaeoecol. 435, 24–37.

Lear, C.H., Bailey, T.R., Pearson, P.N., Coxall, H.K., Rosenthal, Y., 2008. Cooling and ice growth across the Eocene-Oligocene transition. Geology 36, 251–254.

Liu, Z., et al., 2009. Global cooling during the Eocene-Oligocene climate transition. Science 323, 1187–1190.

Luciani, V., et al., 2010. Ecological and evolutionary response of Tethyan planktonic foraminifera to the middle Eocene climatic optimum (MECO) from the Alano section (NE Italy). Palaeogeogr. Palaeoclimatol. Palaeoecol. 292, 82–95.

Lundberg, J.G., 1997. Fishes of the La Venta fauna: Additional taxa, biotic and paleoenvironmental implications. In: Kay, R.F., Madden, R.H., Cifelli, R.L., Flynn, J. J. (Eds.), Vertebrate Paleontology in the Neotropics: The Miocene Fauna of La Venta, Colombia. Smithsonian Institution Press, Washington, DC, pp. 67–91.

Lundberg, J.G., Aguilera, O., 2003. The late Miocene *Phractocephalus* catfish (Siluriformes: Pimelodidae) from Urumaco, Venezuela: additional specimens and reinterpretation as a distinct species. Neotrop. Ichthyol. 1 (2), 97–109.

Magioncalda, R., Dupuis, C., Smith, T., Steurbaut, E., Gingerich, P.D., 2004. Paleocene–Eocene carbon isotope excursion in organic carbon and pedogenic carbonate: direct comparison in a continental stratigraphic section. Geology 32 (7), 553–556.

Marivaux, L., Welcomme, J.-L., Ducrocq, S., Jaeger, J.-J., 2002. Oligocene sivaladapid primate from the Bugti Hills (Balochistan, Pakistan) bridges the gap between Eocene and Miocene adapiform communities in southern Asia. J. Hum. Evol. 42 (4), 379–388.

Marivaux, L., et al., 2005. Anthropoid primates from the Oligocene of Pakistan (Bugti Hills): data on early anthropoid evolution and biogeography. Proc. Natl. Acad. Sci. U. S. A. 102 (24), 8436–8441.

Marivaux, L., et al., 2016. Neotropics provide insights into the emergence of New World monkeys: new dental evidence from the late Oligocene of Peruvian Amazonia. J. Hum. Evol. 97, 159–175.

Marivaux, L., Adnet, S., Benammi, M., Tabuce, R., Benammi, M., 2017a. Anomaluroid rodents from the earliest Oligocene of Dakhla, Morocco, reveal the long-lived and morphologically conservative pattern of the Anomaluridae and Nonanomaluridae during the Tertiary in Africa. J. Syst. Palaeontol. 15 (7), 539–569.

Marivaux, L., et al., 2017b. Earliest Oligocene hystricognathous rodents from the Atlantic margin of Northwestern Saharan Africa (Dakhla, Morocco): systematic, paleobiogeographical and paleoenvironmental implications. J. Vertebr. Paleontol. 37 (4), 1357567.

Marivaux, L., Aguirre-Dias, W., Benites-Palomino, A., Billet, G., Boivin, M., Pujos, F., Salas-Gismondi, R., Tejada-Lara, J.V., Varas-Malca, R.M., Antoine, P.-O., 2020. New record of Neosaimiri (Cebidae, Platyrrhini) from the late Middle Miocene of Peruvian Amazonia. J. Hum. Evol. 146, 102835.

Martínez, C., et al., 2021. Paleoclimatic and paleoecological reconstruction of a late Eocene South American tropical dry forest. Glob. Planet. Chang. (this issue). McKenna, M.C., Wyss, A.R., Flynn, J.J., 2006. Paleogene pseudoglyptodont xenarthrans from Central Chile and argentine Patagonia. Am. Mus. Novit. 3536, 1–18.

Meng, J., McKenna, M.C., 1998. Faunal turnovers of Palaeogene mammals from the Mongolian Plateau. Nature 394, 364–367.

Mianzan, H., et al., 2001. The Río de la Plata Estuary, Argentina-Uruguay. In: Seeliger, U., Kjerfve, B. (Eds.), Coastal Marine Ecosystems of Latin America. Springer, Berlin, Heidelberg, pp. 185–204.

Miller, K.G., Wright, J., Fairbanks, R., 1991. Unlocking the icehouse: Oligocene-Miocene oxygen isotopes, eustasy and margin erosion. J. Geophys. Res. 96, 6829–6848.

Miller, K.G., et al., 2020. Cenozoic sea-level and cryospheric evolution from deep-sea geochemical and continental margin records. Sci. Adv. 6 eaaz1346.

Moreno, F., et al., 2020. Coupled Andean growth and foreland basin evolution, Campanian–Cenozoic Bagua Basin, northern Peru. Tectonics 39 (7) e2019TC005967.

Mudelsee, M., Bickert, T., Lear, C.H., Lohmann, G., 2014. Cenozoic climate changes: a review based on time series analysis of marine benthic δ18O records. Rev. Geophys. 52 (3), 333–374.

Ni, X., Li, Q., Li, L., Beard, K.C., 2016. Oligocene primates from China reveal divergence between African and Asian primate evolution. Science 352 (6286), 673–677.

Noiret, C., et al., 2016. New bio-chemostratigraphic dating of a unique early Eocene sequence from southern Europe results in precise mammalian biochronological tiepoints. Newslett. Strat. 49 (3), 469–480.

Pagani, M., Zachos, J.C., Freeman, K.H., Tipple, B., Bohaty, S., 2005. Marked decline in atmospheric carbon dioxide concentrations during the Paleogene. Science 309, 600–603.

Patterson, B., Roper, S.H., Richards, J.G., 1942. Two Tertiary mammals from Northern South America. Am. Mus. Novit. 1173, 1–7.

Peppe, D.J., Hickey, L.J., Miller, I.M., Green, W.A., 2008. A morphotype catalogue, floristic analysis and stratigraphic description of the aspen Shale Flora (Cretaceous–Albian) of Southwestern Wyoming. Bull. Peabody Mus. Nat. Hist. 49, 181–208.

Peppe, D.J., Royer, D.L., Cariglino, B., Oliver, S.Y., Newman, S., Leight, E., Enikolopov, G., Fernandez-Burgos, M., Herrera, F., Adams, J.M., Correa, E., Currano, E.D., Erickson, J.M., Hinojosa, L.F., Hoganson, J.W., Iglesias, A., Jaramillo, C., Johnson, K.R., Jordan, G.J., Kraft, N.L.B., Lovelock, E.C., Lusk, C.H., Niinemets, U., Penuelas, J., Rapson, G., Wing, S.L., Wright, I.J., 2011. Sensitivity of leaf size and shape to climate: global patterns and paleoclimatic applications. New Phytol. 190, 724–739.

Pérez, M.E., et al., 2019. New caviomorph rodents from the late Oligocene of Salla, Bolivia: taxonomic, chronological, and biogeographic implications for the Deseadan faunas of South America. J. Syst. Palaeontol. 17 (10), 821–847.

Pol, D., Powell, J.E., 2011. A new sebecid mesoeucrocodylian from the Rio Loro Formation (Palaeocene) of North-Western Argentina. Zool. J. Linnean Soc. 163, 7–36.

Pound, M.J., Salzmann, U., 2017. Heterogeneity in global vegetation and terrestrial climate change during the late Eocene to early Oligocene transition. Sci. Rep. 7 (43386), 1–12.

Premoli-Silva, I., Jenkins, D.G., 1993. Decision on the Eocene-Oligocene boundary stratotype. Episodes 16 (3), 379–382.

Pujos, F., De Iuliis, G., Cartelle, C., 2017. A paleogeographic overview of tropical fóssil sloths: towards an understanding of the origin of extant suspensory sloths? J. Mamm. Evol. 24 (1), 19–38.

Ribeiro, A.M., López, G.M., Bond, M., 2010. The Leontiniidae (Mammalia, Notoungulata) from the Sarmiento Formation at Gran Barranca, Chubut Province, Argentina. In: Madden, R.H., Carlini, A.A., Vucetich, M.G., Kay, R.F. (Eds.), The Paleontology of Gran Barranca: Evolution and Environmental Change Through the Middle Cenozoic of Patagonia. Cambridge University Press, New York, pp. 170–181.

Rincón, A.D., Shockey, B.J., Anaya, F., Sol´orzano, A., 2015. Palaeothentid marsupials of the Salla Beds of Bolivia (late Oligocene): two new species and insights into the post-Eocene radiation of palaeothentoids. J. Mamm. Evol. 22 (4), 455–471.

Roddaz, M., et al., 2010. Cenozoic sedimentary evolution of the Amazonian foreland basin system. In: Hoorn, C., Wesselingh, F.P. (Eds.), Amazonia, Landscape and Species Evolution: A Look into the Past. Blackwell-Wiley, Hoboken, pp. 61–88.

Salas-Gismondi, R., et al., 2015. A Miocene hyperdiverse crocodylian community reveals peculiar trophic dynamics in proto-Amazonian mega-wetlands. Proc. R. Soc. B 282, 20142490.

Sánchez Fernández, A.W., Chira Fernández, J.E., Valencia Muñoz, M.M., 1997. Geología de los cuadrángulos de Tarapoto, Papa Playa. In: Utcurarca y Yanayacu 13-k, 13-l, 14-k, 14-l. INGEMMET Boletín A, 94, Lima, p. 237.

Sánchez-Villagra, M.R., 2001. The phylogenetic relationships of argyrolagid marsupials. Zool. J. Linnean Soc. 131 (4), 481–496.

Sánchez-Villagra, M.R., Kay, R.F., 1997. A skull of *Proargyrolagus,* the oldest argyrolagid (late Oligocene Salla Beds, Bolivia), with brief comments concerning its paleobiology. J. Vertebr. Paleontol. 17 (4), 717–724.

Sarkar, A., Sarangib, S., Ebiharac, M., Bhattacharyad, S.K., Raye, A.K., 2003. Carbonate geochemistry across the Eocene/Oligocene boundary of Kutch, western India: implications to oceanic O2-poor condition and foraminiferal extinction. Chem. Geol. 201 (3–4), 281–293.

Savage, D.E., Russell, D.E., 1983. Mammalian Paleofaunas of the World. Addison-Wesley, Reading, MA, p. 432.

Sedor, F.A., Oliveira, ´E.V., Silva, D.D., Fernandes, L.A., Cunha, R.F., Ribeiro, A.M., Dias, E.V., 2017. A new South American Paleogene land mammal fauna, Guabirotuba Formation (southern Brazil). J. Mamm. Evol. 24 (1), 39–55.

Seiffert, E.R., 2007. Evolution and extinction of Afro-Arabian Primates near the Eocene-Oligocene boundary. Folia Primatol. 78, 314–327.

Seiffert, E.R., et al., 2020. A parapithecid stem anthropoid of African origin in the Paleogene of South America. Science 368, 194–197.

Shellis, R.P., Berkovitz, B.K.B., 1976. Observations on the dental anatomy of piranhas (Characidae) with special reference to tooth structure. J. Zool. 180 (1), 69–84.

Shockey, B.J., Anaya, F., 2011. Grazing in a new late Oligocene mylodontid sloth and a mylodontid radiation as a component of the Eocene-Oligocene faunal turnover and the early spread of grasslands/savannas in South America. J. Mamm. Evol. 18 (2), 101–115.

Shockey, B.J., Flynn, J.J., Croft, D.A., Gans, P., Wyss, A.R., 2012. New leontiniid Notoungulata (Mammalia) from Chile and Argentina: comparative anatomy, character analysis, and phylogenetic hypotheses. Am. Mus. Novit. 3737, 1–64.

Simpson, G.G., 1967. The beginning of the Age of Mammals in South America. Bull. Am. Mus. Nat. Hist. 137, 1–259.

Soria, M.F., Hoffstetter, R., 1983. Présence d'un Condylarthre (*Salladolodus deuterotherioides* gen. et sp. nov.) dans le Déséadien (Oligocène inf´erieur) de Salla, Bolivie. CR Acad. Sci. 2 297 (6), 549–552.

Stehlin, H.G., 1909. Remarques sur les faunules de mammifères des couches éocènes et oligocènes du Basin de Paris. Bull. Soc. Geol. Fr. 9 (4), 488–520.

Storme, J.-Y., et al., 2012. Paleocene/Eocene boundary section at Zumaia (Basque-Catabric Basin) revisited: new insights from high resolution magnetic susceptibility and carbon isotope chemostratigraphy on organic matter (δ13Corg). Terra Nova 24, 310–317.

Toledo, C.E.V., Bertini, R.J., 2005. Occurrences of the fossil dipnoiformes in Brazil and its stratigraphic and chronological distributions. Rev. Brasil. Paleontol. 8 (1), 47–57.

Toumoulin, A., et al., 2020. Quantifying the effect of the Drake Passage opening on the Eocene Ocean. Palaeogeogr. Palaeoclimatol. Palaeoecol. 35 e2020PA003889.

Tramoy, R., et al., 2016. Stepwise paleoclimate change across the Eocene-Oligocene transition recorded in continental NW Europe by mineralogical assemblages and δ15Norg (Rennes Basin, France). Terra Nova 28, 212–220.

Traverse, A., 2007. Paleopalynology: Second Edition. In: Topics in Geobiology, 2nd ed. Springer, Netherlands.

Van Mourik, C., Brinkhuis, H., 2005. The Massignano Eocene-Oligocene golden spike section revisited. Stratigraphy 2 (1), 13–30.

Vandenberghe, N., Hilgen, F.J., Speijer, R.P., 2012. Chapter 28: The Paleogene period. In: Gradstein, F.M., Ogg, J.G., Schmitz, M., Ogg, G. (Eds.), The Geological Time Scale 2012. Elsevier Science Ltd, Oxford, pp. 855–921.

Villarroel, C., 2000. Un nuevo Mylodontinae (Xenarthra, Tardigrada) en la fauna de La Venta, Mioceno de Colombia: el estado actual de la familia Orophodontidae. Rev. Acad. Colomb. Cie. Ex. Físicas y Naturales 24 (90), 117–128.

Weissert, H., Joachimski, M., Sarnthein, M., 2008. Chemostratigraphy. Newsl. Stratigr. 145–179.

Westerhold, T., et al., 2020. An astronomically dated record of Earth’s climate and its predictability over the last 66 million years. Science 369, 1383–1387.

Wolff, R.G., 1984. A new early Oligocene argyrolagid (Mammalia: Marsupialia) from Salla, Bolivia. J. Vertebr. Paleontol. 4 (1), 108–113.

Woodcock, D.W., Meyer, H.W., Prado, Y., 2017. The Piedra Chamana fossil woods (Eocene, Peru). IAWA J. 38, 313–365.

Yans, J., et al., 2010. Carbon-isotope of fossil wood and dispersed organic matter from the terrestrial Wealden facies of Hautrage (Mons basin, Belgium). Palaeogeogr. Palaeoclimatol. Palaeoecol. 291, 85–105.

Yans, J., et al., 2014a. First carbon chemostratigraphy of the Ouled Abdoun phosphate

Basin, Morocco: implications for dating and evolution of earliest African placental mammals. Gondwana Res. 25, 257–269.

Yans, J., et al., 2014b. Refined bio- (benthic foraminifera, dinoflagellate cysts) and chemostratigraphy (δ13Corg) of the earliest Eocene at Albas-Le Clot (Corbières, France): implications for mammalian biochronology in Western Europe. Newsl. Stratigr. 47 (3), 331–353.

Yeo, D.C., Ng, P.K., Cumberlidge, N., Magalhaes, C., Daniels, S.R., Campos, M.R., 2007. Global diversity of crabs (Crustacea: Decapoda: Brachyura) in freshwater. In: Balian, E.V., L´evêque, C., Segers, H., Martens, K. (Eds.), Freshwater Animal Diversity Assessment. Springer, Dordrecht, pp. 275–286.

Zachos, J.C., Pagani, M., Sloan, L., Thomas, E., Billups, K., 2001. Trends, rhythms, and aberrations in global climate 65 Ma to present. Science 292, 686–693.

Zachos, J.C., Dickens, G.R., Zeebe, R.E., 2008. An early Cenozoic perspective on greenhouse warming and carbon-cycle dynamics. Nature 451, 279–283.

Zanazzi, A., Kohn, M.J., MacFadden, B.J., Terry, D.O., 2007. Large temperature drop across the Eocene-Oligocene transition in Central North America. Nature 445, 639–642.

Zhifei, L., Shouting, T., Quanhong, Z., Xinrong, C., Wei, H., 2004. Deep-water Earliest Oligocene Glacial Maximum (EOGM) in South Atlantic: Chin. Sci. Bull. 49 (20), 2190–2197.

4.6 INCISOR ENAMEL MICROSTRUCTURE OF WEST INDIAN CAVIOMORPH HYSTRICOGNATHOUS RODENTS (OCTODONTOIDEA AND CHINCHILLOIDEA)

Artigo publicado no periódico *Journal of Mammalian Evolution*, volume 29, p. 969–995, 2022, DOI: 10.1007/s10914-022-09631-7.

Laurent Marivaux[1], Lázaro W. Viñola López[2], Myriam Boivin[3], Léa Da Cunha[1], Pierre-Henri Fabre[1,4], Renaud Joannes-Boyau[5], Gilles Maincent[6], Philippe Münch[7], **Narla S. Stutz[1,8]**, Jorge Vélez-Juarbe[9], Pierre-Olivier Antoine[1]

[1]Laboratoire de Paléontologie, Institut des Sciences de l'Évolution de Montpellier (UMR 5554), Univ Montpellier (UM), CNRS, IRD, cc64, Place Eugène Bataillon, Montpellier Cedex 05 F-34095, France
[2]Florida Museum of Natural History, University of Florida, Gainesville, FL 32611-7800, USA
[3]Laboratorio de Paleontología de Vertebrados, Instituto de Ecorregiones Andinas (INECOA), Universidad Nacional de Jujuy, CONICET, IdGyM, Av. Bolivia 1661, San Salvador de Jujuy 4600, Jujuy, Argentina
[4]Mammal Section, Life Sciences, Vertebrate Division, The Natural History Museum, Cromwell Rd., South Kensington, London SW7 5BD, UK
[5]Geoarchaeology and Archaeometry Research Group (GARG), Southern Cross GeoScience, Lismore Campus, 1 Military Rd., East Lismore, NSW 2480, Australia
[6]Devé, F-97133 Saint-Barthélemy, French West Indies, France
[7]Géosciences Montpellier (UMR 5243, CNRS/UM/Université des Antilles), c.c. 060, Univ Montpellier (UM), Place Eugène Bataillon, Montpellier Cedex 05 F-34095, France
[8]Programa de Pós-Graduação em Geociências (PPGGEO), Universidade Federal do Rio Grande do Sul, Av. Bento Gonçalves, Porto Alegre 9500, 91501-970, Brazil
[9]Department of Mammalogy, Natural History Museum of Los Angeles County, 900 Exposition Boulevard, Los Angeles, CA 90007, USA

Abstract

Analysis of the incisor enamel microstructure of extinct and extant West Indian caviomorph rodents emphasizes a clear microstructural distinction between the Echimyidae (Capromyinae and Heteropsomyinae) among Octodontoidea and the

“Heptaxodontidae”, whose phylogenetic affinities are debated. All capromyines and heteropsomyines have a pattern of enamel characterized by a rectangular crystallite arrangement, which is biomechanically strongest in limiting crack propagation most efficiently (subtype [Sbt.] 3 of multiserial Hunter-Schreger bands [HSBs]). This enamel condition is exclusive to all mainland octodontoids. In stark contrast, “heptaxodontids” sampled here exhibit much less derived enamel subtypes of multiserial HSBs, with parallel to acute angular crystallite arrangement (Sbt. 1 [*Clidomys*], Sbt. 1–2 [*Elasmodontomys*], and low acute Sbt. 2 [*Amblyrhiza*]), less well adapted for prevention of crack propagation. The incisor enamel microstructure of *Amblyrhiza* and *Clidomys* is consistent with a chinchilloid assignment, as reflected by the anatomy of their auditory region and their unusual dental pattern. For *Elasmodontomys*, the primitive condition of its incisor enamel is difficult to reconcilie with its highly nested phylogenetic position within the Octodontoidea clade (among the Capromyinae), as recently inferred from aDNA analyses. The different enamel patterns among extinct and extant West Indian caviomorphs indicate distinct high-level taxonomic groups, but restricted to the Octochinchilloi (Octodontoidea and Chinchilloidea) among Caviomorpha. The great diversity of caviomorphs on the Caribbean islands resulted from intra-archipelago diversification through time, but their high-level phylogenetic diversity can only be explained by distinct sources, implying de facto multiple (potentially time-staggered) natural colonizations of the West Indies. The chinchilloid-compatible enamel and dental pattern characterizing *Borikenomys* from lower Oligocene deposits in Puerto Rico strongly suggest a link with some of the recently-extinct “heptaxodontids”, which would substantiate their much greater antiquity in the Caribbean islands.

Keywords: Caribbean Islands, Caviomorpha, Rodentia, Multiserial enamel, Systematics

Introduction

Rodents are the most diverse and speciose group of living placental mammals (Wilson and Reeder 2005; Burgin et al. 2018; Mammal Diversity Database 2022). Much of the diversity of rodents is found among the hystricognaths of the Neotropics: the caviomorphs (Caviomorpha Wood, 1955), with emblematic forms such as the guinea pigs, capybaras, New World porcupines, chinchillas, spiny rats, and the West Indian hutias. Two main clades are recognized, each divided into two superfamilies (e.g., Fabre et al. 2015; Upham and Patterson 2015; Boivin et al. 2019a): Erethicavioi Boivin, 2019 (comprising Cavioidea Fischer, 1817 + Erethizontoidea Bonaparte, 1845 + stem-

lineages) and Octochinchilloi Boivin, 2019 (comprising Chinchilloidea Bennett, 1833 + Octodontoidea Waterhouse, 1839 + stem-lineages). Caviomorphs can be found in a variety of environments, and their great taxonomical diversity is also ecological, primarily illustrated by a wide range of body sizes (from about 100 g to 65 kg; e.g., Alvarez et al. 2017 and references therein), which results in a large array of lifestyles (arboreal, fossorial, semiaquatic, and terrestrial; e.g., Mares and Ojeda 1982; Patton et al. 2015; Wilson et al. 2016), distinct locomotor behaviors (cursorial, scansorial, swimmers, etc.; Wilson and Geiger 2015; Ginot et al. 2016), different activity patterns (nocturnal, diurnal, cathemeral; e.g., Wilson et al. 2016), and different diets (e.g., Townsend and Croft 2008; Robinet et al. 2020, 2022, and references therein). This astonishing taxonomical and ecological richness of present-day caviomorphs reflects the past 35 million years (at least) of endemic evolution on the South American continent. Their fossil record so far extends back to the end of the Eocene epoch (e.g., Antoine et al. 2012, 2016, 2021; Boivin et al. 2017, 2019a, 2022), initially limited to the tropical forested low latitudes of South America, then rapidly expanding into all higher latitude environments on the South American continent (for a review, see Boivin et al. 2019a), and even to the northeastern Caribbean islands by the early Oligocene (Velez-Juarbe et al. 2014; Marivaux et al. 2020).

West Indian caviomorphs have long been the subject of much debate, not only to explain when and how they arrived/dispersed into these remote islands (over-water versus overland dispersals), but also with regards to their phylogenetic affinities with South American groups (e.g., MacPhee and Iturralde-Vinent 1995, 2005; Woods et al. 2001; Davalos 2004; Hedges 2006; MacPhee 2011; Marivaux et al. 2020). Extant representatives of the West Indian caviomorphs are the hutias, all members of the Echimyidae Octodontoidea, and today recognized as a single subfamily: Capromyinae (e.g., Courcelle et al. 2019). Most of the hutias are threatened with extinction in the Greater Antilles, an IUCN's assessment that is particularly concerning given that these rodents are already the only remnants of a much greater past diversity of caviomorphs on these islands. Several species of hutias have indeed recently become extinct (e.g., MacPhee 2009; Cooke et al. 2017; Turvey et al. 2017; Upham and Borroto-Paez 2017; Orihuela et al. 2020), but so have other endemic West Indian caviomorphs, such as the heteropsomyine echimyids and the iconic “giant hutias”, also known as the “Heptaxodontidae”. The latter inhabited distinct Caribbean islands and provide examples of insular gigantism, with notably a taxon that reached spectacular body size (~ 200 kg; Biknevicius et al. 1993), the famous *Amblyrhiza inundata* (Anguilla Bank;

Cope 1868, 1883; Schreuder 1933). Other known West Indian "heptaxodontids" were not as large but were nevertheless of respectable size (i.e., medium-sized), with *Elasmodontomys obliquus* (Puerto Rico; Anthony 1916, 1917, 1918, 1927), *Quemisia gravis* (Hispaniola; Miller 1929; Ray 1965), *Clidomys osborni* (Jamaica; Anthony 1920; MacPhee 1984; Morgan and Wilkins 2003), *Xaymaca fulvopulvis* (Jamaica; MacPhee and Flemming 2003), and possibly *Tainotherium valei* (Puerto Rico; Turvey et al. 2006). The content and highlevel systematics of the "Heptaxodontidae" have been in a state of flux over the decades. They were originally regarded as a subfamily of Chinchillidae (Anthony 1917, 1918), then subsequently a subfamily closely related to the extinct large/giant South American taxa such as Eumegamyinae, Neoepiblemyinae and Phoberomyinae (these last three subfamilies were considered at that time as Cavioidea; Simpson 1945), then closely related to the Dinomyidae (Ray 1965, but see also Miller and Gidley 1918), or even a full-fledged Family including only West Indian taxa, closely related to the other West Indian rodents, the Capromyidae (e.g., Woods and Hermanson 1985; Woods 1989). Some other rodentologists even kept the family in open nomenclature (incertae sedis) among Caviomorpha (Patterson and Wood 1982; Fabre et al. 2015), while others iteratively regarded Heptaxodontidae together with Capromyidae as Octodontoidea (McKenna and Bell 1997), also redistributing on this occasion the aforementioned related subfamilies of extinct giant rodents of South America among the standard superfamilies (for a detailed summary, see MacPhee 2011). In his study of basicranial morphology, MacPhee (2011) found morphological evidence in favor of the chinchilloid1 status of *Amblyrhiza*, whereas for *Elasmodontomys*, its affinities have remained uncertain inasmuch as the primitive basicranial features observed in this taxon resemble "a wide variety of other taxa" (but not chinchilloids in general). Yet, without much conviction, MacPhee (2011) goes with the idea that the most likely position of *Elasmodontomys* is within the Octodontoidea.

Most of the extinct capromyines, heteropsomyines and "heptaxodontids" are known from Quaternary material, although their evolutionary history on the islands undoubtedly goes back much further (MacPhee and Iturralde-Vinent 1995; MacPhee et al. 2003; MacPhee 2009, 2011). Recent gene-based phylogenies of extant Echimyidae (including West Indian capromyines and South American echimyines and euryzygomatomyines) indicate an early/middle Miocene divergence of hutias from their mainland sister taxon *Carterodon*, a result which hence suggests a Neogene colonization of the West Indies by South American octodontoids (Fabre et al. 2014; Courcelle et al. 2019). Even more recent molecular phylogenetic analyses of

Neotropical Echimyidae, including extant capromyines and, for the first time, ancient DNA (aDNA) of extinct capromyines and heteropsomyines plus *Elasmodontomys*, resolved the latter taxon as closely related to the Hispaniolan capromyine *Plagiodontia*, both taxa being situated at the base of the Capromyinae clade (Woods et al. 2020). Extinct heteropsomyines sampled for these analyses (*Boromys offella* and *Brotomys voratus*) were found as the closest out-groups of the Capromyinae clade (Woods et al. 2020). In this phylogenetic context, the identification of such a West Indian clade gathering heteropsomyines + capromyines-*Elasmodontomys*, led Woods et al. (2020) to consider the origin of these rodents as the result of a single event of colonization of the Caribbean archipelago from a South American *Carterodon*-like echimyid ancestor, sometime during the early/middle Miocene interval. Although the title of their publication2 implies the monophyly of all West Indian caviomorphs, they also suggested that other “heptaxodontids”, notably *Amblyrhiza* and/or *Clidomys*, might represent one or more separate colonizations of the West Indies by other mainland caviomorphs, albeit no Miocene or Quaternary South American caviomorph is known to be closely related to these two West Indian subfossils to date.

The direct evidence of an ancient dispersal of South American caviomorph rodents toward the Caribbean archipelago was first provided by the discovery of dental remains of an echimyid octodontoid from the early Miocene of Cuba (*Zazamys veronicae*; MacPhee and Iturralde-Vinent, 1995). The subsequent discovery of a rodent incisor in lower Oligocene deposits in Puerto Rico (Rio Guatemala [RG], San Sebastian Formation [SB Fm.]) demonstrated that rodents had colonized the Greater Antilles even earlier (Velez-Juarbe et al. 2014). Interestingly, the enamel microstructure of that incisor indicated the presence on this island, at that early time, of a caviomorph with affinities other than Octodontoidea (i.e., rather chinchilloid, cavioid or erethizontoid affinities; Martin in Velez-Juarbe et al. 2014). In 2019, the additional discovery of several dental remains (molars) in these same Puerto Rican deposits (RG, SB Fm.), compatible in size to the former incisor found in the same spot, have allowed to demonstrate the presence of undoubted chinchilloid rodents in Puerto Rico as early as the early Oligocene (Marivaux et al. 2020). This discovery has therefore raised the critical question of a possible link between these Paleogene Puerto Rican chinchilloids and some of the Pleistocene–Holocene West Indian “giant hutias” (“heptaxodontids”, especially *Amblyrhiza* and *Elasmodontomys*) for which a chinchilloid status was also supported from compatible dental morphology and incisor enamel microstructure evidence (Marivaux et al. 2020). Accordingly, the possibility of

a greater antiquity of some of the Quaternary "giant hutias" has been seriously considered, as well as the existence of a pattern of multiple and time-staggered dispersal events to explain the natural colonization of the West Indies by rodents (see Marivaux et al. 2020, 2021).

We explore here the possible link between the Oligocene Puerto Rican chinchilloids and some of the Pleistocene–Holocene West Indian “heptaxodontids” (after Marivaux et al. 2020) versus the relationships between “heptaxodontids” and capromyine/heteropsomyine octodontoids (after Woods et al. 2020) through the analysis of the incisor enamel microstructure. This study substantially complements taxonomically Martin's (1992) first analysis of incisor enamel microstructure of West Indian caviomorph subfossils and provides illustrations of the enamel of these taxa, which had not been made available previously (notably for *Amblyrhiza* and *Elasmodontomys*, and the few hutias sampled initially). The enamel microstructure of the incisor of rodents has proven to be a powerful tool for systematics and phylogeny of the group (e.g., Korvenkontio 1934; Wahlert 1968; Boyde 1978; Koenigswald 1985; Martin 1992, 1993, 1994a, b, 1997; Kalthoff 2000; Marivaux et al. 2004).

The incisor enamel in rodents is primarily composed of two layers (Korvenkontio 1934), the *portio externa* (PE), consisting of radial enamel in which bundles of hydroxyapatite crystallites (= prisms) are oriented in the same direction, and the *portio interna* (PI), which is characterized by decussating bands of prism rows named Hunter-Schreger bands (HSBs) (Martin 1992, 1993; Koenigswald and Sander 1997; Alloing-Seguier et al. 2019). Between the prisms, there is an enamel fraction also formed by parallelly-oriented hydroxyapatite crystallites, but which are not bundled into prisms (Fig. 1). This fraction forms the inter-prismatic matrix (IPM). Ctenohystrican rodents (including Ctenodactylidae, Diatomyidae, and Hystricognathi) display an incisor enamel layer with a PI having decussating multi-prism rows and thin sheets of IPM, which allows describing multiserial HSBs (Korvenkontio 1934; Martin 1992, 1993). On the basis of the angle of the IPM crystallites with respect to the prism long axes, several subtypes of multiserial HSBs can be distinguished (Martin 1992, 1993, 1994a, 1997; see Boivin et al. 2019b). A first subtype (Sbt. 1) can be described when the IPM crystallites run parallel to those of the prisms or slightly deviate from them with a low angle (very low acute angle), and anastomoses very regularly, but without totally surrounding each prism (sheet to sheath-like IPM). A second subtype (Sbt. 2) is identified when the IPM crystallites (thin sheets) anastomose moderately to regularly and form an acute angle (with a wide amplitude range) to the prism crystallite direction.

A third subtype (Stb. 3) is described when the IPM sheets show few or no anastomoses and their crystallites run at a very high acute or right angle to those of the prisms, forming inter-row sheets (i.e., rectangular platelike IPM; Fig. 1). On the biomechanical level, an increasing angulation of the IPM provides a better resistance to the crack propagations, as it strengthens the enamel in the third dimensions (Martin 1992, 1993, 1994a, 1997). A Sbt. 3 of multiserial HSBs characterized by such a rectangular crystallite (prisms and IPM) arrangement is considered as the most derived/specialized condition of enamel, a statement which is corroborated by the successive stratigraphic occurrences of the different subtypes (1 then 2 and finally 3), and the observation of transitional cases (i.e., Sbt. 1–2 and Sbt. 2–3; Martin 1994a, 1997, 2005; Marivaux et al. 2004, 2019; Vucetich et al. 2015; Boivin et al. 2019b). The three subtypes of multiserial HSBs can be found in the different main ctenohystrican clades (see Online Resource 1), with the Sbt. 3 iteratively acquired in most terminal clades. Among caviomorphs, the Sbt. 1, Sbt. 2 and transitional Sbt. 1–2 of multiserial HSBs are found in extinct and extant erethizontoids, chinchilloids and cavioids (Online Resource 1; Martin 1992, 1994b). Modern members of these last three superfamilies have then preserved less advanced and less resistant incisor enamel conditions. In contrast, the derived transitional Sbt. 2–3 and chiefly Sbt. 3 of multiserial HSBs are restricted to octodontoids from an early stage in their evolutionary history (Online Resource 1; Martin 1992, 1994b, 2004, 2005; Boivin et al. 2019b). However, the achievement of Sbt. 3, which can be seen as the best adaptation against crack, seems to have evolved rapidly and iteratively within the Octodontoidea clade (e.g., Vucetich and Vieytes 2006; Vucetich et al. 2010; Boivin et al. 2019b). This incisor enamel condition (Sbt. 3) characterizing virtually all extinct and all extant octodontoids is therefore particularly in stark contrast to the less advanced enamel condition observed by Martin (1992) for the incisor of *Elasmodontomys* (i.e., low acute Sbt. 2; Martin 1992 [but not illustrated]), especially if the latter taxon turns out to be nested high within the Octodontoidea clade, well-into the Echimyidae, as resolved by Woods et al. (2020).

For the purposes of this study, we assembled an importante number of incisors of extinct West Indian caviomorphs, including a newly-discovered incisor of the chinchilloid from the early Oligocene of Puerto Rico, and several incisors documenting “heptaxodontids”, heteropsomyines and capromyines, which all come from Quaternary contexts (see Table 1). With this sampling, we have the opportunity to compare more comprehensively than Martin (1992) the incisor enamel microstructure characterizing each West Indian caviomorph group, to highlight some incompatibilities of previously

suggested phylogenetic affinities, and finally to discuss in favor or against some recently proposed phylogenetic hypotheses concerning "giant hutias". We will discuss the results with a special emphasis on the implications for macroevolutionary and historical biogeographic patterns of some West Indian caviomorphs.

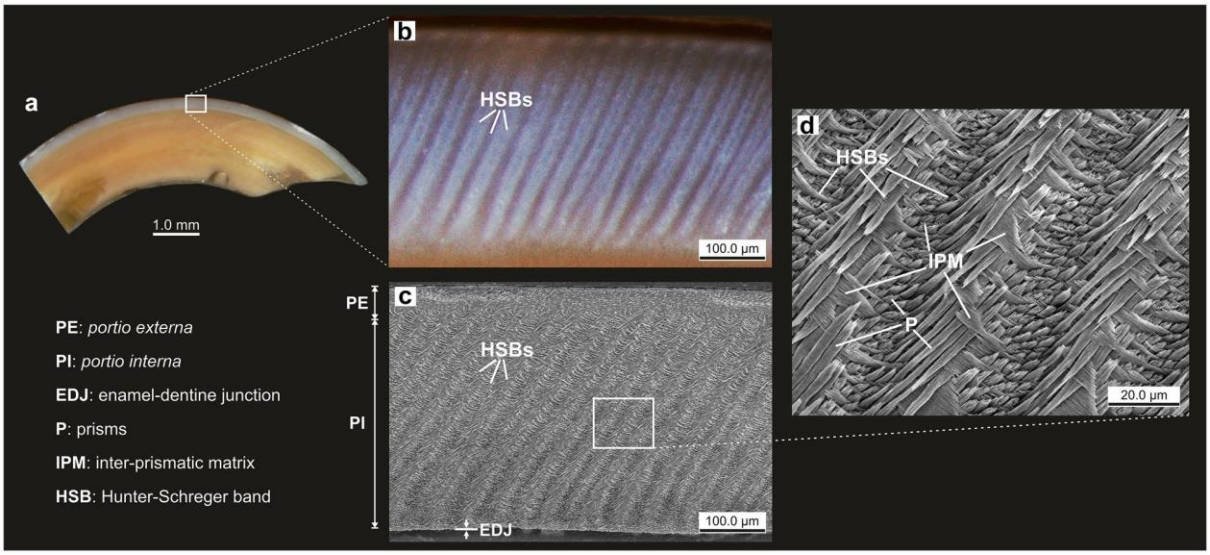


Fig. 1 Optical and scanning electron photomicrographs of an incisor for which the enamel microstructure is revealed in section after polishing and etching. **a.** longitudinal section of the incisor (here *Capromys pilorides*) showing the enamel layer on the labial aspect of the tooth (optical incident light photography); **b.** studied area of the enamel layer at higher magnification, showing inclined Hunter-Schreger bands (HSBs) (optical incident light photography); **c.** studied area of the enamel layer, revealing microstructural details (scanning electron photomicrograph): the *portio externa* (PE) is the outer part of the enamel layer, displaying radial enamel, whereas the *portio interna* (PI), generally representing the largest proportion (%) of the total enamel thickness, displays multiserial HSBs. On this given sample, HSBs are inclined at ~ 35° to the enamel-dentine junction (EDJ); **d.** microstructural detail of '**c**' showing seven decussating HSBs with five to six prisms per band, and the crystallites of the inter-prismatic matrix (IPM) forming thin plates between the prism rows (inter-row sheets) that run perpendicular to the prism long axes (direction), without any anastomosis between prisms.

Table 1 List of sampled taxa for incisor enamel microstructure analyses with indications on their geographic provenance, age and collectors/collections. Abbreviations: CLV, Coleccion Lazaro Vinola; Coll., Collection; FMNH, Florida Museum of Natural History, Division of Vertebrate Paleontology, USA; LACM, Natural History Museum of Los Angeles County, USA; SB, Saint-Barthelemy, French West Indies; UF, University of Florida, USA; UM, Universite de Montpellier, France; UPRMP, University of Puerto Rico, Mayaguez (Paleontology Collection, Department of Geology), Puerto Rico, USA; (frag.) means fragment of incisor. The date format used here is DD/MM/YY

Taxa	Specimen number	Designation (locus)	Provenance	Age	Miscellaneous (collector, collection, date)
Isolobodon portoricensis	UF 520141 (FMNH)	Right lower incisor (frag.) [partial mandible]	Cueva de las Abejas (XD007), Pedernales, Dominican Republic	Late Pleistocene or Holocene (Santarosean)	C. A. Woods (02/1984)
Isolobodon montanus	UF 333712 (FMNH)	Left lower incisor (frag.) [mandible i1 p4–m3]	Trouing Jeremie 5 (XH007), Dept. du Sud, Haiti	Holocene	(07/07/1985)
Hexolobodon phenax	UF 520143 (FMNH)	Right lower incisor [partial mandible]	Trouing Marassa/Trujin Bridge (XH002), Dpt. de l'Ouest, Haiti	Holocene	(10, 35, 21. B; 31/07/1983)
Rhizoplagiodontia lemkei	UF 70850 (FMNH)	Right lower incisor [mandible i1 m1–m2]	Trouing Jeremie 5 (XH007), Dept. du Sud, Haiti	Late Pleistocene or Holocene	C. A. Woods (01/02/1980)
Plagiodontia ipnaeum [velozi]	UF 520142 (FMNH)	Left upper incisor	Trouing Bois Formon 3 (XH019), Dept. du Sud, Haiti	Late Pleistocene or Holocene (Santarosean)	D. Codier (25/01/1984)
Capromys pilorides lewisi	UF 520144 (FMNH)	Left upper incisor	Dolphin Cave (XC018), Grand Cayman Co., Cayman Islands	Late Pleistocene or Holocene	G. S. Morgan (31/03/1993)
Geocapromys caymanensis	UF 520145 (FMNH)	Right lower incisor	Dolphin Cave (XC018), Grand Cayman Co., Cayman Islands	Late Pleistocene or Holocene	G. S. Morgan (31/03/1993)
Geocapromys columbianus	CLV 2595	Right lower incisor	Cueva del Infierno, Mayabeque, Cuba	Middle–late Holocene (Archaeological site)	Coll. S. Diaz Franco
Macrocapromys acevedo	CLV 401	Right lower incisor (frag.)	Cantera J4 # 1, Matanzas, Cuba	Late Pleistocene–Holocene	Coll. L. W. Viñola López (16/05/2012)
Mesocapromys nanus	CLV 2597	Left lower incisor	Cantera J4 # 1, Matanzas, Cuba	Late Pleistocene–Holocene	Coll. L. W. Viñola López (2011)
Mysateles sp.	UM 524N	Left lower incisor [mandible i1 p4–m3]	Cuba (area of capture not specified)	Recent	Old UM collection
Brotomys contractus	UF 333716	Left upper incisor [pmx + mx; I1 P3]	Trou Jean Paul (XH013H) (suf. Layer), Dept. de l'Ouest, Haiti	Not specified	(16/02/1984)
Boromys offella	CLV 2596	Left lower incisor (frag.)	Cueva del Infierno, Mayabeque, Cuba	Middle–late Holocene (Archaeological site)	Coll. S. Diaz Franco
Boromys torrei	CLV 2598	Right upper incisor	Cuevas Blancas, Mayabeque, Cuba	Holocene (see Orihuela et al. 2020)	Coll. E. Fonseca and O. Jimenez (01/05/2001)
Heteropsomys sp.	UPRMP-3229	Left lower incisor	*Elasmodontomys* Shelter, Manati, Puerto Rico	Late Pleistocene (~ 60 ka; Tarentian)	J. Vélez-Juarbe, L. Marivaux et al. (05-06/02/2020)
Elasmodontomys obliquus	UPRMP-3230	Right lower incisor	*Elasmodontomys* Shelter, Manati, Puerto Rico	Late Pleistocene (~ 60 ka; Tarentian)	J. Vélez-Juarbe, L. Marivaux et al. (05-06/02/2020)
Elasmodontomys obliquus	UPRMP-3231	Left lower incisor	*Elasmodontomys* Shelter, Manati, Puerto Rico	Late Pleistocene (~ 60 ka; Tarentian)	J. Vélez-Juarbe, L. Marivaux et al. (05-06/02/2020)
Elasmodontomys obliquus	UPRMP-3232	Right lower incisor	*Elasmodontomys* Shelter, Manati, Puerto Rico	Late Pleistocene (~ 60 ka; Tarentian)	J. Vélez-Juarbe, L. Marivaux et al. (05-06/02/2020)
Clidomys sp. (*osborni*?)	UF 274295	Lower or upper incisor (frag.)	Wallingford 1 (XJ002), St. Elizabeth Parish, Jamaica	Pleistocene	T. H. Patton (06/1966)
Amblyrhiza sp. (*inundata*?)	UM SB-Coco-03	Lower incisor	Fissure-filling 01, Îlet Coco, satellite islet of St. Barthélemy	Middle Pleistocene (~ 415 ka; Chibanian)	L. Marivaux, G. Maincent and P. Münch (25/05/2019)
Amblyrhiza sp. (juvenile)	UM SB-Coco-04	Left small lower incisor (frag.)	Fissure-filling 01, Îlet Coco, satellite islet of St. Barthélemy	Middle Pleistocene (~ 415 ka; Chibanian)	L. Marivaux, G. Maincent and P. Münch (25/05/2019)
Borikenomys praecursor	LACM 162956	Lower incisor (frag.)	LACM Loc. 8060, Rio Guatemala, San Sebastián, Puerto Rico	Late early Oligocene (~29.5 Ma)	J. Vélez-Juarbe, L. Marivaux et al. (10/02/2020)
Lagidium sp.	UM 521N	Left lower incisor [mandible i1 p4–m3]	South America (provenance not specified)	Recent (1946)	Old UM collection
Chinchilla sp.	UM N312	Left lower incisor [mandible i1 p4–m3]	South America (provenance not specified)	Recent	Old UM collection
Cuniculus paca	UM N385	Right lower incisor [mandible i1 p4–m3]	South America (provenance not specified)	Recent	Old UM collection

Materials and methods

The material of this study consists primarily of incisors of subfossil and fossil caviomorphs from the West Indies, which have been recovered over the past few decades (see Table 1 for details on their geographic provenance, age and collectors/collections). We assembled incisors documenting subfossil "heptaxodontids" (notably *Amblyrhiza*, *Elasmodontomys*, and *Clidomys*), subfossil heteropsomyines (*Heteropsomys*, *Boromys*, and *Brotomys*), and subfossil

capromyines (*Isolobodon*, *Hexolobodon*, *Rhizoplagiodontia*, *Plagiodontia*, *Geocapromys*, *Capromys*, *Macrocapromys*, and *Mesocapromys*), the two latter being echimyid octodontoids. We tried to sample as many genera as possible, represented by at least one species (at best two). Regrettably, we were not successful in obtaining incisors documenting the extinct "heptaxodontid" *Quemisia*, *Xaymaca*, and *Tainotherium*. An incisor recovered from lower Oligocene deposits of Puerto Rico (San Sebastian Fm.) was also sampled for enamel microstructure analyses. This incisor was found in the same level as the former one described by Velez-Juarbe et al. (2014) and the lower molars of compatible size that allowed the description of a dinomyid chinchilloid (*Borikenomys*; see Marivaux et al. 2020). Incisors of a few living caviomorphs from South America (*Chinchilla* and *Lagidium* [chinchillid chinchilloids], and *Cuniculus* [cuniculid cavioid]) and from the West Indies (*Mysateles* [capromyine]) were also sampled here for enamel comparison purposes. The latter were retrieved from skulls of available specimens housed in the osteological collection of the *Université de Montpellier* (Table 1). However, our primary reference for enamel microstructure comparisons will be the extensive database of incisor enamel of living caviomorphs assembled by Martin (1992). The latter also includes enamel data on extinct caviomorphs, as well as other extant and extinct rodents in general (Online Resource 1). This database for comparisons will be supplemented by the subsequent work of Martin (1993, 1994a, b, 2004, 2005), and other available work on this topic (e.g., Vieytes et al. 2007; Vucetich et al. 2010, 2015; Arnal et al. 2014; Velez-Juarbe et al. 2014; Assemat et al. 2019; Boivin et al. 2019b; Marivaux et al. 2019, 2020). For our sampling, in most cases (extinct and extant species), the incisors were removed from the embedding bone structure (dentary or maxillary), and only a fragment of less than 1 cm was punctured for analysis. The remaining part of the incisor was repositioned in the bone socket, or preserved separately. In some fossil cases, incisors or fragments of incisors were found isolated. In fossil rodent-bearing localities containing several species, incisor identification was made by morphological comparison with better-preserved specimens from the same localities, whose bony structures bear incisors and molars, as well as on the basis of size compatibility. Lower *versus* upper incisors were identified according to their radius of curvature (lower incisors having a much greater radius than upper incisors of similar overall dimensions).

All selected incisor specimens were embedded in artificial epoxy resin. After hardening, they were cut transversally to observe the incisor in cross-section, and to

draw the outline of the enamel layer (Fig. 2). They were subsequently grounded and polished longitudinally with successive silicon carbide papers (800–4000). The final finely polished sections were etched for 30 s with 37% phosphoric acid (H3PO4), to make the microstructural details of the enamel visible, then rinsed with distilled water. The samples were air-dried and coated with conductive material (palladium) before being examined with a scanning electron microscope (SEM; HITACHI S 4000) at different magnifications (Figs. 1, 3, 4, 5, 6, 7, 8 and 9).

For describing the enamel microstructure, we followed the nomenclature of Koenigswald and Sander (1997) and Martin (1992, 1993) (see Fig. 1). The measurements carried out on the enamel layer observed in longitudinal section follow those proposed by Martin (1992, 1993), Boivin et al. (2019b) and Marivaux et al. (2019). The angle α formed between the direction of the IPM crystallites and that of the prism crystallites was measured at the level of the HSB, where the prism axis is the longest. For describing the variation of α across the diferente incisor sampled, we arbitrarily subdivided its observed range as follows: $0° \leq \alpha \leq 15°$, the IPM crystallites and the prism crystallites are parallel or their respective directions deviate slightly from each other, forming a very low acute angle; $15° < \alpha \leq 40°$, the directions of the two crystallite sets form a low acute angle; $40° < \alpha \leq 70°$, they form a medium to high acute angle; $70° < \alpha \leq 90°$, they form a very high acute to right angle (rectangular crystallite arrangement, plate-like IPM). The identification of a subtype of multiserial HSBs for a given incisor was based on the observation of the whole longitudinal section available of the specimen. The distinction between the main subtypes (and subtle cases of transitional subtypes) was based not only on the value of α, but also on the general organization/configuration of the IPM (i.e., sheets between rows of prisms, sheets inter-prisms, sheath-like sheets, and frequency of the IPM crystallite anastomoses). We note that the recognition of transitional subtypes (especially Sbt. 1–2) is subtle and sometimes difficult to formalize. Nevertheless, we primarily considered the apparent increase in resistance to crack propagation (otherwise, the primitive state as opposed to the successive more advanced/derived states of the IPM configuration, more efficient to limit crack propagation).

Results

All the incisors analyzed (25) in longitudinal section exhibit a double layer enamel consisting of a PE of variable thickness from one tooth specimen to another and composed of radial enamel, and a PI showing decussated multi-prism rows and thin

IPM sheets, which allows the description of multiserial HSBs (Figs. 3, 4, 5, 6, 7, 8 and 9). All observed enamel characters and measurements made on SEM photographs of the studied incisor specimens are reported in Table 2.

Capromyinae Echimyidae Octodontoidea

***Isolobodon portoricensis* †** (Fig. 3a–b) **and *I. montanus* †** (Fig. 3c–d). For both species, the enamel layer in longitudinal section displays HSBs in PI that run straight. The PE, with radial enamel, is weakly extensive, representing Only about 1/10th or less of the enamel thickness. In *I*. *montanus*, the prisms in PE are strongly inclined and lanceolate. In both species, HSBs in PI display four prisms in average per band, which are oval to flattened in cross-section. A prism of transition between two decussating HSBs can be observed on *I*. *portoricensis*, whereas it is not clearly visible/identifiable on *I*. *montanus*. The IPM crystallites in PI are less developed than those of the prisms, whereas in PE it seems equal in strength. In PI, the IPM is thin and lies plate-like between the prism rows (i.e., inter-row sheets), without anastomosis, and with its crystallite Direction nearly perpendicular to the prism main axes. With such an PM crystallite arrangement, the two incisors of these two species of *Isolobodon* illustrate an enamel microstructure characterized by an advanced Sbt. 3 of multiserial HSBs. The enamel layer differs only moderately between the two species, notably in overall thickness (PE + PI), which is thinner in *I*. *montanus* (although the incisor is slightly wider), and in the presence of more inclined HSBs in PI in *I*. *portoricensis*.

***Hexolobodon phenax* †** (Fig. 3e–f). The enamel layer is particularly thick with respect to the width of the incisor (compared to the thickness observed in other capromyines with incisors of comparable size). The PE is limited, accounting for less than 10% of the total enamel thickness. The PI/PE boundary is straight and clearly perceptible. In PI, the HSBs are inclined at ~ 25° (main axis), but they are not straightly arranged from the EDJ to the PI/PE boundary, and instead appear somewhat undulating. Near the EDJ (~ 15% of PI) and the PI/PE boundary (~ 5% of PI), the HSBs are more inclined than in the main central part of PI. Each HSB display four prisms that are particularly flattened in crosssection, and there is no prism of transitional zone between two adjacent HSBs. The IPM crystallites run at a nearly right angle to the prism crystallites, and form thin sheets (platelike) between rows of prisms (inter-row sheets), with only very rare anastomoses. This kind of crystallite arrangement typifies a Sbt. 3 of multiserial HSBs.

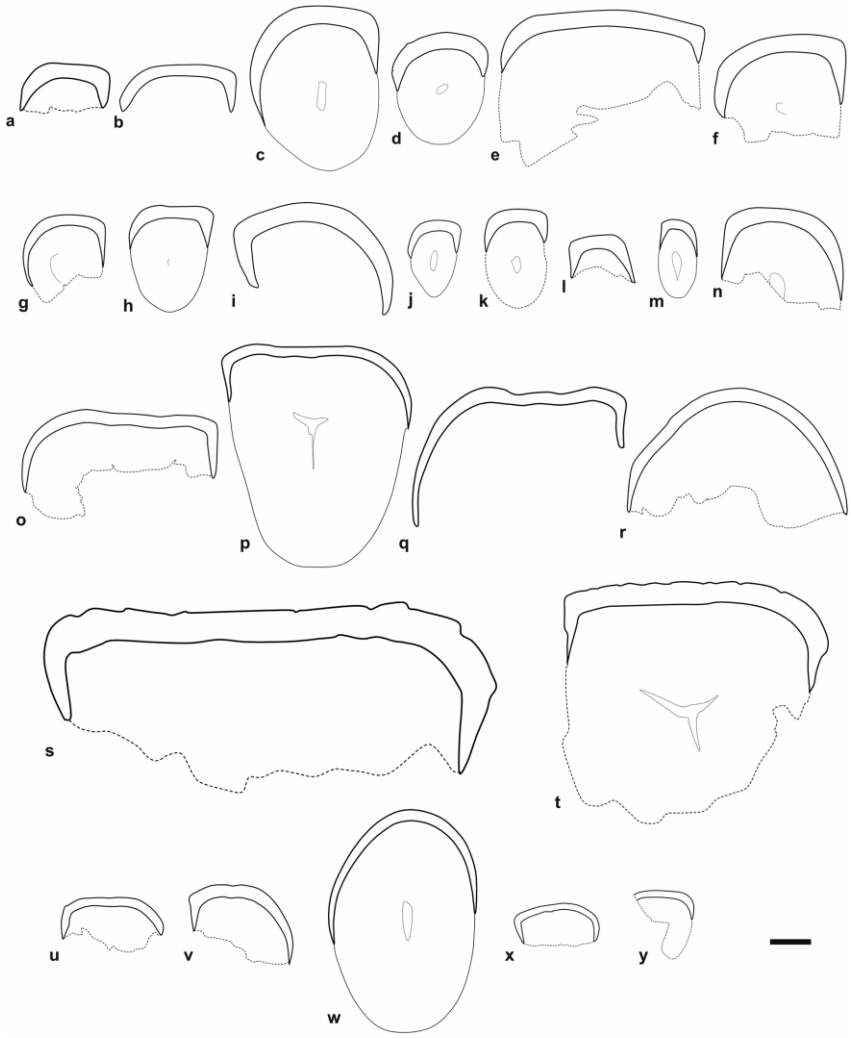


Fig. 2 Incisor cross-sections of sampled hystricognathous rodents from the West Indies and South America. Most of specimens from the West Indies are subfossils (see Table 1). **a.** UF 520141, *Isolobodon portoricensis*; **b.** UF 333712, *Isolobodon montanus*; **c.** UF 520143, *Hexolobodon phenax*; **d.** UF 70850, *Rhizoplagiodontia lemkei*; **e.** UF 520142, *Plagiodontia ipnaeum*; **f.** UF 520144, *Capromys pilorides*; **g.** *Geocapromys caymanensis*; **h.** CLV 2595, *Geocapromys columbianus*; **i.** CLV 401, *Macrocapromys acevedo*; **j.** CLV 2597, *Mesocapromys nanus*; **k.** UF 333716, *Brotomys contractus*; **l.** CVL 2596, *Boromys offella*; **m.** CLV 2598, *Boromys torrei*; **n.** UPRMP-3229, *Heteropsomys* sp.; **o.** UPRMP-3230, *Elasmodontomys obliquus*; **p.** UPRMP-3231, *Elasmodontomys obliquus*; **q.** UPRMP-3232, *Elasmodontomys obliquus*; **r.** UF 274295, *Clidomys* sp.; **s.** UMSB-Coco-03, *Amblyrhiza* sp.; **t.** UM-SB-Coco-04, *Amblyrhiza* sp. (juvenile); **u.** LACM 162956, *Borikenomys praecursor*; **v.** UM 524N, *Mysateles* sp.; **w.** UM N385, *Cuniculus paca*; **x.** UM 521N, *Lagidium* sp.; **y.** UM N312, *Chinchilla* sp. Some specimens have the dentine dammaged (dashed lines). **a–d**, **h–j**,

l, **n–q** and **s–y**: lower incisors. **e–g**, **k** and **m**: upper incisors. **r**: lower or upper incisor. Scale bar equals 1 mm.

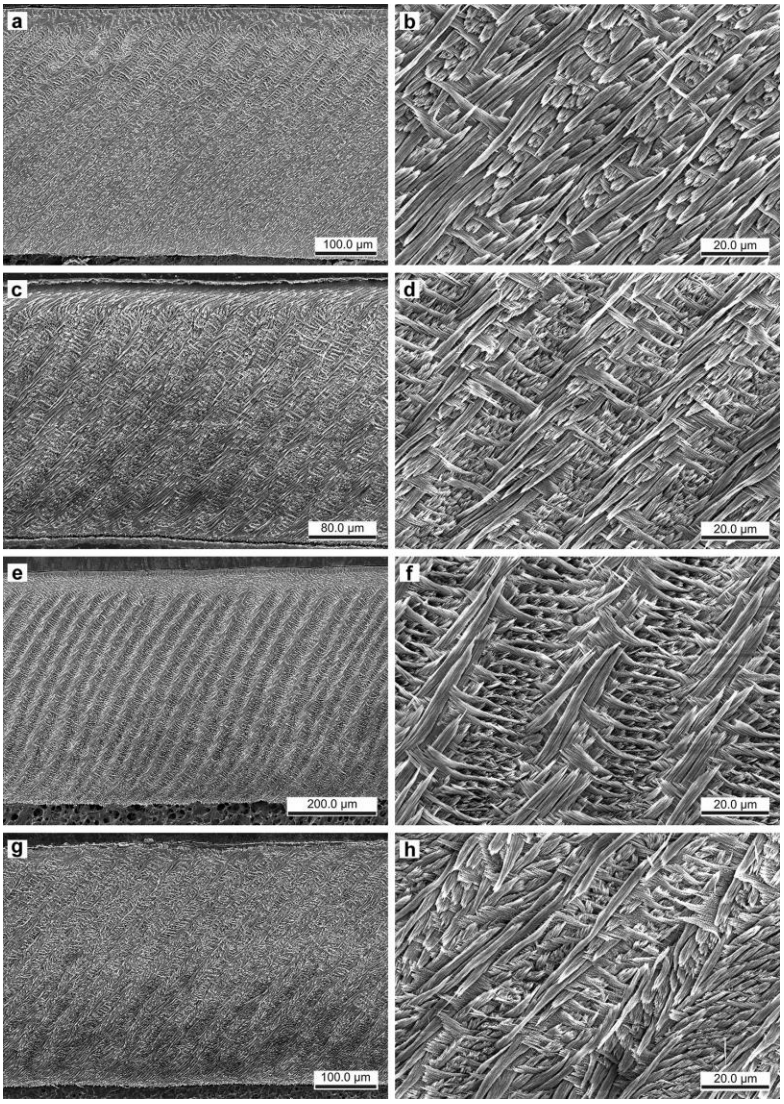


Fig. 3 Scanning electron photomicrographs of incisors of subfossil spiny rat hutias (Echimyidae Capromyinae) from the West Indies, for which the enamel microstructure (multiserial HSBs) is shown in longitudinal section and at different magnifications. The left pictures illustrate an overview of the enamel layer for each specimen, and the associated right ones a detail of the microstructure in PI. **a–b.** *Isolobodon portoricensis* (UF 520141); **c–d.** *Isolobodon montanus* (UF 333172); **e–f.** *Hexolobodon phenax* (UF 520143, reversed); **g–h.** *Rhizoplagiodontia lemkei* (UF 70850).

***Rhizoplagiodontia lemkei* †** (Fig. 3g–h). The enamel layer of this taxon is almost entirely composed of PI, the PE being less than 5%. Furthermore, the PE/PI boundary remains particularly difficult to distinguish. In PI, the HSBs are markedly inclined and straightly arranged, and are composed of three or four oval to flattened prisms, the

fourth being often a prism of transitional zone between two HSBs. At the EDJ, a thin starting zone with a parallel prism progression is observable. The IPM crystallites in PI are almost perpendicular to the crystallites of the prisms, and form thin plates between the prism rows (i.e., inter-row sheets), without any perceptible anastomosis. This type of crystallite arrangement typifies a Sbt. 3 of multiserial HSBs.

Table 2. Enamel characters and measurements of the studied incisor specimens. All incisor sections display multiserial HSBs. Enamel distinctions are made between some incisors depending on the arrangement and direction of the hydroxyapatite crystallites of the IPM, with respect to the crystallites of the prisms, thereby describing different subtypes (Sbt.) or transitional subtypes of multiserial enamel. Arbitrary division of the range of the angle (α) formed between the IPM crystallites and the prism crystallites: parallel to very low acute angle ($0° \leq \alpha \leq 15°$); low acute angle ($15° < \alpha \leq 40°$); medium to high acute angle ($40° < \alpha \leq 70°$); very high acute to right angle ($70° < \alpha \leq 90°$). Abbreviations: HSB, Hunter-Schreger band; IPM, inter-prismatic matrix; mm, millimeters; PE, *portio externa*; PI, *portio interna*; †, extinct; #, slightly different from.

Taxon		Specimen number	Incisor type	Incisor width (mm)	Enamel thickness (µm)	% of PE	Inclination of HSBs	Prisms per HSB	Prisms of transitional zone	Division HSB	Prism cross section in PI	IPM configuration in PI	IPM anastomosis	Angle (α) crystallites of IPM/prisms	Enamel type	Subtype	Figure
Isolobodon portoricensis	†	UF 520141	Lower	2.29	411	11	40°	3–4	Not well-marked (1)	Absent	Oval to flattened	Inter-row thin sheets	None	# Rectangular (83–90°)	Multiserial	3	3a–b
Isolobodon montanus	†	UF 333712	Lower	2.96	307	6	29–32°	4–5	Absent	Absent	Oval to flattened	Inter-row thin sheets	None	# Rectangular (80–84°)	Multiserial	3	3c–d
Hexolobodon phenax	†	UF 520143	Lower	3.18	531	8	23–28°	4	Absent	Absent	Flattened	Inter-row thin sheets	Possible but rare	# Rectangular (81–87°)	Multiserial	3	3e–f
Rhizoplagiodontia lemkei	†	UF 70850	Lower	2.37	400	< 5	40–44°	3(–4)	Not well-marked (1)	Absent	Oval to flattened	Inter-row thin sheets	None	# Rectangular (85–87°)	Multiserial	3	3g–h
Plagiodontia ipnaeum	†	UF 520142	Upper	5.04	388	7	38°	4(–5)	Not well-marked (1)	Absent	Oval	Inter-row thin sheets	None	# Rectangular (84–88°)	Multiserial	3	4a–b
Capromys pilorides lewisi	†	UF 520144	Upper	3.26	508	8	26–27°	5–6	Absent	Absent	Oval to flattened	Inter-row thin sheets	None	Rectangular (89–90°)	Multiserial	3	4c–d
Geocapromys caymanensis	†	UF 520145	Lower	2.07	259	6	36–38°	5	Absent	Very rare	Oval to flattened	Inter-row thin sheets	None	# Rectangular (82–84°)	Multiserial	3	4e–f
Geocapromys columbianus	†	CVL 2595	Lower	2.07	254	3	39°	4–5	Absent	Absent	Oval	Inter-row thin sheets	Possible but very rare	# Rectangular (83–87°)	Multiserial	3	4g–h
Macrocapromys acevedo	†	CLV 401	Lower	3.70	232	7	23°	3(–4)	Not well-marked (1)	Absent	Flattened	Inter-row thin sheets	None	Rectangular (88–90°)	Multiserial	3	5a–b
Mesocapromys nanus	†	CLV 2597	Lower	1.33	208	14	48–50°	3	Present (1)	Absent	Flattened	Inter-row thin sheets	None	Sub–rectangular (75–80°)	Multiserial	3	5c–d
Mysateles sp.		UM 524N	Lower	2.44	298	16	35°	3(–4)	Not well-marked (1)	Very rare	Flattened	Inter-row thin sheets	None	Rectangular (87–88°)	Multiserial	3	5e–f
Brotomys contractus	†	UF 333716	Upper	1.55	279	12	18–22°	3(–4)	Present (1–2)	Absent	Rounded to oval	Inter-row thin sheets	None	Rectangular (~89°)	Multiserial	3	6a–b
Boromys offella	†	CLV 2596	Lower	1.51	298	10	32–33°	3(–4)	Not well-marked (1)	Very rare	Oval to flattened	Inter-row thin sheets	Possible but very rare	Rectangular (85–90°)	Multiserial	3	6c–d
Boromys torrei	†	CLV 2598	Upper	0.92	256	12	20–25°	3(–4)	Present (1)	Rare	Oval to flattened	Inter-row thin sheets	None	Rectangular (90°)	Multiserial	3	6e–f
Heteropsomys sp.	†	UPRMP-3229	Lower	3.04	256	10	35–36°	4(–5)	Present (1)	Absent	Oval	Inter-row thin sheets	Possible but very rare	Sub–rectangular (75–79°)	Multiserial	3	6g–h
Elasmodontomys obliquus	†	UPRMP-3230	Lower	4.88	275	10	27–30°	4–5	Present (1)	Absent	Oval to flattened	Inter-row and often inter-prism thin sheets	Very frequent and regular	Low acute (20–24°)	Multiserial	(1–)2	7a–b
Elasmodontomys obliquus	†	UPRMP-3231	Lower	4.59	232	15	35–37°	4–5	Present (1–2)	Absent	Oval to flattened	Inter-row and often inter-prism thin sheets	Very frequent and regular	Low acute (16–24°)	Multiserial	(1–)2	7c–d
Elasmodontomys obliquus	†	UPRMP-3232	Lower	5.33	232	17	28–31°	4(–5)	Present (1–2)	Very rare	Rounded to flattened	Inter-row and often inter-prism thin sheets	Very frequent and regular	Low acute (23–26°)	Multiserial	(1–)2	7e–f
Clidomys sp.	†	UF 274295	Lower or upper	5.48	254	10	12–15°	(3–)5	Not well-marked (1)	Very rare	Flattened	Inter-row and inter-prism thin sheets (sheath-like)	Permanent	Parallel (~10° or less)	Multiserial	1	7g–h
Amblyrhiza sp.	†	UM SB-Coco-03	Lower	11.26	(660–)752	10–13	25–34°	5(–6)	Present (1–2)	Absent	Oval to flattened	Inter-row and often inter-prism thin sheets	Very frequent and regular	Low acute (28–35°)	Multiserial	2	8a–d
Amblyrhiza sp. (juvenile)	†	UM SB-Coco-04	Lower	6.59	528	9	42° (main axis)	4(–6)	Present (1)	Absent	Oval to flattened	Inter-row and often inter-prism thin sheets	Very frequent and regular	Low acute (28–36°)	Multiserial	2	8e–f
Borikenomys praecursor	†	LACM 162956	Lower	2.59	218	18	37–41°	3(–4)	Not well-marked (1)	Very rare	Rounded to oval	Inter-row and often inter-prism thin sheets	Very frequent and regular	Low acute (29–35°)	Multiserial	2	8g–h
Lagidium sp.		UM 521N	Lower	1.74	144	19	45°	3(–4)	Present (1–2)	Very rare	Oval to flattened	Inter-row and inter-prism thin sheets (sheath-like)	Permanent	# Parallel (~15–22°)	Multiserial	1(–2)	9a–b
Chinchilla sp.		UM N312	Lower	1.70	149	21	46–49°	3(–4)	Present (1–2)	Very rare	Flattened	Inter-row and often inter-prism thin sheets	Very frequent and regular	Low acute (22–28°)	Multiserial	(1–)2	9c–d
Cuniculus paca		UM N385	Lower	3.70	248	22	17°	4	Absent	Frequent	Flattened	Inter-row and inter-prism thin sheets (sheath-like)	Permanent	# Parallel (~15° or less)	Multiserial	1	9e–f

***Plagiodontia ipnaeum* †** (Fig. 4a–b). Whereas this taxon is the largest of the West Indian echimyids sampled capromyines and heteropsomyines), its (large) incisor displays a particularly thin enamel layer, almost similar in thickness to that of taxa with incisors almost twice as small (see Table 2, Incisor width *versus* Enamel thickness). The PE is limited (~ 8% of the total enamel thickness), and the PI/PE boundary is straight and clearly perceptible. In PI, HSBs are moderately inclined, and are composed of at least four prisms that are oval in cross-section. There is an additional prism that appears as a transitional zone between two HSBs. The crystallites of the IPM and prisms are of equal strength. The direction of the IPM crystallites forms a right angle with the main axis of the prisms. The IPM lies platelike, forming well-marked and separated sheets between prism rows (no anastomosis), thereby describing a typical Sbt. 3 of multiserial HSBs.

***Capromys pilorides lewisi* †** (Fig. 4c–d). This táxon displays a tick enamel layer relative to the incisor proportions. The PE is limited and the PE/PI boundary is not well

defined. In PI, the HSBs are slightly inclined, appearing nearly sub-vertical near the EDJ (accounting for 5% of PI). At least five or even six prisms, arranged in a row, can be counted across the width of a HSB. There is no visible transitional prism between two HSBs. The IPM crystallites run perpendicular to those of the prisms, forming thin inter-row sheets, which never anastomose. This type of crystallite arrangement typifies a well-accomplished Sbt. 3 of multiserial HSBs.

***Geocapromys caymanensis* †** (Fig. 4e–f) **and *G. columbianus* †** (Fig. 4g–h). The two incisors sampled in these two species of *Geocapromys* have the same size, and also display a similar thickness of their enamel layer, which may seem relatively thin compared to other capromyines of similar incisor size (Table 2). In both species, the PE is strongly reduced and hardly discernible. In PI, the HSBs are strongly inclined, and include rows of four to five prisms in width, without prism of transitional zone. The prisms are oval in cross-section. The crystallite (IPM and prisms) arrangement in PI is basically similar in the two species. The IPM is well marked and appears as well-defined sheets between the prism rows (plate-like), without IPM inter-prism crystallite in a row (i.e., without anastomosis or very rarely). The crystallites of the IPM sheets run at an almost right angle to the main direction of the prisms. Both species of *Geocapromys* exhibit an incisor enamel microstructure characterized by a Sbt. 3 of multiserial HSBs.

***Macrocapromys acedo* †** (Fig. 5a–b). The analyzed incisor has a thin enamel layer, with a relatively narrow but clearly distinguishable PE of radial enamel, characterized by strongly bent prisms. In PI, the HSBs are only slightly inclined (barely 23°) and straight, with only three prisms wide (in row), and a fourth being a prism of transitional zone between two HSBs. The prisms are strongly flattened, and can even be confused with the IPM sheets (inter-row plate-like), inasmuch as the IPM and prism crystallites seem equal in strength. The IPM crystallites run fully perpendicular to the main direction of the prism crystallites, without any anastomosis. This crystallite arrangement describes a Sbt. 3 of multiserial HSBs.

***Mesocapromys nanus* †** (Fig. 5c–d). The sampled incisor has a “standard” thickness of its enamel layer (i.e., neither thicker nor thinner than the average of all sampled capromyine incisors). It displays a well-developed PE that accounts for about 15% of the total enamel thickness, a feature that distinguishes this genus (as well as *Mysateles*) from other sampled capromyines showing a thinner PE development. The radial enamel of the PE includes prisms and IPM parallel and steeply inclined (almost horizontal). In PI, HSBs are particularly inclined (~ 50°). The prisms (limited to three

per band) are very flattened, and their crystallites seem of equal strength to those of the IPM sheets. There is a welldefined prism of transitional zone between two adjacente HSBs. The IPM crystallites run at a very high acute angle (sub-rectangular) to the prism direction. There is no IPM inter-prism crystallite anastomosis between prism rows. The enamel microstructure of this incisor documents a Sbt. 3 of multiserial HSBs.

***Mysateles* sp.** (Fig. 5e–f). The incisor enamel of this genus is very close to that of *Mesocapromys*, with a proportionally similar thickness of the enamel layer (with respect to the incisor width), including a well-developed PE (16%). Crystallites of prisms and IPM in PE are parallel and steeply inclined. In PI, HSBs are inclined at 35°. They include welldefined and parallel rows composed of three to four prisms, which are particularly flattened. The fourth prism of the row can be a prism of transition between two adjacent HSBs, but the latter is neither well-marked nor regular. The crystallites of the prisms are of equal strength to those of the IPM sheets. The latter are well distinguished, and their crystallites run fully perpendicular to the prism direction, with no inter-prism or inter-row anastomosis. Such a crystallite arrangement describes a well-accomplished Sbt. 3 of multiserial HSBs.

Heteropsomyinae Echimyidae Octodontoidea

***Brotomys contractus* †** (Fig. 6a–b). This small upper incisor displays a moderately thin enamel layer, with a wellmarked PE of radial enamel accounting for 12% of the total enamel thickness. The prisms in PE are parallel and strongly inclined, nearly oriented horizontally. The PI/PE boundary is straight but not well defined linearly, with HSBs in PI protruding irregularly in the PE zone. In PI, HSBs are Only slightly inclined (~ 20°), straight and include successive rows including a maximum of three prisms, which are rounded to oval in cross-section. One to two prisms form a well-marked transitional zone between two adjacent HSBs. The IPM form thin inter-row sheets (plate-like IPM), whose crystallites have a perpendicular orientation to those of the prisms. There is no anastomosis of the IPM sheets. This crystallite arrangement describes a Sbt. 3 of multiserial HSBs.

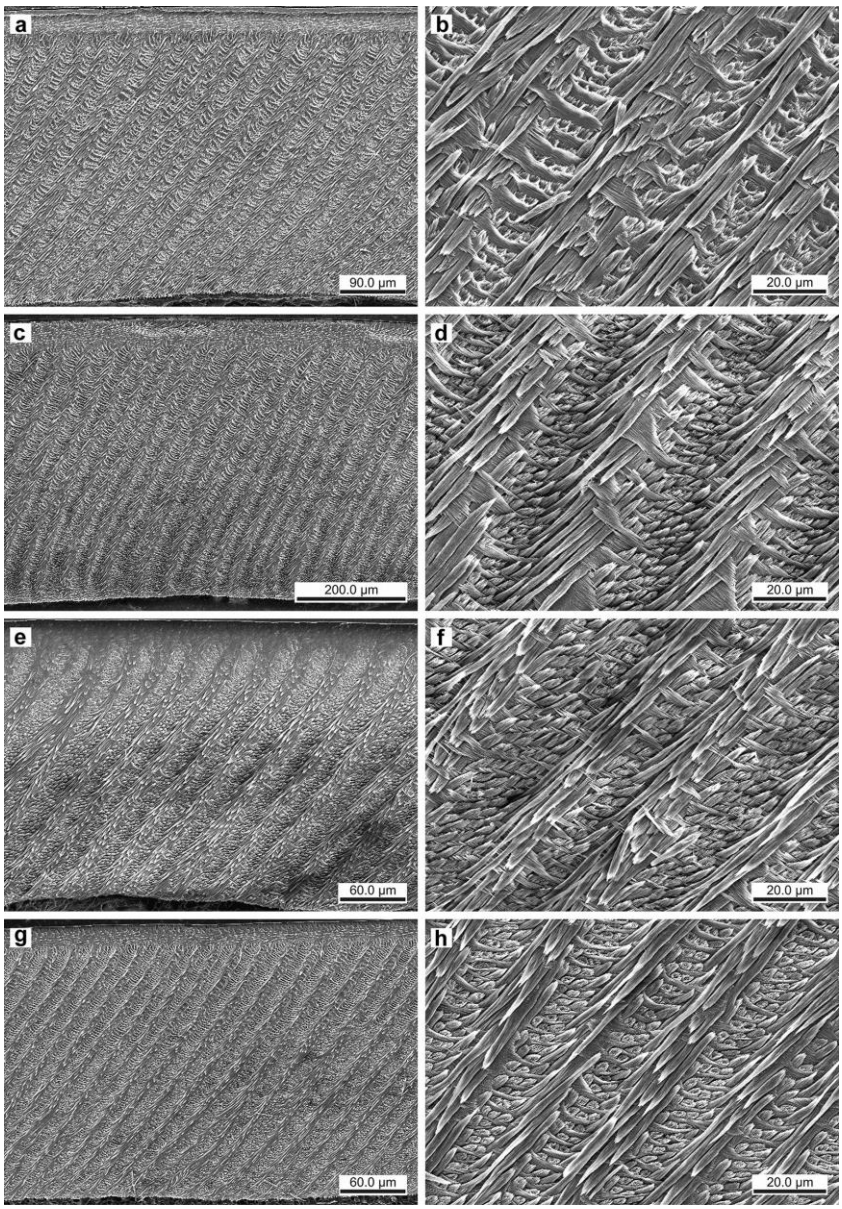


Fig. 4 Scanning electron photomicrographs of incisors of subfossil spiny rat hutias (Echimyidae Capromyinae) from the West Indies, for which the enamel microstructure (multiserial HSBs) is shown in longitudinal section and at different magnifications. The left pictures illustrate an overview of the enamel layer for each specimen, and the associated right ones a detail of the microstructure in PI. **a–b.** *Plagiodontia ipnaeum* (UF 520142); **c–d.** *Capromys pilorides lewisi* (UF 520144); **e–f.** *Geocapromys caymanensis* (UF 520145); **g–h.** *Geocapromys columbianus* (CLV 2595, reversed)

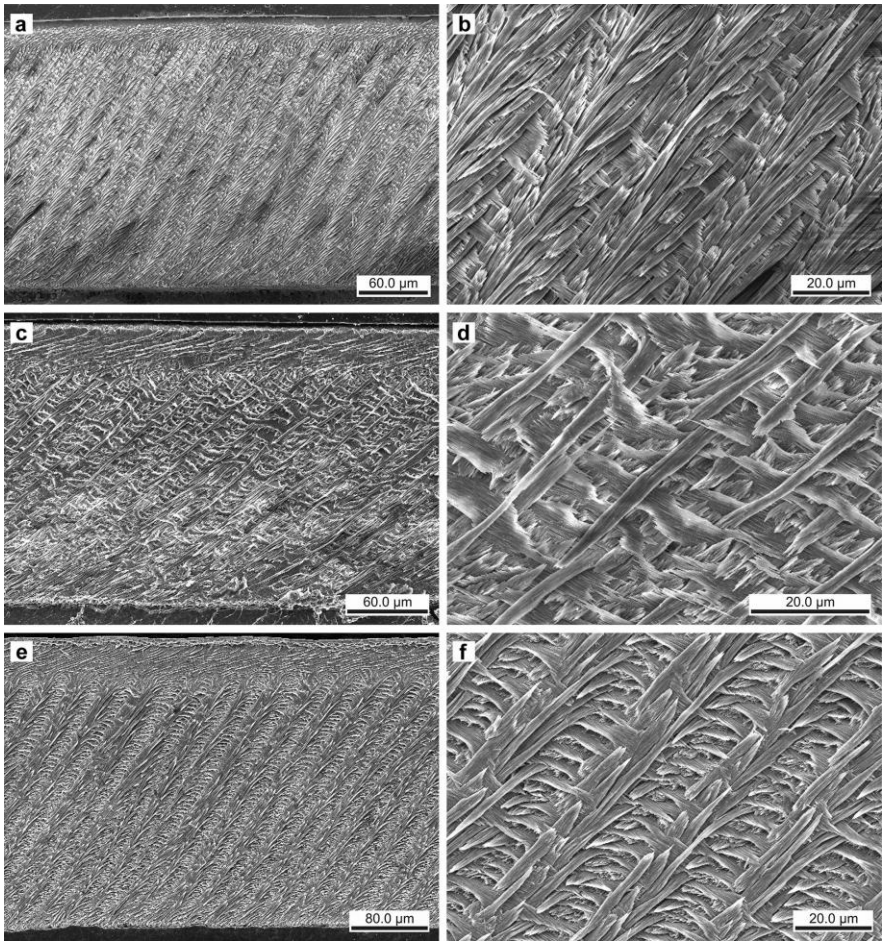


Fig. 5 Scanning electron photomicrographs of incisors of subfossil and extant spiny rat hutias (Echimyidae Capromyinae) from the West Indies, for which the enamel microstructure (multiserial HSBs) is shown in longitudinal section and at different magnifications. The left pictures illustrate an overview of the enamel layer for each specimen, and the associated right ones a detail of the microstructure in PI. **a–b.** *Macrocapromys acedo* (CVL 401, reversed); **c–d.** *Mesocapromys nanus* (UF 520144); **e–f.** *Mysateles* sp. (UM 524N, reversed).

***Boromys offella* †** (Fig. 6c–d) **and *B. torrei* †** (Fig. 6e–f). These two small incisors document two species of *Boromys*, particularly tiny, among the smallest of the species sampled for these analyses. As is the case with *Brotomys*, considering the size of these two incisors (in relation to the measured incisor width), their enamel layer may appear relatively thick compared to the condition observed in capromyines. Both incisors have a PE representing 10–12% of the total enamel thickness. The PE/PI boundary is particularly difficult to distinguish, especially for the incisor of *B*. *offella*, inasmuch as the prisms and IPM are of similar strength, parallel and vertically oriented. This portion of the incisor enamel of *B*. *torrei* was damaged by polishing, which does

not allow for a clear observation of the crystallite orientation in PE. In PI, for both incisors, the HSBs display regular rows including three to four prisms appearing relatively flat in crosssection, the fourth prism forming a well-marked transitional zone between two adjacent HSBs. In both specimens, the IPM lies plate-like between the prism rows (i.e., inter-row sheets), without clear anastomosis (eventually possible but rare for *B*. *offella*). The IPM crystallite direction is perpendicular to the prism main axis. The enamel microstructure of these two incisors is basically similar and describes a well-accomplished Sbt. 3 of multiserial HSBs. The enamel of the two incisors differs in the inclination of the HSBs in PI, which appear more inclined in *B*. *offella* than in *B*. *torrei*, although these differences in inclination might simply reflect a difference in the sampled dental locus (lower *versus* upper incisor, respectively). They also differ in the presence of rare HSB divisions, noticeable in *B*. *torrei*, but not observed in *B*. *offella*.

***Heteropsomys* sp. †** (Fig. 6g–h). Considering the size of this sampled incisor, which is more than twice as large as the incisors of *Brotomys* and *Boromys*, the incisor enamel layer in *Heteropsomys* is particularly thin, similar to that of the incisor of *B*. *torrei*, the smallest species sampled here (see Table 2). PE accounts for 10% of the total enamel thickness, and includes prisms and IPM of similar strength, parallel and strongly inclined. The PE/PI boundary is clearly distinguishable and straight. In PI, the HSBs are moderately inclined, straight and are composed of prism rows including four to five prisms, oval in cross-section, with the fifth prism forming a transitional zone between two HSBs. The IPM is particularly well marked, lying plate-like between the prism rows, with possible (very rare) anastomoses. The crystallites of the IPM sheets run at a very acute to right angle (i.e., sub-rectangular) to the main Direction of the prisms. This crystallite arrangement typifies a Sbt. 3 of multiserial HSBs.

“Heptaxodontidae”

***Elasmodontomys obliquus* †** (Fig. 7a–f). The three available incisors sampled for this taxon are lower ones. They are among the largest incisors in our study, reflecting the medium to large body size of *Elasmodontomys*, approximating that of the capromyine *Plagiodontia*. Despite the large size of these incisors, their enamel layer is proportionally very thin, with a thickness equivalent to that observed on incisors two to three times smaller previously studied (capromyines or heteropsomyines; Table 2). The PE of radial enamel is variable in thickness, accounting for 10 to 17% of the total enamel thickness. Prisms and IPM in PE are of similar strength, and moderately inclined. The boundary between PE and PI is quite distinct, but not smooth and

horizontal, appearing somewhat rough due to the presence of HSBs of PI protruding irregularly in the PE zone. In PI, HSBs are moderately inclined (27–37°) and straightly arranged from the EDJ to the PI/PE boundary. At the EDJ, a thin starting zone with a parallel prism progression is observable. HSBs are noticeably wide, comprising oblique rows of four to five prisms, the fifth prism or even an additional sixth prism, forms a particularly well-defined transitional zone between two adjacent HSBs. Prisms are rounded/oval to slightly flattened in cross-section. The IPM is thin but particularly “invasive”, forming sheets between the prism rows and often between the prisms in a row, thereby describing a pattern of IPM characterized by regular anastomoses. The IPM crystallites run with a low but clearly discernible angular difference to the prism crystallites (low acute angle between the directions of the two crystallite sets). Such na IPM crystallite arrangement with a low value of α, describes among the early stages of a Sbt. 2 of multiserial HSBs, even a transitional Sbt. 1–2 if we consider the very frequent and regular anastomoses of the IPM sheets (inter-rows and frequently inter-prisms in a row).

***Clidomys* sp. †** (Fig. 7g–h). The incisor of this táxon is also among the largest specimens sampled, and like in *Elasmodontomys*, the enamel layer is thin, equivalent in thickness to the incisors two to three times smaller studied previously (capromyines or heteropsomyines; Table 2). The PE represents only 10% of the total enamel thickness. The IPM and prism crystallites in PE are equal in strength as no distinction can be made between the two structures. The PE/PI boundary is discernible, but somewhat discontinuous in appearance due to the presence of protruding HSBs of PI in the PE area. In PI, the HSBs are very slightly inclined (12–15°) and can split or fuse locally, but most often in a limited PI region (about 30%) situated near the PI/PE boundary. The HSBs are straight and particularly wide, composed of poorly defined rows of prisms, which may include up to five prisms (or occasionally more in the split regions or less in the merging regions). There is no clear prism of transition between two HSBs. The prisms are strongly flattened in cross-section. The IPM crystallites form thin sheets that run partly parallel to the prisms, but also partly at a very low angle. The IPM sheets anastomose permanently, so that the prisms are almost completely enveloped (sheath-like IPM). Due to a very close Direction of the IPM and prism crystallites, it may be difficult to distinguish the two structures in cross-section. Such a crystallite arrangement with almost parallel prisms and IPM sheets, the latter anastomosing permanently, corresponds to a Sbt. 1 of multiserial HSBs.

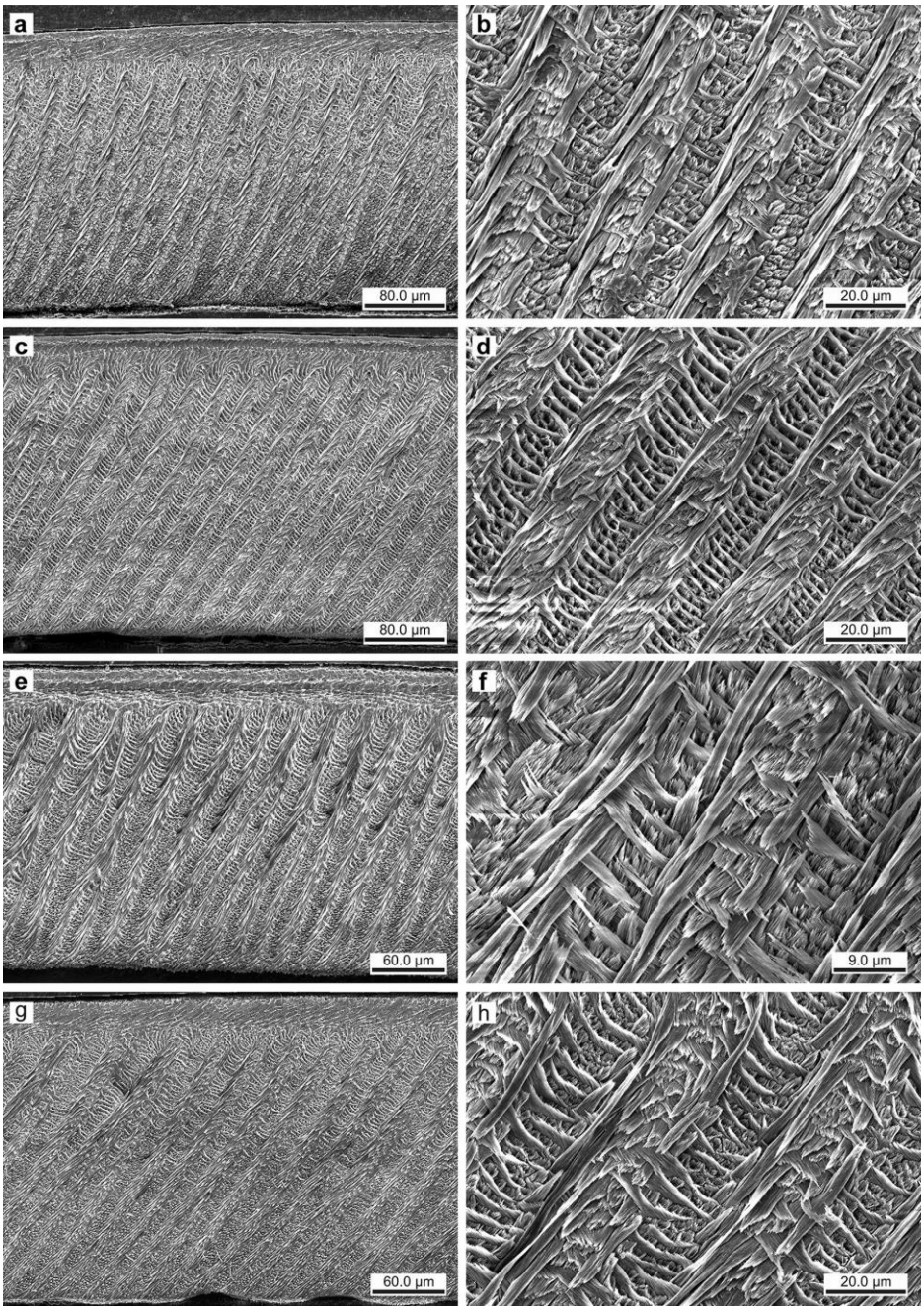


Fig. 6 Scanning electron photomicrographs of incisors of subfossil spiny rats (Echimyidae Heteropsomyinae) from the West Indies, for which the enamel microstructure (multiserial HSBs) is shown in longitudinal section and at different magnifications. The left pictures illustrate an overview of the enamel layer for each specimen, and the associated right ones a detail of the microstructure in PI. **a–b.** *Brotomys contractus* (UF 333716, reversed); **c–d.** *Boromys offella* (CLV 2596); **e–f.** *Boromys torrei* (CLV 2598); **g–h.** *Heteropsomys* sp. (UPRMP-3229, reversed).

***Amblyrhiza* sp. †** (Fig. 8a–d). The incisor of this taxon is the largest specimen sampled for this analysis, reaching at least twice the size of the incisor of *Clidomys*,

and more than twice the size of some of the incisors of *Elasmodontomys*. The thickness of the enamel layer is of the same importance as the incisors of *Clidomys* and *Elasmodontomys*, thereby indicating a relatively thin enamel layer for the size of the incisor, compared to the sampled echimyids (capromyines and heteropsomyines). The PE with radial enamel accounts for 10–13% of the total enamel thickness, including prisms and IPM of similar strength, and as such being not clearly distinguishable from each other. The PE/PI boundary is fairly distinct, but not clearly delineated. In PI, the HSBs are straight and moderately inclined (25–34°), and no division was observed along the analyzed section. The HSBs are rather large, showing inclined multi-prism rows, comprising at least five prisms per band, plus one or two prisms of transition between two adjacent HSBs (not on a regular basis). The prisms have an oval or flat cross-section. The IPM is relatively thick with respect to the prism, and thus well visible, forming sheets between the prism rows and often between the prisms in a row, indicating frequent and regular anastomoses. The crystallites of IPM run at a low acute angle to the prism direction. This crystallite arrangement describes an early stage of a Sbt. 2 of multiserial HSBs.

***Amblyrhiza* sp. † (juvenile)** (Fig. 8e–f). This medium-sized incisor was found in the same fossil locality (and in close proximity) as the one that yielded the large-sized remains attributed to *Amblyrhiza* (Ilet Coco, St. Barth; Table 1). It is almost half the size of the largest *Amblyrhiza* incisors recovered, and its buccal surface is characterized by a crenulated ornamentation, similar to that of the large incisors of the genus. Given that there is no other large-bodied caviomorph rodent other than *Amblyrhiza* recorded/known on the Anguilla Bank to date, it is likely that this smaller incisor specimen corresponds to a juvenile individual of *Amblyrhiza* (*inundata*?). The microstructural pattern in PI (crystallite arrangement of the prisms and IPM) is indeed strictly similar to the one described above (i.e., early stage of Sbt. 2 of multiserial HSBs). The main distinctions are, of course, a thinner enamel layer, but especially the shape and inclination of the HSBs. The latter appear as curved (with a high radius of curvature). They are strongly inclined in the central part of PI, while they become almost vertical when approaching the EDJ.

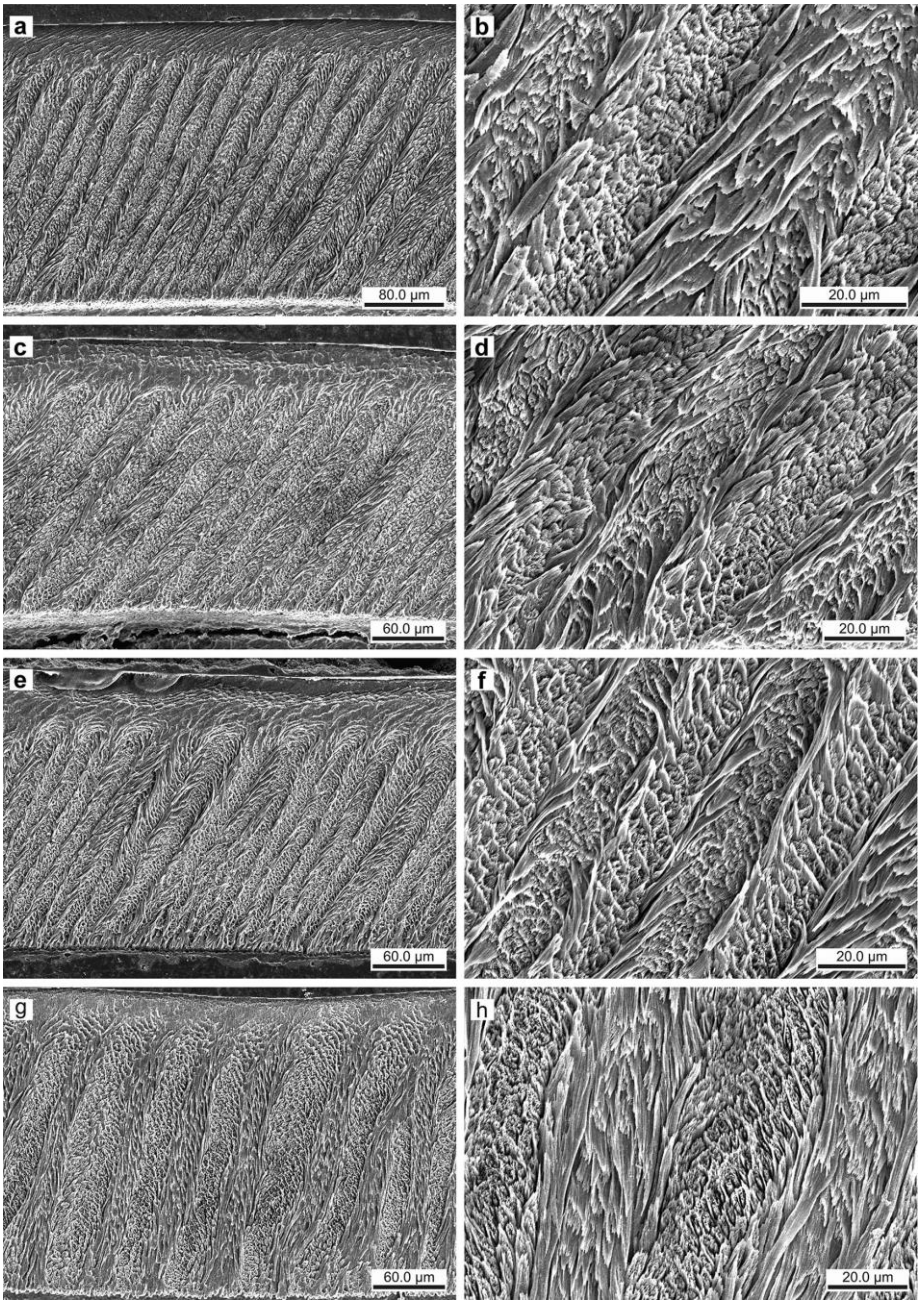


Fig. 7 Scanning electron photomicrographs of incisors of subfossil giant hutias *Elasmodontomys* and *Clidomys* from Puerto Rico and Jamaica, respectively, for which the enamel microstructure (multiserial HSBs) is shown in longitudinal section and at different magnifications. The left pictures illustrate an overview of the enamel layer for each specimen, and the associated right ones a detail of the microstructure in PI. **a–b.** *Elasmodontomys obliquus* (UPRMP-3230); **c–d.** *Elasmodontomys obliquus* (UPRMP-3231); **e–f.** *Elasmodontomys obliquus* (UPRMP-3232); **g–h** *Clidomys* sp. (UF 274295)

Fossil Chinchilloidea and living Chinchilloidea and Cavioidea

***Borikenomys praecursor* †** (Fig. 8g–h). This incisor fragmente displays a moderately thin enamel layer, but somewhat thicker than that covering the former

incisor described by Martin in Velez-Juarbe et al. (2014). Similar to the latter one, the enamel is double-layered, with a PE accounting for 18% of the total enamel thickness (among the thickest PE recorded here). In PI, HSBs are also ~ 40° inclined apically, and comprise three to four prisms per band, which are rounded to oval in cross-section. The fourth prism is often transitory between two adjacent HSBs. The IPM crystallites run at a low acute angle to the prism long axes, and are arranged as thin sheets (hardly visible) between the prism rows, and anastomose regularly, thereby describing an early stage of a Sbt. 2 of multiserial HSBs.

***Lagidium* sp.** (Fig. 9a–b). The enamel layer of this small-bodied species is very thin (much thinner than in the smallest West Indian echimyids sampled here; i.e., *Boromys*, *Brotomys*, *Mesocapromys*, *Geocapromys*, etc.), double-layered with a rather extensive PE, accounting for 19% of the total enamel thickness (one of the thickest PE recorded here). The crystallites of the IPM and prisms are of similar strength in PE (i.e., hardly differentiable), both making structures strongly inclined. The PE/PI boundary is well distinct but not linear. In PI, HSBs are steeply inclined (45°; one of the highest angles recorded here) and straight, with three to four prisms wide, the fourth even a fifth prism being transitional between two HSBs. In cross-section, the prisms are oval to flattened. The IPM is predominantly parallel to the prism direction, but occasionally minor angular differences occur (very low acute angles). It consists of thin inter-row and inter-prism sheets (permanent anastomoses) that almost completely envelop the prisms on all sides (sheath-like IPM). Such a crystallite arrangement typifies a Sbt. 1 of multiserial HSBs, and even transitional Sbt. 1–2 if we take into consideration the minor angular differences between the direction of the IPM crystallites and that of the prism crystallites.

***Chinchilla* sp.** (Fig. 9c–d). The enamel layer is, as for the incisor of *Lagidium*, very thin, with a thick PE (21%). In PE, the crystallites of the IPM and prisms are hardly differentiable, both appearing strongly inclined. The PE/PI boundary is straight/horizontal, and particularly well distinguishable. In PI, the HSBs are strongly inclined (up to 49°), straight, and include three flat prisms per band, with a well-marked transitional zone between two adjacent HSBs, made by one or two additional prisms. The IPM form thin sheets between the prism rows and often between the prisms in a row (frequent/regular anastomoses). The IPM crystallites form a very low to low acute angle to the prism direction. This crystallite arrangement describes an earlier stage of a Sbt. 2 of multiserial HSBs (even a transitional Sbt. 1–2 if we consider the very frequent and regular anastomoses of the IPM sheets).

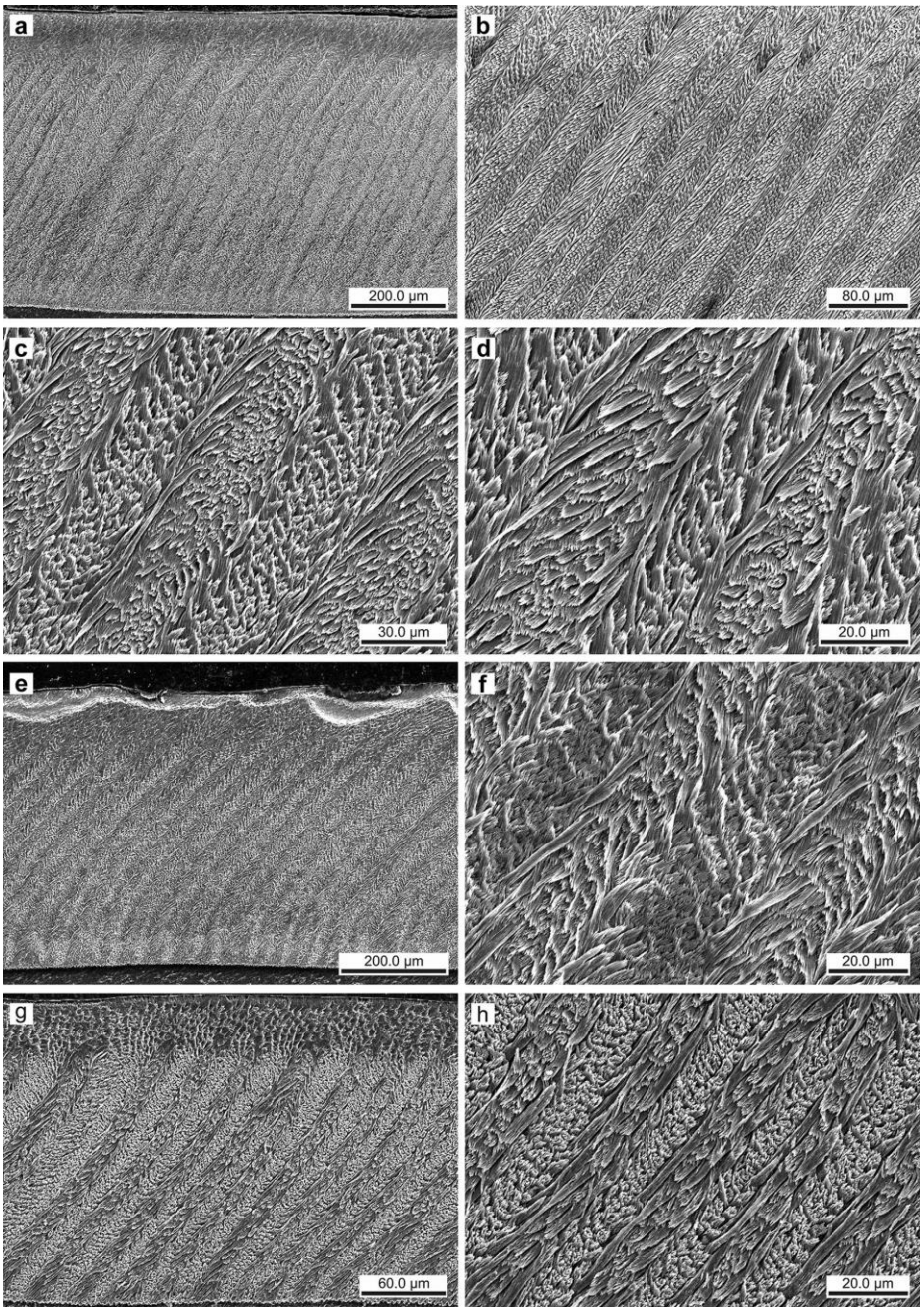


Fig. 8 Scanning electron photomicrographs of incisors of the subfossil giant hutias *Amblyrhiza* from St. Barth, and of the chinchilloid *Borikenomys* from the early Oligocene of Puerto Rico, for which the enamel microstructure (multiserial HSBs) is shown in longitudinal section and at different magnifications (overview of the enamel layer and details of the microstructure in PI). **a–d.** *Amblyrhiza* sp. (UM SB-Coco-03); **e–f.** *Amblyrhiza* sp. (juvenile; UM SB-Coco-04); **g–h.** *Borikenomys praecursor* (LACM 162956)

Cuniculus paca (Fig. 9e–f). This sampled incisor of that medium-sized caviomorph (Cavioidea) displays a moderately thick enamel layer with a PE accounting for a large part of the total enamel thickness (22%). The PE/PI boundary is clearly

distinct and straight. In PI, the HSBs are Only slightly inclined and include frequent divisions. The HSBs appear wide, although including only four prisms, which are large but very flattened in cross-section. There is no prism of transition between the HSBs. The IPM crystallites and prism crystallites are of similar strength, and run parallel to each other. However, it sometimes happens that their respective directions deviate slightly from each other, forming a very small acute angle. The IPM sheets anastomose on a regular basis (inter-row and inter-prism; i.e., sheath-like IPM). This crystallite arrangement corresponds to an advanced Sbt. 1 of multiserial HSBs.

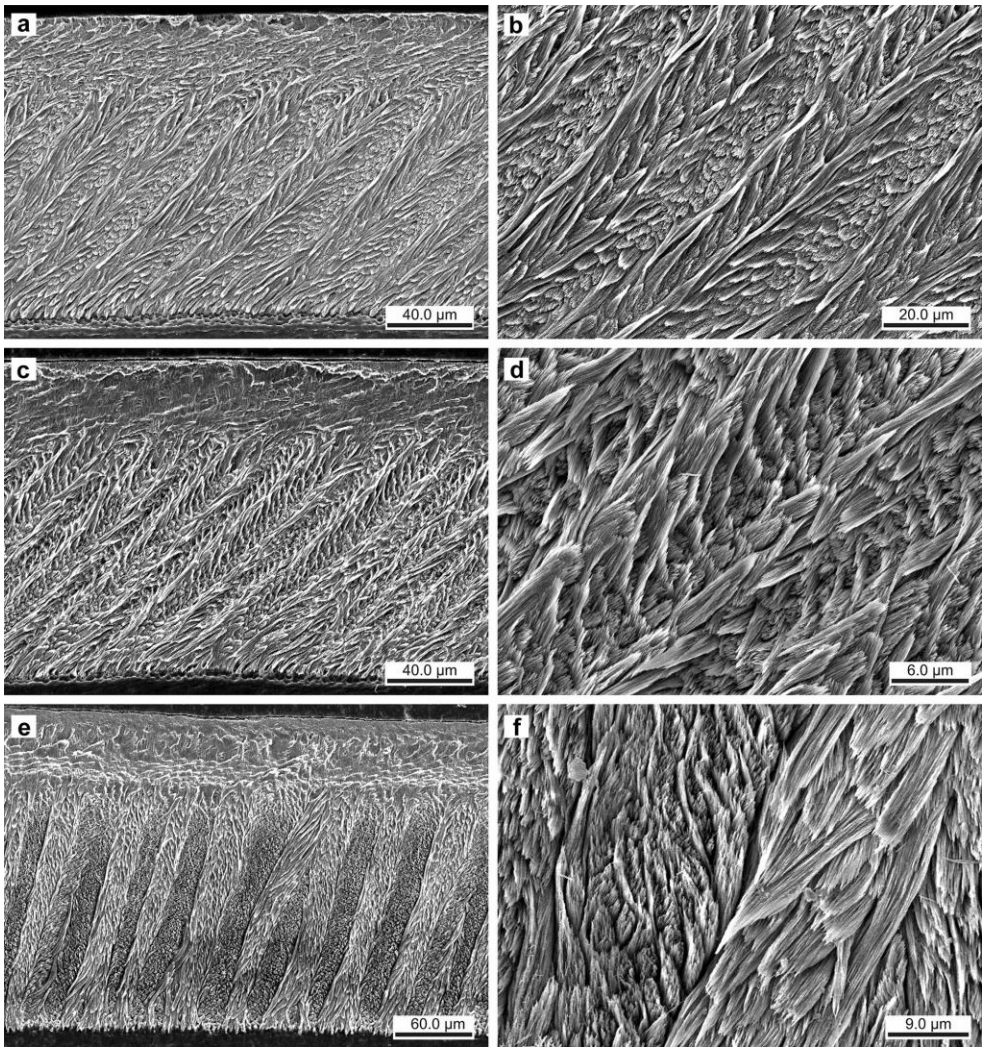


Fig. 9 Scanning electron photomicrographs of incisors of extant caviomorph rodents (Chinchillidae Chinchilloidea and Cuniculidae Cavioidea) from South America, for which the enamel microstructure (multiserial HSBs) is shown in longitudinal section and at different magnifications. The left pictures illustrate an overview of the enamel layer for each specimen, and the associated right ones a detail of the microstructure in PI. **a–b.** *Lagidium* sp. (UM 521N, reversed); **c–d.** *Chinchilla* sp. (UM N312, eversed); **e–f.** *Cuniculus paca* (UM N385).

Discussion and conclusion

In this study, we substantially expanded taxonomically Martin's (1992) first analysis of incisor enamel microstructure of extinct and extant West Indian caviomorphs. Pragmatically, we especially provide here enamel SEM pictures of some of the formerly sampled taxa that had not previously been illustrated (Martin 1992; Martin in Velez-Juarbe et al. 2014). For the taxa treated by both Martin (1992) and ourselves (plus the additional taxa in our dataset), the results are fully consistent, showing a clear distinction between the enamel microstructures of the West Indian Echimyidae Octodontoidea (Capromyinae and Heteropsomyinae) and the West Indian "Heptaxodontidae", whose phylogenetic affinities are still debated. All extinct and extant hutias and spiny rats from the West Indies (capromyines and heteropsomyines, respectively) have enamel crystallites whose configurations, assemblages and/or proportions vary in many respects (e.g., number of prisms per HSB, presence or absence of transitional prisms between HSBs, shape of the prisms in cross section, inclination of HSBs in PI, percentage of PE, etc.; see Table 2), but all describing a pattern of enamel microstructure characterized by a rectangular crystallite (IPM and prisms) arrangement that is biomechanically strongest in limiting crack propagation (i.e., Sbt. 3 of multiserial HSBs; Table 2). This highly derived/specialized condition of the incisor enamel is found in all their echimyid octodontoid counterparts from the South American continent (i.e., Echimyinae, Euryzygomatomyinae, and Carterodontinae; Martin 1992), and more extensively in all related families within the Octodontoidea clade (i.e., Echimyidae, Octodontidae, Ctenomyidae, and Abrocomidae; Martin 1992) (see Online Resource 1). In caviomorphs in general, the Sbt. 3 of multiserial HSBs is not observed in chinchilloids, cavioids and erethizontoids (see Online Resource 1), being exclusive of octodontoids, and this from an early stage in their evolutionary history (Martin 1992, 2004, 2005; Vucetich and Vieytes 2006; Vucetich et al. 2010; Boivin et al. 2019b). Such a highly resistant/efficient enamel microstructure characterizing West Indian echimyids contrasts sharply with that recorded for the “heptaxodontid” taxa sampled here for this analysis, which exhibit much less resistant incisor enamels. Indeed, the incisors of *Clidomys*, *Elasmodontomys* and *Amblyrhiza* display an enamel layer relatively much thinner and characterized by a less complex crystallite arrangement, with the IPM sheets being parallel or at a low acute angle to the prism long axes, and permanently or regularly anastomosing. Such crystallite arrangements describe less advanced subtypes of multiserial HSBs (Sbt. 1 [*Clidomys*], Sbt. 1–2 [*Elasmodontomys*], and low acute Sbt. 2

[*Amblyrhiza*]; see Table 2). The same is true for the incisor of the chinchilloid *Borikenomys* from the early Oligocene of Puerto Rico, which displays an enamel microstructure typifying a low acute Sbt. 2 of multiserial HSBs, strongly reminiscente to that of the incisor of *Amblyrhiza* (regardless of the very large size difference between the two taxa). These less advanced enamel microstructures characterizing West Indian "heptaxodontids" (or "giant hutias") are found in extinct and extant chinchilloids, cavioids or erethizontoids from South America, but never in octodontoids (see Online Resource 1 and Table 2; Fig. 9; Martin 1992).

The absence of highly-derived rectangular crystallite arrangements in the incisor enamel of *Amblyrhiza* and *Clidomys*, does not favor of an octodontoid status for these two taxa, but, in turn, it is consistent with a chinchilloid assignment, as independently reflected by the anatomy of their auditory region (middle-ear of *Amblyrhiza*, MacPhee 2011; innerear of *Amblyrhiza* and *Clidomys*, Da Cunha 2020, unpublished MSc results; Da Cunha et al. in prep.) and their unusual dental pattern (e.g., Marivaux et al. 2020, and cited references herein). For *Elasmodontomys*, it is more complicated since a primitive condition of the IPM crystallite arrangement characterizing its incisor enamel microstructure (i.e., Sbt. 1–2 of multiserial HSBs), is difficult to reconcile with the highlynested phylogenetic position of this taxon within the Octodontoidea clade (among the Echimyidae Capromyinae), as recently inferred from aDNA analyses (Woods et al. 2020). *Elasmodontomys* was indeed found sister to *Plagiodontia* (*P*. *aedium*), and the subclade of both species was resolved at the base of the Capromyinae clade. Species of *Plagiodontia* (*P*. *aedium* and *P*. *ipnaeum*) are smaller-bodied than *Elasmodontomys obliquus*, but their incisors are comparatively very large and robust (Table 2). The incisor of *P*. *ipnaeum* (Fig. 2e) sampled here is of roughly similar width to the incisor of *E*. *obliquus* (Fig. 2o–q), but the two teeth display clearly distinct enamel microstructures (thick layer with Sbt. 3 *versus* thin layer with Sbt. 1–2 multiserial HSBs, respectively). If such a phylogenetic position for *Elasmodontomys* turns out to be correct, this taxon would thus represent the only case of an incisor enamel with a lower degree of resistance, among taxa that have all achieved the highest incisor enamel resistance (Sbt. 3 of multiserial HSBs) since the Paleogene. The acquisition of a Sbt. 1–2 of multiserial HSBs characterizing the incisor enamel of *Elasmodontomys* could then only be explained by a reversion toward this less resistant enamel condition from a very resistant one characterizing all octodontoids. From biomechanical and architectural perspectives, such a loss of three-dimensional enamel reinforcement is, however, hardly conceivable, since the selective pressure is rather

towards strengthening the enamel of the heavily stressed incisor (T. Martin, pers. comm., which we follow). Given this unique case of enamel/phylogeny mismatch, an alternative would be to consider a possible sampling error regarding the extracted aDNA assumed to represent *Elasmodontomys* (after Woods et al. 2020), which could potentially be that of a hutia (capromyine), close to *Plagiodontia*, instead of *Elasmodontomys*. Without definitively calling into question the phylogenetic results of Woods et al. (2020) today, these puzzling incompatibilities then require that the aDNA extraction for *Elasmodontomys* to be duplicated, and new phylogenetic reconstructions to be performed (work in progress). *Elasmodontomys* still represents today a real morphological and phylogenetic *conundrum* as it displays primitive basicranial features that resemble “a wide variety of other taxa” (MacPhee 2011), inner ear traits intermediate between octodontoids and chinchilloids (i.e., Octochinchilloi; Da Cunha 2020, unpublished MSc results; Da Cunha et al., in prep.), some postcranial similarities with octodontoids (Patterson and Wood 1982; Woods and Hermanson 1985), an unusual chinchilloid cheek tooth laminar pattern characterized by a heterogeneous enamel layer (Marivaux et al. 2020), and an incisor enamel microstructure found in extinct and extant chinchilloids, cavioids and erethizontoids, not in octodontoids (Martin 1992; this work).

Considering the phylogenetic significance of the incisor enamel microstructure (e.g., Korvenkontio 1934; Wahlert 1968; Boyde 1978; Koenigswald 1985; Martin 1992, 1993, 1994a, 1994b, 1997; Kalthoff 2000; Marivaux et al. 2004), it is clear for us that the different enamel patterns observed here among the West Indian caviomorphs indicate the presence of distinct high-level taxonomic groups. When crossed with morphological information deriving from dental and basicranial (middle and inner ears) anatomies, extinct and extant West Indian caviomorphs essentially document the Octochinchilloi (Octodontoidea and Chinchilloidea). The diversity of caviomorphs on the Caribbean islands is obviously the result of intra-archipelago diversification through time, but their high-level phylogenetic diversity can only be explained by distinct sources, implying de facto multiple natural colonizations of the West Indies. Recent gene-based phylogenies of extant Echimyidae, including West Indian Capromyinae (e.g., Fabre et al. 2014; Upham and Borroto-Paez 2017; Courcelle et al. 2019), are congruent for proposing a split of the insular forms from their South American relatives (*Carterodon*-like ancestor after Courcelle et al. 2019) sometime during the early/Middle Miocene. The same is true when subfossil representatives of the West Indian capromyines and extinct heteropsomyines are included in these molecular data on

extant Echimyidae (Woods et al. 2020). Capromyinae and Heteropsomyinae are resolved as sister taxa, thereby suggesting that their South American echimyid ancestor (i.e., *Carterodon*-like ancestor) most likely arrived in the Greater Antilles during a single dispersal event (Woods et al. 2020). Regarding the “heptaxodontid” chinchilloids (*Amblyrhiza*, *Clidomys*, and according to us *Elasmodontomys* and *Quemisia*), they most likely result from one (or several) separate dispersal event(s), staggered in time or perhaps concomitant with that of the echimyids. The question of one or multiple colonizations of the West Indies by South American chinchilloids, and the chronology of this or these dispersals, would require formally establishing the relative positions of the insular taxa in a comprehensive and dated phylogeny of Chinchilloidea (including all mainland taxa, i.e., extinct and extant dinomyids and chinchillids, and extinct neoepiblemids [and eventually extinct cephalomyids]). The recent discovery of a dinomyid chinchilloid (*Borikenomys praecursor*) in lower Oligocene deposits of Puerto Rico provides compelling evidence for an early dispersal of South American chinchilloids to the Caribbean islands near the Eocene/Oligocene transition (at the time of the GAARlandia land-bridge; Velez-Juarbe et al. 2014; Marivaux et al. 2020 and references cited therein). With the fossil dental material discovered, including incisors, we have re-analyzed here the incisor enamel microstructure of *Borikenomys* (formerly studied by Martin in Velez-Juarbe et al. 2014), and noticed its strong microstructural similarities with the enamel condition characterizing Quaternary "heptaxodontids", in particular *Amblyrhiza* from the Anguilla Bank (Fig. 8). Similarly, this also suggest chinchilloid or “heptaxodontid” affinities for the late Oligocene unnamed taxon B described in Velez-Juarbe et al. (2014), also from Puerto Rico. Despite the limited fóssil evidence currently assembled for *Borikenomys*, the unusual dental traits of the latter (e.g., laminae with heterogeneous thickness of the enamel layer, and narrow inter-lamina space filled with cement), which are otherwise retrieved only in several mainland chinchilloids (extinct and extant dinomyids and chinchillids) and in the West Indian3 *Amblyrhiza*, *Elasmodontomys* and *Quemisia*, strongly suggest its possible phylogenetic link with these more recent chinchilloid forms of the islands (Marivaux et al. 2020). If this link is proven to be true, it would highlight the long-live insular lineage of the West Indian chinchilloids, including a tendency towards a spectacular island gigantism, as was achieved for some of their South American counterparts (e.g., Mones 1980; Sanchez-Villagra et al. 2003; Rinderknecht and Blanco 2008; Carrillo and Sanchez-Villagra 2015; Alvarez et al. 2017; Rinderknecht et al. 2018; Boivin et al. 2019c; Ferreira et al. 2020). “Giant hutias”

unfortunately never reached modern times, although they potentially evolved on the islands for over 30 million years. Their possible long evolutionary history on the islands needs to be demonstrated/documented by paleontological data, especially for the Miocene epoch. It is in this sense that we are now concentrating our efforts in the field, in order to further document the fossil record of chinchilloids, but also of echimyid octodontoids (capromyines and heteropsomyines), as well as other island vertebrates (e.g., Blackburn et al. 2020; Marivaux et al. 2021; Vinola Lopez et al. 2022).

Acknowledgements

We are indebted to Jonathan I. Bloch (Florida Museum of Natural History, Gainesville, USA) for access to the paleontological collections of his institute, as well as S. Diaz Franco (Cuba) for the donation of his collection to one of us (LWVL). Many thanks to Thomas Martin (Universitat Bonn, Germany) for his useful advice regarding the enamel microstructure of rodent incisors and for sharing enamel microstructure data over the last few decades. We are very grateful to our fossil preparator, Anne-Lise Charruault (ISE-M, France), for her availability and for the preparation and handling of the epoxy resin for the embedding of the incisor specimens, as well as for the access to the polishing facilities of the lab. We warmly thank Chantal Cazevieille (Institut des Neurosciences de Montpellier [INM], France) for access to an electron microscope scanning facility, and also for her welcome and much appreciated help in obtaining detailed images of enamel microstructures. Thank you very much to Odile Maincent (Deve, Saint-Barthelemy, French West Indies) for her hospitality and help during our successive field seasons in Saint-Barth, and for her great interest in our work. We extend our gratitude to Ivan Quintero and Angel Acosta-Colon for assistance with localities in Puerto Rico. We are also grateful to our colleagues Francois Pujos (IANIGLA, Mendoza, Argentina), Hernan Santos-Mercado (UPRM, Mayaguez, Puerto-Rico), Eduardo J. Cruz (UPRM, Puerto Rico), our late colleague and friend Gilles Merzeraud (Geosciences Montpellier, France), Melody Philippon and Jean-Jacques Cornee (Geosciences Montpellier & Pointe-a-Pitre [Guadeloupe, French West Indies]), who contributed to some of the fieldwork seasons in Puerto Rico and Saint-Barthelemy in the framework of the GAARAnti project. Finally, we thank Thomas Martin (Universitat Bonn, Germany), Daniela Kalthoff (Associate Editor; The Swedish Museum of Natural History, Sweden) and another anonymous reviewer, who provided formal reviews of this manuscript that enhanced the final version. This is ISE-M publication 2022-188 Sud.

Funding

This research was supported by the French Agence Nationale de la Recherche (ANR) in the framework of the GAARAnti Project (ANR-17-CE31-0009) and LabEx CEBA (ANR-10-LABX-25–01). Data availability statement Incisor specimens analyzed (polished cross sections and remaining parts of incisors) during the current study are available from the institutions that provided them (see specimen catalog numbers). The figured and extra SEM micrographs generated and analyzed during the current study are available from the corresponding author upon reasonable request.

Declarations

Conflicts of interest The authors declare no competing financial interests.

References

Alloing-Séguier L, Marivaux L, Barczi J-F, Lihoreau F, Martinand-Mari C (2019) Relationships between enamel prism decussation and behavior of the ameloblast layer in rodent incisors. Anat Rec 302:1195-1209. https://doi.org/10.1002/ar.24000

Álvarez A, Arévalo RL, Verzi DH (2017) Diversification patterns and size evolution in caviomorph rodents. Biol J Linn Soc 121:907-922. https://doi.org/10.1093/biolinnean/blx026

Anthony HE (1916) Preliminary report of fossil mammals from Porto Rico, with descriptions of a new genus of ground sloth and two new genera of hystricomorph rodents. Ann N Y Acad Sci 27:193-203.

Anthony HE (1917) New fossil rodents from Porto Rico, with additional notes on *Elasmodontomys obliquus* Anthony and *Heteropsomys insulans* Anthony. Bull Am Mus Nat Hist 37:183-189.

Anthony HE (1918) The indigenous land mammals of Porto Rico, living and extinct. Mem Am Mus Nat Hist, new series 2:331-435.

Anthony HE (1920) New mammals from Jamaica. Bull Am Mus Nat Hist 42:469-475.

Anthony HE (1927) Mammals of Porto Rico, living and extinct - Rodentia and Edentata. Scientific Survey of Porto Rico and the Virgin Islands 9:97-155.

Antoine P-O, Marivaux L, Croft DA et al (2012) Middle Eocene rodents from Peruvian Amazonia reveal the pattern and timing of caviomorph origins and biogeography. Proc Roy Soc B 279:1319-1326. https://doi.org/10.1098/rspb.2011.1732

Antoine P-O, Abello MA, Adnet S et al (2016) A 60-million-year Cenozoic history of western Amazonian ecosystems in Contamana, eastern Peru. Gondwana Res 31:30-59. https://doi.org/10.1016/j.gr.2015.11.001

Antoine P-O, Yans J, Aliaga Castillo A et al (2021) Biotic Community and landscape changes around the Eocene–Oligocene transition at Shapaja, Peruvian Amazonia: regional or global drivers? In: Hoorn C, Palazzesi L, Silvestro D (eds) Exploring the Impact of Andean Uplift and Climate on Life Evolution and Landscape Modification: from Amazonia to Patagonia. Glob Planet Change 202:103512. https://doi.org/10.1016/j.gloplacha.2021.103512

Arnal M, Kramarz AG, Vucetich MG, Vieytes EC (2014) A new early Miocene octodontoid rodent (Hystricognathi, Caviomorpha) from Patagonia (Argentina) and a reassessment of the early Evolution of Octodontoidea. J Vert Paleontol 34:397-406. https://doi.org/10.1080/02724634.2013.808203

Assemat A, Boivin M, Marivaux L, Pujos F, Benites-Palomino A, Salas-Gismondi R, Tejada-Lara JV, Varas-Malca RM, Negri FR, Ribeiro AM, Antoine P-O (2019) Restes inédits de rongeurs caviomorphes du Paléogène de la région de Juanjui (Amazonie péruvienne) : systématique, implications macro-évolutives et biostratigraphiques. Geodiversitas 41:699-730. https://doi.org/10.5252/geodiversitas2019v41a20

Biknevicius AR, McFarlane DA, MacPhee RDE (1993) Body size in *Amblyrhiza inundata* (Rodentia: Caviomorpha), an extinct megafaunal rodent from the Anguilla Bank, West Indies: estimates and implications. Am Mus Novit 3079:1-25.

Blackburn DC, Keefe RM, Vallejo-Pareja MC, Vélez-Juarbe J (2020) The earliest record of Caribbean frogs: a fossil coquí from Puerto Rico. Biol Lett 16:20190947. https://doi.org/10.1098/rsbl.2019.0947

Boivin M, Marivaux L, Orliac MJ, Pujos F, Salas-Gismondi R, Tejada-Lara JV, Antoine P-O (2017) Late middle Eocene caviomorph rodents from Contamana, Peruvian Amazonia. Palaeontol Electron 50:1–50. palaeo-electronica.org/content/2017/1822-eocene-amazonian-caviomorphs

Boivin M, Marivaux L, Antoine P-O (2019a) L'apport du registre paléogène d'Amazonie sur la diversification initiale des Caviomorpha (Hystricognathi, Rodentia) : implications phylogénétiques, macroévolutives et paléobiogéographiques. Geodiversitas 41:143-245. https://doi.org/10.5252/geodiversitas2019v41a4

Boivin M, Marivaux L, Salas-Gismondi R, Vieytes EC, Antoine P-O (2019b) Incisor enamel microstructure of Paleogene caviomorph rodents from Contamana and Shapaja

(Peruvian Amazonia). J Mamm Evol 26:389-406. https://doi.org/10.1007/s10914-018-9430-4

Boivin M, Antoine P-O, Benites-Palomino A, Marivaux L, Salas-Gismondi R (2019c) A new record of a giant neoepiblemid rodent from Peruvian Amazonia and an overview of lower tooth dental homologies among chinchilloids. Acta Palaeontol Pol 64:627-642. https://doi.org/10.4202/app.00609.2019

Boivin M, Marivaux L, Aguirre-Díaz W et al (2022) Eocene caviomorph rodents from Balsayacu (Peruvian Amazonia). Paläontol Zeitsch 96:135-160. https://doi.org/10.1007/s12542-021-00551-0

Boyde A (1978) Development of the structure of the enamel of the incisor teeth in the three classical subordinal groups of the Rodentia. In: Butler PM, Josey KA (eds) Development, Function and Evolution of Teeth. Academic Press, London, pp 43-58.

Burgin CJ, Colella JP, Kahn PL, Upham NS (2018) How many species of mammals are there? J Mammal 99:1-14. https://doi.org/10.1093/jmammal/gyx147

Carrillo JD, Sánchez-Villagra MR (2015) Giant rodents from the Neotropics: diversity and dental variation of late Miocene neoepiblemid remains from Urumaco, Venezuela. Paläontol Zeitsch 89:1057-1071. https://doi.org/10.1007/s12542-015-0267-3

Cooke SB, Dávalos LM, Mychajliw AM, Turvey ST, Upham NS (2017) Anthropogenic extinction dominates Holocene declines of West Indian mammals. Annu Rev Ecol Evol Syst 48:301-327. https://doi.org/10.1146/annurev-ecolsys-110316-022754

Cope ED (1868) Exhibition of bones and teeth of a large rodent from the cave deposits of Anguilla, one of the Virgin West India Islands. Proc Acad Nat Sc Philadelphia 20:313.

Cope ED (1883) Contents of a bone cave in the island of Anguilla (West Indies). Smithson Contrib Knowl 25:1-30.

Courcelle M, Tilak M-K, Leite YLR, Douzery EJP, Fabre P-H (2019) Digging for the spiny rat and hutia phylogeny using a gene capture approach, with the description of a new mammal subfamily. Mol Phylogenet Evol 136:241-253. https://doi.org/10.1016/j.ympev.2019.03.007

Da Cunha L (2020) Oreille interne des rongeurs caviomorphes actuels et fossiles des Antilles: implications systématiques et phylogénétiques. Univ Montp Unpub MSc research internship.

Dávalos LM (2004) Phylogeny and biogeography of Caribbean mammals. Biol J Linn Soc 81:373-394. https://doi.org/10.1111/j.1095-8312.2003.00302.x

Fabre P-H, Vilstrup JT, Raghavan M, Der Sarkissian C, Willerslev E, Douzery EJP, Orlando L (2014) Rodents of the Caribbean: origin and diversification of hutias unravelled by

next-generation museomics. Biol Lett 10:20140266. https://doi.org/10.1098/rsbl.2014.0266

Fabre P-H, Hautier L, Douzery EJP (2015) A synopsis of rodent molecular phylogenetics, systematics and biogeography. In: Cox PG, Hautier L (eds) Evolution of the Rodents: Advances in Phylogeny, Functional Morphology and Development. Cambridge University Press, Cambridge, pp 19-69.

Ferreira JD, Negri FR, Sánchez-Villagra MR, Kerber L (2020) Small within the largest: brain size and anatomy of the extinct *Neoepiblema acreensis*, a giant rodent from the Neotropics. Biol Lett 16:20190914. https://doi.org/10.1098/rsbl.2019.0914

Ginot S, Hautier L, Marivaux L, Vianey-Liaud M (2016) Ecomorphological analysis of the astragalo-calcaneal complex in rodents and inferences of locomotor behaviours in extinct rodent species. PeerJ 4:1-49. https://doi.org/10.7717/peerj.2393

Hedges SB (2006) Paleogeography of the Antilles and origin of West Indian terrestrial vertebrates. Ann Mo Bot Gard 93:231-244.

Kalthoff D (2000) Die Schmelzmikrostruktur in den incisiven der hamsterartigen Nagetiere und anderer Myomorpha (Rodentia, Mammalia). Palaeontogr A 259:1-193.

Kerber L, Negri FR, Ribeiro AM, Nasif N, Pereira de Souza-Filho J, Ferigolo J (2017) Tropical fossil caviomorph rodents from the southwestern Brazilian Amazonia in the context of the South American faunas: systematics, biochronology, and paleobiogeography. J Mamm Evol 24:57-70. https://doi.org/10.1007/s10914-016-9340-2

Kerber L, Bissaro Junior MC, Negri FR, Pereira de Souza-Filho J, Guilherme E, Schmaltz Hsiou A (2018) A new rodent (Caviomorpha: Dinomyidae) from the upper Miocene of southwestern Brazilian Amazonia. Hist Biol 30:985-993. https://doi.org/10.1080/08912963.2017.1327529

Kerber L, Negri FR, Sanfelice D (2019) Morphology of cheek teeth and dental replacement in the extinct rodent *Neoepiblema* Ameghino, 1889 (Caviomorpha, Chinchilloidea, Neoepiblemidae). J Vert Paleontol 38:e1549061. https://doi.org/10.1080/02724634.2018.1549061

Koenigswald W v (1985) Evolutionary trends in the enamel of rodent incisors. In: Luckett WP, Hartenberger J-L (eds) Evolutionary Relationships among Rodents, A Multidisciplinary Analysis. Plenum, New York, pp 403-422.

Koenigswald W v, Sander PM (1997) Glossary of terms used for enamel microstructures. In: Koenigswald W v, Sander PM (eds) Tooth Enamel Microstructure. Balkema, Rotterdam, pp 267-280.

Korvenkontio VA (1934) Mikroskopische Untersuchungen an Nagerincisiven unter Hinweis auf die Schmelzstruktur der Backenzähne. Ann Zoo Soc Zool – Bota Fennicae Vanamo 2:1–274.

Kramarz AG, Vucetich MG, Arnal M (2013) A new Early Miocene chinchilloid hystricognath rodent. An approach to the understanding of the early chinchillid dental evolution. J Mamm Evol 20:249-261. https://doi.org/10.1007/s10914-012-9215-0

MacPhee RDE (1984) Quaternary mammal localities and heptaxodontid rodents of Jamaica. Am Mus Novit 2803:1-34.

MacPhee RDE (2009) Insulae infortunatae: establishing a chronology for Late Quaternary mammal extinctions in the West Indies. In: Haynes G (ed) American Megafaunal Extinctions at the End of the Pleistocene. Springer, Dordrecht, pp 169-193.

MacPhee RDE (2011) Basicranial morphology and relationships of Antillean Heptaxodontidae (Rodentia, Ctenohystrica, Caviomorpha). Bull Am Mus Nat Hist 363:1-70.

MacPhee RDE, Flemming C (2003) A possible heptaxodontine and other caviidan rodents from the Quaternary of Jamaica. Am Mus Novit 3422:1-42.

MacPhee RDE, Iturralde-Vinent MA (1995) Origin of the Greater Antillean land mammal fauna, 1: new Tertiary fossils from Cuba and Puerto Rico. Am Mus Novit 3141:1-30.

MacPhee RDE, Iturralde-Vinent MA (2005) The interpretation of Caribbean paleogeography: reply to Hedges. In Alcover JA, Bover P (eds), Proceedings of the International Symposium on Insular Vertebrate Evolution: the Palaeontological Approach. Monograf Soc Hist Nat Balears, pp 175–184.

MacPhee RDE, Iturralde-Vinent MA, Gaffney ES (2003) Domo de Zaza, an early Miocene vertebrate locality in South-Central Cuba, with notes on the tectonic evolution of Puerto Rico and the Mona passage. Am Mus Novit 3394:1-42.

Mammal Diversity Database. (2022). Mammal Diversity Database (Version 1.9.1) [Data set]. Zenodo. https://doi.org/10.5281/zenodo.4139722

Mares MA, Ojeda A (1982) Patterns of diversity and adaptation in South American hystricognath rodents. In: Mares MA, Genoways HH (eds) Mammalian Biology in South America. Pymatuning Laboratory of Ecology, Pittsburgh, pp 185–192.

Marivaux L, Vianey-Liaud M, Jaeger J-J (2004) High-level phylogeny of early Tertiary rodents: dental evidence. Zool J Linn Soc 142:105-134. https://doi.org/10. 1111/j.1096-3642.2004.00131.x

Marivaux L, Boivin M, Adnet S, Benammi M, Tabuce R, Benammi M (2019) Incisor enamel microstructure of hystricognathous and anomaluroid rodents from the earliest

Oligocene of Dakhla, Atlantic Sahara (Morocco). J Mamm Evol 26:373-388. https://doi.org/10.1007/s10914-017-9426-5

Marivaux L, Vélez-Juarbe J, Merzeraud G et al (2020) Early Oligocene chinchilloid caviomorphs from Puerto Rico and the initial rodent colonization of the West Indies. Proc Roy Soc B 287:20192806. https://doi.org/10.1098/rspb.2019.2806

Marivaux L, Vélez-Juarbe J, Viñola López LW et al (2021) An unpredicted ancient colonization of the West Indies by North American rodents: dental evidence of a geomorph from the early Oligocene of Puerto Rico. Pap Palaeontol 7:2021-2039. https://doi.org/10.1002/spp2.1388

Martin T (1992) Schmelzmikrostruktur in den inzisiven alt-und neuweltlicher hystricognather Nagetiere. Palaeovertebrata Mém extraordin 1–168.

Martin T (1993) Early rodent incisor enamel evolution: phylogenetic implications. J Mamm Evol 1:227-254. https://doi.org/10.1007/BF01041665

Martin T (1994a) African origin of caviomorph rodents is indicated by incisor enamel microstructure. Paleobiology 20:5-13. https://doi.org/10.1017/ S0094 83730 00110 9X

Martin T (1994b) On the systematic position of *Chaetomys subspinosus* (Rodentia: Caviomorpha) based on evidence from the incisor enamel microstructure. J Mamm Evol 2:117-131. https://doi.org/10.1007/BF01464364

Martin T (1997) Incisor enamel microstructure and systematics in rodents. In: Koenigswald W von, Sander PM (eds) Tooth Enamel Microstructure. Balkema, Rotterdam, pp 163-175.

Martin T (2004) Incisor enamel microstructure of South America's earliest rodents: implications for caviomorph origin and diversification. In: Campbell KE (ed) The Paleogene Mammalian Fauna of Santa Rosa, Amazonian Peru. Sci Ser Nat Hist Mus Los Angel Co 40:131–140.

Martin T (2005) Incisor schmelzmuster diversity in South America's oldest rodent fauna and early caviomorph history. J Mamm Evol 12:405-417. https://doi.org/10.1007/s10914-005-6968-8

McKenna MC, Bell SK (1997) Classification of Mammals Above the Species Level. Columbia University Press, New York.

Miller GS (1929) Mammals eaten by Indians, owls, and Spaniards in the coast region of the Dominican Republic. Smithson Misc Collect 82:1-16.

Miller GS, Gidley JW (1918) Synopsis of the supergeneric groups of rodents. J Wash Acad Sci 8:431-448.

Mones A (1980) Un Neoepiblemidae del Plioceno medio (Formacion Urumaco) de Venezuela (Mammalia: Rodentia: Caviomorpha). Ameghiniana 17:277-279.

Morgan GS, Wilkins L (2003) The extinct rodent *Clidomys* (Heptaxodontidae) from a late Quaternary cave deposit in Jamaica. Caribb J Earth Sci 39:34-41.

Orihuela J, Viñola LW, Jiménez Vázquez O, Mychajliw AM, Hernández de Lara O, Lorenzo L, Soto-Centeno JA (2020) Assessing the role of humans in Greater Antillean land vertebrate extinctions: new insights from Cuba. Quat Sci Rev 249:106597. https://doi.org/10.1016/j.quascirev.2020.106597

Patterson B, Wood AE (1982) Rodents from the Deseadan Oligocene of Bolivia and the relationship of Caviomorpha. Bull Mus Comp Zool 149:372-543.

Patton JL, Pardiñas UF, d'Elia G (2015) Mammals of South America. Vol. 2: Rodents. University of Chicago Press, Chicago.

Rasia LL, Candela AM, Cañon C (2021) Comprehensive total evidence phylogeny of chinchillids (Rodentia, Caviomorpha): cheek teeth anatomy and evolution. J Anat 239:405-423. https://doi.org/10.1111/joa.13430

Ray CE (1965) The relationships of Quemisia gravis (Rodentia: ?Heptaxodontidae). Smithson Misc Collect 149:1-12.

Rinderknecht A, Blanco RE (2008) The largest fossil rodent. Proc Roy Soc B 275:923-928. https://doi.org/10.1098/rspb.2007.1645

Rinderknecht A, Bostelmann E, Ubilla M (2018) Making a giant rodent: cranial anatomy and ontogenetic development in the genus *Isostylomys* (Mammalia, Hystricognathi, Dinomyidae). J Syst Palaeontol 16:245-261. https://doi.org/10.1080/14772019.2017.1285360

Robinet C, Merceron G, Candela AM, Marivaux L (2020) Dental microwear texture analysis and diet in extant caviomorphs (Rodentia) from the Serra do Mar Atlantic forest ecoregion (Brazil). J Mammal 101:386-402. https://doi.org/10.1093/jmammal/gyz194

Robinet C, Merceron G, Catzeflis F, Candela AM, Marivaux L (2022) About inter- and intra-specific variability of dental microwear texture in rodents: study of two sympatric *Proechimys* (Echimyidae) species from the Cacao locality, French Guiana. In: Merceron G, Tutken T, Scott R (eds) Understanding Dental Proxies of Ancient Diets. Palaeogeogr Palaeoclimatol Palaeoecol 591:110880. https://doi.org/10.1016/j.palaeo.2022.110880

Sánchez-Villagra MR, Aguilera O, Horovitz I (2003) The anatomy of the world's largest extinct rodent. Science 301:1708-1710. https://doi.org/10.1126/science.10893 32

Schreuder A (1933) Skull of *Amblyrhiza* from St. Martin. Tijdschr Nederl Dierk Vereening 3:242-266.

Simpson GG (1945) The principles of classification and a classification of mammals. Bull Am Mus Nat Hist 85:1-350.

Townsend KEB, Croft DA (2008) Enamel microwear in caviomorph rodents. J Mammal 89:730-743.

Turvey ST, Grady FV, Rye P (2006) A new genus and species of 'giant hutia' (*Tainotherium valei*) from the Quaternary of Puerto Rico: an extinct arboreal quadruped? J Zool 270:585-594. https://doi.org/10.1111/j.1469-7998.2006.00170.x

Turvey ST, Kennerley RJ, Nuñez-Miño JM, Young RP (2017) The Last Survivors: current status and conservation of the non-volant land mammals of the insular Caribbean. J Mammal 98:918-936. https://doi.org/10.1093/jmammal/gyw154

Upham NS, Borroto-Páez R (2017) Molecular phylogeography of endangered Cuban hutias within the Caribbean radiation of capromyid rodents. J Mammal 98:950-963. https://doi.org/10.1093/jmammal/gyx077

Upham NS, Patterson BD (2015) Evolution of caviomorph rodents: a complete phylogeny and timetree for living genera. In: Vassallo AI, Antenucci D (eds) Biology of Caviomorph Rodents: Diversity and Evolution. SAREM Series A, Buenos Aires, pp 63–120.

Vélez-Juarbe J, Martin T, MacPhee RDE, Ortega-Ariza D (2014) The earliest Caribbean rodents: Oligocene caviomorphs from Puerto Rico. J Vert Paleontol 34:157-163. https://doi.org/10.1080/02724634.2013.789039

Vieytes EC, Morgan CC, Verzi DH (2007) Adaptive diversity of incisor enamel microstructure in South American burrowing rodents (family Ctenomyidae, Caviomorpha). J Anat 211:296-302. https://doi.org/10.1111/j.1469-7580.2007.00767.x

Viñola López LW, Core Suárez EE, Vélez-Juarbe J, Almonte Milan JN, Bloch JI (2022) The oldest known record of a ground sloth (Mammalia, Xenarthra, Folivora) from Hispaniola: evolutionary and paleobiogeographical implications. J Paleontol 96: 684-691.https://doi.org/10.1017/jpa.2021.109

Vucetich MG, Vieytes EC (2006) A middle Miocene primitive octodontoid rodent and its bearing on the early evolutionary history of the Octodontoidea. Palaeontogr Abt A 277:81–91. https://doi.org/10.1127/pala/277/2006/81

Vucetich MG, Kramarz AG, Candela AM (2010) Colhuehuapian rodents from Gran Barranca and other Patagonian localities: the state of the art. In: Madden RH, Carlini

AA, Vucetich MG, Kay RF (eds) The Paleontology of Gran Barranca: Evolution and Environmental Change through the Middle Cenozoic of Patagonia. Cambridge University Press, New York, pp 206-219.

Vucetich MG, Arnal M, Deschamps CM, Pérez ME, Vieytes EC (2015) A brief history of caviomorph rodents as told by the fossil record. In: Vassallo AI, Antenucci D (eds) Biology of Caviomorph Rodents: Diversity and Evolution. SAREM Series A, Buenos Aires, pp 11–62.

Wahlert JH (1968) Variability of rodent incisor enamel as viewed in thin section, and the microstructure of the enamel in fossil and Recent rodent groups. Breviora 309:1-18.

Wilson DE, Reeder DM (2005) Mammal Species of the World: a Taxonomic and Geographic Reference. Johns Hopkins University Press, Baltimore.

Wilson DE, Lacher TE, Mittermeier RA (2016) Handbook of the Mammals of the World. Vol. 6. Lagomorphs and Rodents. Lynx Edicions, Barcelona.

Wilson LAB, Geiger M (2015) Diversity and evolution of femoral variation in Ctenohystrica. In: Cox PG, Hautier L (eds) Evolution of the Rodents: Advances in Phylogeny, Functional Morphology and Development. Cambridge University Press, Cambridge, pp 510-538.

Woods CA (1989) The biogeography of West Indian rodents. In: Woods CA (ed) Biogeography of the West Indies; Past, Present, and Future. Sandhill Crane, Gainesville, pp 741–798.

Woods CA, Hermanson JW (1985) Myology of hystricognath rodents: an analysis of form, function and phylogeny. In: Luckett PW, Hartenberger J-L (eds) Evolutionary Relationships Among Rodents: a Multidisciplinary Analysis. Plenum, New York, pp 515-548.

Woods CA, Borroto-Páez R, Kilpatrick CW (2001) Insular patterns and radiations of West Indian rodents. In: Woods CA, Sergile FE (eds) Biogeography of the West Indies: Patterns and Perspectives. CRC Press, Boca Raton, pp 335-353.

Woods R, Barnes I, Brace S, Turvey ST (2020) Ancient DNA suggests single colonisation and within-archipelago diversification of Caribbean caviomorph rodents. Mol Biol Evol 38:84-95. https://doi.org/10.1093/ molbev/msaa189

4.7 NEW STRATIGRAPHIC AND PALEOENVIRONMENTAL CONSTRAINTS ON THE PALEOGENE PALEOGEOGRAPHY OF WESTERN AMAZONIA

Artigo publicado no periódico *Journal of South American Earth Sciences*, volume 124, artigo nº 104256, 2023. DOI: 10.1016/j.jsames.2023.104256

Michele Andriolli Custódio[a,b,c], Martin Roddaz[a,c], Roberto Ventura Santos[a], Pierre-Olivier Antoine[d], Laurent Marivaux[d,h], **Narla S. Stutz[d,e]**, Elton Luiz Dantas[a], Carlos Jaramillo[f], Mélanie Louterbach[g], Christian Hurtado[h], Guilherme de Oliveira Gonçalves[a]

[a] Laboratório de Geocronologia, Instituto de Geociências, Universidade de Brasília, Brasília, DF 70910-000, Brazil
[b] Departamento de Geociências, Universidade Federal do Amazonas, CEP: 69.077-000, Manaus, AM, Brazil
[c] Géosciences-Environnement Toulouse, Université de Toulouse, UPS (SVT-OMP), CNRS, IRD, 14 Avenue Édouard Belin, 31400 Toulouse, France
[d] Institut des Sciences de l'Évolution de Montpellier, Univ Montpellier, CNRS, IRD, Place Eugène Bataillon, 34095, Montpellier, France
[e] Programa de Pós-Graduação em Geociências, Universidade Federal do Rio Grande do Sul (PPGGEO UFRGS). Av. Bento Gonçalves, 9500, 91501-970, Porto Alegre, Rio Grande do Sul, Brazil.
[f] Smithsonian Tropical Research Institute, Roosevelt Avenue, Building 401 Balboa, Ancon, Panama City, Panama
[g] Harvard Graduate School of Design, Department of Landscape Architecture, 48 Quincy Street, MA 02138 Cambridge, USA.
[h] Universidad Nacional Mayor de San Marcos, Av. Venezuela Cda. 34 s/n Lima-Cercado, Lima, Peru.
*Corresponding author
Email address: mi.andriolli@gmail.com (M.A. Custódio)

Abstract

The rise of the Andes and the associated propagation of the retroarc foreland basin during the Mesozoic Cenozoic in western South America shaped the paleogeography and paleoenvironmental settings of Western Amazonia. Much attention has been paid to the Neogene evolution of the Amazonian Basin, but few studies have investigated

in detail the paleoenvironments of Western Amazonia during the Paleogene. We present a multi-proxy study that includes new biostratigraphic and paleontologic data, the interpretation of depositional environments and zircon U-Pb data from the Upper Cretaceous-Paleogene sedimentar sequence exposed in the Huallaga Basi (Northern Peru). The biostratigraphic dating suggests that the lower part of the sequence is Maastrichtian in age. The maximum depositional age and maximum likelihood age according to the U-Pb zircon dating of Paleogene sedimentary rocks indicate Lutetian to Bartonian ages (from 43.5 ± 0.64 Ma to 37.6 ± 0.85 Ma). These results reveal a hiatus in the depositional record during Paleocene time. Two depositional systems can be distinguished: a lacustrine system composed of red mudrocks interbedded with thick sandstone layers and carbonate beds, and a siliciclastic tide-dominated system composed of fine- to medium-grained sandstones associated with tidal bundles, reactivation surfaces and heterolithic stratifications. However, the carbon and oxygen stable isotope values in carbonates tend to characterize a freshwater system, with a transition to brackish conditions toward the upper part of the section (Bartonian), thereby suggesting the presence of an estuary system. Finally, we suggest that the Bartonian shallow marine incursion recorded in the Huallaga Basin occurred from the north through the Caribbean Sea, and that it might have played a role in regional biodiversity patterns in the Paleogene.

Keywords: zircon U-Pb dating, C and O isotopes, shallow marine deposits, Northern Peru, paleogeography

1 INTRODUCTION

Precise knowledge of the geological evolution of Amazonian landscapes and ecosystems is a prerequisite for understanding species diversification in this vast area today biodiversity seems to be deeply rooted in the pre-Quaternary (Hoorn et al., 2010b, and the references therein). The uplift of the Andes reconfigured drainage patterns, involved a vast influx of sediments into the Amazonian basins (Figure 1) (e.g. Roddaz et al., 2010, 2005a), and caused shallow marine incursions in Western Amazonia (Jaramillo et al., 2017; Boonstra et al., 2015; Hovikoski et al., 2010).

Recently, much attention has been paid to the Neogene paleogeographyof the Amazonian basins, especially to the timing of the modern transcontinental Amazon River (Hoorn et al., 2017; van Soelen et al., 2017; Eakin et al., 2014; Gorini et al., 2014;

Sacek, 2014; Shephard et al., 2010; Figueiredo et al., 2009). Attention has also been given to the Neogene paleogeography of Western Amazonia (Hoorn et al., 2010a) and the number and nature of marine incursions that affected this area during the Miocene (i.e., the Pebas megawetland system) (Jaramillo et al., 2017; Antoine et al., 2016; Boonstra et al., 2015; Hovikoski et al., 2010; Hoorn, 1993). However, surface uplift driven by the tectonism and denudation of the present-day Amazonian Andes area started much earlier, as recorded in the Upper Maastrichtian-Paleocene deposits (Hurtado et al., 2018; Louterbach et al., 2018b).

In comparison with the Neogene period, the Paleogene paleoenvironmental changes of Western Amazonian basins have still a poorly documented and poorly dated stratigraphic record. Notable exceptions are the detailed studies of Antoine et al. (2016) and Louterbach et al., (2018b). In the Late Cretaceous (Middle Campanian and Late Maastrichtian), the sedimentary record of the Ecuadorian and northern Peruvian parts of the Western Amazonian Basin (i.e., the Marañón Basin) (Figure 1) indicates thick transgressive-regressive sequences alternating between fluvial-marine paleoenvironments controlled by eustatic processes (Zamora and Gil, 2018). It is nuclear whether or not these conditions prevailed during the Paleogene and how the onset of the Andean uplift affected the landscape and paleoenvironment of Western Amazonia.

Two shallow marine transgressions that occurred during the Paleogene are currently documented in Western Amazonia. The oldest one is a Late Paleocene shallow marine transgression characterized by estuarine and bay paleoenvironments (Louterbach et al., 2014). This latter event has only been documented in the southern part of the Amazonian retroarc foreland basin (Madre de Dios Basin, Peru) (Figure 1), and the entrance of this transgression remain unclear (Louterbach et al., 2014). The second transgression is a Middle to Late Eocene shallow marine incursion known as the “Pozo” embayment or transgression, which flooded the northern part of the Amazonian retroarc foreland basins from the Gulf of Guayaquil or the Caribbean Sea (Roddaz et al., 2010; Santos et al., 2008; Christophoul et al., 2002; Antoine et al., 2016). However, the southwestern margin extension of this Pozo embayment needs to be better constrained. Hence, documenting Paleogene paleoenvironments in other parts of the Western Amazonian Basin may contribute to resolving these issues.

The Cretaceous–Cenozoic sedimentary infilling of the Huallaga Basin (Calderon et al., 2017a; Eude et al., 2015; Hermoza et al., 2005;) has the unique potential to have recorded the Cretaceous–Paleogene paleoenvironmental evolution of the northern

part of Western Amazonia as previous studies show major changes in the sedimentar provenance between the late Cretaceous and the Paleocene (Hurtado et al., 2018). The aim of this work is to characterize the paleoenvironmental evolution of the Huallaga Basin during the late Cretaceous-Paleogene time window, as a key element for unraveling the Andes – Amazon sedimentary evolution.

Our contribution comprises the first detailed stratigraphic analysis of the late Cretaceous–Paleogene sedimentary section, based on new multi-proxy analyses including sedimentological facies, biostratigraphy (palynostratigraphy and vertebrate biochronology), stable isotopes (C, O) in carbonates, and maximum depositional ages based on the U-Pb dating of detrital zircons.

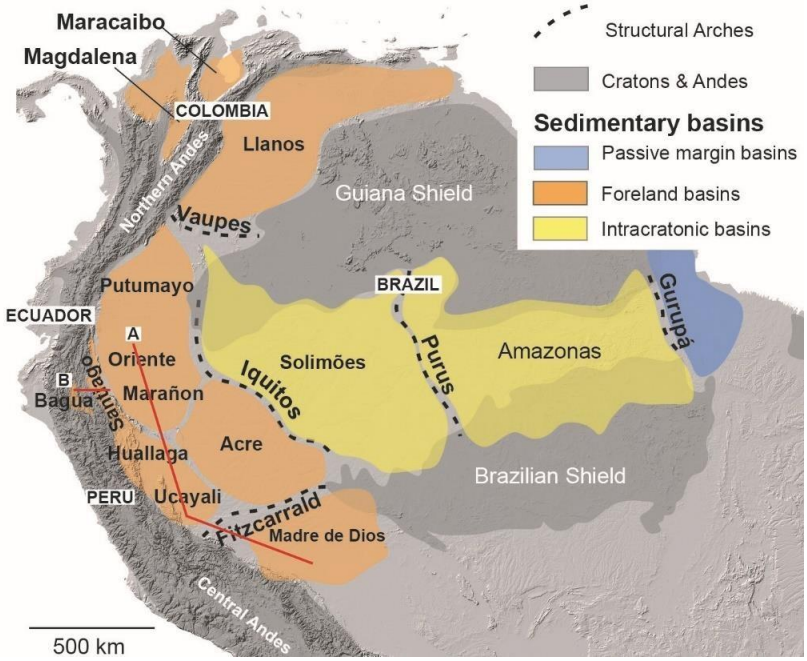


Figure 1. Map of the geographic extent of the major morphotectonic provinces of the northern South America, from west to east, the retroarc foreland basins (Colombia, Ecuador and Peru countries), the intracratonic and passive margin basins (Brazil), partially bounded by structural arches (dashed lines). Northern and Southern Amazon Craton are represented by the Guiana and Brazilian shields, respectively (modified and compiled from Albert et al., 2018; Moreno et al., 2020; Roddaz et al., 2010). The red lines indicate the location of figs 3 A and 3B.

2. GEOLOGICAL BACKGROUND

2.1 Tectonic setting and stratigraphy of the Huallaga Basin

The north-south trending Huallaga Basin (Figure 2) is currently 400 km long with a maximum width of 100 km (Hermoza et al., 2005), and it is part of the northern Peruvian Subandean Zone. It consists of the wedge-top depozone (DeCelles and Giles, 1996) of the North Amazonian retroarc foreland basin (Espurt et al., 2010, 2007; Roddaz et al., 2005b) that formed in response to the tectonic loading of the Andes (Roddaz et al., 2010). To the east, the Huallaga Basin is separated from the Marañón Basin by the Cushabatay High and Chazuta Thrust; the latter corresponds to the thrust front of the Subandean Zone (SAZ) (Figure 2) (Calderón et al., 2017a; Hermoza et al., 2005). To the west, the Huallaga Basin is delimited by the Eastern Cordillera (Figure 2). A sequential restoration based on low-temperature thermochronology and balanced cross-sections suggests that the Eastern Cordillera started to be uplifted between ca. 30 and 24 Ma, which caused thrusts to propagate over a regional detachment level located in the Upper Triassic evaporites (Carrillo et al, 2021; Calderón et al., 2017a, b; Eude et al., 2015). The Cretaceous tectonic configuration of the Huallaga Basin is less constrained. The most recent model suggests that it could be part of a passive margin (Zamora and Gil, 2018) that received sediments from the Amazonian Craton (Hurtado et al., 2018).

The Cretaceous sequences of the Huallaga Basin comprise Albian to Maastrichtian fluvial to shallow marine successions of sandstones, shales and limestones (Cushabatay-Raya, Agua Caliente-Chonta, and Vivian-Cachiyacu-Huchpayacu formations) (Baby et al., 2018; Calderón et al., 2017a, b) (Figure 3). The Albian–Maastrichtian sedimentary rocks of the Huallaga Basin have εNd(0) values (−16.8 to −18.6) consistent with a cratonic source, and a U-Pb zircon age distribution dominated by the easternmost Brazilian Shield terranes (Hurtado et al., 2018).

The Cenozoic stratigraphy of the Huallaga Basin still needs to be better constrained. Calderón et al. (2017) proposed that the Paleocene–lower Eocene sedimentary sequence started with the fluvial and tidal sandstones of the Casa Blanca Formation (Fm.), whereas other authors suggested that the Cenozoic sedimentar sequences started with the Paleogene fluvial sedimentary rocks of the Yahuarango Fm. (Hurtado et al., 2018; Roddaz et al., 2010; Hermoza et al., 2005; Gutierrez, 1982; Kummel, 1948). According to Hurtado et al. (2018), the Paleogene sedimentary rocks of the Yahuarango Fm. have an Andean provenance, with εNd(0) values ranging between -5.6 and -12.0, and up to 16% of U-Pb zircon ages are derived from the Andean volcanic arc.

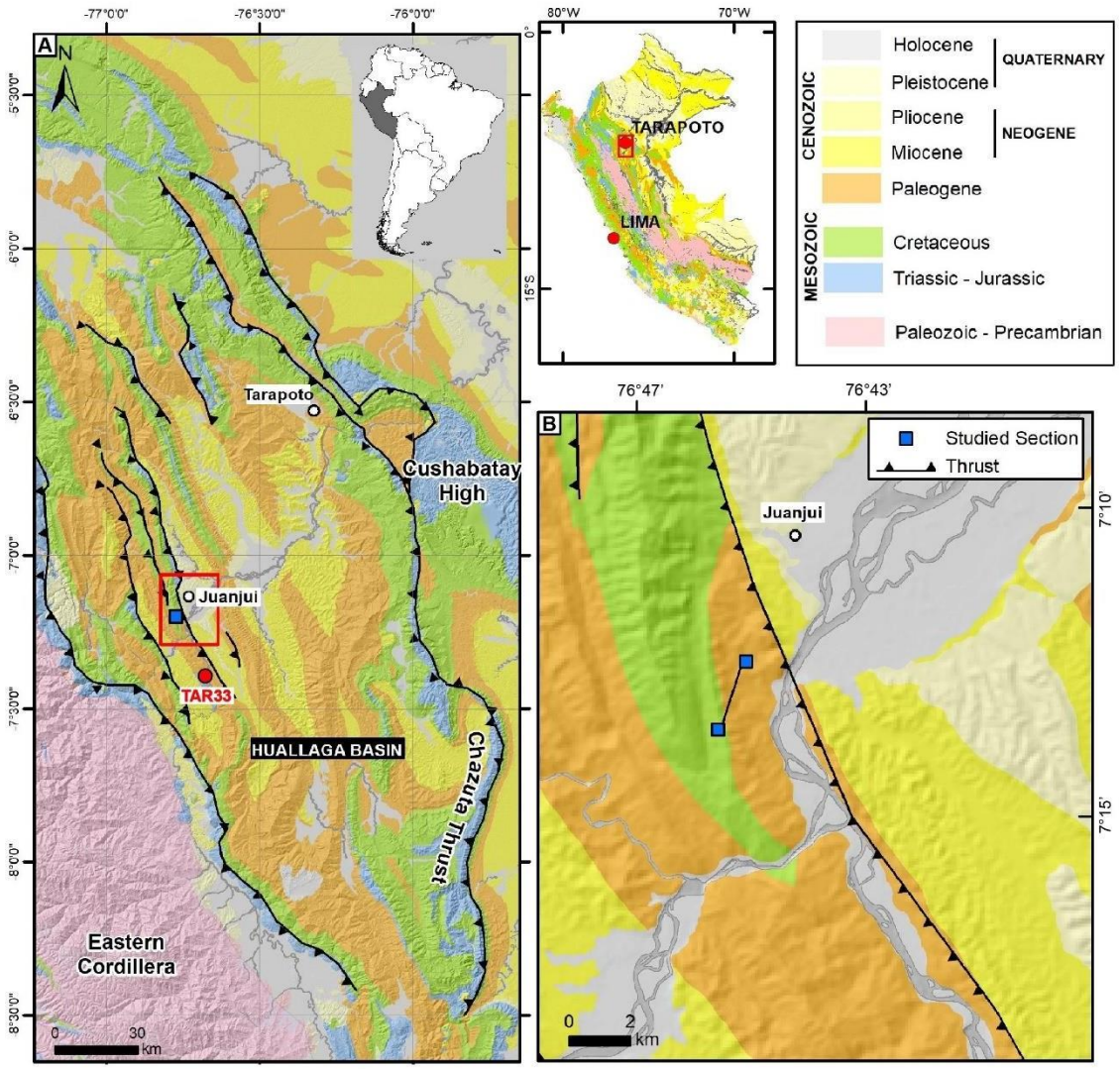


Figure 2. Geological map of the studied area modified from the INGEMMET Geological Map of Peru available at http://geocatmin.ingemmet.gob.pe/geocatmin/. A) Regional geologic map of the Huallaga Basin, which is separated to the west from the Eastern Cordillera and limited, to east, from Marañón Basin by the Chazuta thrust and the Cushabatay High. The red rectangle indicate the location of the Juanjuí stratigraphic section. Location of the large dinosaur tracks is represented by TAR33; B) Detailed geological map showing the Mesozoic-Cenozoic geological contacts and the stratigraphic position of the Juanjui studied section.

2.2 Stratigraphy of other Western Amazonian basins

The Amazonian retroarc foreland basins experienced similar geological evolutions until the Pliocene uplift of the Fitzcarrald Arch (Figures 1 and, 3) (Roddaz et al., 2010; Espurt et al., 2010). An extensional phase in a back-arc basin setting controlled the deposition of the mixed clastic and volcanic deposits of the Triassic Mitu group (George et al., 2019; Calderón et al., 2017), as recorded in the Bagua Basin, the

Eastern Cordillera of Peru and the Santiago Basin (Figure 3). Farther southeast (Marañón-Huallaga-Ucayali basins), a regional extensional basin created due to post-extensional thermal subsidence drove the deposition of the Triassic-Jurassic eolian-fluvial deposits of the Lower Nia Fm. (Calderón et al., 2017a, b). These deposits grade laterally into the shallow marine carbonates of the post-rift Pucara Group and the Sarayaquillo fluvial sequence, as recorded in the Ecuadorian and Peruvian basins (George et al., 2019; Hurtado et al., 2018; Calderón et al., 2017) (Figure 3A; B). The Late Jurassic to Early Cretaceous are marked by a widespread sedimentary hiatus (145-120 Ma) (Hurtado et al., 2018; Calderón et al., 2017) (Figure 3A; B). Overlying this erosional unconformity, the Cretaceous sedimentary rocks comprised Albian to Maastrichtian fluvial to shallow marine deposits, mainly represented by the Goyallarisquizga, Cushabatay-Raya; Agua Caliente-Chonta, and Vivian-Cachiyacu-Huchpayacu formations (Figure 3A, B).

From the Late Cretaceous to the Early Paleogene, the Andean shortening started to control the configuration of the Western Amazonian basins (Horton et al., 2018; Hurtado et al., 2018; Louterbach et al., 2014; 2017; Calderón et al., 2017; Hermoza et al., 2005). The Cenozoic retroarc foreland infill comprises the fluvial and lacustrine siltstones/mudstones of the Paleogene Yahuarango Fm. (Marañon-Huallaga-Ucayali basins) (Hurtado et al., 2018; Roddaz et al., 2010; Hermoza et al., 2005; Gutierrez, 1982; Kummel, 1948), which can be correlated with the Tiyuyacu (Oriente Basin) (Baby et al., 2013) and Huayabamba formations (Madre de Dios Basin) (Louterbach et al., 2014). These formations can be correlated with the Paleocene-lower Eocene braided fluvial deposits of the Rentema Fm. in the Bagua Basin (Moreno et al., 2022; 2020) (Figure 3B).

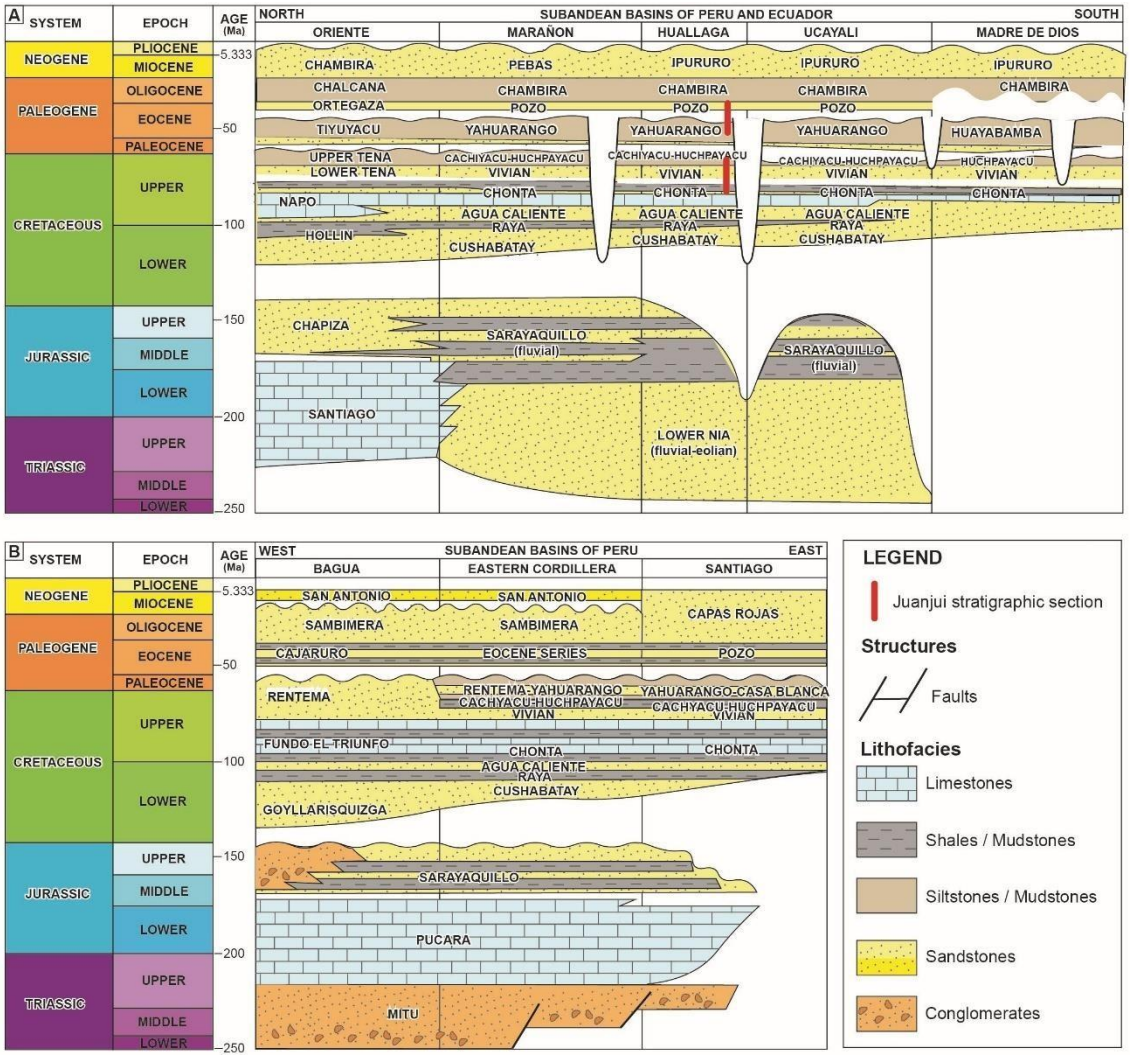


Figure 3. Comparative chronostratigraphic diagram showing the stratigraphic nomenclature, age, lithology, tectonic setting, and stratigraphic discontinuities for (A) the Ecuadorian and Peruvian Subandean Amazonian basins and (B) Peruvian Amazonian foreland basins. The chronostratigraphic diagram (A) was constructed based on Baby et al. (2013); Calvès et al. (2018); Roddaz et al. (2010), Hurtado et al. (2018); Hermoza et al. (2005); Louterbach et al. (2014), and Calderón et al. (2017a, 2017b). The chronostratigraphic diagram (B) is based on Moreno et al. (2020; 2022) and George et al. (2019).

These formations are separated from the youngest formations by a middle Eocene regional unconformity recorded in the Ecuadorian and Peruvian retroarc foreland basins (Figure 3) (Roddaz et al., 2010; Christophoul et al., 2002;). The shallow marine deposits of the middle Eocene-Oligocene Pozo Fm. are recorded in the Santiago, Marañón, Huallaga and Ucayali basins. The Pozo Fm. can be correlated to the north with the Ortegaza Fm. (Oriente Basin) (Baby et al., 2013) and to the west

with the Eocene Series (Eastern Cordillera) and the fluvio-lacustrine Cajaruro Fm. (Bagua basin) (Moreno et al., 2022; 2020) (Figure 3A, B). It is overlaid by the Upper Oligocene-Lower Miocene fluvial deposits of the Chambira Fm. in the Peruvian retroarc foreland basins (Antoine et al., 2016) and by the Chalcana Fm. in the Ecuadorian Oriente retroarc foreland basin (Baby et al., 2013). These formations can be correlated with the Upper Eocene-middle Miocene meandering deposits of the Sambimera Fm. in the Bagua Basin (Moreno et al., 2022, 2020) and Eastern Cordillera, and the Capas Rojas Fm. in the Santiago Basin (George et al., 2019) (Figure 3B). Finally, the Neogene sedimentary deposits are characterized by the fluvial deposits of the Ipururo, Chambira and San Antonio formations in the Bagua Basin, Eastern Cordillera, Huallaga, Ucayali, Madre de Dios basins (Moreno et al., 2022, 2020; George et al., 2019; Calderón et al., 2017; Hermoza et al., 2005) (Figure 3A, B). These deposits can be correlated with those of the Pebas Fm. that belong to the Pebas megawetland system (Hoorn et al., 2022; Jaramillo et al., 2017; Antoine et al., 2016; Boonstra et al., 2015; Hovikoski et al., 2010; Hoorn, 1993) in the Marañón Basin.

3 MATERIALS AND METHODS

3.1 Sedimentology

We studied in detail one Mesozoic–Cenozoic section, the Juanjuí section (Figure 4). The outcrops investigated in this study crop out along the 5N national road close to the Huallaga River and the city of Juanjuí (see Figure 2 for the location and Supplementary Material S1 for the coordinates). To better understand the depositional environment, we measured and described several outcrops along the Juanjuí stratigraphic section. We described the clastic facies in terms of their lithology, geometry, sedimentar structures and paleontological content (Miall, 2006; 1978). The chemical facies (microfacies) were described using Dunham's (1962) classification, which considers the abundances of carbonates, mud and grains; this helps to better constrain the formation process and/or paleoenvironmental conditions. The most commonly used criteria are the depositional texture and fabric, as well as qualitative and quantitative compositional data (Flügel, 2010). As pointed out by Walker (1992), most classifications for carbonates were originally conceptualized for marine systems, but they have also been used for lacustrine deposits with some adjustments. The carbonate thin sections were prepared at the Laboratório de Laminação (LABLAM) of the Universidade de Brasília (UnB). Thirteen sedimentary facies have been identified (Table 1).

Table 1. Summary of the descriptions and interpretations of each sedimentary siliciclastic facies and carbonate microfacies.

Facies/ Microfacies	Lithology and Texture	Sedimentary Structures	Paleontological content	Ichnology	Thickness (m)	Other characteristics/ Geometries	Interpretation
Siliciclastic facies							
Gcm Massive clast-supported conglomerate	Rounded- to sub-rounded mud-clasts (monomictic conglomerates), with cm-dm size (3–15 cm), scattered in the bed. Matrix composed by medium- to coarse-grained arkosik sandstones, with scattered subrounded granules and pebbles (milky quartz pebbles). Poorly-defined fining-upward trend; very poor sorting	Massive	No fossils	No trace fossils	0.3–0.5	Discontinuous and cuneiform beds, marked by concave-up bases	This deposits could be referred as filling of a channel lag deposits, under high sediment concentration and erosive event (Miall, 1978, 1996)
St Trough cross-stratified sandstone	Reddish and brownish, sub-rounded grains, well- to moderately-sorted, fine-to medium-grained arkosic sandstones, with thin mudstone layer drape on the foresets, regular thick-thin (0.1–0.5 cm) alternations in lamina thickeness. Foresets dipping at low angles (5–10°)	Trough cross-stratification	No fossils	No trace fossils	0.2–0.4	Dm-thick wedge-shaped beds. Reactivation surfaces delimiting the foresets.	Migration of subaqueous dunes (3D) by unidirectional flow in lower flow regime. Compound dune/tidal dune of channel infill. Variable energy flow (Miall, 1978, 1996)
Sp Planar cross-stratified sandstone	Sub-rounded grains, well- to moderate-sorted, medium-grained arkosic sandstones, organized in dm-thick	Planar cross-stratification	No fossils	No trace fossils	0.8	Tabular beds, typically flat on the top and concave-up base	Migration of 2D subaqueous dunes by unidirectional flow in lower flow regime (Miall, 1978, 1996)
Sr Climbing ripple cross-laminated sandstone	Rounded grains, well-sorted, very fine- to fine grained arkosic sandstones	Climbing ripple cross-lamination	No fossils	No trace fossils	0.25–0.4	Organized in cm-thick wedge-shaped beds, with flat base	Migration of supercritical climbing ripples by a lower regime unidirectional flow (Miall, 1978, 1996)
Smb Massive sandstone bioturbated	Reddish to brownish, sub-rounded to sub-angular grains, well- to moderate sorted, fine- to medium-grained arkosic sandstone, moderate to highly bioturbated	Massive	No fossils	Vertical and horisontal burrows	0.3–1.0	Tabular beds with flattered top and base. Obliteration of the primary sedimentary structure	Post-depositional modification by bioturbation (Miall, 1978, 1996)
H Heterolithic facies	Grey to beige, well-sorted, sub-rounded grains, very fine- to fine-grained arkosic sandstones with scattered flaser-bedding (mud drapes – 0.1 cm) interbedded with linsen and wavy-bedding (10–20 cm) mudstone layers. Mm- to dm-scale interlamination of thin mud-rich and sand-rich layers, arranged in dm- to m-thick beds	Linsen, wavy and flaser beddings	No fossils	No trace fossils	up to 1	Beds with tabular geometry, normally flattered top and base	They are deposits of shallow bodies of water, under variations in sediment supply and tidal velocity/energy flow (Dalrymple et al., 2003; Dalrymple and Choi, 2007)
Hb Herringbone cross-stratified sandstone	Well- to moderate-sorted, sub-rounded to rounded grains, medium-grained arkosic sandstones	Herringbone cross-stratification	No fossils	No trace fossils	0.3–0.4	Organized in dm-thick wedge-shaped beds. Reactivation surface in association with bidirectional flow evidence	Deposition under opposite-direction currents, dominated either by flood or ebb currents (Dalrymple and Choi, 2007)
F Fines	Red to purple mudstones and siltstones, moderately to highly bioturbated	Massive	Echimonocolpites protofranciscoi, Ulmoideipites krempii, Cricotriporites aff. Macroporus, Proxapertites psilatus, Momipites africanus; Araucariacites sp	Vertical and horisontal burrows	up to 5	Tabular beds	Decantation in subaqueous environment with very low or absent energy (Miall, 1978, 1996)
P Paleosol	Silty shales with mottled aspect; carbonate nodules (2–3 cm); root traces	Massive/ incipient lamination	No fossils	Root traces (undefined)	5 to 10	Tabular beds	Long periods of plants colonization, non-deposition or highly probable low rate of accumulation. Process of evaporation conducting to ions concentration and formation of carbonate nodules (Miall, 2006; Nichols, 2009)
Carbonate facies							
Mp Peloidal Mudstone	Dark brown, fine-grained carbonatic mud matrix (micrite), with scattered peloids grains and minor fine siliciclastic grains	Massive	Peloids	No trace fossils	0.1–0.2	Tabular beds with flattered top and base. Peloids (20–200 µm in diameter) are spherical, ellipsoidal and irregular carbonate grains, with no internal structure, moderately-sorted	Organically induced precipitation (Flügel, 2010; Tucker and Wright, 1990)
Wpo Wackestone with peloids and ostracods	Dark-brown limestones, mud-supported carbonate rock, composed by ostracods and peloids grains (20–45%). Peloids have clotted textures and the ostracods are normally scattered but are occasionally found oriented parallel to stratigraphic bedding by disarticulated valves	Massive/ incipient lamination	Peloids and Ostracods (200–400 µm)	No trace fossils	0.2–0.4	Tabular bed with flattered top and base. Locally, peloids have dense packaging	Deposited under low-energy condition with some water agitations, indicating some transportation (disarticulated valves) (Flügel, 2010; Tucker and Wright, 1990)
Woc Wackestone with ostracods and charophytes	Mainly composed by micrite with scattered bioclasts (>10% grains) such as ostracods and charophyte gyrogonites	Massive	Peloids; ostracods (200 µm); charophyte gyrogonites (600–800 µm)	No trace fossils	0.2–0.5	Tabular beds with flat base and undulated top. Moldic porosity characterized by molds of ostracods and charophyte remains (both broken and intact)	Deposited under low- to medium-energy condition with some water agitations, indicating some transportation (disarticulated valves) (Flügel, 2010; Tucker and Wright, 1990)
Gps Pisolithic Grainstone	Grainstone fabric with dominant occurrence of pisoids. The matrix contain abundant angular to subrounded, moderate to poorly sorted terrigenous quartz grains. Sutured contacts (microstylolitic) and concave-convex contacts (pisoids - quartz grains)	Massive	Pisoids (>2 mm)	No trace fossils	0.1–0.2	Brown to red pisoids with dense or irregular laminations, sub-spherical to irregular, partially replaced by pyrite (?)	Biogenic processes or chemical precipitation. Sutured grains related to compaction and pressure dissolution (Flügel, 2010; Tucker and Wright, 1990)

3.2 Stable isotopes

Forty-six samples of limestones and sandstones in a carbonate matrix were collected along the Juanjuí stratigraphic section (Figure 4). The abbreviations HUA (Huallaga) and JUA (Juanjuí) are used to refer to the samples obtained during field work performed in September 2017 and August 2019, respectively. The carbon and oxygen isotopic compositions are shown in Supplementary Material Table S2.

The samples were analyzed at the Geochronology and Isotope Geochemistry Laboratory of the University of Brasília (LEGGA) on a Delta V Plus mass spectrometer

connected to a Gas Bench II apparatus. The samples reacted with H3PO4 at a temperature of 72 ºC after the flask was flushed with helium. Stable isotope results are reported in delta notation relative to the Vienna Pee Dee Belemnite (V-PDB) reference standard, and they were calibrated against the NBS 18 (δ13CV-PDB = −5.01‰ and δ18OV-PDB = −23.2‰) and NBS 19 (δ13CV-PDB = 1.95‰ and δ18OV-PDB = −2.20‰) reference materials. A linear regression of the standard results followed by correction of the sample data, were performed to account for instrumental bias. To avoid any diagenetic biases, we selected only well-preserved samples. The isotopic composition of carbon and oxygen in a sample was expressed by dividing the isotopic ratio (R) measured in the sample by the isotopic ratio of a standard (V-PDB) using the δ notation; the isotopic composition is expressed in parts per Thousand (‰). δ13C and δ18O were obtained as follows: δ13C(sample) = [(Rsample/RV-PDB) – 1] * 103, and δ18O(sample) = [(Rsample/RV-PDB) – 1] * 103, respectively (Guiguer et al., 2003).

3.3 Palynological analysis

The palynological samples were prepared at the Universidad de Caldas following the standard palynological processing method proposed by Traverse (2007). Carbonates and silicates were removed by digesting the samples in HCl and HF for 12 and 24 hours, respectively. After acid digestion, the samples were neutralized through repeated dilution with distilled water and decanting. The remaining residue was initially sieved with a 250 µm mesh; this was followed by sieving through a 10µm mesh. This residue was cleaned in an ultrasonic equipment for 15 seconds and the organic residue was concentrated by centrifugation, followed by the mounting of a first cover slide in a solution of polyvinyl alcohol. Part of the residue was oxidized in nitric acid for 2–3 minutes, and a second slide was mounted. The slides were sealed with Canadian balsam. A Nikon i80 at the Smithsonian Tropical Research Institute was used to scan the slides. The examination and description of the palynological material were carried out using a 100x Nikon oil immersion planapochromatic objective. The identification of the palynomorphs was performed through a comparison with photographs and descriptions of Cretaceous and Paleocene material published for northern South America that are compiled in an online database (Jaramillo and Rueda, 2021). The palynological zonation of Jaramillo et al. (2011) and the biostratigraphic analysis of Carvalho et al. (2021) and De La Parra et al. (2021) were used to assess the age of the samples.

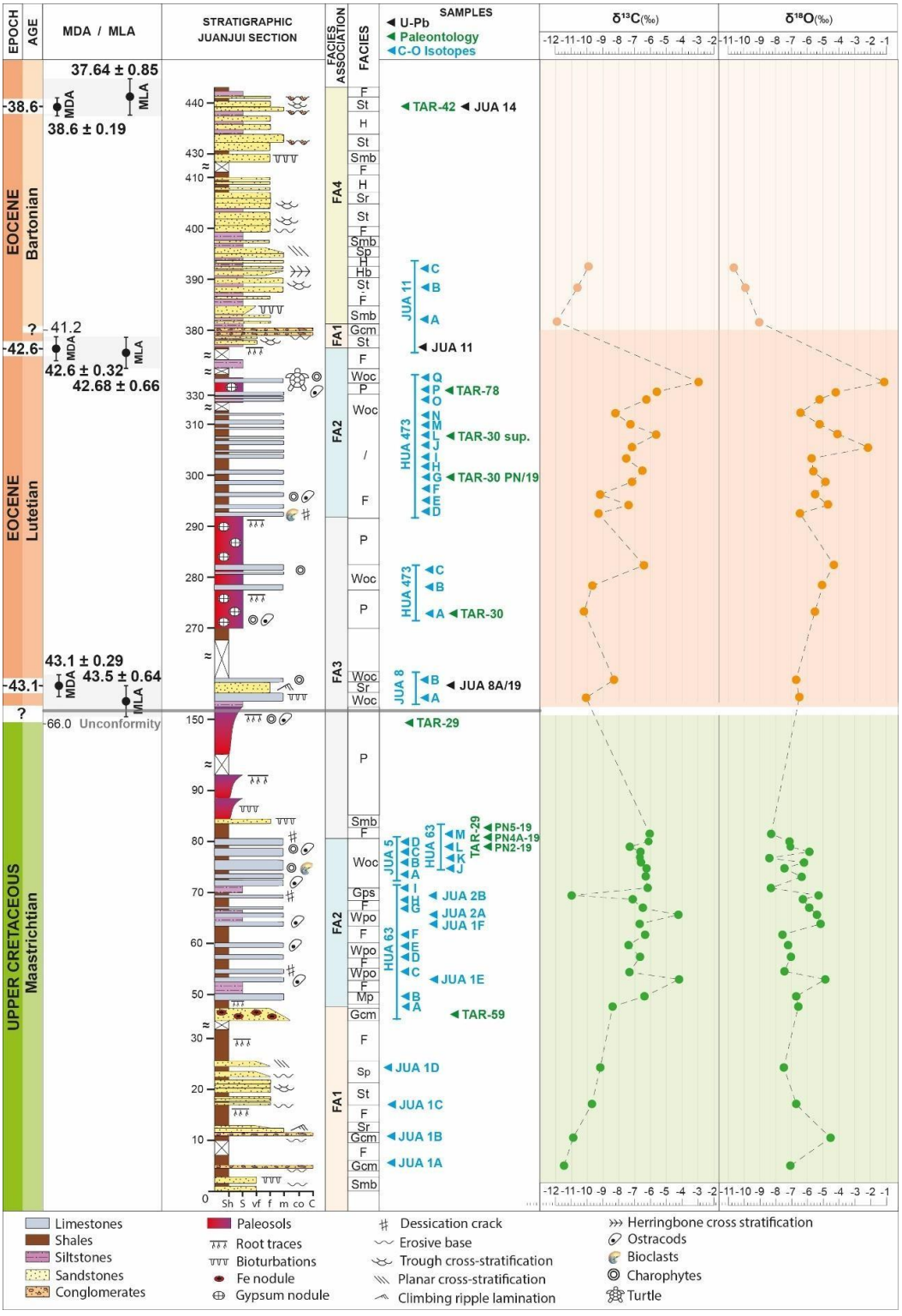


Figure 4. Synthetic Juanjuí stratigraphic section through the late Cretaceous (Maastrichtian) to late middle Eocene (Bartonian) at the Huallaga Basin, constructed from field observations, with location of the analyzed samples for C-O isotopic compositions, paleontological content (biostratigraphic constraints) and U-Pb zircon dating. Siliciclastic facies: massive clast-supported conglomerate (Gcm); trough cross-stratified sandstone (St), planar cross-stratified sandstone (Sp), climbing ripple cross-

laminated sandstone (Sr), bioturbated sandstone (Smb), heterolithic facies (H), herringbone cross-stratified sandstone (Hb), fines (F) and paleosol (P). Carbonate microfacies: peloidal mudstone (Mp); wackestone with peloids and ostracods (Wpo); wackestone with ostracods and charophytes (Woc); and pisolitic grainstone (Gps). FA= Facies association. See text and Table 1 for details.

3.4 U-Pb ages

Zircon grains were obtained from three samples of medium-grained sandstones collected along the Juanjuí section (JUA 8A/19, 11 and 14; Figures 4, S1 and S3–S5). For U-Pb analyses, each sample was prepared and analyzed at the Geochronology and Isotope Geochemistry Laboratory (LEGGA) of the University of Brasília (UnB). The sample preparation process included crushing rock samples, which was followed by heavy mineral separation by panning. Additionally, another separation was performed based on the magnetic properties of the minerals using the Frantz Isodynamic Magnetic Separator. A random selection of the zircon grains was handpicked (~150 grains per sample) under a stereomicroscope, mounted on adhesive tape, enclosed in a 9-mm-diameter plastic ring placed on the tape around the zircons and filled with epoxy resin. Finally, the zircon grains were polished to expose their centers (Gehrels, 2014; Bühn et al., 2009; Gehrels et al., 2008;). The mounts with zircon grains were imaged by a scanning electron microscope (SEM) and back-scattered electron (BSE) detector to identify morphological features and internal structures and to provide a base map for recording laser spot locations.

The masses of interest were measured on a Thermo Finningan Element XR high-resolution single-collector sector field Inductively Coupled Plasma Mass Spectrometry (ICP-MS) coupled to a 193 nm Iridia Excimer (ArF) laser ablation system. The laser ablation system is equipped with a cobalt dual-volume chamber. The mass spectrometer was tuned to improve U and Pb sensitivity while minimizing oxide production prior to each analytical session. Each analysis consisted of 10 s of background measurement followed by 20 s of sample acquisition. Each mass (202, 204, 206, 208, 232, 238) was measured using the triple detection mode (SEM + Faraday) by sweeping the electrostatic sector on each mass. Each sweep lasted 82 ms, resulting in over 800 scans for each ablation. Laser conditions included a spot diameter of 25 µm, 20 Hz and 2.0 J cm-2. The raw data were processed on Iolite 4.0 (Paton et al., 2011) as a time-resolved signal and individual signal inspection was done with the assistance of VizualAge (Petrus and Kamber, 2012). Data correction included

blank subtraction, Laser Induced Elemental Fractionation (LIEF) correction using an exponential plus linear model and normalization using the GJ-1 zircon (Jackson et al., 2004) and 91500 zircon (Widenbeck et al., 1995). Excess variance on the primary calibrant was propagated on each analytical point. A systematic uncertainty of ca. 1% is propagated on each final age. No common lead correction was applied. The ages uncertainties are quoted at 2 sigma (2σ) confidence level.

The data reduction of the U-Pb isotopic results for detrital zircons was conducted using Iolite 4.0 and followed the procedures of Paton et al. (2011). Details regarding the LA-ICP-MS U-Th-Pb dating of the analyzed samples at the LEGGA can be found in Tables S3 to S6 (supplementary dataset).

For the three analyzed samples, we calculated a maximum depositional age using two different statistical methods, the “maximum depositional age’ (MDA) and “maximum likelihood age’ (MLA) (Table S6). The MDA was calculated as the weighted mean average of the overlapped analyses of the three youngest zircons and the associated 2σ uncertainty of this cluster (YC2σ[3+]; Sharman and Malkowski, 2020; Sharman et al., 2018; Dickinson and Gehrels, 2009) . The MLA is a statistical model that assumes that the zircon U-Pb ages are defined as a two-component mixture in which a “fraction of the population is derived from a discrete minimum age peak and the remaining grains follow a (log)normal distribution” (Vermeesch, 2021; Gailbraith, 2005; Galbraith and Laslett, 1993). The MLA was calculated using IsoplotR (Vermeesch, 2021, 2018).

4 RESULTS

4.1 Sedimentary facies

The Juanjuí stratigraphic section is approximately 450 m thick and comprises nine siliciclastic facies and four carbonate microfacies, which are summarized in Table 1.

4.2 Facies associations

4.2.1 Facies association 1 (FA1)

4.2.1.1 Description. Facies association 1 is made up of six facies: Gcm, St, Sp, Smb, Sr and F (Table 1, Figure 4). It vertical succession generally displays a fining- and thinning upward, and it typically has a m-scale thickness (5 m). It starts with the channelized bodies of the coarse-grained facies (Gcm) (Figure 5A, B), which grade to fine-to medium-grained arkosic sandstones with trough (St) (Figure 5C) and planar

(Sp) cross-stratifications, and it ends with cm-scale-thick, very-fine- to fine, climbing-rippled sandstones (Sr) (Figure 5D) interbedded with the fines facies (F), which is marked by root traces. The channel bodies show discontinuous and cuneiform beds, and they laterally change into interbedded fine-to medium-grained arkosic sandstones. Locally, the fine-grained trough cross-bedded sandstones are arranged in wedge-shaped sets with mm-scale mudstone layers draped over the foresets (St facies) (Figure 5F), which are highlighted by reactivation surfaces. There are also dm-scale, very-fine-grained deposits with highly bioturbated sandstone (Smb) (Figure 5E) interbedded with the fines facies (F). FA1 is observed in the lower parts of the Juanjuí section (0 – 30 m) (Figure 4).

4.2.1.2 Interpretation. Channel body geometries, such as those observed in FA1, are common deposits in tidal and fluvial settings. In both systems, channels reveal an erosive base that internally comprises upward-fining and thinning-up strata that grade upwards into shales and siltstone beds. These fines beds at the top of the succession can characterize either tidal flat or fluvial floodplain deposits (Dalrymple and Choi, 2007).

The massive conglomerates (Gcm) or cross-bedded sandstones (St) with mud clasts at erosive basal surfaces can correspond to fluvial channel filling with reworking lag deposits (Miall, 1996). However, the mud clasts in the bottom channel deposits are also common in tide-influenced environments and can occur due to the erosion of thin, muddy tidal-flat deposits made by high-energy currents (Dalrymple and Choi, 2007). Additionally, the occurrence of thin mudstone layers on the foresets of cross-bedded sandstones (St) associated with reactivation surfaces could be used to infer variations in the current speed and may indicate tidal-flow reversals (Dalrymple and Choi, 2007; Mowbay and Visser, 1984); they suggest deposition in a tide-influenced environment. In conclusion, we interpret facies association 1 as channel deposits formed in the inner part (landward) of a fluvial-tidal transition zone during the early-stage of tide-influenced channel settlement.

4.2.2 Facies association 2 (FA2)

4.2.2.1 Description. Facies association 2 is composed of five facies: Mp, Wpo, Woc, Gps and F (Table 1, Figure 4). Laterally, the facies association is represented by dm- to m-scale carbonate tabular beds (Figure 7A), which commonly occur with a flatten top and base, interbedded with m-scale, red to purple, fine-grained facies (F) (Figure

6A). It is characterized by cm-to-dm-thick beds of shelly carbonates composed of dispersed to dense microfossils (mainly ostracods and charophytes) and occasionally contains peloids and pisoids. Some beds are hybrid limestone composed of quartz grains and carbonate bioclasts (pisoids) (Gps). The vertical succession shows a coarsening-upward trend that starts with peloidal mudstones (Mp) (Figure 7B), which grade to the wackestones facies (Wpo; Woc) (Figure 7C–F) and then to the grainstone facies (Gps) (Figure 7G); generally, they are interbedded with mm-to-cm thick fine-grained structureless facies (F) (Figure 4). Poorly developed desiccation-crack surfaces are commonly present at the top of the carbonates and fine-grained beds. The fine-grained facies presented in this facies association contains numerous palynomorphs including *Echimonocolpites protofranciscoi*, *Ulmoideipites krempii*, *Cricotriporites* aff. *macroporus*, *Proxapertites psilatus*, *Momipites africanus* and *Araucariacites* sp. (Figure 6D–G) (Table 1). A microfacies analysis of thin sections made it possible to recognize the micritic matrix, which is mainly attributed to the mudstone facies (Mp) (Figure 7B), as well as the moldic porosity, which generally indicated molds of ostracod and charophyte remains (Figure 7F). FA2 has been observed approximately in two intervals of the Juanjuí stratigraphic section: 50 to 80 m and 292 to 335 m (Figure 4).

4.2.2.2 Interpretation. FA2 indicates minimum water agitation; sediments were deposited in lower-energy conditions (Flügel, 2010; Tucker and Wright, 1990), with some episodic water agitation attributed to the presence of fragmented ostracods (disarticulated valves) and sporadic terrigenous inflow due to an association with detrital quartz grains, suggesting low sedimentary transport or reworking. The peloid features may be organically induced precipitated features (Flügel, 2010). The charophyte-bearing carbonates are commonly attributed to freshwater environments, as they are ubiquitous in many ancient lake deposits (Tucker and Wright, 1990; Burne et al., 1980). The sedimentary succession presented above is indicative of deposition in a shallow lacustrine environment with evaporation and decantation processes, episodic sediment supply events and subaerial exposition.

4.2.3 Facies association 3 (FA3)

4.2.3.1 Description. Facies association 3 consists of four facies: P, Smb, Sr and Woc (Table 1, Figure 4). It is mainly composed of paleosols (P) horizons (Figure 6C) with scattered gypsum nodules in a very fine matrix, with less-common climbing-rippled

sandstone beds (Sr), bioturbated sandstone deposits (Smb) and wackestone with ostracods and charophytes (Woc). The vertical and lateral relations of the facies reveal no significant changes; there are thick paleosol intervals with sparse dm-to-m thick carbonates and sandstones beds.

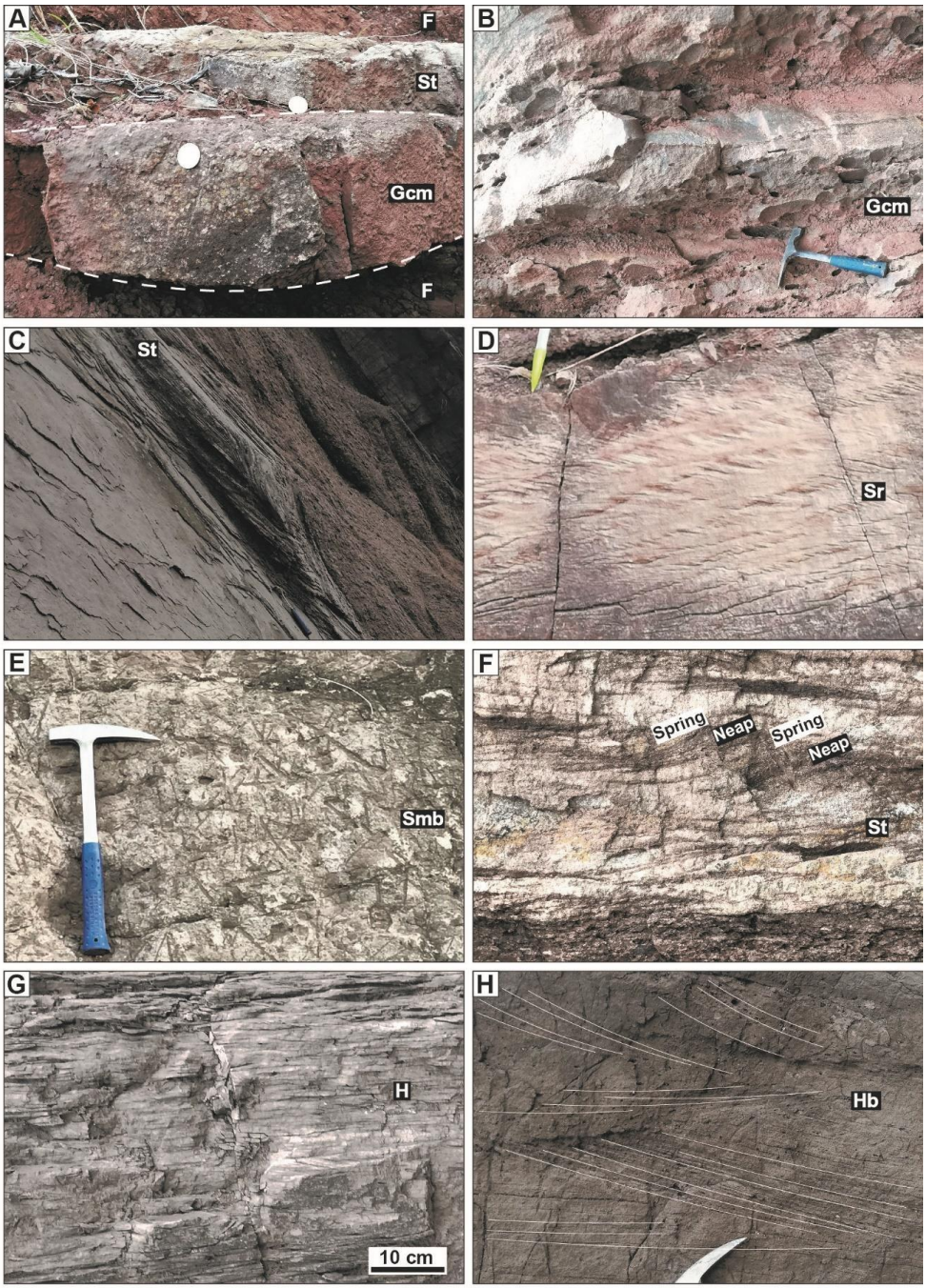


Figure 5. Representative photographs of the siliciclastic facies. A) Massive clast-supported conglomerate (Gcm) with an erosive base, limited between fines with no structures (Fm) (below) and sandstones with through cross-stratification (St) (above); B) Massive conglomerates with scattered clasts (Gcm); C) Fine-grained sandstone with through cross-stratification; D) Fine-grained sandstone with climbing ripples; E) Highly bioturbated deposits (Smb) covering the primary structures in fines bodies; F)

Thin mudstone layer drape on foresets of cross-bedded (St) fine-grained sandstones with regular variations (neap-spring influence); G) Heterolithic facies (H) with flaser bedding; H) Fine to medium-grained sandstones with bi-directional herringbone cross-stratification (Hb).

4.2.3.2 Interpretation. The carbonate nodules occurring in the paleosol intervals represent ions concentrations during processes of evaporation and capillary groundwater flow in arid periods (Nichols, 2009; Miall, 2006), indicating seasonal water fluctuations. Paleosols with root traces can indicate long periods of non-deposition and plant colonization or a low rate of accumulation.

4.2.4 Facies association 4 (FA4)

4.2.4.1 Description. Facies association 4 is composed of seven sedimentary facies: Smb, St, Sp, Sr, Hb, H and F (Table 1, Figure 4). The vertical facies association displays a coarsening and thickening upward into the section, which grades from very-fine- to medium-grained sandstones and cm-to-dm-thick to dm-to-m-thick beds. The section generally varies laterally; it is characterized by the dm-thick heterolithic facies (H) (Figure 5G) interbedded with fines (F) and fine- to medium grained cross-bedded (St) and climbing-rippled (Sr) sandstones. Occasionally, it shows herringbone cross-stratification (Hb) (Figure 5H) or planar cross-bedded (Sp) sandstones. The medium-grained cross-bedded (St) sandstones can present dm-thick wedge-shaped beds, with a concave-up base and mm-scale mudstone layers draped over the foresets (St facies), which are highlighted by reactivation surfaces, grading to climbing-rippled (Sr) sandstones. The highly bioturbated sandstones (Smb) are commonly interbedded with the fines (F) facies, showing no lateral variation. FA4 was recognized in the upper part of the present section, in the interval from about 380 to 442 m.

4.2.4.2 Interpretation. Heterolithic facies with flaser, wavy and linsen bedding, cross-bedded sandstones with thin mudstone drapes on the foresets, reactivation surfaces and herringbone cross-bedded sandstones point to an environment influenced by tidal currents. The presence of reactivation surfaces might have been caused by tidal current reversals (Thomas et al., 1987; De Mowbray and Visser, 1984; Klein, 1970) although these surfaces could also be produced by river-discharge variations in fluvial settings (Dalrymple, 1984). Despite the fact that the H facies can be observed in river-dominated settings (Johnson and Dashtgard, 2014), the mud-sand-mud profile is not

observed in bars further landward (Dashtgard and Gingras, 2012) and is more common in tide-dominated systems (Dalrymple and Choi, 2007; Dalrymple et al., 2003). Reactivation surfaces and mud layers might occur in fluvial point bar deposits (Collinson, 1996; Miall, 1996). The occurrence of bidirectional trough cross-bedding (Figure 5H) suggests a depositional área that received opposite-direction currents, which are characteristic of a tide-dominated environment (Longhitano et al., 2012) and can be either flood or ebb currents. The regular variations in the lamina thickness characterize rhythmic sedimentary structures, which are well documented in subtidal channels (Allen and Homewood, 1984; Visser 1980), and they could be interpreted as the influence of a neap-spring tidal cycle (Flemming, 2012; Dalrymple and Choi, 2007). In conclusion, we interpret facies association 4 as deposits formed in the distal part of a fluvial-tidal transition zone.

4.3 Depositional environments

The integration of the sedimentary facies association, paleontological content and stable isotopic compositions make it possible to characterize two depositional systems during the Maastrichtian-Bartonian: a tide-dominated depositional system and a lacustrine deposition system (Figures 4 and 10).

4.3.1 Tide-dominated environment : The fluvial-tidal transition zone

The tide-dominated depositional system was recognized in the Maastrichtian and late middle Bartonian (Figures 4 and 10A, C). This depositional system is composed of two facies associations: FA1 and FA4.

During the Maastrichtian (0 to 40 m along the section), FA1 generally prevails, and it is mainly composed of m-scale coarse-grained channelized shapes with upward-fining and thinning-up strata. The vertical stacking pattern and lateral changes of conglomerate facies to sandstone and finer facies were most probably related to a proximal area within a fluvial-tidal transition zone (landward) that experienced a less-tide-dominated influence. These Maastrichtian tidal deposits can be correlated with those of the Vivian-Cachiyacu-Huchpayacu formations (Calvès et al., 2018; Hurtado et al., 2018; Louterbach et al., 2014). During the late-middle Bartonian (~350 to 450 m), FA4 is more abundant than FA1. The sedimentary stacking pattern reveals a tide-dominated environment, which is mainly represented by heterolithic facies interbedded with fines and climbing-rippled beds and also by typical tidal-current reversal deposits, such as herringbone cross-bedded sandstones. Reactivation surfaces and

herringbone cross-bedding are more common in the distal area within a fluvial-tidal transition zone (seaward direction), where it is possible to recognize tidal bundles (Dalrymple and Choi, 2007). Compared with the Maastrichtian sedimentary rocks, these deposits are more deeply bioturbated. These Bartonian tide-influenced deposits can be correlated with the shallow marine deposits of the Pozo Fm. (see Roddaz et al., 2010, and the references therein).

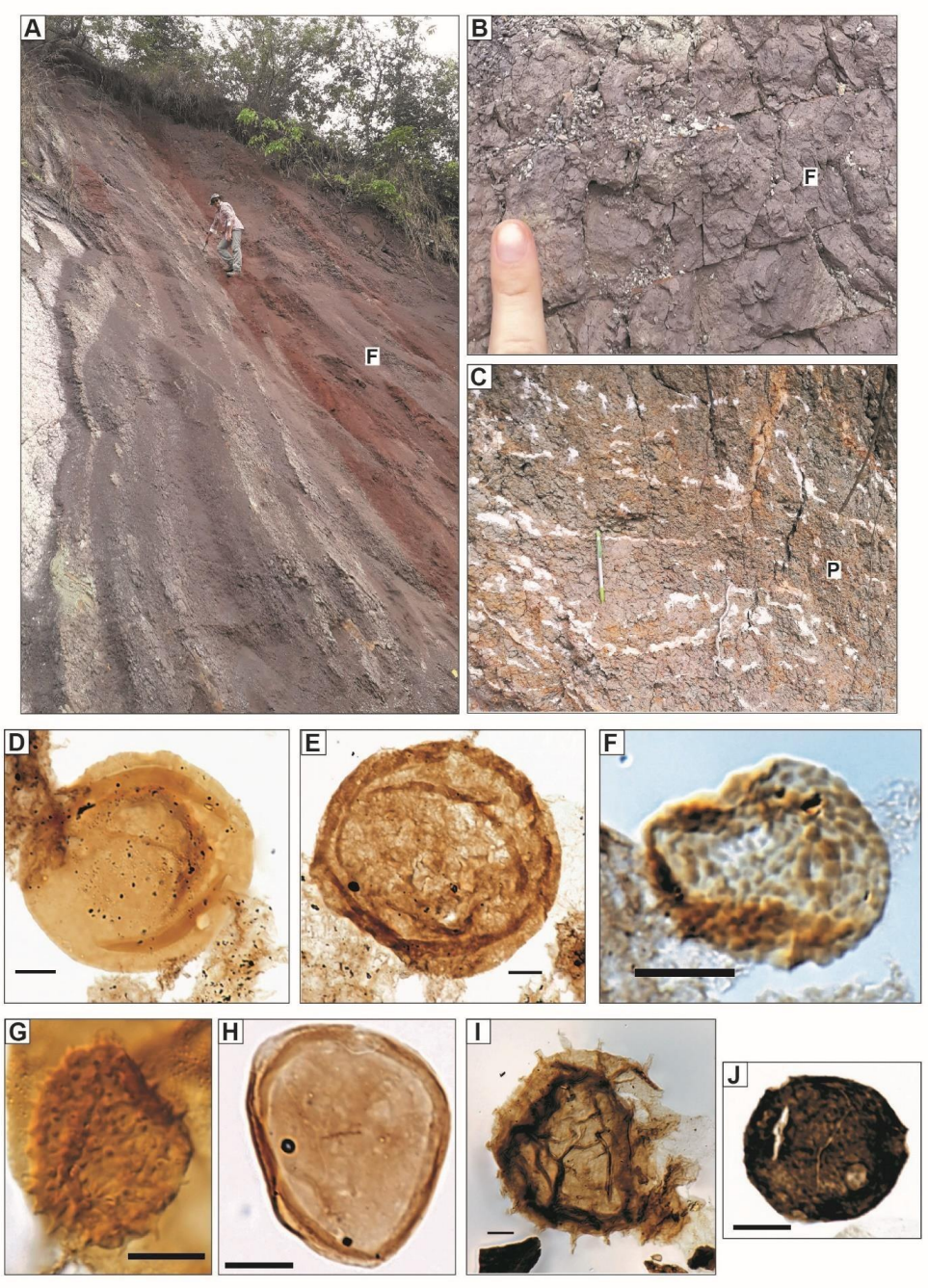


Figure 6. Fine-grained facies; paleosols and palynological content. (A) Overall m-scale view of massive mudstones and siltstones, with red to purple colors, interbedded with cm-dm tabular carbonate beds. (B) Massive siltstones, presenting purple to green-grey colors, latter probably related to weathering processes. (C) Paleosols with incipiente

horizontal lamination, mottled horizons. (D) *Cricotriporites* aff. *macroporus*, slide 47176_A, England Finder (EF) W13; (E) *Araucariacites* sp., slide 47176_A, EF N12/2; (F) *Ulmoideipites krempii*, slide 47176_A, EF S8/4; (G) *Echimonocolpites protofranciscoi*, slide 47176_A, EF Q12/1; (H) *Proxapertites psilatus*, slide 47179_B, EF F15; (I) *Balmeisporites minutus*, slide 47179_B, EF S33/4; (J) *Momipites africanus*, slide 47179_B, EF M5/2. Scale bar= 10um.

4.3.2 Lacustrine environment

The lacustrine depositional system was recognized in the Maastrichtian and the Lutetian (Figures 4 and 10A, B). This depositional system is composed of two facies associations: FA2 and FA3.

The lacustrine setting starts with FA2. The sedimentary stacking pattern is mainly composed of continuous carbonate beds interbedded with shales and siltstone beds with a coarsening-upward trend; Gps and Woc are present at the top of the succession (Figure 4). This facies association occurs from approximately 50 to 80 m and from 292 to 350 m. This facies association was deposited under absent to low-energy hydrodynamic conditions, recording a shallowing-upward succession. The carbonates at the base of the sequence are mainly composed of the mudstone peloidal facies (Mp), which grades to the wackestones (Wpo, Woc) and grainstones (Gps) facies at the top. The sedimentar features observed in FA3 indicate a transition from ephemeral events under arid conditions to a period of low accumulation rates or long periods of non-deposition. The dominance of mudstone facies and the poor development of grainstone facies are interpreted to reflect lower wave energies and point to shallow lake environments (Platt and Wright, 1991). This is in agreement with the presence of charophytes, which are the dominant carbonate producers in low-energy and shallow freshwater settings (Platt and Wright, 1991). The lacustrine carbonates / shelly strata represented by FA2 and FA3 can be correlated with the fluvial-lacustrine Yahuarango Fm. (Roddaz et al., 2010; Hermoza et al., 2005; Gutierrez, 1982; Kummel, 1948).

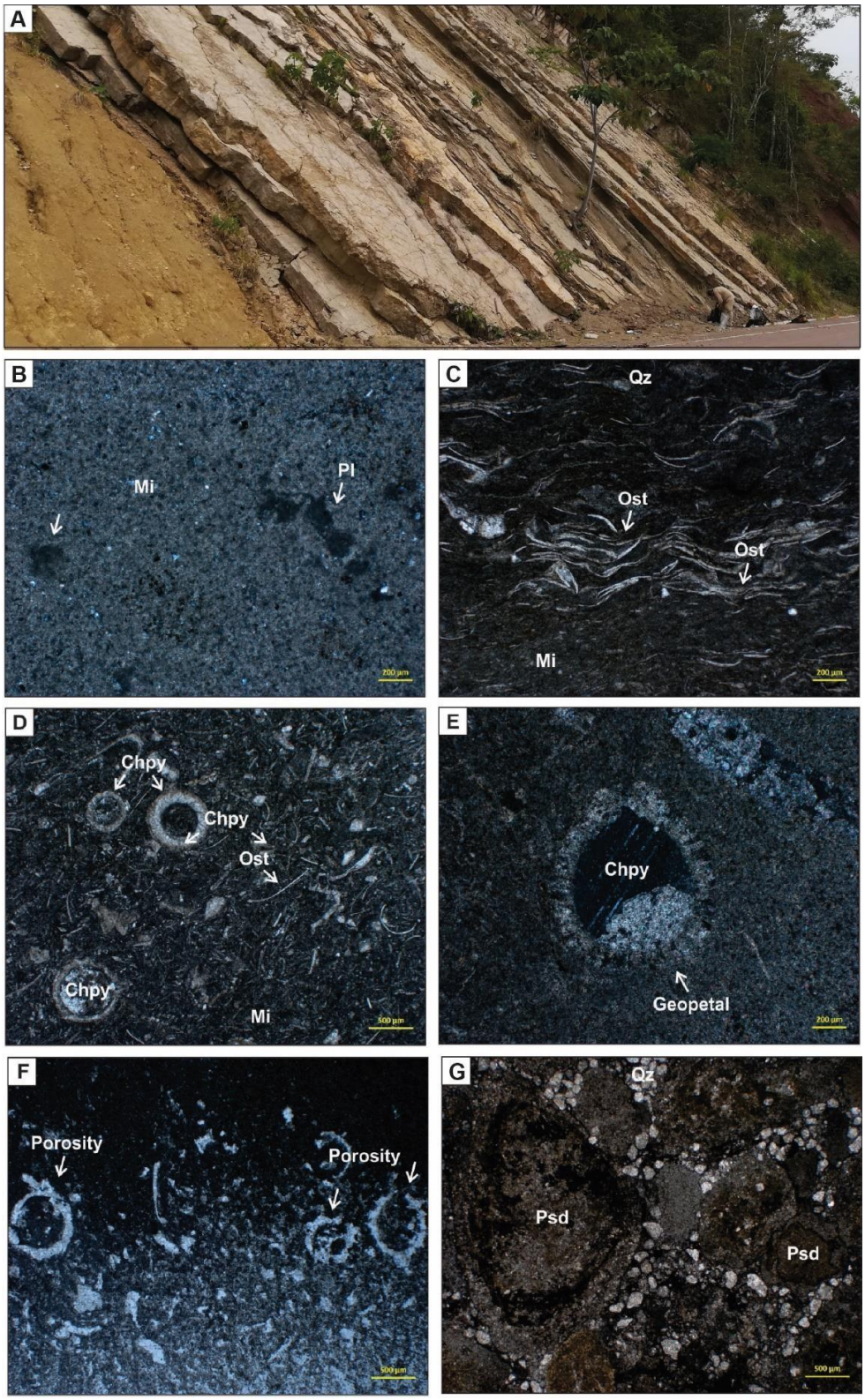


Figure 7. Representative photographs of carbonate microfacies. A) General view of the carbonate outcrops; B) Mudstone deposits with scattered peloids (Mp) with clotted texture (HUA63B); C) Dark-brown wackestones with peloids and ostracods (Wpo) (HUA63C), characterized by disarticulated valves of ostracods oriented parallel to bedding of rock; D) Wackestone with scattered bioclasts as fragmented ostracods and charophytes (Woc) (JUA5A); E) Geopetal structure and recrystallized by spar marked

in the inner part of charophytes (JUA5B); F) Moldic porosity is identified as secondary pores in charophytes (JUA5C); G) Fragments of pisoids partially replaced by pyrite (?) (JUA 2B). Mi= micrite; Pl= peloids; Ost= ostracod; Chpy= charophyte; Psd= pisoid.

4.4 Oxygen and carbon stable isotopes

The results and variations of the stable isotopic compositions (C, O) of the analyzed samples are presented in Figures 4 and 9, and Table S2 (Supplementary Material). The analyzed stable isotopic data were compared with stable isotope values from Amazonian Miocene fossils (Alvim et al., 2021). North American rivers, the Great Lakes, North Atlantic seawater, the Black Sea and the San Francisco Bay estuary (Varol, 2015; Logvina et al., 2004; Ingram et al., 1996; Keith et al., 1964) (Figure 9). It is important to emphasize that, despite using the stable isotopic compositions of modern sites distinct from our localities, the isotopic fractionation processes at these sites are likely to have occurred in similar environments (e.g., lakes, estuaries or seas).

The succession exhibits significant variations in δ13C and δ18O, as shown in Figure 3. In the first 53 m from the base to the top, the δ13C values increase from -11.5 to -4.2‰ (JUA 1A-E) (Figure 4, Table S2). Between 53 and 82 m, most samples range from -7.3 to -6.0‰, except for the sample JUA 2B, which presents a strong negative carbon isotopic value (-11.1‰). Between 82 and 350 m (Lutetian), the δ13C values increase slightly to between -10.0 and -2.8‰, and then they shift to low values (-11.9 to -10.0‰) in the Upper part of the series (Bartonian).

The δ13C and δ18O values for the analyzed samples are negative, varying between -11.9 to -2.8‰ and from −10.2 to -1.1‰, respectively (Figures 4 and 9). The youngest samples (located between 382 and 392 m in Figure 4) are characterized by the most negative δ13C values and plot within the North America river isotopic field. The isotopic compositions of the Lutetian samples are more scattered. Most of the samples have isotopic compositions similar to those of the Contamana Neogene fossils analyzed by Alvim et al. (2021) (dinoflagellate-, oyster- and foraminifer-yielding beds CTA-77 and CTA-58). Four samples are characterized by negative δ18O values and plot between the Great Lakes and NA river fields (Figure 9). The four youngest samples that are associated with the TAR-78 fossil-bearing site have the highest δ18O values and plot close to or within the isotopic field of the San Francisco Bay (Figure 9). The Lutetian samples plot mostly between the NA river and Great Lakes fields, whereas

the Maastrichtian and Bartonian samples have δ13C and δ18O values within or close to the NA river field (Figure 9).

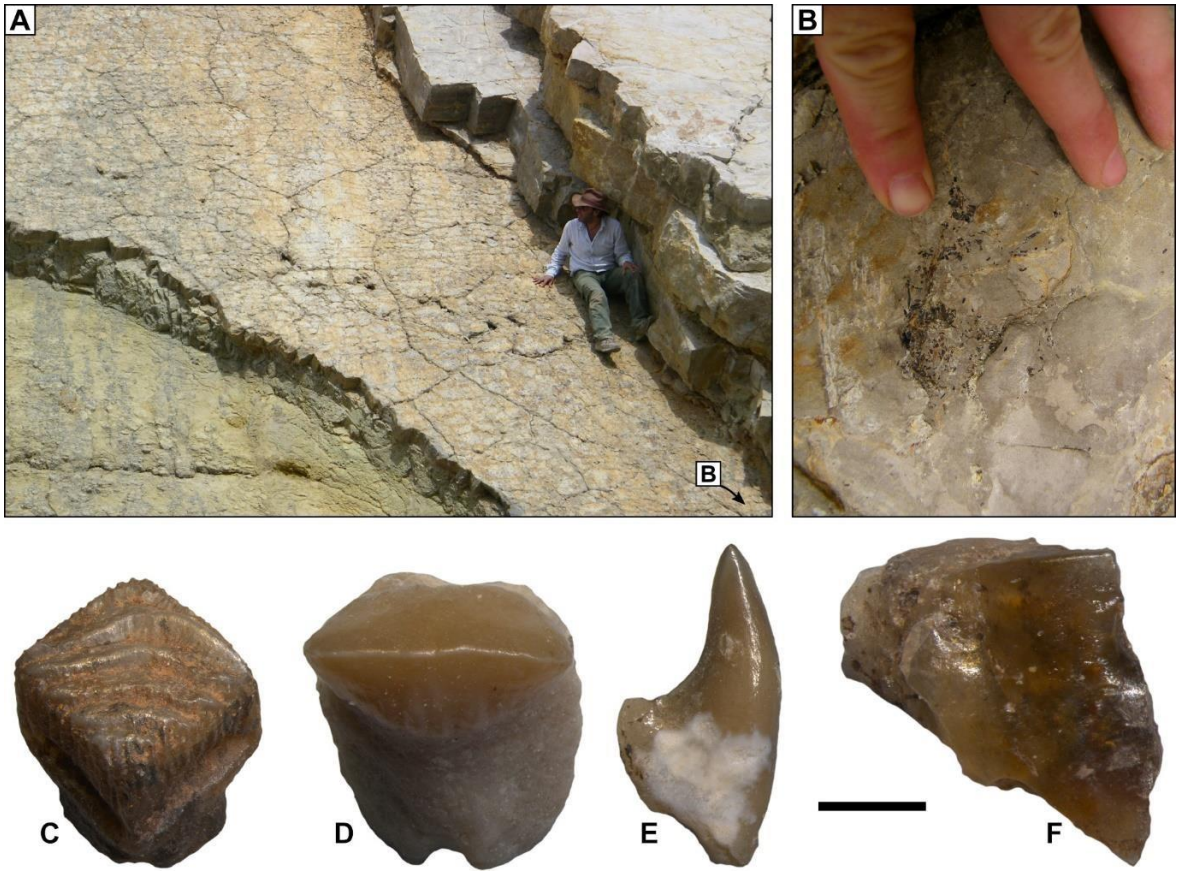


Figure 8. Selected vertebrate-related findings and vertebrate fossils of interest from the Maastrichtian–Paleogene Juanjuí section, San Martín, Peru. A) Paddling-turtle track at TAR-29 (=HUA-63; Maastrichtian). The turtle was moving to the right. The same carbonated layer provided the regurgitation ball seen in B; B) Regurgitation ball (of an aquatic bird?), with fish bones and scales both gathered and split all around (TAR-29 = HUA-63; Maastrichtian); C) *Pucapristis hoffstetteri*, tooth in occlusal view (TAR-41, Maastrichtian); D) *Ouledia* sp., tooth in occlusal view (TAR-30 sup. = HUA-473; Lutetian); E) *Stephanodus* sp., pharyngeal tooth in lateral view (TAR-30 sup. = HUA-473; Lutetian); F) Polypterid polypteriform, fragmentary ganoin scale in external view (TAR-42 = JUA 14; Bartonian). Scale bar = 1 mm (C, E) and 0.5 mm (D, F).

Carbon and oxygen isotopic data exhibit isotopic values that indicate non-marine environmental conditions (δ13C from -11.9 to -2.8‰ VPDB and δ18O from -10.2 to -1.1‰ VPDB (Figures 4 and 9). According to the isotopic signatures, the deposits present a covariance of negative δ13C and δ18O isotopic compositions, which could support predominantly freshwater conditions (Vonhof et al., 1998). The δ13C and

δ18O isotopic values of the upper part of this depositional system (samples HUA 473 N to Q, located from ~ 311 to 333 m; Figure 4) are much less negative (δ13C ranging from -8.2 to -2.8‰ and δ18O from -6.6 to -1.1‰) (Figures 4, 9 and S2), which could reflect a transition to brackish conditions in an estuarine depositional system (Figures 4 and 9) (Ingram et al., 1996). The fossil record is also in agreement with this paleoenvironmental transition, from freshwater to brackish conditions, which is indicated by the presence of i) marine, estuarine or brackish pycnodontiform ray-finned fish and myliobatiform selachians (*Potobatis* and *Ouledia*; Figure 8D) at TAR-30, and ii) pelomedusoid turtles, of brackish affinities at TAR-78.

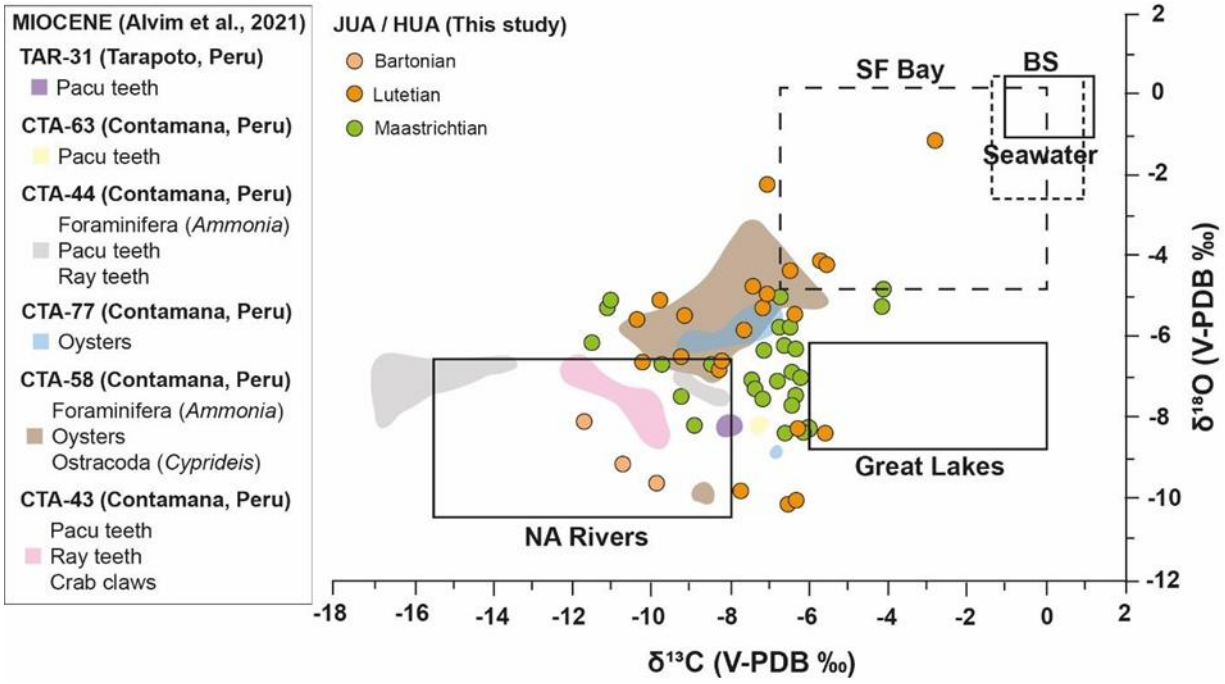


Figure 9. Carbon versus oxygen isotopes cross plot of Miocene (Alvim et al., 2021) and Eocene fossil and carbonates samples. Black boxes represent stable isotopes values of modern mollusks from North Atlantic seawater, Great Lakes, and North American rivers (Keith et al., 1964), the San Francisco Bay estuary (Ingram et al., 1996) and the Black Sea (Varol, 2015).

4.5. Biostratigraphic constraints: Paleontological content of the Juanjuí Maastrichtian–Eocene section

The TAR-59 sample (labeled in green in Figure 4) provided no macrofossil content, but crushed bone fragments, most likely documenting medium-sized dinosaurs, were retrieved from JUA 1B, 30 m below in the same section (Figure 4). Conversely, a palynological sample (TAR-PN-16-09) yielded an assemblage dominated by the freshwater algae *Pediastrum* (about 98% out of 300 grains counted)

and other panchronic taxa, such as the fern spore *Laevigatosporites* sp., dinocysts assignable to *Batiacasphaera*, and reworked acritarchs.

The TAR-29 sample (labeled in green in Figure 4) has yielded charophyte oogonia by the thousands (unidentified), silicified plant cuticles, unidentified turriform gastropods, ostracods (under study), freshwater bony fish remains (pacu-like characiform teeth and loricariid siluriform iridescent dermal scutes), chelonian osteoderm fragments, a paddling-turtle trackway (collapsed in 2015; Figure 8A) and waterbirds regurgitated pellets (with numerous fish scales and spines; Figure 8B) in the uppermost levels of the exposure. Unfortunately, this assembly does not allow any precise biostratigraphic dating. Conversely, palynological samples TAR-29-PN2/19 (stratigraphic meter 79), TAR-29-PN4A-19 (stratigraphic meter 81.4) and TAR-29-PN5-19 (stratigraphic meter 81.6) from the same sample point to a Maastrichtian age (based on the palynological zonation of Jaramillo et al. (2011) and De La Parra et al. (2021)). They are characterized by rich terrestrial organic matter and palynomorphs (Figure 6D–J), including abundant *Araucariacites* (gymnosperm), *Gnetaceaopollenites* (gymnosperm), *Pediastrum* (freshwater algae), *Echimonocolpites protofranciscoi* (angiosperm), *Ulmoideipites krempii* (angiosperm), *Longapertites* (angiosperm, palms), *Cricotriporites* aff. *macroporus* (angiosperm), *Echitriletes selaginelloides* (fern), *Racemonocolpites* (angiosperm, palm), abundant *Proxapertites psilatus* (gymnosperm Araceae), *Momipites africanus* (angiosperm), *Foveotriletes* aff. *margaritae* (fern) and *Balmeisporites minutus* (fern). The additional palynological samples TAR-29-PN1/19, TAR-29-PN3/19 and TAR-29-PN4/19 did not provide useful results.

Aside from unidentified charophyte oogonia and ostracods (under study), the TAR-30 sample (base + top) yielded a species-rich fish assemblage, with ray-finned taxa (characins: pacu- and piranha-like teeth; iridescent dermal scutes of loricariid siluriforms; *Stephanodus* pharyngeal teeth; Figure 8E), selachians (Myliobatiformes: the batoid *Ouledia* sp. (Figure 8D) and the dasyatoid *Potobatis*) and dipnoans (Ceratodontidae/Lepidosirenidae). *Ouledia* (Thanetian–Priabonian) and *Potobatis* (Danian–Thanetian) had also been recognized in shallow marine-influenced Thanetian deposits of the Madre de Dios Basin, in association with pycnodontiform pycnodontids (Louterbach et al., 2014). The TAR-30 fauna also include turriform gastropods, pelomedusoid turtle shell fragments, and crocodylomorph teeth. As a whole, the fauna point to a Thanetian biostratigraphic age, which is supported by close affinities with the

Thanetian ichthyofauna of the Madre de Dios Basin (Louterbach et al., 2014), at least in the absence of younger strata yielding similar assemblages.

The TAR-78 sample yielded charophyte oogonia and half a carapace of a pelomedusoid turtle, of brackish affinities (under study by Edwin Cadena).

At the top of the studied section, the TAR-42 sample yielded a ganoin scale of a polypterid polypteriform (Latinopollia or Dagetella; Figure 8F), as well as turtle shell fragments, a large crocodylomorph osteoderm, and a fragmentary lower molar of a tiny South American native ungulate (SANU), documenting a panperissodactyl (Notoungulata or Litopterna). The last appearance datum (LAD) of polypteriforms in South America is Paleocene in age (Gayet et al., 2002). The occlusal pattern and dimensions of the panperissodactyl are in good agreement with a Thanetian–Ypresian biostratigraphic age and at odds with post-early Eocene SANUs.

4.6 U-Pb ages

Table 2 present the U-Pb zircon ages for the analyzed Cenozoic sedimentary rocks. Details on individual U-Pb zircon ages for each sample can be found in the supplementary material (Tables S2 to S6). The zircon population of the Cenozoic samples is dominated by grains from the Eocene Andean Arc (<0.065 Ga) (Table 2). The other dominant zircon populations are Grenville Sunsás (1.3–0.9 Ga) and to a lesser extent, Rondonia-San Ignacio (1.54–1.3 Ga) and Rio Negro-Jurena (1.82–1.54 Ga). The maximum depositional ages (MDAs), calculated as the weighted mean of YC2σ[+3] following Sharman and Malkowski (2020), are Eocene MDAs. The MDAs decrease up-section from ~43.1 ± 0.29 Ma (Lutetian, JUA 8A/19), to ~ 42.6 ± 0.32 Ma (Lutetian, JUA 11) and ~38.6 ± 0.19 Ma (Bartonian, JUA 14) in the upper part of the section (Figure 4, Table S2). The calculated maximum likelihood ages (MLAs) following Vermeesch (2021) are also Eocene ages. The MLAs range from ~43.5 ± 0.64 Ma (Lutetian, JUA 8A/19) to ~42.68 ±0.66 Ma (Lutetian, JUA 11) and ~37.64 ± 0.85 Ma (Bartonian - Priabonian, JUA 14) (Figure 4, Table S2). Overall, the MDAs and MLAs are quite similar, and they both decrease up-section.

5. Discussion

5.1 Age of the deposits

The first stratigraphic constraint regarding the studied sedimentary section is the biostratigraphic age of the TAR-59 sample. This locality yielded unambiguous dinosaur fossil remains. In addition, large dinosaur footprints were identified at the TAR33

outcrop that can be correlated with the TAR 59 sample (Supplementary Data S7); these footprints are consistent with the Maastrichtian interval (72.1–66.0 Ma) (Figure 4 and Supplementary Data S7). The TAR-59 sample has the same stratigraphic position as the HUA 63 sample (Figure 4), which was previously studied by Hurtado et al. (2018). Originally, a Danian age was assigned to HUA 63 (Hurtado et al., 2018) because it was mistakenly supposed to be intercalated between the TAR-29 fossil site, which yielded a rich charophyte assemblage with a composition similar to the Danian beds of the Ucayali Basin (Agua Caliente, CTA-54 locality; Antoine et al., 2016), and TAR30, which yielded a rich ichthyofauna, notably including the Danian dasyatid marker *Potobatis* sp. (Cappetta and Gayet, 2013). However, our revised fieldwork suggests that HUA 63 is located below the TAR29 sample, and is associated with the TAR-59 fossil site instead (Figure 4). The presence of several key biostratigraphic palynomorphs, including *Echimonocolpites protofranciscoi*, *Ulmoideipites krempii*, *Momipites africanus* and *Foveotriletes* aff. *margaritae*, which were found in the TAR-29 sample (PN2/19, PN4A-19, and PN5-19 located at 79, 81.4 and 81.6 m above the stratum level, respectively) also suggest a Maastrichtian age. Hence, the first 150 m of the Juanjuí sedimentary section as a whole may be ascribed to the Maastrichtian Cachiyacu Fm. Moreover, the contact between Maastrichtian and the overlying Cenozoic sedimentary rocks is located at ~ 150 m in the sedimentary section (Figure 4). Paleosol horizons are found above and below this contact (Figure 4). Paleosol horizons are found above and below this contact (Figure 4).

Above these paleosol horizons, the three analyzed Cenozoic sedimentary rocks presented MDAs that range from the Lutetian (JUA 8A/19, 43.1 ± 0.29 Ma, located at 170 m, and JUA 11, 42.6 ± 0.32 Ma, located at 375 m) to the Bartonian (JUA 14, 38.6 ± 0.19 Ma) located at 440 m (Figure 4). The MLAs of the analyzed samples show similar Lutetian (JUA 8A/19, 43.5 ± 0.64 Ma), and JUA 11, 42.7 ± 0.66 Ma) and Bartonian to Priabonian ages (JUA 14, 37.6 ± 0.85 Ma) (Table S6). These MDAs and MLAs are significantly younger than the biostratigraphic ages obtained from the fossil-rich outcrops TAR-30, TAR-78 and TAR-42. The JUA 8/19A samples, which yield a Lutetian MDA (43.1 ± 0.29 Ma), are stratigraphically below the TAR-30 outcrop, which has a Thanetian biostratigraphical cachet, based on the co-occurrence of the selachians *Potobatis* and *Ouledia* (Paleocene and Thanetian–Priabonian ranges, respectively; Louterbach et al., 2014, and the references therein). Similarly, the Bartonian to Priabonian zircon MDAs and MLAs of sample JUA 14 are significantly younger than the Thanetian–Ypresian biostratigraphical age of TAR-42 (which yielded

polypterid scales of presumed Maastrichtian–Paleocene age and a tiny early-diverging SANU of Paleocene–early Eocene hypothesized affinities), which is situated at the same stratigraphic level. In both cases, this temporal discrepancy may be related to unexpected longer stratigraphical ranges of remarkable fossil taxa, due to last appearances much younger than previously thought for *Potobatis* (world scale) or *Ouledia* and the polypterids (South American scale).

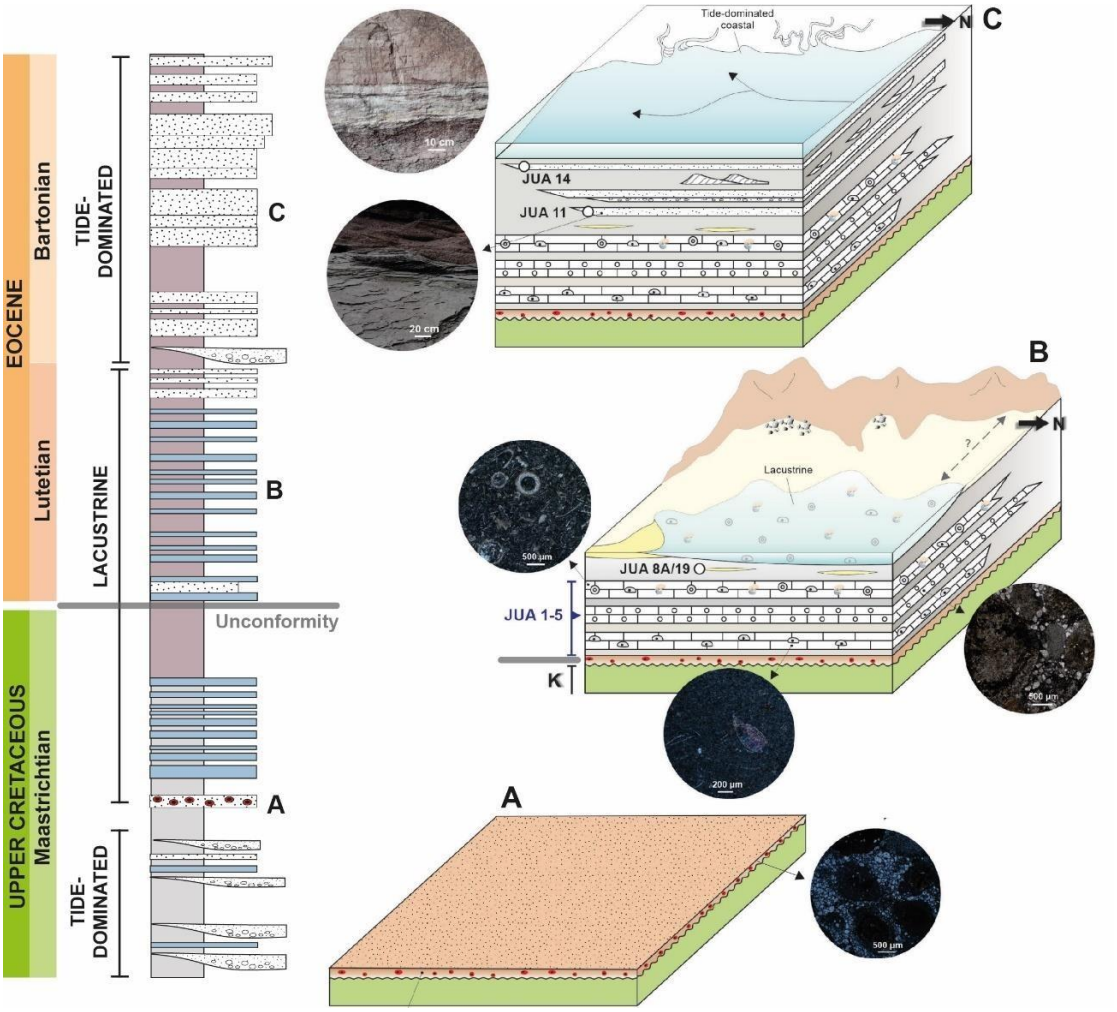


Figure 10. Schematic composite section and 3D sketch representing the paleoenvironmental reconstruction of the (A) Maastrichtian – Paleogene stratigraphic unconformity, (B) Lutetian lacustrine setting, (C) The Bartonian transition from lacustrine system to the tide-dominated setting, represented by the distal part in a fluvial-tidal transition zone. See text for details.

According to the MDAs and MLAs, the faunal content of the fossil site TAR-30 may not be Danian but Lutetian in age and the fossil sites TAR-78 and TAR-42 are Lutetian and Bartonian in age, respectively (Figure 4). These results suggest that i) the

analyzed samples are part of the Eocene Pozo Fm. (Roddaz et al., 2010) and ii) contrary to what was published in Roddaz et al. (2010), the Paleocene Yahuarango Fm. may be absent in the Huallaga Basin.

Table 2. Table showing the number and percentage U-Pb ages of zircons grains by distinct geochronological events in potential source areas on the Amazon craton and the Northern central Andes. Temporal ranges of events according to Bahlburg et al. (2009), Chew et al. (2008) and Reimann et al. (2010). (n) is the number of samples analyzed for the time interval.

Time (Ga)	Province/Event	EOCENE	Lutetian		Bartonian
			JUA 8A-19	JUA 11	JUA 14
			n = 69/77	n = 102/120	n = 102/112
			(%)	(%)	(%)
<0.065	Cenozoic Andean Arc		14	28	38
0.145–0.065	Cretaceous Andean Arc		4	0	2
0.25–0.145	Triassic-Jurassic		0	1	7
0.4–0.26	Paleozoic Magmatic Arc		6	3	3
0.5–0.4	Famatinian		3	4	2
0.7–0.5	Brazilian		12	13	6
0.9–0.7			6	1	2
1.3–0.9	Greenville Sunsás		29	33	25
1.54–1.3	Rondonia - San Ignacio		3	7	8
1.82–1.54	Rio Negro - Jurena		10	6	7
2.0–1.82	Ventuari - Tapajós		6	1	0
2.2–2.0	Maroni - Itacaiunas		6	2	0
>2.2	Central Amazon		1	1	0

5.2 Paleogeographic implications

Our multidisciplinary dataset provides new constraints on the paleoenvironmental evolution of Western Amazonia during the Maastrichtian – Bartonian (late middle Eocene).

Our data suggest that a tide-dominated system occupied the Huallaga Basin during the Maastrichtian. Previous paleogeographic reconstructions of the late Cretaceous configuration of Peruvian Western Amazonia also suggest that the Madre de Dios and Marañon basins were characterized by shallow marine deposits during the Campanian–Maastrichtian (Louterbach et al., 2018b; Zamora and Gil, 2018). In Ecuador, the Maastrichtian basal Tena sandstones of the Oriente Basin are also interpreted to represent tide-dominated deposits (Jaillard et al., 2005). The Upper Cretaceous units in neighboring basins (e.g., Vivian and Cachiyacu formations in the Santiago, Marañon and Madre de Dios basins) are also characterized by shallow marine paleoenvironments (Zamora and Gil, 2018, and the references therein). A coastal paleo-environment is also suggested in the Bagua Basin (Moreno et al., 2020). As already emphasized by previous published studies (Hurtado et al., 2018; Zamora and Gil, 2018), this suggests that Western Amazonia basins were entirely flooded by an epicontinental sea at some point by the Maastrichtian.

At the Cretaceous–Paleogene boundary, a marine-to-continental transition was recorded in the northernmost part of the Andes, coeval with regional records for the onset of compressional deformation in the northern Andes (Central and Eastern Cordilleras) (Zapata et al., 2021; Bayona et al., 2021; George et al., 2019; Gutiérrez et al., 2019; Odoh et al., 2019; Horton, 2018). This transition from shallow marine/coastal to continental paleoenvironments is also recorded in the Huallaga Basin, but it occurred during the Maastrichtian, as indicated by the transition from a tide-dominated depositional system to a continental lacustrine depositional system.

Our new stratigraphic constraints suggest that the Paleocene-to-lower Eocene interval (66–47.8 Ma) may be documented by a 2-m-thick paleosol facies (Figure 4), indicating that a stratigraphic unconformity may separate the Maastrichtian from the Lutetian–Bartonian sedimentary sequences of the Huallaga Basin (Figures 4 and 10). A similar chronostratigraphic hiatus was observed to the north in the Oriente Basin (Ecuador) where the sedimentary deposits of the Lower Eocene Tiyuyacu Fm. unconformably overlie the Upper Cretaceous Tena Fm. (Gutiérrez et al., 2019). In Colombia, a regional unconformity was recognized on the eastern side of the Southern Llanos Basin (Colombia), which separates the pedogenized Cretaceous rocks from the overlying Middle or Upper Eocene rocks (Caballero et al., 2020). To the northwest, in the Bagua Basin (Peru) (Figure 11A), the Paleocene series are also absent, as shown by i) the absence of Paleocene MDAs obtained for U-Pb in zircons in the Upper Cretaceous to

Miocene sedimentary rocks of the Bagua Basin (Moreno et al., 2020), and ii) the presence of a low-angle unconformity between the Campanian–Maastrichtian Fundo el Triunfo Fm. and the overlying Lower Eocene Rentema Fm. (54.2 ± 6.4 Ma) (Naeser et al., 1991). This regional unconformity could be generated by the presence of a migrating forebulge in response to Andean tectonic loading or tectonic quiescence (Horton, 2022). However, we believe that a forebulge unconformity is unlikely to have generated the Maastrichtian-to-Lutetian unconformity recorded in the Huallaga Basin, since an Andean provenance is recorded below and above this unconformity (HUA 63 in Hurtado et al. (2018) and JUA 8A/19 in this study). Following Horton (2022), we propose that a tectonic quiescence marked by a prolonged pause in crustal shortening and flexural loading may have promoted isostatic rebound and the development of an unconformity. In this scenario, we suggest that the Paleocene corresponded to a stage of tectonic quiescence in the Huallaga Basin.

In the Madre de Dios Basin, previous paleogeographic reconstructions suggest that a shallow marine transgression occurred during the late Paleocene (Louterbach et al., 2014). At the time of the publication of this article, the entrance of this shallow marine Transgression (Atlantic Ocean, Pacific Ocean or Caribbean Sea) was still unclear. Here, We suggest a southern connection with the Atlantic Ocean (Bolivia–Argentina) through The Parana Sea (Figure 11A), given the absence of Paleocene deposits in the Huallaga, Bagua and Llanos basins. In this scenario, the upper Paleocene shallow marine deposits of the Madre de Dios Basin may represent the northern end of the Paleocene Parana Sea, which is also recorded by deeper marine deposits in the southern basins, such as the Potosí and Chaco basins (Cappetta and Gayet, 2013; Sempere et al., 1997).

Our data also recorded a shallow marine transgression that may have started during the Bartonian (Late middle Eocene), as indicated by the presence of a tide-dominated coastal depositional system (FA4) (from 42.6 to 38.6 Ma) that overlies the Lutetian lacustrine system (FA2 and FA3). In a tide-dominated estuarine setting, bidirectional currents are likely to be present in the meandering part of the tide-dominated estuary (Dalrymple and Choi, 2007; Dalrymple et al., 1992). This Bartonian shallow marine incursion could be correlated with the Eocene Pozo shallow marine transgression (Hoorn et al., 2010b; Roddaz et al., 2010) that affected the Marañón Basin, which is located east of the studied area (Roddaz et al., 2010; Hermoza et al., 2005; Hermoza, 2004). Moreover, this shallow marine incursion was also recorded in the Santiago Basin (George et al., 2019), within the Pozo and Capas Rojas formations.

Based on i) the absence of Eocene deposits in the southern Peruvian Madre de Dios and northern Bolivian Beni basins (Louterbach et al., 2018a; Louterbach, 2014; Roddaz et al., 2010; Hermoza, 2004), the presence of ii) Upper middle Eocene shallow marine sedimentary rocks (from 42 to 37 Ma) in the Colombian Llanos Basin (De La Parra et al., 2021) and iii) the presence of Eocene shallow marine deposits in the Ecuadorian Oriente Basin (Roddaz et al., 2010; Christophoul et al., 2002), a northern entrance through the Caribbean Sea is suggested for this Bartonian transgression (Figure 11B).

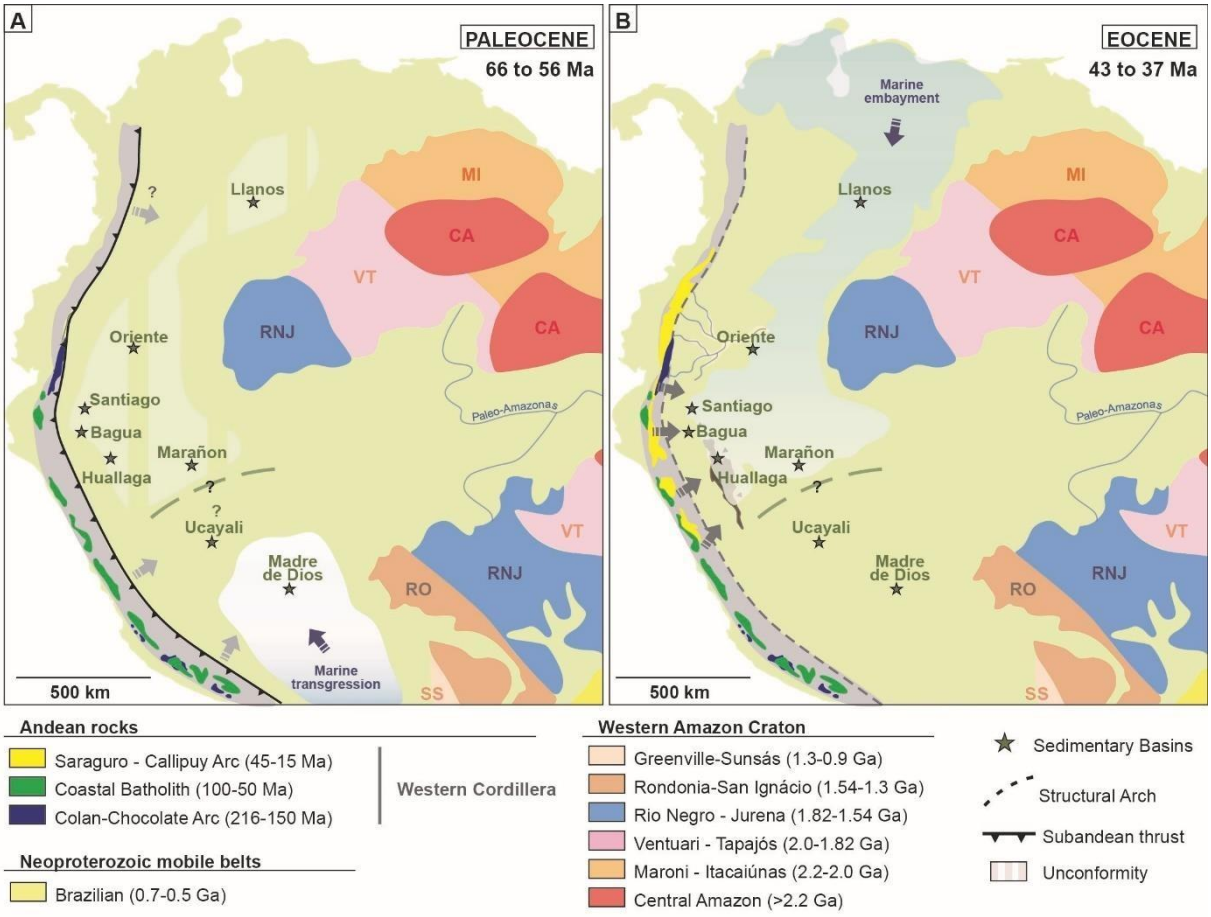


Figure 11. Paleogeographic maps of Western Amazonia in Paleocene (A) Eocene (B) times. A) During the Paleocene, the northern part of the Western Amazonian basins are characterized by the presence of a regional unconformity while the southern part experienced shallow marine transgression (Louterbach et al., 2014). B) During the Eocene, the northern part likely experienced shallow marine embayment during short time-intervals through a connection with the Caribbean Sea while the southern part (the Madre de Dios Basin) is characterized by the absence of Eocene deposits (Louterbach, 2014).

Conclusions

The multi-disciplinary study (biostratigraphy, sedimentological data, U-Pb zircon ages, and stable isotope composition) of the Upper Cretaceous-Paleogene sedimentar rocks documented in the Juanjuí stratigraphic section of the Huallaga Basin yields the following conclusions:

- The maximum depositional U-Pb zircon ages of analyzed samples became younger up-section with peak MDAs at 43.1 ± 0.29 Ma, 42.6 ± 0.32 Ma and 38.6 ± 0.19 Ma, and MLAs at 43.5 ± 0.64 Ma, 42.7 ± 0.66 Ma and 37.6 ± 0.85 Ma. These data make it possible to refine the stratigraphic age of the studied section and reveal that the Maastrichtian sedimentary sequence is separated from the Lutetian–Bartonian sequence by a stratigraphic unconformity.

- The Upper Cretaceous-Eocene sedimentary rocks of the Huallaga Basin are characterized by two depositional systems: a tide-dominated system and a lacustrine system.

- Two marine transgressions occurred during the Maastrichtian and Bartonian epochs. They are dominated by brackish to freshwater tide-influenced siliciclastic sequences that indicate the presence of a regional embayment in northwestern South America during these time intervals.

- The middle Eocene interval (Lutetian) is characterized by the establishment of a lacustrine setting with contrasting seasons (wet and dry).

The presence of a shallow marine incursion in Western Amazonia during the Eocene might have involved biogeographical isolation, and as such, it may have promoted allopatric speciation for terrestrial organisms. This biogeographic context may have thus played a role in shaping the emergence of post-Paleogene regional biodiversity.

Acknowledgments

This work received financial and institutional support from the IRD (Institut pour la Recherche et le Développement). This study was also supported and funded by CAPES-COFECUB program Te 924/18/88881.143095/2017-01 “Paléo-Amazone:

Evolution Néogène de l'Amazonie Brésilienne / O PALEO AMAZONAS: evolução neogênica da Amazônia Brasileira", and CNPq (Proc. 312941/2018-8) "Neogene Evolution of Brazilian Amazon". This work was supported by an "Investissements d'Avenir" grant managed by the Agence Nationale de la Recherche (CEBA, ANR-10-LABX-25-01) and by the cooperative programs ECOS-FonCyT (A14-U01) and CoopIntEER CNRS-CONICET (n°252540), in the frame of the ongoing cooperation agreement between the Museo de Historia Natural de la Universidad Nacional Mayor San Marcos (Lima, Peru) and the Institut des Sciences de l'Evolution-Université de Montpellier. We thank two anonymous reviewers as well as the editor Michelangelo Martini for valuable reviews that improved this contribution.

References

Albert, J.S., Val, P., Hoorn, C. (2018) The changing course of the Amazon River in the Neogene: center stage for Neotropical diversification. Neotrop. Ichthyol. 16, 1–24. https://doi.org/10.1590/1982-0224-20180033.

Alvim, A. M. V., Santos, R. V., Roddaz, M., Antoine, P.-O., Ramos, M. I. F., do Carmo, D. A., et al. (2021). Fossil isotopic constraints (C, O and 87Sr/86Sr) on Miocene shallow-marine incursions in Amazonia. Palaeogeogr. Palaeoclimatol. Palaeoecol. 573. doi:10.1016/j.palaeo.2021.110422.

Antoine, P.-O., Abello, M. A., Adnet, S., Altamirano Sierra, A. J., Baby, P., Billet, G., et al. (2016). A 60-million-year Cenozoic history of western Amazonian ecosystems in Contamana, eastern Peru. Gondwana Res. 31, 30–59. doi:10.1016/j.gr.2015.11.001.

Baby, P., Calderón, Y., Brusset, S., Roddaz, M., Brichau, S., Eude, A., et al. (2018). The Peruvian sub-Andean foreland Basin system: Structural overview, geochronologic constraints, and unexplored plays. AAPG Mem. 117, 91–119. doi:10.1306/13622118M1173767.

Baby, P., Rivadeneira, M., Barragán, R., Christophoul, F. (2013). Thick-skinned tectonics in the Oriente foreland basin of Ecuador. In: Thick-Skin-Dominated Orogens: From Initial Inversion to Full Accretion. (eds) Nemčok, M., Mora, A., Cosgrove, J. W. Geological Society, London, Special Publications, 377, 59–76.

Bayona, G., M. Baquero, C. Ramirez, M. Tabares, A. F. Salazar, G. Nova, E. Duarte, A. Pardo, A. Plata, C. Jaramillo, G. Rodriguez, V. Caballero, A. Cardona, C. Montes, S. Gomez-Marulanda, and A. Cardenas-Rozo. (2021) Unraveling the widening of the

earliest Andean northern orogen: Maastrichtian to early Eocene intra-basinal deformation in the northern Eastern Cordillera of Colombia. Basin Research 33:809-845.

Boonstra, M., Ramos, M. I. F., Lammertsma, E. I., Antoine, P.-O., and Hoorn, C. (2015). Marine connections of Amazonia: Evidence from foraminifera and dinoflagellate cysts (early to middle Miocene, Colombia/Peru). Palaeogeogr. Palaeoclimatol. Palaeoecol. 417, 176–194. doi:10.1016/j.palaeo.2014.10.032.

Bühn, B., Pimentel, M. M., Matteini, M., and Dantas, E. L. (2009). High spatial resolution analysis of Pb and U isotopes for geochronology by laser ablation multi-collector inductively coupled plasma mass spectrometry (LA-MC-ICP-MS). An. Acad. Bras. Cienc. 81, 99–114. doi:10.1590/s0001-37652009000100011.

Burne, R.V., Bauld, J. and deDecker, P. (1980) Saline lake charophytes and their geological significance. J. sedim. Petrol. 50, 281-293.

Caballero, V-M.; Naranjo, J-F.; Rodriguez, G.; Gomez, P-D.; Mora, A.; Villamizar, C.; Miller, F.; Gélvez, J. (2020) Eocene Facies Successions and Environments in The Southern Llanos Basin, Colombia. Ciencia, Tecnologia y Futuro Vol 10, Num 1, 107- 122.

Calderón, Y., Baby, P., Hurtado, C., and Brusset, S. (2017a). Thrust tectonics in the Andean retro-foreland Basin of northern Peru: Permian inheritances and petroleum implications. Mar. Pet. Geol. 82, 238–250. doi:10.1016/j.marpetgeo.2017.02.009.

Calderón, Y., Vela, Y., Hurtado, C., Bolaños, R., Baby, P., Eude, A., et al. (2017b). Petroleum systems restoration of the Huallaga-Marañon Andean retroforeland Basin, Peru. AAPG Mem. 114, 95–116. doi:10.1306/13602026M1143702.

Cappetta, H., and Gayet, M. (2013). A new elasmobranch genus (Myliobatiformes, Dasyatoidea) from the Danian of Potosí (Bolivia). Neues Jahrb. Geol. Palaontologie - Abh. 269, 285–290. doi:10.1127/0077-7749/2013/0351.

Carrillo, E., Barragán, R., Hurtado, C., Calderón, Y., Martín, G., Vázquez-Taset, Y., Parra, M., Rivera, A., Cadena, F.M., Sarmiento, L. 2021. Depositional sequences in northern Peru: new insights on the palaeogeographic and palaeotectonic reconstruction of western Gondwana during late Permian and Triassic. Journal of the Geological Society 2021; 178 (6): jgs2020–186. doi: https://doi.org/10.1144/jgs2020-186

Carvalho, M. R., Jaramillo, C., De la Parra, F., Caballero-Rodriguez, D., Herrera, F., Wing, S., Turner, B. L., D'Apolito, C., Romero-Baez, M., Narváez, P., Martinez, C., Gutierrez, M., Labandeira, C., Bayona, G., Rueda, M., Paez-Reyes, M., Cardenas, D., Duque, A., Crowley, J. L., Santos, C., Silvestro, D. (2021) Extinction at the end-Cretaceous and the origin of modern Neotropical rainforests. Science 372:63-68.

Christophoul, F., Baby, P., and Dávila, C. (2002). Stratigraphic responses to a major tectonic event in a foreland Basin: The Ecuadorian Oriente Basin from Eocene to Oligocene times. Tectonophysics 345, 281–298. doi:10.1016/S0040-1951(01)002177

Collinson, J.D. (1996) Alluvial Sediments. In: Reading, H.G., Ed., Sedimentary Environments: Processes, Facies and Stratigraphy, 3rd Edition, Blackwell Science, Oxford, 37-81.

Dalrymple, R.W. (1984) Morphology and internal structure of sand waves in the Bay of Fundy. Sedimentology 31, 365–382.

Dalrymple, R.W., Zaitlin, B.A., Boyd, R. (1992) Estuarine facies models: conceptual basis and stratigraphic implications. Journal of Sedimentary Petrology, Vol. 62, No. 6, 1130-1146.

Dalrymple, R.W., Choi, K.S. (2007) Morphologic and facies trends through the fluvialmarine transition in tide-dominated depositional systems: a schematic framework for environmental and sequence-stratigraphic interpretation. Earth Science Reviews 81, 135–174.

Dashtgard, S.E., Gingras, M.K. (2012) Chapter 10: marine invertebrate neoichnology. In: Knaust, D., Bromley, R.G. (Eds.), Trace Fossils as Indicators of Sedimentary Environments. Elsevier, New York, pp. 273–295.

De La Parra, F., Pinzon, D., Mantilla-Duran, F., Rodriguez, G., and Caballero, V. (2021). Marine-lacustrine systems during the Eocene in northern South America – Palynological evidence from Colombia. J. South Am. Earth Sci. 108, 103188. doi:10.1016/j.jsames.2021.103188.

De Mowbray, T., Visser, M.J. (1984) Reactivation surfaces in subtidal channel deposits, Oosterschelde, southwest Netherlands. Journal of Sedimentary Petrology 54, 811–824.

DeCelles, P. G., and Giles, K. A. (1996). Foreland Basin systems. Basin Res. 8, 105–123. doi:10.1046/j.1365-2117.1996.01491.x.

Dickinson, W. R., and Gehrels, G. E. (2009). Use of U-Pb ages of detrital zircons to infer maximum depositional ages of strata: A test against a Colorado Plateau Mesozoic database. Earth Planet. Sci. Lett. 288, 115–125. doi:10.1016/j.epsl.2009.09.013.

Dunham, R.J. (1962) Classification of Carbonate Rocks According to Depositional Texture. In: Ham, W.E., Ed., Classification of Carbonate Rocks, AAPG, Tulsa, 108-121.

Eakin, C. M., Lithgow-Bertelloni, C., and Dávila, F. M. (2014). Influence of Peruvian flat-subduction dynamics on the evolution of western Amazonia. Earth Planet. Sci. Lett. 404, 250–260. doi:10.1016/j.epsl.2014.07.027.

Espurt, N., Baby, P., Brusset, S., Roddaz, M., Hermoza, W., and Barbarand, J. (2010). The Nazca Ridge and Uplift of the Fitzcarrald Arch: Implications for Regional Geology in Northern South America. Amazon. Landsc. Species Evol. Look Past, 89–100. doi:10.1002/9781444306408.ch6.

Espurt, N., Baby, P., Brusset, S., Roddaz, M., Hermoza, W., Regard, V., et al. (2007). How does the Nazca Ridge subduction influence the modern Amazonian foreland Basin? Geology 35, 515–518. doi:10.1130/G23237A.1.

Eude, A., Roddaz, M., Brichau, S., Brusset, S., Calderon, Y., Baby, P., et al. (2015). Controls on timing of exhumation and deformation in the northern Peruvian Eastern Andean wedge as inferred from low-temperature thermochronology and balanced cross section. Tectonics 34, 715–730. doi:10.1002/2014TC003641.

Figueiredo, J., Hoorn, C., van der Ven, P., and Soares, E. (2009). Late Miocene onset of the Amazon River and the Amazon deep-sea fan: Evidence from the Foz do Amazonas Basin. Geology 37, 619–622. doi:10.1130/G25567A.1.

Flemming, B.W. (2012). Siliciclastic Back-Barrier Tidal Flats. In: Davis Jr., R., Dalrymple, R. (eds) Principles of Tidal Sedimentology. Springer, Dordrecht. https://doi.org/10.1007/978-94-007-0123-6_10.

Flügel, E. (2010). Microfacies of Carbonates Rocks - Analysis, Interpretation and Application. 2nd ed. , ed. A. Munnecke Springer doi:10.1007/10.1007/978-3-642-03796-2.

Galbraith, R.F. (2005) Statistics for Fission Track Analysis. CRC Press.

Galbraith, R., Laslett, G., (1993) Statistical models for mixed fission track ages. Nucl. Tracks Radiat. Meas. 21 (4), 459–470.

Gayet, M., Meunier, F. J., and Werner, C. (2002). Diversification in Polypteriformes and special comparison with the Lepisosteiformes. Palaeontology, 45(2), 361-376.

George, S. W. M., Horton, B. K., Jackson, L. J., Moreno, F., Carlotto, V., and Garzione, C. N. (2019). Sediment provenance variations during contrasting Mesozoic-early Cenozoic tectonic regimes of the northern Peruvian Andes and Santiago-Marañón foreland Basin. doi:10.1016/b978-0-12-816009-1.00012-5.

Gehrels, G. (2014). Detrital zircon U-Pb geochronology applied to tectonics. Annu. Rev. Earth Planet. Sci. 42, 127–149. doi:10.1146/annurev-earth-050212-124012.

Gehrels, G. E., Valencia, V. A., and Ruiz, J. (2008). Enhanced precision, accuracy, efficiency, and spatial resolution of U-Pb ages by laser ablation-multicollector-inductively coupled plasma-mass spectrometry. Geochem. Geophys. Geosystems 9, 1–13. doi:10.1029/2007GC001805.

Gorini, C., Haq, B. U., dos Reis, A. T., Silva, C. G., Cruz, A., Soares, E., et al. (2014). Late Neogene sequence stratigraphic evolution of the Foz do Amazonas Basin, Brazil. Terra Nova 26, 179–185. doi:10.1111/ter.12083.

Guiguer, K.R.R.A.; Drimmie, R.; Power, M. (2003) Validating methods for measuring d18O and d13C in otoliths from freshwater fish. Rapid Commun. Mass Spectrom. 2003; 17: 463–471

Gutierrez M. (1982). - Evaluación potencial petrolífero cuencas Huallaga, Ucayali y Madre de Dios. Zonación bioestratigráfica del intervalo Cretáceo superior-Terciario inferior. - Petroperú, Rapport interne inédit, Lima, 29 p.

Gutiérrez, E.G., Horton, B.K., Vallejo, C., Jackson, L.J., George, S.W.M. (2019) Provenance and geochronological insights into Late Cretaceous-Cenozoic foreland basin development in the Subandean Zone and Oriente Basin of Ecuador. In: Horton, B.K., Folguera, A. (Eds.),Andean Tectonics. Elsevier, pp. 237–268. https://doi.org/10.1016/B978-0-12-816009-1.00011-3.

Hermoza, W. (2004). Dynamique tectono-sédimentaire et restauration séquentielle du rétro-bassin d'avant-pays des Andes centrales. http://www.theses.fr. Available at: http://www.theses.fr/2004TOU30134 [Accessed January 10, 2022].

Hermoza, W., Brusset, S., Baby, P., Gil, W., Roddaz, M., Guerrero, N., et al. (2005). The Huallaga foreland Basin evolution: Thrust propagation in a deltaic environment, northern Peruvian Andes. J. South Am. Earth Sci. 19, 21–34. doi:10.1016/j.jsames.2004.06.005.

Hoorn, C. (1993). Marine incursions and the influence of Andean tectonics on the Miocene depositional history of northwestern Amazonia: results of a palynostratigraphic study. Palaeogeogr. Palaeoclimatol. Palaeoecol. 105, 267–309. doi:10.1016/0031-0182(93)90087-Y.

Hoorn, C., Bogotá-A, G. R., Romero-Baez, M., Lammertsma, E. I., Flantua, S. G. A., Dantas, E. L., et al. (2017). The Amazon at sea: Onset and stages of the Amazon River from a marine record, with special reference to Neogene plant turnover in the drainage Basin. Glob. Planet. Change 153, 51–65. doi:10.1016/j.gloplacha.2017.02.005.

Hoorn, C., Wesselingh, F. P., Hovikoski, J., and Guerrero, J. (2010a). The Development of the Amazonian Mega-Wetland (Miocene; Brazil, Colombia, Peru, Bolivia). Amazon. Landsc. Species Evol. Look Past, 123–142. doi:10.1002/9781444306408.ch8.

Hoorn, C., Wesselingh, F. P., Ter Steege, H., Bermudez, M. A., Mora, A., Sevink, J., et al. (2010b). Amazonia through time: Andean uplift, climate change, landscape evolution, and biodiversity. Science 330, 927–931. doi:10.1126/science.1194585.

Horton, B. K. (2018). Sedimentary record of Andean mountain building. Earth-Sci. Rev. 178, 279–309. doi:10.1016/j.earscirev.2017.11.025.

Horton, B. K. (2022) Unconformity development in retroarc foreland basins: implications for the geodynamics of Andean-type margins. Journal of the Geological Society, vol. 179.

Hovikoski, J., Wesselingh, F. P., Räsänen, M., Gingras, M., and Vonhof, H. B. (2010). “Marine influence in Amazonia: evidence from the geological record,” in Amazonia, Landscape and Species Evolution, ed. C. Hoorn and F.P. Wesselingh. (Blackwell Publishing), 143–161.

Hurtado, C., Roddaz, M., Santos, R. V., Baby, P., Antoine, P.-O., and Dantas, E. L. (2018). Cretaceous-early Paleocene drainage shift of Amazonian rivers driven by Equatorial Atlantic Ocean opening and Andean uplift as deduced from the provenance of northern Peruvian sedimentary rocks (Huallaga Basin). Gondwana Res. 63, 152–168. doi:10.1016/j.gr.2018.05.012.

Ingram, B. L., Conrad, M. E., and Ingle, J. C. (1996). Stable isotope and salinity systematics in estuarine waters and carbonates: San Francisco Bay. Geochim. Cosmochim. Acta 60, 455–467. doi:10.1016/0016-7037(95)00398-3.

Jackson, S.E., Pearson, N.J., Griffin, W.L., Belousova, E. (2004) The application of laser ablation inductively coupled plasma mass spectrometry to in-situ U–Pb zircon geochronology. Chem. Geol. 211, 47–69.

Jaillard, E., Bengtson, P., and Dhondt, A. V. (2005). Late Cretaceous marine transgressions in Ecuador and northern Peru: A refined stratigraphic framework. J. South Am. Earth Sci. 19, 307–323. doi:10.1016/j.jsames.2005.01.006.

Jaramillo, C., Rueda, M., Torres, V. (2011) A palynological zonation for the Cenozoic of the Llanos and Llanos Foothills of Colombia. Palynology. Volume 35, p. 46-84.

Jaramillo, C., Rueda, M. (2021) A Morphological Electronic Database of Cretaceous-Tertiary Fossil Pollen and Spores from Northern South America V. 2012-2021. Smithsonian Tropical Research Institute. http://biogeodb.stri.si.edu/jaramillo/palynomorph/

Jaramillo, C., Romero, I., D'Apolito, C., Bayona, G., Duarte, E., Louwye, S., et al. (2017). Miocene flooding events of western Amazonia. Sci. Adv. 1–12. doi:10.1126/sciadv.1601693.

Johnson, S.T. and Dashtgard, S.E. (2014) Inclined heterolithic stratification in a mixed tidal–fluvial channel: Differentiating tidal versus fluvial controls on sedimentation. Sedimentary Geology. 301, 41-53.

Keith, M. L., Anderson, G. M., and Eichler, R. (1964). Carbon and oxygen isotopic composition of mollusk shells from marine and fresh-water environments. Geochim. Cosmochim. Acta 28, 1757–1786. doi:10.1016/0016-7037(64)90021-3.

Klein, G. de V. (1970) Depositional and dispersal dynamics of intertidal sand bars. Journal of Sedimentary Petrology 40, 1095–1127.

Kummel, B. (1948). Geological reconnaissance of the Contamana Region, Peru. Geol. Soc. Am. Bull. 12, 1217–1266. doi:10.1130/0016-7606(1948)59.

Logvina, E., Mazurenko, L., Prasolov, E. (2004) Isotopic composition of carbon-13 and oxygen-18 from authigenic carbonates. In: Black Sea Region. AGU Spring Meeting Abstracts.

Longhitano, S. G., Mellere, D., Steel, R. J., and Ainsworth, R. B. (2012). Tidal depositional systems in the rock record: A review and new insights. Sediment. Geol. 279, 2–22. doi:10.1016/j.sedgeo.2012.03.024.

Louterbach, M., Fernández, O., Sisinni, V., Gutierrez, M., and Zamora, G. (2018a). "Stratigraphy, Structure, and Hydrocarbon Potential of the Northern Bolivia Sub-Andean Thrust Belt (Beni Basin)," in Petroleum Basins and Hydrocarbon Potential of the Andes of Peru and Bolivia AAPG Memoirs. (AAPG), 377–413.

Louterbach, M., Roddaz, M., Antoine, P.-O., Marivaux, L., Adnet, S., Bailleul, J., et al. (2018b). Provenance record of late Maastrichtian–late Palaeocene Andean Mountain building in the Amazonian retroarc foreland Basin (Madre de Dios Basin, Peru). Terra Nova 30, 17–23. doi:10.1111/ter.12303.

Louterbach, M., Roddaz, M., Bailleul, J., Antoine, P.-O., Adnet, S., Kim, J. H., et al. (2014). Evidences for a Paleocene marine incursion in southern Amazonia (Madre de Dios Sub-Andean Zone, Peru). Palaeogeogr. Palaeoclimatol. Palaeoecol. 414, 451–471. doi:10.1016/j.palaeo.2014.09.027.

Miall, A. D. (1978). Lithofacies types and vertical profile models in braided river deposits: a summary. Fluv. Sedimentol. 5, 597–600.

Miall, A.D. (1996) The Geology of Fluvial Deposits, Sedimentary Facies, Basin Analysis and Petroleum Geology. Sprin-ger, Berlin.

Miall, A. D. (2006). The Geology of Fluvial Deposits. doi:10.1007/978-3-662-03237-4.

Moreno, F., Garzione, C. N., George, S. W. M., Horton, B. K., Williams, L., Jackson, L. J., et al. (2020). Coupled Andean Growth and Foreland Basin Evolution, Campanian–Cenozoic Bagua Basin, Northern Peru. Tectonics 39. doi:10.1029/2019TC005967.

Moreno, F.; Garzione, C.N.; George, S.W.M.; Williams, L.; Richter, F.; Bandeian, A. (2022) Late Cretaceous through Cenozoic Paleoenvironmental History of the Bagua Basin, Peru: Paleoelevation Comparisons with the Central Andean Plateau. Geosciences, 12, 242. https://doi.org/10.3390/ geosciences12060242

Naeser, C. W., Crochet, J. Y., Jaillard, E., Laubacher, G., Mourier, T., and Sigé, B. (1991). Tertiary fission-track ages from the Bagua syncline (northern Peru): Stratigraphic and tectonic implications. J. South Am. Earth Sci. 4, 61–71. doi:10.1016/0895-9811(91)90018-G.

Nichols, G. (2009). Sedimentology and stratigraphy - Second Edition. 2nd ed. Wiley-Blackwell.

Odoh, S., Saylor, J. E., Higuera, C., Copeland, P., and Lapen, T. J. (2019). Chapter 6: Discriminating mechanisms for coarse clastic progradation in the Colombian foreland Basin using detrital zircon double dating. In: Andean Tectonics, eds. B. K. Horton and A. Folguera (Elsevier), 133–171. doi:10.1016/B978-0-12-816009-1.00008-3.

Paton, C., Hellstrom, J., Paul, B., Woodhead, J., and Hergt, J. (2011). Iolite: Freeware for the visualisation and processing of mass spectrometric data. J. Anal. At. Spectrom. 26, 2508–2518. doi:10.1039/c1ja10172b.

Petrus, J.A. and Kamber, B.S. (2012) VizualAge: A Novel Approach to Laser Ablation ICP-MS U-Pb Geochronology Data Resolution. Geostandards and Geoanalytical Research. Volume36, Issue 3, pages 247-270.

Platt, N.H., Wright, V.P. (1991) Lacustrine carbonates: facies models, facies distributions and hydrocarbon aspects. In: Anado´n, P., Cabrera, L., Kelts, K. (Eds), Lacustrine Facies Analysis. International Association of Sedimentologists, Special Publication 13, pp. 57– 74.

Roddaz, M., Baby, P., Brusset, S., Hermoza, W., and Darrozes, J. M. (2005a). Forebulge dynamics and environmental control in Western Amazonia: The case study of the Arch of Iquitos (Peru). Tectonophysics 399, 87–108. doi:10.1016/j.tecto.2004.12.017.

Roddaz, M., Viers, J., Brusset, S., Baby, P., and Hérail, G. (2005b). Sediment provenances and drainage evolution of the Neogene Amazonian foreland Basin. Earth Planet. Sci. Lett. 239, 57–78. doi:10.1016/j.epsl.2005.08.007.

Roddaz, M., Hermoza, W., Mora, A., Baby, P., Parra, M., Christophoul, F., et al. (2010). Cenozoic Sedimentary Evolution of the Amazonian Foreland Basin System. Amazon. Landsc. Species Evol. Look Past, 61–88. doi:10.1002/9781444306408.ch5.

Sacek, V. (2014). Drainage reversal of the Amazon River due to the coupling of surface and lithospheric processes. Earth Planet. Sci. Lett. 401, 301–312. doi:10.1016/j.epsl.2014.06.022.

Santos, C., Jaramillo, C., Bayona, G., Rueda, M., and Torres, V. (2008). Late Eocene marine incursion in north-western South America. Palaeogeogr. Palaeoclimatol. Palaeoecol. 264, 140–146. doi:10.1016/j.palaeo.2008.04.010.

Sempere, T., Butler, R. F., Richards, D. R., Marshall, L. G., Sharp, W., and Swisher, C. C. (1997). Stratigraphy and chronology of Upper Cretaceous-lower Paleogene strata in Bolivia and northwest Argentina. Bull. Geol. Soc. Am. 109, 709–727. doi:10.1130/0016-7606

Sharman, G. R., Sharman, J. P., and Sylvester, Z. (2018). detritalPy: A Python- based toolset for visualizing and analysing detrital geo-thermochronologic data. Depositional Rec. 4, 202–215. doi:10.1002/dep2.45.

Sharman, G. R., and Malkowski, M. A. (2020). Needles in a haystack: Detrital zircon U-Pb ages and the maximum depositional age of modern global sediment. Earth-Sci. Rev. 203, 103-109. doi:10.1016/j.earscirev.2020.103109.

Shephard, G. E., Müller, R. D., Liu, L., and Gurnis, M. (2010). Miocene drainage reversal of the Amazon River driven by plate-mantle interaction. Nat. Geosci. 3, 870–875. doi:10.1038/ngeo1017.

Thomas, R.G.; Smith, D.G.; Wood, J.M.; Visser, J.; Calverley-Range, E.A.; Koster, E.H. (1987) Inclined Heterolithic Stratification-Terminology, Description, Interpretation and Significance. Sedimentary Geology, 53, 123-179.

Traverse, A. 2007. Paleopalynology, Second Edition. 813 p., Springer, Dordrecht.

Tucker, M. E., and Wright, P. V. (1990). Carbonate Sedimentology. Blackwell Science.

van Soelen, E. E., Kim, J. H., Santos, R. V., Dantas, E. L., Vasconcelos de Almeida, F., Pires, J. P., et al. (2017). A 30 Ma history of the Amazon River inferred from terrigenous sediments and organic matter on the Ceará Rise. Earth Planet. Sci. Lett. 474, 40–48. doi:10.1016/j.epsl.2017.06.025.

Varol, B. (2015). Stable Isotopes (d18O, d13C) of Mollusk Shells in Environmental Interpretations; An Example From Sinop Miocene Succession (Northern TURKEY). Miner. Res Expl Bull 128, 49–60. doi:10.19111/bmre.26386.

Vermeesch, P. (2021) Maximum depositional age estimation revisited. Geoscience Frontiers 12, 843-850. https://doi.org/10.1016/j.gsf.2020.08.008

Vermeesch, P. (2018) IsoplotR: a free and open toolbox for geochronology. Geosci. Front., 9, pp. 1479-1493.

Visser, M.J. (1980) Neap-spring cycles reflected in Holocene subtidal large-scale bedform deposits: a preliminary note. Geology 8:543–546.

Vonhof, H.B., Wesselingh, F.P., Ganssen, G.M. (1998) Reconstruction of the Miocene Western Amazonian aquatic system using moluscan isotopes signatures. Palaeogeogr. Palaeoclimatol. Palaeoecol. 141, 85–93.

Walker, R.G. (1992) Facies, facies models and modern stratigraphic concepts. In: Walker, R.G, James, N.P. (Eds.), Facies Models: Response to Sea-Level Change. Geological Association of Canada, Toronto, pp. 1-14.

Wiedenbeck, M., Allé, P., Corfu, F., Griffin, W. L., Meier, M., Oberli, F., Von Quadt, A., Roddick, J. C., and Spiegel, W. (1995) Three natural zircon standards for U-Th-Pb.Lu-Hf, trace element and REE analyses: Geostandards 1950 Newsletter, v. 19, p. 1-23.